



**A
Symposium
on Noise from
UASs/UAVs**

QUIET DRONES

19 – 21 October 2020

**Paris,
France**

an e-Symposium

PROCEEDINGS - At 9th October 2020

Welcome

Enormous progress has been made on drone technologies in the last decade and the number of professional drones is increasing dramatically and is now much higher than the number of conventional aircraft.

Safety, security and privacy have controlled the development of drones up to now, but noise has become an issue in residential areas and environmentally sensitive areas such as National Parks. On the other hand, ultra-silent machines represent a problem for privacy and security.

The Symposium will provide a venue for researchers on drone noise to meet with manufacturers, users and those engaged in designing innovative applications for this new technology

Because of COVID-19 the Symposium will be held as an e-Symposium.

This Symposium will last 3 days and will be live for 4 or 5 hours a day with invited presentations, panel discussions and informal discussions..

For the rest of the day other material will be available. Some of this may be in fixed time slots - for example exhibitors' presentations - but most will be available on demand such as exhibitor's material, recordings of earlier sessions and cultural tours of Paris.

Here you will find the Programme – correct at 1st October 2020 and all the papers submitted to the Symposium in alphabetical order. This is a PDF Portfolio and the programme and papers should appear as thumbnails on the left.

Jean Turret / Dick Bowdler

Technical Sessions Programme

Clicking on any individual paper in the main technical sessions pages will take you to that paper. Click on the title page will take you to session 1 of the programme.

Some presentations have no paper. If there is no link there is no paper.

OVERALL PROGRAMME

The programme for the symposium will consist of an opening session (Session 1) and nine more technical sessions at which authors will make presentations. At the end of Sessions 2 to 9 there will be a discussion centred round the session topic at which authors will be encouraged to take part. They will each last for one and a half to two and a half hours.

The Opening Session will consist of introductions from INCE Europe, CIDB, International INCE and Year of Sound. After that there will be three key presentations. We are keen that delegates from all time zones will be able to view the opening session before they see the rest of the symposium and with that in mind the whole session will be recorded so that, as well as being available from the symposium opening at 09:00 on Monday it will also be available to delegates in the Americas between 18:00 and 20:00 on Sunday evening.

There will also be "Conversation" sessions which will be informal and where you are invited to join in the conversation on a particular topic with the leaders of the conversation.

Sunday 18th October

18:00 - Prepeat of Opening Session for Delegates in the Americas

Monday 19th October

09:00 - *Session 1* - Opening Session

11:30 - *Conversation* - Come and meet the other delegates - 1 - Jean Turret and Dick Bowdler

14:30 - *Conversation* - Come and meet the other delegates - 2 - Jean Turret and Dick Bowdler

16:00 - *Session 2* - Assessing Noise and its Impact on People and Environment

16:00 - *Session 7* - Acoustic Detection and Identification of Drones

Tuesday 20th October

09:00 - *Session 3* - Specific Noise concerns with packages and deliveries

09:00 - *Session 8* - Drone Audition - Listening with Drones

11:30 - *Conversation* - Mirjam and Roalt brainstorm about Drones - Mirjam Snellen and Roalt Aalmoes

14:30 - *Conversation* - Nathan and Andy's Drone Noise Listening Party - Andrew Christian and Nathan Green

16:00 - *Session 4* - Standardisation and Regulations

Wednesday 21st October

09:00 - *Session 5* - The impact of urban air mobility

09:00 - *Session 9* - Noise generation and mitigation - 1

11:30 - *Conversation* - What's the point of a remote conference? - Andy McKenzie and Dick Bowdler

14:00 - *Session 6* - Tools for measurement, analysis, prediction and control

16:00 - *Session 10* - Noise generation and mitigation - 2

SESSION 1 : OPENING SESSIONS

Sunday 18th October 18h00-19h30 and Monday 19th October 09h00-10h30

Opening Presentations : INCE-Europe, CIDB, International-INCE et International Year of Sound

Opening Presentations :

A summary of the 2018 Workshop on UAS and UAV Noise Emissions and Noise Control Engineering Technology in Washington, DC, National Academy of Engineering.

Robert Hellweg
(Technology for a Quieter America Workshop Steering Committee)

USA

Will Noise become a new Hurdle which could impair the development of Drones

Carine Donzel
(DGAC) et
Henry de Plinval
(ONERA)

FRANCE

Drone Noise, a new public health challenge?

Antonio Torija Martinez
(University of Salford)

GREAT
BRITAIN

SESSION 2 : Assessing Noise and Noise Impact on People and Environment

Monday 19th October 16h00-18h00 (session in parallel with session 7)

Session chaired by : **Patricia Davies** (Purdue University, USA)

European Union legislation on managing noise from drones and e-VTOL	Marco Pavioti (European Commission)	EUROPE
Multi-rotor powered drone noise assessment	Xin Zhang (Hong Kong University of Science & Technology)	CHINA
Aeroacoustic measurements on a free-flying drone in a WindShaper wind tunnel	Roberto Putzu (Univ. Applied Science Geneva)	SWITZERLAND
Assessment of environmental noise characteristics of innovative aerial vehicles	Raphael Hallez (Siemens Digital Industries Software)	BELGIUM
Towards the Incorporation of Auditory Masking Effects into Assessments of Community Noise	Andrew Christian (NASA Langley Research Center)	USA
Methods for Providing Design Guidance to Improve Drone Sound using Community Input	David Bowen (Acentech)	USA
A whole-systems approach to building knowledge about human reaction to drones	Charlotte Clark (ARUP)	GREAT BRITAIN

Discussion : *Is the impact of drone noise on people different from other noise?*

SESSION 3 : Specific Noise Concerns with Packages and deliveries

Tuesday 20th October 09h00-11h00 (**session in parallel with session 8**)

Session chaired by : **Marion Burgess** (UNSW, Australie)
Andy McKenzie (Hayes McKenzie, GB)

Drone delivery and noise regulation in the Australian context

Marion Burgess
(UNSW)

AUSTRALIA

Delivery Drones at La Poste

Philippe Cassan
(DPD group / La Poste)

FRANCE

Commercial Delivery Drone Routing: A Case Study of Noise Impacts

Eddie Duncan
(RSG)

USA

Acceptance of drone delivery is limited (not only) by noise concerns

Hinnerk Eißfeldt
(DLR German Aerospace Center)

GERMANY

Discussion : *Does the Impact on people depend on what is being delivered?*

SESSION 4 : Standardisation and Regulations

Tuesday 20th October 16h00-17h30

Session chaired by : **Christopher Roof** (US Department of Transport / VOLPE, USA)

Research to Support New Entrants
to Public Airspace and Aircraft
Noise Certification

David Read / Christopher Roof
(U.S. Department of Transporta-
tion / Volpe)

USA

EU Drone Regulation

Nicolas Eertmans
(European commission)

EUROPE

ANSI/ASA Standards Activity on
Measurement of UAS Noise

Robert Hellweg
(Hellweg Acoustics)

USA

Noise requirements of Unmanned
Aircraft due to European Regula-
tion 2019/945

Michael Wieland
(UAV DACH e.V)

GERMANY

Discussion : *Should noise from drones be regulated at the European level?*

SESSION 5 : The Impact of Urban Air Mobility

Wednesday 21st October 09h00-11h00 (session in parallel with session 9)

Session chaired by : **Roalt Aalmoes** (Royal Netherlands Aerospace Centre NLR)
Franck Cléro (ONERA, France)

Recommendations for research
on the Noise impact of drones in
an urban environment

Roalt Aalmoes
(Royal Netherlands Aerospace
Centre NLR)

**NETHER-
LANDS**

MOSQUITO Project : a fast estima-
tion approach for urban acoustic
environment

Franck Cléro
(ONERA / DAAA)

FRANCE

From Helicopters to quiet eVTOLs :
A manufacturer's perspective

Julien Caillet
(Airbus Helicopters)

FRANCE

Noise considerations for desi-
gning Skyport Networks

Rohit Goyal
(Uber Elevates)

USA

Achieving quiet flying passenger
vehicles through numerical simu-
lations, a LBM story

Wouter van der Velden
(Dassault Systems)

GERMANY

Assessment of the environmental
impact of drone noise in virtual
flights

Siyang Zhong
(Hong Kong University of Science
& Technology)

CHINA

Discussion

SESSION 6 : Tools for Measurement, Analysis, Prediction and Control

Wednesday 21st October 14h00

Session chaired by : [David Herrin](#) (University of Kentucky, USA)
[François-Xavier Bécot](#) (Matelys, France)

Sound Localisation of Drones
using an Acoustic Camera

[Pablo Alloza](#)
(GFAI Tech GmbH)

GERMANY

Scanning Laser Vibrometer measure-
ments for assessing the origin of
structure borne sound in drones

[Floren Deux](#)
(Polytech France)

FRANCE

UAS Sound Level Prediction using
Panel Contribution Analysis

[David W. Herrin](#)
(University of Kentucky)

USA

Active Noise Cancellation of
Drone Propeller Noise through
Waveform Approximation and
Pitch-Shifting

[Michael Narine](#)
(Georgia State University)

USA

Exploring Noise reduction for
fixed wings UAV

[Michael J. Kingan](#)
(University of Auckland)

NEW
ZEALAND

Discussion

SESSION 7 : Acoustic Detection and Identification of Drones

Monday 19th October 16h00-18h00 (session in parallel with session 2)

Session chaired by : **Lucille Pinel-Lamotte** (MicrodB, France)

Martin Blass (Joanneum Research Forschungsgesellschaft, Austria)

Introduction Anti-Drone Solutions	Lucas Le Bell (Cerbair)	FRANCE
UAV detection from acoustic signature: requirements and state of the art	Lucille Pinel-Lamotte (MicrodB)	FRANCE
A Real-Time System for Joint Acoustic Detection and Localization of UAVs	Martin Blass (Joanneum Research Forschungsgesellschaft)	AUSTRIA
Flight path tracking and acoustic signature separation of swarm quadcopter drones using microphone array measurements	Gert Herold (Technische Universität Berlin)	GERMANY
UAV's localization from a microphone array by exploiting the harmonic structure of the sound produced	Torea Blanchard (LAUM / Le Mans University)	FRANCE
Two Dimensional Convolutional Neural Network Frameworks Using Acoustic Nodes for UAV Security Applications	Theoktisti Marinopoulou (Centre for Research and Technology Hellas / Information Technologies Institute - CERTH/ITI)	GREECE

Discussion : Drone localisation and identification

SESSION 8 : Drone Audition - Listening Drones

Tuesday 20th October 09h00-11h00 (session in parallel with session 3)

Session chaired by : **Antoine Deleforge** (INRIA, France)
Makoto Kumon (Kumamoto University, Japan)

Drone Audition for Search and Rescue: Datasets and Challenges	Antoine Deleforge (INRIA Nancy)	FRANCE
Development of surface-processed low-noise propeller for search and rescue tasks with drone audition	Kotaro Hoshiba (Kanagawa University)	JAPAN
Proposal of Cognitive Drone Audition based on Cognitive Dynamic Systems	Hiroshi Okuno (Waseda University)	JAPAN
3D Sound Source Tracking for Drones Using Direction Likelihood Integration	Taiki Yamada (Tokyo Institute of Technology)	JAPAN
Signal-to-Noise Ratio Enhancement Method for Improving Sound Source Detection of Drone-mounted Phased Microphone Array	Yeong-Ju Go (Chungnam National University)	SOUTH COREA
Advances in Sound and Speech Signal Processing at the Presence of Drones	Oliver Jokisch (Leipzig University of Telecommunications)	GERMANY

Discussion : Drone Audition

SESSION 9 : Noise Generation and Mitigation - 1

Wednesday 21st October 09h00-11h00 (session in parallel with session 5)

Session chaired by : **Young-Min Shim** (Dotterel Technologies, New-Zealand)
Julien Caillet (Airbus Helicopters, France)

Aeroacoustic study of small propellers with Serrated Trailing Edge for a quieter drone

Paolo Candeloro
(UniCusano)

ITALY

Interpolation based acoustic transfer function for drone noise simulation

Hanbo Jiang
(Hong Kong University of Science & Technology)

CHINA

Experimental Investigation of Contra-Rotating multi-rotor UAV Propeller noise

Ryan S. McKay
(Dotterel Technologies)

NEW
ZEALAND

Multi-scale morphological effect on noise level and frequency characteristics of drone propellers

Ryusuke Noda
(Kyoto University)

JAPAN

Drone Noise and the Influence of Support Structure

Simon Watkins
(RMIT)

AUSTRIA

Experimental Investigation of Noise Characteristics of Rotors

Koichi Yonezawa
(Central Research Inst. of Electric Power Industry)

JAPAN

Discussion :

SESSION 10 : Noise Generation and Mitigation - 2

Wednesday 21 October 16h00-18h00

Session chaired by : **Tiziano Pagliaroli** (UniCusano, Italie)
Julio Cordioli (University of Florianopolis, Brazil)

Experiments on UAV rotor noise at low Reynolds and low Mach numbers

Hélène Parisot-Dupuis
(ISAE-SUPAERO / Toulouse)

FRANCE

The Sound of the Drone Uprising' An Exploration into the Aero-acoustic Performance of Drone Blades

Josephine Nixon
(London South Bank University)

GREAT
BRITAIN

Experimental Investigation on Acoustics and Efficiency of Ducted Electric Rotors

Ronja Koenig
(Robert Bosch GmbH)

GERMANY

On the design of acoustic liners for drone ducted fans

Julio Cordioli
(University of Florianopolis)

BRAZIL

Chaotic and wavelet aeroacoustic analysis of twin rotors for drone propulsion

Tiziano Pagliaroli
(UniCusano)

ITALY

CFD-CAA approach for sound generation and propagation in the UAV propeller with subsonic flow

Sergei Timushev
(Moscow Aviation Institute)

RUSSIA

Discussion

Papers

The papers are in alphabetical order of lead author.



CidB

Centre d'information
sur le **Bruit**

QUIET DRONES
International e-Symposium
on
UAV/UAS Noise
Remote from Paris – 19th to 21st October 2020

**SOUND LOCALIZATION OF DRONES USING AN
ACOUSTIC CAMERA**

Pablo Alloza, gfai tech GmbH: alloza@gfaitech.de
Benjamin Vonnheim, gfai tech GmbH: vonnheim@gfaitech.de
Ali Movahed, gfai tech GmbH: movahed@gfaitech.de

Summary

Noise reduction is one of the biggest challenges for the incoming generations of unmanned aerial vehicles (UAV) and unmanned aerial systems (UAS). While for some applications noise reduction in drones can be a desirable feature, for other cases it is an absolute requirement. This paper shows how analysis based on spaced microphone arrays and beamforming algorithms (Acoustic Camera) can be used to establish a relation between noise emission and noise sources depending on other variables such as engine power, rpm or propeller type.

This paper introduces the application of the Acoustic Camera localizing and analysing the sound emissions from two different points of view. First, by determining the noise footprint and the acoustic video of a pass by measurement. Second, by focusing on the propellers, checking several models for benchmarking, using rotational beamforming algorithm in order to provide accurate acoustic pictures.

1. Introduction

The UAV and UAS sector has rapidly expanded in the last years. This is mainly due to two reasons. On the one hand, there is an increase in the use of small drones for recreational purposes like amateur photo and video recording, drone races, etc. And, on the other hand, there is further development of medium and large UAV/UAS for professional uses such as audio-visual acquisition, surveillance and security, industrial tasks, etc. This trend has given rise to a wide variety of devices with different sizes, types of propellers, arms geometry or motors power. But, regardless of this heterogeneity, all of them emit noise.

We can think about the need for noise reduction from two points of view. The first one is related to the human hearing. The noise emitted from drones at a close distance will result in high noise levels at the ears. This noise emission can range from being an annoying sound to representing a health hazard. The second motive for noise reduction is related to situations when a drone is required to minimize its noise emission so that it remains undetected.

Regardless of the purpose of noise reduction, accurately knowing the main noise sources and their frequency range is an important step in order to define solutions and improve the design of future drones. The beamforming systems based on microphone arrays, i.e. Acoustic Cameras, can provide the necessary analysis regarding noise emission. In the field of UAVs and UASs, there is a large variety of possible applications on sound source localization, ranging from the measurement and quick identification of noise sources on propellers, to the visualization of acoustic fingerprints during a drone pass-by.

This publication shows the applications of the Acoustic Camera localizing the acoustic fingerprints of three different drone models flying on top of the microphone array and localizing the sound emissions from propellers in a test bench.

2. Tests

Two different kinds of tests were developed; the first measurement campaign was focused on medium and small drones, flying stable on top of a microphone array and accelerating taking height. The second one focused on the sound emissions from propellers in a test bench.

For both measurement campaigns the same Acoustic Camera was used. The measuring system is based on a multichannel data recorder for the signal acquisition with 192 kHz sampling rate and 32 bits acquisition cards; the microphone array is the RING 48 AC PRO, a circular carbon geometry with 48 electret microphones and a RealSense camera with depth information. This system allows analysis in time and frequency domain, providing noise source localization results in photos and videos.

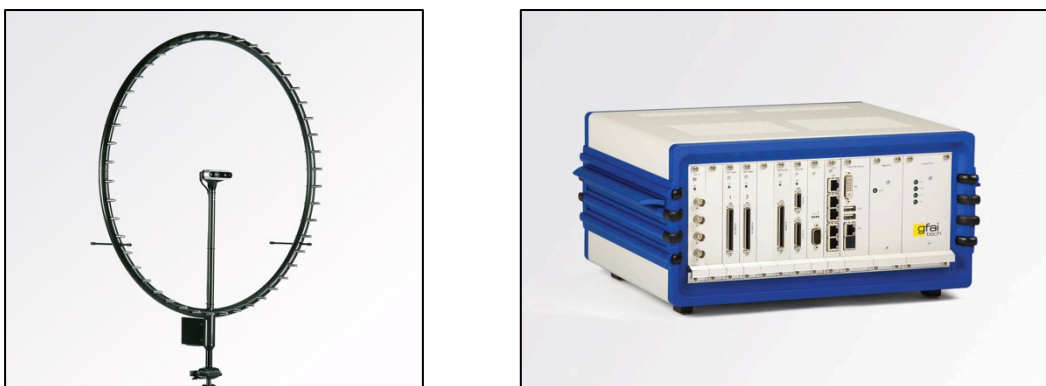


Fig. 1: Microphone array RING 48 AC PRO and data recorder mcdRec by gfaitech

2.1 Drones

The first measurement campaign was developed in a typical room (Dimensions: 56 m² surface, 5 m height) with no acoustic absorption treatment but some absorption panels in the floor around the microphone array. The drones were flown on top of the microphone array at one meter. Three different drones were measured with the next features, all of them mounting technic plastic propellers:

Specimen	Manufacturer	Model	Motor	Propeller
1	DJI	450	M2212 (920 KV)	H9450
2	Homemade	Inspection 250	M2202 (2300 KV)	H5045
3	DJI	Phantom	M2312 (980KV)	H9450

The three models were medium size with four arms, quadcopters, with the propellers mounted on top of the motor. Models 2 and 3 had a short distance between the tips of the propellers when these ones were in front of each other.

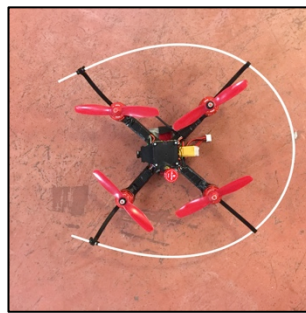
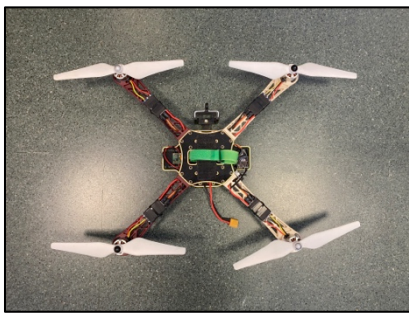


Fig. 2: From left to right: Drones 1, 2 and 3

2.2 Propellers

The second measurement campaign was developed in an anechoic chamber (Dimensions: 25 m², 5 m height). The test bench consisted of a metal support, simulating a drone arm, with a motor (Model U7 V2.0 490 rpm/V), which was set in the middle of the anechoic chamber using a metal platform. The microphone array was installed in front of the test bench, one meter away from the propeller.

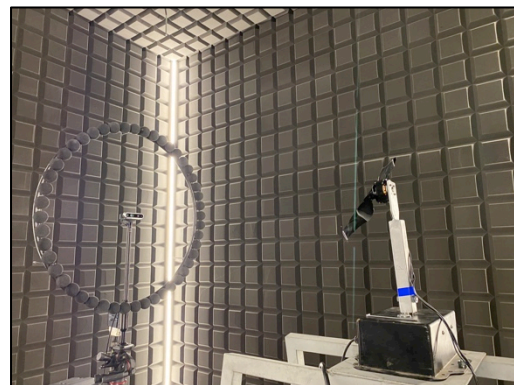


Fig. 3: Set up inside the anechoic chamber

Three different propellers were measured with the features showed in the next table. The three blades were made of carbon, which represent a good balance between toughness and flexibility, albeit at a high price.

Specimen	Manufacturer	Model	Size	Material	Foldable
A	T-Motor	CF Prop	22x6.6R	Carbon	No
B	T-Motor	CF Prop	18x6.0L	Carbon	No
C	T-Motor	CF Prop	18.2x5.9L	Carbon	Yes



Fig. 4: From left to right: Specimen A, B and C

The motor was fed with power supply (Model Polaron SMPS 1500) and controlled with a PWM controller in order to be able to select different speeds. The motor used is not the best choice for this size of blades, so we conducted measurement at maximum and medium power. The rpm at medium power fits better to the recommendations for the propellers under study.

3. Results

On this point the results from the two measurements campaigns are showed. The results are based on acoustic pictures, for both the time and frequency domains.

3.1 Acoustic Fingerprints results

The next results shows a one second integration time while the drone is flying stable on top of the microphone array, one meter distance, by third of octaves from 630 to 8,000 Hz.

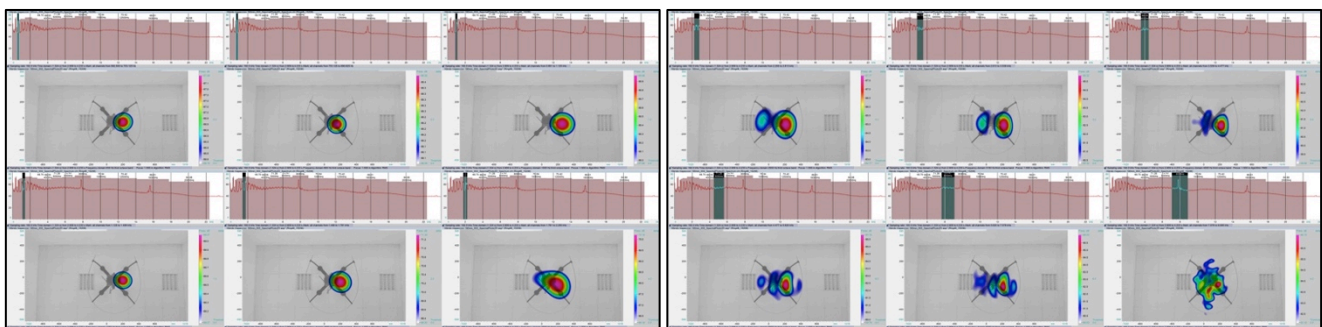


Fig. 5: Drone 1, frequency analysis by third octaves

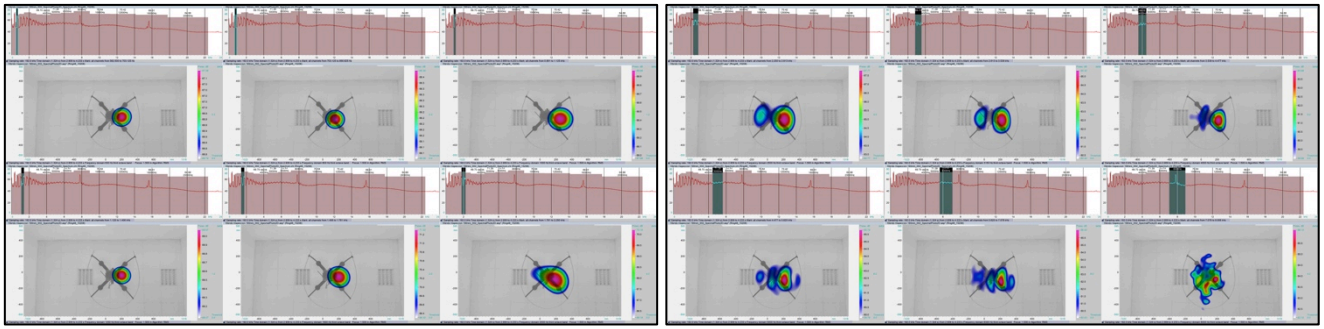


Fig. 6: Drone 2, frequency analysis by third octaves

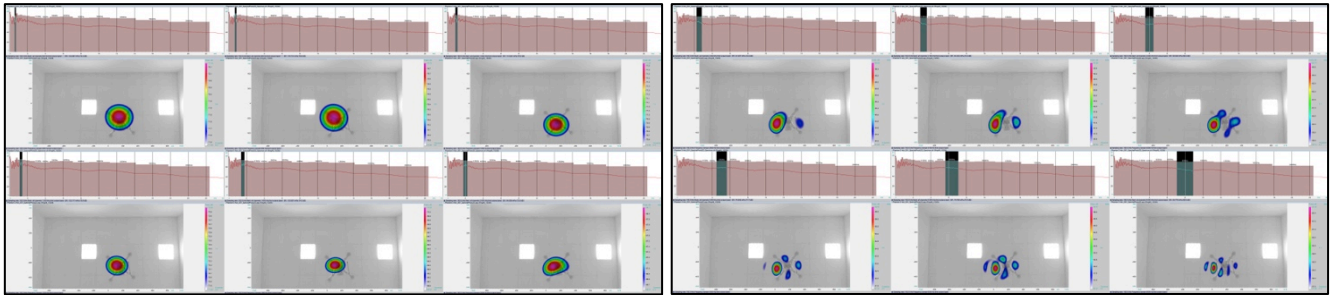


Fig. 7: Drone 3, frequency analysis by third octaves

If we want to evaluate the noise emissions from a human point of view, psychoacoustic analysis is the most suitable option in order to compare results according to universal standards. The focus should not be exclusively on noise level, since the human hearing perception is not a lineal equation, which implies that some frequencies are better identified by human hearing and some types of noises are more disturbing than others. The next results refer to a measurement starting with the drone flying stabilised on top of the microphone array at 1 meter and making a quick acceleration gaining height until approximately 4.5 meters. The graphs show the noise, loudness, sharpness and roughness levels referenced to an 8-second measurement.

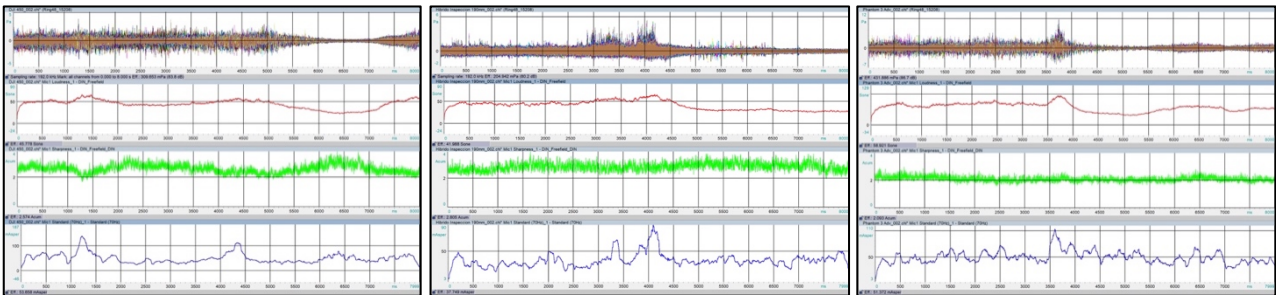


Fig. 8: From left to right, psychoacoustic analysis in drones 1, 2 and 3

According to the results, loudness level increased when the drones accelerated, related to the noise level, especially in the drone #3. Sharpness levels remained constant, regardless of the moment of acceleration; and roughness doubled the level in a peak when the acceleration starts.

Regarding the levels, the overall bigger value is 86.7 dB for drone #3; the more silent one doing this acceleration is drone #2, 80.2 dB. Drone #1 generates 83.2 dB.

3.2 Propellers results

The results developed on propellers are focused on the aerodynamic noise from the blades and the affection within the metal arm, plus the noise emission from the motor; since the measurements were conducted inside an anechoic chamber, no reflections from floor or walls influenced the recordings.

The first measurements were conducted using a downwind position, simulating the receiver position when the drone is flying. Then, the metal arm was twisted 180° in order to take an acoustic picture from the opposite point of view, with the motor in front of the microphone, using an upwind position.

The next results show the results from the time domain, two seconds time selection and using High Dynamic Range (HDR) algorithm in order to increase the dynamic range and localize noise sources with less level than the main one. The HDR is an algorithm based on beamforming and working in the time domain. Moreover, HDR is an iterative deconvolution technique that increases the dynamic of an acoustic photo and therefore facilitates the separation of sources. Hence, the procedure is especially convenient for signals containing several sources that cannot be identified separately because the difference between their sound pressure levels exceeds the dynamic range of the microphone array employed. The acoustic picture shows several noise spots, the main ones (two or three depending on the propeller analysed) are selected with a pushpin icon, with the spectrum related with this point listed on the right. In this way, it is easy to identify the frequencies related with each noise spot. On these tests the motor run at medium power. The results compare downwind position (left) and upwind position (right).

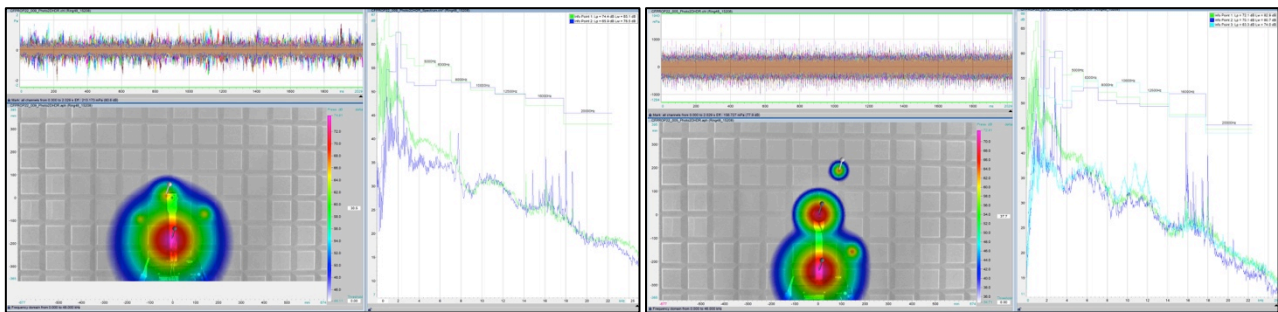


Fig. 9: Spectrum from the points selected in the acoustic photo, propeller A

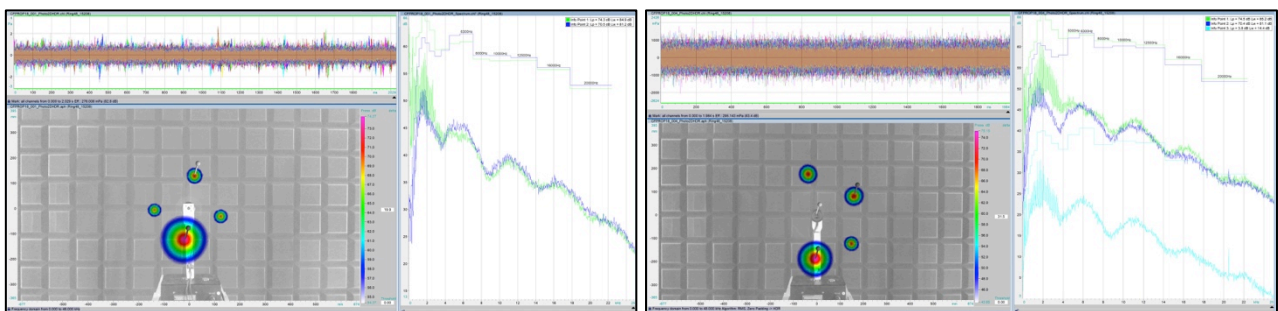


Fig. 10: Spectrum from the points selected in the acoustic photo, propeller B

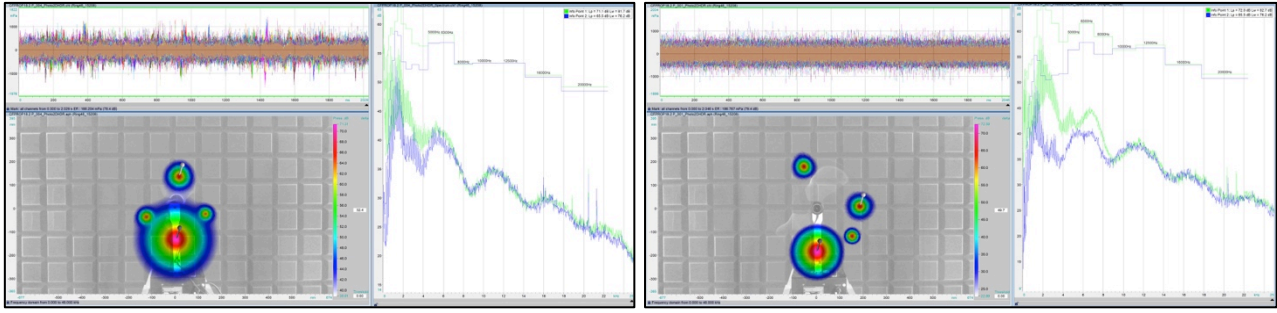


Fig. 11: Spectrum from the points selected in the acoustic photo, propeller C

The following figures compare the results between upwind and downwind positions for each propeller, filtered by third of octaves between 630 and 8,000 Hz, at medium power (around XX rpm), during two seconds recording. The advance algorithm Clean-SC ("Clean based on Source Coherence") has been used in order to increase the dynamic range and visualize more noise spots. This is an algorithm that is widely used for afterward-applied corrections of acoustic maps. In general, the algorithm minimizes the influence of the array-dependent point-spread function (PSF) on a previously calculated map so that various sources can be clearly distinguished from each other and especially from PSF-dependent side lobes, also known as "ghost sources".

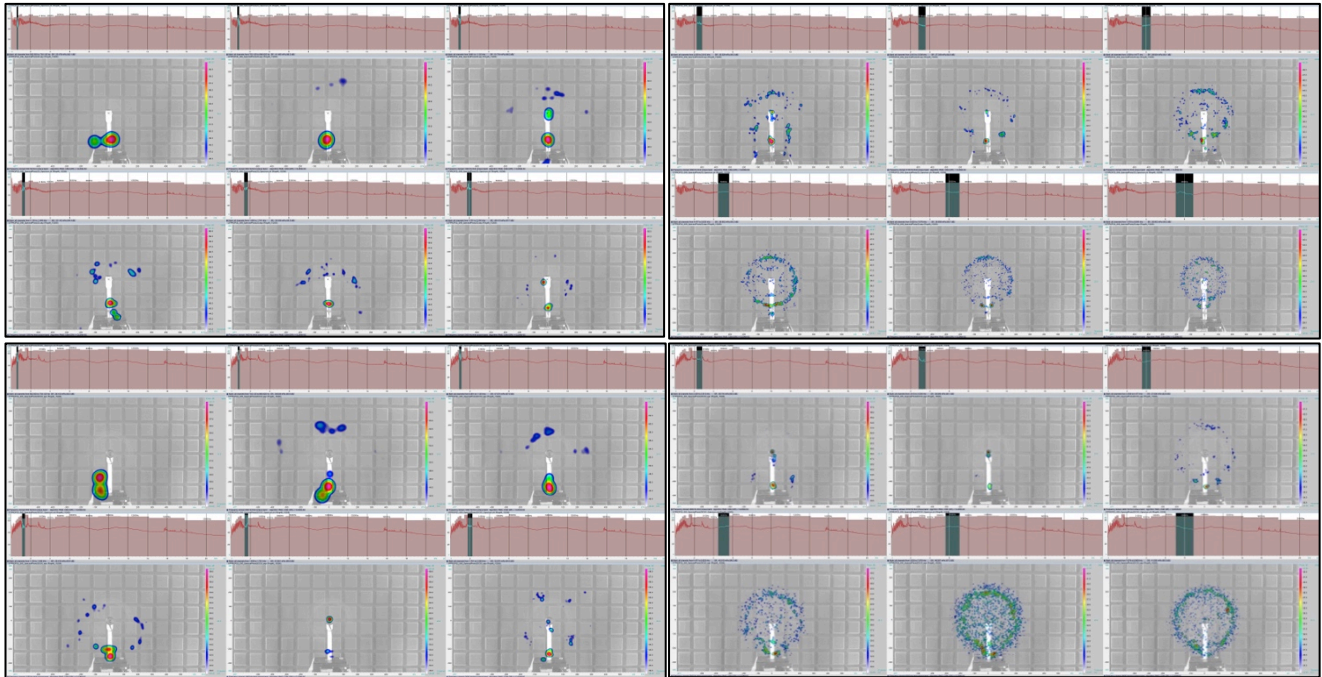


Fig. 12: Freq. analysis by third octaves, downwind (top), upwind (down), propeller A

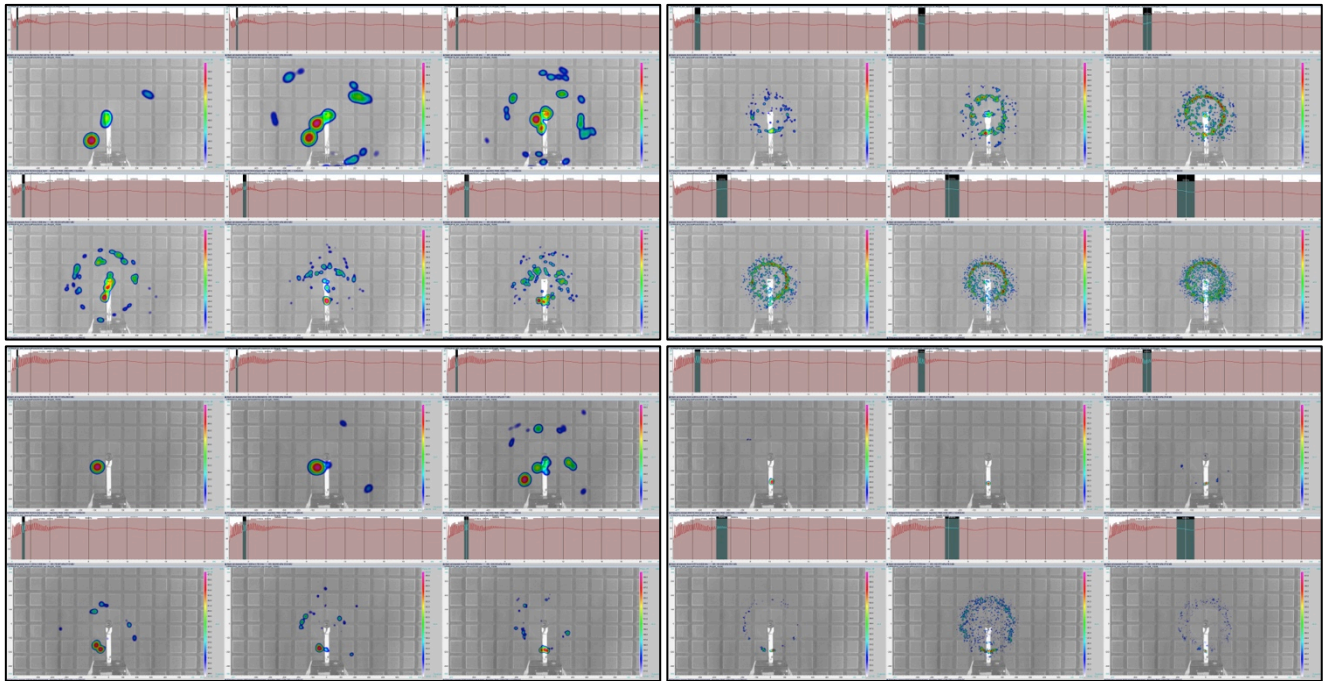


Fig. 13: Freq. analysis by third octaves, downwind (top), upwind (down), propeller B

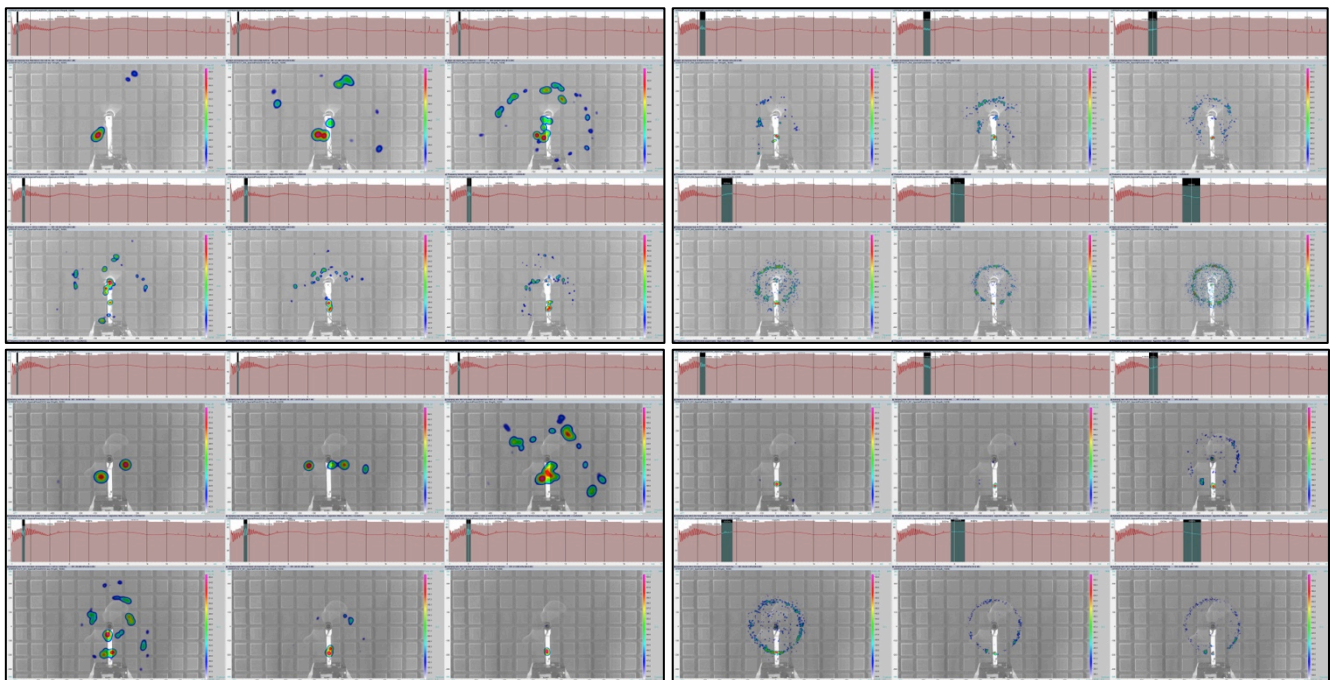


Fig. 14: Freq. analysis by third octaves, downwind (top), upwind (down), propeller C

The results show the influence of the arm, mainly in the low-middle frequency bands. This influence appears in upwind and downwind position, so the vortex created around the arm produce a sound emission in both ways, up and down.

Increasing to maximum power, the noise created around the arm is the loudest one, masking the aerodynamic and the source around the motor. The next figure represents the results from the 22 size propeller rotating at maximum power in upwind and downwind position.

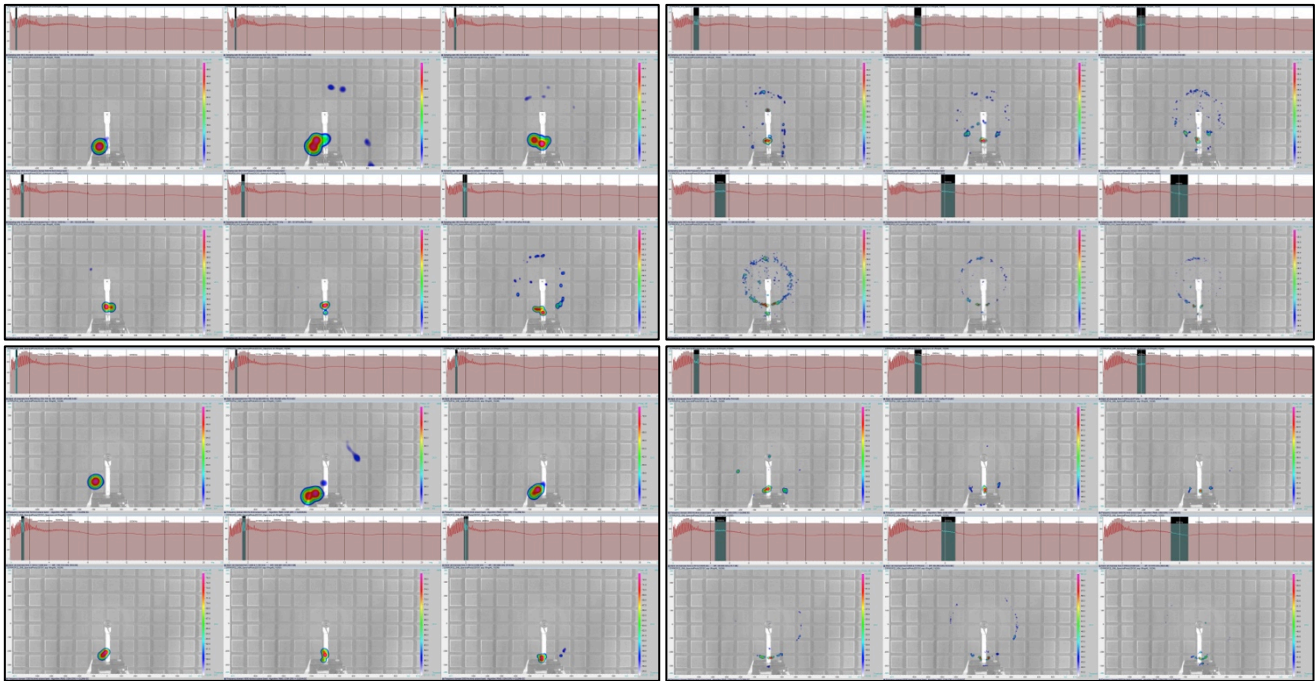


Fig. 15: Freq. analysis by third octaves, downwind (top), upwind (down), propeller A

On the same measurements, at medium and maximum power, psychoacoustic analysis was developed in order to check the difference between different rpms and different propellers. Like in the previous point about acoustic fingerprints on drones, the next graphs show the noise, loudness, sharpness and roughness levels referenced to 8 seconds measurement, starting from zero and accelerating until medium or maximum power. All the results refer to a downwind position.

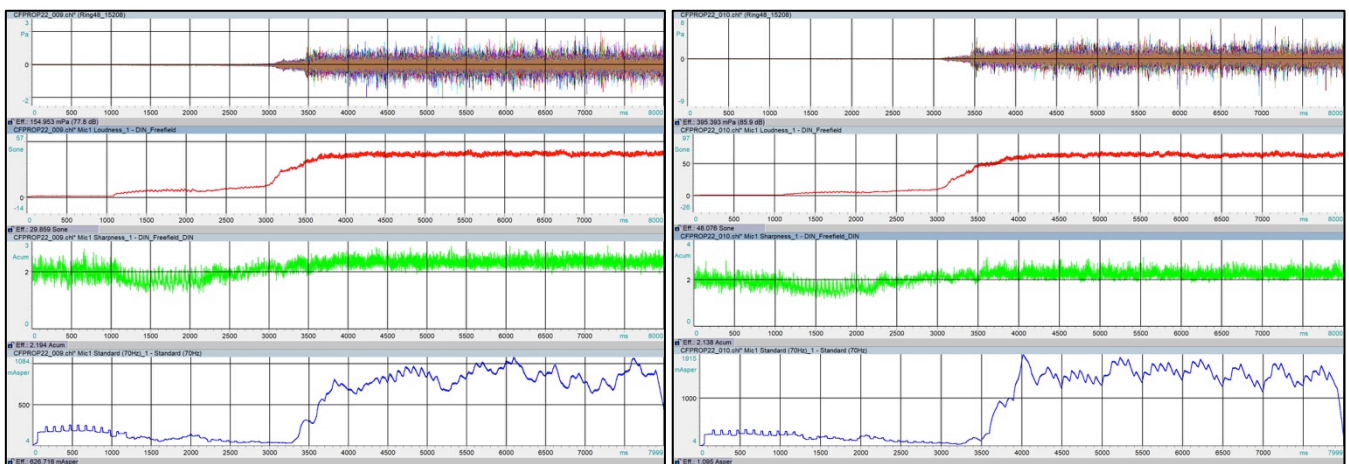


Fig. 16: Psychoacoustic analysis, medium (left) and maximum power (right), propeller A

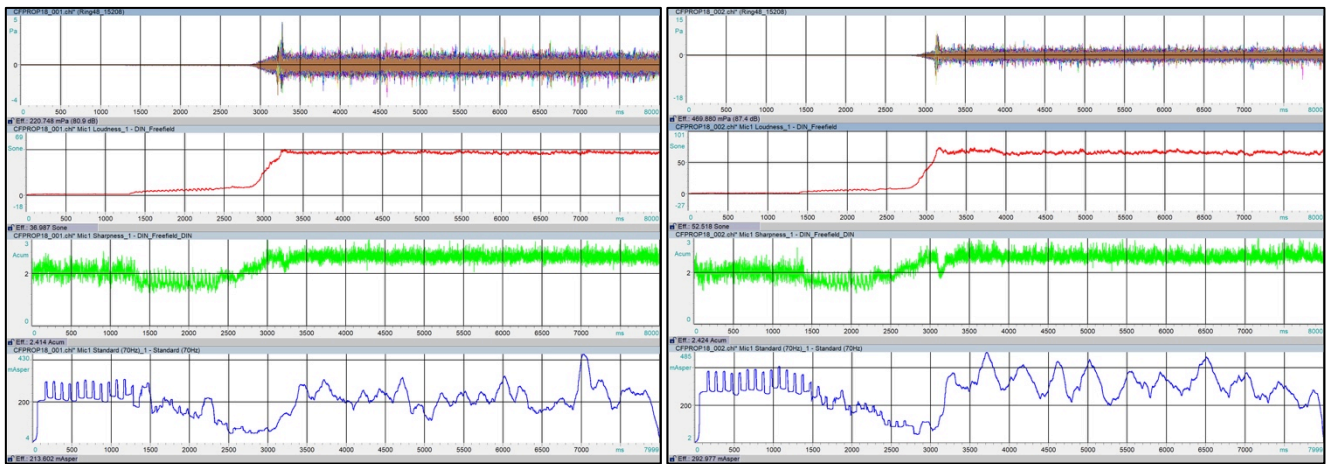


Fig. 17: Psychoacoustic analysis, medium (left) and maximum power (right), propeller B

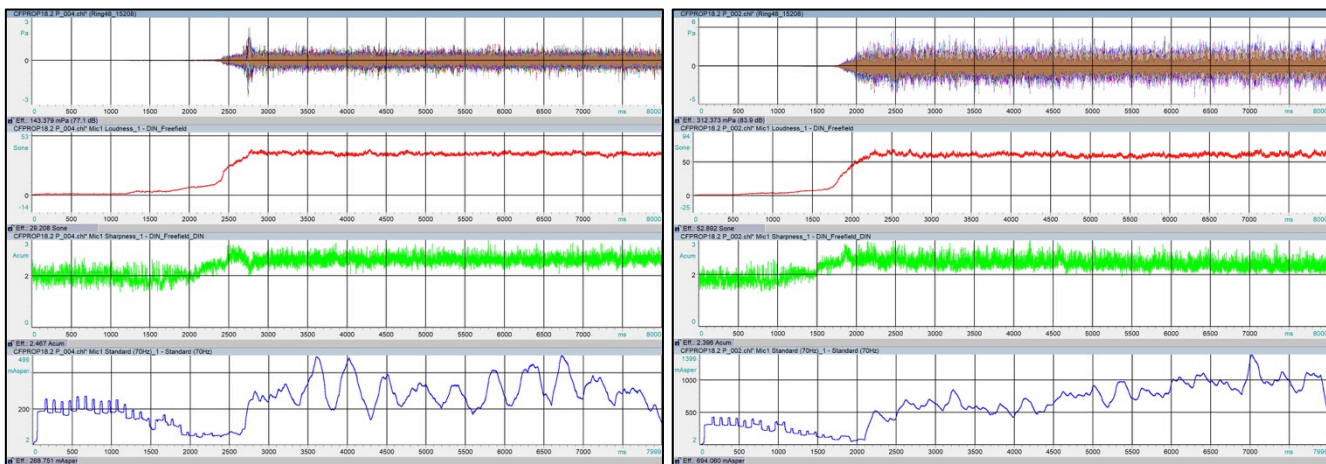


Fig. 18: Psychoacoustic analysis, medium (left) and maximum power (right), propeller C

The second propeller, the louder one, increases the noise level from 80.9 to 87.4 dB. Propeller A increases the noise level from 77.8 to 85.9 dB and propeller C from 77.1 to 83.9 dB. Sharpness stays stable around 2.5 acums for all the propellers, but Roughness doubles in value at maximum power, except for Propeller B (less increase).

For these measurement campaigns it was not possible to measure the rpm signal from the propellers during the test. With the rpm signal it is possible use rotational beamforming, this special algorithm allows for the detection of sound sources on the rotating blades by using a virtual rotation of the microphones. Results using this advance algorithm can be found in the publication “*Validation of Optoacoustic Propeller Noise Examinations*” presented on INTERNOISE 2019.

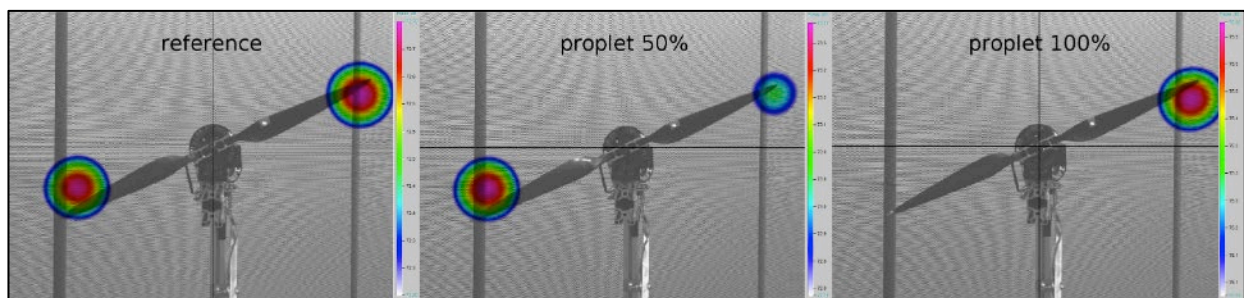


Fig. 19: Fig. 9 from the publication “*Validation of Optoacoustic Propeller...*” INTERNOISE

4. Conclusions

The introduced analyses provides several points of view to approach the localization of noise emissions from UAV/UAS and their components. The results generated by using the Acoustic Camera show the different acoustic fingerprint when a drone is flying on top of a microphone array depending on the frequency. Furthermore, the impact of propellers with different sizes and winglets was analysed in detail, providing useful information for validating the design of models according to low noise emissions.

In addition to the noise level, psychoacoustics analyses can be used to compare different UAV/UAS or even different propeller models, providing the adequate standards for comparison.

The Acoustic Camera is a powerful system able to provide a wide variety of results based on time and frequency domain, pinpointing the noise emissions in easy-to-read acoustic pictures.

References

Stefan Neugebauer, Benjamin Riebold and Dirk Döbler (2013) *Psychoacoustics in Imaging Localization of Sound Sources* DAGA

Konrad Oeckel and Sebastian Kümmritz (2019) *Validation of Optoacoustic Propeller Noise* Examinations INTERNOISE Madrid

Ralph Krause, Christian Friebe, Michael Kerscher and Christof Puhle (2018) *Investigations on noise sources on a contra-rotating axial fan with different modifications* FAN

Michael Kerscher, Jan Heimann, Dr. Christof Puhle, Konrad Oeckel, Christian Friebe and Dr. Ralph Krause (2018) *Application of rotational beamforming algorithms on fast rotating sound sources* BeBeC

Knowledge base of the Acoustic Camera website (2020)

Michael Kerscher, Gunnar Heilmann, Dr. Christof Puhle, Dr. Ralph Krause and Christian Friebe (2017) *Sound Source Localization on a Fast Rotating Fan Using Rotational Beamforming* INTERNOISE Hong Kong



QUIET DRONES
International Symposium
on
UAV/UAS Noise
Remote from Paris – 19th to 21st October 2020

UAV's localization from a microphone array by exploiting the harmonic structure of the sound produced

Torea Blanchard (LAUM, UMR-CNRS 6613 Le Mans Université): torea.blanchard@univ-lemans.fr

Jean-Hugh Thomas (LAUM, UMR-CNRS 6613 Le Mans Université): jean-hugh.thomas@univ-lemans.fr

Kosai Raoof (LAUM, UMR-CNRS 6613 Le Mans Université): kosai.raoof@univ-lemans.fr

1.1.1 Summary

The increasingly widespread emergence of civilian Unmanned Aerial Vehicles (UAV) in recent years has led to major efforts on issues related to the privacy and security of individuals. Although technological improvements have facilitated their access to the public market, with multiple fields of application, their localisation using electromagnetic or optical systems is sometimes hampered. An acoustic approach exploiting the sound emitted by their motorization is then proposed to overcome this problem. A campaign of acoustic measurements made it possible to identify the acoustic signature of a multi-rotor UAV in order to design an acoustic array made up of few microphones. A processing chain based on the use of a pitch detection algorithm and a bank of band-pass filters with zero-phase shift is then proposed upstream of the localization step. This processing aims at selecting the main harmonics in the spectrum of the acoustic signal emitted by the UAV and thus improving the signal-to-noise ratio. Target localization is finally ensured by Delay-and-Sum in the time domain. This study has shown the interest of such a processing for UAV localization by offering a perspective of use in the multi-source case illustrated by numerical simulations. Experimental measurements conducted both in an anechoic room and outdoors are presented for the single source case.

1. Introduction

Unmanned aerial vehicles (UAVs), commonly known as drones, have grown considerably in recent decades, thanks in particular to technological improvements that have made their use increasingly accessible to the public market. Their scope of application is wide, ranging from simple amateur use (e.g. filmmaking) to professional use (e.g. delivery services or maintenance inspections). Drones can also be used for environmental monitoring and conservation. However,

the increasingly widespread emergence of UAVs has led to major efforts on issues related to the privacy and security of individuals. Indeed, UAVs can easily fly near sensitive buildings or strategic airspaces such as ministries, airports or private spaces and show threatening behaviours. Their localization using electromagnetic or optical systems is sometimes hampered. To overcome this limitation, it has become critical to set up effective systems which are able to locate an UAV flying over critical areas. An acoustic approach exploiting the sound emitted by their motorization is then proposed.

Microphone arrays have widely proven their effectiveness in estimating the Direction of Arrival (DOA) of sources for several scenarios. They can be used both indoors (with high reverberation [Tsiami *et al.*, 2014]) and outdoors (embedded on an UAV [Hoshiba *et al.*, 2017] or in submarine conditions [Lopez-Marulanda *et al.*, 2017]). Sound source localization techniques can be separated into two main categories: Time-Direction-of-Arrival (TDOA) estimation methods and beamforming techniques. The first one is based on the cross-correlation function to estimate the time travelling of the acoustic wave emitted by the source between the pairwise of the microphone array. These methods can be viewed as a geometric approach as proposed by E. Van Lancker [Van Lancker, 2002] or X. Alameda-Pineda and R. Horaud [Alameda and Horaud, 2014]. Beamforming techniques reconstruct the acoustic field using the signal recorded by the microphone array [Van Veen and Buckley, 1988]. Signals recorded by the microphones are delayed in order to steer the antenna beam in a desired direction. Signal processing is then used to improve the ability of the array to separate close sources and its resolution.

Significant efforts have been made on the localisation of UAVs by acoustic measurements, and remains an open field of investigation. For instance, E. E. Case *et al.* [Case *et al.*, 2008] designed a low-cost linear 24-microphones array to track the bearing angle of a small UAV using Time-Domain Delay-and-Sum Beamforming (TDDSB). An extended localization for the 3D space case was proposed by X. Chang *et al.* [Chang *et al.*, 2018] using TDOA estimation algorithm based on the Generalized Cross-Correlation with Phase Transform (GCC-PHAT) function. They deployed two arrays of tetrahedron-shaped microphones to ensure localization in 3D space under the near-field hypothesis. Several studies coupled the DOA estimation of multiple microphone arrays (e.g. with two arrays [Busset *et al.*, 2015] or three [Lauzon *et al.*, 2017]) to achieve the 3D localization of the UAV. This work proposes a localization process of a small UAV using only one single 3D fixed microphone array with 10 microphones. The processing chain is based on the use of a pitch detection algorithm and a bank of band-pass filters with zero-phase shift upstream of the localization step. This processing aims at selecting the main harmonics related to the Blade Passing Frequency (BPF) of the rotor in the spectrum of the acoustic signal emitted by the UAV and thus improving the signal-to-noise ratio. Target localization is finally ensured by Delay-and-Sum in the time domain under the far-field hypothesis. The results are compared with estimation based on TDOA technique approach.

The paper is organized as follows: Section 2 presents the theoretical background of the acoustic localization methods used, while Section 3 presents experimental measurements to evaluate the acoustic characteristics of a small UAV. Section 4 describes the experimental measurements which consist of locating the UAV using the microphone array designed for it. Results are presented and discussed.

2. Localization process

2.1 Time-Domain Delay-and-Sum

The Time-Domain Delay-and-Sum Beamforming (TDDSB) consists of steering the array in a "listening" direction by exploiting all of the measured signals. Each signal is delayed or advanced by a time $\tilde{\tau}(\theta)$, depending on the focus direction θ . Thus the signals obtained are summed giving the beamforming output response:

$$p(t, \Theta) = \frac{1}{M} (p_{ref}(t) + \sum_{n=1}^{M-1} p_n(t + \tilde{\tau}_n(\Theta))), \quad (1)$$

where $p_{ref}(t)$ is the acoustic pressure signal measured by the reference microphone, $p_n(t)$ the acoustic pressure signal at the n -th microphone and M the number of microphone of the array. The source localization is ensured by the fact that the signals recorded by the microphones contain similar waveforms, but they are delayed. When the beamformer targets a true sound source position, i.e. $\Theta = \Theta_s$ the steered response power $|p|^2$ of the beamformer's output signal is maximum and the signal components originating from other locations are attenuated. Recall that $\tilde{\tau}_n(\Theta)$ represents the time propagation from the focus direction Θ to the m -th microphone. The source direction is given by the azimuthal φ and the elevation θ angles such that $\Theta = (\varphi, \theta)$ which maximises the output signal of the beamforming given by Eq. (1).

2.2 Pre-processing of the signals

The pre-processing of signals upstream the localization process is often limited to simple bandpass filtering in order to suppress ambient noise and avoid the inherent aliasing in the array geometry and the sampling rate. In this study, the acoustic characteristics of the sound emitted by an UAV are exploited to design a filtering process able to extract specific harmonics of the signal. As shown in a previous work [Blanchard *et al.*, 2019], the sound emitted by a drone has many peaks in its Power Spectral Density (PSD) located at multiples of the frequency rotation of the UAV's rotor. The pre-processing consists of filtering the signal to extract some harmonics using digital zero-phase filters [Oppenheim and Schaffer, 1989]. The fundamental frequency f_d of the signal is estimated using a pitch detection algorithm applied to the reference microphone signal. The Harmonic Product Spectrum (HPS) algorithm is implemented for this task [Schroeder, 1968]. The intuitive approach of this algorithm is based on the fact that the harmonics in the logarithmic spectrum add up coherently. The short-time spectrum $|X(f)|$ of the signal $x(t)$ under consideration is compressed several times by integer factors leading to compressed short-time spectra $|X(2f)|$, $|X(3f)|$, ..., $|X(kf)|$, for $k \in \mathbb{N}^*$. Figure 1 shows the PSDs of a harmonic signal and its two first compressed spectrum versions. One can see that the first harmonic of the uncompressed signal can be coherently added with the second and third harmonics of the two first compressed spectra respectively. The frequency that maximizes the sum of the logarithms of the compressed spectra corresponds to the fundamental frequency of the signal:

$$f_d = \arg \max_f \sum_{k=1}^N \log_{10}(|X(kf)|). \quad (2)$$

The harmonics of the signal are then estimated as multiple integers of the fundamental frequency f_d .

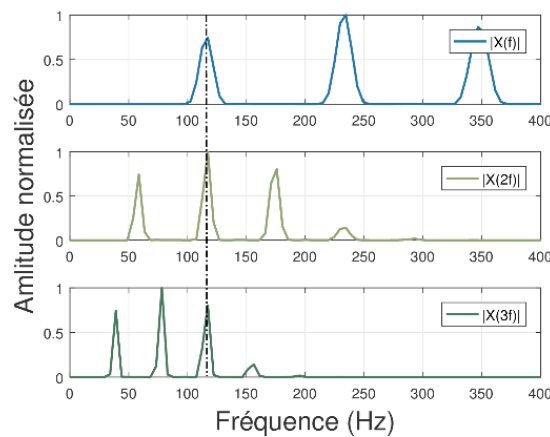


Figure 1: Illustration of the principle of the HPS algorithm for the detection of the fundamental (indicated by the dashed line) of a harmonic signal from 2 compressed spectrum versions.

3. Application to a small multi-rotor UAV

3.1 Array geometry

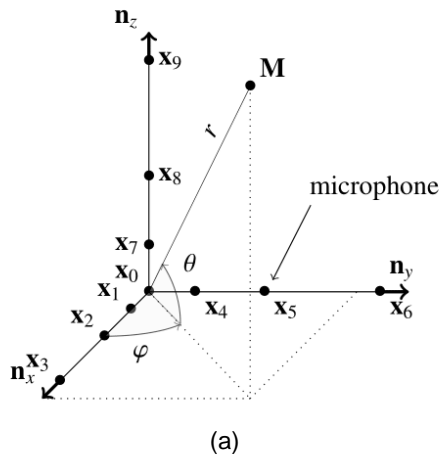
The scheme of the array geometry used is given in figure 2a. A photograph of the microphone array is shown in Figure 2b. The array is composed of 10 microphones distributed on three orthogonal arms. The position of the m -th microphone is identified by its vectorial position \mathbf{x}_m . The reference microphone is chosen to be at the origin of the referential such that $\mathbf{x}_0 = [0 \ 0 \ 0]^T$, where T is the transpose operator. The position of a point \mathbf{M} in the 3D space is given by its direction $\theta = (\varphi, \theta)$ and its range r from the origin. For this study, the microphones are placed such that on each arm, the inter-microphone distances in relation with the reference microphone are

$$\begin{aligned} \|\mathbf{x}_1\| &= \|\mathbf{x}_4\| = \|\mathbf{x}_7\| = 8 \text{ cm}, \\ \|\mathbf{x}_2\| &= \|\mathbf{x}_5\| = \|\mathbf{x}_8\| = 20 \text{ cm}, \\ \|\mathbf{x}_3\| &= \|\mathbf{x}_6\| = \|\mathbf{x}_9\| = 60 \text{ cm}, \end{aligned} \quad (3)$$

for the anechoic condition, leading to the array bandwidth $[220.5, 3430]$ Hz where $\|\cdot\|$ is the l_2 -norm and

$$\begin{aligned} \|\mathbf{x}_1\| &= \|\mathbf{x}_4\| = \|\mathbf{x}_7\| = 5 \text{ cm}, \\ \|\mathbf{x}_2\| &= \|\mathbf{x}_5\| = \|\mathbf{x}_8\| = 20 \text{ cm}, \\ \|\mathbf{x}_3\| &= \|\mathbf{x}_6\| = \|\mathbf{x}_9\| = 110 \text{ cm}, \end{aligned} \quad (3)$$

for outdoor condition, with the array bandwidth $[440.5, 2144]$ Hz. The speed of sound is $c = 343 \text{ m.s}^{-1}$. The low limit frequency of the array bandwidth is defined by the ratio between the speed of sound and the array aperture L . The upper frequency limit is given by the spatial Shannon-Nyquist theorem.



(b)

Figure 2: (a) Scheme of the 10-microphone orthogonal array geometry used for the localization of the UAV. (b) Photograph of the microphone array used during measurements.

3.2 Measurement set-up

3.2.1 Anechoic condition

The measurements aim at validating the proposed signal processing to track the frequency content of the UAV signal for the localization step. The proposed trajectory consists of a vertical path. The trajectory has been modelled as a vertical straight line knowing the height reached by the UAV and its starting and end positions. The drone is placed at a distance of approximately 3 m from the center of the antenna in the direction 45° in azimuth. The elevation is taken at 3.8° considering the center of the drone in the same plane as the propellers.

The localization of the UAV was made over time windowing of $T = 150$ ms without overlapping. The signals recorded by each microphone are pre-processed before the localization step such that only the two first harmonics in the frequency bandwidth of the array are selected. Figure 3a gives in blue lines the estimates obtained in azimuth and elevation. The results are compared with the reference position of the UAV given in black lines. The spectrogram of the reference microphone signal (no filtered) is given in figure 3b for frequencies up to 1 kHz. The black crosses give the fundamental frequency estimated using the HPS algorithm over time (one time windowing out of ten) which corresponds to the BPF of the rotor.

The results show clearly the ability of the process to estimate the UAV positions while the acoustic information is widely restricted to only two harmonics, namely the harmonics at approximately 350 Hz and 525 Hz. The average errors remain low with 2.3° in azimuth and 2.5° in elevation. The HPS algorithm is able to track accurately the fundamental frequency of the reference signal. This frequency is estimated to approximately 175.8 Hz over the whole signal.

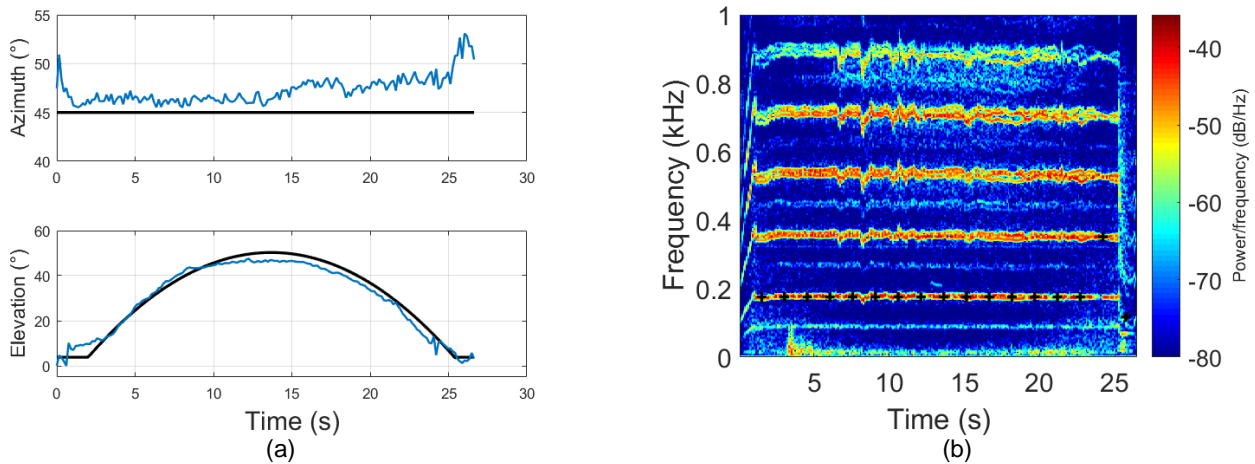


Figure 3: (a) Localization results of the UAV flight performed in the anechoic room using time-domain beamforming. The input signals of the beamformer have been pre-processed to select the 2 first harmonics in the frequency bandwidth of the array. (b) Spectrogram of the reference microphone signal for frequencies up to 1 kHz. Black crosses represent the estimates of the fundamental frequency of the signal over time using the HPS algorithm.

3.2.2 Outdoor condition

For the measurements performed outdoors, the drone was placed at a distance of approximately 18.5 m and flies at a height of about 10 m. The x, y -coordinates of the UAV is calculated from its latitude and longitude gathered by an on-board Global Positioning System (GPS). The z -coordinate is given by an on-board altimeter. The Cartesian coordinates are then converted into spherical coordinates to obtain the azimuthal φ and elevation θ angles of the UAV. The origin of

the coordinates is given by the array center (i.e. the reference microphone) whose GPS coordinates are estimated using a mobile device application.

As the measurements in anechoic condition, the localization of the UAV is made over time windowing of $T = 150$ ms without overlapping. Only the two first harmonics in the frequency bandwidth of the array are selected for the localization step. The estimates of the localization are given in figure 4a in blue and are compared with the reference positions in black. The spectrogram of the reference microphone signal for frequencies up to 1 kHz is also given in figure 4b. The black crosses indicate the fundamental frequency estimated by the HPS algorithm.

In contrast to the previous results, singularity points with high errors occur at some points but the localization and tracking of the device are not significantly affected. The chain process is able to track the UAV with average errors less than 3.6° in azimuth and 2.8° in elevation.

For both conditions, when more harmonics are selected, the average errors are slightly improved and there are fewer singularity points that occur. These results can be particularly interesting in the case of multiple UAVs. For instance, in the case of two UAVs showing different spectral patterns, the pre-filtering step could track the fundamental harmonic of only one source and isolate the sufficient number of harmonics required for location while having a good estimation accuracy. This simple case is discussed in the following section through simulation.

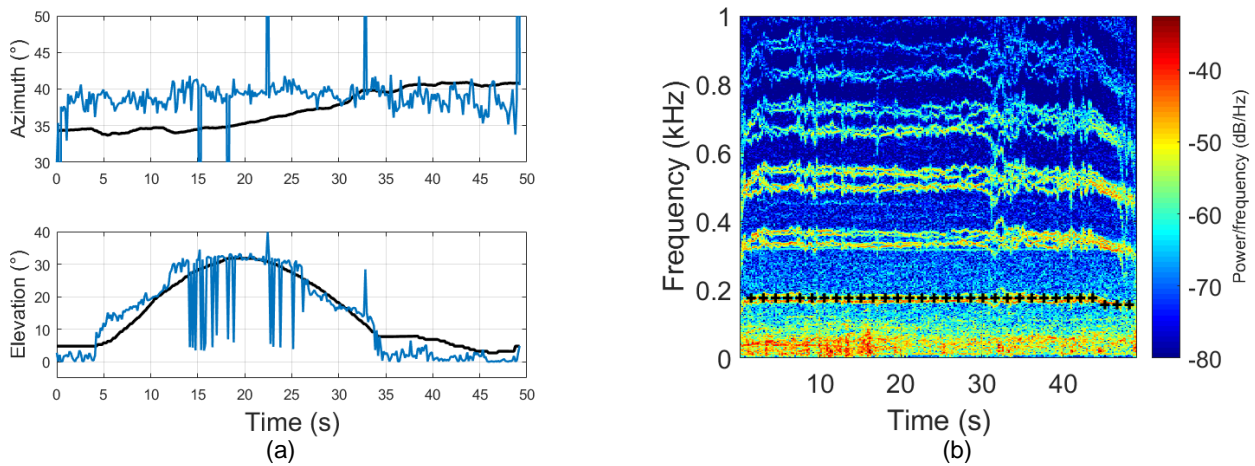


Figure 4: (a) Localization results of the UAV flight performed outdoors using time-domain beamforming. The input signals of the beamformer have been pre-processed to select the 2 first harmonics in the frequency bandwidth of the array. (b) Spectrogram of the reference microphone signal for frequencies up to 1 kHz. Black crosses represent the estimates of the fundamental frequency of the signal over time using the HPS algorithm.

4. Localization and tracking of virtual sources

4.1 Signal Model

The signal model used for numerical simulation is based on the construction of several monopoles for which the frequencies are related by integer factors. The signal $p_m(t)$ recorded by the m -th microphone of the array is written:

$$p_m(t) = \sum_{n=1}^{N_h} \alpha_0(f) \frac{\cos\left(2\pi[2n]f_0\left(t - \frac{r_{ms}(t)}{c}\right)\right)}{4\pi r_{ms}(t)} + \sum_{n=1}^{N_h} \beta \frac{\cos\left(2\pi[2n-1]f_0\left(t - \frac{r_{ms}(t)}{c}\right)\right)}{4\pi r_{ms}(t)}, \quad (4)$$

where $r_{ms}(t)$ is the distance from the source and the m -th microphone at time t and c is the speed of sound. $2N_h$ is the number of harmonics considered into the signal and f_0 is the rotor rotation frequency. It is related with the BPF by a factor 2 ($\text{BPF} = 2f_0$). In this model, the signal

is composed of two terms. The first term models high-energy harmonics for which the amplitude is frequency-dependent (indicated by the parameter $\alpha_0(f)$). The second term is used to consider the low energy harmonics as observed in the signal of a multi-rotor UAV's signal [Blanchard *et al.*, 2019].

4.2 Single source case

The localization process is first tested on a single virtual source using the signal model given in Eq. (4) with a fundamental frequency of $f_0 = 128$ Hz and a number of monopoles $N_h = 30$. The source follows a path reconstructed from the GPS data gathered during experimental measurements made outside. The trajectory is plotted in black in figure 5a. The source begins its take off at a distance of approximately 21 m from the array to a height of almost 6 m. The speed profile is also plotted in figure 5b. The harmonics of the source are estimated using the proposed method. The HPS algorithm is applied over time windowing of $T = 450$ ms on the reference signal. Only the two first harmonics within the array bandwidth are extracted for the localization step. The spectrogram of the entire signal and the PSDs of a time-segment from the reference signal and its filtered version are given in figure 6.

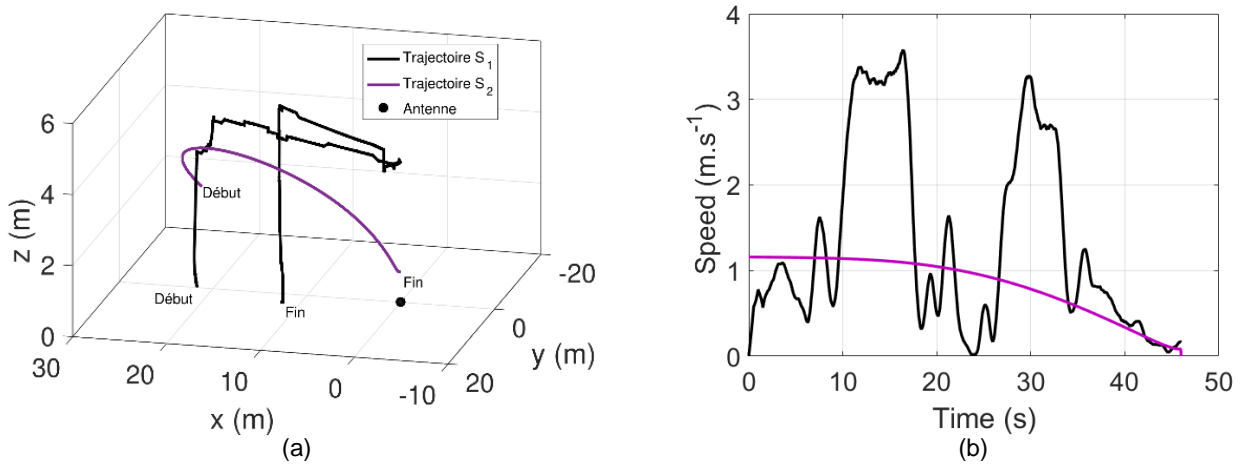


Figure 5: (a) Trajectories of the virtual sources (Note: “Début” = “Start”, “Fin = End”, “Trajectoire” = “Trajectory” and “Antenne” = “Antenna”) and (b) velocity profiles of the sources.

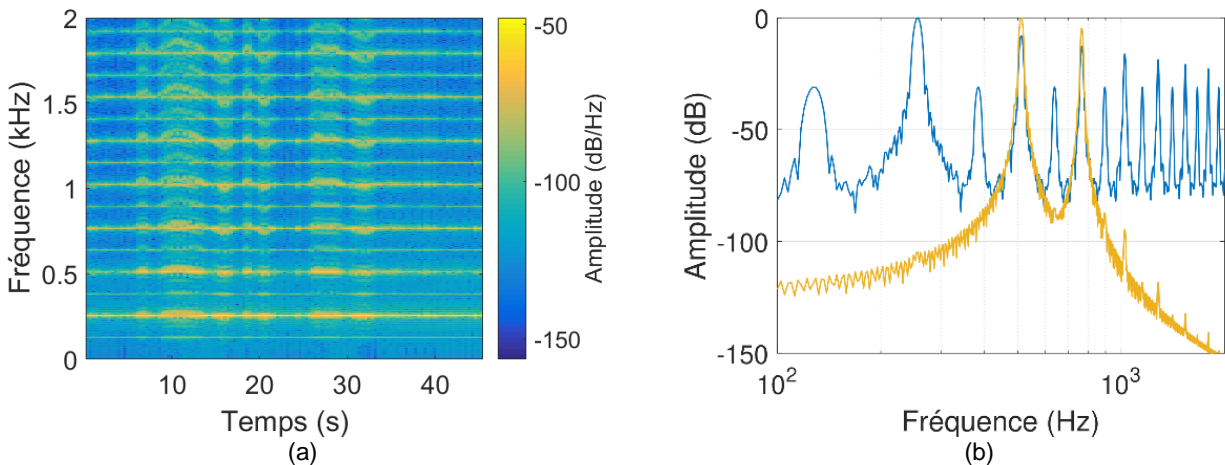


Figure 6: (a) Spectrogram of the reference signal over frequency bandwidth [0, 2] kHz and (b) PSDs of a time-segment of $T = 450$ ms of the reference signal (blue) and its filtered version (yellow) using the proposed method of extracting harmonics. (Note: “Temps” = “Time” and “Fréquence” = Frequency”).

The results of the localization using the TDDSB method on the processed signal are shown in figure 7 where the estimate and the reference positions of the virtual source are plotted on a 3D grid given by the azimuthal and elevation angles over time. The average deviation error, defined

as the average distance in the angle-plane between the reference position and the estimates, is estimated to be 1.9° . These results show that the localization process is able to estimate the source with a low error angle when the signal is strongly limited in frequency to few harmonics.

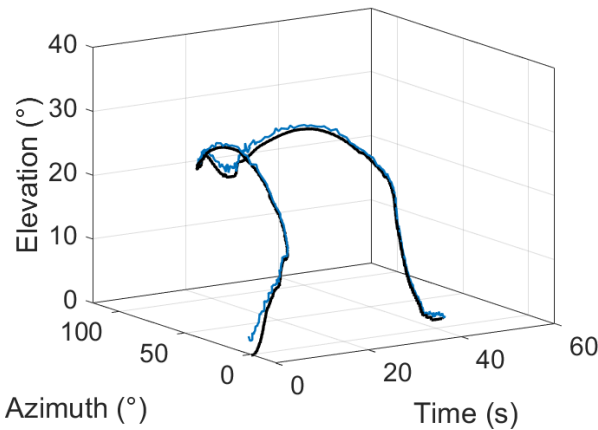


Figure 7: Results of the localization of a single virtual source with a harmonic signal using the TDDSB method. The reference position (black) and the estimates (blue) of the source are plotted on a 3D grid given by the azimuthal and elevation angles over time.

4.3 Two-source case

A second source is now added to the simulation. The path followed by the source is plotted in purple in figure 5a. The source follows a curvilinear trajectory such that its azimuth and elevation vary linearly respectively from -20° to 100° and from 5° to 30° . Its range varies from 25 m to 2 m. The signal of this source is calculated using the model in Eq. (4) with a fundamental frequency of 106 Hz and it is mixed with the signal of the first source.

In the multiple-source case, the goal is to extract the dominant frequency (BPF) of each source and to attenuate the harmonics generated by the other sources to increase the signal-to-noise ratio (SNR). The TDDSB method is then applied to the filtered version of the signal acquired from the array in selective bands centred on the chosen harmonics of the BPF of the concerned source.

Let us consider the two-source case. First, HPS is run to get the BPF of source 1. Then HPS is applied again but in a filtered version of the signal where zero-phase notch filters were used to attenuate the harmonics of source 1, providing the BPF of source 2. This process is repeated until the absolute difference between both BPFs exceeds a certain threshold ε . This assumption assumes that the frequency content of the two sources does not overlap. In this simulation, the threshold is fixed to 10 Hz. If no filtering is operated and if HPS is only run once, the algorithm does not find the same source at each time window.

One can see in figure 8 the localization results in the two-source case in blue circles when no signal processing is applied and in yellow (source 1) and red (source 2) when the proposed separate process is applied. The reference paths followed by the sources are given in black (source S_1) and purple (source S_2). When HPS is run only once, one can see that the beamforming locates at first source S_1 , which is closest to the array, and then source S_2 at approximately 21 s, from which time source S_2 is closer to the array than source S_1 . Indeed, since beamforming is based on constructive interference to search for the noisiest sound source seen by the antenna, the source that will be located first, in this scenario, will be the one closest to the array. The location of the second source is possible if signal processing is used to attenuate the energy from the first source. With the proposed signal processing, the localization of both sources individually is possible. Beamforming is applied twice for each time windowing.

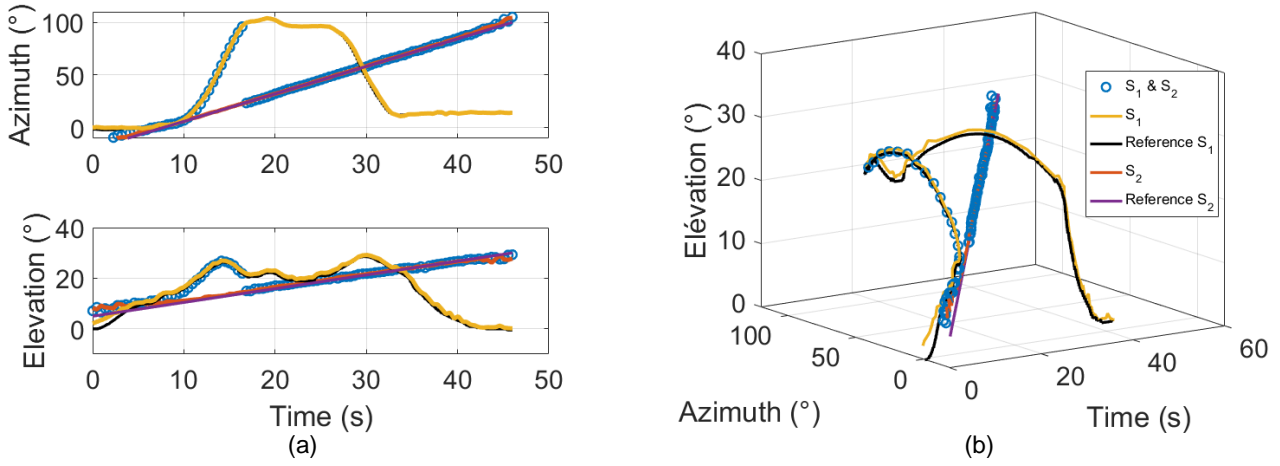


Figure 8: Angular localization results of two sources for three cases: localization without signal processing, localization with extraction of the harmonics of the first source S_1 and then of the second source S_2 . (a) Representation of angles as a function of time and (b) 3D representation of estimates as a function of time.

5. Conclusions

This work deals with the problem of locating UAVs by acoustic measurements. The proposed method exploits the intrinsic harmonic structure of the acoustic signal generated by small UAVs to design a chain process able to select the desired harmonics of the signal. The Blade Passing Frequency is estimated using the Harmonic Product Spectrum pitch algorithm and zero-phase passband filters are used to extract the desired harmonics. Then Time-Domain Delay-and-Sum Beamforming method is applied to the filtered signal to locate the UAV.

Measurements have been done both in anechoic room and outdoors on a small multi-rotor UAV to validate the proposed process. For this study, only the two first harmonics in the array frequency bandwidth have been selected for the beamforming. Results show that the UAV is located accurately while most of the signal information is attenuated. These results show particular interest in the case of multiple UAVs as shown through simulation in the two-source case.

References

- A. Tsiami, A. Katsamanis, P. Maragos, and G. Potamianos, *Experiments in acoustic source localization using sparse arrays in adverse indoors environments*, in Proceedings of the 22nd European Signal Processing Conference (EUSIPCO), IEEE (2014), pp. 2390-2394.
- K. Hoshiba, K. Washizaki, M. Wakabayashi, T. Ishiki, M. Kumon, Y. Bundo, D. Gabriel, K. Nakadai, and H. Okuno, *Design of UAV-embedded microphone array system for sound source localization in outdoor environments*, Sensor **17**(11), 2535 (2017).
- J. Lopez-Marulanda, O. Adam, T. Blanchard, M. Vallée, D. Cazau, and F. Delfour, *First results on an underwater 360° HD audio-video device for etho-acoustical studies on bottlenose dolphins (*tursiops truncatus*)*, Aquatic Mammals **43**(2) (2017).
- E. Van Lancker, *Acoustic goniometry: a spatio-temporal approach*, Ph.D. dissertation, EPFL, Lausanne, Suisse, 1-116 (2002).
- X. Alameda-Pineda and R. Horaud, *A geometric approach to sound source localization from time-delay estimates*, IEEE/ACM Trans. on Audio, Speech, and Language Process. **22**(6), 1082-1095 (2014).

B. D. Van Veen and K. M. Buckley, *Beamforming: a versatile approach to spatial filtering*, IEEE ASSP magazine **5**(2), 4-24 (1988).

E. E. Case, A. M. Zelnio, and B. D. Rigling, *Low-cost acoustic array for small UAV detection and tracking*, in Proceedings of Aerospace and Electronics Conference, IEEE (2008), pp. 110-113.

X. Chang, C. Yang, J. Wu, X. Shi, and Z. Shi, *A surveillance system for drone localization and tracking using acoustic arrays*, in Proceedings of the 10th Sensor Array and Multichannel Signal Processing Workshop (SAM), IEEE (2018), pp. 573-577.

J. Busset, F. Perrodin, P. Wellig, B. Ott, K. Heutshi, T. Rühl, and T. Nussbaumer, *Detection and tracking of drones using advanced acoustic cameras*, in Proceedings of Unmanned/Unattended Sensors and Sensor Networks XI; and Advanced Free-Space Optical Communication Techniques and Applications, International Society for Optics and Photonics (2015), Vol. 9647, p. 96470F.

J.-S. Lauzon, F. Grondin, D. Létourneau, A. L. Desbiens, and F. Michaud, *Localization of RW-UAVs using particle filtering over distributed microphone arrays*, in Proceedings of International Conference on Intelligent Robots and Systems (IROS), IEEE (2017), pp. 2479-2484.

T. Blanchard, J.-H. Thomas, and K. Raoof, *Acoustic localization estimation of an unmanned aerial vehicle using microphone array*, in Proceedings of Inter-Noise and Noise-Con Congress and Conference Proceedings, Institute of Noise Control Engineering (2019), Vol. 259, pp. 6656-6667.



QUIET DRONES
International Symposium
on
UAV/UAS Noise
Remote from Paris – 19th to 21st October 2020

A Real-Time System for Joint Acoustic Detection and Localization of UAVs

Martin Blass: martin.blass@joanneum.at

Franz Graf: franz.graf@joanneum.at

Summary

Unmanned aerial vehicles (UAVs) are commercially available in different types, sizes and pricing. Since no expert knowledge for the use of UAVs is required, they may raise privacy and security concerns, public annoyance due to noise emissions, or even pose a threat to society and public facilities when being used as a means of attack. In this paper, we present a holistic approach for real-time acoustic detection and localization of UAVs using microphone arrays. We describe the array design and an algorithm for 3D UAV localization, the acoustic detection system including audio feature extraction and a defined procedure for acquiring UAV audio training data. The system comprises an MPEG-7 database framework for handling metadata and labeling of audio segments. Labeled audio data is used to train binary classification algorithms to discriminate between the presence and absence of UAVs. For acoustic localization, beamforming techniques are used in combination with a custom source tracking algorithm. The system is evaluated using common classification metrics and a proposed localization error metric. Finally, we outline the real-time implementation and discuss the potentials and challenges about joint detection and localization using beamformed audio signals.

1. Introduction

Within the past years unmanned aerial vehicles (UAVs), such as rotary-wing drones, have gained increased popularity and availability. Nowadays, UAVs are commercially available in different types, sizes and price ranges and their usage does not require any explicit expert knowledge. Due to their autonomous nature and sensing capabilities, UAVs cover a wide range of professional applications such as transportation, tracking, disaster relief, aerial photography, agricultural monitoring and wireless communications [1]–[5]. However, amateur drones may

deliberately or accidentally violate people's privacy, raise public annoyance due to noise or even pose a threat to society and public facilities in case of terrorist attacks [6]–[8]. The incident at Gatwick Airport, London between 19 and 21 December 2018 showed the potential impact and severity of disruption a single drone may cause solely on account of its presence [9].

An increasing number of UAV related incidents [10] have shown that such threats cannot be countered with conventional surveillance and security means. At the moment there is no such system which offers a 100% detection and protection against drones. Current research projects try to increase detection rates by focusing on multimodal approaches, which incorporate different types of sensors and techniques [7], [8], [11]. One such modality is the acoustic domain: By analyzing characteristic sound signatures of UAVs during flights, machine learning algorithms may discriminate between the presence and absence of a drone in real time. In addition, the position or direction-of-arrival (DOA) of a UAV may be estimated with the help of distributed acoustic sensors, such as microphone arrays. Both of these tasks require knowledge about the characteristics of UAV sounds. To this end, several works have been published, which deal with the acoustic measurement and sound analysis of UAV noise, approaches for acoustic source localization and DOA estimation, and the detection and classification of drone sounds.

An experimental study of quadcopter acoustics was conducted in [12], which investigated the main sound components of a multicopter UAV, the rotors and the electric engines, and their noise contributions in different frequency ranges. Similar indoor measurements were performed in [13]–[15]. In field recordings and fly-over measurements of [16]–[19] the impact of UAV flight dynamics on the frequency content was examined in terms of different spectral representations.

Recent works on UAV localization primarily cover the task of DOA estimation using microphone arrays. In [20] two DOA finding algorithms (GCC, SRP-PHAT) were evaluated on five different UAVs with a 3D acoustic array consisting of 12 microphones. In follow-up works of [21], field tests on DOA estimation and detection were performed using three nodes of a 4-channel tetrahedron microphone array and compared to other arrays featuring more sensors. Ramamonjy et al. [22] use compact 2D cross arrays of 13 and 32 MEMS microphones for DOA estimation by computing the sound pressure and particle velocity on two orthogonal axes. Didkovskiy et al. [19] use a 5-element cross-array in combination with a simple phase correlation technique for finding the azimuth DOA angle. In [15] a 3D microphone array with 10 sensors placed on orthogonal axes was set up for indoor and outdoor measurements to assess the localization performance of conventional beamforming versus the acoustic goniometry method using TDOA estimates. A more complex approach was presented in [23] where three distributed 8-channel microphone arrays were deployed to perform 3D sound source localization using triangulation and particle filtering. In the work of Tapolczai et al. [24] a simulation framework for acoustic localization and tracking of moving sound sources using Kalman filters was developed. Other works, such as [25] propose the use of an acoustic camera for tracking small moving objects and the extraction of sound using beamforming for further detection or classification applications.

UAV detection has grown an active field of research within the last years. Early works of [26] and [27] proposed to extract harmonic peaks occurring in the FFT spectrum using the Harmonic Line Association (HLA) method as a prominent feature for UAV sound detection. In a proof-of-concept of [28] a drone detection system is trained using linear predictive coding (LPC) coefficients and generic acoustic low-level features such as spectral slope and zero crossing rate. Mezei et al. [29] uses a correlation-based approach to distinguish drone sounds from noise. In [30] mel-cepstral coefficients (MFCCs) are used together with a GMM and HMM-based classifier. Bernadini et al. [31] and Mandal et al. [32] propose a more generic machine learning system that incorporates preprocessing, short-term audio analysis using temporal and spectral acoustic low-level descriptors as well as MFCCs and Support Vector Machines (SVM) for classification. Garcia-Gomez et al. [33] conducted a detailed analysis of suitable low-level features for UAV sound detection by applying feature selection algorithms, which supports the use of MFCCs. More recent works [34]–[37] apply deep learning strategies such as feed-forward, recurrent and convolutional neural networks based on STFT and MFCC features.

Most of the present works tend to focus either on detection or on localization only, whereas few cover both aspects independently. We want to take a step further in order to arrive at joint UAV detection and localization within a unified framework. In this paper, we present a holistic approach for the development of an acoustic UAV detection and localization system. We give insights about suitable acoustic sensor systems including the construction of a microphone array, present an audio recording procedure for capturing high quality UAV sound data and describe the annotation process to create labeled audio training data. For the UAV localization component, we describe the implementation of a 3D direction-of-arrival (DOA) estimation algorithm, which is capable of tracking multiple sound sources in real-time. For the acoustic detection of UAVs, we outline the design and extraction of relevant audio features as well as the system architecture of a binary classification algorithm to discriminate between UAV and non-UAV sounds. Both localization and detection system components are deployed within a real-time framework that enables the acoustic tracking of single and multiple drones.

The paper is organized as follows: Section 2 describes the acoustic sensor system including UAV sound analysis and microphone array design. In Section 3, we present a 3D DOA estimation algorithm used for acoustic tracking of multiple sound sources and a proposed method to evaluate the UAV localization performance at different distances. Section 4 outlines a machine learning pipeline for UAV sound detection and proposes a distance dependent evaluation scheme similar to Section 3. In Section 5, we present our ideas about joint acoustic UAV detection and localization using beamforming and provide proof-of-concept results. Section 6 describes the implementation of the real time system and Section 7 concludes the work.

2. Acoustic Sensor System

The choice of appropriate acoustic sensors or sensor arrays strongly depends on the application and on the expected type of acoustic signals. In the following, we present a qualitative sound analysis of a commercially available UAV.

2.1 Analysis of UAV sounds

In Figure 1 we investigate spectrograms and corresponding averaged spectrums as power spectral densities (PSDs) of a *DJI Inspire 2*. Audio signals were recorded inside an acoustic laboratory using a *B&K Type 4189* measurement microphone at a distance of 1.5 m from the drone center and at an angle of 30° below the rotor plane. The audio sampling rate and resolution were set to 48 kHz and 16 bit, respectively. For analysis, we used a frame size of 4096 samples (85 ms) with a Hann window, an overlap of 90% and an FFT size of 4096. Spectrograms are normalized with respect to the maximum amplitude corresponding to 0 dB. The fundamental frequency of propeller noise lies at 150 Hz and shows strong harmonics up to 2 kHz. The dynamic range between harmonic lines and noise floor is greater than 10 dB. In Figure 2 an outdoor recording of the same *DJI Inspire 2* hovering near the sensor at a ground distance of 5 m and height of 3 m is illustrated using the same analysis settings as in Figure 1. The hover position corresponds to a similar elevation angle (approx. 31°) as for the indoor recording. The microphone was placed on the ground to minimize ground reflections. Compared to Figure 1 the spectral lines of rotors are less distinct and do not show strictly harmonic behavior (i.e. integer multiples of the fundamental frequency). This is mostly attributed to wind and flight maneuvers causing the rotors to rotate at different speeds to keep the UAV in a stable position. This is typical for multicopter drones performing different kinds of hover and flight maneuvers.

Similar to [12] we conclude that the fundamental frequency of UAV propeller sound typically lies between 100-200 Hz corresponding to the blade passing frequency (BPF) of each rotor. Harmonics of the BPF produce tonal noise that dominates the frequency range up to 2 kHz rotors depending on the distance of the UAV from the sensor. Wind turbulences of propellers and electric motors contribute to broadband noise in the frequency range from 1-12 kHz.

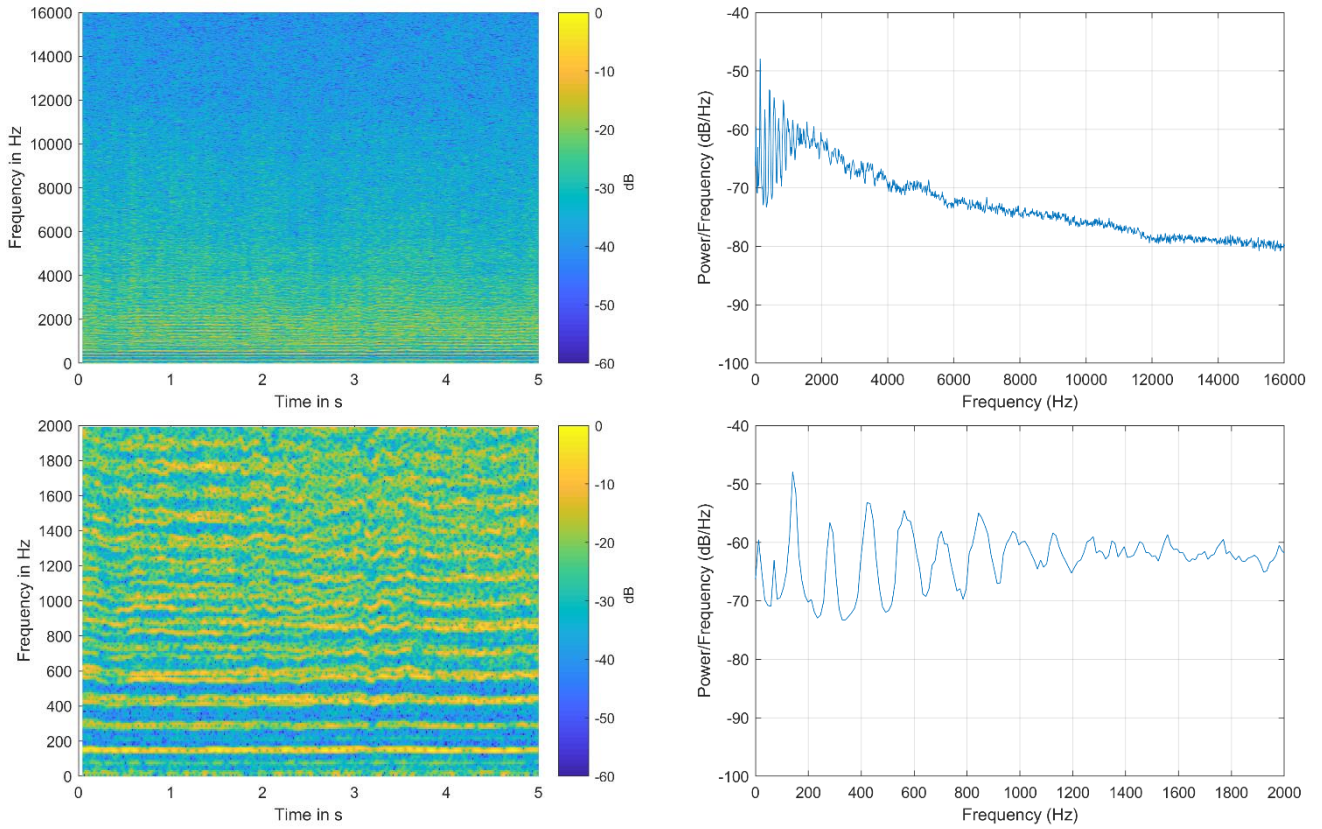


Figure 1: Spectral analysis of a DJI Inspire 2 hovering inside an acoustic laboratory: Spectrogram (top, left) and averaged power spectrum over a duration of 5 s (top, right) with zoomed views on the frequency range 0-2 kHz (bottom).

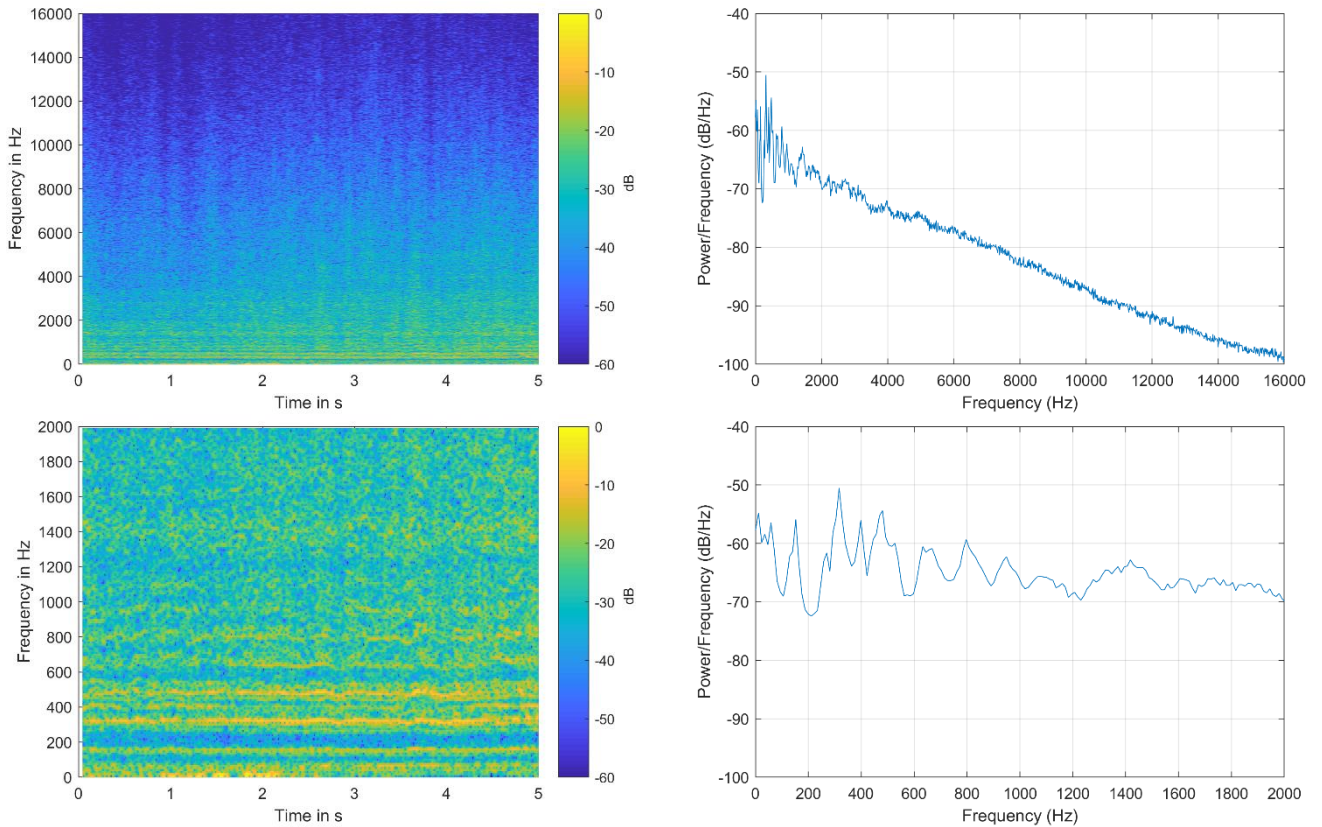


Figure 2: Spectral analysis of a DJI Inspire 2 hovering in the field at a ground distance and height of 5 m and 3 m, resp.: Spectrogram (top, left) and averaged power spectrum (top, right) with zoomed views on the frequency range 0-2 kHz (bottom).

In general, the sound of electro motors may feature narrow frequency peaks above 4-5 kHz [12] depending on the UAV type, which are most of the time masked by wind turbulence noise originating from the rotors. In case of the *DJI Inspire 2* these noise components are completely masked.

2.2 Microphone Array Design

Based on the knowledge about typical drone sound signatures and the desired requirements microphone arrays may be designed suitable for UAV localization tasks. To guarantee a 360° coverage in the azimuth plane, a microphone array needs to feature a rotationally symmetric 2D or 3D geometry. Due to unique time-differences-of-arrival (TDOA) between sensors, a 2D planar array placed on the ground enables 3D DOA estimation within the hemisphere over the array. The number of sensors in an array is always a trade-off between beamforming/localization performance and computational load as well as hardware costs. One critical aspect in array design is the choice of sensor placement since array geometry and size determine the directional characteristic of the spatial filter response, also known as beampattern. The smallest and largest sensor distances define the working frequency range of a microphone array, while the sensor positions determine the spatial separation (beamwidth, mainlobe) and the suppression (sidelobes) of sound sources [38], [39].

Throughout numerical delay-and-sum beamforming simulations, we evaluated different 2D array geometries in terms of their beamwidths and sidelobe levels as proposed in [40]–[42]. As a result, we developed a custom 5-arm spiral geometry with a radius of 0.75 m comprised of 31 measurement microphones of type *PCB 130F22*. The design and quality metrics of the array are listed in Figure 3 (left). Figure 4 shows the spatial response as point spread function (PSF) in the xy-plane and as azimuth beampattern over frequency. A picture of the actual array, in the following referred to as *JR-BigSpiral31*, is displayed in Figure 3 (right).

Parameter	Value
Number of microphones	31
Radius	0.75 m
Lower frequency limit	121 Hz
Upper frequency limit	40 kHz
Half power beamwidth (BW)	15.0°
Maximum sidelobe level (MSL)	-9.3 dB
Directivity (DI)	11.9 dB



Figure 3: List of parameters (left) and picture of the 2D microphone array *JR-BigSpiral31* inside the acoustic laboratory (right). The metrics BW, MSL and DI were evaluated and averaged over octave frequency bands from 125 to 16000 Hz.

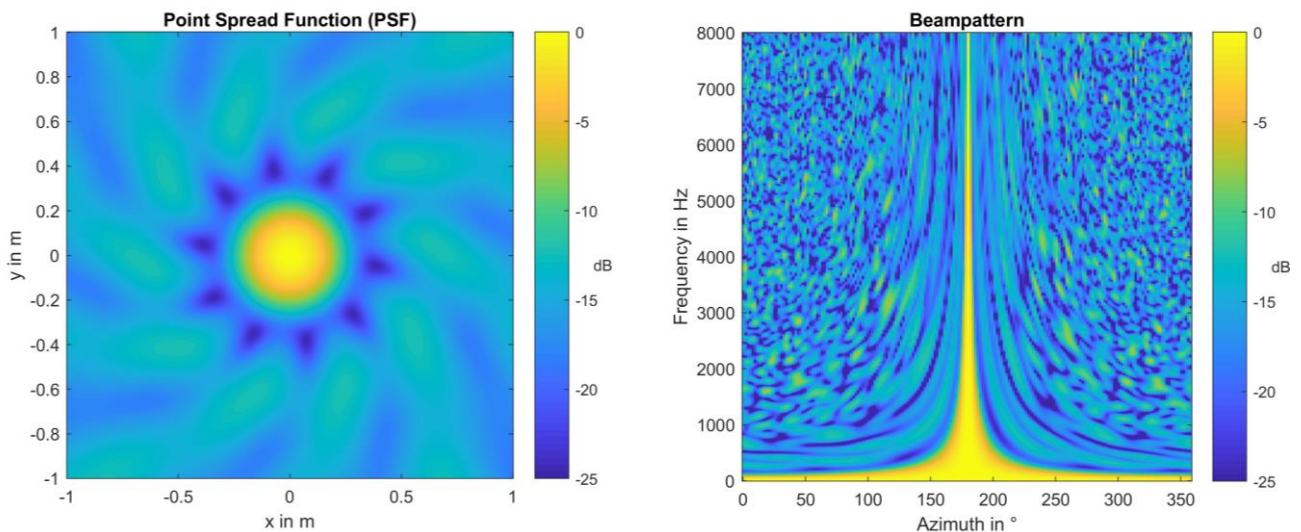


Figure 4: Exemplary far field spatial response visualization using conventional beamforming: point spread function (PSF) for a frequency of 1 kHz and scanning plane height of 1 m (left) and beampattern in the azimuth plane for impact signals of different frequencies from the direction of 180° azimuth and 0° elevation (right).

3. UAV Localization

3.1 DOA Estimation

Using acoustic beamforming principles it is possible to estimate the DOA of multiple sound sources. DOA estimation techniques can be subdivided into two categories [43], [44]: direct methods, which are based on computation of a selection criterion for a preselected set of candidate locations, e.g. steered response power (SRP) of a beamformer output, and indirect methods, which estimate the TDOA of sensors and find source locations by non-linear optimization and parameter fitting. Due to robustness as well as simple implementation and scalability in terms of sensor numbers, we chose SRP-based methods suitable for the task of UAV localization.

As the basis of our localization algorithm, we adapted a model-based of approach of [43], [45], [46] for the use in 3D space with custom frequency and search location settings. The benefits of this approach are manifold: On the one hand, it offers probabilistic modelling and tracking of an unknown number of sound sources plus source extraction using masked beamformer outputs. On the other hand, it provides good localization accuracy even for coarse search grids and the computational load allows application in real-time. The algorithm is originally formulated in 2D space, but was extended to 3D. For details we refer the interested reader to the original papers. The signal model of an array with M microphones is described in the Short-Time Fourier Transform (STFT) domain as [43]

$$\mathbf{X}(k, b) = \mathbf{A}(k)\mathbf{S}(k, b) + \mathbf{V}(k, b), \quad \text{Equation 1}$$

where k and b are discrete frequency bin and frame indices resp., the vector \mathbf{S} denotes Q sound source signals, the matrix \mathbf{A} the propagation vectors from sources to array, \mathbf{V} the disturbing signals (noise and reverberation) at each sensor, and \mathbf{X} the sensor signals. Similar to speech signals, approximate disjointness of sources is assumed, i.e.

$$S_q(k, b)S_{q'}(k, b) \approx 0 \quad \forall q' \neq q, \quad \text{Equation 2}$$

DOA estimation is performed along the azimuth $\theta \in [0^\circ, 180^\circ]$ for each frequency bin of a defined subset $\{k: k_{Lo} < k \leq K/2\}$ by computing the SRP functional $J_{SRP}(\theta, k, b)$ over a preselected grid of search locations. The azimuth estimate is then computed as [43]

$$\hat{\theta}(k, b) = \underset{\theta}{\operatorname{argmax}} J_{SRP}(\theta, k, b). \quad \text{Equation 3}$$

3.2 Sound Source Tracking and Extraction

Under the assumption of time-frequency (TF) disjointness of source signals, each TF point can be attributed to a single dominant source. By clustering estimates of all frequency bins using a univariate GMM a distribution of I active sound sources is obtained for each time frame. Within the GMM model each sound source q is attributed a mean θ_q , a variance σ_q^2 and weight P_q . Since the number of active sources may change from frame to frame each source is assigned a time-to-live (TTL) once it has appeared. By using an age-token-based temporal smoothing method the source locations are updated over time [43]. The principle of source tracking is visualized in Figure 5.

Given the DOA estimates θ_q the corresponding delay-and-sum beamforming (DSB) outputs are computed for each time frame. Since the DSB does not actively cancel interferers and only provides limited signal enhancement, a mask-based approach using the GMM parameters is formulated to achieve better noise suppression. The softmask for source q is computed as the posterior probability that a particular TF point belongs to q , given the GMM model for that frame and the estimates $\hat{\theta}(k, b)$ [45], [46].

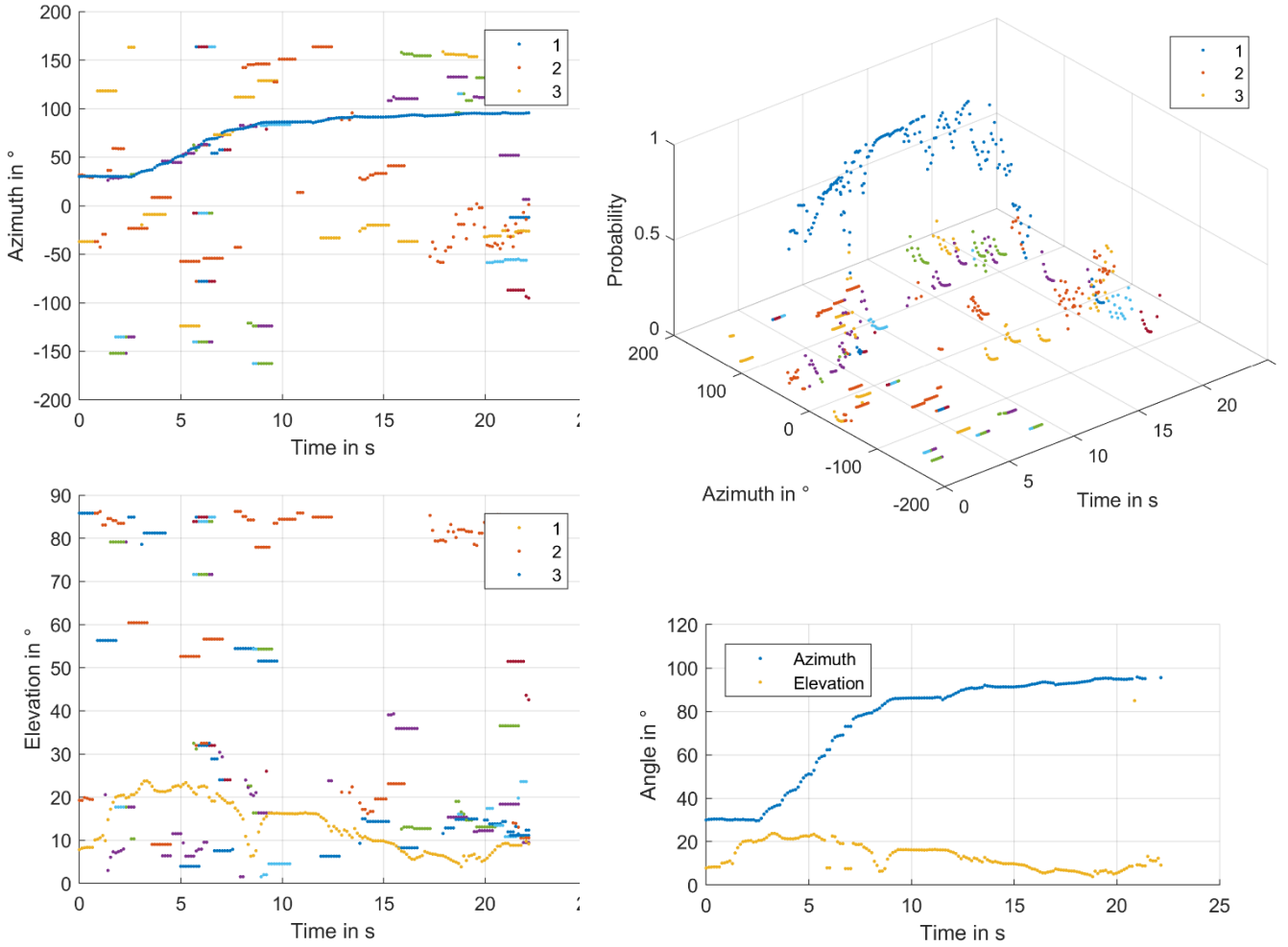


Figure 5: 3D DOA estimation and source tracking example of an AscTec Falcon octocopter based on [43]: Multiple sound sources (colored dots) are tracked over time in terms of azimuth (top left) and elevation angles (bottom left). Each source is attributed a certain weight, which is computed as the a posteriori probability of active sources (top right). The resulting DOA track of the UAV (source 1) is shown in the bottom right subplot.

3.3 Evaluation

For the evaluation of the UAV localization algorithm, different drone types and maneuvers were recorded in the field using the array *JR-BigSpiral31* at a sampling rate of 48 kHz with a resolution of 32 bit. To protect the microphones against wind, a fur windscreen is attached to the array. A GPS-tracker was mounted onto the drone to capture the ground truth positions during flight. The recordings were made under different weather conditions in the occasional presence of background noise sources, e.g. birds, airplanes, cars or speech. Figure 6 (left) shows a picture of the outdoor recording setup.

The algorithm requires a set of predefined parameters, depending on the localization task. For our experiments, we specified a 360° hemisphere scanning area with 200 quasi-uniformly distributed search locations [47] (see Figure 6, right), a search frequency range of 200 to 2000 Hz and the maximum number of sound sources as 3. An example for DOA estimation over time of the dominant sound source (*DJI S900*) is depicted in Figure 7.

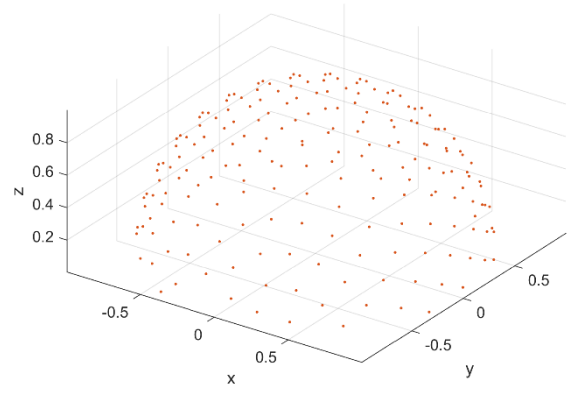


Figure 6: Audio recording in the field with a DJI S900 (left) and 200 predefined search locations quasi-uniformly distributed on a hemisphere over the array yielding an angle resolution of approximately 10° (right).

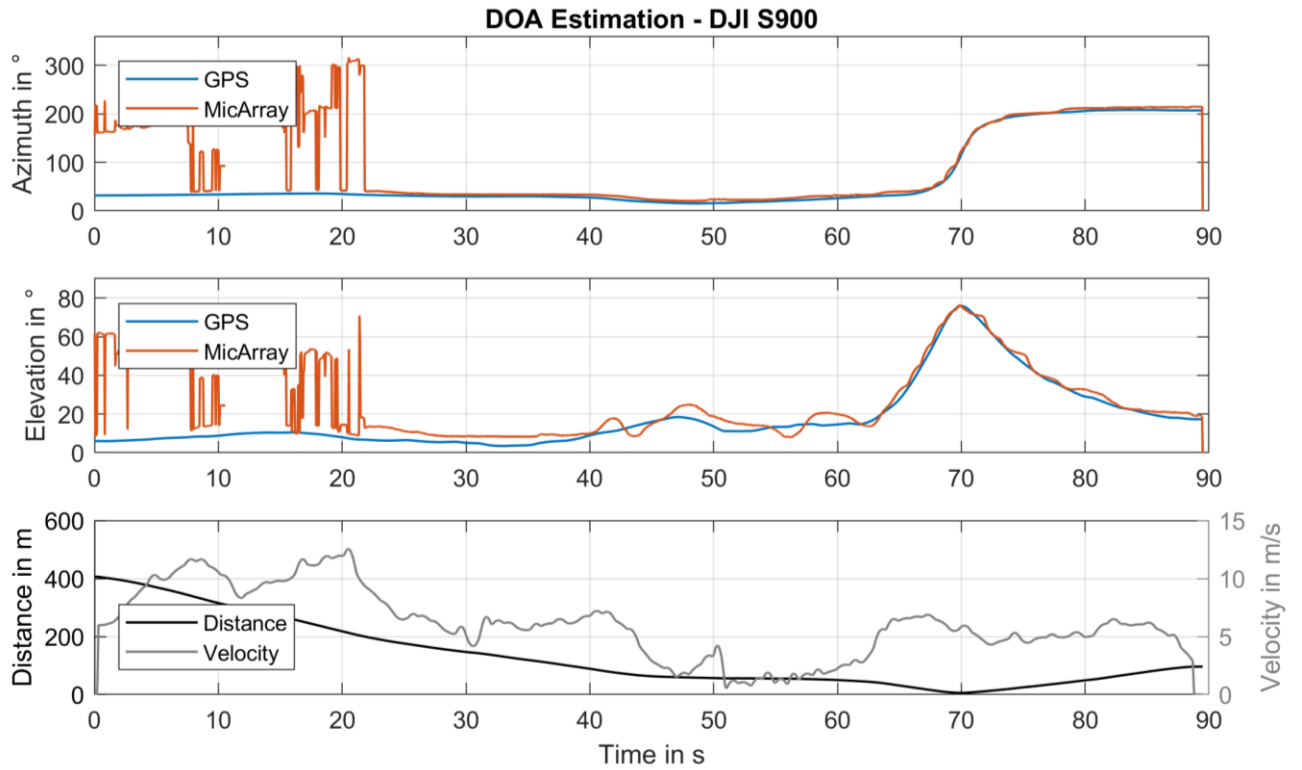


Figure 7: Exemplary DOA estimation result of a DJI S900 flying towards the array from a ground distance of 400 m at a height of approx. 15 m. The UAV is successfully tracked within a range of 200 m (after 22 s). After 70 s the UAV passes the array. The red lines show the estimated DOA for azimuth (top) and elevation (middle), the blue lines the corresponding GPS ground truth. The UAV flight motion (bottom) is visualized as ground distance (black) and velocity (grey) over time.

Since there appears to be no standardized way of assessing the performance of UAV localization in the literature (see references in Section 1), we propose a simple yet comprehensive method to evaluate DOA estimation accuracy and robustness. UAV flights are conducted at different distances from acoustic sensors. GPS trackers mounted onto a drone are used to directly capture the position and transform GPS coordinates into a local Cartesian system with the microphone array center as origin [48]. Using the transformed UAV coordinates the ground truth DOA is given in terms of azimuth and elevation as seen in Figure 7. The absolute estimation error with respect to ground truth is computed for the DOA as well as for azimuth and elevation separately. For a statistical analysis of the error distribution in dependence of the distance we propose to introduce distance ranges, e.g. in steps of 25 m, and to create box plots for each range. By doing so we gain information about the DOA accuracy and precision from the median and the interquartile range (IQR) of the absolute error, respectively. An example is given in Figure 8.

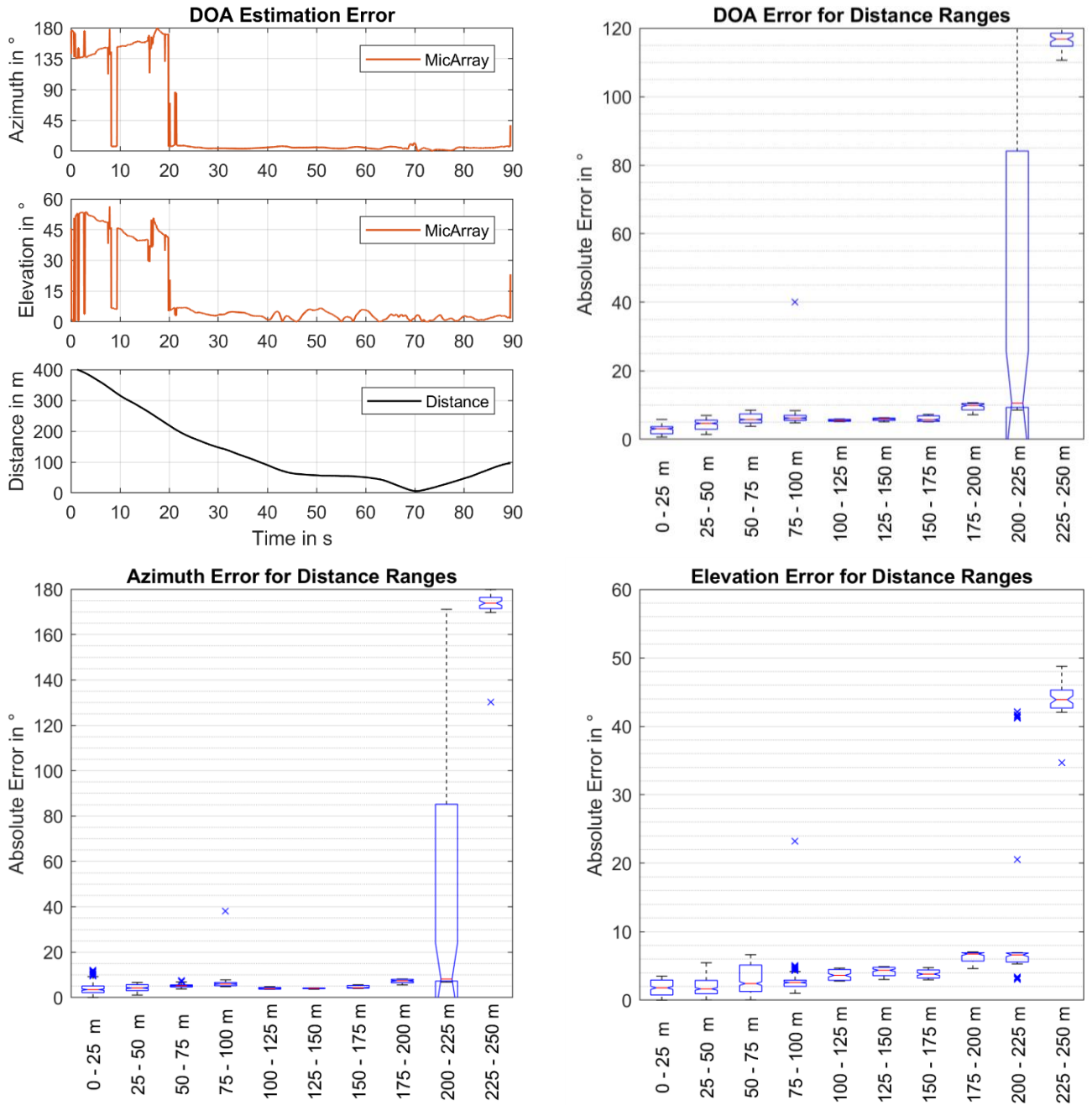


Figure 8: Exemplary analysis of the DOA estimation error in dependence of distance for the flight of a DJI S900 presented in Figure 7: Absolute azimuth and elevation error including distance profile over time (top left) and corresponding boxplots of the absolute error in terms of DOA (top right), azimuth (bottom left) and elevation (bottom right) for different distance ranges.

In this manner, we are able to define a reasonable maximum distance for which the median and the IQR of the absolute DOA error is below a certain threshold. Experimental results for DOA estimation of different UAVs approaching the array are listed in Table 1.

Table 1: Localization distances for different UAVs in terms of the proposed error criterion. The median and the IQR of the absolute DOA error is below 20°. UAVs were approaching the array from 300 m at height of approx. 15 m in strong wind conditions (~10 m/s). The upper performance bound is given by selecting the sound source closest to the GPS reference (oracle source).

UAV Type (DJI)	Number of approaches	Dominant Source Localization Distance (m)	Oracle Source Localization Distance (m)
S900/S1000	8	200	300
Inspire 2	4	75	125
Phantom 4 Pro	7	75	125
Mavic 2 Pro	8	50	100

In presence of background noise, the DOA estimate of the dominant sound source is not reliable. For this reason, it is crucial to consider multiple sound sources as possible candidates. In our field recordings, UAV sound was typically buried within the noise floor until reaching a distance of 50 m for small (e.g. *DJI Phantom 4 Pro*) and 150 m for large UAVs (e.g. *DJI S900*). This limits the localization performance when taking in account the dominant sound source only. By using multiple sources however, we were able to increase the acoustic localization distances of up to 125 m and 300 m for small and large multicopters, respectively.

4. UAV Detection

4.1 Audio Data Acquisition

The acquisition of UAV audio data is an essential step in building a machine learning model for the task of acoustic UAV detection. For the general description of UAV audio recordings we use a defined set of meta-parameters, e.g. UAV and sensor names, date and timestamps, audio codec information, as well as weather parameters such as temperature, wind speed and humidity. Ideally, every audio recording is accompanied by a GPS reference, a video and a text remark. In order to create a high quality data set, each audio file is segmented and annotated using multiple labels describing object (UAV type), events (e.g. *approach*) and context (e.g. *noise*). Labeled audio segments are then stored within an *MPEG-7* database according to *ISO/IEC 15938* [49]. Using database queries [50] a customized collection of labeled audio data is used to create training, validation and test sets. Currently the database contains 10 h of audio data recorded from nine different UAV types.

4.2 Feature Extraction

In the field of audio detection and event classification, there exists a great variety of audio features which are used to describe characteristics of sound. In general, features can be subdivided into temporal, spectral, energy-based and psycho-acoustical features [51]. For the acoustic description of UAV sound, the harmonic content within the frequency range between 100 Hz and 2 kHz and its temporal modulation plays an important role. However, due to multiple rotors and countless flight maneuvers, there is no distinct pattern in the time-frequency domain, which serves as a reliable predictor of UAV sound. Every rotor denotes a sound source on its own and causes a single set of multiple harmonic lines depending on its BPF. During flight each rotor exhibits a different varying BPF, which results in a superposition of multiple non-stationary harmonic lines in the spectrum (see Figure 9, left). Besides these acoustic phenomena, the frequency content of propeller and electro motor noise above 2 kHz may contain additional information relevant to recognizing UAV sound.

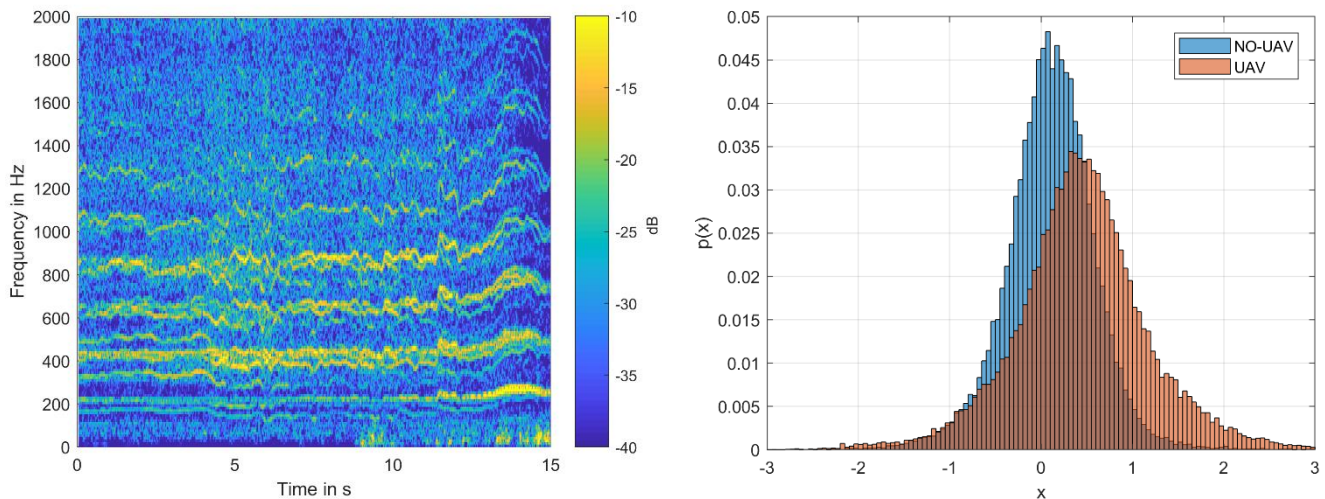


Figure 9: Spectrogram of a *DJI Phantom 4 Pro* showing superposed harmonic lines of multiple rotors (left) and exemplary feature distribution of UAV target and non-target classes computed from the validation dataset containing 1 h of audio data (right).

For this reason, we propose to use a mix of different audio features, such as generic low-level audio descriptors [52], MFCCs with modified frequency ranges, and custom features derived from tracked spectral peaks. In addition, to model temporal characteristics, we apply temporal smoothing and compute statistical functionals, such as minima, maxima or means, over consecutive feature frames. Relevant features may be chosen by using feature selection algorithms or by manually comparing feature distributions of target (UAV) and non-target classes (see Figure 9, right).

4.3 Binary Classification

The acoustic detection of UAV sound poses a binary classification problem to discriminate between *UAV* (target) and *NO-UAV* (non-target) classes. Using block processing, audio signals are subdivided into frames of 20-200 ms and the corresponding feature vectors are computed. In our implementation, we resample audio signals to a sampling frequency of 24 kHz and used frame sizes of 2048 and 4096 samples (85 and 170 ms, resp.) with a frame overlap of 50% for feature processing. We trained and tested different classification algorithms [53] on manually labeled UAV audio data: Support Vector Machines (SVM), Random Forests (RF) as well as Feed-Forward and Recurrent Neural Networks (NN and RNN). Due to simple parametrization, satisfying performance scores and fast execution in real-time, we chose the RF over other classifiers. As a post-processing step, we applied temporal smoothing over frames using a first order IIR filter on the class confidence output of the RF. In this way, predictions made upon single audio frames are given less weight and an ensemble of past predictions determines the current confidence output.

4.4 Evaluation

We evaluated the UAV detector on a separate validation and test dataset using conventional classification scores: accuracy, precision, recall and F1-score. As audio data for training and testing, we used recorded audio from the reference microphone in the center of the array *JR_BigSpiral31*. The dataset covers 12 h of annotated audio data, from which 10 h are used for training and 1 h for validation and testing, respectively. The portion of positives, i.e. the UAV class, is approximately 40% with a similar distribution of UAV types within each dataset. Table 2 shows the detection performance for both validation and test set. An example of the UAV detector output for a flight of a *DJI Mavic 2 Pro* is presented in Figure 10.

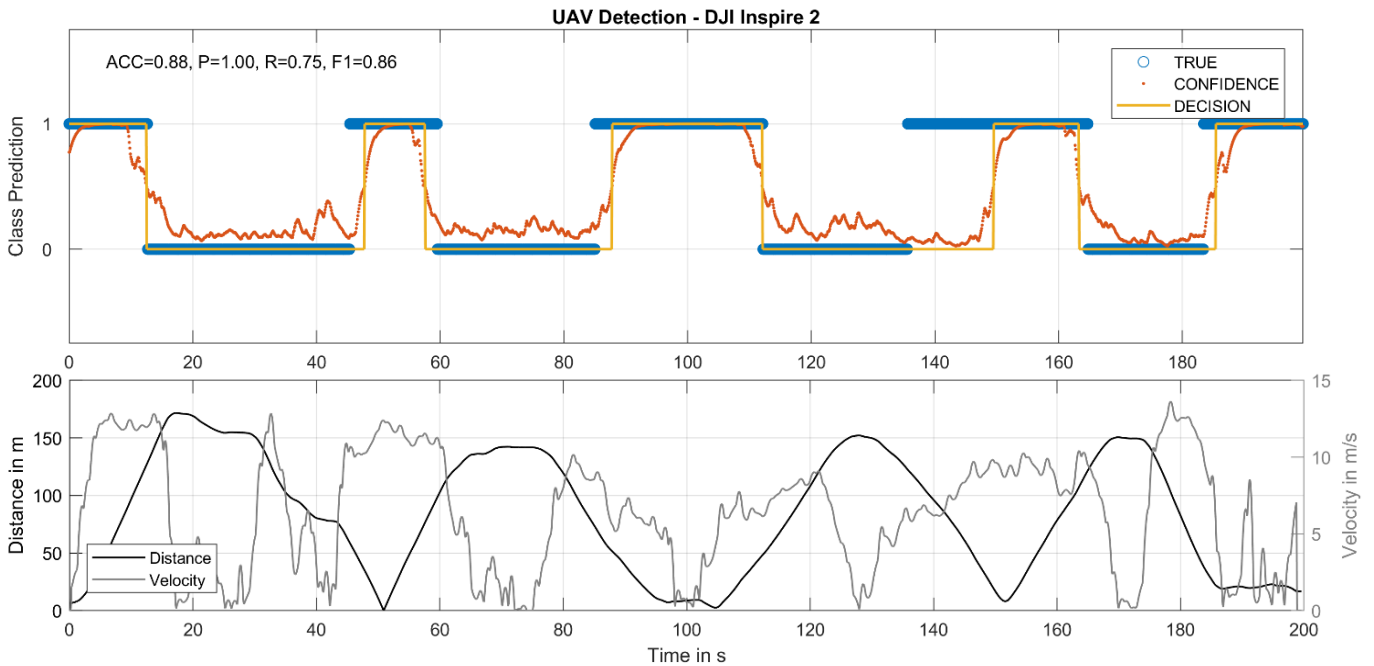


Figure 10: Exemplary UAV detector output (top) with ground truth (blue), confidence (red) and detection (yellow) outputs, and motion trajectory (bottom) for a DJI Mavic 2 Pro. Apart from the fly-over at 140-160 s the drone is reliably detected within 50 m.

Table 2: Performance evaluation of the UAV detection system trained with 10 h audio data of the array reference microphone.

Dataset	Accuracy (%)	Precision (%)	Recall (%)	F1-Score (%)
validation	88.8	90.5	78.1	83.9
test	87.9	87.5	80.8	84.0

Similar to the evaluation of the UAV localizer, we propose to use distance information obtained from ground truth GPS tracks in order to analyze detection performance over different distance ranges. An example corresponding to the flight from Figure 10 is depicted in Figure 11.

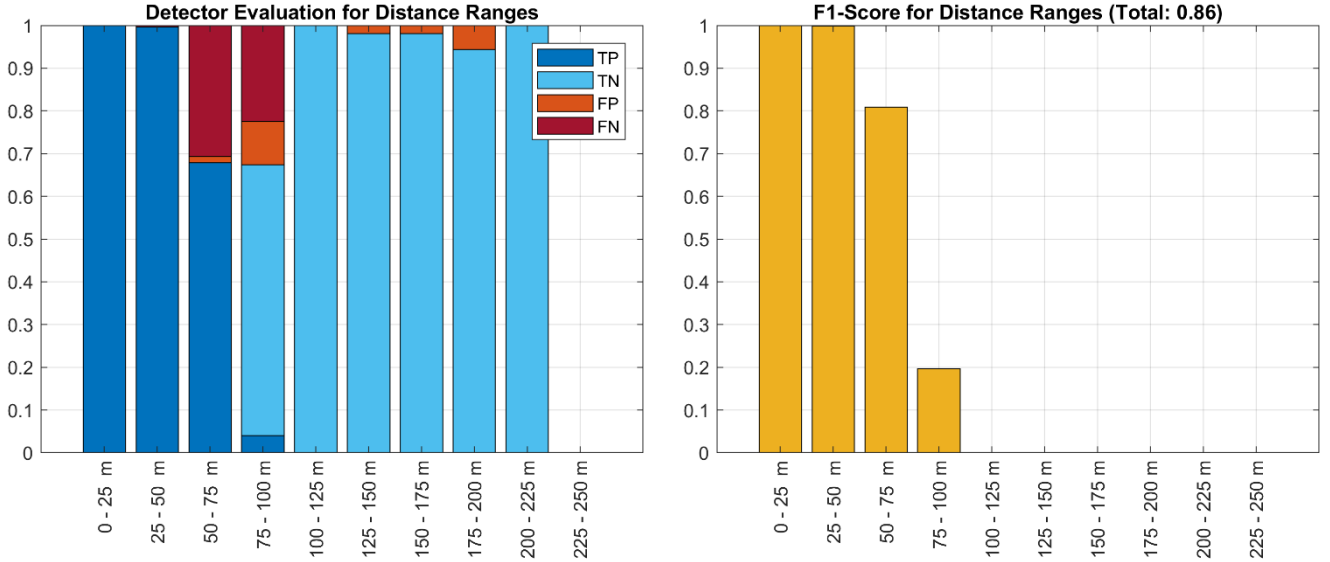


Figure 11: UAV detector evaluation in terms of true positives (TP), true negatives (TN), false positives (FP) and false negatives (FN) over different distance ranges (left) and corresponding F1-scores (right). For distance range 225-250 m no flight data was available. For this flight, detection was reliable up to 75 m with F1-scores above 0.8. In general, the F1-score becomes zero if there are no TP present, as it becomes apparent for 100-250 m.

5. Joint Detection and Localization of UAVs

So far, we have presented acoustic methods to either localize or detect a UAV. The independent usage of localization and detection is sufficient in case a UAV represents the dominant sound source. However, in outdoor environments there are typically multiple sound sources present, which raises the two questions:

- How can we associate a detected UAV sound with the correct sound source?
- How can we detect UAV sound within a noisy mixture of different sound sources?

The answers to these questions may be given by a system, which jointly localizes and classifies multiple sound sources. For this purpose, beamforming signals (BS) of localized sources may be extracted and used as spatially filtered inputs for the UAV detector. As a result, the detector produces a confidence output for each sound source at each time frame. In practice, situations may occur, where the localizer misses the correct DOA of the UAV and captures noise sources from other directions only. In these cases, it is very likely, that the detector misses the UAV since its sound signature is strongly attenuated within the beamforming signals of noise sources. To overcome this problem, we propose to additionally use a single omnidirectional microphone signal (MS) as detector input, which captures the entire sound scene containing the noisy UAV signal. In this way, we increase our chances to detect a drone even when localization fails. At this point, we may expect one of five potential outcomes with respective reasons in case of a positive sample (UAV class) at a specific point in time:

1) Only MS yields a detection:

- Localization failed to capture the UAV sound source.

2) Only one BS yields a detection:

- Beamforming successfully captured and detected the UAV sound source.
- UAV sound is masked by background noise such that detection with MS failed.

3) Multiple BS yield a detection

- Multiple UAV sound sources at different directions are present.
- Captured sound sources are too close or UAV is present from multiple directions (e.g. due to reflections) so that multiple BS extracted the same UAV.

4) Both MS and one BS yield a detection

- UAV was successfully detected by both MS and BS, and correctly localized

5) Both MS and multiple BS yield a detection

- One or more UAVs were successfully detected
- Same reasons as in 3)

To handle these scenarios in a simple and intuitive way we propose to select the sound source q for which the detector yields maximum confidence on the UAV class:

$$\hat{q} = \underset{q}{\operatorname{argmax}} C(q) \quad \text{Equation 4}$$

where C denotes class confidence outputs for Q beamforming signals (BS). This approach assumes that there is only one UAV present at most and hence would not yield satisfying results in case tracking multiple UAVs is desired. Furthermore, it is worth to mention that in either of the discussed scenarios a false positive, e.g. a lawn mower mistaken for a UAV, would mislead the localizer. For this reason, the UAV detection model of the proposed system should feature a high precision score to reject non-UAV sounds. A general system overview for the proposed UAV tracking system is presented in Figure 12.

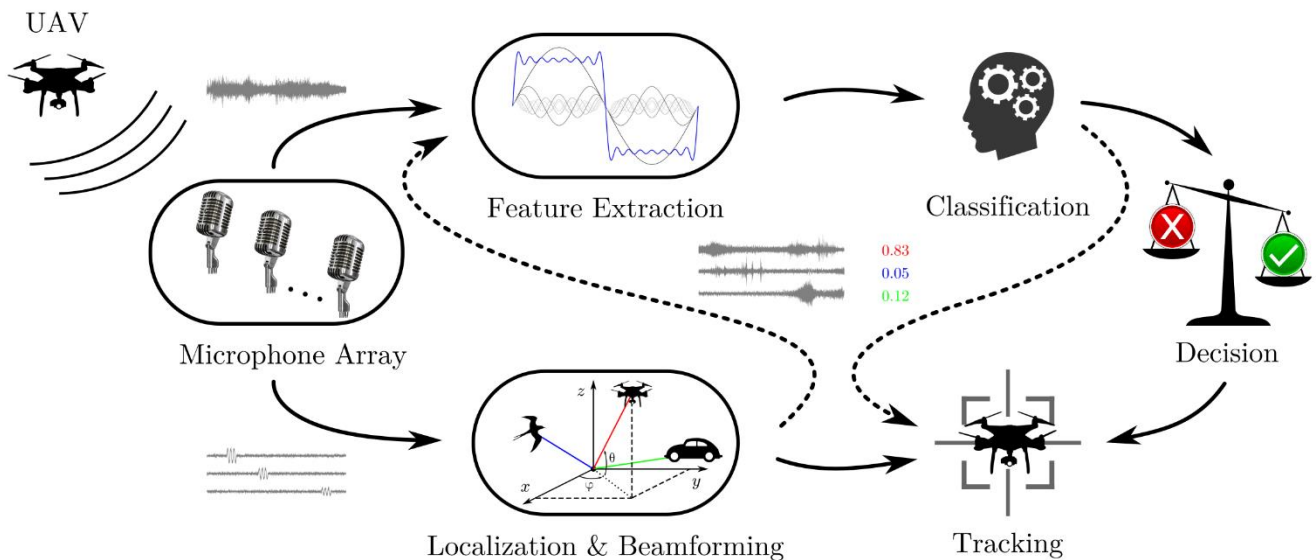


Figure 12: Overview of the proposed system for joint UAV detection and localization. A microphone array captures audio signals, which are used for the acoustic localization of multiple sound sources by DOA estimation. Beamformed audio signals of localized sources and a reference microphone signal serve as inputs for audio feature extraction. Binary classification is performed on beamforming and reference signals to discriminate between UAV and non-UAV classes yielding confidence outputs for sound source tracking and decision-making.

Using the same data and model setup as in Section 4 we evaluated our joint UAV detection-localization system. As BS we chose the delay-and-sum outputs of the three most prominent sound sources estimated by the localizer. In case less than three sources are available, we zero-padded the remaining BS outputs. Consequently, the detector yields four confidence hypotheses:

one for the MS and three for the BS. Applying Equation 4 on MS and BS together for each frame, we generated a new hypothesis based on maximum UAV detection confidence. The results are presented in Table 3.

Table 3: Performance evaluation of the joint UAV detection and localization. Evaluation was performed on the detector hypothesis of maximum confidences as proposed in Equation 4 using the MS and three delay-and-sum BS.

Dataset	Accuracy (%)	Precision (%)	Recall (%)	F1-Score (%)
validation	89.0	88.7	80.6	84.5
test	87.4	83.0	85.2	84.1

Comparing results of Table 3 and Table 2, we see a performance gain of 0.6% and 0.1% in F1-score for validation and test sets, respectively. In other words, the system was capable of extracting UAV source signals, attenuating background noise and other sound sources, which made it easier for the system to correctly discriminate between UAV and other sounds. The relatively small gain in performance may be attributed to a well-trained detector model that already works well under noisy conditions. Further improving detection performance requires either a more accurate DOA estimator together with better interference attenuation using beamforming signals or a more robust UAV sound detector covering more data, better features or improved models.

6. Real-Time System

For the real-time implementation of the proposed system we used the software *MATLAB®* together with *Simulink®* to generate an executable model in C++ [54]–[56]. At runtime, the most computationally expensive part is the SRP-based DOA estimation algorithm: For each FFT frequency bin and scanning point in space, the beamforming output and SRP are computed followed by fitting a bivariate GMM to DOA estimates to track multiple sources. Feature extraction and the random forest classifier are computationally less intensive. Hence, in order to reduce the computational load of the system, we empirically choose a set of parameters for the localizer that still enables fast execution without considerably degrading performance. Using the parameters as listed in Figure 13 (left) we arrive at approx. 20% CPU load on a *Windows 10* PC with an *Intel Core i7 6820HQ* CPU clocked at 2.7 GHz. A screenshot of the system’s user interface is depicted in Figure 13 (right).

Parameter	Value
Number of DOA scanning points	200
Number of FFT frequencies	100
Minimum frequency	200 Hz
Maximum frequency	3 kHz
Number of sources for DOA & BS	4
Number of sources for tracking	16
Processed frames per second	12

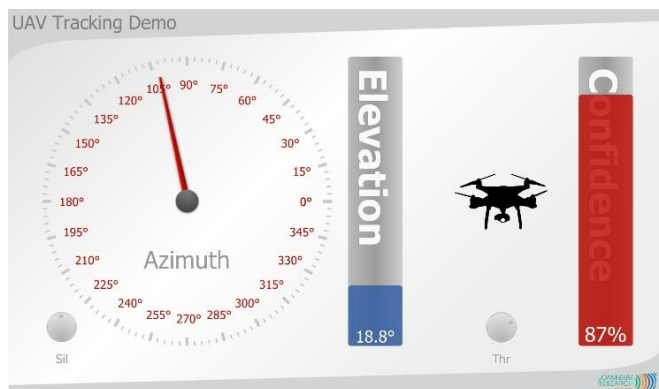


Figure 13: Parameters of the UAV localizer for real-time execution (left) and screenshot of the system’s user interface (right).

7. Conclusions

In this work, we presented a holistic framework for acoustic detection and localization of UAVs in real-time. First, we recorded and analyzed typical sounds of multicopter drones to gain an understanding of the relevant frequency ranges for designing a suitable microphone array. The

constructed array consists of 31 measurement microphones arranged in a spiral shape with a radius of 75 cm. The chosen array geometry yields a good tradeoff between mainlobe beamwidth and sidelobe suppression and provides 360° azimuth coverage due to its rotational symmetry. Next, we presented a DOA estimation algorithm that is capable of tracking multiple sound sources using a GMM-based approach. In experiments, we evaluated the maximum localization distance for different UAV types in the field using a proposed localization error metric. Furthermore, we outlined the UAV detection process consisting of audio feature extraction and binary classification. We argue that the sound signatures of drones require the design of custom features, which model the temporal and spectral modulations that originate from multiple propellers driven at different rotational speeds. The UAV detection model is evaluated using conventional classification metrics and reaches a performance of 83.9% and 84.0% in terms of F1-score for validation and test sets. Similar to the localization evaluation, we assessed the detection performance depending on the distance of the UAV from the sensor. Finally, we presented a proposed concept for joint detection and localization of UAVs. By adding beamforming signals of located sound sources as inputs to the detector, we obtain direction-dependent confidence estimates on the presence of UAV sound. We propose a simple yet effective approach for handling confidence outputs of each sound source to track a single UAV over time. The proposed system was able to improve F1-scores by 0.6% and 0.1% for validation and test sets, respectively. The modular structure of the system facilitates the independent development of more sophisticated system components for UAV detection, localization or tracking of multiple UAVs.

Potential topics for future work are manifold: The use of deep learning strategies for feature extraction and detection, such as state-of-the-art recurrent and convolutional neural network architectures, as well as deep auto-encoders may improve the detection performance and alleviate the need for custom feature design. In addition, data augmentation strategies, such as pitch shifting and mixing UAV sounds with noise, offer opportunities to extend the amount of training data without the need of costly outdoor recordings. The UAV localization and tracking algorithm may profit from state-space models, Kalman filters or particle filters for a more robust DOA estimation over time. Different beamforming algorithms suitable for real-time application may be evaluated in terms of improved UAV detection ranges and performance. Furthermore, multiple distributed microphone arrays may be used to arrive at triangulated sound source localization, which facilitates distance estimation of UAVs.

References

- [1] P. Liu *et al.*, “A review of rotorcraft unmanned aerial vehicle (UAV) developments and applications in civil engineering,” *Smart Struct. Syst.*, vol. 13, no. 6, pp. 1065–1094, 2014.
- [2] F. Nex and F. Remondino, “UAV for 3D mapping applications: a review,” *Applied geomatics*, vol. 6, no. 1, pp. 1–15, 2014.
- [3] T. Adão *et al.*, “Hyperspectral imaging: A review on UAV-based sensors, data processing and applications for agriculture and forestry,” *Remote Sensing*, vol. 9, no. 11, p. 1110, 2017.
- [4] G. Khan, E.-C. Park, and R. Gonzalez, “M3-Cast: A Novel Multicast Scheme in Multi-channel and Multi-rate WiFi Direct Networks for Public Safety,” *IEEE Access*, vol. PP, pp. 1–1, 2017, doi: 10.1109/ACCESS.2017.2749482.
- [5] Z. Fadlullah, D. Takaishi, H. Nishiyama, N. Kato, and R. Miura, “A dynamic trajectory control algorithm for improving the communication throughput and delay in UAV-aided networks,” *IEEE Network*, vol. 30, pp. 100–105, 2016, doi: 10.1109/MNET.2016.7389838.
- [6] B. Custers, “Drones Here, There and Everywhere Introduction and Overview,” in *The Future of Drone Use: Opportunities and Threats from Ethical and Legal Perspectives*, B. Custers, Ed. The Hague: T.M.C. Asser Press, 2016, pp. 3–20.
- [7] D. Mototolea, “A Study on the Methods and Technologies Used for Detection, Localization, and Tracking of LSS UASs,” *Journal of Military Technology*, vol. 1, no. 2, pp. 11–16, Dec. 2018, doi: 10.32754/jmt.2018.2.02.
- [8] M. M. Azari, H. Sallouha, A. Chiumento, S. Rajendran, E. Vinogradov, and S. Pollin, “Key Technologies and System Trade-offs for Detection and Localization of Amateur Drones,” *IEEE Communications Magazine*, vol. 56, no. 1, pp. 51–57, Jan. 2018, doi: 10.1109/MCOM.2017.1700442.
- [9] BBC, *Gatwick Airport: Drones ground flights*. 2018.
- [10] Wikipedia contributors, *List of UAV-related incidents — Wikipedia, The Free Encyclopedia*. 2020.
- [11] G. C. Birch, J. C. Griffin, and M. K. Erdman, “UAS Detection Classification and Neutralization: Market Survey 2015,” Sandia National Lab. (SNL-NM), Albuquerque, NM (United States), 2015. doi: 10.2172/1222445.
- [12] N. Intaratep, W. N. Alexander, W. J. Devenport, S. M. Grace, and A. Dropkin, “Experimental Study of Quadcopter Acoustics and Performance at Static Thrust Conditions,” *22nd AIAA/CEAS Aeroacoustics Conference*, pp. 1–14, 2016, doi: 10.2514/6.2016-2873.
- [13] G. Sinibaldi and L. Marino, “Experimental analysis on the noise of propellers for small UAV,” *Applied Acoustics*, vol. 74, no. 1, pp. 79–88, 2013, doi: 10.1016/j.apacoust.2012.06.011.
- [14] N. Kloet, S. Watkins, and R. Clothier, “Acoustic signature measurement of small multi-rotor unmanned aircraft systems,” *International Journal of Micro Air Vehicles*, vol. 9, no. 1, pp. 3–14, 2017, doi: 10.1177/1756829316681868.
- [15] T. Blanchard, J. Thomas, and K. Raoof, “Acoustic localization estimation of an Unmanned Aerial Vehicle using microphone array,” 2019.
- [16] J. Tong, Y.-H. Hu, M. Bao, and W. Xie, “Target Tracking Using Acoustic Signatures of Light-Weight Aircraft,” *ChinaSIP*, vol. 2, no. 3, pp. 20–24, 2013.
- [17] Y. Zhang, I. Lee, and D. Lin, “Measurement of Noise from a Moving Drone Using a Phased Array Microphone System,” 2017.
- [18] W. N. Alexander and J. Whelchel, “Flyover Noise of Multi-Rotor sUAS,” 2019.
- [19] V. Didkovskiy, S. Kozeluk, and O. Korzhik, “Simple Acoustic Array for Small UAV Detection,” in *2019 IEEE 39th International Conference on Electronics and Nanotechnology (ELNANO)*, Apr. 2019, pp. 656–659, doi: 10.1109/ELNANO.2019.8783262.
- [20] A. Sedunov, H. Salloum, A. Sutin, N. Sedunov, and S. Tsyuryupa, “UAV Passive Acoustic Detection,” Oct. 2018, doi: 10.1109/thS.2018.8574129.

- [21] A. Sedunov, D. Haddad, H. Salloum, A. Sutin, N. Sedunov, and A. Yakubovskiy, "Stevens Drone Detection Acoustic System and Experiments in Acoustics UAV Tracking," 2019.
- [22] A. Ramamonjy, E. Bavu, A. Garcia, and S. Hengy, "Source Localization And Identification With A Compact Array Of Digital Mems Microphones," 2018.
- [23] J.-S. Lauzon, F. Grondin, D. Létourneau, A. L. Desbiens, and F. Michaud, "Localization of RW-UAVs Using Particle Filtering Over Distributed Microphone Arrays," 2017, doi: ng.
- [24] P. Tapolczai, P. Fiala, G. Firtha, and P. Rucz, "Simulation framework for detecting and tracking moving sound sources using acoustical beamforming methods," 2019.
- [25] J. Busset *et al.*, "Detection and tracking of drones using advanced acoustic cameras," *Proc. SPIE*, vol. 9647, p. 96470F—96470F—8, 2015, doi: 10.1117/12.2194309.
- [26] W. Shi, G. Arabadjis, B. Bishop, P. Hill, R. Plasse, and J. Yoder, "Detecting, Tracking, and Identifying Airborne Threats with Netted Sensor Fence," *Sensor Fusion - Foundation and Applications*, no. Figure 1, pp. 139–158, 2011.
- [27] W. Lim, H. Jeong, Y. He, and K. Chang, "Drone Sound Identification and Classification by Harmonic Line Association Based Feature Vector Extraction (TRANSLATED)," *Journal of Advanced Navigation Technology*, vol. 20, no. 6, pp. 604–611, 2016.
- [28] L. Hauzenberger and E. H. Ohlsson, "Drone Detection using Audio Analysis," PhD Thesis, Lund University, 2015.
- [29] J. Mezei and A. Molnar, "Drone sound detection by correlation," *SACI 2016 - 11th IEEE International Symposium on Applied Computational Intelligence and Informatics, Proceedings*, vol. 1, no. 4, pp. 509–518, 2016, doi: 10.1109/SACI.2016.7507430.
- [30] L. Shi, Y. He, and K. Chang, "Acoustic-based Classification for Drone Identification using Hidden Markov Model with MFCC Technique," Electronic Engineering Department, Inha University, 2016.
- [31] A. Bernardini, F. Mangiatordi, E. Pallotti, L. Capodiferro, and F. U. Bordoni, "Drone detection by acoustic signature identification," in *IS&T International Symposium on Electronic Imaging 2017*, 2017, pp. 60–64.
- [32] S. Mandal, L. Chen, V. Alaparthi, and M. Cummings, "Acoustic Detection of Drones through Real-time Audio Attribute Prediction," 2020, doi: 10.2514/6.2020-0491.
- [33] J. Garcia-Gomez, M. Bautista-Duran, R. Gil-Pita, and M. Rosa-Zurera, "Feature selection for real-time acoustic drone detection using genetic algorithms," University of Alcalá, Alcalá de Henares, Spain, 2017.
- [34] S. Jeon, J. Shin, Y. Lee, W. Kim, Y. Kwon, and H. Yang, "Empirical Study of Drone Sound Detection in Real-Life Environment with Deep Neural Networks," *European Signal Processing Conference (EUSIPCO)*, pp. 1858–1862, 2017.
- [35] Y. Seo, B. Jang, and S. Im, "Drone Detection Using Convolutional Neural Networks with Acoustic STFT Features," in *2018 15th IEEE International Conference on Advanced Video and Signal Based Surveillance (AVSS)*, Nov. 2018, pp. 1–6, doi: 10.1109/AVSS.2018.8639425.
- [36] E. Matson, B. Yang, A. Smith, E. Dietz, and J. Gallagher, "UAV Detection System with Multiple Acoustic Nodes Using Machine Learning Models," Feb. 2019, doi: 10.1109/irc.2019.00103.
- [37] S. Al-Emadi, A. Al-Ali, A. Mohammad, and A. Al-Ali, "Audio Based Drone Detection and Identification using Deep Learning," in *2019 15th International Wireless Communications Mobile Computing Conference (IWCMC)*, Jun. 2019, pp. 459–464, doi: 10.1109/IWCMC.2019.8766732.
- [38] J. Benesty, J. Chen, and Y. Huang, *Microphone Array Signal Processing*, vol. 2. Springer, 2009.
- [39] H. L. Van Trees, *Optimum Array Processing*. John Wiley & Sons, 2002.
- [40] Z. Prime and C. Doolan, "A comparison of popular beamforming arrays," *Proceedings of ACOUSTICS 2013*, no. November, pp. 1–7, 2013.
- [41] E. Sarraj, "Optimal planar microphone array arrangements," *Fortschritte der Akustik - DAGA*, no. 2, pp. 220–223, 2015.

- [42] E. Sarradj, "A Generic Approach To Synthesize Optimal Array," *Berlin Beamforming Conference (BeBeC)*, pp. 1–12, 2016.
- [43] N. Madhu and R. Martin, "A Scalable Framework For Multiple Speaker Localization And Tracking," *Proceedings of the International Workshop for Acoustic Echo Cancellation and Noise Control (IWAENC)*, 2008.
- [44] S. K. Dhull, "Review on Acoustic Source Localization Techniques," *European Journal of Advances in Engineering and Technology*, vol. 2, no. 9, pp. 72–77, 2015.
- [45] N. Madhu and J. Wouters, "Localisation-based and situation-adaptive mask and generation for source separation," 2010.
- [46] N. Madhu and R. Martin, "A versatile framework for speaker separation using a model-based speaker localization approach," *IEEE Transactions on Audio, Speech and Language Processing*, vol. 19, no. 7, pp. 1900–1912, 2011, doi: 10.1109/TASL.2010.2102754.
- [47] L. Wimmer, "Gleichmaessige Verteilung von Punkten auf der Einheitskugel," PhD Thesis, Unisersitaet Salzburg, 1992.
- [48] S. P. Drake, "Converting GPS coordinates (phi, lambda, h) to navigation coordinates (ENU)," Surveillance Systems Division Electronics and Surveillance Research Laboratory, 2002.
- [49] MPEG, *MPEG-7*. 2002.
- [50] W3C, *XML Path Language (XPath) 2.0*. 2010.
- [51] G. Peeters, "A large set of audio features for sound description (similarity and classification) in the CUIDADO project," Ircam, Paris, 0, 2004.
- [52] F. Eyben, "Real-time Speech and Music Classification by Large Audio Feature Space Extraction," PhD Thesis, Technische Universität München, 2016.
- [53] PR Sys Design, *perClass*. 2018.
- [54] MathWorks, *MATLAB version 9.3.0.713579 (R2017b)*. Natick, Massachusetts: The Mathworks, Inc., 2017.
- [55] MathWorks, *Simulink version 9.0 (MATLAB R2017b)*. Natick, Massachusetts: The Mathworks, Inc., 2017.
- [56] MathWorks, *Simulink Coder version 8.13*. Natick, Massachusetts: The Mathworks, Inc., 2017.



QUIET DRONES
International e-Symposium
on
UAV/UAS Noise
Remote from Paris – 19th to 21st October 2020

Methods for Providing Design Guidance to Improve Drone Sound using Community Input

David L. Bowen, Acentech Inc., Cambridge, Mass. U.S.A: dBowen@Acentech.com

Summary

Many non-acoustic factors have the potential to contribute to the subjective impressions that sounds convey. For drones, as with many other products and devices, the perspective of the listener can be an important factor influencing these subjective impressions. That is, the reaction of someone who is using/controlling a drone or expecting a drone to appear is likely to be different from that of a bystander who is not necessarily expecting to see (and hear) a drone. Using carefully designed and executed jury studies that expose jurors to an array of virtual/ "what-if" drone sounds, it is possible to develop regression relationships between jury output data (in the form of numerical ratings on a particular subjective attribute such as "acceptability" of the drone sound) and input data consisting of quantifiable changes made to the sounds of the physical components and mechanisms contributing to the overall sound of a drone. These relationships and their resulting response surfaces can then be probed to determine what combinations of component modifications are likely to produce a desired degree of improvement in subjective impression, thus providing valuable design guidance beyond just "make it quieter". An example case study is used to illustrate the methodology as applied to sound recordings made during flyover and hovering operations of a prototype multi-rotor drone. In this case the input variables consisted of changes in the overall levels of broadband aerodynamic noise and motor controller noise, along with changes in the number and overall level of rotor blade passage harmonics, while the output consisted of ratings on subjective attributes as obtained from jurors drawn from a suburban community and listening from a bystander perspective. The results from this study suggested several different approaches for achieving similar degrees of substantial increase in the acceptability ratings of the sound quality of these types of drones.

1. Introduction

The sound that a device produces can contribute to a person's overall perception of the device or brand, in terms of their judgements of, say, the overall acceptability of the sound in the context of its use. Companies are often faced with negative reactions to the sounds of their products or devices, and may be uncertain as to how to improve those sounds so as to increase the general acceptance of their products. These issues, coupled with the need for manufacturers to develop high-end and international markets has made sound quality (SQ) an important product attribute. This can be especially important for completely new categories of products or devices, where people may not be used to hearing the sounds that such devices can produce. The sounds of robotic aerial vehicles - i.e., "drones" - are a fairly recent example of such devices. The potential for large segments of the population to be exposed to drone sounds is fairly high if various visions for using drones to deliver parcels in moderate to densely populated areas become reality. This paper describes the use of a particular type of sound quality jury study to both evaluate the subjective impressions of sounds produced by a proto-type drone, and provide guidance for how to modify the drone so as to "improve" those sounds.

2. Sound Quality Jury Study

To provide input regarding how members of a community may react to the sound of drones in their neighborhood, and in particular to the sound of delivery drones, we recruited people living in suburban environments to take part in listening sessions in which simulated drone sounds were played over a system of loudspeakers arranged to preserve certain spatial aspects of the sounds. The goal of these jury sessions was to quantify how various sound producing components in a prototype drone affected the perception of various subjective "attributes", so that this information could then be used to provide design guidance for subsequent versions of the drone. While it is highly likely that such subjective impressions will depend on whether someone is listening from the perspective of expecting a delivery from a drone, or from the perspective of a neighbor not expecting one, in the jury study described here the jury members were instructed to imagine themselves as being neighbors to a delivery addressee.

"Acceptability" and "Reliability" were chosen as the subjective attributes for which jurors were to provide ratings as they listened to various drone sound samples. Obtaining these ratings required first designing the jury test and then generating the component sounds that comprised the sounds that might be heard from the perspective of a delivery addressee neighbor, followed by the creation of a stimulus set of "virtual" drone sounds obtained by varying the component sounds according to a statistical design-of-experiments type of approach. This stimulus set was then presented to jurors who ranked the sounds in terms of the two attributes. We then developed regression relationships between the component variations and the jury response data, and these were used to come up with candidate drones designed to result in similar degrees of improvement in the attribute ratings. Each of these steps is discussed in more detail in the sections below.

2.1 Design of Jury Test

The SQ jury test described here was designed primarily to determine how various operating "components" within a drone affected the perceptions of Acceptability and Reliability as conveyed by the sounds of the drone as heard during two types of flight that neighbors might experience from a delivery drone – transient flyovers and steady-state hovering over a nearby neighbor's residence. To accomplish this, an approach was used in which jurors listened primarily to the sounds of various "virtual" drones that were created from extracted/simulated component sounds, according to a statistical design-of-experiments (DOE) criteria. Jurors then provided their numerical ratings, on a scale of 0-100, for how "acceptable" they thought each of

these drone sounds were, and also for how “reliable” the drone sounded, again all based on listening from the perspective of a neighbor to the delivery addressee.

The basic idea for this type of sound quality jury study is to break down the total sound of a noise-producing device like a drone into its various primary component sources for a given operating condition, so that we can then create an array of virtual device sounds by mixing together modified versions of these component sounds. The components are varied in a quantifiable way over a range of values centered on their nominal baseline (current) values. This enables us to explore subjective reactions within a space surrounding the existing baseline sounds for each operating condition studied, so that we gain knowledge regarding how these different components affect user perceptions of the subjective attributes that we choose to study. Once the data from the jury test is available, such exploration can be performed by making use of a series of regression equations arising out of response surface methodology that relate changes in the component sounds to the jury ratings of the attributes. The degree of component changes and the number of resulting mix combinations are governed by the particular DOE employed.

For the drone sound study described here we chose to use a central composite DOE, with which we have had experience with in similar sound quality jury studies that we have carried out on consumer products and other devices [1-5]. This design requires creating a number of sound mixes comprised of various unique sounds, with each component varied by a certain number of “steps” (which depends on the number of components varied), plus a number of repeats of the (unvaried) baseline sound. These step changes can be any type of change that is quantifiable in some consistent way. In general, we want a single step to be a noticeable change while not being so large that the largest number of steps called for in the design would put us out of the realm of the type of change that is feasible to implement. For this study, we chose to vary the overall sound levels of the components with a step size of 4.5 dB (exposing the jury to a range of changes over ± 9 dB relative to a baseline level). In addition, we varied the number of audible blade passage harmonics with a step size of 3 harmonics (exposing the jury to a range of 4 to 16 harmonics).

The central composite DOE employed was a full factorial circumscribed type, with the number of center points chosen so as to give uniform precision within the “inference” space. For our targeted jury size of 24 members, we needed to repeat each set of sounds three times (in a randomized fashion). The designs employ both decreases and increases to the component sound levels so that the design space, relative to its existing condition as defined by the “center points” for each component, is fully explored. The center point for the number of harmonics, however, was set to 10, which was midway between 4 (a reasonable lower value) and 16 (which was near the upper end of the number of harmonics apparent in various sound spectra examined).

2.2 Baseline Recordings

The generation of component sounds starts with recordings made of the device in a representative environment, and at a representative listening distance from the device during typical exposure. Since most of the noise from a device like a drone would appear away from (e.g., above) a person, loudspeaker rather than headphone presentation is usually the most effective way to present the sounds to jury members while preserving spatial aspects. While a true binaural recording and playback of an unaltered “baseline” sound may offer more realism to certain listeners, such realism is unlikely to be preserved once component sounds are edited and mixed together. It is unnecessary in any case if the source is mainly above the listener, since such a situation can be adequately simulated by one or more loudspeakers located above the listener (binaural presentations can sometimes also have difficulty simulating sounds that are located above the head).

Most of the baseline recordings used for this study were made at a quiet, grass-covered outdoor location. A microphone was placed at a standing ear level height, and the nominal height of the test drone – a prototype unit with eight, two-bladed rotors – upon closest approach to the microphone was approximately 25 feet. Vehicle loads and flyover speeds were varied, including the case of zero speed for the hovering condition. In addition to sound pressure at the microphone, flight data such as position and motor speed were also captured.

We also acquired representative background sounds such as light traffic, birdsong, distant lawnmowers, etc. for the purpose of mixing into the various sound samples at a low (but constant and unvaried) level, for added realism. However, after evaluating the resulting mixes it was concluded that there was too much risk that such background sounds could be overly distracting to the jurors when they had to be listening to and judging dozens of sound samples over the course of the jury session, so these background sounds were not used.

2.3 Identification and Extraction of Component Sounds

Our analysis and evaluations of the baseline sound recordings made during flyovers and hovering, as well as the associated flight data, suggested a logical breakdown of the drone noise into four different “component sounds” that could be varied for the purposes of creating an array of virtual drone sounds for presentation to a jury. These components were chosen to represent physical characteristics of the prototype drone that could be changed (somewhat independent of each other) in order to affect the total sound as would be experienced by a person on the ground. Generally speaking, these component sounds were identified as (1) broadband aerodynamically-generated noise, (2) a high-pitched, “whistle-like” sound associated with the motor controller, and (3) the blade passage tone and its harmonics. The first two components were varied in terms of their overall sound level, while the latter component was broken down into two aspects that could be varied in a quantifiable way. These were the number of harmonics and their overall sound level. The resulting set of “input variables” used for the jury study was thus as follows:

- A) Change in overall level of broadband noise
- B) Change in overall level of high-pitched motor controller sound
- C) Change in number of blade passage harmonics
- D) Change in overall level of set of blade passage harmonics defined above by (C)

Generation of these component sounds was accomplished primarily by applying to the basic recordings a combination of time-gating and lowpass, highpass, bandpass and notch filtering. Spectral analysis, along with critical listening evaluations, were used to identify frequency values and ranges needed for filter design parameters. Tonal components, for example, were extracted using narrow bandpass filters set to correspond to a range encompassing a desired set of harmonics of the various blade passage frequencies of the different rotors, as well as the high-pitched motor controller component. Captured motor speed data was also used to assist in this procedure. For the baseline sound recording utilized for the hovering condition, the fundamental blade passage frequencies were centered around approximately 162 Hz, while the high-pitched tonal component was in the range of 5900 Hz. These frequencies were slightly higher for the flyover segment used. Figure 1 shows portions of the averaged A-weighted narrowband frequency spectra (up to 6500 Hz) computed from the segments in the baseline recordings used for the hover and flyover conditions.

During the component sound extraction/creation process, checks were made by mixing together the component sounds and comparing the resulting sound to the original recorded sounds. These checks were made both on an objective spectral basis and also on a subjective listening basis until a close match was obtained.

After finalizing the component sounds (including representative sets of blade passage harmonics corresponding to the different steps needed for component C), they were varied in level

according to the DOE discussed above then mixed together and sequenced to form a randomized stimulus set of sounds for the jury to listen to and evaluate.

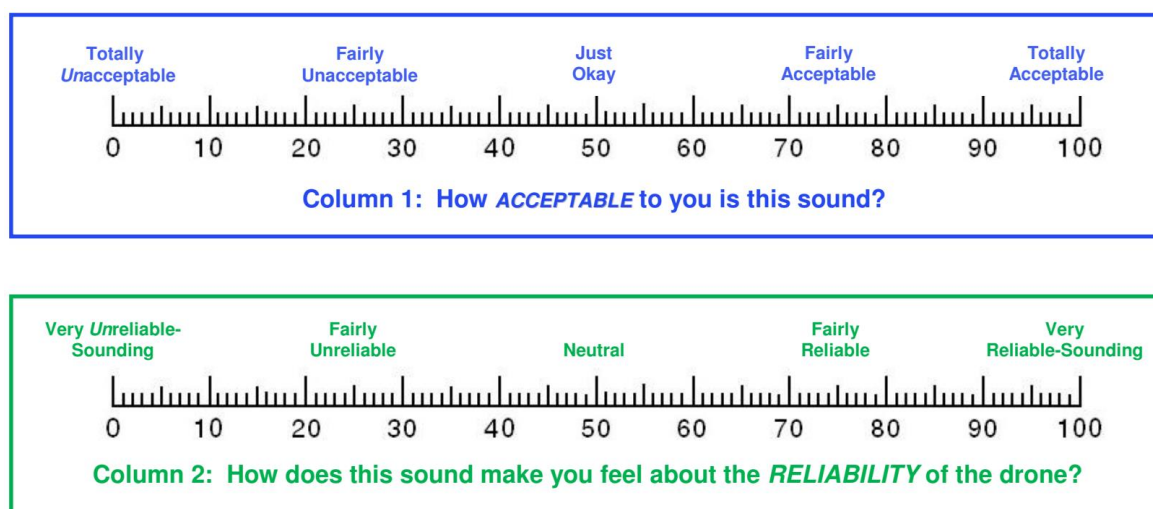
2.4 Execution of the Jury Testing

The jury testing was carried out in a single session approximately 1½ hours in duration, with a total of 27 jurors participating. Each juror was given a cash incentive for their time. A loud-speaker was located above and in front of the jurors, who were seated on chairs facing the speaker inside of a large room with sound absorbing walls and ceiling (these semi-anechoic conditions roughly approximate an outdoor environment). As was mentioned above, this arrangement is generally preferred over headphones since it guarantees that the auditory image will be located away from the listener instead of “inside their head”. The sounds were played out through a computer soundcard, and the gain on a separate amplifier was set such that the overall A-weighted sound levels at the juror locations were approximately what the jurors would experience if the drone were located 25 feet up and 100 feet away.

As described above, the jurors were asked to rate each drone sound sample in terms of the Acceptability and Reliability attributes. They were given 7 seconds after hearing each 5.5 second-long sound sample to provide their rating numbers for these two attributes. The total number of sounds presented for each condition (flyover and hover) was 90. In addition, there were 15 “extra” sounds for the hover condition (presented at the end of the session), in which the payload was varied. These different payloads had the effect of changing the “speed spread” between the individual rotors (i.e., how close the eight individual rotor blade rotation rates were to each other), which has an effect on the general character of the sound.

Before the actual testing began, jurors were first given verbal instructions followed by an example (practice) session using drone sound samples. Jurors were instructed on the meanings of the two attributes, how to fill in their rating forms, to imagine that they were outside in their backyards, etc. They were told to use a fixed interval scale of 0 to 100, with 0 being “totally unacceptable” and 100 being “totally acceptable” for the Acceptability attribute, and, for the Reliability attribute, 0 being “very unreliable-sounding” and 100 being “very reliable-sounding”. A graphical representation of these scales, as shown below in Exhibit 1, was projected onto a screen at the front of the room to remind jurors of the meanings of the rating value ranges. To assist the jurors in picturing the scenario described for them, photographs of different types of drones performing delivery tasks were also put up on the walls inside the jury room. The test then proceeded for the flyover condition, with a brief break before beginning the test for the hover condition.

Exhibit 1: Attribute Rating Scales as Presented to Jurors



2.5 Analysis of Jury Response Data

After first screening the ratings data from all jurors (e.g., checking to see if any particular jurors gave no ratings or egregious ratings such as the same number for all sounds, etc.), the ratings were used as inputs to a response surface analysis procedure. This analysis was configured to utilize a multiple linear regression in order to build a quadratic model of the relationships between the observed Acceptability and Reliability ratings and the component sound changes. Basically, this process tries to fit the entire set of individual juror ratings (i.e., a maximum of $27 \times 90 = 2430$ observations for each of the two flight conditions studied, but reduced slightly due to a few missing ratings from one juror) to a response surface model with all the linear, squared and two-way interaction terms included. After eliminating a first round of observations with large standardized residuals (which amounted to between about 4 and 5.5% of the total number of observations) and eliminating statistically insignificant coefficient terms, the analysis was re-run, resulting in response surface models for each of the two flight conditions.

The equations resulting from this reduced-order regression analyses (i.e., the “models”) are summarized below in Exhibit 2. These relate values predicted for Acceptability and Reliability to *changes* in the component sounds from their baseline conditions. The models can then be used to predict the effect on Acceptability and Reliability of changes in the various sound-producing components of the drones. In these equations, the average Acceptability and Reliability rating values for the baseline condition are given by the constant term located immediately after the equals sign. We can see from this that the average ratings resulting from the current sounds of the prototype test drone examined for this study are slightly lower for the Hover condition than for Flyover, but that the average Acceptability ratings for both are on the lower end of the “Just Okay” range. The average Reliability ratings for both are in the mid to upper end of the “Neutral” range.

Exhibit 2: Reduced-Order Regression Equations Obtained for the “Acceptability” and “Reliability” Attributes

FLYOVER:

$$\text{Acceptability} = 46 - 3.2\mathbf{A} - 0.52\mathbf{B} - 0.77\mathbf{C} - 1.5\mathbf{D} - 0.075\mathbf{C}^2 - 0.043\mathbf{D}^2 + 0.082(\mathbf{AC}) + 0.14(\mathbf{AD}) - 0.077(\mathbf{BD})$$

($R^2=36.2\%$)

$$\text{Reliability} = 58 - 2.0\mathbf{A} - 0.31\mathbf{B} - 0.30\mathbf{C} - 0.35\mathbf{D} - 0.047\mathbf{A}^2 + 0.069\mathbf{C}^2 - 0.026\mathbf{D}^2 + 0.098(\mathbf{AD}) + 0.045(\mathbf{BC}) - 0.049(\mathbf{BD})$$

($R^2=23.1\%$)

HOVER:

$$\text{Acceptability} = 40 - 3.0\mathbf{A} - 0.36\mathbf{B} - 1.4\mathbf{C} - 1.4\mathbf{D} - 0.024\mathbf{B}^2 + 0.16\mathbf{C}^2 - 0.083\mathbf{D}^2 + 0.10(\mathbf{AC}) + 0.19(\mathbf{AD})$$

($R^2=35.8\%$)

$$\text{Reliability} = 53 - 2.7\mathbf{A} - 0.40\mathbf{B} - 0.61\mathbf{C} + 0.53\mathbf{D} - 0.077\mathbf{A}^2 - 0.032\mathbf{D}^2 + 0.048(\mathbf{AC}) + 0.14(\mathbf{AD})$$

($R^2=30.0\%$)

where: **A** = Change in overall level of broadband noise, in dB relative to baseline level
B = Change in overall level of high-pitched motor controller sound, in dB relative to baseline level
C = Change in blade passage harmonic content, in number of harmonics, relative to 10
D = Change in overall level of blade passage harmonics, in dB relative to baseline level

Associated with each of the equations in Exhibit 2 are various statistical indicators arising out of the regression analysis, some of which can be used to help assess the reliability and accuracy of the models. One of the most important indicators is the regression coefficient, R^2 , which is the percentage of the observed variability that can be explained by a given model/equation. We have typically seen R^2 values in the 25 to 45% range in the SQ jury studies we have conducted on products, and the R^2 values shown in Exhibit 2 generally fall within that range. The higher R^2 values observed for Reliability in the 2nd half of the jury session (e.g., Hover) may be due to the jurors getting more used to using the rating scale for this somewhat more abstract attribute by the time they were exposed to the hover sounds.

In any case, the fact that the variability in juror judgments was fairly large does not mean that the predictions of the effect of a component change are wrong, but simply that an associated design change will not necessarily be universally recognized as beneficial. That is simply a fact of how people perceive sounds. The regression equations themselves are just a tool that can be used to potentially guide subsequent engineering effort in the pursuit of increasing a neighbor's positive perceptions of a drone, as conveyed by its sound. A subsequent "verification study" can address some of the uncertainties discussed above by presenting the sounds of drones with supposedly higher sound quality (as determined using results from the current jury study) along with the sound of an unaltered, baseline drone, in order to determine the degree to which people might prefer one version over the other.

To facilitate interpretation of the relationships described by regression equations such as those presented above in Exhibit 2, contour plots of their response surfaces can be produced by varying two of the components at a time, while holding the rest of the variables fixed at some value such as no change from their baseline values. Some examples of such "slices" through the response surfaces are shown by the plots presented in Figures 2 through 4, where colors are used to indicate how the modelled values of the Acceptability and Reliability ratings vary with changes in the component sounds (note that, due to scaling reasons, the color ranges/values are generally different for each plot). The intersection of the solid black lines in the middle of each contour plot represents the (unmodified) baseline condition.

Such contour plots are useful for quickly gauging how sensitive the attribute ratings are to changes in the various components, and for determining the most efficient way to improve the ratings by a certain amount. The regression equations and plots show, for example, that Component "A" (level of broadband noise) is always a strong factor governing how the subjective attributes are rated by the jury, while Component "B" (level of high-pitched motor controller sound) never appears to exert all that much influence. It should be kept in mind that since the regression models essentially result from a curve fitting procedure, the associated confidence in the models will generally decrease as we get closer to the boundaries of the variable space explored (i.e., near and beyond the edges and corners of the contour plots displayed).

The (non-regression) results from the extra sounds presented for the hover condition, where the "speed spread" between the individual rotors was varied by changing payload, is summarized below in Table 1 below. In general, this speed spread increased as the payload decreased, and this was included as a rough way to gauge if/how this factor might affect perception. Since this aspect of the drone sound could not be independently controlled and varied (although an initial effort was made to synthesize such sounds using motor speed data acquired simultaneous with sound data, the resulting sounds were not felt to be realistic enough), the jury ratings for these sounds could not be included in the regression analysis. Instead, these ratings were analyzed only in terms of their means and standard deviations. Both the average Acceptability and Reliability ratings followed a similar pattern in that they tended to increase slightly with speed spread (with the most change – about 10 rating points - occurring from 16 to 15.6 kg). However, given the large standard deviations associated with these ratings, this pattern of change in the average ratings cannot be said to be statistically significant.

Table 1: Mean Ratings and Standard Deviations for "Extra" Sound Samples in Hover Condition

Flight Load (kg)	Avg. Accept. Rating	Standard Deviations for Acceptability Ratings	Avg. Reliability Rating	Standard Dev. for Reliability Ratings
16.39 (least speed spread)	28.5	18.1	41.9	18.3
16.03	27.3	17.7	39.9	19.8
15.64	35.6	21.5	49.8	20.0
15.25	38.3	20.1	52.7	20.9
14.86 (most speed spread)	36.0	22.5	48.0	24.9

3. Using Jury Results to Improve Drone Sounds

The regression equations and their related response surface contour plots described above can be used as guidelines for how to modify the various sound-producing components in the drone so as to achieve targeted improvements in the community's subjective response to the sound of a drone. There will often be more than one way to achieve a given degree of improvement in the mean attribute ratings, and some ways may be more attractive than others due to feasibility and other considerations. For example, the model described above in Section 2 indicates that we could achieve about a 10 point increase in the Acceptability ratings for both the flyover and hover conditions by decreasing only the broadband noise by about 3.5 dB, or by decreasing both the level of broadband and blade passage tones by just 2 dB. The effect on the attribute ratings of also changing the other components can be explored using the regression equations themselves (as presented in Exhibit 2).

3.1 Candidate Designs for Improving Acceptability and Perception of Reliability

We used the general approach outlined above to target improving the Acceptability ratings by about 70% and the Reliability ratings by about 40% over their current average values of around 43 and 55, respectively, for both the flyover and hover conditions. This degree of change was selected so as to cause a significant, but still potentially achievable, increase in the ratings. Such increases would push the ratings from their average present values in the low to mid "Just Okay" and "Neutral" ranges into values firmly within the next higher categories of "Fairly Acceptable" and "Fairly Reliable" (i.e., in the 70-80 range). While targeting increases that are much smaller than this (say, 10%, as initially illustrated above in the introduction to this section) would no doubt be easier to achieve, the statistics of the results indicate that there would be more of a chance of such changes not being noticed.

The most straightforward approach, as suggested by the regression results, for achieving such improvements is to target reductions in the level of the broadband noise. If this level was able to come down by 9 dB, all ratings would be predicted to increase into the 70-75 range, which is slightly below the goals mentioned above. Also reducing the level of the high-pitched motor controller sound, by 6 dB, would increase some of the ratings by another 3 points or so. This sound, since it is fairly high in frequency may be easier to reduce (by deflection or absorption, for example) than some of the other sounds, but it is not a strong driver of the ratings. A similar effect on the Reliability ratings could be achieved by also reducing the number of audible harmonics (to 6) instead of reducing the high-pitched motor controller sound (this change has a more pronounced effect on the Acceptability ratings). Another approach suggested by the results involves a slightly less severe reduction of broadband noise (7.5 dB instead of 9) coupled with a 4 dB reduction in the overall level of the blade passage tone and its harmonics.

A summary of these candidate "target" designs for increasing the attribute ratings so that they all reside close to the 70-80 range follows:

Design 1: Decrease broadband noise level by 9 dB:

- Flyover Acceptability increases from 46 to 74.5, Hover Acceptability increases from 40 to 67.
- Flyover Reliability increases from 58 to 72, Hover Reliability increases from 53 to 71.

Design 2: Decrease broadband noise level by 9 dB and motor-controller tone by 6 dB:

- Flyover Acceptability increases from 46 to 77.5, Hover Acceptability increases from 40 to 68.
- Flyover Reliability increases from 58 to 74, Hover Reliability increases from 53 to 74.

Design 3: Decrease broadband noise level by 9 dB and number of BP harmonics to 6:

- Flyover Acceptability increases from 46 to 82, Hover Acceptability increases from 40 to 79.
- Flyover Reliability increases from 58 to 75, Hover Reliability increases from 53 to 76.

Design 4: Decrease broadband noise level by 7.5 dB and level of BP harmonics by 4 dB:

- Flyover Acceptability increases from 46 to 79, Hover Acceptability increases from 40 to 73.
- Flyover Reliability increases from 58 to 74.5, Hover Reliability increases from 53 to 71.

We can, of course, use information gained from these multiple “2-component-change” designs to create and test designs in which more than just two components are changed. Doing so generally relaxes the reduction requirement on any one component. For example, if the broadband noise level could be reduced by 6.5 dB, the high-pitched motor controller tone by 5 dB, the number of harmonics to 7 and their level by 3 dB, then the model would predict the following improvements in ratings:

- Flyover Acceptability increases from 46 to 79, Hover Acceptability increases from 40 to 75.
- Flyover Reliability increases from 58 to 75, Hover Reliability increases from 53 to 73.

A design such as this one would achieve the goal of moving all ratings into the range between 70 and 80. It should also be noted that if the high-pitched motor controller sound in this design is left unchanged, the resulting new ratings are almost as noted above (78 and 74 for Acceptability of Flyover and Hover, and 73 and 71 for Reliability of Flyover and Hover).

3.2 Additional Steps

Target designs such as those discussed above typically offer different ways to achieve similar improvements in SQ. After several candidate designs have been identified using the results from jury studies, they can then be simulated and listened to for comparison before embarking on actual modifications. As was mentioned above in Section 2.5, such a separate “verification study” can be useful for determining whether there is a real preference for one design over another, and if so to what degree. The main result from this type of study (usually carried out via a paired comparison approach) will be a preference ranking or “score” of the sounds of the different candidate designs (along with, optionally, the baseline sound of the unaltered design). This information can then be used to assess how “close” or “far apart” these drone designs are to each other in terms of preference based on sound, and to help select a final design for implementation and testing.

The analysis and results discussed above all pertain to people reacting to delivery drone sounds from the perspective of a neighbor of the delivery addressee. Results would likely be somewhat different for a person listening from the perspective of an ordering customer. This, of course, could be the focus of an additional jury study if there was interest in potential modifications to increase sound quality from this perspective. The goal here would have to be to find those combination of changes which would increase SQ from both the bystander and addressee listening perspectives, without being detrimental to one or the other.

It is beneficial if physical metrics calculable from the measured sound of a device like a drone can be correlated to existing sound quality ratings that have been obtained for that device. To do this, a modified form of Principal Components Analysis (PCA) or Partial Least Squares (PLS) can be used to reduce the many existing sound quality metrics that can be calculated to just a few custom metrics [3]. Usually these turn out to be weighted combinations of the most “important” metrics found by PCA or PLS, which can then be used to relate physical measures of the sound from existing and future drones to sound quality as determined by existing jury ratings. This can make it convenient to use the recorded/measured sounds of various potential prototype drones to predict subjective reactions to their sounds without necessarily having to carry out further jury studies on different versions.

4. Conclusions

For products and devices, non-acoustic factors have the potential to contribute to the subjective impressions that their sounds convey. The perspective and expectations of the user/listener can be important factors influencing these subjective impressions. In addition, for categories of devices that are fairly new, such as drones, where people may not be used to hearing the sounds that such devices can produce, companies may be uncertain as to how to improve those sounds so as to increase their general acceptance. Jury studies using a representative cross-section of potential users or potentially affected community members can provide valuable information and context that traditional sound quality metrics by themselves cannot necessarily provide.

This paper has described how a particular type of jury study can be designed and used to determine how various sound-producing components/sources in a drone affect subjective impressions. An example case was presented in which the sounds of these components from a prototype 8-rotor delivery drone during two different flight conditions (flyover and hovering) were extracted, varied, and mixed back together to provide a stimulus set of “virtual” drones for a jury to listen to (from the perspective of a neighbor of a delivery addressee) and rate on two different subjective attributes – “acceptability” and “reliability”. The resulting regression relationships between these numerical ratings and the variations introduced into the component sounds resulted in models that could then be used to provide design guidance for how to best achieve improved ratings. Results indicated that reducing the overall level of broadband noise by 9 dB, or by about 6 dB in combination with some smaller reductions in the other components, would increase the rating values from their average present values in the low to mid “Just Okay” and “Neutral” ranges to values firmly in the “Fairly Acceptable” and “Fairly Reliable” range.

References

1. Bowen, D (2015) *Sound Quality and Engineering Noise Control of Various Consumer Products* Invited paper presented at National Academy of Engineering Workshop on Engineering a Quieter America: Progress on Consumer and Industrial Product Noise Reduction, Washington, D.C., 13-17
2. Bowen, D (2010) *Sound Quality Studies of Front-Loading Washing Machines* Sound and Vibration 44(12), 8-13
3. Bowen, D (2008) *Correlating Sound Quality Metrics and Jury Ratings* Sound and Vibration 42(9), 12-15
4. Lyon, R and Bowen, D (2007) *Designing Quiet Products* The Bridge 37(3), 11-17
5. Bowen, D and Lyon, R (2003) *Mapping Perceptual Attributes of Sound to Product Design Choices* Noise Control Engineering Journal 51(4), 271-279

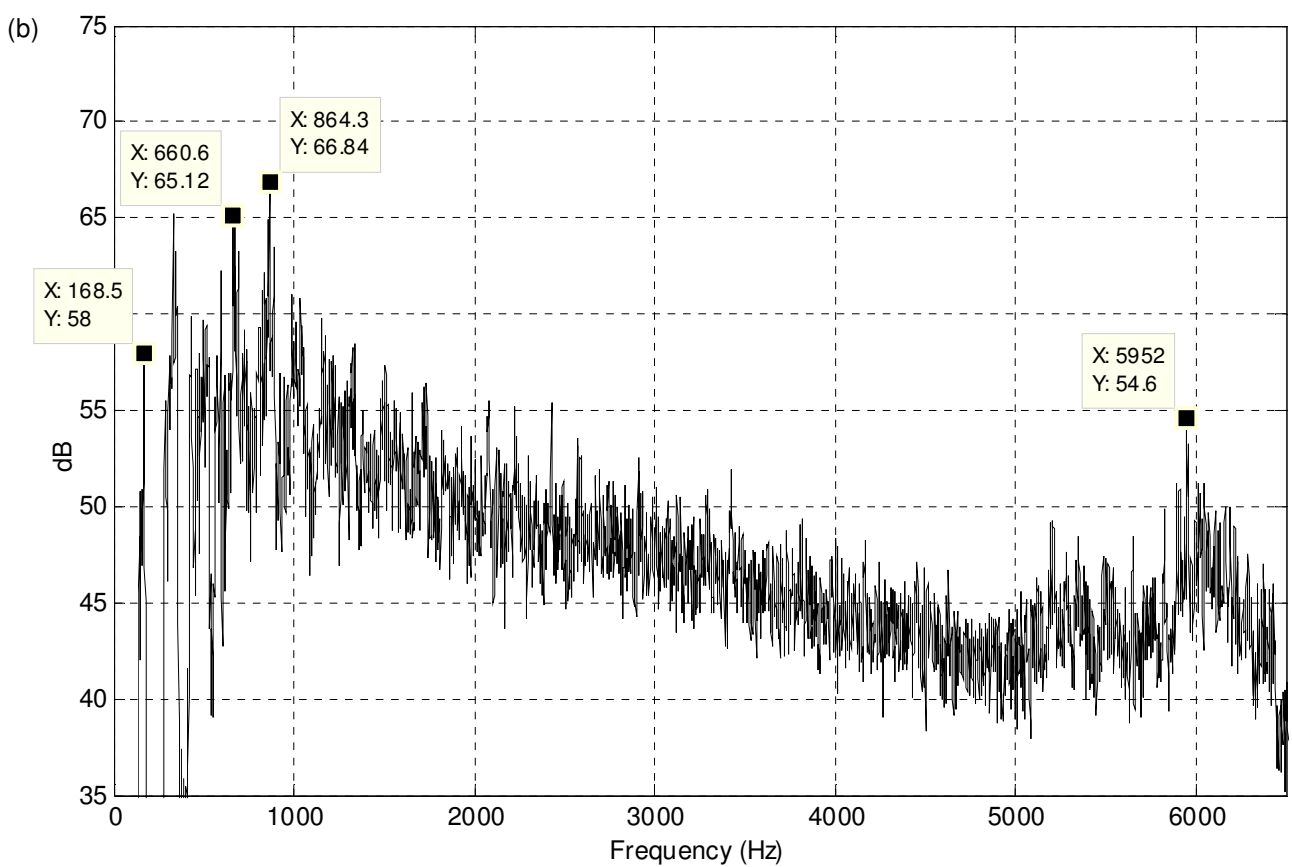
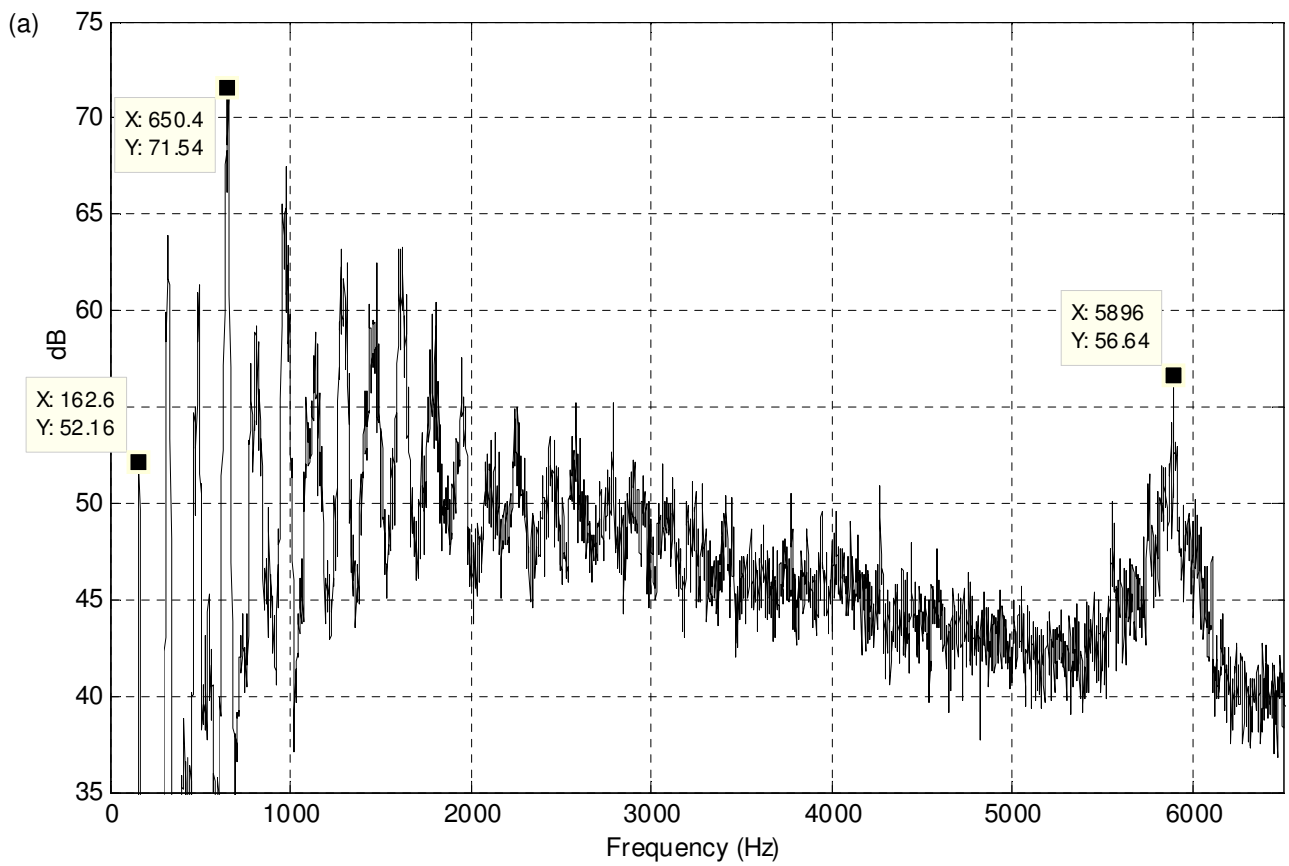


Figure 1: Example averaged A-weighted sound pressure spectra of baseline outdoor recordings utilized for (a) hovering and (b) flyover conditions

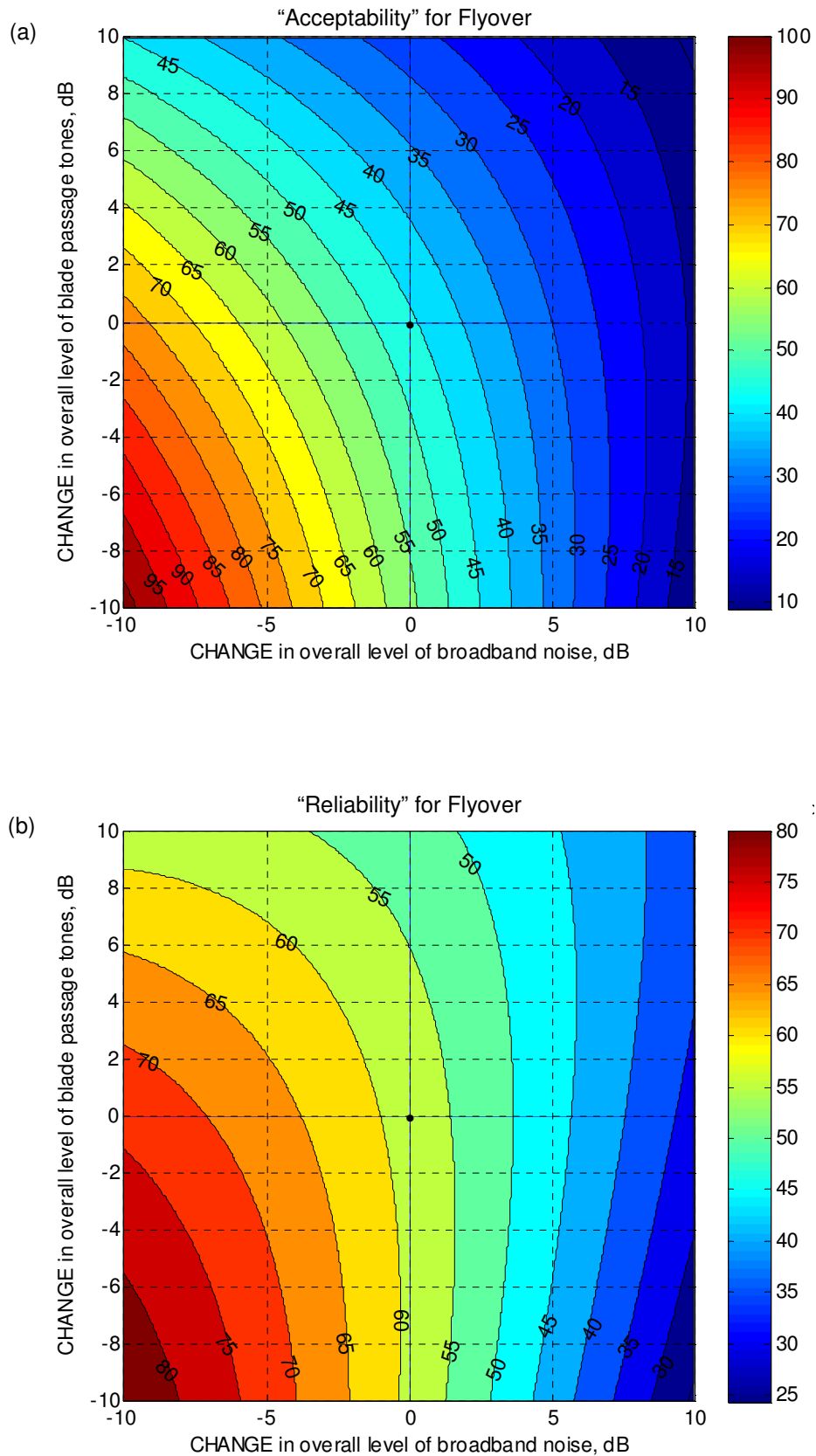


Figure 2: Contour plots of modelled (a) Acceptability and (b) Reliability attribute ratings for Flyover condition, as a function of broadband noise level and overall level of blade passage harmonics (number of blade passage harmonics and level of motor controller sound held fixed at no change from their baseline values)

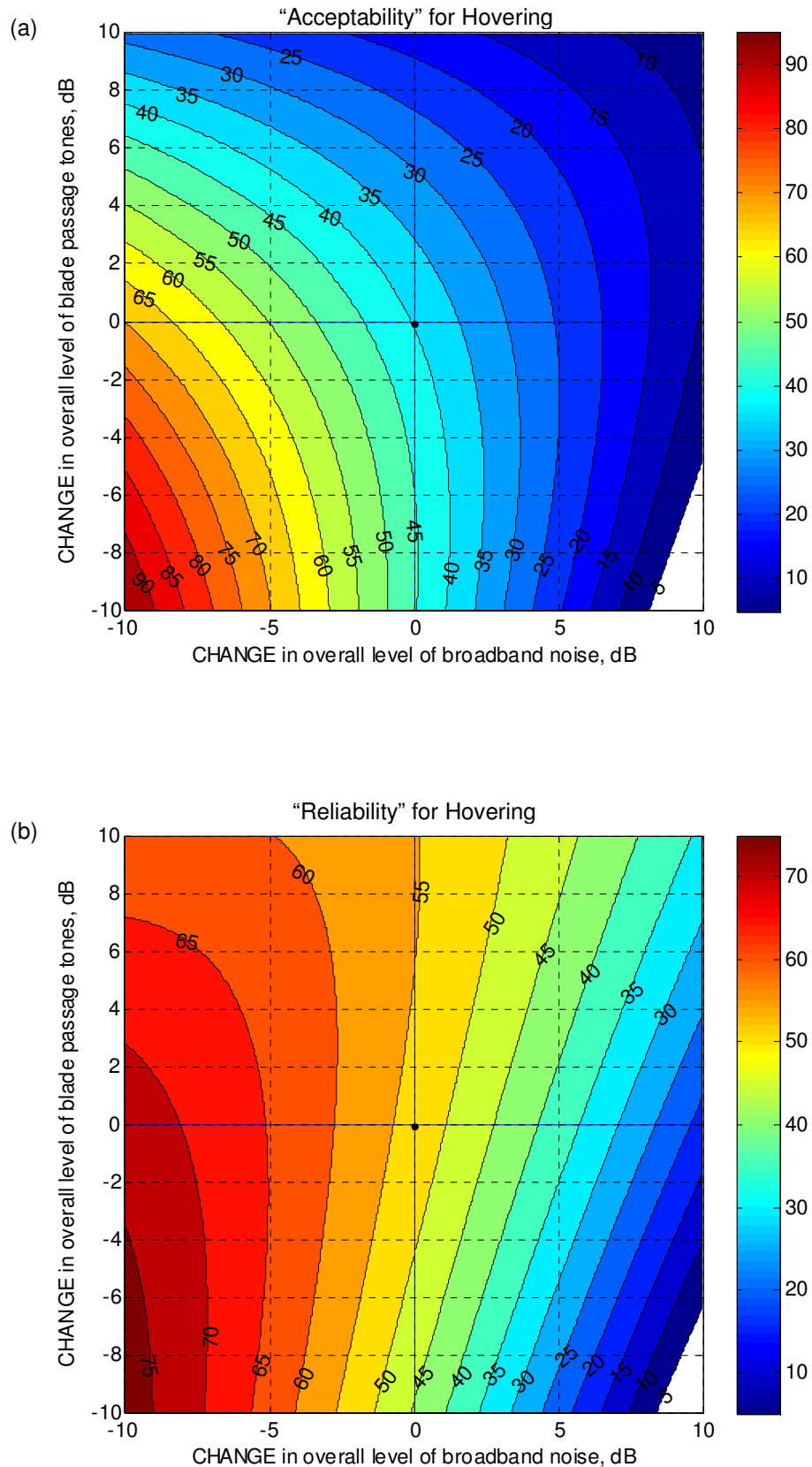


Figure 3: Contour plots of modelled (a) Acceptability and (b) Reliability attribute ratings for Hover condition, as a function of broadband noise level and overall level of blade passage harmonics (number of blade passage harmonics and level of motor controller sound held fixed at no change from their baseline values)

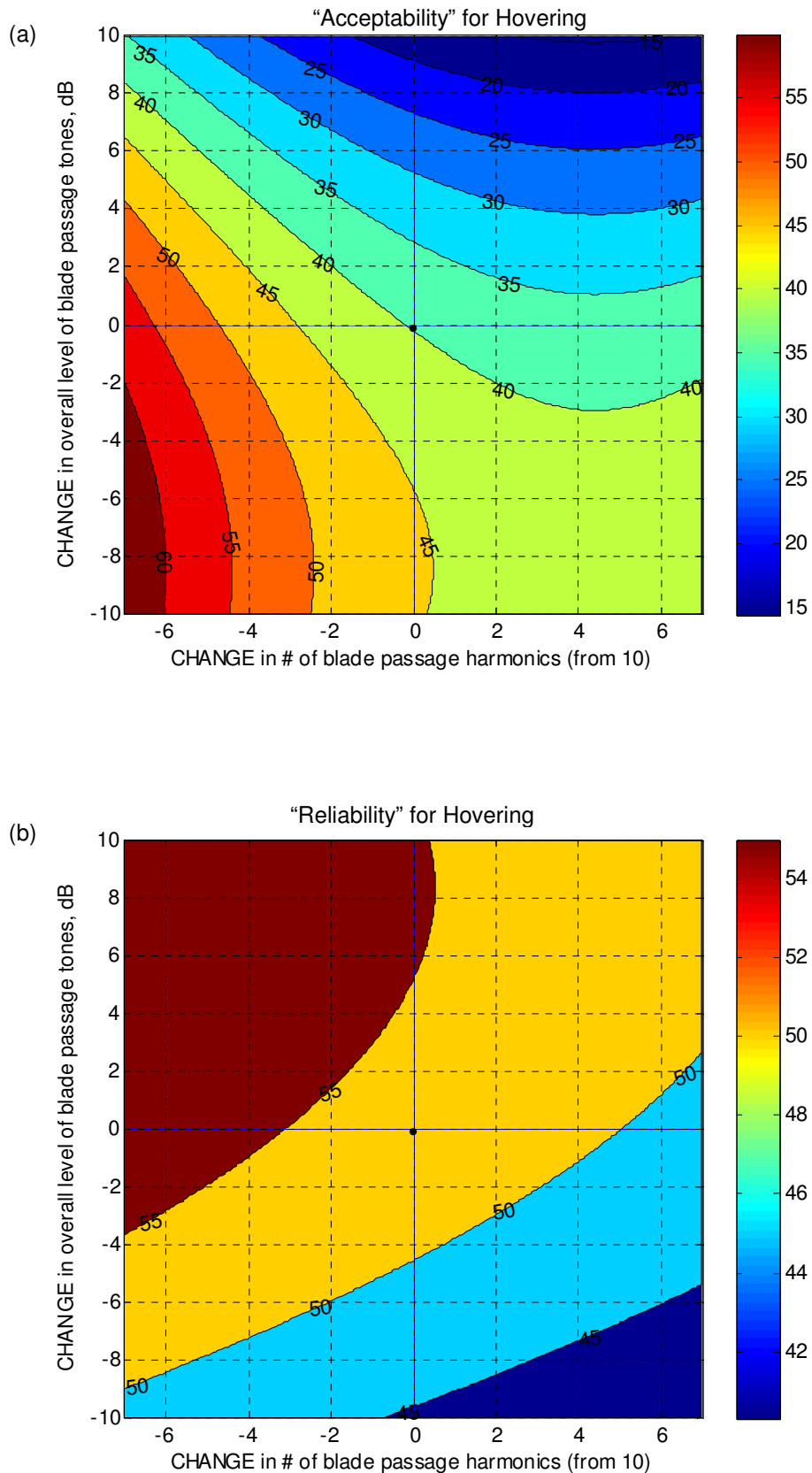


Figure 4: Contour plots of modelled (a) Acceptability and (b) Reliability attribute ratings for Hover condition, as a function of the number of blade passage harmonics and their overall level (levels of broadband noise and motor controller sound held fixed at no change from their baseline values)



QUIET DRONES
International e-Symposium
on
UAV/UAS Noise
Remote from Paris – 19th to 21st October 2020

Drone delivery and noise regulation in the Australian context

Marion Burgess, UNSW Canberra, Australia: m.burgess@adfa.edu.au

Summary

A trial area for drone delivery to residential properties in Australia has been undertaken. The payload of up to 1.5 kg is delivered by a drone designed to keep the package steady and level to avoid spill for products like coffee. After approving the trial and acknowledging that the current noise regulations do not adequately address noise from drones, in 2019, the Federal Department initiated a review. This sought public and organisation submissions to assist with the determination of the appropriate scope and breadth of future noise regulation in relation to drone operations, urban air mobility aircraft as well as specialised and historic aircraft. In this paper the responses from the community exposed to the trial drone delivery noise will be discussed along with the actions taken by the drone delivery company to minimise the noise annoyance. While awaiting the outcome of the review of future regulation, approval was granted for operations in two different jurisdictions. The actions taken to reduce the noise annoyance have led to very few complaints despite many thousands of deliveries being made.

1 Introduction

Delivery of items directly to households and business by drone is one of the so-called 'disruptive' activities that have become available with modern technology. Drone delivery has particular application for suburban residential areas that are some distance from major/local shopping centres. Those living in the areas where it is an option, have embraced this service, especially during the 2020 pandemic when all have been subject to various levels of restriction in our daily life. This paper provides a summary of the experiences with a trial and implementation of drone delivery in Australia.

2. Regulatory Framework for Drone Operations

The company Wing Aviation Pty Ltd considered that the suburban areas of the major cities in Australia provided an ideal test bed for this activity. After careful consideration by the company, an area in the Tuggeranong district to the south of central Canberra, Australian Capital Territory (ACT), was selected for trial in early 2018. The first challenge was to get approval as there was no specific regulatory framework in Australia for commercial drone operations over residential areas.

Airspace in Australia is managed by the Civil Aviation Safety Authority which reports to the Federal Government. Latimore et al (2019) provides a summary of the existing regulatory framework in Australia and discusses options for appropriate noise certification standards and noise metrics. So the first step was to demonstrate that the drone delivery could be undertaken safely with no adverse impact on commercial and general aviation operations from Canberra airport plus the various approved heliports around the city. The next was to deal with concerns about noise impact. Most environmental noise matters in the selected area are managed by the ACT Environmental Protection Authority (ACT EPA) and not by the Federal Government. However it soon became clear that the EPA did not have jurisdiction over the noise from airborne drone delivery.

After careful review, the Federal Government Department formed the view that a range of commercial and recreational drone operations within Australia required approvals under section 17 of the Air Navigation (Aircraft Noise) Regulations 2018 s. (Dept n.d). Part a) of these Regulations (regs, 2018) states

“The owner or operator of an aircraft (other than an aircraft mentioned in paragraph 7(1)(a) or (b) or a supersonic aircraft) may apply to the Secretary for approval for the aircraft to engage in air navigation.”

To allow for the trial of the delivery service and to assess the response from the community, the Secretary did give permission for trial in 2018/19. During this period, the Department provided an Issues Paper in 2018 in preparation for the public review

“to determine the appropriate scope and breadth of future noise regulation in relation to RPAs, such as drone operations and urban air mobility aircraft and Specialised Aircraft, such as supersonic aircraft and historic aircraft”

This issues paper is no longer publicly available but Table 1 from that paper provides some guidance on the options considered to be available to the Department for managing the noise impact. The public review called for submissions and closed in November 2019. A total of 92 submissions were received of which 78 related to remotely piloted aircraft (ie drones) and all the submissions can be viewed from the webpage:

[https://www.infrastructure.gov.au/aviation/environmental/aircraft-noise/noise regulation review for rpa drones and specialised aircraft.aspx](https://www.infrastructure.gov.au/aviation/environmental/aircraft-noise/noise%20regulation%20review%20for%20rpa%20drones%20and%20specialised%20aircraft.aspx).

The outcomes of this review were due in early 2020 but, like much of our life, the production of the final report was overtaken by urgent matters relating to the management of aviation during the pandemic and at the time of preparation of this paper (Aug 2020) is yet to be released.

Following the end of the trial area in the south of Canberra, and even though the report on the review of the regulations had not been completed, approval was granted for a similar delivery service to operate in an area in the northern suburbs of Canberra and an area in the southern suburbs of Brisbane, Queensland.

Table 1 Regulatory options under consideration; extracted from the Issues Paper prepared by the Australian Department of Infrastructure, Transport, Cities and Regional Development in relation to the Review of the Air Navigation (Aircraft Noise) Regulations (no longer publicly available)

Having regard to future development of drone operations in Australia the department is proposing:

- a.** Concentrating Commonwealth noise regulations for drones on their air navigation (not their base of operations) based on:
 - drone size, weight, and design;
 - tested noise levels e.g. effective perceived noise in decibels, sound exposure level, $L_{A_{Max}}$ (the maximum noise level reached) or weighted noise levels which are used for traditional aircraft;
 - operational height and location e.g. commercial/industrial/residential/rural/ remote areas; and
 - particularly in built-up and residential areas, the use of restrictions based on total number of flights per day, the duration of flight, how many flights per hour and time of flights (day/night).
- b.** Regulations not applying to recreational drones, all drones below 250 grams and drones operating under standard operating conditions.
- c.** Regulations not applying to particular types of operations including emergency services, agricultural and other prescribed service operations (e.g. lifesaving patrols, essential medical supply delivery).
- d.** Drones that meet recognised international aircraft noise certification standards not requiring approval under the Regulations (as is the case now with other aircraft types).
- e.** Benchmarking acceptable noise levels for overflying different land use areas (including residential areas) having regard to acceptable noise levels permitted from other similar noise generating equipment under State/Territory legislation.
- f.** Allowing noise regulation of drones by State/Territory Governments where this is consistent with the application of their regulations to other types of noise disturbance from operating equipment and not inconsistent with Commonwealth legislation.

3. Wing Aviation Drone Delivery in Australia

The Wing Aviation delivery in Australia involves the use of custom-designed drones to deliver packages safely, reliably and very quickly. In summary, once a customer submits an order via the Wing mobile app the drone flies to pick up the package, then climbs to a cruise height on average of about 45 metres above ground, flies to the designated delivery destination in several minutes, slows down, hovers, descends to a delivery height of 7 metres above ground, lowers the tether and automatically releases the package in the desired delivery area. Wing's aircraft are designed to deliver small packages that weigh approximately 1.5 kg or less. The drones are equipped with still-image cameras used for back-up navigation in the event GPS is unavailable and the images are grayscale and low resolution. The cameras point downwards and cannot be "aimed" towards particular objects; they instead identify terrain to inform the aircraft of its location. The majority of the deliveries are for fresh food purchases with others including coffee/tea, chemists, hardware, homewares, sport/fitness etc.

The company used the experience from the trial operations plus the developments in drone technology so that the operations in the two new sites use improved and less noisy drones. The specifications for the drones in current use are shown in Figure 1 and an image of the delivery process in Figure 2.

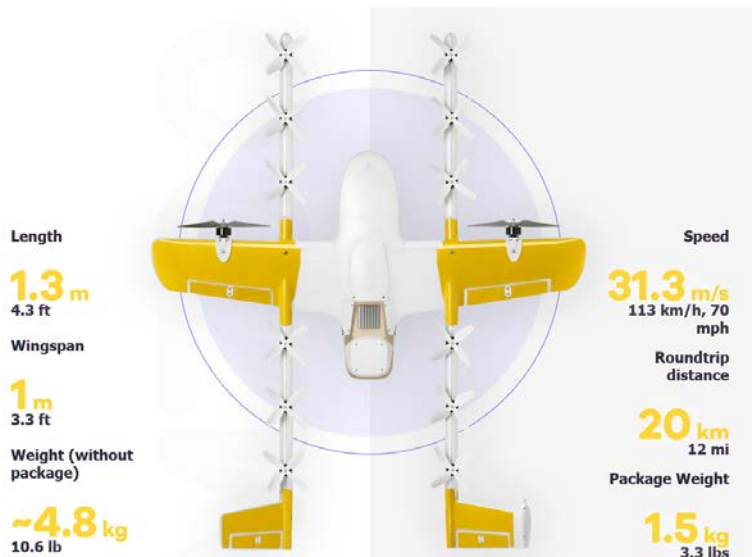


Figure 1 Specification of the drone in current use
from https://wing.com/en_au/how-it-works/



Figure 2 Drone delivery in process
https://wing.com/en_au/press/australia/

4 Conditions on Operations

As mentioned above, although a new regulatory framework had not been released, permission has been granted for two additional areas from February 2020 to February 2021. The conditions for each area are a little different and reflect, to some extent, the different environmental noise legislation in the two areas.

In suburban area to the north of Canberra-

- Tuesday, Wednesday, Thursday and Friday from 7.30am to 7pm (Mondays are used for aircraft maintenance)
- Saturday from 8.00am to 6pm
- Sunday from 9.00am to 6pm
- Operations are not permitted on public holidays.

In suburban area to the south of Brisbane-

- Weekdays from 7.30am to 7pm
- Saturday from 8.00am to 6pm
- Sunday from 9.00am to 6pm

Among the additional conditions on the approval, Wing Aviation must undertake community consultation before commencing the operation and during operation collate all comments received by the company, the local government and the federal government.

5 Changes Based on Findings from the Trial

As is expected with any call for public submissions, the responses to the review came from those who had been exposed to the noise during the trial, those who used and seek expansion of the delivery service and those who have not been exposed but fear the expansion into their area.

Concern about the high noise level and the type of noise ie “buzzing” was a common comment. Wing Aviation has made use of the improvements in drone design to introduce a fleet with lower noise and reduced high frequency components. An independent consultant undertook comparative noise level data at 25m with the former and the current drones operating under the same conditions. This demonstrated a reduction of approximately 7 dB in the overall noise level and a reduction in the tonal noise by approximately 10 to 12 dB (private communication). Comparison of the noise from the drone used in the trial and the drone used in current operations can be found at <https://www.facebook.com/riotactnews/videos/1043923962458934/>.

Another concern during the trial operations was the high number of overflights for those residents near to the base. The bases for the current operations have been located within commercial areas so that houses are not impacted by the regular take off and landing at the base. The flight paths have also been planned to minimise as much as practical repeated overflights of the same houses.

One comment from the trial that is difficult for the company to take action on, is the annoyance to neighbours from repeated deliveries to regular customers. Hopefully the reduced noise of the drones and the other improvements in the current operations will reduce this annoyance.

For the current operation near Canberra and Brisbane, many thousands of deliveries have been made during the time of the pandemic doubling from February to March and doubling again from March to April (<https://www.businessinsider.com.au/alphabets-drone-delivery-service-wing-has-made-thousands-of-deliveries-in-australia-during-the-pandemic-2020-5>). Despite this high number of deliveries, the total complaints received have been only 14 for the Canberra and 9 for the Brisbane operations. Wing Aviation is continually monitoring any complaints and modifying its operation as appropriate.

6 Concluding Comments

The approval for a trial operation of delivery by drone direct to households in a specific area has provided the opportunity for the Federal Government to assess the operation and seek the response from the community as part of the development of a regulatory framework. It has also provided the opportunity for the company to review operation and implement changes to reduce annoyance. The experience from the trial period have led to changes in operation with the use of a drone that has lower noise levels and a less annoying noise signature plus additional attention to flight paths. The success of the trial drone delivery and the actions by the company for reduction of the noise impact, has led to the company gaining approvals for operations in two different jurisdictions. The conditions with approved hours of operation are similar but reflect the varying approaches for managing local noise in different jurisdictions. These new operations have been very successful with very few complaints.

Acknowledgement

The preparation of this paper would not have been possible without the assistance from Jesse Suskin from Wing Aviation Pty Ltd with the provision of information on the noise levels and operations and his cooperation is gratefully acknowledged.

References

Latimore M, Moyo C, Fenner B and Zissermann P (2019) "Remotely Piloted Aircraft Systems (RPAS) noise in an urban environment" Acoustics 2019, Cape Schanck, Victoria, Australia November 10-13, 2019,
Available from https://acoustics.asn.au/conference_proceedings/AAS2019/



QUIET DRONES
International Symposium
on
UAV/UAS Noise
Remote from Paris – 19th to 21st October 2020

**Aeroacoustic Study of Small Propellers with Serrated Trailing
Edge for a Quieter Drone**

Paolo Candeloro: Università Niccolò Cusano, Via Don Carlo Gnocchi 3, 00166 Rome, Italy:
paolo.candeloro@unicusano.it

Ranieri Emanuele Nargi: Università Niccolò Cusano, Via Don Carlo Gnocchi 3, 00166 Rome, Italy:
ranieriemanuele.nargi@unicusano.it

Edoardo Grande: Delft University of Technology, Delft, 2629HS, Netherlands,
e.grande@tudelft.nl

Tiziano Pagliaroli: Università Niccolò Cusano, Via Don Carlo Gnocchi 3, 00166 Rome, Italy:
tiziano.pagliaroli@unicusano.it

Summary

Drone noise is a well-known issue for the European scientific community that develops drones or associated technologies. In general, the increase of endurance and the reduction of the acoustic impact are identified as strategic objectives for the growth of the flying drone market and key issues to improve the safety of this technology. Drones are usually equipped with electric motors, which contribute to simplify operations and significantly reduce the engine

noise signature. Therefore, the main acoustic source from drones turns out to be the propeller/rotor.

It is hereafter described an experimental investigation on the trailing edge noise generated by a small-scale propeller with serrated trailing edge (STE). This control technique is already employed on wind turbines and on fixed wing aerofoil. Nevertheless, a few studies have been devoted to the application of serration on small propellers. The idea of serration comes from nature and mimics owl's wing geometry. Owls are known to be one of the most silent predators in nature, and this feature is related to their characteristics wings, which has not a flat surface and a blunt trailing edge.

Experimental tests were carried out within the anechoic chamber located at Niccolò Cusano University, several blades with the same shape and different STE patterns have been tested to achieve a parametric overview of the noise control strategy effects.

In addition, a spectral and statistical analysis of the pressure time series has been carried out. Results shows a reduction in the broadband noise component and even an unexpected decrease in the tonal component. This effect is relevant for characteristic propagation directions, defined by the polar angle, showing a strong directivity of the noise source. Furthermore, the statistical analysis shows a different probability distribution function at different polar angle suggesting that the serration induces a modification in the wake of the blade. These results are confirmed by the wavelet analysis performed on the time series. Such technique has never been applied to rotor noise and, by its time/frequency definition, looks promising in order to better understand the noise generation mechanism.

1. Introduction

The term "drone" refers to an automatized vehicle with high manoeuvrability, in both hovering and cruise operations. In the most interesting configurations, Unmanned Aerial Vehicle (UAVs), small multicopter Unmanned Aerial Systems (UAS) or Micro Aerial Vehicle (MAV) are already designed with vertical or horizontal take-off and landing capabilities, and can manoeuvre with extremely high versatility and speed. Due to these unique properties, MAVs are often used in tactical surveillance missions or for reconnaissance purposes. In order to gain information about the scouting area without being easily identified, achieving an acoustically stealth-mode is an essential feature for mission success. Despite the different aims, the noise footprint of these vehicles is extremely important even when employed in civilian roles, due to their flight proximity to populated urban areas.

Drones have and will have more and more an enormous social and economic impact. In fact, this technology opens new possibilities in several application fields. The most common mission tasks still require geographical mapping, infrastructure inspections, precision agriculture, delivery and e-commerce but innovative applications comes out every day. Just to give an idea: drones equipped with cameras can resolve the problem of the images taken by satellites (which are often expensive, weather-dependant and in low-resolution) or car-based images (which are limited to human-level perspectives and the availability of accessible roads), farmers can check the quality of crop growth by using cameras mounted on specific UAV, appropriate drones will also enable construction companies to verify work advancement in real time or, for mining companies, the possibility of obtaining precise volumetric data (leading to lower risks for their employers), humanitarian organizations will be able to evaluate and adapt aid efforts for refugee camps, while medical supplies can be delivered quickly by rescue organizations where necessary. By using MAVs for transportation, developing countries that may not have appropriate road networks could deliver goods simply. Inspection drones, vehicles able to fly in confined space, can be used by fire-fighting and emergency units to assess danger faster and safely, or by logistic companies to detect damage to both inner and outer shells of ships, or by road maintenance companies to measure deterioration in bridges or tunnels. Security agencies will be able to improve building safety by monitoring even the areas outside cameras range. Drones will enable disaster mitigation agencies to inspect partially collapsed buildings in the event of obstacles for terrestrial robots. Teams of autonomous drones coordinators will enable missions to last longer than the flight time of a single drone by allowing it to leave the swarm for a short time to replace the battery (Floreano & Wood, 2015).

Therefore, with a so wide range of applications there is a need to address the problem of noise pollution from these vehicles. Furthermore, the classical multi-rotor configuration, preferred for maneuverability, makes drone noise a very central and challenging issue for scientific community with several industrial and academic players working on this task.

The main noise sources for propeller propulsion are the engine and the propeller itself. Therefore, the problem is even more complicated because it requires to optimize both sources at the same time. As reported in literature, MAV are typically equipped with brushless electric motors that significantly reduce the noise signature (Gur & Rosen, 2008, 2009a, 2009b; Tiziano Pagliaroli, Camussi, et al., 2018a) leading to a strong interest of the scientific community to the propeller noise generation mechanism.

In the last few year, several author have addressed the problem of propeller noise (Candeloro, Nargi, Patanè, & Pagliaroli, 2020; Gur & Rosen, 2008, 2009a; Janakiram & Scruggs, 1981; Leslie, Wong, & Auld, 2010, 2008; Nelson & Morfey, 1981; Tiziano Pagliaroli, Camussi, et al., 2018a; Tiziano Pagliaroli, Moschetta, Benard, & Nana, 2014; Rozenberg et al., 2008; Serré, Chapin, Moschetta, & Fournier, 2017; Sinibaldi & Marino, 2013). The topic is even more complicated because achieving proper acoustic and aerodynamics feature are contradictory goals, since a gain in noise generated is always associated with a loss in propulsive force generation.

In the literature, few studies have been devoted to low Reynolds number small-scale propellers. For these kind of propellers the effect of recirculation bubbles, stall cell and non-uniform boundary layer transition are not negligible.

Small-scale UAVs provide a great challenge to the task of noise characterization and prediction. Indeed, the main noise sources remain consistent with those associated with helicopters, but there are numerous unknowns which to investigate, as the effect of reduced size or the balance between tonal noise and broadband noise.

2. Theoretical Background

This section provides a brief explanation of the most common noise prediction model and a description of the passive noise control strategy presented. The aim is to understand the noise generation mechanism and how the serration may mitigate it.

2.1 Noise Model

Generally, the propeller aerodynamic noise is split into two main components: narrow and broad-band contributions (Candeloro et al., 2020; Farassat & Succi, 1980; Tiziano Pagliaroli, Camussi, et al., 2018b; Sinibaldi & Marino, 2013):

$$p'(x, t) = p'_{NB}(x, t) + p'_{BB}(x, t) \quad 1$$

where p'_{NB} is the narrow-band component of pressure fluctuations, whereas p'_{BB} is the broad-band counterpart.

Narrow (or tonal) components are directly associated to the periodic motion of the blade in the surrounding fluid. Therefore, the frequency and magnitude of the radiated noise is related to the rotational regime. For thin blades and low Mach numbers ($M < 1$), the narrow-band contribution is given by the sum of a sound source related to blade thickness, p'_T , and one related to aerodynamic loading, p'_L :

$$p'_{NB}(x, t) = p'_T(x, t) + p'_L(x, t) \quad 2$$

the thickness term takes into account the fluid displacement due to the body shape, while the loading counterpart takes count of the unsteady force distribution over the blade surface.

On the other hand, the interaction of turbulent flow structures with the blade edge is responsible for the broad-band noise radiating from the propeller leading/trailing edge or from the blade tip. Therefore, the main sources that generate this component are:

- I. noise related to the turbulence of the incoming flow (*LE noise*);
- II. noise produced by the interaction of the turbulent boundary layer over the blade surface with the trailing edge (*TE noise*);
- III. noise generated by the possible separation of the flow (*Separation noise*) (Sinibaldi & Marino, 2013).

Therefore, the broad-band contribution can be further divided as:

$$p'_{BB}(x, t) = p'_{LE}(x, t) + p'_{TE}(x, t) + p'_S(x, t) \quad 3$$

where $p'_{LE}(x, t)$ is the leading edge component, $p'_{TE}(x, t)$ is the trailing edge component and $p'_S(x, t)$ is the due to laminar separation bubble term.

Several authors, in the literature, have already addressed the prediction of trailing edge broad-band noise.

Sinibaldi et al. (Sinibaldi & Marino, 2013) in their study present a relation between the Power Spectral Density of the trailing noise, S_{pp}^{TE} and the spanwise velocity correlation length, l_y :

$$S_{pp}^{TE}(r, \theta, \omega) = \frac{B}{8\pi} \left(\frac{\omega c}{2a2} \right)^2 \Delta RD(\theta, \phi) |I|^2 \Phi_{pp} l_y \quad 4$$

where r is the observer position vector, $\omega = 2\pi f$ is the angular frequency, f is the rotational frequency, B is the number of the blades, c is the chord, a is the speed of sound, ΔR is the spanwise length of the blade, $D(\theta, \phi)$ is the directivity function, $|I|^2$ is the square of the absolute value of the radiation integral function and Φ_{pp} is the wall power spectral density of the pressure fluctuations.

There are different models for S_{pp}^{TE} estimation, e.g. the one proposed by Schlinker and Amiet (Schlinker & Amiet, 2001), or the more recent one proposed by Rozenberg et al. (Rozenberg et al., 2008), which takes into account the effect of the adverse pressure gradient. On the other hand, l_y is usually evaluated by means of the Corcos' model (Corcos, 1965).

The noise control strategy analyzed and hereafter described is based on the model proposed in Eq.4. More specifically, since $S_{pp}^{TE} \sim l_y$, a significant modification of l_y , provided by employing a sawtooth pattern to the TE, should correspond to a sensible noise variation in the far field.

2.2 Noise Control Strategy: Serrated Trailing Edge

In Fig.1 two blades are rendered in their three dimensional geometry: one is a commercial blade (APC 9x4e) hereafter denoted as *baseline* (see fig.1 (a)), the other is the custom-made STE blade (fig.1 (b)).

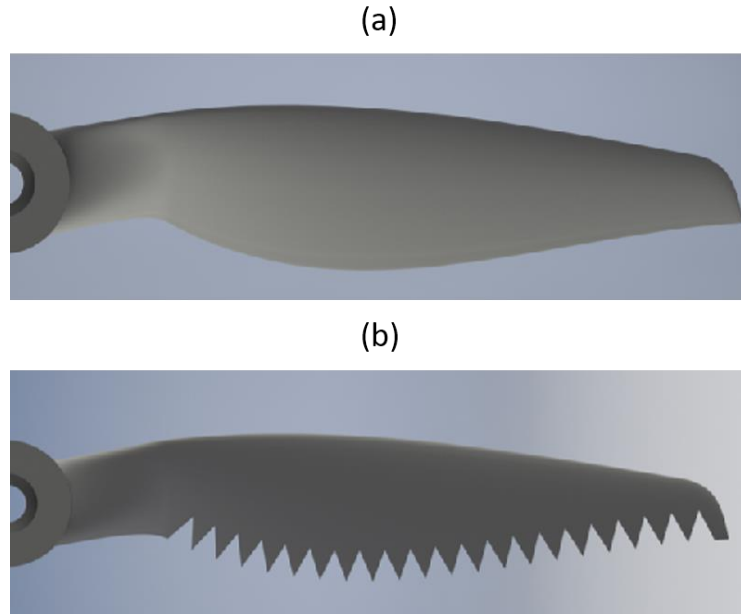


FIGURE 1: 3D RENDERING OF THE PROPELLER: (A) BASELINE, (B) STE PROPELLER.

All blades were manufactured by removing material from the trailing edge of the baseline as represented in Fig.2, where the main geometrical serration parameters are reported: tooth height (h), width (b) and characteristic serration angle (α).

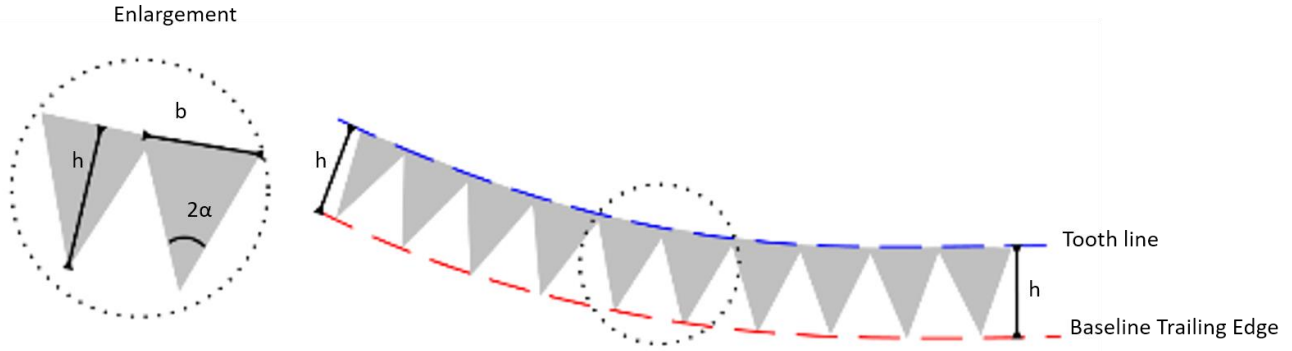


FIGURE 2: SKETCH OF THE PROPELLER GEOMETRY.

Ning et al. (Ning & Hu, 2016) stated that to ensure the mitigation of propeller noise serration must obey three specific geometrical constraints:

- I. $h^* > 0.25$: where $h^* = \frac{h}{2}\delta$ is the dimensionless tooth height, defined as the ratio between the tooth half-height h and the boundary layer thickness δ , otherwise the serration height is too small to have an interaction with the larger eddies convected into the boundary layer;
- II. $\alpha < 45^\circ$: the serratation angle α (defined in Fig.2), must be smaller than 45° , to obtain noise mitigation (Chong & Vathylakis, 2015; Howe, 1991). For the sake of clarity, latter condition is equivalent to $AR_t = 2\frac{b}{h} < 4$;
- III. $St_\delta = \frac{f\delta}{U} > 1$ for significant noise reduction, where St_δ is boundary layer thickness based Strouhal number, as stated by Howe's theory (Howe, 1991).

The effect of tooth height on the aeroacoustics and aerodynamics of propeller, with particular attention to the influence on noise is a central topic for scientific community.

Recently, Intravartolo et al. (Intravartolo, Sorrells, Ashkharian, & Kim, 2017) carried out an experimental analysis on serrated TE showing that an increase in serration height produces a reduction in the intensity of the trailing edge wake. Nevertheless, benefits from the height of the serrations diminished with respect to the overall noise signature of the propeller. When serration height reaches a value comparable to half of the Mean Aerodynamic Chord (MAC), no further gain in aeroacoustic effect can be observed. On the contrary, an increase in the overall noise may occur due mainly to aerodynamic effects.

Serratation height effect was also analysed by Pagliaroli et al. (Tiziano Pagliaroli, Camussi, et al., 2018a) observing a significant noise reduction in the low frequency region of the pressure spectra followed by a loss in propeller aerodynamic efficiency as a main drawback. Furthermore, an analysis of the noise directivity shows that the saw-tooth pattern effect is more important in the propeller wake region.

2.3 Wavelet Transform

Wavelets are a relatively recent mathematical instruments (Farge, 1992) that are becoming a common tool for time series analysis. Wavelet transform (WT) allows decomposing a space/time signal by expanding the choice for a suitable basis from a wide variety of appropriate functions, allowing to adapt the selected wavelet to each specific problem (Ashmead, 2012).

WT may represent the natural development of Fourier transform. Fourier transform decompose a wave function into its components planes wave; in the other hand, wavelet transform decompose a wave function into its wavelet components. Importantly, for non-sinusoidal periodic waveforms, Fourier transform spreads the energy across several sub-harmonics. By contrast, wavelets select only few components with a significant energy content.

One of the main advantages of using wavelet is due to their location in both time and frequency domain resulting in a better fit and a faster convergence for the waves forms usually found in nature than the corresponding Fourier series. Furthermore, there are many different wavelet to choose from giving the possibility to adapt the basis function to our problem. These features have led to use wavelet in several application fields: capturing sea surface thermodynamic variable oscillations in ocean science (C & G, 1998), studying intermittent phenomena in aeroacoustics and solid rocket motors (T. Pagliaroli, Camussi, Giacomazzi, & Giulietti, 2015; Tiziano Pagliaroli, Mancinelli, Troiani, Iemma, & Camussi, 2018) and investigating the acoustic behaviour of meta-surfaces for boundary layer transition control (Tiziano Pagliaroli, Pagliaro, Patanè, Tatí, & Peng, 2020).

The first step for a continuous wavelet analysis (CWT) consists in choosing a proper wavelet function $\psi(t)$, called the *mother wavelet*, in the present manuscript a complex mother wavelet named Morlet has been selected.

$$\psi(t) = \pi^{-1/4} e^{i\omega_0 t} e^{-t^2/2} \quad 5$$

where t and ω_0 are the dimensionless time and wavelet center frequency, respectively (C & G, 1998; Farge, 1992).

Once the $\psi(t)$ has been chosen, a family of continuously and dilated wavelets can be generated and normalized in energy norm:

$$\psi_{s,\tau}(t) = s^n \psi\left(\frac{t-\tau}{s}\right) \quad \text{with } s, \tau \in \mathbb{R}^+ \quad 6$$

where s is the scaling parameter, τ the time shifting and n the normalization exponent $n = -\frac{1}{2} \int_{-\infty}^{\infty} |\psi_{s,\tau}| dt = 1$ having applied a L^2 -normalization.

Finally, the CWT is defined as:

$$w(s, \tau) = s^{-\frac{1}{2}} \int_{-\infty}^{\infty} x(t) \psi^*\left(\frac{t-\tau}{s}\right) dt \quad 7$$

where $w(s, \tau)$ are the wavelet coefficients (T. Pagliaroli et al., 2015; Tiziano Pagliaroli, Mancinelli, et al., 2018) and ψ^* is the complex conjugate of the dilated and translated mother wavelet.

3. Experimental Setup

The propeller baseline, type *APC 9x4e*, selected for the experimental campaign was machining to realize the different test cases: totally 23 propellers with different serration strategy obtained by varying the teeth height h the teeth basis b and the number of teeth n along the blade in spanwise direction. For the present study, the number of teeth was fixed at 10, since measurements have not shown a great influence of the noise generated from this parameter (Candeloro et al., 2020).

For the experimental campaign, performed in anechoic chamber $3 \times 3 \times 1.6 \text{ m}$ in size, a custom-made test bench for measuring both the aerodynamic and aeroacoustic behaviour of small-scale propeller was implemented. Thrust time series was acquired by National Instrument ACQ board type USB-6002 from a load cell, whereas pressure fluctuations were sampled by using Microphone Gefell M360 and National Instrument ACQ board type NI cDAQ-9174.

All signals are acquired for 10 s at sampling frequency $f_s = 51200 \text{ Hz}$.

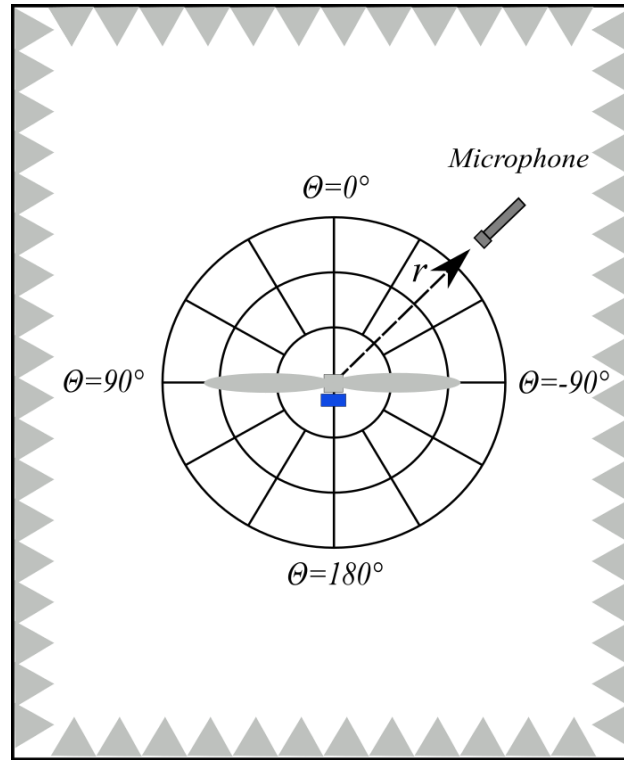


FIGURE 3: SKETCH OF THE EXPERIMENTAL SETUP AND OF THE ANECHOIC CHAMBER USED FOR THE MEASUREMENTS CAMPAIGN.

The microphone was installed on an rotating support which allow us to vary the polar angle θ in a range $[0^\circ - 150^\circ]$, the distance between the microphone and the propeller is: $r = 0.46 \text{ m}$. A sketch of the setup and the polar angle θ are displayed in Fig.3.

In the Tab.1 are reported the test cases for the present manuscript. The idea was to vary the teeth geometry respecting the constraints defined in Sec.2, especially the AR_t is always lower than 4. For each test case, are also reported the markers used in Fig.4-6-7.













<i>Test case</i>	<i>Marker</i>	<i>b</i> [mm]	<i>h</i> [mm]	<i>AR_t</i>
1		$b_1 = 4$	$h_1 = 4$	2.00
2		$b_1 = 4$	$h_2 = 3$	2.66
3		$b_1 = 4$	$h_3 = 6$	1.33
4		$b_1 = 4$	$h_4 = 8$	1.00
5		$b_2 = 5$	$h_2 = 3$	3.33
6		$b_2 = 5$	$h_3 = 6$	1.66
7		$b_3 = 6$	$h_1 = 4$	3.00
8		$b_3 = 6$	$h_3 = 6$	2.00
9		$b_3 = 6$	$h_4 = 8$	1.50
10		$b_4 = 3$	$h_2 = 3$	2.00
11		$b_4 = 3$	$h_3 = 6$	1.00
12		$b_4 = 3$	$h_4 = 8$	0.75

TABLE 1: VALUES ASSUMED BY WIDTH b AND HEIGHT h FOR EACH TEETH AND THE ASSOCIATED MARKER.

4. Results

In this section, the obtained results and some conclusions that can be drawn are reported. Fig.4 reports the OASPL for each blade and for each polar angle considered. The OASPL is defined as:

$$OASPL = 10 \log_{10} \left(\frac{\sigma_p}{p_{ref}} \right)^2 \quad 8$$

where σ_p is the standard deviation of the pressure time series and p_{ref} is the reference pressure equal to $2 \mu Pa$, corresponding to the minimum audible pressure for the human ear. In order to make a comparison a red dotted line has been added which is representative of the baseline propeller. This figure shows a strong directivity of the noise source, it is also interesting to underline that the serration, if are not designed correctly, can produce a stronger noise impact than the baseline.

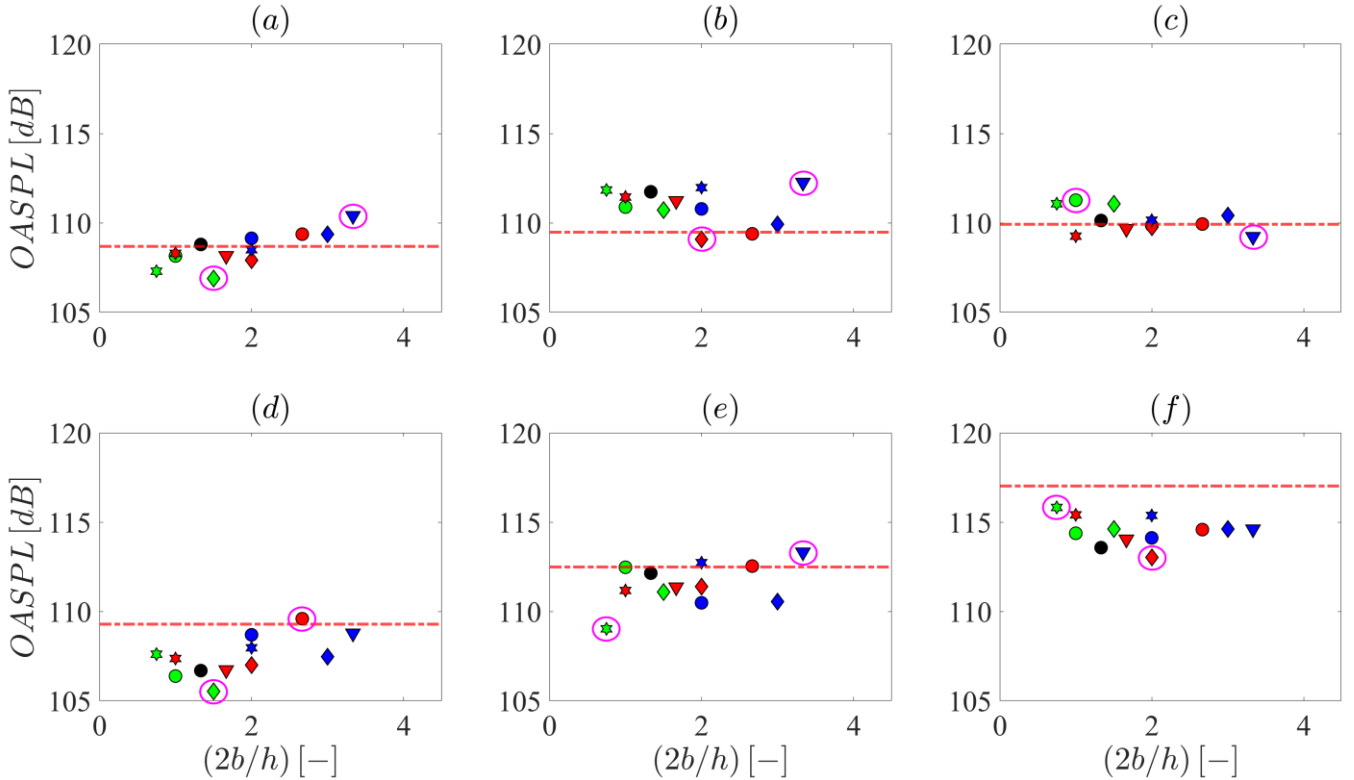


FIGURE 4: OASPL FOR EACH BLADE BY VARYING THE AR_t . THE RED DOTTED LINE IS REPRESENTATIVE OF THE BASELINE PROPELLER. THE POLAR ANGLE UNDER ANALYSIS ARE: $\theta = 0^\circ$ (a); $\theta = 30^\circ$ (b); $\theta = 60^\circ$ (c); $\theta = 90^\circ$ (d); $\theta = 120^\circ$ (e); $\theta = 150^\circ$ (f).

Furthermore, the serration effect seems to be confined in a characteristic polar angle range $\theta > 90^\circ$, see Fig.4 (d)-(e)-(f), this region can be referred as the most interesting for a typical civilian use.

In Fig.4 the best and the worst propeller for each test case are identified (with a circle), from these test cases 2 propeller (b_4h_4 and b_2h_2) has been selected to carry out further analysis in order to investigate the STE propeller aeroacoustic behaviour and to understand the nature of the occurring phenomena.

The following step of the study has been a spectral analysis of the pressure time series for the interest test cases. Results were presented in Fig.5. The spectra are reported in terms of the Sound Pressure Spectrum Level (*SPSL*) defined as:

$$SPSL = 10 \log_{10} \left(\frac{PSD \Delta f}{p_{ref}} \right) \quad 9$$

where *PSD* is the power spectral density of the pressure fluctuations and Δf is the frequency resolution equal to 1 Hz.

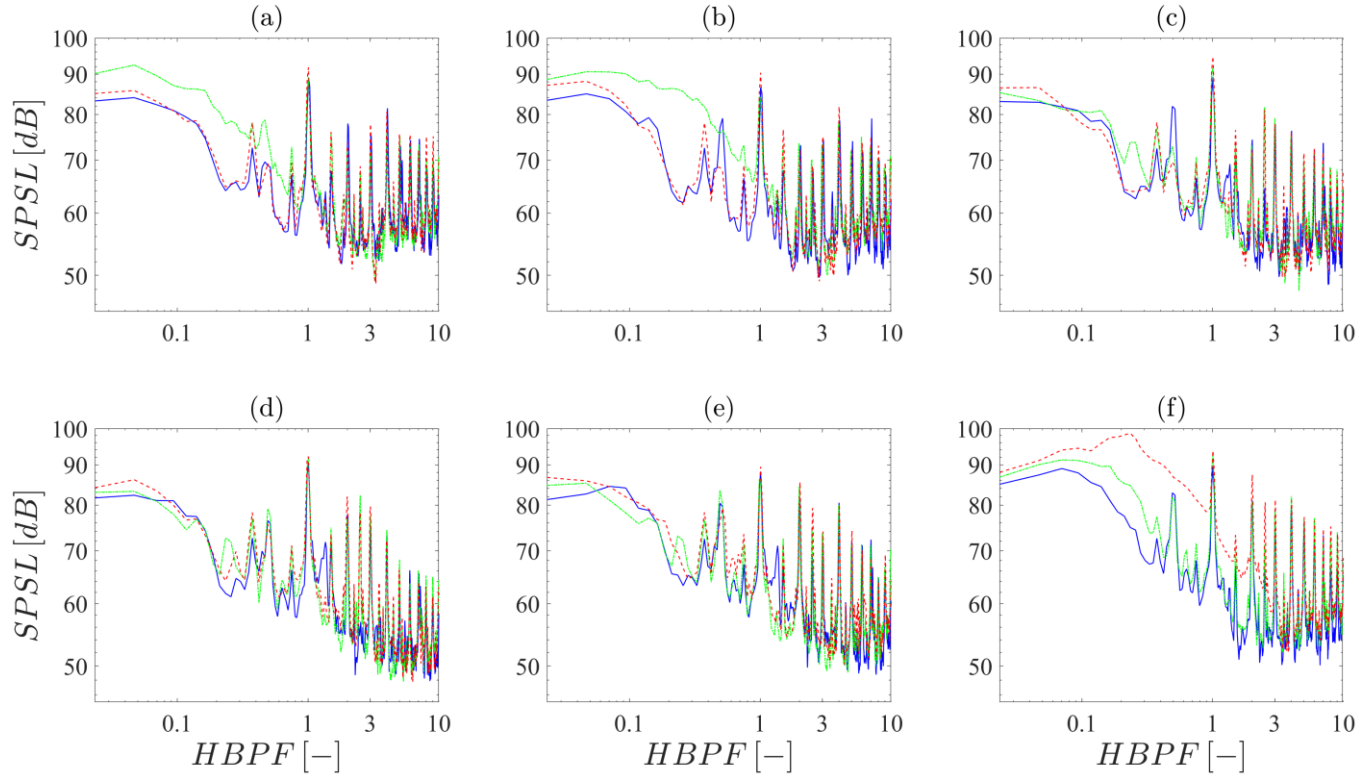


FIGURE 5: SPECTRAL ANALYSIS AT DIFFERENT POLAR ANGLE FOR THE BEST (BLUE LINE), THE WORST (GREEN LINE) AND THE BASELINE PROPELLER (RED DOTTED LINE). THE POLAR ANGLE UNDER ANALYSIS ARE: $\theta = 0^\circ$ (a); $\theta = 30^\circ$ (b); $\theta = 60^\circ$ (c); $\theta = 90^\circ$ (d); $\theta = 120^\circ$ (e); $\theta = 150^\circ$ (f).

Furthermore, the frequency has been normalized with the rotational regime of the propeller as shows in the Eq.10:

$$HBPF = \frac{2 \pi f}{\omega B} \quad 10$$

by having divided for the rotational velocity and the number of blade the first harmonic peak is now associated with the passage of the blade that correspond to $HBPF = 1$ as it is possible to see in Fig.5.

The Fourier analysis seems to confirm what found in the Fig.4. In fact, STE seems to act when the polar angle reach a value of 90° . It is known that the STE modify the broad-band component of the pressure field (Candeloro et al., 2020; Tiziano Pagliaroli, Camussi, et al., 2018a) but, in this figure, even a reduction in the tonal counterpart can be observed for each polar angles (Candeloro et al., 2020). A reduction in the narrow band noise component may be ascribed to a reduction in the aerodynamic loading over the blade surface (see Sec.2). Fig.5 shows that a strong broadband noise reduction in the low frequency region has been achieved in the case of $\theta = 150^\circ$ (Fig.6 (f)), namely in the wake region.

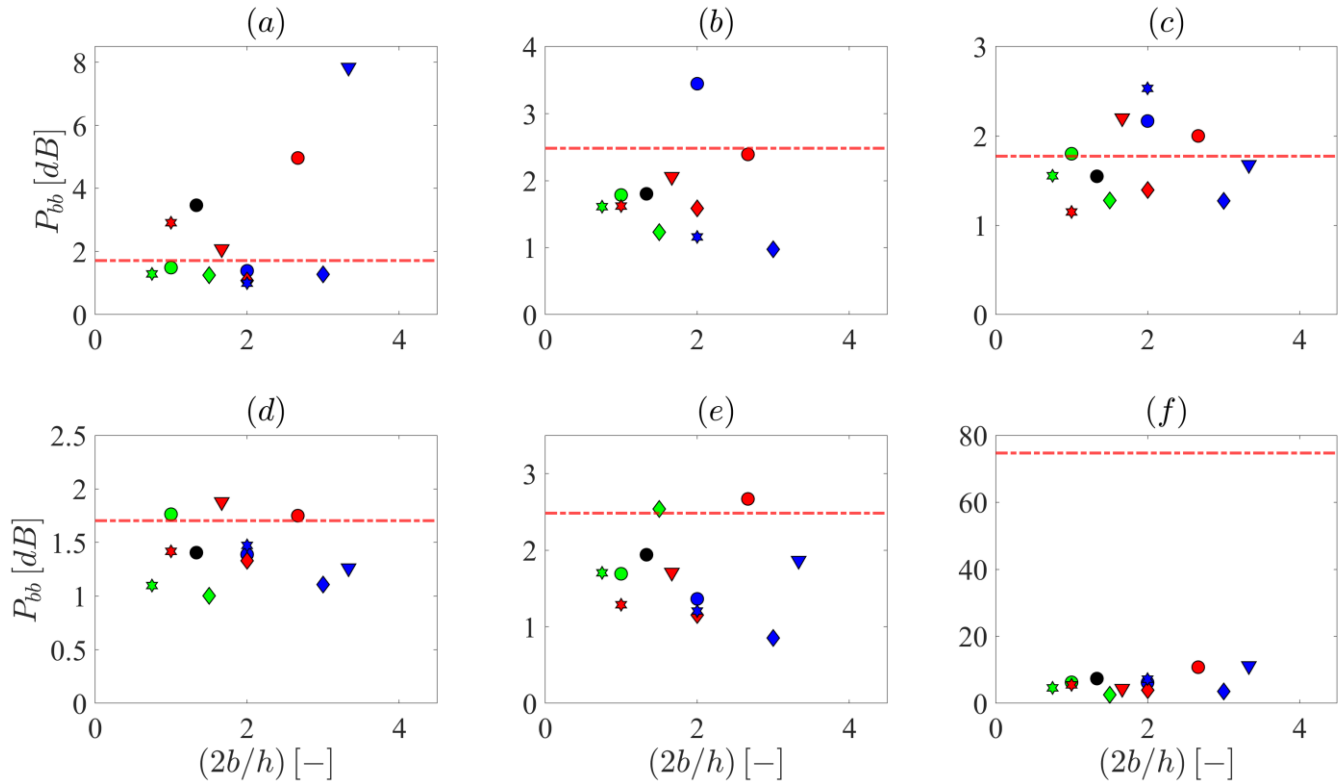


FIGURE 6: BAND INTEGRAL FOR THE BROADBAND COMPONENT IN THE FREQUENCY REGION $\Delta f = [0 - 118]Hz$ AT DIFFERENT POLAR ANGLE. THE RED DOTTED LINE IS REPRESENTATIVE OF THE BASELINE PROPELLER. THE POLAR ANGLE UNDER ANALYSIS ARE: $\theta = 0^\circ(a)$; $\theta = 30^\circ(b)$; $\theta = 60^\circ(c)$; $\theta = 90^\circ(d)$; $\theta = 120^\circ(e)$; $\theta = 150^\circ(f)$.

Having observed a reduction in both the broad-band and narrow band noise components the study continuation has been devoted to a quantification of these effects. For this purpose the Band Integral $P_{\Delta f}$ has been calculated in the frequency range:

- low frequency broad band: $\Delta f_{bb} = 0 - 118 Hz$
- first harmonic of rotor noise $\Delta f_{nb} = 118 - 148 Hz$

The Band Integral is defined as:

$$P_{\Delta f} = \int_{f_1}^{f_2} PSD df \quad 11$$

$P_{\Delta f}$ is representative of the energy content within a specific frequency range, in this sense can give a clear idea of the STE effect, much more than the OASPL.

Fig.6 and 7 report the results for the two band analysed. The results about the broadband component are in perfect agreement to what found before, the STE work in a cone located behind the propeller. By making a comparison with the baseline propeller (represented by the red dotted line in Fig.6), a sensible reduction in the noise generated by the blade has been achieved. On the other hand, despite a tonal noise reduction in not expected by using a control strategy focused on the broad-band, experimental results, see Fig.7, clearly point out that a strong reduction of the fundamental harmonic for each polar angle.

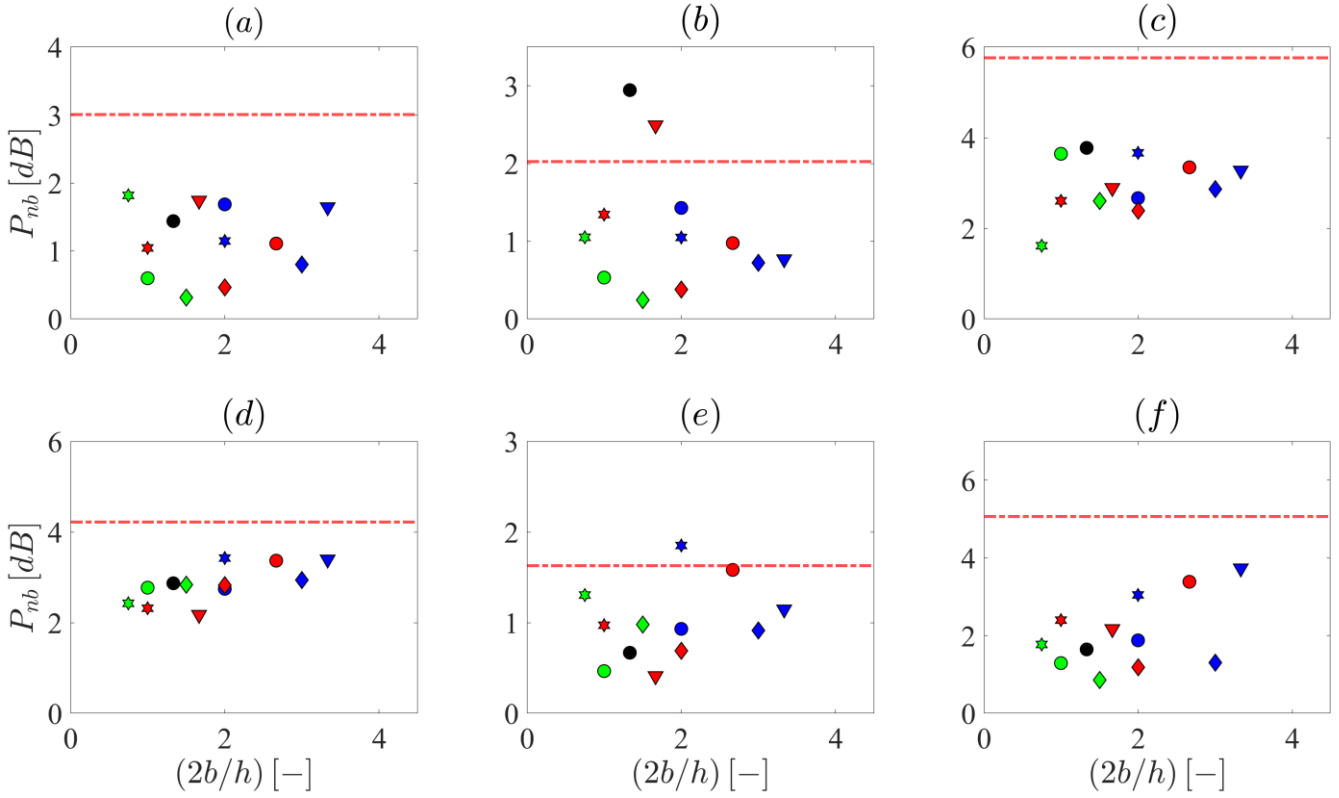


FIGURE 7: BAND INTEGRAL FOR THE NARROW BAND COMPONENT IN THE FREQUENCY REGION $\Delta f = [118 - 148]Hz$ AT DIFFERENT POLAR ANGLE. THE RED DOTTED LINE IS REPRESENTATIVE OF THE BASELINE PROPELLER. THE POLAR ANGLE UNDER ANALYSIS ARE: $\theta = 0^\circ(a)$; $\theta = 30^\circ(b)$; $\theta = 60^\circ(c)$; $\theta = 90^\circ(d)$; $\theta = 120^\circ(e)$; $\theta = 150^\circ(f)$.

Finally, the last analysis performed is a wavelet-based analysis which gives us information in both the frequency and time domain and it is very useful for non-sinusoidal signal as in the case of the present paper. Fig.8-9-10 reports the obtained results for each blade at 3 different polar angle: $\theta = 30^\circ$ (Fig.8), $\theta = 120^\circ$ (Fig.9) and $\theta = 150^\circ$ (Fig.10). The wavelet analysis shed light on the physical mechanism causing the noise reduction. The serration seems to mitigate the intermittency, in fact in Fig.8(c) can be observed a strong broadband component for the b_2h_2 propeller. Such effect can be ascribed to the presence of strong energetic event, which may have produced the uplift of the distribution tails, which is not present in the Fig.8(a) and (b). Thereby, the serration does not eliminate totally the intermittency but they can reduce its frequency.

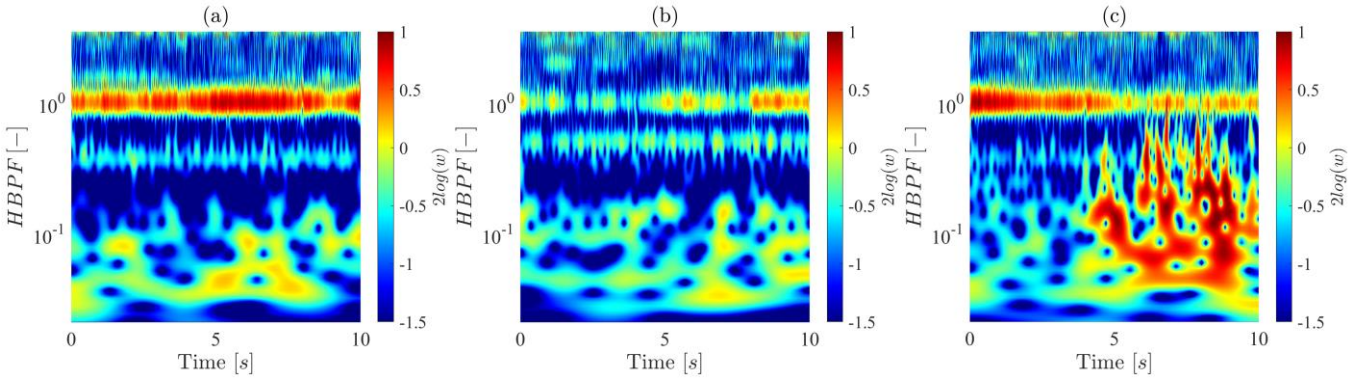


FIGURE 8: WAVELET SCALOGRAM OBTAINED FOR $\theta = 30^\circ$ FOR EACH BLADE: BASELINE PROPELLER (A), b_4h_4 (B), b_2h_2 (C).

Moreover, in Fig.8(b) can be identified a strong reduction of the first harmonic (corresponding to $HBPF = 1$) as seen in the spectral analysis (Fig.5(b)) for the b_4h_4 propeller.

Furthermore, Fig.9 shows another effect due to serration. A decrease in the second harmonics ($HBPF = 2$) can be observed (Fig.9 (b)) in particular for the b_4h_4 propeller. Such effect appear in addition to the well-observed reduction of the broadband component in the low frequency region and of the first harmonic. Therefore, serration may modify even the superior harmonics.

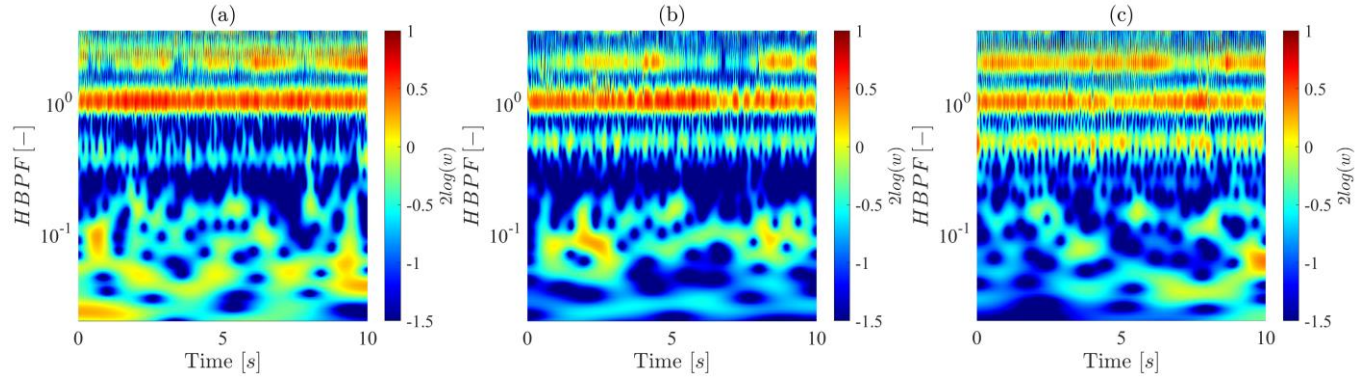


FIGURE 8: WAVELET SCALOGRAM OBTAINED FOR $\theta = 120^\circ$ FOR EACH BLADE: BASELINE PROPELLER (A), b_4h_4 (B), b_2h_2 (C).

However, the main effect can be seen in the wake region (Fig.10) where the difference between the baseline propeller (Fig.10 (a)) and the STE propeller appear clearly. In this figure it is possible to observe both the reduction in the broadband and in the narrow band (with regard to both the first and second harmonics) component with respect to the baseline propeller.

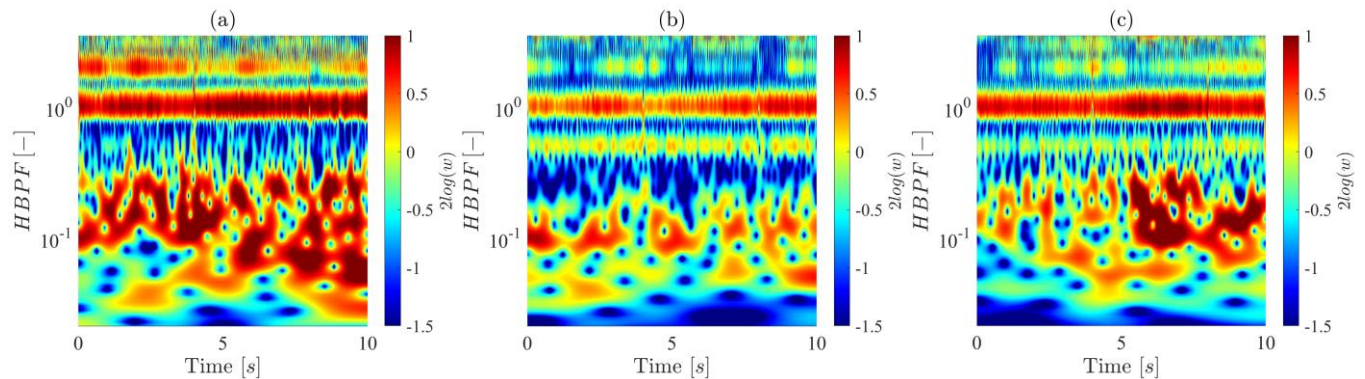


FIGURE 9: WAVELET SCALOGRAM OBTAINED FOR $\theta = 150^\circ$ FOR EACH BLADE: BASELINE PROPELLER (A), b_4h_4 (B), b_2h_2 (C).

Another effect can be seen for $HBPF = 0.5$, in both Fig.9 and 10, this harmonics can be ascribed to the engine noise. In all the three cases the band associated with the engine was different.

For the test case in the wake region one last analysis has been carried out and reported in Fig.11. In this figure can be observed the wavelet coefficient corresponding to $HBPF = 1$ which confirm what said about Fig.10. The wavelet coefficient gives us information of the energy content at a certain frequency of the pressure signal Fig.11 shows that the serration has reduced the energy associated with the first harmonics in particular for the b_4h_4 propeller.

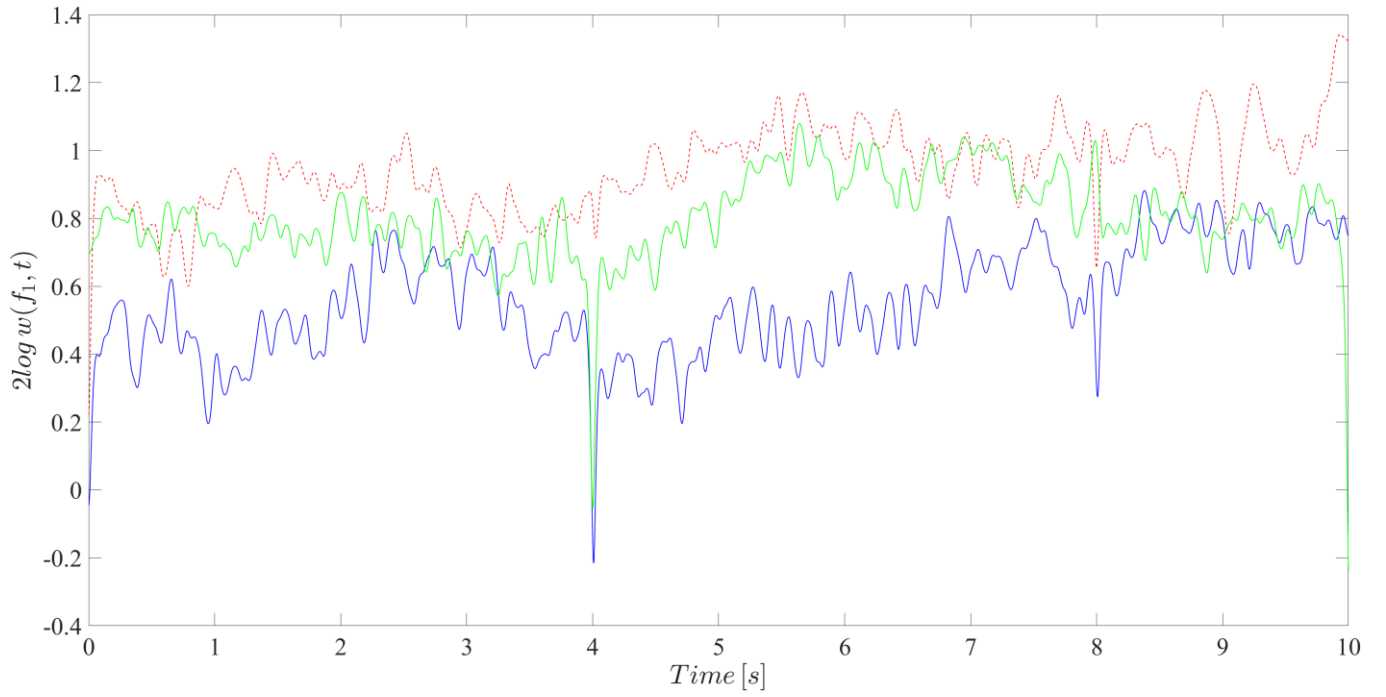


FIGURE 10: WAVELET COEFFICIENT FOR EACH BLADE AT $f = f_1$ (CORRESPONDING TO $HBPF = 1$). THE BLUE LINE IS REPRESENTATIVE OF THE b_4h_4 , THE GREEN LINE OF THE b_2h_2 PROPELLER AND THE RED-DOTTED LINE OF THE BASELINE PROPELLER.

5. Conclusions

An experimental campaign devoted to the aeroacoustic characterization of several propeller with serrated trailing edge has been carried out. The main focus was the effect of serration geometry on the noise generated by custom-made propellers. A specific test bench has been developed and 23 propeller has been designed and tested.

Results shows that, in order to achieve a noise reduction, a great attention has to be kept during the design process, since the noise control strategy proposed may cause an increase in noise generated. A strong directivity of the noise source can be observed suggesting the idea of a quiet cone where STE works located in the propeller wake region. Such effect seems very interesting because that region is the most important for an employee or a civilian.

Spectral analysis indicate that serration modify both the broadband, as expected, and the narrow band component of the pressure field. The effect on the tonal counterpart may be connected to a reduction in the aerodynamic loading over the blade surface that need further analysis. On the other hand, a strong decrease in the broad-band component in the low frequency region can be achieved by using STE, in particular in the wake region. The reduction of the two components has been quantified by calculating the band integrals in the low frequency broad-band region f_1 and the first harmonic of rotor noise, results confirm the spectral analysis outcome.

The wavelet analysis seems to clarify the physical mechanism behind the noise reduction, STE seems to mitigate the intermittency, in fact in the low frequency region results shows a clear reduction of the wavelet coefficient and also underline a mitigation of the first and second harmonics.

6. References

- Ashmead, J. (2012). Morlet wavelets in quantum mechanics. *Quanta*, 1(1), 58–70. <https://doi.org/10.12743/quanta.v1i1.5>
- C, Torrance., & G, Compo. (1998). Practical Guide Wavelet Analysis. *Bams*, 79(1), 1–18.
- Candeloro, P., Nargi, R. E., Patanè, F., & Pagliaroli, T. (2020). Experimental Analysis of Small-Scale Rotors with Serrated Trailing Edge for Quiet Drone Propulsion Experimental Analysis of Small-Scale Rotors with Serrated Trailing Edge for Quiet Drone Propulsion. *J. Phys.* <https://doi.org/10.1088/1742-6596/1589/1/012007>
- Chong, T. P., & Vathylakis, A. (2015). On the aeroacoustic and flow structures developed on a flat plate with a serrated sawtooth trailing edge. *Journal of Sound and Vibration*. <https://doi.org/10.1016/j.jsv.2015.05.019>
- Corcos, G. M. (1965). The structure of the turbulent pressure field in boundary-layer flows. *Deep Sea Research and Oceanographic Abstracts*, 12(6), 1037. [https://doi.org/10.1016/0011-7471\(65\)90880-6](https://doi.org/10.1016/0011-7471(65)90880-6)
- Farassat, F., & Succi, G. P. (1980). A review of propeller discrete frequency noise prediction technology with emphasis on two current methods for time domain calculations. *Topics in Catalysis*. [https://doi.org/10.1016/0022-460X\(80\)90422-8](https://doi.org/10.1016/0022-460X(80)90422-8)
- Farge, M. (1992). Farge1992. *Annual Review Fluid Mechanics*, 395–457.
- Floreano, D., & Wood, R. J. (2015). Science, technology and the future of small autonomous drones. *Nature*, 521(7553), 460–466. <https://doi.org/10.1038/nature14542>
- Gur, O., & Rosen, A. (2008). Optimization of Propeller Based Propulsion System, 46(1), 5–7. <https://doi.org/10.2514/1.36055>
- Gur, O., & Rosen, A. (2009a). Design of a Quiet Propeller for an Electric Mini. <https://doi.org/10.2514/1.38814>
- Gur, O., & Rosen, A. (2009b). Optimizing Electric Propulsion Systems for Unmanned Aerial Vehicles. *Journal of Aircraft*, 46(4), 1340–1353. <https://doi.org/10.2514/1.41027>
- Howe, M. S. (1991). Noise produced by a sawtooth trailing edge. *The Journal of the Acoustical Society of America*, 90(1), 482–487. <https://doi.org/10.1121/1.401273>
- Intravartolo, N., Sorrells, T., Ashkharian, N., & Kim, R. (2017). Attenuation of Vortex Noise Generated by UAV Propellers at Low Reynolds Numbers. In *55th AIAA Aerospace Sciences Meeting*. <https://doi.org/10.2514/6.2017-2019>
- Janakiram, D., & Scruggs, B. (1981). Investigation of performance, noise and detectability characteristics of small-scale remotely piloted vehicle /RPV/ propellers. *7th Aeroacoustics Conference*, 19(12), 1052–1060. <https://doi.org/doi:10.2514/6.1981-2005>
- Leslie, A., Wong, C., & Auld, D. (2010). *Experimental analysis of the radiated noise from a small propeller*.
- Leslie, A., Wong, K. C., & Auld, D. (2008). Broadband Noise Reduction on a mini-UAV Propeller. In *14th AIAA/CEAS Aeroacoustics Conference (29th AIAA Aeroacoustics Conference)*. <https://doi.org/10.2514/6.2008-3069>
- Nelson, P. A., & Morfey, C. L. (1981). Aerodynamic Sound Production. *Journal of Sound and Vibration*, 79(2), 263–289.
- Ning, Z., & Hu, H. (2016). An Experimental Study on the Aerodynamics and Aeroacoustic Characteristics of Small Propellers. In *54th AIAA Aerospace Sciences Meeting*. <https://doi.org/10.2514/6.2016-1785>

- Pagliaroli, T., Camussi, R., Giacomazzi, E., & Giulietti, E. (2015). Velocity measurement of particles ejected from a small-size solid rocket motor. *Journal of Propulsion and Power*, 31(6), 1777–1784. <https://doi.org/10.2514/1.B35490>
- Pagliaroli, Tiziano, Camussi, R., Candeloro, P., Giannini, O., Bella, G., & Panciroli, R. (2018a). Aeroacoustic Study of small scale Rotors for mini Drone Propulsion: Serrated Trailing Edge Effect. In *2018 AIAA/CEAS Aeroacoustics Conference*. <https://doi.org/10.2514/6.2018-3449>
- Pagliaroli, Tiziano, Mancinelli, M., Troiani, G., Iemma, U., & Camussi, R. (2018). Fourier and wavelet analyses of intermittent and resonant pressure components in a slot burner. *Journal of Sound and Vibration*, 413, 205–224. <https://doi.org/10.1016/j.jsv.2017.10.029>
- Pagliaroli, Tiziano, Moschetta, J., Benard, E., & Nana, C. (2014). 49 th International Symposium of Applied Aerodynamics Lille , 24-25-26 March 2014 Noise signature of a MAV rotor in hover, (March), 24–25.
- Pagliaroli, Tiziano, Pagliaro, A., Patanè, F., Tatí, A., & Peng, L. (2020). Wavelet analysis ultra-thin metasurface for hypersonic flow control. *Applied Acoustics*, 157, 107032. <https://doi.org/10.1016/j.apacoust.2019.107032>
- Rozenberg, Y., Roger, M., Moreau, S., Division, D., Cedex, C., Systems, V. T., ... Verri, L. (2008). Fan Blade Trailing-Edge Noise Prediction Using RANS Simulations, 5207–5212.
- Schlinker, R. H., & Amiet, R. K. (2001). Aeroacoustics Conference.
- Serré, R., Chapin, V., Moschetta, J. M., & Fournier, H. (2017). Reducing the noise of Micro–Air Vehicles in hover, 51–59. Retrieved from http://www.imavs.org/papers/2017/65_imav2017_proceedings.pdf
- Sinibaldi, G., & Marino, L. (2013). Experimental analysis on the noise of propellers for small UAV. *Applied Acoustics*. <https://doi.org/10.1016/j.apacoust.2012.06.011>



CidB

Centre d'information
sur le **Bruit**

QUIET DRONES
International e-Symposium
on
UAV/UAS Noise
Remote from Paris – 19th to 21st October 2020

Delivery Drones at La Poste

Philippe CASSAN Drone Programme Director La Poste/dpdgroup

philippe.cassan@dpdgroup.com

Summary

DPDgroup/La Poste is testing drone deliveries since 2014, with two test lines in operation in France.

The future development of these deliveries depends on the regulation and technology, but also on the public acceptance of drone flights, for which noise can be a major issue.

1. Introduction DPDgroup/La Poste

DPDgroup is the parcel delivery network of GeoPost, a holding company owned by Le Groupe La Poste (France).

DPDgroup is the second-largest operator in the CEP (courier express parcel) market in Europe.

Every day our 77,000 experts deliver more than 5.3 million parcels worldwide through our brands DPD, Chronopost, SEUR and BRT.

Our ambition is to be the best delivery partner to work with. We are continuously evolving our customer experience to deliver brilliantly simple solutions that make sending and receiving parcels easier and more flexible.

With our industry-leading Predict service, we are setting a new standard for convenience by keeping customers closely in touch with their delivery.

We believe in building closer connections with all our customers through a network of more than 47,000 Pickup points.

2. DPD group drone project

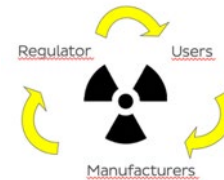
Launched in 2014, our project tests new delivery possibilities (in isolated places, hard-to-access locations, emergency deliveries...) while developing an ecological delivery solution combining security, efficiency & speed.

During this project, DPDgroup is:

- Project Manager (for business expertise),
- Implied in innovation -> we own the Intellectual Property,
- DGAC (French regulator) correspondent.

The objective is to end the “Market vicious circle” in which :

- The users are waiting for technology,
- The manufacturers are waiting for regulation,
- The regulator is waiting for the users.



We selected a French drone company, Atechsys to assist us during the complete value chain of the solution, from R&D to drone delivery service.

2.1 Components

We developed an adaptative platform in order to test our deliveries in real-life conditions: dpd drone G2, with a focus on safety:

- Redundancy Electronics
- Automatic parachute
- Delivery terminal
- Ground control station
- Long range video link
- GPS tracker...



To secure the operators during landing/take off and parcels loading/unloading, we designed a range of Delivery Terminal.

The range is composed of:

- Locker, with embedded parcels locker,
- Light, single-client but can recharge batteries,
- Drop, to receive parcels in isolated areas,
- Mobile, for Delivery Assistant van.





Mobile Terminal

2.2 Lines

Two delivery lines are operated in France, to deliver « real parcels » to « real clients ». The Goal is to demonstrate the reliability, repeatability of deliveries during several months.

First line is located in Saint Maximin (Var) :

- Open in December 2016.
- Deliveries to an isolated SMEs incubator.
- 14 km flight, 2 kg payload.
- Integrated process with Pickup, Chronopost & Colissimo Business Units.
- 260 flights, 6 000 km travelled, 90% success rate.

The second line is in Mont-Saint-Martin (Isère) :

- Open in September 2019.
- 80 inhabitants village, 20 km of dangerous dead-end road
- 8 mn drone flight instead of 40 mn travel by van (2-way).
- The driver uses a « delivery assistant » - equipped van.
- 2 kg payload, up to 10kg next year.
- Reduction of road accidents risks : no CO2 emission during mountain transport.
- 600 test flights, 5 000 km travelled, 37 full delivery flights completed

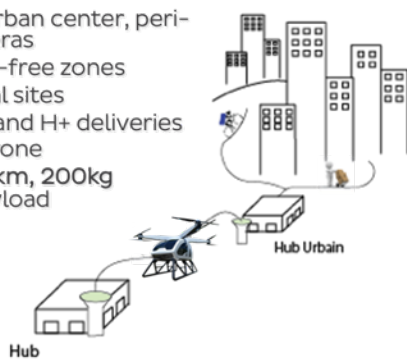
3. Strategy

Our strategy is threefold :

- Routing to unclog urban and peri-urban areas
- Transporting to open up isolated locations
- Transporting to link remote hubs (linehubs)

Routing to **unclog**

- ✓ Dense urban center, peri-urban areas
- ✓ Vehicles-free zones
- ✓ Industrial sites
- ✓ On demand H+ deliveries
- ✓ Cargo drone
 - ✓ 50km, 200kg payload



Transporting to **open up**

- ✓ Mountains
- ✓ Islands
- ✓ Natural disasters
- ✓ « Delivery Assistant »
 - ✓ 20km, 10kg



Transporting to **link**

- ✓ Automated inter-hub links
- ✓ Cut-off avoidance
- ✓ « Secondary cities » service.
- ✓ Long distances / high payloads
- ✓ Drone linehaul
 - ✓ x00km, x00kg CU



The solutions will be adapted to each of the use cases.

3.1 Ecological interest of dpd drone project

Actions we are conducting in this domain:

- Comparative Study in real condition of CO2 emissions (dpd France van vs dpd G2 drone) :
 - ADEME co-financed project in Grenoble : 85% reduction during our mountain trip
 - Country level impact study in 2021
- Research studies on LiPo & LiOn batteries recycling :
 - CIFRE Thesis leaded by LEPMI laboratory & Atechsys
 - Research on second-life, ore recycling and battery usage optimisation
- Our Dpd drone G2 is 100% electric, the Delivery Terminals are self-sufficient, with solar panel alimentation.
- The long-distance drone-planes (linehaul) will be hybrid then electric.
- For the future urban deliveries, the drones will be hybrid (with electric mode for take-off and landing), or 100% electric.
- We are currently integrating air quality sensors (Pollutrack) on our drones to provide altitude pollution report during our deliveries.

3.2 Regulation

DPDgroup is member of « Conseil Français pour le Drone Civil », French Civil Drone Council.

In this Council, we decided the creation of the « Urban Mobility & Logistic » Working Group, co-animated by DPDgroup / Airbus / Thalès / Safran.

Its goals are to study the conditions allowing the execution of routine operations involving air logistics transport drones in an urban environment, under technical and economic conditions that promote the development of the civil drones sector, namely :

- frame the use cases and then define one or more operational concepts (CONOPS),
- define the security policy to be applied, including cyber security aspects,
- study the acceptability of this type of operation, in particular noise pollution.

To address those topics, the Working Group launched sub-working Groups (Mosquito project) in the following domains:

Safety / Acoustics / Electromagnetic environment / Cybersecurity / Infrastructure / Operations / Airspace management.

4. Conclusions

The urban market asks for more frequent, fast deliveries.

Drones can be an useful answer for specific use cases, but people will be challenging on :

- Safety
 - No trade-off on people's security
 - Transported goods safety
 - Cyber-attack protection (diversion)
- Acceptability
 - Privacy : the drones must not be seen as « airborne spies »
 - Drone noise, during take-off and landing phases.

We have several challenges ahead, but we must keep in mind that all this has to be compared with current nuisances: traffic congestion, air pollution, ... and noise !

References

<https://www.dpd.com/group/en/2019/11/07/2nd-line-for-parcel-delivery-by-drone-in-france/>

<https://www.youtube.com/watch?v=t7FxJxe2bxs>



CidB

Centre d'information
sur le Bruit

QUIET DRONES
International e-Symposium
on
UAV/UAS Noise
Remote from Paris – 19th to 21st October 2020

A whole-systems approach to building knowledge about human reaction to UAV/UAS

Charlotte Clark, Acoustics, Ove Arup and Partners, London, UK:

Charlotte.Clark@arup.com

Ryan Biziorek, Acoustics, Ove Arup and Partners, Chicago, IL, USA:

Summary

The aviation revolution to develop low cost, on-demand, point to point aerial transportation of goods and people, and support a range of services (e.g. aerial surveillance and geographic surveys) is developing a pace in many countries. While these new aerial services can ultimately offer many benefits, there is very little known about human and community response to these modes of transport. Undoubtedly these different types of vehicles will lead to noise exposure from new and unfamiliar aerial vehicles in communities that have not experienced aviation or similar transport noise.

We know from working with communities exposed to general and commercial aviation that noise has the potential to become a significant public health issue. A knowledge building process for electric and autonomous flying technology will be required to overcome several challenges related to human response to noise and visual pollution. This evidence is also needed to inform regulation, planning and airspace design policies that will be needed to build social value and acceptance of new systems and infrastructure.

This paper describes lessons that can be learnt from general and commercial aviation for the UAV/UAS industry. A methodological framework is proposed for building knowledge to inform systems and operations development within the short-time frame sought by this emerging market. Arup's ongoing work addressing these challenges through developing immersive auralisations (aural simulations) and visualisations of these vehicles is also summarized. This simulation approach enables a listener to experience simulated acoustic phenomena in different virtual contexts to help with human factors research, policy planning, and stakeholder

engagement to enhance outcomes. We will also report on planned research studies in our immersive aural and visual simulation facilities – SoundLab and iLab – to build knowledge about human response to this mode of transport. Use of these methodologies can inform the development of public acceptability, provides a collaborative tool to engage with OEMs vehicle designers to improve human response and public acceptance, and will aid in identifying appropriate acoustic metrics to describe the exposure and inform certification standards, assessment methods and policy.

1. Introduction

An aviation revolution is underway. New modes of air travel and capability are being developed, and many countries are currently engaged in the development of low cost, on-demand, point to point aerial transportation of goods and people and providing services. In this article vehicles under consideration in relation to electric and autonomous flying technology vary from drones to hybrid electric aircraft that cover short distances (e.g. a few hundred miles). Key vehicle categories being considered include:

- **UAM** (Urban Air Mobility) which are manned vehicles designed to transport people within cities, usually using eVTOL (electric Vertical Take Off & Landing);
- **Drones** which are unmanned aerial vehicles (UAV) that can be small or large and used for pleasure, surveys, emergencies or deliveries. In relation to drones, the term UAS (Unmanned Aerial System) can also be used, to describe a UAV plus all the elements to control it (e.g. remote control, communication system etc);
- **Longer-range electric/hybrid aircraft** for use on regional/short-haul aircraft routes can also be considered as part of the future of aviation.

This paper is focused on UAV/UAS but the content is applicable to all the key vehicle categories.

If implemented correctly, these methods of transport are promoted as having the potential to offer a sustainable alternative to many existing methods of transportation, as they increase mobility, save time, and could reduce the use of other transportation sources (e.g. cars, haulage, commercial aviation).

The introduction of UAV/UAS involves building knowledge and overcoming a number of key challenges related, but not limited to:

- Regulation;
- Vehicle testing and certification;
- Operational Safety;
- Vehicle to vehicle communication;
- Cybersecurity;
- Energy sources;
- Airspace management;
- New infrastructure;
- Developing new business markets;
- Standardisation of noise assessment;
- Human response to noise and visual pollution; and
- Public readiness.

These challenges become more numerous when one considers the different altitudes that these new technologies operate at and the need to integrate them into the existing aviation

airspace, infrastructure and aviation systems and technology. This paper focuses on two specific challenges: human response to noise pollution and public acceptance, highlighting the need to engage with social scientists to build knowledge.

2. What can we learn from General and Commercial Aviation about human response to aircraft noise?

2.1 Overview

At present, very little is known about how people and communities may respond to the introduction of these methods of transport. The acoustic properties of the myriad types of vehicles under development (e.g. drones, EVTOL etc) remain unknown or undocumented at this point in time and have yet to be assessed in terms of human and community response. However, the introduction of these different types of vehicles will lead to communities becoming newly exposed to aviation noise and also exposed to a new unfamiliar noise signature from vehicles, leading to the question of what can we learn from general and commercial aviation about human response to aircraft noise, to inform the knowledge we need to build for these new technologies?

2.2 Community noise annoyance

Annoyance is the most prevalent community response in a population exposed to aircraft noise. The term annoyance is used to describe negative reactions to noise such as disturbance, irritation, dissatisfaction and nuisance (Guski, 1999), as well as an emotional / attitudinal response (Guski, Schreckenberg, & Schuemer, 2017). Annoyance is commonly used to measure the quality of life impact of environmental noise exposure on communities around airports and to derive exposure-response relationships, often referred to as exposure-response functions (ERFs), indicating the percentage of the population highly annoyed (%HA) by the noise source in the community of interest (ISO/TS15666, 2003).

Annoyance is probably one of the key outcomes to assess in relation to new aviation technologies: it is an established measure of community response and standardised questions for its measurement are available (ISO/TS15666, 2003). There is a need to build knowledge about ERFs for different vehicle types, as well as for different operational contexts. This information will need to be built in the laboratory to inform certification, airspace management, infrastructure design and planning, policy, and later verified in the field in communities exposed to these new technologies. The need for establishing ERFs will also be influenced by the development of knowledge about relevant metrics. Where metrics match those typically used for other environmental noise sources, e.g. energy average metrics such as $L_{Aeq, 16h}$, L_{night} , L_{den} , it will be possible to compare annoyance responses for new technologies to annoyance for other sources such as aircraft noise from commercial aviation. This will be important knowledge to build, whilst appreciating that it is likely that other ERFs for new metrics may also need to be established for these new technologies.

In recent years, several studies have suggested that aircraft noise annoyance around major airports in Europe has increased (Babisch, et al., 2009; Janssen, Vos, van Kempen, Breugelmans, & Miedema, 2011; Schreckenberg, Meis, Kahl, Peschel, & Eikmann, 2010). Communities report greater levels of % highly annoyed at the same dB level than in previous decades. There are several reasons that may explain this. Communities have become more organised in their response to aircraft noise, given the greater knowledge about the health

effects of noise and the increased use of social media to organise responses. It is also likely to be linked to an increase in the number of events rather than the noise level per se, as many airports have seen a slight reduction in exposure as assessed by energy averaged metrics but a considerable increase in the number of events. Communities should be considered more organised to oppose increases in aircraft noise exposure or becoming newly overflow than perhaps they were in the past.

Studies of change in aircraft noise exposure, including studies of newly overflowed communities, have found that there is an excess-response in relation to the change in noise exposure, both for decreased and for increased aircraft noise exposures (Breugelmans, et al., 2007; Brown & van Kamp, 2017; Fidell, Silvati, & Haboly, 2002; Nguyen, et al., 2018; Quehl, Muller, & Mendolia, 2017). When noise exposure is changed, subjective reaction may not change in the way that would be predicted by steady-state ERFs (Brown & van Kamp, 2017), i.e., the annoyance response is likely to be slightly higher than that predicted by the noise exposure. This knowledge is likely to be relevant for the introduction of new technologies, where communities will be newly overflowed.

Non-acoustic factors in annoyance responses to environmental noise will also need to be considered (Guski, 1999). There are a variety of individual, social, environmental and situational factors which moderate the relationship between acoustic variables and annoyance or disturbance responses. For example:

- Individual factors, such as noise sensitivity, coping capacity, attitude to the source, such as fear or acceptance, age, gender and socioeconomic status influence annoyance responses (and also vary considerably between people);
- Social factors, for example, the social value placed on the noise source by a community or society;
- Situational factors, related to the immediate context, such as night-noise causing an awakening or an increase in flights over the years; and
- Environmental factors, such as access to quiet or recreational areas or the presence of a quiet side of the home.

Knowledge about these factors will need to be built in relation to new technologies.

2.3 Managing noise

Noise from aircraft is the most significant cause of community reaction around airports. The ICAO Balanced Approach is a useful framework for considering how noise can be managed that will also have applicability for these new technologies. The Balanced Approach puts forward four principles, with the aim of limiting the number of people exposed to noise. The principles are:

- Reduction of noise at source;
- Land-use planning and management;
- Noise abatement operational procedures; and
- Operating restrictions.

It will be important to consider each of these principles through the development and deployment of these new technologies. For example, there exist opportunities to reduce the noise at source through influencing the sound signatures of vehicles; as well as through consideration of infrastructure and operational procedures. Operating restrictions are seen as the last principle to be deployed in most situations - only to be used if the first three principles have been exhausted. Therefore, opportunities to consider and influence the first three

principles need to be constantly reviewed and implemented. As an emerging technology, there is a unique opportunity to influence the Balanced Approach through incorporating knowledge about human response in the design stage.

3. Methodologies to build knowledge about human response to UAV/UAS

There is an urgent need to begin to build knowledge about the human response to UAV/UAS to address these key challenges. Many disciplines will need to work together with OEM (Original Equipment Manufacturers) to develop auralisations (immersive sound recordings) and visualisations of their vehicles to evaluate human response. It is important to highlight the need to engage with social scientists and those with a background in aviation noise effects on health and quality of life, to ensure that the evaluations of human response are being undertaken using methodologically robust approaches.

Using Arup's SoundLabs/iLabs globally, we are developing research studies to build knowledge about human response to auralisations and visualisations of these new vehicles. SoundLab and iLabs have the advantage of offering a well-controlled fully calibrated immersive listening environment for laboratory studies of this nature. In addition, our network of 14 SoundLab/iLab facilities can help bring a diverse and statistically significant number of participants. Arup can apply this simulation approach to address the following challenges in relation to human response and public readiness:

- Develop knowledge about human response to the sound of new vehicles, alongside the development of the vehicles – offering a chance to alter design to improve human response and public acceptance.
- To evaluate the sound emissions of vehicles to identify the appropriate metrics to describe the exposure. This information could also inform certification standards, assessment methods and policy. The development of metrics will need to be informed by human response to noise, as well as ability of individuals to understand what the metric represents for communicating environmental impacts with communities.
- To create virtual reality sound demonstrations to demonstrate new technologies in their context to communities.

Both qualitative and quantitative research methodologies will be needed to develop this knowledge and there would be an advantage from developing standardised methodologies for use in studies that can be used and adapted globally by different teams. This would also enable 'pooling' of data which would speed up knowledge building and add statistical power.

As with any research, all research methodologies have strengths and limitations. It will be important to develop a plan of knowledge development; to conduct studies in an ordered fashion, to enable knowledge to be built; to not overstate the findings of studies; and to acknowledge uncertainties. It will be important to take time to build the knowledge and to resist the temptation to manipulate too many variables at once in a laboratory setting. Initially, more will be learnt from keeping most of the factors of interest stable and manipulating one factor at a time. This will enable further development of studies that manipulate the other factors in turn or in controlled conditions. Knowledge building will be needed to inform holistic knowledge and is tied to developing clear research questions.

A range of metrics will need to be explored in these types of studies including traditional metrics, such as sound quality metrics - loudness, sharpness, tonality, roughness, fluctuation strength, impulsiveness, as well as average metrics and psychoacoustic and soundscape descriptors. A further challenge will be the issue of moving from single sound events in laboratory studies and the need to later build knowledge about human response to operational

metrics that describe typical community exposure. There are also likely to be complex interactions between the sound and visual impacts of these new technologies. Careful definition and manipulation of key factors will be crucial to building knowledge in a timely fashion.

4. Conclusions

Given the sheer scale of the task ahead, it is clear that an approach to building knowledge will need to be large-scale, ambitious and embrace different research methodologies. There is an urgent need to build knowledge to maintain proposed implementation and ultimate acceptance. There is already funding support available in some countries (e.g. Future Flight Initiative in the UK; the Advanced Air Mobility National Campaign in the United States) for research in this field, but it is clear that there will need to be multiple initiatives and collaborations for knowledge to be built to inform the ongoing, rapid development of UAV/UAS technologies. The field of human response to noise exposure is typically undertaken by those with a public health and/or social science background and there will be a need to embrace these disciplines, alongside expertise in public acceptance and community engagement to build this knowledge.

References

- Babisch, W., Houthuijs, D., Pershagen, G., Cadum, E., Katsouyanni, K., Velonakis, M., Dudley, M. L., Marohn, H. D., Swart, W., Breugelmans, O., Bluhm, G., Selander, J., Vigna-Taglianti, F., Pisani, S., Haralabidis, A., Dimakopoulou, K., Zachos, I., & Järup, L. (2009). Annoyance due to aircraft noise has increased over the years--results of the HYENA study. *Environment International*, 35, 1169-1176.
- Breugelmans, O., Houthuijs, D., van Kamp, I., Stellato, R., van Wiechen, C., & Doornbos, G. (2007). Longitudinal effects of a sudden change in aircraft noise exposure on annoyance and sleep disturbance around Amsterdam Airport. In *International Congress on Acoustics*. Madrid.
- Brown, A. L., & van Kamp, I. (2017). WHO Environmental Noise Guidelines for the European Region: A systematic review of transport noise interventions and their health effects. *International Journal of Environmental Research and Public Health*, 14, 873.
- Fidell, S., Silvati, L., & Haboly, E. (2002). Social survey of community response to a step change in aircraft noise exposure. *Journal of the Acoustical Society of America*, 111, 200-209.
- Guski, R. (1999). Personal and social variables as co-determinants of noise annoyance. *Noise Health*, 1, 45-56.
- Guski, R., Schreckenberg, D., & Schuemer, R. (2017). WHO Environmental Noise Guidelines for the European Region: A systematic review on environmental noise and annoyance. *International Journal of Environmental Research and Public Health*, 14, 1539.
- ISO/TS15666. (2003). Acoustics - Assessment of noise annoyance by means of social and socio-acoustic surveys. In (Vol. Reference No. ISO/TC 43/SC 1 N 1313 2003.). Geneva: Reference No. ISO/TC 43/SC 1 N 1313 2003.: International Organization for Standardization.
- Janssen, S. A., Vos, H., van Kempen, E. E., Breugelmans, O. R., & Miedema, H. M. (2011). Trends in aircraft noise annoyance: the role of study and sample characteristics. *Journal of the Acoustical Society of America*, 129, 1953-1962.
- Nguyen, T. L., Nguyen, T. L., Morinaga, M., Yokoshima, S., Yano, T., Sato, T., & Yamada, I. (2018). Community response to a step change in the aircraft noise exposure around Hanoi Noi Bai International Airport. *Journal of the Acoustical Society of America*, 143, 2901.

- Quehl, J., Muller, U., & Mendolia, F. (2017). Short-term annoyance from nocturnal aircraft noise exposure: results of the NORAH and STRAIN sleep studies. *International Archives of Occupational and Environmental Health*, 90, 765-778.
- Schreckenberger, D., Meis, M., Kahl, C., Peschel, C., & Eikmann, T. (2010). Aircraft noise and quality of life around Frankfurt Airport. *International Journal of Environmental Research and Public Health*, 7, 3382-3405.



CidB

Centre d'information
sur le Bruit

QUIET DRONES
International e-Symposium
on
UAV/UAS Noise
Remote from Paris – 19th to 21st October 2020

MOSQUITO Project – a fast estimation approach for urban acoustic environment

Franck Cléro, Onera: franck.clero@onera.fr

Julien Caillet, Airbus Helicopters: julien.caillet@airbus.com

Eric Bouty, Safran Helicopter Engines: eric.bouty@safrangroup.com

Claude Sensiau, Safran Tech: claudio.sensiau@safrangroup.com

Ingrid LeGriffon, Onera: Ingrid.legriffon@onera.fr

Patrice Malbequi, Onera: Patrice.malbequi@onera.fr

Summary

In the framework of development of new services based on drones for Urban Air Mobility and Logistics, the MOSQUITO project aims at performing a first evaluation of the necessary requirements to ensure compliancy with high density population environment. Funded by the DGAC (Direction Générale de l'Aviation Civile), one of its topics is to investigate the acoustical acceptability of drones in urban environment where noise is less and less tolerated.

This paper focusses on the acoustic part of the project which involves Airbus Helicopters, Onera, Safran Helicopter Engines and Safran Tech. These partners have the capacity to simulate the different acoustic sources radiated by a VTOL (Vertical Take-Off and Landing) aircraft, along its flight trajectory, and to propagate the noise toward the ground, without any building. In MOSQUITO, one objective is to add the acoustic effect of the urban environment. Software like MithraSig developed by CSTB, can simulate the acoustic propagation in an urban environment. The existing capabilities of this code are evaluated thanks to the well known source of a full scale helicopter test flying over the Airbus Helicopters center in Marignane. Using this tool, the partners plan on simulating reference cases in order to obtain acoustic correction factors to add the urban effect on a free field noise footprint. Then, 3 different VTOL configurations in three different urban environments are planned to be simulated from the source to the ground integrating the newly developed correction factors. A final auralization step will then be performed to open the way to listening tests. With this complete simulation chain, the partners will have the possibility to study acceptability criteria for new services enabled by Urban Air Mobility and Logistics.

1. Introduction

The fast development of drones opens the way to an opportunity to totally rethink the urban environment. With their wide range of size and design, they can be adapted to many services which, today, are fully managed by ground transportation, with increasing traffic and air pollution. Thus, for logistics, solutions are investigated, going from hub-to-hub delivery of single parcels with small drones, to heavy loads of hundreds of kilogrammes provided to peri-urban hubs by large drones. Urban air taxi is also a new way to envisage the mobility in congested megacities, with reduced travel time.

In this context of development of new services based on drones for Urban Air Mobility and Logistics, the MOSQUITO project aims at performing a first evaluation of the necessary requirements to ensure compliancy with high density population environment. Funded by the DGAC (Direction Générale de l'Aviation Civile), the project addresses four topics: acoustics to prepare acceptability of drones in urban environment where noise is less and less tolerated; safety to identify the hardest technical constraints relative to high level risk environment; cyber security to assess the risk of cyber-attacks taking control of the drone; electro-magnetic compliance to estimate the mutual interaction between drones and urban environment. The project will provide the basis to support the definition of specific regulation of drones in urban areas.

The present paper focuses on the acoustic part of the project, which involves Airbus Helicopters, Onera, Safran Helicopter Engines and Safran Tech, actors of the French aeronautics community and used to deal with airplane and helicopter noise. With drones and their multiplicity of configurations, they had to update their noise simulation tools to cope with new acoustic sources: multi-propellers interaction, shrouded propellers, small rotors, ... and other challenges to be able to estimate the noise radiated to the ground.

In MOSQUITO, the acoustic activities can be summarized in three steps: the adaptation of existing noise simulation tools to drones; the integration of urban effect on the noise radiation; first simulations of noise perceived by the citizens in urban environment. The final result is a complete numerical chain able to simulate the noise radiated by any drone flying above urban areas and to provide time signals for listening tests.

2. Noise footprint estimation

2.1 The noise sources

The noise radiated by a drone can have different sources depending on its configuration: rotor(s) in horizontal plane; propellers in vertical plane, shrouded or not; electric engines; turbine for hybrid configuration and even combustion noise. When moving, additional airframe noise is generated by landing gear, struts, cavities, and more generally every element creating turbulence. However, most of the noise comes from the rotating elements and the engines.

The simulation of these sources can be performed through different approaches from fast estimation tools to high fidelity numerical simulations. The more accurate is the estimation, the more expensive and time costly is the method. Thus, high fidelity numerical simulations are performed on supercomputers with thousands of cores, even for a few numbers of propellers, making it difficult to simulate the full aircraft with accuracy. In MOSQUITO, as the objective is to provide the noise footprint of different kinds of drones, during their different phases of flight, it is necessary to use simplified tools.

Among the MOSQUITO partners, fast estimation tools are available, based on analytical or empirical models. Analytical tools, by simplifying the physics, allow to simulate any kind of aircraft, even non-existent ones; however, they need preliminary comparisons with experimental results to validate their range of use. On the contrary, empirical models, by nature, are already validated and therefore are trustworthy, as long as they are applied to

similar sources and configurations. For years, MOSQUITO partners have been developing their own approach guided by their future use of the tool.

In general, Onera has been working on a Noise prediction tool for several years now, making it possible to calculate noise sources on an aircraft, evaluate the installations effects and propagate the sound through the atmosphere to the ground. The calculation of noise sources and installation effects permits to evaluate the pressure field radiated during take-off, landing and cruise, taking into account the aircraft configurations [LeGriffon 2015] (engine thrust, high-lift devices and landing gear position, etc.), at each discretisation step of the flight trajectory. The overall structure of Onera's tool chain is described in Figure 1. Based on previous works on helicopters, Onera has developed an analytical model of rotor noise including thickness noise, loading noise and blade-vortex interaction noise (BVI) [Reboul & al. 2012; Reboul 2014]. Several rotors can be simulated simultaneously, however each rotor is considered as independent from the others, which is not the case when they are close to each other. This is a limitation that has to be investigated in the future. Nevertheless, at first order, the information provided by the model is sufficient to have a quick and rough idea of the noise footprint on the ground. Several post-processing possibilities are then available, such as the calculation of sound quality metrics or the creation of audible sound files for listening tests.

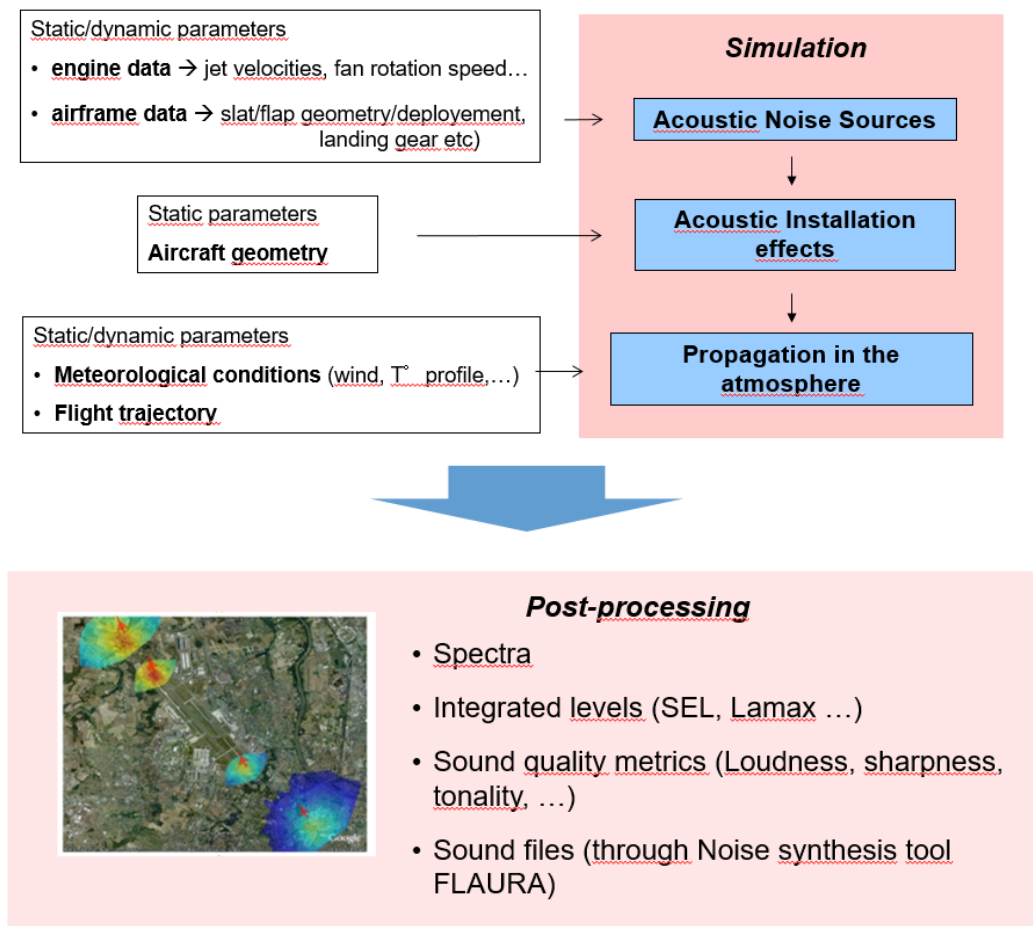


Figure 1: Structure of Onera's Noise prediction tool chain

Airbus Helicopters has been working on tool chains for predicting helicopter noise for years, to design quiet helicopter products and to propose noise abatement procedures as an efficient mean to alleviate helicopter noise impact on population. In particular, a computation tool based on noise hemispheres (see Figure 2) is used to accurately simulate the noise footprint of an arbitrary trajectory flown by a helicopter.

A noise source database is obviously required to evaluate noise footprint and an extensive experience has been gathered in building such empirical sources databases for helicopters, from flight test campaigns with ground microphones [Guntzer & al. 2014].

Noise sources can also be generated from various simulation methods, ranging from semi-empirical to comprehensive high-fidelity numerical modelling approaches. For new eVTOL configurations, these methods still require validation, which now becomes possible thanks to preliminary acoustic measurements results on new vehicles such as Vahana or City Airbus demonstrators (Figure 3). Airbus Helicopters can thus provide reliable source data that can be used to evaluate acceptance in cities.

The global noise footprint calculation tool chain, based on the available helicopter tool chain, is being improved in the frame of MOSQUITO to include these new sources models and their specificity, as well as to include new capabilities such as auralization of the simulated signals on ground.

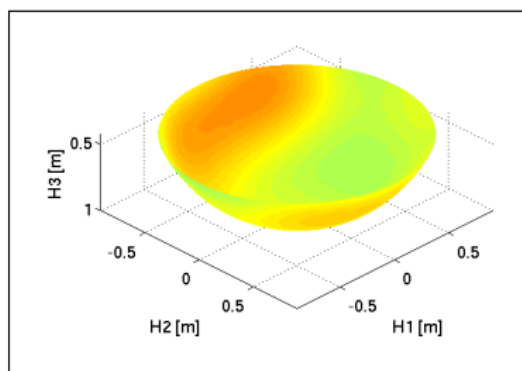


Figure 2 – A-weighted level of a 1m-radius hemisphere helicopter source



Figure 3 – Vahana and City Airbus demonstrators

Safran already had a modern, modular framework for simulating in-flight aircraft noise impact on ground, but noise sources were mostly described in 2D, assuming their axisymmetric radiation. Trajectory is simplified as a succession of linear segments. This model can prove sufficient for airplanes, due to airplane geometry and the important distance between emitter and receiver. This is not the case anymore for UAM, as distance to listeners may be very short, and included noise sources may have significantly different geometric orientations. MOSQUITO helped to update the whole framework to 3D representation of noise sources. Moreover, additional noise sources models have been implemented: empirical simple flux engine (per noise source), analytical rotor noise. Finally, a small post-processor module has been added for generating audible sound from predictions.

One typical workflow for helicopter noise modelling is shown in Figure 4.

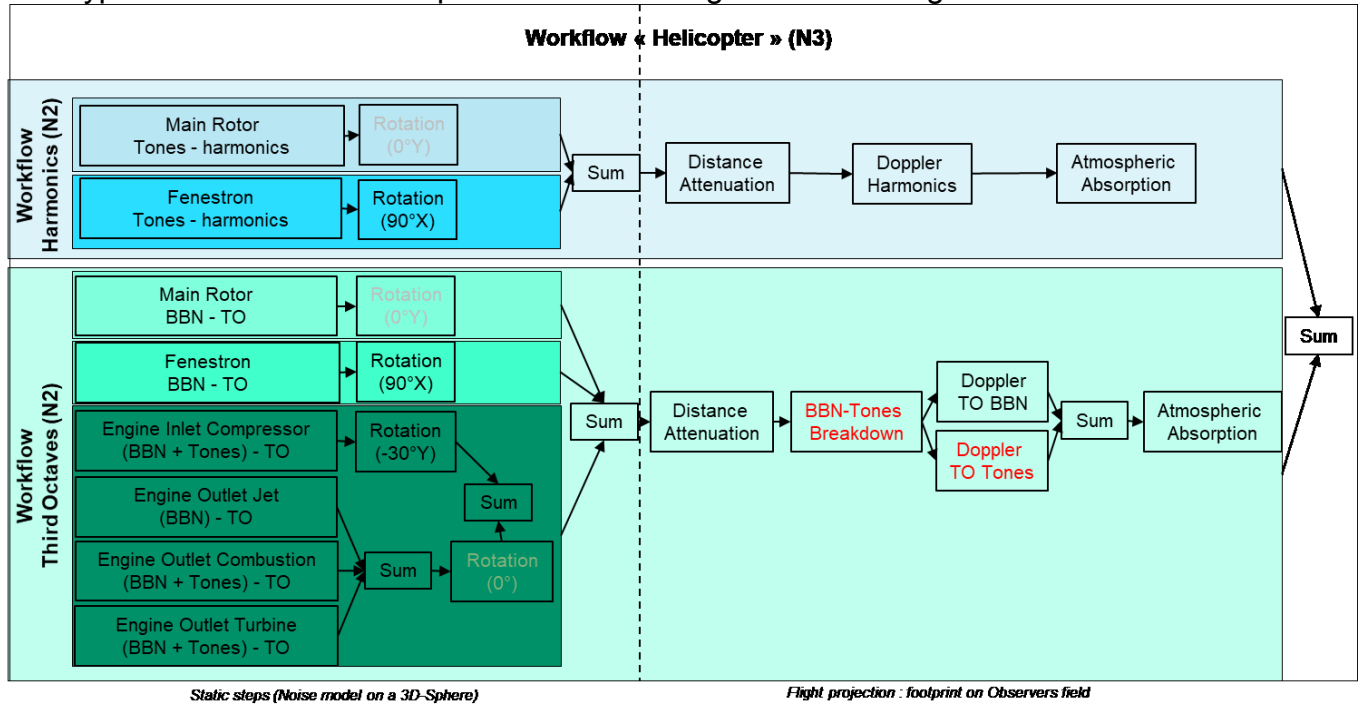


Figure 4 : Typical in-flight helicopter noise prediction workflow (angle values given as examples)

If analytical methods still need some validation works, the whole methodology is ready to take into account any UAM vehicle.

In a general manner, acoustic installation effects such as shielding, reflection, or diffraction can strongly modify the directivity of the source. Therefore, it cannot be neglected if accurate levels on the ground are expected. Installation effects can be treated thanks to preliminary calculation of the radiation of each source in presence of the aircraft, which can be done with the Boundary Element Method or Ray Tracing. Some empirical models already integrate these effects because they are based on measurements including them.

Whatever the method, for all partners, the result is always a sphere surrounding the aircraft providing acoustic pressure generated by the different sources in each direction. Its radius is usually 100 meters to ensure that far field hypothesis is reached.

In MOSQUITO, three typical aircraft are considered: a helicopter as strongly documented reference case; a large drone able to accept a load of several hundreds of kilogrammes, and a small drone adapted to parcels of a few kilogrammes.

2.2 The propagation to the ground

From the noise source sphere, the next step is to compute the sound propagation to the ground. A number of methods are available to predict the sound propagation in a heterogeneous atmosphere, such as the Gaussian beams, the parabolic equation or the Fast Field Program and MOSQUITO partners do not necessarily used the same method.

Recent computations solving the Euler's equations are now available to solve the sound propagation in the atmosphere at short distances. These methods are accurate and allow us to take into account the diffraction effects and the topography. However, again they still require a large amount of computing resources.

As an alternative, the standard ray-method is used. The ray-equations are integrated using a Runge-Kutta method of 4th order. The sound propagation module propagates the pressure field from the sphere to the airport surroundings, taking into account the wind profiles, the temperature gradients, the atmospheric absorption, as well as the Doppler effect generated by the moving aircraft. While it is based on a high frequency approximation, in practice this method

can also handle the sound propagation at mid frequency. Another advantage of the Ray-model is its capability to straightforwardly integrate the atmospheric absorption along the ray path, which, at long distances, dominates the sound pressure level reduction, in addition to the spreading law. In practice, for small distances of propagation of typically a few hundreds of meters, while the curvature of the rays can be neglected, the ray trajectory from the emission to the reception on the ground can be considered as straight lines, and the ray equations integration is no more required, saving significant CPU time [Malbéqui 2012].

3. Urban effect on noise radiation

3.1 State-of-the-art

For decades, the scientific community has developed methods to propagate the sound in urban environment which involves multiple reflections and diffractions due to the presence of buildings. In acoustics, the usual classification of propagation methods distinguishes the geometric methods (sometimes described as energetics) from wave methods. For propagation in urban environment, geometric methods are the most commonly used, even if recent progresses in numerical techniques have also allowed the application of wave methods such as Euler equations or even the Lattice Boltzmann Method.

MOSQUITO does not aim at developing a new urban propagation code, but rather at exploiting validated existing codes. According to a bibliography study, it appears that the macroscopic methods characterizing the influence of a set of buildings are mainly based on the ray tracing method. This is an effective method to take into account multiple reflections encountered in urban environment. The addition of diffraction terms to this asymptotic method, assuming the acoustic wavelength is small compared to the characteristic dimensions of the medium, makes it possible to account for the physics in the shadow zone formed behind an obstacle. Thanks to its anteriority to more modern numerical methods, ray tracing theory is integrated into many codes dedicated to propagation in urban areas. In the majority of these codes, the rays are straight line: there is no integration of the system of partial differential equations allowing heterogeneous atmosphere leading to curved rays. This simplification allows to apply high-performance algorithms to find intersections between rays and buildings. Nowadays, the ray-tracing method still offers a shorter computation time than other methods.

Therefore, MithraSIG and Mithrasound software, developed by CSTB have been chosen for numerical simulations. However, as these codes have been designed for ground transportation such as cars, trucks, motorbikes or trains, currently they do not propose the possibility to implement acoustic sources with full 3D directivity such as drones. It appears necessary to evaluate the capabilities of these tools for flying aircraft.

3.2 Validation

As a first step to evaluate the capability of the tools to simulate the sound radiated from a VTOL aircraft to the ground in urban environment, the case of a helicopter flying over the Airbus Helicopters site in Marignane is taken.

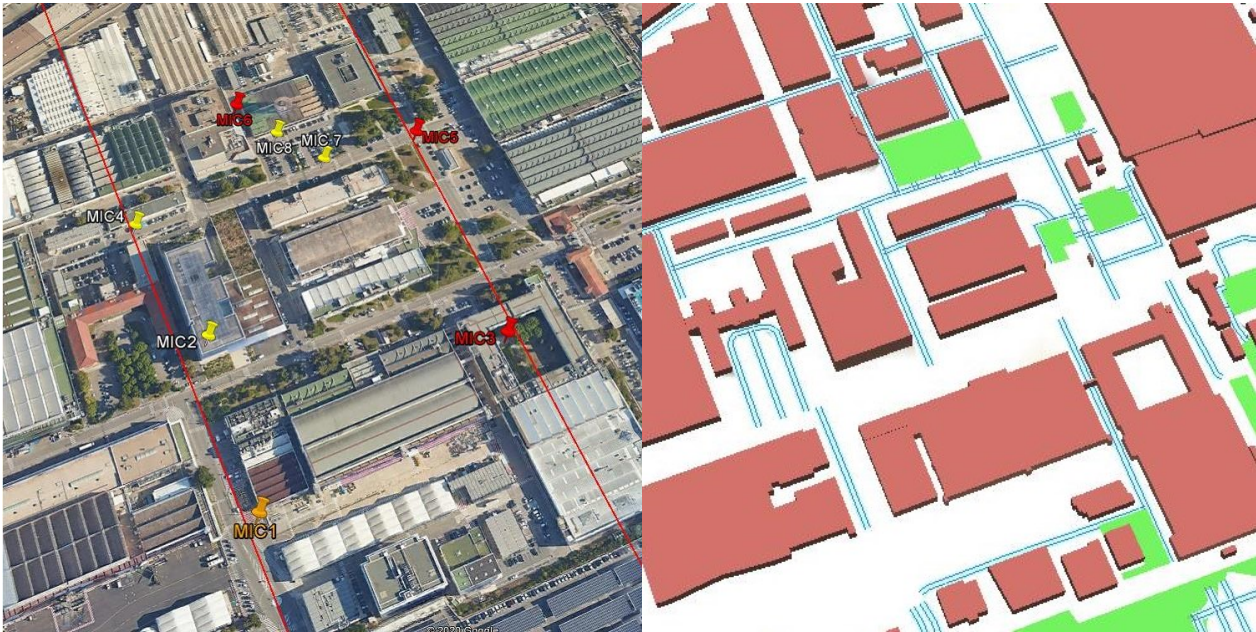


Figure 5 – Microphone location on Airbus Helicopters site – Open Streetmap/MithraSIG modelisation

In June 2020, during evening to limit background noise perturbation, a H130 helicopter performed several flights above the Airbus Helicopters facilities in Marignane, where 8 microphones were installed as depicted in Figure 5. Noise data, as well as trajectory and meteorological data were recorded for all the helicopter runs, each run consisting in a straight flight following a given flight axis, in a given direction, at a constant height and a constant speed.

Two flight axes were considered as represented on Figure 5, flown in both north and south directions. Flights were performed for 2 different altitudes (500ft and 1000ft), and 2 cruise speeds (95kt and 129kt), for a total flight duration of approximately 3 hours.

Acoustic measurements have been made by eight microphones placed at specific locations on the Airbus Helicopters site, so as to represent several propagation phenomena that could occur in an urban environment: masking effects, reflections and refractions on buildings. Some microphones are located undertrack of flight axes (e.g. Microphone 5 for flight axis 2). Other microphones are more or less close to buildings (e.g. Microphone 3 is in a kind of courtyard, thus surrounded by buildings, see Figure 5). Microphone 2 is on the rooftop of a building, which is 23m-high. All microphones except Microphone 2 are installed at 1.7m height above ground. Microphone 2 is installed at 7mm height above the roof ground upon an aluminium plate.

The noise source model of the H130 had been derived previously in the frame of an extensive flight test campaign in a quiet and flat area, and enables the comparison of these measurements with free-field noise propagation simulations. This comparison will enable to assess the influence of the “urban-like” environment on the noise propagation.

Therefore, MithraSIG and Mithrasound are currently used to reproduce the Marignane test campaign. This activity involves the urban environment effect, but also the evaluation of their capabilities to take into account aircraft noise provided by the source sphere described in §2.1. This work is still under progress.

3.3 Perspective for correction factors

As presented previously, the existing tools are able to simulate the noise radiated by an aircraft and to propagate the acoustic waves to the ground without any obstacle [Guntzer & Al 2014]. On the other hand, the ability of urban propagation software to simulate flying sources is to be validated thanks to comparisons with the Marignane measurements, for realistic helicopter flyovers procedures. The idea proposed in MOSQUITO is to estimate the urban effect on the propagation by correction factors allowing the change from free field propagation to urban one. Of course, this approach will not be able to provide the same accuracy as would an urban

propagation software, but it should be sufficient to provide the right order of magnitude. The principle of this approach is illustrated in Figure 6.

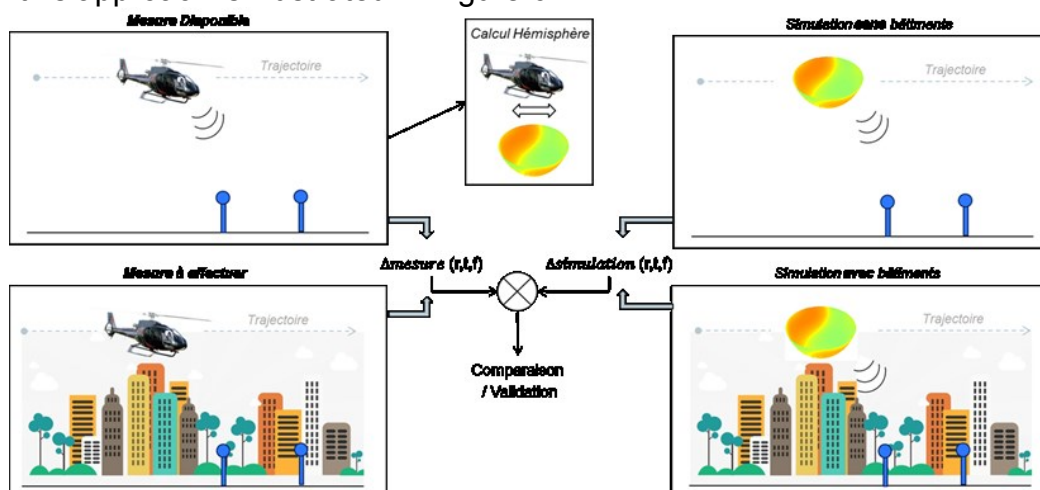


Figure 6 – Principle of simplified approach for urban environment effect

As the environment can be very different, three typical urban landscapes have been defined (Figure 7): a suburban city mainly composed of individual houses with small streets; a large city with small buildings of 3 or 4 floors with a mix of small and large streets; a dense district with high buildings and potential urban canyon effect.

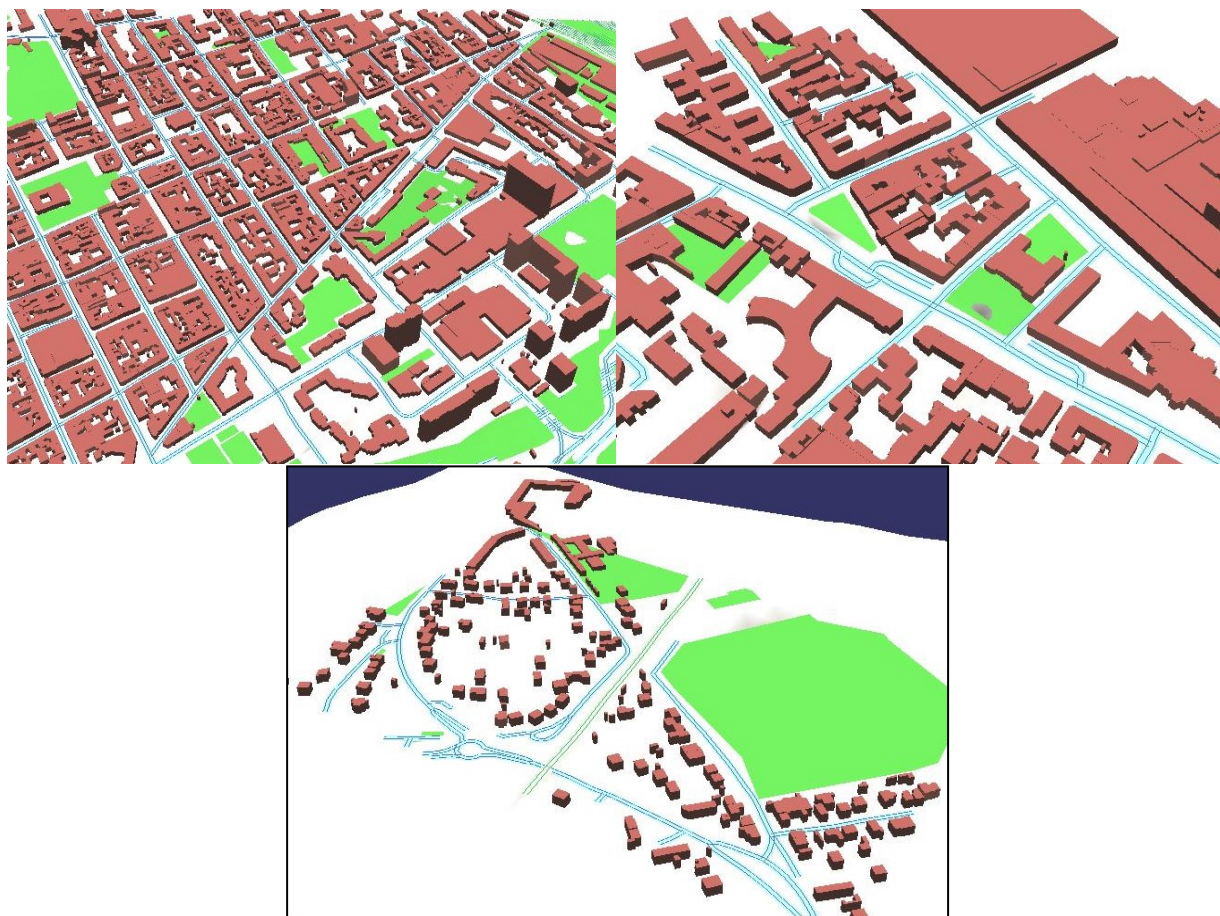


Figure 7 – Urban environment type from high to low density population from open streetmap/ MithraSIG: Levallois, Neuilly-sur-Seine, Igny

4. Perception of noise

One of the main goals of establishing realistic noise impact estimations of VTOL in the urban environment is the evaluation of acceptability. Indeed, sustainability and acceptability will be keys to the success of the introduction of Urban Air Mobility or Logistics, and most importantly, its ability to persist in time to become a natural addition to existing traffic means.

In the frame of MOSQUITO, a state of the art of noise perception and annoyance in urban environment has been performed, leading to a better understanding of its multifactorial nature. In fact, an urban environment stands for multiple expositions. The fact that one is exposed to a multitude of very different noise sources, all at the same time makes it quite complicated to pin point with certainty what contributes to the perception of annoyance. In the same manner, it is not straightforward to evaluate the impact that the introduction of a new type of noise source would have on the general soundscape and even less on the perceived noise annoyance. Factors that are not at all linked to the acoustic source itself become extremely important in the reaction to noise. This may refer to sociodemographic data such as age or social status, but also activity, time and space. The perception of a soundscape varies whether one is at work or shopping, whether it is early winter morning or a sunny weekend afternoon, whether one is in a park or a public square etc.

Taking into account these factors is extremely delicate, however there is absolutely no way around the good understanding of people's perception to an urban soundscape if we want to evaluate the annoyance impact of VTOL.

There certainly is an impact to be expected if things are not prepared correctly. The aircraft itself presents a noise signature that is uncommon to classic urban soundscapes yet. Its spectral content is very different from already present noise sources and its occurrence very VTOL specific (time varying, over a certain duration, low flights, hovering etc.).

Moreover, we not only add a new noise source but also factors that come along, such as the surprise of a source coming from the sky, the fear of a drone falling, or even the sensation of perhaps being "spied on". Thus, many factors are to be investigated, in order to ensure a deployment of these new services compatible with urban citizen acceptability.

5. Conclusions

MOSQUITO is a preliminary study, funded by DGAC, aiming at setting the basis for future activities about the implementation of Urban Air Mobility and Urban Logistics new services enabled by VTOL aircraft such as drones. The present paper has presented only the acoustic fold of the project, but similar investigations are carried out on safety, cyber risks and electromagnetic compliance. On the basis of their existing background, partners are preparing a full software chain able to simulate the noise sources from most of VTOL aircraft configurations, to propagate the acoustic waves to the ground with urban effects and to use these results for listening tests thanks to an auralization phase.

Unfortunately, the overall planning of MOSQUITO has been impacted by the COVID19 crisis preventing the authors to complete this presentation of the project with concrete results.

At medium-term, the work performed in MOSQUITO will open the way to studies to understand annoyance factors generated by VTOL aircraft with a perfect control of the acoustic sources at the origin.

References

- Legriffon, I. (2015) *Aircraft noise modelling and assessment in the IESTA program with focus on engine noise*, Proceedings of the 22th International Congress on Sound and Vibration, Florence, Italy, 12-16 July
- Reboul G. et Taghizad A. (2012) *Semi-analytical modelling of helicopter main rotor noise*, Proceedings du 38th European Rotorcraft Forum, Amsterdam, Netherland
- Reboul G. (2014) *A parametrized BVI prediction code* Greener Aviation 2014, Bruxelles, Belgique

Guntzer F., Gareton V., Gervais M., Rollet P., *Development and testing of optimized Instrument Flight Rules (IFR) noise abatement procedures on EC155*, Proceedings of American Helicopter Society Forum, 2014

Malbéqui, P., Legriffon, I., and Sanders, L. (2013) *Prediction of aircraft noise propagation using the ray model: comparison with flyovers*, 17th workshop of the aeroacoustics Specialists' Committee of CEAS, 3rd scientific workshop of the European X-Noise EV network, Sevilla, Spain



CidB

Centre d'information
sur le Bruit

QUIET DRONES
International Symposium
on
UAV/UAS Noise
Paris – 19th to 21st October 2020

Drone audition for search and rescue: Datasets and challenges

Antoine Deleforge, Inria Nancy – Grand Est: antoine.deleforge@inria.fr

Summary

Processing audio signals recorded from a microphone array embedded in an unmanned aerial vehicle (UAV) has received increasing research interest in the recent years and has been referred to as *drone audition*. An important field of application is search and rescue, where humans in disaster areas need to be quickly found. UAVs equipped with high-resolution cameras have already been used in humanitarian responses, while audio-based UAV-embedded sound localisation remains an open research challenge. Microphones could provide a critical complementary modality to vision in situations where visual feedbacks are limited due to bad lighting conditions (night, fog) or obstacles limiting the field of view. This paper provides an overview of the technical and methodological challenges faced by drone audition in the context of search and rescue and presents two publicly available datasets that aim at fostering research in this area. Some localisation and noise-reduction results obtained using baseline methods are also presented. While static localisation of speech sources from a distance of four meters can be efficiently achieved, in-flight localisation from larger distances remains a challenge.

1. Introduction

Unmanned aerial vehicles (UAV), commonly referred to as drones, have been of increasing influence in recent years. Applications such as autonomous human transport machines or delivery devices for postal services are being envisioned [1]. Search and rescue scenarios where humans in emergency situations need to be quickly found in areas difficult to access also constitute a potentially large field of application. Drones have already been used by humanitarian organizations in places like Haiti and the Philippines to map areas after a natural disaster, using high-resolution embedded cameras, as documented in a recent United Nation report [2]. While a number of UAV-embedded tools to address such situations have been developed using video cameras [3], audio-based source localization from UAVs has received relatively less research attention. UAVs equipped with a microphone array could present several advantages in emergency situations, especially whenever there is a lack of visual feedback due to bad lighting

conditions (night, fog, etc.) or obstacles limiting the field of view [4]. Sound signals primarily capture two types of information: (i) Geometrical information via the sound propagation path, e.g., the position of emitting sources with respect to the receiving microphone array and (ii) the semantic content of emitted sounds, e.g., speech or an emergency whistle. Methods for retrieving information of the first type include sound source localization or acoustic echo retrieval. Methods for retrieving information of the second type include speech recognition or sound event detection and classification.



Figure 1: Microphones embedded in a drone may help localizing people for search and rescue in disaster area.

In the specific context of drone audition, these traditional audio signal processing (ASP) tasks are made challenging by a variety of effects. One major issue is the noise produced by the UAV itself, generically referred to as *egonoise* in robotics [5]. Due to the quickly changing speed of motors to stabilize the vehicle in the air or to change its position, the noise profile is highly non-stationary. Additionally, since the microphones are mounted on the drone itself, they are very close to the noise sources leading to high noise levels. Because of this, the signal-to-noise ratio (SNR) can easily reach -15 dB or less [6]. Another factor affecting ASP performance is wind noise. The wind is produced by the rotating propellers, the UAV movement in the air and may occur naturally in outdoor scenarios. This wind noise has high power and is of low-frequency. Hence, it easily overlaps with speech signals that typically occur in a similar frequency range [7]. Last, UAV often encounter very dynamical situations. This means that drone-audition methods must be designed to adapt to quickly changing spatial configurations (direction, distance, etc.) environment (presence of reflecting surfaces, wind, etc.) and noise (level, type, etc.). All these challenges need to be tackled at the same time and in near real-time for real world applications such as search and rescue.

On the bright side however, using microphones embedded in a UAV comes with interesting opportunities. Additionally to audio signals, other signals recorded by various embedded sensors (camera, lasers, gyroscope, motor controllers, inertial measurement unit, compass, etc.) may be available. Multimodal approaches fusing information from multiple sensors in order to enhance drone perception and navigation present a promising research avenue, as investigated in [8, 9, 10, 11].

The remainder of this paper is organized as follows. Section 2 provides a brief overview of the recent literature in drone audition, in particular on ego-noise reduction, sound source localization, echolocation and datasets. Section 3 reviews two recently created datasets, namely, the collaborative drone egonoise datasets from the IEEE Signal processing Cup 2019 (SPCup19, [26]) (Section 3.1), and the DREGON dataset [6] dedicated to UAV-based sound localization (Section 3.2). Finally, concluding remarks and outlooks are provided in Section 4.

2. Related Work

2.1 Egonoise Reduction

Egonoise reduction is a topic of interest in robot audition for some years [5]. A first category of methods performs egonoise reduction solely based on audio signals. This includes the work in [12], which compares *unsupervised* methods such as beamforming, blind source separation (BSS) and time-frequency filtering algorithms on UAV-embedded recordings. More recently, the same authors proposed a framework combining time-frequency filtering and BSS for egonoise reduction [13]. It shows very promising performance in a realistic outdoor flight scenario involving a human speaker at a 4 meters distance. Alternatively, the *supervised* methods proposed in [14, 15, 16] rely on pre-recorded noise-only signals to learn a dictionary that represents the egonoise via techniques such as nonnegative matrix factorization (NMF) or K-SVD. This dictionary is then used to model the noise characteristics in noisy recordings and improve its reduction. These methods have been successfully applied to ground robots but not yet to UAVs to the best of our knowledge.

A second category of methods makes use of additional sensors than audio to improve egonoise reduction performance, and in particular, *motor data* such as the rotors' speed or inertial measurements. These include dictionary-based methods [17, 18, 19] as well as Gaussian process [8] or neural-network based approaches [9]. The idea is to predict the spectral characteristics of the egonoise at runtime by learning its relationship to the current motor and/or inertial status of the robot.

2.2 Sound Source Localization

Sound source localization (SSL) is a long standing and extensively studied topics in robotics [20], but is still relatively new in the specific context of drone audition. Many robotic SSL approaches developed in recent years are different variations of the Multiple Signal Classification (MUSIC) algorithm, e.g., [8, 21, 22, 23, 28]. Generalized Cross Correlation (GCC) methods [24] and their variants were also successfully used in robot SSL [4, 25, 6] and are generally less computationally expansive than their MUSIC counterparts. They were notably applied to UAV-embedded SSL in [4, 6], and used as a baseline in the recent SPCup19 drone SSL challenge [26] (see Section 4). An open-source python implementation of this baseline is available at [27]. Reducing ego-noise using the multichannel Wiener filter as a pre-processing step to GCC-based SSL was shown to significantly improve performance in [6].

In [8], a UAV-embedded SSL method using both pre-recorded and on-flight propeller speed data is proposed. These data are used to estimate an adaptive noise correlation matrix in a Gaussian process regression model. This matrix is then used to improve robustness to noise of a MUSIC-like method. In the same spirit, [9] presents a Deep Neural Network (DNN) approach to UAV-embedded SSL. To overcome the large training data requirements of DNNs, a partially shared network learning multiple tasks at the same time is implemented. In [28], two different UAV microphone array designs are proposed and MUSIC variants are compared on an outdoor SSL scenario. Good SSL success rates are obtained in relatively mild SNR conditions (around 0 dB). The authors propose to adapt the algorithms depending on the considered scenario and emphasize their high computational costs as a drawback for real-time applicability.

2.3 Echolocation for Navigation

Another more recent and emerging research topic in drone audition is the use of acoustic echoes for navigation in closed environments, and in particular for auditory *simultaneous localization and mapping* (SLAM), which is relevant for search and rescue. When sound propagates from a source in an environment, early reflections of the sound on nearby surfaces result in delayed and attenuated copies of the emitted signals at receivers, commonly referred to as *echoes*. The

timings of these echoes contain rich information on the geometry on the environment and can be used to detect obstacles, a principle used in nature by echoing bats to orientate themselves. This principle is referred to as *active echolocation* when a perfectly known and controlled source signal is used and as *passive echolocation* using a partially known or unknown source signal. In the context of UAVs, using a sound emitter placed on the drone (active) or even the drone egonoise itself (passive) is an attractive avenue for navigation in closed-environments where vision cannot be fully relied on. This idea has recently received some research attention. In [29, 30] a perfectly known source placed at the center of a circular array mounted on a drone is used to detect nearby surfaces. The method is validated on simulated data only, but using real drone egonoise. In [31], the same approach is successfully used for a real-world ground-robot navigation demo, where the noise level is much lower than in typical UAV scenarios. Conversely, in [10], cameras, depth sensors and laser sensors are used to identify reflectors in an environment and build a corresponding acoustic model that can localize non-line-of-sight sound sources in a ground-robot navigation scenario.

2.4 Datasets

While the following sections focus on the SPCup-Egonoise [26] and DREGON [6] datasets, at least two other recently published datasets for drone audition are worth mentioning. The AIRA-UAS dataset was captured indoor with an 8-channel circular microphone array mounted on three types of drones [32]. The recording drone is flying either alone or in the presence of other drones. It aims at evaluating UAV-embedded sound source localization and separation methods, which could be applied to search-and-rescue but also to unauthorized drone operation detection. Also of interest is the AVQ dataset, consisting of outdoor, synchronized audio-visual recordings from a flying drone equipped with an 8-microphone-array as well as a camera [11]. The dataset includes scenarios for source localization and sound enhancement with up to two static sources, and a scenario for source localization and tracking with a moving sound source.

3. Drone Audition Datasets

3.1 The SPCup-Egonoise dataset

The IEEE Signal Processing Cup is a yearly international competition involving teams of undergraduate students. The 6th edition (SPCup19) took place from November 2018 to May 2019 and was focused on UAV-embedded sound localization for search and rescue [26]. On top of the main required SSL tasks, a bonus task asked participants to gather their own sound recordings using microphones mounted on a UAV. Eleven teams participated to this task, which resulted in the *SPCup-Egonoise dataset*, now publically available online for research purpose at [33]. The dataset includes recordings using 1- to 16-channel microphone arrays and features a variety of drone model and array geometries. The diversity of this dataset is illustrated in Figure 2. As can be seen, noise levels vary widely depending on the setup. Team *Idea! SSU* placed their sensors the farthest away from the UAV propellers, resulting in relatively mild low frequency noise, while recordings from teams *ChuMS* and *Maverick* feature clipping (microphone saturation) due to extreme noise loudness. It can also be observed that different drone models feature different harmonic comb patterns, from very distinct and spectrally spread patterns (teams *KU Leuven* and *NSS Chellamma*) to less distinct ones (team *Shout COOE*), through sparser spectra (team *AGH*) or lower frequency ones (team *Diagonal Unloading*).

Common to all these recordings is the presence of recognizable patterns that characterize drone egonoise. These correspond to wind (low frequency, sporadic bursts), propeller rotations (harmonic combs) and other electronic and mechanical sources (random stationary background). These patterns are better seen in Figure 4, showing the spectrogram of a speech source recorded from a flying UAV [6]. As can be seen, wind noise is particularly detrimental to speech, as it lies within the same frequency range and is very loud. However, it rarely occurs in all

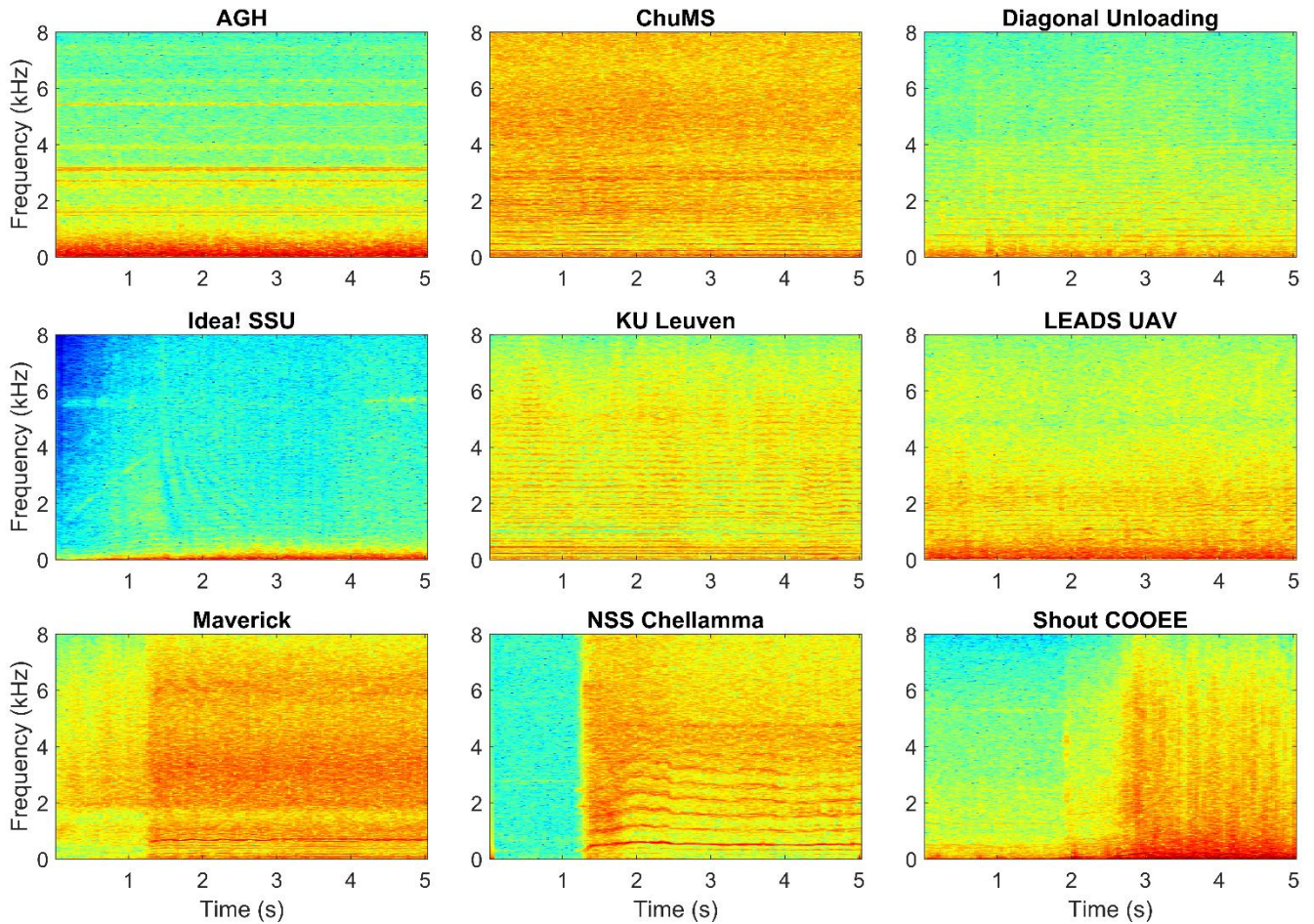


Figure 2: Example spectrograms of 5-second excerpts of egonoise recordings made by different teams that participated to the IEEE Signal Processing Cup 2019 [26]. The same color scale from blue to red is used to represent log-magnitudes (dB) in each spectrogram.

channels at the same time, suggesting the use of wind noise detection for adaptive channel selection. Wind noise reduction using NMF has also been explored in [7]. The random stationary background components are the easiest to remove using statistical methods such as the multichannel Wiener filter (MWF), as showed, e.g., in [6]. MWF can also be used to efficiently remove harmonic components, assuming that the harmonic pattern is known and constant over time. While this assumption is reasonable for stationary or constant-velocity flights, it is no longer valid in scenarios that are more dynamic, with numerous changes of velocities and directions. For such situations, a promising avenue is to use motor-speed data to predict harmonic patterns, as illustrated in Figure 5 and as explored in [42] on a ground robot.

3.2 The DREGON Sound Localization dataset



Figure 3: DREGON setup.

The DREGON dataset was published in 2018 [6] with the aim of fostering research in UAV-embedded SSL for search-and-rescue applications. It is publicly available online at [34]. The setup used is a MikroKopter quadrotor UAV equipped with a cube-shaped 8-microphone array mounted under the drone via a 3D-printed structure, as depicted in Figure 3. The dataset contains both noisy (motors on) and clean (motors off, hand-held) in-flight and static audio recordings. These are continuously annotated with the 6 degrees-of-freedom placements of both the target source and microphone array using a precise VICON motion capture system.

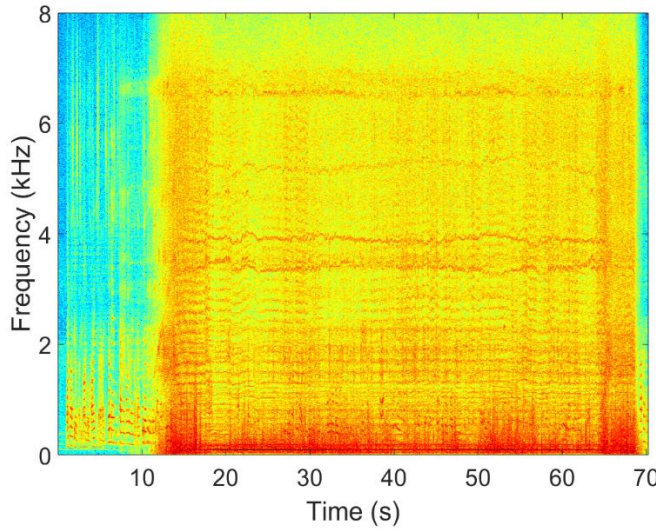


Figure 4: Spectrogram of the recording of a speech source by a microphone embedded in a drone [6]. First the drone is idle, then the motors are powered on and the drone takes off.

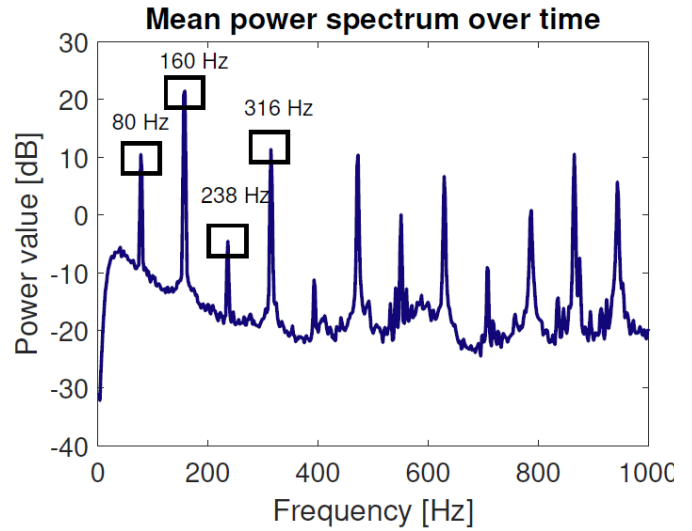


Figure 5: Mean power spectrum of the sound generated by an individual drone rotor spinning at 80 rotations per second [6]. Peaks at harmonics proportional to 80 Hz can be observed.

Different flight patterns featuring varying dynamics are available. The target source is a static loudspeaker on the ground, emits either speech or white (broadband) noise, and is placed 2 to 4 meters from the UAV. In addition to audio and position signals, the rotational speeds of each of the four individual rotors as well as inertial measurements data are available at all time, and all signals are time-stamped for synchronization. The dataset features in-flight recording sessions in two different rooms with respective volumes 10m x 10m x 2.5m and 12m x 12m x 3.5m and mild reverberation times ($RT60 < 200\text{ms}$).

Figure 6 shows some of the sound source localization results obtained on the dataset using GCC-PHAT [24] after pre-processing the signals with multichannel Wiener filtering (MWF). The noise statistics used for MWF were pre-computed from recordings of each individual rotors spinning at 80 rotations per second, and were fixed over time. As can be seen, very satisfactory SSL results can be obtained with this approach when the emitting sound source is broadband, even in harsh noise conditions ($\text{SNR} < -10 \text{ dB}$). However, when the emitted signal is speech, much poorer results are obtained under similar SNR, in particular when speed and position change. This can be explained by the strong spectral overlap between speech, wind, and propeller noises, and suggest that a fixed MWF does not sufficiently reduces these noises for SSL in these conditions (See Section 3.1).

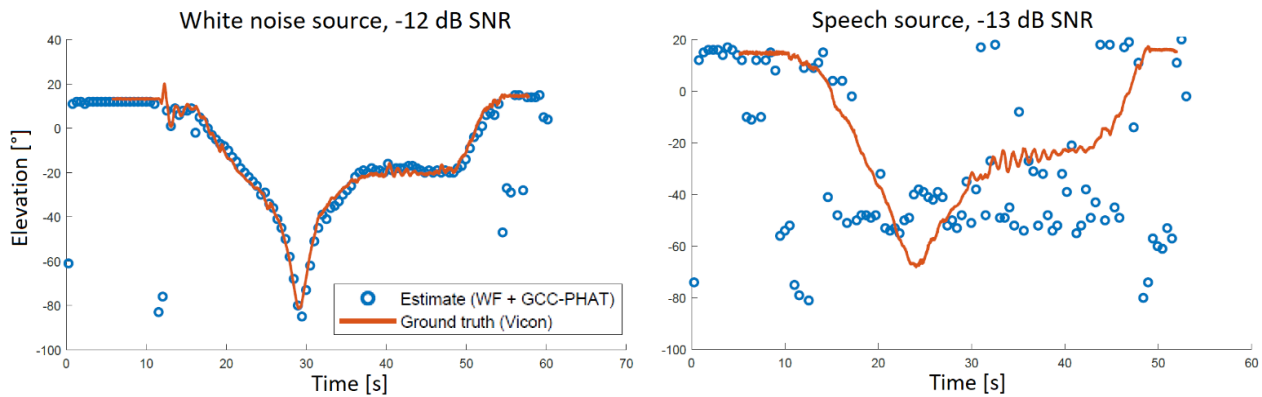


Figure 6: Estimated elevation angles of a static, ground sound source recorded from a flying drone using multichannel Wiener filtering (WF) followed by GCC-PHAT, versus ground truth [6]. Left: the source emits white noise. Right: the source emits speech.

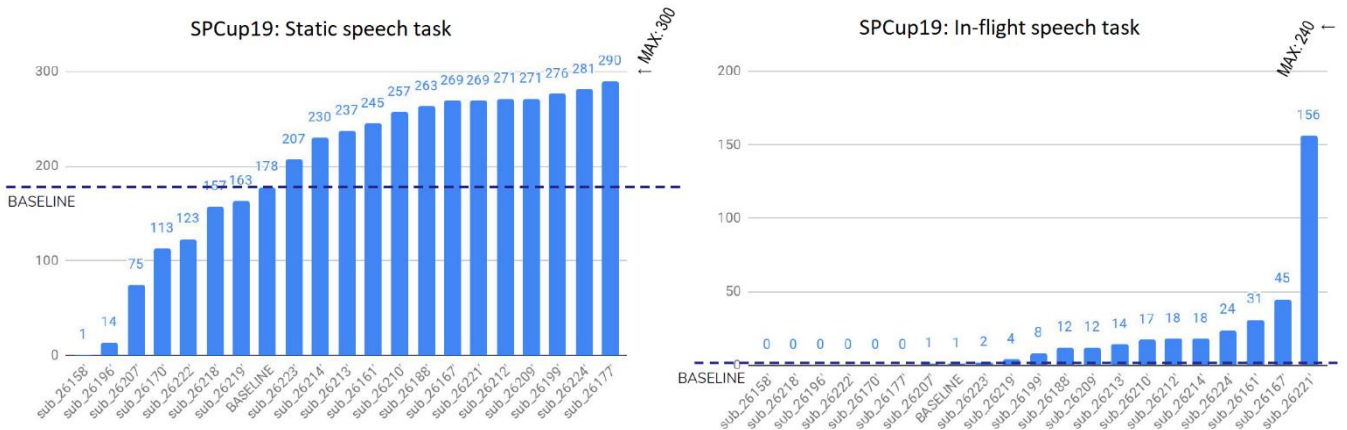


Figure 7: Results obtained by the 20 student teams that participated to the SPCup19 [26]. Left: number of correctly localized static speech sources from a stationary drone (angular error $<10^\circ$). Right: number of correctly localized speech source from a flying drone.

Finally, some of the results obtained on the SSL tasks of the SPCup19, which were based on a subset of DREGON, are shown in Figure 7. Note that the baseline used for this challenge was also GCC-PHAT, but without Wiener pre-filtering. Here, it can be observed that while near-perfect results are obtained by several teams on the static speech localization task, the in-flight speech localization task proves much more challenging, despite similar SNR conditions. The best performing team nevertheless achieves an encouraging 65% localization accuracy on that realistic task. Crucially to this success, the team used Kalman filtering to smooth estimated trajectories, pre-filtered signals using an adaptive MWF, fused localization estimates of both MUSIC and GCC-PHAT methods via k-mean clustering, and processed the angular spectra obtained from these methods using handcrafted heuristics.

Amongst the top 12 performing teams, the most popular pre-filtering method was MWF, and the most popular SSL method was GCC-PHAT. About half of the team used motor speeds provided with audio signals to estimate noise characteristics and about half used some form of angular trajectory smoothing and post-processing. Other notable ideas included the use of a speech activity detector or channel selection to reduce the effect of wind noise. Interestingly, only two teams made use of machine learning techniques such as deep neural networks, probably owing to the limited amount of data available for training. The newly released SPCup19-egonoise dataset could constitute a first step towards employing such approaches in the future.

4. Conclusion

In this paper, we have explored some of the numerous challenges and research opportunities brought by the recent and emerging topic of drone audition. An important application for this new field is audio-based search and rescue, which involves a large number of audio signal processing tasks, from sound source localization to echolocation, from noise reduction to sound event and speech detection and recognition. While many of these tasks have long been studied, the specific setting of drone audition, involving compact arrays near loud noise sources and very dynamic soundscapes make them particularly challenging. Most of these problems remain open as of today, but emerging research efforts in noise reduction and source localization along the past few years have shown promising results, notably fostered by the recent development of publicly available datasets.

References

- [1] R. D. Andrea (2014), "Guest Editorial Can Drones Deliver?" IEEE Transactions on Automation Science and Engineering, vol. 11, pp. 647–648.
- [2] U.N.O. for the Coordination of Humanitarian Affairs (2014), "Unmanned aerial vehicles in humanitarian response," [Online].
- [3] L. Lopez-Fuentes, J. van de Weijer, M. Gonzalez-Hidalgo, H. Skinnemoen and A. D. Bagdanov (2017), "Review on computer vision techniques in emergency situations," Multimedia Tools and Applications.
- [4] M. Basiri, F. Schill, P. U. Lima, and D. Floreano (2012), "Robust acoustic source localization of emergency signals from micro air vehicles," in IEEE/RSJ International Conference on Intelligent Robots and Systems, pp. 4737–4742.
- [5] H. W. Löllmann, H. Barfuss, A. Deleforge, S. Meier, and W. Kellermann (2014), "Challenges in acoustic signal enhancement for human-robot communication," in Speech Communication; 11. ITG Symposium; Proceedings of VDE, pp. 1–4.
- [6] M. Strauss, P. Mordel, V. Miguët, and A. Deleforge (2018), "Dregon: Dataset and methods for uav-embedded sound source localization," in IEEE/RSJ International Conference on Intelligent Robots and Systems (IROS).
- [7] M. Schmidt, J. Larsen, and F.-T. Hsiao (2007), "Wind Noise Reduction using Non-Negative Sparse Coding," in Machine Learning for Signal Processing 17 - Proceedings of the 2007 IEEE Signal Processing Society Workshop, MLSP, pp. 431 – 436.
- [8] K. Furukawa et al. (2013), "Noise Correlation Matrix Estimation for Improving Sound Source Localization by Multirotor UAV," in IEEE/RSJ International Conference on Intelligent Robots and Systems (IROS), pp. 3943–3948.
- [9] T. Morito et al. (2016), "Partially Shared Deep Neural Network in Sound Source Separation and Identification Using UAV-Embedded Microphone Array," in IEEE/RSJ International Conference on Intelligent Robots and Systems (IROS), pp. 1299–1304.
- [10] I. An, M. Son, D. Manocha, and S.-e. Yoon (2018), "Reflection-Aware Sound Source Localization," in IEEE International Conference on Robotics and Automation (ICRA), pp. 66–73, IEEE
- [11] L. Wang, R. Sanchez-Matilla and A. Cavallaro, "Audio-visual sensing from a quadcopter: dataset and baselines for source localization and sound enhancement," in IEEE/RSJ International Conference on Intelligent Robots and Systems (IROS), pp. 5320-5325.
- [12] L. Wang and A. Cavallaro (2017), "Microphone-Array Ego-Noise Reduction Algorithms for Auditory Micro Aerial Vehicles," IEEE SENSORS, vol. 17, no. 8, pp. 2447–2455.
- [13] L. Wang and A. Cavallaro (2020), "A blind source separation framework for ego-noise reduction on multi-rotor drones," in IEEE/ACM Transactions on Audio, Speech, and Language Processing.
- [14] A. Deleforge and W. Kellermann (2015), "Phase-optimized K-SVD for signal extraction from underdetermined multichannel sparse mixtures," in IEEE International Conference on Acoustics, Speech and Signal Processing (ICASSP) (pp. 355-359).
- [15] N. Mae, M. Ishimura, S. Makino, D. Kitamura, N. Ono, T. Yamada and H. Saruwatari (2017), "Ego noise reduction for hose-shaped rescue robot combining independent low-rank matrix analysis and multichannel noise cancellation," in International Conference on Latent Variable Analysis and Signal Separation (pp. 141-151). Springer, Cham.
- [16] T. Haubner, A. Schmidt and W. Kellermann (2018), "Multichannel Nonnegative Matrix Factorization for Ego-Noise Suppression," in Speech Communication; 13th ITG-Symposium, pp. 1-5.

- [17] A. Deleforge, A. Schmidt and W. Kellermann (2019), "Audio-motor integration for robot audition," *Multimodal Behavior Analysis in the Wild* (pp. 27-51). Academic Press.
- [18] A. Schmidt, A. Deleforge and W. Kellermann (2016), "Ego-noise reduction using a motor data-guided multichannel dictionary," in *IEEE/RSJ International Conference on Intelligent Robots and Systems (IROS)*.
- [19] A. Schmidt, H. W. Löllmann and W. Kellermann (2018), "A novel ego-noise suppression algorithm for acoustic signal enhancement in autonomous systems," in *IEEE International Conference on Acoustics, Speech and Signal Processing (ICASSP)*.
- [20] C. Rascon and I. Meza (2017), "Localization of sound sources in robotics: A review," *Robotics and Autonomous Systems*, vol. 96, pp. 184–210.
- [21] K. Nakamura et al. (2009), "Intelligent Sound Source Localization for Dynamic Environments," in *IEEE/RSJ International Conference on Intelligent Robots and Systems (IROS)*, pp. 664–669.
- [22] T. Ohata et al. (2014), "Improvement in Outdoor Sound Source Detection Using a Quadrotor-Embedded Microphone Array," in *IEEE/RSJ International Conference on Intelligent Robots and Systems (IROS)*, pp. 1902–1907.
- [23] K. Okutani et al. (2012), "Outdoor Auditory Scene Analysis Using a Moving Microphone Array Embedded in a Quadcopter," in *IEEE/RSJ International Conference on Intelligent Robots and Systems (IROS)*, pp. 3288–3293.
- [24] C. Knapp and G. Carter (1976), "The generalized correlation method for estimation of time delay," *IEEE Transactions on Acoustics, Speech, and Signal Processing*, vol. 24, no. 4, pp. 320–327.
- [25] F. Grondin, D. Létourneau, F. Ferland, V. Rousseau, and F. Michaud (2013), "The ManyEars open framework," *Autonomous Robots*, vol. 34, no. 3, pp. 217–232.
- [26] A. Deleforge, D. Di Carlo, M. Strauss, R. Serizel and L. Marcenaro (2019), "Audio-Based Search and Rescue With a Drone: Highlights From the IEEE Signal Processing Cup 2019 Student Competition [SP Competitions]," in *IEEE Signal Processing Magazine*, vol. 36, no. 5, pp. 138-144.
- [27] <https://github.com/Chutlhu/SPCUP19>
- [28] K. Hoshiba et al. (2017), "Design of UAV-Embedded Microphone Array System for Sound Source Localization in Outdoor Environments," *Sensors*, 17, 2535, pp. 1–16.
- [29] U. Saqib, J. R. Jensen (2019), "Sound-based Distance Estimation for Indoor Navigation in the Presence of Ego Noise", *27th European Signal Processing Conference (EUSIPCO)*, 1-5.
- [30] U. Saqib, S. Gannot, J. R. Jensen (2020), "Estimation of acoustic echoes using expectation-maximization methods", *EURASIP Journal on Audio, Speech, and Music Processing* (1), 1-15.
- [31] U. Saqib and J. R. Jensen (2020) "A Model-based Approach to Acoustic Reflector Localization with a Robotic Platform," in *IEEE/RSJ International Conference on Intelligent Robots and Systems (IROS)* [Accepted].
- [32] O. Ruiz-Espitia, J. Martinez-Carranza and C. Rascon (2018), "AIRA-UAS: an Evaluation Corpus for Audio Processing in Unmanned Aerial System," in *International Conference on Unmanned Aircraft Systems (ICUAS)*, pp. 836-845.
- [33] <http://dregon.inria.fr/datasets/the-spcup19-egonoise-dataset/>
- [34] <http://dregon.inria.fr/datasets/dregon/>



CidB

Centre d'information
sur le **Bruit**

QUIET DRONES
International e-Symposium
on
UAV/UAS Noise
Remote from Paris – 19th to 21st October 2020

**Scanning Laser Vibrometer measurements for assessing the
origin of structure borne sound in drones**

Florent Deux, Polytec France SAS, f.deux@polytec.fr

Jochen Schell, Polytec GmbH, j.schell@polytec.de

Summary

We report on a modal test for vibrations in the body of a drone, using an automated, robot-assisted version of a 3D scanning Vibrometer, leading to 3D deflection shapes of the full body over a broad frequency range. We furthermore show measurements of the deflection shapes of a rotating propeller, using a 1D scanning Vibrometer together with a Derotator to track the rotating blades.

1. Introduction

Vibrations produce sound. In order to develop quieter drones, the precise determination of the vibration behavior of the drone body and the propellers is a mandatory step. Scanning Laser Doppler Vibrometers have the potential to show the detailed surface vibration of the structure, on the complete visible surface, in all 3 directions, in a contactless way and across the entire needed frequency spectrum. Such measurements can therefore be used either directly for finding experimentally the zones of high vibration, important e.g. for finding a suitable position for an on-board camera. Or, even more important, they can also be used to validate and improve Finite Element (FE) simulations of the vibration behavior. If the FE model is first adjusted and then validated, design improvements towards quieter flight can be initiated via this model. This is also true for the vibrations of the rotating propellers, which are an important noise source. Using a so-called Derotator, the beam of a scanning Vibrometer follows the rotating blade and can also measure the deflection shapes of vibration over the entire frequency range of interest.

2. Test equipment

2.1 3D Scanning Vibrometer

A PSV 500 3D Scanning Vibrometer from Polytec GmbH was used for the vibration measurement of the drone body. With such a laser-based device complete 3D deflection shapes of complex surfaces can be measured. The PSV 500 3D uses Laser Doppler Vibrometry, an established method for non-contact vibration measurement [1]-[4]. Basically it is an interferometric method. If the emitted laser beam hits a vibrating surface, the backscattered light is modulated in its phase and frequency. By measuring this modulation, the movement of the point of impact of the laser beam is measured with very high precision. Depending on the frequency of the oscillation, displacement resolutions in the nm - pm range are possible.

In a scanning system a whole grid of measurement points is sequentially scanned with the help of deflection mirrors. This allows the representation of deflection shapes of complex surfaces with very high spatial resolution. The scanning process, the data acquisition and the visualization of the deflection shapes is done in the PSV software, which is an integral part of the system. Furthermore the system also contains a frequency generator, also integrated in the software, which can be used for vibration excitation. The PSV thus allows, for example, to excite a component to vibrations in a broadband manner, to scan the surface and then, immediately after the end of the measurement, to display the vibration modes for each excited frequency in an animated form.

Since coordinates are also stored for all points, this data can be exported and used for a numerical comparison with simulation data from finite element simulations.

With the 3D system used, each measurement point is not only measured along a single beam direction (1D vibration data), but with the help of 3 measurement heads with beams from 3 different directions. Thus 3D vibration data can be measured and visualized. More details about the operation of a 3D Scanning Laser Doppler Vibrometer can be found in [5].

The figure below shows the 3 measurement heads of a 3D Scanning Vibrometer. The scan mirrors that steer the beams to the desired positions are visible.



Figure 1: 3 measurement heads of 3D Scanning Vibrometer

2.2 RoboVib

With a 3D Scanning Vibrometer the 3D movement of all surface points which are reachable by all 3 measurement heads can be measured. The scanning range of the deflection mirrors is 50 x 40°. If points are to be measured which are outside the possible scanning range or which are shaded by other parts of the measurement object, the scanning heads mounted on tripods can be manually moved to another location from which these points can be reached. The new position is then taught-in. This makes it possible to combine the measurements from different views into one single result file. However, this is a manual process: the scan heads must be moved and the new position must be taught-in with the help of a new so-called 3D adjustment.

To facilitate and automate this process, an automated procedure for this has been developed: the use of a so-called RoboVib test bench. This is a combination of a 3D Scanning Vibrometer with industrial robotics from KUKA for positioning the measuring heads. The following picture shows the RoboVib test bench used.



Figure 2: RoboVib test bench at Polytec GmbH in Waldbronn.

When using the RoboVib system, a geometry teach-in has to be performed only once at the beginning of the measurement. When the measurement heads are repositioned by the industrial robot, the new position is exactly known by the robot encoders and the necessary new 3D alignment is calculated automatically. With this system an automated measurement of many different views of a complex 3D body is now possible.

The measurement sequence is therefore approximately as follows: First, the geometry data are acquired at 4 prominent points of the object to be measured and used for teach-in. Then a measurement grid is either imported if a simulation already exists, or successively generated for the visible area from each robot position. Then robot positions are taught-in manually, from which all measurement points can be reached step by step. The software automatically calculates which points can be reached best from which position. After a manual test of the robot program created in this way, a fully automatic measurement can then be started: the robot positions the measurement heads at the first position, loads the 3D alignment valid there and the set of points

that can be reached. The measurement is then performed on these points. When the measurement is finished, the robot moves to the next position, loads the 3D alignment and the points that can be reached, etc. until all points are measured.

2.3 Derotator

An important noise source of a flying drone are the rotating propeller blades. To assess this noise contribution, measurements at standstill are not fully sufficient. Measurements in operation lead to much more reliable data.

Using the Scanning Laser Doppler (SLDV) technique typically only continuous rotating objects like brake disks could be measured under rotation. On such continuous surface, besides brake disks also on belt pulleys or drive shafts SLDV's are routinely used. Segmented parts like propellers and rotor blades could not be examined under rotation and so only could be investigated using experimental modal analysis and measuring the frequency transfer function (FRF) for non-rotating conditions. The real excitation under operating conditions is quite different from a modal test at standstill and is moreover hard to simulate exactly. Stiffening effects by centrifugal forces also influence the result under working conditions. It is therefore mandatory to measure segmented parts in rotation.

With a special rotating optical unit whose rotation speed is synchronized to the object rotation it is possible to "derotate" the rotating object and measure the operational deflection shapes. The laser beam measuring the vibration of each scan point needs to follow a fixed position on such a rotating object.

As shown in figure 3 an external optical unit called "Derotator" is positioned in front of the standard SLDV sensor. In the Derotator a "Dove Prism" rotates with half the rotational speed of the rotating object to let the object seem to stand still for the SLDV sensor head.

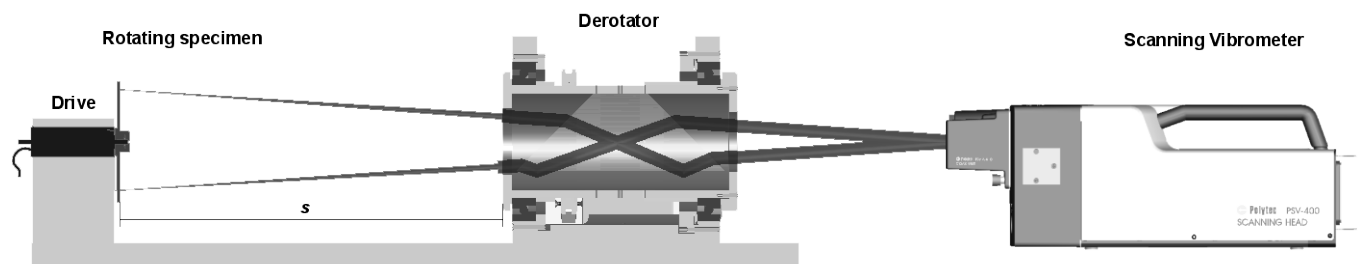


Figure 3: Principle of derotating a rotating specimen using an external rotational unit called "Derotator"

The central element of the derotator is the rotating Dove-Prism, whose RPM is controlled and adjusted by a rotary encoder. By rotating the Dove-Prism in the Derotator about 90° the image of the object gets rotated by 180° . To synchronize the rotational unit of the Derotator with exactly half the object RPM a PID controller is used. By processing an external encoder signal from the object and the internal encoder signal from the internal driving motor of the optical unit the PID controller delivers a certain voltage to the drive motor to set the Derotator RPM. With this setup, constant RPMs and also high accelerations as in run-ups can be synchronized and scanning vibration measurements can be performed as for objects at standstill.

More details on the Derotator setup can be found in [6].

3. Vibration modal test of drone body

To predict noise that originates from structural vibrations of a drone body, extensive FE simulations are performed. As drones have a complex shape and are mainly made of novel lightweight material, these FE simulations absolutely need to be verified against real test results,

a so-called FE model correlation has to be done. One important step in this process is to simulate the Eigen-Modes at standstill by FE, then perform an experimental vibration modal test, extract modes from the test results by curve fitting and correlate the modes from simulation and test. The FE model can then be updated, until the FE modes are in satisfactory agreement with the experimentally determined “true” modes.

As the drones are made of lightweight material, typically the mode shapes at acoustic frequencies are already quite complicated, hence the need for a spatially well resolved measurement. Classical accelerometers can hardly be used for this purpose as a large number of these would be necessary and their weight and damping would alter the true vibration behaviour. Therefore, a robot assisted 3D Scanning Vibrometer, as described above, is used to measure the resonance deflection shapes in a non-contact manner with the required high spatial resolution.

3.1 Modal test setup

Figure 4 shows the used setup. The drone body is suspended with soft rubber strings to be close to free-free conditions, often used in simulations. Its vibration response is excited by an electro-dynamical shaker, connected to the drone body via a thin beam, a so-called stinger, and the input force measured with a force transducer. The 3D SLDV on its robot arm is moved all around the structure to measure the entire deflection shape from all surfaces.

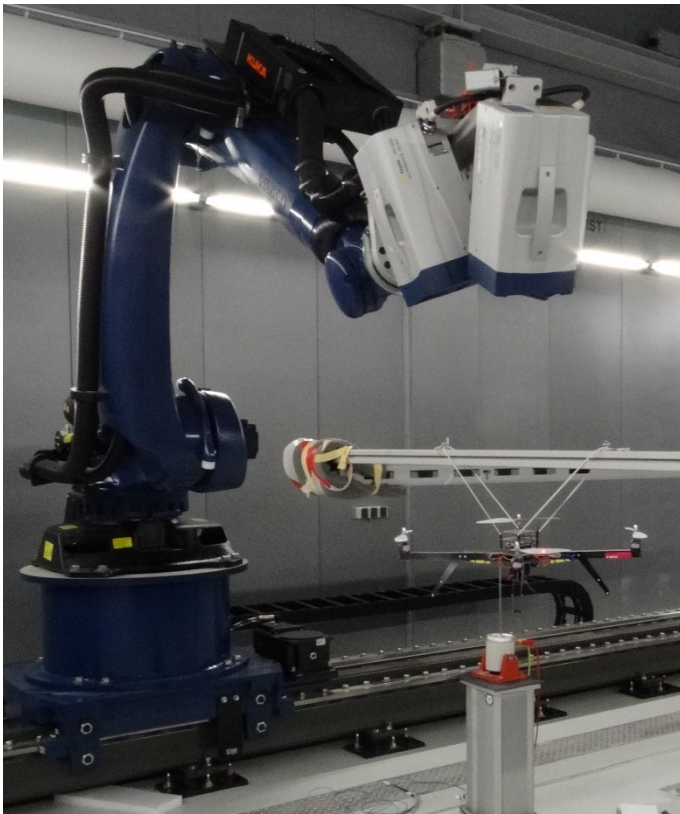


Figure 4: modal test setup with RoboVib, suspended drone body and excitation shaker.

3.2 Results

During the measurement, a full set of transfer functions (surface velocity as a result of the input force) for all points is acquired. The software displays the corresponding deflection shapes as a function of frequency by simply selecting a frequency from the FRF spectrum. Figure 5a and b shows 2 of the acquired deflection shapes, together with their position in the spectrum, indicated by the vertical cursor lines. The deflection shapes of the blades and the supporting beam

structure is clearly visible. Due to the high point density and the non-contact nature of the measurement, a very detailed and undisturbed study of the deflection shapes is possible.

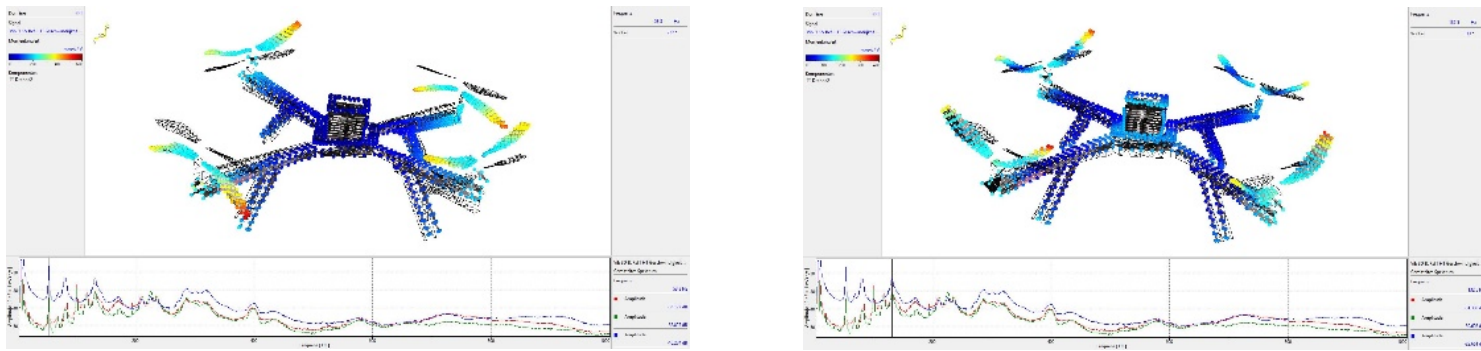


Figure 5 a and b: 2 example deflection shapes measured with the setup above.

These data are a very good base for a subsequent modal analysis, which will then be used for FE model correlation and –updating. The result is then an updated FE model which predicts the vibration behaviour with high confidence.

4. Vibration measurement of rotating propeller blades

The vibration behaviour of the rotating blades is obviously a large contribution to the observed noise of a drone. Measurement of this vibration behaviour as close to operation conditions as possible is therefore a crucial step, when assessing noise from a drone. The first step is a modal test at standstill and correlation to FE models, as described above. Nevertheless, for the rotating blades, this is not sufficient. The rotation itself changes the behaviour due to centrifugal forces and the interaction with the air flow is not an easy task in modelling. Further effects like mode splitting for rotating parts complicate this task even further. Therefore, additional measurements in rotating conditions are very beneficial for the accuracy of models.

Rotating blades can be measured with scanning vibrometers when using an accessory called “Derotator”. This device keeps the measurement beam on a fixed location on the rotating blade, therefore enabling the measurement as if the blade was non-rotating. Hence the name Derotator.

4.1 Derotator Setup

The figure below shows a typical setup of a scanning vibrometer together with a Derotator, as used for the tests described here. The scanning head sits on an adjustable table and looks through the blue box in front of it, which contains the rotating prism. The prism rotates with exactly half the speed of the rotating object, keeping the beam on a fixed location on the blade. Furthermore, a reference laser (the smaller head on the adjustable table) is also coupled into the prism. Its beam stays therefore on a fixed position on the blade, while the beam of the scanning head scans through all the measurement points sequentially. The single point laser head serves as the needed phase reference for animation of the deflection shapes. The adjustable table is needed, as the position tracking via the prism only works for exact coaxial alignment of the beam path with the rotation axis of the blades.

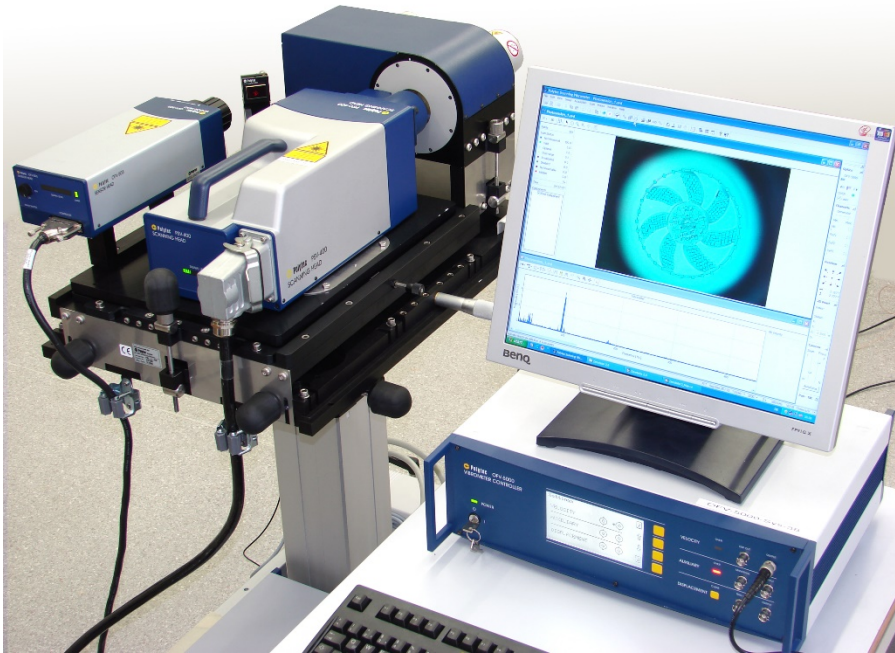
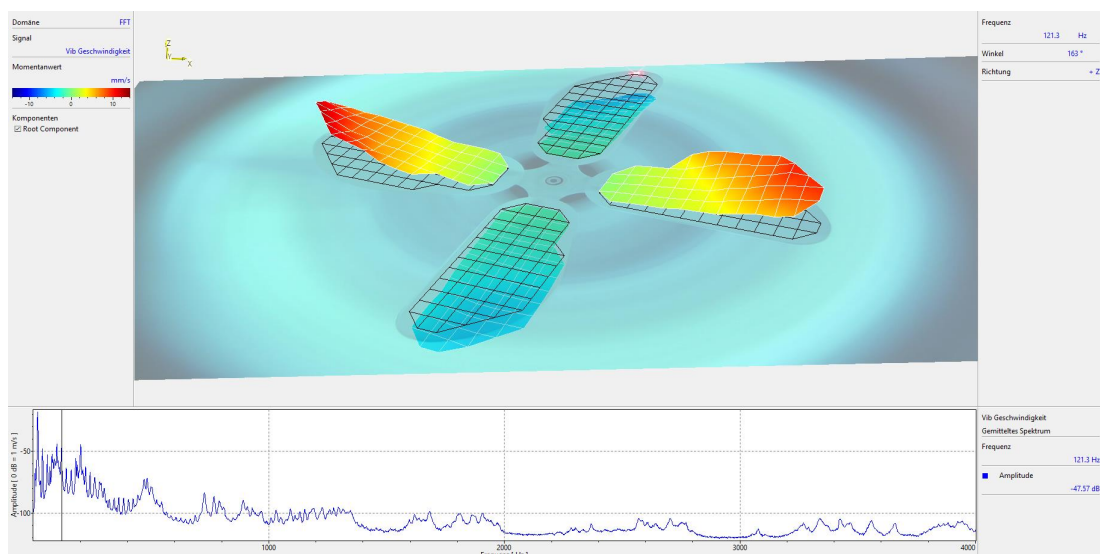


Figure 5: Derotator Setup

Once the axis of the prism is aligned to the axis of the rotating shaft and the RPM is synchronized via the 2 rotary encoders, the scanning beam steps through the points like for a non-rotating object while the beam of the single point Vibrometer serves as the phase reference for the animation of the acquired deflection shapes.

4.2 Results

The following figures show 2 example deflection shapes that have been acquired on a rotating propeller. The cursor position defines again which frequency is selected for the animation. In the first picture at the top, a bending shape is clearly visible, in the second one below a torsion shape of the blades can be seen at a slightly higher frequency.



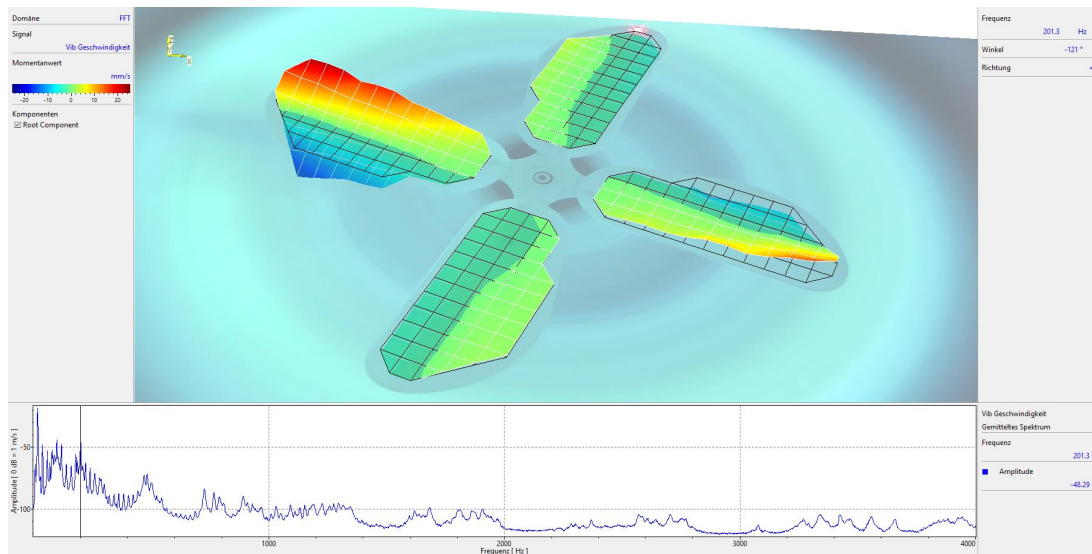


Figure 6: Example deflection shapes obtained by Derotator measurements

5. Conclusions

To assess the origin of drone noise, 2 kinds of tests have been performed: a modal test of the drone body for correlation and updating of FE models and a direct vibration measurement of deflection shapes of rotating blades. For the modal test, a robot-assisted 3d Scanning Vibrometer has been used, for the tests on the rotating blades a scanning Vibrometer together with a Derotator for tracking the blades have been used.

Both tests measure the vibration behaviour with excellent spatial resolution over the entire frequency range of interest.

In the modal test, detailed deflection shapes have been acquired that are the basis for a detailed correlation with a FE simulation model, leading to an improved model that can be used for predicting the vibration behaviour of drones under different conditions.

The measurement of the rotating blades also lead to spatially well resolved deflection shapes under real load conditions without influencing the behaviour of the sample. As modelling of the blades under real load conditions is a difficult task, such data is precious for improving the quality of the underlying models or also for direct trouble shooting of prototypes.

References

- [1] Drain, L (1980) *The Laser Doppler Technique* Wiley
- [2] Lewin, A (1985) *Non-contact surface vibration analysis using a monomode fiber optic interferometer* SCI. Instrum. Vol, 18
- [3] Lewin, A (1988) *Introduction to interferometric Measurement Systems*
- [4] Stoffregen, B and Felske, A (1985) *Scanning Laser Doppler Analysis System* SAE paper, series 850327
- [5] Johansmann, M and Sauer, J (2005): A new tool for three- dimensional non-contact vibration measurements in automotive applications, SAE Paper No. 2005-26-052
- [6] Johansmann, M, Fritzsche, M and Schell, J (2011) *A new method for measurement of rotating objects utilizing Laser Doppler Vibrometry combined with an optical Derotator with focus on automotive applications* SIAT conference paper



CidB

Centre d'information
sur le Bruit

QUIET DRONES
International e-Symposium
on
UAV/UAS Noise
Remote from Paris – 19th to 21st October 2020

Commercial Delivery Drone Routing: A Case Study of Noise Impacts

Eddie Duncan, RSG, Eddie.Duncan@rsginc.com

Kenneth Kaliski, RSG, Kenneth.Kaliski@rsginc.com

Isaac Old, RSG, Isaac.Old@rsginc.com

Erica Wygonik, RSG, Erica.Wygonik@rsginc.com

Justin Culp, RSG, Justin.Culp@rsginc.com

Summary

Many efforts are underway to understand the efficiency, climate impact, and privacy issues surrounding the routing of commercial drone deliveries from central distribution centers, and while potential noise impacts are a notable concern, only now are we starting to quantify them. This paper uses a case study to explore the use of community noise mapping as a tool to reduce noise impacts by optimizing flight routes to both increase sound masking and reduce population exposure to noise. The primary purpose of this paper is to explore a methodology using sound propagation modeling of drones coupled with existing community noise maps and background sound level data to assess various flight route options and flyover and hover levels in the context of a residential neighborhood.

The case study considers four different routing scenarios and, as discussed in Section 3.3, finds that routing options over undeveloped lands and waterways result in the lowest overall exposure of drone noise to the case study population, but that routes over higher populated areas following roadways may result in lower impacts due to masking by traffic noise. The case study also considers the short-term sound exposure of individual flyovers and hovering for delivery. For flyover levels, when compared to background sound levels for different areas, as discussed in Section 3.1, flight path setbacks may be established to reduce potential impacts to residential areas.

1. Introduction

Unmanned aerial vehicles (UAVs) and systems (UASs), or what are commonly referred to as drones, are being used commercially in such applications as package delivery and point-to-point medical product delivery. For example, Wing has developed pilot programs for package delivery in Australia, Finland, and the U.S., and United Parcel Service's UPS Flight Forward has a pilot program with the WakeMed Hospital campus in Raleigh, North Carolina, U.S. to deliver urgent medical supplies between hospital campuses.

Given the success of these pilot projects, there is an expectation that these systems will achieve widespread adoption. For example, some municipalities are planning for "drone highways" to manage aerial traffic congestion and to improve safety. However, just as noise from ground-based highways is a planning consideration, the impacts of drone highways on the communities below should also be considered in the planning process.

This paper discusses strategies for reducing noise impacts on communities by adopting existing noise mapping techniques to site drone delivery paths. These strategies assume drone operations originate from a single depot outside an urban core and are routed in various ways to residential destinations. Four main routing strategies are investigated:

- 1) Straight line – The shortest path from the depot to the destination. While this route is the most efficient for drones due to travel distance and other related factors, drones may fly over residential communities with low ambient sound. In addition, homes below well-used paths, such as from a hospital to a clinic, would have outsized impacts.
- 2) Corridors over existing highways – From the depot, drone corridors are created over existing highways. While population density over these corridors is relatively high, the ambient sound is also high, maximizing the masking of drone sound.
- 3) Corridors over undeveloped land – From the depot, drone corridors are created over power lines or waterways before spurring off to delivery locations. These areas have the least human activity and would thus result in lower noise exposure. However, these areas also have the lowest ambient sound level, so drone sound is the least masked.
- 4) Corridors over industrial and undeveloped land – From the depot, drone corridors are created over railways before spurring off to delivery locations. Often passing through industrial areas and undeveloped land, railway corridors may result in lower noise exposure, and may have varying degrees of masking along the corridor.

2. Method

The approach taken in this study is to use existing sound modelling used for community noise mapping and adapt it to drone noise to assess the level of sound and the degree of masking from background sound associated with drone use. As such, to the extent practical, existing commercial software and methods are relied upon. These are described below.

2.1 Sound Propagation Modelling

The framework for sound propagation modelling was the Chittenden County Noise Map, which encompasses the urban core of Burlington, Vermont, U.S. (Kaliski, 2005; Cowan & Kaliski, 2006; Kaliski, Duncan, Cowan, 2007; Kaliski 2019). The sound map includes traffic and rail noise, but it excludes aircraft noise. The model is based in the Cadna/A software package, produced by Datakustik, GMBH. The resulting sound is the annual average daytime equivalent continuous sound level during the day (L_d).

The Chittenden County model has been validated to both daytime and night-time sound levels; however, this work assumes only daytime drone operations will occur. The daytime sound levels from the model are further broken down into 1/3 octave bands using actual monitored

sound levels at various locations throughout the county. The locations were representative of three categories of areas where residences may be located and are generally described as:

1. Busy Road
2. Suburban Neighbourhood
3. Rural Residence

The 1/3 octave band sound levels from these areas are used as the background sound levels for the masking analysis.

2.2 Drone Sound Emissions

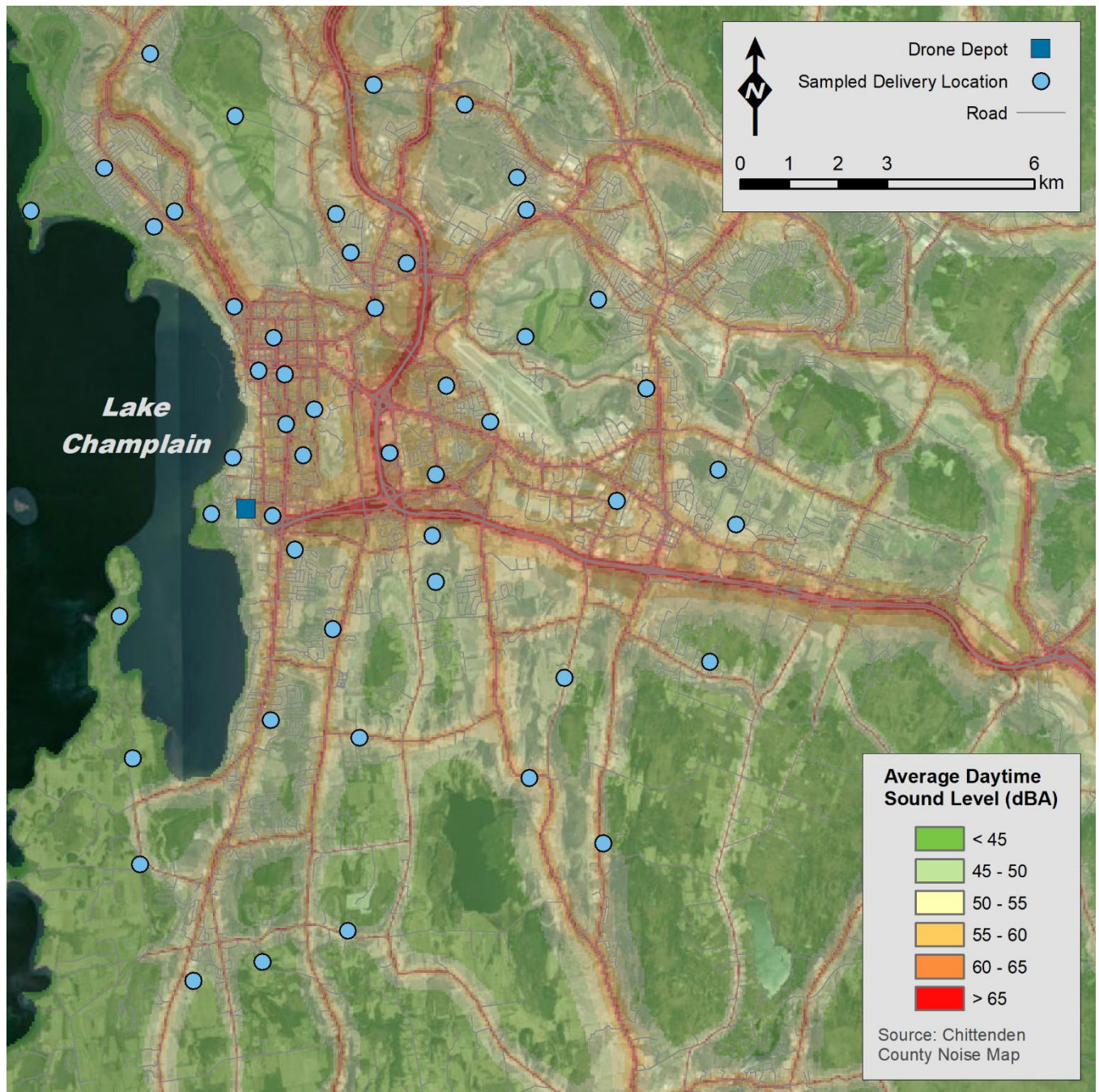
Sound emissions for the modelled drone was provided by W. Nathan Alexander, an assistant professor at Virginia Polytechnic Institute and State University. The drone captured in the measurements is the DJI Matrice 600 Pro. This drone is a commercial grade hexacopter (six rotors) with a total unloaded weight of about 10 kg and a diameter of about 1.67 meters. Both flyover and hover data were used. Hover data was measured with the drone at an elevation of 9.14 meters, and the hover data was measured with the drone at an elevation of 7.5 meters. This data was then used to calculate sound power levels for model inputs.

More details about the measurement methodology can be found in Virginia Tech's 2019 InterNoise paper (Alexander and Whelchel 2019).

2.3 Flight Routes

The first step in choosing flight paths is to establish the location of the drone depot from which deliveries will originate. Given no commercial drone delivery service is currently available in Chittenden County, the authors chose a depot location for use in this study. The criteria were a location within flying distance to residences, near a highway network to support stocking the depot, and within an existing industrial area. A map of the study area, showing the chosen drone depot and the background L_d , is shown in Figure 1.

Once the depot location was chosen, routes were developed from the depot to a sample of 50 delivery locations at residences within 12 kilometers of the depot. The drone was assumed to travel vertically from the hub to a height of 61 meters, then along the given route, at a speed of 113 kilometers per hour, to the destination where it would drop to 7 meters and hover for 60 seconds. While delivery routes were only modelled to a sample of 50 residential locations spread throughout the study area, for the purposes of evaluating the relative magnitude of noise exposure of the route options, sound levels from drone flight and deliveries were evaluated at over 26,000 residential addresses within the study area. For a specific delivery application, actual distribution delivery locations may differ. For example, there may be clusters within a specific region where more deliveries occur than in other areas. The purpose of modelling over 26,000 residential addresses was not to produce an accurate sound level projection for a specific neighbourhood or receptor, but rather to provide a general means of comparing the relative magnitude of noise exposure for different routing options in a region.



Service Layer Credits: Source: Esri, DigitalGlobe, GeoEye, Earthstar Geographics, CNES/Airbus DS, USDA, USGS, AeroGRID, IGN, and the GIS User Community

Figure 1: Study Area Map & Daytime Background Sound Levels

Four sets of routes, shown in Figure 2, were considered including:

- Direct routes, shown in orange, from the depot to the 50 delivery locations,
- Roadway routes, shown in red, following most direct roadway paths along major roads,
- Waterway routes, shown in blue, using Lake Champlain as a low-population corridor with spurs, and
- Railway routes, shown in yellow, using the railway as a low-population corridor with spurs.

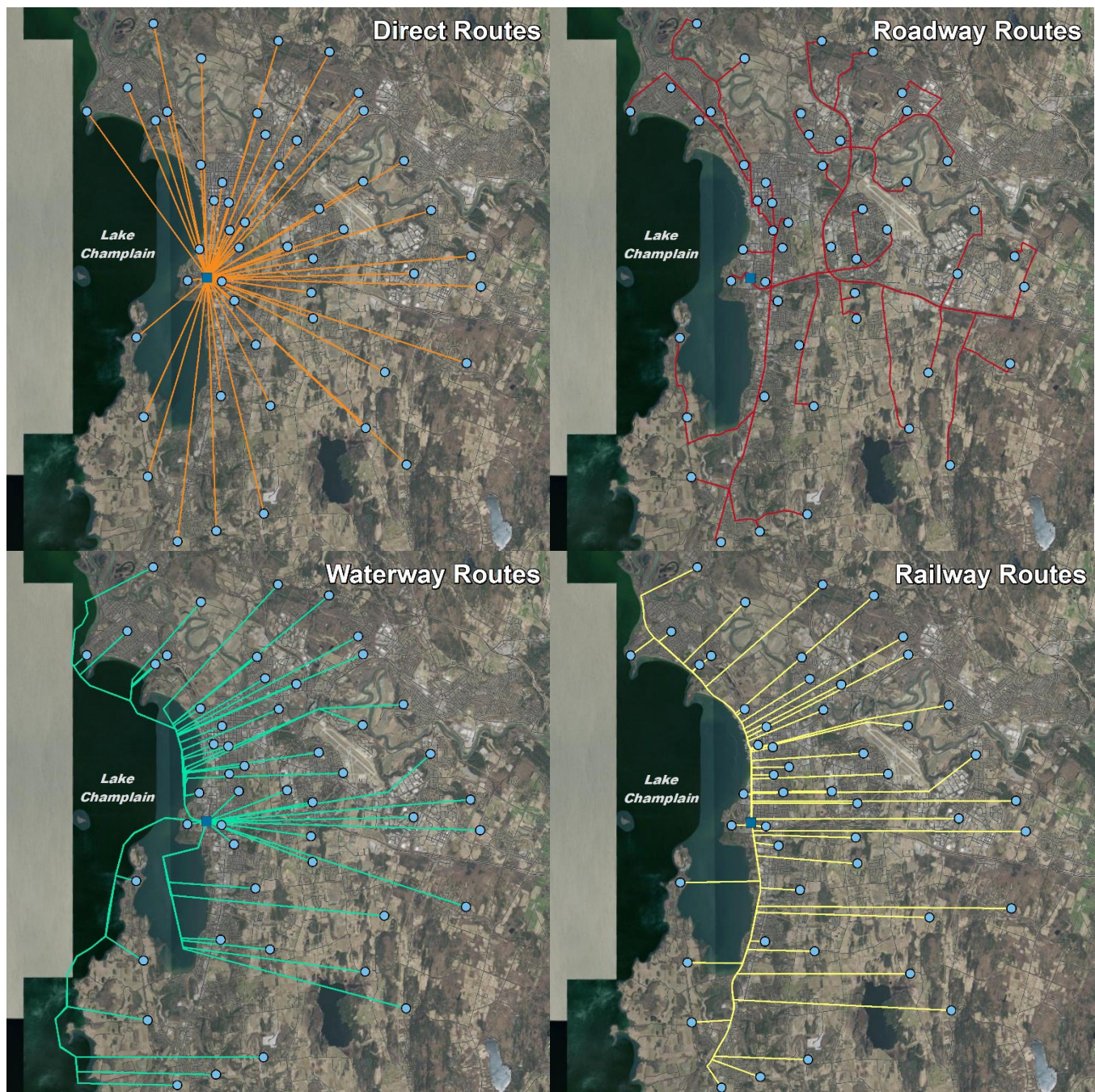


Figure 2: Maps of Evaluated Drone Routes

3. Results

The model was used to evaluate sound levels in a variety of ways as a means of comparing route options including short-term flyover levels, short-term levels due to hover delivery, and average hourly sound levels. These results are reported in the following sections.

3.1 Flyover Sound Levels

Flyover sound levels are dependent on the sound emissions of the specific drone being used for delivery service. The sound generated from any drone are related to several factors including rotor speed, number of rotors, and blade design, among others. In addition to sound emissions, speed, elevation, terrain, and distance from flight path are also variables that will affect the flyover level at any given receptor. The results in this section are only representative of the hexacopter data and flight path elevation used in this case study.

Figure 3 provides a comparison of modelled flyover levels with background sound levels for different representative areas within Chittenden County. The distance listed for each flyover represents the horizontal distance between the receptor and the flight path which is 61 meters above grade. The background sound level ranges represent the L_{90} up to the L_{10} for a given representative area. For example, the daytime background for a residence in a “Busy Road” area ranges from 48 dBA (L_{90}) to 57 dBA (L_{10}), while the daytime background for a residence in a “Rural” area ranges from 33 dBA (L_{90}) up to 43 dBA (L_{10}).

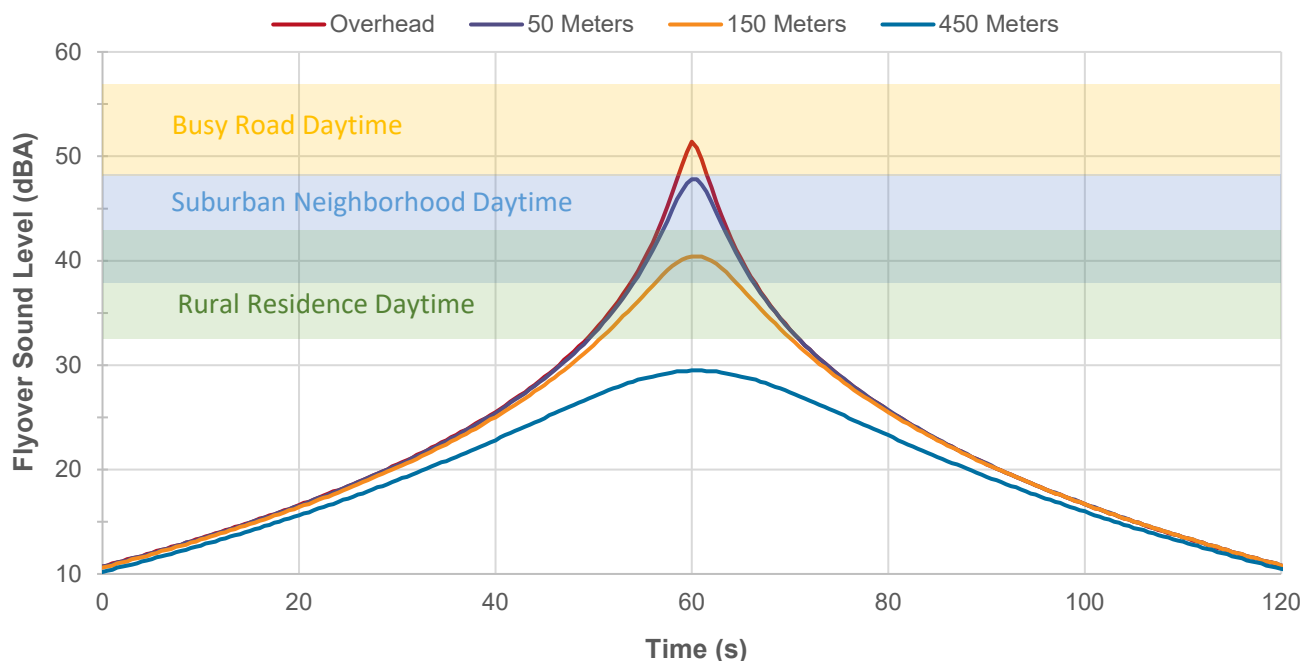
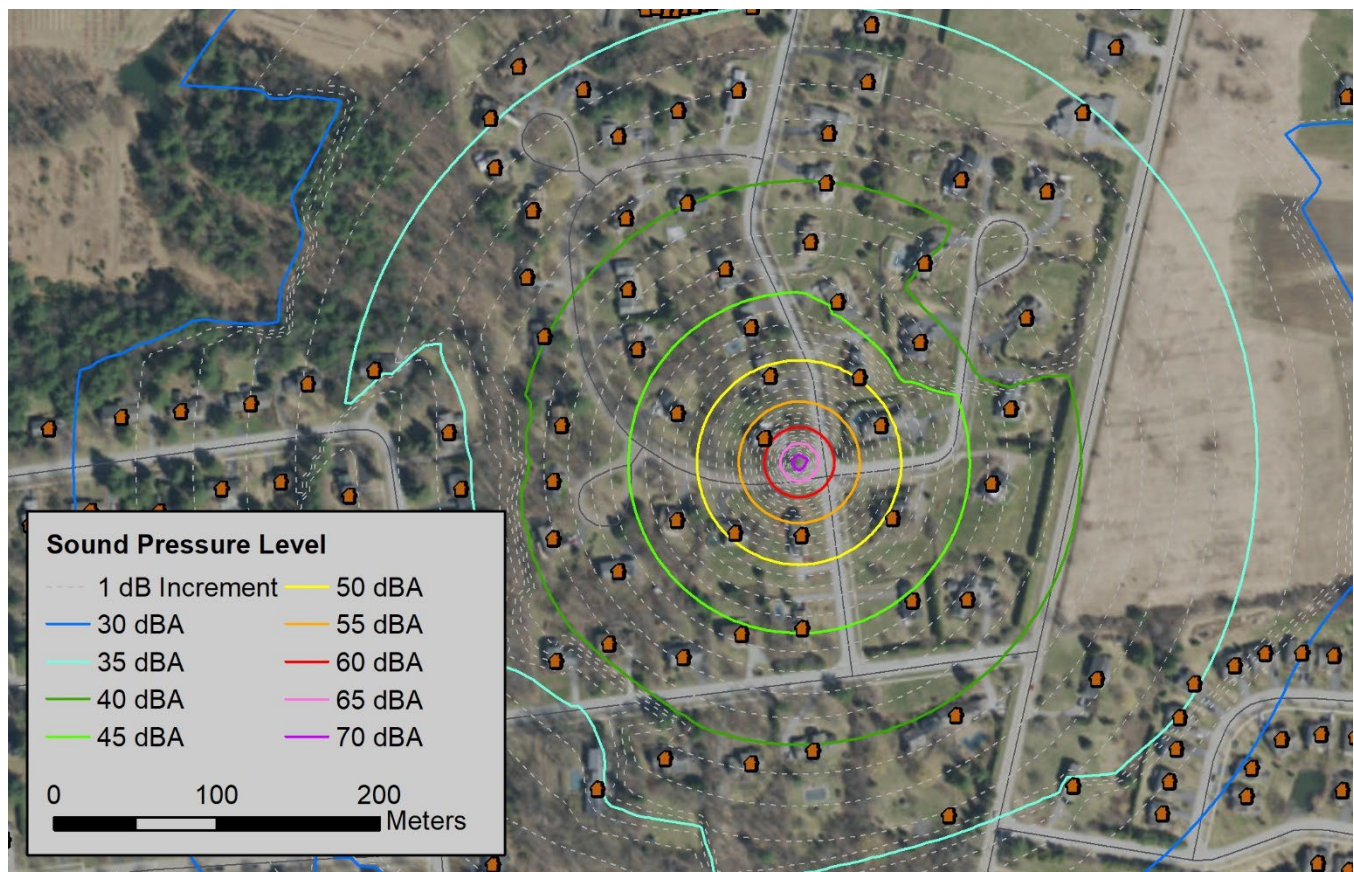


Figure 3: Graph of Flyover Sound Levels Compared to Background Sound Levels in Different Areas of Chittenden County by Horizontal Distance between the Receptor and the Flight Path

As shown in Figure 3, a flyover directly overhead results in a sound level of 51 dBA at ground level which would likely be clearly audible at a rural residential location and suburban neighbourhood area and noticeable some of the time in a busy roadway area. A horizontal route setback of approximately 150 meters is needed before the flyover level is reduced to 40 dBA, and a horizontal route setback of approximately 450 meters is required before to reduce the flyover level to 30 dBA.

3.2 Hover Levels

In this case study, as a drone approaches the delivery location, it reduces its altitude to 7 meters above grade, hovers, and lowers the package for delivery. Given the potential proximity of residential receptors to the delivery point, hover delivery results in the highest sound exposure for a given receptor. As shown in Figure 4, depending on the distance between receptor and a drop point the sound level during delivery could range between 60 and 70 dBA for the receiver of the package. Sound levels throughout a residential neighbourhood will vary during delivery depending on the spacing and density of the residential area. A nextdoor residence at 35 meters would be exposed to sound levels in the range of 55 dBA, while further residences, out to 120 meters, would experience sound levels between 45 and 55 dBA in areas that are not shielded by building structures.



Service Layer Credits: Source: Esri, DigitalGlobe, GeoEye, Earthstar Geographics, CNES/Airbus DS, USDA, USGS, AeroGRID, IGN, and the GIS User Community

Figure 4: Map of Sound Levels due to Hovering during Delivery

3.3 Masking of Overhead Passbys

Negative community reaction to drone noise is, to some extent, a function of audibility. That is, audibility precedes annoyance in most cases. Thus, if the background sound masks the drone sound, the drone will not be audible and will probably not be annoying due to noise.

Since the drone sound is largely characterized by tones generated by the rotation of the blades, the primary concern is with the audibility of those tones, as they will stand out from the largely broadband background sound. The proper calculation of audibility of tones is complex and can be described in such standards as ISO 1996-2, IEC 61400-11, and ANSI S1.13. These standards use narrowband measurements of the sound with the tones. ANSI S12.9 Parts 3 and 4 also provide simplified analysis approaches to determine whether a tone is prominent and discrete using 1/3 octave bands.

This paper is a demonstration of methods, but sufficient narrowband data from a representative delivery drone is not available to conduct a full analysis. However, we provide a simple analysis of the masking using 1/3 octave bands.

Figure 5 charts the 1/3 octave bands from a drone passby at 61 meters above the ground by 1/3 octave bands. The top line is the drone sound power level. Note the presence of tonal prominences at 100 Hz, 1 kHz and 6.3 to 8 kHz. The greatest prominence occurs at the higher frequencies between 6.3 and 8 kHz, rising 23 dB above the 5 kHz band. The darker blue line shows the sound pressure level of the zone passby from an observer on the ground. We see that the high frequency tones are diminished, largely due to atmospheric absorption, which is more efficient at high frequencies. In this case, the difference between the 5 kHz and 8 kHz sound pressure level is 11 dB. In contrast, the low frequency tonal prominence at 100 Hz is

less effected by atmospheric absorption and rises about 14 dB above its neighbouring 1/3 octave bands.

The dashed lines of Figure 5 show the sound pressure level (daytime L₅₀) of representative background sound monitoring locations in Chittenden County. These locations include busy road, suburban, and rural soundscapes. They all are low-frequency dominated and lack tonal prominences. As shown, the drone sound is largely masked by the busy road background sound, except in the higher frequencies above 2 kHz. Even then, the tonality of the drone sound is reduced, since the tones are partially masked by the background sound. However, there is less masking in the suburban example, and almost no masking in the rural example.

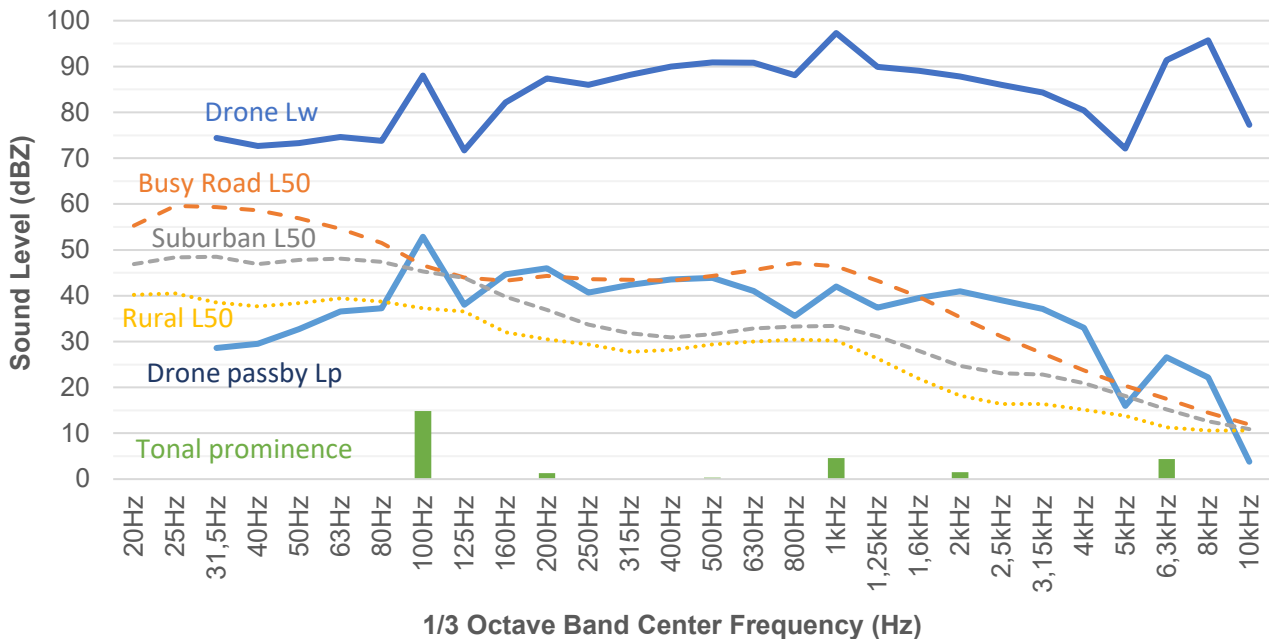


Figure 5: Maximum Passby Sound Level (L_p) Compared to Background L₅₀, Drone Sound Power Level (L_w), and ANSI S12.9 Part 4 Tonality of a Drone Passby

This example points out the potential for effective masking of drone sound by routing delivery corridors over existing ground highways and the potential impacts to audibility of broadband and tonal sound from drones over less populated areas.

3.4 Flight Route Comparisons

For each flight route scenario, an average hourly sound level was modelled for over 26,000 residential receptors accounting for take-off from the hub, a round trip flight from the depot to the 50 delivery locations, and hovering at the delivery location. Full implementation of a delivery service could involve a greater number of round-trip flights and delivery locations resulting in higher average hourly sound levels than what were modelled in this case study, and a specific delivery service may result in clustering of deliveries to certain areas. Nonetheless, the average hourly sound level of the spatially sampled delivery locations serves as a suitable metric for evaluating the relative magnitude of noise exposure of the routing options. It is important to note, however, that this analysis is specific to the Chittenden County case study area. Flight path comparisons will vary under different land use planning regimes. Different areas may also have different densities of roadways, waterways, residences, and railways, affecting which routing schema will result in different average sound levels.

The distribution of average hourly sound levels for all receptors is provided in Figure 6. Given that much of the flight path was over uninhabited area, the routing option with the lowest average hourly sound level across all receptors was the Waterway Routes at 18.9 dBA, but

there would likely be fewer sources to mask drone sound for recreational users of the lake. The Direct Routes scenario had the second lowest average hourly sound level of 19.1 dBA across all receptors. This result is likely due to many of the flight paths being over large plots of undeveloped land and over sections of the lake in some cases. The Roadway and Railway Routes resulted in very similar average hourly sound levels across all receptors, 20.1 dBA and 20.2 dBA, respectively. The higher levels for the Roadway Routes are reasonably expected given the proximity of residential development to roadways. The higher results of the Railway Routes may be less expected, but given that there are residences within 40 meters of the railway particularly in the northern portion of the case study area, and that many of the Railway route spurs involve flight over more populated portions of the city to reach western delivery locations, the results are reasonable.

While the Roadway and Railway Routes resulted in higher levels at a greater number of residences, these results do not necessarily indicate that those options would result in higher impact. As discussed in the previous Section, those routes may result in higher masking which could reduce the potential impact.

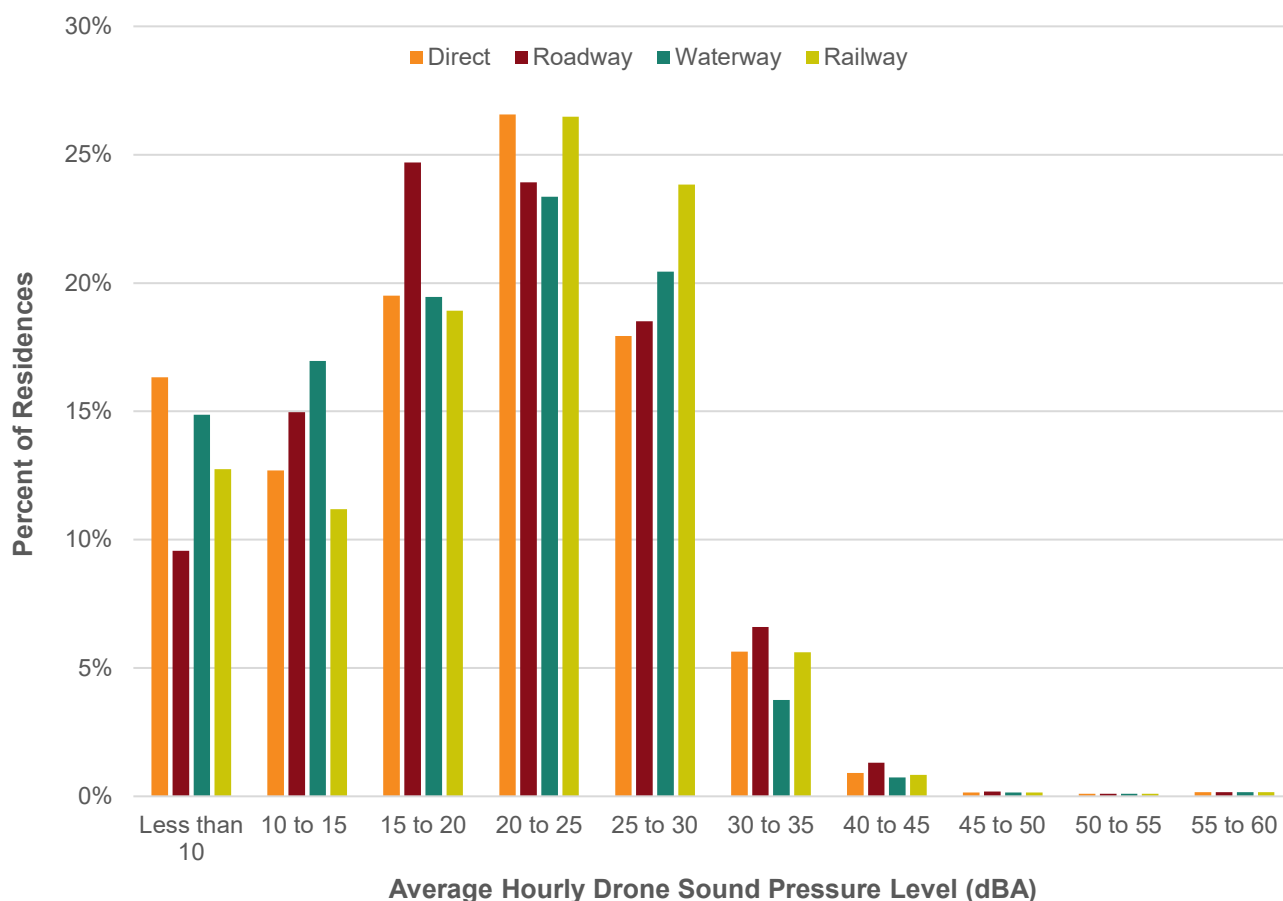


Figure 6: Distribution of Average Hourly Sound Levels across All Case Study Residences

4. Conclusions

This case study explored a methodology using sound propagation modelling coupled with existing community noise maps and background sound level data to assess various flight route options and short-term flyover and hover levels in the context of residential package delivery. Four different routing options were assessed for a hypothetical drone depot located in an

industrial area at the edge of an urban area in Chittenden County, VT, U.S. These routing options included Direct, Roadway, Waterway, and Railway Routes.

Given the location of the drone depot, the Waterway and Direct Routes were found to result in the lowest overall sound exposure at residential receptors, but the Roadway Routes provide more masking, at least along busier roadways. Path routes could be further randomized to reduce impacts. This would be especially useful near the drone depot or where the same source/destination pair are used frequently, such as between a hospital and clinic. While the randomization would not reduce the sound from single flyover events, it does reduce the compounded daily noise exposure. This strategy was reportedly successfully used by Wing (a subsidiary of Alphabet, Inc.) in a pilot project in Canberra, Australia, in response to complaints from residents who live near the hub (Nagle, 2020).

For sound levels from individual flyovers, if passing directly overhead, the drone in this study would likely be clearly audible at a rural residential location and suburban neighbourhood area and noticeable some of the time in a busy roadway area. For a route that is setback horizontally at a distance of 150 meters, the drone would likely be clearly audible in a rural residential location, noticeable in a suburban neighbourhood area, but masked in a busy roadway area. At a horizontal setback of 450 meters, the overall sound level of a flyover is reduced to 30 dBA which would be masked in busy roadway and suburban areas and likely masked in a rural residential area.

Similarly, we evaluated tonal audibility of a passby event using a simple evaluation of 1/3 octave bands of an example drone and background soundscapes. For an overhead passby, the low, and mid frequency tones generated by the drone are masked completely or almost completely by a busy road. However, the high frequency tones are only partially masked. For suburban and rural soundscapes, there is much less masking of tones, and these would thus be expected to be more highly audible. This type of analysis can be done more effectively using narrowband analysis, but for this type of analysis to be conducted, the quality and quantity of sound information provided by drone manufacturers needs to be markedly improved. Currently, as there are few noise regulations that drones are subject to, there appears to be little incentive to drone manufacturers and delivery companies to provide this information.

Assuming a drone depot is not located within a residential area, the highest noise exposure, although relatively short in duration, is likely to occur while hovering during package delivery. This is the point at which the drone would be closest to residential receptors. While a function of density in a residential area, the representative delivery presented in Section 3.2 resulted in 11 residences above 45 dBA and 4 residences above 50 dBA. This is above the background sound levels in the suburban neighbourhood which generally range from 38 to 48 dBA.

There are several opportunities to improve and expand upon this case study including:

- Using more detailed sound emissions data for a variety of package delivery drone models.
- Investigating different flight route elevations, hover elevations, and speeds.
- Accounting for expected delivery distribution for specific applications where deliveries may be more clustered in some areas than others.
- Developing more detailed customized routes that focus on hybrid routes over uninhabited working landscapes and zones where masking is likely to occur.

With these improvements, noise mapping can be a powerful tool to quantify and mitigate noise impacts from drone delivery. Indeed, these tools can also be used for other advanced aviation initiatives such as the siting of air taxi depots and their routing.

References

Alexander, W. N. and Whelchel, J. "Flyover Noise of Multi-Rotor sUAS." *Internoise 2019*. June 2019.

Cowan, J. and Kaliski, K. "Tools for Expedited Regional Transportation Noise Mapping," Presented at the *Transportation Research Board Summer Meeting*, 2006.

Kaliski, K. "Using Transportation Demand Models to Assess Regional Noise Exposure," *Proceedings of the 2005 Institute of Noise Control Engineers NOISECON 2005*.

Kaliski, K., Duncan, E., and Cowan, J. "Community and Regional Noise Mapping in the United States," *Sound & Vibration Magazine*, Vol. 41 No. 9, September 2007.

Kaliski, K., "Practical Uses of Transportation Noise mapping in the U.S." presented at the Transportation Research Board annual meeting, January 2019

Nagle, M., "We're with the IPP and We're Here to Help," panel discussion during U.S. Federal Aviation Administration UAS Symposium, August 18, 2020.

Acknowledgement

Thank you to W. Nathan Alexander and Virginia Tech for sharing the sound level data from their hexacopter measurements. Publicly available detailed sound level data on drones that could be used for package delivery is sparse, and we appreciate their assistance.



QUIET DRONES
International e-Symposium
on
UAV/UAS Noise
Remote from Paris – 19th to 21st October 2020

Acceptance of drone delivery is limited (not only) by noise concerns

Hinnerk Eißfeldt
DLR German Aerospace Center, Department of Aviation and Space
Psychology, Hamburg, Germany.

Summary

In recent years, civil drones have become increasingly present in the media and in everyday life. There has been a high level of interest in drone delivery from the very beginning, yet public acceptance of drone delivery still seems limited, with acceptance rates usually ranging from 30 to 40%. The present paper reports findings of a representative national study about the acceptance of civilian drones in Germany. Several factors limiting the support of drone delivery are identified, such as concerns about transport safety, noise, and animal welfare. In addition, effects of drone experience are discussed, showing all areas of concern being reported at higher rates by participants who had no prior experience with civil drones. For noise concerns however, a more detailed look into the kind of experience with drones revealed a significantly higher percentage of noise concern among those who reported having heard a drone compared to those who reported that they had not. Moreover, an effect of NIMBYism is confirmed in the context of drone delivery. Even residents who envision using drones for the delivery of their own parcels frequently report that they would not agree to flights over their own homes. This particular effect is termed NOMOH ('Not Over My Own Home'). Finally, the need for regulation is discussed, as well as potential measures to increase acceptance of drone delivery. Besides defining topographical conditions, urban areas and time restrictions, installing means of noise control or providing residents with tools for participatory

noise sensing can also be viable measures to increase public support. If the acceptance level among residents remains in the range of below one third, drone delivery will not become a successful service in Western cities.

1. Introduction

Drones are becoming increasingly visible in public perception. Applications range from parcel delivery to animal welfare, from the production of live images of major events to law enforcement, and from the inspection of industrial facilities to the design of artificial fireworks. Many drone applications, such as precision farming, are considered to have high potential for conserving resources, and drone technology often is regarded as having a disruptive effect on certain markets and industries. In addition, the use of drones might reduce ground traffic, shorten travel time, and help achieve sustainable transportation. However, when comparing the energy consumption of truck-based and drone-based parcel delivery, these hopes have been called into question for urban areas in particular (Kirschstein 2020). On a global level, the International Transport Forum of the OECD described opportunities and challenges of future drone usage in a recent report (ITF 2018).

Several surveys in different countries have studied public support for drone delivery. A representative national survey (N = 2007) in the United States reported that 44% of respondents liked the idea of drone delivery while 34% disliked this concept, with strong effects of gender, age, region and rurality. Male millennials with an urban background in western regions liked the idea of drone delivery most (Soffronow et al, 2016). In Great Britain, a survey for the Royal Aeronautical Society conducted in 2016 reported support for drone delivery at 32% and opposition at 51% (Comres 2017). Another study reported 44% opposition to drone usage for parcel delivery (Nesta 2017), and in a 2019 study (N = 2010), support for drone delivery in the UK was found to be only 23% (IME 2019).

In Germany, a recent multi-method study found the general support for drone delivery among the public to be 25%, with only 21% indicating they would use it themselves (Dannenberg et al., 2020). A further distinction was made between the usage of drones for delivering one's own consumer goods in general, or exclusively in cases of emergency (e.g. for delivering pharmaceuticals). While only 21% of the sample would use drones for delivering parcels and consumer goods (vs 68% opposing), 60% would use drone delivery for urgently needed pharmaceutical products (vs 28% opposing).

Results for the public perception of drones in Germany based on online surveys for the years 2017 and 2019 have been published by the German Unmanned Aviation Association (VUL 2017, 2019). Here the results for parcel delivery by drones were broken down into three geographical areas of service, with more support for drone delivery in remote areas (small villages in the mountains, or small islands in the sea) and rural areas, and the lowest levels of support in large cities. In the 2017 study, the results from respondents who 'support' vs 'oppose' online delivery were 67 vs 24% for remote areas, 46 vs 44% for rural areas, and 27 vs 64% for large cities. About two years later, the respective results reported were 68 vs 23% for remote areas, 47 vs 43% for rural areas, and 30 vs 60% for large cities, showing a slight increase in support for drone delivery reported in each area over the two-year period.

Differences concerning rurality have also been reported for the United States. As opposed to the German survey, US study participants from urban areas liked the idea of drone delivery better (51% 'like' vs 27% 'dislike') than those from rural or remote locations (37 vs 41%; Soffronow et al, 2016).

Exploring factors affecting attitudes to drone delivery, Yoo et al. (2019) report differences when comparing urban and suburban/rural groups in an online survey among US citizens. While speed and ease of delivery were significant factors for both groups, performance risk was an additional negative factor for the urban group, whereas for the suburban/rural group, environmental friendliness and personal innovation both had significant positive effects on their attitude towards drone delivery.

In order to shed further light on people's attitudes towards drone delivery, this paper reports findings of a representative national study about the acceptance of drones in Germany, considering both the attitude toward parcel delivery by drones in general and how respondents anticipate their own usage of drone delivery.

2. Method

The study was conceptualized at DLR and a prototype fielded early in 2018 by infas Institute for Applied Social Sciences as a Computer Assisted Telephone Interview (CATI). Using a dual frame technique with 70% landline and 30% mobile phones, a random digital-dial design was used with the aim of reaching conclusive results representative for the German population.

The questions were asked in a standardized manner by specially trained employees in a telephone interview with a duration of about 20 minutes. The answers were coded according to the appropriate template directly online. For quality assurance, online supervision could be performed occasionally by senior staff listening in on the calls. The study fully adhered to the professional code of conduct for telephone interviews agreed on in Germany (ADM 2016).

832 respondents took part in the study, which was conducted between March and May 2018, and answered all questions. Respondents were 51.8% male and 48.2% female, with ages ranging from 14 to 94 years ($M = 51.5$ years, $SD = 18.2$ years), and the average size of household was 2.5 persons ($SD = 1.3$ persons). The response rate was calculated at 3.8% following statistical procedures published by the American Association for Public Opinion Research (AAPOR 2016). This means that about every 25th eligible phone number led to a full interview. Following the same procedures, the cooperation rate for the study was calculated to be 9.4% (defined as percentage of interviews completed, divided by sum of interviews completed (832), plus sum of partial interviews (5), plus sum of refusals (6.952), and sum of other nonresponses (1.048)).

3. Results

After explaining the purpose of the study and gaining consent for participation, at the beginning of the interview, subjects were asked whether they knew of the term 'drones' in aviation. The 95% of participants who answered 'yes' were subsequently posed an open question that invited them to mention what they associate with a drone. 794 participants gave answers ranging from single-word responses to several complex sentences, all of which were transcribed by the interviewer. Participants mentioned between 1 and 9 different aspects, with a majority mentioning 2 aspects ($M = 2.44$, $SD = 1.26$). Terms were automatically translated into English using standard software. A total of 1.926 words underwent translation, of which the term 'parcel delivery' (comprising brand names and service descriptions) was mentioned most frequently ($N = 119$), followed by 'surveillance/monitoring' ($N = 105$), 'toy' ($N =$

98), with the terms 'military' and 'dangerous' being mentioned 89 times each. Seven subjects just responded with the word 'nothing'.

After providing their associations with the term 'drone', study participants were informed that the drones to be discussed in the remainder of interview were unmanned aircraft that look like small helicopters with several rotors, typically four or more, and that only civil applications were relevant for this study. They were then asked how they would describe their general attitude towards civil drones ('rather positive' vs. 'rather negative'). If they could not decide, the answer was coded as 'undecided'. Results ($N = 832$) revealed an attitude slightly more in favour of drones: 49% of the participants responded 'rather positive', 43% 'rather negative', and about 8% were 'undecided'. (For further information regarding the influence of sociodemographic factors such as gender, age, income, and place of residence in the context of the present study, see Eißfeldt et al., 2020).

During the telephone interview, 7 different areas of concern that had been identified in the literature were asked in randomized order so as to avoid sequence effects. When asked whether they are 'rather concerned' or 'rather unconcerned' about certain aspects of civil drone usage, most of the respondents indicated their concern about misusing drones for criminal purposes (91%), followed by privacy concerns (86%, see also Figure 1). Issues related to accidents (liability and insurance, transport safety, as well as damages and injuries) all raised concerns in the range of 72 to 75%, followed closely by concerns about animal welfare (68%). Concerns about noise were mentioned less frequently (53%). On the whole, a large majority of respondents named at least three or more subjects of concern regarding civil drone usage (91%). However, the number of aspects mentioned varied with the age and gender of the respondent, with women and older respondents being more concerned than younger or male respondents.

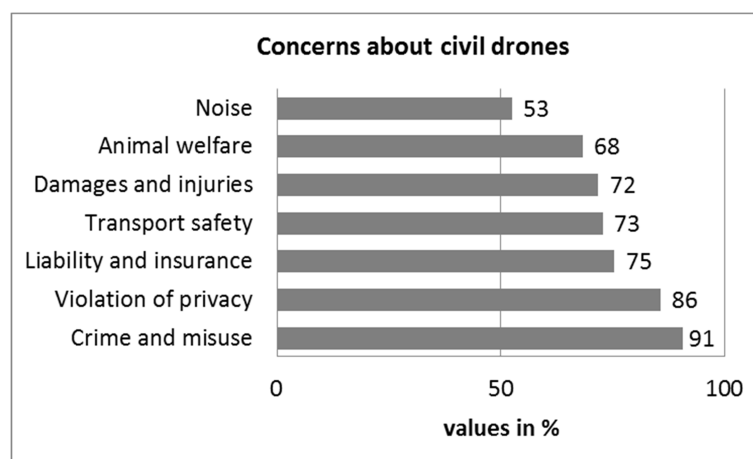


FIG. 1: Concerns about civil drones (%)

About half of the participants (47%) reported having prior experience with drones in their personal lives (37%), on the job (4%), or in both contexts (6%). All areas of concern were reported at higher rates by participants who had no experience with civil drones. Chi-square tests at the 10% level revealed significant differences for concerns about damages and injuries, $\chi^2 (1) = 3.09$, $p = .08$, OR = .76, animal welfare, $\chi^2 (1) = 4.29$, $p = .04$, OR = .73, and traffic safety, $\chi^2 (1) = 3.39$, $p = .07$, OR = .75.

It is somewhat remarkable that the level of concern about drone noise was rather low (53%), as this had been discussed in previous literature as being a potential barrier to drone proliferation (ITF 2018). However, the relatively low level of noise concern in the results of present study might be due to a lack of acoustic experience among participants. Among those reporting having experience with drones ($N = 387$), a more detailed look into the kind of experience with drones revealed a significantly higher percentage of noise concern among those who reported having heard a drone compared to those who reported that they had not, $\chi^2 (1) = 3.29, p = .07, OR = 1.45$. During the interview, the respondents were also asked to what extent they would accept various drone applications in general. Answers were given on a 4-point Likert scale ranging from 1 (totally agree) to 4 (totally disagree). The questions regarding acceptance of the various purposes were asked in a randomized order so as to avoid sequence effects. Acceptance was the highest for official uses such as ‘catastrophe response’ ($M = 1.43$), ‘life-saving efforts and rescue operations’ ($M = 1.56$), and ‘science and research’ ($M = 1.59$). Medium acceptance levels were reported for ‘monitoring of infrastructure’ ($M = 1.82$), ‘transporting medicine or medical samples’ ($M = 1.83$), and ‘agriculture’ ($M = 2.07$). There were low acceptance levels for ‘photo and video recordings for news media’ ($M = 2.40$), ‘leisure time activities’ ($M = 2.62$), and surprisingly for ‘parcel delivery’ ($M = 2.73$) as well. ‘Photo and video recordings for advertisement’ ($M = 3.09$) received the least acceptance (see also Figure 2).

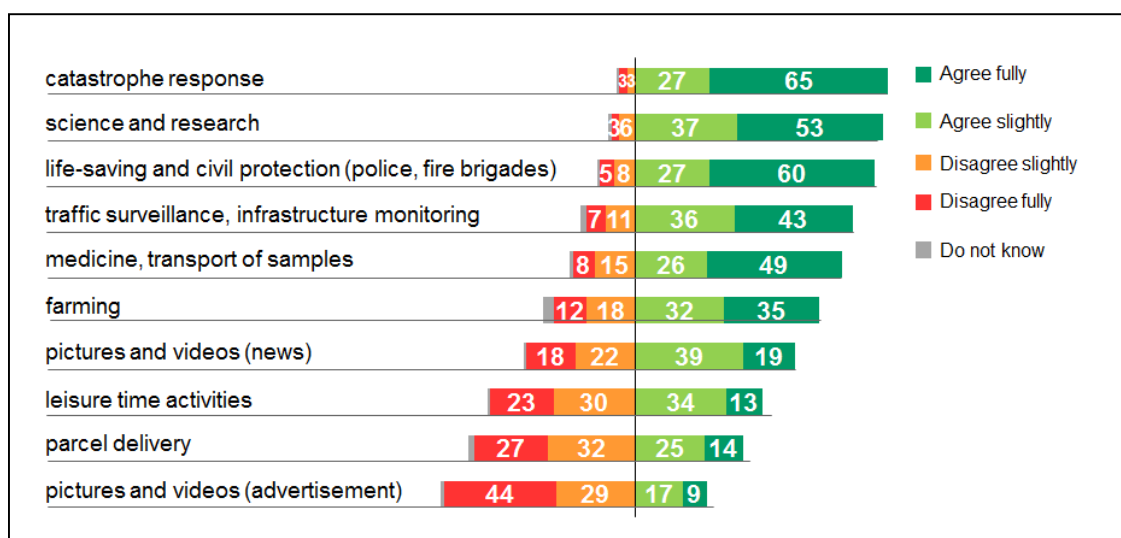


FIG. 2: Acceptance of various drone applications (%)

For 9 out of these 10 applications, the agreement varies according to gender, with females being substantially less supportive of drone applications; only for the purpose of ‘transporting medicine or medical samples’ was the acceptance slightly higher among female respondents.

A subsequent question asked respondents for which purposes they would accept drone usage for their own benefit: for ‘leisure time activities’, ‘first aid’, ‘parcel delivery’, ‘police and fire services’, or as an ‘unmanned taxi’. Answers were given on the same 4-point scale mentioned above. Again, the purposes were asked in randomized order.

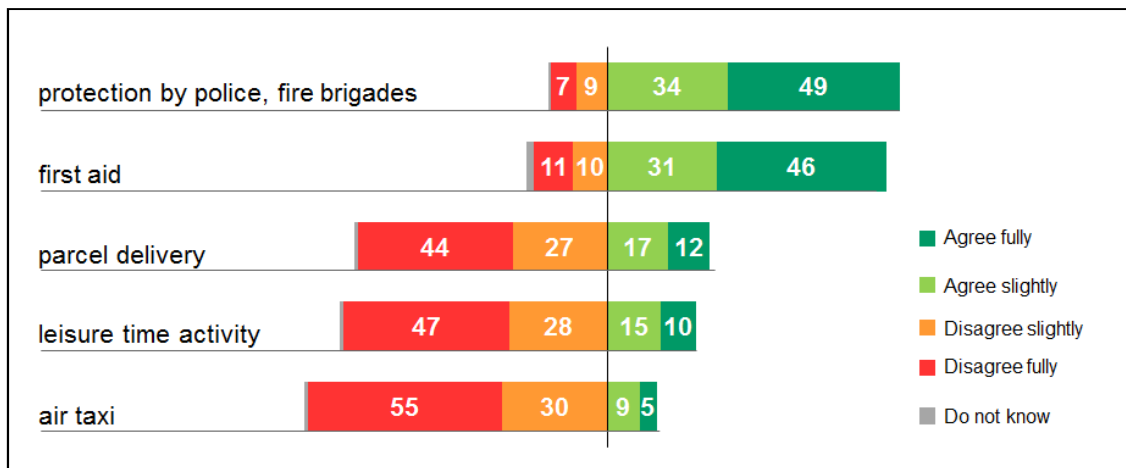


FIG. 3: Acceptance of drone use for own purposes (%)

Interestingly, the willingness to use a drone personally is low for the applications that have the highest economic interest ('parcel delivery', $M = 3.03$) and are featured most prominently in the news ('air taxi', $M = 3.37$, see also Figure 3). The two applications that receive the highest acceptance levels are 'protection by police and fire brigades' ($M = 1.74$) and 'first aid' ($M = 1.87$), which the urban population is already accustomed to because of helicopter overflight.

When asked about their own potential use of drones, the agreement among female respondents is significantly lower for all the applications listed in Figure 3. For 'air taxi', 'leisure time activity', 'parcel delivery' and 'protection by police, fire brigades', these differences are significant at $p < 0.01$, whereas for 'first aid' the difference is significant at $p < .05$.

Taking a closer look at the acceptance of drones for delivering one's own parcels, not only does gender produce a significant difference, $\chi^2(1) = 8.77$, $p = .004$, $OR = 1.58$, but the corresponding distributions (see Figure 4) seem to indicate that male and female distribution in general show the same linear pattern from 'agree fully' to 'disagree fully'. However, the disapproval from the female respondents seems to be more distinctive.

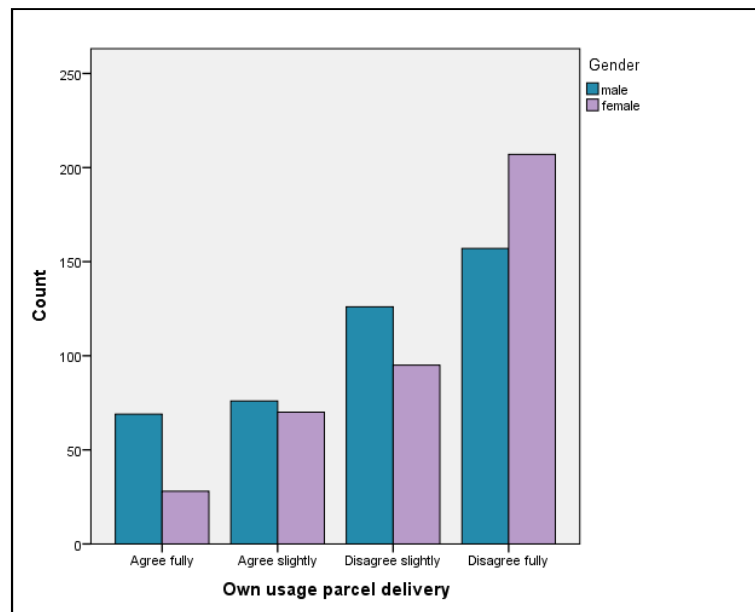


FIG. 4: Acceptance of drone usage for delivery of respondents' own parcels by gender

According to the regulations in Germany, any overflight of people's homes is prohibited unless the owner has provided prior consent. The same is valid for flying over groups of people, industrial facilities or public institutions. However, among the public, there is concern about how such an overflight ban could be enforced. When the respondents of the present study were asked about their general acceptance of flights over their own homes during the daytime using the same 4-point scale, results showed slight disagreement ($M = 2.8$, $SD = 1.0$). Overflight at night was even less accepted, with an average rating of 3.1 ($SD = 0.9$), which reflects clear disapproval. However, for the official functions of rescue and protection, respondents agreed slightly with home overflight of drones ($M = 2.2$, $SD = 0.9$).

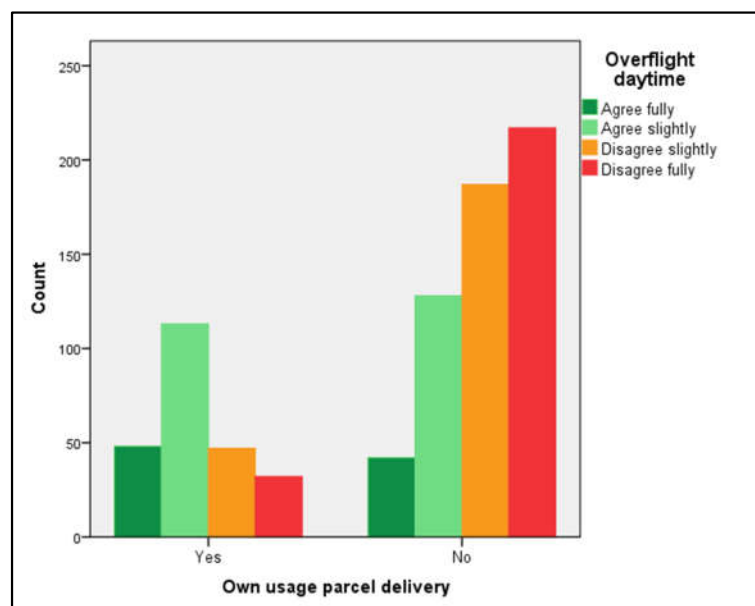


FIG. 5: Own usage of parcel delivery envisioned and acceptance of home overflight at daytime.

As shown in Figure 3, 71% of the respondents indicated they would not use drone delivery. However, even having a positive attitude towards using drones for parcel delivery does not necessarily mean accepting drones flying above one's own dwelling. Among the 29% of respondents who agreed either fully (12%) or slightly (17%) with the prospect of using drone delivery themselves, only two out of three (67%) would accept drones flying above their home at daytime (Figure 5), and less than half (44%) would agree to night-time flyovers.

Whereas parcel delivery is the most prominent association when asked about drones, respondents tend to disapprove of this application. In order to further investigate this attitude, the influence of the various concerns about civil drones on the acceptance of drone delivery for oneself was analysed using Chi-square Automatic Interaction Detection (CHAID). This method partitions a contingency table produced from cross-tabulation by using a semi-hierarchical, sequential procedure (Perreault et al. 1980) and has the advantage that it can be used with non-parametric survey data. In this study, it has been used to explain the extent to which each of the concerns explains the public acceptance of civil drones in Germany, finding that, out of all areas of concerns (listed in Figure 1), being or not being concerned about noise best explained the attitude towards civil drones $\chi^2 (2) = 38,6$, $p = .000$, $OR = .41$ (Eißfeldt et al., 2020).

With drone delivery under special scrutiny in the present analysis, the acceptance of parcel delivery by drones was defined as a parent group variable that was split according to the different categories of concerns. Out of all areas of concerns that were assessed, being rather concerned or rather unconcerned about transport safety best explained the attitude towards parcel delivery by drones among all respondents, $\chi^2 (1) = 52.7$, $p < .001$, and entered the analysis first. Concerns about noise among those concerned about transport safety followed on the second level. On the third level of the CHAID model, concerns about animal welfare entered the analysis among those who were concerned about traffic safety and noise. Overall, the analysis yielded groups of 59% approval (node 1) down to 23% approval (node 6) of the use of drones for parcel delivery (see Figure 6).

In comparison, a decision tree for the usage of drones for one's own parcels revealed a nearly identical model, with slightly lower acceptance levels at each node (node 1: 49%; node 5: 14%). Again, traffic safety entered the analysis first, with noise following on the next level for those concerned with traffic safety, and animal welfare further explaining concern among those who were also concerned about noise and about traffic safety. Acceptance of parcel delivery in general and personal usage of parcel delivery were highly correlated (Spearman rho = .76).

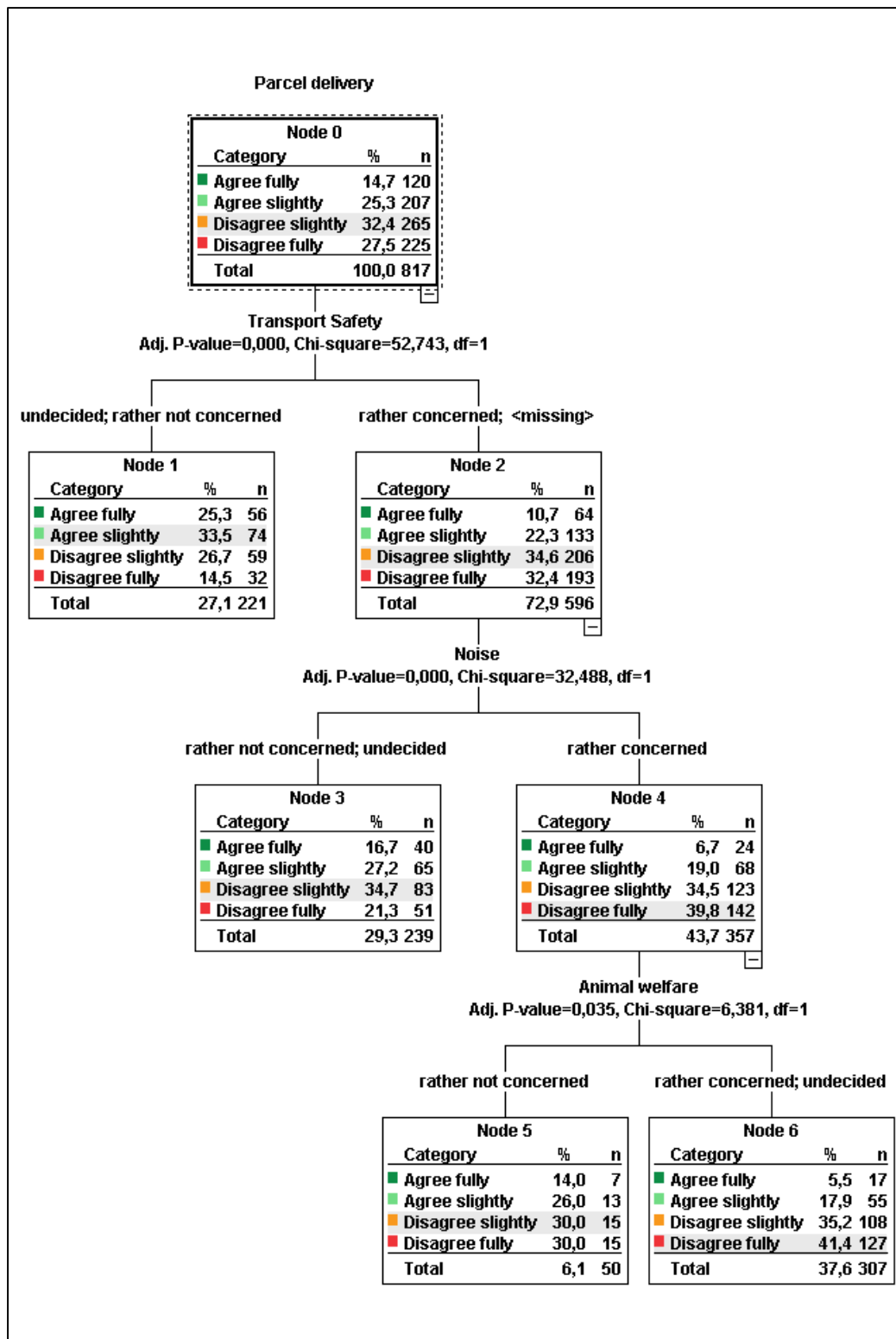


FIG. 6: CHAID decision tree model for agreement with parcel delivery by drones, partitioned by areas of concern.

4. Discussion

The attitude towards drone delivery among the German population is rather critical; about 6 out of 10 respondents disapprove of this application in general, and 7 out of

10 do not envision using it themselves. This is well in line with findings for other Western countries and has been quite stable for several years.

The disapproval rates are higher among females than males, with the gender dimension again being well in line with other countries. An important aspect is that this could be related to women being underrepresented in e-commerce. However, in recent years, females statistically pulled even with men in online shopping, as two thirds of both men and women have ordered products or services online in Germany (Statista 2020). Gender differences can be found throughout nearly all aspects of drone acceptance: Women display lower acceptance levels, have more and higher concerns, are more critical of different applications in general and are critical of home overflight in particular. This attitude might be driven by the technology used and the impacts anticipated, thus also leading to the support for drone delivery being especially weak among women. However, when asked about using drones for transporting medical samples or urgently needed medication, the picture changes. Not only are approval rates in the total sample much better then, with 3 out of 4 approving this usage, but furthermore, in this case women demonstrate even slightly higher approval of drone delivery than men. It might be that women value health-related usages of drones higher than men, an interesting aspect in times of pandemic when special neighbourhood deliveries are being tested (Fuller 2020). In those trials, the noise of the drone used for delivery (a popular consumer model) was measured to be in the range of 47 to 50 dB while hovering at an altitude between 100 and 200 feet, with about 68 dB while landing. The report takes this as proof of concept in terms of not being harmful to hearing and only a little more than the ambient noise level of 42 dB. Ambient noise is sometimes discussed as softening the noise impact of drones, however it underlies certain variation too. When investigating the effects of drone noise from a small multicopter (same model as above) added to various audio-visual scenarios, Torija et al. (2020) found that in soundscapes with reduced traffic noise, subjects in the position of a pedestrian reported higher perceived loudness and annoyance than they did in scenes highly impacted by road traffic noise, although the drone noise was held constant at 65 dBA across all scenarios. Instead of seeing this as proof for the potential of masking drone noise by street traffic, the results rather underlines the impairing aspects of drone noise on residents of such roads: As traffic varies over the day, there will be times with low traffic volume when local residents experience loudness and annoyance of drones much more ("annoyance up to 6.4 times higher than without drone noise" p. 18), e.g. at night. Furthermore, even in psychoacoustic tests comparing different outside noise using the same drone model, subjects rated the sound of drones as more annoying than that of road vehicles, at an equal level of sound pressure (Christian & Cabell, 2017). Other noise issues to be considered with drone delivery include the special aspects of tonality typical for quadcopters (Kloet et al., 2017), special influences of ambient weather conditions on sound levels and quality (Alexander et al., 2019), or the effects of load. In addition, quadcopters are controlled by varying the speed of every rotor individually, inducing pitch and yaw of the vehicle and changing the sound constantly, leading to more content at higher frequencies compared to conventional aircraft (Senzig et al., 2019). Cherney (2018) provides an example of how this led to problems in the neighbourhood of a testing site. While these trials took place in Canberra and even led to parliamentary review in Australia (Gothe-Snape, 2019), it is interesting to note that a follow-up of this drone model has recently been added to the collection at the Smithsonian National Air and Space Museum as being the first drone to make an official U.S. home delivery in Christiansburg VA (Fox 2020).

The imbalance between a generally supportive attitude towards a new, often technological development and the lack of acceptance of change in one's direct environment connected with it has been described as the NIMBY ('not in my backyard') effect in literature. According to Pol et al. (2006): 'Different factors can generate a NIMBY effect, especially fear of loss of the perceived quality-of-life status and economic value of property' (p.44). This effect is considered to be somewhat 'normal' and seems to be relevant in the context of drone delivery too. Even among those who support drone usage and would consider using drone delivery themselves, the motivation to accept drones as part of their personal environment is limited. As is the case with other new developments that are accepted in general, NIMBYism will be a factor when it comes to the acceptance of drones flying over one's own dwelling. In this special setting however, the term NOMOH ('not over my own home') seems more appropriate. There is hope that providing transparent information and careful communication can limit the influence of such phenomena on the acceptance of civil drones in daily life.

Based on the results of this study, the critical attitude toward drone delivery in general is based on concerns about transport safety, noise, and animal welfare. The same combination of concerns determines the attitude towards using drone delivery for one's own purposes. The special role of noise in shaping the attitude towards drone delivery has been confirmed in a recent study on using drones for parcel transportation in German towns. Asking for positive and negative factors, noise was confirmed as a disadvantage of drone delivery by two-thirds of the respondents. Other important problem areas that were foreseen included 'job-loss effects' (68%), 'stress due to drones flying around' (67%) and 'visual clutter' (57%). On the other hand, 'environmental friendliness' (79%) and 'reliability of service' (73%) were the top-rated benefits anticipated for drone delivery (Dannenberg et al., 2020).

After years of limited trials of drone delivery services, the start of large-scale services authorized by the government is coming. An online survey conducted late in the year 2019 among 528 online shoppers reports that 31% of the respondents are feeling 'excited', 19% are 'anxious', and 50% 'uncertain' about drone delivery (Panko 2020). As another survey has shown, residents do not support a general right to drone deliveries ('agree' 24%, 'disagree' 31%) whether or not people in their area have agreed beforehand. Instead, they largely agree (73% 'agree', 16% 'disagree') that communities should be consulted on drone deliveries (IME 2019).

Therefore, the results of this study attest to the need for regulation. Besides defining favourable topographical conditions and certain urban areas where drone delivery should be allowed, time restrictions can also be a viable measure to increase support. In addition, installing measures of noise control or providing tools for participatory noise sensing to residents could increase general acceptance (Eißfeldt 2020). If the acceptance level among residents remains in the range of below one third, drone delivery of commercial products will not become a successful service in Western cities. Thus, further research should closely monitor drone delivery services and their perception in the public, while taking into account relevant aspects such as the different usages, in order to avoid undesirable developments and to foster community agreement.

References

- AAPOR American Association for Public Opinion Research (2016). Response Rate Calculator-4-0-Clean-18_May_2016. <https://www.aapor.org/Education-Resources/For-Researchers.aspx>.
- ADM Arbeitskreis Deutscher Markt- und Sozialforschungsinstitute e.V. (2016). Richtlinie für telefonische Befragung. <https://www.adm-ev.de/standards-richtlinien/>.
- Alexander, W. N., Whelchel, J., Intaratep, N., Trani, A. (2019) Predicting Community Noise of sUAS. 25th AIAA/CEAS Aeroacoustics Conference, Delft. <https://doi.org/10.2514/6.2019-2686>.
- Cherney, M.(2018). Delivery drones cheer shoppers, annoy neighbours, scare dogs. Wall Street Journal Dec 26, 2018. <https://www.wsj.com/articles/delivery-drones-cheer-shoppers-annoy-neighbors-scare-dogs-11545843552>.
- Christian, A. & Cabell, R. Initial Investigation into the Psychoacoustic Properties of Small Unmanned Aerial System Noise. AIAA-2017-4051. 23rd AIAA/CEAS Aeroacoustics Conference, Denver. 2017. <https://doi.org/10.2514/6.2017-4051>.
- COMRES (2017) Royal aeronautical society drones polling. https://www.comresglobal.com/wp-content/uploads/2016/06/160513_Royal-Aeronautical-Society_DronesPolling_Tables.pdf
- Dannenberger, N., Schmid-Lörtzer, V., Fischer, L., Schwarzbach, V., Kellermann, R. & Biehle, T. (2020). [Traffic solution or technical hype? Representative population survey on delivery drones and air taxis in Germany](https://skylimits.info/wp-content/uploads/2020/06/Sky-Limits-_Results_Survey_english.pdf). https://skylimits.info/wp-content/uploads/2020/06/Sky-Limits-_Results_Survey_english.pdf.
- Eißfeldt, H., Vogelpohl, V., Stolz, M., Papenfuß, A., Biella, M., Belz, J. & Kügler, D. (2020) The acceptance of civil drones in Germany. CEAS Aeronautical Journal. 1-12. DOI: 10.1007/s13272-020-00447-w.
- Eißfeldt, H. (2020) Sustainable Urban Air Mobility Supported with Participatory Noise Sensing. Sustainability 2020, 12, 3320. <https://doi.org/10.3390/su12083320>.
- Fox, A. (2020) This Drone Made the First Home Delivery in the United States. <https://www.smithsonianmag.com/smithsonian-institution/this-drone-made-first-home-delivery-united-states-180975463/>
- Fuller, J. (2020). Operation Last-Mile: Critical drone delivery testing. <https://resources.droneup.com/view/338698/>.
- Gothe-Snape, J. (2020) 'Obnoxious' drone noise to get national review as hobby pilots, Google face crackdown. <https://www.abc.net.au/news/2019-06-18/drones-noise-review-after-complaints-about-google-trial/11219808>.
- IME Institution of mechanical engineers (2019). Public perceptions: drones. Survey results 2019. <https://www.imeche.org/docs/default-source/1-oscar/reports-policy-statements-and-documents/imeche-drones-report-final.pdf>.
- ITF International Transport Forum (OECD) (2018). (Un)certain Skies? Drones in the World of Tomorrow. Retrieved from <https://www.itf-oecd.org/uncertain-skies-drones>
- Kirschstein, T. (2020). Comparison of energy demands of drone-based and ground-based parcel delivery services. Transportation Research Part D: Transport and Environment, Volume 78, <https://doi.org/10.1016/j.trd.2019.102209>.
- Kloet, N., Watkins, S., Wang, X., Prudden, S., Clothier, R. & Palmer, J. (2017). Drone on: A preliminary investigation of the acoustic impact of unmanned aircraft systems (UAS), in ICSV24 Proceedings, London, England, 23 - 27 July 2017, pp. 1-8. 2017 <https://researchbank.rmit.edu.au/view/rmit:46120>.
- Nesta (2018). Drones in our cities by 2020, predict a quarter of people. <https://www.nesta.org.uk/press-release/drones-in-our-cities-by-2020-predict-a-quarter-of-people-rising-to-half-by-2024/>.

Panko, R. (2020). Drone delivery: Benefits and Challenges. <https://clutch.co/logistics/resources/drone-delivery-statistics-benefits-challenges>

Perreault, W. D., & Barksdale, H. C. (1980). A model-free approach for analysis of complex contingency data in survey research. *Journal of Marketing Research*, 17(4), 503-515. <http://dx.doi.org/10.2307/3150503>.

Pol, E., Di Masso, A., Castrechini, A., Bonet, M.R. & Vida, T. (2006). Psychological parameters to understand and manage the NIMBY effect. *Revue européenne de psychologie appliquée* 56 (2006) 43–51.

Senzig, D. A., Marsan, M., Downs, R. S., Hastings, A. L., Cutler, C. J., Samiljan, R. W. (2017). UAS Noise Measurement and Certification Status Report. <https://rosap.ntl.bts.gov/view/dot/32569>.

Soffronoff, J., Piscioneri, P., Weaver, A. (2016). Public Perception of drone delivery in the United States. RARC-WP-17-001). <https://www.uspsoig.gov/document/public-perception-drone-delivery-united-states>.

Statista (2020). Number of e-commerce users by age and gender. <https://www.statista.com/statistics/786579/e-commerce-users-by-age-gender-germany>.

Torija, A.T., Li, Z., Self, R. (2020). Effects of a hovering unmanned aerial vehicle on urban soundscapes perception. *Transportation Research Part D: Transport and Environment*, Vol. 78. <https://doi.org/10.1016/j.trd.2019.11.024>.

Verband unbemannte Luftfahrt (VUL) (2017). Drohnenumfrage 2017. <https://www.verband-unbemannte-luftfahrt.de/umfrage-2017/>.

VUL Verband unbemannte Luftfahrt (2019). Was denken die Deutschen über unbemannte Luftfahrt? <https://www.verband-unbemannte-luftfahrt.de/wp-content/uploads/2019/11/Akzeptanzumfrage.pdf>.

Yoo, W., Yu, F., Jung, J. (2018). Drone delivery: Factors affecting the public's attitude and intention to adopt, *Telematics and Informatics*, Volume 35, Issue 6, pages 1687-1700, <https://doi.org/10.1016/j.tele.2018.04.014>.



QUIET DRONES
International e-Symposium
on
UAV/UAS Noise
Remote from Paris – 19th to 21st October 2020

Signal-to-Noise Ratio Enhancement Method for Improving Sound Source Detection of Drone-mounted Phased Microphone Array

Yeong-Ju Go, Chungnam National University, South Korea: yjgo@cnu.ac.kr
Jong-Soo Choi, Chungnam National University, South Korea: jchoi@cnu.ac.kr

Summary

There is a request to detect the location of the sound source using drones for the purpose of saving lives and detecting abnormalities in disaster and security situations. This technique extends the limits of detection methods based on images of current drones, and is meaningful in securing improved detection methods by adding a new sense of sound. In order to detect sound, a microphone is attached to the drone to acquire sound pressure, and the noise generated by the drone's operation acts as a direct factor in reducing the signal-to-noise ratio of the sound source that the drone wants to detect. This paper described the method of detecting the location of the sound source generated on the ground level by using phased microphone array mounted on drones. To eliminate propeller noise and flow noise, the main noise, the spectral subtraction method was applied and the signal-to-noise ratio of the detection sound source was improved. The filtered signals were then used to estimate the arrival angle of the sound source based on the beamforming method and experimentally confirmed that the location of the ground noise source could be detected by merging with the flight information of the drone.

1. Introduction

Various technologies using drones are being developed. The area that is currently best applied commercially is the field of imaging. Video information measured using a drone-mounted camera is used in civil engineering, architecture, environmental analysis, and film industry and can be considered the most successful application case. Development of drones for disaster and security surveillance is required. Although video equipment is essential for monitoring equipment, a new monitoring system is required to respond to unpredictable sites, and acoustic detection in

the area of the incident is one of them. A request for the development of a monitoring system was made to detect possible explosions at the fire site and distress signals at the accident site and to respond quickly to them. The sound-detecting monitoring system can supplement the limitations of the image-monitoring system, which is only recognized within a fixed angle of view, and can be expected to improve detection capabilities for the target by providing additional senses.

Currently, most commercial drones use propeller propulsion systems. The propeller must physically generate flow induced noise when operated, and since the microphone attached to the drone is close to the source of noise, strong sound pressure is continuously measured together. The masking effect occurs because the sound pressure produced by the operating noise of the drone is greater than the sound pressure level of the target sound source. This makes it difficult to detect sound sources. Therefore, it is essential to apply the signal-to-noise improvement method to accurately recognize the target sound source.

The location detection study of sound source using phased microphone array is continuously studied in various fields for noise reduction study. The application of phased microphone array related to drones has also been developed to detect the sound source generated by drones for anti-drone purposes and apply it to an acoustic radar system that detects the approach and movement path of drones.

The study is about how to detect the location of sound sources on the ground using a microphone array mounted on a drone. As a concept study for applying the microphone array system for location detection of sound source to drones, the method of improving the signal-to-noise ratio for the target sound source from the removal of drone self-noise measured in the microphone and detecting the location of the sound source of interest using filtered signals were described.

2. Method of Sound Source Detection

2.1 Spectral Subtraction

Improving the signal-to-noise ratio of the sound source of interest from the measured original signal is essential for clarifying the signal and reducing the error of the arrival angle estimation algorithm to identify the target sound source. The study limited the target sound source to impulse signals assuming an explosion sound and focused on eliminating the surrounding noise and background noise generated during operation with propellers in low frequency bands with large sound pressure levels in the spectrum. The figure 1 illustrates the process of deriving time domain signals with improved signal-to-noise ratio. It is not clear, but the short time Fourier transform is calculated by detecting the abnormal signal interval detected by the drone during operation. The sound pressure signal measured just before the abnormal signal was detected was used to remove it from the detected signal and the filtered signal in the frequency domain was restored to the time domain signal again.

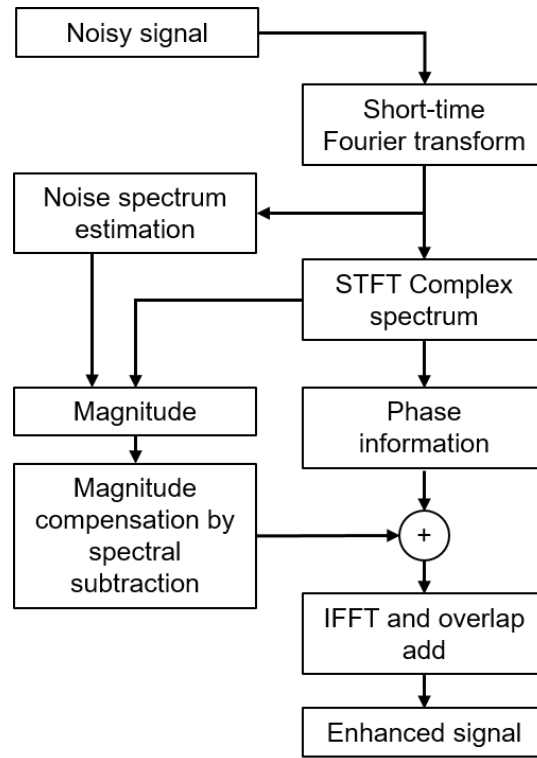


Fig. 1 Spectral subtraction process

2.2 Beamforming method

The beam formation method was applied to estimate the arrival angle of the sound source. The beam power was calculated using the conventional time domain beamforming method using signals with improved signal-to-noise ratio by spectral subtraction. The beam power was calculated by calibrating the phase difference between each microphone by the angle of incidence expressed in a vertical angle and the horizontal angle relative to the drone (fig. 2). As shown in figure 3, the direction representing the maximum beam power through interpolation from the calculated beam power contour was estimated as the arrival angle of the sound source by setting 10242 equally divided direction vectors in the downward hemisphere of the drone. The grid resolution for directional vectors affects the angle of arrival error. Appropriate settings were needed because of the problem of higher resolution lowering the estimated error of the arrival angle, but increasing the amount of calculations. Normally, the maximum beam power was considered to be the effective beam width up to -3 dB, but was estimated as a directional vector with the maximum value.

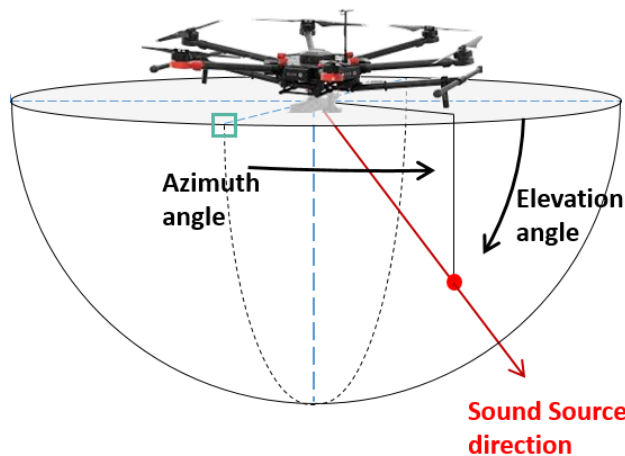


Fig. 2 Definition of the angle of arrival

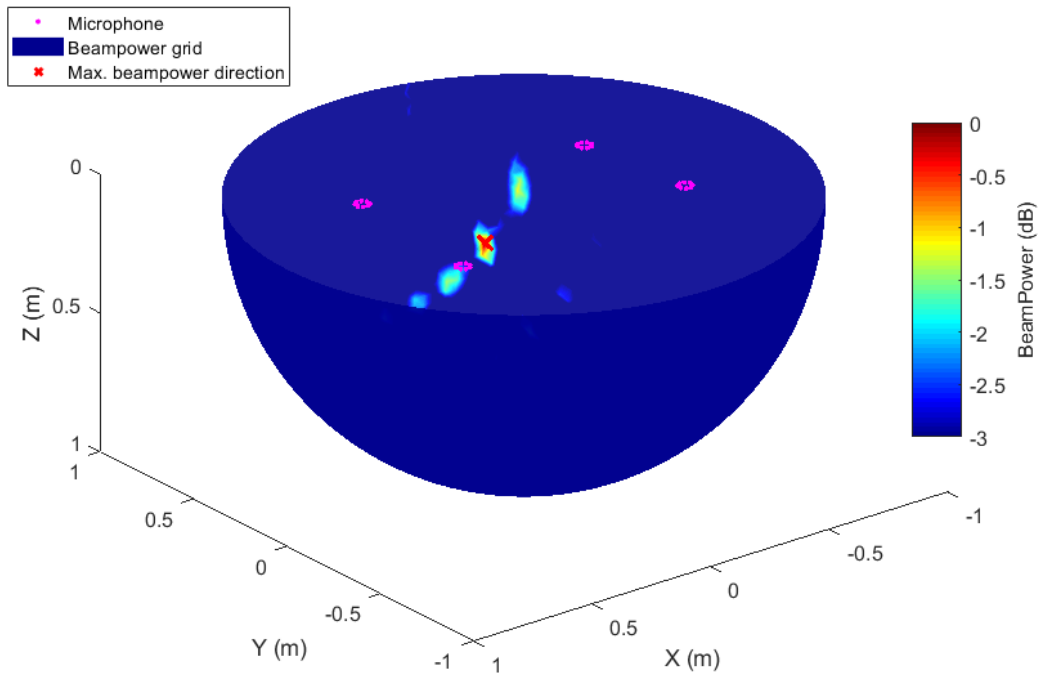


Fig. 3 Estimation of the arrival angle of sound wave by the calculation of beam power

2.3 Sound Source Localization Method

The beamforming method calculates the difference in beam power relative to the difference in phase of sound waves from the difference in geometric position of fixed microphone to estimate the arrival angle. The drone-mounted microphone array uses a fixed coordinate system for the drone and the sound source exists on a fixed ground. Therefore, it is necessary to link the direction of arrival defined by drones to the location on the ground. The relative position relationship between the ground and the drone was defined as a GPS system, and the posture of the microphone was corrected by the yaw, pitch, roll angle of the drone. Because the position and posture constantly change when the drone is operated, synchronized positions and posture angles must be applied to the trigger time of the measured acoustic signal to estimate the correct position on the ground.

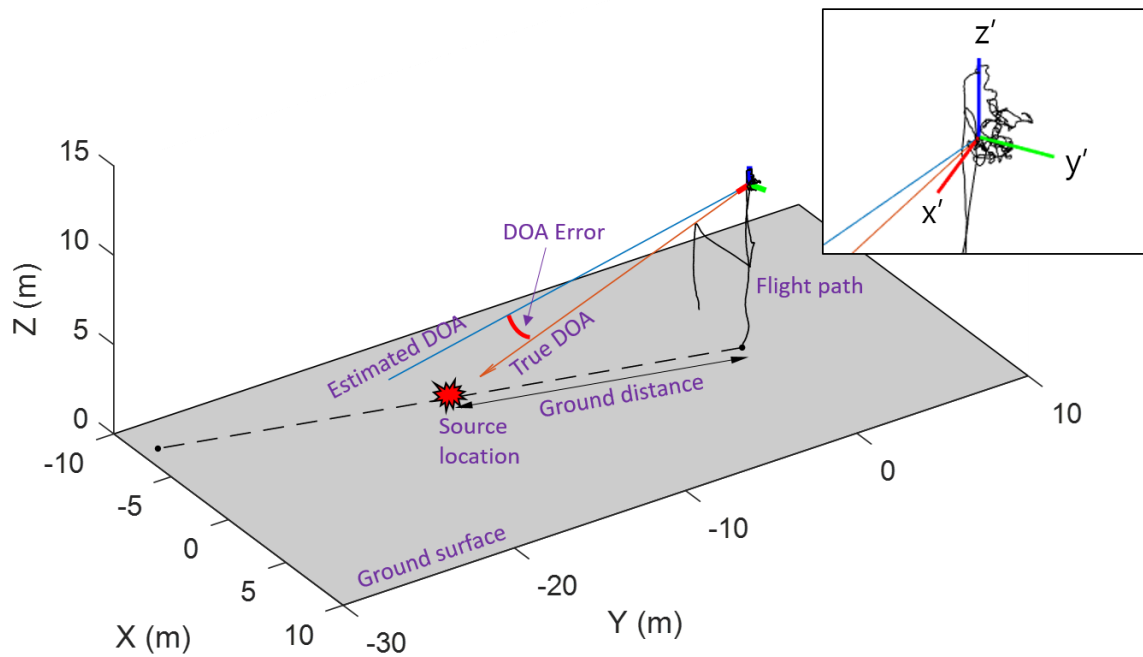


Fig. 4 A concept of location detection of ground source using arrival angle detected by drone

3. Experiment

3.1 Drone mounted phased microphone array

The direction of arrival was measured based on the phase difference microphone array. In this study, a phased microphone array consisting of 32 channels was used. Figure 5 shows a drone equipped with a microphone array. The drone is DJI Matrice 600pro and four modules of eight MEMS microphones are X-shaped at the drone's camera mount position as shown in figure 6. The measured sound pressure on 32 microphones is time-synchronized and can be recorded in real time.



Fig. 5 32-channel microphone array system mounted on drones

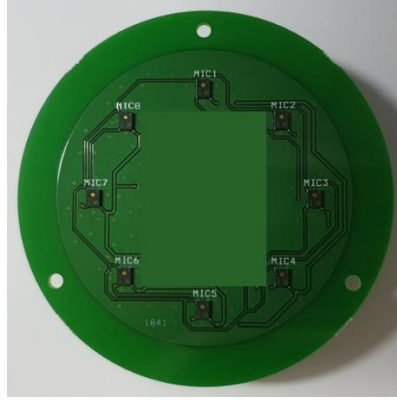


Fig. 6 8-channel microphone module

3.2 Experimental setup

Experiments on location estimation of sound sources were conducted in standard soccer stadiums as shown in figure 7. The target sound source used a toy firecracker to simulate an impulse signal. The experiment measured the firing of firecrackers three times each in order at positions 1 to 6 for about 25 minutes of the time the drone was capable of one flight. During this time, the drone maintained hover at an altitude of 15 meters and movement was recorded within a radius of about 0.5 meters due to atmospheric flow.

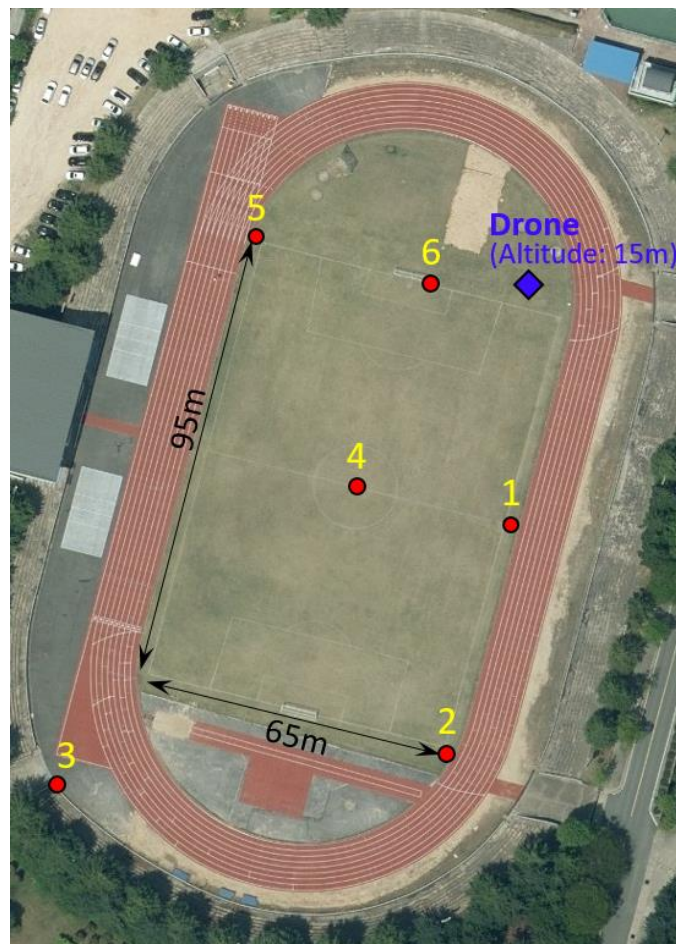


Fig. 7 Experimental site.

Firecracker explosion location (red dot) and drone hover location (blue dot).

3.3 Results

The figure 8 and 9 shows the estimated arrival angle error from the experiment divided into horizontal and vertical angles. With the heading of the drone as the reference angle, the straight path from the center of the drone to the sound source on the ground was set to zero error, and the difference from the estimated angle of arrival was calculated as error. At each point where the firecracker was set off, the error was checked for three measurements. It averaged three times at No. 3 (about 151m), where the ground distance to the drone and explosion point, and measured at ± 8.8 degrees of horizontal angle error and ± 10.3 degrees of vertical angle error. For all experimental cases carried out within a radius of approximately 150 m, errors of an average of 3.7 degrees and a vertical angle of 6.2 degrees were identified. As the location of the sound source is further away from the drone, it can be seen that the margin of error increases, and the error for the vertical angle is greater than the horizontal angle.

4. Conclusions

In this study, in order to detect the location of acoustic sources on the ground using phased microphone array mounted on drones, the location estimation performance was confirmed by extracting the sound source of interest using the spectral subtraction method and applying the arrival angle estimation method by beamforming method.

Spectral subtraction improved the signal-to-signal noise ratio of the sound source of interest by removing propeller noise and ambient background noise from the measured sound pressure signal and made it possible to distinguish the sound source signal to be measured. In addition, the signal-to-signal noise ratio was improved without distortion of phase and the beamforming method confirmed that it was appropriate to estimate the direction of arrival of sound waves.

In the location detection of sound sources, it was confirmed that the performance of estimating direction of arrival of sound waves by beamforming method is important as well as that the convergence of navigation information of drones is a very important factor and is a direct factor in location detection accuracy.

Recognizing a specific sound wave signal or human language, not an impulse signal, is another research topic and a real problem to solve. Thus, depending on the various sound sources, it is considered that an effective application of the spectral subtraction method or other background noise reduction methods or the application of speech recognition algorithms will be further necessary.

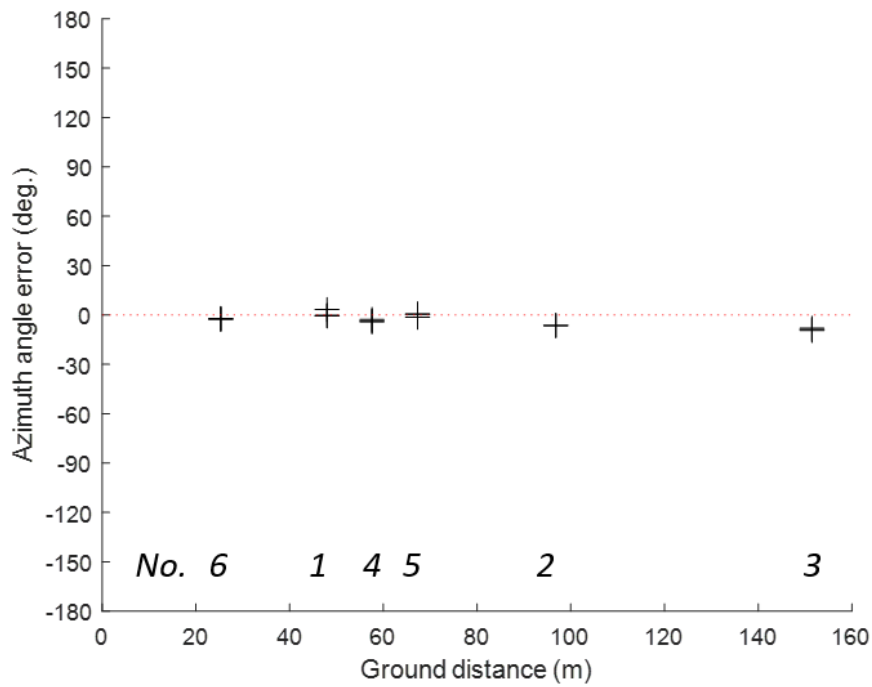


Fig. 8 Horizontal angle detection errors by distance

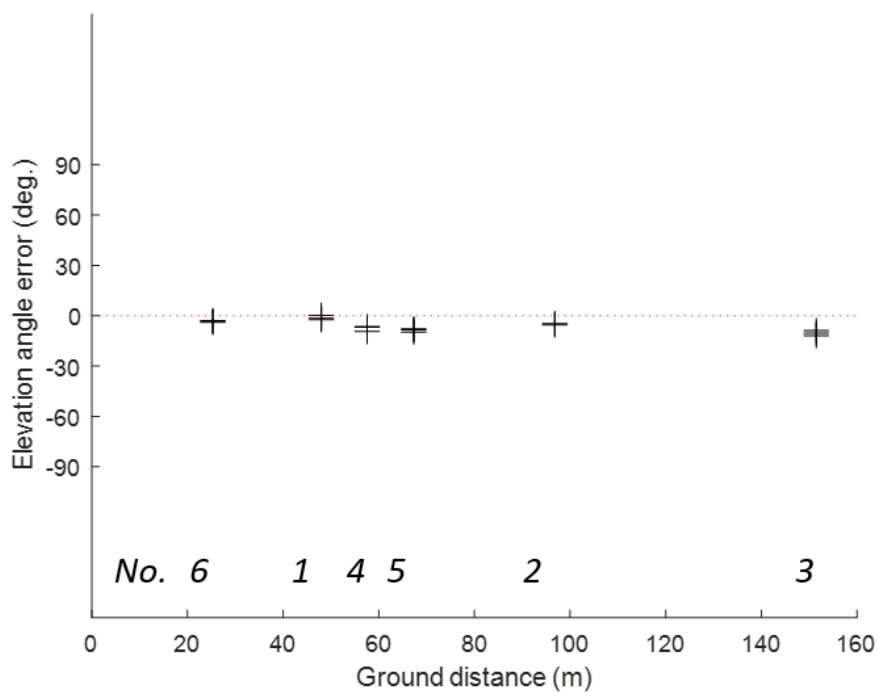


Fig. 9 Azimuth angle detection errors by distance

References

- Lee, J. W., Go, Y. J., Kim, S. K. and Choi, J. S. (2018) *Flight Path Measurement of Drones Using Microphone Array and Performance Improvement Method Using Unscented Kalman Filter* Journal of the Korean Society for Aeronautical and Space Sciences 46(12), 975-985
- Van Trees, H. L. (1971) *Optimum Array Processing*, Wiley, New York



CidB

Centre d'information
sur le Bruit

QUIET DRONES
International e-Symposium
on
UAV/UAS Noise
Remote from Paris – 19th to 21st October 2020

Assessment of noise characteristics of innovative aerial vehicles

Raphaël Hallez, Nicolas Gass, Claudio Colangeli, Siemens Digital Industries Software,
raphael.hallez@siemens.com

Summary

Vertical mobility is a potentially disruptive technology which is expected to thrive in the coming years. One of the most important elements for the development of Vertical Take Off and Landing (VTOL) aircraft and Unmanned Aerial Vehicles (UAV) is their acceptance from the community and in this domain, the emitted noise plays a very important role. Engineering teams need to use the right techniques to efficiently assess the acoustic performance of such innovative vehicles and improve their design to enable flight in densely populated area. This paper gives an overview of experimental techniques available for the assessment of noise radiated by aerial vehicles. Fly-over noise measurement techniques currently used for aircraft noise certification are presented, as well as more detailed acoustic engineering techniques such as sound source localization and sound quality analysis. The case of an electrically-propelled aircraft is used to show how to obtain a detailed acoustic characterization of the aircraft and gain insights into noise generation mechanisms. These techniques can be successfully applied to investigate the signature and the sound quality implications of the noise emitted by UAVs and improve their acoustic performance. This is highlighted here for the case of a quadcopter drone.

1. Introduction - UAV noise challenges

Similar to the automotive industry, electric propulsion could provide many new possibilities for more efficient, flexible and greener air transportation. New concepts, such as VTOL vehicles based on all-electrical or hybrid propulsion, are currently being studied to enable urban air mobility [1]. However, next to the many technological challenges associated with such innovative concepts, important regulatory barriers still need to be overcome to make flight in urban areas come true. One area of special attention is the environmental noise impact. Although electric motors are typically less noisy than traditional combustion engines, aiming to fly above densely

populated urban areas sets challenging acoustic signature requirements. Experts expect the targeted noise profile of such vehicles to be about 65 decibels (dB) A-weighted at 300 feet, which registers at one fourth the noise emitted by the smallest four-seat helicopter currently on the market [2]. Such programs will only be viable if environmental noise requirements are met so it is crucial that developers of such VTOL vehicles include noise mitigation as one of the primary objectives. It is important for engineering teams to have a good view of the techniques available to efficiently support them in the assessment of radiated noise and to improve the acoustic design.



Figure 1: Aircraft programs for urban air mobility can only succeed if community noise impact is limited.

Providing a superior cabin comfort is also a way for aircraft manufacturers to differentiate themselves from competitors. This applies to traditional aircraft already flying but will also most certainly apply to future UAVs carrying passengers. Next to the thermal comfort, the acoustic comfort should be addressed to deal with passengers' elevated expectations for an enjoyable flight experience. Noise reduction and sound engineering are continuous challenges in the aircraft design process. Acoustic requirements are frequently in conflict with requirements for lighter and more eco-friendly aircraft. Engineering teams have a clear need for tools and solutions to measure, analyze and get insight into noise generation mechanisms and validate quiet designs. Test teams need to handle a number of measurement tasks to verify aircraft performance or troubleshoot design issues. There is often time pressure to perform these measurements quickly and get deep insight into noise issues.

The goal of this paper is to give an overview of the technologies available today to assess acoustic performance of aircraft and understand to what extent it can be used to also address noise from innovative aerial vehicles such as drones. Examples of measurements performed on traditional fixed wing aircraft and rotorcraft will be presented, as well as measurements performed on a small quadcopter drone. The techniques to address exterior noise will first be presented and followed by an overview of techniques useful for acoustic comfort improvement.

2. Exterior noise radiation assessment

2.1 Overall exterior noise measurement

For acoustic engineering teams involved in aircraft development, it is crucial to ensure the final design meets target noise objectives. For traditional aircraft developed till now, noise limits are defined by certification authorities and must be met to commercialize the aircraft [3]. For instance, this applies to aircraft flyover noise certification measurements, static noise tests for aircraft engines and noise certification for installed auxiliary power units and associated aircraft systems during ground operations. Such noise certification requires detailed measurement procedures, as described in the ICAO environmental technical manual [4]. Critical elements of the procedure are the measurement system and processing software, which should ensure proper data quality and full traceability of the results. The measurement setup typically includes several microphones on the ground positioned at a specific location with respect to the aircraft trajectory.

Measurements are performed for various manoeuvres, including take-off and approach and microphone data should be accurately synchronized with the aircraft position. Each microphone is connected to a data acquisition system, which enables the user to record the noise data while the aircraft is flying over it. Simcenter Testlab software and SCADAS hardware are well suited for such measurements. The system, already approved by certification authorities, provides full processing capabilities and data traceability to support noise certification.



Fly-over noise reduction with electric propulsion	Δ LAMax
Low altitude (50 feet)	6.7 dB(A)
High altitude (1000 feet)	14.5 dB(A)

Figure 2: Impact of electric propulsion estimated with a fly-over noise measurement setup.

Overall noise from an aircraft measured during flyover is expressed in effective perceived noise level or A-weighted maximum sound level (LAMax) depending on the aircraft type. Such noise metrics are obtained by processing the raw time signals from the microphones, applying third-octave filtering and corrections for environmental conditions. Flyover noise level is a good indicator of the overall aircraft noise, including sources from the engine and aero acoustic sources from the airframe. It can be helpful to understand how innovative technologies such as electric propulsion can impact aircraft environmental noise. Highlighted here as an example is a comparison of the acoustic performance of two variants of the same aerobatic aircraft, one equipped with a conventional piston engine and the other with an electric motor based on flyover noise measurements [5]. As shown in the figure 2, calculating overall aircraft noise level using Simcenter Testlab shows reductions of up to 14.5 dB, which confirms the great potential of electric propulsion for greener and quieter aircraft. Similar procedure can be applied to UAV and VTOL vehicles to estimate the overall exterior noise radiated during specific manoeuvres like fly-over or hovering conditions.

2.2 On-board sensors

Using on-board sensors such as microphones, accelerometers or strain gages can also be useful to characterize noise sources during flight and identify potential issues linked to noisy or vibrating components. Very compact data acquisition systems like the Simcenter SCADAS XS, as shown in figure 3, can be installed on the aerial vehicle and record the data during the entire flight on a memory card. Such data acquisition system has weight and allows to connect a wide variety of sensors which is ideal for on-board measurements even for small UAVs. Data is then processed afterwards on the ground.



Figure 3: Simcenter SCADAS XS system used for on-board data acquisition.

Figure 4 shows the frequency spectra obtained from on-board microphones placed near each propeller of a small quadcopter (Potensic T35) during flight and measured in a semi-anechoic room. It is interesting to note that the noise generated by the different propellers (2-bladed) is not identical. Front left and right propellers exhibit higher overall levels. Front left microphone spectrum also exhibits higher response in the 80, 160 and 500 Hz octave bands. Note that the quadcopter was clamped at a fixed position to ensure consistency and repeatability of the measurements.

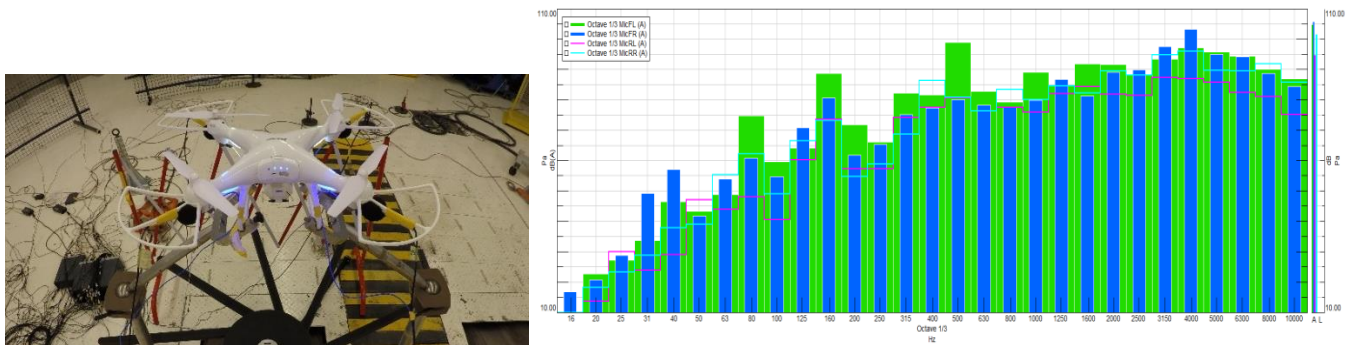


Figure 4: On-board microphones measurement – test set-up and 3rd octave noise spectra.

Figure 5 shows the narrow band spectrum obtained for the front left microphone. The main Blade passing frequency (BPF) around 100 Hz and harmonics can clearly be seen and also observed on the acceleration signal measured with accelerometers on the corresponding drone arm.

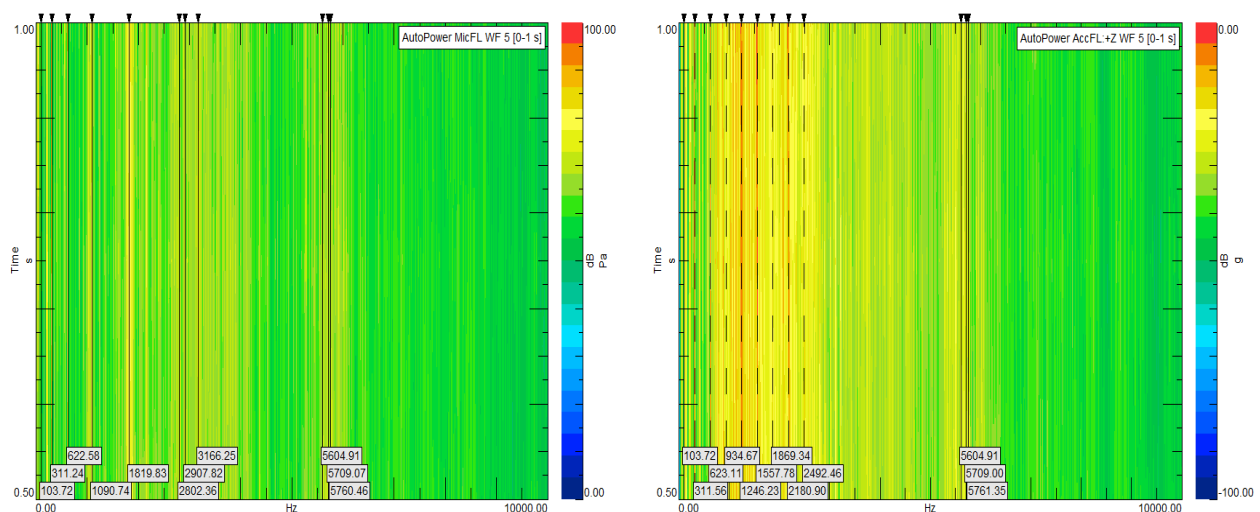


Figure 5: On-board microphones (left) and accelerometer (right) narrow-band spectra.

2.3 Sound quality engineering

Keeping overall aircraft noise level under control is important but designing an improved aircraft acoustic signature might require going one step further. Sounds can generate a variety of feelings of annoyance for a listener. For instance, a fluctuating tonal sound is typically more annoying than a steady broadband sound even though both might have the same energy level. Shaping a sound so the human ear likes it is the domain of sound quality engineering and can be useful for engineering teams working on aircraft noise. Sound quality metrics allow to process the recorded noise and provide quantified indicators on various aspects of annoying or pleasing sounds. Such metrics consider how the human ear perceives certain characteristics of sound such as fluctuation in time, spectral content or interaction between multiple sources. Sound quality can help improve exterior aircraft noise – certainly in the context of new urban air mobility where the impact on the community is critical – and design improved cabin comfort to respond to the higher expectations of passengers.

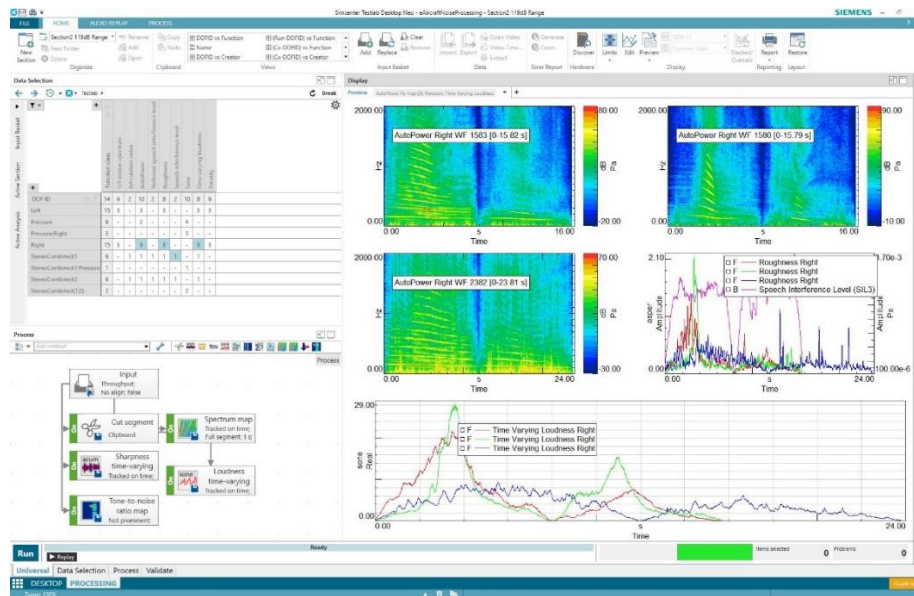


Figure 6: Detailed sound quality engineering performed using Simcenter Testlab software.

The process of sound quality engineering involves the recording of different sounds, which can be done using a binaural recording device, such as Simcenter SCADAS XS hardware and the binaural headset. Detailed sound quality engineering can then be efficiently performed using Simcenter Testlab. Equalized and calibrated playback allows to listen to recorded sounds as if the listener were sitting in the plane during flight or on the ground during flyover. Interactive filtering enables subjective evaluation of original and modified sound. Objective evaluation is possible thanks to a wide range of sound quality metrics, such as time-varying loudness, speech interference level (SIL), articulation index, fluctuation strength, tonality, etc.

Figure 7 shows the sound quality results obtained by using an arc of microphones around the quadcopter drone. This layout allows to plot the value of the specific metric as a function of the azimuthal angle between the drone and the listener. This shows that the overall sound level is quite homogeneous across the different angles and the source has quite an omnidirectional acoustic radiation. However, some more noticeable differences are observed across different angles for Loudness, sharpness or fluctuation strength metrics.

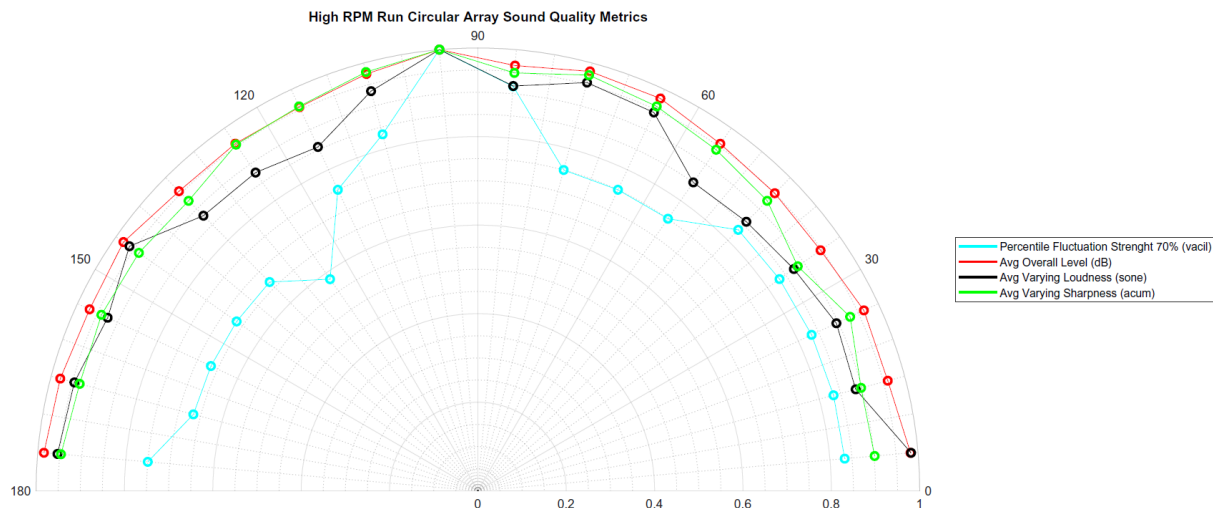


Figure 7: Directivity analysis of overall sound and sound quality metrics.

2.4 Exterior sound source localization

Aircraft noise results from the contribution of multiple complex sources. Getting a good understanding of noise generation mechanisms and the relative contribution of each source is crucial to develop noise control measures that significantly improve aircraft acoustic performance. Ranking the contributing sources can also be useful for calibrating and validating numerical models. However, for both exterior and interior noise, precisely identifying the location and amplitude of a sound source is a challenge and can be quite time-consuming.

Sources can be different in nature: low or high frequency, tonal or broadband, air-borne or structure-borne, steady or impulsive, and they may only appear during certain flight conditions. Engineering teams need measurement techniques that can deal with such complexity. Moreover, measurement techniques should be quick and easy to set up so test teams can deliver results as quickly as possible because flight testing typically is expensive.

Acoustic arrays can be efficiently used to address these challenges. They are made of multiple microphones arranged in a specific spatial pattern that all record the sound at the same time. The principle of the array technique is quite simple but powerful; it considers the relative delay of the sound waves reaching each microphone to localize the noise sources. The great advantage of such method is it captures the entire sound field at once and only requires a few seconds of measurement to provide the source map. Dedicated arrays have been designed for optimal source localization and quantification in interior or exterior sound fields [6]. State-of-the-art processing methods have also been implemented to produce results that are accurate and easy to interpret.

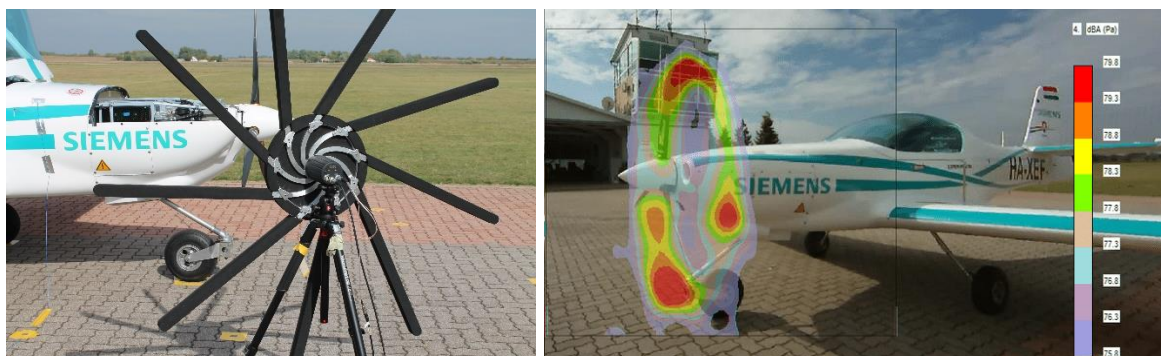


Figure 8: Using the Simcenter Sound Camera for propeller noise analysis.

The Simcenter Sound Camera Digital Array, as shown in figure 8, is a modular, high-quality digital microphone array for sound source localization. The system has been designed to be a versatile solution, with arms that can be added or removed. Adjusting the size of the array and the number of microphones allows to handle a variety of testing situations. Reference sensors such as additional microphones or accelerometers can be used for coherence analysis and to get deeper insights into airborne or structure-borne sources. For instance, this array can be conveniently used to analyze engine or propeller noise sources as illustrated in figure 8.

Sound source localization can also be performed on the flying aircraft. In this case, the array is placed on the ground towards the aerial vehicle. Its size should be scaled to the altitude of the aerial vehicle to ensure proper spatial resolution. Using such array allows to capture sources contributing to the aircraft noise, including engines and airframe sources. Figure 9 illustrates such measurement. It can be seen that some propellers have a higher radiation than others during flight. This technique can be very useful to evaluate the impact of design changes such as blade geometry.

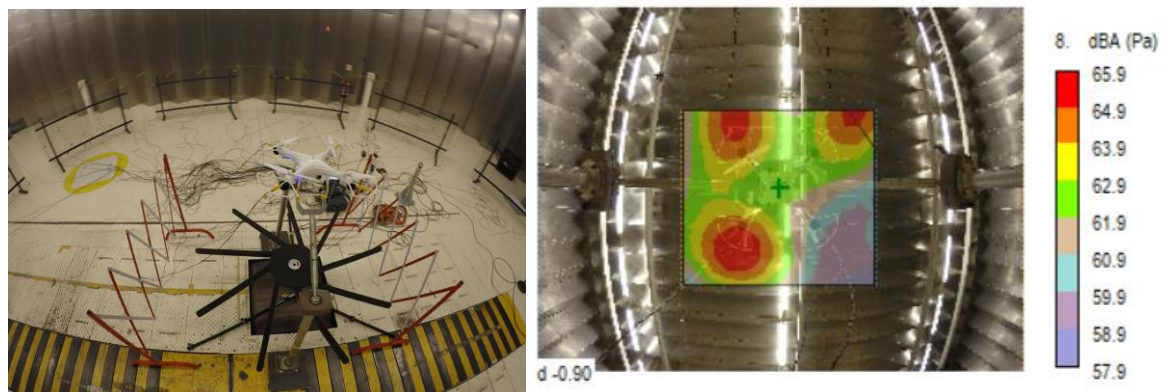


Figure 9: Sound source localization on the drone during flight.

2.5 Wind tunnel measurements

Aeroacoustics measurements based on acoustic arrays in wind tunnels also provide a detailed understanding of complex aircraft noise sources. Wind tunnel tests help the user to investigate new aircraft concepts, verify performance of innovative designs and validate prediction models. Wind tunnel testing is the ultimate way to validate such models long before the aircraft can fly. However, measuring in such a facility is expensive and must be performed efficiently to get the most out of the limited testing time. Detailed insights can be obtained thanks to real-time visualization of results during measurements and directly comparing results from several acoustic arrays or multiple runs. Optimal array design combined with state-of-the-art processing algorithms such as deconvolution ensure superior accuracy [7]. Figure 10 shows an example of such measurement performed on a scaled model in a wind tunnel and highlighting the airframe noise source generation mechanisms.

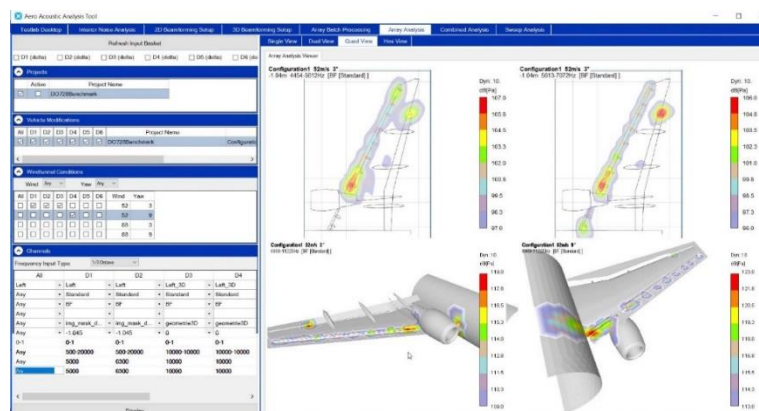


Figure 10: Dedicated measurement and analysis solution for productive aeroacoustic wind tunnel testing.

3. Interior noise analysis

Compact and scalable data acquisition systems exist to acquire operational noise and vibration data during flight. The process consists in recording the data for the entire flight on a solid-state CompactFlash card and downloading it later for further analysis. Built-in signal conditioning eliminates the need for additional equipment and ensures the highest possible data quality for various types of microphones or vibration sensors (including accelerometers and strain gages). Simcenter SCADAS XS for instance is a pocket-size and lightweight device that is well suited for such in-flight measurements inside tiny cockpits or cabins. In-flight measurements aboard an electrically propelled aircraft are illustrated in figure 11 and compared with the same aircraft equipped with a traditional combustion engine. Cabin noise level is clearly seen to be reduced and less tonal thanks to the electric propulsion. Vibration level measured using accelerometers on the aircraft structure reveals that some of the low-frequency tones heard in the cabin are propagating dominantly via a structure-borne path. This indicates that locally changing the structural design or applying vibration treatments such as damping patches would help reduce the acoustic contribution of these tones. On the other hand, variation of vibration levels at higher frequencies don't correlate with cabin noise level, which proves that acoustic radiation is mostly airborne in this case. Acoustic insulation would be an efficient noise control measure to improve cabin comfort in such a frequency range.

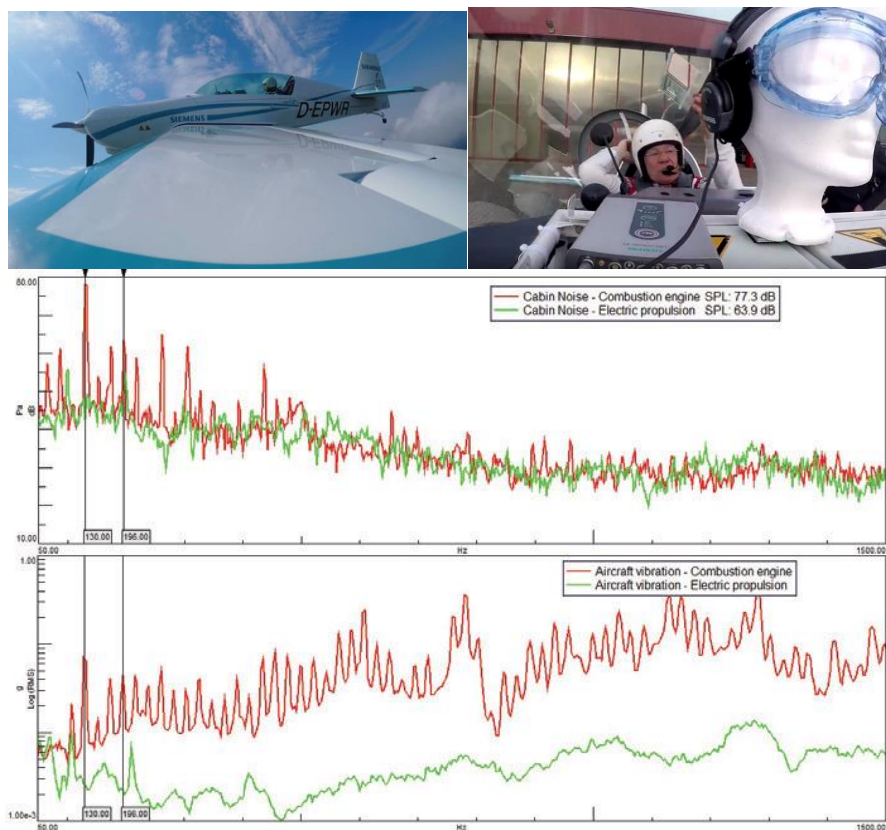


Figure 11: In-flight operational measurements performed on two variants of an aerobatic aircraft. Comparison of noise levels (top) with vibration levels (bottom).

3.1 Interior sound source localization

Interior sound source localization for cockpit or cabin noise and acoustic leak detection can be efficiently performed using acoustic arrays. The rigid spherical acoustic array shown on figure 12 drastically speeds up aircraft acoustic testing compared to traditional scanning methods. It allows for one-shot sound source localization, enabling to perform measurements in a few seconds that provide acoustic maps, back calculated and projected on a 3D view of the cabin or equipment. This yields on-the-spot accurate and comparable results. To improve the localization maps,

microphones are inserted in a full rigid sphere. This allows the user to increase the spatial resolution in comparison to an open sphere design as it better separates direct incident waves coming from one side of the array from scattered waves coming from the other side [8]. As such, it allows to capture sources from all directions and provides a detailed 360-degree view of the sources in the aircraft interior. This technique can be employed not only for source localization, but also for quantification and ranking. A full acoustic view of radiating sound is obtained in a short time, even from transient sounds. Such technique quickly reveals the full sound field of the aircraft interior in various ground and flight conditions and offers excellent spatial resolution to clearly separate sound sources. Figure 12 shows the dominant sound sources measured in-flight in the cabin of a helicopter.



Figure 12: Spherical array allows rapid sound source localization throughout the entire aircraft cabin.

3.2 Transfer path analysis

Aircraft interior noise arises from exterior sources transmitted through a variety of paths into the cabin and from interior noise sources linked to the environmental control system or auxiliary systems. Pinpointing the root causes of the sound and understanding how the energy is transferred from the sources to the receiver in the cabin is essential to derive efficient noise control measures. For instance, one may wonder how the operational vibrations in the propellers of a VTOL vehicle propagate to the frame and how much noise is radiated in the cabin. With the increased usage of distributed electric propulsion, understanding how the vibration energy from these sources propagates through the aircraft structure and how they interact with each other is also important to achieve improved cabin comfort. The source-transfer receiver approach helps to gain engineering insight into these phenomena. The principle of this technique is to decompose the different transmission paths through the aircraft structure from the sources to the receiver to identify possible issues.

The source-transfer-receiver method decomposes operational data, measured from a target or receiver location, into a sum of individual partial contributions. These partial contributions can be written as operational quantities at the source, multiplied with the transfer function between the source and the target. The procedure to build a conventional transfer path analysis (TPA) model consists of two steps: first, identify operational loads from in-operation tests in-flight or on the ground and then estimate the frequency response functions (FRF) between the load interfaces and target locations. The data is then processed to obtain contribution plots, highlighting possible issues at the source side along the transmission path (like a structural resonance) or due to dynamic interaction between the source and the structure. This systematic vibro-acoustic analysis approach is fully supported in commercial packages such as Simcenter testing solutions. Guidance is provided to engineering teams at each step of the process, including vibroacoustic modal identification, operational data measurement at source and receiver, vibro-acoustic transfer function measurements using calibrated vibration and noise sources (such as Simcenter Qsources hardware) and detailed transfer path analysis.

4. Conclusions

A lot of UAV and VTOL vehicles are currently being developed and aim to fly in densely populated areas. These programs will only be viable if environmental noise impact is limited. For future aerial vehicles carrying passengers, cabin comfort is also an important element to consider. Engineering teams have the difficult task of reaching interior and exterior aircraft noise objectives without compromising the overall aircraft weight and performance. Ground and in-flight acoustic measurements are essential to achieve these goals. Various experimental techniques have been presented here to enable efficient acoustic design of aircraft. Most of the techniques currently used in the context of traditional aircraft development can also be used for new aerial vehicles such as drones or UAVs. Commercially available data acquisition and processing systems allow to address exterior and interior noise measurement tasks and verify that target noise objectives meet certification standards or internal requirements. Operational measurements can be executed in a flexible, efficient and reliable way to assess noise levels and be able to shape the right sound quality while minimizing flight testing time. State-of-the-art technologies, including array-based sound source localization and transfer path analysis, are available to provide a deep understanding of the noise generation mechanisms and efficiently design noise control measures. This combined set of capabilities offer a complete and scalable acoustic engineering solution for aircraft noise design.

References

- [1] Uber Elevate White paper (2016), *Fast-Forwarding to a Future of On-Demand Urban Air Transportation*, www.uber.com/elevate.pdf.
- [2] Porsche Consulting management consultancy study, *The future of vertical mobility*, 2018. <https://www.porsche-consulting.com/en/press/insights/detail/study-the-future-of-vertical-mobility>.
- [3] ICAO Annex16 Volume I, *environmental protection – Aircraft noise*, www.icao.int/environmental-protection/pages/Reduction-of-Noise-at-Source.aspx.
- [4] Environmental technical manual – Volume 1, *Procedures for the noise certification of aircraft*, Doc 9501-1.
- [5] Hallez, R.; Colangeli, C.; Cuenca, J.; De Ryck, L., *Impact of electric propulsion on aircraft noise – all-electric light aircrafts case study*, AIAA/IEEE Electric Aircraft Technologies Symposium 10.2514/6.2018-4982, 2018.
- [6] Hallez, R.; Beebe, S.; Finez, A., *Detection and analysis of interior and exterior noise sources in a MD902 helicopter*, AHS 72nd Annual Forum, West Palm Beach, Florida, 2016.
- [7] Picard, C.; Lepercque, F.; Le Magueresse, T.; Minck, O.; Hallez, R.; Lanslots, J., *Microphone array deconvolution methods for efficient aeroacoustic testing in wind tunnels*, Internoise 2019 Madrid, 2019.
- [8] Hallez, R.; Paillasseur, S. ; Lamotte, L. ; Caillet J.; Roulois G., *Acoustic comfort optimization in a H175 helicopter*, 42nd European Rotorcraft Forum, France, 2019.



CidB

Centre d'information
sur le **Bruit**

QUIET DRONES
International e-Symposium
on
UAV/UAS Noise
Remote from Paris – 19th to 21st October 2020

ANSI/ASA Standards Activity on Measurement of UAS Noise

Robert D. Hellweg, Jr., Hellweg Acoustics: Hellweg@HellwegAcoustics.com

Kevin Herreman, Owens Corning Science & Technology,
kevin.herreman@owenscorning.com

Summary

The American Standards Committee S12 on Noise is developing an American National Standard for the measurement of sound power levels from small (under 55 pounds) unmanned aerial systems (UAS) in an anechoic chamber. This paper presents an update on the development of this American Standard.

1. Introduction

American Standards Committee S12 (Noise) Working Group 58 (WG58), "Small Unmanned Aerial System Sound Measurement," was formed in October 2017 with Kevin Herreman as its chair. The scope of the WG58 is to develop and maintain a new American national standard for the measurement of sound power levels from small (under 55 pounds) unmanned aerial systems in an anechoic chamber.

The working group has approximately thirty individual expert members, representing acoustic test labs, consultants, the public, U.S. government agencies - Federal Aviation Administration (FAA) and National Aeronautics and Space Administration (NASA), U.S. military, professional societies, world-wide UAS manufacturers, UAS commercial users, and other interested parties from the United States and Europe.

The goal of the working group is to develop a small UAS sound power level measurement standard that is:

- repeatable and independent of the environment, i.e., temperature, wind, background sounds, precipitation, etc.;

- a uniform test procedure following specified operating conditions;
- a method that provides users with data that can be used to predict ground sound pressure levels at specified locations in many different environmental and geographical conditions.

2. ANSI/ASA process for developing noise standards

American Standards Committee (ASC) S12 on Noise is an ANSI-approved standards committee on noise, which is administered by the Acoustical Society of America (ASA).

Once an ASC S12 working group develops and reaches consensus on a draft standard, the draft standard is submitted to the ASC S12 committee for approval. ASC S12 is composed of approximately 40 institutional members, representing general interest organizations, U.S. government agencies and military departments, manufacturers, trade associations, and user groups. Standards approved by ASC S12 are designated as “ANSI/ASA S12” standards.

3. ASC S12 Working Group 58 Activities

3.1 Initial working group activities (2018)

WG58 activities in 2018 were focused on validating the scope of the standard development and on reviewing the published papers that were relevant to this effort. Herreman (2016) presented data and rationale for the procedure. Mobley (2015) demonstrated that sound power level data from fixed wing and small quadcopter UAS obtained in anechoic rooms for input to advanced modeling software enables prediction of inflight ground sound pressure levels.

The working group had little issue with testing fixed wing UAS in an anechoic chamber. However, there were issues raised with testing rotary-wing UAS in an anechoic chamber. Stephenson (2019) demonstrated problems with recirculating air in anechoic chambers that raised the sound power levels. Other issues involved flight angle effects and the temporal nature of flight control inputs. It was agreed that additional measurements were needed on rotary wing to quantify these effects.

3.2 Working group activities (2019)

After the 2018 Technology for a Quieter America (TQA) workshop on UAS/UAV noise in Washington DC in December 2018, the WG58 membership increased from 12 to 29. Two WG58 meetings were held in 2019 -- one in conjunction with the bi-annual ASA meeting in Louisville, Kentucky in May, and the other at NOISE-CON 2019 in San Diego, California in August.

The concerns from some members on testing rotary-wing craft indoors continues, and the working group is considering outdoor testing of rotary wing aircraft. Some believe that flight testing is the best method to capture accurate sound levels. However, the group continues to have little issue with testing small fixed-wing aircraft indoors.

NASA continued the noise measurements of unmanned systems, and others also planned additional measurements.

WG58 considered and discussed the newly adopted European Commission UAS regulation (2019), which has a requirement to report UAS A-weighted sound power levels and a measurement procedure based on ISO 3744 in “essentially free field conditions over a reflecting plane”. Many WG58 members did not believe the EU regulation test method will

produce usable results, and it was agreed that WG58 should not use this type of measurement as described in the EU Commission regulation.

3.3 Working group activities (2020)

The planned WG58 meeting scheduled in conjunction with the bi-annual ASA meeting in Chicago, Illinois in May was cancelled due to the cancellation of the ASA meeting.

Herreman (2020) will present a paper at the virtual NOISE-CON 2020 in November 2020 with the results from sound power level measurements of an octocopter in an anechoic chamber. He concludes that “the testing process of this study has already been used to evaluate fixed wing and small quadcopter UAV systems, and components, with reasonable repeatable results.”

A virtual working group 58 meeting is planned for the fall of 2020 to discuss data taken including the NASA data and the new Herreman data. WG58 will continue development of the standard and make a decision on how to handle rotary-winged UAS. It is expected there will be working group draft standard available in 2021. The concerns from some members on testing rotary-wing craft indoors continues, and the working group is considering outdoor testing of rotary wing aircraft. Some believe that flight testing is the best method to capture accurate sound levels. However, the group continues to have little issue with testing small fixed-wing aircraft indoors.

4. Conclusions

When approved, the ANSI/ASA standard will provide small UAS sound power levels that can be used for:

- product-to-product comparisons,
- determining effects of noise control methods on specific models,
- purchase specifications,
- determining community sound pressure levels using advanced software programs or directivity information (which can be determined during the sound power level measurements in an anechoic chamber).

References

Mobley, Frank (2015), “Interpolation of aircraft source noise directivity patterns modeled by spherical” *Proc. Mtgs. Acoust.* 25, 045003 (2015); [This is based on the presentation at the 170th meeting of ASA: Mobley, Frank S., “Acoustic measurements of the noise generated by the Silver Fox Unmanned Aerial System” *J. Acoust. Soc. Am.* 138, 1829 (2015)]

Herreman, Kevin (2016), “Proposed Measurement Method for UAV Sound Levels”, NOISE-CON 2016, 2016, INCE-USA

Stephenson, Weitsman, Zawodny, “Effects of flow recirculation on unmanned aircraft system (UAS) acoustic measurements in closed anechoic chambers (L)”, *J. Acoust. Soc. Am.* 145(3), 1153-1155 (2019)

Technology for a Quieter America, *UAS and UAV (Drone) Noise Emissions and Noise Control Engineering Technology*, Workshop Final Report, December 13 – 14, 2018, INCE/USA
<https://www.inceusa.org/publications/technology-for-a-quieter-america/#Drone%20Noise>

European Commission Delegated Regulation (EU) 2019/945 “on unmanned aircraft systems and on third-country operators of unmanned aircraft systems”. March 12, 2019.

Herreman, Kevin (2020), "Anechoic Chamber Measurement of an Octocopter", NOISE-CON 2020, November 2020, INCE-USA



CidB

Centre d'information
sur le Bruit

QUIET DRONES
International e-Symposium
on
UAV/UAS Noise
Remote from Paris – 19th to 21st October 2020

A summary of the 2018 Workshop on UAS and UAV Noise Emissions and Noise Control Engineering Technology in Washington, DC.

Robert D. Hellweg, Jr., Hellweg Acoustics: Hellweg@HellwegAcoustics.com

Adnan Akay, Bilkent University: akay@bilkent.edu.tr

Gregg Fleming, United States Department of Transportation – Volpe National Transportation Systems Center: Gregg.Fleming@dot.gov

George C. Maling, Jr., Managing Director Emeritus INCE-USA:
georgemaling.nae@gmail.com

Eric W. Wood, Acentech Inc.: ewood@acentech.com

Summary

The U.S. National Academy of Engineering (NAE) hosted a workshop “UAS and UAV (Drone): Noise Emissions and Noise Control Engineering Technology” on December 13-14, 2018 in Washington, DC. The workshop was organized by the INCE Foundation in cooperation with the U.S. National Aeronautics and Space Administration (NASA) and the U.S. Federal Aviation Administration (FAA). The workshop had presentations from representatives of world-wide unmanned aerial systems (UAS)/unmanned aerial vehicles (UAM) manufacturers, UAS users, U.S. government agencies, universities, consultants and professional societies. There were many presentations on a wide-range of topics, including modelling and testing, psychoacoustics, community impact, and noise reduction strategies, measurement techniques, and uses of UAS/UAVs. There were a series of presentations on urban air mobility (UAM) which covered projected noise impacts from future activities, including air taxis. There were also two panel discussions on legal issues. A final report of the workshop was published in early 2020 and includes a summary of each presentation and images of selected slides. This paper presents a brief summary of the papers presented.

1. Introduction

Workshop opening remarks were provided by NAE President C. Daniel Mote and workshop organizing committee member George Maling (NAE member, and INCE-USA Managing Director Emeritus).

Adnan Akay (Bilkent University) highlighted some issues important to UAS/UAV stakeholders. According to Akay, it is unclear how the public will react to noise from drones, and there will be an evolutionary process as the public is increasingly exposed to this type of noise. Akay suggested, “This workshop represents an unusual opportunity to recognize needs in advance, and to proactively consider technologies and policies, whether they’re self-regulated or not.”

Gregg Fleming (Volpe Center, U.S. Department of Transportation) characterized drones as a transformative, if not disruptive, technology. Some ask why studying drone noise emissions would constitute a high priority, he said, and the answer may lie in unintended consequences—such as a highly annoyed community response—to these noise emissions, which deserve to be understood.

2. Keynote Addresses

2.1 UAS/UAV Noise Overview

The first keynote address was by Carl Burleson (acting deputy administrator for FAA), who said that FAA economists predict there could be more than two million drones operating in the United States by 2021, and that personal passenger drones could soon operate in cities. Integrating these unmanned aircraft into aerospace systems will be a real challenge, with the first step being to frame the relevant questions to be asked. He said that the importance of the issue of noise should not be underestimated, and gave the example of noise issues arising from the NextGen approach to modernizing the national aerospace system.

Quieter drones would ease the way to public acceptance, and the FAA is receptive to working with industry and researchers toward designing low-noise drone technology, Burleson stated. He discussed helicopters as a possible model for learning about drone noise, given that helicopters don’t always fly in predictable flight paths, and often fly lower than, and use rotors with a different frequency than, fixed-wing aircraft.

In his closing remarks, Burleson said “That’s my hope for folks in this room—that you will stay with the problem and work with us to solve it. I’m confident that, working in partnership, we will find ways to effectively integrate drone technology, with all its benefits to users, our economy, and our citizens.”

2.2 UAS Noise Emissions and Control - An Industry Perspective

The second keynote speaker was Mark Blanks (director of the Virginia Polytechnic Institute and State University Mid-Atlantic Aviation Partnership), who spoke on behalf of the Association for Unmanned Vehicle Systems International (AUVSI). He said that the drone industry has the economic potential to grow to tens of billions of dollars. He pointed out that the industry is very different from the current aircraft industry in that drone noise can affect the public in general, not just those living around airports. Blanks identified three “hot topics”: safety, security, and privacy. While noise is not on this list, public acceptance is required in order for the industry to achieve its economic potential, and noise is a big large part of that acceptance, he emphasized.

Blanks also discussed the FAA UAS Integration Pilot Program (IPP), which involves implementing drone programs to integrate emerging technology into current state and federal regulations. Blanks said that IPPs represent a “golden opportunity” to engage with communities and get feedback on issues, including noise effects, to point the way to solutions.

3. Introductory Presentations

3.1 UAS/UAV Noise Oversight: The U. S. Federal Aviation Administration (FAA) Perspective

Rebecca Cointin (FAA) also spoke to the importance of noise issues. She highlighted two key issues: control of source noise emissions through certification regulation, and perception of noise by the community. Even a low-noise vehicle can become a problem if a community is exposed to noise many times a day, she pointed out, stating that there is a lack of noise emission data for drones and that the FAA is enthusiastic about creating partnerships for noise measurements. Cointin identified the FAA UAS Integration Pilot Program as a good source of data, and noted that the FAA planned to gather a large amount of data in the upcoming year.

3.2 Brief History of Unmanned Flying

While most presentations during this UAS/UAV noise workshop focused on current and future UAS/UAV technologies, Eric Wood (Acentech) presented a historical overview of unmanned flight—very broadly defined. He covered a historic span of thousands of years—providing a serious perspective interjected with insightful observations.

4. Concerns from Three U.S. Government Agencies about UAS/UAV Noise Emissions

4.1 U.S. National Park Service

Brent Lignell said that the National Park Service has a mission to protect, maintain, and restore acoustical environments throughout the U.S. national parks. He pointed out benefits and noise issues associated with UAS operations within the parks. He also pointed out that drones have proven useful for many applications, including the ability to reach locations that are difficult or hazardous to access.

4.2 U.S. Department of Energy (DOE)

Matthew Balderree said that, while package delivery by drones has attracted great interest, less attention has been paid to the energy required for drones to function. He noted that differences in energy consumed by different platforms may affect what platform should be used for delivery systems. The DOE conducts physical testing in controlled environments to characterize the energy impact and other implications of freight delivery by drone. With a lack of drone energy characterization by companies, DOE is helping to fill in knowledge gaps, and the department's findings can potentially support policymakers' decisions going forward.

4.3 U.S. Department of Defense (DoD)

Warner Ward said that his department's focus is on fixed-wing unmanned vehicles, and that historically noise has not been an issue of great concern for DoD. However, interest has grown in recent years, and DoD has implemented a noise abatement program throughout the United States and host nations to minimize the impact of noise whenever possible—first and foremost, to protect the health and welfare of those affected by DoD-created noise, and also to reduce community annoyance.

DoD's concerns about UAS noise and approaches to mitigation are in some respects far different from private-industry considerations for applications such as package delivery. In some ways, however, DoD's approaches—such as engaging communities affected by this type of noise—resemble private-sector strategies.

5. Standards for determination of UAS/UAV noise emissions

5.1 Noise Regulation: Federal Standards or Self-Certification by the Private Sector

Robert Hellweg (Hellweg Acoustics) and George Maling discussed how noise emission standards for information technology equipment and wind turbines could serve as a model for UAS/UAV standards. The noise emission measurement standards for IT equipment and wind turbines both use sound power level as the noise metric, which can be used to determine receiver sound pressure levels. They pointed out that the IT industry developed measurement standards for IT equipment noise emissions became the basis for government regulations and requirements and for customer purchase specifications.

5.2 ANSI/ASA Standards Activity on Measurement of UAS Source Noise

Robert Hellweg discussed the work of the American National Standards Institute (ANSI) Standards Committee S12, Working Group 58, which is developing a noise emission measurement standard for sound power level of small UAS/UAVs (less than 55 pounds) for measurement in an anechoic chamber. The measurement must be simple to enable manufacturers to test their UAS craft for potential labelling purposes and should provide data that could be used to determine sound pressure levels from UAS overflights. Many technical issues have been discussed during working group meetings. The working group has 29 members and includes representatives of UAS/UAM manufacturers and commercial users, as well as government, military, academia, consultants, and acoustical test laboratories, and other industries.

5.3 Mitigating the Pitfalls of Testing UAS Vehicles in Anechoic Chambers

James Stephenson (U.S. Army) presented additional work that is needed in the development of a UAS noise measurement standard in an anechoic chamber. He pointed out that one problem with measurements in a closed anechoic chamber is the recirculation of turbulent air through propeller blades, which leads to an undesired increase in noise level. He said that the recirculation effect is a significant consideration in this type of testing and that further research is needed.

6. UAS/UAV noise emissions and noise reduction

There were eight presentations on noise emissions from and noise reduction for UAS/UAVs.

6.1 Overview of UAS Noise Modeling and Experimental Capability at NASA Langley Research Center

Michael Doty (NASA) focused on the UAS modeling and experimental work at the Langley Research Center. Among NASA Langley's 2018 areas of study include propeller-airframe interaction aeroacoustic effects; broadband noise; phasing of propellers for noise reduction; and recirculation effects in static test facilities. Areas of emphasis included ongoing noise modeling prediction and experimental capabilities under development. Propeller phasing is one of several key technologies, which requires identical rotation rates for two propellers arranged so that the (pure tone) noise emissions are 180 degrees out of phase.

6.2 Psychoacoustic Considerations for UAS/UAV and UAM

Andrew Christian (NASA) spoke about psychoacoustic considerations related to UAVs and UAMs, opening his presentation by laying out the three major aspects of psychoacoustics that are under study in this context:

- The human hearing mechanism, including the ear, and how this mechanism shapes perception

- The qualitative aspects of human perception
- Psychosocial factors that lead from sound perception to attitudes (annoyance) and behaviors (complaints).

Christian discussed NASA research in all of these areas and concluded that there are many avenues showing promise with none promising to be a panacea. Techniques have been developed to quantify subjective aspects of sound beyond loudness. These techniques measure sound quality metrics such as tonality/tone prominence; fluctuation strength; roughness; sharpness; and impulsiveness.

He reported on a NASA study to determine the annoyance in response to various small UASs versus road vehicles of the type that might be used for package delivery. It was found that the UASs produced more annoyance than cars; on average cars need to be 6 dB(A) louder than UASs to be at the same level of annoyance. Christian pointed out helicopters may share more operational and psychosocial qualities with UAS/UAV and UAM than any other contemporary noise source.

6.3 Noise from Multirotor UAS and Community Impact

Nathan Alexander (Virginia Tech) shared information about his UAS community impact research, sponsored by Virginia Tech's Institute for Critical Technology and Applied Science and by Aurora Flight Sciences. Topics being studied include strategies for reduction of noise emissions as well as flyover studies in an outdoor test facility to build up a database of information for a tool to predict noise impact on communities. Virginia Tech is helping to unravel the complex issues associated with UAS noise. By advancing the understanding of noise from these unmanned vehicles, Virginia Tech's findings promise, in turn, to guide strategies for reducing community noise and annoyance.

6.4 Research into Aeroacoustic Emissions of Unmanned Aircraft Systems

Frank Mobley (U.S. Air Force) said the U.S. Air Force has made consequential strides in UAS aeroacoustic emissions research. Based on sophisticated data gathered at its own advanced research facility in White Sands, New Mexico, and at other modern test sites, the Air Force is translating theoretical measurements toward achieving quieter UAS flights in the real world. He said that the Air Force is making efforts to share what it can about its research in the area of UAV noise prediction and modelling, including information about Air Force-developed technologies and facilities. He discussed his organization's research site, source characterization, and UAV noise analysis.

6.5 Measurement Surface Contribution Analysis on a UAS and Field Testing

David Herrin (University of Kentucky) discussed panel contribution analysis (PCA)— a discretized form of the Helmholtz integral equation— as a method of characterizing the noise emissions of a source. The University of Kentucky has conducted panel contribution analyses (PCA) and pass-by noise testing on UAVs. In these tests, PCA was successfully applied to predict sound pressure levels for hovering UAVs, and showed significantly higher levels off the top of the UAV compared to the bottom. Then, pass-by tests showed repeatable findings.

6.6 Simulation Method for Use in Design of Quieter Multirotor UAS

Sheryl Grace (Boston University) said that different multirotor UAS designs have different performance and noise characteristics. Simulation methodologies that can predict both performance and noise of a multirotor UAS in real-world situations would enhance the design process. It is argued that important effects that contribute to the performance and noise characteristics of multirotor UAS are only captured if the multiple rotors and fuselage are simultaneously simulated. Grace introduced these basic findings about the noise from different UAV designs:

- UAVs that utilize a single propeller have tones that are very narrow and hence the blade passing frequency (BPF) dominates.
- UAVs with multi-rotors have tones with broader peaks and the higher harmonics can have amplitudes higher than the main BPF.

She said that the characteristics of the two noises are very different, which may result in a big difference in annoyance and distinct mitigation techniques.

6.7 Noise Reduction Strategies for UAS

Noah Schiller (NASA) said that NASA Langley conducts research in many areas, including UAS and UAM acoustics. This includes experimental characterization of vehicle noise, modelling, psychoacoustics, and noise control technologies.

Schiller presented strategies for reducing noise, focusing on two categories:

- Design “solutions.” These are applicable to individual vehicles, and include minimizing the wake interaction, using stacked rotors, synchronizing rotors, controlling propeller phase, and active noise control. Wake interference can be minimized by increasing the clearance, at least in hover, and the harmonic content can be significantly reduced.
- Acoustically aware operations. This strategy, which can be applicable to a variety of vehicles, involves modifying either the operating conditions or flight trajectory of the vehicle to meet acoustic, safety, or other mission requirements. The goal may be to fly from point A to point B as quickly as possible without exceeding noise constraints in a noise-sensitive region.

6.8 How You Can Help Reduce Noise from UAS/UAV

Nesrin Sarigul-Klijn (University of California, Davis) said that collaboration across various groups—including engineers, pilots, public health specialists, educators, and policymakers—is key to reducing UAS noise. Each group can contribute to noise reduction, according to their respective areas of expertise, to help protect both people and wildlife. The Transportation Noise Control Center of UC Davis is working to improve computational simulations so they match with flight test results and ultimately provide a reliable indication of noise from real-world UAS flights.

7. International UAS/UAV activities

7.1 Activities of the French Civil Drones Council Related to Noise

Frédéric Guntzer (Airbus Helicopters, France) presented an overview of the French Civil Drones Council’s efforts related to noise. The French Civil Drones Council (CDC) works with Airbus Helicopters and other industry partners on UAV and UAM issues including noise. Each partner brings its respective expertise in areas such as urban air mobility and urban air logistics, toward realizing the promise of drones for the industry and ultimately the public. His presentation covered the organization’s efforts from the perspectives of Airbus and these additional partners: the French Civil Aviation Authority (DGAC), aerospace lab ONERA, and rotorcraft turbine manufacturer SAFRAN. Airbus Helicopters is involved in two CDC technical committees, one of which is dealing with noise issues. The three areas that they are working related to the acceptance of drone noise are: source noise control; routes and procedures; and ground impact and annoyance.

7.2 NATO Activities: Assessment and Reduction of Installed Propeller and Rotor Noise from Unmanned Sector

On Behalf of Philip Morris (Pennsylvania State University), Kenneth Brentner (also of Penn State) provided an overview of the new NATO Science and Technology Organization (STO)

Research Task Group AVT-314 “Assessment and Reduction of Installed Propeller and Rotor Noise from Unmanned Aircraft.” Morris and Theo van Veen (Netherlands Aerospace Center) are the co-chairs of this new research Task Group. The overall objective of the Task Group is to assess the state of the art in UAS noise prediction and reduction, and to provide a technical assessment of the noise from UAS operations.

Key topics for the Task Group’s review include: the state of the art in the measurement and prediction of UAS propeller and rotor noise; methods for UAS rotor and propeller noise reduction, with a focus on the effectiveness of UAS operations; and the role of new materials and computational tools in the design and development of quiet and efficient propellers and rotors. The task group was set to officially begin its work in January 2019 and planned to meet for presentations and discussions at least twice a year for two years through December 2021 and will submit a technical report on its findings.

8. Legal Panel Discussions

Legal experts led the two panel discussions. The first, on governance, addressed the roles of federal, state, and local governments, including issues such as pre-emption of regulations and standards by the federal government. The second panel addressed privacy and security.

8.1 Panel Discussion: Governance— Federal (U.S.), State, and Local

Panelists Anne Swanson (Wilkinson Barker Knauer LLP) and Steven Ucci (Adler Pollock & Sheehan P.C.) discussed the important issue for the UAV industry of the division of regulatory responsibility among federal, state, and local governments in the United States. State and local governments often wish to enact laws and ordinances that address noise and other issues related to UAS/UAV operations, creating challenges for manufacturers and operators that may be faced with a myriad of legal requirements. The two panelists discussed how those who govern may deal with U.S. federal preemption and other issues, while representing the public interest.

8.2 Panel Discussion: Privacy and Security

Privacy and security issues were addressed by the second panel, composed of panel moderator Anne Swanson and her law partners Aaron Burstein and Clete Johnson. While industry focuses on unmanned aerial vehicles’ potential benefits, there is the possibility, that must be recognized, for drones in the wrong hands to invade privacy and jeopardize security. The panel discussion painted the picture of an evolving legal and regulatory framework with gaps that must be filled to protect the privacy and security interests of individuals and the country.

Aaron Burstein explained how the broad term “privacy” applies to diverse, ever-changing issues both commercial and governmental.

Clete Johnson provided an overview of security issues, pointing out that technology advances raise questions in the national security world about “what can go wrong?” With an unmanned vehicle such as a drone, there is no need to risk a person’s life or risk their capture during an operation, and drones can be excellent spies and saboteurs because they can place a sensor or cyber capability in a physical space that otherwise might be inaccessible. The biggest near-term threat is the terabytes of data that are collected by interception or hacking, given the criminal groups affiliated with adversarial nation-states and the money that is at stake.

9. Uses and Noise Considerations of UAS/UAV in the Private Sector

There were three presentations on the uses of UAS/UAV in the private sector and noise considerations.

9.1 How the Private Sector Uses UAVs

In a second presentation, Eric Wood gave various examples of how drones are being used in the private sector. He said that UAVs are already in use to support of both leisure and business pursuits. He provided a tour of many current uses—including applications in the energy, mining, agriculture, and other industries—and gave a glimpse of prospective uses that could make noise a front-and-center concern.

9.2 UAS Use Cases

Lisa Malloy (Intel) pointed out that for many businesses the value of UASs has already become clear as drones are used to great advantage in various industries. Four examples of industries in which drone systems can improve efficiency and reduce costs are construction, utilities, insurance, and oil and gas. Malloy highlighted that flight is only a small portion of what makes the data collected by drones valuable to companies and individuals. “The whole cycle of how the data is turned into actionable information for farmers, construction companies, and insurance companies - all the things that we've talked about [at the workshop] - is a really important part of the value that drones offer to society and the economic benefits that they provide to industry.”

Intel is in favor of a continuing dialogue about drone regulation, and in fact “is very eager for rules,” Malloy stated. She added that, where noise is in fact not a significant issue, the topic should not overshadow the benefits of an activity to industry and society.

9.3 Small UAS Noise: Policy and Technology Considerations in the Private Sector

Brendan Schulman (DJI) highlighted several examples of drones’ beneficial uses including aircraft safety inspections (such as fuselage inspections), disaster response, and human rescue applications.

He pointed out that DJI has proactively considered sound in its drone designs. For example, the DJI Mavic Pro Platinum was “much quieter” when it was released in 2017 than its predecessor, the Mavic Pro. The noise reduction was achieved in two ways: with a quieter electronic speed control and with a redesigned propeller that improved aerodynamics by changes such as the addition of more pointed, raked propeller tips. He also said the newer design had a “less irritating sound” since the frequency spectrum was different.

Schulman also discussed the proposed European Union drone noise regulations and had concerns that the original measurement procedure did not represent actual drone operation. He opined that drone noise does not seem to represent a significant problem—at least not yet.

At the end of his talk Schulman said the UAS industry may benefit from addressing noise-related issues in designs for global products. “We want there to be social acceptance of our technology, so that all those great uses you’ve heard about actually take place.”

10. Urban Air Mobility (UAM)

The final section of the workshop was devoted to urban air mobility with a goal to use vertical lift vehicles such as air taxis for human transport in crowded cities.

10.1 Noise Considerations and Urban Air Mobility

Susan Gorton (NASA) pointed out that NASA is investing heavily in the field of vertical lift applications, and is making crucial headway in its wide-ranging research across the areas of source noise modeling and validation, low-noise design, low-noise flight path management, and human annoyance from UAM vehicle noise.

She spoke of four major elements of NASA's approach in eVTOL (electric as well as hybrid electric vertical takeoff and landing vehicles) noise modelling and technology:

- Source noise modelling, prediction, and validation
- Low-noise design capability
- Low-noise flight path management and assessment tools
- Human response (lower sound levels do not always correlate with reduced annoyance).

10.2 Scaling up Unmanned Aircraft Systems (UAS): Characterizing Noise Impacts from Future Air Taxis

Brock Lascara (MITRE) addressed the characterization of noise impacts from future urban air taxis. Lascara emphasized that many challenges exist in terms of integrating air taxi service into an already-complex national airspace system. At the system level, for example, operational integration and safety challenges exist, and one important question is how a self-piloted aircraft would be certified. Lascara discussed the noise implications of these aircraft of the future including the following factors:

- Flights where there currently are none
- Vehicles flying closer to the ground and in high-population areas
- Airspace integration effects.

10.3 UAS/UAV) Perspective

Steven Morris (Aurora Flight Sciences, a Boeing Company) spoke of design and analysis for UAM community noise. UAMs promise to alleviate traffic problems, but vehicle design challenges abound, including technical hurdles and the difficulty of anticipating government and community requirements of the future. Concepts being considered in designing vehicles include open rotors, ducted rotors, and tilted rotors, with primary issues including interactions between rotors and those between rotors and structure.

10.4 Design for UAM Community Noise Acceptance—Vehicles and Operations

David Josephson (Josephson Engineering) spoke on behalf of Uber Elevate on UAM noise and community impact. Uber Elevate's admittedly hard-to-reach goal is to drive development of UAM vehicles that are to a listener in a neighborhood as loud, or even half as loud, as compared with a delivery truck. He spoke of psychoacoustic issues that are vitally related to the acceptance of UAM vehicles. He pointed out that sound is the most direct piece of community impact that aircraft designers can control. Community noise costs boils down to how many people can hear a flight, and whether they find the noise disturbing. He said that the main issue is one of noisiness, not loudness; however, loudness is the primary component of noisiness.

11. Conclusions

The workshop report provides information on the many new and useful private, government, and commercial applications for UAS/UAVs that are available and expected to be implemented over the next few decades. Operations near populated residential areas can be expected to introduce environmental sounds unwanted by the general public unless industry, responsible government agencies, and the engineering community plan for and implement steps to reduce noise emissions from UAS/UAVs. During this workshop, experts from government, academe, and the private sector addressed future uses, noise emissions, and noise control technologies in this context.

This workshop focused on noise emissions of UAS/UAVs in sizes up to and including those capable of carrying packages. Pilot programs for fast delivery of medical supplies already exist and delivery of consumer products is on the horizon. Less emphasis was placed on larger

devices proposed, for example, for urban air mobility (UAM), whose implementation is expected further in the future.

Workshop attendees expressed a common commitment to partnering with others in government, industry, and the public toward integrating drones into the national airspace.

12. Future workshop

During the first week of December, 2020, a virtual workshop on aerial mobility and noise will be hosted by the National Academy of Engineering and organized by the same group that organized the 2018 workshop in Washington, D.C. The larger issue is how aerial mobility vehicles such as air taxis will be integrated into the national airspace. Other small unmanned aerial vehicles (UAS/UAVs) generally known as drones will also be considered in the workshop. The noise from all of these vehicles is a focus area for both the FAA and NASA, which are cooperating in this virtual workshop. The objective of this virtual workshop is to move the understanding of these sources and effects on communities forward to assist government, industry, and academia in formulating plans to advance noise control technology for aerial vehicles. This December virtual workshop will be a follow-on to the 2018 Washington workshop and the 2020 Quiet Drones e-Symposium in October 2020.

References

Technology for a Quieter America, 2020. *UAS and UAV (Drone) Noise Emissions and Noise Control Engineering Technology*, Workshop Final Report, December 13 – 14, 2018, INCE/USA <https://www.inceusa.org/publications/technology-for-a-quieter-america/#Drone%20Noise>



QUIET DRONES
International e-Symposium
on
UAV/UAS Noise
Remote from Paris – 19th to 21st October 2020

Flight path tracking and acoustic signature separation of swarm quadcopter drones using microphone array measurements

Gert Herold*, Adam Kujawski, Christoph Strümpfel, Svenja Huschbeck, Maarten Uijt de Haag, Ennes Sarradj

Technische Universität Berlin

Summary

Unmanned aerial systems (UAS) are used for a wide variety of applications, including agriculture, law enforcement, search and rescue, mapping, and journalism. The number of applications can be expected to increase in the near future, as is the impact of such systems on the environment – urban or rural. Moreover, unknown UAS penetrating airport areas pose an increasing security threat to flight operation.

In this contribution, flight paths and individual acoustic signatures of up to four simultaneously flying quadcopter drones are calculated from measurements with a 64-channel microphone array. The data processing consists of two steps. First, a frequency-domain beamforming method is used to reconstruct the individual flight trajectories. The separation of the sound signals from the drones is accomplished in a second step using a moving-focus time-domain beamforming method.

The accuracy of the flight paths calculated from the array measurements is evaluated by comparing them to paths reconstructed from additional synchronous camera recordings. The quality of the separated acoustic signatures is assessed via reference measurements of a single drone of the same type.

*Corresponding author: gert.herold@tu-berlin.de

1. Introduction

The noise emitted by unmanned aerial systems (UAS) differs in many ways from conventional aircraft or road vehicle noise. A study conducted by the NASA Langley Research Center concluded that UAS noise was perceived by study participants as more annoying than road noise [1]. It can also be expected that UAS will generally operate closer to people on the ground and that their use will not be limited to a specific area (e.g. around airports). Against this background it must be assumed that previous noise certification procedures – e.g. according to ICAO Annex 16 [2] – are only partially applicable to the new and very specific UAS noise.

A study performed by the German Federal Environmental Agency investigated sound emissions of multiple quadcopter UAS with a maximum take-off mass below 2 kg, including (psycho-)acoustic measurements during both indoor and outdoor flight campaigns as well as the definition of horizontal and vertical noise directivity patterns [3]. The vulnerability of the measuring method for determining the sound power level according to ISO 3744 [4] for slight changes of the 3D position was identified. Furthermore, the use of the aforementioned measurement method to determine a reproducible sound power level is only useful for UAS in hovering, which represents only a very specific operating mode. Typically, such devices are also intended to perform translatory movements.

Performing measurements including flight tests, on the other hand, poses challenges regarding the reproducibility or tracking of the flight paths, which is necessary for a correct source characterization. The reconstruction of flight paths using acoustic sensors has been the subject of recent research [5, 6, 7]. Flight tests of larger UAS usually have to be performed in open spaces, where additional noise sources might be present. This makes it necessary to additionally filter signals emitted by the measured object. Moreover, with increasing number of applications for UAS, monitoring the noise impact caused by the drones will become important. If several drones are present in the vicinity, it is necessary to acoustically separate the immissions from the individuals, i.e. follow multiple trajectories at once.

In this contribution, a method for reconstructing trajectories of multiple simultaneously flying quadcopter drones and isolating their respective acoustic signatures using microphone array measurements is presented. The method was tested in an anechoic chamber with up to four UAS flying at the same time in five different flight scenarios. The accuracy of the acoustic position detection is quantified by calculating the deviations to positions detected using a dual-camera setup for 3D localization. Coherent trajectories with time-dependent position and velocity information are calculated and attributed to the individual drones. Using these trajectories, the microphone array is dynamically focused, following the path of each drone and filtering the respective acoustic signals.

2. Materials and methods

2.1 Measurement setup

Measurements were performed in the anechoic chamber at the Department of Engineering Acoustics at TU Berlin. For acoustic recording, a planar array consisting of 64 wall-mounted microphones with an aperture of 1.5 m was oriented towards the ceiling. While not ideal for 3D localization, this setup ensures that the equipment does not interfere with the flight paths. Battista et al. [8] showed that source positions in 3D can be obtained from measurements with a planar array even though the resolution capability perpendicular to the array plane is lower than in lateral direction.

Additionally, synchronous video recordings were done with two cameras. One of the cameras was positioned near the array center with the same orientation as the array. The other camera was fixed to the chamber wall, with its principle axis pointing towards the focus area above the array. The setup as viewed from above is depicted in Figure 1.

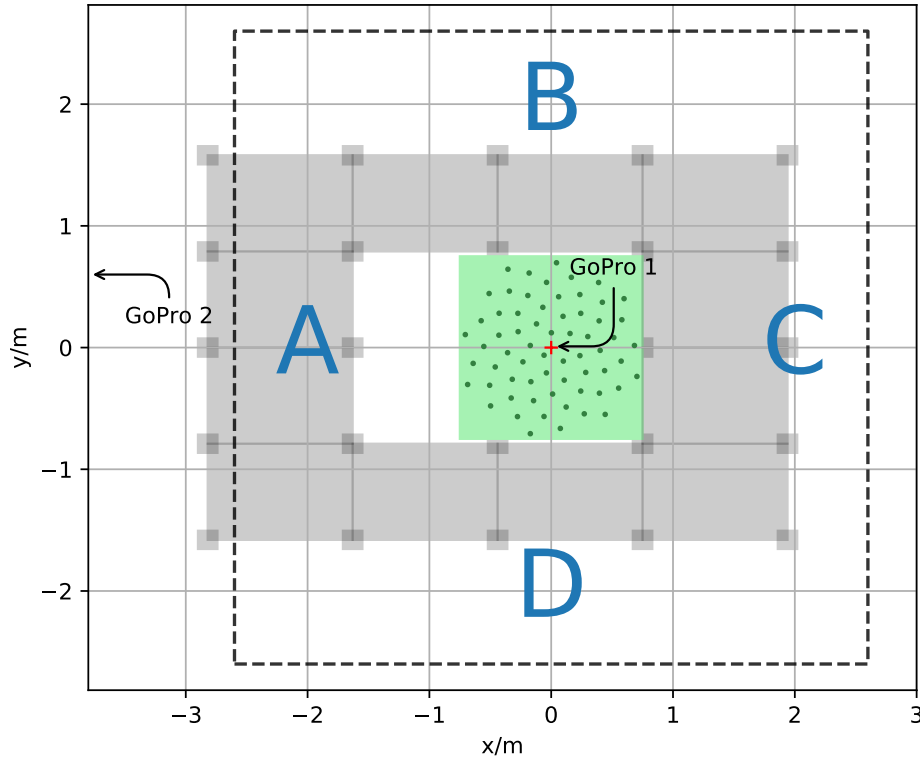


Figure 1: Measurement setup with the 64-channel microphone array and the FATO sites A-D. The dashed line marks the x - y -extent of the area monitored by the array.

2.2 Measurement object

Four small quadcopter UAS (Type: Tello EDU, Manufacturer: Ryze Technology, see Fig. 2) were used for the flight experiments, enabling remote-controlled as well as pre-programmed auto piloted swarm-like flights above the microphone array. The Tello EDU is a small UAS (sUAS), with a weight of 87 g (incl. propellers and batteries), sizing 9.8 cm by 9.2 cm (without propellers and protection guards) and a propeller diameter of 7.6 cm. As the Tello EDU only uses optical flow sensors and an inertial measurement unit for inflight positioning, it is suitable for indoor flights and comparable small flight distances, where global navigation satellite systems like GPS or GALILEO are not available. All sUAS were integrated into a WiFi network and controlled via a Python-based programming interface. In this experimental setup, the Tello EDU only accepts vector- and speed-based control inputs (up-, down-, for- and backwards, yaw along z axis, speed control), thus an implementation of flight plans consisting of several 3D coordinates and time was not possible.

Five flight scenarios above the array were designed, from single flights to swarm flights using four sUAS. The setup of final approach and take-off (FATO) sites (A, B, C, D) is shown in Figure 1. Due to suboptimal flight conditions (e.g. low light and uneven floor), the navigation performance in vertical and lateral extension repeatedly deviated from the target flight path.

- Scenario 1: One sUAS is taking off from FATO A upwards to 1.3 m flight height and flies towards FATO C, where it lands.
- Scenario 2: Two sUAS are taking off from FATO A and FATO C respectively, upwards to 1.3 m flight height, and simultaneously fly in opposite directions above the array center towards the opposite FATO.
- Scenario 3: Two sUAS are taking off from FATO A and FATO C respectively, upwards to 1.3 m flight height, and simultaneously fly in opposite directions towards the array center, where a



Figure 2: Tello EDU (left) and preparation of measurement flights with 4 identical Tello EDU sUAS (right)

static hover maneuver with a 90° turn towards FATO B and FATO C is performed.

- Scenario 4: Four sUAS are taking off from FATO A-D and fly at different flight heights to the opposite FATO.
- Scenario 5: Four sUAS fly remote-controlled along arbitrary paths.

Schematics for the first 4 scenarios are given in Fig. 3.

2.3 Flight path reconstruction

Flight records with 4D-trajectory information (3D position + time) of the sUAS are not available directly but could be calculated based on parsing raw measurements of the IMU (translatory acceleration and rotation rates). However, due to drift effects and non-accurate timestamps, this approach is not accurate enough to determine the true position above the array. Hence, the IMU information was not used and the flight paths of the drones were only reconstructed by evaluating video and audio recordings respectively.

2.3.1 Optical tracking

To visually monitor the trajectory of the moving drones during the experiment, consumer-grade cameras (GoPro Hero 7 black) were used in a stereo setup. Each of the cameras covered a different view of the volume of interest. However, their exact alignment was not known a-priori. GoPro 1 was positioned near the center of the microphone array, with its field of view covering the ceiling of the chamber; GoPro 2 was mounted on the wall in “A”-direction, oriented towards the opposite wall. Figure 4 shows the views of the respective cameras.

A shooting mode with an aspect ratio of 4:3 (2704×2028), 2.7k resolution, and a frame rate of 50 fps was selected to capture the spatially limited recording area. The wide field of view of the camera’s fisheye lens made it possible to observe a large area in the volume of interest. However, the images contained additional radial and tangential distortion.

In order to use the measured 2D images to reconstruct the drones’ flight path in the real world 3D coordinate system, the lens distortion and the relative positioning, including rotation and translation of the camera views, must be known. The determination of unknown lens parameters (tangential

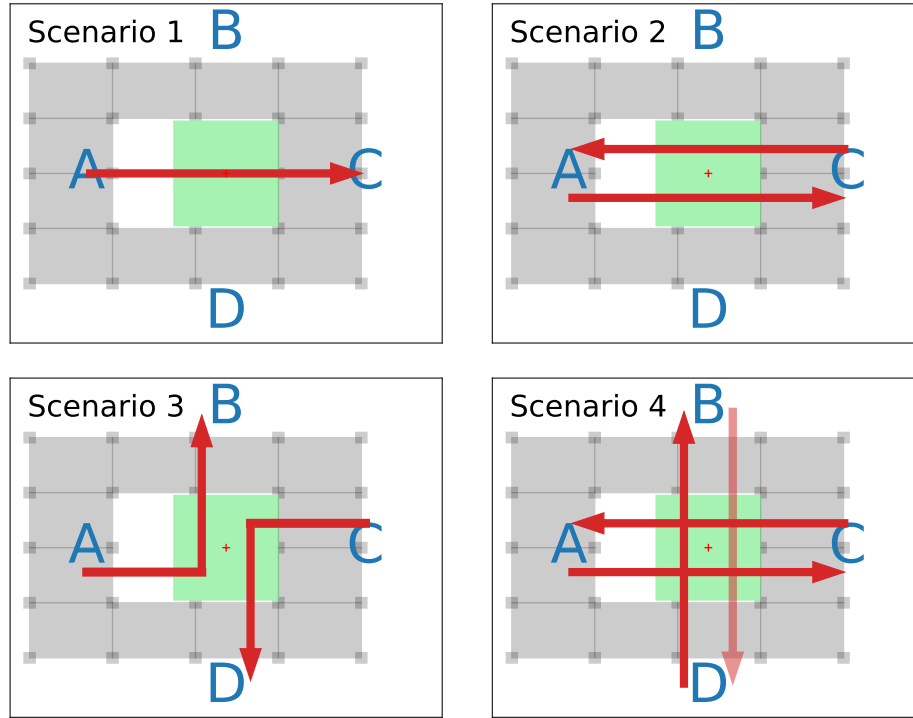


Figure 3: Pre-programmed flight scenarios of the drones.

and radial distortion coefficients, focal length, principal points) and alignment of optical sensors is an often encountered problem in computer vision [9], widely known as camera calibration.

As described by Abdel-Aziz et al. [10], the mapping from measured image points to object space involves a two-step transformation, which they introduced as Direct Linear Transform (DLT). The DLT coefficients can be determined using the Sparse Bundle Adjustment (SBA) method [11], which solves the nonlinear least-squares problem based on multiple measurements of a calibration object with known position in the field of view projected on the image plane. Due to the size of the observation volume, no object that completely fills the measuring field and has known 3D dimensions could be used for calibration. Instead, two blue balls attached to a rod with fixed and known distance, often referred to as a “wand” in the literature [12], were moved in the field of view as shown in Figure 4. A total of 200 frames with paired points was used for the calibration.

The edges of several visible absorbing wedges and the lamps were used as additional 64 points that project from the real world coordinate system on the image plane of the two cameras for calculating the camera parameters. For tracking of the wand and calculation of the DLT coefficients via SBA, the Python-based software *Argus* was used [13]. The world coordinate frame was chosen to be aligned with that of the camera positioned on the microphone array. To ensure that the camera coordinate system also matches that of the microphone array, a small loudspeaker was positioned at a distance of 1 m to the center of the array and used as visual and acoustic reference point. The center of the camera coordinate system was then adjusted accordingly in x , y and z direction so that the position of the reference point in the camera coordinate system coincides with that of the microphone array. It should be noted that this step only accounts for a possible translation between the two coordinate systems but did not compensate any rotation. However, based on the comparison of acoustically obtained trajectories and those determined from image data, it is assumed that the rotation is negligible.

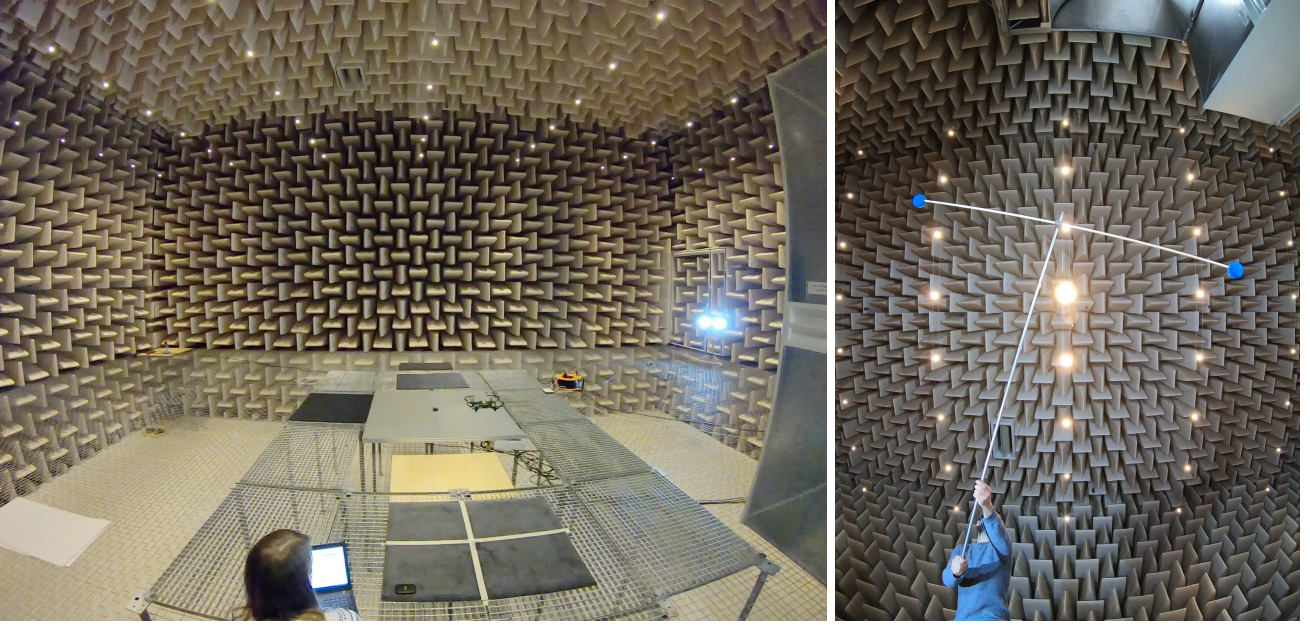


Figure 4: Fields of view of the wall-mounted GoPro 2 (left) and the GoPro 1 positioned at the array center including camera calibration procedure with the “wand” (right).

2.3.2 Acoustic tracking

The reconstruction of the flight paths from microphone array measurements is done in a multi-step process. In a first step, the recording is divided into short tracks of $\Delta t = 0.1$ s length, with the assumption that within that time, a moving drone has changed its position sufficiently little to still be detectable with stationary frequency domain beamforming.

Using Welch’s method [14] with a block length of 512 and an overlap of 50 %, a cross-spectral matrix (CSM) is estimated for each discrete frequency by:

$$\mathbf{C} = \frac{1}{K} \sum_{k=1}^K \mathbf{p}_k \mathbf{p}_k^H, \quad (1)$$

with the number of averaged cross-spectra $K = 19$ in this case. The vector $\mathbf{p}_k \in \mathbb{C}^M$ contains the complex spectral data for each of the M microphones.

For beamforming in the frequency domain, the sound propagation model (i.e. phase shift and amplitude correction according to distances of microphones to focus points $r_{s,m}$) is described via the steering vector \mathbf{h} , whose entries are calculated by

$$h_m = \frac{1}{r_{s,m} \sqrt{M \sum_{l=1}^M r_{s,l}^{-2}}} e^{-jk(r_{s,m} - r_{s,0})}, \quad m = 1 \dots M, \quad (2)$$

with $s = 1 \dots N$ being the focus positions of interest. The reference distance at which the levels are evaluated is set to $r_{s,0} = 1$ m for all focus points. The formulation in (2) ensures the correct detection of a local maximum at the location of a source [15].

For this step, the major objective consists of finding the sources, whereas the exact quantitative information about its strength is not of importance. Therefore, the main diagonal of the CSM is set to zero (as are its resulting negative eigenvalues) and Functional Beamforming [16] can be applied:

$$b(\mathbf{x}_s) = \left(\mathbf{h}^H(\mathbf{x}_s) \mathbf{C}^{\frac{1}{\nu}} \mathbf{h}(\mathbf{x}_s) \right)^{\nu}. \quad (3)$$

Table 1: Measurement and data processing parameters for the beamforming.

Total number of microphones	64
Array aperture	1.5 m
Sampling rate	51 200 Hz
Focus grid (excl. mirror) ($l_x \times l_y \times l_z$)	5.2 m \times 5.2 m \times 1.7 m
Focus grid resolution	0.05 m
FFT window	512 samples, von Hann
Averaging time	0.1 s
Beamforming	Functional Beamforming ($\nu = 8$) Removed main diagonal of CSM
Reference position	$r_{s,0} = 1$ m

The exponent $\nu = 8$ ensures sufficient side lobe suppression. The beamforming is done using the Python package *Acoular* [17] for a three-dimensional, regularly discretized area in which the drones are to be tracked. Acoustic data processing details are summarized in Table 1.

In the next step, local maxima in the focus area are detected using the multi-dimensional maximum filter from the *SciPy* package [18]. To avoid false positives, a hard level threshold below which source candidates are discarded, is set. Furthermore, a slight position resolution enhancement is achieved by calculating the center of mass of the focus grid point containing the maximum and its neighboring points (including up to three neighbors in every direction).

The above steps are repeated for every time step, yielding positions where acoustic sources are detected, which are assumed to be attributed to a drone. A quantitative comparison of the positions calculated from the video recordings to those calculated from the microphone array measurements is done in Section 3.1.

The extracted positional information is, however, still insufficient in two aspects. Firstly, it is not ensured that a movement along the reconstructed points is physical, and secondly, for the case of multiple drones being present in the monitored area, it is necessary to attribute the points to the respective trajectories of the individuals. Both problems are assessed via a two-step process consisting of trajectory prediction combined with solving a linear assignment problem (LAP), based on the method described by Wu et al. [19].

Let the time-dependent state $\mathbf{x}(t)$ of a moving object be described by its 3D position and velocity:

$$\mathbf{x}(t) = (x, y, z, u, v, w)^T \quad (4)$$

With the assumption that the current state exclusively depends on the previous state, one can postulate that

$$\mathbf{x}(t) = \mathbf{F} \mathbf{x}(t-1) + \sigma_p(t), \quad (5)$$

with the transition matrix

$$\mathbf{F} = \begin{pmatrix} 1 & 0 & 0 & \Delta t & 0 & 0 \\ 0 & 1 & 0 & 0 & \Delta t & 0 \\ 0 & 0 & 1 & 0 & 0 & \Delta t \\ 0 & 0 & 0 & 1 & 0 & 0 \\ 0 & 0 & 0 & 0 & 1 & 0 \\ 0 & 0 & 0 & 0 & 0 & 1 \end{pmatrix} \quad (6)$$

and some process noise σ_p . The observed quantities are only the current positions $\mathbf{z}(t)$, which are described by

$$\mathbf{z}(t) = \mathbf{H} \mathbf{x}(t) + \sigma_m(t), \quad (7)$$

with the observation matrix

$$\mathbf{H} = \begin{pmatrix} 1 & 0 & 0 & 0 & 0 & 0 \\ 0 & 1 & 0 & 0 & 0 & 0 \\ 0 & 0 & 1 & 0 & 0 & 0 \end{pmatrix} \quad (8)$$

Table 2: Parameters for the trajectory generation.

Source level threshold	0 dB
Max distance of trajectory points	0.83 m
Max. number of frames w/o source	5
Min. number of valid trajectory points	5
Smoothing filter	$\alpha = \beta = 0.2$

and the unknown measurement noise σ_m .

With a known state $\mathbf{x}(t-1)$ and following Eq. (5), the current state can predicted via

$$\hat{\mathbf{x}}(t) = \mathbf{F} \mathbf{x}(t-1) . \quad (9)$$

This prediction may not necessarily agree with the associated observation $\mathbf{z}(t)$. However, the prediction can be updated to estimate the true state with

$$\mathbf{x}(t) = \hat{\mathbf{x}}(t) + \mathbf{G}(\mathbf{z}(t) - \mathbf{H} \hat{\mathbf{x}}(t)) . \quad (10)$$

Equations (9) to (10) describe a Kalman filter [20]. While it is possible to determine an optimal Kalman gain \mathbf{G} , an efficient simplification is given by the α - β filter with fixed coefficients:

$$\mathbf{G} = \begin{pmatrix} \alpha & 0 & 0 \\ 0 & \alpha & 0 \\ 0 & 0 & \alpha \\ \frac{\beta}{\Delta t} & 0 & 0 \\ 0 & \frac{\beta}{\Delta t} & 0 \\ 0 & 0 & \frac{\beta}{\Delta t} \end{pmatrix} , \quad (11)$$

where α and β are weight factors between measurement and prediction. In this case, values of $\alpha = \beta = 0.2$ yield satisfactory results.

Before applying Eq. (10), the observation $\mathbf{z}(t)$ associated to the prediction $\hat{\mathbf{x}}(t)$ has to be identified. This is trivial in case of a single drone, but can be challenging in case of multiple drones flying in close vicinity of each other. Therefore, a linear assignment problem (LAP) is formulated with a cost matrix \mathbf{D} :

$$D_{ij} = \|\mathbf{z}_i(t) - \mathbf{H} \hat{\mathbf{x}}_j(t)\| , \quad (12)$$

where i and j denote the specific observations and predictions respectively. The LAP is solved using *SciPy*'s linear sum assignment implementation [18].

This process is repeated for every time step, including all detected maxima. If a maximum can not be associated with an existing trajectory, a new trajectory state is initialized. Furthermore, if no associated points can be found for an active trajectory, the drone is assumed to remain at constant speed for a fixed number of time steps. If, after that time, no further valid points are detected, the trajectory is set to inactive and the presumed trajectory states are discarded. Only trajectories with a minimum number of points are regarded as valid. Table 2 summarizes important parameter for the trajectory generation.

2.4 Moving focus time domain beamforming

For filtering the time signal of an individual drone from a measurement where multiple drones were present, beamforming in the time domain (TD) with a moving focus is performed. The formulation of a TD beamformer for one focus point is [21]:

$$p_{\text{out}} = \sum_{m=1}^M h_m p_m(t + \Delta t_m) , \quad (13)$$

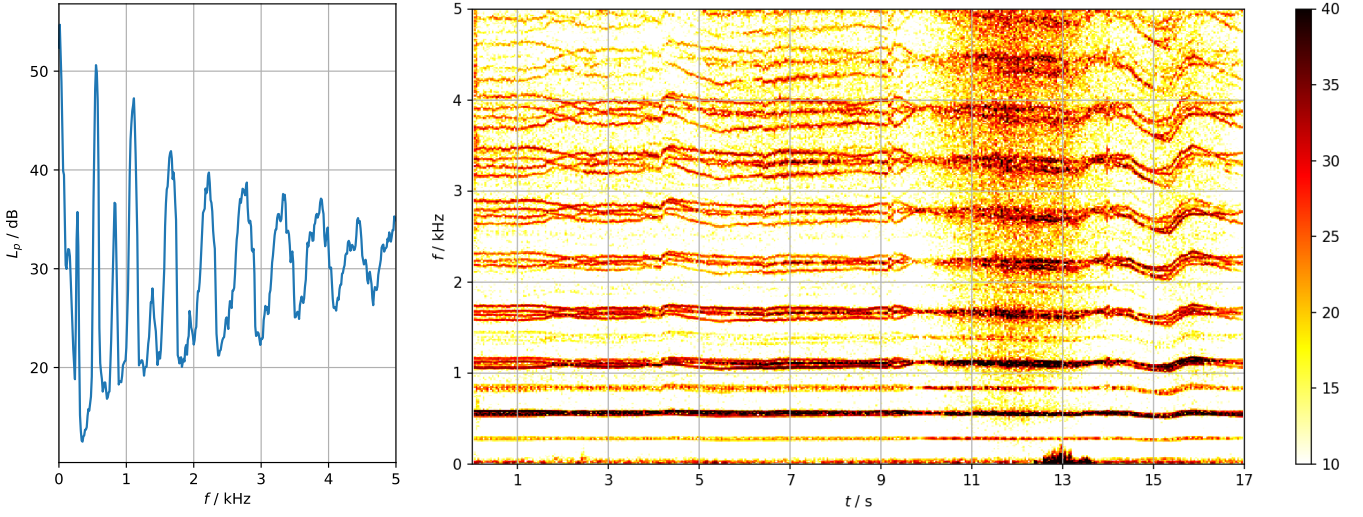


Figure 5: Narrow band spectrum (left) and spectrogram (right) of a single-drone flight (Scenario 1).

with the time delays $\Delta t_m = \frac{r_{s,m}}{c}$ from the M microphones to the focus point, and the steering factor

$$h_m = \frac{1}{r_{s,0} r_{s,m} \sum_{l=1}^M r_{s,l}^{-2}}, \quad m = 1 \dots M, \quad (14)$$

which, in contrast to the formulation in Eq. (2), weighs the signals such that, given the focus point contains an actual sound source, the reconstructed signal *amplitude* is correct [15].

If the focus point is moving, the distance from this point to the microphones is time-dependent $r_{s,m} = r_{s,m}(t)$. Furthermore, the reference position at which the sound pressures are evaluated is set to be in the array center, so the distance $r_{s,0}$ may also change over time. Thus, Δt_m and h_m have to be recalculated for each evaluated time sample according to the trajectory of the observed source. Beamforming again is performed with *Acoular* [17] for each trajectory calculated according to the process described in Section 2.3.2, using one focus point moving along the respective trajectory.

3. Results

The measured drones emit a very characteristic humming noise while flying. Figure 5 shows an averaged narrow-band spectrum ($\Delta f = 12.5$ Hz) and spectrogram for the single drone of Scenario 1, measured at the center-most microphone of the array. The spectrum features strong tonal components, with multiples of the 558 Hz average blade passing frequency (BPF). With two rotor blades on each rotor, this amounts to an average rotor speed of 16 740 rpm. As can be seen from the spectrogram, the actual BPFs of the four individual rotors differ slightly. This is likely due to the internal electronics regulating rotor speed to fulfill different lift requirements for keeping the drone steady while hovering, during acceleration as well as during deceleration.

The measurement starts when the drone is already hovering at an initial position. It then rises another 0.5 m between seconds 4 and 6, where it remains hovering for another 3 seconds. Shortly after second 9, the drone accelerates, entering the space above the array around second 12 and passing the evaluated microphone at around second 13, inducing flow noise on the microphone. This is visible in the spectrogram through an increase of the level at the lowest frequencies. Having passed the array, the drone decelerates at 14 seconds, stabilizes, and begins descent at around second 16.

For the acoustic detection of the position, only the information within small frequency bands of 558 Hz bandwidth is used. With the block size of 512, this amounts to an evaluation of 6 discrete

frequencies per band. The center frequencies for the evaluations in the following section are multiples of 2, 5, 8, 10, 12, and 15 times the BPF.

3.1 Positional accuracy

For the verification of the accuracy of the drone tracking by the array, the drone positions obtained from short-time beamforming of Scenario 1 were compared to the positions yielded by the dual-camera system. It should be mentioned that the camera data can not serve as an exact ground truth of the trajectory, since the accuracy of the camera system itself highly depends on the quality of the calibration, which was not validated in the case and can also vary spatially. However, since the two methods for path detection work completely independent of each other – one relying purely on video while the other only evaluates acoustic data – both results can be compared against each other to quantify the uncertainty.

Acoustic positions were calculated with 10 frames per seconds, optical positions with 50 frames per seconds. Frame recording was not synchronized initially. Therefore, the position determined with the microphone array at one respective time step was compared with the position from image data at the closest time step.

Table 3 shows the average deviation of the acoustically obtained positions from the optically determined positions along x , y and z direction over a number of snapshots for different frequencies. Along the x direction, slightly higher position deviations can be observed on average than along

Table 3: Mean value μ and standard deviation σ of the differences Δx , Δy , Δz of the drone trajectory detected via camera vs. array setup ($\Delta x = x_{\text{cam}} - x_{\text{mic array}}$).

f/Hz	$\mu_{\Delta x}/\text{m}$	$\mu_{\Delta y}/\text{m}$	$\mu_{\Delta z}/\text{m}$	$\sigma_{\Delta x}/\text{m}$	$\sigma_{\Delta y}/\text{m}$	$\sigma_{\Delta z}/\text{m}$
1116	-0.085	0.021	-0.024	0.126	0.029	0.077
2790	-0.059	0.015	-0.048	0.077	0.015	0.027
4464	-0.072	0.018	-0.026	0.078	0.018	0.033
5580	-0.069	0.016	-0.034	0.072	0.016	0.030
6696	-0.086	0.016	-0.044	0.088	0.015	0.035
8370	-0.075	0.016	-0.035	0.077	0.016	0.030

the other directions. However, the mean spatial difference is always below 9 cm. A very good fit with deviations of about 2 cm can be observed along the y dimension. In general, the accuracy of the tracking does not vary a lot for the tested frequencies. At the lowest evaluated frequency of 1116 Hz, the standard deviation increases in all directions.

Figure 6 shows detected points for both methods. As image processing was done at a higher frame rate than acoustic processing, more positions could be determined with the cameras. While the results are in very good agreement towards the C side, on the A side the positions appear to deviate more. This could be attributed to the camera calibration being mostly done with video recordings where the wand was on this side. The comparison proves that for this setup, acoustic tracking can be used as an alternative with similar accuracy as camera tracking.

3.2 Reconstruction of drone trajectories

For the trajectory detection of the different scenarios, all evaluations were done using data recorded with the array and following the multi-step data processing described in Section 2.3.2 at a frequency of 5580 Hz.

The calculated trajectory plots are shown in Figures 7 to 11. The lines indicate the calculated flight paths, with their color (blue to yellow) matching the velocity of the drone at that position. The

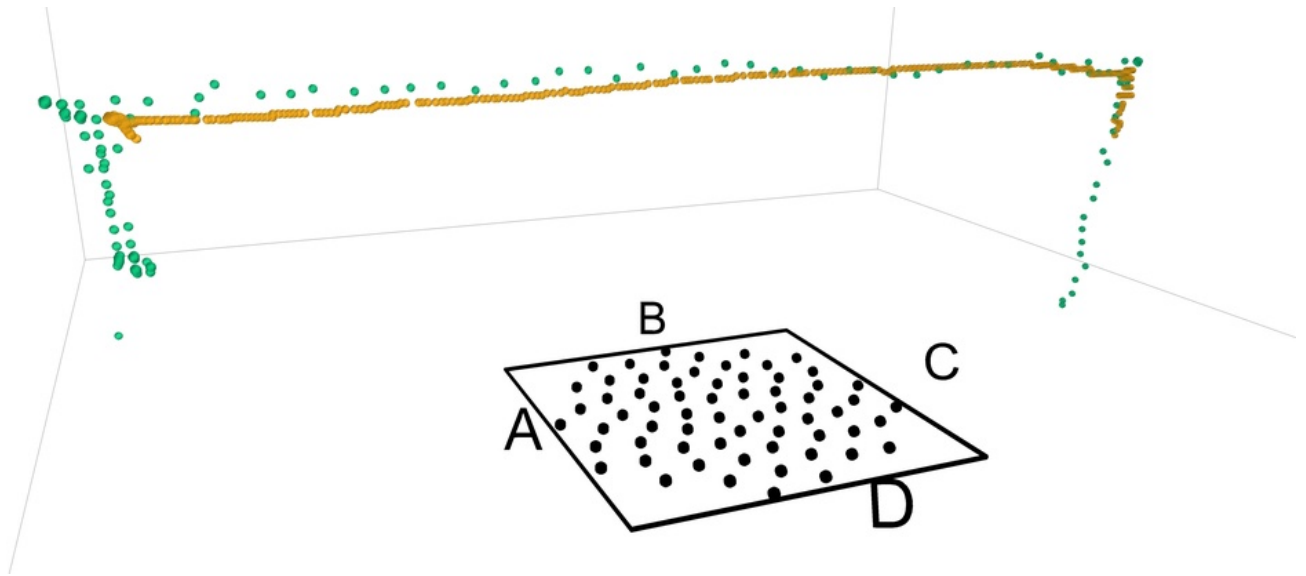


Figure 6: Detected positions of the drone flying Scenario 1. Orange: from video recordings, green: from array measurements (evaluated at 5580 Hz).

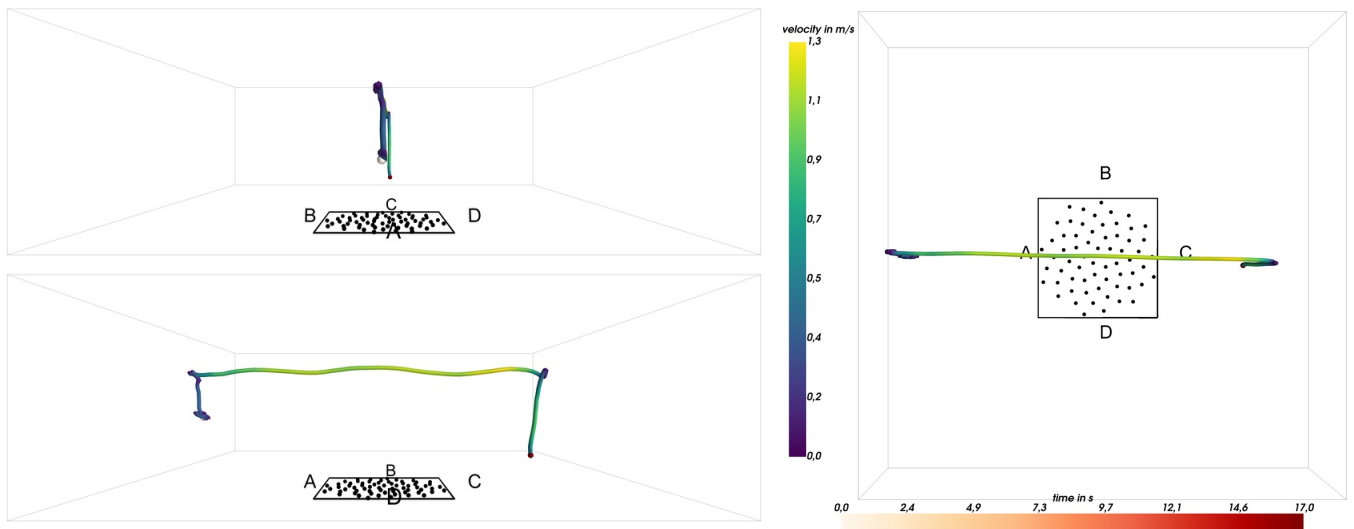


Figure 7: Scenario 1: Single drone flying from FATO A to FATO C.

corresponding scale is given on the vertical colorbar. Each trajectory line begins and ends with a colored sphere, whose color (from white to red) indicates the instance in time at this position. The corresponding horizontal colorbar shows the respective times, which do not necessarily start at zero, since the evaluated acoustic measurement may have started some time before the event of interest happened.

On several occasions, trajectories begin after the start of the recording time or end before recording has stopped. This may indicate several phenomena: drones starting or stopping to fly, drones leaving the monitored area, multiple sound sources on the drones that are sufficiently far away from each other to be detected as individual maxima, or changes in the flying configuration such that in the observed frequency band not enough energy is present to be considered as source by the algorithm. Furthermore, a sudden change of the velocity may lead to the predicted position to be too far from the actual one, so that the flight path of one drone may be cut into several trajectory pieces. Several views of the trajectory of Scenario 1 are shown in Fig. 7. The recording started shortly after take-off, when the drone is hovering for a couple of seconds before it climbs another 50 cm and commences its path from FATO site A to C, where it lands. As can be seen in the side view from B

towards D, the horizontal part of the path is not completely straight. This may either be caused by the drone adjusting its path when its sensors encounter the array or a slight positional error due to an incorrect sound propagation model – e.g. the flow caused by the drone itself is not accounted for. This particular characteristic is not observed in the other scenarios.

Additionally, the climb and landing paths appear to be somewhat slanted away from the array. This is not plausible and was also not physically observed. It can therefore be concluded that this is due to a mapping error by the algorithm, which may be caused by the elongated point spread function lateral sources exhibit at large angular deviations from the array axis, or by different visibility of noise-emitting parts of the drones from the microphones. In the other scenarios, the apparent slanting of vertical climb or descent trajectories at lateral positions can be seen as well.

Scenario 2 is depicted in Fig. 8. The acoustic tracking starts with the drones being already in-flight to the opposite sites. The calculated trajectories are more straight than in the previous case, which may be influenced by the flight height of the two drones being (inadvertently) lower than that of the single drone.

Scenario 3 featured two opposite drones flying towards the center and performing a 90° left turn in front of each other (Fig. 9). Apart from different velocity profiles the drones' trajectories are very similar. It is visible that the drone flying from FATO A to B exhibited a more unsteady hovering behavior while performing the turn.

In general, all pre-programmed flight maneuvers performed as intended during the preliminary tests. However, the poor lighting conditions and the uneven floor in the anechoic chamber led to the drones repeatedly deviating from their projected behavior.

This becomes most apparent for Scenario 4, where one of the drones did not take off. As shown in Fig. 10, the remaining three drones performed as expected. However, the reconstructed trajectory of the drone flying from A to C, with its path being the most elevated of the three, shows several peculiarities. Firstly, the trajectory during hovering was split into three parts. Secondly, the path over the array seems to considerably vary in height, which was not visually observed. Aside from the flight height, this drone intersecting with the drone flying from D to B (in (x, y) positions) at almost the same time might impact the position detection as well.

Finally, a segment of the recording of Scenario 5 is presented in Figure 11. Each of the four drones was individually remote-controlled by a person, and flying was not constrained to the monitored area, which was however extended by 1 m in z direction. As is visible, the reconstructed path is interrupted several times¹. Apparently, the filter configuration with fixed coefficients α and β is not sufficient for obtaining a continuous trajectory in this case. However, in general, the found trajectories are plausible and match the visual observations.

3.3 Separation of acoustic signatures

The emissions of the individual drones are filtered using time-domain beamforming as described in Section 2.4. For each detected trajectory, one time signal is extracted.

Figure 12 shows the filtered spectrogram of the drone flying in Scenario 1. Since there are no other sources present in this case, the characteristics of the spectrogram are very similar to that of a single microphone as displayed in Fig. 5. There are, however, two notable differences: the sound pressure level is generally a little lower for the filtered spectrogram than for the one from the single microphone and the low-frequency noise at second 13 is no longer present.

As is mentioned in Section 2.4, the beamforming calculation spatially filters the sound immission and thus will only yield a correct level if the array is correctly focused to a source position. Here, only one focus point is chosen for each drone, representing all its respective components. Inevitably, this leads to some of the components being slightly “out of focus” and therefore not represented

¹ It should be noted that the two most-closely spaced dark-red points between the letters C and D do *not* mark a falsely detected trajectory interruption but an actual collision of two drones in mid-air.

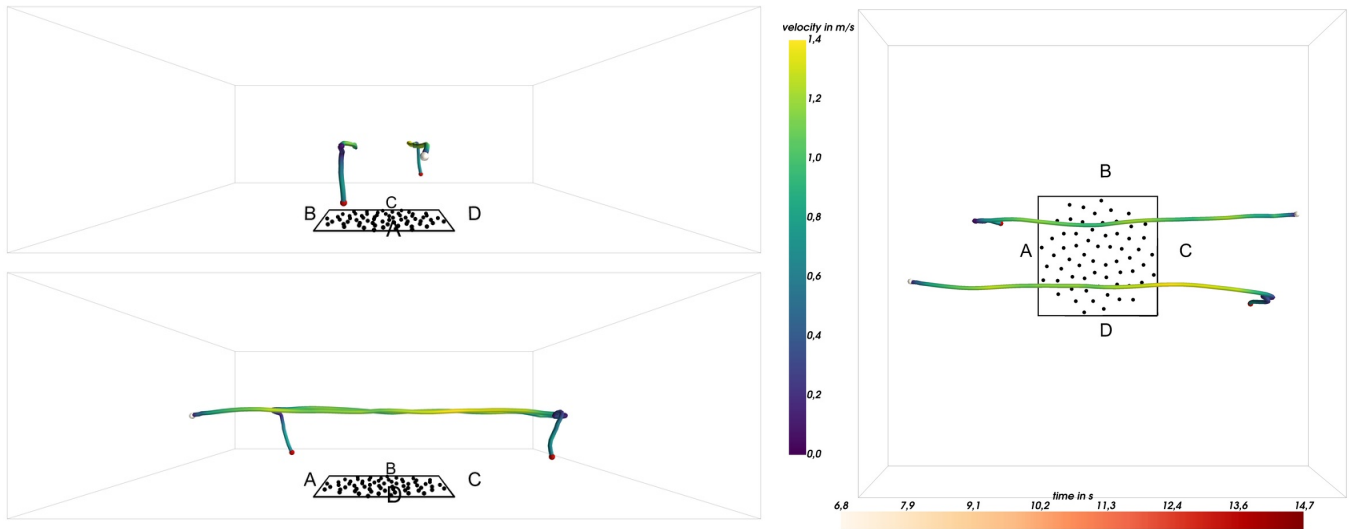


Figure 8: Reconstructed trajectories of Scenario 2: Two drones at FATO A/C flying in opposite direction towards FATO C/A.

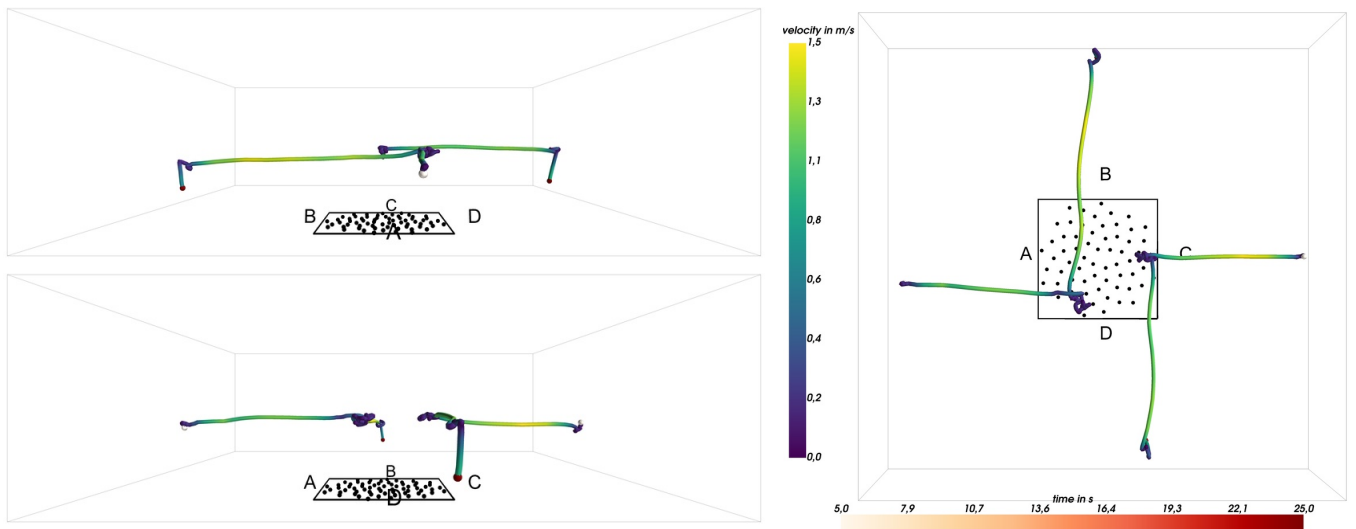


Figure 9: Reconstructed trajectories of Scenario 3: Two drones starting from opposite FATOs A/C, flying towards array, where they perform a left turn and fly towards FATOs B/D.

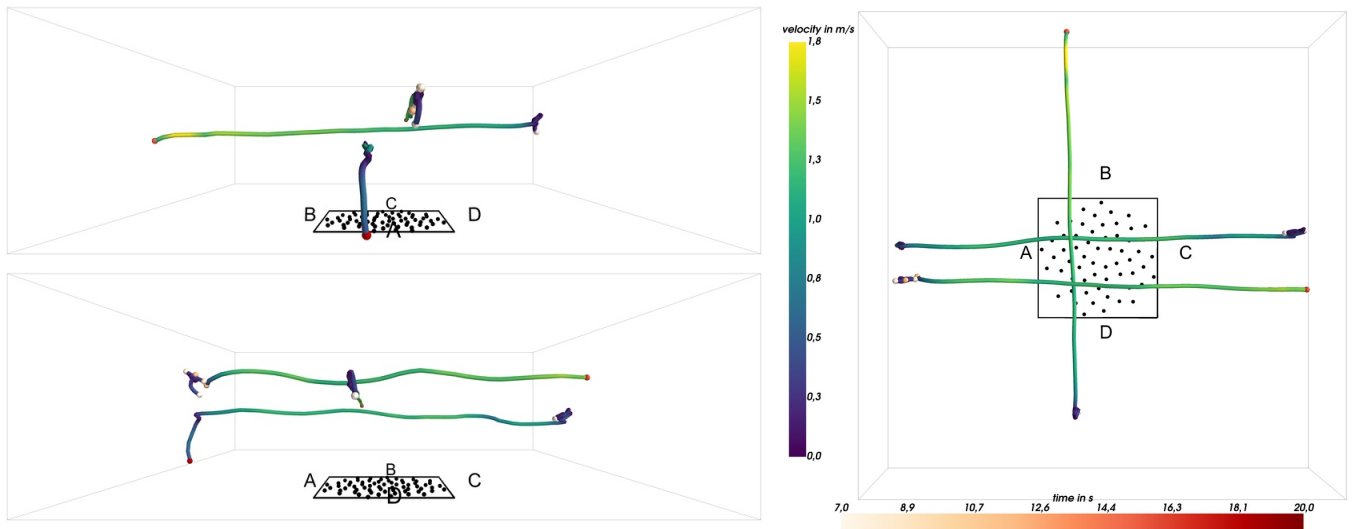


Figure 10: Reconstructed trajectories of Scenario 4: Three drones from FATOs A/C/D flying to the opposite FATO.

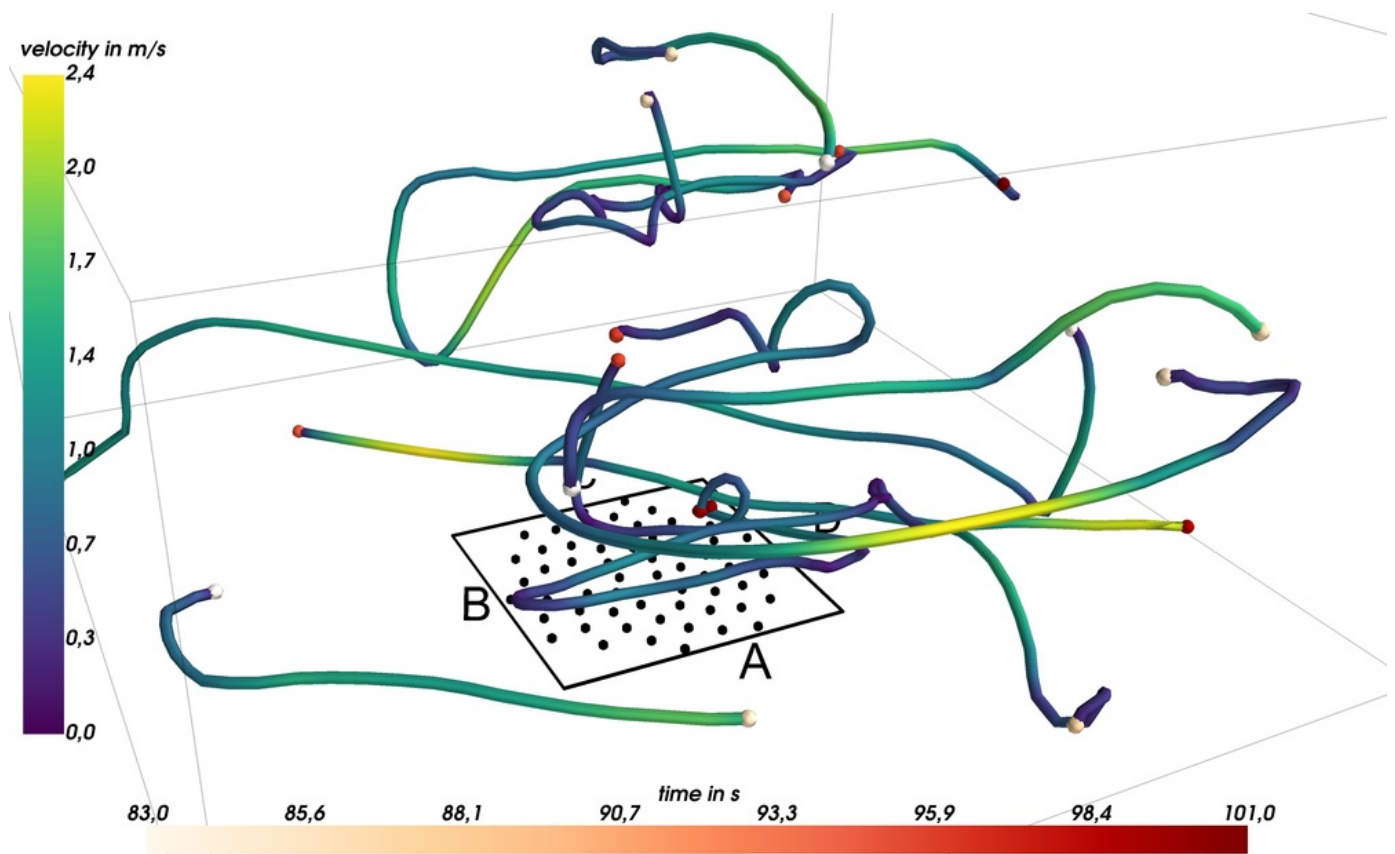


Figure 11: Reconstructed trajectories of a short time segment of Scenario 5: Four drones flying remote-controlled and arbitrarily.

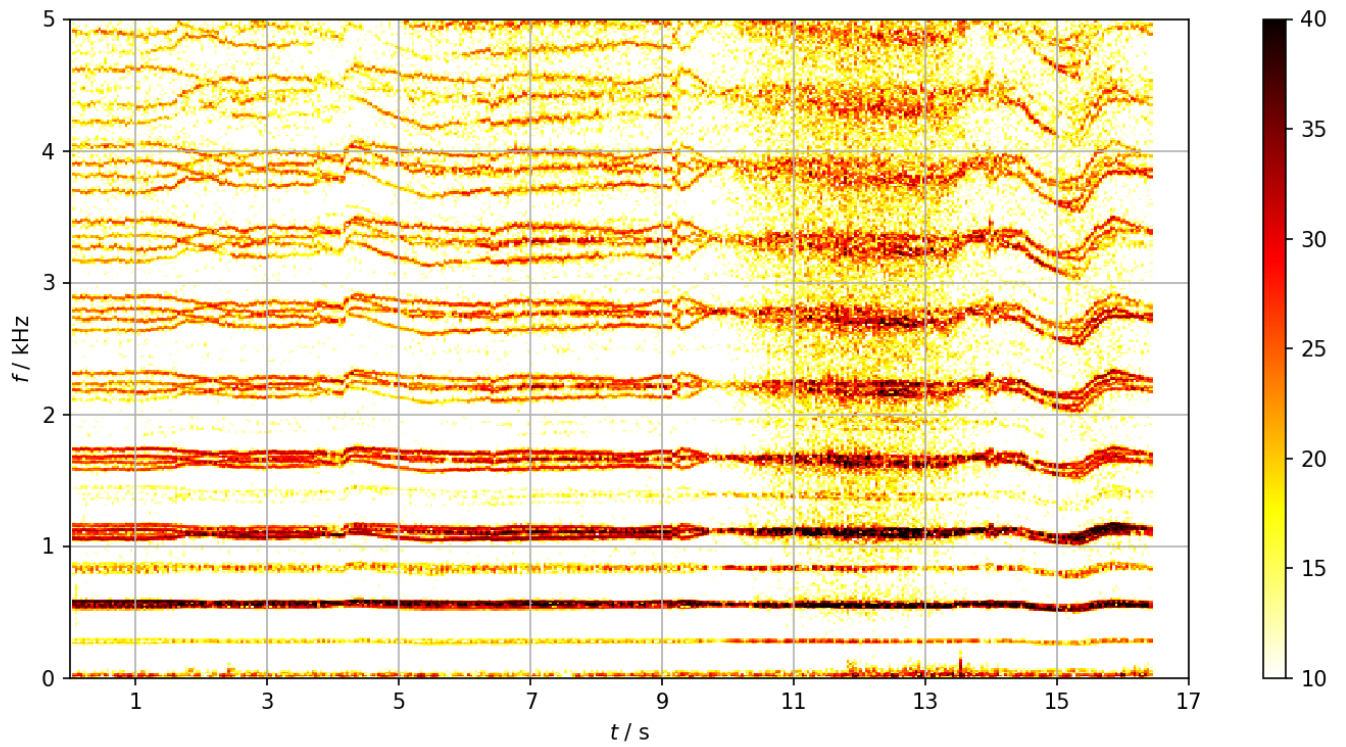


Figure 12: Scenario 1 (1 drone, straight flight): spatially filtered spectrogram of the trajectory (see also Figures 5 and 7).

with their full level. A possible way to avoid this effect would be to encompass each trajectory with a grid of multiple focus point to ensure that all important noise-generating components are accounted for. However, due to imaging artifacts in beamforming, the results would have to be energetically weighted before adding them to a single time track again.

Other possible factors that can lead to an incorrect sound pressure level are the assumed characteristics of the medium – only the average current temperature is taken into account and all flow is ignored – and not taking into account the directivity of the sources. All errors have an larger effect at higher frequencies.

Classic beamforming consists of an averaging of all measured signals, which leads to signal portions only recorded by one sensor – such as the flow-induced noise at the reference sensor at second 13 – being significantly attenuated in the output.

Figure 13 shows the acoustic separation result for Scenario 2. In the single-microphone spectrogram, the BPF-harmonics of all rotors are visible, as can be seen by the 8 lines around the average BPF multiples. The spatial filtering reveals which rotor tones can be attributed to to which of the two trajectories. Furthermore, it can be seen that at the A side of the A-to-C trajectory as well as throughout the whole C-to-A trajectory, one pair of rotors appears to always rotate significantly faster than the other, indicating the tipping of the drone in order to move it horizontally.

The different rotor speeds can also be observed, most prominent on the A side, in the filtered spectrograms of Scenario 4 (depicted in Fig. 14). Moreover, the rotor pairs appear to converge in speed or even switch upon approaching the microphone array, which might be the drone's electronics having to compensate the changing ground conditions (from flow-permeable net to rigid array and surroundings) to maintain undisturbed horizontal flight.

While the drones are within the region above the array, the tonal components of the spectrum are not as clearly distinguishable anymore as the downward flow from the drones interacting with the array disturbs the signal. This is also visible in the other scenarios. For this scenario, the spectrograms corresponding to two of the drones were “stitched” in post-processing, as the

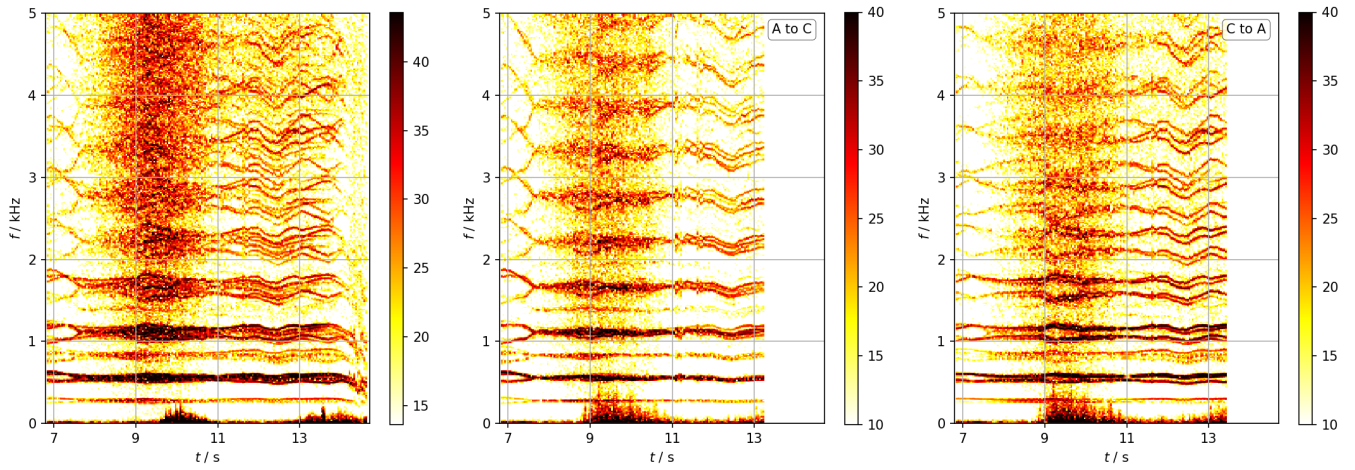


Figure 13: Scenario 2 (2 drones, straight flight): spectrogram at one microphone (left) and spatially filtered spectrograms of the two trajectories (see also Fig. 8).

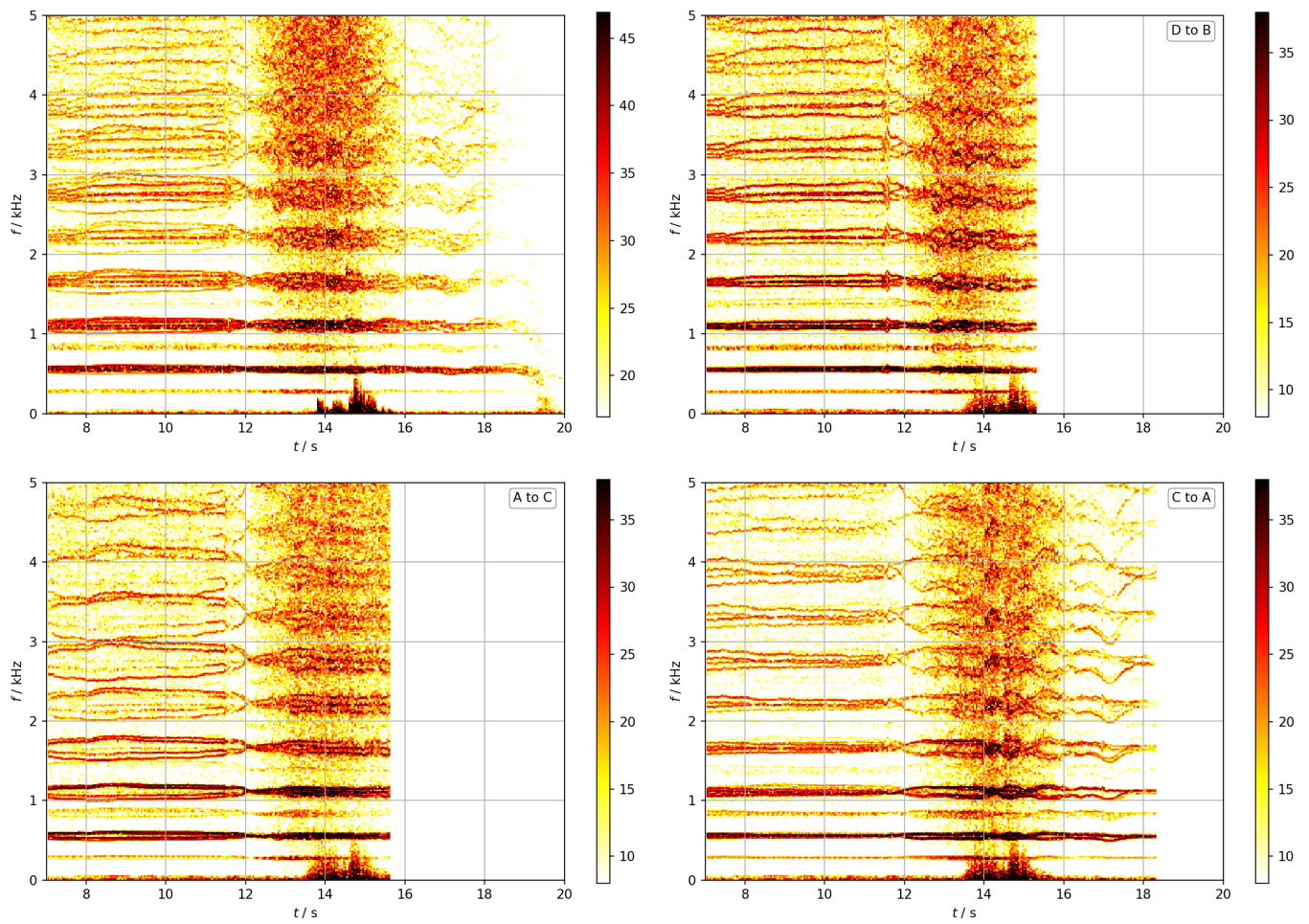


Figure 14: Scenario 4 (3 drones, 3 directions): spectrogram at one microphone (top left) and spatially filtered spectrograms of the three trajectories (see also Fig. 10).

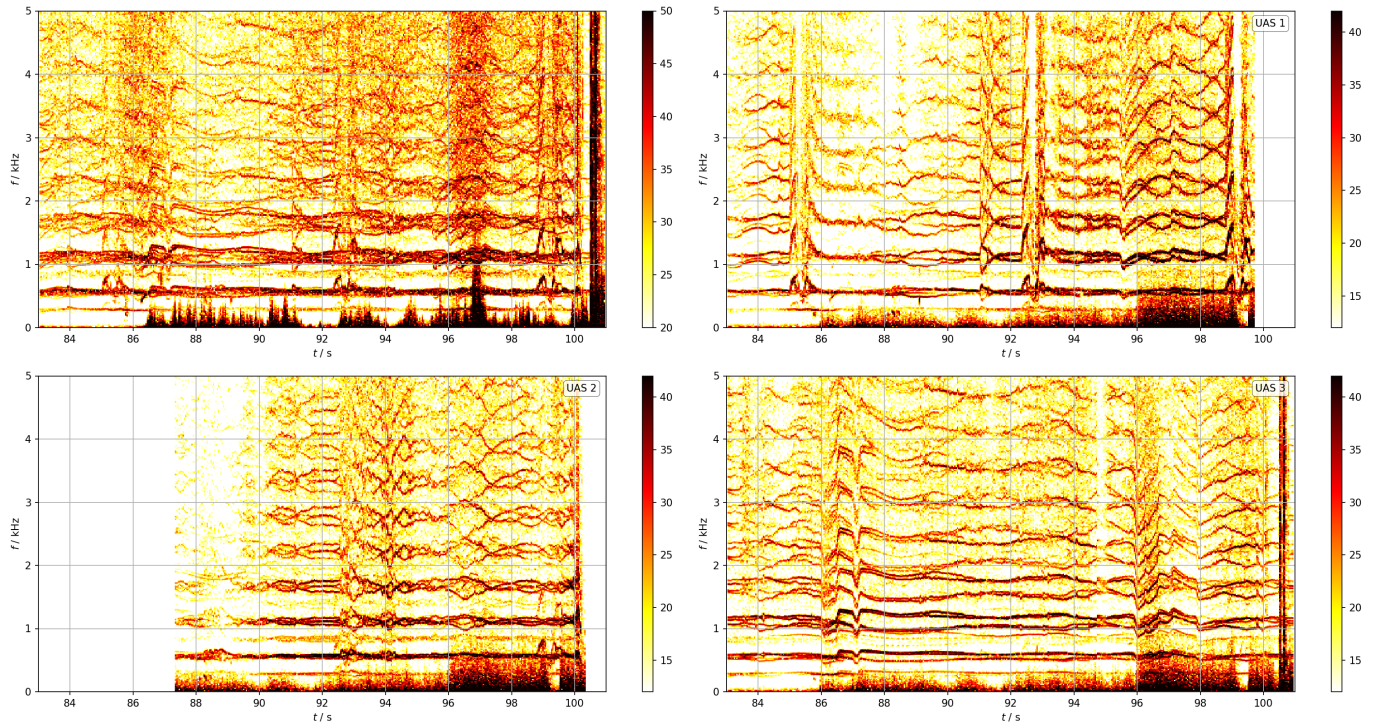


Figure 15: Scenario 5 (4 drones, arbitrary, excerpt): spectrogram at one microphone (top left) and spatially filtered spectrograms of three of the four trajectories (see also Fig. 11).

reconstructed trajectories were interrupted (see Fig. 10). This was done for the excerpt from Scenario 5 as well.

In Figure 15, filtered spectrograms for three of the four arbitrarily flying drones are displayed. During the 18-seconds-period depicted here, the fourth drone only passed the observed volume for short time segments. Compared to the other scenarios, the rotor tones of the drones vary very dynamically. The more elaborate maneuvers flown cause the rotor speed significantly here. For example, the sudden increase-decrease-increase characteristics at around seconds 85, 93, and 99 in the spectrogram of UAS 1 mark a flip performed by this drone.

The spectrograms of UAS 1 and UAS 2 end around second 100, where both drones collided. Even though two impact impulses from these drones falling onto the array are visible in the spectrogram of UAS 3, that drone was not influenced by this event, and the impulses can be attributed to imperfect filtering.

3.4 Computational cost

All calculations were done on a DELL XPS 13 9360 Laptop with 8 GB RAM and an Intel i5-8250U 4×1.60 GHz CPU. The detection of the source candidates with frequency-domain beamforming on the extensive grid is the computationally most costly part of the method, with a runtime of ≈ 80 s per real-time second. The signal extraction with time-domain beamforming adds up to another ≈ 12 s per real-time second.

The presented methods were not optimized for speed. Only one of the available CPUs was used for each calculation, thus it would easily be possible to decrease calculation time through parallelization. Further acceleration, e.g. for real time applications, could be achieved by using less sensors, an adaptive focus grid definition for frequency-domain beamforming, decreased sampling frequency, and by calculating the functional beamforming result with only one discrete frequency or for less time steps.

4. Conclusion

The tracking of multiple synchronously flying UAS and the separation of their respective acoustic signatures using microphone array measurements have been successfully demonstrated. Although the resolution of a planar array as the one used in this contribution is limited, it has been shown to be capable of reconstructing the trajectories in 3D space, even with the drones flying in close vicinity to each other and crossing paths. The used filter setup allows a fast calculation, but can lead to short-time interruptions of some trajectories.

A comparison with position detection from video recordings has shown that acoustic positioning can perform similarly. Several flight scenarios were tested, ensuring the robustness of the method. Therefore, this technique can be applied for cases where the trajectory of moving sound-emitting objects is of interest, be it as redundant unit to video monitoring or stand-alone system.

The acoustically reconstructed trajectories were used as basis for time domain beamforming with moving focus. This allowed the isolation of the signals of the individual drones. The method can therefore be employed for measuring and monitoring acoustic in-flight characteristics of UAS in realistic, non-optimal, i.e. noisy, environments.

The evaluation setup was not optimized for real-time processing. However, with suitable adaptations, achieving such calculation speeds appears possible.

References

- [1] A. Christian and R. Cabell, "Initial investigation into the psychoacoustic properties of small unmanned aerial system noise," *23rd AIAA/CEAS Aeroacoustics Conference, 2017*, no. June, 2017.
- [2] ICAO, "ANNEX 16 to the Convention on International Civil Aviation, Environmental Protection. Volume I - Aircraft Noise. 5th edition, incorporating Amendments 1-9," 2008.
- [3] J. Treichel and S. Körper, "Untersuchung der Geräuschemission von Drohnen," *Lärmbekämpfung*, vol. 14, no. 4, pp. 108–114, 2019.
- [4] ISO, "ISO 3744:2010 – Acoustics – Determination of sound power levels and sound energy levels of noise sources using sound pressure – Engineering methods for an essentially free field over a reflecting plane," 2010.
- [5] X. Chang, C. Yang, J. Wu, X. Shi, and Z. Shi, "A Surveillance System for Drone Localization and Tracking Using Acoustic Arrays," in *2018 IEEE 10th Sensor Array and Multichannel Signal Processing Workshop (SAM)*, vol. 2018-July, pp. 573–577, IEEE, jul 2018.
- [6] V. Baron, S. Bouley, M. Muschinowski, J. Mars, and B. Nicolas, "Drone localization and identification using an acoustic array and supervised learning," in *Artificial Intelligence and Machine Learning in Defense Applications* (J. Dijk, ed.), p. 13, SPIE, sep 2019.
- [7] T. Blanchard, J. H. Thomas, and K. Raoof, "Acoustic localization estimation of an unmanned aerial vehicle using microphone array," *INTER-NOISE 2019 MADRID - 48th International Congress and Exhibition on Noise Control Engineering*, 2019.
- [8] G. Battista, P. Chiariotti, G. Herold, E. Sarradj, and P. Castellini, "Inverse methods for three-dimensional acoustic mapping with a single planar array," in *Proceedings of the 7th Berlin Beamforming Conference*, pp. 1–23, 2018.
- [9] R. Hartley and A. Zisserman, *Multiple View Geometry in Computer Vision*. USA: Cambridge University Press, 2 ed., 2003.

- [10] Y. I. Abdel-Aziz, H. M. Karara, and M. Hauck, "Direct Linear Transformation from Comparator Coordinates into Object Space Coordinates in Close-Range Photogrammetry," *Photogrammetric Engineering & Remote Sensing*, vol. 81, no. 2, pp. 103–107, 2015.
- [11] M. I. A. Lourakis and A. A. Argyros, "SBA: A Software Package for Generic Sparse Bundle Adjustment," *ACM Trans. Math. Softw.*, vol. 36, no. 1, 2009.
- [12] D. H. Theriault, N. W. Fuller, B. E. Jackson, E. Bluhm, D. Evangelista, Z. Wu, M. Betke, and T. L. Hedrick, "A protocol and calibration method for accurate multi-camera field videography," *Journal of Experimental Biology*, vol. 217, no. 11, pp. 1843–1848, 2014.
- [13] B. E. Jackson, D. J. Evangelista, D. D. Ray, and T. L. Hedrick, "3D for the people: multi-camera motion capture in the field with consumer-grade cameras and open source software," *Biology Open*, vol. 5, no. 9, pp. 1334–1342, 2016.
- [14] P. D. Welch, "The Use of Fast Fourier Transform for the Estimation of Power Spectra: A Method Based on Time Averaging Over Short, Modified Periodograms," *IEEE Transactions on Audio and Electroacoustics*, vol. 15, no. 2, pp. 70–73, 1967.
- [15] E. Sarradj, "Three-Dimensional Acoustic Source Mapping with Different Beamforming Steering Vector Formulations," *Advances in Acoustics and Vibration*, vol. 2012, pp. 1–12, 2012.
- [16] R. P. Dougherty, "Functional beamforming," in *Proceedings of the 5th Berlin Beamforming Conference*, (Berlin), pp. 1–25, 2014.
- [17] E. Sarradj and G. Herold, "A Python framework for microphone array data processing," *Applied Acoustics*, vol. 116, pp. 50–58, 2017.
- [18] P. Virtanen, R. Gommers, T. E. Oliphant, M. Haberland, T. Reddy, D. Cournapeau, E. Burovski, P. Peterson, W. Weckesser, J. Bright, S. J. van der Walt, M. Brett, J. Wilson, K. J. Millman, N. Mayorov, A. R. J. Nelson, E. Jones, R. Kern, E. Larson, C. J. Carey, I. Polat, Y. Feng, E. W. Moore, J. VanderPlas, D. Laxalde, J. Perktold, R. Cimrman, I. Henriksen, E. A. Quintero, C. R. Harris, A. M. Archibald, A. H. Ribeiro, F. Pedregosa, P. van Mulbregt, and SciPy 1.0 Contributors, "SciPy 1.0: fundamental algorithms for scientific computing in Python.," *Nature methods*, 2020.
- [19] H. S. Wu, Q. Zhao, D. Zou, and Y. Q. Chen, "Automated 3D trajectory measuring of large numbers of moving particles," *Optics Express*, vol. 19, p. 7646, apr 2011.
- [20] B. D. O. Anderson and J. B. Moore, *Optimal filtering*. Englewood Cliffs, N.J.: Prentice-Hall, 1979.
- [21] D. H. Johnson and D. E. Dudgeon, *Array Signal Processing: Concepts and Techniques*. Englewood Cliffs: Prentice Hall, 1993.



QUIET DRONES
International e-Symposium
on
UAV/UAS Noise
Remote from Paris – 19th to 21st October 2020

UAS Sound Level Prediction using Panel Contribution Analysis

Gong Cheng, Jiazhui Li, and D. W. Herrin
University of Kentucky
dherrin@engr.uky.edu

This paper is adapted from: Cheng, G. and Herrin, D. W., Noise Level Prediction of a Small UAV using Panel Contribution Analysis, Inter-Noise 2018, August 26-29, Chicago, IL (2018).

Summary

The sound pressure level is predicted 5.5 m away from a small UAS in a hemi-anechoic space using panel contribution analysis. The particle velocity and sound pressure were measured using a P-U probe on six surfaces forming a grid encompassing the UAS. Acoustic transfer functions between the source and the receiver location were measured reciprocally. The noise level was predicted at the receiver location from measurements close to the UAS assuming correlated and uncorrelated sources. The sound pressure level calculated by the correlated model compared well with direct measurement. The method was then used to predict the sound pressure level in a room that was not anechoic. The earlier particle velocity and sound pressure measurements were combined with newly measured transfer functions to predict the sound pressure level. The predicted sound pressure level compared well with direct measurement.

1. Introduction

Recreational use of small unmanned aerial vehicles or UAS has expanded because of improvements in technology along with decreased cost. Likewise, commercial applications are becoming more widespread due to the ability to easily manoeuvre a payload without a pilot onboard. UAS are now commonly used in agriculture, film making, 3D mapping, wildlife ecology management, logistics, and other applications [1-2]. As the use of UAS in public areas has increased, noise has been recognized as problematic [3] and the FAA is becoming increasingly concerned [4].

The objective of the current research is to make a series of measurements close to the UAS and then to predict the sound pressure level at some distance away. Once a source model is developed, it is relatively simple to predict the sound pressure level at any distance away from the source in both outdoor and indoor environments.

The approach used is a simple and approximate method commonly referred to as panel contribution analysis or PCA. The method was developed by Fahy [5-6] and Verheij [7-8] over 20 years ago. It has been applied in several different industries [9-10], including aerospace [11]. PCA consists of the following steps.

1. A source is discretized into a collection of panels or patches. These patches should surround a source but need not be on the source.
2. Acoustic transfer functions are measured between the patch volume velocity and the sound pressure and sometimes particle velocity at the receiver position. These transfer functions are most easily measured reciprocally.
3. The volume velocity and sometimes the sound pressure is measured for each patch.
4. The sound pressure in the field can be predicted by summing the products of volume velocities (and sound pressures) and the respective transfer functions.

In this paper, the relevant theory is discussed and then it is applied to a small UAS of the type commonly used by hobbyists.

2. Panel Contribution Analysis

A discrete version of the Helmholtz integral equation can be used to express the sound pressure at a receiver position P in the field. This is expressed as

$$p(P) = \sum_{i=1}^N \left[(v_n)_i \left(\frac{p_i}{Q_R} \right)_{TF_i} - p_i \left(\frac{(v_n)_i}{Q_R} \right)_{TF_i} \right] \Delta S_i \quad (1)$$

where $(v_n)_i$ is the normal velocity and p_i is the sound pressure at the center of patch i . Transfer functions $(p_i/Q)_{TF_i}$ and $((v_n)_i/Q)_{TF_i}$ are measured reciprocally by placing a volume velocity source Q_R at the intended receiver position in the field and measuring the sound pressure and particle velocity at the center of each patch. The UAS should be in the correct position but not operating. For most applications, the second term on the right-hand side in Eq. 1 can be neglected. If a source is relatively rigid, the transfer function $((v_n)_i/Q)_{TF_i}$ will be small since the source will vibrate little when insonified. However, it is included in this case because patches surround the source but are not on the source.

The next phase of the measurement campaign is to identify the volume velocity $(v_n)_i \Delta S_i$ and sound pressure p_i for each patch i with the UAS operating. If phase is not ignored, the volume velocity and sound pressure at the center of each patch can be measured directly using a P-U Probe [12] or a traditional intensity probe. Phase is preserved in the measurements so long as there is an appropriate reference signal. Alternatively, sources may be assumed to be uncorrelated with respect to one another. In that case, the average sound intensity from each patch I_i is measured and the volume velocity Q_i expressed as

$$Q_i^2 = (I_i \cdot \Delta S_i) \frac{2\pi c}{\rho \omega^2} \quad (2)$$

where Q_i replaces $(v_n)_i \Delta S_i$ in Equation (1).

3. Objective

The objective of PCA is to determine the sound pressure level at 5.5 m away from the UAS as shown in Fig. 1. For the baseline measurement of sound pressure level, the UAS was hovering in one corner of the University of Kentucky hemi-anechoic chamber and the sound pressure level was measured in the other corner. A small quad propeller (DJI Mavic Pro) was used.

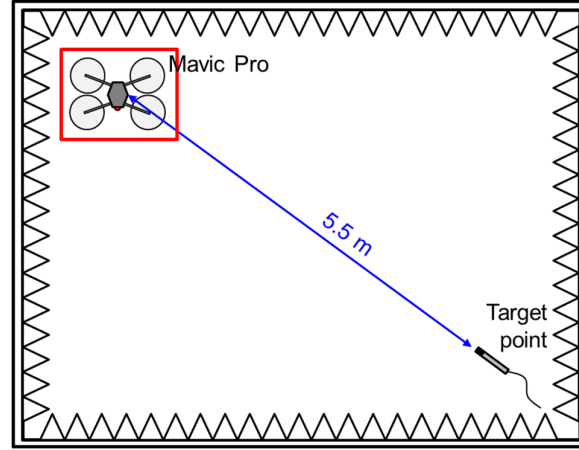


Fig. 1 Sound pressure level 5.5 m from a small drone.

Propeller noise is the dominant noise source for small UAS [12-13]. Tonal noise components dominate at lower frequencies with broadband noise due to turbulence becoming more important at higher frequencies. Fig. 2 shows a measurement of sound pressure level at 5 m away from the UAV. The blade pass frequency is ~200 Hz and there are important harmonics at ~400, 600, and 800 Hz. The blade diameter is 0.2 m and the corresponding tip speed is ~60 m/s while hovering.

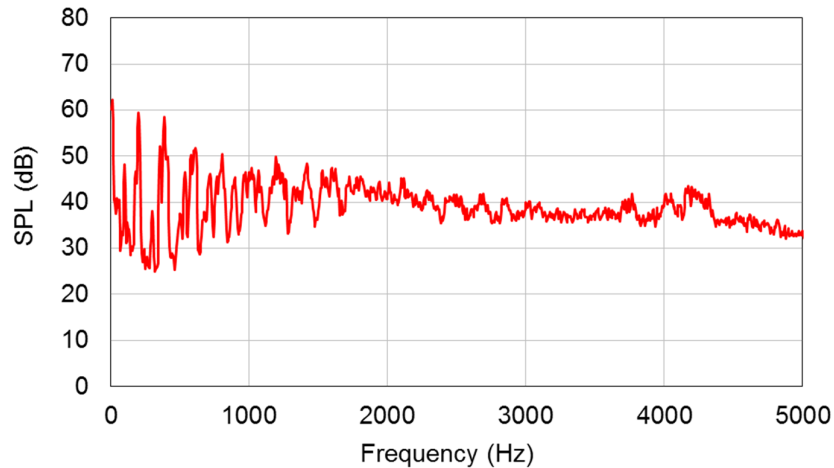


Fig. 2 Sound pressure level 5 m from a small drone.

4. Sound Pressure Level Prediction of UAS

A rectangular cuboidal grid was constructed around the UAS and discretized into patches. The discretization is shown in Fig. 3 with each patch having an area of 10 cm × 10 cm for a total of 64 patches.

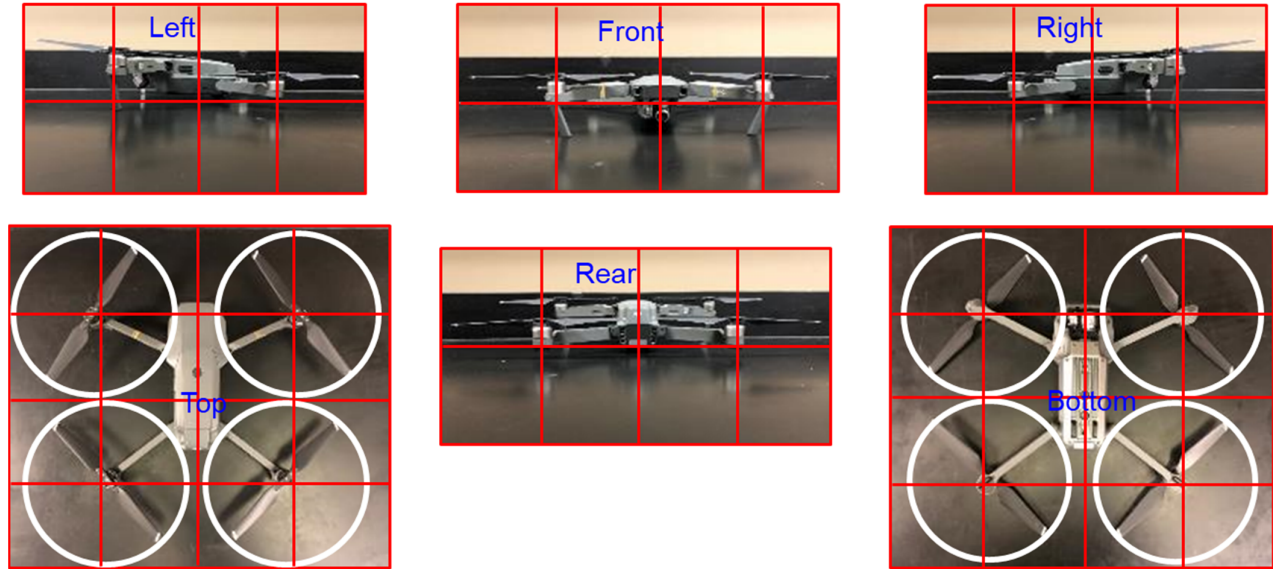


Fig. 3 Patch Discretization on the imaginary box.

Transfer functions were measured with the UAS suspended from a metal frame in the hemi-anechoic chamber at the University of Kentucky as shown in Fig. 4. The UAS is turned off and is positioned 0.8 m above the floor of the chamber. The volume velocity source was placed at a receiver location 5.5 m away from the UAS, and 1.5 m above the ground (i.e., approximately ear level). A microphone positioned 0.8 m away from the source is used to calibrate the sound source. The sound source consists of shop air connected to a metal throat attached to a whiffle ball. This source was validated in Ref. 15. With the P-U probe at the center of each patch, transfer functions $(p_i/Q)_{TF_i}$ and $((v_n)_i/Q)_{TF_i}$ were measured.

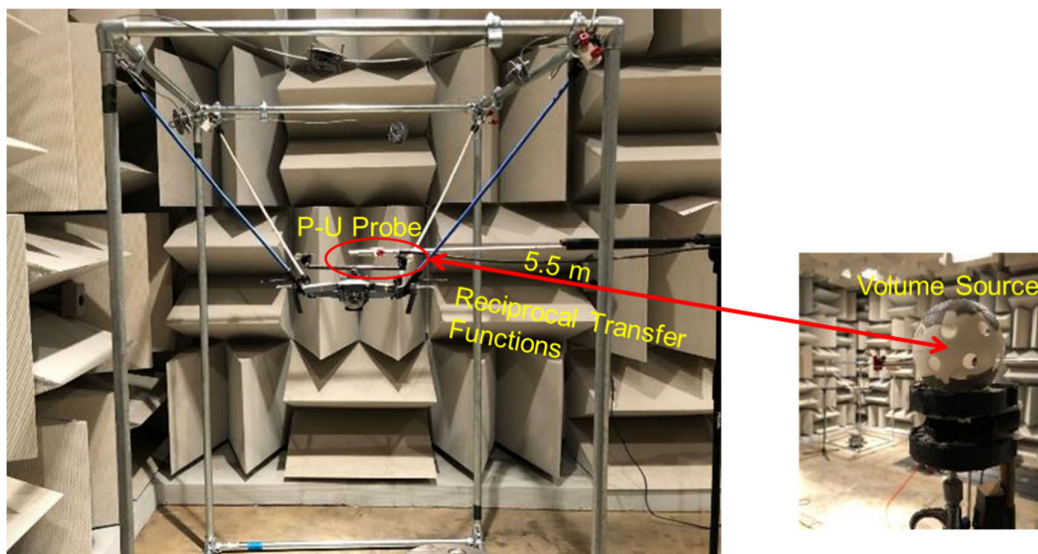


Fig. 4 Transfer functions measurement.

For the operating measurements, the UAS was flown to the same position where it had been suspended in the prior step. The P-U Probe was then used to measure particle velocity, sound pressure and sound pressure at the center of each patch on the rectangular cuboidal surface. Pictures of measurements above and below the UAS are shown in Fig. 5. With the help of a forward and downward vision sensor and motion sensor, the UAS stably hovered in place. Fig. 5 shows the spectrogram for one patch during a 15 second testing period. As the spectrogram shows, the signal was very consistent in the testing window with very little fluctuation in frequency. Hence, measurements were made without the benefit of any holding stand.

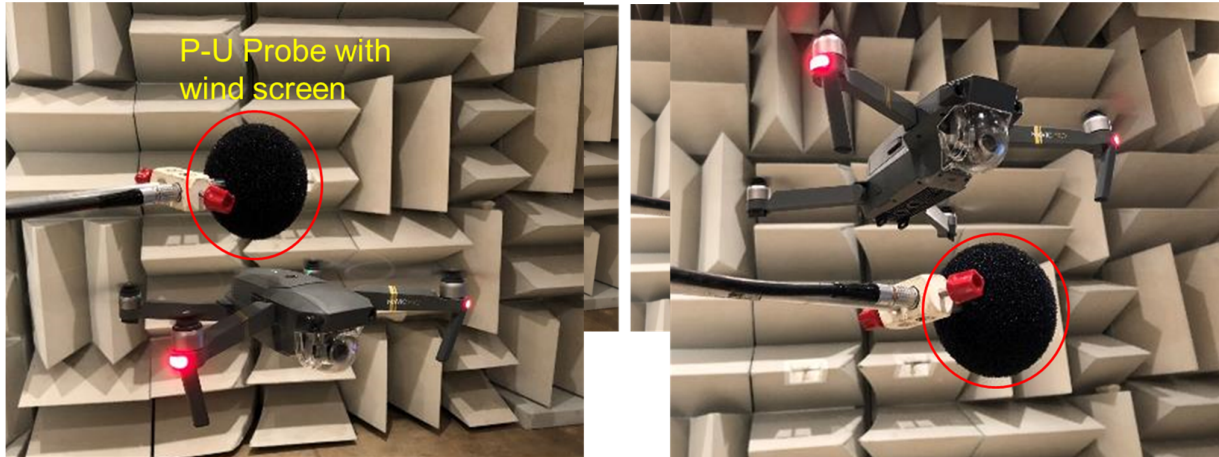


Fig. 5 Particle velocity and sound pressure measurements.

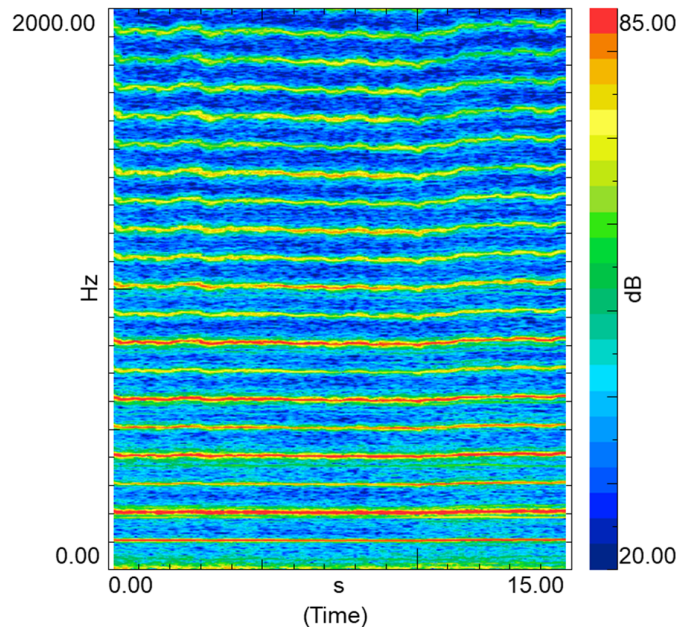


Fig. 6 Spectrogram using P-U prove.

Figure 7 shows the measured sound pressure level at a position below the UAS on the left and the sound intensity level measured at the same location on the right. Notice that two blade pass frequencies from the front and rear blades are identifiable in the sound pressure measurement. However, sound intensity is the product of the sound pressure and particle velocity, and so the sound intensity measurement is directional because particle velocity is a vector quantity. Observe that the sound intensity measurement discriminates between the blade pass frequencies and only picks up that which it is aimed towards.

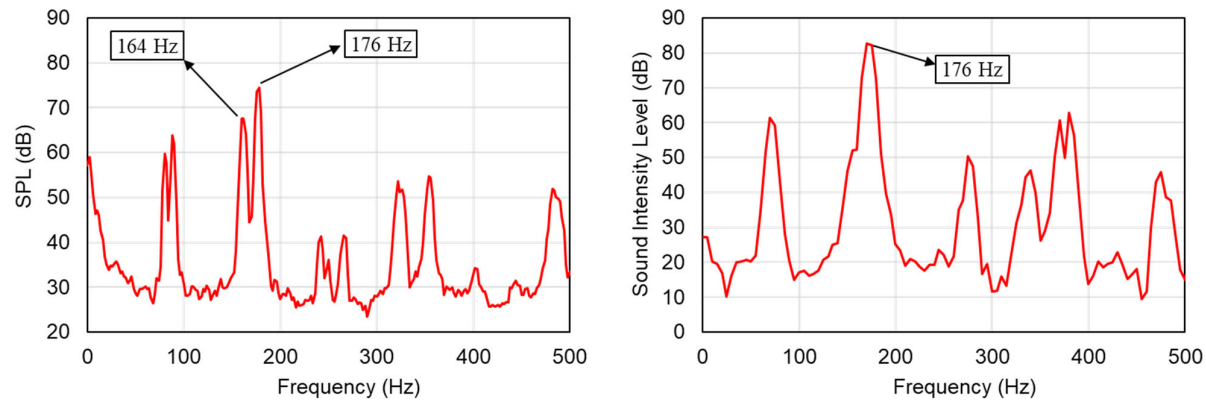


Fig. 7 Sound pressure level and sound intensity level at location below propeller.

Predictions were then made for both correlated and uncorrelated assumptions. The reconstructed and measured sound pressures in narrow band and 1/3 octave bands at the receiver point are shown in Fig. 8. Results based on the correlated source assumption compare very well with measured results. This was anticipated since blade pass noise produces a strong dipole pattern [13] and so the phase information should not be ignored.

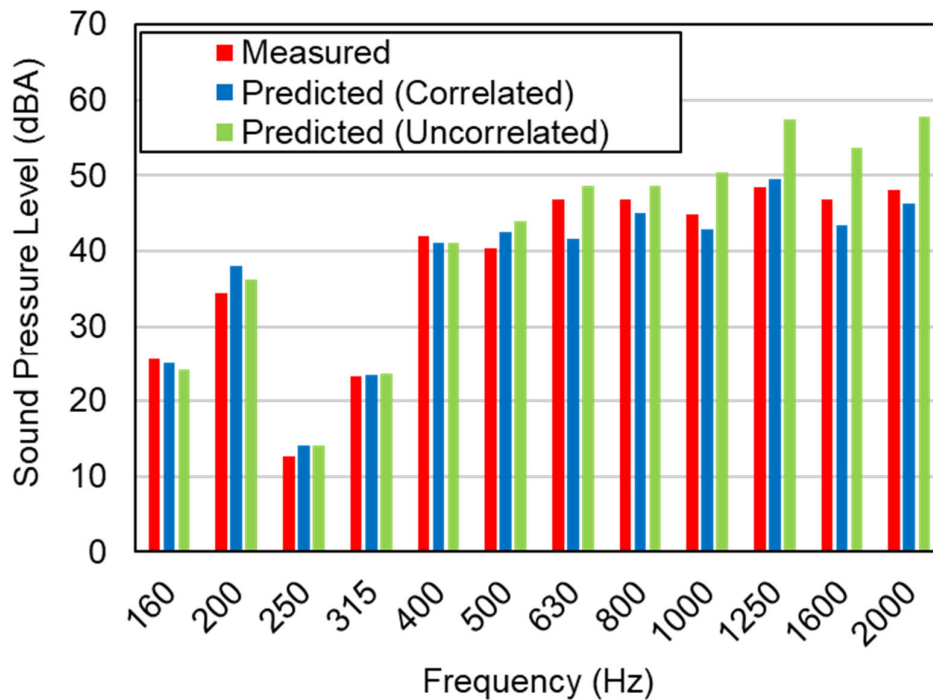


Fig. 8 Sound pressure level at target location.

The sound pressure level contributions from each surface assuming correlated sources are compared in Fig. 9. It can be seen that the top surface is the primary contributor. This result agrees with microphone measurements which showed the sound pressure level to be over 10 dB higher above the UAS compared to below the UAS.

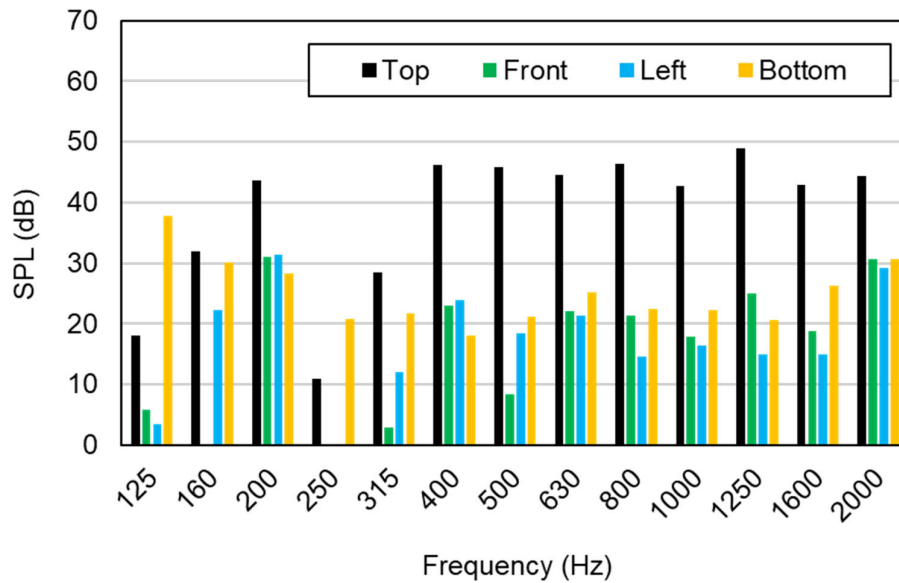


Fig. 9 Contribution analysis.

The UAS was then hovered inside the loft of a bakery as shown in Fig. 10. The loft had hard surfaces on 3 sides, the floor, and ceiling. The sound pressure level was measured at a distance of 4.2 m from the UAS. PCA was used to predict the sound pressure level. The operating measurements from earlier were used again. Transfer functions were measured in the loft using the same procedure described earlier. The PCA predicted sound pressure level is compared to direct measurement in Fig. 11. It can be observed that the agreement is excellent.

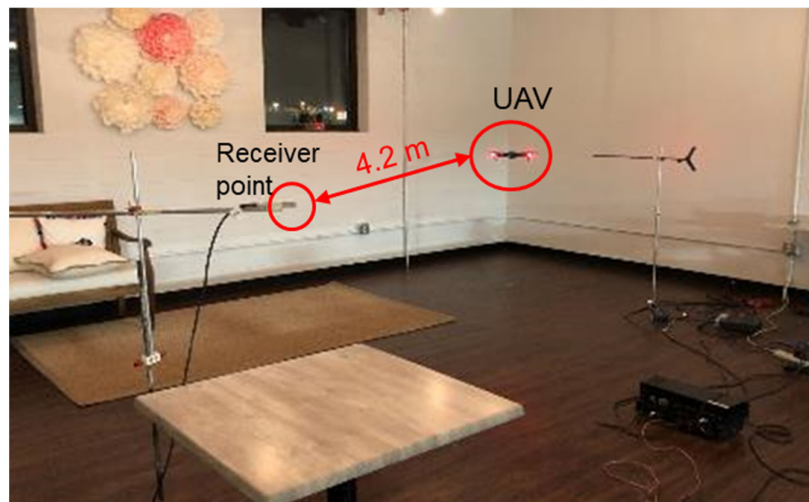


Fig. 10 UAS hovering inside bakery.

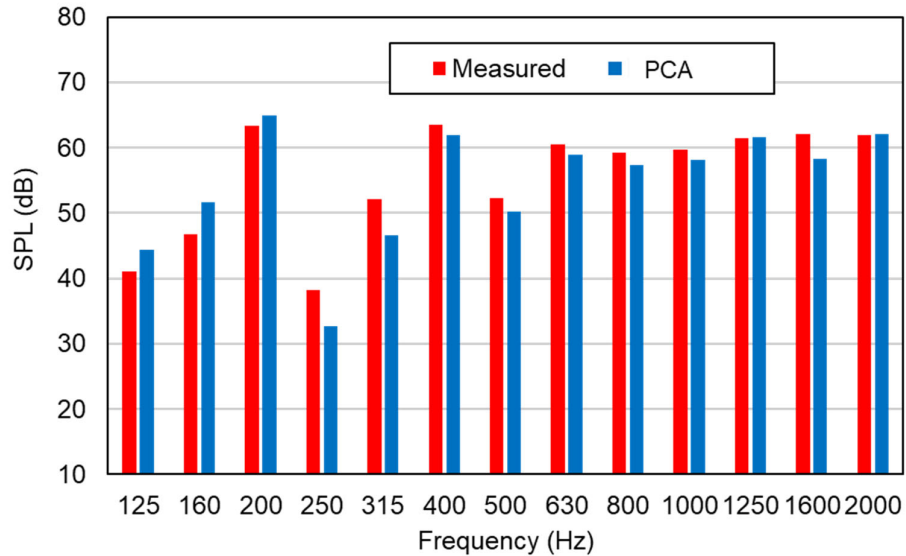


Fig. 11 Sound pressure level comparison.

5. Conclusion

PCA was used to predict the noise radiation from a small UAS. The receiver location was located 5.5 m away from the source in a hemi-anechoic chamber. Transfer functions were measured reciprocally between patches on a rectangular grid encompassing the UAS and the receiver location with the UAV suspended. After which, the volume velocity, sound pressure, and sound intensity for each patch measured using a P-U Probe with the UAS hovering. The sound pressure level at the receiver point was estimated with good agreement compared to direct measurement. The contribution from each surface of the imaginary rectangular cuboidal was compared and the dominant contribution was from the top surface of the UAS. The procedure was then repeated inside a bakery loft with hard surfaces on the walls and ceiling. The results demonstrated that the sound pressure emissions could be predicted after operational measurements are completed.

Acknowledgements

The authors gratefully acknowledge the support of the Vibro-Acoustics Consortium.

References

1. H. Xiang and L. Tian, "Development of a Low-cost Agricultural Remote Sensing System Based on an Autonomous Unmanned Aerial Vehicle (UAV)," *Biosystems Engineering*, vol. 108, Issue 2, February 2011, Pages 174-190 (2011).
2. K. Anderson and K. J. Gaston, "Lightweight Unmanned Aerial Vehicles will Revolutionize Spatial Ecology," *Frontiers in Ecology and the Environment*, Vol. 11, No. 3, pp. 138-146, Apr (2013).
3. B. Berglund, T. Lindvall, and D. H. Schwela, "Guidelines for Community Noise," in *Guidelines for Community Noise*, ed: OMS (1999).
4. C. Burleson, "Aviation Leadership, Economy and Security," *Commercial Aviation: A New Era*, Workshop hosted by the National Academy of Engineering, ed. A. Akay, G. G. Fleming, R. D. Hellweg, G. C. Maling, Jr., and E. W. Wood (2017).

5. F. J. Fahy, "The Vibro-Acoustic Reciprocity Principle and Applications to Noise Control," *Acustica*, Vol. 81, pp. 544-558 (1995).
6. F. J. Fahy, "Some Applications of the Reciprocity Principle in Experimental Vibro-Acoustics," *Acoustical Physics*, Vol. 49, No. 2, pp. 217-229 (2003).
7. J. W. Verheij, "Inverse and Reciprocity Methods for Machinery Noise Source Characterization and Sound Path Quantification. Part 1: Sources," *International Journal of Acoustics and Vibration*, Vol. 2, No. 1, pp. 11-20 (1997).
8. J. W. Verheij, "Inverse and Reciprocity Methods for Machinery Noise Source Characterization and Sound Path Quantification. Part 2: Transmission Paths," *International Journal of Acoustics and Vibration*, Vol. 2, No. 3, pp. 103-112 (1997).
9. J. Zheng, F. J. Fahy, and D. Anderton, "Application of a Vibro-Acoustic Reciprocity Technique to the Prediction of Sound Radiated by a Motored IC Engine," *Applied Acoustics*, Vol. 42, pp. 333-346 (1994).
10. O. Wolff and R. Sottek, "Panel Contribution Analysis – An Alternative Window Method," *SAE Noise and Vibration Conference*, Traverse City, MI, May 16-19 (2005).
11. J. M. Mason and F. J. Fahy, "Development of a Reciprocity Technique for the Prediction of Propeller Noise Transmission through Aircraft Fuselages," *Noise Control Engineering Journal*, Vol. 34, No. 2, pp. 43-52 (1990).
12. F. Jacobsen and H.-E. de Bree, "A Comparison of Two Different Sound Intensity Measurement Principles," *J. Acoust. Soc. Am.*, Vol. 118, No. 3, pp. 1510-1517 (2005).
13. Jack E. Marte and Donald W. Kurtz, "A Review of Aerodynamic Noise from Propellers, Rotors, and Lift Fans," *NASA, Jet Propulsion Laboratory, Technical Report 32-1462* (1970).
14. Rod H. Self, "Propeller Noise," *Encyclopedia of Aerospace Engineering*, online published in Wiley Online Library, December 15 (2010).
15. G. Cheng, D. W. Herrin, J. Liu, and J. M. Stencel, "Determination of Acoustic Emissions using Panel Contribution Analysis and Scale Modeling," *Applied Acoustics*, Vol. 155, pp. 63-74 (2019).



CidB

Centre d'information
sur le **Bruit**

QUIET DRONES
International e-Symposium
on
UAV/UAS Noise
Remote from Paris – 19th to 21st October 2020

Development of surface-processed low-noise propeller for search and rescue tasks with drone audition

Kotaro Hoshiba, Department of Electrical, Electronics and Information Engineering,
Faculty of Engineering, Kanagawa University: hoshiba@kanagawa-u.ac.jp

Ryusuke Noda, Department of Aeronautics and Astronautics, Kyoto University:
noda@kuaero.kyoto-u.ac.jp

Toshiyuki Nakata, Graduate School of Engineering, Chiba University: tnakata@chiba-u.ac.jp

Hao Liu, Graduate School of Engineering, Chiba University: hliu@chiba-u.ac.jp

Kei Senda, Department of Aeronautics and Astronautics, Kyoto University:
senda@kuaero.kyoto-u.ac.jp

Kazuhiro Nakadai, Department of Systems and Control Engineering, School of
Engineering, Tokyo Institute of Technology / Honda Research Institute Japan Co., Ltd.:
nakadai@ra.sc.e.titech.ac.jp

Makoto Kumon, Graduate school of Science and Technology, Kumamoto University:
kumon@gpo.kumamoto-u.ac.jp

Hiroshi G. Okuno, Kyoto University / Future Robotics Organization, Waseda University:
okuno@nue.org

Summary

In disaster-stricken areas, prompt search and rescue operations are required to increase the survival rate according to a "First 72 Hour Response" guideline. UAV (unmanned aerial vehicle) assisted sensing of people is effective in such disastrous situations because a UAV enables prompt operation regardless of the situations on the ground. Because sensing techniques of a UAV rely mainly on vision, it is vulnerable to poor lighting conditions or occlusions. To solve these problems, we instead have focused on audition and developed a sensing technique by localizing human-related sound sources with a UAV-embedded microphone array. One critical issue in localizing sound sources with a UAV is its large ego-noise. To achieve high noise-robustness of sound source localization, we developed two approaches for drone audition. First, we developed a novel microphone array consisting of 12 or 16 microphones embedded in a small spherical-

shaped body. Thanks to this spherical structure, the target sound and ego-noise could be separated properly, and thus noise robustness was improved. Second, we developed an active spectral filtering for sound source localization by dynamically adjusting a frequency range to input signals, and demonstrated its high noise-robustness and low calculation cost. As a next step of a drone audition system, aiming at suppressing the ego-noise level of the multicopter-typed UAV, we developed a surface-processed low-noise propeller in this paper. Inspired by a Gurney flap for the lift enhancement of an airfoil, we designed three models with different structures. The performance of developed propeller models was evaluated in indoor and outdoor flying situations with sound source localization. The evaluation experiments validated the developed propeller models on a drone audition system.

1. Introduction

Researches on search and rescue techniques in disaster-stricken areas are becoming more important due to disasters occurring all over the world. To increase the survival rate, prompt search and rescue operations in 72 hours after a disaster occurs are required, which is known as the "golden 72 hours". In such a situation, sensing using a UAV (unmanned aerial vehicle) is effective because it enables a prompt operation regardless of the ground situations. Such sensing techniques with a UAV mainly rely on vision, and thus are vulnerable to poor lighting conditions or occlusions. To solve this problem, sensing technique by localizing human-related sound sources with a UAV-embedded microphone array has been studied. An international competition was also held [1]. One critical issue in localizing sound sources with a UAV is its large ego-noise. A low SNR (signal-to-noise ratio) deteriorates the success rate of sound source localization. For the challenge to achieve high noise robustness in sound source localization, several methods have been proposed. Xu et al. reported the method to create a frequency mask for MUSIC (multiple signal classification) [2] processing using LSTM (long short term memory), which is a kind of machine learning technique [3]. Wang et al. reported the method to estimate sound source directions and enhance the target sound by time-frequency processing [4]. Lee et al. reported a sound source localization algorithm with two directional microphones using a band pass filter, an improved minima controlled recursive averaging method and a Wiener filter to reduce ego-noise [5].

We have tackled this challenge through two approaches based on drone audition that is an extension of robot audition [6-8]. The first approach is to develop a high-performant sound source localization algorithm with low computational cost. In this approach, various MUSIC-based, noise-robust sound source localization methods have been reported. For example, iGSVD-MUSIC (MUSIC based on incremental generalized singular value decomposition), which calculates a noise correlation matrix from received signals and whitens ego-noise by generalized singular value decomposition, suppresses the dynamically changing ego-noise [9]. We have proposed AFRF-MUSIC (MUSIC with active frequency range filtering), which calculates a frequency filter using only the four simple arithmetic operations with a low computational cost for real-time sound source localization [10]. The second approach is to develop a microphone array which provides highly robust sound source localization. The developed small spherical microphone array with 12/16 microphones could separate the target sound and ego-noise easily, and thus noise robustness improved [11-13].

This paper, as a next step of drone audition system, aims at suppressing the noise level of the multicopter-typed UAV with a microphone array by a surface-processed low-noise propeller to enhance the audibility for drone audition system. Inspired by a Gurney flap for the lift enhancement of an airfoil, we designed three models with different structures to suppress the sound-pressure levels of propeller noise and to improve the flight efficiency. The performance of developed propeller models on a drone audition system was verified through indoor and outdoor flying experiments in terms of sound source localization.

2. Materials and Method

This section describes the design of low-noise propeller models and sound source localization algorithm used in evaluation.

2.1 Design of low-noise propellers

2.1.1 Propeller Model

The commercial propeller of Inspire 2 (1550T Quick Release Propeller, DJI Ltd., China) was employed as the basic propeller model. The three-dimensional shape of the propeller was reconstructed with the laser scanner images to determine the design parameters of the low-noise propeller based on the original parameters such as chord length and angle of attack at each cross section. The basic model and reconstructed shape are illustrated in Fig. 1. All of the measured parameters of the basic propeller model are summarized in Table 1. Based on the nominal weight ($= 3.44$ kg) and the number of rotors ($= 4$) of Inspire 2, we assumed that the required lift force of a single propeller for the “hovering condition” is 8.4 N, and the rotational speed was adjusted manually for generating the required lift force. Note that the “wing length, R ” we call in this paper expresses the half length of the propeller diameter.

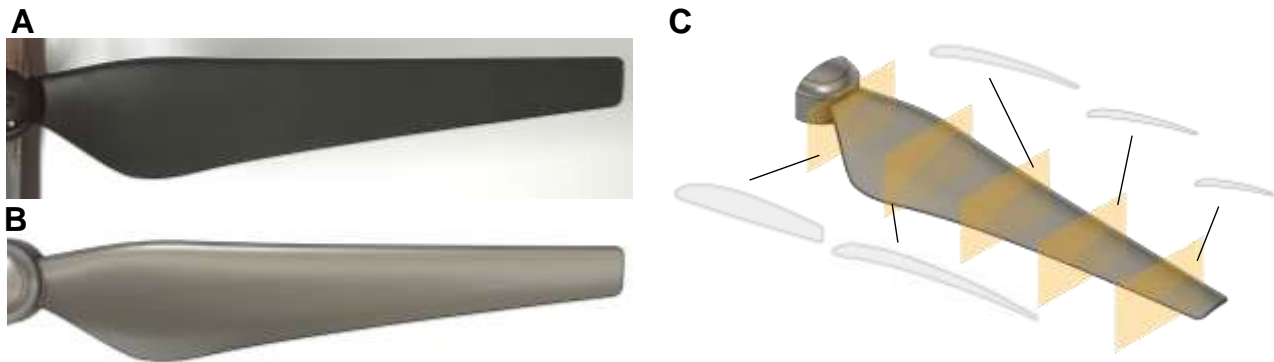


Fig. 1 Top views of (A) Basic propeller model and (B) Reconstructed three-dimensional shape. (C) Reconstructed cross-section at 10%, 30%, 50%, 70% and 90% of the wing length.

Table 1 Parameters of the basic propeller.

Propeller diameter (mm)	380.40
Wing length, R (mm)	190.20
Hub diameter (mm)	27.39
Mean chord length (mm)	25.47
Rotational speed (rpm)	4100
Wing tip velocity (m/s)	81.66
Reynolds number	1.35×10^5

2.1.2 Low-Noise Propeller Model

Inspired by many previous studies on the lift enhancement of an airfoil with a Gurney flap [14–16], we designed three types of the attachments with different span-wise lengths (30.0, 160.4 mm) and different heights (2.0, 3.0, 4.5 mm) located at the trailing edge on the lower surface of the propeller as illustrated in Fig. 2. Fig. 2(A) and (C–E) show the photos of the basic and developed propellers, and (F–H) are the schematics of the attachments for (C–E), respectively. All attachments consist of the series of cylinders with the diameter of 1 mm and the gaps of 1 mm. The attachments for the experiment were fabricated by a 3D printer (Finder, Zhejiang Flashforge3D technology Co., Ltd., China). In addition, the commercial propeller of Inspire 2 for high-altitude operations (Quick Release High-Altitude Propeller, DJI Ltd., China) equipped with

the large propeller pitch and the large chord length was adopted in anticipation of the noise suppression by reducing the rotational speed comparing to the basic propeller model under the hovering condition. Fig. 2(B) shows the photo of the high-altitude propeller.

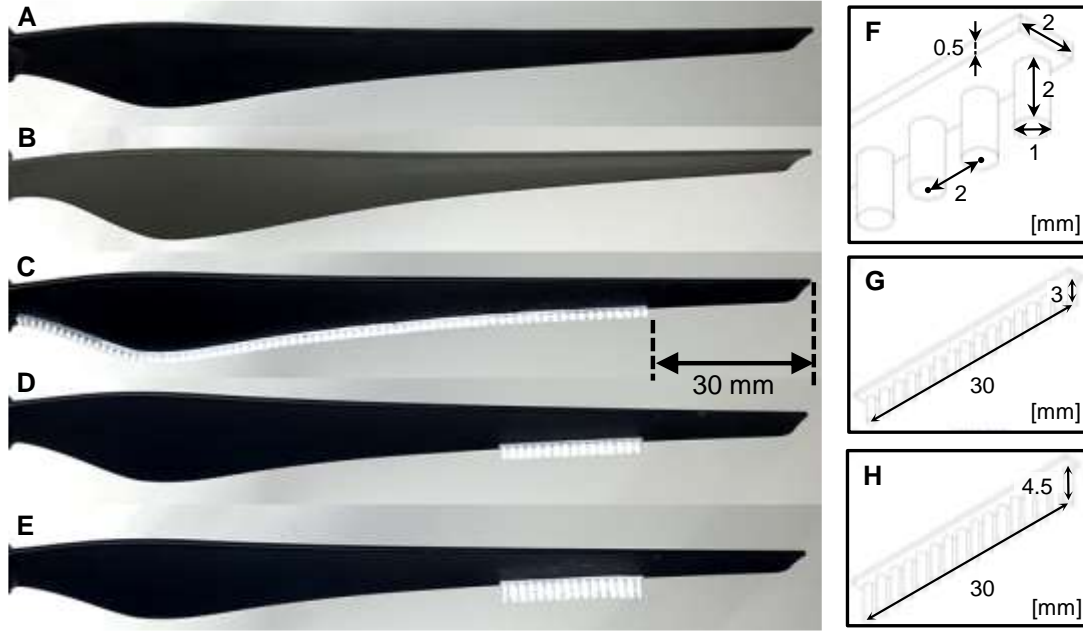


Fig. 2 Upstream-side frontal views of tested propeller models. (A) Basic, (B) High-altitude and (C-E) Gurney flap inspired models. All of the attachments equipped in a Gurney flap inspired models were glued on the trailing edge of the lower surface of the propeller and they were located at a horizontal distance of 30 mm from the wingtips. (F-H) Schematics of the attachments for C-E, respectively. (Hereinafter referred to C-E as "H_2mm_wide", "H_3mm", "H_4.5mm", respectively.)

2.2 Sound Source Localization Algorithm

To evaluate designed low-noise propeller models in terms of robot audition system, SEVD-MUSIC (MUSIC based on Standard Eigen Value Decomposition), which is an original MUSIC method [2], is used as sound source localization method. Our drone audition system developed in previous study used SEVD-MUSIC, iGSVD-MUSIC and AFRF-MUSIC as a sound source localization algorithm. Unlike iGSVD-MUSIC or AFRF-MUSIC, SEVD-MUSIC does not include explicit noise suppression besides sub-space division based on Eigen value decomposition. Therefore, SEVD-MUSIC is suitable to evaluate the noise of designed propeller models simply. The algorithm of SEVD-MUSIC is described below.

The f -th frame of M -channel input acoustic signals are Fourier transformed to $\mathbf{Z}(\omega, f)$. Using \mathbf{Z} , a correlation matrix $\mathbf{R}(\omega, f)$ is defined as follows:

$$\mathbf{R}(\omega, f) = \frac{1}{T_R} \sum_{\tau=f}^{f+T_R-1} \mathbf{Z}(\omega, \tau) \mathbf{Z}^*(\omega, \tau) \quad (1)$$

where ω is the frequency bin number, T_R is the number of frames used for averaging of the correlation matrix and \mathbf{Z}^* is a complex conjugate transpose of \mathbf{Z} . In the SEVD-MUSIC method, eigenvectors are calculated by the eigenvalue decomposition of the $\mathbf{R}(\omega, f)$ as

$$\mathbf{R}(\omega, f) = \mathbf{E}(\omega, f) \mathbf{\Lambda}(\omega, f) \mathbf{E}^*(\omega, f) \quad (2)$$

where $\Lambda(\omega, f)$ is a matrix with diagonal components that are eigenvalues in descending order and $E(\omega, f)$ is a matrix containing eigenvectors corresponding to $\Lambda(\omega, f)$. Using $E(\omega, f)$ and a transfer function $G(\omega, \psi)$ corresponding to the sound source direction ψ in the microphone array's coordinates, MUSIC spectrum $P(\omega, \psi, f)$ is calculated as follows:

$$P(\omega, \psi, f) = \frac{|G^*(\omega, \psi)G(\omega, \psi)|}{\sum_{m=L+1}^M |G^*(\omega, \psi)e_m(\omega, f)|} \quad (3)$$

where L is the number of target sound source and e_m is the m -th eigenvector contained in E . ψ is defined as $\psi = (\theta, \phi)$ with azimuth θ and elevation ϕ in this paper. $P(\omega, \psi, f)$ is averaged over ω direction to estimate the sound source direction as

$$\bar{P}(\psi, f) = \frac{1}{\omega_H - \omega_L + 1} \sum_{\omega=\omega_L}^{\omega_H} P(\omega, \psi, f) \quad (4)$$

where ω_H and ω_L are indices corresponding to the upper and lower limits of used frequency bin, respectively. $\bar{P}(\psi, f)$ represents the power of the sound coming from the direction ψ at the f -th frame. To detect sound source direction, threshold processing and peak detection are performed for $\bar{P}(\psi, f)$.

3. Indoor Experiment

To evaluate the noise level and the aerodynamic efficiency of the developed low-noise propellers under the hovering condition with a single propeller, an indoor experiment was performed first. In this experiment, aerodynamic performances and noise characteristics were measured in an indoor environment with a single propeller.

3.1 Experimental Procedure

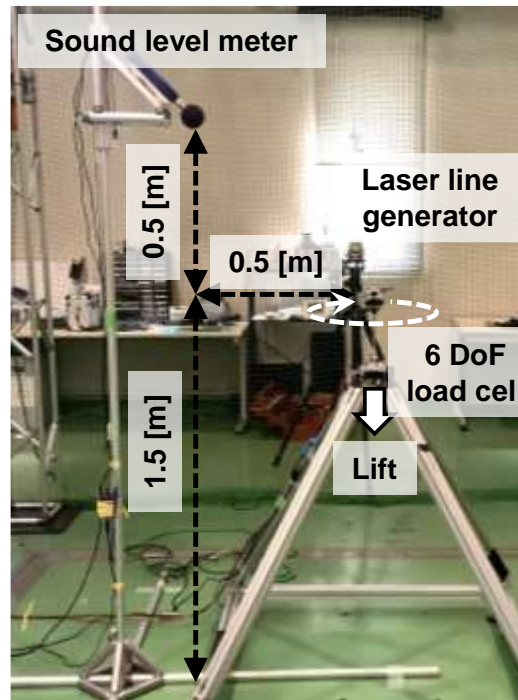


Fig. 3 A snapshot of experimental setup. The propeller models were mounted so that the upper surfaces of the propellers are in the downward direction.

As illustrated in Fig. 3, the propeller models and the brushless DC motor (DR55-M, Shinano Kenshi Co., Ltd., Japan) were attached onto a 6 DoF (degree of freedom) load cell (CFS034CA101U, Leptrino Inc., Japan). The wing tips on the left and right sides of the propeller models were adjusted to be horizontal with a laser line generator for keeping the propeller balance accurately. The force and noise of a single propeller were measured in a quiet room (18 x 9 x 8.4 m). The horizontal distances between the wingtips and the building walls are at least 20 times longer than the wing length, so the wall effects due to the flow interaction are likely to be quite small in this condition. Time-varying dynamic forces (600 Hz) acting on the propeller models were measured for 60 seconds and their averaged values were taken as the steady forces in this study. A precision sound level meter (NL-52, RION Ltd., Japan) was located at a vertical and horizontal distances of 0.5 m from the center of the propeller hub. The noise was measured simultaneously with the force measurements. The Z-weighted sound pressure levels (SPLs) averaged over 60 seconds were obtained in a quiet indoor environment. Note that the noise level in the indoor environment without the rotor noise is about 30 dB while nearly 70 dB was observed with the rotor noise in all tested models.

3.2 Results

In order to evaluate the efficiency of the tested model, the figure of merit (FM) of a propeller is defined as

$$FM = \frac{P_{RF}}{P_{exp}} \quad (5)$$

where P_{exp} expresses the actual power given by the product of the measured torque about the rotational axis and the angular velocity. P_{RF} is the ideal power that means the minimum power for generating the resultant lift force obtained from the experiment, and can be derived by using the Rankine-Froude momentum theory as bellow [17].

$$P_{RF} = \frac{L^{3/2}}{\sqrt{2\rho A}} \quad (6)$$

where A is the area of the actuator disk. A summary of the measured lift forces, torques, rotational speeds, FM s and overall SPL s is given in Table 2, and the measured noise characteristics are illustrated in Fig. 4.

Table 2 Lift forces, torques, rotational speeds, FM s and SPL s of five propeller models.

Model	Lift (N)	Torque (N · m)	Rotational speed (rpm)	FM	SPL (dB)
Basic_1	8.34	0.163	4050	0.671	70.7
Basic_2	8.44	0.165	4125	0.662	70.4
Basic_3	8.42	0.164	4125	0.665	70.5
High-altitude	8.38	0.210	3225	0.659	68.6
H_2mm_wide	8.36	0.214	3525	0.590	68.9
H_3mm	8.45	0.199	3825	0.594	69.2

The three tested basic models show good agreements with each other in terms of all of the values shown in Table 2, and the noise characteristics are also well matched as in Fig. 4. Note that because the resultant lift forces are time-averaged values and considering that there were fluctuations in the forces, we decided to allow for this level of the force variations from the ideal force (= 8.4 N). The high-altitude propeller model has higher angle of attack and can generate

the same amount of the lift force with the basic propeller models at the lower rotational speed. The reduction in rotational speed decreases the overall SPL since the noise from the propeller generally can be proportional to the fifth [18, 19] or sixth power [20, 21] of rotational speed due to the dipole source under the tested flow condition. As can be seen in Fig. 4, the noise levels are significantly reduced from 1.5 kHz to 10kHz while increase below 1.5 kHz. The cause of the increase in this range is not clear, but it is potentially due to the characteristics of the motor. The FM of the high-altitude propeller model is decreased slightly as a result of the increase in the angle of attack that makes the shape of the airfoil suboptimal. The attachment of the Gurney flap in this study modified the performance of the basic propeller models similarly with the increase of the angle of attack. The Gurney flap models reduce the rotational speeds and the overall SPLs down to a similar level of the high-altitude propeller model. The FM of the Gurney flap models were reduced severely, probably because the airfoil shapes as a result of the attachment were not well optimized yet. However, in terms of the noise characteristics, there is a decrease in a different manner with the high-altitude propeller model. Up to 1.5 kHz, the noise levels are maintained at the same level as the basic models and the significant decrease can be seen from 10 kHz to 20 kHz only in the H_2mm_wide model. In the H_3mm model, the increase of the torque from the basic propeller model is suppressed compared to that of the high-altitude propeller model. It can avoid an overload applied to a motor and can reduce a crash due to abnormal heat of motor or ESC after a long flight. Considering the development of “drone audition”, it is expected that there will be a wide range of sounds that should be detected and it will be essential to develop various propeller models with different noise characteristics.

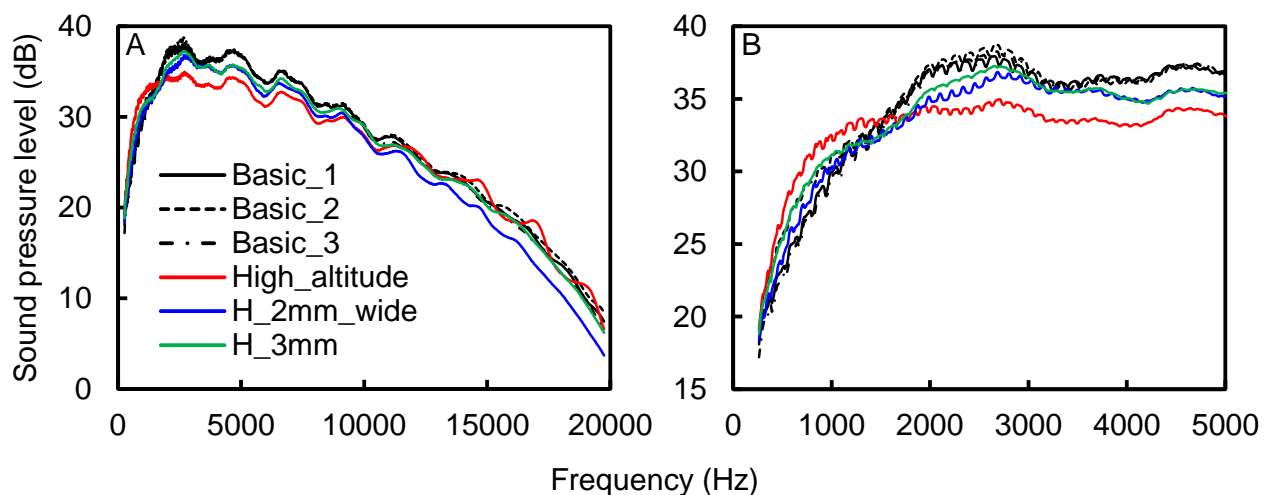


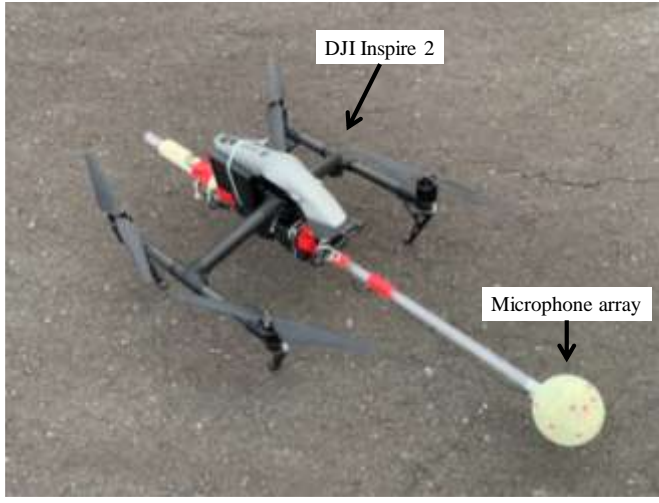
Fig. 4 (A) Moving-average sound pressure levels of tested propeller models. (B) Enlarged view.

4. Outdoor Experiment

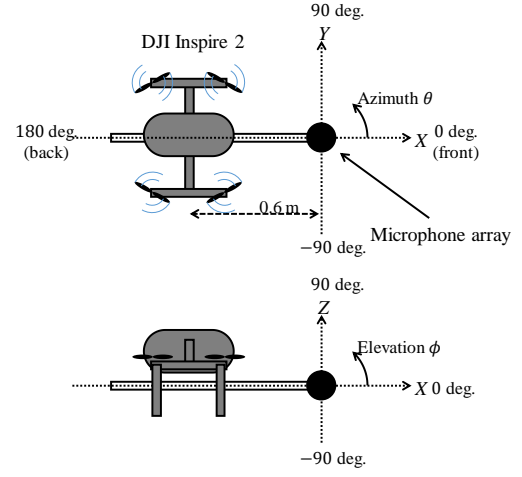
Second, the performance of the designed propeller models on a drone audition system was evaluated in an actual flying situation. In this experiment, five models: basic, high-altitude, H_2mm_wide, H_3mm, H_4.5mm were compared.

4.1 Experimental Procedure

To perform a flying experiment, the drone audition system was developed. As shown in Fig. 5(a), the microphone array developed by Hoshiba et al. [12] was assembled to Inspire 2 with an acrylic pipe at the distance of 600 mm between centers of Inspire 2 and the microphone array. The coordinate system of the microphone array is shown in Fig. 5(b). In a spherical body of the microphone array, sixteen MEMS microphones are embedded as shown in Fig. 5(c) and (d).



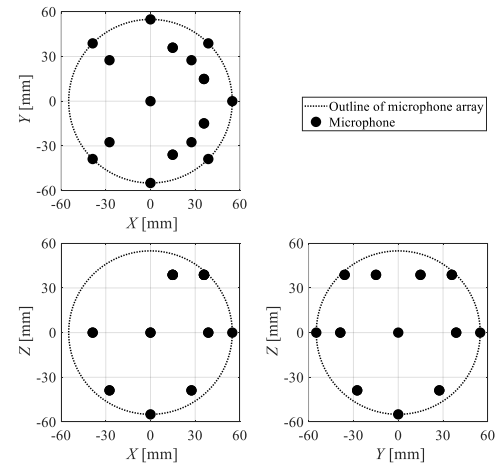
(a) UAV with the microphone array



(b) layout and the coordinate system of the microphone array



(c) closeup view of the microphone array



(d) coordinates of 16 microphones in the microphone array

Fig. 5 Drone audition system.

Acoustic signals were recorded at a sampling frequency of 16 kHz, and a quantization bit rate of 24 bits. Using this microphone array, propeller sounds were recorded in a hovering state. Moreover, a male voice was recorded without UAV as the target sound and clear signals coming from various directions were created through numerical simulations. Directions of the target sound were set as every 10 deg. in the azimuth range of $-180 \sim 180$ deg. and the elevation range of $-90 \sim 0$ deg. The spectrogram of the recorded voice is shown in Fig. 6. To create acoustic signals for sound source localization evaluation in various situations, the target sound with different sound level was added to the propeller sound. Because the drone audition system cannot measure the SPL of the target sound, SNR between the target sound and the basic propeller model's sound was used as the relative index of the target sound level. This index is hereinafter referred as SNR. The range of SNR was $-10 \sim 10$ dB. For each condition, 25 seconds acoustic signal (50 frames) was created. Created signals were processed with SEVD-MUSIC. A transfer function G used in Eq. (3) was derived from the geometric calculation. The parameters set for SEVD-MUSIC are given in Table 3. For visualization of the MUSIC spectrum \bar{P} in Eq. (4), the coordinate system shown in Fig. 7 was defined.

Table 3 Parameters of sound source localization method.

M	2
T_R	50 frame (0.5 s)
ω_H	3 kHz
ω_L	1 kHz

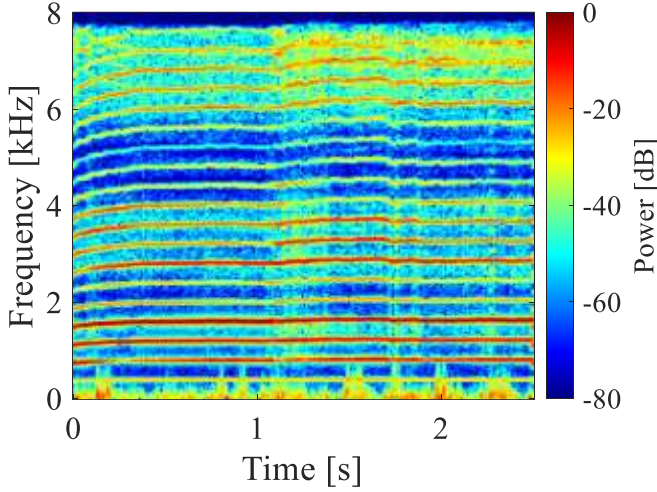


Fig. 6 Spectrogram of the target sound.

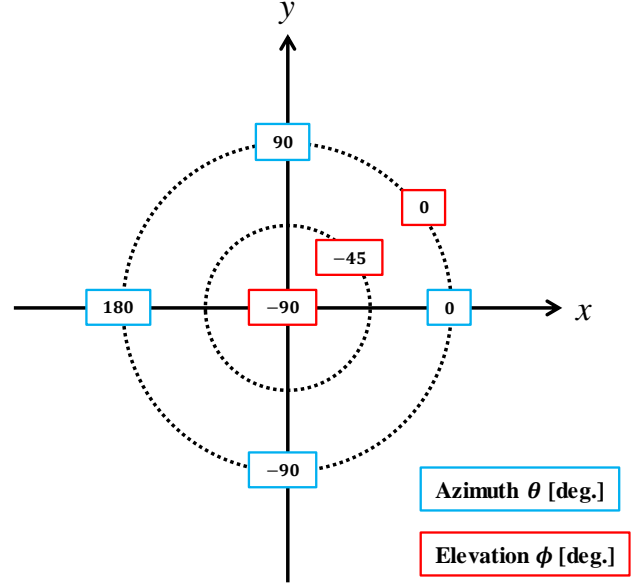
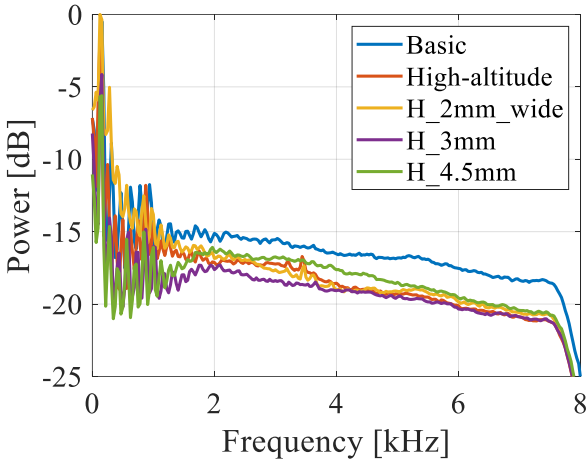
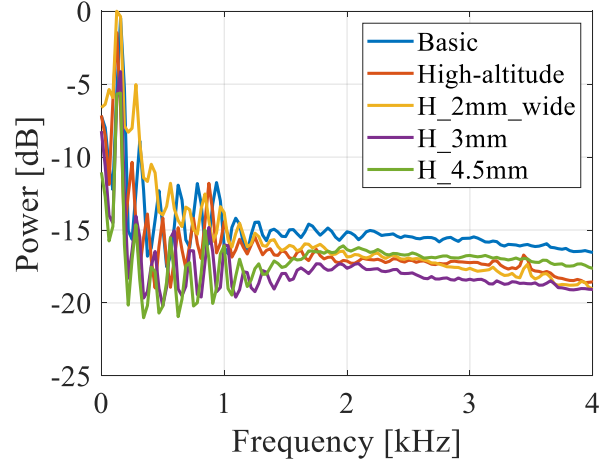


Fig. 7 Coordinate system of visualization of MUSIC spectrum.



(a) full scale



(b) enlarged view

Fig. 8 Frequency spectra of the noise of five propeller models recorded by the microphone array. Spectra were calculated as time-averaged values of spectrograms.

4.2 Results

First, noise characteristics recorded by the microphone array in the actual flying situation are compared. Fig. 8 shows frequency spectra of the noise of five propeller models. The horizontal axis represents the frequency, and vertical axis represents the normalized power. These spectra were calculated as time-averaged values of spectrograms. Compared with the results under the single propeller condition in Fig. 4, the noise characteristics are different because recording

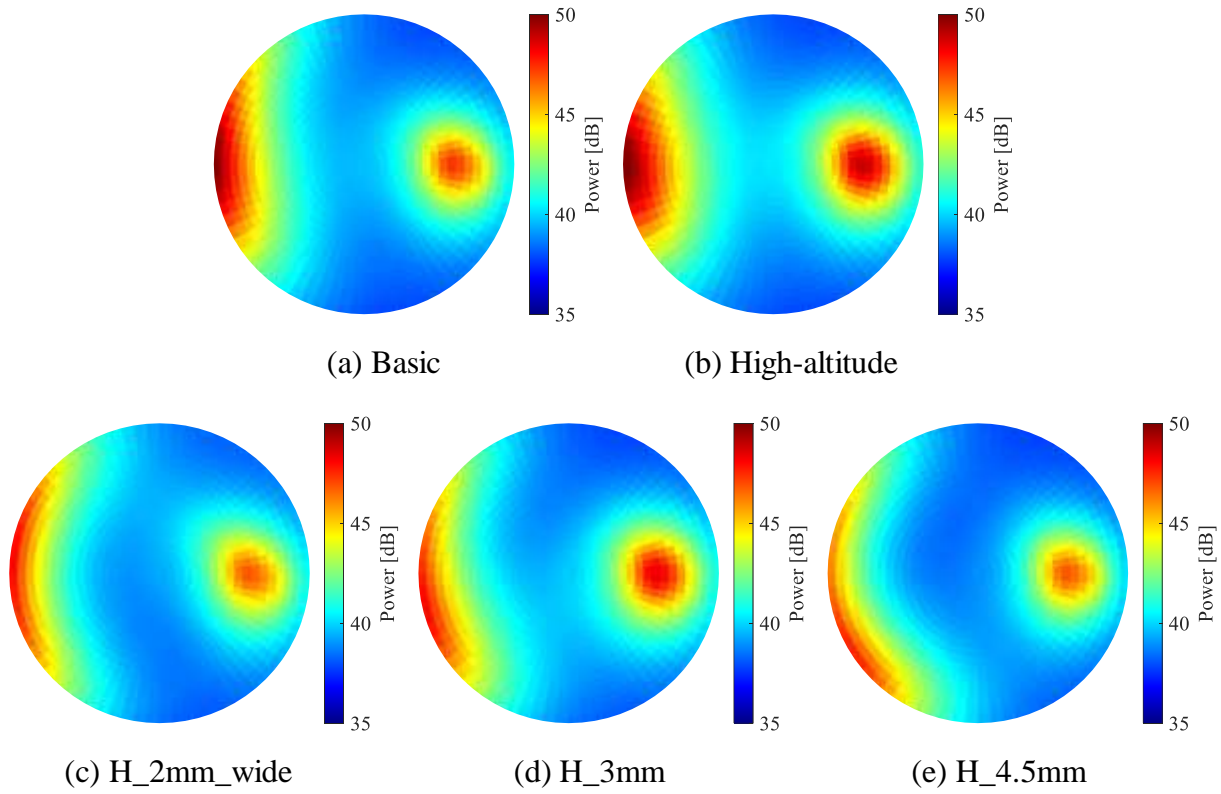


Fig. 9 MUSIC spectra when SNR was 0 dB, azimuth and elevation of target sound direction were 0 deg. and -40 deg.

conditions such as the number of rotors, surrounding environments, and the position of a microphone are different. The noise power of every propeller model at the frequency of 2 kHz or lower in the flying situation was larger than that of the indoor experiment. Moreover, the noise power of developed three propeller models was smaller than that of the basic propeller model at every frequency band, especially the H_3mm model was the smallest. The noise power of the H_4.5mm model was as small as that of the H_3mm model at the frequency of 1 kHz or lower. However, at the frequency of 1 kHz or higher, it was the second-largest of five models.

Second, MUSIC spectra are compared. Fig. 9 shows an example of MUSIC spectra when SNR was 0 dB, the azimuth and elevation of the target sound direction were 0 deg. and -40 deg. MUSIC spectra are plotted with the axis defined in Fig. 7. The color indicates the power of the sound coming from each direction. Two peaks in target sound and propeller noise directions can be seen. MUSIC spectrum of target sound is approximately the same shape in all propeller models. However, the spectra of propeller noise have not only different power but also different distribution. The spectra of basic and high-altitude models spread in the negative direction of elevation, and those of H_2mm_wide, H_3mm and H_4.5mm models spread only around $\phi = 0$. It is considered that the flow field pressure fluctuations around the microphone array can be suppressed by the Gurney flap-inspired attachments and the direction of noise reached to the microphone array could be also changed. Because of the distribution of the spectrum of three developed propellers' noise, it is expected to improve the accuracy of sound source localization, especially the sound coming from downward and backward of the microphone array.

4.3 Discussion

To discuss about the performance of proposed propeller models in sound source localization, the success rate of localization is calculated. When the direction of the maximum point of MUSIC spectrum matched the set sound source direction, it is defined that the localization succeeded. In case the localization using SEVD-MUSIC, the limitation of detection angle range is effective to

avoid the effect of noise which appears in one direction constantly and increase the accuracy of localization [11]. However, in this paper, the maximum point was detected in all directions to evaluate noise characteristics. The success rate was defined as (the number of successful frames) / (the total number of frames: 50 frames \times 325 directions), and calculated the success rates for five propeller models and different target sound levels were compared. Fig. 10 shows the calculated success rate. The horizontal axis represents SNR, and the vertical axis represents the success rate. As shown in the figure, the success rates for developed three propeller models are higher than those of basic and high-altitude models. Because the noise power of the H_3mm model is the smallest in five propeller models, the success rate of the H_3mm model is the highest. However, even though the noise power of the H_4.5mm model was the largest except basic model, the success rate of the H_4.5mm model is the second highest. This is because of the distribution of MUSIC spectrum of the H_4.5mm model's noise. Therefore, it is found that the design of propeller considering the distribution of noise is also important for sound source localization in addition to the noise power. In this experiment, the success rates of developed propeller models were improved up to approximately 60 % compared to the basic model. These results confirm the validity of developed propeller models and the possibility to control the noise power and distribution. However, the relationship between the success rate and the length or height of attachment is not clear. Therefore, further validation using different processed propeller models is needed.

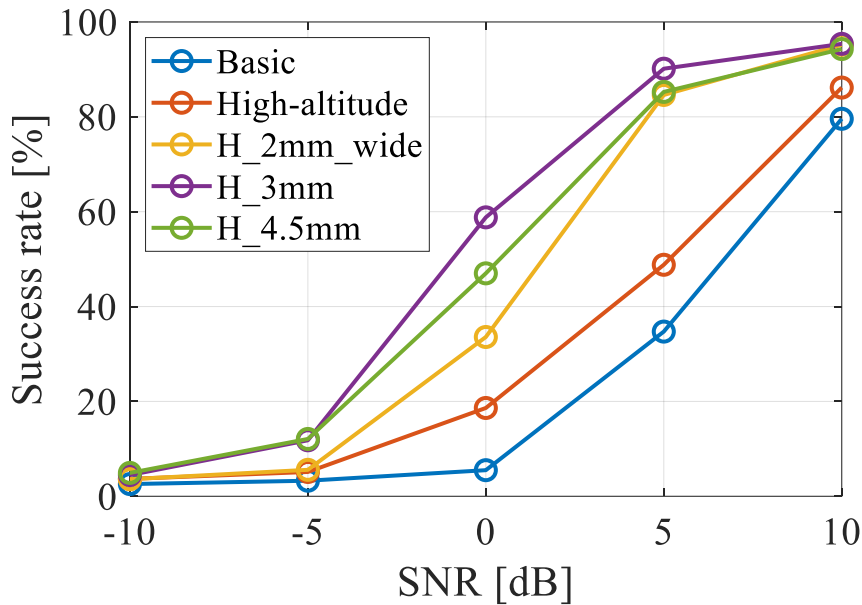


Fig. 10 Success rate of localization.

5. Conclusion

In this paper, aiming at suppressing the noise level of the multicopter-typed UAV with a microphone array and enhancing the audibility for drone audition system, the surface-processed low-noise propeller was developed. Three models with different structures were designed and evaluated in indoor and outdoor flying situations. The results of evaluation experiments confirmed the validity of developed propeller models on drone audition system and the possibility to control the noise power and distribution. Future work includes to clear the relationship between the performance of drone audition system and the structure of propeller, as well as further validation using different processed propellers.

Acknowledgement

This work was supported by JSPS KAKENHI Grant Number 19H00750 and General Research Grant from the SECOM Science and Technology Foundation.

References

- [1] IEEE Signal Processing Cup 2019: Search & Rescue with Drone-Embedded Sound Source Localization: <https://signalprocessingsociety.org/get-involved/signal-processing-cup>
- [2] Schmidt, R O (1986) *Multiple emitter location and signal parameter estimation* IEEE Trans Antennas and Propagation 34(3), 276-280
- [3] Xu, C, Xiao, X, Sun, S, Rao, W, Chng E S and Li, H (2017) *Weighted Spatial Covariance Matrix Estimation for MUSIC Based TDOA Estimation of Speech Source* Proc INTERSPEECH 2017, 1894-1898
- [4] Wang, L and Cavallaro, A (2018) *Acoustic Sensing From a Multi-Rotor Drone* IEEE Sensors Jnl 18(11), 4570-4582
- [5] Lee, D, Jang, B, Im, S and Song, J (2019) *A New Sound Source Localization Approach Using Stereo Directional Microphones* Proc IEEE 2nd International Conference on Information Communication and Signal Processing (ICICSP), 504-508
- [6] Nakadai, K, Lourens, T, Okuno H G and Kitano, H (2000) *Robot audition: Its rise and perspectives* Proc 17th National Conference on Artificial Intelligence (AAAI), 832-839
- [7] Okuno, H G and Nakadai, K (2015) *Active audition for humanoid* Proc 2015 IEEE International Conference on Acoustics, Speech and Signal Processing (ICASSP), 5610-5614
- [8] Okuno, H G and Nakadai, K (2017) *Special Issue on Robot Audition Technologies* Jnl Robotics and Mechatronics 29(1), 15-267
- [9] Ohata, T, Nakamura, K, Mizumoto, T, Tezuka, T and Nakadai, K (2014) *Improvement in outdoor sound source detection using a quadrotor-embedded microphone array* Proc IEEE/RSJ International Conference on Robots and Intelligent Systems (IROS), 1902-1907
- [10] Hoshiba, K, Nakadai, K, Kumon, M, Okuno H G (2018) *Assessment of MUSIC-Based Noise-Robust Sound Source Localization with Active Frequency Range Filtering* Jnl Robotics and Mechatronics 30(3), 426-435
- [11] Nakadai, K, Kumon, M, Okuno, H G, Hoshiba, K, Wakabayashi, M, Washizaki, K, Ishiki, T, Gabriel, D, Bando, Y, Morito, T, Kojima, R and Sugiyama, O (2017) *Development of Microphone-Array-Embedded UAV for Search and Rescue Task* Proc IEEE/RSJ International Conference on Intelligent Robots and Systems (IROS), 5985-5990
- [12] Hoshiba, K, Washizaki, K, Wakabayashi, M, Ishiki, T, Kumon, M, Bando, Y, Gabriel, D, Nakadai, K and Okuno H G (2017) *Design of UAV-Embedded Microphone Array System for Sound Source Localization in Outdoor Environments* Sensors 17(11), 1-16
- [13] Nonami, K, Hoshiba, K, Nakadai, K, Kumon, M, Okuno, H G, Tanabe, Y, Yonezawa, K, Tokutake, H, Suzuki, S, Yamaguchi, K, Sunada, S, Takaki, T, Nakata, T, Noda, R, Liu, H and Tadokoro, S (2019) *Recent R&D Technologies and Future Prospective of Flying Robot in Tough Robotics Challenge* Disaster Robotics - Results from the ImPACT Tough Robotics Challenge, Satoshi Tadokoro Ed., 143-193
- [14] Storms, B L and Jang, C S (1994) *Lift enhancement of an airfoil using a Gurney flap and vortex generators* Jnl Aircraft 31(3), 542-547
- [15] Li, Y C, Wang, J J and Zhang, P F (2002) *Effect of Gurney flaps on a NACA0012 airfoil Flow Turbul Combust* 68(1), 27-39
- [16] Wang, J J, Li, Y C and Choi, K S (2008) *Gurney flap-Lift enhancement, mechanism and applications* Prog Aerosp Sci 44(1), 22-47
- [17] Ellington, C P (1984) *The aerodynamics of hovering insect flight. Part V: a vortex theory* Phil Trans R Soc B 305, 115-144
- [18] Powell, A (1964) *Theory of vortex sound* Jnl Acoust Soc Am 36(1), 177-195
- [19] Howe, M S (1975) *Contributions to the theory of aerodynamic sound, with application to excess jet noise and the theory of the flute* Jnl Fluid Mech 71(4), 625-673

- [20] Lighthill, M J (1952) *On sound generated aerodynamically. Part I : General theory* Proc Roy Soc Lond A 211, 564-587
- [21] Curle, N (1955) *The influence of solid boundaries upon aerodynamic sound* Proc Roy Soc Lond A 231, 505-514



QUIET DRONES
International e-Symposium
on
UAV/UAS Noise
Remote from Paris – 19th to 21st October 2020

Interpolation based acoustic transfer function for drone noise simulation

Hanbo JIANG,

Department of Mechanical and Aerospace Engineering, The Hong Kong University of Science and Technology, Hong Kong, China: hjiangan@ust.hk

Siyang ZHONG,

Department of Mechanical and Aerospace Engineering, The Hong Kong University of Science and Technology, Kowloon, Hong Kong, China: zhongsy@ust.hk

Xin Zhang,

Department of Mechanical and Aerospace Engineering, The Hong Kong University of Science and Technology, Hong Kong, China: aexzhang@ust.hk

Summary

In this paper, we describe an efficient method to compute the broadband noise scattering of drone fuselage based on boundary element method. The acoustic transfer function is a well-known concept for multi-frequency problems in combination with repeated analyses for modified boundary conditions. It was initially proposed to accelerate the boundary element analysis by interpolating instead of directly assembling influence matrices. In this work, a new frequency-interpolation algorithm is proposed by incorporating the proper orthogonal decomposition and a discrete matrix interpolation method. The former is imposed on those pre-computed transfer functions to construct a reduced-order subspace where the later interpolation is implemented, resulting in efficiency gain in both computer storage and data interpolation. Both computational performance and accuracy are investigated to verify the algorithm. Finally, the capability of the proposed method is demonstrated in a drone-noise scattering problem.

1. Introduction

Small-scale drones have been widely used in many areas, which attracts increasing attentions to their noise problems. The related acoustic phenomena usually involve sophisticated noise

generation due to unsteady motion of propellers and acoustic wave reflections due to complicated geometries, which need expensive computational resources to simulate [1][2].

Acoustic boundary element method (BEM) is a well-established numerical method to render sound emission and propagation in acoustic media [1], based on which a concept of the acoustic transfer vector [3], was proposed for repeated analysis [4]. In this method, the acoustic transfer function (ATF) values at some slave frequencies were evaluated by the BEM technique and stored on the hard disk. Then, those ATFs at the other intermediate frequencies were interpolated using the pre-calculated ATFs other than those assembled directly. The linear interpolation of ATFs was first proposed by Benthien [5]. Other interpolation methods such as a global spherical approximation [6], a Green's function interpolation [7] were extensively discussed in a series of investigations [8][9], and similar interpolation/approximation methods were also extended for the multi-frequency boundary element analysis [10][11][12][13]. Overall, using ATFs demands pre-computing and storing of the acoustic influence coefficients for a certain number of discrete frequencies, which are then used to reconstruct a new ATF using interpolation methods. As a result, the computation efficiency lies in storing, loading, and interpolating these pre-computed ATFs, especially for a large number of boundary elements.

In this work, the proper orthogonal decomposition (POD) is imposed on these ATFs, and then the discrete matrix interpolation method (DEIM) [14] is used to produce new ATFs for given parameters based on the POD-basis. Therefore, in contrast to previous linear or spline interpolation methods, this approach first compresses the collected ATFs with regard to any prescribed tolerance and then runs matrix interpolation in a subspace with small dimensions. The resultant efficiency gain in both storage and interpolation enables the proposed approach to be used to generate significant cost-saving predictions within an optimization framework. Finally, the proposed method is applied to a drone-noise scattering problem.

2. BEM-based ATFs

For general time-harmonic acoustic scattering problems, the waves are governed by the Helmholtz equation

$$\nabla^2 p(\mathbf{x}) + k^2 p(\mathbf{x}) = 0, \quad (1)$$

where p is the acoustic pressure, $k = \omega/c$ the wavenumber, ω the angular frequency, and c the speed of sound in the acoustic median domain D . Typically, the principle theory of BEM is to represent the solution of Eq. (1) in an integral form [15]

$$C(\mathbf{x})p(\mathbf{x}) = \int_S \left[G(\mathbf{y}, \mathbf{x}) \frac{\partial p(\mathbf{y})}{\partial n(\mathbf{y})} - p(\mathbf{y}) \frac{\partial G(\mathbf{y}, \mathbf{x})}{\partial n(\mathbf{y})} \right] dS(\mathbf{y}) + p^{inc}(\mathbf{x}), \forall \mathbf{x} \in S, \quad (2)$$

where the constant $C(\mathbf{x}) = 1/2$ if the boundary S of the domain D is smooth around \mathbf{x} [15]. \mathbf{x} is the observer point, and \mathbf{y} is the source point on the boundary S . The term $n(\mathbf{y})$ describes outward normal vector at \mathbf{y} and $(\cdot)^{inc}$ indicates the incident wave. The function G represents the free-field Green's function:

$$G(\mathbf{y}, \mathbf{x}) = \begin{cases} \frac{i}{4} H_0(kr), & \text{in two dimensions,} \\ \frac{e^{ikr}}{4\pi r}, & \text{in three dimensions,} \end{cases} \quad (3)$$

where $r = |\mathbf{x} - \mathbf{y}|$, i is the unit imaginary number and H_0 represents the Hankel function of first kind of order 0. In the case of a pure acoustic scattering problem with rigid wall condition $\partial p(\mathbf{y})/\partial n(\mathbf{y}) = 0$, Eq. (2) can be simplified as

$$C(\mathbf{x})p(\mathbf{x}) = \int_S -p(\mathbf{y}) \frac{\partial G(\mathbf{y}, \mathbf{x})}{\partial n(\mathbf{y})} dS(\mathbf{y}) + p^{inc}(\mathbf{x}), \forall \mathbf{x} \in S. \quad (4)$$

The semi-discretized form of Eq. (4) can be written in a compact representation

$$\{M_k p\}_{\Delta S}(\mathbf{x}) + \frac{1}{2}p(\mathbf{x}) = p^{inc}(\mathbf{x}), \forall \mathbf{x} \in S, \quad (5)$$

where

$$\{M_k p\}_{\Delta S}(\mathbf{x}) = \int_{\Delta S} \frac{\partial G(\mathbf{y}, \mathbf{x})}{\partial n(\mathbf{y})} p(\mathbf{y}) dS(\mathbf{y}), \quad (6)$$

Then the collocation method is adopted to discretize Eq. (5), which states that the centroid of each element is used as a collocation point \mathbf{x} and Eq. (6) holds exactly in each element. By assuming that the number of boundary elements is N and all boundary elements are constant, a linear system of equations for scattered pressure field can be obtained as follows

$$\left[\mathbf{M} + \frac{1}{2} \mathbf{I} \right] P_s = P^{inc}, \quad (7)$$

where

$$M_{ij} = \frac{\partial G(\mathbf{y}_j, \mathbf{x}_l)}{\partial n(\mathbf{y}_j)} \Delta S_l, l, j = 1, 2, \dots, N, \quad (8)$$

$$P_s = [p_1, p_2, \dots, p_N]^T, P^{inc} = [p_1^{inc}, p_2^{inc}, \dots, p_N^{inc}]^T. \quad (9)$$

The $(\cdot)^T$ represents the transpose operation and \mathbf{I} is unit diagonal matrix. Finally, solving the linear equation Eq. (7) for both boundary elements and field points would yield the expected transfer function

$$P_f(k) = -\mathbf{M}_f(k) \left[\mathbf{M}(k) + \frac{1}{2} \mathbf{I} \right]^{-1} P^{inc}(k), \quad (10)$$

where $P_f(k)$ represents the radiated sound waves at observation points in the field and the element of matrix \mathbf{M}_f is obtained by setting \mathbf{x}_l in Eq. (8) as the observer location. From the numerical perspective, the ATF is an array of transfer functions between the incident wave on the surface and the total sound pressure at the field point. For practical application, usually more than one frequency would be considered and the ATF has to be evaluated repeatedly for every single frequency. This calls for special treatments to reduce the computation time, among which employing frequency interpolation techniques is widely used to accelerate multi-frequency simulations.

2.1 ATFs interpolation

Typically, the first step of applying ATFs is to collect some snapshots, i.e., a series of ATFs obtained by assembling the systems (7) at a prescribed series of wavenumbers, which are then reshaped into column vectors $f_j, j = 1, 2, \dots, N_s$, with N_s being the total number of snapshots. f_j depends on the frequency range in which the ATFs shall be applied and the number N_s is related to the required interpolation accuracy. These snapshots can be assembled into a compact representation

$$F = [f_1, f_2, \dots, f_{N_s}] \in \mathbb{C}^{N \times N_s}, \quad (11)$$

Then the singular value decomposition is performed on the matrix F ,

$$U \Sigma V^H = F F^H, \quad (12)$$

where $(\cdot)^H$ is the conjugate transpose operation. The diagonal terms of matrix Σ are singular values, $\sigma_1 \geq \sigma_2 \geq \dots \geq \sigma_{N_s}$. Afterwards, an integer M is obtained such as the leading M singular values satisfy a prescribed truncation tolerance. A reduced-dimension basis Ψ is obtained by the POD algorithm

$$\Psi = \text{POD}(F, \epsilon_{POD}), \quad (13)$$

where ϵ_{POD} is a prescribed tolerance. Usually, it is found that storing the POD basis $\Psi_{N \times M}$ is much more efficient than storing the original snapshots $F_{N \times N_s}$. The second step is to perform

matrix interpolation. Given a new wavenumber k , a target $f(k)$ is projected onto a low-dimensional subspace spanned by the DEIM basis Φ (here we deploy $\Phi = \Psi$)

$$f(k) \approx f_M(k) = \Phi\theta(k), \quad (14)$$

where θ is the coefficient. DEIM selects some proper entries from the basis Φ . Then θ is obtained based on the selected entries $I \subset \{1, \dots, N_s\}$ with $|I| = M$:

$$\Phi_I\theta(k) = f_I(k), \quad (15)$$

where $\Phi_I \in \mathbb{R}^{M \times M}$ is the matrix formed by the I rows of matrix Φ and $f_I(k)$ is a low-dimension vector related to the given k . As a result,

$$f_M(k) = \Phi\Phi_I^{-1}f_I(k). \quad (16)$$

3. Results and discussion

3.1 Verification

The test example is an infinite cylinder scattering problem in two dimensions as shown in Fig. 1(a). A cylinder of radius $a=1$ m is centred at $(0, 0)$ and is impinged upon by a planar incident wave, e^{-ikx} . The cylinder boundary is uniformly discretized into 512 segments. The acoustic medium is assumed to have a sound speed of $c=340$ m/s and a unit density. Fig. 1(b) shows the polar plot of the ratio of the scattered wave to the incident velocity potential at $r = 5a$ from the centre of the cylinder at $ka = \pi$. The amplitude of the scattered wave is normalized by that of the incident wave. The two numerical solutions compare very well with each other, and both agree well with an analytical solution given by Morse and Ingard [17]. Therefore, the accuracy of the DEIM based BEM algorithm is verified.

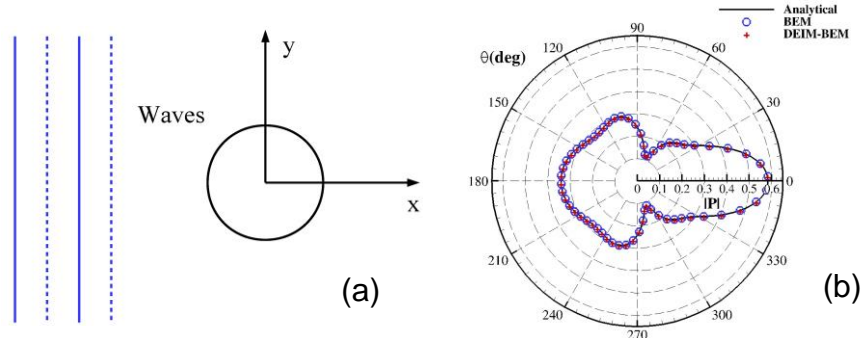


Figure 1 (a) Sketch of the representative case with planar incident waves scattered by a rigid cylinder; (b) Comparison of directivity patterns of the scattered field predicted by the proposed new BEM, the conventional BEM and the analytic solution with all data

3.2 Application

The proposed BEM solver is used to simulate a simple monopole source scattering by a quad-rotor drone fuselage as shown in Fig. 2(a), where the surface is discretized into 7446 constant triangle elements. The monopole is placed close to the rotor centre in order to simulate rotor noise, and the resultant incident sound field is given in Fig. 2(b). The real part of the total sound field and the corresponding sound pressure level contours are plotted in Fig. 3(a) and 3(b), where the scattering effect of the drone fuselage is clearly observed. For this problem, the overall computational time is reduced by about 50% using the proposed BEM with the AAF computed using interpolation. For practical broadband noise computations, the computational time can be greatly reduced for the repeated computation at various frequencies.

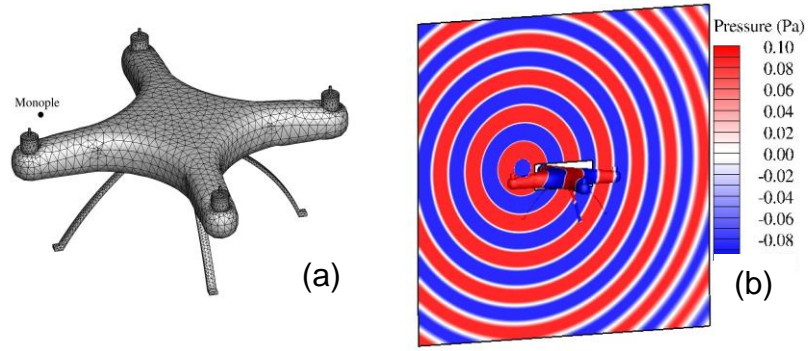


Figure 2 Sketch of the application to drone noise problem where a monopole source is placed close to the rotor centre. (b) The real part of the incident waves by a monopole source.

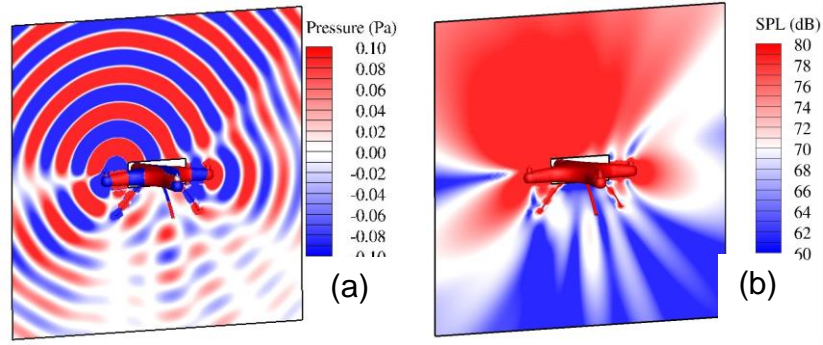


Figure 3 (a) the total sound pressure using the BEM; (b) The corresponding sound pressure level contours of (a). The frequency of the incident wave is 3.0 kHz.

3.3 Efficiency

The whole in-house BEM solver including the DEIM module is implemented on the platform of MATLAB[®]. Cases are tested on a computer with an Intel Xeon[®] CPU E5 – 1620 @ 3.5GHz. The time costs of the case in Fig. 2 are summarized in Table. 1 with the element number varied from 256 to 4096. Since the proposed method interpolates the system matrices based on several slave frequencies instead of being assembled directly, here attention should be focused on computational time reduction of this part. A maximum time saving percentage of 94.1% regarding to the system setup is observed from the third column of Table. 1 over different element numbers. However, the solution time is almost the same with and without DEIM interpolation, which is not surprising because the corresponding linear system of equations has the same dimensions. Nevertheless, the overall time saving as a percentage is observed up to 84.7% in comparison with the total computation time.

4. Conclusions

A BEM based acoustic transfer function incorporating with a matrix interpolation algorithm has been presented for multi-frequency scattering analysis. In this approach, system matrices in BEM analysis are interpolated from some pre-calculated results, which are compressed using the POD technique to the storage space. The accuracy of the proposed algorithm is verified by comparing with the conventional BEM and an analytical solution. The new method uses a pure data-based interpolation, which can be easily included in any existing BEM code as a standalone module to enable multi-frequency analysis. For problems of small to moderate size, this new technique has been demonstrated saving up to 94.1% and 84.7 % of the setup time and total time, respectively.

Table 1 Comparison of computation times including setup time and solution time for the conventional BEM and the proposed DEIM based BEM with the number of elements varied from 256 to 4096. The computation time is obtained using the average of 10 evaluations

	Elements	Setup time (s)	Solution time (s)	Total time (s)
BEM	256	0.03799	0.00172	0.03971
DEIM-BEM	256	0.00447	0.00176	0.00623
Saving	-	88.2%	-2.3%	84.3 %
BEM	1024	0.52627	0.05179	0.57806
DEIM-BEM	1024	0.03490	0.05340	0.08830
Saving	-	93.4%	-3.1%	84.7 %
BEM	4096	8.25118	2.0327	10.28383
DEIM-BEM	4096	0.48687	2.0047	2.49154
Saving	-	94.1%	1.4%	75.8 %

5. Acknowledgements

The work is supported by the Hong Kong Innovate Commission (ITS/387/17FP), the Hong Kong Research Grant Council (RGC 16202520).

References

- [1]. P. R. Cook (2002), *Real sound synthesis for interactive applications*, AK Peters/CRC Press.
- [2]. D. L. James, J. Barbic, D. K. Pai (2006), *Precomputed acoustic transfer: output sensitive, accurate sound generation for geometrically complex vibration sources*, ACM Transactions on Graphics (TOG) 25, 987–995
- [3]. S. Marburg, H. Hardtke, R. Schmidt, D. Pawandenat (1997), *Application of the concept of acoustic influence coefficients for the optimization of a vehicle roof*, Engineering Analysis with Boundary Elements 20(4), 305–310.
- [4]. S. Marburg, B. Nolte (Eds.) (2008), *Computational acoustics of noise propagation in fluids: Finite and Boundary element methods*, Berlin Heidelberg: Springer.
- [5]. G. Benthien (1989), *Application of frequency interpolation to acoustic-structure interaction problems*, Tech. rep., Navel Ocean Systems Center Technical Report 1323.
- [6]. O. von Estorff, O. Zaleski (2003), *Efficient acoustic calculations by the BEM and frequency interpolated transfer functions*, Engineering analysis with boundary elements 27(7), 683–694.
- [7]. T. Wu, W. Li, A. Seybert (1993), *An efficient boundary element algorithm for multi-frequency acoustical analysis*, The Journal of the Acoustical Society of America 94(1), 447–452.
- [8]. O. Von Estorff (2003), *Efforts to reduce computation time in numerical acoustics– an overview*, Acta Acustica United with Acustica 89(1), 1–13.
- [9]. O. Von Estorff, S. Rjasanow, M. Stolper, O. Zaleski (2005), *Two efficient methods for a multifrequency solution of the Helmholtz equation*, Computing and Visualization in Science 8(3-4), 159–167.
- [10]. C. Vanhille, A. Lavie (1998), *An efficient tool for multi-frequency analysis in acoustic scattering or radiation by boundary element method*, Acta Acustica united with Acustica 84(5), 884–893.
- [11]. J.-P. Coyette, C. Lecomte, J.-L. Migeot, J. Blanche, M. Rochette, G. Mirkovic (1999), *Calculation of vibro-acoustic frequency response functions using a single frequency*

boundary element solution and a pad´e expansion, Acta Acustica united with Acustica 85(3), 371–377.

- [12].S. Li (2005), *An efficient technique for multi-frequency acoustic analysis by boundary element method*, Journal of sound and vibration 283(3-5), 971 – 980.
- [13].J.-S. Oh, S.-K. Youn (2018), *An efficient technique for the indirect BEM for multifrequency acoustic analysis using green’s function approximation*, Journal of Mechanical Science and Technology 32(5), 1965–1973.
- [14].D. Wirtz, D. C. Sorensen, B. Haasdonk (2014), *A posteriori error estimation for deim reduced nonlinear dynamical systems*, SIAM Journal on Scientific Computing 36(2), 311–338.
- [15].L. Shen, Y. Liu (2007), *An adaptive fast multipole boundary element method for three-dimensional acoustic wave problems based on the Burton–Miller formulation*, Computational Mechanics 40(3), 461–472.
- [16].Y. Zhang, L. Feng, S. Li, P. Benner (2015), *An efficient output error estimation for model order reduction of parametrized evolution equations*, SIAM Journal on Scientific Computing 37(6), 910–936.
- [17].P. M. Morse, K. U. Ingard, *Theoretical acoustics*, Princeton University.



QUIET DRONES
International Symposium
on
UAV/UAS Noise
Remote from Paris – 19th to 21st October 2020

Advances in Sound and Speech Signal Processing at the Presence of Drones

Oliver Jokisch, Leipzig University of Telecommunications, Germany: jokisch@hftl.de
Ingo Siegert, Otto von Guericke University Magdeburg, Germany: ingo.siegert@ovgu.de

Summary

The civilian and military use of drones (unmanned aerial vehicles, UAVs) for surveillance tasks, for inspection of industrial structures, for monitoring in agriculture and science-data collection is steadily growing. A sound or speech signal processing directly at drones or at the presence of drones nearby is challenging because of the significant rotor and maneuver-related noise components. The signal processing has to consider various sound sources, and the wanted signals (e.g. environmental sounds or voice signals) have to be separated from the flight and surrounding flow noises. For many tasks, other sources of information (e.g. electromagnetic-wave signals) need to be analyzed in parallel, with an adequate concept of data fusion.

Recently, a lot of effort has been invested in more quiet drones, but due to several application requirements with regard to drone size, flight stability, robustness or price, the noise issue is still immanent. A noticeable proportion of noise is affecting sensible applications, such as the analysis of acoustic drone signatures by other surveillance drones, the intelligibility of speech transmission in disaster operation, or the recognition of human speech and animal sounds.

The paper introduces some acoustic scenarios and experiments at a typical small, commercial drone (DJI Mavic Pro). We recorded different sound and speech signals by a lightweight eight-micro array that allows for an improved signal-to-noise ratio, and we tested different noise-filtering methods. The test signals were processed in a free field environment with a battery-powered Raspberry Pi 3, attached to the drone. We briefly discuss the factors of influence and selected quality criteria, such as the resulting signal-to-noise ratio and word recognition rate. The article concludes with lessons learned for acoustic drone interactions and measurements.

1. Introduction

In the last decade, the civilian operation areas of unmanned aerial vehicles (UAV, drone) grew steadily, including surveillance tasks, the inspection of industrial structures, monitoring tasks in agriculture, data collection tasks in science, as well as the rescue of persons during disasters (Hassanalain and Abdelkefi, 2017). Many applications, such as the use of drones for parcel delivery, autonomous flight taxis, wildlife monitoring, or the support of lockdown enforcement are currently under development.

Besides the improvement of application-specific techniques such as image processing, flight-maneuver planning, multi-drone communication, and battery lifetime, also the drone noise is a critical issue (Teichel and Körper, 2019). Noises are among the immissions that, depending on their type, extent, and duration, can lead to health problems or other impairments. Within public areas, the noise can be perceived as heavily disturbing. Hence, applying drones with a reduced noise emission is very helpful to keep silence in an already noisy environment.

The presence of more quiet drones opens up further application possibilities, which benefit from the low flight altitude, good maneuverability, and relatively low investment costs – sound and speech processing at drones.

Applications that record and analyze acoustic signals with a rotary-wing drone are still quite experimental and challenging, mainly due to a strong, non-stationary noise generated by such an aircraft. The acoustic or speech event analyses directly at drones have some advantages over video-only analyses, including the lower transmission bandwidth of acoustic signals in comparison to video signals (Siegert et al., 2016) as well as the possibility of intuitive drone interaction (Carroll, 2013).

Nevertheless, sound or speech analyses with drones are still rarely investigated: Typical audio applications are the recording of acoustic UAV signatures by other surveillance drones (Rascon et al., 2019), the sound immission in humans, the measurements of the sound pressure level (Miesikowska, 2017) and spectral analyses of overflight noise (Cabell et al., 2016).

In our previous contributions, we therefore analyzed the main aspects of sound and speech processing at typical small drones from the end-costumer market. For this purpose, we had recorded speech samples directly at a flying Mavic Pro drone (DJI Technology, 2018). Our first review of the audio characteristics for this UAV type in the free field showed the dominating and significantly varying blade passing frequencies (BPFs), and associated harmonic components depending on the recording position and flight maneuver (Jokisch and Fischer, 2019, March). The underlying single-channel analysis of environmental sounds or even of nearby speech commands, involving standard methods of noise suppression, turned out to be challenging. In Jokisch (2019, April), we tried to obtain more acoustic insights at the same but affixed drone in a semi-anechoic chamber to ensure reproducible conditions, based on a two-channel microphone approach, with limited success. In a next step (Jokisch et al., 2019, August), we generalized the preliminary results and discussed a few drone-based communication scenarios and challenges in a more generic style. We suggested, amongst others, a design of specific ‘low-noise drones’ to improve the signal-to-noise ratio, e.g. by compromising on less-dynamic flight-stabilizing maneuvers that are hardly relevant for audio versus video-oriented tasks (which usually require higher flight stability).

In most recent experiments, we were focusing on the enhancement of the signal-to-noise ratio in drone-recorded speech signals by constructive methods to improve the signal capturing and analysis, including a lightweight microphone array for beamforming, supplemented by post-filtering (Lösch et al., 2020). The respective experiments and results were summarized in Jokisch et al. (2020) with a focus on speech processing.

In this contribution, we want to compare our results with other contributions in this field, and to discuss the implications for new or adjusted scenarios that are relevant to a drone-based sound and speech processing. In Section 2, we are revisiting relevant scenarios of sound and speech-signal processing at drones, including the latest developments in 2020. Section 3 is illustrating a few current, drone-related challenges and measures of audio signal processing, with a focus on external literature. In Section 4, we demonstrate the mentioned challenges and measures in

a drone context by selected audio-processing examples from both, external sources and own experiments. Afterwards, we briefly summarize and discuss the previous findings in Section 5, completed by some conclusions.

2. Relevant Scenarios of Sound and Speech Signal Processing at Drones

In this section, we want to illustrate selected scenarios of drone operation that are posing challenges in sound and speech signal processing, by not making any claim to be complete.

2.1 Flexible and Resilient Communication Infrastructure

Many studies deal with the intelligent extension of mobile communication concepts, e.g. from manned flight or marine missions to autonomous systems or self-organized groups of systems (swarms) and with the necessary transmission of control and mission data via advanced radio or even optical wireless data links. For that matter, UAVs can be used as flexible components in a more resilient communication and sensing infrastructure, e.g. in disaster management (Fadelli, 2018; Magid et al., 2019) as visualized in Figures 1 and 2.

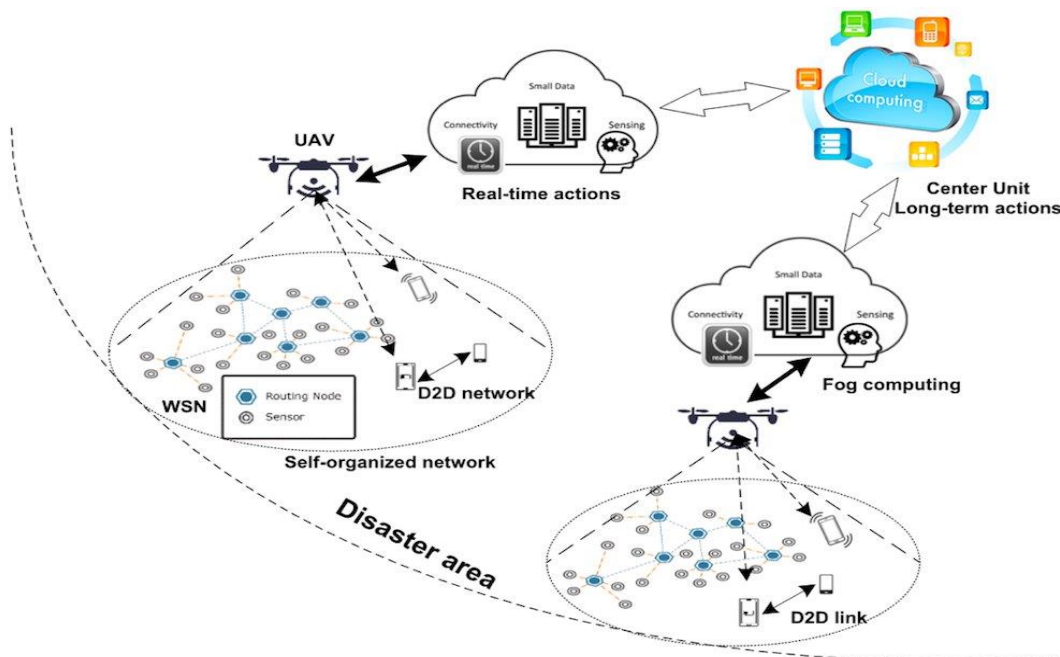


Fig. 1. Resource allocation for UAV communication systems in disaster management (Fadelli, 2018).

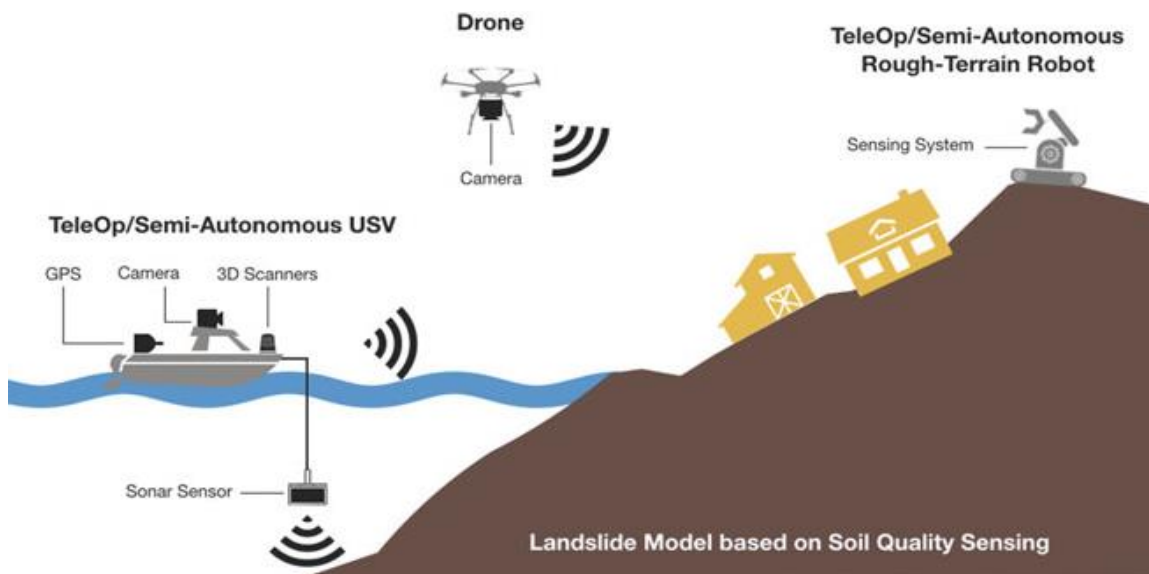


Fig. 2. Multimodal sensing architecture, including UAVs for landslide disasters (Magid et al., 2019).

In such scenarios, smaller drone systems up to 25 kg are primarily used as airborne transmitter or sensor platforms for the surveillance, monitoring, documentation and disaster management (Restas, 2015; Erdelj and Natalizio, 2016). However, the surveilled or supervised people are usually not linked to the drone or swarm infrastructure, and thus they cannot communicate with drones or their operators, as no simple interaction interface is available. A possible solution for trained people e.g. in rescue teams is a visual UAV control by a gesture alphabet for operations management (Schelle and Stütz, 2018). Nonetheless, such a gesture-based solution is not applicable for untrained humans in disaster scenarios. In a previous article (Jokisch, Siegert et al., 2019) we therefore suggested a speech-based interaction interface for UAVs, as speech is a very efficient and intuitive communication channel (Figure 3).

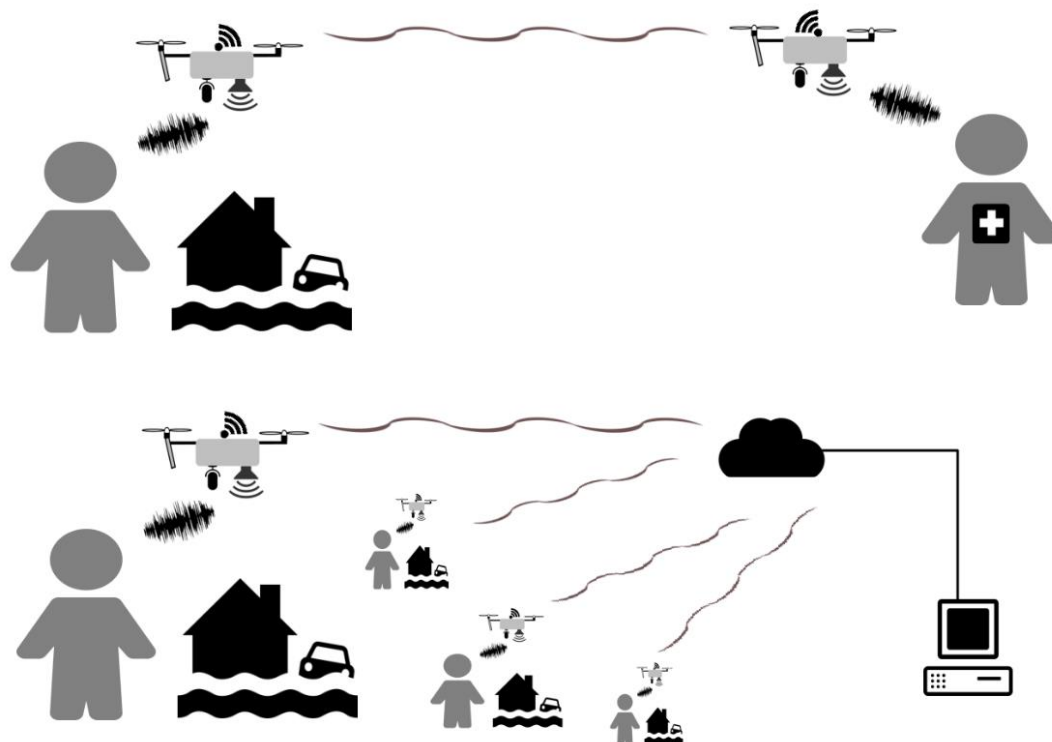


Fig. 3. UAV-supported disaster communication – bidirectional voice communication (top) and cloud-supported operation (bottom) from Jokisch, Siegert et al. (2019).

2.2 Surveying and Measurement Tasks at Challenging Locations

Especially in different industrial tasks, the drones can demonstrate their strengths. Topological surveying is at the very top of the list of applications, as the surveying market is characterized by extremely low-profit margins (Unger et al., 2017). For this kind of applications, drones can support to capture the topology and to reach inaccessible areas. Furthermore, without drone use, inspection and mapping tasks are personnel-intensive, time-consuming, and sometimes dangerous, e.g. the inspection of wind-power plants or high-voltage lines (Zhou et al., 2016).

Another application, closely related to sound processing is the determination of sound-power levels of inaccessible sound sources (chimney pots, air vents etc.) by using drones (Figure 4). The measurement of noise emissions directly at the source is often impractical, as many typical sound sources are inaccessible. Since noises are among the immissions that, depending on their type, extent, and duration, can lead to serious impairments or health problems, better protection against noise impacts on humans and nature is a central social task. The major challenge is that a UAV itself represents a noise source. Hence, various approaches to exclude the disturbing influences of UAV systems have to be investigated.



Fig. 4. UAV-based measurement at unapproachable industry locations (Jokisch, Siegert et al., 2019).

2.3 Detection of Drones and Flight-Operation Diagnostics by Acoustic Signatures

The detection of drones in restricted air zones (e.g. around airports) or their flight tracking plays an important role, e.g. in the civil and military security (Güvenç et al., 2017), and even in indoor scenarios (Iannace et al., 2020; Ciaburro et al., 2020). The majority of detection and tracking methods is based on well-known techniques of air-traffic control for manned systems by using electromagnetic signals, as in radio detection and ranging (Radar), in global positioning system or in surveying radio communication (i.e. radio frequency/RF transmission, Azari et al., 2018).

Alternatively, light detection and ranging (Lidar) or sound navigation ranging (Sonar) can be used. Although such conventional methods cover a broad range of detection and tracking scenarios, there are some specific disadvantages, e.g. in the case of a disconnected radio communication or with respect to stealth drones. Some video-based approaches use ground cameras for a flight dynamics-based recovery of the UAV trajectory (Rozantsev et al., 2017).

The analysis of RF or other signatures from autonomous systems is a huge field of research as well as the sensor and control networks for flight operations, including the air and ground-based (terrestrial) surveillance (e.g. Bernardini et al., 2017; Azari et al., 2018), exemplified in Figure 5.

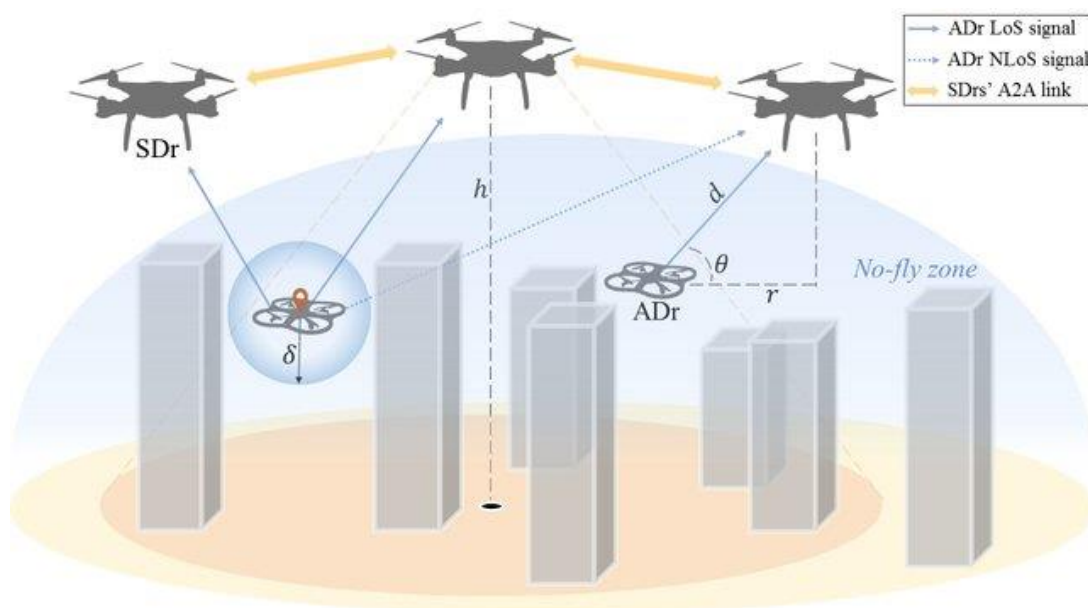


Fig. 5. Passive radio spectrum monitoring of amateur drones by surveillance drones (Azari et al., 2018).

Due to the higher line-of-sight (LoS) probability at high altitudes, the use of a surveillance drone (SDr) guarantees higher SNRs for better detection and less shadowing for accurate localization compared to terrestrial surveillance. As the transmit power of a targeted amateur drone (ADr) is unknown, the estimated location of the ADr is represented by a sphere of radius δ . Although the air-to-air (A2A) links are dominated by LoS propagation, the impact of multipath fading due to ground or building reflections cannot be ignored (i.e. non-line-of-sight/NLoS components).

A common strategy to deal with the shortcomings of the methods above and to increase the resilience or precision of the detection and tracking includes a data fusion from multimodal signal analyses. It is obvious that a relatively small and loud signal source as a UAV offers the opportunity for subsidiary acoustic methods. The so-called acoustic signature and further sounds of UAVs allow for a general detection of drone activities in air zones, the identification of a concrete drone model or even the localization and tracking of respective point sources in the air sector.

The concrete acoustic-signature processing exceeds the scope of this article, but the research objectives are similar to our general, drone-related challenges and measures in audio signal processing, raised in the next section.

Beyond, acoustic analyses can facilitate a diagnostics of flight-operation (Jokisch and Fischer, 2019, March) or a fault diagnosis of UAV components, e.g. rotor blades (Iannace et al., 2019).

2.4 Further Drone-related Scenarios

The relatively small size of a customer drone enables the use beyond conventional applications of aircrafts. Recently, drones were used by several city administrations for the enforcement of lockdowns in the COVID-19 crisis – also by loudspeaker-enabled UAVs to urge people to wear a mask, to maintain a safe distance outside of the house and to discourage travel (Bourdon and Moynihan, 2020).

The indicated solutions are quite easy, e.g. to prevent people from taking the pandemic far too lightly, but these quick solutions still have some flaws, as no back-channel communication is possible. Hence, people cannot explain their behavior, although there may be compelling reasons for them. Furthermore, the employed drones represent an additional source of noise pollution, which is perceived as very disturbing, in particular due to their small size and weight of about 30 cm diameter and 800 g (Teichel and Körper, 2019).

Another promising research area to exploit advanced drone technology is wildlife monitoring. A UAV can observe animals in their natural environment, is much cheaper, and applicable in bad weather conditions, compared to conventional aerial techniques (Hodgson and Koh, 2016), and even anesthesia can be avoided. Currently, UAVs are primarily used to accurately estimate the numbers of wildlife animals or to easily survey their migration routes (Šimek et al., 2017).

In contrast, a drone can stress the wild animals, e.g. wild horses reacted to a flying fixed-wing drone with a significantly faster heartbeat, and they stopped grazing and were visibly alarmed. Furthermore, some birds of prey have already attacked flying UAVs (Hodgson and Koh, 2016). Therefore, more research is needed on the noise signatures of different UAV models, including respective frequencies that are inaudible to humans.

3 Drone-related Challenges and Measures in Audio Signal Processing

A drone detection task represents only a part of the relevant applications, but it demonstrates typical acoustic challenges. Compared to Radar, RF or video methods, Azari et al. (2018) listed the advantages of audio processing as: cheap sensors, limited processing load, and available equipment, but they also named significant disadvantages such as: sensitivity to ambient noise, limited range, need of a microphone array, large datasets for training, and fixed installations. In general, the acoustic peculiarities of UAVs are manifold, mainly caused by ego-noise due to a complex multirotor design, but also associated with a variety of drones / monitoring tasks and

ambient noises. Although the physical and mechanical principles of sound generation are known from classic flight engineering, a practical localization or separation of the different sound sources as well as noise elimination or reduction is application-specific and elaborative. In this section, we briefly describe selected acoustic findings in the context of our illustrated application scenarios in Section 2, with a focus on noise sources and reduction approaches.

3.1 Noise Sources

Sources of UAV noise can be distinguished into the engine / motor(s), an exhaust system if applicable, propellers, and airframe noise (Miljković, 2018, January). The propulsion system (propeller and motor combinations) of the drones is usually the main source of the noise. Kloet et al. (2019) have characterized the aerodynamic and acoustic performance of multirotor propellers. The performance values (thrust and RPM) correlate well with their three-component velocity measurements taken of the wake. The propeller geometry seems to have a larger effect on the overall acoustic profile than any supporting structure. The authors suggest more investigations into the vortex shedding from supporting structure and the distance between supporting structure and propeller plane as well as into psychoacoustic noise contributions. The propeller noise can be reduced by specific designs (e.g. tip vortex design of Mavic Pro Platinum results in an SPL reduction of 6 dB against Mavic Air), by less weight, the motor RPM, prop design, or size and number of prop overlap. For the considered UAVs, an electric motor is mostly utilized, commonly brushless direct current (BLDC) motors, due to the energy efficiency. The acoustic noise in BLDC motors is associated with mechanical resonances caused by the stator excitation. Electric motors operate at high RPMs when used in drones, while the motor speed is related to its “Kv rating” in unloaded operation – e.g. 10,350 RPM is a starting speed of the motor that can even reach 41,400 RPM (unloaded). Basically, there are two components, broadband and tonal components, which contribute to the propeller noise. The propeller plane shows the biggest noise proportion, concerning directivity. The product of propeller RPM and number of blades per propeller is called blade passing frequency (BPF). The tonal noise is usually less significant and widely covered by broader harmonics of the BPF. In Figure 6, the BPF and dominant harmonics can be observed in the marked frequency range, up to 3 kHz. Characteristic peaks in the marked frequency ranges above 3.9 kHz and 6.5 kHz are related to the engine sounds. The overall decline of the red curve (below) characterizes the frequency response of the microphone line (recorded at silence, as a reference).

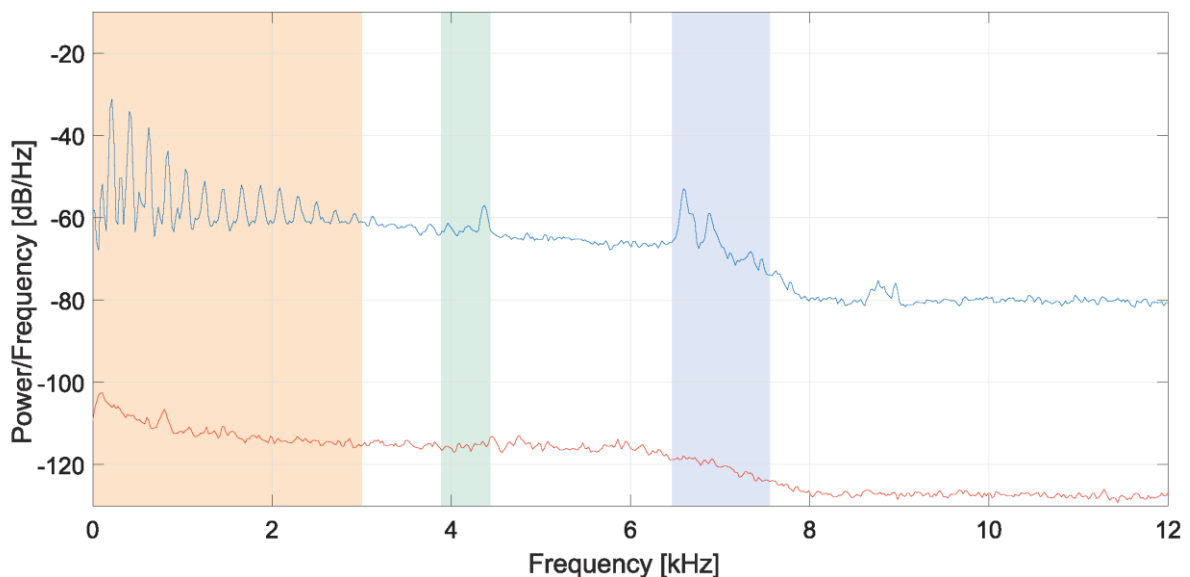


Fig. 6. Power density spectra of DJI Mavic Pro, hovering 2 s (upper curve) from Jokisch et al. (2019, August).

Wang et al. (2019) observed and simulated that a bottom-mounted UAV propeller configuration causes more noise, due to an increase in the amplitude of BPF harmonics and high-frequency noise. They concluded that the slight increases could be attributed to a distorted inflow caused

by the airframe. The airframe in such a configuration does not only produce large periodic turbulent structures, which can cause tonal noise, but it can also cause smaller turbulent structures to continually impact the rotor, resulting in broadband noise.

3.2 Noise Reduction Techniques

To reduce the noise of the UAV itself and to increase the usability for the application scenarios in Section 2, two methods can be distinguished: passive and active methods. Passive Methods mainly focus on modifications of the propulsion system, e.g. the shape modification of propeller blades, a propeller design with more blades, absorptive and reflective barriers, or a shielded (ducted) propeller with sound absorbers.

The propeller noise can be reduced (a few dB) by modifying the shape of the airfoil section and the blade. A detailed investigation of the impact of the geometry of propeller blades to its noise level was conducted by Štorch et al. (2016).

Another possibility is the design of multi-blade propellers. Mostly in UAVs, double blades are used. The same thrust, as from a two-blade propeller, can be obtained by using more blades with a smaller diameter that results in a lower tip speed, which also slightly reduces the noise (by ca. 4.5 dB). In contrast, the power efficiency decreases, and the flight balance needs more attention (Miljković, 2018, May).

In Sibo et al. (2019), specific sound radiations are decreased by using absorptive and reflective barriers. Using a dampening foam fixed at the propeller guards of a Parrot Mini UAV, they achieved a maximum of 6 dB noise attenuation. This approach can be even improved by using ducted propellers, in which the propeller is mounted inside a shroud (Headrick, 2015). Meta-surface absorbers based on a Helmholtz resonator can be integrated to especially reduce the mid and low-frequency noise (Figure 7).



Fig. 7. Carbon-fiber duct around propeller lowers noise level of aircraft (Headrick, 2015).

According to McKay and Kingan (2019), the noise spectrum of a propeller with a nominally constant speed contains a multitude of tones at integer multiples of the nominal BPF. They propose that the cause of the tones is an unsteady loading and thickness noise by the small variations in the angular speed of the propeller driven by an electric motor, and hence they measure the angular speed with a shaft encoder as input for a time-domain noise prediction. Castro et al. (2017) proposed an active noise cancellation system with an overall weight of ca. 120 g as an affordable payload for medium UAVs that performs quite well in canceling low-frequency noises, and without causing interferences to further UAVs or other nearby vehicles. The acoustic challenge for the drone and application design is concerning the best trade-off between low-noise measures and potential effects on further operation criteria like payload, on-board processing power, or interferences (e.g. with other drone systems in swarms).

4 Selected Audio Experiments and Results

4.1 Noise Characteristics

So far, there are only a few well-founded studies available on noise generated by drones. Teichel and Körper (2019) measured the horizontal and vertical directional characteristics of various UAV models under different flight maneuvers (hovering, overflight, sinking, climbing). The sound power level varied between 57.8 dBA (hovering) and 73.7 dBA (maneuvering). In Jokisch et al. (2020), even sound pressure levels up to 98 dBA are reported. Both surveys furthermore state that the flight speed, a momentary wind force, the load, and the acceleration have an influence on the noise profile of the drones. In addition, a strongly demonstrated directional characteristic is discussed (Christian and Cabelly, 2017). Upwards or downwards, an increased sound pressure level of about 10 dB versus side movements was observed. Furthermore, psychoacoustic measurements were performed to determine the parameters loudness and sharpness. Essentially, UAVs can be perceived as disturbing, due to their frequency composition, but they do not have a particular proportion of low-frequency sounds.

4.2 Flight Maneuvers and Environmental Signals

In Jokisch and Fischer (2019, March), our sample quadcopter (DJI Mavic Pro) with a weight of 734 g was supplemented by mounted equipment of 102 g comprising a recording smartphone and the omnidirectional micro Rode smartLav+ (frequency range 20 Hz to 20 kHz). To analyze the effect of recording positions onto different flight maneuvers, use cases and environments, the microphone was placed at different positions at the UAV. The acoustic measurements at a flying UAV pose some challenges, which affect the reducibility of the signal analysis and the potential of noise filtering. The flight control together with micro-movements, varying rotor speeds, and other dynamic factors, such as turbulent flow or reflections, can hardly be synchronized with a simple harmonic or other analysis. All sounds were sampled at 44.1 kHz for the five flight maneuvers including hovering, indoor and outdoor, and we also recorded environmental sounds from a quiet modern car, a loud motorcycle, and a church bell.

By the sketched experimental setup, the flight maneuvers showed the expected acoustic effects, associated to the BPFs and their variations – e.g. at the beginning of a climb, the rotation speeds are shortly increased for drone acceleration, before they turn back to the previous level, as demonstrated in Figure 8 within the time interval 1.1...2.5 s.

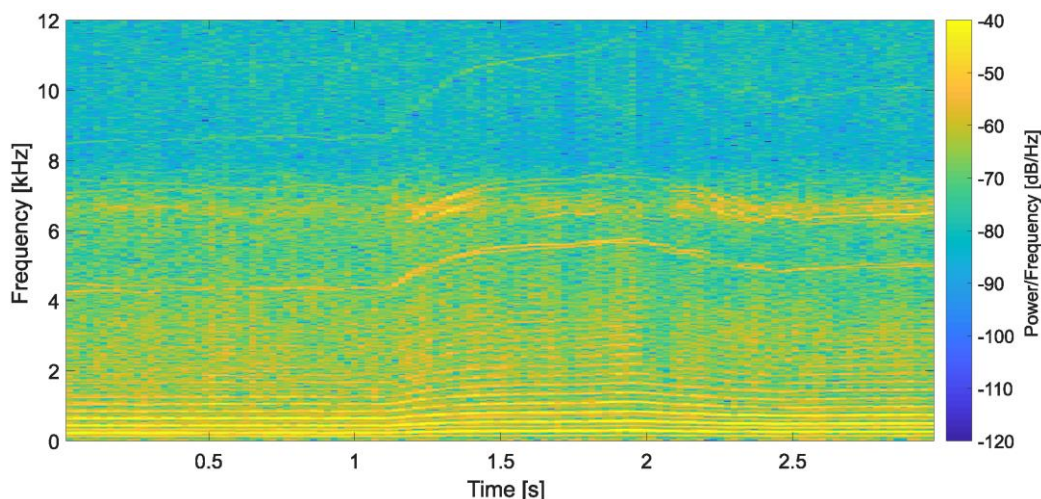


Fig. 8. Spectrogram of drone climbing (starting at 1.1 s and ending at 2.5 s).

By contrast, we could not find reproducible spectral patterns related to different in and outdoor flight environments – even in very short distances of 30...60 cm over ground or under ceiling. Although the recorded signals are effected by sound reflections and absorption, the spectra were dominated by the influences of micro position and flight maneuver. The car sounds are

almost completely masked by the drone sound, i.e., not really audible or detectable in the spectrogram, apart from a short level reduction, which is presumably caused by the air blast in the moment of passing (Figure 9). In contrast, the motocross sounds (Figure 10) and the bell-ringing (Figure 11) are still audible and detectable at a close range.

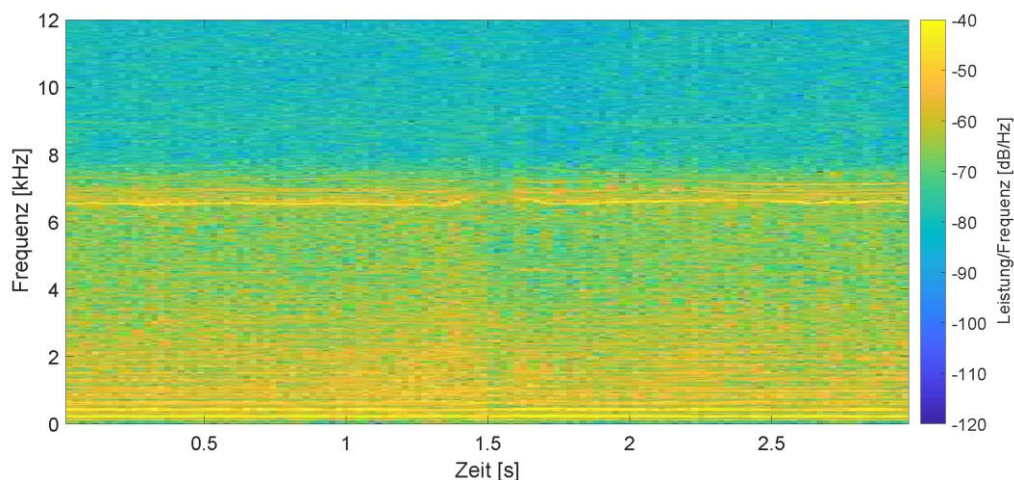


Fig. 9. Spectrogram of 3 s UAV-noise masked car sound – quiet car passing at 80 km/h on country road.

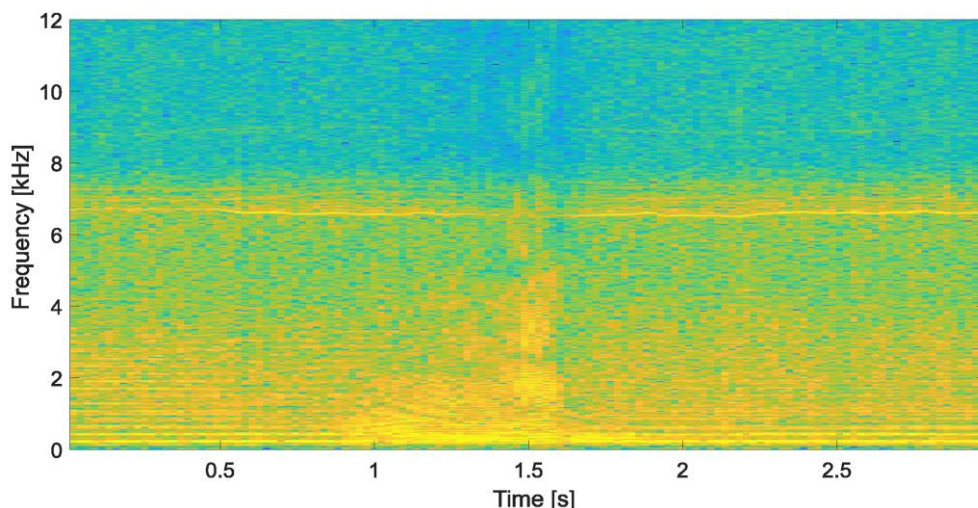


Fig. 10. Spectrogram of 3 s UAV-noise masked motocross sound – loud motorcycle at 30 km/h on a field.

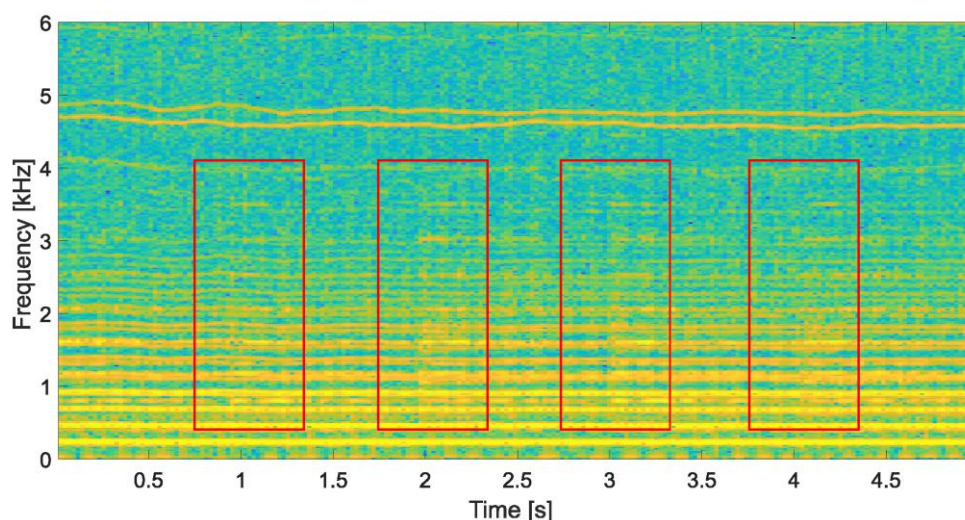


Fig. 11. Spectrogram of 5 s UAV-masked church-bell ringing at 5 m distance (bell components marked red).

4.3 Acoustic Signatures and Detection of Drones

Bernardini et al. (2017) used different short-term parametrization in time and frequency domain of environmental audio data to develop a machine-learning based, UAV-warning system with support vector machines (SVMs) for recognizing a drone-audio fingerprint (Figure 12).

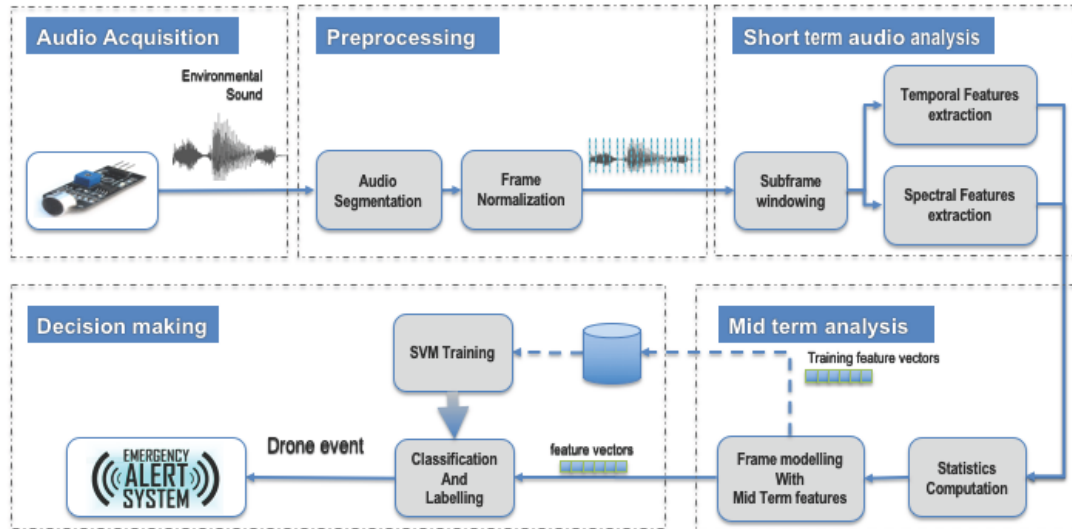


Fig. 12. Acoustic-signature identification framework for drones (Bernardini et al., 2017)

To evaluate the system, a dataset with five typologies of environmental sounds (drone is flying, nature daytime, street with traffic, train passing, crowd) from the web was automatically created that corresponds to six hours of environmental sounds. Each audio file was manually verified, whether it is correctly associated with the automatic label, and then divided in frames of 5 s, resulting in at least 840 segments per label class. To train binary SVM classifiers, the authors determined optimal discriminative subsets, and they assessed the performance by k-fold cross-validation to prevent overfitting. Their classification performance is indicated in Table 1.

Tab. 1. Classification performance of ten SVMs (Bernardini et al., 2017)

SVM classifier	Accuracy	Precision
drone vs. crowd	0.964	0.984
drone vs. nature daytime	0.992	0.983
drone vs. train passing	0.978	0.983
drone vs. street with traffic	0.964	0.987
crowd vs. nature daytime	0.959	0.919
crowd vs. train passing	1.000	1.000
crowd vs. street with traffic	0.891	0.782
nature daytime vs. street with traffic	0.991	1.000
nature daytime vs. train passing	0.996	0.991
street with traffic vs. train passing	1.000	1.000

For overall testing, the current frame was fed to all ten SVM at the same time. By using a max-wins strategy, the appropriate output label was identified, with a resulting precision in the drone recognition of 98.3 % that demonstrated the feasibility of a drone-sound recognition.

4.4 Speech Analysis at Drones

The development of automatic speech recognition systems has made enormous progress in recent years (Chiu et al., 2018). The systems can meanwhile recognize very noisy speech recordings in relatively low quality (Siegert et al., 2020). Jokisch and Fischer (2019) showed that even with a minimal preprocessing (notch filter) it is possible to recognize voice commands directly recorded at drones with a recognition rate up to 96.2 % (Figure 13 and Table 2).

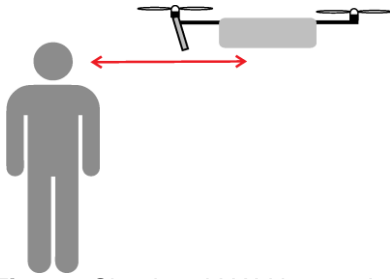


Fig. 13. Simulated UAV interaction.

Tab. 2. Speech recognition of 343 test signals (Jokisch and Fischer, 2019).

Noise reduction	SNR	Rejection rate (%)	Recognition rate (%)	Recognition w/o rejections (%)
without	0	100.0	0	-
ANR	20 dB	89.8	10.2	100.0
Notch & LP	5 dB	69.4	28.6	93.3
Notch & ANR	25 dB	53.1	32.6	69.6
Notch	3 dB	46.9	51.0	96.2

Nonetheless, the problem is the unacceptable percentage of rejections (heavily distorted voice commands for which no recognition is possible) of ca. 50 %. In general, UAV sound emissions at the microphones can be reduced, or intelligent preprocessing techniques can be used to lower the rejection rates significantly. In the described baseline setup, the noise reduction reaches an SNR improvement of about 20 dB, but an adequate speech recognition in these cases is still not possible due to the high rejection rates.

4.5 Advanced Recording Setup and Filtering Methods

To facilitate a significant SNR improvement for recordings of environmental or speech sounds, Lösch et al. (2020) proposed a lightweight microphone array for beamforming, directly mounted at the drone. In conjunction with a host system, the parameters directivity, main reception direction, and signal amplification can be configured dynamically. The overall weight of this experimental measuring system including cabling and battery amounts to 242 g (Figure 14).

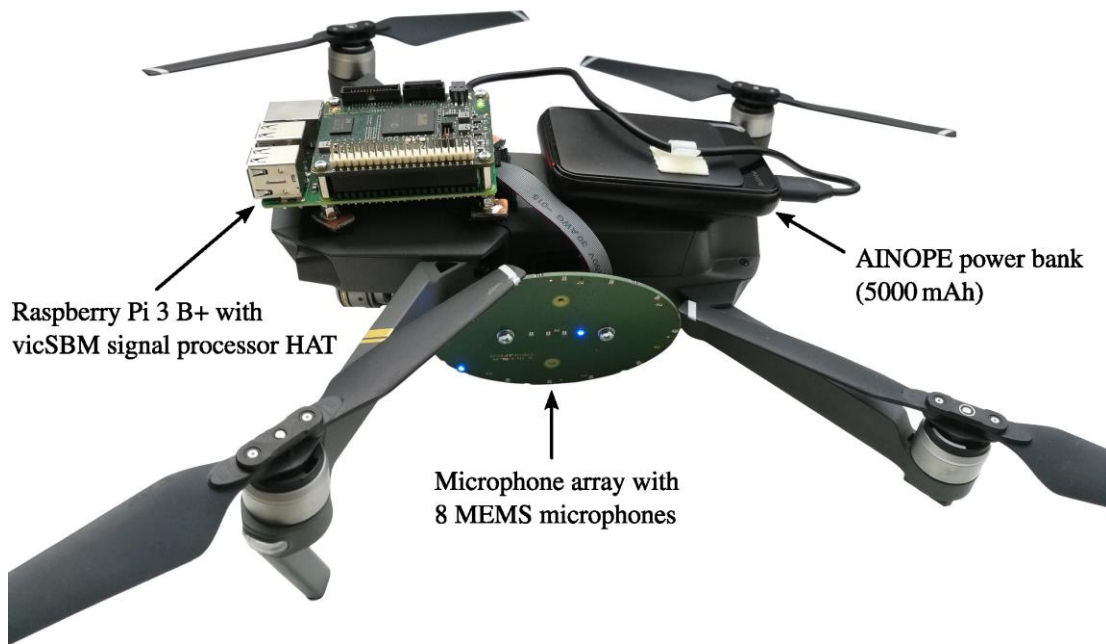


Fig. 14. UAV-mounted audio system with an 8-MEMS microphone array (Lösch et al., 2020).

The test signals were recorded at 16 kHz in a quiet rural area at wind speeds below 10 km/h, and a loudspeaker simulated speech commands directed to the drone that was either hovering 2 m above the speaker or flying in 3.2 m ground distance to the speaker (Figure 15). Additionally, the directivity (from 0 dB \triangleq bypass till 30 dB) and the azimuth angle (from 0° \triangleq highest sensitivity towards front till 90° \triangleq highest sensitivity towards ground) were varied.

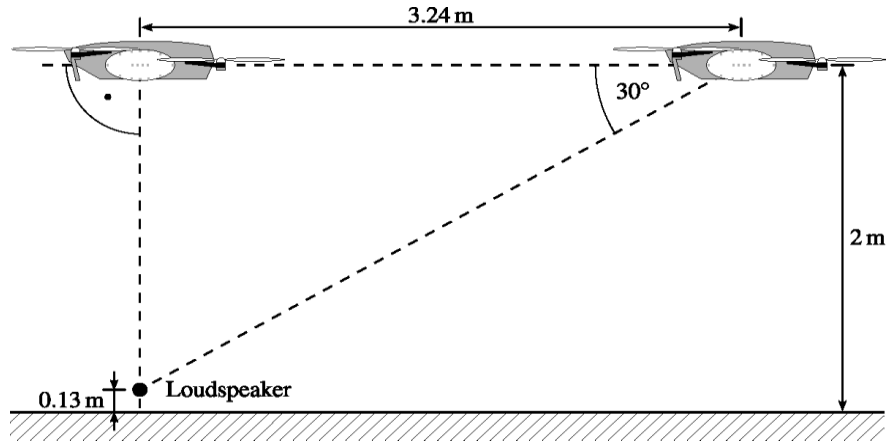


Fig. 15. Audio recording setup in Lösch et al. (2020).

In total, 80 settings were analyzed, comprising (a) the inherent UAV noise (without any voice signal), (b) the voice signal (no UAV-induced noise), and (c) the voice under flight conditions (voice overlaid by UAV's noise). In (b), the deactivated UAV was mechanically fixed at the respective positions. The host system (vicSBM) realized the beamforming and steering. The resulting SNR was enhanced in the best case by 35 dB for signals above 3 kHz (Figure 16).

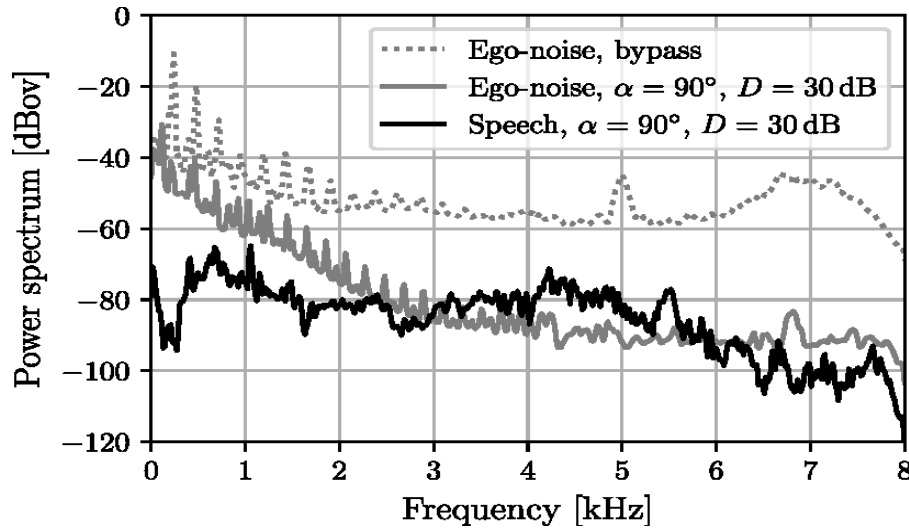


Fig. 16. Target speech vs. UAV ego-noise in best-case scenario (bypass \triangleq omnidirectional; D: directivity).

In the optimal case, the main beam has to be aligned to the signal source with a maximum directivity. Nevertheless, the noise attenuation significantly decreases for values below 3 kHz, hindering a proper speech processing. Compared to omnidirectional micro setups, a realistic SNR improvement of 10 dB only can be achieved around 1 kHz. A consecutive noise reduction by the Quantile Based Noise Estimation (Stahl et al., 2000) or Adaptive Quantile Based Noise Estimation (Bonde et al., 2006) did not result in a significant signal enhancement either.

5 Discussion and Conclusion

Although the use of drones and the application areas are considerably expanding since the last decade, the acoustic signal processing at, nearby or with drones is still an under-researched field. Furthermore, the growing use of drones in urban or natural areas significantly increases the requirements to reduce the noise emissions of UAVs.

Even though acoustic sensors have much fewer demands on the communication infrastructure in terms of transmission bandwidth, signal processing or post-processing, and their usage can be beneficial for many applications, a major disadvantage of acoustic processing at UAVs are their distinctive noises. Both aspects – the usage of drones in urban or natural areas as well as the acoustic investigations at and with drones – require further specific investigations of noise

emissions and radiation directions of UAVs to find best-possible generic solutions for noise reduction measures as depicted in Sections 3 and 4.

After an explosive growing of UAV functionalities, including sensing and control technologies, our attention has to turn to qualitative improvements in selected components, which includes audio sensors and processing in the UAV context. Such a paradigm shift has to involve specific acoustic standards and regulations (rather than usage limitations), more efforts in governmental and private sponsorships of research and development, and generally a higher sensibility for the acoustic topics among the UAV developers/producers and other innovation communities. Noise protection in both urban and natural areas is a high-relevant social and technical target, which deserves more conviction and attention in a way of “green drones”.

With respect to the manifold application scenarios illustrated in Section 2 and the several constructive and algorithmic possibilities sketched in Section 3, a careful engineering can open even more innovative research and business fields, by optimizing the tradeoff between the discussed advantages and deficits of UAV technologies, specifically by silent components and better methods of audio signal processing.

Besides aspects of flight security, privacy, or data protection in restricted areas that shall not be discussed here, a superior target could be the possible usage of drones in nearly all urban and natural areas.

The intermediate results of our survey, mainly demonstrated in Section 4, can be used to optimize the design of “silent UAVs” as well as the placement of acoustic sensors at UAVs. So far, most UAV bodies are designed to provide a maximal flight stability and to allow for optical sensors, but acoustic noise does not represent a specific limitation. The findings of Teichel and Körper (2019) about lower noise emissions in the horizontal versus vertical direction should be taken into account, if integrating acoustic sensors that are usually lightweight.

A standard integration of acoustic sensors into a UAV can enable a variety of new applications, e.g. to conduct voice interactions with a wide range of actors (rescuers and injured persons in a disaster situation, recipients parcel of deliveries, etc.). The technical infrastructure like on-board processors (managing the sensing and control parts) as well as distributed geometric positions for a microphone-arrays setup is already available. A necessary technical enhancement would be less costly (with an estimated range of 5...30 Euro in mass production). An additional weight of acoustic sensors and cabling should be uncritical – optimized only a few grams (compared to the mounted test equipment of 100...240 g used in Section 4) that do not significantly affect the payload profiles of UAVs.

Assuming a dynamic, ambient acoustics in outdoor and indoor scenarios, future challenges will deal with acoustic interferences of the local UAV system with other surrounding systems and their constructive measures (e.g. an active noise cancellation), and environmental objects in general. Furthermore, a stable distinction between speech, other ‘useful sounds’ and noise will remain difficult in many application scenarios, due to the high flexibility of the drone usage in changing environments that are generally critical for audio, speech and music applications.

Last, but not least, most environmental sounds are not only noise sources but also important sources of information. Acoustic scene detection could be improved by using silent drones with acoustic sensors, which closes the loop between constructive and algorithmic methods.

References

- Azari, M.; Sallouha, H.; Chiumento, A.; Rajendran, S.; Vinogradov, E.; Pollin, S. (2018). *Key technologies and system trade-offs for detection and localization of amateur drones*. IEEE Communications Magazine 56(1), pp. 51–57, Jan. 2018. <https://arxiv.org/pdf/1710.08478.pdf>
- Bernardini, A.; Mangiatordi, F.; Pallotti, E.; and Capodiferro, L. (2017). Drone detection by acoustic signature identification. J. Electronic Imaging 2017(10), pp. 60-64, January 2017. <https://doi.org/10.2352/ISSN.2470-1173.2017.10.IMAWM-168>

- Bourdon, M.; Moynihan R. (2020). *One of the largest cities in France is using drones to enforce the country's lockdown after the mayor worried residents weren't taking containment measures seriously*. Business Insider France, March 2020. <https://www.businessinsider.com/coronavirus-drones-france-covid-19-epidemic-pandemic-outbreak-virus-containment-2020-3>
- Bonde, C.; Graversen, C.; Gregersen, A.; Ngo, K. H.; Nørmark, K.; Purup, M.; Thorsen, T. and Lindberg, B. (2006). *Noise robust automatic speech recognition with adaptive quantile based noise estimation and speech band emphasizing filter bank*. Proc. Nonlin. Analyses & Algor. for Speech Processing (NOLISP), Barcelona, 2005. Springer LNCS, vol. 3817, pp. 291–302, 2006. https://doi.org/10.1007/11613107_26
- Cabell, R.; Grosveld, F. and McSvan, R. (2016). *Measured noise from small unmanned aerial vehicles*. In: Proc. Internoise/Noise-Con, vol. 252, pp. 345–354. June 2016. <https://ntrs.nasa.gov/archive/nasa/casi.ntrs.nasa.gov/20160010139.pdf>
- Carroll, J. M. (2013). *Human computer interaction - brief intro*. In M. Soegaard and R. F. Dam (eds.), The Encyclopedia of Human-Computer Interaction, The Interaction Design Foundation, Aarhus, Denmark, Second Edition, 2013. <https://www.interaction-design.org/literature/book/the-encyclopedia-of-human-computer-interaction-2nd-ed/human-computer-interaction-brief-intro>
- Castro, V., Contreras, V., Cea, A., Collado, G., & García, L. (2017). *Active Noise Cancellation System for UAVs*. In: Proc. 13th PEGASUS-AIAA Student Conference (American Institute of Aeronautics and Astronautics), Berlin, April 2017.
- Chiu, C.; Sainath, T.; Wu, Y.; Prabhavalkar, R.; Nguyen, P.; Chen, Z.; Kannan, A.; Weiss, R.; Rao, K.; Gonina, E.; Jaitly, N.; Li, B.; Chorowski, J.; Bacchiani, M. (2018) *State-of-the-art speech recognition with sequence-to-sequence models*. Proc. IEEE ICASSP, pp. 4774–4778. Calgary, April 2018.
- Christian, A.; Cabelly, R. (2017). *Initial Investigation into the Psychoacoustic Properties of Small Unmanned Aerial System Noise*. NASA Langley Research Center, Hampton, USA.
- Ciaburro, G.; Iannace, G. and Trematerra, A. (2020). *Research for the presence of unmanned aerial vehicle inside closed environments with acoustic measurements*. J. Buildings, 10(5), 96, May 2020. <https://doi.org/10.3390/buildings10050096>
- DJI Technology (2018). DJI Mavic Pro. <http://www.dji.com/en/mavic> retrieved 28/01/2020.
- Erdelj, M.; Natalizio, E. (2016). *UAV-assisted disaster management: applications and open issues*. In: 2016 Intern. Conference on Computing, Networking and Communications (ICNC), pp. 1–5, February 2016. <https://doi.org/10.1109/ICCNC.2016.7440563>
- Fadelli, I. (2018). *Optimal resource allocation for UAV communication systems in disaster management* (Tech Xplore). <https://techxplore.com/news/2018-09-optimal-resource-allocation-uav-disaster.html> retrieved 11/08/2020.
- Güvenç, I.; Ozdemir, O.; Yapici, Y.; Mehrpouyan, H.; Matolak, D. (2017). *Detection localization and tracking of unauthorized UAS and Jammers*. In: Proc. IEEE/AIAA 36th Digital Avionics Systems Conference (DASC), pp. 1-10, 2017. <https://doi.org/10.1109/DASC.2017.8102043>
- Hassanalian, M. and Abdelkefi, A. (2017). *Classifications, applications, and design challenges of drones: A review*. J. Progress in Aerospace Sciences, vol. 91, pp. 99–131, May 2017. <https://doi.org/10.1016/j.paerosci.2017.04.003>
- Headrick, S. (2015). *AeroTestra MK10 Ducted Multi Rotor Aircraft*. Retrieved 25/02/2020. <https://aerotestra.com/projects-updates/2015/2/24/aerotestra-mk10-ducted-multi-rotor-aircraft>
- Hodgson, J.C.; Koh, L.P. (2016). *Best practice for minimising unmanned aerial vehicle disturbance to wildlife in biological field research*. J. Current Biology, 26(10), pp. 404–405. <https://doi.org/10.1016/j.cub.2016.04.001>

- Iannace, G.; Ciaburro, G. and Trematerra, A. (2019). *Fault Diagnosis for UAV Blades Using Artificial Neural Network*. J. Robotics 2019, 8(3), 59. <https://doi.org/10.3390/robotics8030059>
- Iannace, G.; Ciaburro, G. and Trematerra, A. (2020). *Acoustical unmanned aerial vehicle detection in indoor scenarios using logistic regression model*. J. Building Acoustics/OnlineFirst, May 2020. <https://doi.org/10.1177/1351010X20917856>
- ITU-T P.501 (2017). *Test signals for use in telephony, Recommendation P.501*. <http://www.itu.int/rec/T-REC-P.501-201703-I/en> , March 2017.
- Jokisch, O. and Fischer, D. (2019, March). *Drone sounds and environmental signals – a first review*. In: Proc. 30th ESSV Conference, pp. 212–220. Dresden, Germany, March 2019. http://www.essv.de/pdf/2019_212_220.pdf
- Jokisch, O. (2019, April). *A Pilot Study on the Acoustic Signal Processing at a Small Aerial Drone*. Proceedings 14th Intern. Conference on Electromechanics and Robotics "Zavalishin's Readings" (ER-ZR), Kursk, Russia. In: Springer Smart Innovation, Systems and Technologies, vol. 154, chapt. 25, pp. 305–317, April 2019. https://doi.org/10.1007/978-981-13-9267-2_25
- Jokisch, O.; Siegert, I.; Maruschke, M.; Strutz, T.; Ronzhin, A. (2019, August). *Don't Talk to Noisy Drones - Acoustic Interaction with Unmanned Aerial Vehicles*. Proc. 21th International Conference on Speech and Computer (SPECOM), Istanbul. In: Springer LNAI, pp. 180–190, August 2019. https://doi.org/10.1007/978-3-030-26061-3_19
- Jokisch, O.; Siegert, I.; Loesch, E. (2020, March). *Speech Communication at the Presence of Unmanned Aerial Vehicles*. Proc. 46th Annual German Conf. on Acoustics (DAGA), Hannover, pp. 952–955, March 2020. https://pub.dega-akustik.de/DAGA_2020/data/articles/000474.pdf
- Kloet, N.; Watkins, S.; Wang, X. (2019). *Aeroacoustic investigation of multirotor unmanned aircraft system (UAS) propellers and the effect of support structure*. Internoise Conference, Madrid, June 2019. http://www.sea-acustica.es/fileadmin/INTERNOISE_2019/Fchrs/Proceedings/1596.pdf
- Lösch, E.; Jokisch, O.; Leipnitz, A.; Siegert, I. (2020). *Reduction of Aircraft Noise in UAV-Based Speech Signal Recordings by Quantile Based Noise Estimation*. Proc. 31th ESSV Conference, Magdeburg, pp. 149-156, March 2020. http://www.essv.de/pdf/2020_149_156.pdf
- Magid, E.; Pashkin, A.; Simakov, N.; Abbyasov, B.; Suthakorn, J.; Svinin, M. and Matsuno, F. (2019). *Artificial Intelligence Based Framework for Robotic Search and Rescue Operations Conducted Jointly by International Teams*. 14th Intern. Conf. Electromechanics and Robotics "Zavalishin's Readings" (ER-ZR), Kursk, Russia. In: Springer Smart Innovation, Systems and Technologies, vol. 154(2), pp. 15-26, April 2019. https://doi.org/10.1007/978-981-13-9267-2_2
- McKay, R.; Kingan, M. (2019). *Multirotor Unmanned Aerial System Propeller Noise Caused by Unsteady Blade Motion*. 25th AIAA/CEAS Aeroacoustics Conference, Delft, May 2019. <https://doi.org/10.2514/6.2019-2499>
- Miesikowska, M. (2017). *Analysis of signal of x8 unmanned aerial vehicle*. In Proc. IEEE Conf. Signal Processing: Algorithms, Architectures, Arrangements & Applications (SPA), pp.69–72. September 2017. <https://doi.org/10.23919/spa.2017.8166840>
- Miljković, D. (2018, January). *Active Noise Control in Light Aircraft Cabin Using Multichannel Coherent Method*. J. Automatika, vol. 57, number 4, pp. 1056-1069, January 2018. <https://doi.org/10.7305/automatika.2017.12.1706>
- Miljković, D. (2018, May). *Methods for attenuation of unmanned aerial vehicle noise*. Proc. 41st Intern. Convention on Information and Communication Techn., Electronics and Microelectronics (MIPRO), pp. 914-919, Opatija, May 2018. <https://doi.org/10.23919/MIPRO.2018.8400169>

- Rascon, C.; Ruiz-Espitia, O. and Martinez-Carranza, J. (2019). *On the use of the AIRA-UAS corpus to evaluate audio processing algorithms in unmanned aerial systems*. Sensors, 19(18), pp. 3902–3921, September 2019. <https://doi.org/10.3390/s19183902>
- Restas, A. (2015). *Drone applications for supporting disaster management*. World J. Eng. Technol. 3, 316–321, 2015. <https://doi.org/10.4236/wjet.2015.33C047>
- Rozantsev, A.; Sinha, S.; Dey, D.; Fua, P. (2017). *Flight dynamics-based recovery of a UAV trajectory using ground cameras*. In: Proc. IEEE Conference on Computer Vision and Pattern Recognition (CVPR), Honolulu, July 2017.
- Schelle, A., Stütz, P. (2018). *Gestural transmission of tasking information to an airborne UAV*. In: Yamamoto, S., Mori, H. (eds.) HIMI 2018. LNCS, vol. 10904, pp. 318–335. Springer, Cham 2018. https://doi.org/10.1007/978-3-319-92043-6_27
- Sibo, H.; Xinsheng, F.; Wang, X.; Badreddine, A.; Qian, C.; Yong, Y. (2019). *Acoustic perfect absorbers via Helmholtz resonators with embedded apertures*. J. Acoustical Society of America (JASA), vol. 145, number 1, pp. 254–262, 2019. <https://doi.org/10.1121/1.5087128>
- Siebert, I.; Lotz, A. F.; Duong, L. L. and Wendemuth, A. (2016). *Measuring the impact of audio compression on the spectral quality of speech data*. In Proc. ESSV Conference, pp. 229–236. Leipzig, March 2016. http://www.essv.de/pdf/2016_229_236.pdf
- Siebert, I.; Sinha, Y.; Jokisch, O.; Wendemuth, A. (2020). *Recognition Performance of Selected Speech Recognition APIs – A Longitudinal Study*. In: Proc. 22th International Conference on Speech and Computer (SPECOM), St. Petersburg. In: Springer LNAI, October 2020 (in print).
- Šimek, P.; Pavlík, J.; Jarolínek, J.; Očenášek, V.; Stočes, M. (2017). *Use of Unmanned Aerial Vehicles for Wildlife Monitoring*. In: Proc. 8th International Conference on Information and Communication Technologies in Agriculture, Food and Environment (HAICTA 2017), pp. 795–804. Chania, Greece, September 2017.
- Stahl, V.; Fischer, A. and Bippus, R. (2000). *Quantile based noise estimation for spectral subtraction and wiener filtering*. IEEE International Conference on Acoustics, Speech, and Signal Processing. Proceedings, vol. 3, pp. 1875–1878. June 2000. <https://doi.org/10.1109/icassp.2000.862122>
- Štorch, V.; Nožička, J.; Brada, M.; Gemperle, J.; Suchý, J. (2016). *Measurement of noise and its correlation to performance and geometry of small aircraft propellers*. EPJ Web of Conferences. Vol. 114. <https://doi.org/10.1051/epjconf/201611402112>
- Treichel, J. and Körper, S. (2019). *Untersuchung der Geräuschemission von Drohnen (Investigation of the noise emission of drones, in German)*. Lärmbekämpfung: Zeitschrift für Akustik, Schallschutz und Schwingungstechnik, Springer VDI, vol. 14, issue 4, pp. 108–114.
- Unger, L.; Knopf, P.; Monetti, D. (2017). *Praxis der Datenerfassung mit Drohnen für GIS und Vermessung (in German)*. Proc. 22nd Intern. Conference on Urban & Regional Development and Spatial Planning in the Information Society (REAL CORP), Wien, pp. 717–722, Sept. 2017. https://programm.corp.at/cdrom2017/papers2017/CORP2017_36.pdf
- voice INTER connect GmbH (2019). *vicDIVA – A development kit for the distant voice acquisition*. https://www.voiceinterconnect.de/en/sdk_beamforming retrieved 28/01/2020
- Wang, Z.; Henricks, Q.; Zhuang, M.; Pandey, A.; Sutkow, M.; Harter, B.; McCrink, M. and Gregory, J. (2019). *Impact of rotor–airframe orientation on the aerodynamic and aeroacoustic characteristics of small unmanned aerial systems*. J. Drones (MDPI) 3(3):56, July 2019. <https://doi.org/10.3390/drones3030056>
- Zhou, G.; Yuan, J.; Yen, I. and Bastani, F. (2016). *Robust real-time UAV based power line detection and tracking*. In Proc. IEEE International Conference on Image Processing (ICIP), Phoenix, USA, pp. 744–748, Sept. 2016. <https://doi.org/10.1109/ICIP.2016.7532456>



QUIET DRONES
International Symposium
on
UAV/UAS Noise
Paris - 19th to 21th October 2020

Experimental Investigation on Acoustics and Efficiency of Ducted Electric Rotors

**Ronja Koenig, Robert Bosch GmbH, ronja.koenig@de.bosch.com,
Jochen Fassnacht, Robert Bosch GmbH,
Felix Albrecht, Robert Bosch GmbH,
Eike Stumpf, RWTH Aachen University, eike.stumpf@ilr.rwth-aachen.de.**

Summary

Aerial vehicles based on distributed electric propulsion systems have gained great interest. Several designs apply ducts at rotors. Ducts are used for various reasons like safety and efficiency. Furthermore, benefits in acoustics are expected.

Focus of this paper is to understand the influence of ducts at single and coaxial rotor configurations regarding efficiency and acoustics while hovering. Results from experimental investigations done in a hover-test-bench are presented. Rectangular, symmetric blades with a radius of 106 mm are used. Ducts are developed considering the rotor streamtube, which is visualized using Particle Image Velocimetry (PIV). Experiments are done varying the inner surface of the duct, the duct length and the duct position at the rotors.

Results show, that ducts can improve efficiency and acoustics. The position of a duct has huge influence, especially when increasing duct length. Best results were found using ducts leading the rotor streamtube and positioning the rotor at the beginning of the duct. Reduction in Sound Pressure Level (SPL) at higher harmonics of the blade passage frequency were found. Positioning a duct at the bottom rotor of a coaxial rotorsystems can be recommended according to the experimental results. However, ducting both rotors at a coaxial rotorsystem cannot be recommended. It was also found that a decrease of tip clearance up to 3 mm leads to increase in SPL. Porous surfaces and rounded inlet showed positive influence on SPL at single rotors. Finally, conclusions for duct design at aerial vehicles are derived from experimental results.

1. Introduction

Aerial vehicles based on distributed electric propulsion have gained great interest. Development of aerial vehicles for search and rescue missions [1], surveillance missions [2], transportation of parcels [3], or people [4] and medical aid [5], [6] takes place. Aerial vehicles with distributed electric propulsion apply rotors, which often create loud and annoying [7] noise. This leads to problems regarding acceptance and obstructs market success. One feature, which can be observed on emerging designs is a duct around rotors. Ducts are used for various reasons like safety and efficiency. Furthermore benefits in acoustics are expected.

This paper presents an experimental analysis on ducts at single and coaxial contrarotating rotor configurations while hovering. The influence of ducts on efficiency and acoustics is analyzed. The rotor streamtube is taken into consideration. The main contributions of this paper are:

1. Extensive experimental investigation of ducted rotors while hovering:
 - Analysis of the influence of duct position at single and coaxial rotors on acoustics and efficiency. For a single rotor, a duct above the rotor, at the rotor or below the rotor is evaluated. These positions are also measured at coaxial configuration at the top and bottom rotor. In addition ducting both rotors is analyzed as well.
 - Analysis of influence of duct length on acoustics and efficiency.
 - Analysis of influence of inner surfaces of ducts on acoustics and efficiency: Application of straight design, porous surface, rounded inlet and designs inspired by rotor streamtube.
2. Derivation of design rules for acoustic optimization of ducts based on the experimental results.

The paper is structured as follows. First, related work is presented including analysis of emerging concepts. An overview regarding the experimental setup follows. Subsequently, selection and analysis of the rotor configurations are explained. After describing the developed duct designs, experimental results are presented: Methodology, single rotors, coaxial rotors. The influence of ducts on the aerial vehicle is discussed and design rules are proposed.

2. Related Work

Ducts around rotors have been studied in the past. A theoretic overview of ducted propellers is given by [8]. Properly designed ducts can reduce tip losses in a propeller and thus increase thrust compared to a propeller of the same diameter alone. Duct thrust is produced by suction force on the inner duct surface [8]. In the following, experimental investigations and studies of ducted rotors are presented. Afterwards emerging concepts applying ducts are discussed. Studies, that investigated the influence on acoustics and efficiency are described in the following. These configurations of ducts and rotors are abstracted in Fig. 1. It can be observed, that the outer contours vary widely and might have different influence on efficiency and wind susceptibility in horizontal flight. This paper however is focussing on the design of the inner contours.

Rotor-duct interactions were studied by [9] on a rotor for low Reynolds numbers, see Fig. 1 (1). Un-tapered, untwisted rectangular blades with a radius of 136 mm were used. Two ducts with 5 mm and 10 mm rotor tip clearance and 20 mm height were used. Positive effects on rotor performance regarding Figure of Merit (FOM), even if the duct is not designed for thrust generation, were found. Smaller rotor tip clearance showed better performance results, due to reduced tip losses. Overall SPL was about the same for ducted and un-ducted cases, but higher tonal content

for cases with higher vortex core/duct interactions was found [9]. The influence on lift force and energy due to a shrouded rotor with different blade tip clearances and heights was investigated experimentally by [10] for a rotor with 254 mm diameter, see Fig. 1 (1). However, it resulted that small blade tip clearance performed worse than larger blade tip clearance, which were worse than the results of the open rotor.



Figure 1: Abstract setup of ducted rotors investigated: left (1) by [9] and [10], middle (2) by [11], middle (3) by [12], right (4) by [13].

Experimental analysis of ducts were done by [11] with a rotor diameter of 160 mm at low Reynolds numbers, see Fig. 1 (2). Increase in thrust up to 94 % at the same power consumption and reductions in power up to 62 % at the same thrust were found. The following parameters were identified for optimal duct design: Increase of lip radius, decrease of blade tip clearance, diffuser angle at 10° and diffuser length at 50 % of shroud diameter [11]. A negative effect due to increased blade tip clearance on broadband noise level and efficiency was also found by [14] for a ducted axial fan with a diameter of 300 mm. Diameter and strength of the tip vortex increased as well.

Analysis of a shrouded coaxial rotor while hovering were done by [12], see Fig. 1 (3). It was shown that a negative pressure region around the shroud lip is the main source for thrust generation. Moreover it was found, that the shrouded rotors produced larger thrust with less power consumption. A three bladed, single and coaxial rotor system with a diameter of 4.05 ft was experimentally investigated by [13], see Fig. 1 (4). Rotor spacing, duct inlet shape, position of rotors within the duct and tip clearance were analyzed regarding efficiency. It was found, that single rotors almost always improved system performance. However, only one setup (rotor spacing of 0.15 blade radius, cambered duct, rotors down within the duct) of the ducted coaxial rotor showed better performance than the open rotor. Design parameters were found to be different for single and coaxial rotor [13].

These studies show, that the following design factors have influence on duct performance: Rotor tip clearance, lip radius, length of duct, design of inner surface of duct. However no general statements can be derived, since different boundary conditions and experimental setups were applied.

Some emerging concepts for transportation of goods and people apply ducts around rotors. Concepts with ducts are analyzed based on published photographs and categorized in the following. Fig. 2 shows an abstract design of ducts at emerging aerial vehicles.

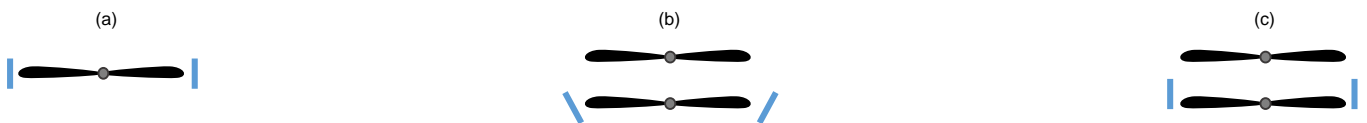


Figure 2: Abstract design of ducts at emerging aerial vehicles.

One of Amazon Prime Air's package delivery drones has a duct structure around four rotors, looking like a safety feature. Rotors are positioned at the middle of the duct structure Fig. 2 (a). The concept PopUp.Next by Audi/Airbus has a three-bladed coaxial rotor. The bottom rotor is ducted and seems to be located at the lower end of the duct. The duct seems to have a straight inner surface, see Fig. 2 (c). The concept City Airbus is similar. However the duct around the bottom rotor seems to be in the middle of the duct. Moreover the duct looks slightly beveled towards the lower end, see Fig. 2 (b). Another example is the concept Bell Nexus. It has ducts around five-bladed single rotors, which seem to be placed at the middle of the rotor plane. Moreover a stator seems to be placed at the lower end of the duct and below the duct.

As described, it is known from earlier analysis, that ducts can be used for thrust generation. Safety and acoustic functions are discussed. This paper extends experimental analysis of ducted single and coaxial rotors in hover conditions for the following topics: Geometric parameters with constant boundary conditions regarding not only efficiency but acoustics are also analyzed. In addition ducts at emerging concepts, like ducting the bottom rotor only are investigated. Moreover analysis of acoustic measures inside of ducts, like porous surfaces are done.

3. Experimental Setup

A hover-test-bench, which has been presented in detail in [15], is used. The hover-test-bench is based on a propulsion system of the type DJI 4114. It includes torque and force sensors measured in 6 degrees of freedom, rotational speed measurement and PIV (Particle Image Velocimetry) measurements. The adaption of pitch control for rotor blades is available. All walls of the hover-test-bench are covered with acoustic foam (Basotect G+). In this study, the blades X-Blades X106 are selected. These are un-tapered, untwisted rectangular blades with a radius of 106 mm. A two-bladed configuration is used for single as well as coaxial configurations.

Acoustic measurement are done with a mobile frontend (SQobold, head-acoustics) and three microphones (1/2" Microtech Gefell, MM215). The positioning of the microphones in the hover-test-bench is shown in Fig. 3. Microphones are positioned in a circle around the sound source at even distances, following enveloping surface methods. Number and distances are chosen by the following constraints: Sufficient distance from the walls, possibility to place microphone stands and microphone position out of the air flow to avoid incorrect measurement.

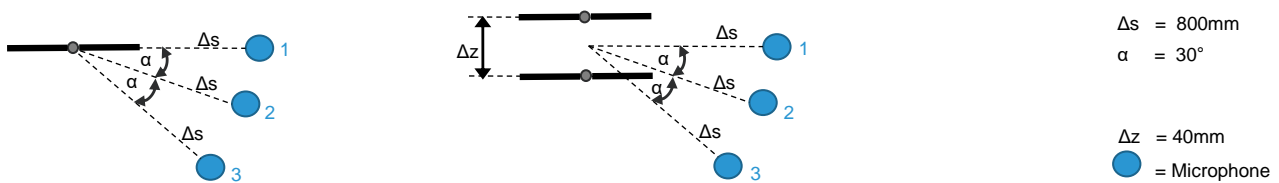


Figure 3: Position of three microphones inside the test-bench. Left: Position in case of one rotor. Middle: Positions in case of a coaxial rotor.

To measure the influence of ducts on efficiency, the duct designs are attached at the motor housing. Thus, it is connected to the top measurement unit. The position of a duct at a rotor is adjusted using a threaded rod, see Fig. 4. A measurement mode using ramp-ups with rotational speeds from 3000 rpm to 7000 rpm for 8 s each is used. Synchronisation between acoustic and efficiency measurements is provided. For subsequent calculations, an evaluation tool is built using Matlab.



Figure 4: Attachment of duct at top rotor at hover-test-bench.

4. Rotor Configuration without Duct

In the following, the selection of the rotor configurations and analysis regarding efficiency, acoustics and rotor streamtube are presented. This is the basis for comparing the effect of ducts. First, the rotor systems are adjusted concerning pitch angle of the blades. Therefore, measurements are done and hover efficiency is calculated using the Figure of Merit (FOM), as defined by [16]:

$$\text{FOM} = \frac{P_{\text{ideal}}}{P_{\text{real}}} \quad (1)$$

with P_{ideal} defined for single and coaxial configurations:

$$P_{\text{ideal, single}} = \frac{T^{3/2}}{\sqrt{2\rho A}} \quad (2)$$

$$P_{\text{ideal, coax}} = P_{\text{ideal, top}} + P_{\text{ideal, bottom}} \quad (3)$$

and P_{real} for single and coaxial configurations:

$$P_{\text{actual, single}} = 2\pi M n \quad (4)$$

$$P_{\text{actual, coax}} = P_{\text{actual, top}} + P_{\text{actual, bottom}} \quad (5)$$

The variables P_{ideal} and P_{real} describe the ideal and real power. T describes thrust, ρ air density, A rotor disk area, M torque and n revolutions per minute.

A constant pitch angle of 17° is selected due to best efficiency results for all configurations. For coaxial rotor configurations, the same rotational speed is selected for the top and bottom rotor. Rotors are chosen contrarotating and thus are balanced regarding torque. Minimal packaging space for a aerial vehicle is kept in mind selecting the vertical distance Δz between coaxial rotors, see Fig. 5. Extensive research has been done regarding the optimal Δz in the past. Analysis done by [17] support the conclusion of [18] that for $\frac{\Delta z}{D} > 0.05$ little effect on performance occurs. In [15] it was presented, that the vertical distance between two coaxial rotors, rotating at the same rpm, leads to only slight deterioration of the combined FOM for increased distance, with optimum at $\frac{\Delta z}{D} = 0.13$. The overall performance of a coaxial rotor is according to [19] independent of axial separation for $\frac{\Delta z}{D} > 0.15$.



Figure 5: Rotor diameter and vertical distance between coaxial rotors.

A vertical distance Δz of 40 mm between the rotors is selected, which is equal to $\frac{\Delta z}{D} = 0.16$. Fig. 6 shows the resulting thrust and efficiency of the selected configurations.



Figure 6: Thrust and efficiency (FOM) of the selected single and coaxial rotor configurations at the test-bench with X-Blades X106.

To compare results, operating points are required. Typical operating points of systems^{1 2} using similar blade length are analyzed. It follows, that single rotors at real systems typically operate at around 3.5 - 5 N while hovering. An operating point for single rotors at 5 N (5000 rpm) and 10 N (5000 rpm) for coaxial rotors is selected.

Fig. 7 shows acoustics of the selected rotor configurations. Single and coaxial rotor configurations shows similar characteristics. The propeller blade passage frequency f_1 of the system is given by [20]:

$$f_1 = B \cdot \frac{n_P}{60} \quad (6)$$

with B as number of blades and n_P as rotational speed in rpm. It follows, that f_1 for a single rotor lies at 166 Hz. In this case f_1 is most dominant at microphone 1 (see marker X1, Fig. 7). Higher harmonics are, however, more dominant at microphone 2 and especially 3 (see marker X2, Fig. 7). It is observed, that SPL increases from microphone 1 to 3 at higher harmonics.

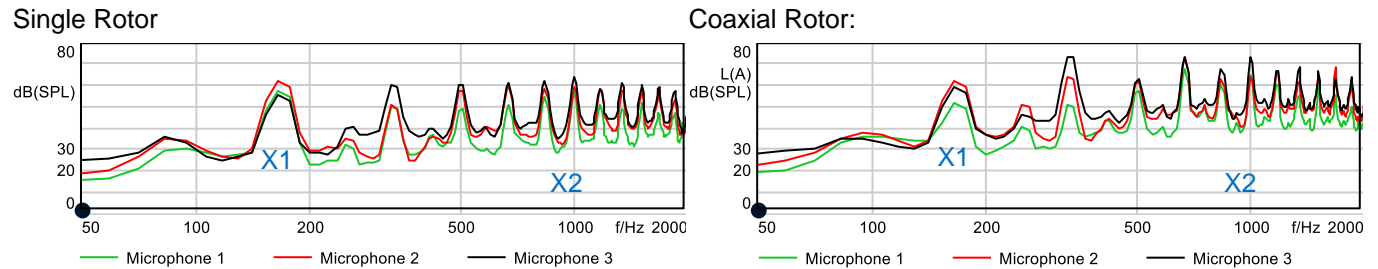


Figure 7: Frequency spectra of the SPL for selected rotor configurations at at 5 N (single) and at 10 N (coaxial).

To investigate the position and direction of velocity (V_y) and vorticity ($vorticity_z$) of the air flow, PIV measurements are conducted, averaging 100 measurements each, see Fig. 8. The position of the rotor streamtube is particularly interesting for designing ducts, which lead the air flow or do not disturb the air flow. It results, that the rotor streamtube does not change significantly for different thrust values, however, vorticity and velocity increase applying higher thrust. The rotor streamtube at 5 N for single rotors and 10 N for coaxial rotor systems is used for development of the inner surfaces of the ducts. Fig. 8 shows vorticity and velocity of the single and coaxial configurations at these operating points.

¹<https://www.lumenier.com/commercial/qav500> [last visited 10.07.2020].

²<https://www.dji.com/phantom-4> [last visited 10.07.2020].

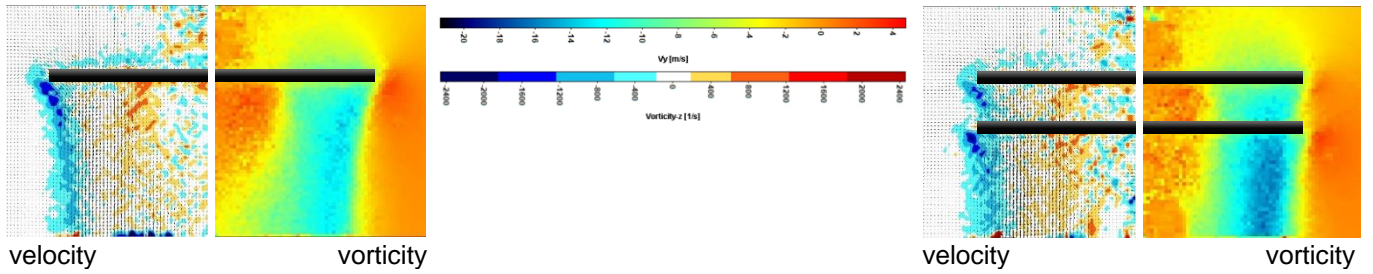


Figure 8: PIV measurements: Single rotor (left) at 5 N and coaxial rotor (right) at 10 N. The presented scales are constantly used throughout this paper.

5. Duct Design

As analyzed in chapter 2, studies of thrust generation and efficiency of ducts have been done in the past. Experimental investigations with constant boundary conditions regarding geometric parameters (duct length, inlet geometry), short ducts at one rotor of a coaxial rotor system and acoustic treatment inside of ducts, like porous surfaces are added in this paper. In this paper, ducts are designed to analyze these topics. Ducts with different inner surface geometries, porous surfaces and different length are created. Position of the ducts at rotors is varied. The geometries are designed considering the rotor streamtube of the open rotor system, which is visualized using Particle Image Velocimetry (PIV), see chapter 4.

Based on the emerging concepts analyzed in chapter 2, a duct length H_b of 20 mm is selected as basic configuration. The length H_b matches roughly 15% of the rotor diameter. This not only allows to analyze air flow concepts, but also meets requirements of manufacturing and robustness for experimental testing. To analyze the influence of the duct length on acoustics and efficiency, three versions (length H_b , $2H_b$ and $3H_b$) are designed as well. Longer versions enable to analyze a coaxial rotor configurations with both rotors ducted and simulate situations where a rotor is included into the body of an aerial vehicle. The concepts and integration of ducts as well as the chosen designs are described in the following.

5.1. Concept and Integration

The duct concept is based on an outer part, that is mounted at the test-bench and variable inner geometries. The outer and inner parts are centered with grooves, see Fig. 9. In addition, they are locked at three positions with screws and metal threads inside the material. The components of the duct have been manufactured using 3D-printing. A Fortus 450mc from alphacam is used. Acrylic Styrene Acrylonitrile (ASA) is used in black to enable PIV measurements without reflections.

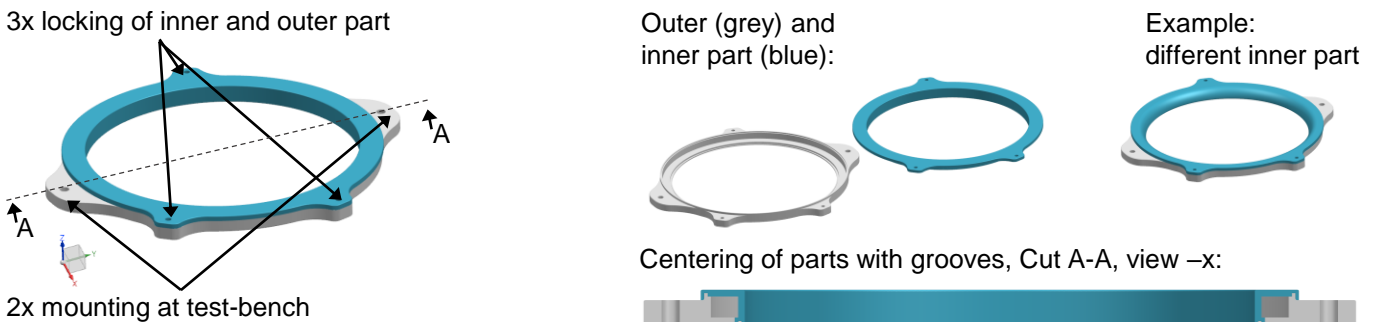


Figure 9: Duct concept: Outer and variable inner part including mounting positions at the test bench and locking of parts with screws and grooves.

5.2. Straight Inner Surface

Three different inner designs of ducts with straight inner surfaces are created. A tip clearance t_c of 10 mm is selected, see Fig. 10. This distance positions the duct outside the rotor streamtube (visualization see chapter 4), which avoids disturbance of the air flow. In addition, it serves as safety distance in case of vibrations at high rotational speeds. To investigate the influence of a reduced tip clearance of 3 mm, foamed tape is applied. To analyze the influence of porous material at the inner surface, ducts with a fence are designed to lock porous material in place. Fig. 10 shows the summary of the described ducts with examples of the length H_b , positioned symmetrical to the rotor planes. The included streamtube is taken from the open rotor configuration and is used for design purposes only.

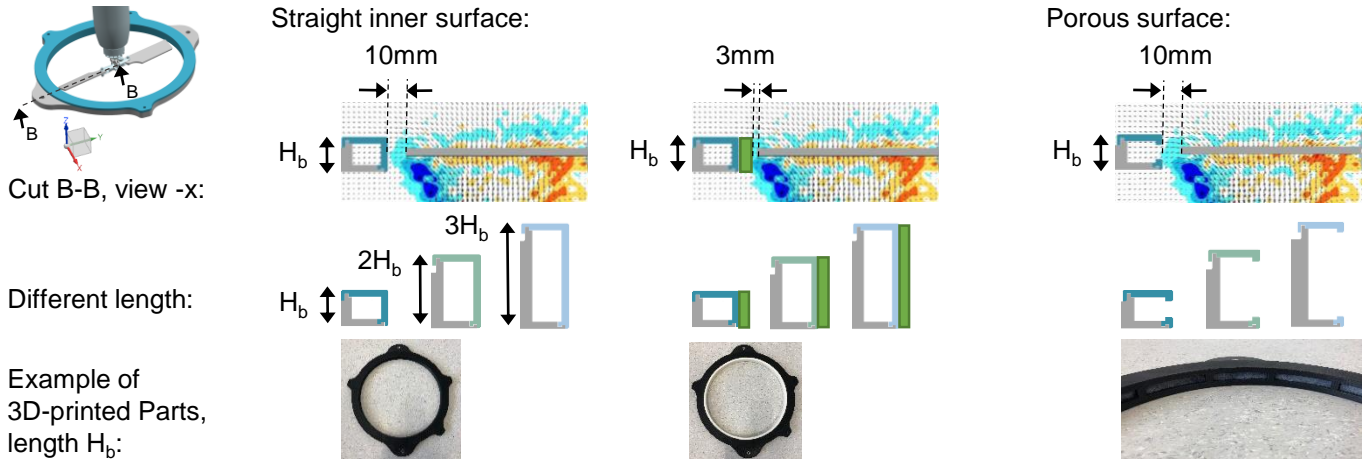


Figure 10: Duct with straight inner surface (tip clearance 10 mm and 3 mm) and ducts with porous surface (tip clearance 10 mm). Examples shown for the length H_b . Colorbar PIV-result see Fig. 8.

5.3. Rounded Inlet

To analyze if a rounded inlet improves acoustics and efficiency in comparison to a straight design, a duct with the length H_b is designed. The streamtube of the open rotor configuration is considered. Fig. 11 shows this duct positioned symmetrical to the rotor plane, straight surface (left) and rounded inlet (right). The included streamtube is taken from the open rotor configuration and is used for design purposes only.

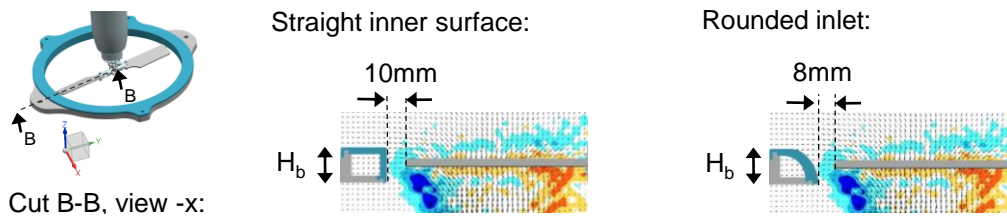


Figure 11: Rounded inlet based on PIV measurement (right), straight inner surface (left), with length H_b positioned symmetrical to rotor plane. Colorbar PIV-result see Fig. 8.

5.4. Ducts inspired by Rotor Streamtube

Variants of the inner surface, which consider the position of the rotor streamtube and especially the vorticity, are designed with the lengths H_b and $2H_b$. Fig. 12 shows these ducts including vorticity measurements of the open rotor configuration. The ducts are positioned below the rotor-plane to enable the inflow of air. Reason is, that the PIV-measurements show the inflow of air in the rotor-plane of the open rotor configuration. It is assumed, that blocking this inflow could lead

to worse acoustics or efficiency. The aim is to evaluate, if such a guidance of the rotor streamtube can optimize acoustics while having no or a positive effect on efficiency.

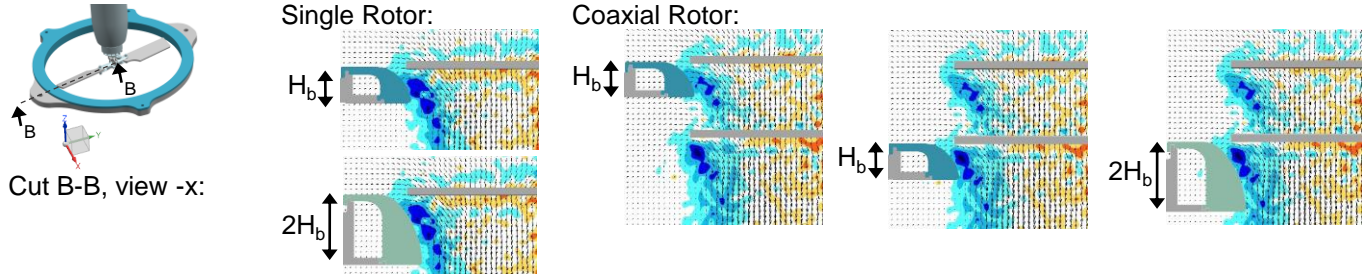


Figure 12: Ducts inspired by the rotor streamtube of the open rotor configuration. PIV measurements of vorticity done at 5 N (single rotor) and 10 N (coaxial rotor). Colorbar PIV-result see Fig. 8.

6. Experimental Results and Discussion

In the following the used methodology of the experimental investigation is described. Afterwards, results for single and coaxial rotor configurations are explained. The influence of ducts regarding the weight are discussed. Finally, sign rules optimizing acoustics and efficiency of ducts are summarized.

6.1. Methodology

All results presented in the following are shown as a comparison to the basic open rotor configuration, which is presented in chapter 4. Changes of efficiency due to duct influence are presented in Δ FOM [%]. Changes of Sound Pressure Level due to duct influence are shown as Δ SPL [dBA]. SPL is presented in this paper using a lowpass at 1900 Hz. It is used to focus on the rotor acoustics itself and leave out high-frequency noise, which is caused by the motor.

The designed ducts are measured regarding efficiency, acoustics and PIV at different positions. Due to that, the influence of length and position as well as the influence of overhang of duct material in both directions of the rotor plane can be analyzed. Positions of the rotor at the end of the duct, the rotor at the center of the duct and the rotor at the beginning of the duct are regarded. Fig. 13 shows these positions for the single rotor configuration and for the coaxial configuration. Ducting both rotors at coaxial configurations is done at position C_c for ducts of the lengths $2H_b$ and $3H_b$. Moreover, Fig. 13 shows the distinction of cases at position C_c , C_{c+} and C_{c-} depending on duct length. Reason is that ducting both rotors is only reasonable with ducts of the length of minimum $2H_b$.

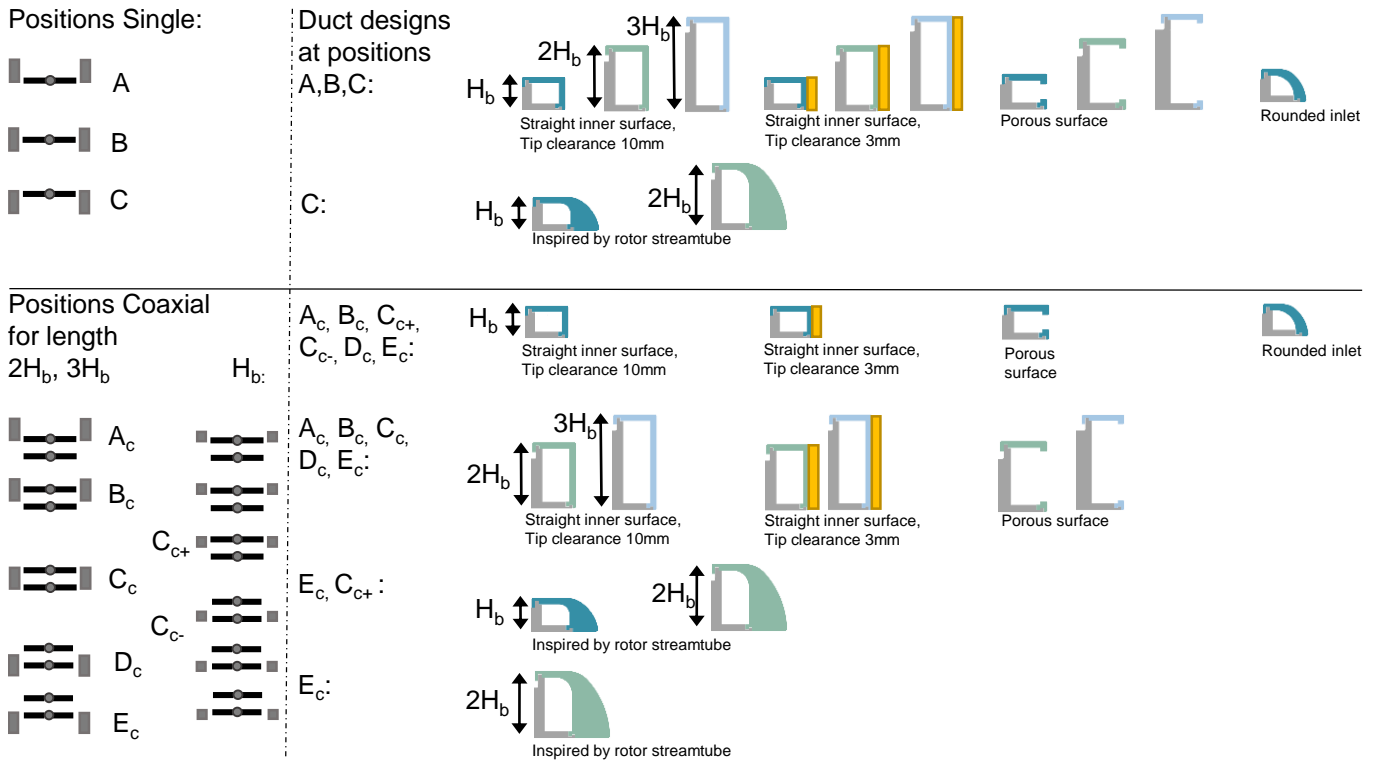


Figure 13: Positions of ducts and different inner designs analyzed at single rotors and coaxial rotors in this paper.

6.2. Single Rotors

In the following, results of the experimental investigation of ducted single rotors are presented. Since comparable behaviour is found over the whole analyzed thrust range, results are presented for the earlier defined operating point of 5 N only. Moreover similar behaviour is found regarding changes in SPL from microphone 1 to 3. Therefore, only microphone 3, which shows highest SPL, is presented in the following.

Fig. 14 shows the influence of the analyzed ducts at a single rotor regarding SPL and efficiency at 5 N. The influence is presented with the difference of the ducted cases compared to the open rotor configuration. For efficiency changes, the deviation of FOM in [%] and for acoustic changes, the difference in SPL in [dBA] is shown. Green areas in Fig. 14 represent positive changes (better FOM, smaller SPL). The duct position is presented on the y-axis. The legend illustrates the following characteristics: Colors represent the different duct designs, focussing on the inner surface, like "rounded inlet" or "straight". The markers (O, X, *) represent the three duct lengths H_b , $2H_b$ and $3H_b$. The abbreviation "tc" is used to present different tip clearances, like "10 mm".

Results presented in Fig. 14 display, that efficiency and acoustics can be improved using ducts at single rotors while hovering compared to an open rotor configuration. The parameters of the designed ducts (details see chapter 5) "inner surface", "duct length", "acoustics treatment", "rounded inlet" and "considering rotor streamtube" are discussed in the following.

Ducts with straight inner surface, tip clearance 10 mm and porous measures (red, yellow) show positive influence on efficiency and acoustics for the length H_b . Negative influence results, when increasing the duct length, especially at position B. It can be observed that ducts with straight surface and acoustic measure (yellow), show better results for efficiency and SPL than without acoustic measure (red). Reducing the tip distance at straight inner surfaces from 10 mm (red) to

3 mm (violet), shows improved efficiency, while the SPL is worse. Again, increasing duct length can not be recommended.

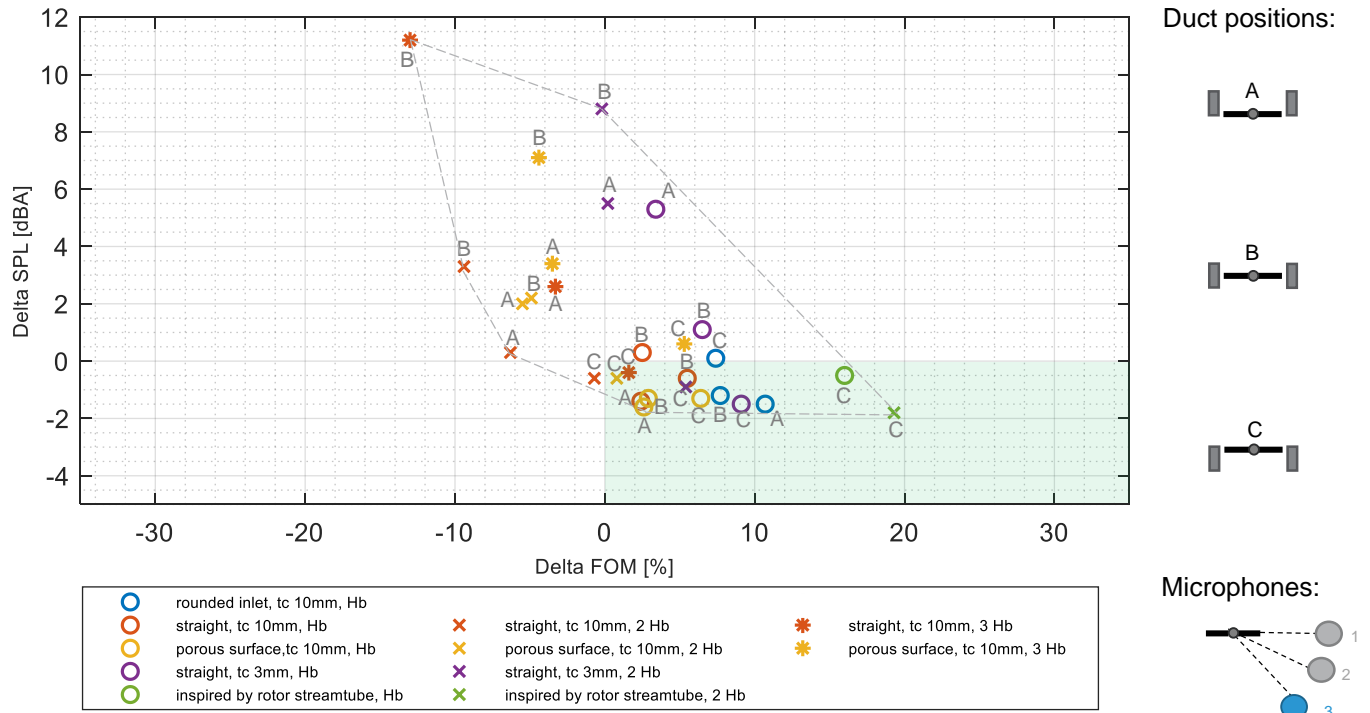


Figure 14: Results for changes of FOM (left) and SPL (right) due to ducts on single rotors at a thrust of 5 N compared to the open rotor configuration.

Comparing straight (○) with round (○) inner surfaces at the length H_b , indicates, that a rounded inlet improves efficiency. This is expected due to previous experimental investigations like [11]. Moreover a rounded inlet improves SPL at position B compared to a straight inner surface at length H_b .

Ducts, whose inner surface is inspired by rotor streamtube and therefore leads the current without disturbing it (X, O), result in improved efficiency and SPL. Increased duct length shows positive impact in this case.

In general, it is observed, that most ducts provide positive effects on efficiency and acoustics at position C . Ducts with short lengths tend to be more flexible regarding position.

In the following, the worst and best results are discussed in detail. Decrease in efficiency and increase in SPL results for a duct with straight inner surface, length $3H_b$ at position B . Details regarding acoustics as well as velocity and vorticity are presented in Fig. 15. Position and value of velocity and vorticity do change significantly compared to the open rotor configuration. The flow gets wider and values decrease. The airflow expands after passing the duct exit, which indicates, that the air flow is underexpanded. This could explain reduced efficiency and increase in SPL. The frequency spectrum shows increase in SPL especially over 200 Hz, as well as blurred higher harmonics of the propeller blade passage frequency.

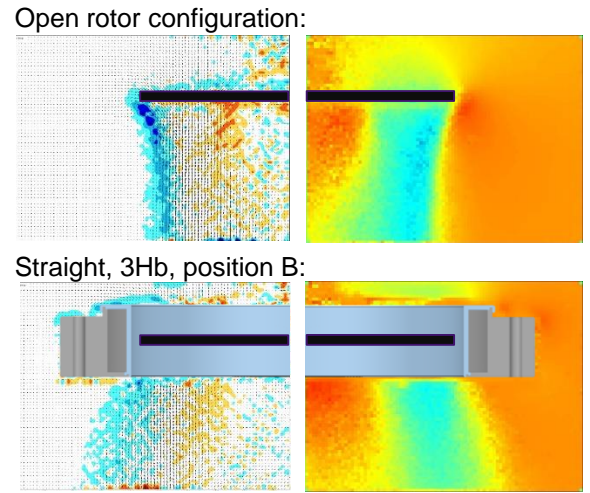
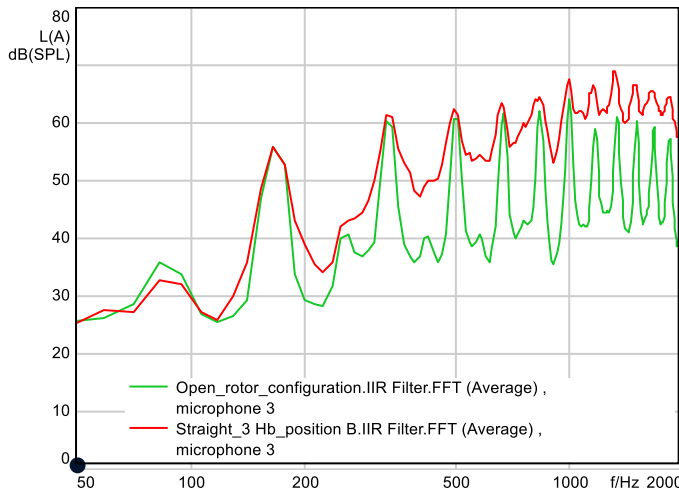


Figure 15: Frequency spectrum and vorticity/velocity results for a straight duct, length of $3H_b$, position B , compared to the open rotor configuration at microphone 3. Colorbar PIV-result see Fig. 8.

Best efficiency was found for a duct with inner surface inspired by rotor streamtube, length $2H_b$ at position C (see X in Fig. 14). Position and value of high velocity and vorticity do not change significantly, see Fig. 16. This indicates that the exit pressure equals ambient pressure, which characterizes a properly expanded air flow, which produces maximum efficiency. SPL at microphone 3 is nearly 2 dBA less compared to the open rotor configuration. The frequency spectrum shows reduction in SPL at higher harmonics of the propeller blade passage frequency.

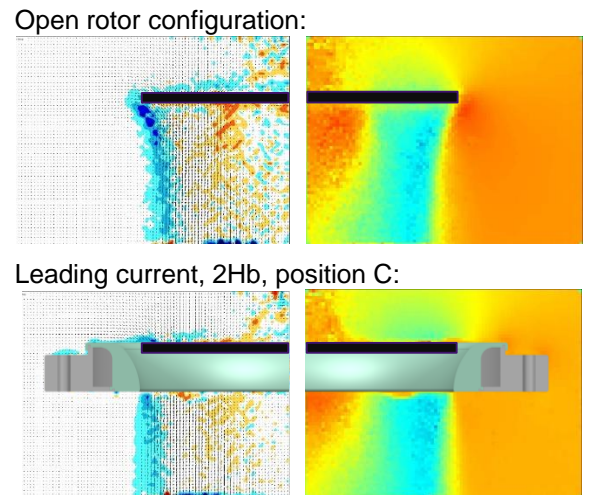
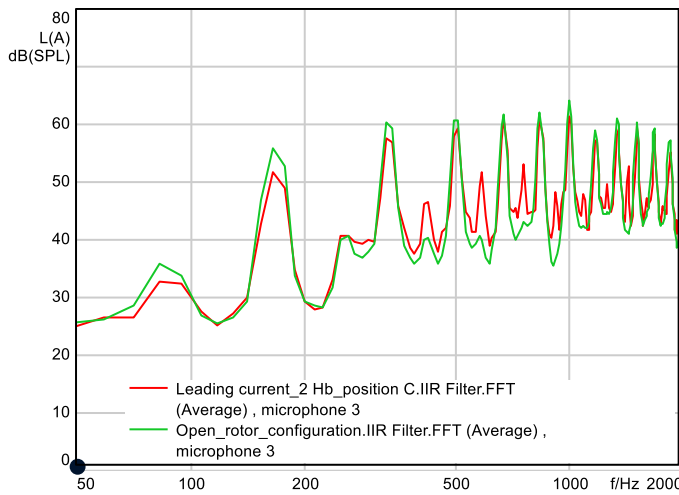


Figure 16: Frequency spectrum and vorticity/velocity results for a duct which leads the current, length of $2H_b$, position C , compared to the open rotor configuration at microphone 3. Colorbar PIV-result see Fig. 8.

6.3. Coaxial Rotors

In the following, results of the experimental investigation of ducted coaxial rotors are presented. The legend and diagrams are designed as explained for single rotors in chapter 6.2. Fig. 17 shows the influence of the analyzed ducts at coaxial rotors regarding FOM and SPL at 10 N.

Results presented in Fig. 17 show, that efficiency and acoustics can be improved using ducts at coaxial rotors while hovering compared to an open rotor configuration. The parameters of the designed ducts (details see chapter 5) "inner surface", "duct length", "acoustics treatment",

"rounded inlet" and "considering rotor streamtube" are discussed in the following.

Ducts with straight inner surface, tip distance 10 mm and porous measures (red, yellow) show positive influence an efficiency for the length H_b at the bottom rotor (position C_{c-} , D_c , E_c). However, an increase in SPL results. Negative influence results, when increasing duct length, especially when positioning the duct at the top rotor. Exception is a better efficiency performance of ducts with length $2H_b$ at position E_c compared to length H_b . Ducts with straight surface and acoustic measure (yellow), show slightly better results for efficiency and SPL than without acoustic measure (red). Reducing the tip distance at straight inner surfaces from 10 mm (red) to 3 mm (violet), shows improved efficiency. However, SPL is worse with exception of position E_c . Again, increasing duct length can not be recommended.

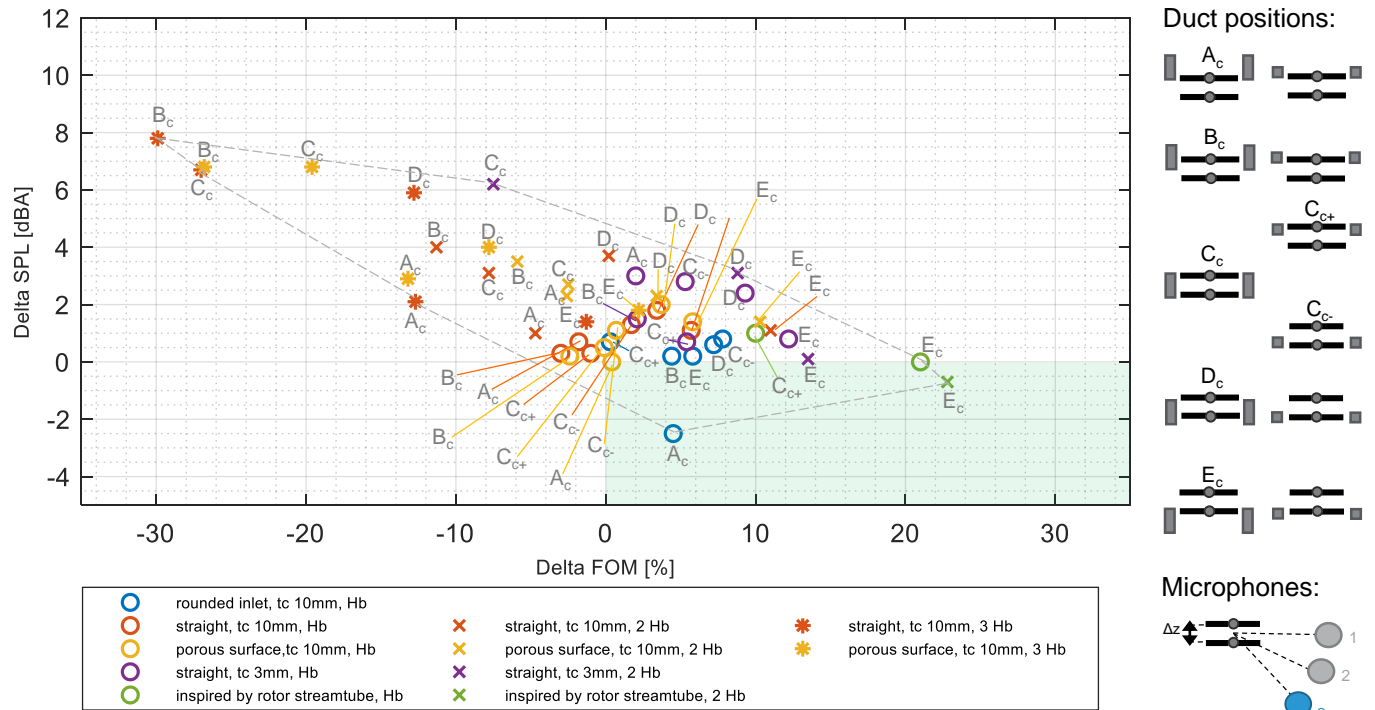


Figure 17: Results for changes of FOM (left) and SPL (right) due to ducts on coaxial rotors at a thrust of 10 N compared to the open rotor configuration.

As observed at single rotors, ducts with rounded inlet (\circ) with length H_b show better efficiency than straight (\circ) inner surfaces. However, a duct with rounded inlet at coaxial rotors worsened SPL with exception of position A_c , where a reduction of SPL results.

As observed at single rotors, ducts, whose inner surface is inspired by rotor streamtube (\times , \circ), result in improved efficiency. However improvement in SPL was only found for length $2H_b$. Increased duct length shows positive impact in this case.

In general, it is observed, that most ducts provide positive effects on efficiency at position E_c . Ducts with short length tend to be more flexible regarding position.

In the following, the worst and best results are discussed in detail. Decrease in efficiency and increase in SPL results for a duct with straight inner surface, length $3H_b$ at position C_c (see \dots in Fig. 17, both rotors ducted). Details regarding acoustics as well as velocity and vorticity are presented in Fig. 18. As earlier described for the single rotor configuration, results show again an air flow, that expands after passing the duct exit. This could explain reduced efficiency

and increase in SPL. The frequency spectrum shows increase in SPL, as well as blurred higher harmonics of the propeller blade passage frequency.

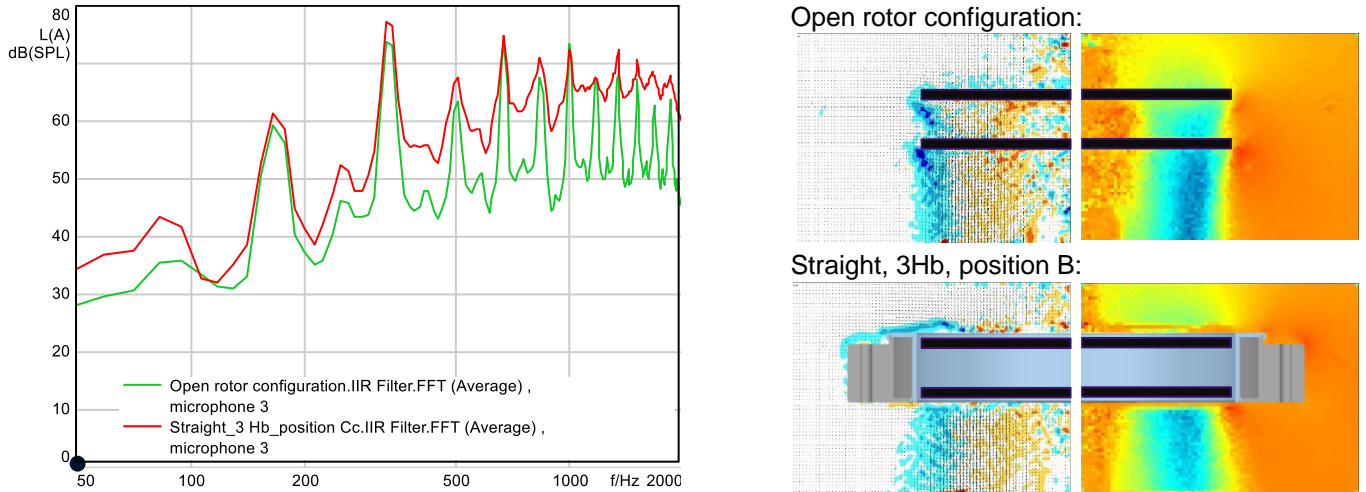


Figure 18: Frequency spectrum and vorticity/velocity results for a straight duct, length of $3H_b$, position C_c , compared to the open rotor configuration at microphone 3. Colorbar PIV-result see Fig. 8.

Best efficiency combined with improvement of SPL was found for a duct with inner surface inspired by rotor streamtube, length $2H_b$ at position E_c (see X in Fig. 17). As earlier described for the single rotor configuration, results show a properly expanded air flow, see Fig. 19. SPL at microphone 3 is slightly decreased. The frequency spectrum does not show significant deviation as compared to the open rotor configuration.

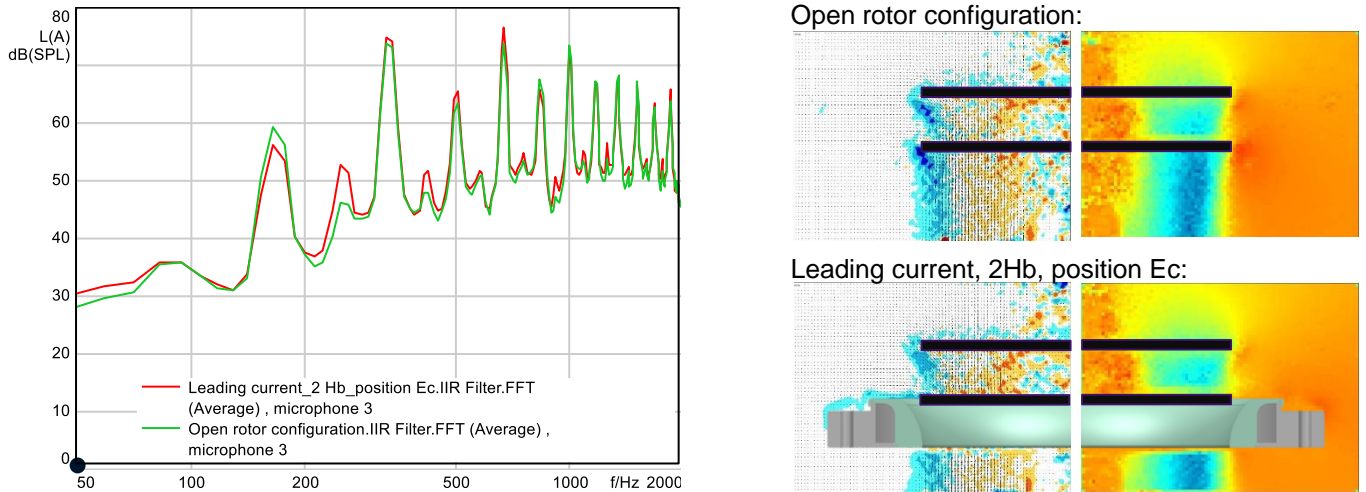


Figure 19: Frequency spectrum and vorticity/velocity results for duct leading the current, length of $2H_b$, position E_c , compared to the open rotor configuration at microphone 3. Colorbar PIV-result see Fig. 8.

6.4. Evaluation of experimental results

The positive influence of certain ducts on efficiency and SPL has been presented in chapter 6.2 and 6.3. If a duct is applied for safety reasons only, the additional weight might already be considered. If however a duct is applied for acoustic reasons only, additional thrust due to better efficiency is required to compensate the duct weight.

Exemplarily the maximum duct weight for a coaxial rotor configuration is calculated in the following. Fig. 20 shows the additional thrust generated due to a duct, length $2H_b$, leading current, position E_c at a coaxial rotor configuration.

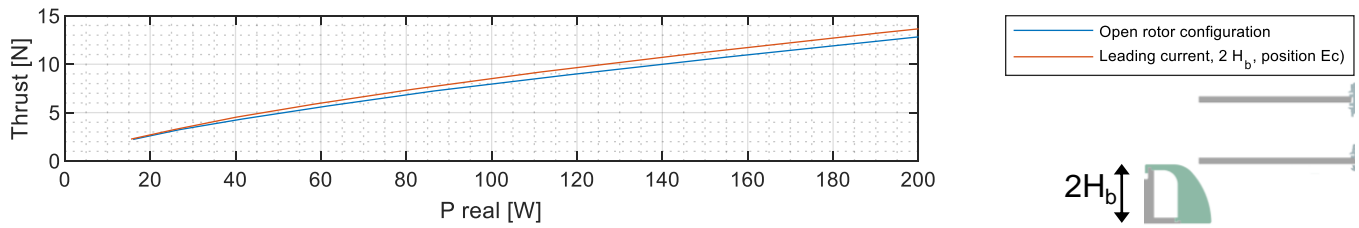


Figure 20: Thrust generated by a open coaxial rotor configuration compared to a configuration with duct, length $2H_b$, leading current, position E_c .

To get a thrust of 10 N, 140 W are needed for the open rotor configuration, see Fig. 20. Applying this power to the ducted version would lead to circa 11 N of thrust. Considering the thrust as product of mass and gravitational acceleration, a duct weight of maximum 100 g results. The duct was not designed for thrust generation itself. Focussing thrust generation could improve the possible maximum duct weight.

6.5. Proposed Design Rules

Duct design rules are derived from experimental results. The experimental investigation shows that applying ducts at an aerial vehicles, even for safety reasons only, should be done carefully. Improvement of efficiency and acoustics is possible, however deterioration is also possible. Design features showed similar behaviour at single and coaxial rotor configurations.

Best efficiency combined with improvement of SPL was found for a duct with inner surface inspired by rotor streamtube, length $2H_b$ at position C (single rotors) and position E_c (coaxial rotors). Rotor streamtube should be considered during design.

If the inner surface of duct is not inspired by rotor streamtube, ducts of the length H_b can be recommended. In this case, reduced tip distances enable highest efficiency with, however, an increased SPL. Highest SPL reduction can be achieved with rounded inlet. Longer ducts, which would also be heavier and need more packaging space are not necessary and showed worse influence for many cases. When using longer ducts or integrating coaxial rotors into a fuselage, the design of a properly expanded airflow should be focused to avoid deterioration regarding acoustics and efficiency.

Porous surfaces and rounded inlet indicated positive influence on SPL at single rotors. Further potential for acoustic improvement at same efficiency due to acoustic measures like porous surfaces is assumed. More detailed analysis focussing different materials would be needed to give detailed advice.

The position of a duct has huge influence on efficiency and acoustics, especially when increasing duct length. Considering all results for single and coaxial rotors presented in Fig. 14 and Fig. 17 it can be recommended to position a rotor at the beginning of a duct (position C at single rotors and E_c at coaxial rotors).

7. Conclusion

This paper presented the influence of ducts on single and coaxial rotor systems, with a blade radius of 106 mm, on efficiency and acoustics while hovering. Experimental investigations were done in a hover-test-bench, using efficiency measurement and acoustic measurement with three microphones. Particle Image Velocimetry was used to visualize the rotor streamtube, velocity and vorticity of the airflow. Ducts were designed based on rotor streamtubes of the open rotor systems. Different inner features, like geometry (rounded inlet, straight surface), porous surface and leading of the rotor streamtube were applied. Ducts length of 15 %, 30 % and 45 % rotor diameter were selected. In addition different positions at the rotor were analyzed to evaluate the optimal overhang of duct material in both directions of the rotor plane. Rotors were positioned at the beginning of a duct, at the center of a duct and at the end of a duct. For coaxial rotors, these positions were investigated at the bottom rotor and at the top rotor. In addition both rotors were ducted, too.

Results show, that ducts can improve acoustics and efficiency. However deterioration of acoustics and efficiencies also possible. Applying ducts at an aerial vehicles, even for safety reasons only, should be done carefully. The main findings are:

- Design features showed similar behaviour at single and coaxial rotor configurations.
- Best increase in efficiency (circa +19 % for single rotors, circa +23 % for coaxial rotors) combined with improvement of SPL (circa -2 dBA for single rotors, circa -1 dBA for coaxial rotors) was found for a duct with inner surface inspired by rotor streamtube and the length $2H_b$ (equate to 30 % of the rotor diameter).
- Ducts improving acoustics and efficiency indicated no significant change of the rotor streamtube. The frequency spectra display reduction in SPL at higher harmonics of the blade passage frequency. Ducts which deteriorated acoustics and efficiency, indicated expansion of air flow and decrease of velocity and vorticity. The frequency spectra display increased SPL as well as blurred higher harmonics of the blade passage frequency.
- If the inner surface of the duct is not inspired by rotor streamtube, ducts of the length H_b (equal to 15 % of the rotor diameter) can be recommended.
- Reduced tip distances enable better efficiency with, however, an increased SPL.
- Porous surfaces and rounded inlet showed positive influence on SPL at single rotors.
- The position of a duct has huge influence on efficiency and acoustics, especially when increasing duct length. Results suggest to position a rotor at the beginning of a duct. For coaxial rotors a duct at the lower rotor shows performs better in most cases. Ducts with short length tend to be more flexible regarding position.
- Ducting both rotors with a duct with straight inner surface cannot be recommended according to experimental results.

In future work, combinations of the analyzed features as well as additional acoustic measures will be evaluated with ducts.

Acknowledgement

We would like to thank Joachim Bartel for his strong support with duct development and 3D printing as well as Henry Schmidt for his assistance during extensive measurements at the hover-testbench.

References

- [1] Y. Karaca, M. Cicek, O. Tatli, A. Sahin, S. Pasli, M. F. Beser, and S. Turedi, "The potential use of unmanned aircraft systems (drones) in mountain search and rescue operations," *The American Journal of Emergency Medicine*, vol. 36, no. 4, pp. 583–588, Apr. 2018.

- [2] A. Otto, N. Agatz, J. Campbell, B. Golden, and E. Pesch, "Optimization approaches for civil applications of unmanned aerial vehicles (UAVs) or aerial drones: A survey," *Networks*, vol. 72, no. 4, pp. 411–458, Dec. 2018.
- [3] A. Goodchild and J. Toy, "Delivery by drone: An evaluation of unmanned aerial vehicle technology in reducing CO₂ emissions in the delivery service industry," *Transportation Research Part D: Transport and Environment*, vol. 61, pp. 58–67, Jun. 2018.
- [4] W. Johnson, C. Silva, and E. Solis, "Concept Vehicles for VTOL Air Taxi Operations," in *AHS Technical Conference on Aeromechanics Design for Transformative Vertical Flight*, San Francisco, CA, Jan. 2018.
- [5] J. E. Scott and C. H. Scott, "Drone Delivery Models for Healthcare," in *Proceedings of the 50th Hawaii International Conference on System Sciences*, 2017.
- [6] J. C. Rosser, V. Vignesh, B. A. Terwilliger, and B. C. Parker, "Surgical and Medical Applications of Drones: A Comprehensive Review," *JSLS : Journal of the Society of Laparoendoscopic Surgeons*, vol. 22, no. 3, p. e2018.00018, 2018.
- [7] S. A. Rizzi, D. L. Palumbo, J. Rathsam, and Christian, "Annoyance to Noise Produced by a Distributed Electric Propulsion High-Lift System," in *AIAA Aviation*, 2017.
- [8] P. M. Sforza, "Propellers," in *Theory of Aerospace Propulsion*. Elsevier, 2012, ISBN 978-1-85617-912-6, pp. 409–437.
- [9] D. Shukla and N. Komerath, "Rotorduct aerodynamic and acoustic interactions at low Reynolds number," *Experiments in Fluids*, vol. 60, no. 1, Jan. 2019.
- [10] I. Penkov and D. Aleksandrov, "Propeller shrouding influence on lift force of mini unmanned quadcopter," *International Journal of Automotive and Mechanical Engineering*, vol. 14, no. 3, pp. 4486–4495, Sep. 2017.
- [11] J. L. Pereira, "Hover and Wind-Tunnel Testing of Shrouded Rotors for Improved Micro Air Vehicle Design," Doctor of Philosophy, Faculty of the Graduate School of the University of Maryland, Aug. 2008.
- [12] H. Han, C. Xiang, B. Xu, and Y. Yong, "Experimental and Computational Analysis of Microscale Shrouded Coaxial Rotor in Hover," in *2017 International Conference on Unmanned Aircraft Systems (ICUAS'17)*, Miami Marriott Biscayne Bay, Miami, FL 33132, 2017.
- [13] T. L. Lee, "Design and Performance of a ducted coaxial rotor in hover and forward flight," Master-Thesis, Faculty of the Graduate School of the University of Maryland, Department of Aerospace Engineering, 2010.
- [14] M. Alavi, M. H. Meinke, W. Schroeder, and M. Seyed, "Analysis of the Acoustic Field of a Ducted Axial Fan," in *23rd AIAA/CEAS Aeroacoustics Conference*. Denver, Colorado: American Institute of Aeronautics and Astronautics, Jun. 2017.
- [15] M. Kraenzler, S. Dufhaus, and E. Stumpf, "Studies on the influence of rotor distance on the efficiency of a coaxial rotor system," in *44th European Rotorcraft Forum*, Delft, The Netherlands, Sep. 2018.
- [16] J. G. Leishman and M. Syal, "Figure of merit definition for coaxial rotors," *Journal of the American Helicopter Society*, vol. 53, no. 3, pp. 290–300, 2008.
- [17] D. A. Wachspress and T. R. Quackenbush, "Impact of Rotor Design on Coaxial Rotor Performance, Wake Geometry and Noise," in *American Helicopter Society 62nd Annual Forum*, Phoenix, AZ, May 2006.
- [18] C. P. Coleman, "A Survey of Theoretical and Experimental Coaxial Rotor Aerodynamic Research," Tech. Rep. NASA-TP-3675, NAS 1.60:3675, A-975555, Jan. 1997.
- [19] M. Ramasamy, "Measurements Comparing Hover Performance of Single, Coaxial, Tandem, and Tilt-Rotor Configurations," in *69th American Helicopter Society International annual forum 2013*, Phoenix, AZ, USA, May 2013.
- [20] G. J. J. Ruijgrok, *Elements of aviation acoustics*. Delft: Univ. Press, 1993, ISBN 978-90-6275-899-9.



QUIET DRONES
International e-Symposium
on
UAV/UAS Noise
Remote from Paris – 19th to 21st October 2020

Introducing anti-drone solutions

Lucas Le Bell, CERBAIR's CEO, lucas.lebell@cerbair.com

1. INTRODUCTION	2
2. DETECTION TECHNOLOGIES	2
2.1 COST-EFFECTIVENESS, ACCESSIBILITY AND EASE OF USE: A THREE FACTORS APPROACH TO A MARKETABLE SOLUTION	2
2.2 THE NEED FOR A MULTI-TECHNOLOGY SYSTEM	2
2.3 PRIMARY MEANS OF DETECTION	3
2.3.1 RADIOFREQUENCY SPECTRUM ANALYSIS	3
2.3.2 RADAR-BASED DETECTION	4
2.4 SECONDARY MODES OF DETECTION	4
2.4.1 OPTRONIC SENSORS	4
2.4.2 ACOUSTIC SENSORS	5
3. NEUTRALIZATION TECHNOLOGIES	5
3.1 KINETIC NEUTRALIZATION METHODS	6
3.2 ELECTRONIC WEAPONS	6
3.3 DIRECTED ENERGY WEAPONS	7

1. Introduction

In 2018 the Gatwick Christmas drones incidents, during which drones flyovers blocked just shy of 1000 flights and 140.000 passengers, proved the necessity of reliable antidrone solutions accessible to sensitive civilian infrastructure, with an emphasis on cost-effectiveness, accessibility and ease of use. UAV are not purely acoustic nuisances but can represent real threats to national security: attacks, collisions, espionage, and smuggling operations.

We hereby analyse the drawbacks and benefits of counter-drone systems. To this end, the notion of “C-UAV kill-chain” will be introduced, as well as the primary means of detection and neutralization.

2. Detection Technologies

2.1 Cost-effectiveness, accessibility and ease of use: a three factors approach to a marketable solution

For an anti-UAV detection method to be marketable, a few key factors should be met. With the rise of threats directed towards the public, sensitive civilian infrastructures are at the center of security concerns. Stadiums, airports, or outdoor events need to be protected. However, contrary to military sites, these locations are often secured by private entities. Thus, **cost effectiveness**, **accessibility** and **ease of use** should be decisive factors in the development of such a solution.

Cost effectiveness could, in this instance, be defined as the ratio between costs (initial and operational) and effectiveness (range, coverage and availability). As private entities rarely enjoy unlimited budgets, this factor should be the main driver in development-related decision-making. A security company will not opt for the most effective system, with the longest ranges and the highest level of coverage: such a solution would fall way outside the realm of its budget. Instead, its choice will go to the system offering a relevant range (no more than a few kilometers), with coverage against realistic threats (civilian drones), marketed at a reasonable price. Herein lies the difference between the operational requirements of a private security company, and an army. Secondly, the question of legal **accessibility** should be raised. In most countries, regulatory constraints prohibit non-state actors from possessing and using military hardware. An offer aimed towards private entities should take this legal dimension into consideration.

Lastly, labor and system integration represent a good share of operating costs. As such, an offer need to easily fit into existing security procedures. A solution should not rely on external highly qualified operators, but rather on quickly trainable internal personnel. Finally, the end-user should not be left with the burden of analyzing raw datasets. Instead, the solution should provide the client with an ergonomic display and a facilitated decision-making, so as to fulfill the **ease of use** requirement.

2.2 The need for a multi-technology system

As the following parts will explain it, each mean of detection has its own flaws and benefits. While some excel in rural environments, others lack usability in urban theaters. Each method varies in **coverage**, **accuracy** and **efficiency**, according to the external constraints (weather, obstacles, nature of the target). To maximize the aforementioned factors, combining multiple technologies would make for a reliable, thorough and comprehensive solution. Furthermore, redundancy would ensure a minimal operational availability in case of a malfunction.

For instance, here is how such a system would work:

- An omni-directional radiofrequency sensor would make the initial detection, based on the analysis of the surrounding RF spectrum
- The radar module would then take the lead, giving the user a more accurate location of the target, provided that no physical obstacles lie between the UAV and the solution. In rural environment, an acoustic sensor could complement the radar.
- Finally, an optronic pod using EO/IR (Electro-Optical/Infra-Red Imaging) would record the incident, track the object at long distances, and identify the specific model of the drone using Image Reconnaissance combined with Machine Learning algorithms.

Thus, a multi-technology solution is the only way to ensure the detection of all types of UAV, through all environmental constraints, on a day-round basis.

2.3 Primary means of detection

Not all detection methods are equal. Some excel in rural and quiet environments; others can only be used in featureless landscapes. But since most UAVs can operate regardless of any external factors (buildings, cloud covers, urban noise...), so should a detection system. Thus, the latter should be ranked according to their availability level across all conditions.

2.3.1 Radiofrequency spectrum analysis

The communication between the drone and its radio command (operator by the pilot) is established using pre-set protocols. The ascending and descending signals should be dissociated. The former, going from the pilot to the drone, contains flightpaths orders (turns, altitude...), while the latter, going the other way, contains the updated GPS location, as well as the video feed. As the data is transmitted through radiofrequency, a compromise has to be reached between extended operational ranges (requiring longer wavelengths) and signal “payload” capacity (requiring shorter wavelength). Recreational and professional UAV use pre-set bandwidths to exchange data with their user: communication protocols. According to the manufacturer’s level of transparency, this protocol can be fully disclosed to the public.

An RF-based C-UAV (Counter Unmanned Aerial Vehicle) system would work as follows:

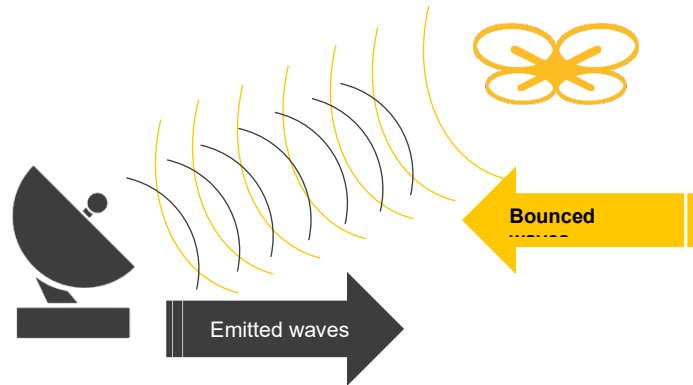
- 1) Communication protocols are pre-recorded by the anti-drone solution manufacturer
- 2) These signatures are then compiled into a dedicated database
- 3) Once deployed on ground, the system, mainly a spectrometer, can analyse the surrounding RF environment. The latter can be composed of Wi-Fi, AM/FM, TV emissions...
- 4) The system compares every signature to the database, looking for similarities
- 5) Once a match is confirmed, a drone has been detected.

Such a system presents a few benefits. First, RF sensors are relatively cheap compared to other detection sensors such as radar. Secondly, the core technology has long been developed, further removing R&D (Research and Development) costs. Furthermore, this solution would work regardless of external conditions, such as buildings, urban noise pollution or weather. As a passive mean of analysis, no disturbing emissions are to be accounted for. Lastly, the presence of two links (descending and ascending) allows for the localisation of both the drone and its pilot, a prowess which only RF analysis can achieve. However, to work properly on all drone models, most UAV RF signature would need to be recorded.

2.3.2 Radar-based detection

A radar is an electronic system which detects entities by emitting waves which, once they reach the target, bounce off of its structure, and reaches back the emission source.

As both the speed of the RF wave (light speed) and the time it took to reach the target are known, the distance of the target can be calculated by a simple, well-known formula ($Speed * Time = Distance$).



This technic, which widespread use can be traced back to the second world war, is commonly used for air detection in civilian and military airspaces. Thus, no insurmountable technological barrier would need to be overcome for its potential UAV detection application.

However, a few drawbacks could worsen this picture. First, radar can't be used in packed urban environments as malicious drones could find shelter behind walls, hiding away from the radar emissions. Secondly, small radars would have a high false alarm rates, as most birds and drones share roughly the same dimensions and speed. Lastly, if deployed in cities, such a system would cause RF disruption due to its active nature.

2.4 Secondary modes of detection

These technologies have been deemed “secondary” due to their high dependency on external factors: favourable weather conditions, absence of noises and obstacles...

2.4.1 Optronic sensors

Optronics is the combination of optic sensors and electronics. It involves the simultaneous use of cameras (“traditional”, infrared, etc...) and image processing algorithms.

Applicated to the UAV context, optronic sensors could procedurally analyse the sky. For the detection to be fully automated, the system would have to be able to recognize drones by itself. To this end, Machine Learning could have a pivotal role in the process. Carried out prior to the deployment by the solution manufacturer, it would require the time-consuming procedure of teaching the algorithm the difference between a drone and other aerial entities (planes, birds, shades...).

An optronics-based system would present the perk of self-perfecting its algorithms through time, as more encounters would tend to refine its capabilities. Furthermore, optronic sensors are among the least expensive detection items. However, this technology would have the same flaws as radar. The longer the range, the higher the difficulty to differentiate a bird and a drone. Buildings would completely limit its visual range, and its capabilities would be extremely sensitive to weather conditions, such as fog, clouds, or even rain.

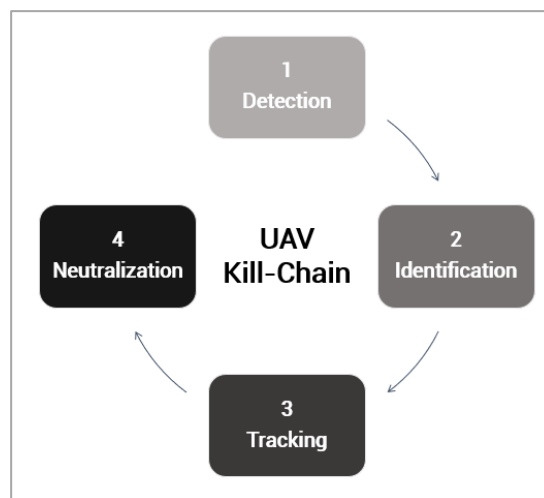
2.4.2 Acoustic sensors

This method relies on a passive process of surrounding acoustic environment analysis. Similarly, with the RF-based detection method, pre-recorded sound signatures can be stored in databases. A detection is confirmed once the sensor detects similarities between these signatures, and the surrounding acoustic environment. Once more, Machine Learning will be used to train the system into discriminating drone noises.

This technology would present the perk of having a low physical footprint, as sensors of this kind are getting increasingly smaller. Furthermore, as modern submarines have proved, passive acoustic monitoring can provide an extremely accurate assessment of its surrounding. However, urban noise pollution could tend to decrease its range. But even as improvements are being noticed, civilian UAV will never completely quiet. Far from obsolete, this technology could prove to be very promising in the coming years.

3. Neutralization technologies

When it comes to deterring aerial threats, detection and identification are only the first two steps. The “kill-chain” can be defined as the sequence of action leading to the UAV neutralization.



This last step can bear many forms: from its impossibility to keep flying, all the way to the complete destruction of the device. For a neutralization system to be effective and usable, a few key factors should be met.

First, a substantial proportion of sensitive sites are not governmental: power plants, airports, gatherings... Thus, a system aimed at protecting these locations should be accessible to civilians. This accessibility would rely on purchase authorizations, as well as regulation in favour of its proper use, should a threat arise. These two conditions alone exclude military hardware from being used by private actors.

Secondly, as most drone incidents tend to occur near and within urban areas, characterized by the presence of unarmed innocent civilians, a neutralization system should be usable in such environments. This solution would require to rely on non-kinetic technologies, and maximize the level of accuracy, so as to minimize, if not cut out, collateral damages.

Finally, in a more practical sense, the integration between the detection and neutralization processes should be seamless. UAV are fast, responsive and reactive. So should the system aimed at countering them.

3.1 Kinetic neutralization methods

Kinetic methods are often considered of last-resort, due to their short-range accuracy and the level of training required to use them.

- Classic ballistic systems (firearms and anti-air batteries) are irrelevant in this civilian context. Unsuitable for urban environments, unable to be used by private entities, inaccurate at medium and long ranges and intensive in human resources. Furthermore, as Patriot Missiles were tested to shoot down quadcopters in 2017, the price asymmetry between the target and its countermeasure becomes overwhelming.
- Birds of prey, especially hawks and eagles, can be trained to take down civilian drones. In 2015, after a few illegal flights took place above the Elysée Palace, the French Army started to train four hawks for C-UAV purposes. Able to detect a drone at more than a mile away, the animal can reach speed of up to 200 km/h, exerting 500 pounds per square inch of pressure on the device. However, as effective as it can get, this system required years of training for the birds and their operators, implying extensive initial costs.
- Using a similar method, counter-drone drones can be used to intercept aerial threats. Once a UAV is detected, a dedicated device will take off and scramble to the targeted area. Such drones already exist and are physically made to this end: their blades are protected by metal rings, their structure is impact-resistant, and their speed and agility allow them to compensate for their relative high weight. However, swarms of drones would require equal amounts of anti-UAV devices, raising the issue of onsite counter-measures physical print.
- Finally, nets are the most marketed physical anti-drone solutions. Shot from the barrel of a dedicated rifle, the synthetic lines composing its structure jam the blades rotating mechanism, immediately stopping the UAV. However, these nets are the very definition of a last resort weapon: extremely limited ranges, inability to counter swarms and relatively low accuracy.

3.2 Electronic weapons

Communication hacking and Electronic Counter Measures (ECM) are the most widely used methods of civilian UAV neutralization. Both present the benefits of being swarm-proof (multiple targets can be treated at any given time), with no ammunition's costs. Finally, as non-kinetic radiofrequency-based solutions, they can be used in urban environments, regardless of crowds, buildings, weather conditions... It should be noted that the use of electronic weapons isn't necessarily aimed at destroying the drone, but rather to prevent it from reaching its destination.

Radiofrequency jamming is perhaps the most known method. Ever since the first "jamming rifles" started to erupt around 2012, its use has been considered the most promising neutralization method by the public. The system has not changed much since its invention: by saturating the surrounding with RF noise, the drone loses contact with its pilot. Unable to communicate, the action will trigger one of three emergency protocols: the device can hover until its batteries get drained out, land immediately, or return to the last known position of its owner. Two types of jamming exist, considering the variable level of sophistication of the solution:

- The C-UAV system can identify the specific band on which the drone and the radio command communicate and choose only to jam this part of the RF spectrum. Accurate and reliable, it requires time-consuming pre-deployment development.
- If no communication protocol detection method has been engineered, the operator can choose to jam broadly, by saturating all bands with RF noise, in the hope that the device will be prevented from communicating with its owner. Considered as a low-cost method, it causes massive RF disruption on all nearby devices, including Wi-Fi hotspots, phones, TV signals... As no distinction is being made between the drone and other communication protocols, digital collateral damages are great.

However, **drone hacking** goes even further. The process usually relies on two steps: jamming and spoofing. A commonly used method is called “GPS spoofing”:

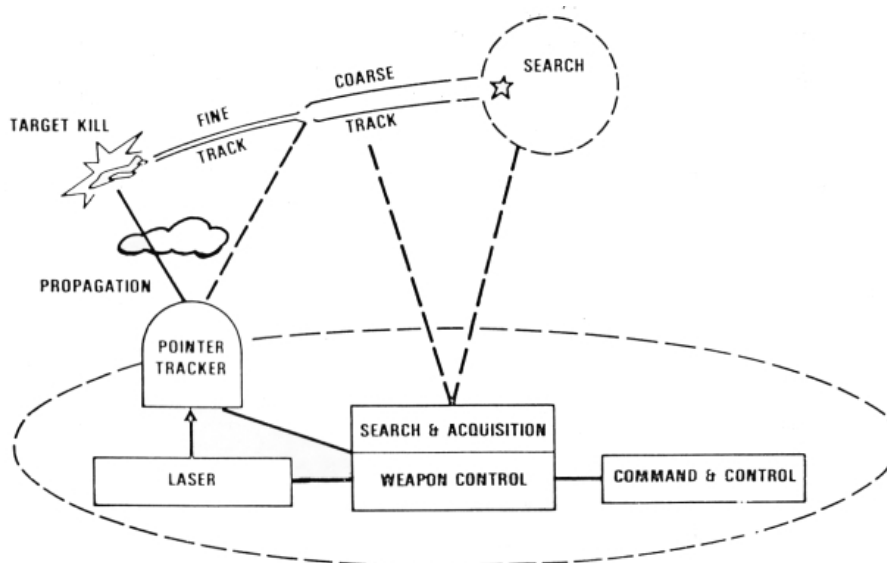
- The link between the UAV and its pilot is jammed, leaving the device unable to communicate with its operator
- The hacking module then sends false GPS data to the UAV, tricking it into thinking it successfully located itself
- With the GPS location spoofed, the hacker can ‘wait’ for the drone to land to, what it thinks, is its proper emergency destination.
- Using this method, the Iranian Revolutionary Guard Corps successfully hijacked an American RQ-170 drone in 2011, making it land on an Iranian airbase instead of its home base in Afghanistan.

However, each drone models possessing a fairly different Operating System than the others, the hacking method cannot be simply extended to every UAV. Instead, every device would have to be individually hacked prior to the operation. Furthermore, once the drone manufacturer identifies the cyber vulnerability, a software patch can be applied.

3.3 Directed Energy Weapons

DEW (Directed Energy Weapons) treat their objective by targeting it with a concentrated beam of energy. By altering their aerodynamics or the microcomputers controlling it, DEW cause the UAV to crash. One of the main benefits is the lack of ammunitions. Access to electricity, the main ‘fuel’ to their operation, is virtually unlimited. For this analysis, two categories can be distinguished.

High-power microwave (HPM) weaponry sends out a short, extremely high voltage burst of electromagnetic energy capable of disrupting computer systems for a fraction of a second. If



sustained long enough, micro-circuits within the UAV computer could burn, disrupting its flying software.

High Energy Laser (HEL) work by aiming towards the objective with an extremely powerful laser. Upon hitting the target, the heat created by the HEL turns the outer layer of the specific impact point into a plasma. The latter will “eat” into the surface, destroying the drone. THOR, manufactured by Raytheon, is an HEL-based C-UAV system.

However, both HPM and HEL systems suffer from numerous flaws. First, they are extremely expensive, with prices beginning at a few millions of dollars apiece. Furthermore, as their operation require a lot of hardware, software and batteries, their physical print can reach the size of a vehicle, with weights up to a thousand kilograms. Lastly, as HEL induce extreme level of heat, trials conducted by the US Army concluded that a resting period was necessary after every few ‘shots’.

4. Conclusion

As drones have the potential to pose increasingly pressing threats to national security, it seemed, until a few year ago, that the issue was not taken seriously. Until industrials, policy makers and research centres gathered and strengthened their respective arsenals.

Efforts seemed to orbit around a “UAV Kill-Chain”. While institutions put the emphasis on the necessity to dissociate malevolent from innocent drones, some manufacturers focused on the three remaining steps. Slowly, engineers started to consider the threat asymmetry they were facing: if drones are cost-effective, easy-to-use and accessible, so should be their countermeasures.

As a vector of progress, it seems logical that forecasts are predicting a ten-fold increase in their use for the coming years. However, the bigger the flock, the greater the wolves. Hence, the necessity to monitor, track down and neutralize malicious drones has never been more potent.



CidB

Centre d'information
sur le Bruit

**QUIET DRONES
International Symposium
on
UAV/UAS Noise
Remote from Paris – 19th to 21st October 2020**

**Two Dimensional Convolutional Neural Network Frameworks
Using Acoustic Nodes for UAV Security Applications**

Theoktisti Marinopoulou, Centre for Research and Technology Hellas (CERTH),
Information Technologies Institute (ITI): tmarinop@iti.gr

Anastasios Vafeiadis, Centre for Research and Technology Hellas (CERTH), Information
Technologies Institute (ITI): anasvaf@iti.gr

Antonios Lalas, Centre for Research and Technology Hellas (CERTH), Information
Technologies Institute (ITI): lalas@iti.gr

Christian Rollwage, Fraunhofer Institute for Digital Media Technology (IDMT):
christian.rollwage@idmt.fraunhofer.de

Danilo Hollosi, Fraunhofer Institute for Digital Media Technology (IDMT):
danilo.hollosi@idmt.fraunhofer.de

Konstantinos Votis, Centre for Research and Technology Hellas (CERTH), Information
Technologies Institute (ITI): kvotis@iti.gr

Dimitrios Tzovaras, Centre for Research and Technology Hellas (CERTH), Information
Technologies Institute (ITI): dimitrios.tzovaras@iti.gr

Abstract

Unmanned Aerial Vehicles (UAVs) have become increasingly popular to the public with a multitude of associated applications in real life. However, malicious applications of UAVs, such as terrorism and air transport disturbance may occur with devastating consequences. Therefore, counter-UAV (C-UAV) systems are required to efficiently address these undesired situations. Artificial intelligence approaches, such as deep neural networks (DNNs), are deemed crucial for high accuracy detection and real-time response of the next generation C-UAV systems. UAV detection based on acoustic sensors has received a great research interest over the past years, however the performance of the proposed solutions may vary in different

environments, since sound signals from UAVs are multi-source and unstructured. In this work, three different 2D Convolutional Neural Networks (CNNs) using short-time Fourier transform spectrograms as input, for UAV binary classification in real-world settings, are compared. The results confirm that 2D CNNs, along with data augmentation techniques in the image domain, can capture the spatio-temporal information of the UAV sound signals, even in noisy environments, and obtain a 95.35% macro average F1-Score in a dataset collected from two different environments.

1. Introduction

Unmanned Aerial Vehicles (UAVs) or Systems (UASs) are becoming a part of citizens' everyday life. UAVs bring a continuous market increase in a growing number of useful applications such as construction [1], agriculture [2], insurance [3] and internet communications [4]. However the rapid spread of UAVs is generating serious security issues. In recent years, newspapers and mass media have reported dozens of incidents involving drones flying over restricted areas and around critical infrastructures or during public events. On December 2018, a UAV was spotted flying close to Gatwick airport ultimately causing the closure of Britain's second largest airport for 36 h and disrupting 1000 flights [5]. Moreover, in September 2013, Chancellor Merkel has been threatened by a Parrot AR Drone which landed at her feet without any reaction from her security service. It turned out that the drone was sent by the Pirate Party, in an attempt to raise her awareness about drones' dangerous potential [6]. As a consequence, it has become important to develop effective and affordable countermeasures to report of a drone flying over critical areas.

Various types of sensors such as thermal [7], electro-optical [8] and radar [9] have been proposed in the literature for the data acquisition in the UAV detection field. However, C-UAV systems consisted of the above sensors may contain some drawbacks. First, although thermal sensors are excellent for night-time surveillance, they face issues with humidity and other adverse environmental settings [10]. Moreover, electro-optical sensors are able to detect the target when it is visible but the occlusions, night-time and low visibility affect their performance [11]. Finally, radar is invariant to environmental settings but may lack in classification capabilities. On the other hand, acoustic sensors overcome these drawbacks using a low cost infrastructure as well. Acoustic sensors are robust to environmental settings and provide adequate classification capabilities which make them a reliable choice [12] [13].

In this paper an audio-based UAV binary classification approach in real-world settings is proposed. The main contributions are summarized as follows:

- A large drone flight dataset was collected under a variety of conditions. Various types of drones were recorded in two different environments under diverse weather conditions and background noises.
- An end-to-end procedure was implemented since the model was trained on features learnt by the DNN in contrast to computationally intensive hand-crafted ones.
- Three different deep learning architectures were compared achieving high classification performances. Their results were evaluated and each one's limitations and applications were analyzed.

2. Related Work

Over the last few years, many researchers have worked on acoustic scene classification, by recognizing single events in monophonic recordings [14]. Different feature extraction techniques [15] and data augmentation [16] have been explored. Jeon et al. [17] showed that the classification performance increased when using data augmentation methods. The ability of DNNs to extract unique features from raw data and the high processing speeds of modern Graphic Processing Units (GPUs) lead these networks to receive a lot of attention in audio classification field. Particularly, CNNs have been applied and compared with other deep

learning architectures [18], resulting in better performance and making them the dominant methodology option.

In the field of audio-based detection of UAVs many different approaches have been proposed. Liu et al. [19] used the Mel Frequency Cepstral Coefficients (MFCCs), commonly used in the field of speech recognition, and a Support Vector Machine (SVM) classifier to detect UAVs. Recently, Kim et al. [20] introduced a real-time drone detection and monitoring system, using one microphone. This system used the k-nearest neighbors and plotted image learning algorithms to learn from properties of the Fast Fourier Transform (FFT) spectra. The authors extended their work [21] and increased the classification accuracy of their proposed system from 83% to 86%, using an artificial neural network. In all circumstances, there was a strong need for the collection of a real world UAV audio dataset and application of methods that overcome the noise sensitivity and the functionality in a confined dataset only.

3. Methodology

In this Section the methodology followed for a binary classification problem based on UAV's audio data is presented. According to Figure 1, after data annotation, the first step relies on audio-pre-processing which consists of trimming, resampling, adding silence as well as data augmentation techniques. Afterwards, a feature extraction procedure is implemented including the audio transformation to short-time Fourier spectrograms. The following phases include the training of three different CNNs as well as their performance evaluation based on precision, recall and F1-score metrics.

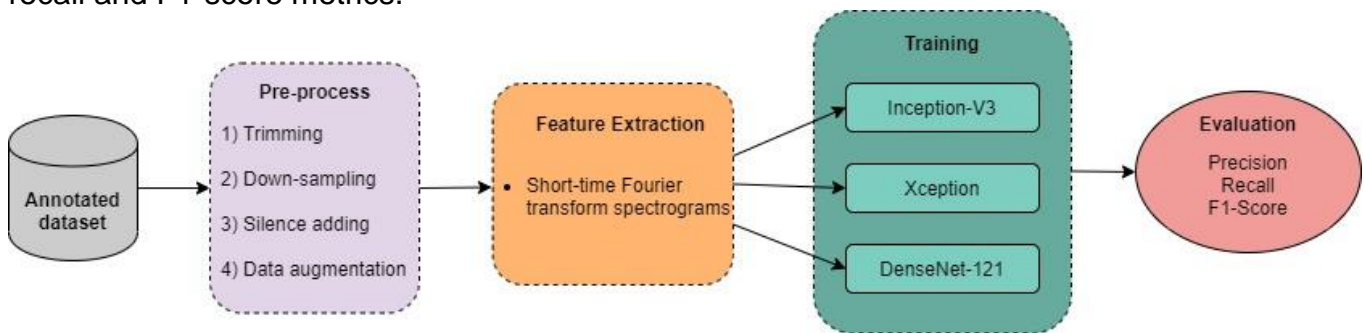


Figure 1: A general view of the applied methodology.

3.1 Audio data description

A critical issue in the UAV detection applications is the limited number of the public available datasets, both in number and size [22]. In this work, a large dataset was collected from two different environments under a variety of real-world conditions. During this investigation, various capturing sessions took place at the Markopoulo Training Facility, in Athens among 30/9/2019 – 4/10/2019. Furthermore, an additional dataset was recorded by Fraunhofer Institute for Digital Media Technology (IDMT), in Hude, Germany during the time period from 2017 to 2019. Both datasets were recorded by three eight-channel arrays with a sampling rate of 48 KHz and a 32-bit depth.

The dataset contained drone flights data in large areas. The flights altitudes ranged from 0 meters to 20 meters and the horizontal distances between a drone and the system, ranged from 1 meter to 200 meters. The final dataset contained 149982 seconds of monophonic audio data and was separated into two target classes, drones and false alarms (FA).

The annotation procedure was carried out manually by human annotators. In particular Information Technologies Institute of Centre for Research and Technology Hellas (CERTH), conducted the Markopoulo dataset annotation and Fraunhofer IDMT the one in Hude. The drone target class contained samples from different types of drones such as DJI Mavick, DJI Phantom 4, DJI Matrice 200, AAlign 470L, Sky hero Little Spyer, DJI F450, Parrot Disco (surfaceplane), Unique Taifun H520 – Hexacopter and some unknown drones. The aforementioned drone class included various drone flight scenarios such as drone in short and long distances, drone

with commercial aircraft background sound and drone with vehicles background sound. Accordingly, the false alarm class (not drone-class) included sound samples of animals, moving vehicles, wind noises and commercial aircrafts flights.

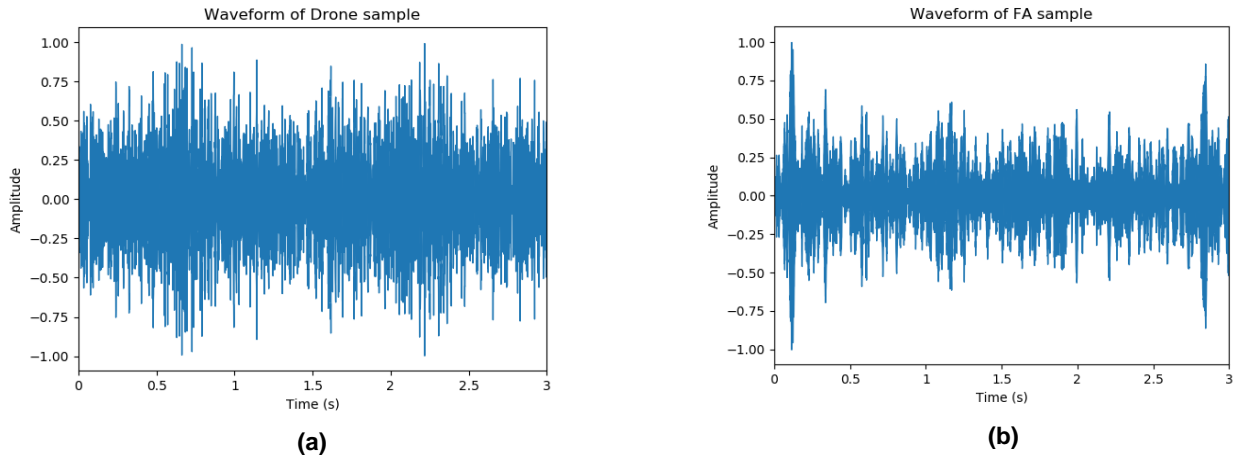


Figure 2: Audio waveform of (a) a drone class sample and (b) a false alarm class sample. The x-axis represents the time and the y-axis represents the amplitude of the sound.

3.2 Pre-process

One necessary step before the audio feature extraction procedure is the audio data pre-processing. Considering that the final system should operate in real-time, it was important to minimize the computational cost as much as possible. Therefore, the input signal was trimmed into smaller chunks of a constant interval. After several tests, three seconds of audio appeared to be sufficient for the network learning. Since some recordings had smaller duration than the appropriate one, an audio sample of silence was added in order to re-structure the collected information into a global form of data.

Furthermore, it was observed that the main energies of the drone frequencies reached up to approximately 8 kHz. Above that frequency, some harmonics had minimal energy in the frequency domain. Therefore, the information can be considered as insignificant for the network training. Hence, the 48 kHz recordings were down-sampled to 16 kHz and the computational cost was minimized.

To further increase the robustness of the network and avoid overfitting as much as possible, data augmentation techniques in the image domain were applied. Specifically, the height and width of the image were shifted randomly by 25% resulting in new, additional training data without changing the semantic meaning of the labels. Therefore, the performance of the CNN was enhanced and its ability of generalization was increased.

3.3 Feature Extraction

The feature extraction is an important step in pattern recognition systems. It transforms originally high-dimensional patterns into lower dimensional vectors by capturing the essence of their characteristics. Various feature extraction techniques have been proposed in the literature for environmental sound analysis. A few of them include Zero crossing rate [23], MFCCs [24], Mel band energy spectrograms [25] and Spectral centroids [26]. This work is focused on spectrogram based image features using the short-time Fourier Transform (STFT). Therefore, the two-dimensional CNN learns the spatio-temporal representation of the target classes.

After the 3-s audio trimming process and the 16 kHz resampling, the audio input signal was transformed in the time-frequency domain using STFT. For STFT, the discrete Fourier transform with a sliding Hanning window was applied to overlapping segments of the signal. Varying the window length, results in a trade-off between frequency and time resolution. By

using a window size of 512 samples and a hop length of 256, an equal significance was attributed on the aforementioned parameters.

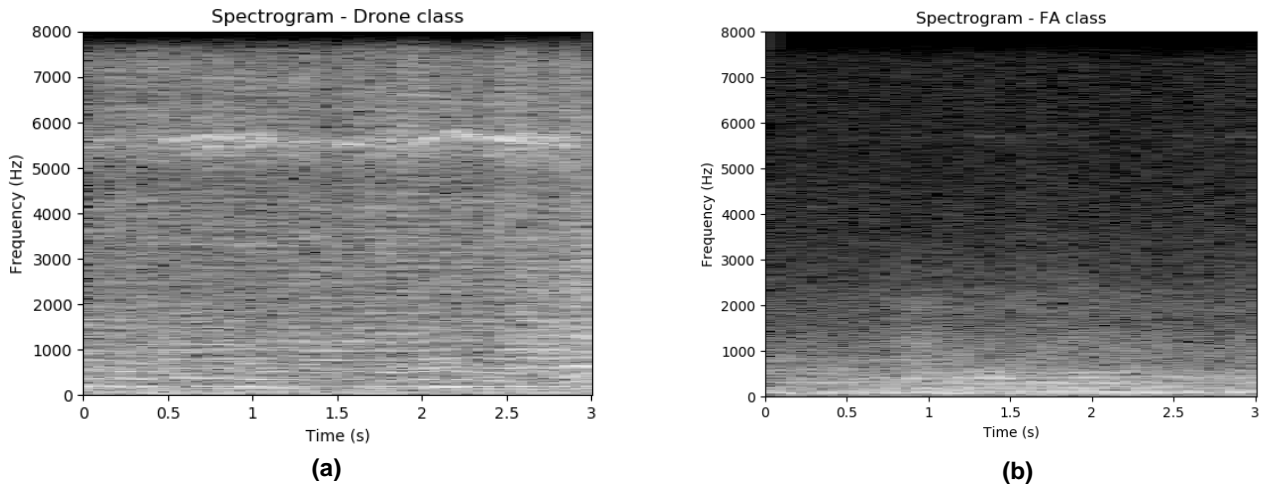


Figure 3: Grayscale spectrogram images of (a) a drone and (b) a false alarm sample. The x-axis represents the time (s) and the y-axis the frequency (Hz). The colour represents the amplitude of a particular frequency with darker colours corresponding to low energies and bright colours corresponding to progressively higher energies.

Afterwards, the values were converted to a logarithmic scale (decibels) then normalized from [0, 255] to [0, 1], generating single-channel greyscale images (Figure 3). The dimensions of the aforementioned images were 257x188 pixels.

3.4 Network architecture

This work focused on the comparison of various two-dimensional CNN architectures under real world conditions. In particular, the Inception-V3 [27], Xception [28], and DenseNet-121[29] were applied in the context of this investigation in order to evaluate the impact of different architecture structures and sizes in UAV detection applications.

The initial annotated dataset consisted of 22,501 drones and 27,493 FA samples (Figure 4a). In the terms of the two-dimensional CNN learning, the aforementioned dataset was divided into training and validation set with a ratio of 70 (15,750 drones – 19,245 FA) and 30 (6,750 drones – 8,247 FA) percent respectively. Furthermore, the networks were tested on an unseen dataset, consisted of 1651 drones and 1309 FA samples (Figure 4b).

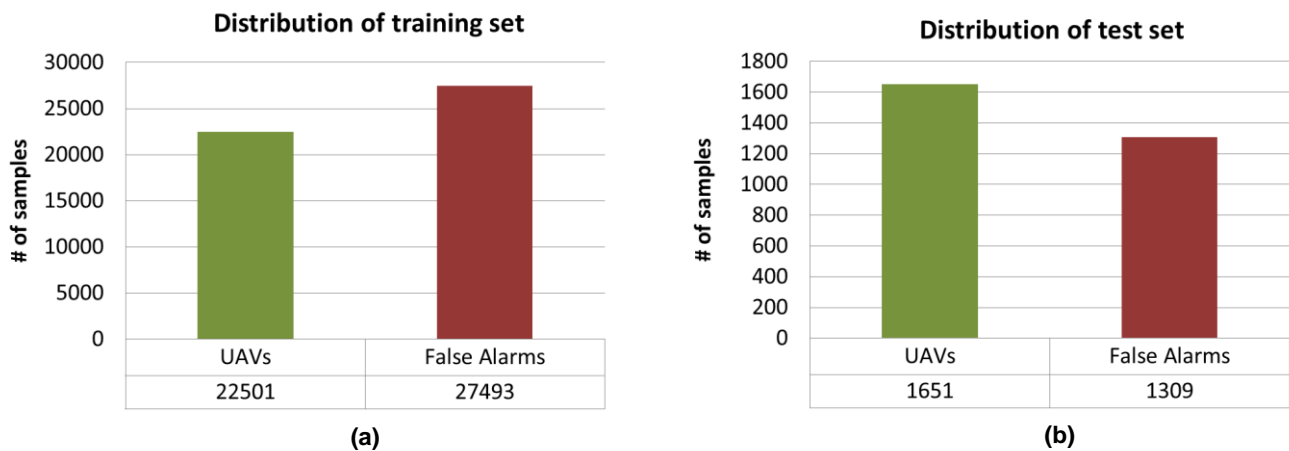


Figure 4: Dataset distribution of (a) training and (b) test set for each class.

After the data pre-processing described in Section 3.2, the original and the augmented images were fed into the networks in batches of eight images per iteration. For this binary classification problem, the Adam [30] optimizer with an initial learning rate of 0.001 and the binary cross

entropy loss function for optimization were used. Moreover, the learning rate was reduced by a factor of 0.1 when there was no improvement after 5 epochs. The initial epoch number for the CNNs was 200 with an early stopping patience of 10 epochs.

4. Experimental results

In order to compare the deep learning architectures performance, the precision, recall and F1-Score for each class were calculated as well as their macro average scores (Table 1). According to Table 1, all experiments produced satisfactory results, since the capability of distinguishing very efficiently between drones and false alarm samples, is revealed. Particularly, Inception-V3, a 42-layer deep learning architecture, adding batch normalisation to the auxiliary layers results to a great classification performance. Nevertheless, the network size is large due to the high parameters count (24 million).

Table 1: Precision, recall and F1-Score metrics of the training set for each experiment.

Architecture		Precision	Recall	F1-Score
Inception-V3	Drones	99.34%	97.59%	98.45%
	False Alarms	98.05%	99.47%	98.75%
	Macro-avg	98.69%	98.53%	98.60%
Xception	Drones	99.37%	98.58%	98.97%
	False Alarms	98.84%	99.49%	99.17%
	Macro-avg	99.11%	99.03%	99.07%
DenseNet-121	Drones	97.81%	97.26%	97.53%
	False Alarms	97.77%	98.22%	97.99%
	Macro-avg	97.79%	97.74%	97.76%

Moreover, the Xception network succeeded the highest average scores, achieving 99.07% F1-Score. Xception is an adaptation from Inception, replacing Inception modules with depth-wise separable convolutions and there are residual connections originally proposed in ResNet [30], placed for all flows. The number of its parameters is quite high too (23 million). Based on the concept of dense connections and features reuse, DenseNet-121 allows better gradient flow using much fewer parameters (8 million). However, its F1-Score exhibited a decrease of 1.31% in contrast to Xception model.

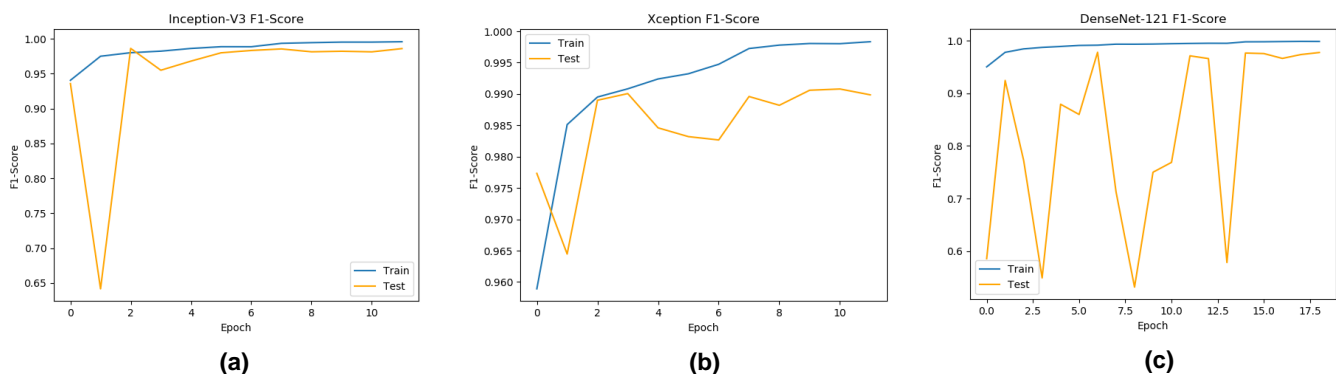


Figure 5: F1-Score plots of (a) Inception-V3, (b) Xception and (c) DenseNet-121 classification model. The x-axis represents the epochs and the y-axis the F1-Score value.

The F1-Score plots for each epoch of the above-mentioned experiments are depicted in Figure 5. According to these plots, Inception-V3 and Xception converged in 12 epochs and DenseNet-121 in 18. The curve's fluctuations occur due to the data shuffling during training.

In order to further evaluate the classification performance of the two-dimensional CNNs, they were tested on an unseen during training dataset as described in Section 3.4. The relevant metrics resulting from this procedure are illustrated in Table 2.

Table 2 shows that even on new data, the CNNs can classify correctly the largest part of the drones despite the presence of environmental noise. In particular, Xception and DenseNet-121 succeeded better results than Inception-V3. Nevertheless, Inception's results remain satisfactory, meaning that the model is able to generalize. The choice of the most appropriate model therefore, depends on the nature of the application and its requirements.

Table 2: Precision, recall and F1-Score metrics of the test set for each experiment.

Architecture		Precision	Recall	F1-Score
Inception-V3	Drones	97.61%	86.49%	91.71%
	False Alarms	85.10%	97.33%	90.81%
	Macro-avg	91.36%	91.91%	91.26%
Xception	Drones	96.16%	95.58%	95.87%
	False Alarms	94.47%	95.19%	94.82%
	Macro-avg	95.31%	95.38%	95.35%
DenseNet-121	Drones	93.59%	98.24%	95.86%
	False Alarms	97.64%	91.52%	94.48%
	Macro-avg	95.68%	94.88%	95.17%

5. Conclusion

This work presented a binary classification model approach that uses audio data to detect the existence of a drone. A large dataset was collected from two different environments under real-world conditions and a manual annotation was applied separating them to drones and false alarms. The next steps included the audio recordings pre-processing and the spectrograms extraction via STFT, in order to train two-dimensional CNNs. Utilising data augmentation techniques, three different deep learning architectures were trained, Inception-V3, Xception and Densenet-121 keeping the same optimizer, learning rate and early stopping patience criteria. Their performances were compared and evaluated in terms of precision, recall and F1-Score metrics on a training and test set as well.

The applied experiments showed that all three models achieved high classification scores and are capable of generalizing and detect drones in noisy environments. The Xception model specifically, achieved the highest F1-Score (95.35%) on unseen during training data. Nevertheless, depending on the application's nature, different deep learning models could be implemented. In a real time detection task for example, it is more appropriate to use a model with a small number of parameters (such as DenseNet-121) if the trade-off between number of parameters and classification performance is small. Otherwise, in applications where the accuracy of the model plays the most crucial role, the Xception model would be a better option. In any of those cases, the aforementioned models show great potential for a variety of applications related to critical infrastructure monitoring or public safety and privacy.

Acknowledgments: This work was supported by the EU funded project ALADDIN H2020 under Grant Agreement No. 740859.

References

- [1] Tatum, M. C., & Liu, J. (2017, June). Unmanned aerial vehicles in the construction industry. In *Proceedings of the Unmanned Aircraft System Applications in Construction, Creative Construction Conference, Primosten, Croatia* (pp. 19-22).
- [2] Adão, T., Hruška, J., Pádua, L., Bessa, J., Peres, E., Morais, R., & Sousa, J. J. (2017). Hyperspectral imaging: A review on UAV-based sensors, data processing and applications for agriculture and forestry. *Remote Sensing*, 9(11), 1110.
- [3] Lim, B. J. (2018). *System and method for processing of UAV based data for risk mitigation and loss control*. U.S. Patent No. 9,978,030. Washington, DC: U.S. Patent and Trademark Office.
- [4] Fadlullah, Z. M., Takaishi, D., Nishiyama, H., Kato, N., & Miura, R. (2016). A dynamic trajectory control algorithm for improving the communication throughput and delay in UAV-aided networks. *IEEE Network*, 30(1), 100-105.
- [5] Guardian, T. Gatwick Drone Disruption Cost Airport Just £1.4 m. 2018. Available online: <https://www.theguardian.com/uk-news/2019/jun/18/gatwick-drone-disruption-cost-airport-just-14m> (accessed on 16 March 2020).
- [6] Gallagher, S., "German chancellor s drone attack shows the threat of weaponized UAVs," (2013). Available online: <https://arstechnica.com/information-technology/2013/09/german-chancellors-drone-attack-shows-the-threat-of-weaponized-uavs/> (accessed on March 2020).
- [7] Thomas, A., Leboucher, V., Cotinat, A., Finet, P., & Gilbert, M. (2019, September). UAV Localization Using Panoramic Thermal Cameras. In *International Conference on Computer Vision Systems* (pp. 754-767). Springer, Cham.
- [8] Nalamati, M., Kapoor, A., Saqib, M., Sharma, N., & Blumenstein, M. (2019, September). Drone detection in long-range surveillance videos. In *2019 16th IEEE International Conference on Advanced Video and Signal Based Surveillance (AVSS)* (pp. 1-6). IEEE.
- [9] Molchanov, P., Harmanny, R. I., de Wit, J. J., Egiazarian, K., & Astola, J. (2014). Classification of small UAVs and birds by micro-Doppler signatures. *International Journal of Microwave and Wireless Technologies*, 6(3-4), 435-444.
- [10] Palmowska, A., & Lipska, B. (2018). Research on improving thermal and humidity conditions in a ventilated ice rink arena using a validated CFD model. *International Journal of Refrigeration*, 86, 373-387.
- [11] Weiss-Wrana, K. R. (2004, February). Influence of atmospheric turbulence on imaging quality of electro-optical sensors in different climates. In *Optics in Atmospheric Propagation and Adaptive Systems VI* (Vol. 5237, pp. 1-12). International Society for Optics and Photonics.
- [12] Klein, D. J., Venkateswaran, S., Isaacs, J. T., Burman, J., Pham, T., Hespanha, J., & Madhow, U. (2013). Localization with sparse acoustic sensor network using UAVs as information-seeking data mules. *ACM Transactions on Sensor Networks (TOSN)*, 9(3), 1-29.
- [13] Case, E. E., Zelnio, A. M., & Rigling, B. D. (2008, July). Low-cost acoustic array for small UAV detection and tracking. In *2008 IEEE National Aerospace and Electronics Conference* (pp. 110-113). IEEE.
- [14] Barchiesi, D., Giannoulis, D., Stowell, D., & Plumbley, M. D. (2015). Acoustic scene classification: Classifying environments from the sounds they produce. *IEEE Signal Processing Magazine*, 32(3), 16-34.
- [15] Serizel, R., Bisot, V., Essid, S., & Richard, G. (2018). Acoustic features for environmental sound analysis. In *Computational Analysis of Sound Scenes and Events* (pp. 71-101). Springer, Cham.
- [16] Salamon, J., & Bello, J. P. (2017). Deep convolutional neural networks and data augmentation for environmental sound classification. *IEEE Signal Processing Letters*, 24(3), 279-283.

- [17] Jeon, S., Shin, J. W., Lee, Y. J., Kim, W. H., Kwon, Y., & Yang, H. Y. (2017, August). Empirical study of drone sound detection in real-life environment with deep neural networks. In *2017 25th European Signal Processing Conference (EUSIPCO)* (pp. 1858-1862). IEEE.
- [18] Li, J., Dai, W., Metze, F., Qu, S., & Das, S. (2017, March). A comparison of deep learning methods for environmental sound detection. In *2017 IEEE International Conference on Acoustics, Speech and Signal Processing (ICASSP)* (pp. 126-130). IEEE.
- [19] Liu, H., Wei, Z., Chen, Y., Pan, J., Lin, L., & Ren, Y. (2017, April). Drone detection based on an audio-assisted camera array. In *2017 IEEE Third International Conference on Multimedia Big Data (BigMM)* (pp. 402-406). IEEE.
- [20] Kim, J., Park, C., Ahn, J., Ko, Y., Park, J., & Gallagher, J. C. (2017, March). Real-time UAV sound detection and analysis system. In *2017 IEEE Sensors Applications Symposium (SAS)* (pp. 1-5). IEEE.
- [21] Kim, J., & Kim, D. (2018). Neural network based real-time UAV detection and analysis by sound. *Journal of Advanced Information Technology and Convergence*, 8(1), 43-52.
- [22] Jeon, S., Shin, J. W., Lee, Y. J., Kim, W. H., Kwon, Y., & Yang, H. Y. (2017, August). Empirical study of drone sound detection in real-life environment with deep neural networks. In *2017 25th European Signal Processing Conference (EUSIPCO)* (pp. 1858-1862). IEEE.
- [23] Gouyon, F., Pachet, F., & Delerue, O. (2000, December). On the use of zero-crossing rate for an application of classification of percussive sounds. In *Proceedings of the COST G-6 conference on Digital Audio Effects (DAFX-00)*, Verona, Italy (p. 26).
- [24] Ardiansyah, M., Rahmat, R. F., Adnan, S., & Anugrahwaty, R. (2019, June). Application of Digital Sound Recognition on Piano Tones Using MFCC and LVQ. In *Journal of Physics: Conference Series* (Vol. 1235, No. 1, p. 012087). IOP Publishing.
- [25] Sakashita, Y., & Aono, M. (2018). Acoustic scene classification by ensemble of spectrograms based on adaptive temporal divisions. *DCASE2018 Challenge*.
- [26] Ferdoushi, M., Paul, M., & Fattah, S. A. (2019, November). A Spectral Centroid Based Analysis of Heart sounds for Disease Detection Using Machine Learning. In *2019 IEEE International WIE Conference on Electrical and Computer Engineering (WIECON-ECE)* (pp. 1-6). IEEE.
- [27] Szegedy, C., Vanhoucke, V., Ioffe, S., Shlens, J., & Wojna, Z. (2016). Rethinking the inception architecture for computer vision. In *Proceedings of the IEEE conference on computer vision and pattern recognition* (pp. 2818-2826).
- [28] Chollet, F. (2017). Xception: Deep learning with depthwise separable convolutions. In *Proceedings of the IEEE conference on computer vision and pattern recognition* (pp. 1251-1258).
- [29] Huang, G., Liu, Z., Van Der Maaten, L., & Weinberger, K. Q. (2017). Densely connected convolutional networks. In *Proceedings of the IEEE conference on computer vision and pattern recognition* (pp. 4700-4708).
- [30] Zaheer, M., Reddi, S., Sachan, D., Kale, S., & Kumar, S. (2018). Adaptive methods for nonconvex optimization. In *Advances in neural information processing systems* (pp. 9793-9803).
- [31] He, K., Zhang, X., Ren, S., & Sun, J. (2016). Deep residual learning for image recognition. In *Proceedings of the IEEE conference on computer vision and pattern recognition* (pp. 770-778).



CidB

Centre d'information
sur le Bruit

QUIET DRONES
International Symposium
on
UAV/UAS Noise
Paris – 25th to 27th May 2020

Experimental Investigation of Contra-Rotating Multi-Rotor UAV Propeller Noise

Ryan S. McKay - Dotterel Technologies: rmck910@aucklanduni.ac.nz

Michael J. Kingan - University of Auckland: michael.kingan@auckland.ac.nz

S. T. Go - Dotterel Technologies: sqo587@aucklanduni.ac.nz

Summary

Contra-rotating propellers could increase efficiency and lifting capacity of multi-rotor unmanned aerial vehicles (UAVs); however, they are notoriously loud. This work experimentally investigated the noise from static contra-rotating UAV propellers. The effects of propeller diameter were studied by testing different configurations of 12" and 15" propellers. The propeller spacing and rotational speed were also investigated. In total, 1400 propeller configurations were tested. This paper will focus on the errors and uncertainty in the experimental method. The microphones are shown to be in the acoustic far-field which. A study of the repeatability of the automated method used to collect the acoustic and performance data is presented and confirms that the measurements are repeatable. Finally, the anechoic chamber measurements are compared to a quadcopter with contra-rotating propellers flying outdoors.

1. Introduction

Small unmanned aerial systems (UASs) are a rapidly growing technology which is driven by affordability and a wide range of applications. Multi-rotor unmanned aerial vehicles (UAVs) are rotary-wing aircraft with multiple propellers that are commonly used in UASs. Although multi-rotor UAVs can have many propeller configurations (e.g. quadcopters, hexacopters or octocopters), they typically use a number of conventional single propellers all rotating in the same plane to generate thrust. An alternative propeller arrangement are contra-rotating propellers which are two co-axially aligned propellers that rotate in opposite directions. The main benefit of contra-rotating propellers in large scale aircraft is the increase in efficiency resulting from the reduction of swirl by the downstream propeller [1]. Contra-rotating propellers can be used on multi-rotor UAVs to provide additional thrust without increasing the size of an aircraft. The additional propeller can also provide redundancy. The well-known downside of contra-rotating propellers is that they are often louder than equivalent conventional single propellers. There is little research

on contra-rotating multi-rotor UAVs, with almost all published literature focusing on the aerodynamics rather than the acoustics. This paper presents experimental acoustic data for contra-rotating multi-rotor UAV propellers in hover and investigates the repeatability and validity of the method used to collect this data.

The noise from conventional single multi-rotor UAV propellers is predominantly caused by steady loading and thickness noise in directions near the plane of the propeller [2]. They are caused by the force and volume-displacement effects exerted by the rotating propeller on the air and cause tonal noise generated at integer multiples of the blade-passing frequency ($BPF = B\Omega/2\pi$, where BPF has units of Hz, B is the number of blades and Ω is the rotational speed in rad/s) and typically 2 to 3 harmonics that are above the broadband level. Static conventional single propellers can also generate unsteady loading noise due to turbulence ingestion [3] which produces quasi-tonal noise with peaks in the sound pressure level spectrum at a multitude of BPF harmonics. The turbulence ingestion noise typically generates noise at higher harmonics of the BPF than the steady loading and thickness noise. Rapid, low-amplitude, periodic fluctuations in the rotational speed of brushless DC motors that are typically used on multi-rotor UAV may also cause tonal noise at harmonics of the shaft rotational speed [4].

The noise produced by contra-rotating propellers contains an additional noise source which is caused by the unsteady loading on each propeller due to its interaction with the flow-field from the adjacent contra-rotating propeller. The unsteady loading can be caused by wake interactions, aerodynamic potential field interactions and tip vortex interactions [5]. The periodic component of the unsteady loading generates tonal noise at the sum and difference of the blade passing frequencies, i.e. at $\omega_{n_1, n_2} = n_1 B_1 \Omega_1 + n_2 B_2 \Omega_2$, where n_1 and n_2 are integers (positive and negative) and the subscripts, 1 and 2, indicate that a parameter is associated with the upstream or downstream propeller, respectively. Another parameter for describing contra-rotating propeller interaction tones is the azimuthal mode order, $\nu = n_2 B_2 - n_1 B_1$. The azimuthal mode order is an important parameter which influences the directionality of the interaction tones which has previously been discussed by the authors [6]. Interactions of the downstream propeller with the turbulent flow from the upstream propeller can also be a source of broadband noise [7].

Although there have been several studies investigating the aerodynamics of contra-rotating UAV propellers (e.g.[8]–[12]), the authors know of very few studies on the acoustics of contra-rotating UAV propellers. Liu et al. [13] performed a computational study on a micro UAV with 6.5 cm diameter contra-rotating propellers. Their simulations showed that the tip vortex from the upstream propeller interacted with the downstream propeller which led them to their conclusion that tip vortex interaction was a major noise source. Horváth et al. [14] provide some guidelines for the design of quiet contra-rotating UAV propellers based on the radiation efficiency of different interaction tones.

In this study, the noise from various configurations of contra-rotating UAV propellers in hover is experimentally investigated. The configurations that were tested generated maximum thrusts of 3.5-6.5 kg. The experimental results have previously been analysed by the authors and the effect of propeller spacing, propeller diameter and number of blades on the interaction tones is presented in [6], [15]. This paper will focus on demonstrating the validity of the experimental method by demonstrating that the microphones are in the acoustic far-field and showing that the measurements are repeatable. A comparison between the anechoic chamber results and a quadcopter with contra-rotating propellers will also be presented to show these results are comparable to a multi-rotor UAV in hover.

2. Methods

The purpose of the experiments performed for this work was to investigate the noise produced by contra-rotating UAV propellers in hover. This was done by testing various configurations of contra-rotating UAV propellers mounted statically in an anechoic chamber. A common configuration for contra-rotating UAV motors is to have two motors mounted either side of the UAV frame. This configuration typically has a large propeller spacing and it is difficult to adjust the distance between propellers. Furthermore, the support which protrudes into the flow between the propellers may alter the flow and generate additional noise. Another approach is to use a single motor unit consisting of two connected motors with coaxial shafts. In this configuration, the lower motor's shaft runs through that of the upper motor. This configuration has an upper limit on propeller spacing but does allow for moderate variation in the propeller spacing (including very close spacings) and does not disrupt the flow between the propellers. We decided to use a coaxial motor unit to limit the noise sources to propeller interactions rather than interactions with support structures.

The motor was mounted on a single-axis Honeywell Model 151 S-type load cell. The load cell was used to measure the static thrust generated by the two propellers. The contra-rotating motor used in this study was constructed from two T-Motor MN501 motors and is shown in Figure 1. The motor was controlled by two T-Motor Alpha electronic speed controllers (ESCs) which enabled the speed of the upstream and downstream propellers to be varied separately. Constant 48 V power supplies powered the motors and the current was measured using two Mauch PL-050 hall current sensors. The ESCs output the rotational speed of each motor. The thrust, current and rotational speed were acquired for all tests using a National Instruments MyRio.



Figure 1. Contra-rotating motor unit with two 15" propellers spaced 48 mm between the hubs. The motor was mounted on a load cell in the University of Auckland's anechoic chamber.

2.1 Parameter study

To demonstrate the effect of different parameters on contra-rotating propeller noise, we conducted an initial experimental campaign in which we varied the rotational speed, the propeller spacing, the propeller diameter and the number of blades on a propeller. The rotational speed of each propeller was varied from stationary to maximum speed by changing the pulse width modulation (PWM) signal sent to the ESC. The PWM signal was varied in 10 to 13 equal increments, depending on the tested configuration which meant between 99 and 168 tests were performed for each propeller configuration. A total of 1408 tests were performed in this part of the experimental campaign.

Commercially available 15" \times 5" ¹ (381 mm \times 127 mm) two-blade propellers, 12" \times 4" (305 mm \times 102 mm) two-blade propellers and a 12.5" \times 4.3" (318 mm \times 109 mm) three-blade propeller were tested. We will denote a contra-rotating propeller configuration with two-blade propellers by $D_1 - D_2$ where D_1 and D_2 are the diameters of the upstream and downstream propellers, respectively. For example, a contra-rotating propeller with 15" diameter propellers upstream and downstream will be denoted as 15"-15". Tests with a three-blade propeller upstream will be denoted as $3 \times D_1 - D_2$; note that the convention adopted in this paper is that the blade numbers of two-blade propellers are not explicitly included in the configuration designation.

At observation locations close to the axis of rotation of the propellers, it was expected that tones with zero azimuthal mode order would have very high amplitudes. The amplitude and number of such tones can be reduced by selecting blade numbers such that there are fewer tones with zero azimuthal mode order occurring over a given frequency range. We used a three-blade propeller in a 3×12.5 "-12" configuration to demonstrate this effect.

Propeller spacing can change the position at which the tip vortex impinges on the downstream propeller, and the strength of the potential field and wake interactions. Each of the propeller configurations was tested at the default propeller spacings for the motor set of 17 mm and 48 mm between the hubs of the propellers. The list of configurations tested over a wide speed range is:

1. 15"-15" with 17 mm spacing
2. 15"-12" with 17 mm spacing
3. 12"-15" with 17 mm spacing
4. 12"-12" with 17 mm spacing
5. 15"-15" with 48 mm spacing
6. 15"-12" with 48 mm spacing
7. 12"-15" with 48 mm spacing
8. 12"-12" with 48 mm spacing
9. 3×12.5 "-12" with 48 mm spacing

The significant number of rotational speeds that each configuration was tested resulted in a significant time requirement for each test. This process was automated to reduce the total time and to greatly reduce the time demand for the person performing the tests. Matlab was used to acquire the acoustic data and to loop through the data. LabView was used to generate the PWM signal for the motors and to acquire the thrust and rotational speed data.

2.2 Acoustic methodology

The tests were performed in the University of Auckland's anechoic chamber, which has internal dimensions of 5.3 m \times 5.3 m \times 5.3 m (wedge tip to wedge tip) and has a cut off frequency below 80 Hz. Acoustic measurements were taken with 11 G.R.A.S 46AE 1/2" microphone and preamplifier sets connected to National Instrument NI9234 modules in an NI cDAQ-9178 chassis. Microphones were positioned at polar angles, measured from the propeller axis with origin at the hub of the downstream propeller, every 15° from $\theta=0^\circ$ (directly above the propeller) to $\theta=150^\circ$ on a C-shaped frame, as shown in Figure 2. No measurement was made at, or close to, $\theta=180^\circ$ as these positions were in the wake of the propeller and would have been corrupted by flow noise. All acoustic data was corrected to 1.5 m assuming spherical spreading. This distance is in the acoustic far-field for conventional single UAV propellers of a similar size [16] and it is shown in Section 3.1 to be in the acoustic far-field for significant rotor-alone tones, interaction tones and broadband noise produced by the contra-rotating propellers. Acoustic measurements were taken

¹ UAV propellers are typically specified in inches as diameter \times pitch. The pitch is the theoretical distance that the propeller will move through the air in a single revolution assuming no slip.

over 30 s and were acquired at 51.2 kHz. A relatively long averaging time is required for contra-rotating UAV propellers because the speed of the UAV motors vary over time. This means that the interactions between propellers occur at random azimuthal locations. If the averaging time is too short, then the azimuthal directivity effects may not be adequately averaged. Reflective surfaces, with the exception of the mount directly beneath the load cell shown in Figure 1, were covered with 10 mm thick polyester acoustic absorbing material to minimise reflections (the mounting surface was not covered as doing so would have made a larger obstruction downstream of the propeller, which may have affected the noise generation). The acquired acoustic data were processed using Welch's PSD estimate [17] with a Hanning window of 50% overlap and a frequency resolution of 1 Hz. The rotational speed measurements were used to identify the BPF and other tones related to the rotational speeds of the upstream and the downstream propellers.

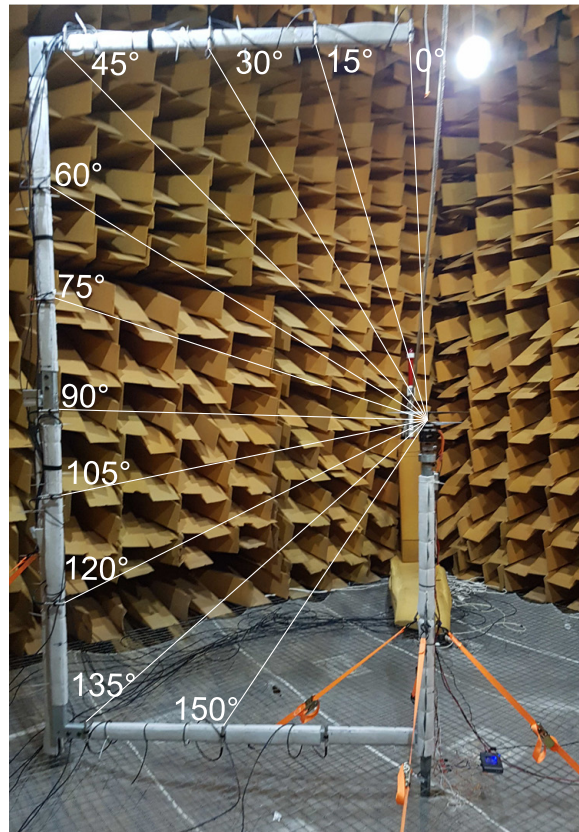


Figure 2. An array with 11 microphones spaced every 15° around the contra-rotating propeller acquired the acoustic data.

2.3 Repeatability tests

The repeatability of the automated test procedure was investigated by testing 15"-15" and 12"-15" contra-rotating propeller at six different upstream and six different downstream PWM settings. This set of 36 tests was performed five different times to quantify the variability of the thrust, power and OASPL data.

2.4 In-flight test

A test on a 4 kg quadcopter with contra-rotating propellers was performed to demonstrate the applicability of static testing of an isolated propeller in an anechoic chamber. The quadcopter with contra-rotating 12"-12" propellers spaced 86 mm apart, shown in Figure 3, was tested in hover approximately 5 m above the ground. Microphones were positioned at ground height at $\theta=180^\circ$ and approximately $\theta=135^\circ$ (angles use the same convention as the static tests which are defined in Figure 2 but defined from the centre of the quadcopter). In order to remove the

influence of ground reflections, the microphones were positioned in the centre of wooden boards measuring $0.9\text{ m} \times 0.9\text{ m} \times 5\text{ mm}$ and measured sound pressure levels were corrected with a -6 dB correction. Hemispherical windscreens were placed on the microphones to reduce flow noise from the quadcopter. The tests were performed on a still day with the quadcopter maintaining a relatively constant height and position using on-board sensors.



Figure 3. The custom built 4 kg quadcopter with 12"-12" propellers used for in-flight testing.

3. Results

The results are presented in three parts. The first part demonstrates that the microphones are in the acoustic far-field. The second part demonstrates the repeatability of the measurements. The final section presents in-flight data to show the applicability of testing a single contra-rotating propeller in an anechoic chamber.

3.1 Acoustic pressure decay

Data were measured using a linear microphone array positioned at $\theta=135^\circ$ with microphones located at various distances measured from the centre of the downstream propeller. The purpose of these tests was to show the decay of the acoustic pressure with distance. A 15"-15" propeller producing 2.0 kg of thrust was used for this test. The upstream propeller was rotating at 5670 rpm and the downstream at 4290 rpm. Figure 4 plots the OASPL summed over 500 Hz to 10 kHz, the lower frequency BPF tone and two interaction tones against the distance from the centre of the downstream propeller. The overall sound pressure level (OASPL) was summed from 500 Hz as flow noise had an obvious effect below 500 Hz on measurements made using the closest microphones. However, the tones below 500 Hz each had higher amplitude than the flow noise; hence, these tones were used in plotting the decay. The measurements for the $\{0,1\}$ tone at 0.3 and 0.35 m were the only tones $<10\text{ dB}$ above the flow noise; hence, they have been excluded

from Figure 4. The $\{1,1\}$ interaction tone and the $\{2,1\}$ interaction tones were chosen as their sonic radii² lay inboard and outboard of the propeller blade tip, respectively. Kingan and Sureshkumar [18], [19] have shown that the field is evanescent inboard of the sonic radius in the propeller plane. The spherical decay law is shown by the dashed $1/r$ lines in Figure 4, which shows that all metrics follow the spherical decay law for microphones positioned at, and outboard of, 1.5 m; hence, it is valid to correct for distance using the spherical decay law at all microphone locations used during the experiments reported here.

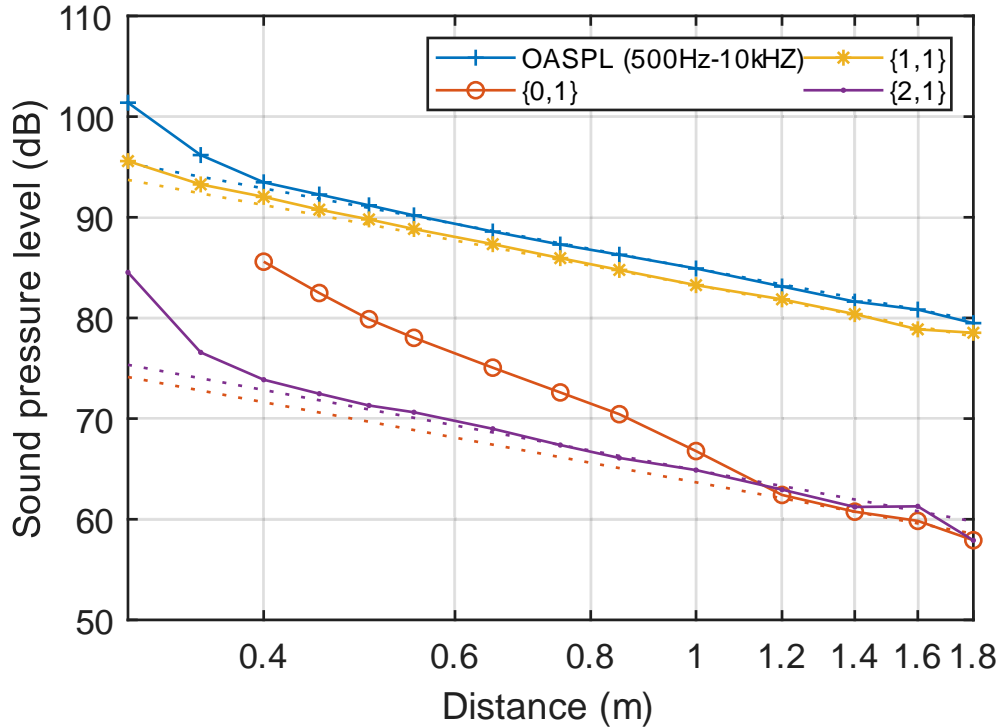


Figure 4. Pressure decay along a linear microphone array compared with the spherical decay law ($1/r$) for a 15"-15" contra-rotating propeller. The test was performed using a 15"-15" propeller which was producing 2.0 kg of thrust. The upstream propeller was rotating at 5670 rpm and the downstream at 4290 rpm.

3.2 Repeatability

The data for the five repeatability tests for the 15"-15" contra-rotating propeller is shown in Figure 5. This figure shows the spread of the data by using error bars to show the maximum and minimum value for each tested configuration. The OASPL was calculated from 50 Hz to 10 kHz for the microphone at 135°. The average variation in thrust for the 15"-15" contra-rotating propeller was 43 g with a maximum variation of 120 g. The average variation for power was 7.6 W with a maximum variation of 22 W. Some variation is expected as the rotational speed of the motor can vary for a specific pulse length.

The OASPL for the 15"-15" configuration had an average variation of 0.72 dB and a maximum variation of 4.2 dB. The maximum value occurred for the case where both upstream and downstream motors were set at the lowest PWM pulse length of 1140 μ s. The motor speeds seemed to vary more significantly when the PWM pulse lengths were set to these low values. If the tests at 1140 μ s are excluded then the average variation is 0.58 dB and the maximum variation is 1.3 dB, which we deemed an acceptable variation between five tests.

The 12"-15" configuration had an average variation in thrust of 19 g and a maximum variation of 51 g, an average variation in power of 2.0 W and a maximum variation of 7.4 W, and an average variation in OASPL of 0.30 dB and a maximum variation of 1.7 dB (not excluding the 1140 μ s tests).

² See equations 6.4.4 [20]

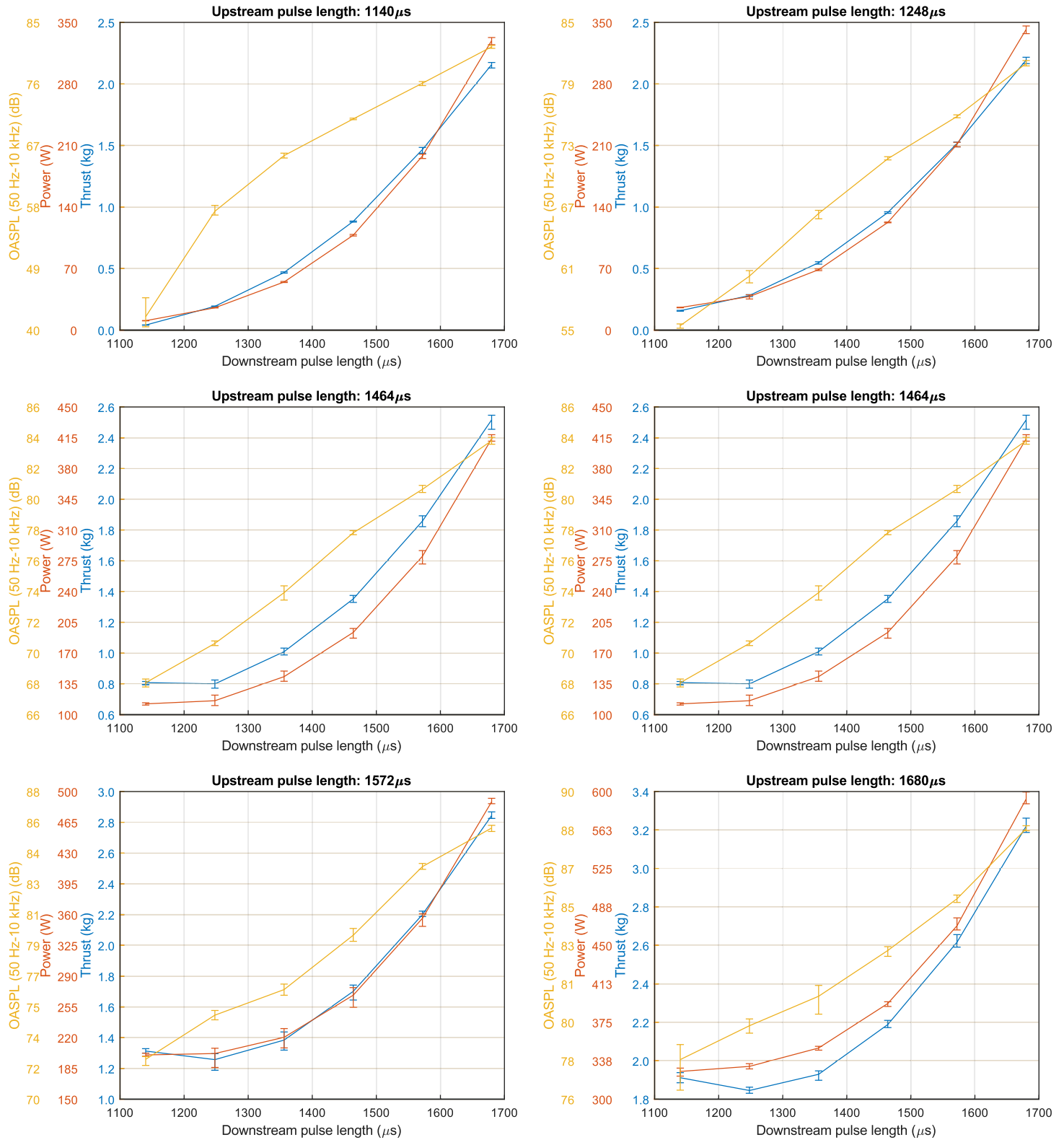


Figure 5. Variation in the power, thrust and OASPL over five repeated tests.

3.3 In-flight testing

Acoustic tests were performed on a 4 kg quadcopter with 12"-12" contra-rotating propellers spaced 86 mm apart. Spectrograms of the results at $\theta=135^\circ$ and 180° are shown in Figure 6 and Figure 7, respectively. The speed of the upstream and downstream propellers for each set of contra-rotating propellers on the quadcopter was the same due to limitations of the flight controller. This meant that the $\{1,1\}$ interaction tone was the same frequency as the second BPF harmonic. The BPF for the quadcopter's propellers was approximately 180 Hz, although the BPF

varied over time as the flight-controller varies the speed of each propeller to maintain stability. Figure 7 shows the BPF tone is the highest amplitude tone at $\theta=135^\circ$; however, Figure 6 shows that the $\{1,1\}$ tone (which is at the same frequency as the second BPF tone) is the highest amplitude tone at $\theta=0^\circ$. This result is also demonstrated by the time averaged spectra from the in-flight tests shown in Figure 8 which have been scaled, assuming spherical spreading, to an observer distance of 1.5 m. The broad tones in Figure 8 are likely due to the variation in the rotational speed of the propellers over time. The dual peaks near BPF and subsequent harmonics are likely due to each of the propeller sets having different rotational speeds to maintain stability.

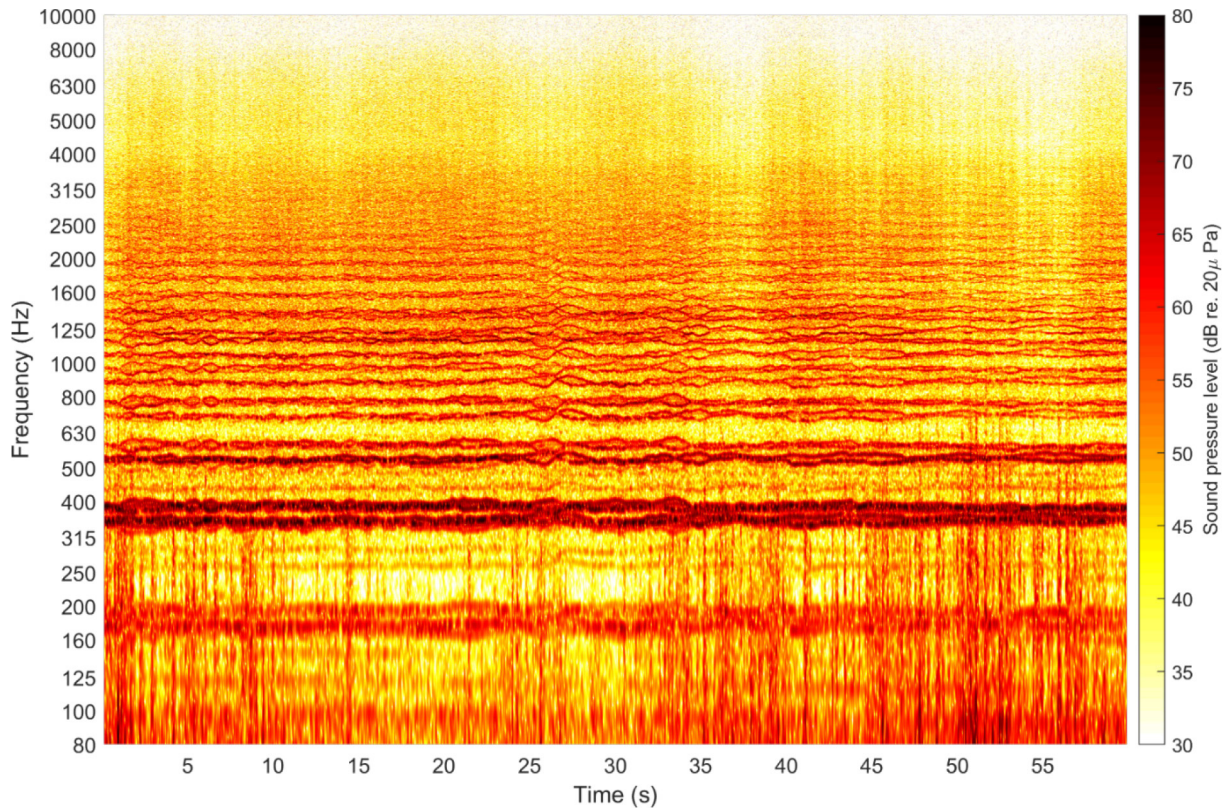


Figure 6. Inflight testing of a quadcopter with contra-rotating propellers at $\theta=0^\circ$

The sound pressure level spectra for a configuration with 12"-12" contra-rotating propellers spaced 48 mm apart statically tested in the anechoic chamber is shown in Figures 9 and 10 at $\theta=0^\circ$ and 135° . This result shows similar trends with the BPF tone being the highest amplitude tone at 135° but the $\{1,1\}$ interaction tone being the highest amplitude tone at 0° . Additionally, the interaction tones decrease in amplitude with decreasing frequency. The qualitative consistency between results demonstrates that the static testing in the anechoic chamber is valid for making comparisons to the noise from a quadcopter. Quantitative agreement is seen between the anechoic chamber tests and the in-flight tests for the first two interaction tones at $0^\circ/180^\circ$ and the $\{1,1\}$ interaction tone at 135° . The overlaid in-flight tones are found by summing the energy in the broad tones and then, assuming they are incoherent sources, subtracting 6 dB to account for the four sources. The anechoic chamber and in-flight tests do not agree well for the BPF tone and the second harmonic. However, the lack of agreement is possibly due to differences in the turbulent inflow between the outdoor test and the anechoic chamber. Another source of discrepancy is that the motor configurations were also different. The quadcopter had a support between the two propellers and the two propellers had a much greater spacing (86 mm) than the static test (48 mm) – these effects require further investigation.

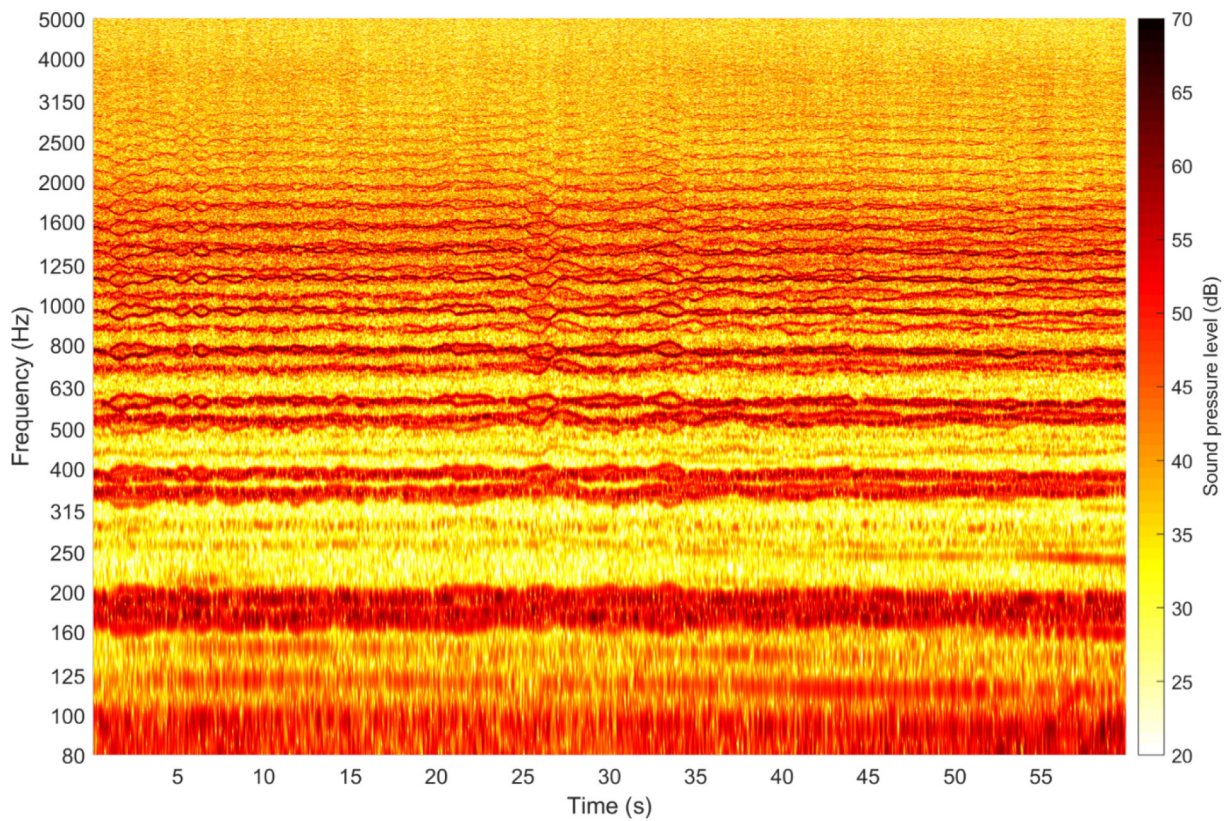


Figure 7. Inflight testing of a quadcopter with 12"-12" contra-rotating propellers at $\theta=45^\circ$

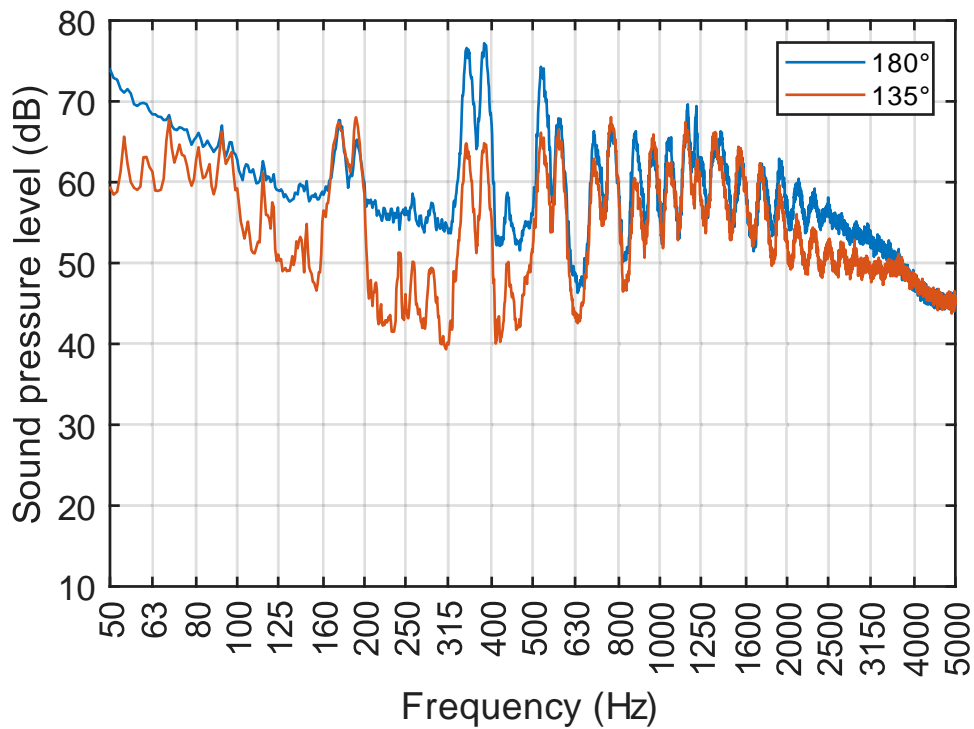


Figure 8. Spectrum from a quadcopter with 12"-12" contra-rotating propellers averaged over 60 s. The levels are adjusted to match the observer distance of 1.5 m from the anechoic chamber tests assuming spherical spreading.

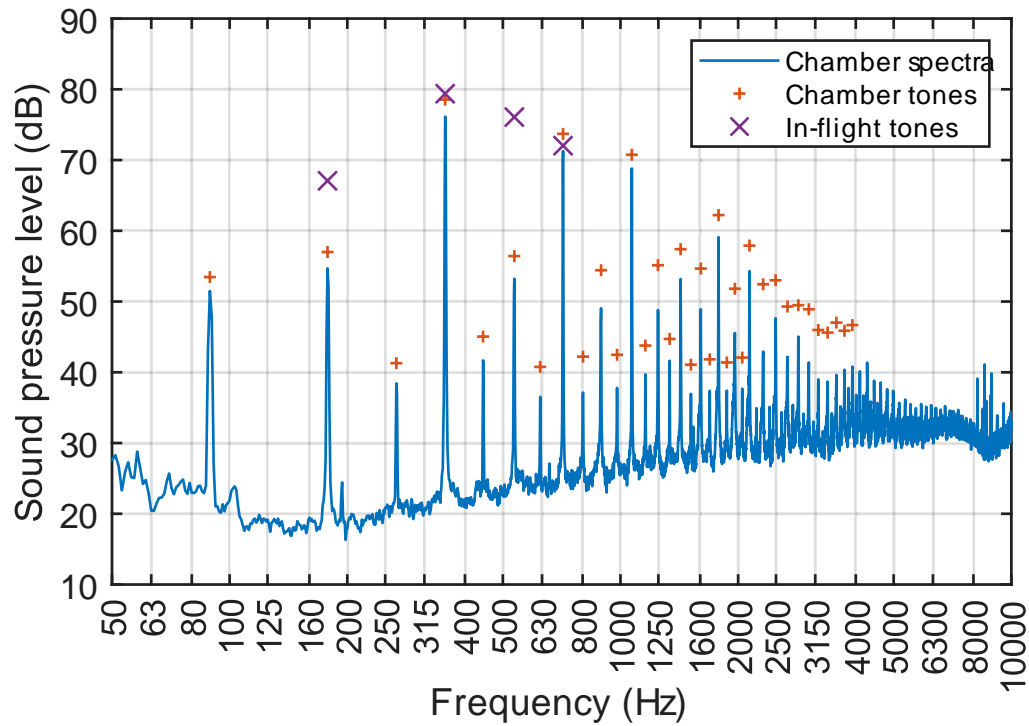


Figure 9. Sound pressure level spectrum from an anechoic chamber test of a 12"-12" contra-rotating propeller spaced 48 mm apart with the upstream and downstream propellers operating at the same rotational speeds. This configuration generated around 1 kg of thrust, which is around the same thrust required by the quadcopter at hover. The microphone was located at $\theta=0^\circ$. The in-flight tones are for a microphone at $\theta=180^\circ$ and corrected for distance and four sources.

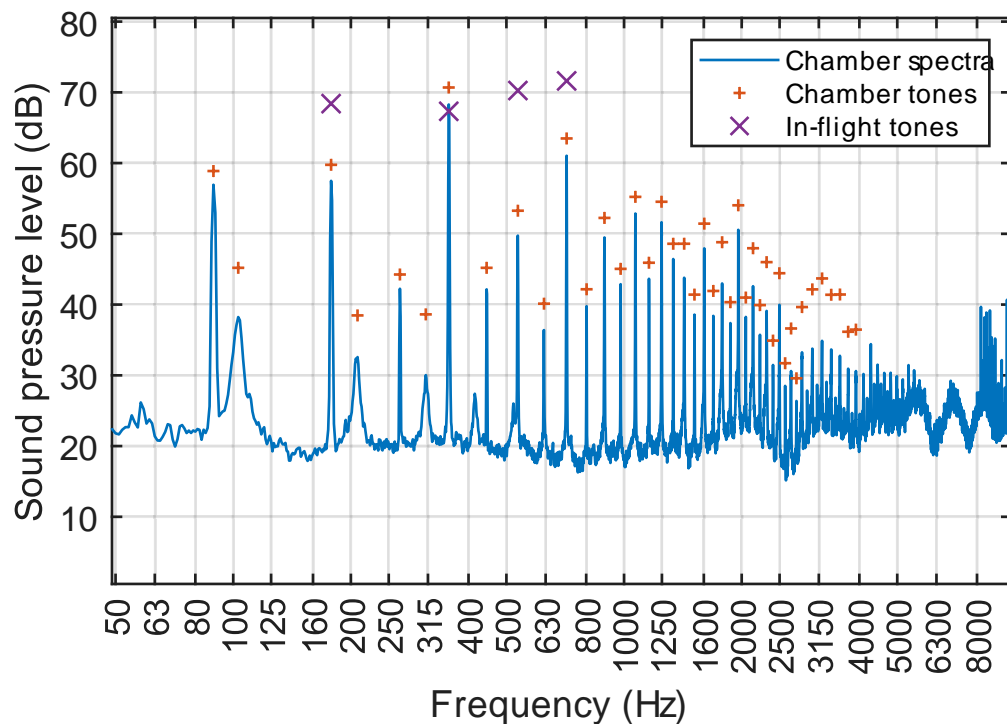


Figure 10. Anechoic chamber test of a 12"-12" contra-rotating propeller spaced 48 mm apart with the upstream and downstream propellers operating at the same rotational speeds. This configuration generated around 1 kg of thrust, which is around the same thrust required by the quadcopter at hover. The microphone was located at $\theta=135^\circ$. The in-flight tones are for a microphone at $\theta=135^\circ$ and corrected for distance and four sources.

4. Conclusions

This paper discusses the errors and uncertainty of a large experimental campaign on contra-rotating propellers for multi-rotor UAVs in hover. The experimental campaign investigated the effect of rotational speed, propeller diameter and propeller spacing. This paper has shown that the microphone location is in the acoustic far-field, which validates the assumption of spherical spreading made by the authors. A repeat of a sub section of the experiments has shown that there is minimal variance in the thrust, power and OASPL data which indicates that the test procedure is repeatable. Finally, the static tests in the anechoic chamber have been compared to an in-flight test of a quadcopter with contra-rotating propellers which showed qualitative agreement between the in-flight and anechoic chamber tests and quantitative agreement for the first two interaction tones.

References

- [1] W. C. Strack, G. Knip, A. L. Weisbrich, J. Godston, and E. Bradley, "Technology and Benefits of Aircraft Counter Rotation Propellers," NASA Technical Memorandum 82983, 1981.
- [2] N. S. Zawodny, D. D. Boyd Jr., and C. L. Burley, "Acoustic Characterization and Prediction of Representative, Small-Scale Rotary-Wing Unmanned Aircraft System Components," in *AHS International 72nd Annual Forum*, 2016, pp. 34–48.
- [3] C. Nardari, D. Casalino, F. Polidoro, V. Coralic, P.-T. Lew, and J. Brodie, "Numerical and Experimental Investigation of Flow Confinement Effects on UAV Rotor Noise," in *25th AIAA/CEAS Aeroacoustics Conference*, 2019, no. May, pp. 1–17.
- [4] R. McKay and M. J. Kingan, "Multicopter Unmanned Aerial System Propeller Noise Caused by Unsteady Blade Motion," in *2019 AIAA/CEAS Aeroacoustics Conference*, 2019, no. May.
- [5] N. Peake and A. B. Parry, "Modern Challenges Facing Turbomachinery Aeroacoustics," *Annu. Rev. Fluid Mech.*, vol. 44, no. 1, pp. 227–248, 2012.
- [6] R. S. McKay, S.-T. Go, R. Jung, and M. J. Kingan, "Noise from unmanned aerial vehicle contra-rotating propellers," in *18th International Symposium on Transport Phenomena and Dynamics of Rotating Machinery*, 2020.
- [7] M. J. Kingan, "Open rotor broadband interaction noise," *J. Sound Vib.*, vol. 332, no. 17, pp. 3956–3970, 2013.
- [8] D. Shukla and N. Komerath, "Drone scale coaxial rotor aerodynamic interactions investigation," *J. Fluids Eng. Trans. ASME*, vol. 141, no. 7, pp. 1–10, 2019.
- [9] V. K. Lakshminarayanan and J. D. Baeder, "Computational Investigation of Small Scale Coaxial Rotor Aerodynamics in Hover," in *47th AIAA Aerospace Sciences Meeting*, 2009, no. January.
- [10] V. K. Lakshminarayanan and J. D. Baeder, "Computational investigation of microscale coaxial-rotor aerodynamics in hover," *J. Aircr.*, vol. 47, no. 3, pp. 940–955, 2010.
- [11] F. Bohorquez, "Rotor Hover Performance and System Design of an Efficient Coaxial Rotary Wing Micro Air Vehicle," University of Maryland, 2007.
- [12] S. D. Prior and J. C. Bell, "Empirical Measurements of Small Unmanned Aerial Vehicle Co-Axial Rotor Systems," *J. Sci. Innov.*, vol. 1, no. 1, pp. 1–18, 2011.
- [13] Z. Liu, C. Bu, X. Kong, D. Yang, and B. Li, "Computational investigation of noise interaction for a nano counter-rotating rotor in a static condition," *Int. J. Comput. Mater. Sci. Eng.*, vol. 07, no. 01n02, p. 1850004, 2018.
- [14] C. Horváth, B. Fenyvesi, and B. Kocsis, "Drone Noise Reduction Via Radiation Efficiency Considerations," 2018.
- [15] R. S. McKay, M. J. Kingan, and R. Go, "Experimental investigation of contra-rotating multi-rotor UAV propeller noise," in *Acoustics 2019*, 2019, pp. 1–10.
- [16] C. E. Tinney and J. Sirohi, "Multicopter Drone Noise at Static Thrust," *AIAA J.*, vol. 56, no. 7, pp. 2816–2826, 2018.

- [17] P. D. Welch, "The Use of Fast Fourier Transform for the Estimation of Power Spectra: A Method Based on the Time Averaging Over Short, Modified Periodograms," *IEEE Trans. Audio Electroacoust.*, vol. 15, no. 2, pp. 70–73, 1967.
- [18] M. J. Kingan and P. Sureshkumar, "Open rotor centrebody scattering," *J. Sound Vib.*, vol. 333, no. 2, pp. 418–433, 2014.
- [19] P. Sureshkumar, M. J. Kingan, and A. B. Parry, "Predicting the noise of an open rotor in a wind tunnel," *Int. J. Aeroacoustics*, vol. 18, no. 4–5, pp. 414–443, 2019.
- [20] A. B. Parry, "Theoretical prediction of counter-rotating propeller noise," University of Leeds, 1988.



CidB

Centre d'information
sur le Bruit

QUIET DRONES
International e-Symposium
on
UAV/UAS Noise
Remote from Paris – 19th to 21st October 2020

**Active Noise Cancellation of Drone Propeller Noise Through
Waveform Approximation and Pitch-Shifting**

Michael Narine, Georgia State University: mnarine1@student.gsu.edu

Richard Howard, WINLAB/Rutgers University: rich@richardehoward.com

Ashwin Ashok, Georgia State University: aashok@gsu.edu

Summary

The use of drones introduces the problem of noise pollution due to the audio noise generated from its propeller rotations. To mitigate the noise pollution from drone propellers, this paper explores a method of using active noise cancellation (ANC). This paper hypothesizes that by analysing the waveform of the drone propeller noise, an approximated wave function can be produced and used as an anti-noise signal that can effectively nullify the drone noise. In order to align the phase of the anti-noise signal to maximize drone noise reduction, this paper presents a signal pitch-shifting approach, to guide areas of destructive interference to a desired target such as a microphone, at a desired location. Through experimental evaluation using a prototype of the proposed Pitch-Aligned Active Noise Cancellation system (PA-ANC), this paper reveals that the proposed technique can achieve a 43.82% reduction of drone noise.

1. Introduction

Drone technology has become widely integrated into many commercial and industrial applications, and with a large range of cost variation of drones, they have become much more accessible for recreational use. The conveniences that drones present are starting to be exploited by many companies where drones can be used as a means of package delivery. In the film industry, drones are being used to obtain footage from angles that would have been difficult to obtain before. Drones have also been used to gather research data in environments where the terrain is difficult to navigate or at high altitudes. While drones have many benefits, drones also present drawbacks such as noise pollution.

Noise pollution can be defined as an abundance of noise that may annoy or harm humans or animals in the surrounding environment. Prolonged exposure to noise pollution can have significant negative impacts to an individual's physical and mental health. Due to rapid urbanization in recent times, urban areas are a hotspot for high amounts of noise pollution. Although noise is regulated in residential areas, in urban environments, noise pollution is highly unregulated and usually the result of poor planning and rapid urban development. Fatigue and hearing loss are common issues caused by noise pollution. With noise pollution already being a prominent issue, the widespread use of drones in these environments further exacerbates this issue. Furthermore, the use of drones is introducing the problem of noise pollution to areas that were not previously affected, such as residential and rural areas.

Large corporations are beginning to incorporate drones as a means to deliver products over large distances. Because these drones must be able to carry heavy loads, more powerful rotors are used which further increase the noise produced. With these delivery drones becoming more abundant, the impact of noise pollution will become much more widespread. According to a NASA study, the noise produced by drones was found to produce a higher negative reaction compared to the noise produced by various land vehicles (Christian et al.). It was suggested that people are used to noise produced by automotive vehicles because they heavily rely on these vehicles for transportation, and therefore, tolerate this form of noise. However, drones are a novel source of noise and are not heavily integrated in everyday life, therefore, drones can be seen as an unnecessary source of noise.

Noise cancellation, or noise control, is the process of attenuating, or reducing, the noise using passive and active methods. Passive noise cancellation involves the use of acoustic insulating or absorbing materials to reduce the ambient noise or noise produced by specific sources. Active noise cancellation involves the use of a second sound source to produce destructive interference and reduce the overall volume, or amplitude, of the target noise source. Applications of noise cancellation usually implement both active and passive methods in order to maximize the reduction of noise. Although noise cancellation techniques are relatively effective at reducing noise, both passive and active noise cancellation have specific uses and limitations, such as its effectiveness in certain frequency ranges (Lifei) (Kottayi et al.) (Liang et al.).

2. Problem Statement and Contributions

As drones become more abundant, the level of noise pollution is further increased to being dangerous. Many attempts at noise cancellation have proved to be effective, such as altering the propeller shapes, reducing the weight of the body of the drone (Miljković), and implementing active noise cancellation techniques (Kang et al.) (Miljković). However, such methods can be expensive to implement or can negatively impact the performance of the drone.

This paper hypothesizes that it is possible to actively cancel the drone noise using an external anti-noise signal. In this regard, this paper proposes Pitch-Aligned Active Noise Cancellation (PA-ANC) approach, which aims to efficiently reduce the noise produced by a drone's propellers without affecting the performance of the drone itself. In order to align the anti-noise signal to the drone noise signal, the PA-ANC system takes advantage of the principle of beats, the oscillations in amplitude as a result of two signals of different frequencies. The oscillations in amplitude due to beats are a result of oscillations in the phase between the two signals over time. By manipulating the dominant frequency or pitch of the anti-noise, the PA-ANC system can determine when the phase between the anti-noise and drone noise signals is exactly 180° , which correlates to a maximum reduction in noise.

The key contributions of this paper include the frequency domain analysis of drone propeller noise, dominant spectral frequency estimation, and exploration and development of the use of pitch-shifting as a form of phase alignment.

3. Related Work

Active noise cancellation, or active noise control (ANC), is a widely explored method of noise reduction in various fields and applications. Despite this, ANC technology has only recently begun to be integrated into drones. Different ANC techniques implemented for various applications can be adapted to better target drone propeller noise and maximize the noise reduction effect.

Passive noise control involves the use of sound insulating or absorbing materials to reduce the noise being produced. In manned aerial vehicles, such as airplanes and helicopters, the structure of the aircraft is altered and contains such vibration absorbing materials in order to reduce the vibrations and noise experienced by the passengers. However, in unmanned aerial vehicles (UAV), such materials have little effect in noise attenuation to observers and can have a significant impact in performance. Instead of reducing overall noise through the use of these materials, the noise can be redirected such that the level of noise that reaches the observer is minimized. Mohamud et al. aimed to reduce the noise emitted by a drone's propellers by forming shrouds composed of sound insulating foam as well as aluminum to reflect the noise back towards the drone. In this method, the level of noise was measured from different angles of the drone. It was found that the sound insulating foam performed the best at reducing the noise emitted from the propellers, especially from the front of the drone. Dotterel, a company specializing in noise reduction in UAVs, also developed such a method similar to this. This method involves the use of a lightweight material arranged in a cone around each of the propellers of the drone. The noise produced by the propellers bounce off this material and is redirected upwards, greatly reducing the level noise that reaches the observers on the ground without significantly affecting the performance of the drone (Rotherhan).

While many UAVs used for industrial and military purposes used fuel in order to provide power to the propellers, the majority of recreational UAVs used electrical power in order to operate the propellers. In the study of UAV noise by Tansel et al., it was found that electrically powered UAVs produced less noise compared to fuel powered UAVs. The engine used to convert the fuel to power produced vibrations that significantly increased the amount of overall noise produced by the UAV. While the electrically powered UAV produced less noise, electricity has a lower power density than fuel, thus these UAVs cannot operate for long periods of time.

In *Methods for attenuation of unmanned aerial vehicle noise*, aspects of unmanned aerial vehicle noise and various methods of noise reduction in propeller technology are explored. The tips of the propellers have a significant impact on the level of noise produced by the propellers. The shape of the blades controlled the formation of air vortices above the wingtips which were found to be a source of noise produced by the propellers. By altering the shape of the tips of the propeller blades, the airflow around the blades can reduce the formation of these vortices and reduce the noise produced by the propellers. The number of propeller blades was also found to contribute the noise produced. Traditionally, drone propellers are composed of two blades. However, the same amount of lift produced by two-bladed propellers can be replicated by propellers with a smaller diameter but larger number of blades. The reduction in the diameter of the propeller correlates to a slower wingtip speed. The speed of the wingtips is proportional to the noise produced by the propeller, therefore, as the diameter of the propeller decreases, the amount of noise produced also decreases (Miljković) (Marte et al.).

ANC methods applied to propellers were also explored in *Methods for attenuation of unmanned aerial vehicle noise*. In one explored ANC method, he used an array of 12 single-channel speakers arranged in a circle surrounding a single propeller. Each of the 12 speakers plays the same synthesized waveform at a 30-degree phase shift from the previous speaker in the array. In this setup, the noise produced by the propeller is cancelled as the propeller wings pass in front of each speaker. Another explored method of ANC is the use of a synchrophaser, which synchronizes the rotational speed and phases of a multi-propeller setup. In this method, the synchrophaser was implemented in a four engine C-130 aircraft with two propellers and was used to alter the phase of the second propeller relative to the first propeller. The noise produced by the second propeller cancels the noise from the first propeller. This setup was able to achieve a 3-5 dB reduction in noise. In this last explored ANC method, Miljković describes a method patented by RotoSub® technology, which is implemented for computer cooling fans, but a similar approach can be potentially implemented for drone propellers as well. By switching on and off the electricity flowing through a coil within the propeller frame, the magnetic fields produced interact with magnets placed inside the tips of fan blades. These brief interactions with the magnetic fields create slight modulations in the rotational movements of the blades, and thus, creates an anti-noise signal. Because this anti-noise signal originates from the target noise source itself, the speed and phase of the signal exactly matches the target.

A noise reduction method through spatial filtering was proposed by Wang et al. In this method a multi-microphone setup was implemented in order to localize and isolate the noise produced by the drone propellers. By determining the direction in which the noise is produced relative to a microphone, the resulting filter is further enhanced by being directionally aware. The spatial frequencies of both stationary and nonstationary drone noise were analyzed and measured against a normal frequency distribution using the kurtosis measurement. By combining both the direction of the noise as well as its spatial characteristics, a filter can be produced. This filter can be used while recording live recordings in order to reduce the noise and leave target sounds intact.

In *A software platform for noise reduction in sound sensor equipped drones*, a hybrid approach to drone noise reduction through both ANC and spectral subtraction was developed. In this method, a drone is equipped with two microphones. One microphone captures the target sound signals, such as speech, as well as the noise from the drone and its propellers. The other microphone captures only the drone noise signal. To reduce noise, first, ANC is applied by emitting an inverse signal of the drone only noise signal. This will reduce the drone noise to a certain degree. This interference is then captured and processed using a spectral subtraction filtering method to further reduce the drone's noise. The ANC method is applied first, because spectral subtraction methods tend to produce better results when the power of the frequencies within the frequency spectrum is weaker. While the effect of noise reduction in this method is observable in the real world, the effect of the spectral subtraction filtering is done programmatically and is not observable in the real world. This method was able to produce a reduced noise signal with a 67.5% similarity to the original target noise signal.

4. Exploration of Acoustic Noise from Drones

Acoustic noise can be defined as the propagation of pressure waves through a medium, such as air. Acoustic signals are composed of many complex characteristics that have significant impacts of the interactions of noise cancellation systems. During preliminary research, these characteristics were analyzed to better comprehend the design requirements for a noise cancellation system.

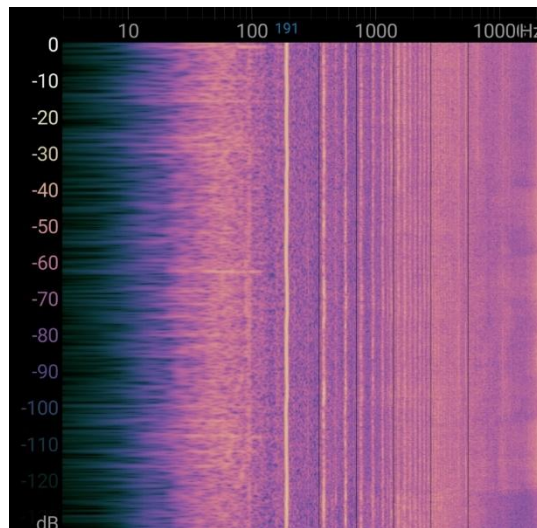


Figure 1: Spectrogram of Propeller Noise (obtained using the Spectroid application (Reinke))

4.1 Spectral Frequencies

By mapping the spectral frequencies of the drone propeller noise over time, the dominant and harmonic frequencies can be determined. In order to determine the spectral frequencies of the drone propeller noise, the drone propeller was mounted to a stand and operated at its maximum speed setting. Using the Spectroid application (Reinke), the drone propeller noise signal was recorded through the use of a mobile device's microphone, which was located approximately three feet away from the propeller. The noise was recorded over a length of ten seconds. The Spectroid application is able to display the spectral frequencies of the real time noise signal and determine the frequency with the largest amplitude, which is the dominant frequency of the noise signal. Figure 1 depicts the frequency spectrum of a ten second recording of the drone propeller noise. In this recording, the dominant frequency is 196 Hz, and its harmonic frequencies are multiples of 196. The strength of the harmonic frequencies relative to the dominant frequency as well as the number of harmonic frequencies are characteristics closely related to the waveform of the noise. A single frequency noise is composed of a simple sinusoidal wave. When multiple sinusoidal waves of varying frequencies and amplitudes are compounded, harmonic frequencies are produced. These compounding waves also contribute to the waveform of the noise as well.

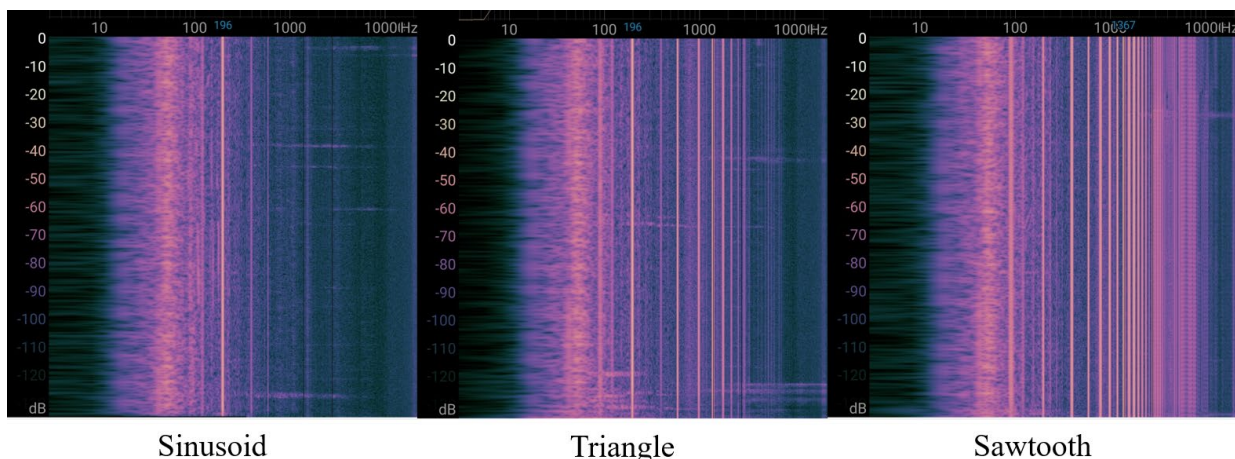


Figure 2: Spectral frequencies of sinusoid, triangle, and sawtooth waves

In Figure 2, the spectral frequencies of a sinusoid, triangle and sawtooth waveform playing a 196 Hz tone are shown. The sinusoid waveform generates a single dominant frequency at 196 Hz. The triangle waveform has a dominant frequency at 196 Hz as well as harmonic frequencies that are multiples of 196. However, there is a quick falloff in strength as the harmonic frequencies increase. A sawtooth waveform also has a dominant frequency at 196 Hz as well as harmonic

frequencies being multiples of 196, however, the falloff in strength of each of the harmonic frequencies is much slower.

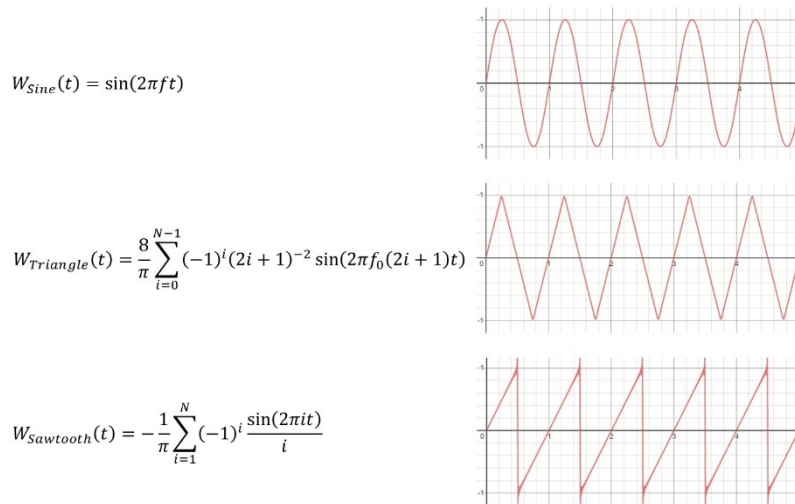


Figure 3: Time series equations used to approximate triangle and sawtooth waves

Although these waveforms have a single dominant frequency at 196 Hz, the observable loudness and noise are much different. These differences can be explained using the formulas that approximate these waveforms, as shown in Figure 3. Triangle waveforms are approximated using a compound of sinusoidal waves. These frequencies are multiples of the dominant frequency and the amplitude, which correlates to the strength of the signal, of each compounded sinusoidal wave is proportional to the inverse squared of the amplitude of the dominant frequency. The inverse squared relationship is the cause of the quick falloff in strength of the harmonic frequencies. Sawtooth waves are similar to triangle waves in that it is composed of compounded sinusoidal waves, however, each harmonic frequency has an inverse of the amplitude of the dominant frequency. This characteristic explains the slow falloff of the harmonic frequencies.

These approximations also contribute to the loudness of the noise as well. The number of harmonic frequencies as well as the falloff in strength correlates to the loudness of the overall noise. Each harmonic frequency can be considered its own noise source with a certain loudness, and the compounding of these noise sources will increase the overall loudness of the noise. Therefore, a noise signal with many harmonic frequencies is observably louder than a noise signal with few harmonic frequencies but the same falloff rate. Sawtooth waves must use a nearly infinite amount of harmonic frequencies in order to approximate its waveform, while triangle waves can be closely approximated with few harmonic frequencies. This explains why sawtooth waves are louder than triangle waves despite having the same maximum amplitude. To confirm this, a loudness of a triangle wave and sawtooth wave of 196 Hz and same amplitudes were compared. The triangle wave was observed to have a loudness of 97 dB, while the sawtooth wave was observed to have 111 dB.

The spectral frequencies of drone propeller noise are very similar to that of a triangle wave. Using this information, it is possible to generate anti-noise signals using triangle waveforms in order to target certain frequencies. This process is known as spectral subtraction. Spectral subtraction is able to reduce the strength of certain frequencies while ignoring other frequencies. This is useful for applications where a background noise needs to be reduced but a target noise, such as speech, can be preserved.

4.2 Interference Patterns

Acoustic pressure waves from different sources can be superimposed and interact. Acoustic noise is the propagation of periodic high and low pressure. When the noise from different sources interact, these high and low pressures are compounded. This is referred to as constructive and destructive interference. When similar pressures (high + high pressures or low + low pressures) interact, the resulting pressure becomes more intense than its individual components. This is constructive interference. During destructive interference, areas of differing pressures (low + high pressures) interact, and the resulting pressure is less intense than either of its original components. ANC utilizes destructive interference to cancel sound. The anti-noise signal used to cancel sound is generally an inverse of the target sound. The areas of high and low pressure in the target noise correlates to the areas of low and high pressure in the anti-noise signal, respectively. Another key component of ANC is the phase of the anti-noise signal.

4.3 Phase of Acoustic Noise

The phase between two or more noise signals is the alignment of each signal with respect to the corresponding points. In osculating signals, such as sinusoidal waves, these corresponding points are the peaks of each wavelength. The phase determines whether two signals experience constructive or destructive interference. In order to achieve destructive interference, the phase between two signals must be 180° . In order to achieve this, the polarity of one of the signals is inverted. However, small delays in a signal can also affect the phase between signals as well. ANC systems aim to minimize or eliminate delays and latency in order to minimize changes in phase when emitting the anti-noise signal.

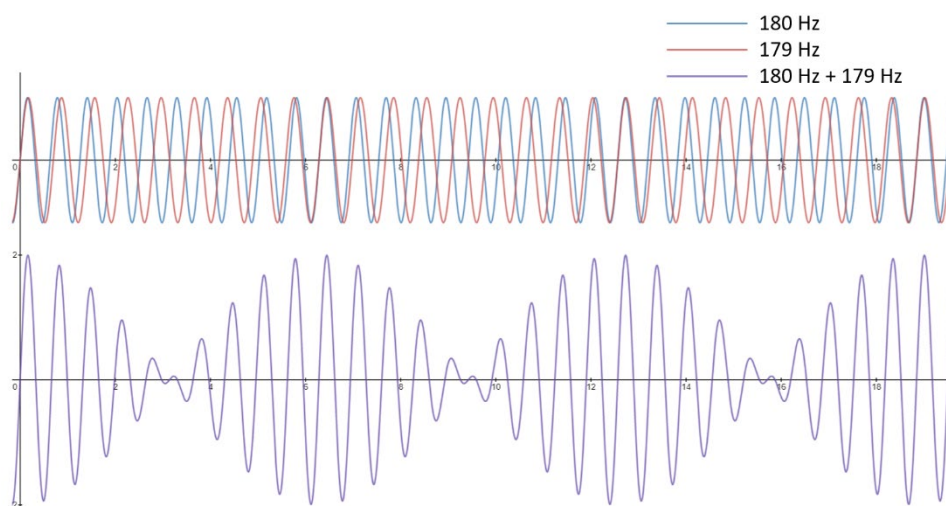


Figure 4: The interference pattern between signals of differing frequencies

While two signals with the same frequency do not experience changes in phase over time, when two signals have differing frequencies, the phase between the two signals will change over time. These changes in phase over time can be observed as oscillations in maximum amplitude over time. These oscillations are referred to as beats, the difference between the two frequencies are referred to as the beat frequency. In Figure 4, two sinusoidal waves of differing frequencies are superimposed, and the resulting wave experiences periodic points of total destructive interference.

Acoustic noise signals propagate in three-dimensional space in all directions, therefore, the interference between two signals can also be mapped in three-dimensional space. In Figure 5, the interference pattern between two signals of the same frequency is mapped in two-dimensional space. The cyan areas represent the destructive interference in which the noise signals are completely cancelled out. These areas also represent points in which the two signals have a phase of 180° . There are other regions in the mapping where the noise signals are not cancelled. This is due to the speed of sound affecting the time it takes an acoustic noise signal

to reach a location. This creates a delay which misaligns the phase of the signals. Because sinusoidal signals are periodic, the delay can realign the phase such that the peak of one signal is superimposed on the next peak of the other signal. In Figure 6, the interference pattern of two signals with differing frequencies is mapped. When two signals have differing frequencies, the phase between the signals changes over time. Because the rate in which the signal repeats is different between the signals, the superposition of the signals changes over time as the difference between wavelengths cause the phase to drift over time. In oscillating waves, the changes in phase will also oscillate, the signals will experience repeating periods of constructive and destructive interference.

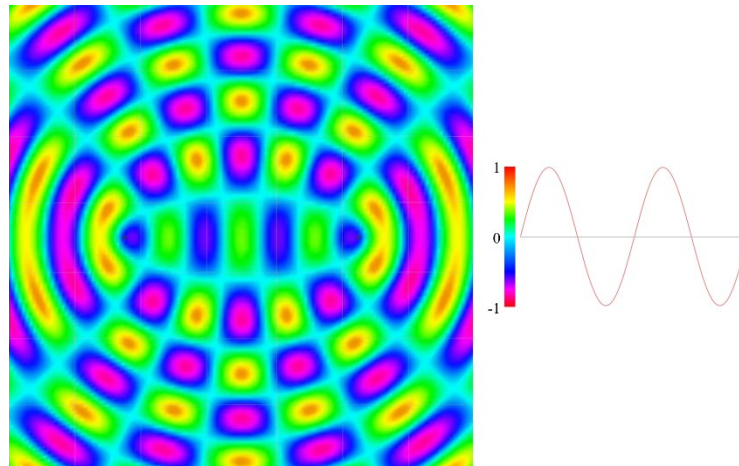


Figure 5: 2D mapping of interference between signals with the same frequency

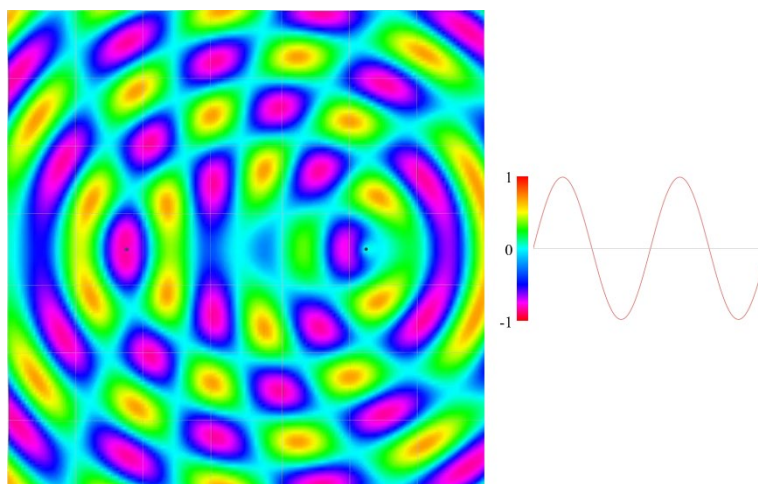


Figure 6: 2D mapping of the interference between 2 signals of differing frequencies

Methods for aligning phases rely on compensating for latency in an ANC system. However, the phase between oscillating signals can also be aligned if the signals have differing frequencies. Because phase alignment between signals of differing frequencies changes periodically over time, a phase of 180° can be predicted.

4.4 Waveform Filtering

In traditional ANC systems, the input noise signal is inverted and used as the anti-noise signal. While this method is effective at reducing the overall noise, it affects all sources of noise equally. In applications of ANC where the goal is preserving a target noise while reducing ambient noise, the input noise signal must be pre-processed or analyzed before an anti-noise signal can be produced. Many implementations of the ANC system incorporate a sophisticated filtering algorithm in order to target certain spectral frequencies. In order to successfully implement these filtering techniques, the hardware used must be able to handle such computationally expensive tasks.

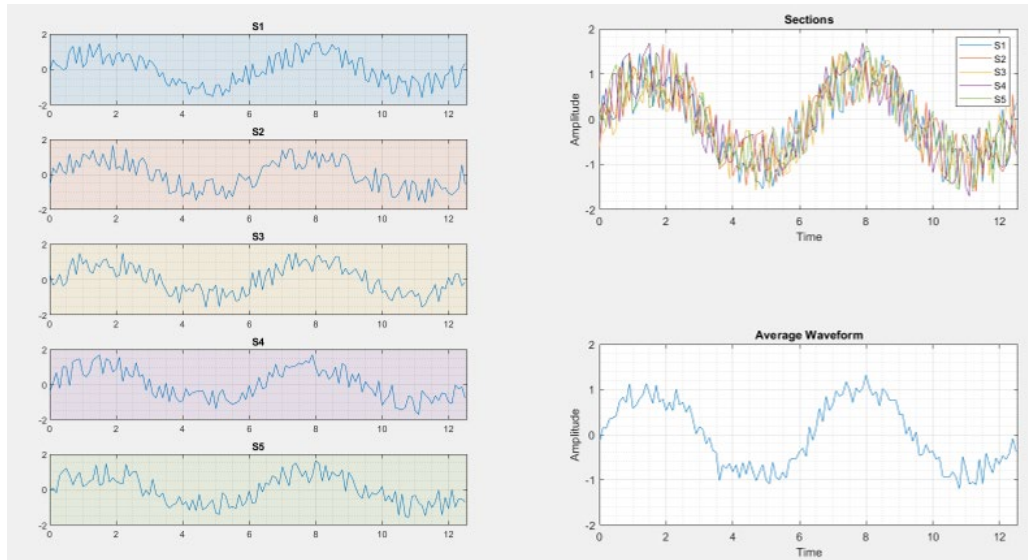


Figure 7: The averaged waveform is produced through from the original noise signal

The noise produced by a propeller, when the drone is stationary, is composed of highly repetitive waveform patterns. In order to use these waveform patterns, the errors in the signal (due to data noise) must be removed. Waveform averaging can take advantage of the repetitive nature of the propeller noise to filter out the noise data while obtaining the noise signal produced solely by the propeller. By superimposing the individual waveforms of a signal into a single wavelength, the corresponding individual points of data can be averaged. The nonrepetitive data, such as speech and ambient sounds, have a negligible impact on the average. The repetitive data produced by the drone propellers will converge to a single waveform that will represent the true waveform of the propeller noise. This is due the waveform of the propeller noise being present in the entirety of the noise signal. Once the averaged waveform is produced, it can be used as an anti-noise signal. Figure 7 illustrates this process. The colored sections represent the wavelengths of the original input noise signal. Superimposing these sections of data reveals the true nature of the waveform of the propeller noise.

This signal will contain the spectral frequencies of the propeller noise, therefore, it will only target frequencies similar to that of the propeller noise, leaving target noises unaffected. This process of waveform averaging is relatively computationally inexpensive and can also be parallelized to further increase computation speed. Also due to the repetitive nature of the propeller noise, the averaged waveform does not need to be continuously updated in order to accurately reduce the propeller noise. This averaged waveform will only need to be updated when the drone's propellers change the nature of its noise, or over a long period of time to avoid error due to phase drifting.

4.5 Preliminary Exploration and Experimentation

Traditionally, ANC systems will use the unfiltered inverted noise signal as the anti-noise signal to cancel the sound. In order to test the effectiveness of the traditional technique, the drone propeller noise was recorded, inverted, and emitted from a loudspeaker. When the noise produced by the drone propeller and the anti-noise signal emitted from the loudspeaker interacted, the superimposed signals were aligned such that the high pressure areas of one signal overlapped the low pressure areas of the other signal, creating destructive interference and reducing the strength of the resulting noise signals. The interference between the propeller noise and the anti-noise signal was able to achieve a reduction of 27.64%. However, this technique also achieved a 14.46% increase in noise as well. This was due to the lack of phase alignment techniques needed to produce destructive interference. Without a phase alignment technique, the phase between the noise and anti-noise signals may produce constructive interference which will

increase the overall level of noise. In traditional ANC systems, phase alignment techniques are implemented using delayless signal transferring methods which allows a system to immediately emit the anti-noise signal and eliminate any changes in phase. While this may be practical for unfiltered anti-noise signals, filtered anti-noise signals must also implement a delayless filtering algorithm in order to minimize the computation time and change in phase between the two signals.

During early exploration of the waveforms, the waveform of the drone propeller noise closely resembled the triangle waveform, however, due to a high level of noisy data, it was difficult to determine any compounded waveform structures hidden within the noise. A triangle wave with the same dominant frequency was used as the anti-noise signal against the drone propeller noise. This method was able to achieve up to 4% reduction in overall level of noise. While the failure of this method was partially due to the lack of a phase alignment method, this method also made the true nature of the propeller noise waveform apparent. The waveform of the drone propeller noise resembled a triangle wave; however, it was also slightly skewed and slightly resembling a sawtooth wave. It was determined that this phenomenon was a result of rotational Doppler shifting caused by the high rotational speed of the propeller blades. As the propeller approaches a high rotational speed, the pressure ahead of the propeller blade experiences a sharp pressure gradient, while the pressure behind the propeller blade experiences a gradual pressure gradient. These differing pressure gradients correlate to a skewed waveform, which may increase the strengths of the harmonic frequencies as the waveform approaches a form similar to that of a sawtooth waveform. Through this experiment, it was determined that the waveform approximation algorithm must take into account the rotational speed of the propeller to better adapt to rotational Doppler shifting.

5. Design

The proposed system was tested using a single propeller in order to test its effectiveness. The propeller is attached to a three-phase brushless motor, which is mounted to a stand. A Raspberry Pi, controlled over a Wi-Fi connection, is used to control the rotational speed of the motor (Raspberry Pi). A Bluetooth speaker attached to a tripod is used as the loudspeaker that emits the anti-noise signal. A microphone, attached to a stand, is used as the primary microphone as well as the error microphone. The propeller, loudspeaker, and microphone are arranged such that the speakers are located 30 inches apart, and the microphone is located 45 inches from each of the speakers. This setup is located in a sound booth lined with sound insulating foam, which prevents reverberations from flat surfaces. The PA-ANC system was developed using MATLAB in order to take advantage of its audio and signal processing toolkits (MATLAB).



Figure 8: The setup of preliminary experiments includes a microphone, blue speaker (unaltered) and a red speaker where the polarity of the input signal is hardwired. In the PA-ANC

experiments, the red speaker is replaced by the drone propeller, which is mounted to a stand, and the Raspberry Pi controlling it is also mounted to the stand.

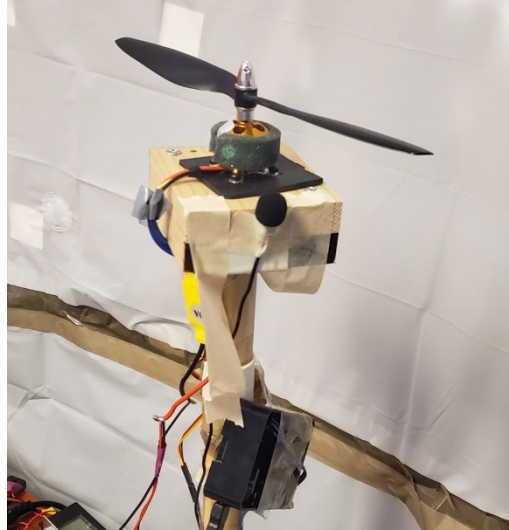


Figure 9: Drone propeller and Raspberry Pi mounted to the stand

Figure 8 depicts the sound booth in which the experiments were conducted. The propeller in Figure 9 replaces the red speaker during experimentation. In future implementations, the system will experiment with a multi-propeller drone capable of flight.

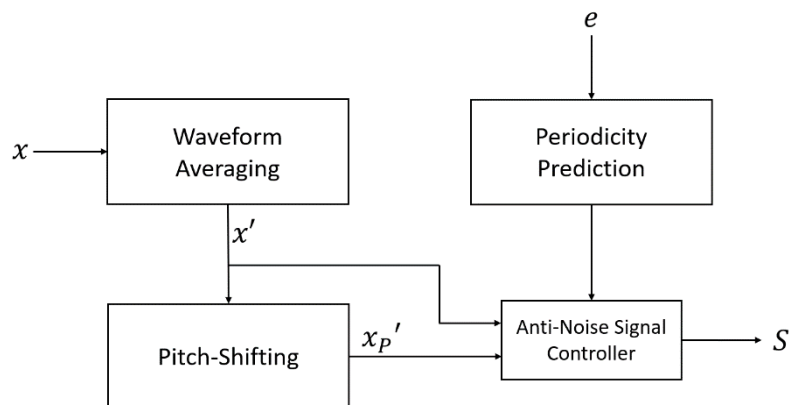


Figure 10: System design of the PA-ANC system

In Figure 10, the system design is illustrated. The proposed PA-ANC system is designed as a feed-forward configuration. x represents the input noise (propeller noise). The input is analyzed by the waveform averaging algorithm, and the averaged waveform x' is transferred to the anti-noise signal controller and the pitch-shifting algorithm. After the anti-noise signal is pitch-shifted, it is then transferred to the anti-noise controller. The error signal e is analyzed by the periodicity prediction algorithm which controls the anti-noise signal controller. The anti-noise signal controller determines if the output signal S is the averaged waveform x' or the pitch-shifted averaged waveform x'_p .

6. Experiment and Results

Experimental results demonstrated that the pitch-shifting method successfully produced patterns of constructive and destructive interference when played against the drone propeller. At points of maximum destructive interference, this method was able to reliably achieve 20-40% reduction in noise from the overall noise produced by the drone propeller.

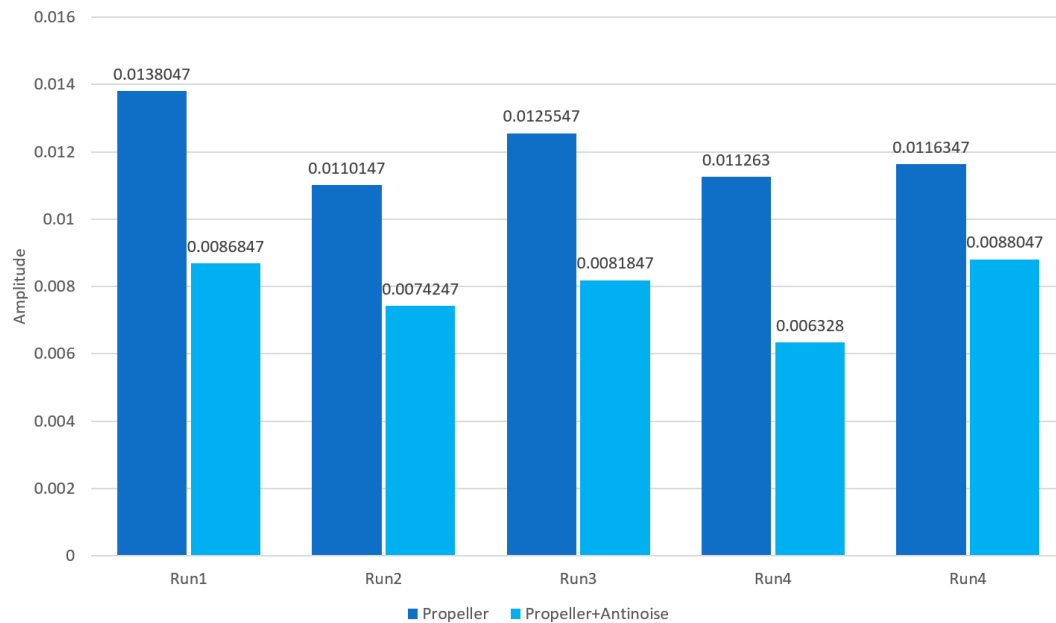


Figure 11: The averaging amplitude of the propeller noise signal compared to the lowest amplitude measured from the PA-ANC system

Figure 11 illustrates the results of the PA-ANC system during five runs of the experiment. The PA-ANC system achieved its highest level of noise reduction of 43.82% during Run4 and its lowest level of noise reduction of 24.32% during Run5 at its lowest point of maximum destructive interference when compared to ambient levels of noise. The pitch-shifting alignment strategy was able to reliably align the anti-noise signal against the propeller noise signal to reliably favor destructive interference.

The waveform averaging algorithm was able to produce an anti-noise signal that had high similarity to the recorded drone noise. It was also able to successfully smooth out the ambient noise and recreate the waveform produced solely by the propeller. During the tests of the PA-ANC system, the averaged waveform proved to be effective as it was able to significantly reduce the level of noise produced by the propeller.

The periodicity algorithm was able to accurately predict the periods of maximum destructive interference in linear noise signals (signals with static dominant frequencies), however, due to slight changes in the rotational speed of the propeller, interference patterns changed drastically and unpredictably. In practice, the prediction algorithm performed poorly to predict a future point of destructive interference.

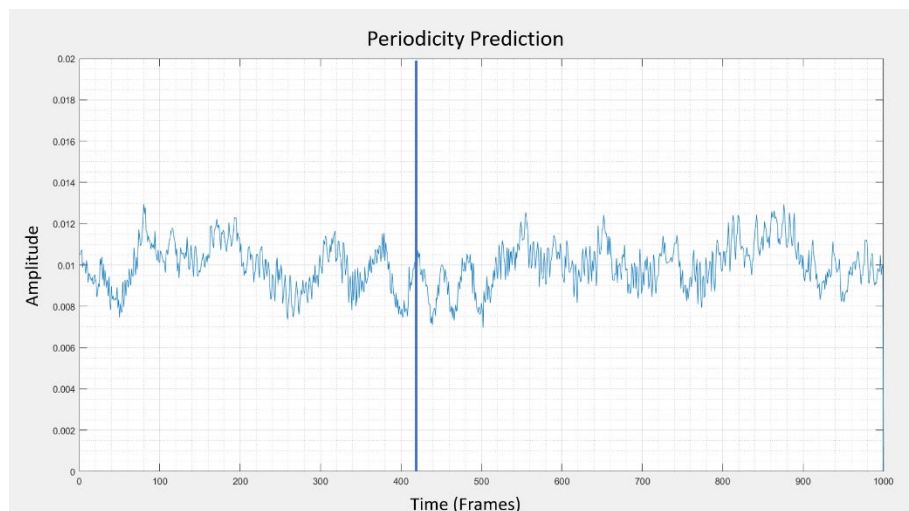


Figure 12: Recorded interference pattern before and after switch at frame 421

As an alternative, the system will find a minimum amplitude and shift the pitch when the current amplitude is less than the minimum measured value with a tolerance of 5%. This alternative algorithm performed well in practice. In Figure 12, the alternative algorithm was able to pitch shift at a point of maximum destructive interference. It is apparent that the propeller is changing frequencies, as the distance between any two consecutive points of interference differ greatly, this alternative algorithm provides a reliable, computationally inexpensive method to determine at what point to shift the pitch of the anti-noise signal.

In order to compare the effectiveness of the PA-ANC system, various benchmarks were implemented. The effectiveness of the PA-ANC system was compared to traditional ANC techniques as well as a control test of the PA-ANC system using generated tones.

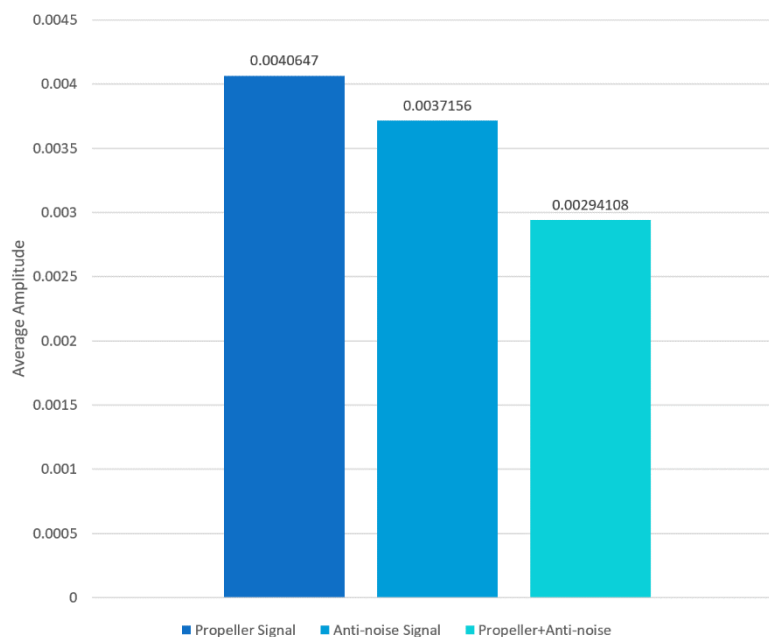


Figure 13: Noise reduction between propeller and unfiltered anti-noise signals

Traditional ANC systems use the unfiltered drone noise signal as the anti-noise signal. As a baseline measurement of the effectiveness of ANC systems on drone propellers, the traditional ANC technique was implemented and tested against the drone propeller. In the first experiment, the anti-noise signal was a one-minute recording of the drone propeller noise. The recording was inverted and emitted from a loudspeaker located 45 inches from the propeller. The interference was then recorded, and the average amplitude of the interference was determined. Using this method, a 27.64% reduction in noise was observed as seen in Figure 13.

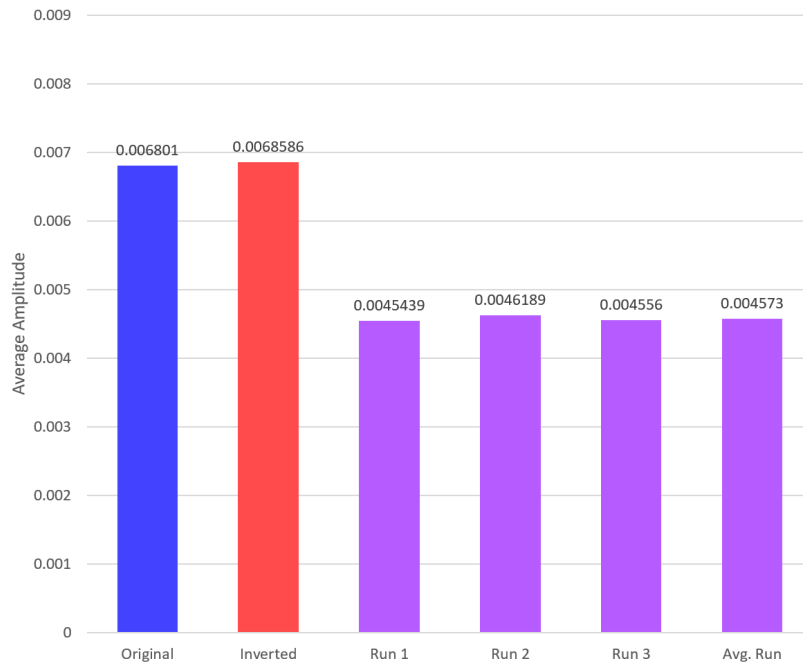


Figure 14: Noise reduction of traditional ANC using speakers

The traditional ANC system was then implemented using two speakers. One speaker, used instead of the propeller itself, emitted the recorded drone propeller audio signal in order to replicate the noise produced by the drone propeller. The other speaker was altered such that the polarity of the input signal is reversed. This speaker will emit an inverted noise signal relative to the input signal, therefore, this speaker is used as the anti-noise speaker. Figure 14 displays the results of 3 runs of this experiment. This ANC method was able to achieve a 33.47% reduction in noise level. This experiment was used in order to measure the effect of noise reduction on the same signal and measure the expected level of noise reduction on linear signals.

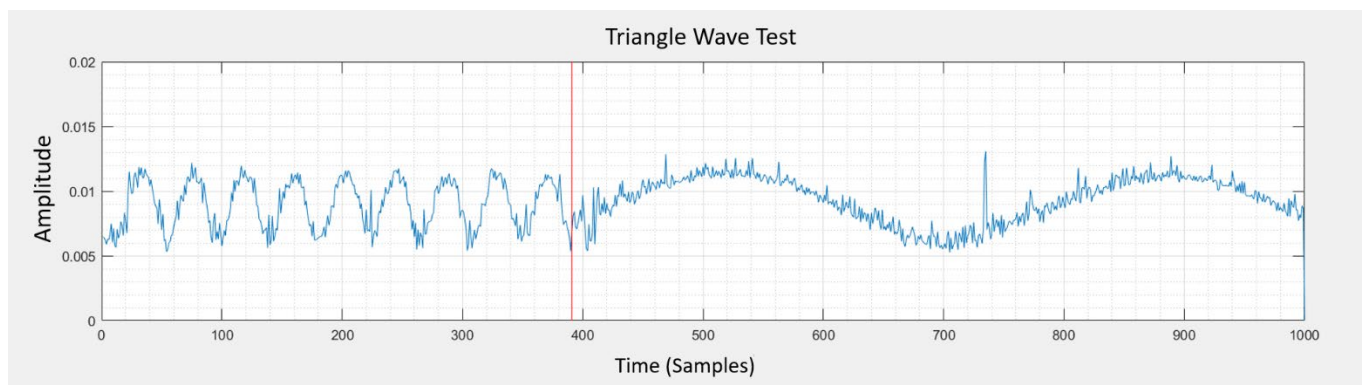


Figure 15: PA-ANC system tested against 186 Hz Triangle wave

As a benchmark of the PA-ANC system's performance against drone propeller noise, this system was tested using a 186 Hz triangle wave signal. The PA-ANC relies on the dominant frequency of a noise signal. If the noise signal is linear in nature, the system should perform exceptionally well to reduce the noise. In Figure 15, the periodicity of interference increases significantly after the anti-noise signal is shifted back to its original pitch. As the periodicity increases, the difference between of pitch between the anti-noise and propeller noise signals decrease. The original pitch of the anti-noise signal must differ very slightly to the pitch of the noise due to the observed interference pattern after the shift to the original pitch. This may be due integer window size computed in the waveform averaging algorithm. The pitch of a noise signal can have a non-integer wavelength. When playing the anti-noise signal, a drift in phase occurs. This effect can be observed over relatively long periods of time.

7. Conclusions

Drone noise further exacerbates the issue of noise pollution. While noise pollution can have negative effects such as overpowering and ruining audio recordings, it may also contribute to the negative mental and physical illnesses linked to noise pollution such as fatigue, hearing loss, and hypertension. The proposed PA-ANC system aimed to solve this problem by implementing methods of spectral analysis and active noise cancellation to reduce the overall noise produced by a drone propeller. By isolating the dominant frequencies of the propeller noise and phase-shifting a generated anti-noise, this method of noise control was able to achieve a 43.82% reduction in noise.

While this reduction in noise could not be sustained, these experiments revealed the characteristics of drone propeller noise signals and highlighted key features that may improve the effectiveness of future ANC systems. Harmonic frequencies contribute largely to the observed loudness of a noise signal. The waveform of the noise signal determines the number and strength of the harmonic frequencies and, therefore, the observed loudness of the noise. Periodic signals, such as the drone propeller noise signal, can be approximated by averaging the wavelength of the noise signal, and by using the generated waveform as the anti-noise signal, the spectral frequencies of the drone propeller noise can be targeted and reduced. The waveform averaging algorithm was able to accurately reproduce the true nature of the noise produced by the drone propeller by smoothing the noisy data from the input signal and preserving the waveform of the propeller noise signal. Pitch-shifting the anti-noise signal presented an effective method of aligning the phase of the signals by relying on the produced beat frequency in order to predict the points of maximum destructive interference and maximum the noise reduction effect.

Future improvements to this system will incorporate factors such as hardware specifications as well as parallel computing in order to reduce latency of certain computations and allow the system to better adapt to changes in noise over time. The use of software or hardware that supports dynamic sampling rates may also reduce the latency of the system by eliminating the need to resample the anti-noise signal and, instead, instantly change the sample output rate. A dynamic sampling rate may also facilitate continuous updating after aligning the phase in order to sustain the noise reduction effect. Periodic updating of the averaged waveform as well as continuous error signal checking may also improve the effectiveness and robustness of the PA-ANC system.

References

Reinke, C (2018) *Spectroid*

Christian, A and Cabell, R (2017) *Initial investigation into the psychoacoustic properties of small unmanned aerial system noise* Jnl 17th AIAA Aviation Technology, Integration, and Operations Conference (AVIATION 2017)

Lifei, J (2010) *A design of an adaptive active noise control system in driver's cab* Jnl 2010 The 2nd International Conference on Computer and Automation Engineering (ICCAE) 3, 560-563

Kang, B and Anh, H and Choo, H (2019) *A software platform for noise reduction in sound sensor equipped drones* Jnl IEEE Sensors Journal 19(21), 10121-10130

Kottayi, S and Althomali, R and Thasleema, T M and Narayanan, N K (2016) *Active noise control for creating a quiet zone around mobile phone* Jnl 016 International Conference on Communication and Signal Processing (ICCSP), 73-77

Liang, J and Zhao, T and Zou, L and Zhang, L and Li, Z (2015) *Adaptive active noise control system of power transformer* Jnl 2015 Fifth International Conference on Instrumentation and Measurement, Computer, Communication and Control (IMCCC), 1394-1397

Marte, J E and Kurtz, D W (1970) A review of aerodynamic noise from propellers, rotors, and lift fans Technical Report

MATLAB (2018) *The MathWorks Inc.*

Miljković, D (2018) *Methods for attenuation of unmanned aerial vehicle noise* Jnl 41st International Convention on Information and Communication Technology, Electronics and Microelectronics (MIPRO), 914-919

Mohamud, A and Ashok, A (2018) Drone noise reduction through audio waveguiding Jnl 4th ACM Workshop on MicroAerial Vehicle Networks, Systems, and Applications, DroNet'18, 92-94

Raspberry Pi (2017) *The Raspberry Pi Foundation*

Rotherhan, F (2016) *Kiwi startup dotterel wins innovation award for noise reduction drone technology*

Tansel, I and Uragun, B (2014) *The noise reduction techniques for unmanned air vehicles* Jnl 2014 International Conference on Unmanned Aircraft Systems, 800-807

Wang, L and Cavallaro, A (2018) Acoustic sensing from a multi-rotor drone Jnl IEEE Sensors Journal 18(11), 4570-4582



QUIET DRONES
International e-Symposium
on
UAV/UAS Noise
Remote from Paris – 19th to 21st October 2020

‘The Sound of the Drone Uprising’

An Exploration of the Aero-acoustic Performance of Drone Blades

Josephine Nixon, London South Bank University jn1828@my.bristol.ac.uk

Stephen Dance, London South Bank University dances@lsbu.ac.uk

Abstract

This study considers the acoustic emission from a Dji Phantom 4 commercial drone using different rotor blades. Measurements were taken from a hovering drone with four blade configurations. Three blades were commercial products and one was designed and built specifically for this drone. Measurements were taken in accordance with (BS) EN ISO 3741: 2010 ‘Acoustics – Determination of sound power levels and sound energy levels of noise sources using sound pressure – Precision methods for reverberation test rooms’. The aim of the project was to reduce the sound emission level of the drone, whilst still allowing the drone to fly and hover. The results show that it is possible to reduce sound emission and tonality by altering the blades but flight performance can be affected in terms of duration (flight-time).

Introduction:

Drones have become increasingly common in our skies and have both recreational and commercial use. Existing research has tended to focus on health, safety and security, (Finn *et al*:2012, Clarke *et al*:2014, BBC:2019) with a limited amount of research being undertaken on the acoustics of drones (Intaretep: 2016, Bown:2018, Oecket *et al*: 2018). This study considers the acoustic emission from a Dji Phantom 4 commercial drone using different rotor blades. The study aims to reduce the sound emission level of the drone, utilising four different blade configurations.

The Drone and Blade Design:

A DJi Phantom 4 drone was utilised, a 'high end' drone designed for recreational use. It weighs 1380g and has a diagonal dimension of 350mm and uses four rotate blades each with a 234mm diameter (Dji:2019), see Figure 1. The Phantom 4 drone is usually sold with the original quick release blades.



Figure 1 – Dji Phantom IV Drone

Aerodynamic noise is very strongly dependent on airflow speed. Two important areas when looking at aerodynamic noise within aeroacoustics is the blade passing frequency and the proportionality of airflow to noise emissions.

The blade passing frequency is important as this determines any fundamental tones and harmonics from a blade. The blade passing frequency (BPF) is the fundamental frequency, f_0 , created by the number of times a blade passes a particular point, equation 1:

$$f_0 = N * \text{RPM} / 60 \quad (\text{Equation 1})$$

Where N is the number of blades.

Research, such as Klei et al: 2014, Pechan et al: 2015 and Muller et al: 2014, amongst others have looked at the frequency spectrum produced in relation to blades from aircraft. The shape of the blade and speed at which it travels can affect the noise emission. The quicker the blade spins, the more turbulence the blade tip would cause. The speed or velocity of the wing tip affects the noise emission from the blades; it is an interlinked relationship. The shape of the blades prop, could therefore impact the speed in which the rotor has to turn to ensure the drone hovers

The excessive noise, E, created by changing the design of the blade is given by equation 2.

$$E = 10 \lg \left(\frac{V}{V_0} \right)^6 \quad (\text{Equation 2})$$

Where V is the velocity of the new blade tip (m/s), V_0 is the blade tip velocity of the original blade (m/s).

The noise emission level was measured with the following blades fitted: original quick release blade, quick release blades with shaped props, altered quick release blades and carbon fibre blades, see Figures 2,3,4,5 respectively.



Figure 2 – Photograph of Original Blade



Figure 3 – Photograph of Blade with Shaped Props



Figure 4 – Photograph of Altered Blade



Figure 5 – Photograph of Carbon Fibre Blade

Three of the blades types are available on the commercial market; the exception is the altered blade. The blades with shaped props have been sold as a low noise propeller by DJi and tend to be fitted to the more modern Mavic Drone. The carbon fibre blades are sold as a quiet option by a third party manufacturer.

The thicker the blade the more resistance there would be through the air, increasing air turbulence, vibration and thus noise. Leslie et al: 2008 explored the possibility of broadband noise reduction through boundary layer tipping from a mini UAV / Drone. They considered the blades tonal components and concluded “these tones are manifesting themselves as a large broadband hump due to the range of velocities across the propeller range.” (Leslie et al: 2008).

Intaretep et al: 2016 explored four different commercially available propeller configurations for a DJi Phantom 4 drone, along with their rotors and concluded that “[t]he acoustic spectra of the Quadcopter is dominated by high and sustained noise at the blade passing frequency and shaft rate and their harmonics up to the mid frequency range” (Intaretep et al:2016). The blade shape was noted to remain the same; however, different materials were used (e.g. white carbon, original plastic, black carbon). The shape and size of the blade will be to determine if this impacts the tonality or sound emissions.

According to a recent study by NASA, the noise made by roads traffic was “systematically judged less annoying” than the high-pitched buzzing made by drones” (Bown: 2018). The blade design expands on Leslie et al: 2010 argument by looking at the level and type of noise emitted in relation to the shape, material, size/dimensions (length and width) and weight of the blades. The simplest method to assess the sound emissions is determining the sound power level produced.

The altered blade has electrical tape layered over the surface as smoothly as possible and are shaped to take on a toothmark / v-shape edge, like modern jet engines and stealth fighters. The design follows research for a quieter blade.

Figure 6 provides the Blade Specification and dimensions:

Blade Type	Weight (g)	Material	Max width (mm)	Blade length (mm)	'Known as'
Quick Release Original	42	Coated Smooth Plastic Surface	30.8	236	Original
Quick Release Shaped	44	Coated Smooth Plastic Surface	32.2	238	Shaped
Quick Release Altered	49	Electrical Tape on Plastic Surface	36.4	236	Altered
Carbon Fibre	56	Smooth Carbon Fibre	30.8	234	Carbon Fibre

Figure 6 – table of Blade Specification

Methodology:

The free-field method to determine sound power, as prescribed in BS EN ISO 3745: 2012 (*Acoustics – Determination of sound power levels and sound energy levels of noise sources using sound pressure – Precision methods for anechoic rooms and hemi-anechoic rooms*), could not be undertaken due to constraints by the available anechoic chambers construction. To fly unassisted the drone requires a compass, GPS Signal or Signalling Point. These signals are blocked within the anechoic chamber due to the mass of the wall construction and amount of steel in the chamber design. Previous research (Nixon: 2017) tried to undertake measurements within the anechoic chamber, but the drone was unstable, flipping over and breaking the blades on the grated floor. This was caused by a lack of signal, which automatically forced the drone to land as a safety measure.

The testing methodology selected was (BS) EN ISO 3741: 2010 '*Acoustics – Determination of sound power levels and sound energy levels of noise sources using sound pressure – Precision methods for reverberation test rooms*'. The reverberation chamber was utilised as the drone could locate a reference/signalling point to enable it to fly and hover. Three 1/3 octave band measurements of the drone hovering for 30 seconds were undertaken for each blade type. These values were then averaged for each blade type investigated. Six class 1 sound level meters, NTi XL2, were used to take the measurements. Four were located at 1.6m distance at hover height (1.2m high). The remaining two SLM's were located above and below the drone using extension cables. An FFT was also taken per blade type using another sound meter.

Background and reverberation time measurements, T_{20} , were then undertaken under identical conditions. Reverberation time was taken in five positions using two different sound source locations in accordance to ISO 3382-2. The sound source used was a floor mounted hemi-dodecahedron producing interrupted pink noise.

Results:

The average sound pressure results per blade type can be seen in figure 7. The amount of sound can be seen to change per blade type with the quick release and carbon fibre blades generally producing the highest sound levels. The altered blades can be seen to be more dominant in the lower frequencies at 80Hz and 125Hz.

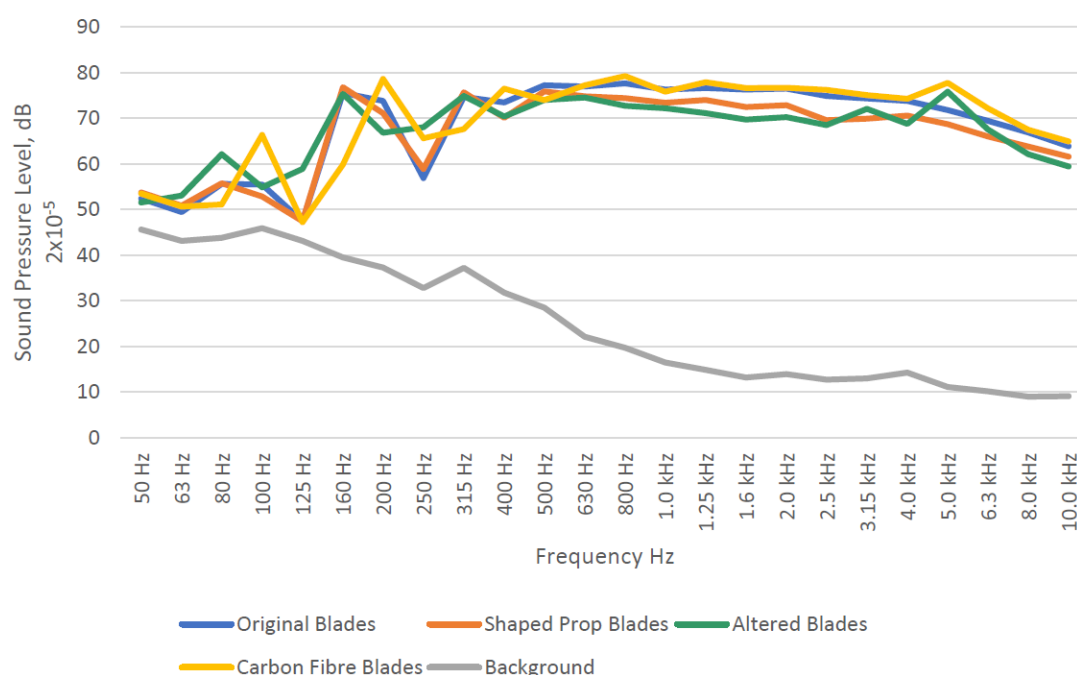


Figure 7 - Averaged 1/3 Octave Sound Pressure Levels per Blade Type for the Phantom 4 in a hover

Figure 8 illustrates the averaged measured 1/3 octave reverberation times in the occupied reverberation chamber.

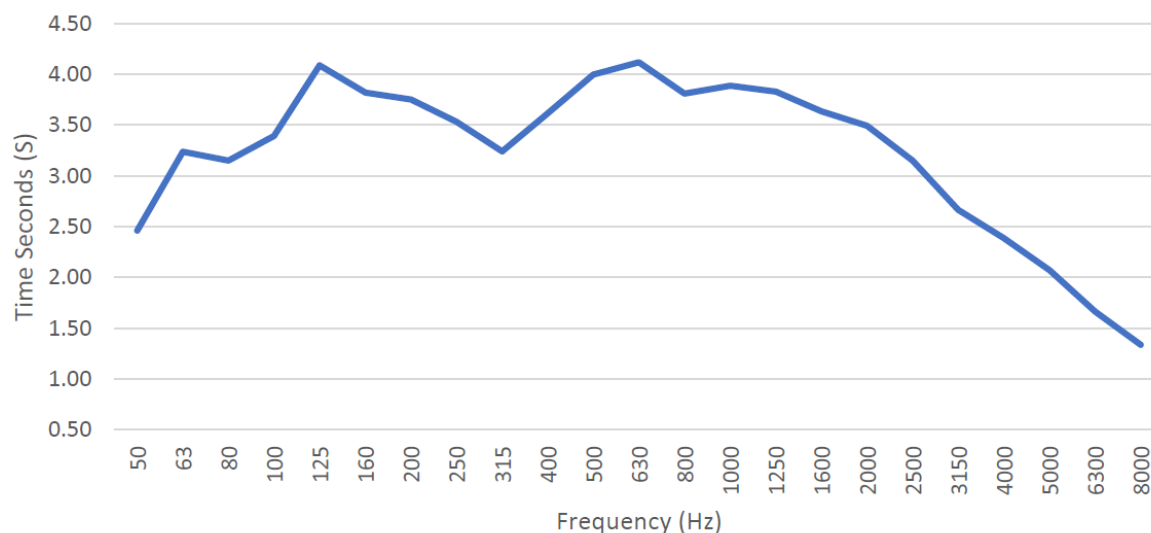


Figure 8 – Averaged Reverberation Time, T20 in the Occupied Reverberation Chamber

The sound power level was determined per blade type from the sound and reverberation measurements, and is shown in figure 9. The Carbon fibre blades were found to be the loudest. Both the shaped prop blades and Altered blades were quieter than the Original blades.

	LWz	LWA
Original Blades	84.6	83.7
Shaped Prop Blades	82.3	80.6
Altered Blades	81.7	80.0
Carbon Fibre Blades	85.4	84.6
Background Noise	45.6	28.8

Figure 9 – Calculated Average Sound Power Levels of the Drone per Blade Type

The Altered blades were the quietest with the lowest emission with a 3.7dB A-weighted sound power level reduction from the Original blade valves.

Discussion:

From figure 7 it can be seen that all blade types appear to be broadband in nature but that specific peaks can be seen for the different blade types at certain frequencies, indicating a possible presence of tonality. Significant noise emission is noted (figure 7) to occur at 160 Hz for the plastic blades (Original, Shaped and Altered) and 200 Hz, the next 1/3 octave band, for the Carbon fibre blades. At 250 Hz there was a significant dip in sound emission for the Original and Shaped blades that was lessened by 10 dB for the Altered Blades, this dip was also present for the Carbon fibre blades again at the next 1/3 octave band. This more balanced sound spectra for the Altered blades produced less noticeable tonality than for the other blades.

Subjective and objective tonality was assessed in accordance with BS 4142: 2014 +A1: 2019. Subjectively, the Altered blades were unanimously agreed to be the quietest by those undertaken measurements. The most tonal were the Carbon fibre blades.

One of the BS4142 recommended objective methods is to look for peaks in the spectrum, see Figure 7. No significant peaks were found in the spectrum for the Original blades or for the Shaped blades. Certain frequencies, however, are noted as dominant for the Carbon fibre and Altered blades. Once assessed using the objective method the carbon fibre blades were found to be tonal.

Finally, an FFT is an alternative approach to explore the relationship of tonality and blade types. Figure 10 shows the results of the FFT's for all blade types.

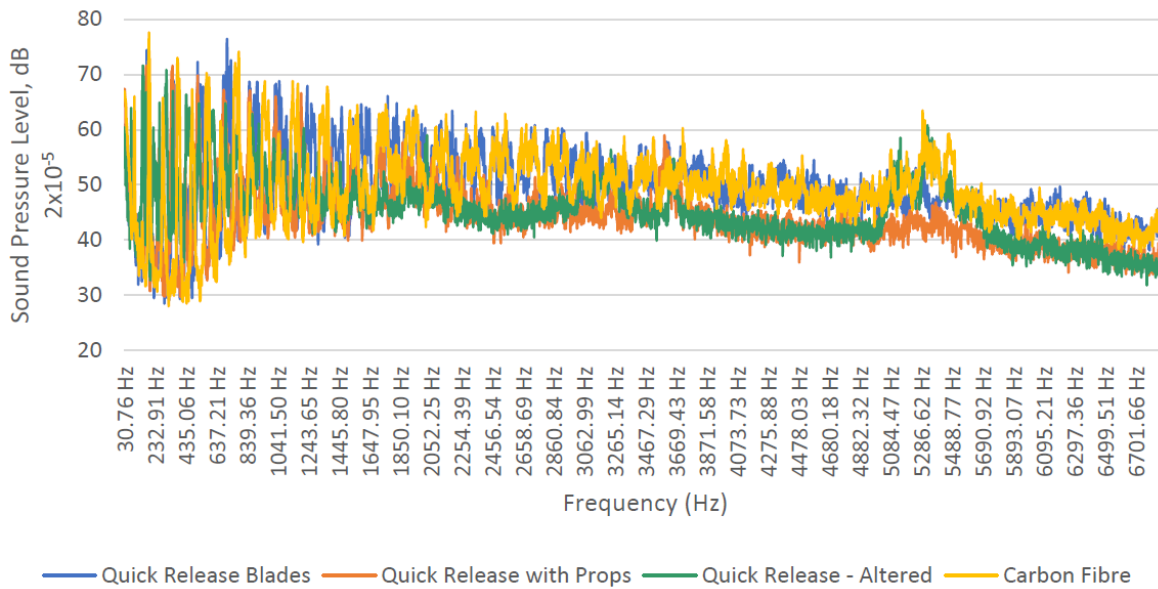


Figure 10 – FFT per Blade Type

From figure 10 it can be clearly seen that the Altered blade (green line) was significantly lower in the mid-high frequencies with a lowered fundamental frequency, 151 Hz. The Original blade had a 177 Hz fundamental frequency, the Shaped prop blade had a fundamental frequency at 171 Hz and the Carbon fibre blade the highest fundamental frequency of 190 Hz. Harmonics of the fundamental frequency can also be seen from figure 10.

Using equation 1 it is possible to calculate the rotor speed per blade type based on the fundamental frequency. By calculating the RPM, whilst the drone hovers, the work rate of the motor was found. The lower the RPM the more lift the blade was producing, but the harder the motor must work. This was observed by touching the motor after the hovers were completed. The Altered blade were by far the hottest to touch.

Using the blade dimensions given in figure 6, the blade tip velocity was calculated. The excess sound produced by the blade due to air turbulence could be calculated using equation 2. Figure 11 provides the calculated blade rotation rate, blade tip velocity and excess sound per blade type.

	Rotation Speed (RPM)	Blade Tip Velocity (m/s)	Excess Sound (dB)
Original Blades	5310	65.58	n/a
Shaped Prop Blades	6130	63.90	-0.67
Altered Blades	4530	55.95	-4.14
Carbon Fibre Blades	6700	69.80	1.63

Figure 11: The blade rotation rate, blade tip velocity and excess sound emission per blade type

The predictions based on blade tip speed closely agreed with the measurement of the fundamental sound emission for the different blade types, see Figures 9 and 11. A reduction of 3.6 dB was achieved compared to a prediction of 4.1 dB for the Altered blades.

To summarise, the quietest blades were noted to be the Altered blade even when considering penalties for tonality. The Altered blades were 3.6dBA quieter than the Original blade. This could be due to a number of factors, such as the additional lift created by the larger surface area, which allow the blade to rotate more slowly but create the same amount of lift force, the v-cut teeth smoothing the airflow and hence help create less turbulence.

Conclusion:

In conclusion, this study considers the acoustic emission from a recreational Dji Phantom 4 drone with various different rotor blade types fitted. The study aimed to reduce the sound emission level of the drone, by evaluating each blade type. The rotation speed of the blade was found to be the determining factor for sound emission and this would be the optimisation criteria for acoustic emission in future blade designs. The quietest blade measured is the Altered blade, which was 3.6dBA quieter than the Original blade. The motors on the drone were noted to be significantly hotter after the three consecutive 30 second flights when the Altered blades were fitted. The increased heat will have taken power so it is likely that this could compromise the maximum flying time of the drone.

References:

- (BS) EN ISO 3741: 2010 'Acoustics – Determination of sound power levels and sound energy levels of noise sources using sound pressure – Precision methods for reverberation test rooms'.
- BS EN ISO 3745: 2012 'Acoustics – Determination of sound power levels and sound energy levels of noise sources using sound pressure – Precision methods for anechoic rooms and hemi-anechoic rooms'.
- BBC (2019), Coventry City Council set to ban Drones, <https://www.bbc.co.uk/news/ukengland-coventry-warwickshire-46751423>, published 3/1/2019 accessed 27/01/2019
- Bown, Jessica (2018), Why your pizza may never be delivered by drone, Technology of Business Reporter, BBC news <https://www.bbc.co.uk/news/business-46483178>, published 14/12/2018 accessed 27/01/2019
- Clarke, Roger, (2014), Understanding the Drone Epidemic, Computer Law and Security Review 30 (2014) p230-246

- Finn, Rachel L., and Wright, David (2012), Unmanned Aircraft Systems: Surveillance, Ethics and Privacy in Civil Application, Computer Law and Security Review 28 (2012) p184 – 194.
- Intaratep N., Alexander W. N., Devenport W. J., Grace A. M., and Dropkin A., (2016) Experimental Study of Quadcopter Acoustics and Performance at Static Thrust Conditions, American Institute of Aeronautics and Astronautics, Aeroacoustics Conferences (22nd AIAA/CEAS) 30 May – 1 June 2016, Cross Mark AIAA 2016-2873 Lyon, France
- ISO 3382-2: 2008 Measurement of room acoustic parameter – Part 2: Reverberation time in ordinary rooms Geneva, Switzerland
- Leslie A., Wong K. C., and Auld D., (2008), Broadband Noise Reduction from a Mini-UAV Propeller through Boundary Layer Tripping, Acoustics and Sustainability: How Should Acoustics Adapt to Meet Future Demands? AAS 2008, 24-26 November, Geelong Australia
- Leslie A., Wong K. C., and Auld D., (2010), Experimental Analysis of the Radiated Noise from a Small Propeller, Proceedings of 20th International Congress on Acoustics, ICA 2010, 23-27 August 2010 Sydney, Australia
- Klei, Christine E., Buffo, Rainer M and Stumpf E. (2014), Effects of Wing Tip Shaping on Noise Generation, InterNoise 2014 Conference, Melbourne, Australia, Institute of Aerospace Systems, RWTH Aachen University, Germany.
- MilijkoVIC Dubravko (2018), Methods for Attenuation of Unmanned Aerial Vehicle Noise, DOI: 10.23919/MIPRO.2018.8400169
- Nixon J., (2017), 'Attack of the Drones! Noise Impact from Recreational Drone use in a Rural Area, Roxwell', London South Bank University, Diploma thesis
- Oeckel Konrad, Heimann Jan, Kersscher Michael, Angermann Sven, Heilmann Gunnar (2018), Comparative Acoustic Examination of UAV Propellers, Inter-Noise 2018 26-29 August, Impact of Noise Control Engineering,
- Pechan T. and Sescu A.(2015), Experimental Study of Noise Emitted by Propeller's Surface Imperfections, Applied Acoustics, 2015 Issue 92, p12-17



QUIET DRONES
International e-Symposium
on
UAV/UAS Noise
Remote from Paris – 19th to 21st October 2020

Multi-scale morphological effect on noise level and frequency characteristics of drone propellers

Ryusuke Noda, Department of Aeronautics and Astronautics, Kyoto University:
noda@kuaero.kyoto-u.ac.jp

Toshiyuki Nakata, Graduate School of Engineering, Chiba University: tnakata@chiba-u.ac.jp

Kei Senda, Department of Aeronautics and Astronautics, Kyoto University:
senda@kuaero.kyoto-u.ac.jp

Hao Liu, Graduate School of Engineering, Chiba University: hliu@chiba-u.ac.jp

Summary

Drones have huge potential for various missions such as delivery and surveillance, and they will likely be operated in the urban areas. In this situation, drones are expected to cause noise pollution and the solutions are required immediately for preventing that. In this study, we developed a method to reduce the noise that utilizes the attachment at trailing edge of the propellers. The effect of the attachment on the aerodynamic and acoustic performance is investigated by the single propeller experiments. Through the parameter sweeps, we found that the trailing-edge attachment can reduce the rotation speed, but the microstructure of the trailing-edge is necessary to prevent the greatly increase in the noise level. The trailing-edge attachment with microstructures at proper locations can reduce the noise level down to the level lower than the basic one while reducing the efficiency. The results point out that the trailing-edge attachment still requires the optimization but may improve the acoustic performance of the propellers with the minimal reduction in efficiency.

1. Introduction

For the various missions such as surveillance and delivery, multicopter-type unmanned aerial vehicles (UAVs), called drones, have become widespread during the past few years (Rothstein, 2015; Nonami, 2016). Since drones are expected to fly around urban areas or to be used for the

acoustic surveillance, their noise level needs to be suppressed (Christian et al, 2017). Noise of drones are mainly generated from their propellers along with the generations of the aerodynamic lift and, therefore, the three-dimensional shape of the propellers strongly affects both of the aerodynamic and acoustic performances of drones.

Under the identical lift generation, the noise of propeller can be reduced by decreasing the rotation speed (Lighthill, 1952; Curle, 1955; Powell, 1964; Howe, 1975). The enhancement of the lift coefficient (lift normalized by the reference length and speed) is, therefore, a promising strategy to improve the acoustic performance of propellers. We have recently developed a low-noise propeller (Noda et al, 2017; Nonami et al, 2019) by attaching a curved plate to appropriately increasing the wing area of propellers, which can generate the same amount of lift with the basic one, and can reduce the noise from propellers. The power consumption of the low-noise propellers, however, is considerably increased since the attachment makes the airfoil shapes suboptimal.

In this study, we have utilized another kind of a trailing edge device, called Gurney flap (Liebeck 1978; Fig. 1), that helps the flow stay attached around the trailing edge and hence enhance the lift coefficient. By attaching a trailing edge device to the commercial propellers for drones, we have estimated the aerodynamic and acoustic performances of propellers with Gurney flaps experimentally. In addition, inspired by the low-noise device on the owl feathers, called serrations (Graham, 1934; Lilley, 1998), the effect of the shapes and locations of the attachments are further investigated to explore the possibility to reduce the noise while keeping the reduction of the efficiency minimal.

2. Materials and methods

2.1 Propeller Model

The commercial propeller of Inspire 2 (1550T Quick Release Propeller, DJI Ltd., China) was employed as the basic propeller in this study. The three-dimensional shape of the propeller was reconstructed with the laser scanner images to determine the design parameters of the low-noise propeller based on the original parameters such as chord length and angle of attack at each cross section. The basic propeller and reconstructed shape are illustrated in Fig. 2. All of the measured parameters of the basic propeller model are summarized in Table 1. Based on the nominal weight (= 3.44 kg) and the number of rotors (= 4) of Inspire 2, we assumed that the required lift force of a single propeller for the “hovering condition” is 8.4 N, and the rotational speed was adjusted manually for generating the required lift force. Note that the “wing length, R ” we call in this paper expresses the half length of the propeller diameter.

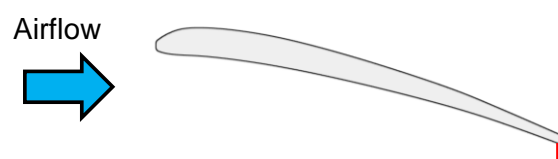


Fig. 1 Schematic diagram of the airfoil with Gurney flap (red line).

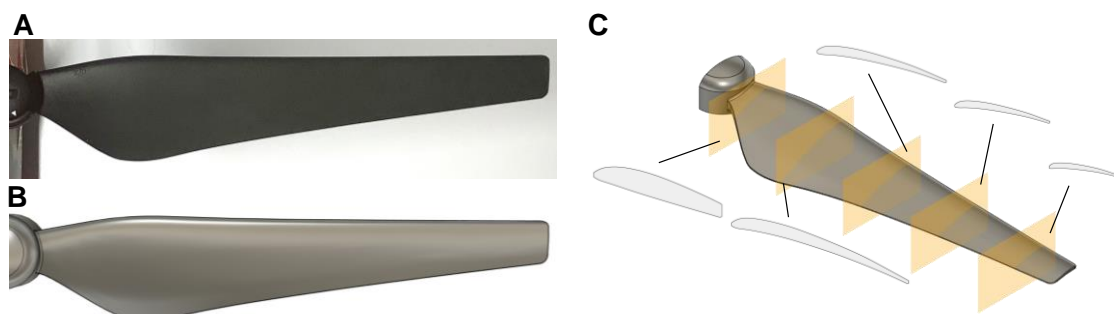


Fig. 2 Top views of (A) the propeller and (B) the reconstructed three-dimensional model.
(C) Reconstructed cross-sections at 0.1R, 0.3R, 0.5R, 0.7R and 0.9R.

Table 1 Parameters of the basic propeller.

Propeller diameter (mm)	380.40
Wing length, R (mm)	190.20
Hub diameter (mm)	27.39
Mean chord length (mm)	25.47
Rotational speed (rpm)	4100
Wing tip velocity (m/s)	81.66
Reynolds number	1.35×10^5



Fig. 3 (A) The basic propeller and (B) the propeller with trailing-edge attachment. (C) The dimensions of micro-structured attachment.

2.2 Low-Noise Propeller Models

Inspired by many previous studies on the lift enhancement of an airfoil with a Gurney flap (Storms et al, 1994; Li et al, 2002; Wang et al, 2008), we designed the attachments with different span-wise lengths and different heights located at the trailing edge on the lower surface of the propeller as illustrated in Fig. 3. All attachments consist of the series of cylinders with the diameter of 1 mm and the gaps of 1 mm. The attachments for the experiment were fabricated by 3D printer (Finder, Zhejiang Flashforge3D technology Co., Ltd., China).

2.3 Force and Noise Measurements

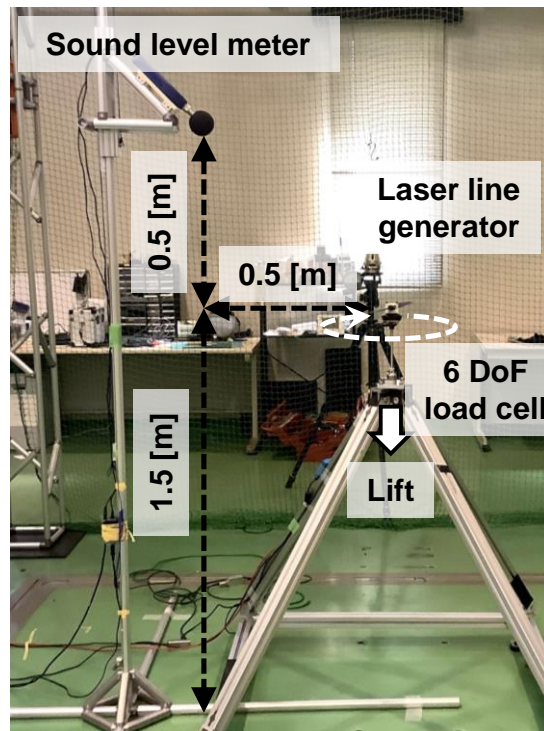


Fig. 4 Experimental set-up for force and noise measurements.

As illustrated in Fig. 4, the propeller and the brushless DC motor (DR55-M, Shinano Kenshi Co., Ltd., Japan) were attached onto a 6 DoF (degree of freedom) load cell (CFS034CA101U, Leprino Inc., Japan). The wing tips on the left and right sides of the propeller models were adjusted to be horizontal with a laser line generator for keeping the propeller balance accurately. The force and noise of the single propellers were measured in a quiet room (18 x 9 x 8.4 m). The horizontal distances between the wingtips and the building walls are at least 20 times longer than the wing length, so the wall effects due to the flow interaction are likely to be quite small in this condition. Time-varying dynamic forces (600 Hz) acting on the propeller models were measured for 60 seconds and their averaged values were taken as the steady forces in this study. A precision sound level meter (NL-52, RION Ltd., Japan) was located at a vertical and horizontal distances of 0.5 m from the center of the propeller hub. The noise was measured simultaneously with the force measurements. The Z-weighted sound pressure levels (SPLs) averaged over 60 seconds were obtained in a quiet indoor environment. Note that the noise level in the indoor environment without the rotor noise is about 30 dB while nearly 70 dB was observed with the rotor noise in all tested models.

In order to evaluate the efficiency of the tested model, the figure of merit (FM) of a propeller is defined as

$$FM = \frac{P_{RF}}{P_{exp}}, \quad (1)$$

where P_{exp} expresses the actual power given by the product of the measured torque about the rotational axis and the angular velocity. P_{RF} is the ideal power that means the minimum power for generating the resultant lift force L obtained from the experiment, and can be derived by using the Rankine-Froude momentum theory as bellow (Ellington, 1984).

$$P_{RF} = \frac{L^{3/2}}{\sqrt{2\rho A}}, \quad (2)$$

where ρ is the density of air and A is the area of the actuator disk.

3. Results and discussion

The trailing edge attachments are found to reduce the rotational speed to generate the same amount of lift, because of the enhancement of the lift coefficients. The effect of the trailing edge attachment on the SPL and FM are summarized in Fig. 5. In comparison with the basic propeller (solid lines in Fig. 5), the simple attachment of the plate with the height of 1mm at the trailing edge (broken lines in Fig. 5) generates considerably greater noise with slightly lower efficiency. However, the noise level can be suppressed even lower than the basic one by replacing the plate with the series of the cylinders and gaps except the model with the height of 8 mm. The FMs are linearly decreased in comparison with the basic one with increasing the height of the cylinder in all models. It can be observed that there is a trade-off relationship between the noise suppression level and efficiency. The significant increase of the SPL in the model with the height of 8mm is potentially due to the characteristics of the motor or the flow interaction in a different manner with the other models. In this study, considering the increase of the actual torque about the rotational axis and to avoid an overload applied to the motor due to the attachments, we adopted the model with height of 3 mm for further parametric study as discussed below.

Fig. 6 shows the effect of the tip position of the attachment from the wing tip on the overall SPL and FM. Both SPL and FM become closer to the basic models with increasing the distance, because the wing base doesn't affect the force and noise due to the lower speed. The overall SPL is peaked at $L = 5$ cm but is decreased to the lower level than the basic one when 2 cm shorter to the tip than the 5 cm except the model with $L = 11$ cm. The mechanism of the reduction

of the noise at $L = 3$ cm is unclear yet, but it is probably associated with the location of the high pressure, and turbulence generations. Based on the results, the spanwise section from $L = 3$ to 5 cm from the wing tip is identified as the important location where the noise can be suppressed by attaching a Gurney flap.

The effect of the height of the partial attachment is summarized in Fig. 7. The noise is lower when the attachment is high, but the efficiency is also decreased. Therefore, the series of cylinders (1 mm diameter, 3 mm height) attached at 3 to 5 cm is found to be the best design in the range of the study. The effect of the diameter, gap, and the shape of the cross sections will be investigated in the future study.

The spectrum and its moving average values of the noise from the basic propeller (black lines), the propeller with simple plate attachment (blue lines), and the propeller with the partial attachment with best height (red lines) are shown in Fig. 8. In comparison with the basic one, the trailing edge attachments can reduce the rotational speed as can be seen at blade pass frequency ranging from 115 to 138 Hz. The simple plate attachment greatly increases the noise especially at higher frequency, probably due to the flow separations and periodic vortex generations at the trailing edge plate. The attachment micro-structured by the cylinders and gaps are found to reduce such increase of the noise at higher frequency, while reducing the rotation speed. In comparison with the basic propeller, the noise level of the propeller with partial attachment is reduced especially at around 1,500–6,000 Hz. The improvement of the performance is thought to be due to the suppression of the large-scale flow separations at trailing edge plate in the similar manner with the noise suppression by the leading-edge serrations of the owl feather (Rao et al, 2017, Ikeda et al, 2018). Therefore, the microstructure at the trailing edge have a great potential to reduce the noise level of propellers for drones.

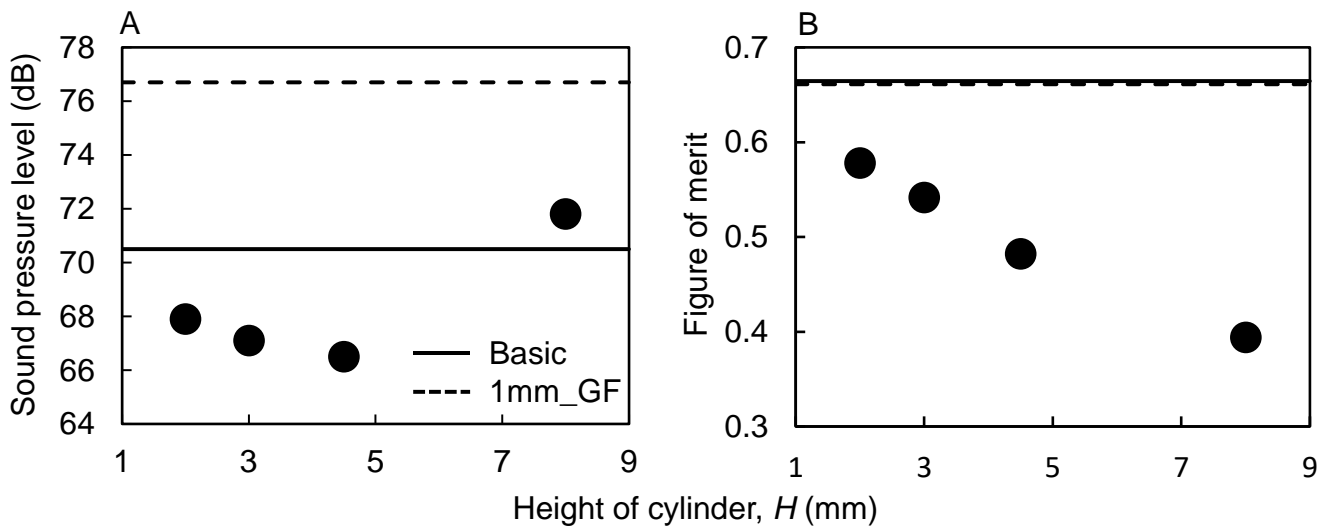


Fig. 5 Effect of height of the attachment on (A) the overall sound pressure level and (B) the figure of merit of the propellers. The solid and broken lines indicate the basic propeller and the propeller with the simple plate attachment.

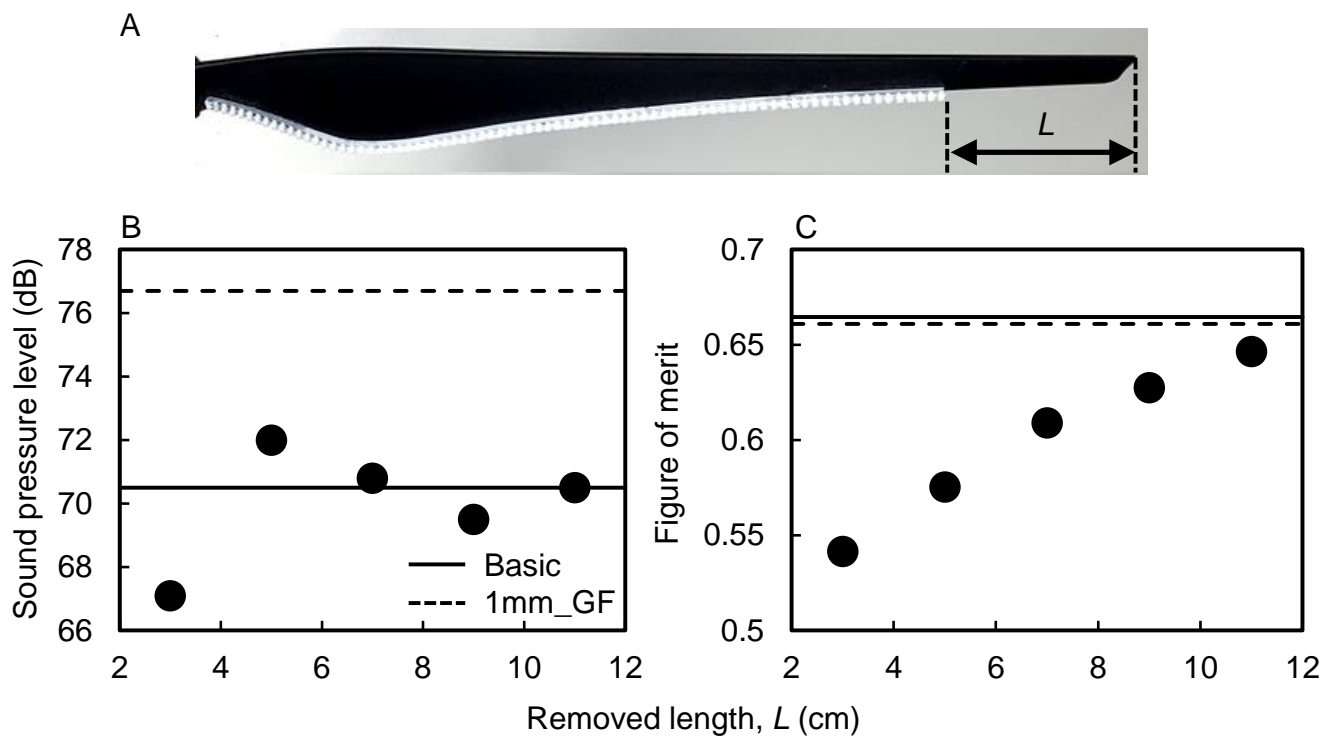


Fig. 6 Effect of the tip position of the attachments from the wing tip (A) on (B) the overall sound pressure level and (C) the figure of merit of the propellers with the trailing-edge attachments.

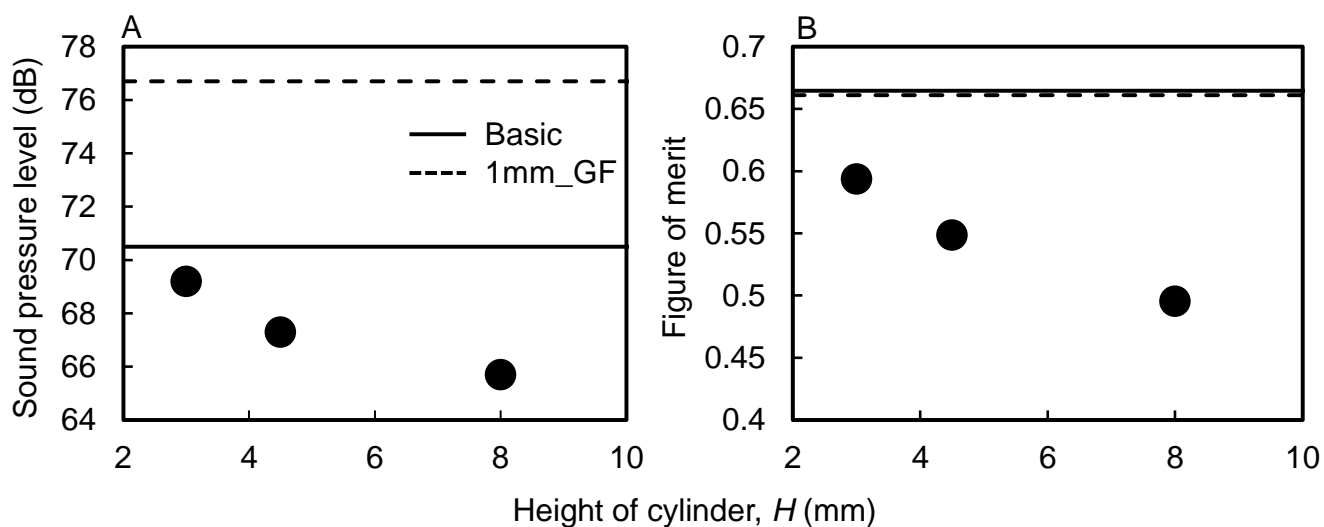


Fig. 7 Effect of height of the partial attachment on (A) the overall sound pressure level and (B) the figure of merit of the propellers.

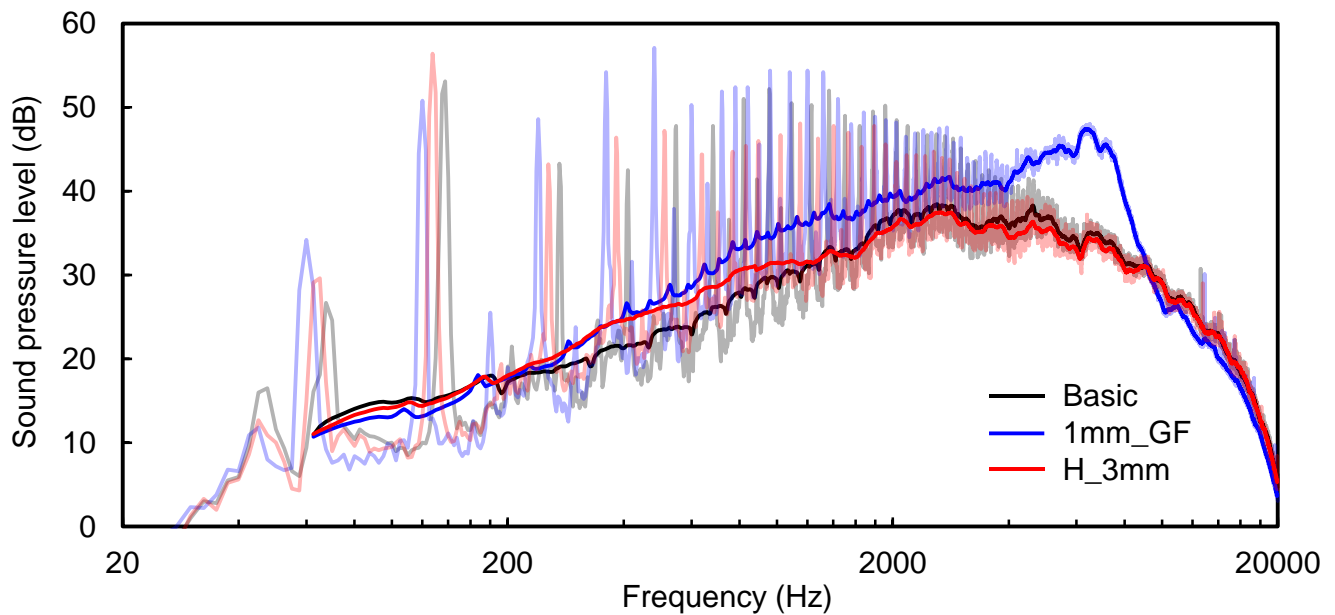


Fig. 8 Frequency spectrum of noise from the basic propeller, the propeller with the simple plate attachment, and the propeller with the micro-structured partial attachment.

4. Conclusions

In this study, we have investigated the effect of the trailing-edge attachment, like Gurney flap, on the aerodynamic and acoustic performances of the propellers for drone experimentally. It is found that the simple plate attachment greatly increases the noise level of the propeller, but the noise can be reduced lower than the basic propeller by replacing the plate with the series of cylinders and gaps. The design of the microstructure needs further optimizations for reducing the noise and improving the efficiency of the propeller with trailing-edge attachment, but our results indicate the great potential of the trailing-edge attachment in order to improve the acoustic performances.

Acknowledgement

This work was supported by JSPS KAKENHI Grant Number 19H00750 and General Research Grant from the SECOM Science and Technology Foundation.

References

- Christian, A. and Cabell, R. (2017) *Initial investigation into the psychoacoustic properties of small unmanned aerial system noise* AIAA Aviation Technology, Integration, and Operations Conf. (AVIATION 2017), Denver, CO, June 5-9
- Curle, N (1955) *The influence of solid boundaries upon aerodynamic sound* Proc. Roy. Soc. Lond. A 231, 505-514
- Ellington, C. P. (1984) *The aerodynamics of hovering insect flight. Part V: a vortex theory* Phil. Trans. R. Soc. B 305, 115-144
- Graham, R. R. (1934) *The silent flight of owls* J. Roy. Aeronaut. Soc. 38(286), 837-843
- Howe, M. S. (1975) *Contributions to the theory of aerodynamic sound, with application to excess jet noise and the theory of the flute* J. Fluid Mech. 71(4), 625-673
- Ikeda, T., Ueda, T., Nakata, T., Noda, R., Tanaka, H., Fujii, T. and Liu, H. (2018) *Morphology effects of leading-edge serrations on aerodynamic force production: An integrated study using PIV and force measurements* J. Bionic Eng. 15, 661-672

- Li, Y. C., Wang, J. J. and Zhang, P. F. (2002) *Effect of Gurney flaps on a NACA0012 airfoil* Flow Turbul. Combust. 68(1), 27-39
- Liebeck, R. H. (1978) *Design of subsonic airfoils for high lift* J. Aircraft 15(9), 547-561
- Lighthill, M. J. (1952) *On sound generated aerodynamically. Part I : General theory* Proc. Roy. Soc. Lond. A 211, 564-587
- Lilley, G. M. (1998) *A study of the silent flight of the owl* 4th AIAA/CEAS Aeroacoustics Conference, Toulouse, France, 1-6
- Noda, R., Nakata, T., Ikeda, T., Chen, D., Yoshinaga, Y., Ishibashi, K., Rao, C. and Liu, H. *Development of bio-inspired low noise propeller for a drone* J. Robot. Mechatron. 30(3), 337-343
- Nonami, K. (2016) *Drone technology, cutting-edge drone business, and future prospects* J. Robot. Mechatron. 28(3), 262-272
- Nonami, K., Hoshiba, K., Nakadai, K., Kumon, M., Okuno, H. G., Tanabe, Y., Yonezawa, K., Tokutake, H., Suzuki, S., Yamaguchi, K., Sunada, S., Takaki, T., Nakata, T., Noda, R., Liu, H. and Tadokoro, S. (2019) *Recent R&D Technologies and Future Prospective of Flying Robot in Tough Robotics Challenge, Disaster Robotics - Results from the ImPACT Tough Robotics Challenge* Springer Tracts in Advanced Robotics, 128, 77-142
- Powell, A. (1964) *Theory of vortex sound* J. Acoust. Soc. Am. 36(1), 177-195
- Rao, C., Ikeda, T., Nakata, T. and Liu, H (2017) *Owl-inspired leading-edge serrations play a crucial role in aerodynamic force production and sound suppression* Bioins. & Biomim. 12, 1-13
- Rothstein, A. (2015) *Drone (Object Lessons)* Bllomsbury Publishing, New York, Chapter 1
- Storms, B. L. and Jang, C. S. (1994) *Lift enhancement of an airfoil using a Gurney flap and vortex generators* J. Aircraft 31(3), 542-547
- Wang, J. J., Li Y.C. and Choi, K. S. (2008) *Gurney flap-Lift enhancement, mechanism and applications* Prog. Aerosp. Sci. 44(1), 22-47



CidB

Centre d'information
sur le **Bruit**

QUIET DRONES
International Symposium
on
UAV/UAS Noise
Remote from Paris – 19th to 21st October 2020

Proposal of Cognitive Drone Audition based on Cognitive Dynamic Systems

Makoto Kumon, Kumamoto University: kumon@gpo.kumamoto-u.ac.jp

Hiroshi G. Okuno, Kyoto University/Waseda University: okuno@nue.org

**Kazuhiro Nakadai, Honda Research Institute Japan/Tokyo Institute of Technology:
nakadai@jp.honda-ri.com**

Kotaro Hoshiba, Kanagawa University: hoshiba@kanagawa-u.ac.jp

Ryosuke Noda, Kyoto University: noda.ryusuke.6a@kyoto-u.ac.jp

Summary

Quiet drone is critical for anti-sound pollution for humans as well as for drone audition. Current drone audition, a hearing capability of a drone with a microphone array mounted on it, can localize and trace sound sources by coping with strong ego-noise generated by rotors and air-flow and environmental noise. In this paper, we propose a novel “*cognitive drone audition*” modeled by a cognitive dynamic system (CDS) [Haykins, 2012]. CDS is motivated by the bat echolocation which is based on cognition. Then we present our current activities of drone audition including open sourced robot audition software called HARK, MUSIC-based sound source localization (SSL) methods, and field demonstrations of search-and-rescue tasks. The problems with current drone audition are robustness against ego-noise and multiple sound sources. Most drone audition assumes a single sound source, which does not hold in real-world situations. Finally, we present current activities towards cognitive drone audition. Data association between tracked sound sources and observed SSL is solved by using sound source identification. Silent propeller models designed for quiet drone show power reduction in a lower frequency band, which may make. MUSIC with active frequency range filter exploits this characteristic to improve SSL. Kite planes, a UAV with a delta-shaped wing, provides a rotor stall mechanism to reduce ego-noise and thus improve SSL. Through these preliminary activities, we set the stage for cognitive drone audition.

1. Introduction

Drones are expected to help humans reduce human-to-human contacts in an era of Covid-19 or to support human activities damaged by natural disasters and accidents. One of the main problems posed by drones is noise originated from the sky which usually cannot be prevented or reduced outdoors. A psychoacoustic test suggests that the noise of the recorded drones (small unmanned aerial systems, sUAS) is not of the same quality of that of a set of recorded road vehicles (Christian & Cabell, 2017). The noise of the sUAS may be a different annoyance to human subject listeners. The authors conclude as follows:

This result casts doubt on the idea that sUAS operators can expect their operations to be greeted with minimum noise-based opposition as long as the sound of their systems are [sic] “no louder than” conventional package delivery solutions.

Quiet drone is thus critical in deploying drones to measurement, monitoring, logistics, delivery, as well as to search and rescue activities. In the latter activities, well-known guidance of “*First 72 Hour Response*” expects drones to be deployed for monitoring, logistics, and search and rescue mission because they are free from most ground restrictions (Tadokoro et al., 2019) (Nonami et al., 2019). To improve the quality and performance of the search and rescue mission, more sensory capabilities are critical. The current drones exploit LiDAR (Light Detection and Ranging (Wallace et al., 2012) (Chisholm et al., 2013), and cameras (Yuan et al., 2009) (Carrillo et al., 2012). Although vision sensors are powerful due to visual precision devices and powerful deep-learning-based software, they have critical weaknesses such as occlusion and ill-illumination conditions. Therefore, drones should exploit other sensors to compensate for such weaknesses.

Computational auditory scene analysis (CASA) tries to recognize and understand the auditory scene by sounds (Rosenthal & Okuno, 1998). As CASA models computer listening, it should provide sound source localization (SSL), sound source separation (SSS), and recognition of separated sounds. If a separated sound is a speech signal, automatic speech recognition (ASR) is conducted. If music, automatic transcription is conducted. If environmental sound, sound event detection is conducted. CASA is applied to robots to provide listening capabilities to robots by using microphones attached to them, which is called “*robot audition*” (Nakadai et al., 2000) (Okuno & Nakadai, 2015). As a natural and reasonable consequence, robot audition has been applied to drones, which is also called “*drone audition*” (Okutani et al., 2012) (Kumon et al., 2013) (Ishiki et al., 2014) (Wakabayashi et al., 2020a). One of the challenging problems in robot audition is the strong *ego-noise* generated by the robot’s movements and fans. This problem of *ego-noise* becomes much more severe in drone audition because the noise generated by rotors and airflow around the drone is much louder and dynamically changing (Nakadai et al., 2017) (Wang & Cavallaro, 2020). The performance of SSL, sound source tracking deteriorates severely. Therefore, quiet drone is also critical for improving the performance of drone audition.

This paper presents cognitive drone audition, then overviews our activities of drone audition up to date, summarizes the problems of current drone audition, and finally presents the possibility of cognitive drone to cope with the problems. Cognitive drone audition is based on cognitive dynamic systems (CDS) (Haykin, 2012) inspired by animals such as bats, dolphins, and whales.

2. Cognitive Drone Audition

Since search-and-rescue activities with sound have similar aspects of search-and-pray ones of animals such as bats, dolphins, and whales, biomimetic echolocation by “*see with sound*” may be promising (Baker et al., 2014). Bats detect, identify, locate, navigate, and capture its prey through echolocation. They use echolocation pulse consisting of short bursts of sound at

frequencies ranging from 30 kHz to 200 kHz, which provides information such as distance, range, angular position, shape, and texture of an object (Lawrence & Simmons, 1982). They perceive the environment and then take action to it based on the perception and cognition with memory.

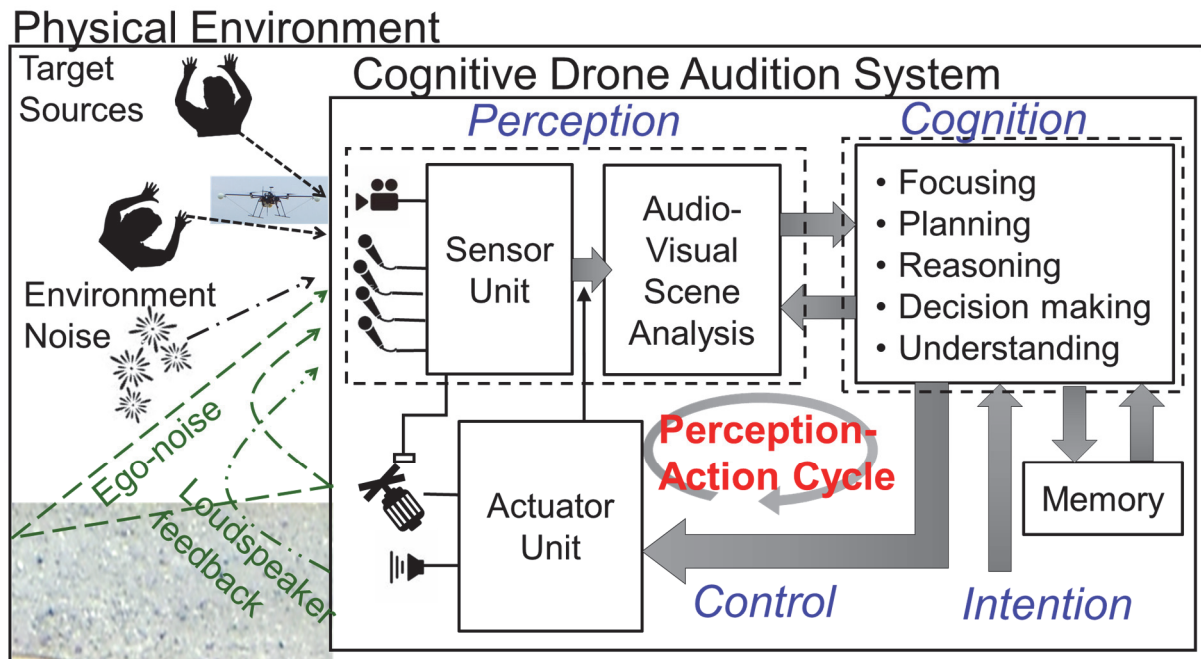


Fig. 1 Cognitive Drone Audition (adopted to drone (Schmidt et al, 2019))

In other words, bat echolocation is based on CDS and the perception-action cycle plays a critical role in cognition dynamic systems (Haykin, 2014). Since radar and sonar systems are man-made echolocation system, cognitive radar and sonar systems have been extensively studied to improve the performance of object detection. Cognitive radar is trying to integrate recent outcome of increased signal-to-interference ration, adaptive beamforming and sidelobe reduction, and improved spatial resolution by understanding their capabilities and the environments (Haykins, 2006) (Baker et al., 2014).

Drone audition mainly detects, identifies, locates sound sources by sound, and facilitates perception with visual and auditory scene analysis and navigation. The current drone audition lacks understanding of the environments and actions. Cognitive drone audition extends drone audition by incorporating the perception-action cycle. Figure 1 illustrates the scheme of cognitive drone audition. When the drone searches people of screaming for help, the system captures (*senses*) sounds by a microphone array. Usually, input sounds comprise ones originating from target sound sources, environment noise, ego-noise, and reflection of ego-noise. Sensor unit includes proprioceptors such as mechanical control information and GPS or GNSS as well as vision and audition. It analyses (*perceives*) data obtained by sensor unit by audio-visual scene analysis. Audio-visual scene analysis provides information such as how many people call for help where? which is used for memory-driven cognition. “Focusing” attention is to allocate and direct the sensing resources toward relevant information. “Planning” is to determine what actions to take how and when, that is, motion-planning and path-planning. “Reasoning” is needed to improve the understanding of the situation by using data stored in memory. For example, as the drone flies towards an object or downwards to the terrain, the reflection of ego-noise becomes stronger, and thus ghost sound sources are usually detected. Most current drone audition system uses a specialized filter to discard such ghost sound sources. “Decision making” determines the attention and decides the planning. Cognition consists of perception, memory, attention, and intelligence. Deep learning, deep neural network, or Bayesian reasoning is a tool for cognition. By summarizing obtained information the system improves the understanding of the situation, and decision making and related information is stored in memory.

2.1 Perception-Action Cycle in Cognitive Drone Audition

Figure 2 shows the scheme of cognitive drone audition, with the perception-action cycle and memory occupying the “drone” and the “brain” of the drone audition system. The drone is responsible for cognitive flight control, while the brain is responsible for cognitive audition. The drone and brain have each control that is driven by the perception-action cycle and memory. The control of the drone consists of model predictive control and reflective control, both of which interact with multi-scale executive memory to specify appropriate cognitive actions to the sound-visual environment. Multi-scale executive memory is organized in timescale from stable information, plan, and task. Usually, model predictive control stores and uses high-level data of multi-scale executive memory, while reflexive control stores and uses low-level data. Essential data in multi-scale executive memory are extracted and stored in the dynamical model library for long-term memory. Such data may be restored on-demand in multi-scale executive memory.

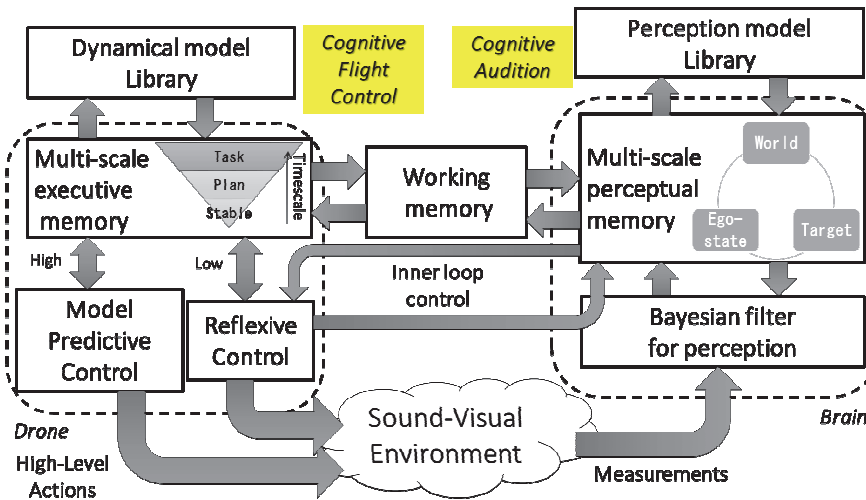


Fig.2 Perception-Action Cycle in Cognitive Drone Audition

The control of the brain obtains measurements from the sound-visual environment and applies a Bayesian filter for perception. Perception is conducted on filtered measurements and information stored in multi-scale perceptual memory. The information obtained by perception is stored in multi-scale perceptual memory. Multi-scale perceptual memory stores data about ego-state, targets, and world, which can be stored in or extracted from the perception model library. Through a sound-visual environment, the drone and brain have a global feedback loop. They also have an inner feedback loop through working memory. To realize this scheme, we are planning to apply the model to our past activities explained later in this paper.

2.2 Robot audition

Robot audition proposed by Nakadai and Okuno is the capability of listening to several things at once with its own “ears” (Nakadai et al., 2000). It plays an important role in improving symbiosis between humans and robots. Before emerging of robot audition, most studies of human-robot interaction assumed that humans wore a head-set microphone or talked to a microphone close to the speaker. In other words, a robot did not use its microphone even if it was equipped with a microphone or microphones (Okuno & Nakadai, 2015). The critical issues in robot audition are real-time processing and robustness against noisy environments. Some important functions of robot audition are SSL, sound source tracking, SSS, and ASR of separated speech.

2.3 HARK: Open-sourced robot audition software

Based on our experience with robot audition applications, we have developed an open-sourced robot audition software called HARK¹ (Nakadai et al., 2010) (Nakadai et al., 2017a). Its design focused on realtime processing and high flexibility to support various kinds of robots and hardware configurations as well as providing a rich set of functions required by robot audition. We assume that a robot is equipped with a microphone array. The main functions are summarized below:

1. Sound source localization (SSL): HARK provides several noise-robust SSL based on MUSIC (Multiple signal classification) (Schmidt, 1986). In addition to original MUSIC, generalized eigenvalue decomposition of correlation matrices for noise robustness (GEVD-MUSIC) (Nakamura et al., 2009), generalized singular value decomposition (GSVD-MUSIC) (Nakamura et al., 2013). Since both GEVD- and GSVD-MUSIC require a noise correlation matrix, it is usually estimated in advance. GEVD-MUSIC can keep SSL performance down to -20dB noisy environments in batch processing, while GSVD-MUSIC can cope with -10dB noisy environments in real-time. HARK also provides an incremental estimation of a noise correlation matrix for GEVD- and GSVD-MUSIC to cope with dynamic changing acoustic environments, that is, for drone. These extended versions are called iGEVD-MUSIC (Okutani et al., 2012) and iGSVD-MUSIC (Ohata et al., 2014), which can detect a sound source at up to 20m under dynamically changing noise conditions.
2. Sound source tracking: HARK provides naïve tracking and particle filter based tracking. Both methods run in realtime by accepting the outputs of SSL.
3. Sound source separation (SSS): HARK provides twelve sound source separation algorithms, which are classified into four categories.
 - 1) Fixed beamformer (BF) -- delay-and-sum BF, null-BF, weighted delay-and-sum BF, and indefinite term and least square estimator based BF.
 - 2) Explicit use of noise information – maximum likelihood BF, and maximum signal-to-noise ratio BF
 - 3) Linearly constrained minimum variance (LCMV) – minimum variance distortion-less response (MVDR) BF, LCMV-BF, and Griffith-Jim type BF
 - 4) Linearly constrained blind separation – geometric source separation (GSS), geometric independent component analysis (GICA), and geometric high-order decorrelation based source separation (GHDSS).
4. Speech enhancement and noise estimation: HARK provides histogram-based recursive level estimation (HRLE), semi-blind independent component analysis (SB-ICA), ego-noise estimation, and online robust principal component analysis (ORPCA).
5. Automatic speech recognition (ASR): HARK provides two interfaces to state-of-the-art ASR engine, Julius and Kaldi. HARK usually use Mel-scale log spectrum (MSLS) as an acoustic feature in addition to the conventional Mel-frequency cepstrum coefficient (MFCC).

¹ HARK is an acronym of Honda Research Institute Japan Audition for Robots with Kyoto University. It is a middle English meaning “listen”. HARK is available at <https://hark.jp/>

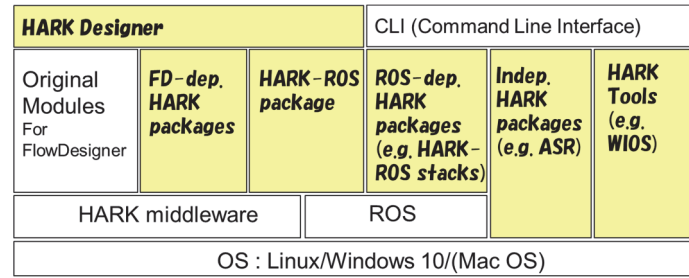


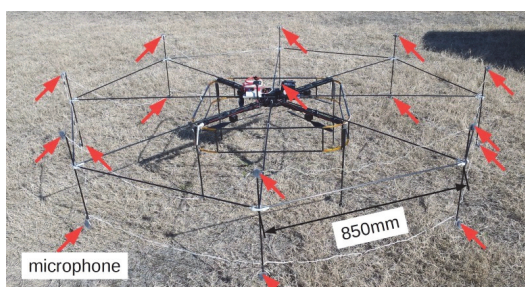
Fig.3 Architecture of HARK

HARK is based on HARK-middleware on either Windows 10 or Ubuntu (cf. Figure 3). HARKDesigner is a web browser-based GUI, which provides network-like programming. The first version of HARK was opened to the public in 2008 with rich document and cookbooks in Japanese and English and annual updates have been conducted with free tutorials and hackathons both domestic and abroad. HARK has been downloaded more than 150 thousand times up to date.

2.4 Drone Audition

The first capabilities of drone audition are sound source localization (SSL) and tracking. Drone audition localizes sound sources by extracting the directional information of a sound source in azimuth, the horizontal direction, and elevation, the vertical one. Then it traces sound sources by associating new directions to extracted directions. Ego-noise is much stronger to drone audition than robot audition because the sources of ego-noise are quite close to a microphone array and the power of rotor noise, airflow around the drone is much stronger than that of ego-noise generated by a robot. To cope with strong ego-noise at the signal processing level, HARK provides variations of MUSIC, which searches peaks in MUSIC spectra by sub-space division based on eigenvalue decomposition. Ordinal MUSIC yields a much sharper peak than one by beam-formers, they are more robust against ego-noise. Since original MUSIC assumes that the signal level should be greater than that of noise sources and this assumption does not hold for drone audition, HARK provides extended MUSICs; GEVD-MUSIC based on GEVD and GSVD-MUSIC based on GSVD, both of which assume a noise correlation matrix. The correlation matrix is either prepared in advance or obtained incrementally. The latter methods are called iGEVD-MUSIC and iGSVD-MUSIC.

In addition to ego-noise suppression at the signal processing level, the configuration of the microphone setting is critical at the device level. Many configurations are possible by choosing directional or omnidirectional microphones, the number of microphones, the configuration of microphones, linear, circular, sphere, and so on (Ishiki & Kumon, 2015) (Hoshiba et al., 2017) (Ishiki & Kumon, 2017). Another critical aspect of microphone arrays is the easiness of deployment. Even if some configuration of microphone array provides better performance of SSL, a ready-to-use microphone array with not the best performance is preferable for actual



(a) 16-ch 2-layered microphone array



(b) 16-ch sphere microphone array coloured orange (counterweights coloured white)

Fig.4 Two kinds of microphone array

drone audition systems. For example, it takes about two hours to prepare a 16-ch 2-layered microphone array depicted in Figure 3(a), while it took about twenty minutes to prepare a 16-ch spherical microphone array depicted in Figure 3(b). Both microphone arrays used MEMS omnidirectional microphones. The former outperformed the latter concerning SSL.

Since SSL provides only azimuth and elevation of a sound source and not its distance, we adopt the information of the drone obtained by GPS and GNSS. Figure 5 depicts the scheme of sound source position estimation. By using sound source direction and the height, the sound source position can be estimated. In an earlier implementation, a planar terrain model with GPS was adopted, but its performance was poor because the estimated position is wrong or a ghost. Poor performance in estimating sound source position caused by several factors; the information obtained by GPS fluctuates and thus the height is not so accurate. A planar terrain model does not hold. A ghost position appears depending on the surface of the terrain. If it is covered by grass or other objects or is uneven, the reflection of ego-noise is so weak, ghost positions are possible. If it is not covered and even, ghost positions are probable. Our current drone audition uses GNSS in place of GPS to obtain an accurate position of the drone and 3D point clouds in place of the planar terrain model. Ghost positions are eliminated by a pre-defined program.

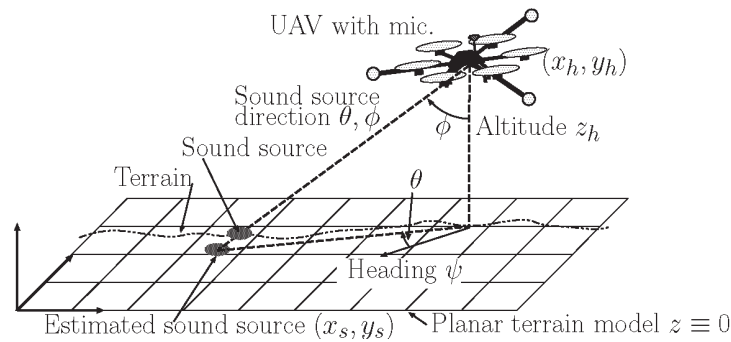


Fig.5 Schema of Estimating Sound Source Position (Wakabayashi et al., 2020)

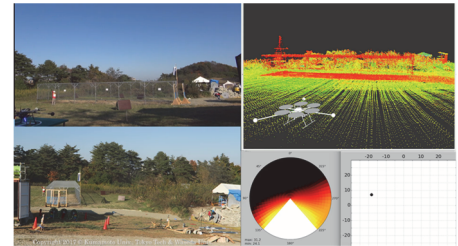
3. Experience with Drone Audition

This section first reports our activities with the ImPACT (Impulsing Paradigm Challenge) Tough Robotics Challenge (TRC) (Tadokoro, 2019), which was supported by the Japanese Cabinet from 2014 to 2019. The robot audition team consisting of Tokyo Institute of Technology, Kumamoto University, and Waseda University demonstrated human search tasks by sounds to the public for four times (Nakadai et al., 2017b) (Nonami et al., 2019) (Wakabayashi et al., 2020c).

1. 2016/October at a field of Tohoku University, Japan
The drone is a UAV of quadrotor of enRoute with a 12-ch sphere microphone array. It is connected to the base station via 2.4GHz Wifi with a powered Yagi antenna. Their distance is about 20 m and the planar terrain model was used. The drone successfully detected and estimated a moving whistleblower.
2. 2017/October at a field of Tohoku University, Japan
The drone is a UAV of quadrotor of enRoute with a 12-ch sphere microphone array. It is connected to the base station via 2.4GHz Wifi with a powered Yagi antenna. Their distance is about 20 m and the terrain was covered by grass. A 3D point cloud map was used. A professional operator operated the drone. The drone successfully detected and estimated a standing man and a man hiding in a pipe both shouting “Ohi” successively.
3. 2018/June at the Fukushima Robot Test Field, Japan
The drone is a UAV of quadrotor of PF-1 Survey in ACSL with a 16-ch sphere microphone array with an embedded ARM processor. It is connected to the base station via 920MHz/169MHz link with a relay drone. Their distance is about 750 m and the terrain was even without grass. A professional operator operated the drone. The drone successfully detected and estimated a standing man near a building and a man near a fallen cottage shouting “Ohi” successively.
4. 2018/Oct. at the Fukushima Robot Test Field, Japan
The drone is a UAV of quadrotor of PF-1 Survey in ACSL with a 16-ch sphere microphone array with an embedded ARM processor. It is connected to the base station via 920MHz/169MHz link with a relay drone. Their distance is about 250 m and the terrain was even without grass. The drone successfully detected and estimated a standing man near a fallen cottage shouting “Ohi”.



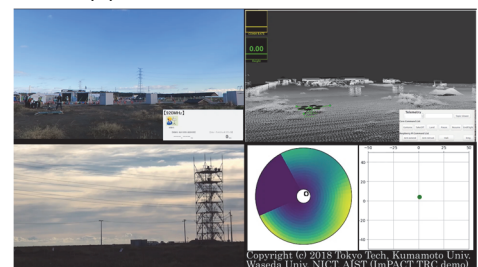
(a) The first demonstration



(b) The second demonstration



(c) The third demonstration



(d) The fourth demonstration

Fig. 6 A Series of Demonstrations

3.1 Lessons Learned on Drone Audition – Why is Cognitive Drone Audition mandatory?

Based on our over-ten-year experience with drone audition, we have learned lessons on drone audition. In this subsection, we summarize the lessons learned and present why cognitive drone audition is needed. In particular, the design and implementation of the perception-action cycle shown in Figure 2 should be established and its effect should be evaluated. Although the perception-action cycle and CDS are effective in cognitive radar and cognitive radio (Haykin, 2006) (Haykin, 2007) (Haykin, 2012), (Haykin et al., 2012) (Haykin, 2014) cognitive drone audition is just proposed without evaluation.

1. *Issues of auditory function:* Real-time processing of localization and position estimation; the targets are multiple moving sound sources. (1) In tracking multiple moving sound sources, uncertainties remain in the data association between the sound source position estimation result and observed data. (2) Reflection of strong ego-noise from an object or the ground surface causes uncertainty in estimated sound sources. (3) No integrated processing in drone audition. Sound source localization, position estimation, separation, and sound source identification are processed independently of each other.

The research questions are how CDS models auditory function based on perception-action cycle; whether CDS modeling of auditory functions can perceive a dynamic auditory environment and perform adaptive signal processing effectively; and how cognitive drone audition outperforms conventional drone audition in performance and speed.

2. *Issues of Flight control*: (1) Flight control near a target is difficult due to increasing dynamic fluctuations of airflow compared to flight in free space, restricted availability of GPS and camera images. (2) More sensors and devices such as vision, audition, and silent propeller models, increase the complexity of control and integration. In addition to the development of sensor technologies such as vision, audition, silent propeller models, it is essential to realize the cognition of “situation judgment, utilization of past knowledge, and appropriate control planning”. Flightpath planning is also needed.

The research question is whether the flight control by CDS improves the performance against dynamic airflow fluctuated from a long distance to a near target.

3. *Issues of the integrated system*: (1) Various kinds of maps are needed in advance and on-demand; audition creates auditory maps while the flight control needs them to create flight planning and path planning. After the flight is done, cognitive drone audition should understand the flight and upgrade the maps. This feedback cycle should extract know-how and create higher-level knowledge.

The research questions are whether cognitive drone audition can construct perception, memory, attention, and intelligence to improve the performance of sound source localization and tracking of multiple moving sound sources and how cognitive drone audition can scale up.

4. *Issues in elemental technology*: Estimation of multiple moving sound sources is the first goal to attain. In addition to developing novel technologies for quiet drone in audition, vision, and 3D position estimation, ego-noise suppression and silent propeller models are mandatory. Kite planes with gliding is also promising.

The research question is whether innovation of elemental technology can contribute quiet drone, improve perception, and outperform conventional robot audition.

4. Preliminary Activities in Cognitive Drone Audition for Quiet Drone

This section reports our three current activities in cognitive drone audition towards quiet drone: data association for sound source tracking, silent propeller models, AFRF-MUSIC, and kite planes.

4.1 Data Association by integrating sound localization and separation

Most of the current implementations of robot audition focus on a single sound source (Basiri et al., 2012) (Hoshiba et al., 2017) (Nonami et al., 2019) (Wang & Cavallaro, 2020). We focus on the estimation of multiple sound source positions from acoustic signals captured by a drone equipped with a microphone array. Due to ego-noise such as rotor and airflow noise around the drone, the estimation of the sound source position is obscured and prone to error even for a single sound source. When a drone hears sounds originating from multiple sound sources, its sound-source localization function determines their directions. If two sources are very close to each other, the localization function cannot determine whether they are crossing or approaching-then-departing. This ambiguity in tracking multiple sound sources is resolved by data association. In particular, in the case of multiple sound sources, data association between localization information and sound sources is critical to the performance of such estimation. Figure 7 depicts the scheme of data association for SSL.

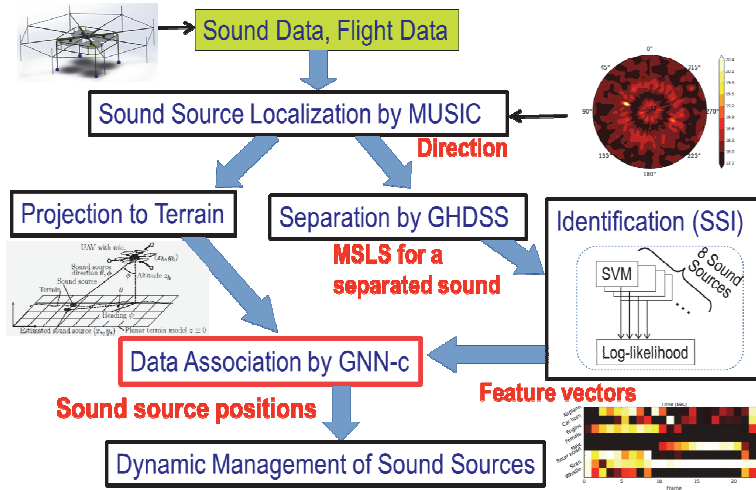


Fig. 7 Scheme of Data Association for SSL

Sound data and flight data are captured by microphone array and sensors of the drone. Then GSVD-MUSIC performs SSL to obtain the direction in azimuth and elevation. The direction is projected to the terrain with flight data to estimate the sound source position. It is also given to GHDSS, which separates sound source originated from the designated direction. Then separated sound source is identified by a set of 8 SVMs to obtain a set of log-likelihood as feature vectors. To cope with uncertainty in data association, we extend Global Nearest Neighbor (GNN) to exploit sound source features (GNN-c) because drone audition needs real-time or minimum latency (Wakabayashi et al., 2020b). Finally, GNN-c conducts data association between sound source positions under tracking and feature vectors of a newly separated sound source. This dynamic management of sound sources allows drone audition to detect and track multiple sound sources simultaneously. The effectiveness of the proposed approach is validated through simulations and experiments conducted in the field (Wakabayashi et al., 2020b). The resulting system demonstrates that it can estimate multiple sound source positions with an accuracy of about 3 m (Wakabayashi et al., 2020a).

4.2 Silent Propeller Models

The design of silent propeller models with the analogy of flying birds is an idea that has been known for a long time, and until now, a trial and error approach was the mainstream. Recently computational fluid dynamics (CFD) approach emerges to design a biological norm for the purpose of noise reduction and stable flight (see Figure 8). To search for silent propeller models, bio-norm structure, wing area increased structure, and the surface of the resin wing have been investigated (Noda et al., 2020). Extensive studies of various potential silent propeller models, five propeller modes for DJI Inspire 2 were designed by CFD (Hoshiba et al., 2020).

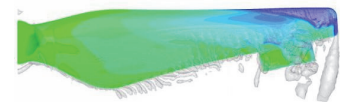


Fig. 8 CFD of a Propeller Model

The acoustic features of the five proper models shown in Figure 9 were analyzed in the laboratory and actual flights. The power of noise generated by each propeller models is shown in the right graph of Figure 9. The graph indicates that each propeller model has its intrinsic acoustic characteristics. Compared to the basic propeller model provided by the manufacture, 1550T Quick Release Propeller, DJI, the other propeller models have lower power from 100 to 1,500 Hz. The propeller model E has the least noise power in the whole frequency region. Therefore, cognitive drone audition should understand the acoustic characteristics of its propeller models and record such acoustic information into memory. Then, cognitive drone audition should exploit this information to improve SSL and other drone audition functions. One possible exploitation is explained in the next subsection.

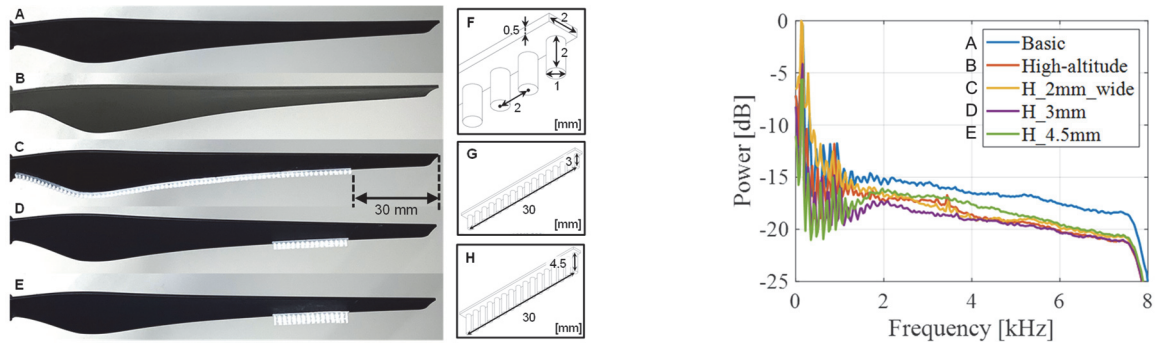


Fig. 9 Five Propeller Models and their frequency-power of propeller noise (adopted from (Hoshiba et al., 2020))

4.3 MUSIC with Active Frequency Range Filtering (AFRF-MUSIC)

MUSIC-based methods are one of the most powerful SSL that demonstrates noise-robustness and real-time processing. From the viewpoint of drone audition, in particular, strong ego-noise and real-time processing, we have to solve a problem of a trade-off between noise robustness and real-time processing. Among MUSIC-based methods, SEVD-MUSIC (original MUSIC) is fast but not so robust against noise, while iGSVD-MUSIC is slow but robust against noise and ego-noise. The operations of these methods are Fourier transform (FT), correlation matrix calculation (CM), and eigenvalue decomposition (SEVD) of the recorded sound to calculate the MUSIC spectrum. Since a frequency range filter narrows the frequency range of processing and makes a data matrix sparser, the processing becomes less expensive and shorter latency. For example, the latency of SEVD-MUSIC with 500-3000Hz range filter and with 2500-3000 Hz range is 0.533 sec and 0.194 sec, respectively. That of iGSVD-MUSIC is 3.219 sec (see Table 1). Since the difference in the frequency range between target signals and noise can be estimated online, we proposed the MUSIC with Active Frequency Range Filtering (AFRF) called AFRF-MUSIC (Hoshiba et al., 2018).

Their difference in operations is schematized in Figure 10. A frequency range filter plays an important role in making the matrix sparse and can be calculated by simple arithmetic functions, its computing cost is much less expensive than other MUSIC methods. The active frequency range is calculated by estimating the difference between signals and noise. Table 1 presents the results of three MUSIC methods in terms of latency of processing and the success rate of SSL. By this comparison, AFRF-MUSIC demonstrates its effectiveness by extracting a frequency range that consists of the target signal.

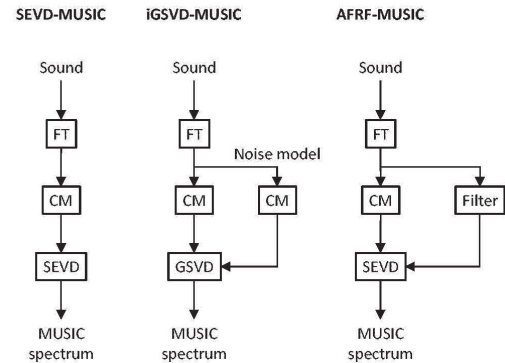
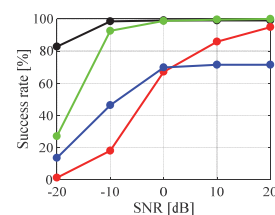


Fig. 10 Flowcharts of SEVD-, iGSVD-, and AFRF-MUSIC (adopted from (Hoshiba et al., 2018))

FT: Fourier Transform, CM: Correlation Matrix calculation

Table 1 Comparison among iGSVD-MUSIC, SEVD-MUSIC, and AFRF-MUSIC in latency of processing and the success rate of SSL

Method	Latency [s]
● iGSVD-MUSIC	3.219
● SEVD-MUSIC (500-3,000 Hz)	0.533
● SEVD-MUSIC (2,500-3,000 Hz)	0.194
● AFRF-MUSIC	0.204



As mentioned above, silent propeller models enhance the lower frequency characteristics compared with the basic propeller models. Cognitive drone audition should exploit such information. It should record the frequency characteristics of silent propellers in memory and create a corresponding frequency range filter so that AFRF-MUSIC is expected to perform SSL with less latency and more accurate SSL. This integrated work is important future work.

4.4 Kite plane with Flying and Gliding

Kite planes, UAV (unmanned aerial vehicle) with a delta-shaped main wing, have a long history as UAV. In Japan, kite planes have been used to monitor the Antarctic since 2007 (Hirasawa et al., 2019). But the recent rapid progress of multi-motor drones has forced kite planes to be forgotten. This black history may be reverted by recent increasing interests in quiet drone, in particular, from the viewpoints of sound pollution and drone audition. We have focused on kite planes from the viewpoint of drone audition. Figure 11 depicts our kite plane of an electric motor model with a circular 8-ch microphone array. Figure 12 shows that the power spectrum of ego-noise decreases when the rotor is off and the kite plane glides. Ego-noise generated by the rotor is shown in the right part of the spectrum and disappears when the rotor stops (Kumon et al., 2015) (Nagayoshi et al., 2016). Figure 13 illustrates the flight path to search for a man shouting “Ohi” repeatedly and the results of sound source localization during gliding while turning. The left-lower figure shows the power and MUSIC spectrums for the green trajectory of 5 sec. The drone audition localizes an area of sound source positions because the height of the kite plane obtained by GPS fluctuates so much. Therefore, we replace GPS with GNSS and we use a 3D point cloud map to improve the estimation of the sound source position as mentioned in Section 3 of current drone audition activities.

Another important issue with kite planes is flight-path planning and control of switching the rotor. When the rotor is stalled and ego-noise decreases, sound source localization improves. But the rotor stall period becomes longer, the flight height and horizontal movement interfere each other, which deteriorates the performance of sound source

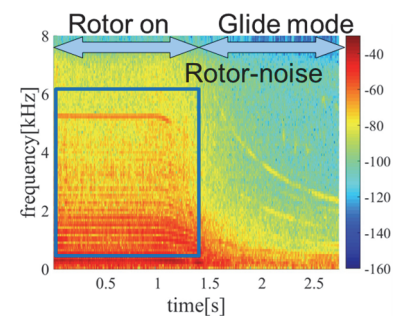
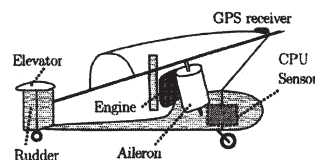


Fig. 11 Kite plane of electric motor model and its microphone array

Fig. 12 Spectrogram at flying and gliding

localization. Periodical stall of the rotor with flight path planning guided towards a sound source demonstrates the stable performance of sound source localization (Kumon et al., 2015) (Nagayoshi et al., 2016). This new method needs to be verified by actual flight.

The kite plane system should be reconstructed by CDS. Since the kite plane is fragile against aerodynamic environments, its control seems much

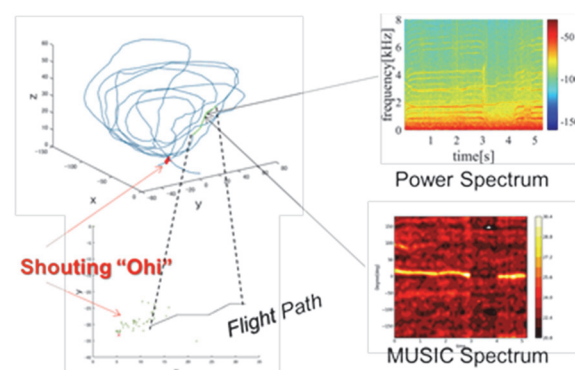


Fig. 13 Position estimation and Tracking of Sound source

more difficult than rotor-based UAVs. The design of the dynamical model library, model predictive control, and reflexive control for cognitive flight control is challenging.

5. Conclusions

Through our experience on drone audition, in particular, a series of field demonstrations of drone audition in search-and-rescue tasks, we realized that a more systematic approach to drone audition was needed to redesign the system and improve the total performance. Inspired by the bat echolocation, CDS-based redesign of radar systems demonstrates significant improvement of the performance of search and track tasks of the radar systems, which is called cognitive radar. In this paper, we proposed cognitive drone audition which is based on CDS. The next step is to design and implement cognitive drone audition for rotor-based drones and kite planes. For rotor-based drones, the integration of silent propeller models and AFRF-MUSIC is the first task. For kite planes, control of rotor-stall duration with path-planning for sound source tracking is the first task. The progress and results will be reported shortly.

References

- Baker, C.J, Smith, G.E, Balleri, A, Holderied, M. and Griffiths, H.D (2014) *Biomimetic Echolocation With Application to Radar and Sonar Sensing* Proc IEEE 102(4), 447-458 doi:10.1109/JPROC.2014.2306252
- Basiri, M, Schill, F.S, Lima, P.U, and Floreano, D (2012) *Robust acoustic source localization of emergency signals from micro air vehicles* Proc 2012 IEEE/RSJ Int'l Conf Intelligent Robots & Systems (IROS), 4737-4742 doi:10.1109/IROS.2012.6385608
- Carrillo, L.R.G, López, A.E.D, Lozano, R, and Pégard, C (2012) *Combining Stereo Vision and Inertial Navigation System for a Quad-Rotor UAV* Jn; Int'l Robot Syst (65), 373–387 doi:10.1007/s10846-011-9571-7
- Chisholm, R.A, Cui, J, Lum, S.K.Y, and Chen, B.M (2013) *UAV LiDAR for below-canopy forest surveys* Jnl Unmanned Vehicle Systems, 1(1), 61-68 doi:10.1139/juvs-2013-0017
- Christian, A and Cabell, R (2017) *Initial Investigation into the Psychoacoustic Properties of Small Unmanned Aerial System Noise* 23rd AIAA/CEAS Aeroacoustic Conf, 15p doi:10.2514/6.2017-4051
- Haykin, S (2006) *Cognitive radar: A way of the future* IEEE Signal Process Mag 23(1), 30-40
- Haykin, S (2007) *Cognitive dynamic systems* Proc 2007 IEEE Int'l Conf Acoustics, Speech & Signal Process (ICASSP), 1369-1372 doi:10.1109/ICASSP.2007.367333
- Haykin, S (2012) *Cognitive Dynamic Systems: Perception-action Cycle, Radar and Radio* Cambridge UK: Cambridge University Press
- Haykin, S, Xue, Y, and Setoodeh, P (2012) *Cognitive Radar: Step Toward Bridging the Gap Between Neuroscience and Engineering* Proc IEEE 100(11), 3102-3130 doi:10.1109/JPROC.2012.2203089
- Haykin, S (2014) *Cognitive Dynamic Systems* Proc IEEE 102(4), 414-41 doi:10.1109/JPROC.2014.2306249
- Hirasawa, N, Hayashi, M, Higashino, S, Okabe, K, Oishi, H, Saito, K, Alimasi, N, and Funaki, M (2019) *UAV observation in Japanese Antarctic Research Expedition (JARE) (in Japanese)* Proc JSSI & JSSE Joint Conf – 2019 in Yamagata, S2-6 doi: 10.14851/jcsir.2019.0_13
- Hoshiba, K, Washisaka, K, Wakabayashi, M, Ishiki, T, Kumon, M, Bando, Y, Gabriel, D, Nakadai, K, and Okuno, H.G (2017) *Design of UAV-embedded Microphone Array System for Sound Source Localization in Outdoor Environments* Sensors 17(11), 2535 doi:10.3390/s17112535

- Hoshiba, K, Nakadai, K, Kumon, M, and Okuno, H.G (2018) *Assessment of MUSIC-Based Noise-Robust Sound Source Localization with Active Frequency Range Filtering* Jnl Robotics & Mechatronics 30(3), 426-435 doi:10.20965/jrm.2018.p0426
- Hoshiba, K, Noda, R, Nakata, T, Liu, H, Senda, K, Nakadai, K, Kumon, M, and Okuno, H.G (2020) *Development of surface-processed low-noise propeller for search and rescue tasks with drone audition* Proc Quiet Drone, to appear
- Ishiki, T and Kumon, M (2015) *Design model of microphone arrays for multirotor helicopters* Proc IEEE/RSJ Int'l Conf Intelligent Robots & Systems (IROS), 6143-6148 doi:0.1109/IROS.2015.7354252
- Ishiki, T, Washizakki, K, and Kumon, M (2017) *Evaluation of microphone array for multirotor helicopters* Jnl Robotics & Mechatronics 29(2), 154-176 doi:10.20965/jrm.2017.p0168
- Kumon, M, Udo, Y, Michihira, H, Nagata, M, Mizumoto, I, and Iwai, Z (2006) *Autopilot System for Kiteplane* IEEE/ASME Trans Mechatronics 11(5), 615-624 doi:10.1109/TMECH.2006.882994
- Kumon, M, Ito, Y, Nakashima, T, Shimoda, R, and Ishitobi, M (2007) *Sound source classification using support vector machine* IFAC Proc 40(13), 465-470 doi:10.3182/20070829-3-RU-4911.00072
- Kumon, M., Oda, Y, and Mizumoto, I (2013) *Simple Adaptive Control for a Class of Mechanical Systems and its Application to a Quadrotor Helicopter* AIAA Guidance, Navigation, and Control (GNC) Conference, 16p doi:10.2514/6.2013-4515
- Kumon, M, Tajima, S, and Nagayoshi, H (2015) *Sound Source Search by Kiteplane (in Japanese)* JSAI Tech Rep SIG-Challenge-043-10 (11/12), 48-53
- Nakadai, K, Lourens, T, Okuno, H.G. and Kitano, H (2000) *Active audition for humanoid* Proc 17th Nat'l Conf Artificial Intelligence (AAAI), 832-839
- Nakadai, K, Takahashi, T, Okuno, H.G, Nakajima, H, Hasegawa, Y, and Tsujino, H (2010) *Design and Implementation of Robot Audition System "HARK" – Open Source Software for Listening to Three Simultaneous Speakers* Advanced Robotics 24(5-6), 739–761 doi:10.1163/016918610X493561
- Nakadai, N, Okuno, H.G, Mizumoto, T (2017a) *Development, Deployment and Applications of Robot Audition Open Source Software HARK* Jnl Robotics & Mechatronics 27(1), 16-25 doi:10.20965/jrm.2017.p0016
- Nakadai, K, Kumon, M, Okuno, H.G, Hoshiba, K, Wakabayashi, M, Washizaki, K, Ishiki, T, Gabriel, D, Bando, Y, Morito, T, Kojima, R, and Sugiyama, O (2017b) *Development of microphone-array-embedded UAV for search and rescue task* Proc 2017 IEEE/RSJ Int'l Conf Intelligent Robots & Systems (IROS), 5985-5990 doi:10.1109/IROS.2017.8206494
- Nagayoshi, H, Kumon, M, Washizaki, K, and Okabe, K (2016) *Sound source recognition on the ground by the gliding flight of Kiteplane (in Japanese)* Proc JSME ann Conf Robotics & Mechatronics (Robomec) 1A2-18a3 doi: 10.1299/jsmermd.2016.1A2-18a3
- Nakamura, K, Nakadai, K, Asano, F, Hasegawa, Y, and Tsujino, H (2009) *Intelligent sound source localization for dynamic environments* Proc 2009 IEEE/RSJ Int'l Conf Intelligent Robots & Systems (IROS), 664-669 doi:10.1109/IROS.2009.5354419
- Nakamura, K, Nakadai K, and Okuno, H.G (2013) *A real-time super-resolution robot audition system that improves the robustness of simultaneous speech recognition* Advanced Robotics 27(12), 933–945 doi:10.1080/01691864.2013.797139
- Noda, R, Nakata, T, Senda, K, Liu, H (2020) *Multi-scale morphological effect on noise level and frequency characteristics of drone propeller* Proc Quiet Drone, to appear

Nonami, K, Hoshiba, K, Nakadai, K, Kumon, M, Okuno, H.G, Tanabe, Y, Yonezawa, K, Tokutake, H, Suzuki, S, Yamaguchi, K, Sunada, S, Takaki, T, Nakata, T, Noda, R, and Liu, H (2019) *Recent R&D Technologies and Future Prospective of Flying Robot in Tough Robotics Challenges* Disaster Robotics, Springer Tracts in Advanced Robotics (STAR) 128, 77-142 doi:10.1007/978-3-030-05321-5_3

Okuno, H.G and Nakadai, K (2015) *Robot Audition: Its Rise and Perspective* Proc 2015 IEEE Int'l Conf Acoustics, Speech & Signal Process (ICASSP), 5610-5614 doi:10.1109/ICASSP.2015.7179045

Okutani, K, Yoshida, T, Nakamura, K, and Nakadai, K (2012) *Outdoor auditory scene analysis using a moving microphone array embedded in a quadcopter* Proc 2012 IEEE/RSJ Int'l Conf Intelligent Robots & Systems (IROS), 3288-3293 doi:10.1109/IROS.2012.6385994

Ohata, T, Nakamura, K, Mizumoto, T, Taiki, T, and Nakadai, K (2014) *Improvement in outdoor sound source detection using a quadrotor embedded microphone array* Proc 2014 IEEE/RSJ Int'l Conf Intelligent Robots & Systems (IROS), 1902-1907 doi:10.1109/IROS.2014.6942813

Rosenthal, D.F and Okuno, H.G (Eds.) (1998) *Computational Auditory Scene Analysis* Mahwah, NJ: Lawrence Erlbaum Associates Pub

Lawrence, B.D and Simmons, J.A (1982) *Measurements of atmospheric attenuation at ultrasonic frequencies and the significance for echolocation by bats* Jnl Acoustical Soc America 71(3), 585-590 doi:10.1121/1.387529

Schmidt, A, Loellmann, H.W, and Kellermann, W (2020) *Acoustic Self-awareness of Autonomous Systems in a World of Sounds* Proc IEEE 108(7), 1127-1149 doi:10.1109/JPROC.2020.2977372

Schmidt, R (1986) *Multiple emitter location and signal parameter estimation* IEEE Trans Antennas & Propagation 34(3), 276-280 doi:10.1109/TAP.1986.1143830

Tadokoro, S (2019) *Overview of the ImPACT Tough Robotics Challenge and Strategy for Disruptive Innovation in Safety and Security* Disaster Robotics - Results from the ImPACT Tough Robotics Challenge, STAR 128, 3-22 doi:10.1007/978-3-030-05321-5_1

Yuan, C, Recktenwald, F, and Mallot, H.A (2009) *Visual Steering of UAV in Unknown Environments* Proc 2009 IEEE/RSJ Int'l Conf Intelligent Robots & Systems (IROS), 3906-3911 doi:10.1109/IROS.2009.5354361

Wakabayashi, M, Okuno, H.G, and Kumon, K (2020a) *Drone Audition Listening from the Sky Estimates Multiple Sound Source Positions by Integrating Sound Source Localization and Data Association* Advanced Robotics 34(11), 744-755 doi:10.1080/01691864.2020.1757506

Wakabayashi, M, Okuno, H.G, and Kumon, M (2020b) *Multiple Sound Source Position Estimation by Drone Audition Based on Data Association between Sound Source Localization and Identification* IEEE Robotics & Automation Letters 5(2), 792-789 doi:10.1109/LRA.2020.2965417

Wakabayashi, M, Washizaka, K, Hoshiba, K, Nakadai, K, Okuno, H.G, Kumon, K (2020c) *Design and Implementation of Real-Time Visualization of Sound Source Positions by Drone Audition*, Proc 2020 IEEE/SICE Int'l Conf System Integration (SII), 814-819 doi:10.1109/SII46433.2020.9025940

Wallace, L, Lucieer, A, Watson, C, and Turner, D (2012) *Development of a UAV-LiDAR System with Application to Forest Inventory* Remote Sensing, 4(6), 1519-1543 doi:10.3390/rs4061519

Wang, L and Cavallaro, A (2020) *A blind source separation framework for ego-noise reduction on multi-rotor drones* IEEE/ACM Trans Audio, Speech, and Language Process in print doi:10.1109/TASLP.2020.3015027



QUIET DRONES
International e-Symposium
on
UAV/UAS Noise
Remote from Paris – 19th to 21st October 2020

Chaotic and wavelet aeroacoustic analysis of twin rotors for drone propulsion

Tiziano Pagliaroli: Niccolò Cusano University: tiziano.pagliaroli@unicusano.it

Paolo Candeloro: Niccolò Cusano University: paolo.candeloro@unicusano.it

Ranieri Emanuele Nargi: Niccolò Cusano University: ranieriemanuele.nargi@unicusano.it

Luca Flamini: NHOE srl: luca.flamini@nhoe.it

Roberto Camussi: University of Roma Tre: roberto.camussi@uniroma3.it

Luca Cucinella: NHOE srl: luca.cucinella@nhoe.it

Roberto Pasta: NHOE srl: roberto.pasta@nhoe.it

Summary

In recent years, small scale unmanned aerial vehicles have received significant attention for a wide range of applications. In the multirotor configuration, the rotor interaction phenomenon occurs severely because the rotors are located in close proximity. Therefore, the distance between the adjacent rotor tips has a strong effect on the flow structures in the wake, on the aerodynamic performance and on the noise generated by the multirotor vehicles.

In the present study, an experimental investigation in semi-anechoic chamber under hover flight conditions is conducted to analyse the mutual rotor-to-rotor interactional effects on the near field of the pressure fluctuations. Experimental data for the twin rotor configurations with different separation distances show an increase in the tonal noise component due to the rotor-rotor interaction, a rotation of the directivity pattern as the rotor distance is varied, and a time-dependent cancellation of the narrow band noise.

1. Introduction

Drones are often identified as Unmanned Aerial Vehicle (UAVs) or Micro Aerial Vehicle (MAV). In the most interesting configurations, drones are already designed with vertical or horizontal

take-off and landing capabilities, and can be manoeuvred with extremely high versatility and speed. MAVs are often used in tactical surveillance missions or for reconnaissance purposes. The noise footprint of these vehicles is highly important even when employed in civilian roles, due to their flight proximity to populated urban areas.

To give an idea of public acceptance of large-scale use of drones in residential areas, information about the effects on the population of a large-scale test drone for delivering can be found in an article from the Wall Street Journal: "Delivery Drones Cheer Shoppers, Annoy Neighbors, Scare Dogs" (Cherney, 2018). Indeed, drone noise is indicated as the main obstacle to widespread public acceptance of this technology.

For this reason, the scientific community has been studying the phenomenon very carefully for the last few years. Specifically, since the main source of drone noise are the rotors, significant efforts are focusing on the aeroacoustic studies of the blades. In the past, the topic of rotor noise has been extensively addressed also on helicopter rotor, but these studies cannot be automatically extended to drone rotor. This hindrance is strongly linked to the difference in scale of the drone blades compared to helicopter ones. The use of small scale blades on drones implies that the Reynolds number assumes values between 10^4 and 10^5 (Lee & Lee, 2020). This range of values is associated with transitional fluid dynamic fields, where Tollmien-Schlichting instability and recirculation bubble dynamics play an important role in term of generation of pressure fluctuations (Sinibaldi & Marino, 2013).

The scientific community has tackled the study of drone aeroacoustics by following mainly two strategies: the study of the phenomenon associated with the single rotor (isolated rotor), or the investigation of the noise generated by the complete drone.

Zhou et al. have performed an experimental investigation of the impact of the distance between the twin rotors on both the thrust force and noise level (Zhou, Ning, Li, & Hu, 2017). Tinney and Sirohi have assessed the aerodynamic performance and the near-field acoustics of isolated rotor, quadcopter, and hexacopter configurations through a six-degree-of-freedom load cell and an azimuthal array of microphones to demonstrate the effects of the number of rotors (Tinney & Sirohi, 2018).

Jia and Lee have investigated the interactional aerodynamics and acoustics of the coaxial rotor and quadrotor VTOL aircraft using high fidelity CFD simulations (Jia & Lee, Impulsive loading noise of a lift-offset coaxial rotor in high-speed forward flight, 2020) (Jia & Lee, Acoustic analysis of urban air mobility quadrotor aircraft, 2020). Also Ko et al. have analysed the noise directivity patterns depending on the diamond and square multirotor configuration (Ko, Kim, & Lee, 2019).

Recently Lee and Lee have performed a numerical aeroacoustic study of rotor-rotor interaction by varying their mutual distance (Lee & Lee, 2020).

Although several studies on the multirotor UAVs have been extensively conducted through experiments and the numerical simulations, the analysis of the interactional aeroacoustics have not yet been discussed in detail. In particular, the rotor interactional phenomena occurring around the multirotor vehicles are significantly influenced by the separation distance between the adjacent rotors (Lee & Lee, 2020).

In this work, we aim to study from an experimental point of view the aeroacoustic behavior of a couple of rotors by varying the separation distance, in this way the phenomenon is simplified compared to the study of a complete drone, but still takes into account the interaction between rotors. In fact, the aeroacoustic performance of small UAVs is not simply proportional to the number of rotors. Particular attention is hereafter given to two different aspects: i) the directivity of the noise due to the rotor-rotor interaction; ii) the tonal and intermittent noise dynamics in time-pseudo frequency domain. Moreover, a preliminary chaotic analysis is performed to evaluate if recurrence analysis quantification (RQA) is a suitable mathematical tool to characterize this kind of problem.

1. Theoretical Background

Generally, the propeller aerodynamic noise is split into two main components: narrow and broad-band contributions (Candeloro, Nargi, Patané, & Pagliaroli, 2020)

$$p'(x, t) = p'_{NB}(x, t) + p'_{BB}(x, t)$$

1

where p'_{NB} is the narrow-band (or tonal) component of pressure fluctuations, whereas p'_{BB} is the broad-band counterpart. To further clarify this aspect, the two components have been represented in the Fourier domain in Figure 1.

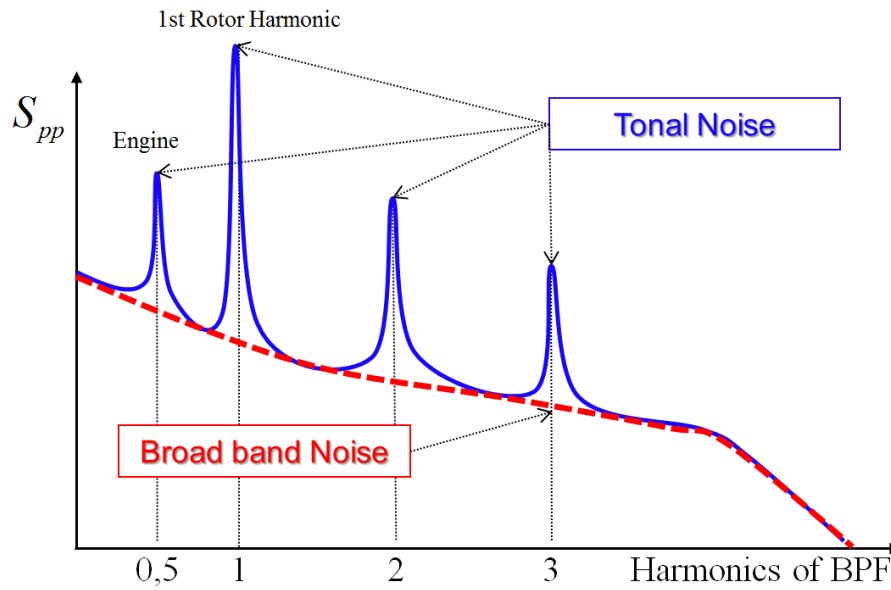


Figure 1 Narrow and broad band component of the pressure fluctuations represented in Fourier domain. Frequency axis is normalised with respect to the blade passing frequency (BPF).

Narrow (or tonal) components are directly associated to the periodic motion of the blade in the surrounding fluid. Therefore, the frequency and magnitude of the radiated noise is related to the rotational regime. For thin blades and low Mach numbers ($M < 1$), the narrow-band contribution is given by the sum of a sound source related to blade thickness, p'_T , and one related to aerodynamic loading, p'_L :

$$p'_{NB}(x, t) = p'_T(x, t) + p'_L(x, t)$$

2

the thickness term takes into account the fluid displacement due to the body shape, while the loading counterpart takes count of the unsteady force distribution over the blade surface. On the other hand, the interaction of turbulent flow structures with the blade edge is responsible for the broad-band noise radiating from the propeller leading/trailing edge or from the blade tip. Therefore, the main sources that generate this component are:

- I. noise related to the turbulence of the incoming flow (*LE noise*) (Pagliaroli, et al., 2018);

- II. noise produced by the interaction of the turbulent boundary layer over the blade surface with the trailing edge (*TE noise*);
- III. noise generated by the possible separation of the flow (*Separation noise*) (Sinibaldi & Marino, 2013)

Therefore, the broad-band contribution can be further divided as follows:

$$p'_{BB}(x, t) = p'_{LE}(x, t) + p'_{TE}(x, t) + p'_S(x, t) \quad 3$$

where $p'_{LE}(x, t)$ is the leading edge component, $p'_{TE}(x, t)$ is the trailing edge component and $p'_S(x, t)$ is the due to laminar separation bubble term.

Another important aspect of pressure fluctuations generated by rotors is the presence of intermittent events. Such events, related to the coherent flow structures, are extremely energetic and characterized by a low probability of occurrence. A normalized time history of the pressure fluctuations is sketched in Figure 2, where a couple of highly energetic intermittent events can be seen.

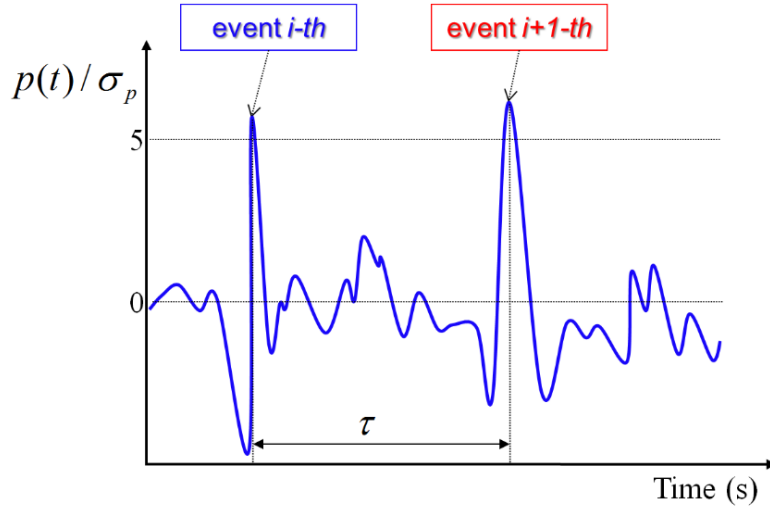


Figure 2 Sketch of a couple of intermittent events occurring in the normalized pressure fluctuations time history.

Since these events exhibit a finite time scale, their projection on a compact support, like the wavelet transform, is particularly useful for their identification in time and the extraction of some of their characteristics. This is one of the reasons that motivated the use of the wavelet transform for data analysis in the present manuscript.

1.1 Wavelet Transform

Wavelets are a relatively recent mathematical tool for time series analysis (Farge, 1992). Wavelet transform (WT) decomposes a space or time signal by expanding the choice for a suitable basis from a wide variety of appropriate functions, allowing to adapt the selected wavelet to each specific problem.

In the last two decades, wavelet transform (WT) has been used for a number of studies, e.g. capturing sea surface thermodynamic variable oscillations in ocean science (Torrence & Compo, 1998), studying coherent structures in turbulent flows (Farge, 1992), studying intermittent phenomena in aeroacoustics (Pagliaroli, Mancinelli, Troiani, Iemma, & Camussi, 2018), in solid rocket motors (Pagliaroli, Camussi, Giacomazzi, & Giulietti, 2015), and within combustor (Pagliaroli & Troiani, 2020). Very recently, WT is used for investigating the acoustic behaviour of meta-surfaces for boundary layer transition control (Pagliaroli, et al., 2020). WT

permits to decompose a space/time history expanding the choice for a proper basis among a great variety of suitable functions, allowing to tailor the selected wavelet to each specific problem.

One of the main properties of wavelet basis functions is their localization in both time and frequency domains. As a result, wavelet series better fit wave forms usually found in nature and often converge faster than corresponding Fourier series.

The first step for a continuous wavelet analysis (CWT) consists in choosing a proper wavelet function $\psi(t)$, called the *mother wavelet*, in the present manuscript a complex mother wavelet named Morlet has been selected.

$$\psi(t) = \pi^{-1/4} e^{i\omega_0 t} e^{-t^2/2} \quad 4$$

where t and ω_0 are the dimensionless time and wavelet centre frequency, respectively (Farge, 1992). Once the $\psi(t)$ has been chosen, a family of continuously and dilated wavelets can be generated and normalized in energy norm:

$$\psi_{s,\tau}(t) = s^n \psi\left(\frac{t-\tau}{s}\right) \quad \text{with } s, \tau \in \mathbb{R}^+ \quad 5$$

where s is the scaling parameter, τ the time shifting and n the normalization exponent. Finally, the wavelet coefficients are defined as:

$$w(s, \tau) = s^{-\frac{1}{2}} \int_{-\infty}^{\infty} x(t) \psi^*\left(\frac{t-\tau}{s}\right) dt \quad 6$$

where ψ^* is the complex conjugate of the dilated and translated mother wavelet.

1.2 Pseudo-phase portrait

In the study of dynamical systems, a delay embedding theorem gives the conditions under which a chaotic dynamical system can be reconstructed. The reconstruction preserves the properties of the dynamical system that do not change under smooth coordinate changes.

First of all, the pseudo-phase space is reconstructed using the Time Delay Embedding (TDE) method (Takens, 1980), after the estimation of the optimal time delay τ_{opt} and the proper embedding dimension d_0 , determined by the Average Mutual Information (AMI) and the Average False Nearest Neighbor (AFNN) algorithm, respectively (Cao, 1997).

Once τ_{opt} and d_0 are obtained, the pseudo-phase space is reconstructed creating a d_0 dimensional time series $y(t)$ from the original one-dimensional $x(t)$ (Pagliaroli & Troiani, 2020):

$$y(t) = [x(t), x(t + \tau_{opt}), \dots, x(t + (d_0 - 1)\tau_{opt})] \quad 8$$

2. Experimental setup

The aeroacoustic measurements campaign was performed within a semi-anechoic chamber. A test bench was realized as described in the following, in order to measure the near field noise generated by the interaction of the twin propellers. Three bladed propellers, type KDE-CF155-TP, were mounted on custom-made vertical support that allows to modify the distance d between them (see Figure 3). For the present study, the propellers rotated in the same direction at two different rotational regimes: 2200 and 3600 *rpm*. Rotational speed was measured by using a Kubler incremental encoder characterized by 500 *ppr*. For the sake of brevity, only the results related to the lower rotational regime are presented and hereafter discussed.

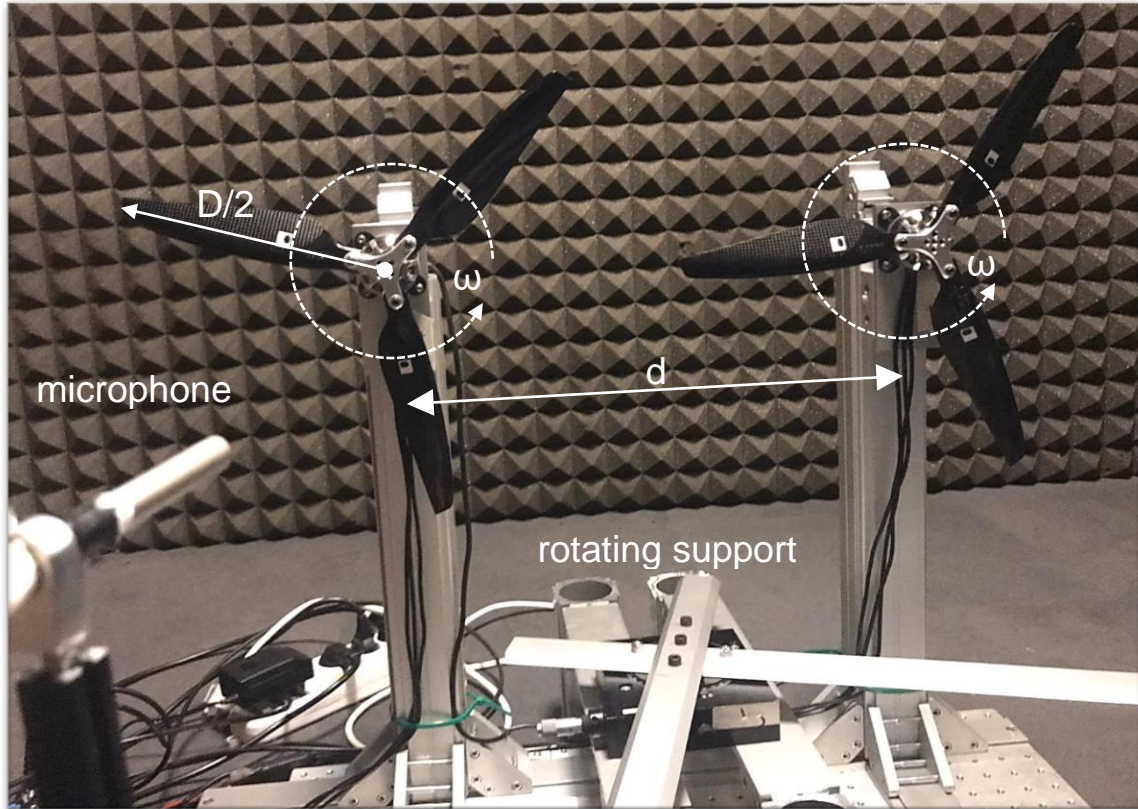


Figure 3 Picture of the experimental setup located within the semi-anechoic chamber (an anechoic wall was used as a background only to take the present picture).

The rotors were driven by a KDE4012XF-400 engines and two KDEXF-UAS55 electronic speed controllers. A NI LabVIEW software was implemented to control the engine, measure the rotational regime and acquire the pressure fluctuations time series. Pressure fluctuations were sampled by using a Microphone Gefell M360 and an ACQ board type NI cDAQ-9174. All signals were acquired for 30 s at sampling frequency $f_s = 51200 \text{ Hz}$. The microphone was mounted on a manual rotation stage in order to characterize the rotor noise directivity pattern, with a polar angle ranging from 0° to 230° , to measure the pressure fluctuations in the inflow field and wake regions as sketched in Figure 4.

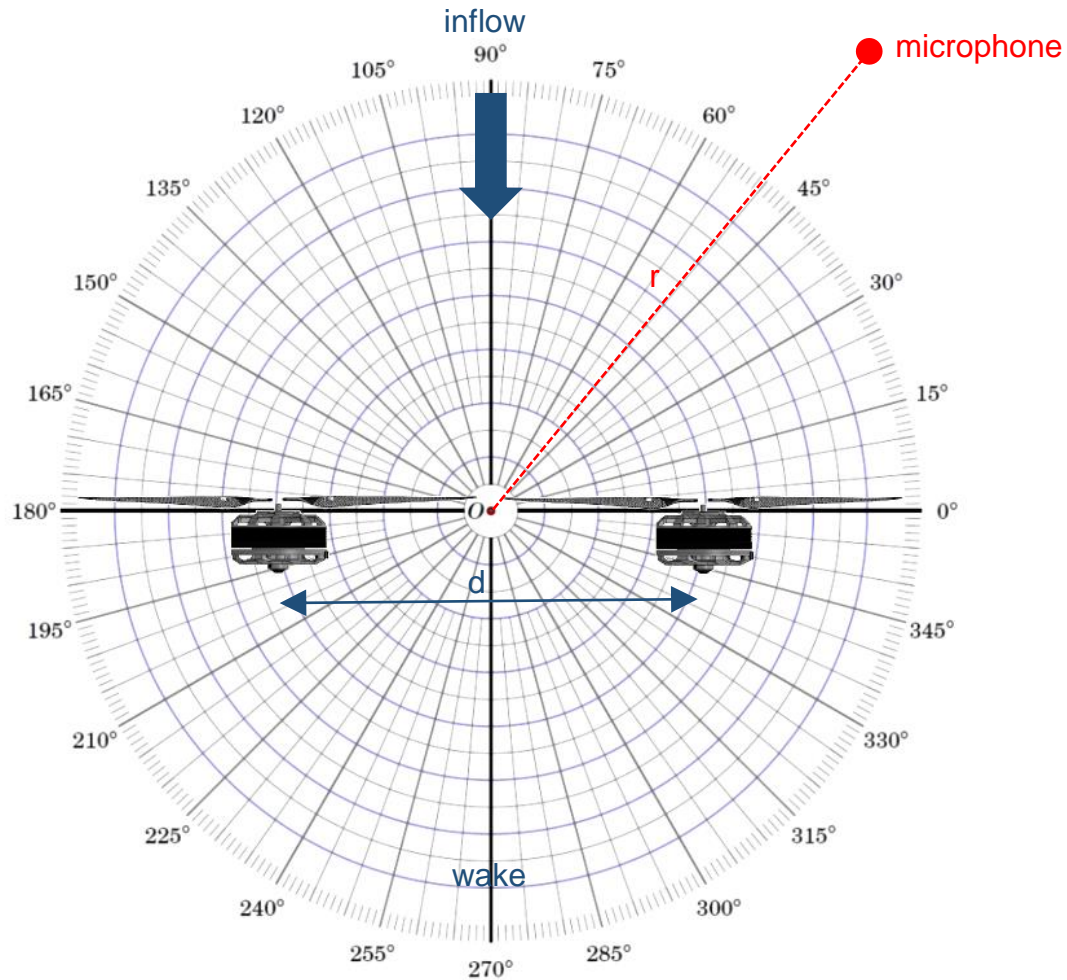


Figure 4 Sketch of the experimental setup.

3. Results

The Over All Sound Pressure Level (OASPL) is represented on a polar diagram for the three different rotor distances (see Figure 5). For the all three cases, there is an asymmetry in the angular region ranging from 0° to 180° . OASPL exhibits the same behavior for the distances between the rotational axes of 42 and 47 cm: from 0° to 90° the OASPL increases, from 90° to 100° a reduction is observed, from 100° to 180° it follows a constant trend, and between 210° and 230° there is a considerable increase due to the effect of the wake. Very different behavior is observed by increasing the distance between the rotors, from 47 to 52 cm: the OASPL trend is constant between 0° and 90° , then there is an increase from 90° to 180° , and the wake effect appears at smaller angles with respect to the previous cases. In summary, the reduction of the rotors mutual distance has a very important effect on the directivity, giving rise to a reinforcement of the noise in the right inflow region and a reduction in the left inflow region. In other words, the interaction between rotors results in directivity angular rotation.

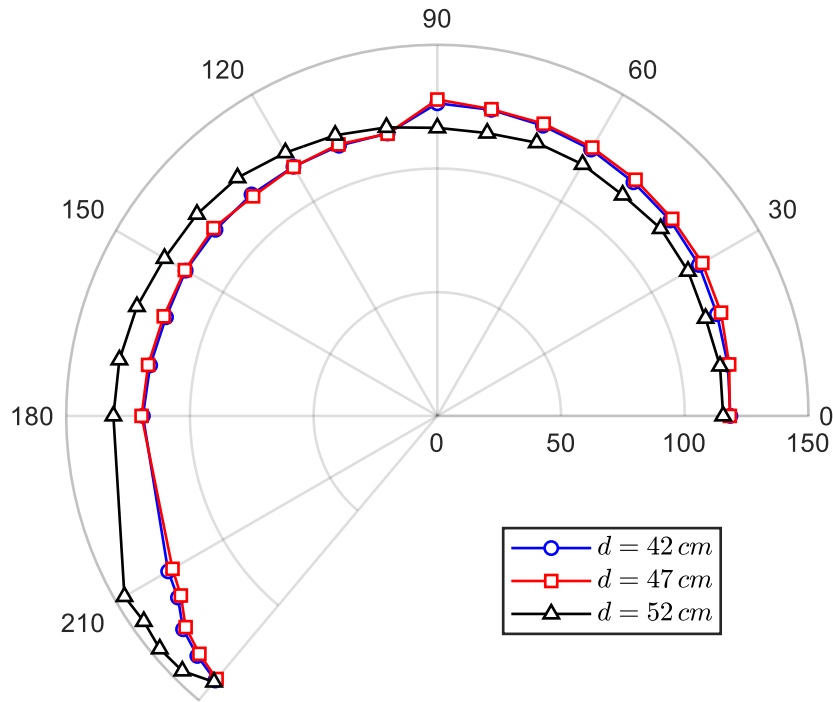


Figure 5 Over All Sound Pressure Level upon the polar angle represented for the three different distances between rotors.

The spectral analysis, represented in normalized frequencies (HBPF) in Figure 6, shows that the SPSLs differ considerably when the distance d is varied, except for the positions 0° where the tonal noise component dominates, and 230° where the broadband component dominates. In these two angular positions the spectra collapse on each other (see Figure 6 a and f).

For angles of 60° and 90° the first effect of the interaction can be clearly distinguished: for $d = 42$ and 47 cm the broadband component is very important while for $d = 52$ cm, as expected for an isolated rotor, the narrowband component is higher in amplitude than the broadband (see Figure 6 b and c).

Furthermore, for polar angle of 120° , only one interesting characteristic is observed: the peak at HBPF=1 is reduced in amplitude while a second one appears in close proximity (at HBPF=1.2), as shown in Figure 6 d.

It is noticeable that in Figure 6 e, for angle equal to 180° , the peak at HBPF=1.2 exceeds in amplitude the other occurring at HBPF=1. This phenomenon, that happens only for $d = 52$ cm, apparently could be explained as an energy transfer from the first tonal component to another one. In Figure 6 e, it is interesting to note that for $d = 52$ cm the broad band component becomes important starting from 180° forward, whereas for $d = 42$ and 47 cm such a characteristic is significant already from 60° . This last aspect contributes to confirm that approaching propellers causes directivity rotation.

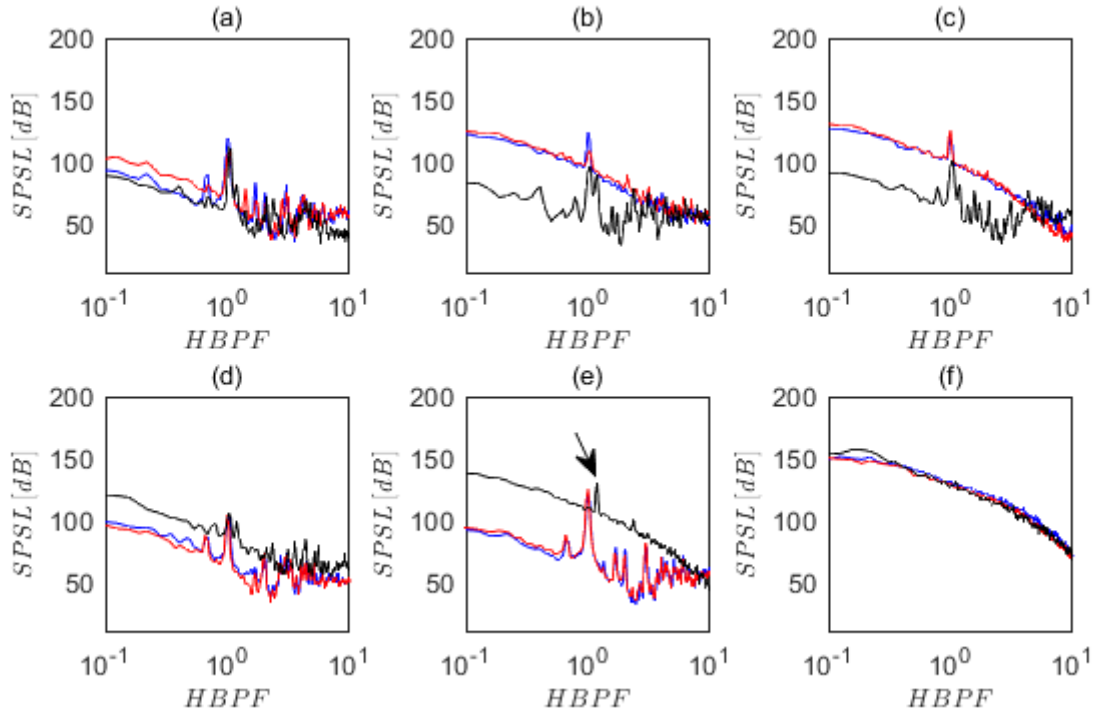


Figure 6 Sound pressure spectral level (SPSL) calculated for $d=52$ cm (black line), 47 cm (red line) and 42 cm (blue line). Spectra are provided for several angular positions: 0° (a), 60° (b), 90° (c), 120° (d), 180° (e), and 230° (f).

In order to highlight what effect the interaction between propellers has on the tonal component, the value assumed by the SPSL at an $HBPF=1$ upon the angular position is represented in Figure 7 a. The asymmetry, previously described in Figure 5, is more evident when the propellers are closer, whereas it is negligible for the pair of propellers separated by a higher distance. The effect of the rotor interaction on the tonal noise as the mutual distance is varied can be summarized in two main features: directivity rotation and SPSL reinforcement. Between 0° e 90° , the closer the propellers, the higher the tonal noise which is produced.

With reference to the assumed energy transfer mechanism from the first ($HBPF=1$) to the harmonic at $HBPF=1.2$, in Figure 7b the SPSLs of the two harmonics are plotted as a function of the angular position. A comparison between the two polar diagrams points out that they are specular (symmetric with respect to the vertical axis $0-90^\circ$). It is also interesting to note that SPSLs increase when the microphone is closer to the rotor disks (at the angular position of 15° and 165°). The underlying origin of the last observation will be object of future investigations.

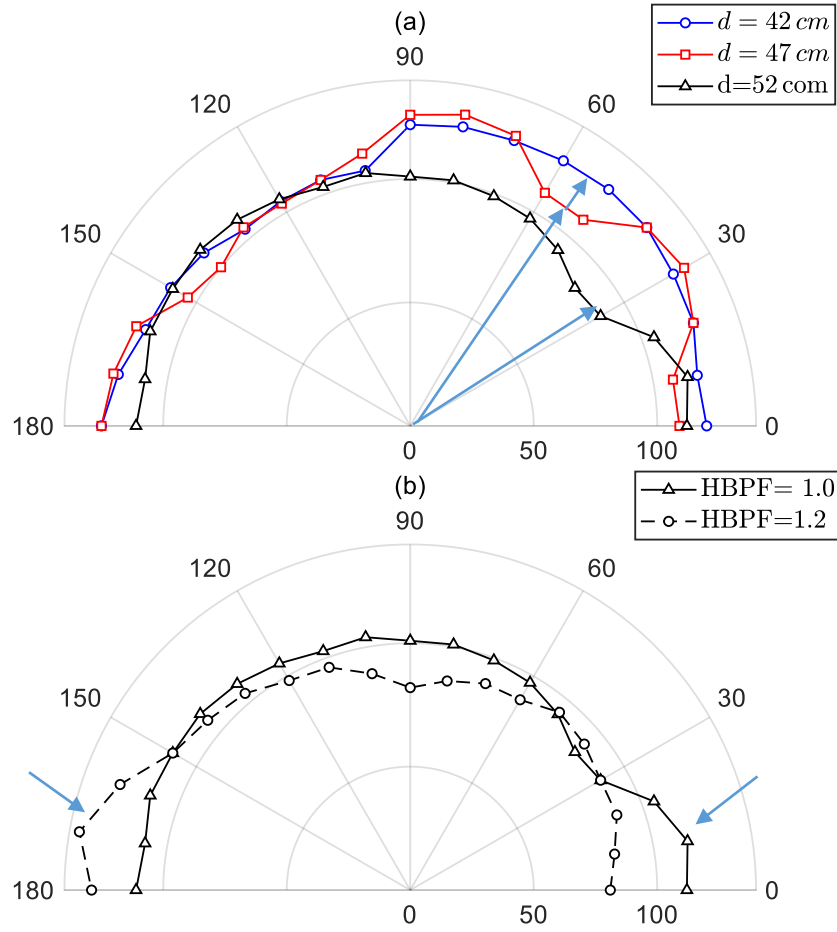
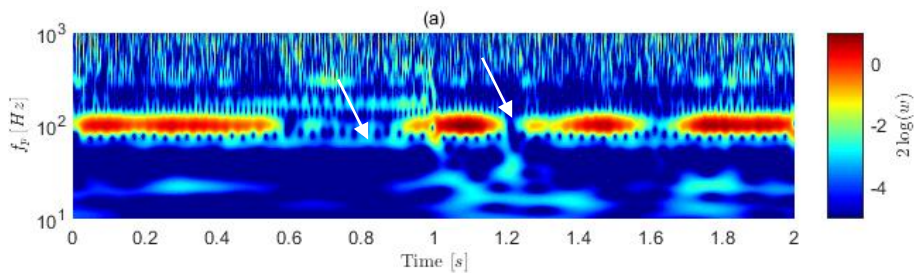


Figure 7 Polar diagram of the SPSL calculated for HBPF=1 for all distances (a); polar diagram of the SPSL calculated for HBPF=1 and HBPF=1.2 for $d=52$ cm (b).

In order to investigate the aeroacoustic behavior of the two propellers, wavelet coefficients are calculated in time and pseudo-frequencies domains for the two configurations $d = 42$ and 52 cm. Generally, Figure 8 and Figure 9 show that the first tonal component is not continuous in time. More specifically, in Figure 8a several time windows can be distinguished indicating a complete cancellation of the first harmonic.

On the other hand, in Figure 9a, by increasing the distance between the propellers, there is a greater continuity of the tonal component that seems to be modulated in intensity. In addition, it is worth noting that for larger angles (see Figure 9b) the tonal component is fragmented becoming intermittent.

Lastly, Figure 8b reveals the passage of large time scale structures significantly contributing to the broad band component.



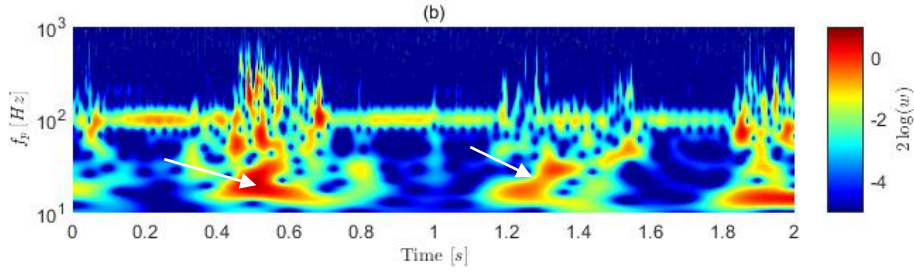


Figure 8 Wavelet coefficients calculated in time and pseudo-frequency domain for $d=42$ cm and angular position of 0° (a) and 90° (b).

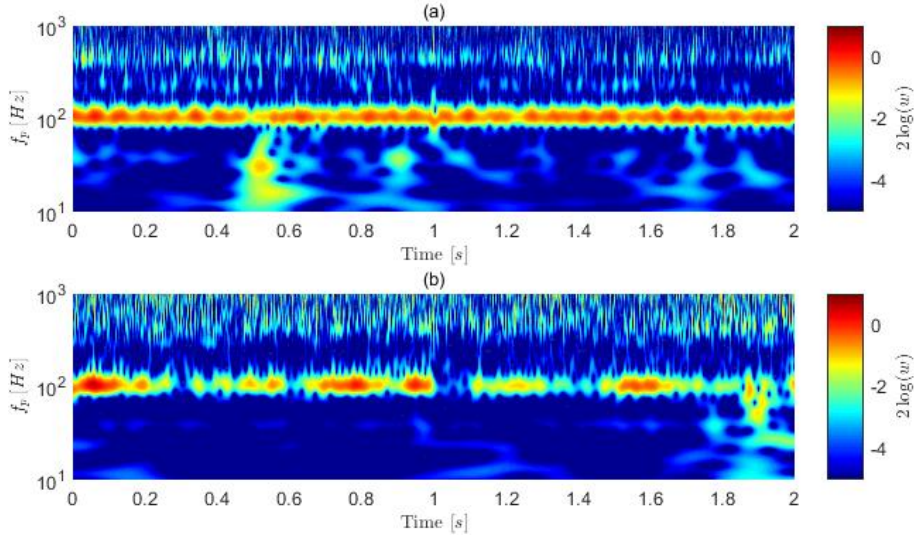


Figure 9 Wavelet coefficients calculated in time and pseudo-frequency domain for $d=52$ cm and angular position of 0° (a) and 90° (b).

The representation of pressure fluctuations in pseudo-phase space confirms what has been discussed so far. As a matter of fact, in Figure 10 a and Figure 11 a-b, the attractors are not elliptical orbits, as expected for pseudo-sinusoidal signals, but they are spiral attractors with a fixed point located in the origin of the axes. These orbits are representative of the temporal dependence of the first harmonic of the rotor noise which is sporadically cancelled. The noise cancelling forces the orbit to restart from the fixed point in the origin. Instead, in Figure 10 b the attractor is not evident because there are some orbits, i.e. the extreme values, with a low frequency of occurrence being ejected from the attractor and reinjected in the more common orbits. Such trajectories are related to intermittent phenomena embedded in the pressure signal. These events are detected by using wavelet transform and appear as bumps in the low frequency region (see white arrows in Figure 8 b).

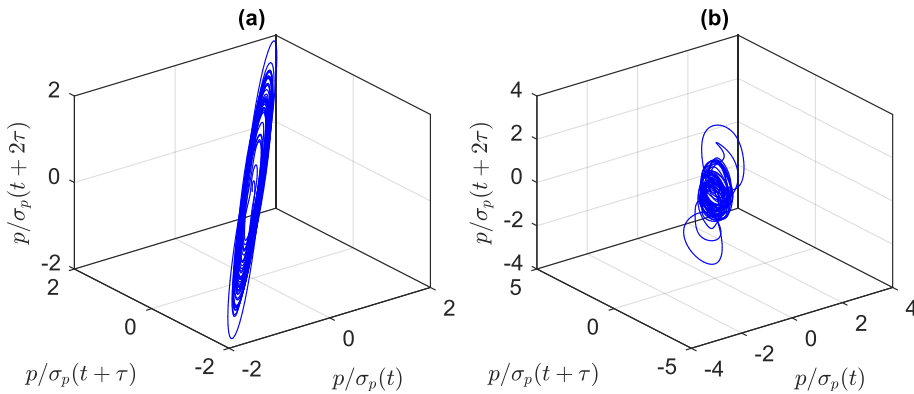


Figure 10 Attractors in pseudo-phase space calculated for $d = 42$ cm at the angular position 0° (a) and 90° (b).

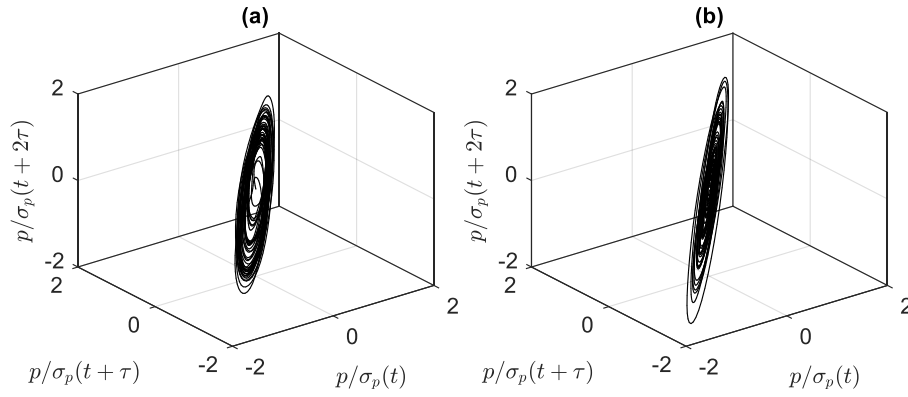


Figure 11 Attractors in pseudo-phase space calculated for $d = 52$ cm at the angular position of 0° (a) and 90° (b).

4. Conclusions

The aeroacoustic behavior of twin rotors for drone propulsion has been experimentally studied in a semi-anechoic chamber. As a main outcome, the shortening of the distance between rotors induces a significant increase in noise amplitude from 0° to 90° , especially for the tonal component. The noise increase is due to rotor-rotor interaction, which is demonstrated to exhibit a strong directivity.

In addition to the increase in the noise tonal component, rotor-rotor interaction is observed to generate a further effect: the rotation of directivity as the distance between rotors is varied.

Wavelet coefficients have allowed to reveal a temporally discontinuous behavior of the narrowband component, which appears to be totally erased in several time intervals. Such a phenomenon may result from the destructive interference of the tonal noise produced by the two propellers. Wavelet analysis has also identified intermittent phenomena occurring in the time series of the pressure signal that contribute significantly to the broadband component in the Fourier domain. Lastly, despite pseudo-phase inspection is a basic approach borrowed from chaotic analysis, it has proved to be a valid and promising mathematical tool for the investigation of rotor noise.

References

- Candeloro, P., Nargi, R. E., Patané, F., & Pagliaroli, T. (2020). Experimental Analysis of Small-Scale Rotors with Serrated Trailing Edge for Quiet Drone Propulsion. *In Journal of Physics: Conference Series* (p. Vol. 1589, No. 1, p. 012007). IOP Publish.
- Cao, L. (1997). Practical method for determining the minimum embedding dimension of a scalar time series. *Physica D*, 110, 43.
- Cherney, M. (2018). Delivery Drones Cheer Shoppers, Annoy Neighbors, Scare Dogs. *Wall Street Journal*.
- Farge, M. (1992). Wavelet transforms and their applications to turbulence. *Annual review of fluid mechanics*, 24(1), 395-458.
- Jia, Z., & Lee, S. (2020). Acoustic analysis of urban air mobility quadrotor aircraft. *In Vertical Flight Society*.
- Jia, Z., & Lee, S. (2020). Impulsive loading noise of a lift-offset coaxial rotor in high-speed forward flight. *AIAA Journal*, 58(2), 687-701.
- Ko, J., Kim, J., & Lee, S. (2019). Computational study of wake interaction and aeroacoustic characteristics in multirotor configurations. *In INTER-NOISE and NOISE-CON Congress and Conference Proceedings*, (pp. Vol. 259, No. 4, pp. 5145-5156).
- Lee, H., & Lee, D. J. (2020). Rotor interactional effects on aerodynamic and noise characteristics of a small multirotor unmanned aerial vehicle. *Phys. of Fluids*, 32(4), 047107.
- Pagliaroli, T., & Troiani, G. (2020). Wavelet and recurrence analysis for lean blowout detection: An application to a trapped vortex combustor in thermoacoustic instability. *Physical Review Fluids*, 5(7), 073201.
- Pagliaroli, T., A., P., Patané, F., Tatí, A., & Peng, L. (2020). Wavelet analysis ultra-thin metasurface for hypersonic flow control. *Applied Acoustics*, 157, 107032.
- Pagliaroli, T., Camussi, R., Candeloro, P., Giannini, O., Bella, G., & Panciroli, R. (2018). Aeroacoustic Study of small scale Rotors for mini Drone Propulsion: Serrated Trailing Edge Effect. *AIAA/CEAS Aeroacoustics Conference*, (p. p. 3449).
- Pagliaroli, T., Camussi, R., Giacomazzi, E., & Giulietti, E. (2015). Velocity measurement of particles ejected from a small-size solid rocket motor. *Journal of Propulsion and Power*, 31(6), 1777-1784.
- Pagliaroli, T., Mancinelli, M., Troiani, G., Iemma, U., & Camussi, R. (2018). Fourier and wavelet analyses of intermittent and resonant pressure components in a slot burner. *Journal of Sound and Vibration*, 413, 205-224.
- Sinibaldi, G., & Marino, L. (2013). Experimental analysis on the noise of propellers for small UAV. *Applied Acoustics*, 74(1), 79-88.
- Takens, F. (1980). Detecting strange attractors in turbulence. *In Dynamical systems and turbulence*, Vol. 898 pp. 366–381.
- Tinney, E., & Sirohi, J. (2018). Multirotor drone noise at static thrust. *AIAA Journal*, 56(7), 2816-2826.
- Torrence, C., & Compo, G. P. (1998). A practical guide to wavelet analysis. *Bulletin of the American Meteorological society*, 79(1), 61-78.
- Zhou, W., Ning, Z., Li, H., & Hu, H. (2017). An experimental investigation on rotor to rotor interactions of small UAV. *35th AIAA applied aerodynamics conference*, (pp. 2017-3744). Denver.



QUIET DRONES
International e-Symposium
on
UAV/UAS Noise
Remote from Paris – 19th to 21st October 2020

Experiments on UAV rotor noise at low Reynolds and low Mach numbers

Parisot-Dupuis H., Université de Toulouse, ISAE-SUPAERO: Helene.Parisot-Dupuis@isae-superaero.fr

Gojon R., Université de Toulouse, ISAE-SUPAERO: Romain.Gojon@isae-superaero.fr

Jardin T., Université de Toulouse, ISAE-SUPAERO: Thierry.Jardin@isae-superaero.fr

Jo Y., Hanseo University, yminjo@hanseo.ac.kr

Doué N., Université de Toulouse, ISAE-SUPAERO: Nicolas.Doue@isae-superaero.fr

Moschetta J.-M., Université de Toulouse, ISAE-SUPAERO: Jean-Marc.Moschetta@isae-superaero.fr

Summary

The present work outlines efforts at ISAE-SUPAERO to reduce the acoustic footprint of rotors operating at low Reynolds and low Mach numbers typical of small and medium scale drones.

An experimental campaign that aims at characterizing rotor noise is presented. The latter serves as a basis for validation of numerical approaches and to investigate the noise mechanisms. Data are obtained in an anechoic room with dimensions (wedge tip to wedge tip) 5.02x5.24x5.34 m3 and cut-off frequency 80 Hz. Aerodynamic loads as well as acoustic fields are recorded for two off-the-shelf (APC 9x6 SF and 11x4.7 SF) and four canonical rotors with different numbers of blades. Both near and far acoustic fields are measured using one microphone located one diameter away from the rotor plane and 13 microphones mounted on a directivity antenna. A range of rotation speed from 1,000 to 10,000 RPM is addressed, corresponding to Mach and Reynolds numbers up to 0.23 and 130,000 respectively.

Results presented in this article are related to two-bladed rotors and are validated using existing experimental data from the literature. They are then used to assess in-house numerical simulations (NL-VLM and CFD) and unravel the physics behind rotor noise at low Reynolds and low Mach numbers. This fundamental understanding will help draw general guidelines for the design of low noise rotors.

Introduction

The great development of Unmanned Air Vehicles (UAV) in the last decade may considerably increase city noise pollution in the near future. This will lead FAA and EASA to put in place more stringent certification standards to protect civilian population, addressing especially UAV noise. The understanding of UAV noise generation mechanisms becomes then an important research topic to develop future UAV designs suitable for these new standards.

The study of rotor noise is not new but was since recently essentially focused on helicopters (Brentner *et al.* 1994). While helicopters operate at relatively high Reynolds and Mach numbers with usually only one rotor, UAV often present multiple rotors configurations operating at much lower Reynolds and Mach numbers. This makes the knowledge on helicopter noise not directly transposable to all UAV configurations.

The aeroacoustics of low Reynolds and Mach numbers rotors have been recently addressed by Zawodny *et al.* 2016 which reported experiments on small scale rotors operating under hovering conditions. They pointed out that the farfield radiation is characterized by tonal noise at the Blade Passing Frequency (BPF) and harmonics, and broadband noise in the mid and high frequency range. Tonal and broadband noises in the low frequency range coming from the motor during their experiments were also reported. They additionally presented comparison of experimental results with numerical predictions using low fidelity (blade element analysis) and high fidelity (CFD) simulations associated to Ffowcs Williams-Hawkings approach (FW-H) and broadband models. Rotor tonal noise was found to be reasonably well predicted by both approaches.

In Intarattep *et al.* 2016, the aerodynamic and acoustic performances of a quad rotor drone DJI Phantom II were investigated in different configurations. They observed notably that the noise was dominated by tone noise at the blade passing frequency and their harmonics. In Tinney *et al.* 2018, several multirotor drones were studied in an anechoic room with propeller diameters ranging from 20 to 30 cm. An azimuthal array of microphone was used to assess the acoustic near field. The sound pressure of the first few harmonics was shown to decrease with both the number of propellers and the increase of propeller diameter.

More recently, Jo *et al.* 2019 used a Non-Linear Vortex Lattice Method (NL-VLM) associated with a FW-H analysis to study the effect of blades number on the aeroacoustics of hovering rotors. It was demonstrated that, for a given target thrust, rotor performance was enhanced in the case of three blades and that, despite the increasing influence of blade-vortex interactions, noise monotonically decreased with the number of blades. Serré *et al.* 2019 also performed an aeroacoustic optimization of hovering rotor using low order models (blade element analysis, FW-H and broadband models). The overall rotor noise appeared to be significantly reduced with low order approaches in comparison to conventional off-the-shelf rotors. Further investigations using high fidelity (LES) simulations gave some insights on the hierarchy of noise sources mechanisms.

In order to obtain further guidelines for the development of low noise UAV rotors in hovering conditions, this paper presents an experimental campaign that aims to be a database for the validation of numerical approaches. First, acoustic fields and aerodynamic loads measured for off-the-shelf two-bladed rotor APC 11x4.7 SF were validated using existing experimental data from the literature. Then, a canonical two-bladed rotor was used to assess the performance of in-house CFD and NL-VLM simulations and to unravel the physics behind hovering rotor noise at low Reynolds and low Mach numbers.

1. Experimental and numerical setup

1.1 Experimental setup

A view of the experimental setup used in this study is provided in Figure 1.

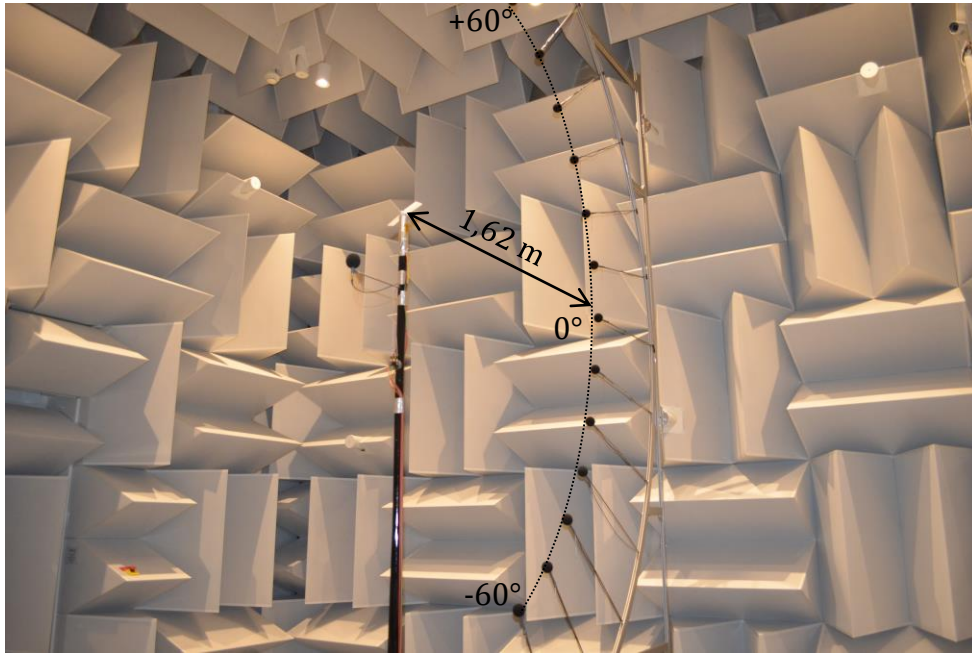


Figure 1: Experimental setup for UAV rotor testing within ISAE-SUPAERO anechoic room.

Experiments were performed in the ISAE-SUPAERO anechoic room. This facility is acoustically treated down to a cut-off frequency of 80 Hz and has interior dimensions of (wedge-tip to wedge-tip) of 5.02x5.24x5.34 m³. Tested UAV rotors were positioned at the center of the anechoic room, at the top of a rotor test stand. They were driven by means of a Faulhaber 3274G024BP4 3692 electric brushless motor, which was chosen for its low noise emission. Real time Revolution Per Minute (RPM) are directly given by the associated Motion Controleur MC5010 for an accurate speed control.

A six-axis ATI Nano17 load cell is located just beneath the motor for measuring aerodynamic loads. One can notice that only two components are of interest here: the rotor thrust $T(N)$ and torque $Q(N.m)$. These data were acquired at a sampling rate of 2 kHz for a duration of 16 s.

A total of 14 GRAS 40PH microphones were used for acoustic measurements. One of them was placed in the nearfield 25 cm below the rotor plane and 25 cm away from the rotor axis. Others were mounted on a directivity antenna to measure farfield noise radiated at distance of 1.62 m from the rotor center. They were positioned every 10° from -60° to 60°, where 0° corresponds to the rotor plane. Acoustic data were acquired at a sampling frequency of 51.2 kHz during 16 s.

Several UAV rotors have been tested on this setup. First, 2 two-bladed commercial rotors APC 9x6 SF and 11x4.7 SF. Then, 4 homemade 3D-printed rotors with NACA0012 blade profile and blade numbers from 2 to 5. Characteristics of these different rotors are given in Table 1. Please note that only results obtained for two-bladed rotors APC11x4.7 SF and ISAE 2 are presented in this article. All the results will be available in a few months as an open database for the UAV acoustic community.

Name	Diameter (m)	Blades number	Profile	Chord (m)	Pitch (°)
APC 9x6 SF	0.23	2	Eppler E63 / Clark-Y*	varying	varying
APC 11x4.7 SF	0.28	2	Eppler E63 / Clark-Y*	varying**	varying**
ISAE 2-5	0.25	2-5	NACA0012	0.025	10

Table 1: Rotors characteristics (* from www.apcprop.com, ** see Zawodny *et al.* 2016)

The experimental test matrix used for aerodynamic and acoustic measurements is presented Table 2.

Rotors	RPM	Additional RPM
APC	0:1000:7000	3600; 4200; 4800
ISAE	0:500:9000	N/A

Table 2: Experimental test matrix used for UAV aeroacoustic rotors testing.

1.2 Numerical setup

The flow past the two-bladed ISAE rotor at 6000 RPM is simulated using two numerical approaches; namely a low order Non-Linear Vortex Lattice Method (NL-VLM) and higher fidelity Computational Fluid Dynamics (CFD) simulations.

The CFD simulations are performed with the CFD commercial software Star CCM+ v13.04. The rotor geometry includes the two blades and a short part of the hub, as shown on Figure 2.

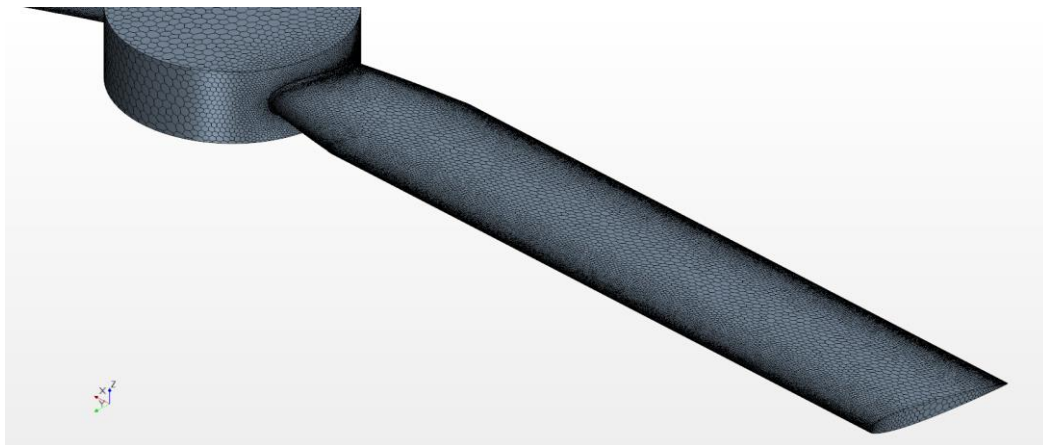


Figure 2: Rotor surface mesh.

The computational domain is split into two parts: an inner rotating part including the rotor, and an outer static part for the farfield boundary conditions, see Figure 3. The rotating part is meshed with polyhedral cells and prism layers at blade walls for the discretization of the boundary layers. The thickness of the near wall prism layer is set to target a value of 1 for Y^+ . The static part is meshed with trimmed cells, whose size increases from the rotor center to the farfield boundaries. The inner and outer regions communicate thanks to interfaces. The blades are modelled as non-slip walls. Upstream, downstream and lateral boundaries are modelled as stagnation inlet, pressure outlet and slip walls, respectively. Convergence with respect to spatial resolution is

tested using three different unstructured meshes with a total number of cells of 3.4, 5.7 and 11.4 millions for the coarse, base and fine meshes, respectively.

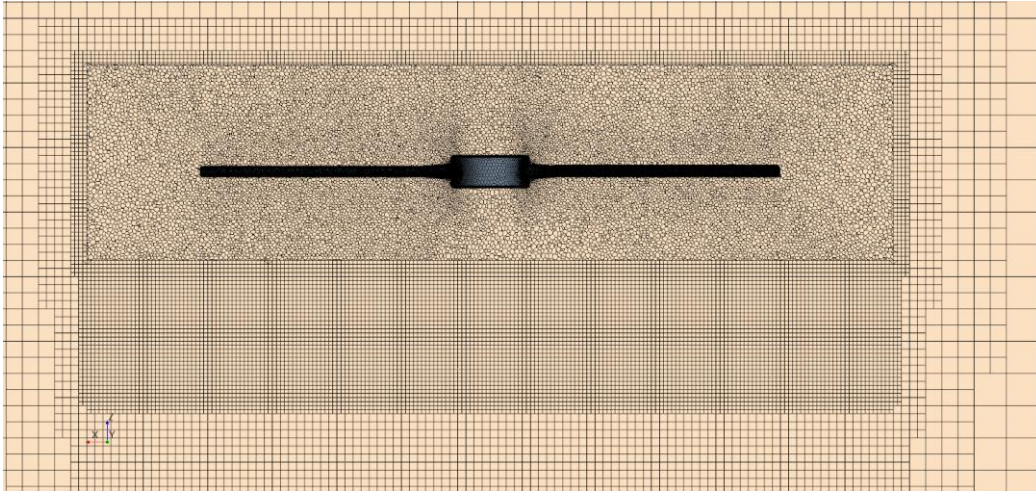


Figure 3: Split of the volume mesh.

Since the flow is incompressible, a segregated solver with constant density is selected. Note that the local Reynolds number based on the local blade speed and chord length increases from approximately 20 000 at the blade root to 120 000 at the blade tip. The laminar boundary layers will be predominant, and fully turbulent URANS simulations are not appropriate with such Reynolds numbers. We thus test two laminar/turbulent simulations: implicit Large Eddy Simulation (implicit LES), and the $k\omega$ -SST turbulence model with Gamma transition model ($k\omega$ -SST).

With implicit LES, Navier-Stokes (N-S) equations are solved directly without turbulence or sub-grid model. However the mesh was generated according to RANS requirements and only the largest turbulence length scales can be simulated. In a classical $k\omega$ -SST turbulence model is fully turbulent. We enabled the Gamma transition model to consider the laminar part of the flow, especially in the boundary layer.

The spatial and temporal discretization schemes are second order, and the time-step for the implicit unsteady solver is defined to obtain a rotation of 1 degree every time-step. The mean and maximal values of the convective Courant number in the rotating part are around 1 and below 10, respectively.

The NL-VLM simulations are achieved using the in-house code described in Jo *et al.* 2017 and Jo *et al.* 2019. Specifically the blade surface is discretized into two-dimensional panels on which Laplace equation for the velocity potential ϕ is solved. Non-penetration condition at the blade surface and Kutta condition at the trailing edge are applied to close the system. Non-linearity is introduced using a table look-up procedure, with blade section polars obtained using Xfoil. The rotor wake is modelled using vortex particles released at the trailing edge, leading to an N-body problem whose resolution is accelerated through a Fast Multiple Method (FMM) and with Message Passing Interface (MPI) for parallelization. The code is further detailed and validated on cases similar to those addressed thereafter in Jo *et al.* 2017 and Jo *et al.* 2019.

Both CFD and NL-VLM approaches are coupled with a Ffowcs Williams-Hawkings model that propagates acoustic waves from the rotor surface to the farfield.

The whole rotor (blades and hub) is defined as the source surface and acoustic receivers are placed at 1.68m of the rotor center, every 5 degrees.

1.3 Data reduction and post-processing

This part presents the data reduction and post-processing of physical aerodynamic and acoustic quantities used in this article.

Please note that in the following:

- aerodynamic loads are presented in their non-dimensional form, using time-averaged thrust and torque coefficients: $\overline{C_T} = T/\rho f^2 D^4$ and $\overline{C_Q} = Q/\rho f^2 D^5$, where ρ , f and D are respectively the fluid density, the rotational frequency and the rotor diameter.
- acoustic spectra presented corresponds to Sound Pressure Levels (SPL) computed using a Hanning window with 50% overlap and a frequency resolution of 3.125 Hz.

2. Experimental setup validation

First, mounting and environment effects are investigated in order to find the best testing configuration. Then, as aerodynamic (Brandt *et al.*) and acoustic (Zawodny *et al.* 2016) results are already published on APC rotors, they are used to validate the experimental setup.

2.1 Experimental setup assessment

The APC 11x4.7 SF rotor is used to assess mounting and environmental effects.

First, the impact on measurements of airflow direction respect to the rotor test stand is investigated.

Comparison between aerodynamic measurements performed in the case of upstream airflow (clockwise rotation) and downstream airflow (anti-clockwise rotation) for different rotational speeds are presented Figure 4.

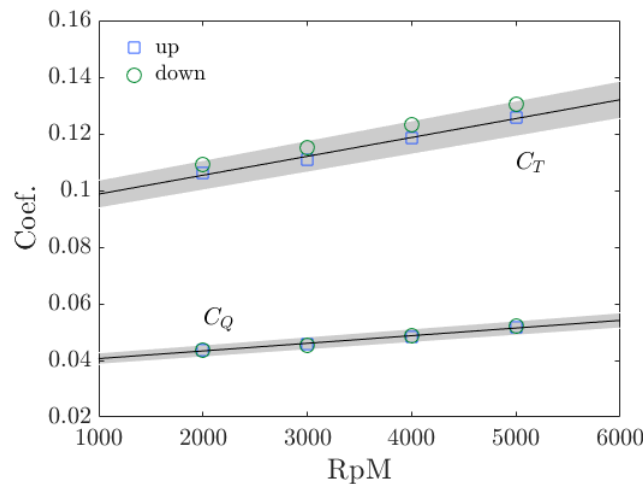


Figure 4: APC 11x4.7 SF time-averaged thrust and torque coefficients as a function of rotor RPM for upstream and downstream airflows.

Thrust and torque coefficients $\overline{C_T}$ and $\overline{C_Q}$ obtained for upstream (blue squares) and downstream (green circles) airflows are comparable and in good agreement with Brandt *et al.* data corresponding to black lines. Grayed regions indicate an arbitrary $\pm 5\%$ of the fitted values obtained by Brandt *et al.*. Small differences observed on $\overline{C_T}$ between upstream and downstream airflows stay within this range of values.

Acoustic measurements were also compared for both airflow directions. Figure 5 shows farfield SPL obtained in the rotor plane for 3000 and 5000 RPM. In the case of 5000 RPM, a repetition of each measurement is also plotted to emphasize the measurement repeatability.

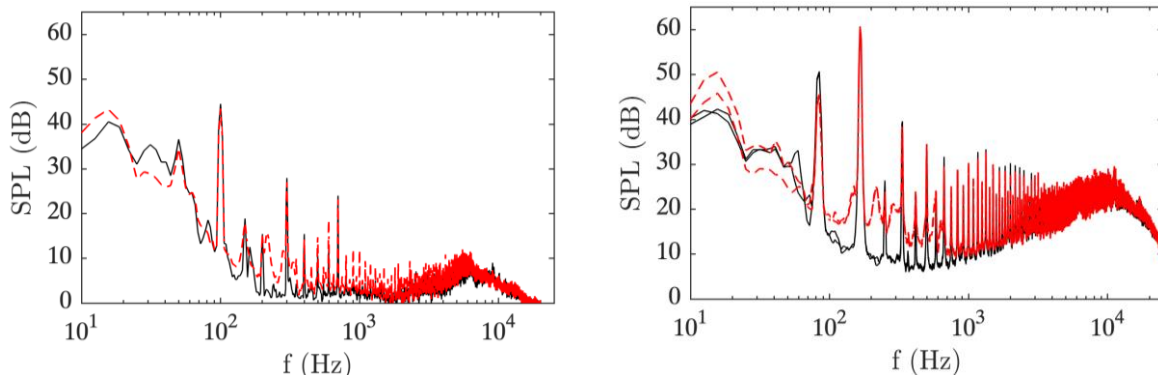


Figure 5: APC 11x4.7 SF farfield SPL in the rotor plane for 3000 RPM (left) and 5000 RPM (right): upstream airflow (---) and downstream airflow (- - -).

Some differences can be noticed for the tonal noise corresponding to the rotational speed (first tone) and for the broadband noise in the frequency range 100-800 Hz. This increase of broadband noise for downstream airflow can be explained by the interaction of the airflow with the test stand, which creates additional noise. However, results obtained for the main tone associated with the BPF and high frequency broadband noise due to trailing edge noise are very similar for both airflow directions.

In order to limit mounting impact on the results, it was decided to keep in the following the upstream airflow direction, except for the comparison with Zawodny *et al.* 2016 results.

Secondly, the effect of airflow recirculation in the anechoic room on the measurements is assessed.

Indeed, Stephenson *et al.* 2019 recently showed that airflow recirculation in small anechoic rooms can result in a significant increase of higher harmonic rotor tones. They observed an increase of more than 15 dB of some harmonics for a 24 cm diameter rotor in an anechoic room of wedge-tip to wedge-tip dimensions 3.65x2.56x3.26 m. In order to verify this point, a spectrogram of 60 s length with a sampling frequency equals to 0.1 s is presented in Figure 6 in the rotor plane. The rotor is driven from 0 to 5000 RPM and reaches its maximum speed at $t = 13.5$ s.

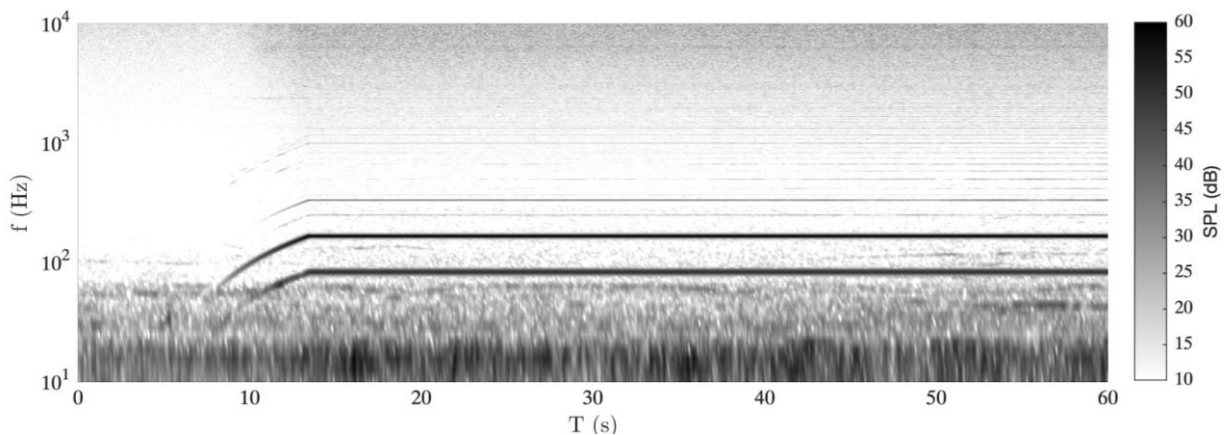


Figure 6: APC 11x4.7 SF SPL spectrogram in the rotor plane: 0 to 5000 RPM.

The main tones appear to be very stable over time but some small discrepancies can be visible on higher harmonics. This shows that the effect of airflow recirculation seems thus acceptable for the thrust tested.

2.2 Aerodynamic validation

Aerodynamic measurements are validated by comparison with Brandt *et al.* reference database for APC 11x4.7 SF and Zawodny *et al.* 2016.

Thrust and torque coefficients $\overline{C_T}$ and $\overline{C_Q}$ measured by the ATI Nano 17 load cell for rotational speeds ranging from 2000 to 6000 RPM are presented Figure 7.

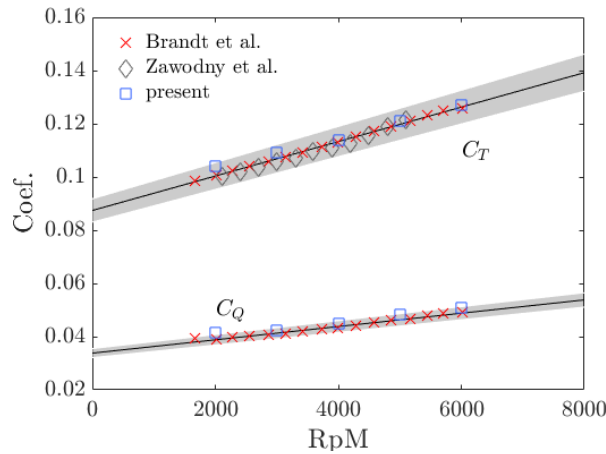


Figure 7: APC 11x4.7 SF time-averaged thrust and torque coefficients as a function of rotor RPM: Brandt *et al.*, Zawodny *et al.* 2016 and present data.

Results obtained with the three datasets are consistent and globally stay within the grayed regions.

2.3 Acoustic validation

Commercial rotor APC 11x4.7 SF is now used to validate acoustic measurements against results published by Zawodny *et al.* 2016 for 3600, 4200 and 4800 RPM.

Zawodny *et al.* 2016 measurements were performed with airflow going on the rotor test stand and farfield spectra presented correspond to a microphone situated 190,5 cm away from the rotor center at an angle of 45 degrees with respect to the rotor plane. To allow this comparison, an amplitude scaling assuming spherical wave propagation in freefield is applied to our 40 and 50 degrees spectra in the case of downstream airflow (anti-clockwise rotation). Results are shown Figure 8.

The main tone, which corresponds to the BPF, is very comparable to Zawodny *et al.* 2016 data as its amplitude is always located between 40 and 50 degrees spectra as expected. Differences can be observed on its harmonics that present globally higher levels than Zawodny *et al.* 2016 measurements which show numerous other tones related to their motor above 500 Hz. Broadband noise is well comparable except on the frequency ranges for which the motor used for Zawodny *et al.* 2016 experiments generates broadband noise: lowest frequencies for 3600 and 4200 RPM and on the frequency range 500-2000 Hz.

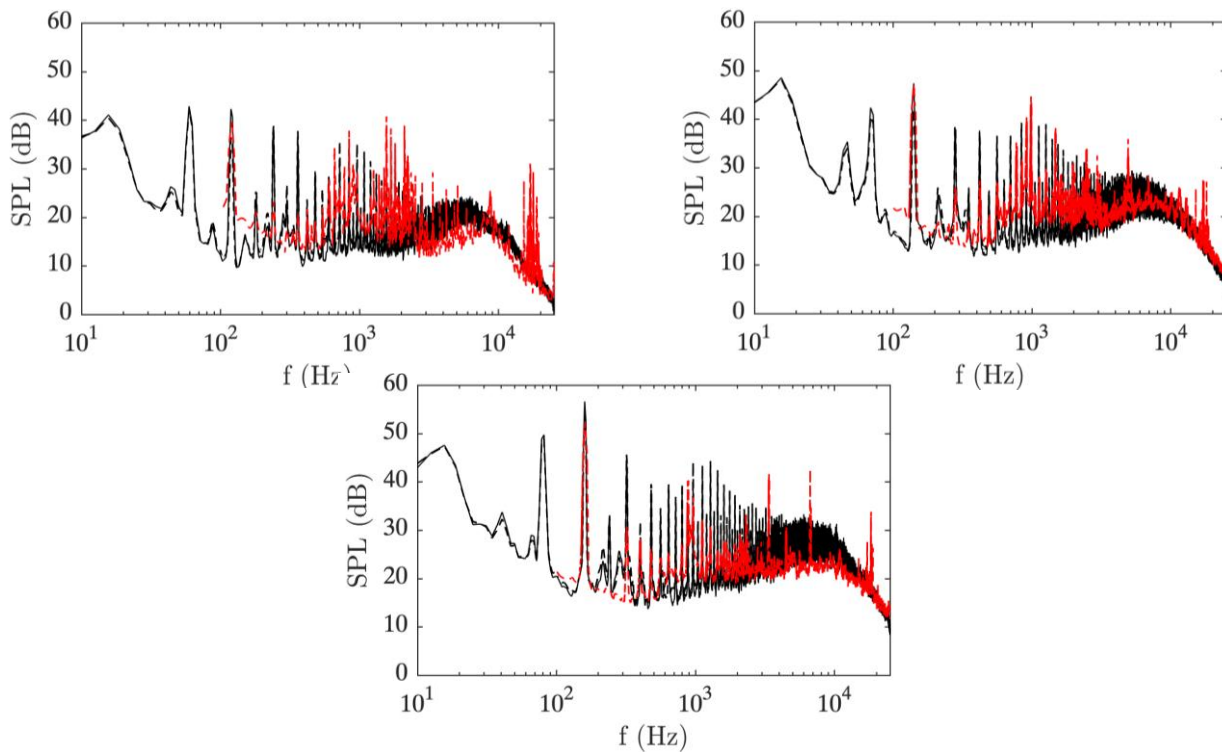


Figure 8: APC 11x4.7 SF SPL at 190,5 m for 3600 RPM (top left), 4200 RPM (top right) and 4800 RPM (bottom): 40° (---), 50° (- - -) and 45° (- - -) (Zawodny *et al.* 2016).

3. Numerical approaches assessment

In this section, we investigate the aerodynamics and aeroacoustics of the two-bladed ISAE canonical rotor. Recall that the latter has NACA0012 blade sections with uniform chord length and a constant pitch angle of 10 degrees. The diameter and the chord length are 12.5 cm and 2.5 cm, respectively. The rotor is 3D-printed using stereolithography and tested experimentally using the setup described earlier. In addition, NL-VLM and CFD simulations are performed and the results are compared with experimental data for 6000 RPM.

3.1 Global assessment

Table 3 reports aerodynamic (thrust and torque coefficients) and acoustic (BPF SPL) data obtained at 6000 RPM for NACA0012 two-bladed rotor using experimental and numerical approaches.

Methods	CT	CQ	BPF SPL (dB)
Experiments	0.0503	0.0033	62.2
CFD (implicit LES) - coarse/base/fine	0.0571/0.0571/0.0575	0.0036/0.0036/0.0036	64.7/64.8/64.8
CFD ($k\omega$ -SST) - coarse/base/fine	0.0566/0.0569/0.0573	0.0035/0.0035/0.0034	64.7/64.8/64.8
NL-VLM	0.0493	0.0032	58.9

Table 3: Comparison of aerodynamic (thrust and torque coefficients) and acoustic (BPF amplitude on the rotor plane) data for ISAE two-bladed rotor at 6000 RPM.

Aerodynamic results show that the effect of meshes and laminar/turbulent methods is negligible for CFD simulations. In the following only implicit LES results with fine mesh are presented. These

results appear to slightly overestimate thrust and torque coefficients with respect to experimental data, whereas NL-VLM and experimental aerodynamic results are very consistent.

The comparison of BPF SPL obtained with the three approaches shows that implicit LES overestimates the BPF whereas NL-VLM underestimates it. The higher levels obtained with implicit LES might be explained by higher thrust and torque coefficients that might be linked to a higher blade loading. In the case of NL-VLM, differences may be explained by the nature of the low order model, which uses 2D approximation. Even with the good thrust and torque coefficients, the aerodynamic loading may be locally less accurate. Please note that numerical acoustic results are corrected assuming spherical wave propagation in free field in order to be comparable to experimental data measured 1,62 m from the rotor center.

3.2 Aeroacoustic performance

Now aeroacoustic performance of both numerical approaches (implicit LES and NL-VLM) is assessed.

First, farfield acoustic spectra measured and simulated at 40° from the rotor plane and in the rotor plane are presented Figure 9.

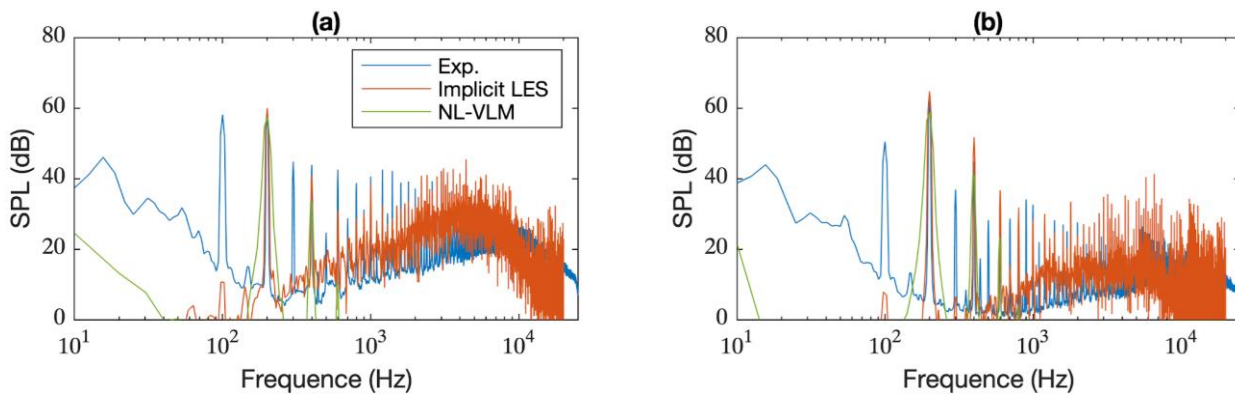


Figure 9: Acoustic spectra measured at 40 degrees (left) and in the rotor disk plane (right) for ISAE two-blade rotor at 6000 RPM.

Tonal noise at the shaft rate, the BPF and their harmonics as well as mid and high frequency broadband noise dominate the rotor spectra for both radiation angles. Data comparison shows that implicit LES is able to predict the main tones (BPF and first harmonics) and a part of the high frequency broadband noise due to trailing edge noise, whereas NL-VLM, which is a low order numerical approach, is only able to estimate the SPL of the BPF and its first harmonic.

When looking at the directivity, several characteristics of the spectra can be studied. The Overall Sound Pressure Level (OASPL) on the frequency range [80-16000] Hz, the amplitude of the BPF and its first harmonic, as well as the high frequency broadband noise on the frequency range [7500-16000] Hz are plotted Figure 10. Please note that for NL-VLM simulations, only the amplitudes of the BPF and of its first harmonic are plotted as only those values can be predicted by the NL-VLM method.

In terms of physical behaviour, the OASPL radiation pattern seems omnidirectional as expected. The BPF presents a horizontal dipole pattern with a slight dissymmetry: the maximum is located between angles 10 and 20°. This is consistent with results obtained by Zawodny *et al.* 2016 for other two-bladed rotors (DJI 9443 and APC 11x4.7 SF). Experimental results show a similar directivity for the first harmonic of the BPF with lower levels. High frequency broadband noise presents a vertical dipole noise pattern with a minimum level at -10°, typical of trailing edge noise.

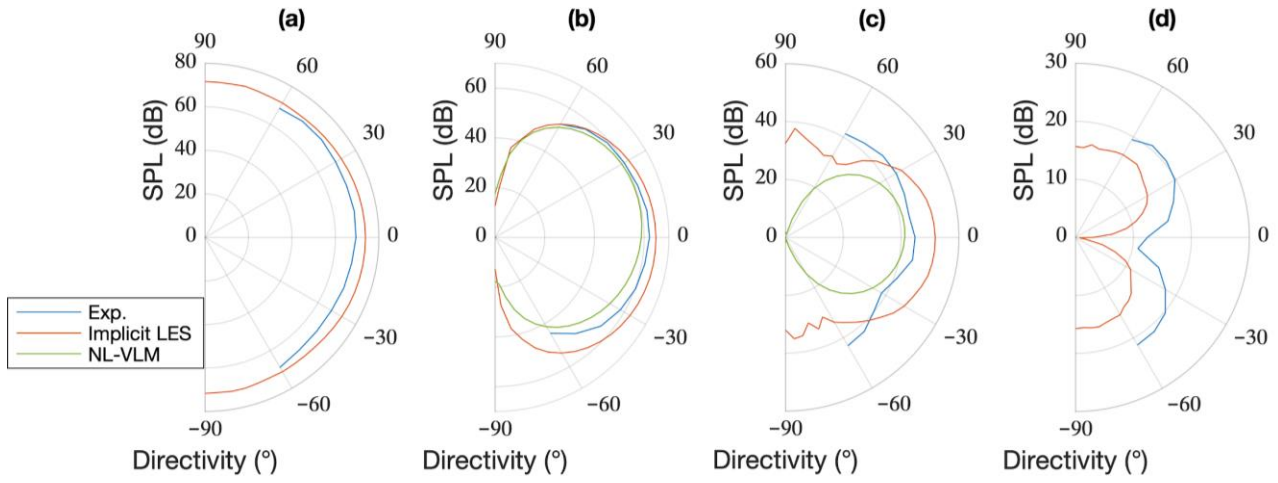


Figure 10: OASPL (a), BPF (b), first harmonic (c) and high frequency broadband noise (d) directivity results from experimental (blue), implicit LES (red) and NL-VLM (green) approaches.

Experimental and numerical directivities and associated levels are consistent for OASPL. The slight dissymmetry observed with experimental and NL-VLM approaches for the BPF seems not reproduced by implicit LES. Differences appear for the first harmonic where the radiation pattern is more directive in the case of numerical results, especially those obtained with NL-VLM method, and SPL seems to be overestimated by implicit LES. For the high frequency broadband noise, implicit LES predicts lower levels than measurements but the directivity pattern is well estimated. Indeed, implicit LES is not able to reproduce the smallest eddy scales that are part of the acoustic sources related to the trailing edge noise. As an illustration, Figure 11 shows the largest eddy scales that can be simulated by implicit LES at the blade tip.

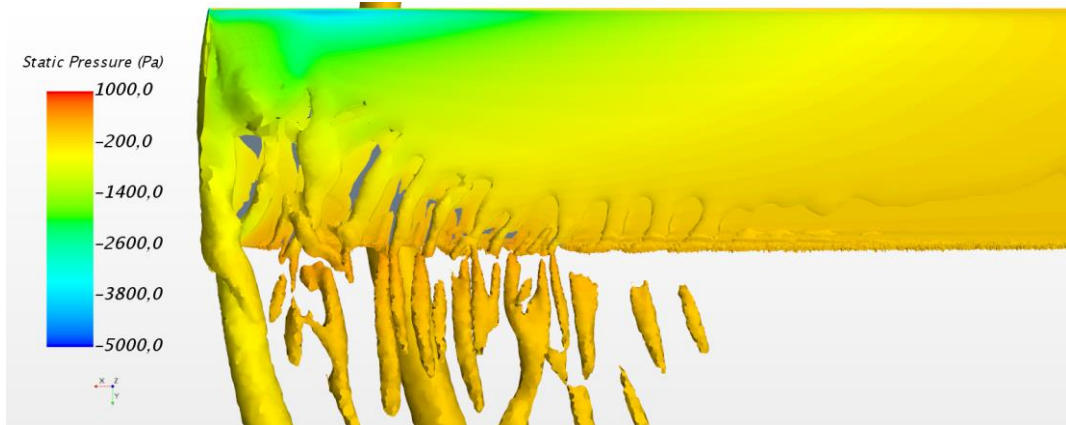


Figure 11: Isosurface of Q -criterion= $1e6 \text{ s}^{-2}$ colored by gauge static pressure predicted by implicit LES for two-bladed NACA0012 rotor at 6000 RPM.

4. Conclusions

This paper presents an experimental campaign that aims at characterizing rotor noise operating at low Reynolds and low Mach numbers typical of small and medium scale drones.

First, the experimental setup reliability is assessed showing that airflow recirculation in the ISAE-SUPAERO anechoic room seems negligible for the thrust studied. It is pointed out that the interaction of the airflow with the test stand creates additional broadband noise. In order to limit mounting impact on the results, the upstream airflow direction was recommended.

Secondly, experimental results were assessed against literature. Aerodynamic and acoustic data obtained for the off-the-shelf two-bladed APC 11x4.7 SF rotor were validated by comparison with

Brandt *et al.* reference database and Zawodny *et al.* 2016. Aerodynamic and acoustic results coming from the different setups are very consistent. Some differences can be observed on BPF harmonics and broadband noise on the frequency ranges for which the motor used in Zawodny *et al.* 2016 generates additional tones and broadband noise.

The physics behind two-bladed UAV rotor noise was then studied using a two-bladed canonical rotor with NACA0012 blade profile. Farfield noise is characterized by tones at the shaft rate, the BPF and their harmonics and high frequency broadband noise. The radiation patterns of the OASPL, the BPF, its first harmonic and high frequency broadband noise had been identified. Particularly, the vertical dipole directivity associated with high frequency broadband noise typical of trailing edge noise had been highlighted.

Measurements made on the latter rotor were also used to assess two numerical approaches: a low order Non-Linear Vortex Lattice Method (NL-VLM, Jo *et al.* 2019) and implicit Large Eddy Simulations (implicit LES). For aerodynamic loads, implicit LES results appear to slightly overestimate thrust and torque coefficients, whereas NL-VLM and experimental aerodynamic results are very consistent. In terms of acoustics, data comparison shows that implicit LES is able to predict the main tones (BPF and first harmonics) and a part of the high frequency broadband noise, whereas NL-VLM is only able to predict the BPF and its first harmonic. The farfield radiation pattern of different noise components (OASPL, BPF, 1st harmonic and high frequency broadband) is quite well estimated by numerical approaches, except for the first harmonic. Some differences on levels can be noticed, especially in the case of high frequency broadband noise for which implicit LES underestimates SPL due to the lack of small eddy scales noise sources.

Only results on APC 11x4.7 SF and two-bladed NACA0012 rotor were presented here, but APC 9x6 SF and NACA0012 rotors with blade numbers from 2 to 5 were also tested on this setup. All the results will be available in a few months as an open database for the UAV acoustic community to help drawing general guidelines for the design of low noise rotors.

Acknowledgements

This work was funded by the French DGA and the authors would like to acknowledge all the ISAE-SUPAERO technical team for the success of this campaign.

References

- Brentner, K. and Farassat, F. (1994) *Helicopter noise prediction: the current status and future direction* J. Sound Vib.170 (1), 79–96
- Zawodny, N. S. and Boyd Jr, D. D. and Burley, C. L. (2016) *Acoustic characterization and prediction of representative, small-scale rotary-wing unmanned aircraft system components* In 72nd American Helicopter Society (AHS) Annual Forum
- Intaratep, N., Alexander, W. N., Devenport, W. J., Grace, S. M., & Dropkin, A. (2016) *Experimental study of quadcopter acoustics and performance at static thrust conditions* In 22nd AIAA/CEAS Aeroacoustics Conference (p. 2873)
- Tinney, C. E., & Sirohi, J. (2018) *Multicopter drone noise at static thrust* AIAA Journal, 56(7), 2816-2826
- Jo, Y., Jardin, T., Gojon, R., Jacob, M. C. and Moschetta, J.M. (2019) *Prediction of Noise from Low Reynolds Number Rotors with Different Number of Blades using a Non-Linear Vortex Lattice Method* In 25th AIAA/CEAS Aeroacoustics Conference (p. 2615)

Jo, Y., Lee, H., and Lee, D. J. (2017) *Prediction of Rotor Flow for Unmanned Aerial System Using Nonlinear Vortex Lattice Method* 6th Asia/Australian Rotorcraft Forum / Heli Japan 2017, Kanazawa, Japan

Serré, R., Gourdain, N., Jardin, T., Jacob, M. and Moschetta, J. (2019) *Towards silent micro-air vehicles: optimization of a low Reynolds number rotor in hover* Int. J. Aeroacou. 18 (8), 690–710

Brandt, J.B., Deters, R.W., Ananda, G.K. and Selig M.S. *UIUC Propeller Database*, University of Illinois at Urbana-Champaign, <http://m-selig.ae.illinois.edu/props/propDB.html>

Stephenson, J. H., Weitsman, D. and Zawodny, N. S. (2019) *Effects of flow recirculation on unmanned aircraft system (UAS) acoustic measurements in closed anechoic chambers* Journal of the Acoustical Society of America, 145(3), 1153-1155



QUIET DRONES
International e-Symposium
on
UAV/UAS Noise
Remote from Paris – 19th to 21st October 2020

UAV detection from acoustic signature: requirements and state of the art

Lucille PINEL LAMOTTE, MicrodB: lucille.lamotte@microdb.fr

Valentin BARON, MicrodB: valentin.baron@microdb.fr

Simon BOULEY, MicrodB: simon.bouley@microdb.fr

Summary

The detection, identification and classification of micro-Unmanned Aerial Vehicles (UAVs) using their acoustic signature is at an early stage where the current performances do not meet the market requirements. They are targeted to complete electro-optical and radio frequency sensors acting in short distances (between 200 and 500 meters). This study firstly defines the detailed requirements to develop effective and affordable countermeasures to report of UAV flying over critical areas, especially in urban areas. It concerns Signal-to-Noise Ratio (SNR) required by the environment and UAV type/distance, the operational frequency domain with the best SNR, the localization accuracy required for neutralization, the real time capabilities to act as soon as possible...

The sound landscape observation is a complex task which has to isolate the noise sources of interest in short delay. The second part of the study establishes a state of the art of the available technologies on the market and the academic works addressing this topic and details how the current solutions cover the complete procedure from detection to classification. For the detection, the system tries to measure the acoustic signature using a single microphone or more complex sensors for a better directivity. For the identification and classification, a Machine Learning procedure is well-suited to recognize UAV audio fingerprint. For now, many academic papers demonstrate the low maturity of the procedure and the need to improve its reliability.

1. Introduction

The detection, identification and classification of micro-Unmanned Aerial Vehicles (UAVs) requires the combination of different sensors to generate low levels of false negatives and false

positives. The use of multiple detection modalities is intended to increase the probability of a successful detection, given that no individual detection method is entirely fail proof. This is difficult to achieve. A detailed study [1] counted in February 2018 155 counter-drone products either on the market or under active development for detection. Those systems rely on a variety of techniques for detecting drones: Radar, Radio Frequency (RF), Electro-optical (EO), Infrared (IR), Acoustic. 95 appear to employ a single sensor type, while at least 60 employ a combination of several sensor types. Roughly an equal number of systems employ radar, RF detection, IR and EO sensors while only 21 systems employ an acoustic sensor. The acoustic sensor detects drones by recognizing the unique sounds produced by their propulsion system. The limited number of solution based on acoustic may points out the low effectiveness of such a sensor in many situations. The first part of this paper analyses the requirements and foreseen limitations of the use of acoustic sensor, especially in urban area. Then a second part lists the current technology based on acoustic sensors with their adequacy to those requirements.

2. Requirements for effective acoustic UAV detection

2.1 UAV none covered by usual detection system

UAVs group a numerous variety of flying autonomous systems from small ones of few centimetres to the largest ones of real plane size. As traditional surveillance systems cope with the largest objects, the ones of interest are “*small UAVs, including cheap Commercial off the Shelf (COTS) and easy to assemble UAS components*” as described in the recent last H2020 call “Capabilities to detect, classify, track, identify and/or counter UASs in defence scenarios ID: EDIDP-CUAS-2020 (European Defence Industrial Development Programme)” (<https://ec.europa.eu/info/funding-tenders/opportunities/portal/screen/opportunities/topic-details/edidp-cuas-2020>). The below Table 1 extracted from the call lists them with their characteristics.

TAXONOMY (coherent with NATO)	Reference information regarding UAV threats	Reference information regarding UAV threats	Reference information regarding UAV threats	Reference information regarding UAV threats	Reference information regarding UAV threats
Threat	Weight [kg]	Reference size [cm ³]	Max speed [km/h]	Typical altitude [m]	Typical RCS (Radar Cross Section) [dBm ²]
Class I (a) and (b) - micro	< 2 kg	25 x 25 x 30	80	100	-20 (objective -30) (Human in the loop)
Class I (c) - mini	> 2 & < 20	40 x 40 x 30	100	1 000	-13 (objective -20)
Class I (d) - small	> 20 & < 150	200 x 150 x 50	150	1 500	-10
Class II - tactical	> 150 & < 600	1 000 x 700 x 100	300	3 000	-3

Table 1 : UAV classification from H2020 call “Capabilities to detect, classify, track, identify and/or counter UASs in defence scenarios ID: EDIDP-CUAS-2020.

The Class I micro UAV are flying at low altitude and are very small compared to other ones, permitting them to evolve in urban area, hardly detected by conventional radars. Their very low RF, thermal and acoustic signatures make them difficult to also detect by other sensors. The

acoustic sensor can help in detecting and identifying those Class I UAV with typical distance from 100 to 1000 m for which one they are sensitive.

2.2 UAV acoustic signature

Class I UAS group a numerous variety of flying autonomous systems with multi-rotor or fixed-wings, electric or thermic propulsion. As a consequence, their acoustic fingerprint can be very different, without prior knowledge of their frequency content and noise level.

One of the primary applications of unmanned aerial vehicles is surveillance. As surveillance often needs to be quietly conducted, the capability of silent flight has led to very low noise system with preferable electric propulsion systems but usually reserved to professional with expensive costs. Most of the systems are COTS but those systems can also be home made with unpredictable acoustic signature but keeping some of the characteristics of usual technology and noise level. The picture below gives some averaged sound pressure level for DJI quadricopters (from <https://www.airbornedrones.co/drone-noise-levels/>). This range is close to the European Aviation Safety Agency drone regulations published in their Easy Access Rules for Unmanned Aircraft Systems (Regulations (EU) 2019/947 and (EU) 2019/945). These do mention maximum sound power L_{WA} at 85 dB with a future target to 81 dB.



Spark	74cB
Mavic Air	76dB
Mavic Pro	79dB
Mavic Pro w/New Props	75,5dB
Mavic Platinum	70dB
Phantom 4 Pro	81dB
Phantom 4 Pro w/New Props	79,5dB
Phantom 4 Pro 2.0	76,5dB

Table 2 : DJI sound power level

There are two different UAV types: the fixed-wings or multi-propellers. The measured noise of those vehicles is dominated by propeller-related noise, including narrowband deterministic noise and broadband noise. Both are characterized by prominent tonal components. The multicopter spectra have significant noise at higher harmonics of the blade passing frequency (BPF), and in some cases the levels at higher harmonics exceeds levels at the BPF compared to fixed-wings [4].

Multi-copter drone flyovers noise emission have been conducted in many studies [2,3,4] including the basic manoeuvres of hover and forward flight. Three distinct frequency regions are identified in the sound spectra as illustrated on Figure 1 for DJI Matrice 600 Pro or Figure 2 for home-made Quad-rotor MUAS. Below 2 000 Hz, tones at harmonics of the BPF correspond to the narrowband peaks in the spectra. Broadband noise between 2 000 and 5 000 Hz is also an important noise source for these vehicles, including noise caused by unsteady pressure fluctuations due to turbulence and boundary layer interactions with the edges of the blade broadband. Over and up to 10 kHz the rotor self-noise is also very typical. It is caused by the electric motors with force pulses as the magnets and armature interact, and variations in forces caused by phase changes in the motor drive signal. Although atmospheric absorption at these high frequencies will attenuate such noise, it could still be an important part of the emission at closer distance.

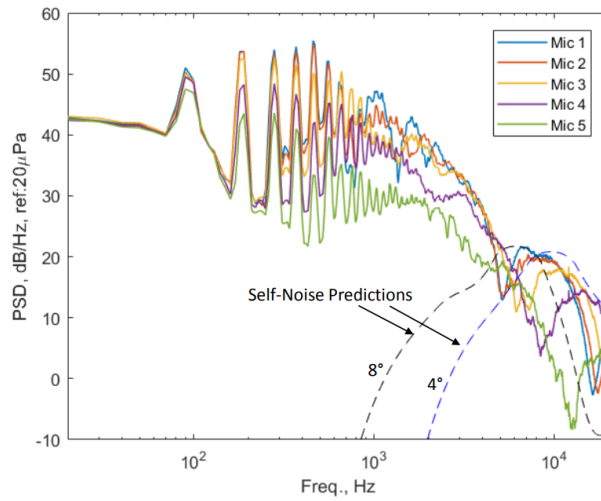


Figure 9. Acoustic frequency spectra for the five microphone positions during hover above Mic 1 at an altitude of 9.18 m

Figure 1: UAV spectrum DJI Matrice 600 Pro from [2]

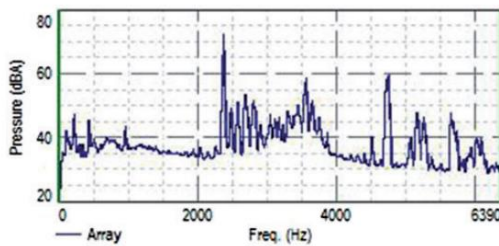


Figure 16. Frequency levels for test with all motors running but no propellers. Top of MUAS facing array.

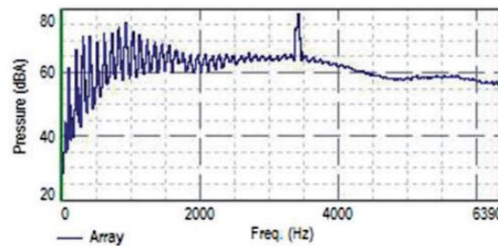


Figure 18. Frequency levels for test with all motors and propellers running. Top of MUAS facing array.

Figure 2 : home-made Quad-rotor UAS from [3]

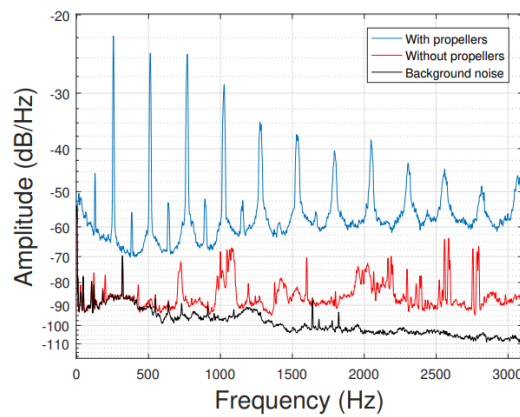
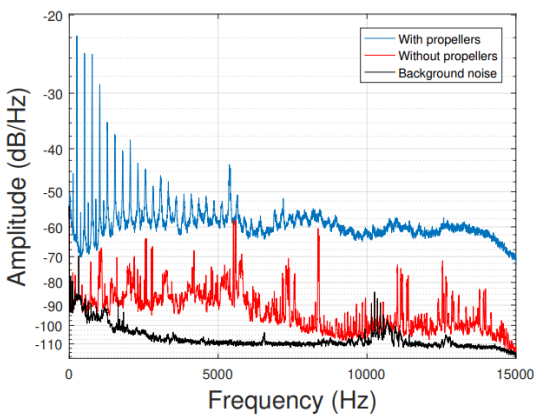


Figure 2: (left) Power Spectral Densities of the sound emitted by the drone with propellers (blue), without (red) and the background noise (black) of the anechoic room and (right) a zoom up to 3 kHz.

Figure 3: DJI Phantom IV acoustic signature from [6]

2.3 Signal-to-noise ratio

For acoustic detection, the own UAV emission cannot be considered as a single source of noise because it usually flies over noisy environment. For VIP events or in urban site the threat can act at short distance but usually with high background noise level. On the opposite, sensitive site protection requires middle range detection but in usual less noisy environment with constant and

regular levels. At last in military operational theatres or airports, the background noise can be at a large scale with unpredictable additive noisy events of different nature. So the signal-to-noise ratio is a parameter to consider to isolate the UAV acoustic signature from the other noise sources of an acoustic scene.

The Figure 4 superimposes on the same graph the environment background level and the Sound Pressure Level of UAVs with decreasing distance. This estimation is given from average DJI sound power level with a decrease of 6 dB per doubling of distance. Those approximations are confirmed in [3] and [4] whose some results are presented in Figure 5. It points out that a negative SNR is mostly envisaged for short distances and quickly below – 25 dB over 500 m. From usual microphone sensitivity, the maximum audible distance with acoustic sensors would be 1 km.

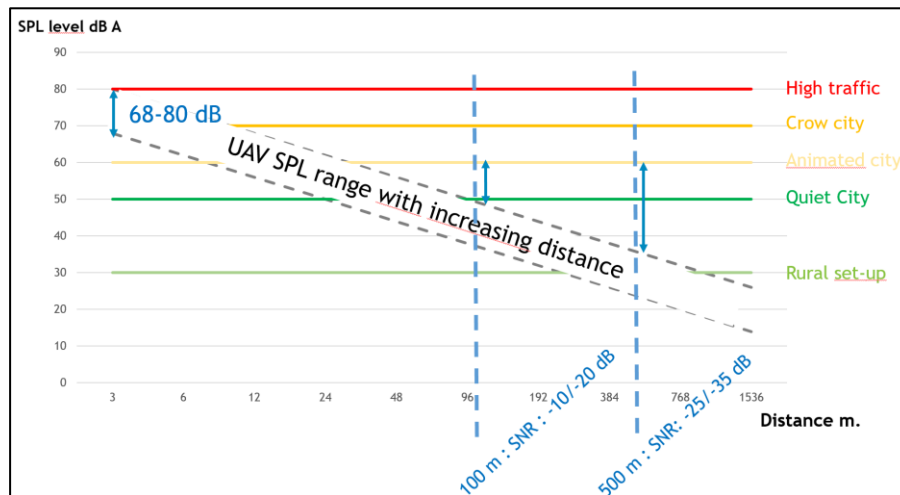
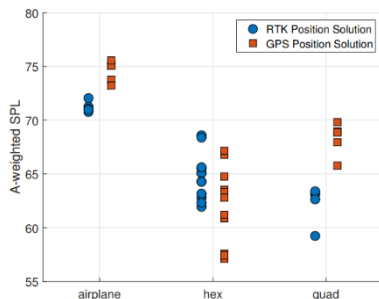


Figure 4 : superimposition of usual UAV sound emission with distance and typical background noise level



(a) LAmax normalized to 15 m from microphone.

Vehicle Name	Type	Flight Weight (kg)	Max Speed (m/s)	Power	Location
Edge 540 ^[1]	fixed-wing	~11.3	27	gas engine	42VA
DJI Phantom 2 ^[2]	quadcopter	1.6	15	electric motor	42VA
3DR Y6 ^[3]	tricopter	2.5	15	electric motor	42VA
Prioria Hex ^[4]	hexcopter	7.3	15	electric motor	AP Hill

Figure 5 : interpolated noise level from [4]

2.4 Implementation requirements regarding acoustic sensor and processing

One point of interest which is to consider in the development of methodology is real time processing. As much as possible, the system has to deliver the results of detection/identification in real time. The state of the art will prove that this constraint limits the fitting processing and implies optimization in those last ones. The Table 1 indicates speed of 100 km/h, 27 m/s for UAVs class I (c) mini. It means that with the previous analysis indicating that UAV could be detected from 500 meters, it remains 18 seconds to act for neutralization.

The system must cover a 3D sound landscape without prior knowledge of any privileged direction. In some cases like VIP events, the system has to be easily deployed on the field. It implies low power consumer, easy positioning to communicate the drone position in GPS coordinate system,

low cumbersome and handled hardware, and robustness regarding harsh environmental exposition.

3. State of the art for UAV detection/identification from their acoustic signature

3.1 Actors and history

The first publication referring drone detection dates from 2004 [23] with the TTCP-AG6 mission leaded by United States US to explore the use of acoustic sensor technology against UAVs. Although the first good results they present and claim, no further work from this group could be founded later about acoustic sensor. Besides, only one publication could be founded until 2015 also in US [7].

But most of the work were done after 2015. UAV detection/identification is therefore a recent topics of interest with mainly academic publications and theoretical experiments. Only two commercialized solutions can be found with brochures and associated patent in US and Norway [25, 26, 27] indicating performances which do not completely answer to the previous requirements.

Area	Objectives/methods	Publication date	Ref.
US	Mission to explore the use of acoustic sensor technology (Music)	2004	23
	Beamforming for tracking with low cost array	2008	7
	Dronesield patented solution (parabolic antenna / ML)	2017	24,25
	Patent : Delta signature from different UAV manoeuvre	2016	20
	Patent for system with audio/video/RF detection from multi-arrays	2018	26
	Detection and Acoustic Scene Classification with Deep Learning	2018	14
China	Patent for wearable system with audio/video/ultrasonic detection	2019	21
	Patent :UAV identification with ML and vibration velocity vector signal	2019	19
	TDOA and tracking with Kalman filter	2018	8
	Doppler effect and the matching method for UAV straight line flying	2016	9
Europe	Beamforming and Tracking with Kalman filter	2020	18
	Beamforming TDOA comparison	2019	6
	Acoustic/video based detection/identification solution with micro array	2018	17,10
	Patent for audio/video detection/identification system with micro array	2017	27
	Micro Array Methodology coupling beamforming and SVM	2019	16
	Identification/classification with SVM	2017	15
	Correlation first approach	2016	12
	Identification/classification with ML (LPC & freq spec slope)	2015	13
Korea	Beamforming for noise source tracking	2015	5
	Identification and classification with Deep Learning	2017	28
Australia	laboratory prototype for embedded flying system to detect and avoid UAV (TDOA)	2011	22

Figure 6 : list of main publications relating UAV detection, identification and classification

3.2 Detection

In most of the publications, the detection consists of locating in the space the UAV as a source of noise. The methodology is based on microphone array measurement and processing. There are three categories of algorithm which allow to localize the source.

The first one is TDOA (Time Direction Of Arrival) or goniometry. It is usually calculated through the generalized cross-correlation function between two microphones. But four microphones or more are required to localize a sound source in 3D with better accuracy. They are arranged over a tetrahedral shape. This processing is interesting for its low computational complexity and time domain, large frequency range using low cost microphone array. This method is already used in gunshot detection with usually good signal-to-noise ratio and one or few noise sources.

The experimental tests carried out in laboratory-like conditions with determined and controlled sound scape [11] show good results. But its application for UAV detection meets the difficulties of multi-path effect, multi drone and the low signal-to-noise ratio (SNR) condition in complex environment (e.g. presence of buildings in city scape).

TDOA method for UAV detection is detailed by Martin in 3D [11] with two to four microphones. The Phase transform function (GCC-PHAT) is usually applied as a window to attenuate the effects of the intensity difference in the generalized cross-correlation function.

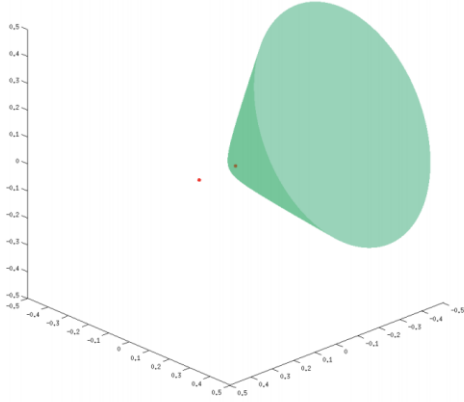


Figure 2.3: Solution space in \mathbb{R}^3 (green), for two microphones (red)

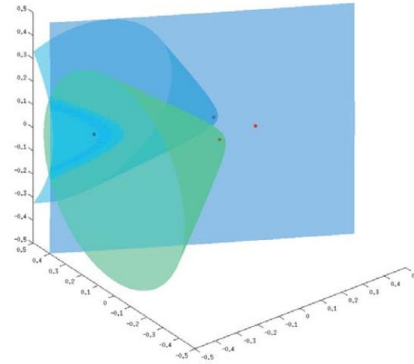


Figure 6.1: Array microphones in red, intersection point in blue

Figure 7 : sound source localization with TDOA methods from [11]

In [10], the tetrahedral shape acoustic array is upgraded to seven microphones to increase the frequency range and localization accuracy. In [8] two arrays of tetrahedron-shaped microphones are used to ensure accurate localization in 3D space.

The regular movement of the UAV can also be used to improve its localization knowing that at succeeding time window analysis, the localization is close. [8] proposes a new TDOA algorithm based on the Gaussian prior probability density function which mainly makes use of the relevance of the TDOA estimation results for a flying drone between time k and time $k-1$ with the peak of cross-correlation function at time k will appear near the peak of one at time $k-1$. The results are improved but at larger distance (80-100 m) and on large incident angle, the error range is quickly increasing.

The second family groups maximum energy methods with mainly the usual beamforming method. It can be applied in time or frequency domains. The second one is at higher computation cost with Fast Fourier Transformations but allows a frequency selection where the source of interest emits noise. Thus, the energy of undesirable frequencies coming from other sources is attenuated and therefore the Signal-to-Noise Ratio (SNR) is improved. The method to select the frequency range of interest is manually set-up in most of the experiments. [23,6] propose to identify the harmonics of the rotor blades and focuses localization algorithms on those ones.

In [17], localization is performed with an original method estimating the pressure and the particle velocity components on two orthogonal axis at the center of the microphone array from multiple microphone pairs. A Chinese patent from its abstract seems to use the same approach [19].

Blanchard in [6] compares beamforming to the previous TDOA methods using a dedicated ten microphone array distributed over three arms. The low accuracy of the GPS for the outdoor case did not allow to evaluate the actual performances of the methods while the results are good consistent between TDOA (goniometry) and beamforming (named "TFDSB") referring Figure 8.

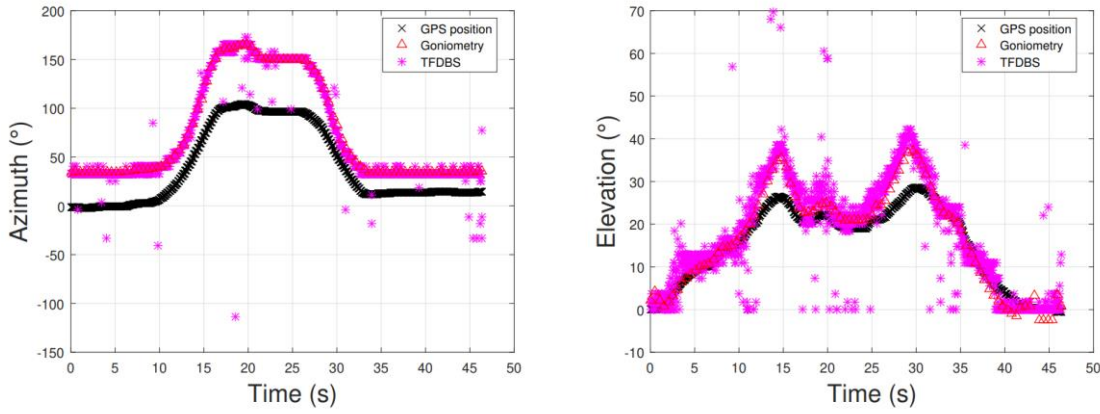


Figure 11: Results of the localization estimation of the drone using the TFDSB algorithm (magenta) with 4 harmonics selected and the acoustic goniometry method (red) for the outdoor measurement conditions in azimuth (left) and elevation (right).

Figure 8 : trajectory comparison between TDOA (goniometry) and beamforming (TFDSB) from [6]

Beamforming is also successfully used in [5] determining that drones can be tracked from 160 to 250 meters.

The last category groups high resolution methods. MUSIC (Multiple Signal Classification) has been early applied in [23] with good results. But those methods are sensitive to correlated sources and low Signal-to-noise ratio. In the publication they indicate that wind speed is below 5 knots. [8] criticizes this method with “very low accuracy and fails to track the target”. No other publication refers to this type of method.

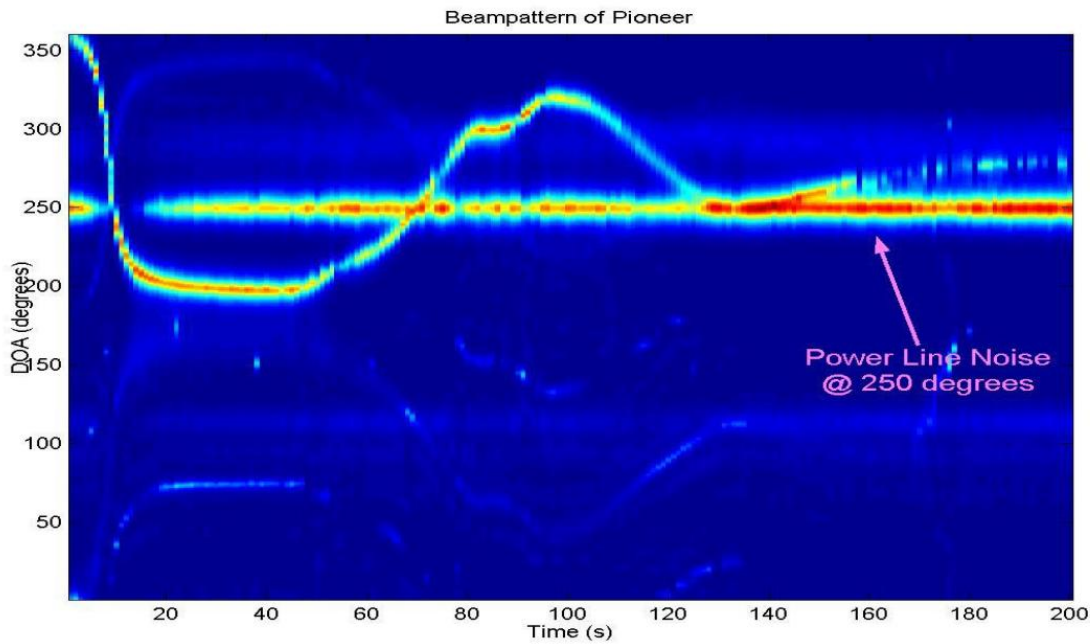


Fig. 4: Pseudo-spectrogram (DOA estimates vs. time) of a low-flying, medium-size, gasoline-engine tactical UAV.

Figure 9 : trajectory with MUSIC method from [23]

3.3 Trajectory

Whereas a microphone array usually provides only angular position, using the combined output of several arrays enables to obtain the source distance. This triangulation problem can be solved by different algorithms. It implies technical constraint to ensure the signal synchronisation between several data recording systems and their accurate relative position. A calibration procedure is proposed in [7] using TDOA.

Kalman filters are used in several publications to reconstruct the drone trajectory to obtain continuous trajectory from discretized position [8, 18]. This filter is widely used in tracking problems because of good real-time and low computational complexity. A method for reconstructing trajectories of multiple simultaneously flying quadcopter drones from microphone array measurements is presented in [18]. The method was tested in an anechoic chamber with up to four UAS flying at the same time in five different flight scenarios.

[9] provides an original algorithm using the total least square estimate of the target trajectory combining beamforming and Doppler effect evolution over harmonics emitted by propellers but under the assumption of constant target height, direction, and speed.

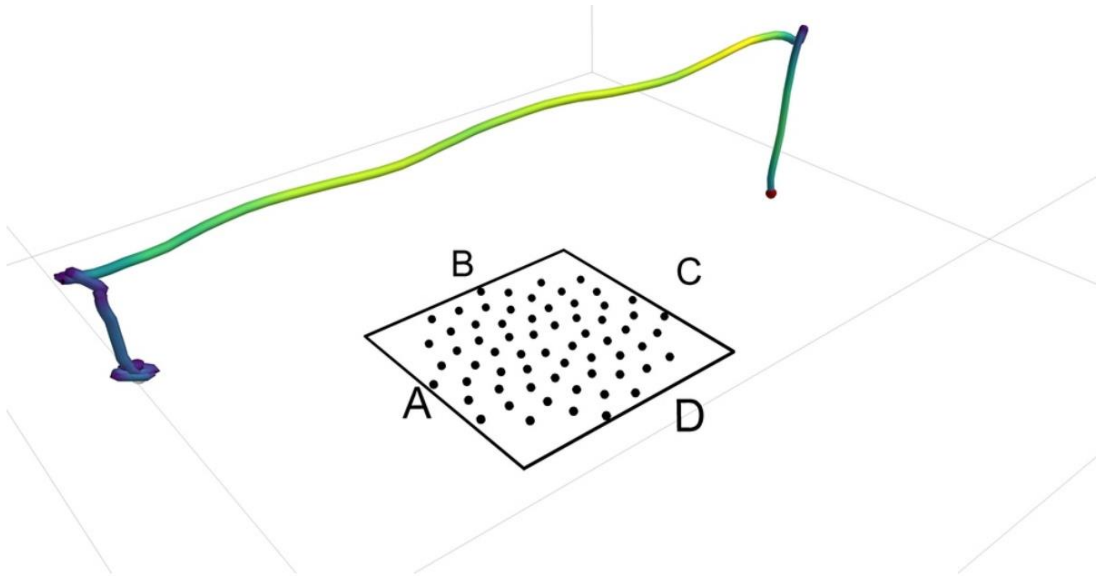


Figure 7: Scenario 1: Single drone flying from FATO A to FATO C.

Figure 10 : trajectory reconstruction with speed level indicating by colours from [18]

The output of the sound source localization algorithm can be processed exactly as traditional mono-channel signals for the case of beamforming. This class of algorithm presents an advantage compared to other ones which cannot reconstruct the “denoised” acoustic signature of the UAV acoustic source. The focused signal presents better signal-to-noise ratio than single microphone recording and as a consequence it will bring better performance in the identification step.

3.4 Identification

Features for acoustic characteristics

While the previous “detection” processing allows to localize a moving sound source like a UAV, the identification processing recognizes this sound source in the audio scene as a UAV by its acoustic signature. The identification is performed by comparing the similarities on selected features between the detected sound source and values in a database from UAV recording and other environmental noises in training stage. The intelligent machine listening systems identifies acoustic sources similar to human listeners. This technology has been widely used for speech recognition based on machine learning well known as Automatic Speech Recognition (ASR). Many academic works try to apply similar methodologies for acoustic scene classification, with among them an application for drone identification [12,13].

When detecting human speech the three most used techniques are linear predictive coding (LPC), Mel-Frequency Cepstral Coefficients (MFCCs) and perceptual linear predictive (PLP) analysis. MFCC and PLP analysis are both based on how humans perceive sound. The methods could therefore be unsuitable for identifying UAV. LPC requires the analysed sounds to have spikes in the spectral envelop as human speech does. The acoustic signature of UAV presented

in the first chapter showed similarities to human speech with harmonics, which made LPC a possibility used in [13]. The zero crossing rate which counts the average number of times where the audio signal changes its sign within the short-time window useful for voiced sub-frame has not met the same efficiency for UAV identification.

Among features based on the spectral content of the UAV signature, it is also commonly used Spectral Centroid and Spectral roll-off which represent the balancing point of audio spectrum and the frequency below which a certain amount of the spectral energy is concentrated, respectively [15].

Other features relate to the energy of the signal. The slope of the frequency spectrum is used in [13]. In [15], the Short Time Energy provides a measure of the energy variations of the environmental sound over time.

In [16], 32 features are computed over three different domains: the temporal, spectral and cepstral domains. They describe the input signals by means of statistical oriented, entropy oriented or shape oriented descriptors maximising the success of classification.

[12] introduces the use of correlation to identify a drone from its sound emission. With the help of correlation, the tightness of the relationship between two sets of data can be given.

Those previously described features are calculated on small time window describing the perceptual physical property of the audio frame for UAV source of interest and other environmental sources. Then those ones can directly be aggregated into global vector or statistically processed on a mid-term time window to reduce variability sensitivity [15]. This task allows to look into long-term dependencies with statistical, polynomial, regression and transformations functions applied to the instantaneous features. For example in [14], to classify an acoustic scene, the model needs to initially compute all the events happening during the scene, followed by identifying the relationship between those events to make the final prediction. An original approach of machine learning has been patented [20] working on the difference of acoustic signature between two manoeuvres (stationary, moving, changing direction) types to identify the UAV. The acoustic signature delta may be correlated with acoustic signature deltas of various types of UAVs.

Classifier for UAV

The UAV classification problem can be addressed formulating a multiclass environmental audio recognition problem using preceding features. A SVM (Support Vector Machine) based classifier is usually trained for estimating the multidimensional audio descriptors [15,16]. The “one against all” and the “one against one” are the two most popular strategies for multi-class SVM. The first one consists of building one SVM per class, trained to distinguish the samples in a single class from the samples in all remaining classes while the “one against one” builds one SVM for each pair of classes. In any case, a labelled training data set is required to implement a SVM. In [16], two different learning models are tested: the first one uses two classes : UAV and noise, with a classic SVM model while the second one is based on an One Class Support Vector Machine algorithm where only the UAV class is learned. In [15], the “one against one” strategy is adopted. A boundary is defined by the hyperplan that separates the two classes with a maximum margin. The classification accuracy is given by the ratio of number of correct predictions to the total number of samples in the dataset. Identification results on the tested database in [15,16] give accuracies over 95 % for the two or one classes approaches. It is also pointed out that this high accuracy is reached thanks to the intrinsic separability of the created data obtained by the different features that have been chosen to compute.

[14,28] explore the use of Convolutional Neural Network (CNN) and Recurrent Neural Network (RNN) to detect the presence of multi-drone. [14] uses hand engineered features extracted from large-scale feature extraction schemes as inputs to Deep Neural Networks. [28] uses the most popular combination of feature and classification Mel-frequency Cepstrum Coefficients (MFCC) with the Gaussian Mixture Model (GMM). In both works, custom datasets were collected for different classes: multiple drone detection which includes background noise, a single drone in

the scene and two drones in the scene. The results in [14] prove that large-scale extraction schemes with Deep Neural Network or CNN with Spectrograms are possible with limited availability of data. [28] concludes from their experiments that the RNN model showed the best score. Both agree with the use of data augmentation to synthesize raw drone sound with diverse background sounds to alleviate the shortage of drone training data

In the state of the art, a Chinese patent [19] also relates to “a UAV positioning system based on a vector detecting unit”, with *“the following steps: training a UAV recognition model to obtain a trained UAV recognition model; allowing a vector detecting unit to acquire an ambient sound vector signal of a detection area; preprocessing the sound vector signal acquired by the vector detecting unit.”*

3.5 Strategy

This section is interested into the implementation of the preceding technologies into industrial tools.

Some patents relate to the use of acoustic sensor for UAV detection combined with other sensors without detailing the technology envisaged with acoustic sensors [21, 26].

In [22], they apply the TDOA using a small array of microphones located on board an UAV or aircraft to characterise the temporal variation of the received tone of an approaching aircraft/UAV and estimate its propeller blade rate (and hence type), together with its speed, time and distance to the point of closest approach. This work is interesting by the fact that the acoustic sensors and processing are envisaged to be embedded on UAV but requiring to maximise effectiveness of the adaptive cancellation techniques of the own UAV noise embedded the array.

In [17] and [10], a network of compact microphone arrays is used to detect and localize a potential target in real time, and the 3D DOA of this potential target is then transferred to an optical system for a multi-modal audio/video accurate identification. First, spatial filtering is achieved using differential beamforming to focus the array on four principal directions in order to enhance the initial detection. Then, the video system with a limited view angle is oriented towards the target before triggering the tracking.

In [24], DroneShield details their patented technology based on audio. They use the difference of spectral content between time sample with and without flying UAV to detect a drone. They identify it using matching between background/UAV combination database from the spectral density. This company commercializes their solution with an acoustic sensor which is an omnidirectional microphone or one mounted on parabolic structure to focus on target and to improve SNR. With this last solution, [25] indicates detection for distance up to 100-250 m in Urban environment, 250-500 m in Suburban environment, and 500-1000 m in rural environment which coincide with the signal-to-noise analysis done in section 1.

In [27], SquareHead technology details their patented technology associating video and audio sensors with a commercialized solution named “Discovair”. They use differential beamforming map associated to video for detection and machine learning for identification/classification.

4. Conclusions

Many academics works are dealing with UAV detection/identification and classification from acoustic sensors since 2015. China, Europe, US mostly published. The maturity of the published technologies does not permit to have commercial solutions answering to the complete market requirements defined in the first chapter.

The foreseen solution is based on a first detection stage which would localize the sound sources in 360° soundscape. It requires multi-microphone arrays of few sensors if TDOA processing is applied or more microphones if other methods are preferred. The processing has to be real time, preferably without human actions. Nevertheless, the automatization of the source extraction in the space and in the frequency spectrum with the best SNR needs to develop artificial intelligence on that topics. First approaches have been investigated with harmonics extraction, trajectory

coherence. The second stage is to apply machine learning for UAV sound recognition. The selection of the right features and good training are the success keys before any neural network methodology. The SVM is preferred to deep neural network due to the few available data. There are few academic works working on both stage detection/identification processing. Anyway the complete processing has to be evaluated together to optimize it.

The experiments meet several difficulties. The GPS technology is not an easy task to retrieve the right trajectory limiting the evaluation of results. UAV flying requires authorization, and large area for test over 200 m. The UAV database are usually limited to few quadcopters. It leads to limited experiments usually not realistic. When system are then tested with true scenario, they failed to cope with the customer requirements. UAS detection must be sensitive enough to detect all drones operating within the area of use, but systems that are too sensitive may create an overwhelming number of false positives, rendering the system unusable. Systems that aren't sensitive enough might generate false negatives, which is even less desirable from the operator's standpoint.

References

1. MICHEL, Arthur Holland, "Counter-drone systems", Center for the Study of the Drone at Bard College, 2018
2. Alexander, W. Nathan, Whelchel, Jeremiah, "Flyover Noise of Multi-Rotor sUAS", InterNoise 2019
3. N Kloet, S Watkins and R Clothier, "Acoustic signature measurement of small multi-rotor unmanned aircraft systems", International Journal of Micro Air Vehicles 2017, Vol. 9(1) 3–14
4. Randolph Cabell , Robert McSwain, Ferdinand Grosveld, "Measured Noise from Small Unmanned Aerial Vehicles", NOISE-CON 2016 2016 June 13–15
5. Joël Busset, Florian Perrodin, Peter Wellig, Beat Ott, Kurt Heutschi, Torben Rühl and Thomas Nussbaumer "Detection and tracking of drones using advanced acoustic cameras", Proc. of SPIE Vol. 9647 96470F-3
6. Blanchard, Torea, Thomas, Jean-Hugh, Raoof, Kosai, "Acoustic localization estimation of an Unmanned Aerial Vehicle using microphone array", InterNoise 2019
7. Ellen E Case, Anne M Zelnio, and Brian D Rigling, "Low-cost acoustic array for small uav detection and tracking", Aerospace and Electronics Conference, NAECON 2008. IEEE National, pages 110–113. IEEE, 2008
8. Xianyu Chang, Chaoqun Yangz, Junfeng Wu, Xiufang Shi and Zhiguo Shiz, "A Surveillance System for Drone Localization and Tracking Using Acoustic Arrays",
9. Jianfei Tong, Wei Xie, Yu-Hen Hu, Ming Bao, Xiaodong Li, and Wei He, "Estimation of low-altitude moving target trajectory using single acoustic array," The Journal of the Acoustical Society of America, vol. 139, no. 4, pp. 1848–1858, 2016.
10. Frank Christnacher, Sebastien Hengy, Martin Laurenzis, Alexis Matwyschuk, Pierre Naz, Stephane Schertzer, and Gwenael Schmitt, "Optical and acoustical UAV detection," in Proceedings of SPIE Conference on Security+ Defence, 2016, pp. 1–13
11. Juan Luis Gamella Martin, "A prototype for positioning Aerial Vehicle Through Acoustic source localization", Undergraduate Thesis, 2016
12. József Mezei, András Molnár "Drone Sound Detection by Correlation", 11th IEEE International Symposium on Applied Computational Intelligence and Informatics, May 12-14, 2016
13. Louise Hauzenberger, Emma Holmberg Ohlsson "Drone Detection using Audio Analysis", Master's Thesis, Department of Electrical and Information Technology, Faculty of Engineering, LTH, Lund University, June 2015
14. Hari Charan Vemula "Multiple Drone Detection and Acoustic Scene Classification with Deep Learning", B.Tech, Department of computer science and Engineering, Wright State University, 2018
15. Andrea Bernardini, Emiliano Pallotti, Frederica Mangiatordi, Licia Capodiferro; Fondazione Ugo Bordoni "Drone detection by acoustic signature identification", © 2017, Society for Imaging Science and Technology

16. Valentin Baron, Simon Bouley, Matthieu Muschinowski, Jérôme Mars, and Barbara Nicolas, "Drone localization and identification using an acoustic array and supervised learning", Artificial Intelligence and Machine Learning in Defense Applications, Sep 2019, Strasbourg, France. pp.13,
17. Aro Ramamonjy, Eric Bavu, Alexandre Garcia , Sébastien Hengy "SOURCE LOCALIZATION AND IDENTIFICATION WITH A COMPACT ARRAY OF DIGITAL MEMS MICROPHONES", ICSV 25, July 2018
18. G. Herold, A. Kujawski, C. Strumpf, S. Huschbeck, M. de Haag, and E. Sarradj "Detection and Separate Tracking of Swarm Quadcopter Drones Using Microphone Array Measurements", 19. Berlin, 2020
19. FANG ERZHENG; ZU WENLIANG; QIN YIN; WANG HUAN; GUI CHENYANG, "UAV positioning system based on vector detecting unit", patent CN109283491 (A) — 2019-01-29
20. NAGUIB AYMAN [US]; ISLAM NAYEEM [US], "DEVICE FOR UAV DETECTION AND IDENTIFICATION", patent US2017234724 (A1) — 2017-08-17
21. ZHANG RUOTIAN, "Wearable acoustic detection and recognition system", patent CN209525006 (U) — 2019-10-22
22. Anthony Finn & Stephen Franklin, Defence and Systems Institute (DASI), University of South Australia « Acoustic Sense & Avoid for UAV's », December 2011, DOI: 10.1109/ISSNIP.2011.6146555
23. Pham, Tien, Srour, Nino, "TTCP AG-6: acoustic detection and tracking of UAVs", SPIE Defense and Security, 2004, Orlando, Florida, United States
24. FRANKLIN JOHN [US]; HEARING BRIAN [US], DRONESHIELD LLC [US], "DRONE DETECTION AND CLASSIFICATION WITH COMPENSATION FOR BACKGROUND CLUTTER SOURCES", patent WO2017139001 (A2) — 2017-08-17
25. Droneshield, product information <http://www.m2ktechnologies.com/admin/fileuploads/1503552100.pdf>
26. WEINSTEIN LEE [US]; GAINSBORO JAY [US], « Method and apparatus for drone detection and disablement », patent US9862489 (B1) — 2018-01-09
27. HAFIZOVIC INES [NO]; NYVOLD STIG OLUF [NO]; AASEN JON PETTER HELGESEN [NO]; DALENG JOHANNES ALMING [NO]; OLSEN FRODE BERG, SQUAREHEAD TECH AS [NO]; SAMUELS ADRIAN JAMES [GB] + "UAV DETECTION", Patent WO2017077348 (A1) — 2017-05-11
28. Sungho Jeon, Jong-Woo Shin, Young-Jun Lee, Woong-Hee Kim, YoungHyouon Kwon, and Hae-Yong Yang, "Empirical Study of Drone Sound Detection in Real-Life Environment with Deep Neural Networks", arXiv:1701.05779 2017



Centre d'information
sur le **Bruit**

QUIET DRONES
International e-Symposium
on
UAV/UAS Noise
Remote from Paris – 19th to 21st October 2020

**Aeroacoustic measurements on a free-flying drone
in a WindShaper wind tunnel**

Roberto Putzu, HES-SO Genève, roberto.putzu@hesge.ch
Romain Boulandet, HES-SO Genève, romain.boulandet@hesge.ch
Benjamin Rutschmann, HES-SO Genève, benjamin.rutschmann@edu.hesge.ch
Thierry Bujard, HES-SO Genève, thierry.bujard@hesge.ch
Flavio Noca, HES-SO Genève, flavio.noca@hesge.ch
Guillaume Catry, WindShape, guillaume.catry@windshape.ch
Nicolas Bosson, WindShape, nicolas.bosson@windshape.ch

Summary

In the near future, drone usage in inhabited areas is expected to grow exponentially. The inherent noise generated is one of the concerns for this kind of vehicle.

Conventional aeroacoustic wind tunnels can be used to investigate uniform-flow generated noise. Flyers are generally solidly tethered to a sting in these wind tunnels. However, the interaction of complex environmental flows with the drone fans is expected to generate different harmonic content, especially during unsteady maneuvers. Being able to probe the aeroacoustic signature of a free-flying drone in a realistic urban and wind environment is a necessity, in particular for future certification procedures.

We have developed a new family of wind tunnels, the “WindShaper” (Noca et al. 2019 Wind and Weather Facility for Testing Free-Flying Drones, AIAA Aviation Forum), able to generate complex unsteady flows reproducing environmental gusts and shear flows. The WindShaper

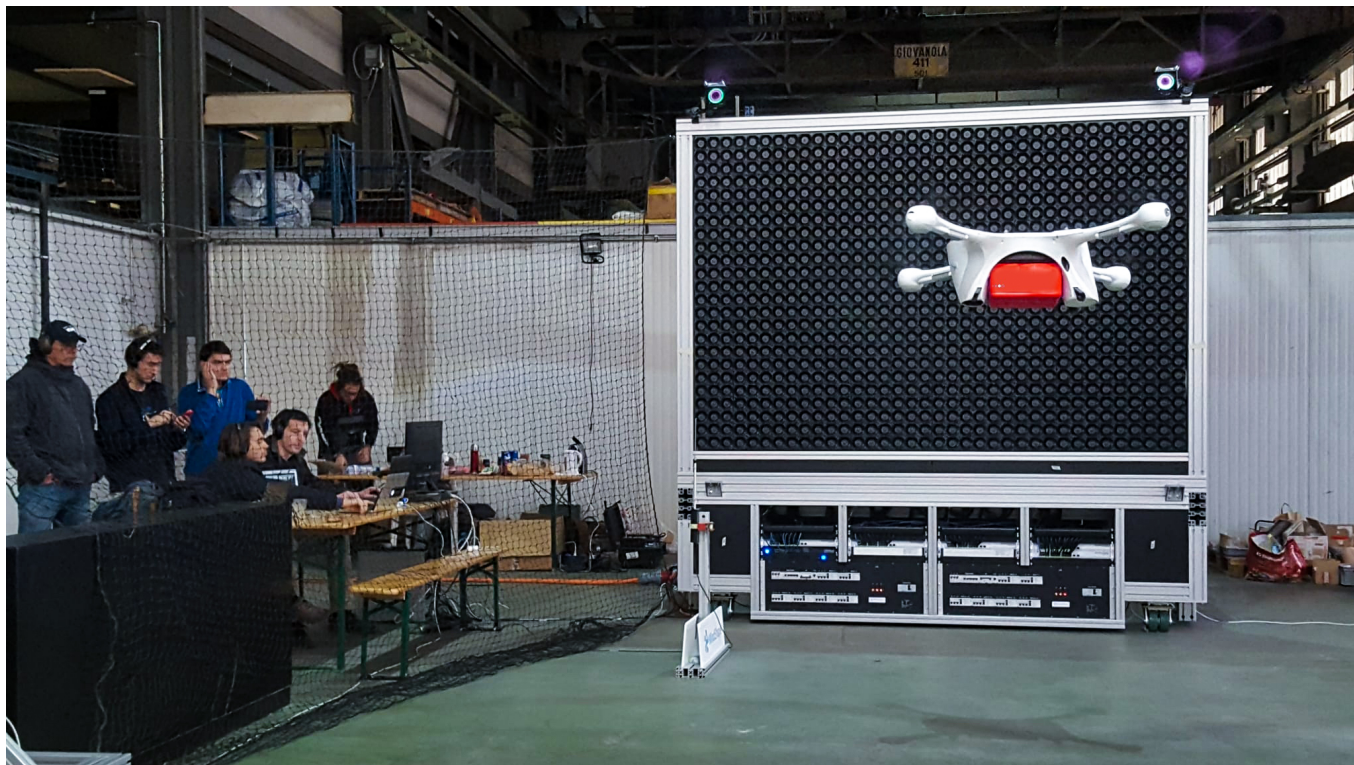


Figure 1: In November 2019, WindShape tested Matternet drone in various wind conditions within a WindShaper.

consists of an array of a large number of fans (wind-pixels) that may be arranged in various patterns on demand. It is in some ways a digital wind facility that can be programmed to generate arbitrary winds of variable intensity and direction. Various weather conditions (such as rain, snow, hail, fog etc.) that reflect real world situations can be introduced. Drones are in a free-flight configuration (untethered) as in their natural state. These tests can rate drones according to their capacity in maintaining a proper flight attitude and tackling flight perturbations, especially in an urban environment.

A WindShaper was modified in order to allow aeroacoustic measurements around a free-flying drone in a turbulent flow. Particular attention was given to a design that allows the drone aeroacoustic signature to be segregated from the aeroacoustic signature of the multi-fan facility. Details on the results achieved in this new infrastructure will be presented and discussed.

1 Introduction - Why drones need to be tested and certified

Drones are aerial vehicles that fly without an onboard pilot. In the past, the terminology *drone* was restricted to military platforms. The word *drone* is today accepted worldwide to refer to both military and civilian systems. If they are unmanned, they are classified officially by the FAA (Federal Aviation Administration) and the ICAO (International Civil Aviation Organization) as Unmanned Aircraft Systems or UAS (which also include associated ground systems), although they are also commonly called Unmanned Aerial Vehicles (UAV). If they carry a handful of passengers, drones are known as Urban Air Mobility (UAM) aircrafts, drone-taxis, or Advanced Air Mobility (AAM) vehicles, although no official label yet exists since these vehicles are still experimental. UAVs are used nowadays for multiple applications, from recreational to industrial and commercial activities such as mapping/cartography/inspection and delivery. In turn, UAMs are expected to thrive in the coming decade through the efforts of traditional aircraft or helicopter manufacturers as well as a

number of burgeoning startups.

Drones can be remotely piloted (as in traditional recreational radio-controlled flyers), but the trend is towards fully *autonomous* systems, whether for unmanned or manned drones. However, such automation entails a number of risks and challenges that need to be mitigated.

Similarly to the aircraft industry, the performance of drones needs to be assessed in order to minimize the occurrence of such risks in the future. Above a certain size or weight (yet to be standardized), drones will be certified to fly following traditional aircraft procedures (which will need to be amended for the autonomous aspect).

However, for smaller size drones (including single passenger drone-taxis), certification procedures will need to be greatly revised since these vehicles are extremely prone to weather conditions, including gusts and shear, which could also affect their noise signature.

Additionally, these flyers will evolve closer to the ground and to people. Therefore the social acceptance of this technology is another great challenge. Certifying drones with respect to their noise emission could offer access to populated areas only to those drones that respect a given noise rating.

Nowadays, it is natural for most drone manufacturers to run operational demonstrators or obtain waivers for specific operations but in the near future this industry will need to rely on performance and safety standards. Various international regulatory agencies are in the process of setting up regulations for the operation of drones. It is for the good of the industry that drones will have to pass official testing procedure (as it is the case today for traditional transportation systems), and will be rated according to their ability to tackle realistic scenarios (Figure 1), such as adverse weather conditions [2], but also according to aspects such as noise emission performance.

2 Background - WindShape technology

2.1 General description

In order to resolve the issues associated with traditional wind tunnels or outdoor testing protocols, we have developed a real wind and weather simulator [9, 10] for testing flying vehicles in various and controllable atmospheric conditions, including arbitrary wind speed, temperature and direction (even vertical flow for simulating landing/descent configurations), as well as turbulence, hail, rain, snow, and sandstorms. The novel wind facility allows free-flight maneuvering, is completely modular, can be assembled in any desired geometry, and can be made as large as desired while maintaining a small footprint. It is capable of generating gusts (temporally varying winds) and arbitrary wind profiles (shear flows) in any direction. Foremost, the flyer is always at hands-reach from the tester while performing actual flight maneuvers. A motion tracking system (motion capture cameras or mocap) is integrated into the facility in order to measure the drone position and attitude (Figure 2).

2.2 Multiple-fan technology

The wind facility is based on a multiple-fan technology, which is not novel in itself. A number of conventional tunnels use multiple-fan, although they are made to rotate at the same speed (such as in the National Full-Scale Aerodynamics Complex at NASA Ames Research Center, Moffet Field, CA, USA). Atmospheric boundary layers have been simulated with arrays of individually-controlled jets [14] and fans [8, 13, 15]. Fan arrays have been used to generate gusts and shears around pliable structures [6, 3] or micro-air vehicles (MAVs) [5]. One hundred years ago, the single-fan technology used by Eiffel and Prandtl was not novel either (the Wright brothers and

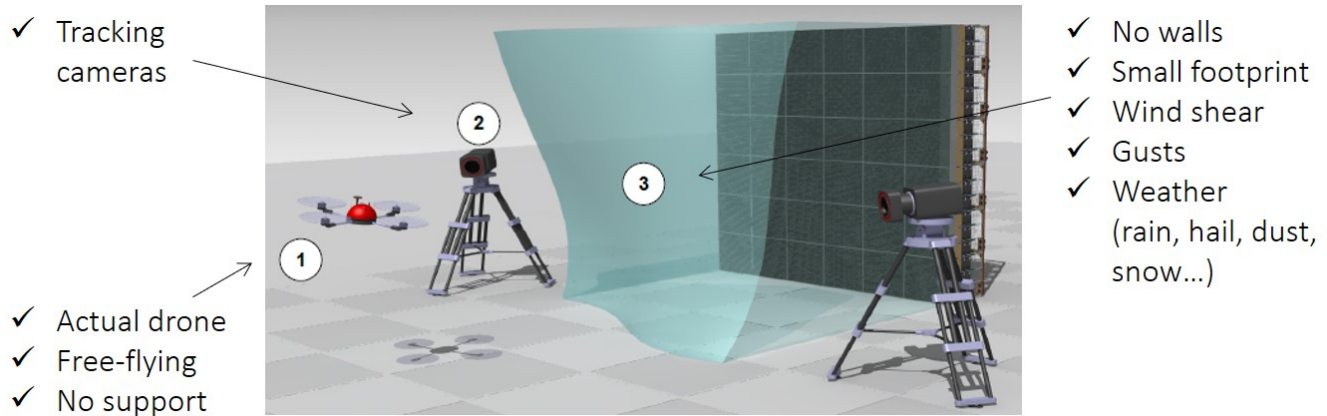


Figure 2: Wind facility for drone-testing based on multiple-fan technology [9].

others had experimented with similar devices), but the tunnels they designed were a unique and innovative tool for the aircraft industry. Similarly, WindShape technology is distinctive as it addresses the needs of the drone industry. In particular, the patented modular fan system [9] enables the stacking of an unlimited number of fans (1'296 for the Caltech facility CAST) for high resolution and fast response, as well as arbitrary wind-generating geometries that can be modified at will and over time.

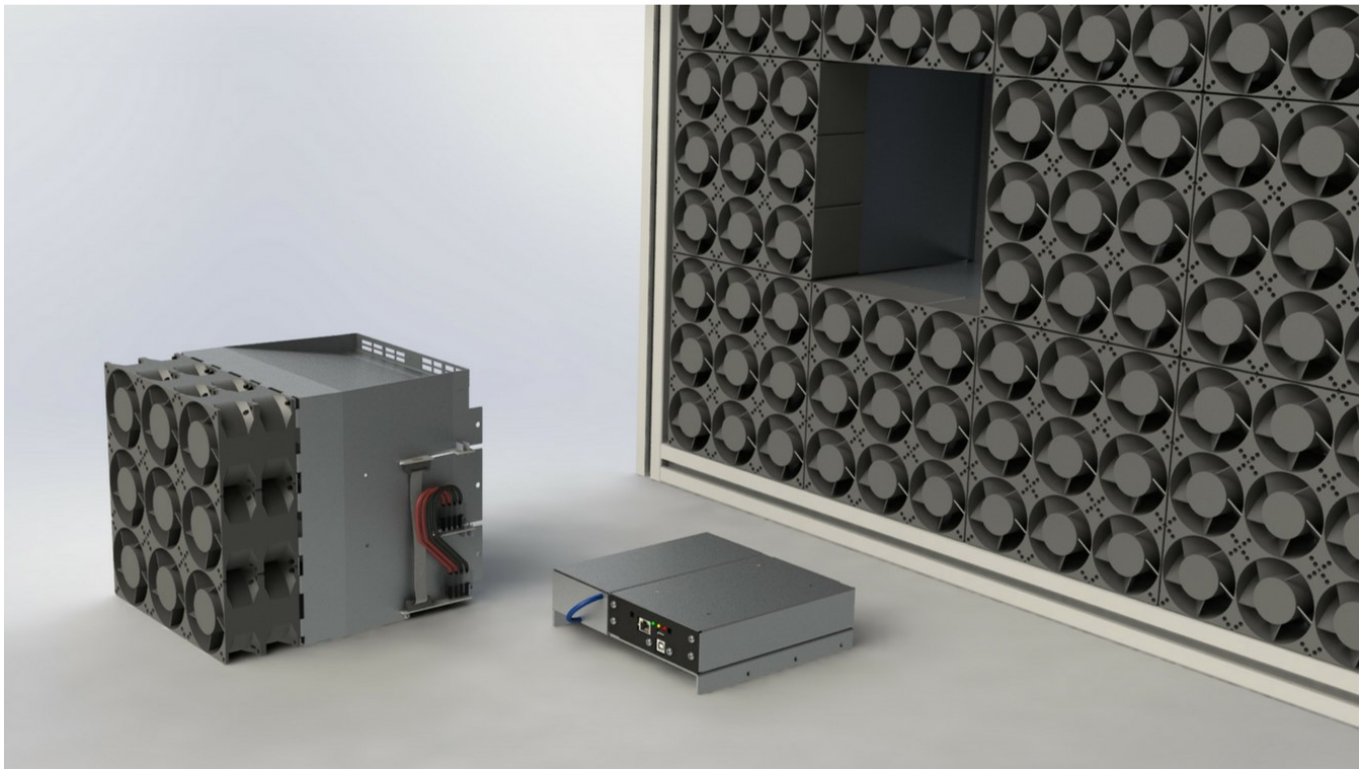
2.3 Wind pixels

The technology consists of an array of a large number of fans (approximately 150 fans per square meter) stacked in arbitrary fashion. Each single fan can be controlled independently and can, thus, be assimilated to a wind pixel (wpix). WindShape wind walls are composed of a great number of wind pixels (12.5 wpix/m in the Caltech configuration). This feature allows fine control over the generated wind properties, which in traditional tunnels requires extra flow management devices (proper nozzle geometry, flow control devices, vanes etc.). In addition, the low inertia of small-size fans enables fast changes in wind speed. Gusts of wind and shear flows can be faithfully reproduced. Laminar wind conditions, with a turbulence intensity below 1 %, can be achieved by adding screens and honeycombs in front of the fans, while preserving the independent character of every single wind pixel. Alternatively, traditional wind testing can be performed by placing the model on the aspiration side and by integrating appropriate tunnel walls.

2.4 Wind modules

The basis of the product is what we call a wind module – a wind generation unit composed of nine small fans (Figure 3a), acting like a building brick or Lego™ block. These modules are designed to be assembled manually into an array to shape surfaces of fans (Figure 3b). These modules can be arranged onto surfaces of any shapes (Figure 3c). One current version of the module has a square section of 0.058 m², can generate winds up to 16 m/s, and requires about 1.1 kW of electrical power at maximum output.

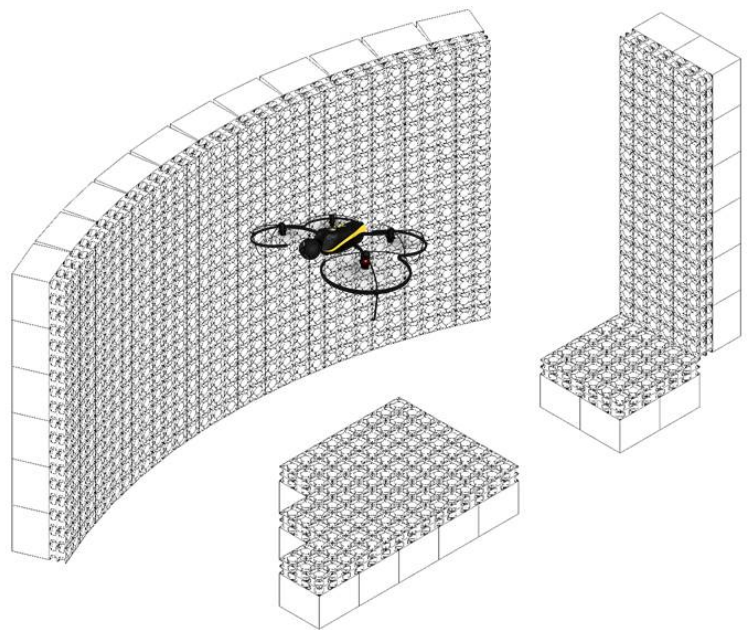
The facility being highly modular, thus, lends itself to an unlimited variety of wind configurations, spatially or temporally (Figure 3b): a wind wall can be enlarged simply by adding more modules to the wall; by moving the modules around, one can change the aspect of the wall (rectangular, square, etc.); the wall orientation can be easily modified: for instance, one can recreate the apparent wind of the descent (landing) phase of a multirotor by choosing to place the wind modules in a horizontal plane.



(a)



(b)



(c)

Figure 3: (a) The basis of WindShape technology is what we call a wind module – a wind generation unit composed of nine small fans with integrated power, which acts like a building brick or Lego™ block. (b) These modules can be rapidly assembled into an array to shape surfaces of fans. (c) Wind modules can be stacked into arbitrary shapes and sizes, thus enabling the testing of drones of various dimensions, from small UAVs up to drone-taxis, in arbitrary wind configurations (cruise flight, descent, cross-winds etc.).

3 Experimental methodology

3.1 Instrumentation

Wind facility A WindShaper with 3x6 modules (9x18 fans) is used. The cross-sectional dimension of the free jet is 1.50 m x 0.75 m, and is 0.80 m from the floor. Background details are given in Section 2. The WindShaper can be supplemented with a settling chamber that acts as a flow management device, composed of a series of screens with varying porosity and a honeycomb structure. It has the same cross-sectional area as the WindShaper and is 1 m in length. In such a configuration, the flow turbulence level varies between 0.5% and 1.0% depending on wind speed.

Acoustics Acoustic measurements are carried out with and without flow using a *01dB Fusion* sound level meter (SLM) and the *01dB dBTrait* and *dBInside* softwares for the post-processing of the data. Reverberation time (RT60)[4], defined as the time in seconds for a signal to decay to 1/1000 or 60 dB of its original amplitude, is used to assess the ability of the wind tunnel environment to synthesize a free sound field. Blank pistol shots creating a sufficiently loud noise were used as sound source to assess the reverberation time. In this study, RT60 is calculated from RT20, which is the RT value extrapolated from the time required for sound to decay by 20 dB. The calculation of sound pressure level is used to provide baseline data on the background noise.

Drones The test subjects considered in this study are well known, small commercial drones - either a *Parrot Bebop 2* or a *DJI Mavic Pro*. Both of these drones use a down-facing camera along with inertial sensors for stabilization and present a good ability in maintaining flight position when subjected to perturbations.

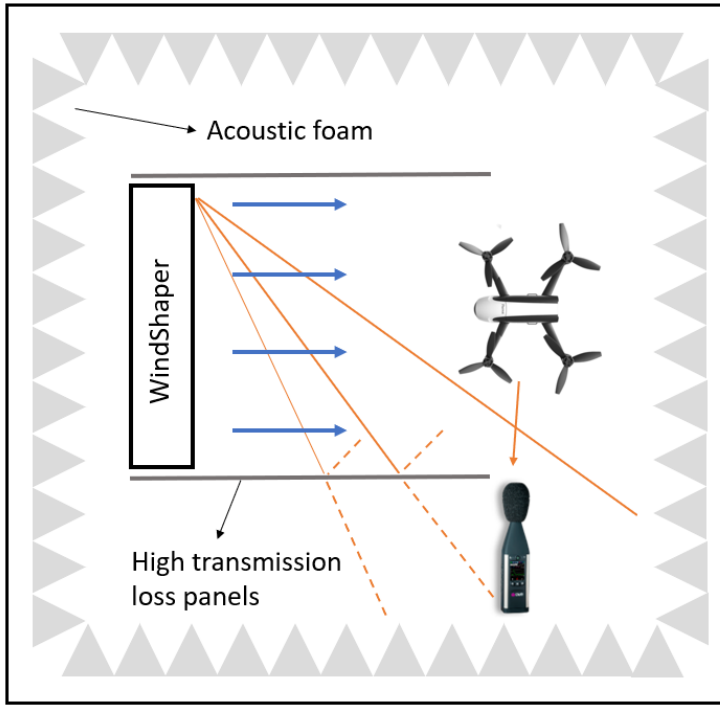
3.2 Aeroacoustic environment for WindShapers

In addition to the aeroacoustic design aspect of the wind tunnel, appropriate acoustic treatment is also required in order to achieve the aeroacoustic signature of a free-flying drone. The challenge is therefore to provide a test environment capable of generating high-quality fluid dynamic and acoustic measurements. Acoustic treatment in the aeroacoustic wind tunnel is needed: 1) to prevent the fan and fan motor noise from propagating into the test section and 2) to create an anechoic sound field and simultaneously reduce background noise in the test environment.

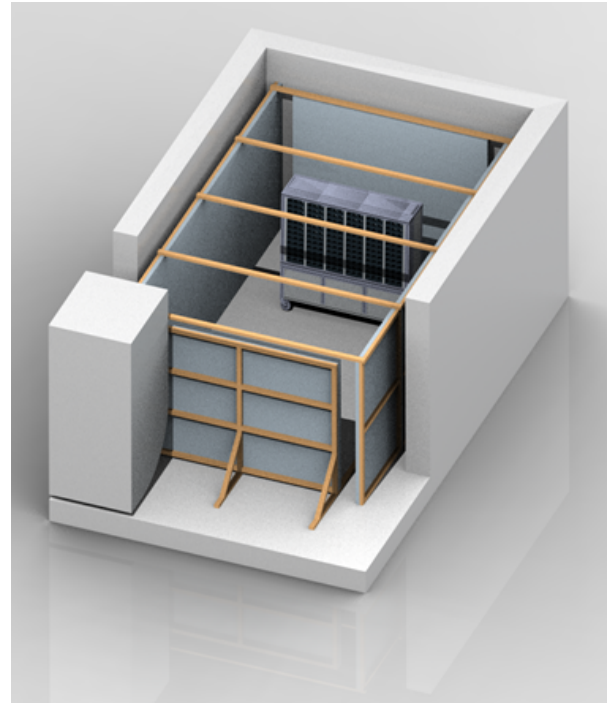
Conventional aeroacoustic wind tunnels [7, 12, 11, 1] damp these disturbances by a twofold approach based on the use of silent blocks to minimize structure-borne sound transmission and on the use of aerodynamic mufflers and acoustic liners to diminish the sound propagation along the wind tunnel ducts.

Due to the unique architecture of the WindShaper, the use of silent blocks and lined ducts was not deemed a viable solution to reduce background noise to levels compatible with aeroacoustic measurements. As shown in Figure 4a, in order to limit the influence of direct sound radiation from the WindShaper's fans on the measuring microphones, heavy panels characterized by a high transmission loss were used on the sides of the wind tunnel. Moreover, the wind tunnel itself was placed within a semi-anechoic environment to damp reflected sound that would contribute to increase the background noise.

Figure 4b shows the semi-anechoic environment that was designed to fit around the wind tunnel. The semi-anechoic environment of the test room (4.5 m x 2.7 m x 2.0 m) is composed by: 1) 48 mm thick melamine foam panels (Keller Lärmschutz Dinaphon® B810) placed at a distance of 20 cm from the walls; 2) 30 mm thick polyurethane foam panels with profiled surface (Keller Lärmschutz Dinaphon® M 8041) placed at a distance of 60 cm from the ceiling. The floor



(a)



(b)

Figure 4: (a) Aeroacoustic environment foreseen for the WindShaper; (b) CAD drawing of the semi-anechoic environment designed for the WindShaper.

is left tiled (no acoustic treatment). The heavy panels with high transmission loss used to line the exit of the wind tunnel are of type Keller Lärmschutz Idikell(R) M4021-05.

3.2.1 Acoustic performances of the semi-anechoic environment

To take quality acoustic measurements, walls, ceilings and floors should not reflect sound back into the room. To this end, an anechoic chamber would best fit the task. However, due to wind tunnel manipulation issues and measurement simplification, a semi-anechoic environment was designed and built on purpose (Figure 4b). The acoustic performance of the aeroacoustic wind tunnel is first evaluated without airflow from the measurement of the reverberation time (RT). Reverberation time is generally on the order of 0.1 s (or less) in fully anechoic chambers. Based upon the size of a room, standing waves will occur at certain frequencies. When there is a standing wave, there is maximum pressure at an anti-node and no pressure variation at a node. In order to account for this uneven distribution of acoustic pressure, RT measurements were taken at several different positions in the room and the results were averaged.

Figure 5 shows the RT values calculated by one-third octave bands in comparison to the data measured in a traditional anechoic chamber (64 m³, cut-off frequency $f_c = 100$ Hz). As can be seen in Figure 5, there is a good agreement for frequencies higher than 800 Hz, meaning that the current aeroacoustic wind tunnel provides a free sound field environment in the mid-high frequency range. In low-mid frequencies, however, further acoustic improvements are needed to increase the sound absorption capacity within the test environment. This discrepancy was expected in the design phase and is consistent with a foam thickness of 5 cm and wall-foam distance of 20 cm.

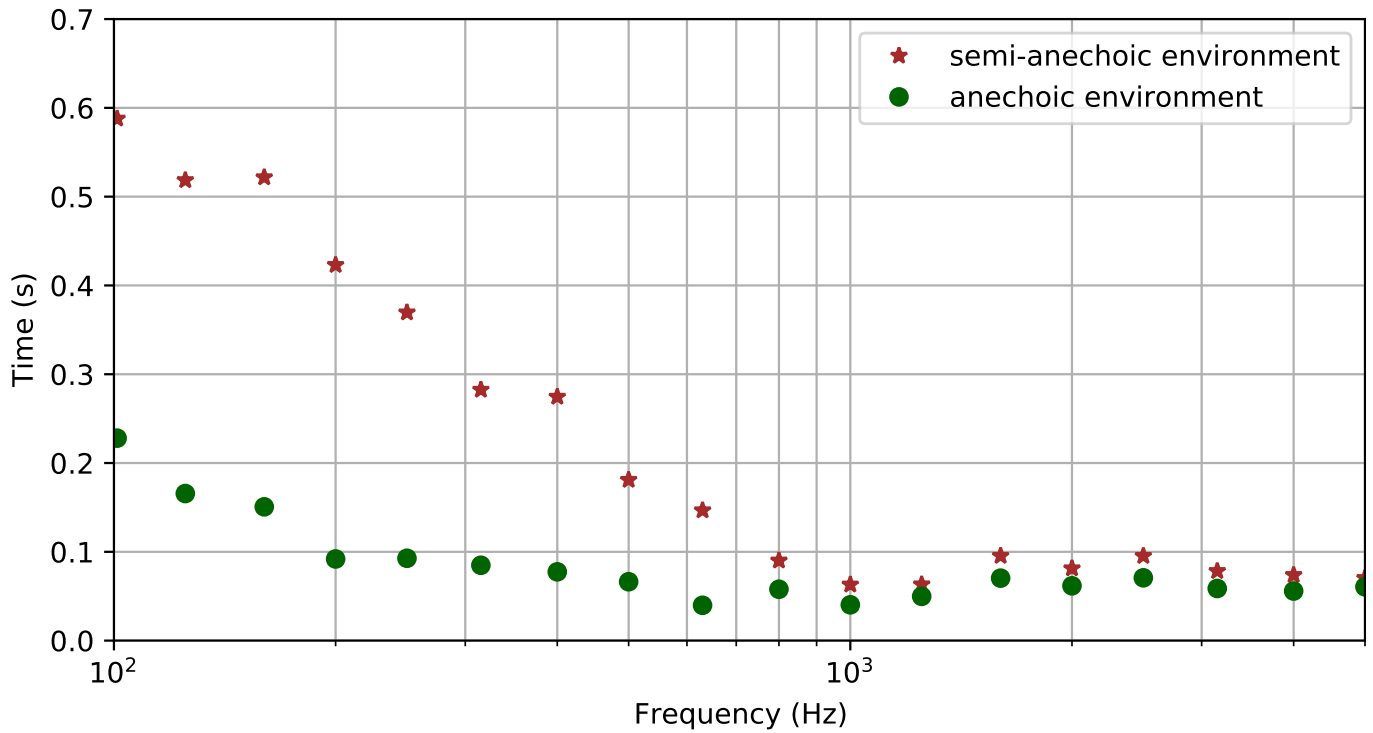


Figure 5: Anechoic chamber Vs Semi-anechoic environment RT60 reverberation times comparison.

3.2.2 Wind tunnel background noise

In order to properly assess the aeroacoustic signature generated by the drone-airflow interactions, the background noise level within the WindShaper environment should be as low as possible. The background noise determines the nominal effective noise floor at a given speed setpoint. As is generally accepted, a signal-to-noise ratio of at least 10 dB is required to make quality noise measurements. As depicted in Figure 6, four configurations were tested in order to attenuate the self-induced noise from the WindShaper:

- **Configuration A** The bare WindShaper was placed in the semi-anechoic environment (Figure 6a and Figure 4b);
- **Configuration B** A wooden structure lined in high transmission loss panels was placed around the flow to impair direct sound propagation from the WindShaper fans to the microphone;
- **Configuration C** A wooden settling chamber, of the same cross-sectional area as the WindShaper and 1.0 m in length, was placed at the exit of the WindShaper;
- **Configuration D** Both settling chamber and high transmission loss panels were placed at the exit of the wind tunnel.

The sound level spectrum was measured in these four configurations to determine the frequency response of the aeroacoustic wind tunnel at different nominal wind speeds. The position of the measurement microphone relative to the wind tunnel air exit (Figure 6) is given in Table 1.

The acoustic spectra measured for each configuration are shown in Figures 7 and 8 when the WindShaper is operating at 50% and 80% of nominal wind speed, respectively.

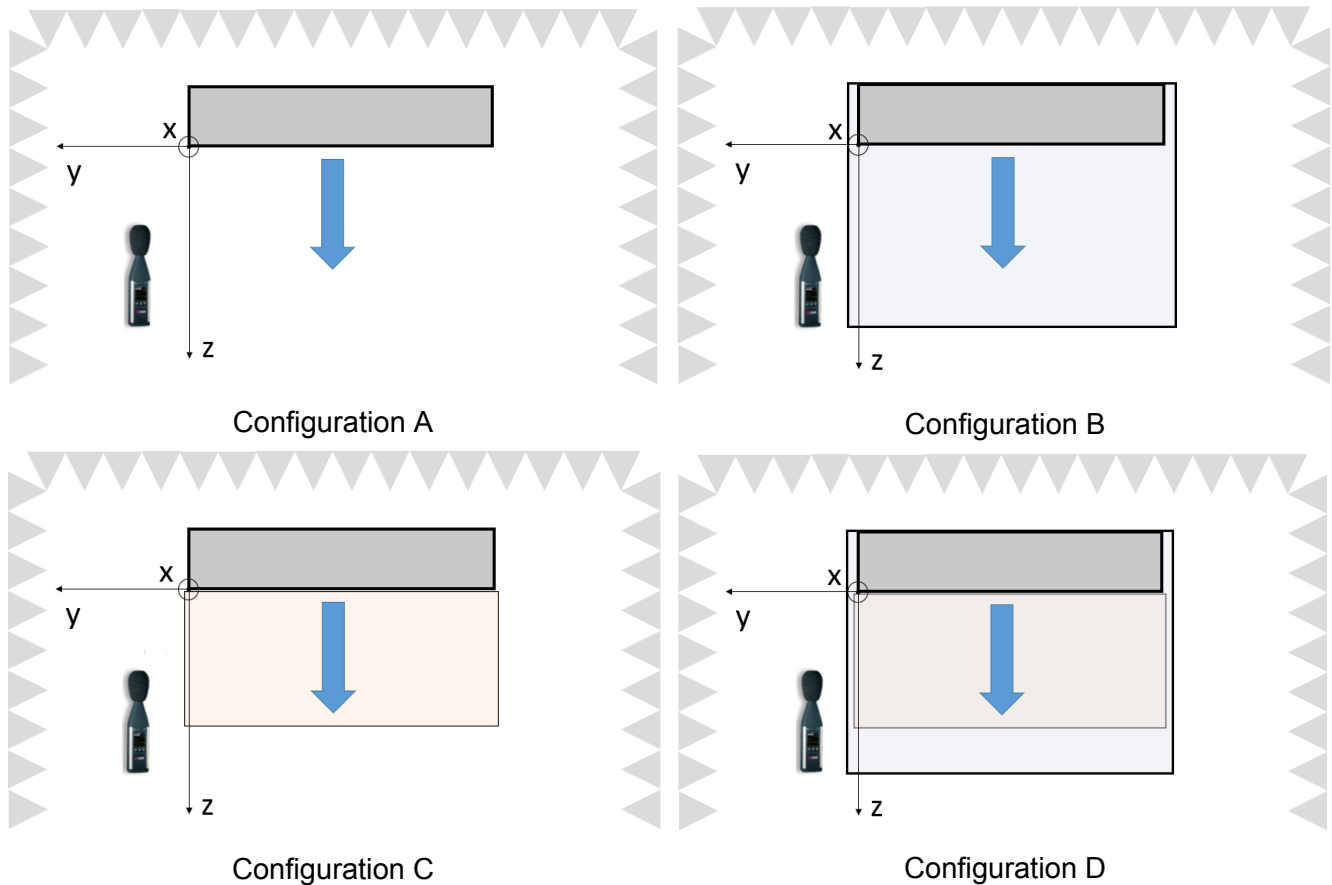


Figure 6: WindShaper's background noise investigation configurations in the semi-anechoic environment. Configuration A: bare wind tunnel; Configuration B: heavy panels lining wind tunnel exit; Configuration C: settling chamber lining the wind tunnel exit; Configuration D: settling chamber and heavy panels lining the wind tunnel exit.

X	Y	Z
1200 mm	150 mm	600 mm

Table 1: Microphone position relative to the wind tunnel exit.

As can be seen in Figures 7 and 8, the background noise when the WindShaper is operating contains tonal components typical of a fan noise source. On Figure 7, at 50% of the regime, two peaks at 525 Hz and 850 Hz respectively, correspond to the rotation speeds of the counter-rotating fans fitted to the WindShaper. The frequency and sound level of these peaks increase with the nominal wind speed, and in Figure 8, at 80% regime, the peaks move respectively at 800 Hz and 1275 Hz.

As expected, a decrease in the background noise level is observed by installing either the high transmission loss panels or the wooden settling chamber. This decrease is observed to be comparable in the two configurations.

At 50% of the nominal speed (Figure 7), the use of both high transmission loss panels and wooden settling chamber results in a reduction of the background noise of approximately 9 dB in the frequency range between 400 and 1000 Hz. The background noise reduction increases for higher frequencies up to 25 dB.

At 80% of the nominal speed (Figure 8), the same configuration reduces the background noise of approximately 12 dB in the frequency range between 400 and 1000 Hz. For higher frequencies, the reduction increases up to 25 dB.

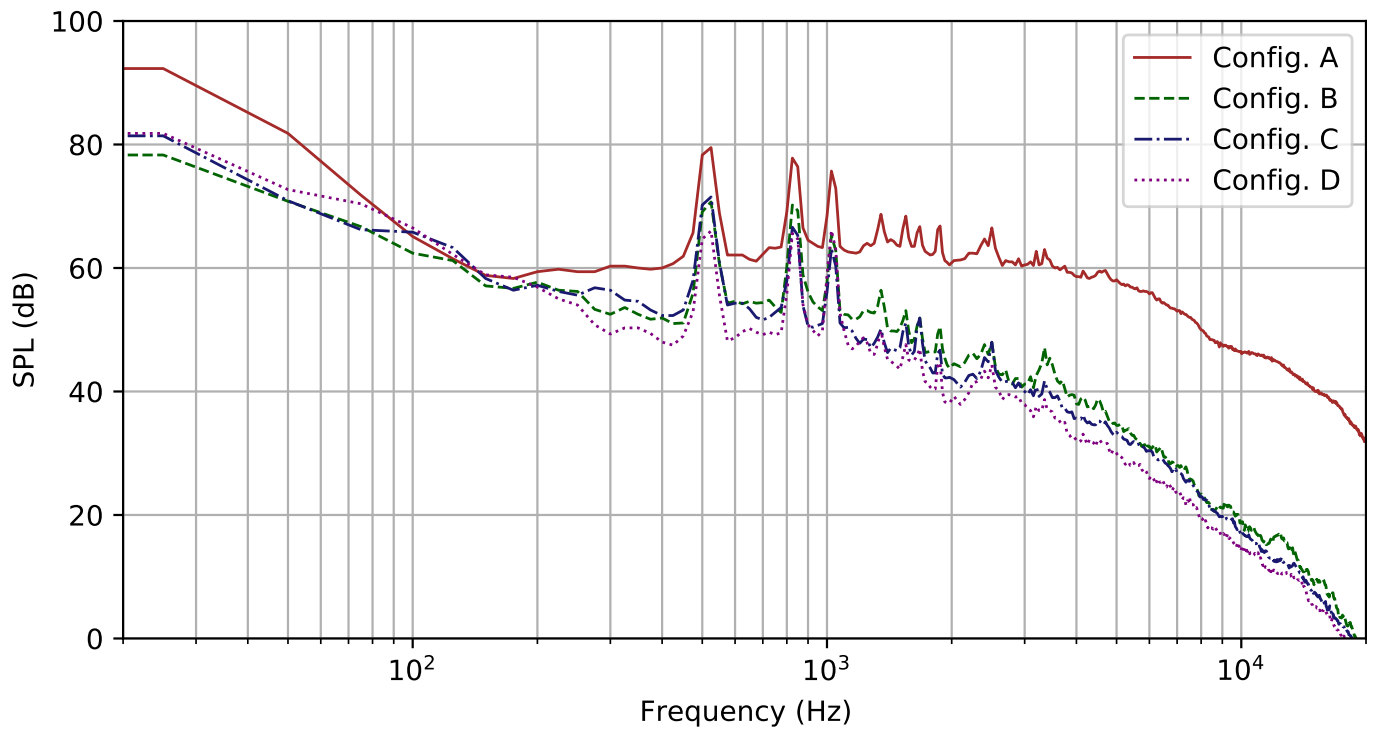


Figure 7: WindShaper Background noise SPL spectrum at 50% of maximum velocity.

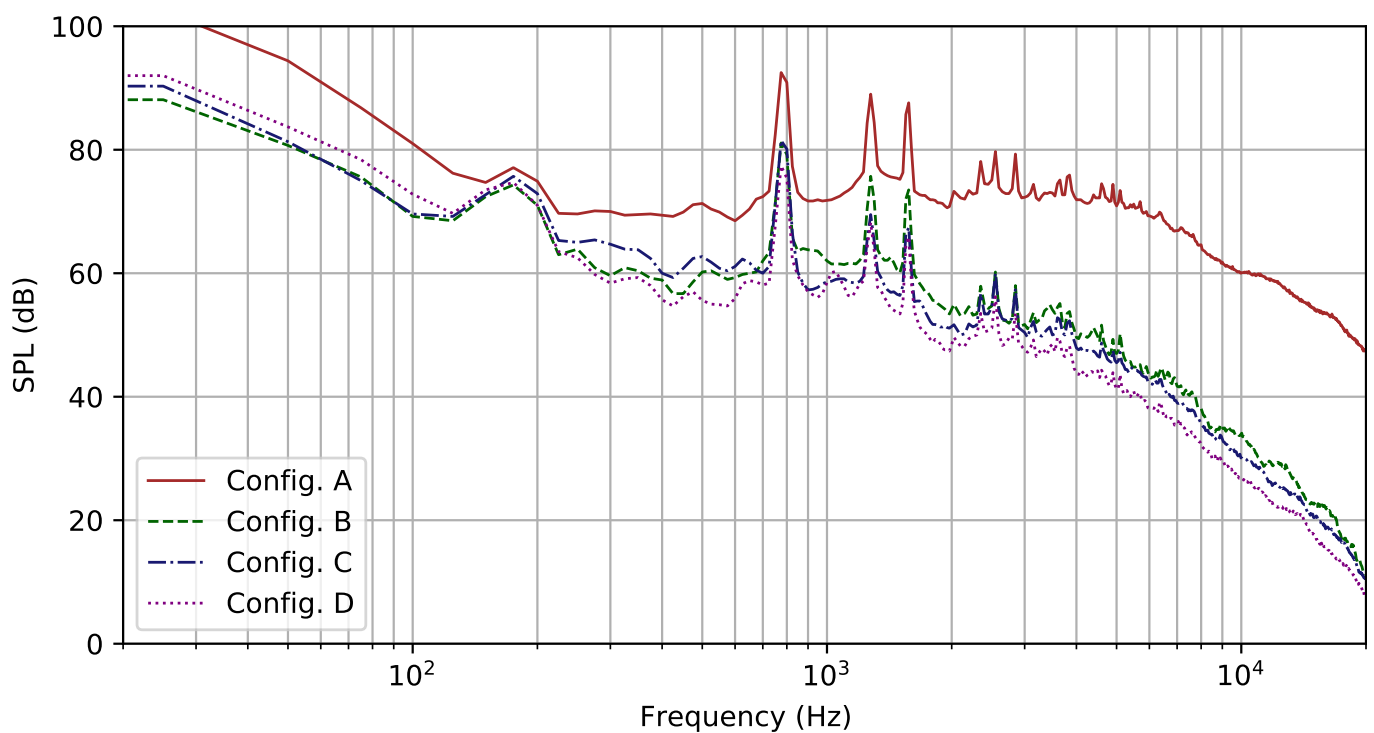


Figure 8: WindShaper Background noise SPL spectrum at 80% of maximum velocity.

Between 400 Hz and 1000 Hz the use of both settling chamber and heavy panels reduces the noise by approximately 12 dB, whereas for higher frequencies the reduction increases up to approximately 25 dB.

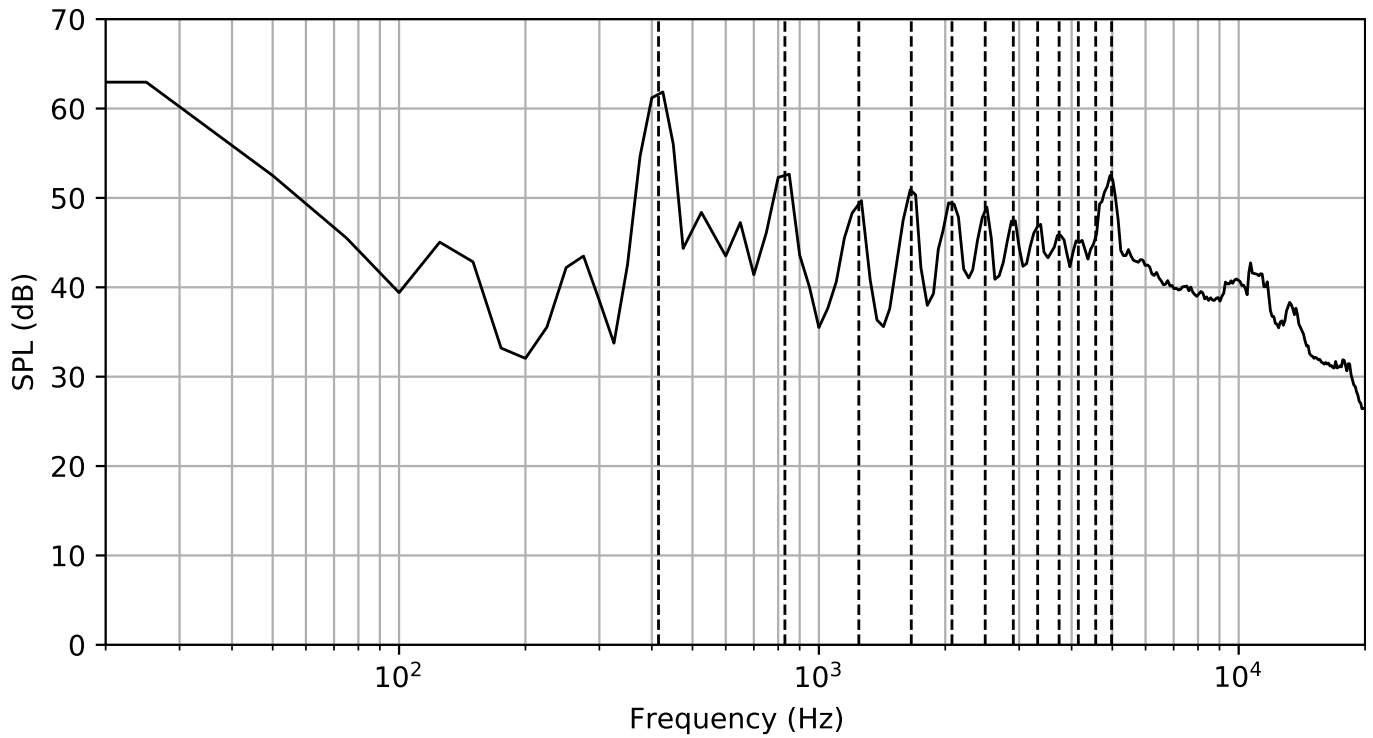


Figure 9: Drone SPL noise spectrum in the semi-anechoic environment.

3.2.3 Drone noise testing in the WindShaper

A lightweight *Parrot Bebop 2* drone in steady flight was tested both in the anechoic chamber and in the semi-anechoic environment with comparable results. Figure 9 shows its SPL spectrum in wind-off semi-anechoic environment. As can be seen in Figure 9, the prominent noise in hovering flight is the tonal noise of the blade passing frequency at 415 Hz and its harmonics.

Acoustic investigations were also carried out on the drone with WindShaper operating at 30%, 40%, 50% and 60% of its nominal wind speed. During these tests, the WindShaper was equipped with both high transmission loss panels and settling chamber as depicted in Figure 6d. Figures 10 and 11 show the SPL spectrum of the drone and of the WindShaper at 30% and 40% of its nominal speed.

Figure 10 shows that operating the WindShaper at 30% of its nominal velocity, the sounds emitted by the drone for frequencies higher than 2000 Hz can be considered more than 10 dB above the background noise. For frequencies ranging between 1400 Hz and 2000 Hz, the 10 dB difference with respect to the background noise cannot be guaranteed. For frequencies lower than 1400 Hz, the magnitude of the drone noise becomes comparable or lower than the WindShaper's.

Figure 11 shows that for higher wind speeds the WindShaper's background noise becomes more important, and the exploitable frequency range gets smaller. For WindShaper at 40% of its nominal velocity, a 10 dB difference with respect to the background noise can be observed above approximately 8000 Hz.

Due to clear superposition of the background noise with the drone's emissions for higher wind speeds, the measurements for these configurations are not shown in the present paper.

4 Conclusions

An overview of the aeroacoustic wind tunnel has been presented including the several acoustic treatments implemented. The current semi-anechoic environment generates a free field for frequencies higher than 800 Hz ($TR_{60} < 0.1$ s). Room improvements will aim at increasing the free

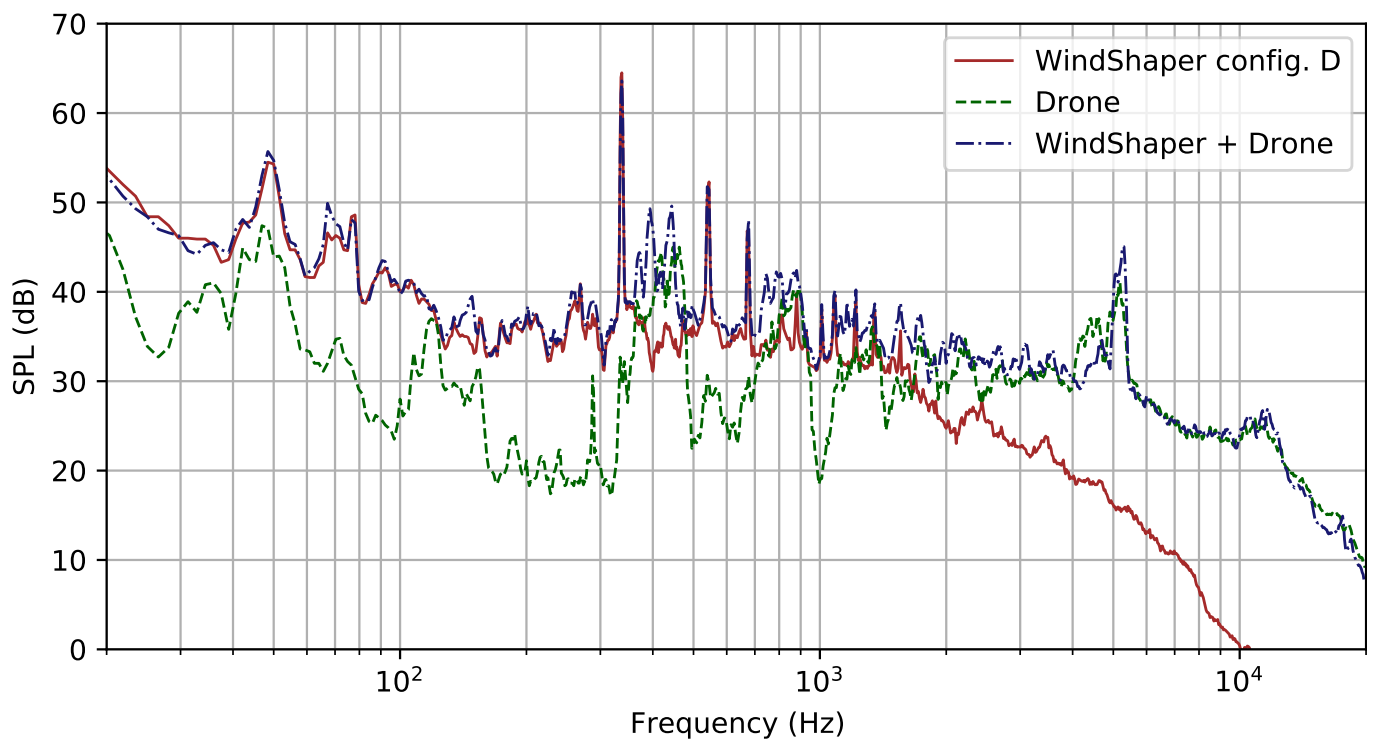


Figure 10: Drone SPL noise spectrum in the semi-anechoic environment with wind-tunnel at 30% of its nominal velocity.

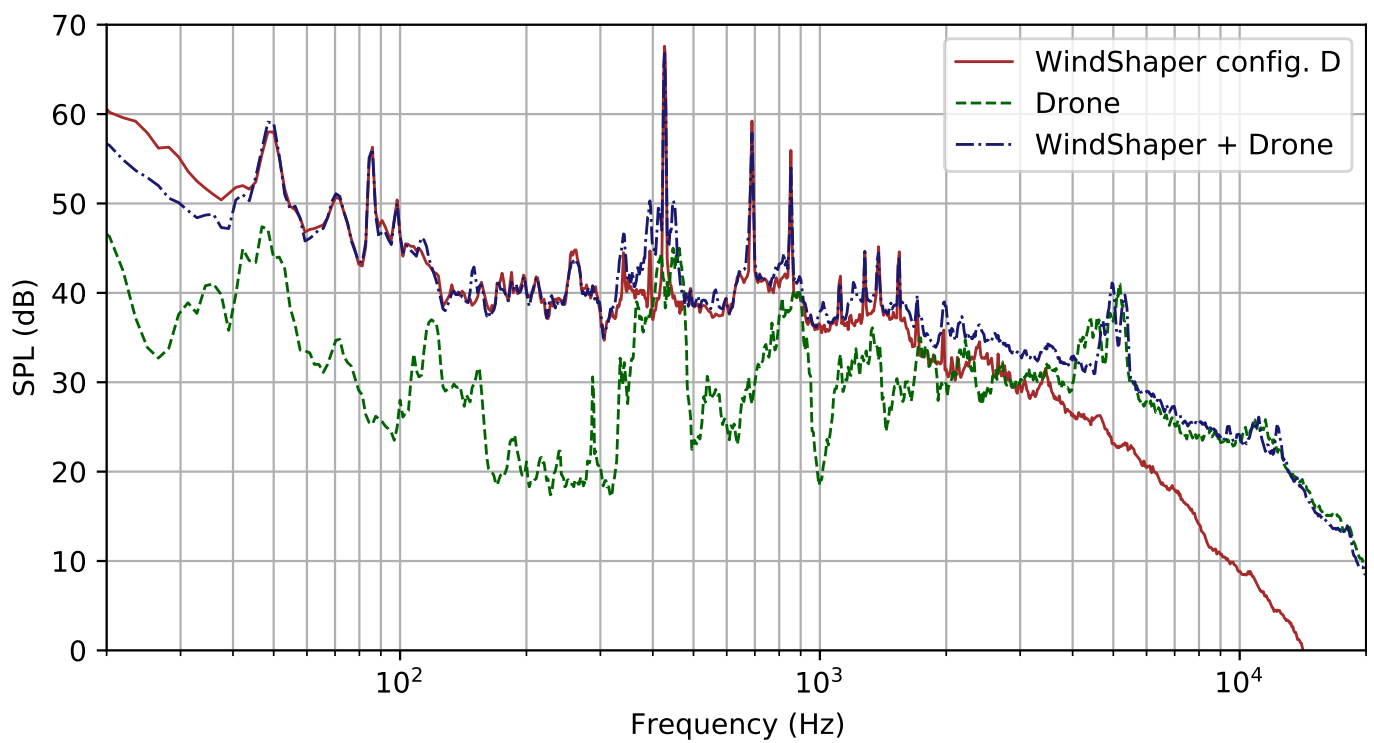


Figure 11: Drone SPL noise spectrum in the semi-anechoic environment with wind-tunnel at 40% of its nominal velocity.

field frequency range.

With airflow, background noise levels are competitive, but further reduction is desired to achieve sufficient signal-to-noise ratio. Acoustic sidewalls surrounding the WindShaper used to prevent the propagation of fan motor noise have been found to be effective, reducing the background noise by 9 to 25 dB depending on the configuration. Nevertheless, this noise damping is observed to be not sufficient to make use of the WindShaper at higher regimes. For a *Bebop 2* like drone, at 30% regime the frequencies where the WindShaper is considered to be exploitable for aeroacoustic investigations are 1400 Hz and higher. At 40% regime, the lowest exploitable frequency is considered to be 8000 Hz.

On the other hand, it has to be noted that the sample drone used here to investigate the WindShaper's acoustic capabilities is a lightweight device that constitutes a worst case scenario: commercial drones that will need certifications are likely to be heavier, and to produce louder sounds. However, particular attention will have to be paid in further investigations to damp the WindShaper's background noise and harmonic behaviour, whose frequencies vary with the wind speed in a range of amplitudes common to many drones. In future developments, effort will be put in the identification of the background noise sources in order to damp the acoustic disturbances at their origin. Moreover, investigating the properties of different sidewall configurations will be useful to establish a baseline reference for designing future experimental setups. On this topic, on-purpose designed resonant systems such as acoustic liners are likely to be effective both on the broadband and tonal noises.

From the measurement system point of view, single microphone techniques are suited to measure the overall sound level occurring at a certain position, which makes it impossible to distinguish whether a sound is generated by the drone or by the WindShaper. In future works it is planned to study how accurately aeroacoustic sound sources can be detected and quantified within a WindShaper using phased array microphone techniques.

Acknowledgements

This work has received support from HEPIA - HES-SO University of Applied Sciences; the Swiss Confederation; the Fondation pour l'Innovation Technologique (FIT).

References

- [1] Christopher S. Allen et al. Springer. Springer, 2002.
- [2] G Catry, F Noca, and A Thurling. "Novel Drone Airworthiness Validation and Assessment Method Addressing ICAO DRONE ENABLE/4 (2020) RFI Problem Statement a)UA Performance Requirements in a UTM Environment". In: *International Civil Aviation Organization 2020* (2020).
- [3] Julia Theresa Cossé. "On the Behavior of Pliable Plate Dynamics in Wind: Application to Vertical Axis Wind Turbines". PhD thesis. California Institute of Technology, 2014.
- [4] *Acoustics – Measurement of room acoustic parameters – Part 2: Reverberation time in ordinary rooms*. en. Standard. Geneva, CH: International Organization for Standardization, 2008. URL: <https://www.iso.org/standard/54029.html>.
- [5] Eric Johnson and Jamey Jacob. "Development and Testing of a Gust and Shear Wind Tunnel for NAVs and MAVs". In: *47th AIAA Aerospace Sciences Meeting including The New Horizons Forum and Aerospace Exposition* (May 2009).

- [6] Daegyoum Kim et al. "Flapping dynamics of an inverted flag". In: *Journal of Fluid Mechanics* 736 (2013), R1.
- [7] T. Mueller et al. "The design of a subsonic low-noise low turbulence wind tunnel for acoustic measurements". In: July 1992. DOI: 10.2514/6.1992-3883.
- [8] A Nishi and H Miyagi. "A computer-controlled wind tunnel". In: *Journal of Wind Engineering and Industrial Aerodynamics* 54 (1995), p. 493.
- [9] Flavio Noca and Guillaume Catry. *Wind Generation Means and Wind Test Facility Comprising the Same*. PCT/EP2017/064451. 2016.
- [10] Flavio Noca et al. "Wind and Weather Facility for Testing Free-Flying Drones". In: *AIAA Aviation 2019 Forum* (2019). DOI: 10.2514/6.2019-2861. eprint: <https://arc.aiaa.org/doi/pdf/10.2514/6.2019-2861>. URL: <https://arc.aiaa.org/doi/abs/10.2514/6.2019-2861>.
- [11] Roberto Putzu, Davide Greco, and David Craquelin. "Design and Construction of a Silent Wind Tunnel for Aeroacoustic Research". In: *4th CEAS Air & Space Conference, FTF Congress: Flygteknik 2013*. July 2013.
- [12] Ennes Sarradj et al. "Acoustic and aerodynamic design and characterization of a small-scale aeroacoustic wind tunnel". In: *Applied Acoustics* 70.8 (2009), pp. 1073–1080. ISSN: 0003-682X. DOI: <https://doi.org/10.1016/j.apacoust.2009.02.009>. URL: <http://www.sciencedirect.com/science/article/pii/S0003682X09000577>.
- [13] J.T. Smith et al. "A simplified approach to simulate prescribed boundary layer flow conditions in a multiple controlled fan wind tunnel". In: *Journal of Wind Engineering and Industrial Aerodynamics* 109 (2012), pp. 79–88.
- [14] H. W. Teunissen. "Simulation of the planetary boundary layer in a multiple-jet wind tunnel". In: *Atmospheric Environment* (1967) 9.2 (1975), pp. 145–174.
- [15] Jia-Ying Wang et al. "A multiple-fan active control wind tunnel for outdoor wind speed and direction simulation". In: *Review of Scientific Instruments* 89 (2018), 837–846.



CidB

Centre d'information
sur le Bruit

**QUIET DRONES
International e-Symposium
on
UAV/UAS Noise
Remote from Paris – 19th to 21st October 2020**

Research to Support New Entrants to Public Airspace and Aircraft Noise Certification

David Read, United States Department of Transportation – Volpe National Transportation Systems Center: david.read@dot.gov

Christopher Roof, United States Department of Transportation – Volpe National Transportation Systems Center: christopher.roof@dot.gov

Summary

This paper identifies some of the reasons why existing aircraft noise certification methods might not fully address the integration of new entrants to public airspace, and describes ongoing research measurement programs to obtain data that can inform future noise policy and methodologies for noise certification of such aircraft.

1. Introduction

Aircraft noise certification is a mechanism promulgated by civil aviation authorities such as the U.S. Federal Aviation Administration (FAA) to fulfil statutory requirements including those in the United States under U.S.C. 49, section 44715, “Controlling aircraft noise and sonic boom”. When such requirements were first introduced, the purpose was to control aircraft noise at its source (the aircraft) where it had the greatest potential to impact the public the most: in the vicinity of airports, during typical operations, such as take-offs and landings. (Figure 1)

Trajectory and Certification Locations

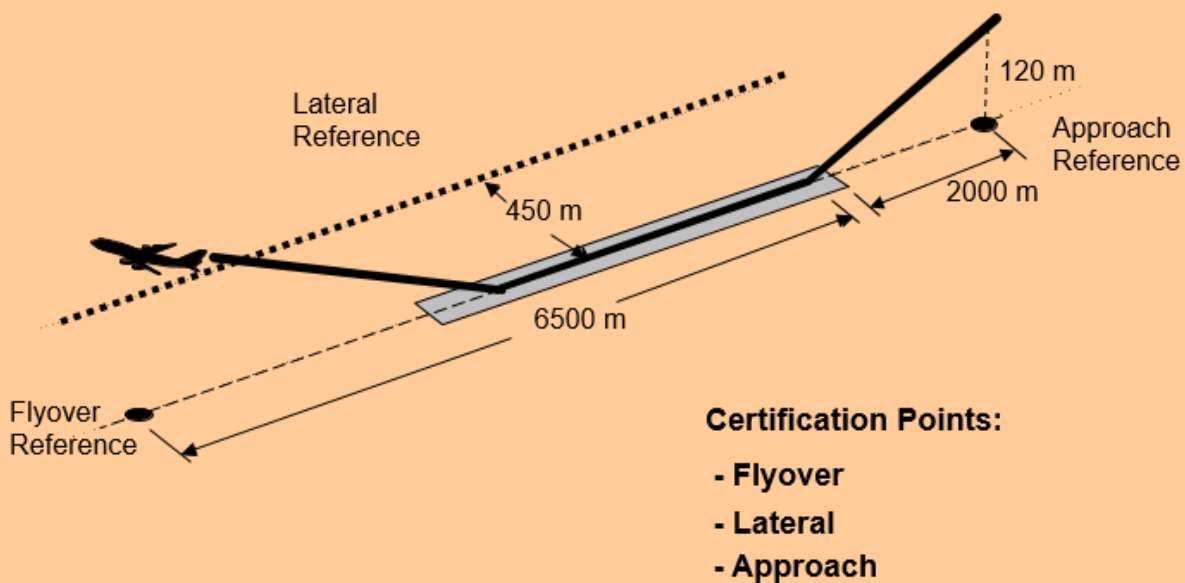


Figure 1 - Aircraft Noise Certification - Flight Operations for Transport Category Aircraft evaluated under 14 CFR Part 36, Appendix 1 (FAA Office of Environment & Energy)

Today, technology improvements are allowing previously unavailable flexibility in aircraft configuration, size, propulsion, and control mechanisms; and the missions and typical operations of such aircraft have the potential to affect the environment in previously unanticipated ways: Noise from some of these aircraft is likely to extend to communities beyond the vicinity of an airport into areas not previously experiencing aircraft noise. The qualities of such noise may cause public reaction in a variety of ways not anticipated by conventional aircraft noise regulation. In addition, due to the novel design techniques being employed, and the operational capabilities enabled by those designs, the ability of conventional noise metrics to reliably represent the effects of noise from these aircraft may not be a certainty.

2. The role of aircraft noise certification

Currently, certification is the primary mechanism used to regulate and reduce aircraft source noise. The process, developed and agreed to internationally¹, is managed on a national level by aircraft authorities. The underlying philosophy is to motivate manufacturers and operators to employ current best-practices in design – and to operate aircraft featuring these design elements - in order to meet increasingly stringent noise level limits based on existing aircraft categories: small propeller-driven aircraft; small helicopters; and “transport-category” aircraft such as jets, large propeller-driven aircraft, helicopters, and tilt-rotors, using takeoff mass as the primary correlating

¹ The United States Government is a member-state of the United Nations (UN), and participates in the UN's International Civil Aviation Organization (ICAO) Committee on Aviation Environmental Protection (CAEP) Working Group 1 – Noise Technical. ICAO Noise Standards are documented in Annex 16 Volume 1.

element. Other than stringency increases (quieter noise limits) associated with various “stages” or “chapters”, and small updates to the details regarding technical procedures and methodology for noise measurement and analysis, the rules – and noise metrics - have remained mostly the same as when first introduced in the mid-to-late 1960’s (in the US) and early 1970’s (for ICAO member states).

2.1 Unwritten assumptions behind existing aircraft noise certification requirements and specifications

When the standards for noise certification were established, it was impossible, for example, for an aircraft to be piloted entirely by computer control. Also, it was impractical to design for exclusively electrical propulsion systems, or for an aircraft (other than toys or model replicas) to be small enough to be operated within a community from areas other than aerodromes or airports.

All of these aircraft functional concepts have either already been implemented or are entirely plausible, and represent issues being introduced by the consideration of new entrants to the public airspace. None of them were addressed in the formulation of noise certification procedures because they did not exist at the time. Improvements in computer-processing power and software-aided simulation and design techniques, in combination with the development of new materials and construction methods; as well as developments in electrical energy storage technology, have converged to make the current moment possible. Previously impossible aircraft are now a reality. These new entrants and novel aircraft designs will enable previously impossible missions and flight profiles, in places where aircraft operations were never anticipated.

2.2 Unique characteristics of noise from new entrants

Some of the new aircraft design and operational differences may result in the introduction of community noise with substantially different qualities than that from conventional aircraft. For example, electric propulsion systems currently available exhibit different spectral content from conventional internal-combustion or jet-powered aircraft.

Observations have been made that aircraft with electrical propulsion may actually result in lower noise levels, than from conventionally-powered aircraft when quantified using conventional noise metrics. In contrast, multi-rotor eVTOL aircraft that make use of computer-controlled, differential-thrust for manoeuvring have raised public awareness of a characteristic sound that some have compared to the sound of swarming bees – due perhaps to the presence of multiple, dynamic, enharmonic tones.

Additionally, operations in and around neighbourhoods - such as package delivery or infrastructure inspections – could result in relatively short sound propagation paths, which could minimize or negate any beneficial effects of high-frequency atmospheric absorption of sound. (Such absorption is typical for high-altitude aircraft overflights.) The proximity of aircraft operations in itself, may be a contributing factor to human annoyance, and the unnattenuated high-frequency content may be perceived as characteristic of such proximity.

Abrupt onsets and cut-offs of the sound may be more likely, due to intermittent line-of-sight blockage by local objects and structures, as the aircraft travel through neighbourhoods. The absence of human occupants on an aircraft may allow for performance profiles that would not be otherwise acceptable, but may also contribute to the dynamic, time-variant nature of this noise.

Long-term operations involving sustained hovering, where an aircraft may be performing a local survey (weather conditions, surface traffic volume, insect population estimates, mapping, etc.) or reconnaissance (automobile license plate capture, census-taking, fugitive searches, etc.), or may be providing temporary access to Wi-Fi or cellular radio service, may also create new noise characteristics that the public are not accustomed to.

2.3 Aircraft noise metrics

Traditionally, broadband frequency-weighted noise levels in various forms are used to characterize noise in communities. For aircraft certification, several such metrics are used, including the maximum, slow (1-second time-constant) time-averaged, A-weighted Level ($L_{A_{\text{smx}}}$), for small propeller-driven aircraft under 19,000 lbs (8618 kg). This value is provided in decibels re: 20 micro-Pascals, and is directly available as an output from any calibrated, class 1 sound level meter (SLM). A-weighted Sound Exposure Level (ASEL or L_{A_e}), also referenced in decibels re: 20 micro-Pascals, is used for small helicopters under 7,000 lbs. (3175 kg). This ASEL is a time-integrated metric, and so it not only includes the maximum broadband noise level, but also reflects the duration effect of the noise by integrating the noise energy over the 10 dB-down duration in reference to the standard duration of 1 second. This metric is available as a direct output from any calibrated, class 1, *integrating* SLM.

The Effective tone-corrected Perceived Noise Level (EPNL) is specifically used for noise certification of any jet-powered aircraft, large, propeller-driven aircraft, helicopter or tilt-rotor. Similar to SEL, EPNL is another time-integrated, broadband metric, but is derived from one-third octave band (OTOB) spectral analysis at one-half second increments of the time-varying pressure signal from a calibrated, class 1 measurement microphone system. EPNL is similar in nature to SEL, in that it integrates the noise energy over time, but in this case, the reference duration is 10 seconds, and the time-integration is performed using Tone-corrected Perceived Noise Level (PNLT), which is a broadband metric representing the spectral and tonal content at any one-half second instant in time. Rather than applying a simple frequency-weighting to the noise energy, each OTOB sound pressure level (SPL) in a particular spectrum is converted to Noys – an indicator of perceived loudness, based on amplitude and frequency – then summed together to obtain Perceived Noise Level (PNL). The maximum tonal content in each spectrum is identified and quantified to determine the Tone-corrected Perceived Noise Level (PNLT) for that spectrum, and then the time-history of PNLT is integrated to obtain EPNL. Current noise certification regulations only require that OTOB analysis be evaluated over the range of bands having nominal center frequencies of 50 Hz to 10 kHz. It should be noted that tonal content is only evaluated to identify the *maximum single tone correction* within a given spectrum. (Figure 2)

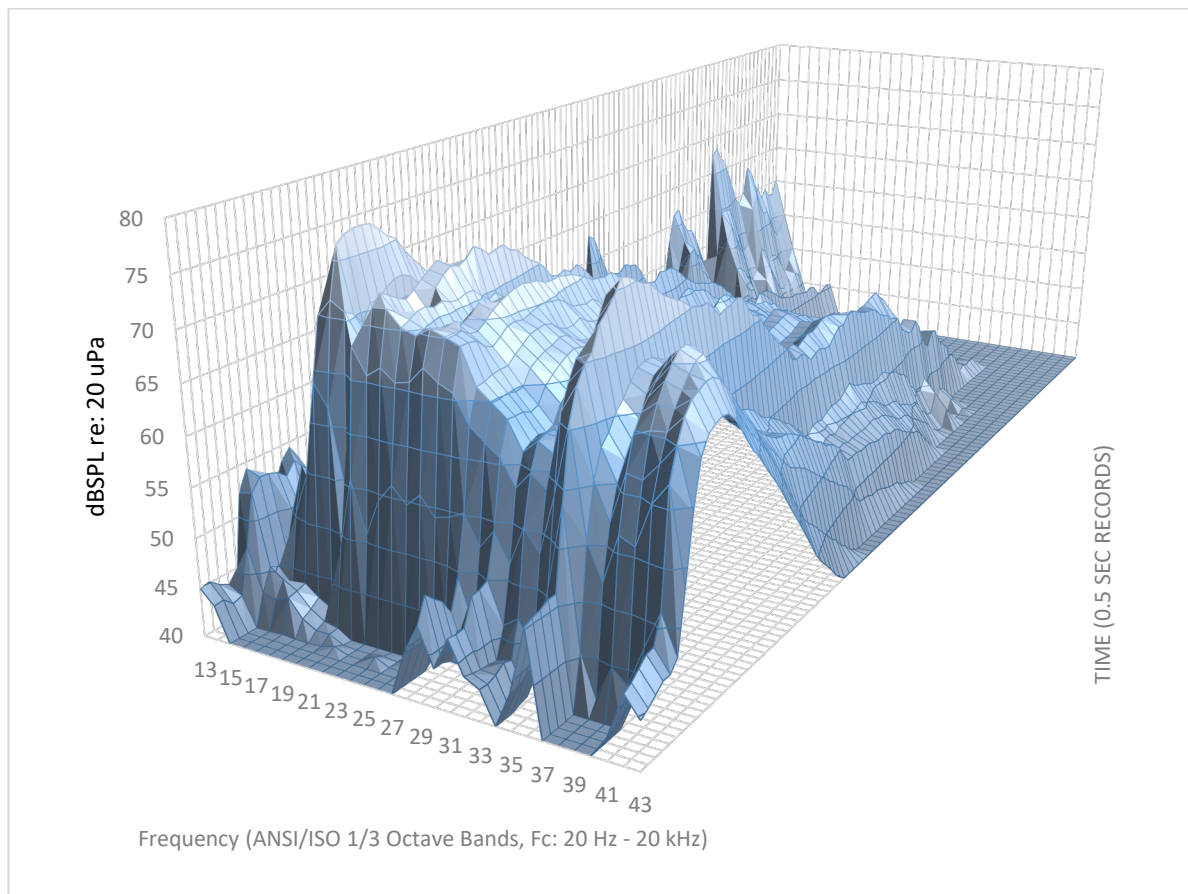


Figure 2- OTOB SPL time history (slow time-weighting response): octocopter vertical take-off, ground plane microphone illustrating energy above 10 kHz and presence of multiple tones (Volpe)

Noise metrics used in the modelling and prediction of aircraft noise in communities are also primarily based on broadband frequency-weighted levels and include some of the metrics already mentioned, but also – for cases such as Day-Night Average Sound Level (DNL) and Community Noise Equivalent Level (CNEL), the metrics are intended to represent cumulative noise during 24-hour periods – with “penalty” offsets applied to account for the intrusive effects for sounds occurring during evening or night-time hours - and may present specific challenges when used to manage operational noise from novel aircraft.

2.4 Exploring additional metrics for noise certification

As noted previously, there are indications that the new entrants being discussed may exhibit noise signatures that contain substantial energy in the high-frequency region beyond 10 kHz (between 10 kHz and 20 kHz) due to the noise generating mechanisms involved, as well as due to the lack of attenuation of higher frequencies from atmospheric absorption, since propagation distances may be very short. The EPNL metric used for many types of aircraft considers noise within the 50 Hz to 10 kHz OTOB range, thus potentially excluding a portion of the sound energy that may be found to be typical of these new entrants. Substantial work might be required to modify the existing EPNL calculation procedures to adapt this metric to accommodate these higher-frequency bands. SEL (A-weighted, or with other frequency-weightings) could accommodate the higher frequency content because for each weighting curve the response vs. frequency is expressed as a continuous function (whereas the PNL and Tone-correction frequency-dependencies used for EPNL are defined in the form of OTOB constants for the previously identified range of bands only) but may have other weaknesses in representing noise effects from these aircraft.

Additionally, it is anticipated that much of the noise energy from such aircraft – especially electrically-powered and/or multirotor - could be in the form of multiple, dynamic tones, which are likely to be important in possible future human-response evaluations. None of the metrics currently in use for aircraft noise certification address perceived annoyance related to the presence of multiple tones.

Furthermore, close operating distances in urban or suburban environments - in combination with near-instantaneous, computer-controlled manoeuvring systems, and the potential absence of human occupants - suggest that, in addition to sudden onsets and cut-offs of the sound, there are likely to be rapid fluctuations of the noise energy content over time, which would likely not be captured using any of the current noise metrics.

Although initial noise rules and specifications for such aircraft are likely to be based on conventional metrics, new metrics employing finer resolution in both time and frequency – as well as the ability to track and quantify multiple simultaneous tones - might be needed for future noise regulations for noise certification, as well as for quantifying contribution of noise from these aircraft in the community..

3. FAA-Sponsored noise measurements & research related to new entrants

In order to prepare for noise certification or other noise-related evaluations of these new entrants and novel aircraft, FAA's Office of Environment & Energy (AEE) is funding noise measurement research by the US DOT Volpe Center (Volpe) to obtain operational noise data and audio recordings from production models of existing aircraft and prototypes of future aircraft, such as drones, UAVs, Air Taxis, UAMs, etc.

3.1 Noise data collection and measurement methodology

Volpe's Unconventional Aircraft Noise Team is undertaking noise measurement campaigns through various avenues using high-quality audio recording to capture the fundamental noise data. Rugged, multichannel audio recorders with high sample rates and frequency bandwidth beyond 20 kHz are used to store the audio pressure time waveform from the microphone signals and time-synchronize them using GPS-based Universal Coordinated Time (UTC). (Figure 3)

Volpe Acoustics UAS IPP System Instrumentation Block Diagram

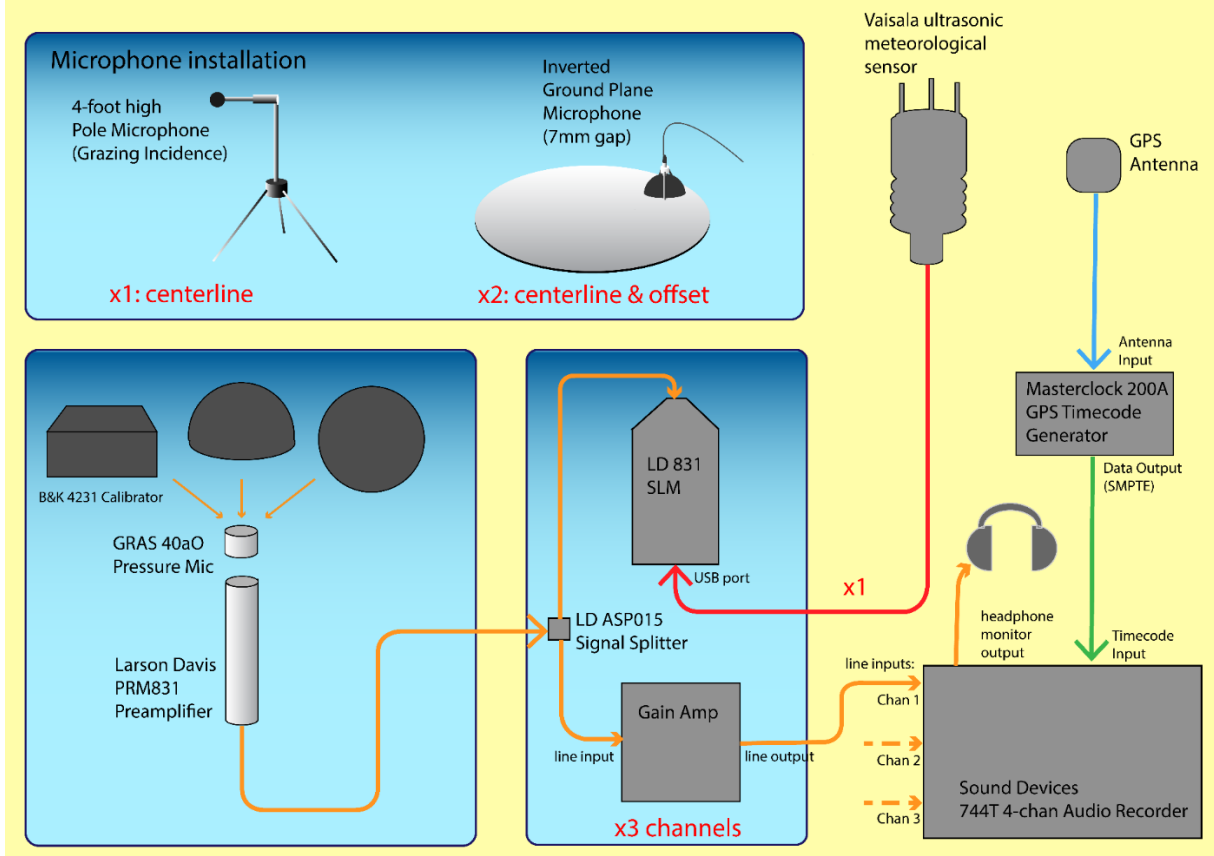


Figure 3 - Volpe UA Noise Team Instrumentation (Volpe)

Microphones are deployed in both 4-foot-high pole-mount and ground-plane configurations, directly under a notional flight path, with a second ground plane microphone positioned about 20' off to one side of the flight path. (Figure 4)

The microphones are all class 1, one-half inch diameter measurement microphones with predominantly flat pressure response from ~10 Hz to ~20 kHz. The pole mic is mounted for primarily grazing incidence relative to the aircraft flight path, while the ground plane microphones are installed in an inverted position, parallel to and 7mm above a flat aluminium disc, 14 cm in diameter and 2.5 mm in thickness, which has been installed into the local ground surface in a manner intended to minimize edge effects caused by the impedance boundary between the plate and the local ground material. (Figure 5)



Figure 4 - Microphone deployment for IPP (Volpe)

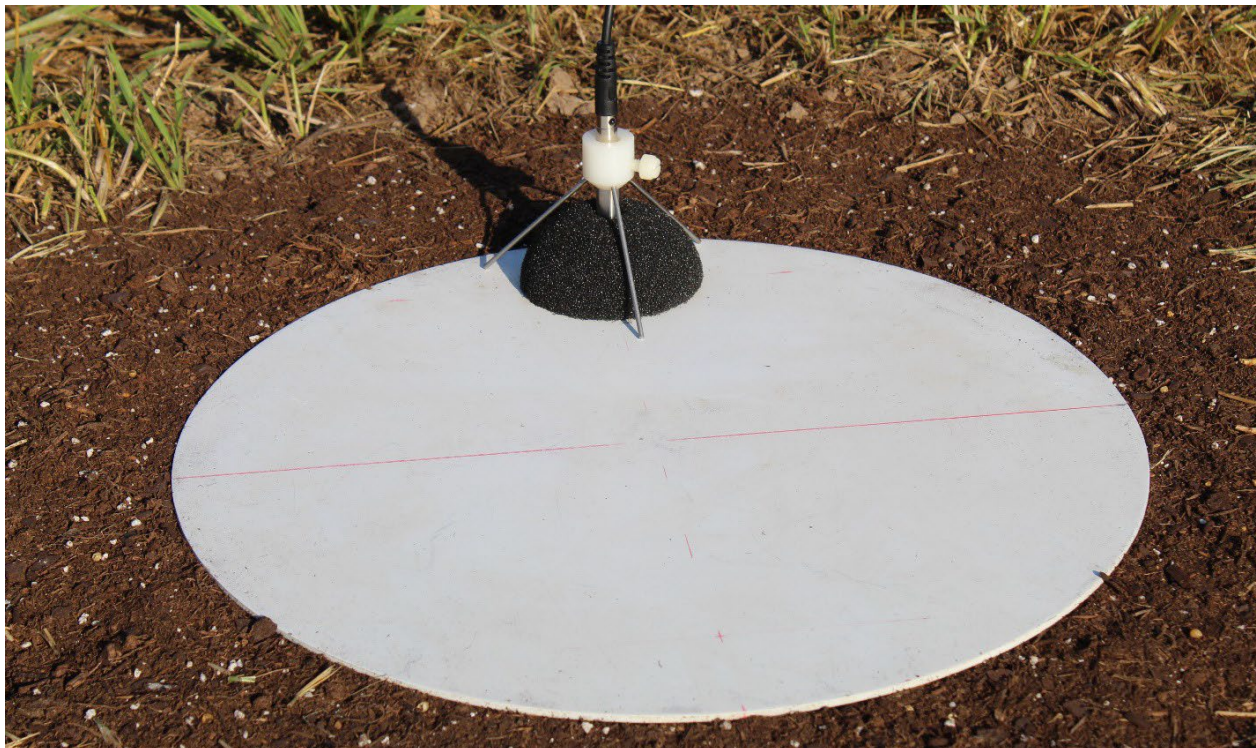


Figure 5 - Inverted ground-plane microphone: ground plate installation in local surface (Volpe)

Edge effects can introduce irregularities into the higher-frequency response of the system, which otherwise substantially provides a uniform pressure-doubling effect in the microphone response to sound pressure. The pressure-doubling effect becomes less uniform with lower sound incidence angles, such as when the source is at a low elevation or a very long distance relative to the microphone location. The frequency bandwidth of the effective pressure zone varies with the physical size of the microphone and of the gap between the microphone and the plate. (Note: Members of the Volpe Team are also actively participating in ICAO technical efforts that include evaluation and comparison of conventional aircraft noise measured using ground plane microphones vs. the pole-mounted microphones specified for noise certification.)

During testing, the subject aircraft is flown past the microphones in a series of operations intended to characterize typical flights that might occur in a neighborhood: ideally a variety of higher-speed ("dash") and lower-speed ("cruise") level overflights are completed, at a variety of heights above

the ground, with the aircraft maintaining stable flight conditions. Overflights are performed in both directions in order to minimize influences of measurement site topology, and prevailing wind, as well as to provide data from both sides of the aircraft to the “sideline” microphone. These operations also allow for comparison to the level overflights required for conventional noise certification for large and small rotorcraft and tilt-rotors.

For any fixed-wing aircraft evaluated during these programs, simulated takeoffs are also performed for comparison to the noise certification requirements for small and large propeller-driven aircraft.

For each individual aircraft evaluated during these programs, an effort is made to identify typical missions and modes of operation, such as package-delivery, infrastructure inspection, hovering surveys, etc. Test flight procedures are then established to simulate the noise effects of such typical operations.

In most cases for rotorcraft, a takeoff/landing target is identified, and specific flight operations are performed in relation to this location, which is typically close to the measurement microphones. Horizontal approaches, followed by complete vertical or near-vertical landings are not unusual for many such aircraft, as are complete vertical takeoffs, followed by horizontal departures from the measurement area. In some cases, hovers or orbits are included, as appropriate. For delivery missions where a parcel is lowered to the local ground while the aircraft hovers over the target, such operations – or appropriate simulations - will be included in these tests. (Figure 6)

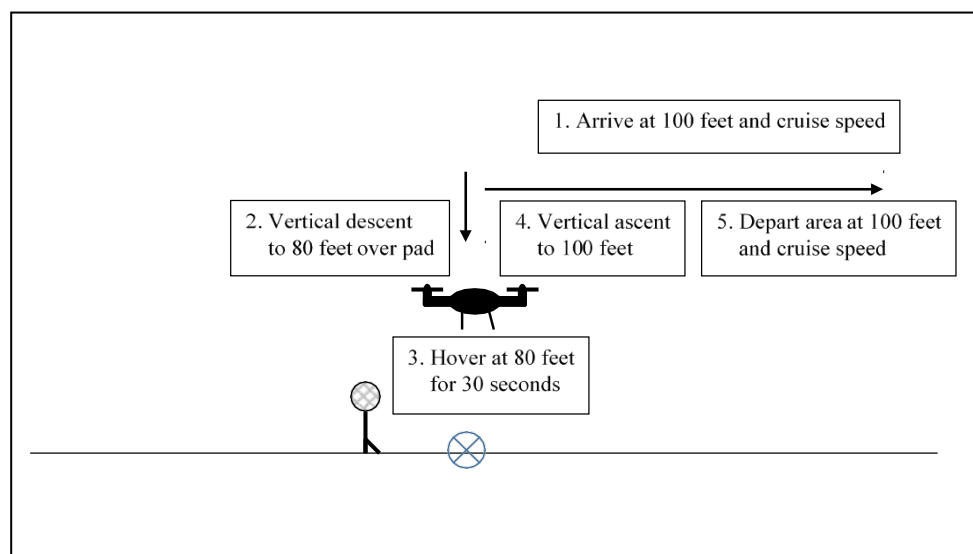


Figure 6 - Schematic for Infrastructure inspection operation specific to a particular multirotor (Volpe)

In most cases, prior to noise flight testing, aircraft are fitted with miniature, independent, Volpe-developed, RTK GPS instrumentation system (Figure 7), comprised of components that capture and record high resolution, time-synchronized aircraft position data. The time-space-position-information (TSPI) datasets obtained from this system are then used in coordination with the time-synchronized audio recordings and local meteorological data to characterize the aircraft noise appropriately.



Figure 7 - Installation of Volpe miniature tracking system components on hexacopter sUAS (Volpe)

Test reports primarily include as-measured data sets, using conventional noise metrics, with some distance-normalized levels also provided. The availability of time-synchronized audio recordings allows for a variety of future analyses and re-analyses to be performed as needed. It is anticipated that such analyses will include finer time and frequency resolutions than are currently required for noise certification purposes.

The audio recordings may also prove useful for auralization experiments, where representative sounds for a particular aircraft type or configuration may be synthesized or modified from the recorded audio for use in human perception evaluations.

As additional data are collected, they may also be used to evaluate scalability factors, such as identifying characteristics of UAV noise that might apply to air-taxis as well. The database may also be useful for development of noise modelling procedures and methodologies, as the models currently in use may not otherwise effectively represent the community noise effects from new entrants.

3.2 Opportunities for data collection

AEE and Volpe are leveraging various existing and new relationships with the National Aeronautics and Space Administration (NASA), industry, local governments and other FAA programs and activities in order to maximize data collection opportunities. The scheduling and logistical preparations for such noise measurement programs can be difficult, and optimal opportunities can be hard to find, due to various limitations – including:

- legal restrictions on commercial or institutional operation of such aircraft within the U.S. National Airspace (NAS);
- preferred measurement site conditions that are crucial for smaller and quieter aircraft, such as low ambient background noise levels, and calm wind conditions;
- obtaining cooperation from owners /operators of such aircraft, who are willing to allow a such noise measurements to be made – and who have the appropriate clearances and authorizations;

The situation has become especially problematic during the current pandemic environment, due to travel restrictions, and quarantining conventions.

Some of the avenues and opportunities for noise data-collection being considered are listed below:

3.2.1 FAA's UAS National Airspace Integration Pilot Program (IPP)

With nine lead participants at various locations around the US, the IPP offers a variety of aircraft and applications. As of this writing, a small assortment of UAVs were measured at the Oklahoma site. Measurements were in planning stages for multiple UAVs at several additional sites around the country, but the program ended on 30 September, 2020. Additional opportunities may be available during future programs.

3.2.2 Other programs

AEE and Volpe's relationships with NASA have enabled various collaborative research measurement programs including ones that address noise from new entrants and should continue to allow for these in the future.

Industry-sponsored events such as the GoFly Personal Flight Competition FlyOffs, held at Moffett Federal Airfield in February, 2020 (Figures 8 & 9), may provide opportunities to capture sound from experimental, prototype aircraft, and NASA's Advanced Air Mobility (AAM) National Campaign (Formerly Urban Air Mobility Grand Challenge) may make available some larger aircraft, designed for passenger flights.



Figure 8- Team Verticycle - GoFly FlyOffs Finalist (Volpe)



Figure 9 - Team Tetra - GoFly FlyOffs Finalist (Volpe)

Volpe is also in discussion with various manufacturers, and operators, some of which are open to the idea of supporting this work by allowing Volpe to perform side-by-side noise measurements during in-house flight testing.

3.2.3 Individual Noise Certification projects

Volpe is supporting FAA/AEE and the various aircraft directorate Noise Certification Specialists (NCSs) in the development of noise certification procedures for new entrants, including the potential for supplemental flight operations that do not currently have associated noise limits, but may help provide needed noise data for future decision-making. Volpe is also involved in discussions with FAA technical specialists regarding development of long-term approaches to aircraft noise certification for new entrants.

4. Other activities related to noise from new entrants

AEE and Volpe are also engaging in other activities related to new entrants, including participation in public discussions, working groups and technical committees, such as the following:

- NASA's UAM Noise Working Group (UAMNWG or UNWG) to develop guidance and flight-testing standards for noise related to Urban Air Mobility – now included under the newly-named Advanced Air Mobility (AAM) vehicles;
- The Vertical Flight Society (VFS) and General Aviation Manufacturers' Association (GAMA) have joined efforts to form a VTOL Noise Assessment Working Group (NAWG), which has similar goals to the NASA group, but from an Industry-centric perspective;
- INCE-USA (and I-INCE, and INCE-Europe) Workshops and symposiums on drone noise;
- SAE International's A-21 Subcommittee on Aircraft Noise is supporting development in cooperation with ANSI and ASA of the noise section of the ANSI Unmanned Aircraft Systems Standardization Collaborative (UASSC)'s Standardization Roadmap for Unmanned Aircraft

Systems, now available as version 2, and has established a Project Working Team to address UAM noise;

- ICAO Working Group 1- Volpe has been supporting FAA by bringing reports of activities related to noise from new entrants in the US to the international arena, as well as engaging in brainstorming and idea exchange discussions with noise certification experts from other nations (including EASA, DGAC France, CAA UK, Transport Canada, ANAC Brazil, and Australian CASA, among others) in order to help find meaningful solutions to the issues being presented by such aircraft.

Additionally, Volpe team members serve as advisors to many of FAA's ASCENT Center Of Excellence projects, including current and coming projects related to UAS/UAM noise modelling, testing and noise certification. Volpe has continuously supported FAA's Office of Environment & Energy in efforts related to Aircraft Noise Certification for over 40 years.

5. Considerations for Future Research and Analyses

Volpe's Unconventional Aircraft Noise Team has identified some unique noise characteristics and analysis approaches we think could be most valuable for moving research and understanding forward. The following are recommendations are based on opinions, but those opinions are based on discussions with various organizational and individual stakeholders and on first-hand experiences with our own noise measurements and those we've participated in or have observed.

It should be noted that the opinions expressed herein do not necessarily reflect the opinions of FAA.

5.1 High-quality noise data collection

The need for real noise measurement data related to typical flight operations of these aircraft cannot be overstated: prevailing business and legal concerns have created an environment where it is extremely difficult to obtain noise data suitable for research purposes – due not only to the particular physical requirements for research-quality noise measurements, such as calm wind conditions and low background noise levels – but also due to the competitive nature of the industry and the concern for protecting what may be proprietary information, while opportunities for performing noise measurement flight testing is hampered by concerns about operational approvals by authorities at various levels. There is a fundamental need for “research-quality” data: wide frequency bandwidth, high-dynamic range audio recordings of typical flight operations at locations representing typical sound propagation distances, time-synchronized to high-resolution position information, at sites with suitable environments as described above. Careful capture and clear field documentation of the data collection efforts are also needed. Such recordings could be used to analyse and re-analyse noise data using various metrics and methodologies, as well as provide source material (time-pressure waveforms) for human-response testing and public awareness sessions via auralization techniques.

Currently, the scarcity of such data is considered the primary gap in moving forward with research related to the noise from new entrants.

Since there is a scarcity of measurement data, the following characteristics have been identified as priorities in the selection of test subject aircraft to be considered for research-quality noise measurements:

- Larger – and heavier – aircraft – among the new entrants, these seem to be most problematic in terms of measurement scheduling availability; also, most likely to exhibit any unique noise characteristics associated with novel propulsion systems, or physical configurations;
- Unique physical configurations – to broaden knowledge of potential noise-generating mechanisms;
- Common physical configurations – such as put forward by organizations anticipating high levels of market infiltration (Major package delivery firms, popular hobbyist models, etc.) – to better represent typical community noise source-composition;
- Differential-thrust designs – especially for larger numbers of rotors/propulsors, since these have already been identified as having characteristic noise signatures AND seem to be extremely popular;
- Hybrid designs that combine vertical lift and fixed-wing/forward propulsion – due to potential acoustic interaction effects that might result from such unusual design;
- Hybrid propulsion systems, such as electric motors with on-board internal-combustion or turbine-based electrical generators that may run on limited duty-cycle schedules – or at reduced output - during flight operations – such designs seem likely to prevail for larger aircraft, at least until better battery capacity technology arrives;
- Any design incorporating intentional noise-reduction technology – these may provide insight into potential areas and methods, and might also be helpful in revealing possible weaknesses in conventional noise metrics;
- Aircraft capable of – or designed specifically for – unique operations such as long-term station-keeping, or local package delivery, or herding of livestock – such operations may introduce noise having unique characteristics into the community;
- Aircraft intended to operate within close proximity of humans or wildlife – useful in evaluation of extended high-frequency bandwidth for instrumentation and metrics;

5.2 In-situ noise data from existing operations in their intended environment

Although less useful for research purposes due to potentially suboptimal measurement conditions and constraints, noise data from new entrants measured during actual flight operations will likely be needed in order to monitor community noise levels and to validate any noise modelling, prediction, or correction methodologies.

5.3 Exploration and evaluation of current aircraft noise certification approaches, metrics, and methodologies to address noise from new entrants

Initial impressions regarding the typical characteristics of noise from new entrants suggest that conventional methods of quantifying such noise – including metrics, noise limits and certification procedures – could benefit from exploratory experimentation to evaluate their effectiveness in addressing the noise from new entrants, but until additional data are available for such aircraft, specific recommendations cannot be made.

5.4 Experimentation to identify potential benefits of increased “granularity” in methods, techniques and metrics for characterization of noise in the community from new entrants

As noted, the variation of noise over time from some of these new entrants will be more dynamic than for conventional aircraft noise, due to control system concepts – like differential thrust – and

potentially abrupt onset and cutoff of sound due to line-of-sight blockages. Additionally, close proximity to sensitive receivers may result in shorter-duration “events”, where the entire 10 dB-down “envelope” may have a duration of only a few seconds – or even less – in contrast to noise envelopes from conventional aircraft flyovers, where such duration can stretch out to 30 seconds or more. In the frequency domain, closely-spaced tones, or other spectral irregularities may result in characteristic noise signatures that differ substantially from conventional aircraft. All of these elements may require analyses of the sound with substantially higher time and frequency resolution – or granularity – than is currently applied. (OTOB frequency analysis, and one-half second time samples are the current “granules” used for aircraft noise certification.)

5.5 Development of noise generation source modelling and prediction techniques

In order to begin consideration of potential noise-reduction technologies, source prediction methodologies will need to be developed and optimized to address the unique characteristics of new entrants and novel aircraft designs, some of which have been identified in other sections of this paper. The variety of proposed designs and missions suggests that this modelling effort may need to be considered as an ongoing task, as technology and conceptual innovations continue to be introduced in the fleet.

5.6 Evaluation of important considerations for – and development of methodologies specific to - prediction and modelling of noise in the community from new entrants

Current state-of-practice aircraft noise modelling methods need to be evaluated for applicability to noise from new entrants, and innovative techniques and considerations for successfully predicting community noise effects for the introduction of these aircraft to the public airspace may be needed. The sheer number and anticipated variability of flight operations, combined with the introduction of such operations into an acoustically complex environment, close to the ground, where structures and terrain features may influence the perceived noise in a substantial manner, suggest that such modelling may need to be profoundly different from the current state of practice.

6. Conclusions

New entrants to public airspace and novel aircraft are becoming a reality and in the U.S. the FAA is already working through a list of Applications for noise certification for such aircraft. Noise from these aircraft may be substantially different from what the public has previously experienced. The variety of configurations, propulsion systems, flight controls, physical size, and potential mission objectives may require an entirely new framework for classifying similar groups of aircraft, and for determining appropriate noise certification procedures and specifications. New methods, rules, limits, procedures and even metrics may be required to address community noise from such aircraft, and while research is ongoing in various arenas, the greatest gap seems to be the scarcity of representative noise data sets. Evaluating these data sets will be the next step in determining whether any updates are needed to the existing noise certification paradigm.

References:

Acoustical Society of America, American National Standards Institute. (2013), *S1.1 – American National Standard Acoustical Terminology*, Melville, NY.

ANSI Unmanned Aircraft Systems Standardization Collaborative (2020), *Standardization Roadmap for Unmanned Aircraft Systems – Version 2.0*,

ASCENT – THE AVIATION SUSTAINABILITY CENTER webpage, FAA, Center Of Excellence, Washington, DC.

<https://ascent.aero/>

Cabell, R., McSwain, R. & Grosveld, F. (2016), *Measured Noise from Small Unmanned Aerial Vehicles*, Noise-Con, INCE-US, Providence, RI.

Christian, A. & Cabell, R. (2017), *Initial Investigation into the Psychoacoustic Properties of Small Unmanned Aerial System Noise*, 17th AIAA Aviation Technology, Integration, and Operations Conference (AVIATION 2017), Denver, CO.

GAMA EPIC eVTOL Committee (2019), *Noise Certification for Emerging VTOL Aircraft*, General Aviation Manufacturers Association, Washington DC/Brussels, Belgium.

International Civil Aviation Organization (2017), *ICAO International Standards and Recommended Practices – Annex 16 to the Convention on International Civil Aviation – Environmental Protection, Volume I – Aircraft Noise*, Eighth Edition, July 2017, International Civil Aviation Organization, Montreal, Quebec.

International Civil Aviation Organization (2018), *ICAO Doc 9501 Environmental Technical Manual, Volume I – Procedures for the Noise Certification of Aircraft*, Third Edition, 2018, International Civil Aviation Organization, Montreal, Quebec.

International Civil Aviation Organization (2020), *Noise from new aircraft concepts* webpage, International Civil Aviation Organization, Montreal, Quebec.

https://www.icao.int/environmental-protection/Pages/noise_new_concepts.aspx

Read, D., Senzig, D. A., Cutler, C., Elmore, E. & He, H., (2020) *Noise Measurement Report: Unconventional Aircraft – Choctaw Nation of Oklahoma – July 2019* FAA report # DOT/FAA/AEE/2020-4, USDOT Volpe Center, Cambridge, MA.

Senzig, D.A., Marsan, M. & Downs, R.(2017), *UAS noise certification and measurement status report*, FAA report # DOT/FAA/AEE/2018-01, USDOT Volpe Center, Cambridge, MA.

Senzig, D. A. & Marsan, M., (2018) *UAS Noise Certification*, InterNoise 2018, I-INCE, Chicago, IL.

Senzig, D. A., Marsan, M., Cutler, C.J., & Read, D. R. (2018), *Sound Exposure Level duration adjustments during UAS rotorcraft noise certification*, FAA report # DOT-VNTSC-FAA-18-07, USDOT Volpe Center, Cambridge, MA.

Sparrow, V. et al (2019), *Aviation Noise Impacts White Paper*, Chapter two of ICAO Environmental Report for 2019, International Civil Aviation Organization, Montreal, Quebec.

Technology for a Quieter America (2020) *UAS and UAV (Drone) Noise Emissions and Noise Control Engineering Technology: Workshop Final Report* ISBN: 978-1-7325986-2-1, Washington, DC.

<http://www.inceusa.org/publications/technical-reports/>

U.S. Department of Transportation, Federal Aviation Administration (2017), *Advisory Circular: NOISE STANDARDS: AIRCRAFT TYPE AND AIRWORTHINESS CERTIFICATION, AC36-4D*, FAA Office of Environment & Energy, AEE, Washington, DC.

U.S. Federal Government (2019) *Code of Federal Regulations, Title 14, Part 36, Amend. 31, - NOISE STANDARDS: AIRCRAFT TYPE AND AIRWORTHINESS CERTIFICATION*, Federal Register, Washington DC

<https://www.ecfr.gov/cgi-bin/text-idx?rgn=div5&node=14:1.0.1.3.19>

Volpe Aircraft Noise Certification Support webpage, United States Department of Transportation, Volpe National Transportation Systems Center, Environmental Measurement & Modeling Division, Cambridge, MA.

<https://www.volpe.dot.gov/environmental-energy-systems/environmental-measurement-and-modeling/AC-Cert>

Willshire, W. & Nystrom, P (1982) *Investigation of Effects of Microphone Position and Orientation on Near-Ground Noise Measurements*, NASA Technical Paper 2004, Langley Research Center, Hampton, VA



QUIET DRONES
International e-Symposium
on
UAV/UAS Noise
Remote from Paris – 19th to 21st October 2020

Noise reduction methods for a fixed wing UAV

Young-Min Shim. Dotterel Technologies Ltd. young-min.shim@dotterel.co.nz

Michael Kingan, Sung Tyaek Go, Ruil Jung, Ryan McKay. University of Auckland

Con Doolan, Yendrew Yauwenas, Chaoyang Jiang, Jiawei Tan, Paul Croaker. University of New South Wales

Dries Verstraete, Rens MacNeil. The University of Sydney

Alex Skvortsov. Defence Science and Technology (Australia)

Summary

This paper describes a project exploring a number of different methods for reducing the noise produced by a small fixed-wing unmanned aerial vehicle (UAV). The methods which were investigated included the use of optimised propellers, ducted propellers and shielding surfaces. A range of experimental and numerical techniques were used to assess each of these methods and these techniques are also described in this paper.

1. Introduction

Small fixed wing UAVs, such as the Skywalker X8 – shown in figure 1, are well suited for use in aerial surveillance applications where low noise emissions are desirable. This paper describes a project exploring a number of different approaches for reducing the noise produced by the Skywalker X8 UAV. It is assumed that the primary source of noise is the pusher propeller system and therefore the noise reduction methods involve either reducing noise from the propeller system itself or shielding an observer from the noise which is produced.

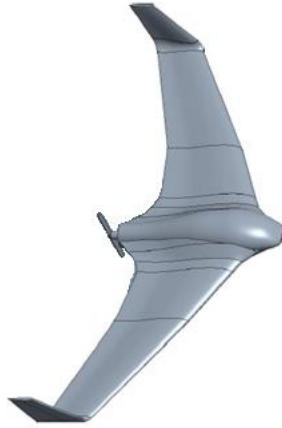


Figure 1. Skywalker X8 UAV

2. Propeller noise reduction

The goal of this section of work was to design a propeller system for this UAV which was optimised to minimise noise during flyover whilst maintaining reasonable efficiency.

2.1 Optimised propeller design

The propeller optimisation was performed using an in-house multi-disciplinary propeller analysis tool which has been developed at the University of Sydney. This tool combines aerodynamic, structural and acoustic modelling. Aerodynamic performance is calculated using an efficient unsteady free-wake panel method [1]. The blade loads obtained from the unsteady panel method are input into a nonlinear beam structural model, based on that described in Ref. [2], to calculate the stress within and deformation of the blade. The blade loading, rotational speed and deformation are used as input to the acoustic prediction model which is based on a source-time-dominant implementation of Farassat's formulation 1A [3]. The propeller geometry was defined using spanwise distributions of chord, twist and sweep. The blade section profile was parameterised using polynomial functions for the upper and lower surfaces. The propeller rotational speed was also set as an additional variable. Propeller installation effects were not taken into account in the performance calculation. The propeller optimisation tool uses the PyOptSparse optimisation framework [4]. The optimisation algorithm selected for use in this study was based on the sequential quadratic programming (SQP) method. This algorithm is well suited for optimisation studies which contain a large number of design variables and constraints.

The propeller design was optimised for several design cases including optimum efficiency and minimum noise. The method predicted that the low noise propeller produced an A-weighted overall noise level 5 dB lower than the maximum efficiency propeller, but required 13% more power at the design operating condition.

A ducted propeller design was also assessed using numerical methods. The ducted propeller aerodynamics were calculated using an LES simulation performed using ANSYS Fluent. The radiated acoustic pressure was predicted using a Ffowcs-Williams and Hawkings solver with the radiated field being calculated using the loading and thickness sources on the surface of the duct and propeller. Figure 2 shows a visualisation of the instantaneous flow structures around the ducted propeller predicted by this simulation. The primary goal of these simulations was to demonstrate the capability of performing such simulations.

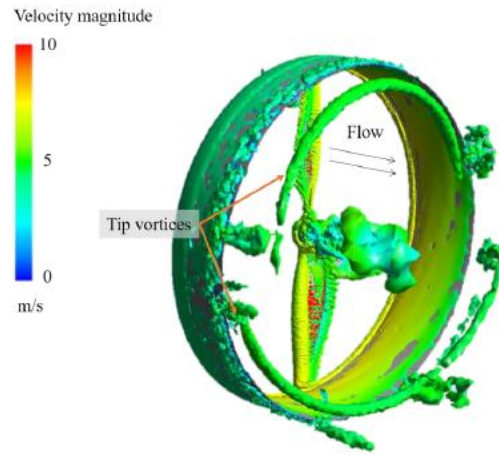


Figure 2. CFD simulation of a ducted UAV propeller. This figure shows Isosurfaces of constant λ_2 vortex criterion, coloured by velocity magnitude.

2.2 Propeller design assessment

Experiments were carried out within the UNSW anechoic wind tunnel facility [5] to measure the noise produced by a propeller system installed on a Skywalker UAV operating within an air stream. In these experiments the body of the UAV was mounted between two end-plates spanning the width of the test section. Acoustic measurements were made using a 64 microphone array located just outside the wind tunnel exit jet. Photographs of the experimental setup are shown in figure 3.

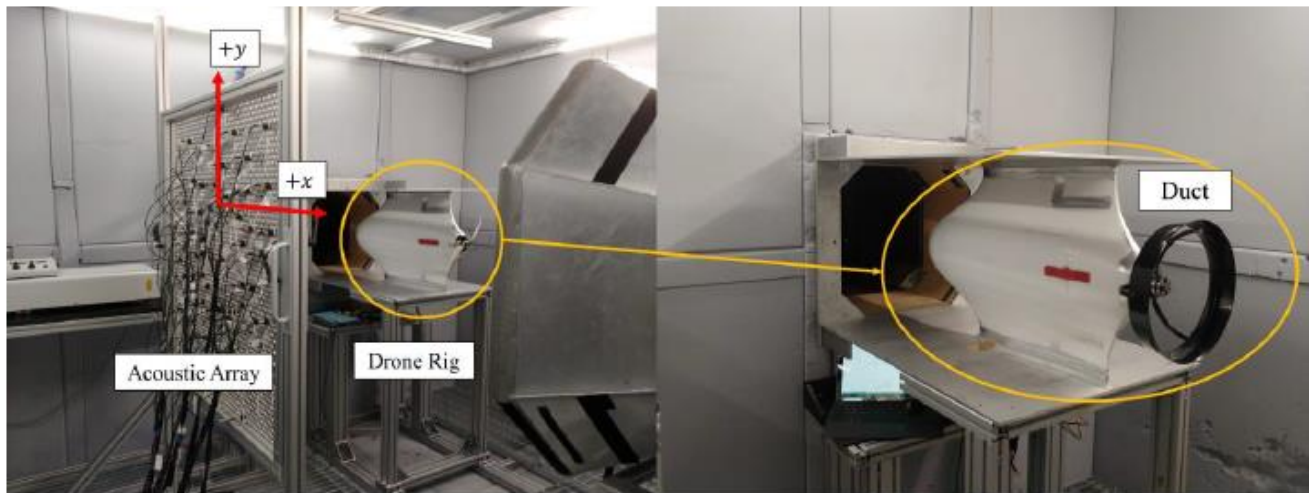


Figure 3. Photographs of the experimental rig with the UAV and propeller system mounted between two endplates. The left photograph shows the microphone array and an open propeller. The right photograph shows a ducted propeller.

Six different propellers were tested. One of these was a commercially available 12" diameter UAV propeller. The other five were custom made and were manufactured from ABS plastic. These propeller designs included: (1) a reference 12" diameter propeller with unswept blades; (2) a 12" diameter propeller with a gradually swept profile and serrated leading edges; (3) a 13.7" diameter propeller; (4) a 10" propeller which had been optimised to achieve maximum efficiency; (5) an 8" diameter propeller which was optimised to produce low noise levels. This propeller was tested with and without a duct (shown in figure 3, right). Photographs of three of the tested propellers are shown in figure 4.

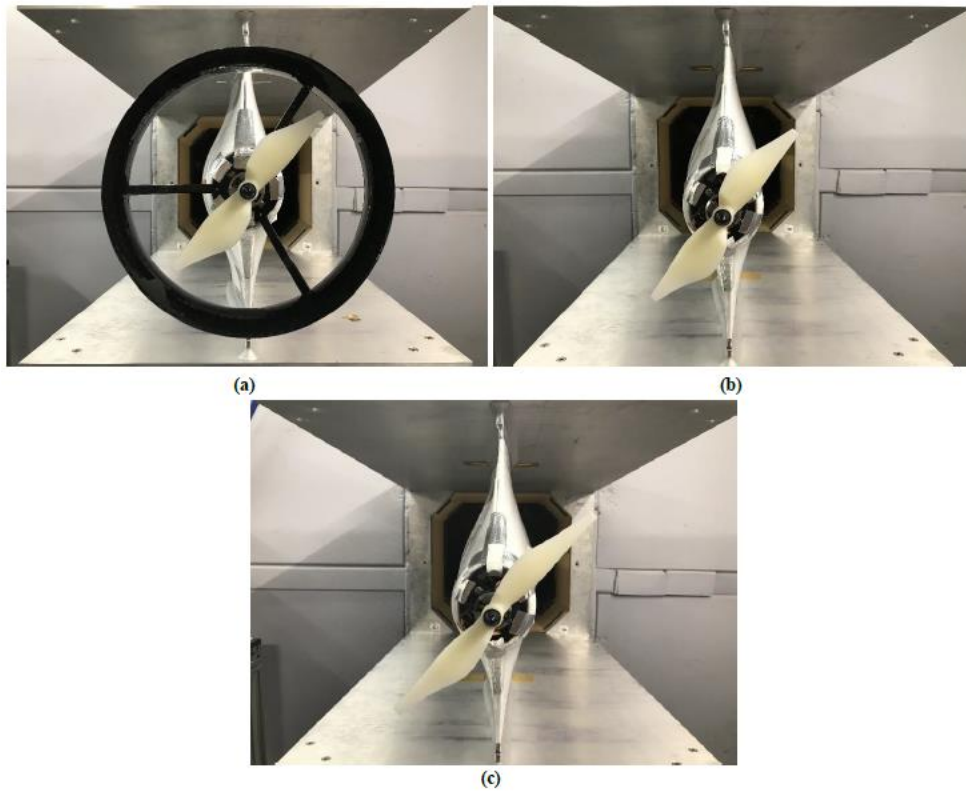


Figure 4. Photos of 3 of the installed propeller configurations. (a) 8" diameter ducted propeller, (b) 8" diameter open propeller, (c) 10" diameter open propeller.

Figure 5 plots the measured narrowband sound pressure level (SPL) spectra produced by the 3 different propeller configurations shown in figure 4. During these experiments the free-stream velocity was 15 m/s and each propeller was operated at approximately 5000 RPM. All propellers produce significant levels of tonal noise at integer multiples of the propeller shaft rotational frequency. The prominence of the tones at odd harmonics of the shaft rotational frequency indicates that the propellers may have been unbalanced or there may have been significant differences in the blade-to-blade geometry of the propellers. The cause of these tones requires further investigation. The multitude of tones at even harmonics of the shaft rotational frequency (i.e. at harmonics of the blade passing frequency) could also be caused by the unsteady loading on the propeller blades due to their interaction with the wake from the UAV body. The ducted propeller is also observed to produce slightly higher noise levels (both tonal and broadband) than the other configurations. This could be partially attributed to: the ducted propeller producing more thrust and thus larger steady loading tonal noise; noise produced by the interaction of the wakes from the duct struts with the propeller; and separated flow around the duct. Noise from the electric motor is also likely to have contributed to the noise spectrum at higher frequencies. These noise generation mechanisms all require further investigation.

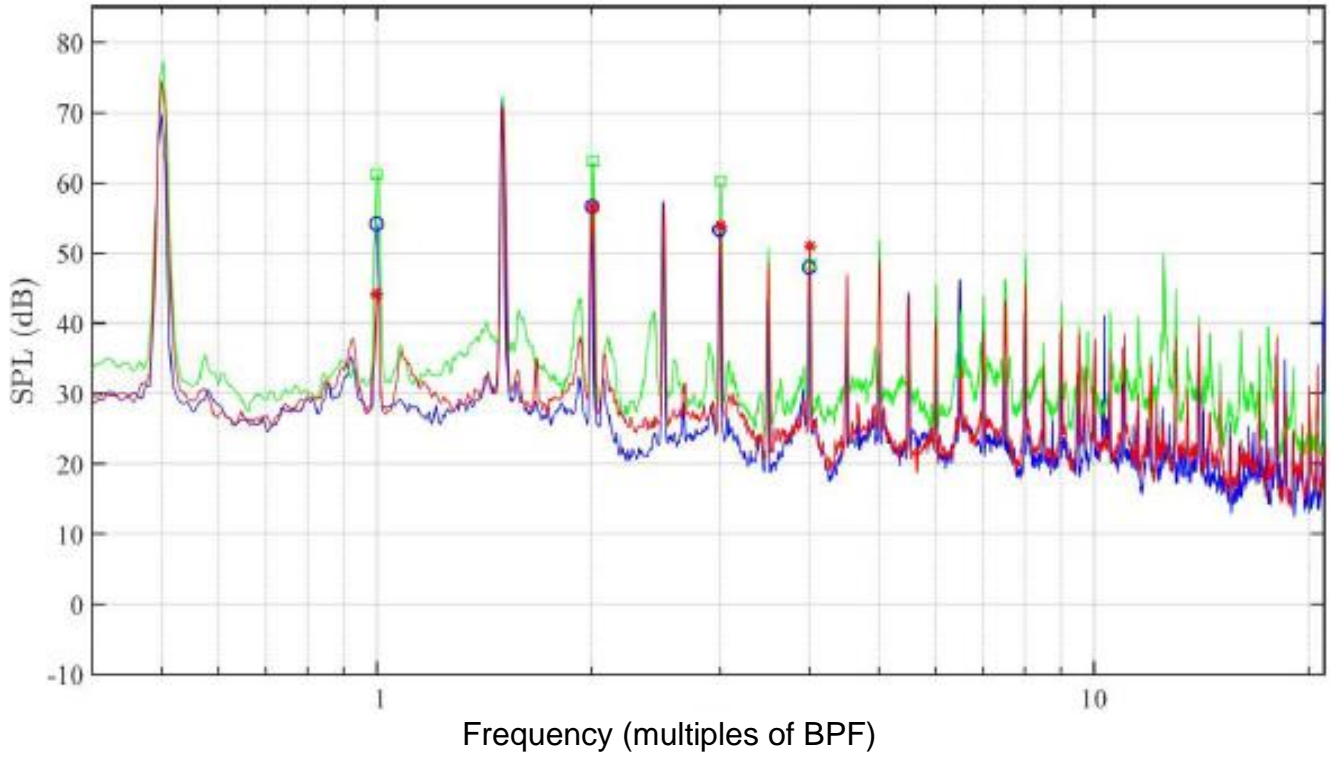


Figure 5. Narrowband SPL spectra produced by 3 different propeller configurations. 8" diameter ducted propeller (green), 8" diameter open propeller (blue), (c) 10" diameter open propeller (red).

3. Propeller noise shielding

Work was undertaken to assess the effect of lightweight shielding surfaces close to and beneath the propeller, such as shown in figure 6. The method assumed that the rotor-alone tones produced by the propeller could be modelled as equivalent to those produced by a rotating point source. The acoustic pressure at location \mathbf{x} and circular frequency $\omega_m = mB\Omega$ produced by B point sources rotating at speed Ω of strength Q is given by

$$\tilde{p}_r(\mathbf{x}, \omega_m) = ik_m \rho_0 c_0 Q \frac{B}{2\pi} \int_0^{2\pi} \tilde{G}(\mathbf{x}|\mathbf{y}, \omega_m) \exp\{imB\phi_s\} d\phi_s, \quad (1)$$

where $i = \sqrt{-1}$, $k_m = \omega_m/c_0$ is the acoustic wavenumber, ρ_0 is the density of the ambient air, c_0 is the speed of sound in the ambient air, ϕ_s is the azimuthal angle (through which the blade rotates) and $\tilde{G}(\mathbf{x}|\mathbf{y}, \omega_m)$ is the Green's function between the source position \mathbf{y} and observer position \mathbf{x} at frequency ω_m .

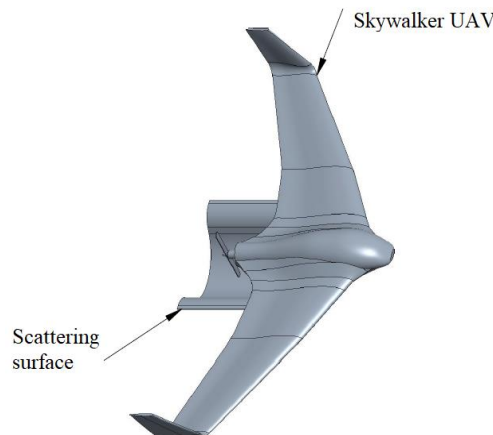


Figure 6. Skywalker UAV with installed shielding/scattering surface.

The Green's functions were measured experimentally using the principal of reciprocity. A microphone on a rotating arm was mounted in the propeller position at the rear of the UAV which was mounted in the anechoic chamber at the University of Auckland. The experimental setup is shown in figure 7. Speakers were positioned at five different polar angles directly beneath the aircraft. The Green's functions were measured with and without the scattering surface and measurements were made for each speaker position at 180 microphone positions by rotating the microphone through a complete revolution in 2° increments.

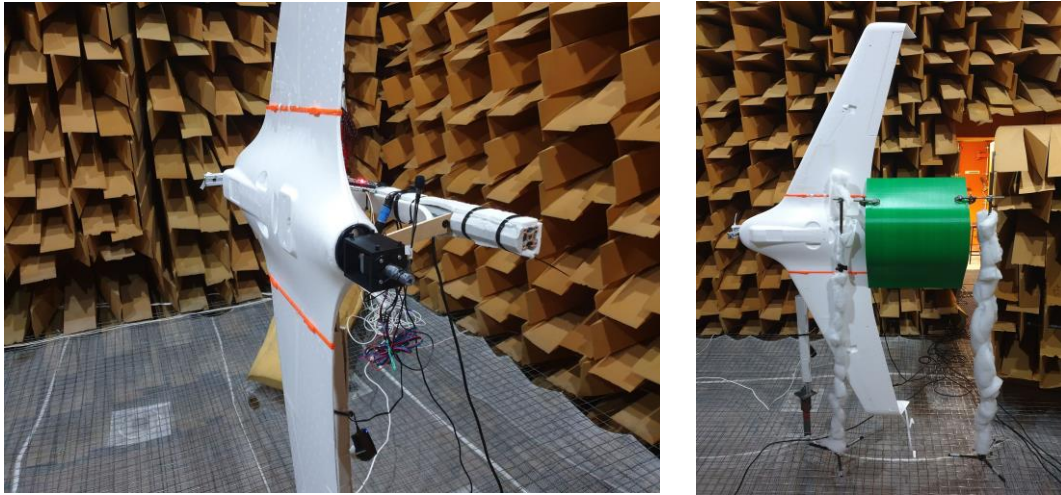


Figure 7. Rotating microphone installed at rear of UAV (left). Scattering surface installed beneath UAV (viewed from the speaker position) (right)

The measured Green's functions were used in eq. (1) to calculate the sound pressure level produced by the rotating sources at the five speaker positions. The results are shown in figure 8 and show that the shielding surface is capable of producing significant reductions in the measured noise levels (assuming the propeller sources are unaffected). These results were compared with BEM predictions and showed moderate agreement. Further work is required to validate the experimental method presented here and to explore different scattering surface geometries and acoustic linings. It is also intended to extend the method to account for impulsive noise sources (in order to simulate the noise generated when the propeller blade passes through the wake of the UAV).

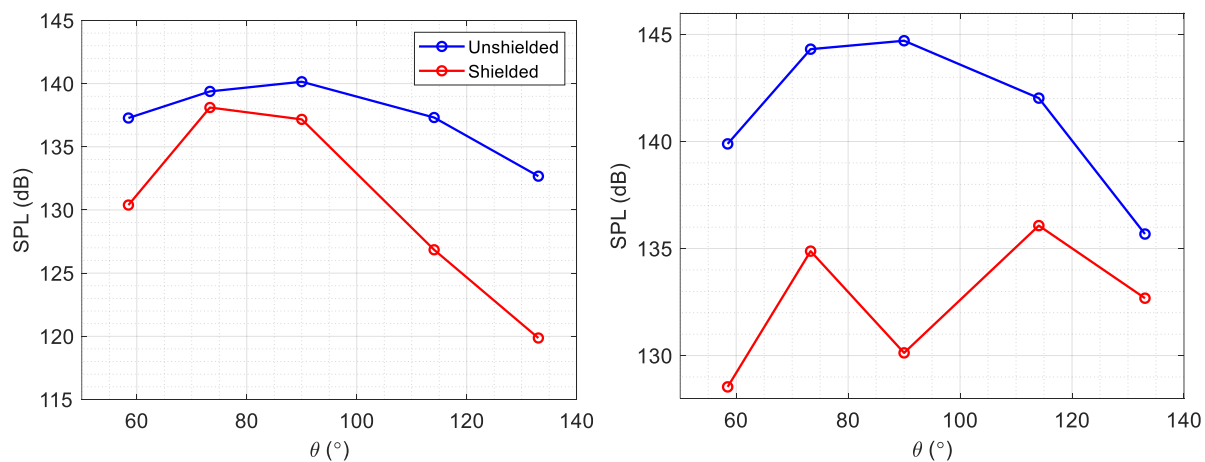


Figure 8. Plot of SPL versus polar angle predicted for the first two tones produced by two rotating point sources adjacent to the Skywalker UAV – with and without the acoustic shielding surface. First rotor-alone tone (left), second rotor-alone tone (right)

4. Fuselage vibration assessment

A scanning laser vibrometer was used to measure the vibration velocity over the surface of a statically mounted UAV with propeller operating. The purpose of these experiments was to assess the importance of noise generated by the fuselage vibration caused by the attached motor and propeller. Figure 9 shows the vibration velocity magnitude on the surface of the UAV for one such test. Estimates of the noise radiated from the vibrating surface indicated that surface vibrations would not produce significant levels of noise.

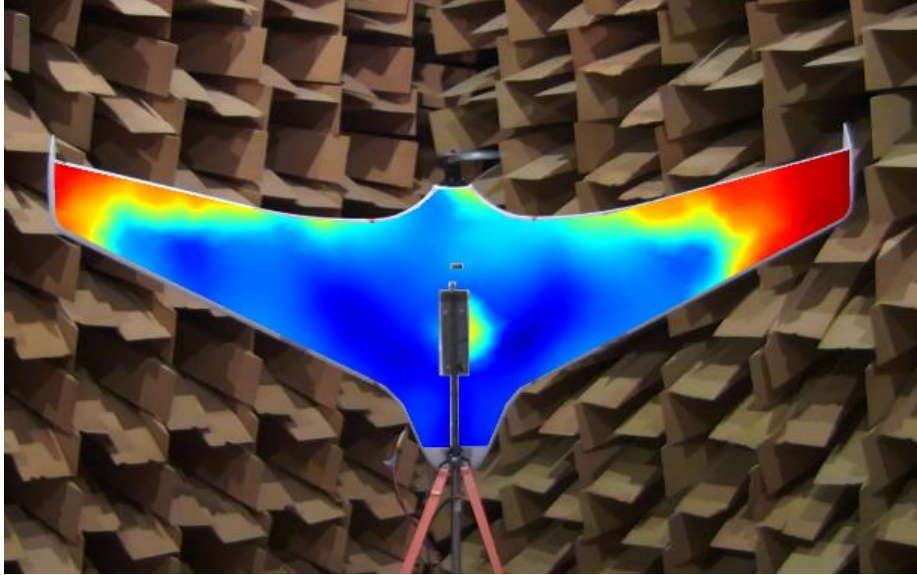


Figure 9. Colourmap showing the measured vibration velocity amplitude on the surface of a statically mounted UAV with propeller. Red indicates high vibration velocity amplitude and blue indicates low vibration velocity amplitude.

5. Conclusions and future work

This paper has provided an overview of a project exploring methods for reducing the noise produced by a Skywalker X8 fixed wing UAV. The project investigated the use of optimised propellers, ducted propellers and acoustic shielding surfaces for this purpose.

The optimised propellers were predicted to provide significant reductions in the rotor-alone tones produced by an isolated propeller. Further work is required to extend the noise prediction method to include installation effects and broadband noise sources.

The noise produced by a number of different propellers installed on a Skywalker UAV were assessed in the low noise wind tunnel at UNSW. The sound pressure level spectra measured during these tests indicated that the noise produced by the installed propeller system was likely caused by a number of different source generation mechanisms which were not included in the noise optimisation method. Further investigation is required to understand these noise generation mechanisms.

A high-fidelity CFD/CAA simulation was also conducted to predict the noise produced by a ducted propeller. Further work is required to validate this prediction method against experimental results.

A novel method based on the principal of acoustic reciprocity was used to assess the noise reduction potential of a shielding surface placed beneath the propeller. This method showed that the scattering surface could produce significant reductions in noise level. The predicted noise reductions were validated against BEM predictions. Further work is required to assess different

scattering surface geometries and acoustic surface linings. The method will also be extended to allow impulsive noise sources to be modelled.

Measurements of the surface vibration of the UAV during static testing indicated that surface vibration was not a significant source of noise.

Acknowledgements

This project was funded by a Small Business Innovation Research for Defence (SBIRD) grant from the Australian Department of Defence.

References

- [1] S.Y. Wie, S. Lee and D.J. Lee, Potential Panel and Time-Marching Free-Wake Coupling Analysis for Helicopter Rotor, *Journal Of Aircraft*, 46(3), pp. 1030-1041, 2009.
- [2] P. Minguet and J. Dugundji, Experiments and Analysis for Composite Blades Under Large Deflections Part 1: Static Behavior, *AIAA Journal*, 28(9), pp. 1573-1579, 1990.
- [3] F. Farassat, Derivation of Formulations 1 and 1A of Farassat, NASA-TM-2007-214853, 2007.
- [4] R.E. Perez, P.W. Jansen and J.R.R.A. Martins, pyOpt: A Python-Based Object-Oriented Framework for Nonlinear Constrained Optimisation, *Structural and Multidisciplinary Optimization*, 45(1), pp. 101-118, 2012.
- [5] C. Doolan, D. Moreau, M. Awasthi, and C. Jiang. The UNSW anechoic wind tunnel. *Proceedings of WESPAC*, 2018.



QUIET DRONES
International e-Symposium
on
UAV/UAS Noise
Remote from Paris – 19th to 21st October 2020

On the design of acoustic liners for ducted fans of drones

Andre M. N. Spillere – Federal University of Santa Catarina, Florianópolis, Brazil:
andre.spillere@lva.ufsc.br

Julio A. Cordioli – Federal University of Santa Catarina, Florianópolis, Brazil:
julio.cordioli@ufsc.br

Summary

The so-called acoustic liners are the main noise control treatment applied to traditional turbofan engines and are responsible for a considerable reduction of different components of the engine noise, especially the fan noise. Therefore, the application of liners to the reduction of drone noise seems an interesting alternative at first. However, the many different applications and concepts of drones make the design of a liner for drones a very complex task. Traditional liners are designed to maximize the attenuation of propagating modes inside the nacelle of a turbofan engine in the presence of high flow velocities and sound pressure levels. Clearly, different conditions will be found in the case of drones. In this study, we consider ducted fans of geometry and operating conditions expected to be found in distributed propulsion systems, such as in electric vertical takeoff and landing aircraft. By employing a typical liner design methodology, it is shown that acoustic liners remain an attractive alternative to reduce fan noise of drones if a proper design procedure is followed.

1 Introduction

The terminology "drone" has been loosely applied to describe eVTOL (electrical vertical takeoff and landing) aircraft, which may have very different applications. More recently, there has been a large interest in using drones for urban logistics (T. Jones 2017) or as an air taxi vehicle (Holden and Goel 2016). The adoption of such means of transportation in the urban environment

has also raised several concerns, specially in terms of the community noise impact. In general, it is expected that drones will have a lower noise signature when compared to other traditional aircraft, such as fixed-wing commercial aircraft or helicopters. However, the potential of these new applications of drones, and the possible large demand, may lead to a much larger traffic than traditional aircraft and, consequently, a much higher cumulative noise impact.

In the last few year, some studies have been carried out to understand drone noise, the human perception and possible associated problems (Zawodny, Boyd Jr, and Burley 2016; Henderson and Huff 2018; Christian and Cabell 2017). However, many questions are still open, and noise is still considered a potential risk to this new business model. Therefore, in order to ensure that drones can be adopted as an alternative to urban mobility, its noise generation needs to be minimized as much as possible. In this sense, the application of technologies already available, such as acoustic liners, seems an obvious first choice.

The acoustic treatment of the nacelle of turbofan engines is one the main noise reduction techniques applied to commercial aircraft, and it is responsible for a considerable reduction of engine noise (McAlpine et al. 2006; Sugimoto, Murray, and Astley 2012). The so-called acoustic liners are in general composed of a perforate facesheet over a honeycomb core and backed by a rigid plate. Liner parameters need to be carefully selected in order to provide an acoustic impedance that maximizes noise attenuation within the engine duct. In this sense, much effort has been undertaken to understand the physics involved in noise attenuation by liners and on design methods used in the project of such treatment. However, the vast majority of the literature remains focused on commercial aircraft turbofan engines, and the study of the possible application of such treatments to other aircraft, such as drones, is very limited.

A great number of design configuration for drones can be found in the literature (Bacchini and Cestino 2019). The majority of designs rely on a multi-rotor configuration for lift and propulsion, with the rotor becoming the main noise source. As a consequence, much attention has been given to the design of reduced noise blades, mitigating the noise directly at the noise source (D. Moreau, Brooks, and Doolan 2012; Aleix, Ethan, and Syamir 2018). On the other hand, the so-called silent blades usually also lead to a performance degradation in terms of lift generation. Another alternative seldom explored is the use of noise control treatments. In the case of drones with open rotors, the application of noise control treatment is restricted to the drone structure, making it less effective due the small applicable area. On the other side, drones with ducted fans can considerably gain from this strategy, since the treatment of the duct can be highly effective as seen in turbofan engines of traditional aircraft. However, the design of liners from ducted fan of drones remain an open question since the conditions (flow velocity, duct diameter, sound pressure levels, etc) can be considerably different than turbofan applications. In the same line, the applicability of liners to reduce the noise of drones also needs to be verified in view of the reduced number of blades and vanes, which lead to tonal components in lower frequencies, and the reduced space available to accommodate the liners.

The present study aims at providing a first analysis on the use of acoustic liners to attenuate the noise of ducted fans used in eVTOL aircraft. Two examples are considered: (i) the Lilium Jet and (ii) the Bell 4EX aircraft. In what follows, Section 2 provides an overview of the two aircraft considered in the analysis and the estimated operational conditions. Section 3 describes the liner design methodology traditionally applied to the design of liners for turbofan engines, which will be used to design the liners for the cases described in Section 2. Finally, Section 4 presents the design procedure for each case and the results in terms of selected modes, optimum impedance and expected noise reduction in terms of noise transmission loss. The final remarks and the study conclusions are given in Section 5.

2 EVTOL aircraft cases

In order to evaluate the possible noise reduction provided by liners, two eVTOL aircraft have been selected: the Lilium Jet and the Bell 4EX aircraft. Both aircraft are vectored-thrust eVTOL aircraft, but with considerable design differences as can be seen in Figure 1. While Lilium jet relies on 36 ducted fans with small diameter, the Bell 4EX uses only four large diameter ducted fans. The latter also display a much shorter nacelle than the Lilium Jet, what may have a key hole on the noise reduction by a liner since it is directly related to the area that can be treated. A summary of the estimated operation conditions for each eVTOL is given in Table 1, which are then used for the design of acoustic liners and to evaluate the potential noise reduction. It is important to note that the information in Table 1 has been estimated based on data published online (*Electric VTOL News* 2020) and pictures of the aircraft and their rotors.

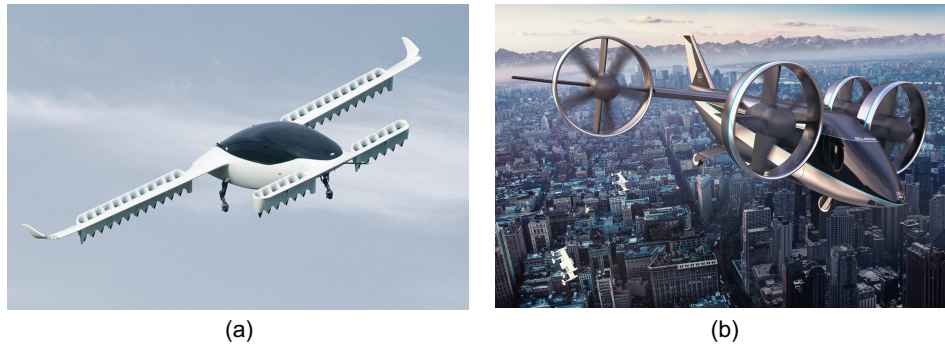


Figure 1: EVTOL aircraft cases considered in the study: (a) Lilium Jet and (b) Bell 4EX.

Table 1: Duct geometry and estimated operation conditions.

	Lilium Jet	Bell 4EX
Duct diameter	0.3 m	2.5 m
Flow velocity	30 m/s	30 m/s
Number of fan blades	27	5
Number of stator vanes	8	4
Fan rotation speed	6000 RPM to 10 000 RPM	1000 RPM to 1500 RPM
First blade passing frequency	2700 Hz to 4500 Hz	83 Hz to 125 Hz

3 Liner design methodology

Traditional liners are composed of a perforated sheet over a honeycomb core and backed by a rigid plate as seen in Figure 2. The main parameters of a liner are: (i) the number and diameter of holes, which lead to a Percentage of Open Area (POA), (ii) the perforate sheet thickness, and (iii) the cavity height. These parameters must be properly selected to maximize the noise attenuation provided by the liner. To do so, it is first necessary to define the propagating modes within the fan duct, what must take into account the presence of the liner. The equations governing the acoustic propagation in the presence of a uniform flow and an impedance wall (representing the liner) are reviewed in Section 3.1. In general, the acoustic field inside the duct is dominated by a few modes, which should be target by the liner (attenuating low energy modes is very little effective). The definition of the dominant modes is usually done by means of the Tyler-Sofrin rule, which is described in Section 3.2. Once the target mode is selected, it is possible to define an optimum impedance that maximize the attenuation of that mode, and the procedure to calculate the optimum impedance is briefly presented in Section 3.3. Finally, semi-empirical models of the liner impedance can be used to defined the liner parameters (mainly POA and cavity height) in order to achieve the optimum impedance, what is described in Section 3.4

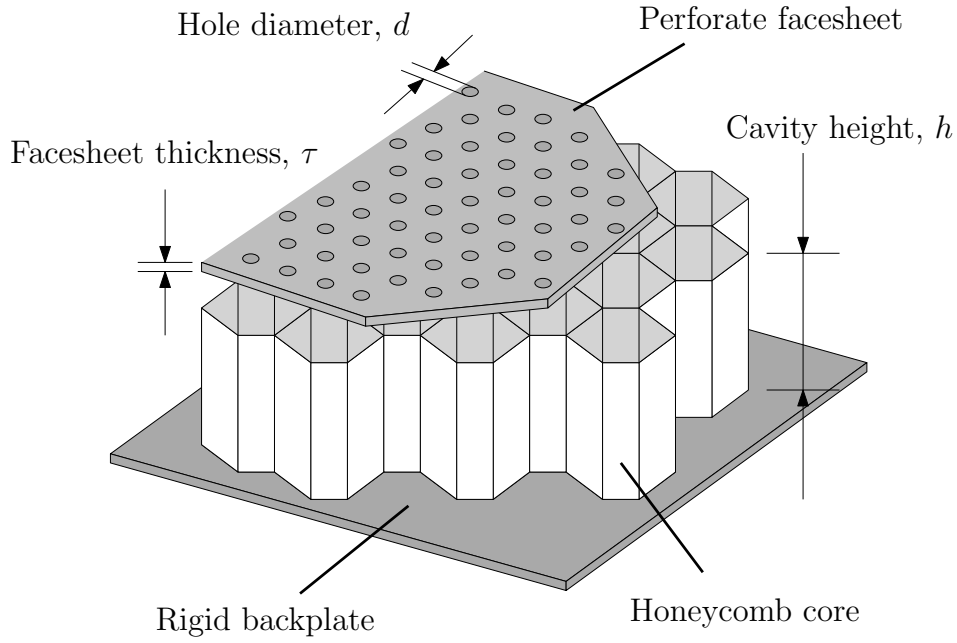


Figure 2: Schematic of a typical single degree of freedom acoustic liner.

3.1 Governing equations

In general, analytical modelling of acoustic propagation in turbofan engines is represented by acoustic modes. For brevity, we consider only the nacelle intake, which can be represented by a straight cylindrical duct of radius a with polar coordinates (r, θ) and axial coordinate x , with flow in the positive x -direction, as shown in Figure 3. Assuming a uniform mean flow and its properties (density $\rho_0 \approx 1.2 \text{ kg/m}^3$ and speed of sound $c_0 \approx 343 \text{ m/s}$) inside the nacelle, acoustic propagation in the form of $p(x, r, \theta, t) \propto \hat{p}(r) \exp(i\omega t - ik_x x - im\theta)$ is governed by the Convected Helmholtz equation,

$$\frac{d^2 \hat{p}}{dr^2} + \frac{1}{r} \frac{d\hat{p}}{dr} + \left((k - Mk_x)^2 - k_x^2 - \frac{m^2}{r^2} \right) \hat{p} = 0, \quad (1)$$

where $k = \omega/c_0$ is the free-field wave number, ω is the wave frequency, k_x is the axial wave number, m is the azimuthal wave number and M is the mean flow Mach number. Solution to Eq. (1) is given in form of Bessel functions of the first kind, $\hat{p}(r) = J_m(k_r r)$, where k_r is the radial wave number that satisfies the dispersion relation

$$k_{x,m\mu}^\pm = \frac{-kM \pm \sqrt{k^2 - (1 - M^2)k_{r,m\mu}^2}}{1 - M^2}, \quad (2)$$

where $+$ and $-$ denote downstream and upstream propagating modes, respectively. The pair of subscripts $m\mu$ indicate the azimuthal and radial mode orders. Thus, the acoustic field is given by a sum of left- and right-propagating modes (time dependence omitted) as

$$p(x, r, \theta) = \sum_{m=-\infty}^{\infty} \sum_{\mu=1}^{\infty} (A_{mn}^+ J_m(k_{r,m\mu}^+ r) \exp(-ik_{x,m\mu}^+ x - im\theta) + A_{mn}^- J_m(k_{r,m\mu}^- r) \exp(-ik_{x,m\mu}^- x - im\theta)), \quad (3)$$

where $A_{m\mu}^\pm$ are the modal amplitudes. In particular, tones exhibit dominant duct modes which are the main target of acoustic liners. Although the exact amplitudes are necessary to correctly assess the far-field radiated noise, it is sufficient to identify the correct dominant mode order when designing optimal acoustic liners at preliminary stages.

At the lined wall, acoustic pressure and normal particle velocity are related by the normalized effective impedance $Z_{\text{eff}} = \hat{p}(a)/\hat{v}(a)$ as seen by the acoustic field in a uniform flow, which takes into account the liner normalized impedance Z and refraction/viscothermal effects through the

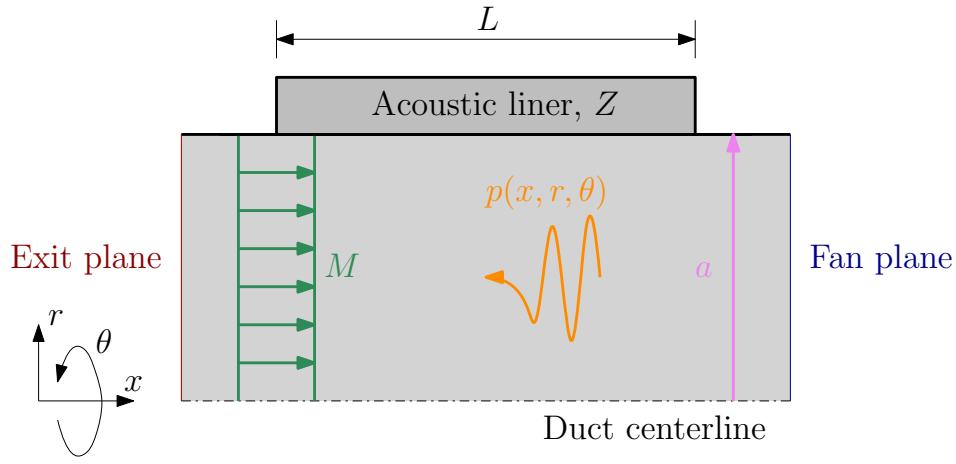


Figure 3: Schematic of the duct intake.

boundary layer. Assuming an inviscid fluid and infinitely thin boundary layer thickness leads to (Ingard 1959; Myers 1980)

$$Z_{\text{eff}} = \frac{kZ}{k - Mk_x}, \quad (4)$$

With aid of the momentum equation in transverse direction,

$$\frac{d\hat{p}}{dr} + i\rho_0 c_0 (k - Mk_x) \hat{v} = 0, \quad (5)$$

it is possible to derive the eigenvalue equation,

$$ikZ = (k - Mk_{x,m\mu})^2 \frac{J_m(k_{r,m\mu}a)}{k_{r,m\mu} J'_m(k_{r,m\mu}a)}, \quad (6)$$

which can be solved for $k_{m\mu}$ (given Z) or Z (given $k_{m\mu}$). Eq. (6) is particularly important because it relates the modal axial decay rate $\text{Im}(k_{m\mu})$ to the liner impedance Z .

3.2 Tyler-Sofrin rule

If the fan blade tip speed is subsonic ($M < 1$), then noise generation is dominated by the rotor-stator interaction (Tyler and Sofrin 1962). The so-called Tyler-Sofrin rule relates the dominant azimuthal order m of the acoustic field to the number of fan blades B and stator vanes V , as follows

$$m = jV + nB, \quad (7)$$

where n is the harmonic order and j is an integer. Note that not every excited mode m propagates since it depends on its cut-on frequency f_c ,

$$f_c = \frac{j'_{m\mu} c_0}{2\pi a} \sqrt{1 - M^2}, \quad (8)$$

where $j'_{m\mu}$ is a root of $J'_m(k_{r,m\mu}a) = 0$, which is the eigenvalue equation for a rigid wall. Therefore, the mode propagates only if the blade passing frequency BPF_n ,

$$\text{BPF}_n = nBf, \quad (9)$$

is above its cut-on frequency. A helpful measure of the mode cut-on frequency relative to the blade passing frequency is the cut-off ratio, defined as

$$\zeta_{m\mu} = \frac{2\pi a \text{BPF}_n}{c_0 j'_{m\mu} \sqrt{1 - M^2}}. \quad (10)$$

Cut-off ratios close to 1 indicate “nearly cut-off” modes, and therefore should be well attenuated by the liner. Higher cut-off ratios (e.g. $\zeta_{m\mu} > 2$) indicate “well cut-on” modes, which are poorly absorbed. A physical interpretation (McAlpine et al. 2006) is related to ray acoustics: nearly cut-off modes propagate mostly in the radial direction, leading to multiple reflections per unit length. On the other hand, well cut-on modes propagate mostly in the axial direction, which severely limit liner attenuation. As a result, the cut-off ratio is closely related to the maximum achievable attenuation of an acoustic liner.

As a final remark, the Tyler-Sofrin rule does not predict the modal amplitude since it depends on the rotor-stator distance, stator geometry, and flow turbulence, for example.

3.3 Optimal impedance

A lined wall results in different attenuation rates for each mode. Once the dominant azimuthal order is known, the liner impedance can be determined. Given the short nacelle length, it is desirable to maximize liner attenuation, which can be achieved by means of the optimal impedance. A quick analytical estimate was proposed by Cremer (1953) based on the merge of the two least-attenuated modes, which is related to the existence of exceptional points in lined waveguides (Xiong et al. 2017). In the presence of uniform flow, it is given by Spillere and Cordioli (2019) as

$$\frac{2MJ_m(k_r a)}{(1 - M^2)k_x + kM} + \frac{a(k - Mk_x)}{k_r J'_m(k_r a)} \left(J'_m(k_r a)^2 + \left(1 - \frac{m^2}{(k_r a)^2} \right) J_m(k_r a)^2 \right) = 0, \quad (11)$$

which is solved for k_r (or k_x) and valid for hollow cylindrical ducts. This equation contains multiple roots, therefore care must be taken to ensure that it corresponds to the merge of the two least-attenuated modes (see Spillere, Zhang, et al. (2019) for details). The same concept can be applied to annular ducts (Qiu et al. 2019), as in the bypass duct of turbofan engines or aft-fan of eVTOL aircraft. The optimal wave numbers $k_{x,\text{opt}}$ and $k_{r,\text{opt}}$ can be substituted in the eigenvalue equation to yield the optimal impedance Z_{opt} so that

$$Z_{\text{opt}} = \frac{(k - Mk_{x,\text{opt}})^2}{ik} \frac{J_m(k_{r,\text{opt}} a)}{k_{r,\text{opt}} J'_m(k_{r,\text{opt}} a)}. \quad (12)$$

The corresponding attenuation can be estimated by

$$\text{TL} = 8.68 \text{Im}(k_{\text{opt}})L, \quad (13)$$

where L is the lined length. In this work, we consider a fixed length of $L = 0.1$ m for both eVTOL aircraft. It is possible to include boundary layer effects on the optimal impedance (Spillere and Cordioli 2019). However, it should have minimal impact on low Mach number velocities, such as in eVTOLs and similar applications.

3.4 Predictive semi-empirical impedance models

In order to relate the optimal impedance to the liner geometrical parameters, semi-empirical models are required. Many different semi-empirical models of liner impedance can be found in the literature, but in general they are found by analytical derivation of viscous and backing effects, and best-fitting non-linear effects (high SPL and flow) to experimental data. These effects are generally summed up to provide the liner impedance in the form of

$$Z = Z_{\text{visc}} + Z_{\text{backing}} + Z_{\text{flow}} + Z_{\text{SPL}}, \quad (14)$$

where Z_{visc} and Z_{backing} are the impedances due to the viscous and backing effects respectively, and Z_{flow} and Z_{SPL} are the impedances due to non-linear effects associated with flow and high SPL. The high SPL contribution can be neglected for $\text{SPL} < 130$ dB and will not be considered

here. In this work, the model of Yu, Ruiz, and Kwan (2008) is used for the other terms. The impedance due the viscous effects is given by

$$Z_{\text{visc}} = \frac{i\omega(\tau + \epsilon d)}{\sigma c_0} \left(1 - \frac{4}{k_s d} \frac{J_1(k_s d/2)}{J_0(k_s d/2)} \right)^{-1} \quad (15)$$

where τ is the facesheet thickness, d is the hole diameter, σ is the percentage of open area, J_0 and J_1 are Bessel functions of the first kind, $\epsilon = \frac{(1-0.7\sqrt{\sigma})}{1+305M^3}$ is the hole correction end, and $k_s = \sqrt{\frac{i\omega}{\nu}}$ is the Stokes wave number, with $\nu \approx 1.5 \times 10^{-5} \text{ m}^2/\text{s}$ the air kinematic viscosity. Flow effects are given by

$$Z_{\text{flow}} = \frac{M}{\sigma \left(2 + 1.256 \frac{\delta^*}{d} \right)} \quad (16)$$

where δ^* is the boundary layer displacement thickness, assumed as laminar with $\delta = 0.01a$. The backing effect is purely reactive and given by

$$Z_{\text{backing}} = -i \cot \left(\frac{\omega h}{c_0} \right), \quad (17)$$

with h the cavity height.

The standard procedure is to select the facesheet thickness and hole diameter, and find the percentage of open area and cavity height that match the optimal impedance. In this work, it is assumed a facesheet thickness of 0.635 mm and hole diameter of 0.889 mm, which are typical values for turbofan engine liners.

It must be noted that the model of Yu, Ruiz, and Kwan (2008) was best-fitted to experimental data in the frequency range from 500 Hz to 3000 Hz, whereas most of the expected blade passing frequencies for the Lilium Jet and Bell 4EX designs are outside this range. Therefore, the liner geometries presented in Section 4 should be considered as reference values to be confirmed by experimental testing.

4 Results

Both intake and exhaust of ducted fans are considered. In general, very similar results are obtained due to the relatively low flow velocity, and therefore the discussion makes no distinction between intake and exhaust results.

4.1 Lilium Jet

The excited modes as predicted by the Tyler-Sofrin rule are shown in Table 2. At the first BPF, azimuthal modes of order $m = 3$ (clockwise) should dominate the acoustic field, with a cut-off ratio ranging from $\zeta = 1.8$ (low rotation speed) to $\zeta = 3.0$ (high rotation speed). Azimuthal modes of order $m = -5$ (counterclockwise) are also excited, but should be easily attenuated due to the lower cut-off ratios. At the second BPF, similar mode orders are excited, however with a much higher cut-off ratio. These modes should be very difficult to attenuate, even in the presence of an optimized liner. Therefore, care should be taken in the rotor-stator design to minimize the modal amplitude of the second BPF modes. Higher order cut-on modes for the second BPF have been omitted for brevity.

It is difficult to determine which mode and BPF contribute mostly to the far-field radiated noise without knowledge of their respective modal amplitudes. In spite of that, we focus on the mode $m = 3$ at the first BPF in order to illustrate the liner design process. Fig. 4 shows the optimal impedance for intake as a function of frequency. The optimal resistance increases with frequency, whereas

Table 2: Excited modes as predicted by the Tyler-Sofrin rule for Lilium jet.

RPM	First BPF		Second BPF	
	Mode order, m	Cut-off ratio, ζ	Mode order, m	Cut-off ratio, ζ
6000	3	1.8	-2	4.9
	-5	1.2	6	2.0
10000	3	3.0	-2	8.1
	-5	1.9	6	3.3

the optimal reactance decreases with frequency. Once a target frequency has been selected e.g. 8000 RPM, the corresponding liner geometry can be determined. Also shown in Fig. 4 is the liner impedance for the selected geometry. It is possible to observe that the liner resistance is close to the optimal resistance over the whole frequency range. However, liner reactance exhibits a different tendency when compared to the optimal reactance due to the $-\cot(\omega h/c_0)$ term. For this reason, liner attenuation should be concentrated over a narrow frequency range, as expected for typical SDOF liners.

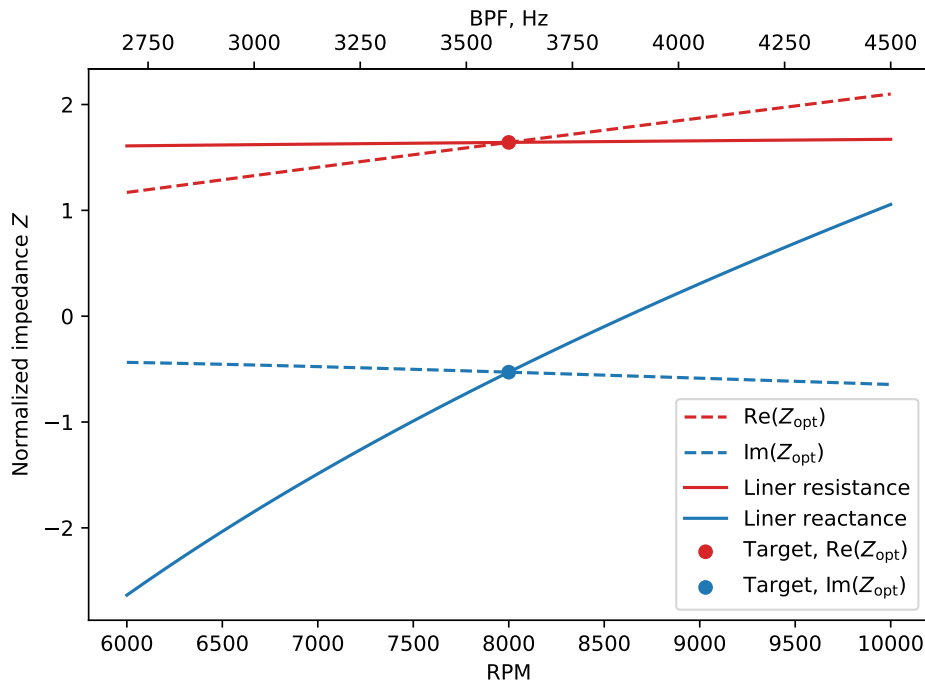


Figure 4: Optimal impedance for intake as a function of frequency (dashed lines). Also shown is the target optimal impedance for 8000 RPM (circles) and the corresponding liner design (solid lines).

The optimal impedance, expected transmission loss (TL) and corresponding liner for different fan rotation speeds are shown in Table 3. The maximum transmission loss decreases with frequency, from approximately 17.6 dB at 6000 RPM to 6.7 dB at 10 000 RPM. This tendency is closely related to the cut-off ratio and highlights that higher frequencies, which propagates predominantly in the axial direction, are more difficult to attenuate. Additionally, noise generation is higher at these power settings, and therefore should be the frequency of interest when designing acoustic liners. It is also noted that the liner facesheet porosity decreases with frequency. Since a constant flow velocity is assumed, the facesheet porosity must increase in order to accompany the optimal resistance. In practice, flow velocity is a function of fan rotation speed, which would contribute to increase the liner resistance. In all considered cases, the facesheet porosities are relatively low for SDOF liners (typically $< 5\%$). This indicates that (i) the liners would be very sensitive to non-linear effects i.e. flow and high SPL, and (ii) drag increase due to the liner presence would be minimal.

The cavity depth also decreases with frequency, which is relatively small compared to SDOF

Table 3: Optimal liner design and expected transmission loss (TL) for different fan rotation speeds in the Lilium Jet case.

RPM	1st BPF, Hz	Intake				Exhaust			
		Z_{opt}	TL, dB	POA, %	L_c , mm	Z_{opt}	TL, dB	POA, %	L_c , mm
6000	2700	$1.17 - 0.44i$	17.59	3.70	8.53	$0.98 - 0.20i$	16.66	4.42	10.81
7000	3150	$1.41 - 0.48i$	12.24	3.11	5.64	$1.11 - 0.26i$	12.37	3.94	7.39
8000	3600	$1.64 - 0.53i$	9.45	2.70	3.90	$1.24 - 0.31i$	9.72	3.57	5.27
9000	4050	$1.87 - 0.59i$	7.80	2.39	2.80	$1.38 - 0.36i$	8.03	3.24	3.86
10 000	4500	$2.10 - 0.65i$	6.69	2.15	2.08	$1.52 - 0.40i$	6.87	2.97	2.92

liners (typically > 20 mm). At maximum rotation speed, the optimal liner should have a total thickness (facesheet thickness + cavity depth + backplate thickness) between 4 mm and 5 mm, which corresponds to approximately 3 % of the duct radius. Therefore, the installation of an acoustic liner should be realizable in terms of required space.

Although most of the liner geometries presented in Table 4 are similar, the corresponding liner impedances as a function of frequency are rather considerably different. As a consequence, a liner design with target frequency of 8000 RPM will perform poorly at 10 000 RPM, and vice versa, as illustrated in Fig. 5. Also shown is the maximum achievable TL at each frequency. The liner design for 8000 RPM presents a significant attenuation over a broader frequency range when compared to the liner design for 10 000 RPM. However, noise generation at 10 000 RPM may be critical to the perceived noise levels in the nearby community, in which case the optimal liner design for this frequency will be required, even if it penalizes attenuation at lower frequencies. Moreover, the optimal liner for 6000 RPM would be very effective at this frequency, but almost nonexistent at higher frequencies. Together with the required cavity depth, it is unlikely that this low-frequency liner design would be used in this specific application.

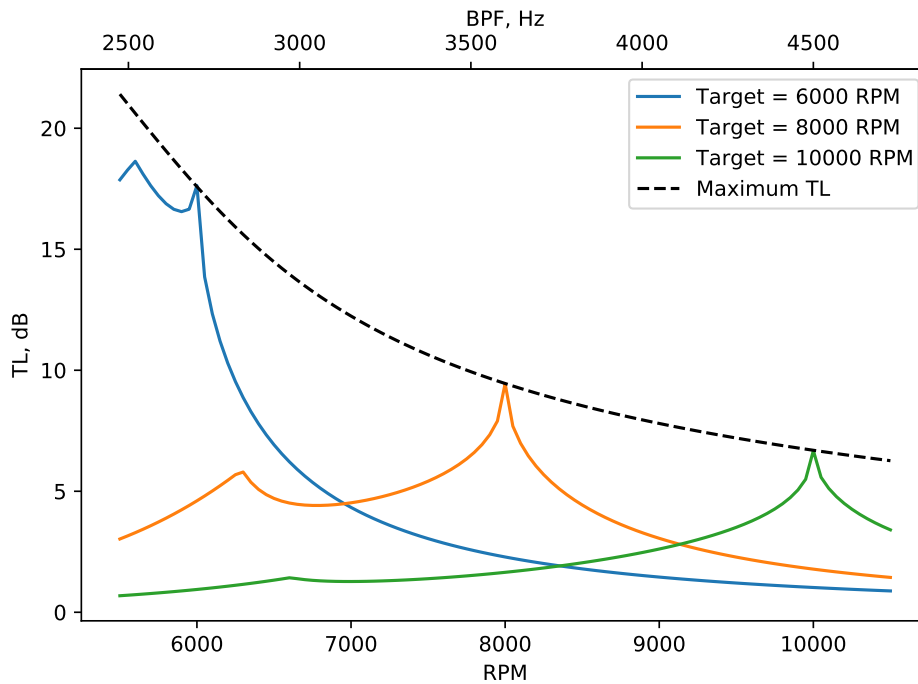


Figure 5: Transmission loss of the least attenuated mode of azimuthal order $m = 3$ as a function of frequency for different liner designs.

4.2 Bell 4EX

Despite the relative small ratio between duct length and duct diameter, it is still assumed that the Tyler-Sofrin applies. In contrast with the Lilium jet design, all excited modes present lower cut-off

ratios, as shown in Table 4. In consequence, acoustic liners should be very effective in terms of attenuation. On the other hand, the longer wavelengths at this BPF and large duct radius may contribute to insufficient liner absorption for such short nacelle lengths.

Table 4: Excited modes as predicted by the Tyler-Sofrin rule for Bell 4EX.

RPM	First BPF		Second BPF	
	Mode order, m	Cut-off ratio, ζ	Mode order, m	Cut-off ratio, ζ
1000	1	1.0	-2	1.3
	-	-	2	1.3
1500	1	1.6	-2	1.9
	-	-	2	1.9

Since the first BPF is considerably low for such liner application, we focus on mode $m = 2$ at the second BPF. The optimal geometries and maximum transmission loss are shown in Table 5. The optimal facesheet porosities are similar to the Lilium Jet case and will not be discussed. However, cavity depth is considerably larger due to the lower BPF. At maximum rotation speed, the total liner thickness corresponds to almost 15 % of the duct radius. It is very unlikely that space restrictions will be satisfied unless novel liner designs are applied, such as folded cavities (Sugimoto, Murray, and Astley 2012) or spiral-shaped cavities (Versaevel, L. Moreau, and Lacouture 2016). The small attenuation of a short lined length may also contribute to discourage the use of conventional liners, and motivate the research of over-the-rotor liners (Sutliff and M. G. Jones 2009).

Table 5: Optimal liner design and expected transmission loss (TL) for different fan rotation speeds for Bell 4EX case.

RPM	2nd BPF, Hz	Intake				Exhaust			
		Z_{opt}	TL, dB	POA, %	L_c , mm	Z_{opt}	TL, dB	POA, %	L_c , mm
1000	166.7	$0.66 - 0.38i$	3.33	2.28	337.30	$0.62 - 0.03i$	3.02	2.44	438.42
1250	208.3	$0.85 - 0.41i$	2.78	1.79	242.20	$0.76 - 0.11i$	2.49	1.99	309.13
1500	250	$1.04 - 0.44i$	2.11	1.46	178.40	$0.89 - 0.18i$	1.93	1.72	224.95

5 Conclusion

It is likely that drone noise will face stringent regulations in the near future, and, therefore, it is important to minimize noise generation and propagation. In the latter case and considering drones with ducted fans, it is possible to apply acoustic liners at the nacelle internal walls of the propulsion system to partially absorb the acoustic waves, as usually used in turbofan engines. It is unclear, however, if the liner geometry would remain feasible in practice due to the different conditions found in ducted fans of drones.

In this work, a liner design methodology has been applied to ducted fans which are expected to operate in eVTOLs. In particular, the proposed propulsion systems of the Lilium Jet and Bell 4EX have been evaluated in terms of achievable noise reduction and the respective liner geometry. The high number of blades and rotation speed of Lilium jet leads to a relatively high blade passing frequency. As a consequence, the optimal liner requires very small cavity heights, which would comply with space restrictions typically found in aerospace applications. The maximum achievable transmission loss also encourages the application of acoustic liners in small-size ducted fans. On the other hand, conventional acoustic liners should have limited usage in the Bell 4EX due to the low-frequency signature of this propulsion system, leading to very large cavity heights, together with a small transmission loss. In this case, researchers should pursue novel liner technologies, such as folded cavities or over-the-rotor liners. In terms of percentage of open area, both vehicles would require very low values, which should have a limited impact on drag increase due to the liner, and consequently on fuel consumption. Regarding the Lilium Jet case, further research is necessary to assess the liner impedance of such geometries at high-frequencies with flow, and manufacture constraints of acoustic liners for small-size duct diameters, for example.

Acknowledgements

The authors acknowledge funding from CNPq (National Council for Scientific and Technological Development), FINEP (Funding Authority for Studies and Projects) and Embraer S.A.

References

- Aleix, C., P. Ethan, and A. Syamir (2018). "Investigation Towards a Better Understanding of Noise Generation from UAV Propellers". In: *AIAA Paper* 3450.
- Bacchini, A. and E. Cestino (2019). "Electric VTOL configurations comparison". In: *Aerospace* 6.3, p. 26.
- Christian, A. W. and R. Cabell (2017). "Initial investigation into the psychoacoustic properties of small unmanned aerial system noise". In: *23rd AIAA/CEAS aeroacoustics conference*, p. 4051.
- Cremer, L. (1953). "Theory regarding the attenuation of sound transmitted by air in a rectangular duct with an absorbing wall, and the maximum attenuation constant produced during this process". In: *Acta Acustica united with Acustica* 3.4. (In German), pp. 249–263.
- Electric VTOL News* (2020). URL: <https://evtol.news/> (visited on 08/13/2020).
- Henderson, B. S. and D. Huff (2018). "Electric Motor Noise for Small Quadcopters: Part II-Source Characteristics and Predictions". In: *2018 AIAA/CEAS Aeroacoustics Conference*, p. 2953.
- Holden, J. and N. Goel (2016). "Fast-forwarding to a future of on-demand urban air transportation". In: *San Francisco, CA*.
- Ingard, U. (1959). "Influence of Fluid Motion Past a Plane Boundary on Sound Reflection, Absorption, and Transmission". In: *The Journal of the Acoustical Society of America* 31, pp. 1035–1036. DOI: 10.1121/1.1907805.
- Jones, T. (2017). *International commercial drone regulation and drone delivery services*. Tech. rep. RAND.
- McAlpine, A. et al. (2006). "Acoustic scattering by an axially-segmented turbofan inlet duct liner at supersonic fan speeds". In: *Journal of Sound and Vibration* 294.4, pp. 780–806. DOI: 10.1016/j.jsv.2005.12.039.
- Moreau, D., L. Brooks, and C. Doolan (2012). "On the noise reduction mechanism of a flat plate serrated trailing edge at low-to-moderate Reynolds number". In: *18th AIAA/CEAS aeroacoustics conference (33rd AIAA aeroacoustics conference)*, p. 2186.
- Myers, M. K. (1980). "On the Acoustic Boundary Condition in the Presence of Flow". In: *Journal of Sound and Vibration* 71, pp. 429–434. DOI: 10.1016/0022-460X(80)90424-1.
- Qiu, X. et al. (2019). "The Cremer concept for annular ducts for optimum sound attenuation". In: *Journal of Sound and Vibration* 438, pp. 383–401. DOI: 10.1016/j.jsv.2018.09.029.
- Spillere, A. M. N. and J. A. Cordioli (2019). "Optimum acoustic impedance in circular ducts with inviscid sheared flow: Application to turbofan engine intake". In: *Journal of Sound and Vibration* 443, pp. 502–519. DOI: <https://doi.org/10.1016/j.jsv.2018.12.007>.
- Spillere, A. M. N., Z. Zhang, et al. (2019). "Optimum Impedance in the Presence of an Inviscid Sheared Flow". In: *AIAA Journal* 57.3, pp. 1044–1054. DOI: 10.2514/1.J057526.
- Sugimoto, R., P. Murray, and R. J. Astley (2012). "Folded Cavity Liners for Turbofan Engine Intakes". In: *Aeroacoustics Conferences*. 18th AIAA/CEAS Aeroacoustics Conference (33rd AIAA Aeroacoustics Conference). American Institute of Aeronautics and Astronautics. DOI: 10.2514/6.2012-2291.
- Sutliff, D. L. and M. G. Jones (2009). "Low-Speed Fan Noise Attenuation from a Foam-Metal Liner". In: *Journal of Aircraft* 46.4, pp. 1381–1394. DOI: 10.2514/1.41369.
- Tyler, J. M. and T. G. Sofrin (1962). "Axial Flow Compressor Noise Studies". In: *SAE Technical Paper*. SAE International. DOI: 10.4271/620532.
- Versaavel, M., L. Moreau, and E. Lacouture (2016). "Folded spiral-shaped cavities for nacelle acoustic liners: Impedance and attenuation modelling and comparison to experimental results". In: *3AF Greener Aviation* 2016.

- Xiong, L. et al. (2017). "Sound attenuation optimization using metaporous materials tuned on exceptional points". In: *The Journal of the Acoustical Society of America* 142.4, pp. 2288–2297. DOI: 10.1121/1.5007851.
- Yu, J., M. Ruiz, and H.-W. Kwan (2008). "Validation of Goodrich Perforate Liner Impedance Model Using NASA Langley Test Data". In: *Aeroacoustics Conferences*. 14th AIAA/CEAS Aeroacoustics Conference (29th AIAA Aeroacoustics Conference). American Institute of Aeronautics and Astronautics. DOI: 10.2514/6.2008-2930.
- Zawodny, N. S., D. D. Boyd Jr, and C. L. Burley (2016). "Acoustic characterization and prediction of representative, small-scale rotary-wing unmanned aircraft system components". In:



QUIET DRONES
International e-Symposium
on
UAV/UAS Noise
Remote from Paris – 19th to 21st October 2020

CFD-CAA Approach for Sound Generation and Propagation in the UAV Propeller With Subsonic Flow

Sergey Timushev, Alexey Yakovlev, Dmitry Klimenko Moscow Aviation Institute (National Research University), Moscow, Russia: TimushevSF@mai.ru

Andrey Aksenov, Vladimir Gavriluk TESIS LTD, Moscow, Russia: andrey@tesis.com.ru

Pyotr Moshkov Irkut Corporation: p_moshkov@ssj.irkut.com

Summary

Subsonic flow air blade machines like UAV propellers generate intensive noise thus the prediction of acoustic impact, optimization of these machines in order to reduce the level of emitted noise is an urgent engineering task. Currently, the development of calculation methods for determining the amplitudes of pressure pulsations and noise characteristics by CFD-CAA methods is a necessary requirement for the development of computer-aided design methods for blade machines, where the determining factors are the accuracy and speed of calculations. The main objective is to provide industrial computer-aided design systems with a highly efficient domestic software to create optimal designs of UAV blade machines that provide a given level of pressure pulsations in the flow part and radiated noise. It comprises: 1) creation of a method for the numerical simulation of sound generation using the correct decomposition of the initial equations of hydrodynamics of a compressible medium and the selection of the source of sound waves in a three-dimensional definition, taking into account the rotation of blades and their interaction with the stator part of the UAV; 2) decomposition of the boundary conditions accounting pseudo-sound disturbances and the complex acoustic impedance at the boundaries of the computational domain 3) development of an effective SLAE solver for solving the acoustic-vortex equation in complex arithmetic (taking into account the boundary conditions in the form of complex acoustic impedance); 4) testing of a new method at all stages of development using experimental data on the generation of pressure pulsations and aerodynamic noise, including a propeller noise measurements.

1. Introduction

Small unmanned aerial systems (SUAS), also known as drones are becoming increasingly useful for commercial, private activities. Despite their usefulness, drones create noise that is annoying to the public [1-4]. Surprisingly, there are a lack of adequate safety and noise regulations for drones [5]. Given the need to reduce noise and develop appropriate standards, new research is required to understand the nature of drone noise production and develop novel methods of control [6]. Drone noise is dominated by the small propellers used as part of their propulsion systems. Acoustic signatures consist of strong harmonics occurring at multiples of the blade pass frequency as well as a broad-band component [7, 8]. The dramatic increase of the UAV market for civil purposes shows that the quietness and the efficiency of the propulsive system are key aspects in the design of advanced aerial vehicles and very often can lead to the success or failure of the mission [9]. From other hand, the acoustic signature of commercial propeller aircraft is becoming a key design parameter as airlines shift from turbofan to turboprop engines for short-duration flights [10, 11] and restrictions on the noise pollution surrounding airports become more stringent. The new International Civil Aviation Organization noise standard in Annex 16, Vol. 1, Chapter 14 constitutes a 7 dB increase in stringency of the effective perceived noise level and will apply to propeller aircraft under 55 ton in 2020 [12]. Propeller aircraft noise also has a direct impact on the health of those living or working near airports [13, 14].

Propeller noise can be classified into three categories: harmonic noise, broadband noise, and narrow-band random noise [15,16]. Harmonic noise is the periodic component, that is, its time signature can be represented by a pulse which repeats at a constant rate. If an ideal propeller with B blades is operating at constant rotational speed N , then the resulting noise appears as a signal with fundamental frequency BN . The blade-passage period is $1/BN$. Typically the generated pulse is not a pure sinusoid, so that many harmonics exist. These occur at integer multiples of the fundamental frequency. The first harmonic is the fundamental, the second harmonic occurs at twice the fundamental frequency, and so on. Broadband noise is random in nature and contains components at all frequencies. The frequency spectrum is continuous, although there may be a "shape" to it because not all frequencies have the same amplitude. Narrow-band random noise is almost periodic. However, examination of the harmonics reveals that the energy is not concentrated at isolated frequencies, but rather it is spread out. The frequency spectrum shows discrete components, but these spread out, particularly at the higher frequencies. Steady sources are those which would appear constant in time to an observer on the rotating blade. They produce periodic noise because of their rotation. Noise sources are usually divided into three categories: linear thickness, linear loading, and (nonlinear) quadrupole. Thickness noise arises from the transverse periodic displacement of the air by the volume of a passing blade element. The amplitude of this noise component is proportional to the blade volume, with frequency characteristics dependent on the shape of the blade cross section (airfoil shape) and rotational speed. Thickness noise can be represented by a monopole source distribution and becomes important at high speeds. Thin blade sections and planform sweep are used to control this noise. Loading noise is a combination of thrust and torque (or lift and drag) components which result from the pressure field that surrounds each blade because of its motion. This pressure disturbance moving in the medium propagates as noise. Loading is an important mechanism at low to moderate speeds. For moderate blade section speed, the thickness and loading sources are linear and act on the blade surfaces. Unsteady sources are time dependent in the rotating-blade frame of reference. They include periodic and random variation of loading on the blades. A typical example of periodic blade loading in propellers is the effect of shaft angle of attack. When the propeller axis is tilted relative to the inflow, each blade sees a cyclic change in local angle of attack. Therefore, the loading on the blade varies during a revolution. The loading change may be once per revolution or several times per revolution, depending on the source of inflow distortion. All inflow distortion which is invariant with time results in blade-loading changes which repeat exactly for every propeller revolution. The resulting periodic unsteady-loading noise occurs at harmonics of

blade-passage frequency. Unsteady loading is an important source in the counterrotating propeller. Although the counterrotating propeller does not contain any additional or unique sources of noise, the aerodynamic interference between the two rotors gives rise to significant levels of unsteady-loading noise which are particularly significant at low flight speeds, such as during takeoff and landing. Aerodynamic interaction is a significant source of noise for low-speed operation. Under certain conditions blade loading which is nearly periodic can occur. An example of this is the ingestion of a vortex, which could be induced by the propeller and attached to the fuselage or to the ground ahead of the propeller. Random sources give rise to broadband noise. For propellers there are two sources which may be important, depending on the propeller design and operating conditions. The first broadband noise source is the interaction of inflow turbulence with the blade leading edges. Because the inflow is turbulent, the resulting noise is random. The importance of this noise source depends on the magnitude of the inflow turbulence, but it can be quite significant under conditions of high turbulence at low speeds. In the second broadband mechanism, noise is generated near the blade trailing edge. A typical propeller develops a turbulent boundary layer over the blade surfaces, which can result in fluctuating blade loading at the trailing edge. The noise is characterized by the boundary-layer properties. A related mechanism occurs at the blade tips, where turbulence in the core of the tip vortex interacts with the trailing edge. As such, propeller noise testing and prediction are active fields of research.

The first successful acoustic theory was developed by Gutin in 1936, when he represented the steady aerodynamic forces on the propeller as a ring of acoustic dipole sources acting at a certain effective radius [17]. Gutin's theory, however, was limited to loading noise for propellers with axial flow, simple geometry, low tip speed, and no forward speed. Since then, there have been significant advances in acoustic theory due to the work of many researchers who have removed these limitations [18-20]. A thorough review of propeller noise prediction methodology, detailing these advances, has been published by multiple authors [21-23].

Noise prediction methods are typically grouped into two categories: frequency-domain methods and time-domain methods. Time-domain methods retain the pressure time history and allow the propeller geometry to be treated with superior precision. However, they require the computation of retarded blade locations and, due to their sensitivity to aerodynamic error, need high-quality aerodynamic data to obtain accurate results.

The physical mechanisms of aerodynamic noise generation in bladed machines are fairly well studied, in particular with the example of fans [24], where it was noted that the noise spectrum of fans consists of broadband noise and tonal components at frequencies that are multiples of the Blade Passing Frequency of the rotor blades (BPF). Various analytical and semi-empirical methods for computation the fan wideband noise take into account physical phenomena such as turbulence at the rotor inlet, turbulent boundary layer on the blades, the influence of the blade outlet edge, the flow in the radial clearance at the rotor periphery, and flow separation on the blades. With the development of computational fluid dynamics, methods have been developed for calculating pressure pulsations in blade machines based on solving RANS equations. In particular, D. Croba et al. proposed a method for computing a non-stationary two-dimensional flow in a centrifugal impeller and a pump volute based on the solution of the averaged Navier-Stokes equations and the k- ϵ turbulence model [25, 26].

Another approach using the Reynolds equations was proposed by S. Chu et al. [27]. Unsteady pressure is obtained by integrating the Reynolds equation, where all terms depending on the velocity field are determined experimentally by the laser-anemometric method.

A similar approach is developed in the work of M.S. Thompson et al. [28], who also use laser anemometry data, but pressure pulsations are calculated by solving equations of the Blokhintsev-Howe type [29] with respect to the stagnation enthalpy.

Currently existing approaches for modeling the noise of blade machines are based mainly on the application of the Lighthill equation [30]. Later, the works of Curle [31], Flowcs-Williams and Hawkings [32] formulated the theoretical basis for the development of methods for calculating

the aerodynamic noise of blade machines based on the so-called aero-acoustic analogy, as well as the application of Kirgoff's theorem [33, 34].

As is known, in blade machines, where the Mach number at the periphery of the rotor is lower than 0.5, the noise is emitted mainly by the type of a dipole source. Aeroacoustics' analogy introduces a certain simplification of the physical processes of noise generation for the purpose of their analytical description. The dipole nature of the radiation is due to pressure forces acting on the rotor and stator blades from the flow. These forces, steady or unsteady, are the cause of the tonal noise of the BPF and its higher harmonics, which is generated by the rotor blades, and also, as a result of the interaction of the rotor - stator, with guide stator blades. The analytical formulation of these processes is based on the formalization proposed, in particular, by Sears [35], and represents the emitted sound in the form of the so-called spiral modes [36, 37, 38].

In connection with the development of the possibilities of using methods of computational fluid dynamics and acoustics, approaches based on the numerical simulation of unsteady flow in blade machines using modern methods of computational fluid dynamics, for example, LES with subsequent determination of acoustic radiation, are gaining wider development [39-41]. In combination with the aeroacoustic analogy, other methods are also being developed, such as, for example, RANS + LEE + SNGR [42], as well as DDES [43] in conjunction with the Lighthill or Ribner equation [44].

The key issue in computational aeroacoustics studies is an adequate source definition. It should also be noted that the Lighthill equation obtained under the assumption of small oscillations in the turbulent flow of a compressible medium, while in the bladed machines pressure pulsations and the generation of emitted sound occur in a wide range of wave numbers when large-scale vortex disturbances decay in a cascade process into a small-scale turbulence [45], and the generation of acoustic waves occurs in this process.

A drawback of most methods, which leads to a significant modeling error of up to 10 dB or more, is associated with an error in solution to the decomposition problem — the separation of the acoustic and vortex (pseudo-sound) modes in the region of the oscillation source.

The method developed bases on decomposition of the velocity vector on a vortex and acoustic mode. This leads to the acoustic-vortex wave equation and boundary conditions with using complex acoustic impedances.

2. Acoustic-Vortex Method

The key issue in computational aeroacoustics studies is an adequate source definition. It should also be noted that the Lighthill equation obtained under the assumption of small oscillations in the turbulent flow of a compressible medium, while in the bladed machines pressure pulsations and the generation of emitted sound occur in a wide range of wave numbers when large-scale vortex disturbances decay in a cascade process into a small-scale turbulence [45], and the generation of acoustic waves occurs in this process.

A drawback of most methods, which leads to a significant modeling error of up to 10 dB or more, is associated with an error in solution to the decomposition problem — the separation of the acoustic and vortex (pseudo-sound) modes in the region of the oscillation source.

The method developed bases on decomposition of the velocity vector on a vortex and acoustic mode. This leads to the acoustic-vortex wave equation and boundary conditions with using complex acoustic impedances.

2.1 Main Equations

The acoustic model describing the isentropic inviscid flow is constructed based on the decomposition proposed by Crow S. [46] and K. Artamonov. [47]. Currently, the acoustic-vortex decomposition method and the acoustic radiation source are analysed. The equations of aeroacoustics are derived in terms of the parameters of the hydrodynamic flow and, as indicated in the works of Doak P. [48] and Goldstein M. [38] cannot be considered as purely

sound. The right-hand sides, or source terms, in these equations describe the generation of perturbations of the flow parameters without distinguishing the acoustic component proper, and the left-hand sides describe the spatiotemporal propagation of wave-type acoustic-vortex perturbations, taking into account convective transport and spatial inhomogeneity of sound speed. The initial equations of aeroacoustics are linearized with respect to their perturbed values.

We represent the velocity as the sum of the velocity of the main flow and the velocity of acoustic motion that leads to the wave equation. The use of decomposition with the representation of enthalpy in the form (angle brackets means that the time average value of the expression enclosed in them is taken, and a stroke indicates its component pulsating relative to the average value), we obtain the equation

$$\frac{1}{c^2} \frac{d^2 h'}{dt^2} - \Delta h' = f \quad (1)$$

With a source member

$$f = \nabla(\mathbf{u} \nabla) \mathbf{u} - (\mathbf{u} \nabla) \nabla \mathbf{u} - \frac{1}{c^2} \frac{d^2 \langle h \rangle}{dt^2} + \Delta \langle h \rangle \quad (2)$$

Such linearization allows one to carry out the Fourier transform of the obtained equations and impedance boundary conditions and formulation of the boundary value problem.

$$\frac{1}{c^2} \left(i\omega + \langle \mathbf{v}_i \rangle \frac{\partial}{\partial x_i} \right) \left(i\omega + \langle \mathbf{v}_j \rangle \frac{\partial}{\partial x_j} \right) h' - \frac{\partial^2 h'}{\partial x_i^2} = \Phi(\omega)(f) \quad (3)$$

$$\Phi(\omega)(f) = \Phi(\omega) \left(\frac{\partial \mathbf{v}_i}{\partial x_k} \frac{\partial \mathbf{v}_k}{\partial x_i} \right) \quad (4)$$

The momentum equation and continuity equation for modeling the vortex mode motion are [49]

$$\frac{\partial \rho \cdot V}{\partial t} + \nabla(\rho \cdot V \times V) = -\nabla P + \nabla(\mu \cdot (\nabla V + (\nabla V)^\tau) \quad (5)$$

$$\frac{\partial \rho}{\partial t} + \nabla(\rho V) = 0 \quad (6)$$

2.2 Boundary Conditions

The boundary conditions of the impedance type are written in terms of perturbations of the flow parameters relative to their average value.

Assuming the flow perturbations in the vicinity of impedance boundary are isentropic then boundary conditions can be represented as follow:

$$\frac{\partial h'}{\partial n} + \left(i\omega + \langle \mathbf{v}_i \rangle \frac{\partial}{\partial x_i} - \frac{\partial \langle \mathbf{v}_i \rangle}{\partial x_k} n_i n_k \right) \left(\frac{\partial p}{\partial h} \right)_s \frac{h'}{\rho c Z} = 0 \quad (7)$$

Non-reflecting condition on the outer boundary of the computational domain

$$\frac{\partial h'}{\partial n} + \left(i\omega + \langle v_i \rangle \frac{\partial}{\partial x_i} - \frac{\partial \langle v_i \rangle}{\partial x_k} n_i n_k + \frac{ic^2}{2\omega} \Delta_n \right) \left(\frac{\partial p}{\partial h} \right)_s \frac{1}{\rho c} h' = 0 \quad (8)$$

3. Validation With Flow Data Around A Cylinder

Another validation task completed for a 3D flow pass a cylinder of 4 mm diameter [50].

Table 1 Cylinder case parameters

Parameter	Unit	Value
Velocity	m/c	20
Diameter	mm	4
Length	mm	400
Re number	-	5300

Using local adaption, the grid size near the cylinder wall reached 0.08 mm. In Fig. 1 there is outlined a comparison of pressure pulsation amplitude on the cylinder surface along the polar coordinate starting from the frontal point. Computation data using ILES are shown by red columns corresponding to symmetrical points on both parts of cylinder wall.

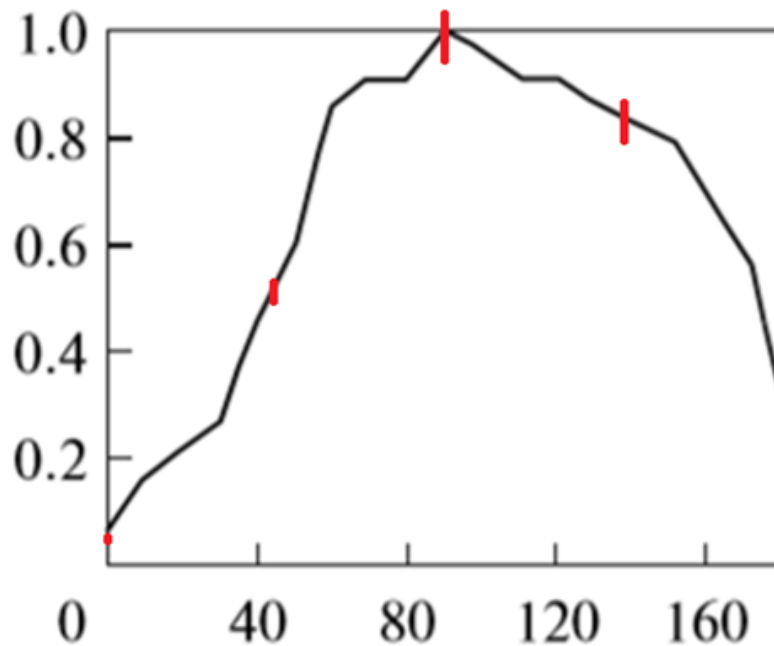


Figure 1. Comparison with [50]

4. Feasibility Study on a Quadcopter Propeller

Feasibility computational study is undertaken of a quadcopter propeller with 70 mm diameter under rotation speed 12,000 RPM. In Fig. 5, b) there is shown the instantaneous velocity field in the rotor plane scaling from zero (blue) to 5 m/s (red). In Fig. 5, a) pressure isolines and the source function are presented. To represent the source spatial structure two iso-surfaces are

introduced for the level $\pm 50,000 \text{ s}^{-2}$. The positive level is marked by red, and negative – by blue color. In the zone of blades, the source function zeroed.

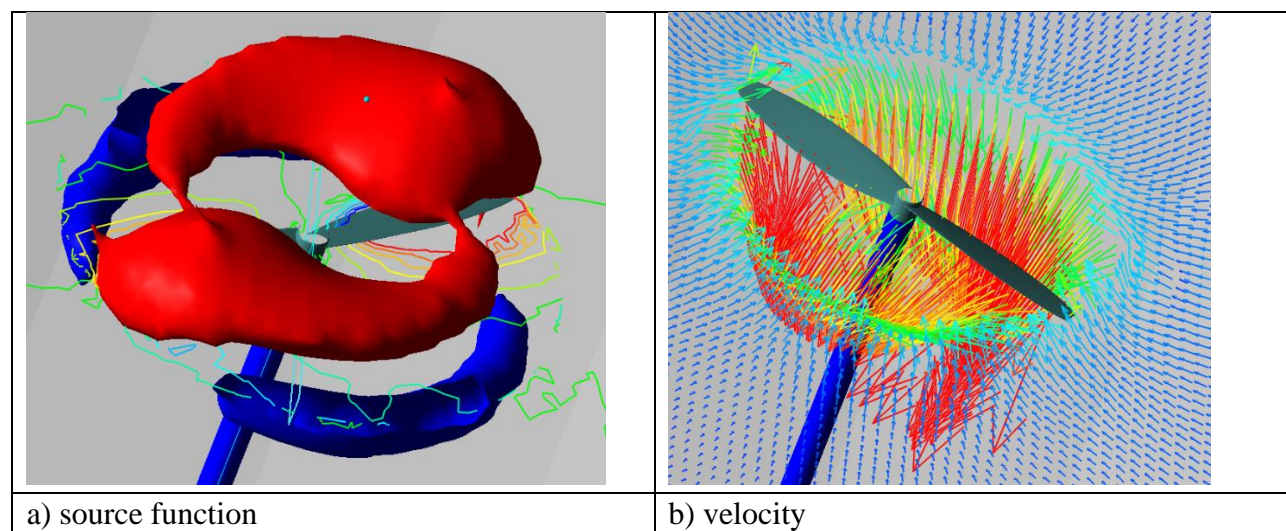


Figure 2. Comparison with [50]

The presented in Fig. 3 acoustic pressure field is determined from the acoustic-vortex wave equation solved by explicit approach using equations (1, 2) for the first BPF harmonic oscillations. Near the rotor domain pseudo-sound perturbations of pressure field accounted from the solution of turbulent flow equations (5, 6).

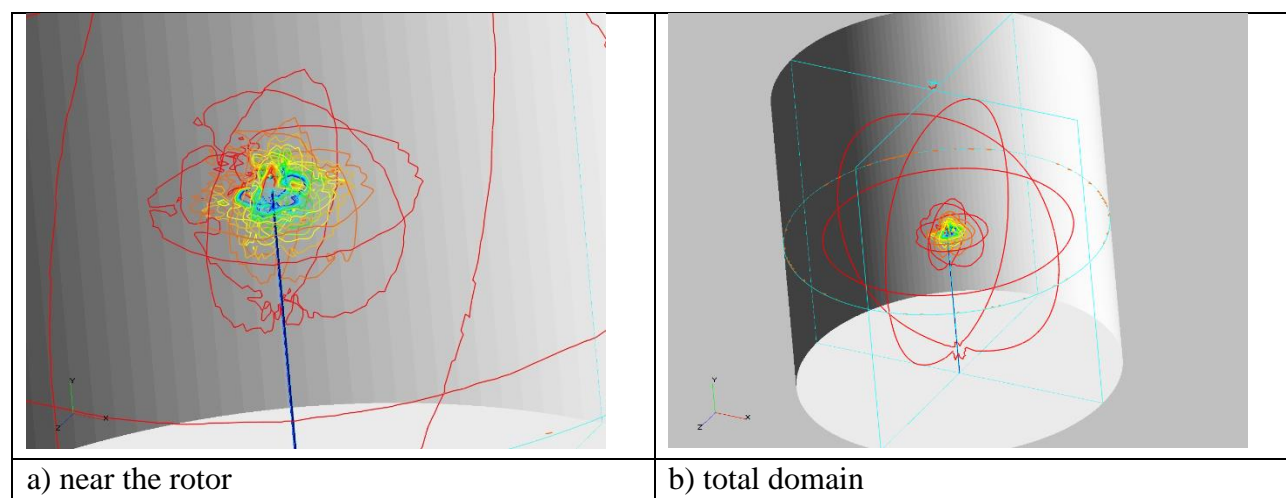


Figure 3. Acoustic pressure field

One can see the effect of non-propagating modes near the propeller (a) and almost spherical waves far away the rotor. A small deflection is made by the propeller “shaft” that has a surface with infinite impedance.

5. Conclusion

CFD-CAA method based on acoustic-vortex decomposition is under development for prediction of quadcopter propeller acoustic field. It gives the explicit and infinite approaches for resolving emitted noise accounting boundary conditions with using the complex acoustic

impedance. Validation and verification work is ongoing for the case of turbulent flow pass a cylinder and BPF noise of a single propeller.

References

- Jones, A and McKenna T (2010) *A new method for statistical analysis: the two part reverse interrogation of sparse data* Jnl Reverse Statistics 55(2), 65-219
- [1] "ABCNews: Whining drones bringing burritos and coffee are bitterly dividing Canberra residents." <https://www.abc.net.au/news/2018-11-09/noise-from-drone-delivery-service-divides-canberra-residents/10484044>. Accessed: 11-03-2019.
- [2] "BBC News: Why your pizza may never be delivered by drone." <https://www.bbc.com/news/business-46483178>. Accessed: 11-03-2019.
- [3] Moshkov P.A., Samokhin V.F., Yakovlev A.A. Selection of an audibility criterion for propeller driven unmanned aerial vehicle // Russian Aeronautics. 2018. Vol. 61. No. 2. pp. 149-155. DOI: 10.3103/S1068799818020010
- [4] Moshkov P., Ostrikov N., Samokhin V., Valiev A. Study of Ptero-G0 UAV Noise with Level Flight Conditions // 25th AIAA/CEAS Aeroacoustics Conference. 2019. AIAA Paper No. 2019-2514. <https://doi.org/10.2514/6.2019-2514>
- [5] N. Kloet, S. Watkins, and R. Clothier, "Acoustic signature measurement of small multi-rotor unmanned aircraft systems," *International Journal of Micro Air Vehicles*, vol. 9, pp. 3–14, Feb. 2017.
- [6] Abhishek Kumar Sahai "Consideration of aircraft noise annoyance during conceptual aircraft design" (PhD thesis) June 2016 <http://publications.rwth-aachen.de/record/668901>. Accessed: 27-02-2020.
- [7] C. E. Tinney and J. Sirohi, "Multirotor Drone Noise at Static Thrust," *AIAA Journal*, vol. 56, pp. 2816–2826, July 2018
- [8] N. Intaratep, W. N. Alexander, W. J. Devenport, S. M. Grace, and A. Dropkin, "Experimental Study of Quadcopter Acoustics and Performance at Static Thrust Conditions," 22nd AIAA/CEAS Aeroacoustics Conference, June 2016
- [9] Giorgia Sinibaldi, Luca Marino, "Experimental analysis on the noise of propellers for small UAV," *Applied Acoustics* Volume 74, Issue 1, January 2013, Pages 79-88
- [10] Peterson, R., "Regional Turboprop Resurgence Continues; Jet Demand Shifts Upward," *Aircraft Engineering and Aerospace Technology*, Vol. 80, No. 2, 2004. doi:10.1108/aeat.2008.12780baf.008
- [11] Ryerson, M. S., and Hansen, M., "The Potential of Turboprops for Reducing Aviation Fuel Consumption," *Transportation Research Part D: Transport and Environment*, Vol. 15, No. 6, 2010, pp. 305–314. doi:10.1016/j.trd.2010.03.003
- [12] Holsclaw, C., "Stage 5 Airplane Noise Standards," *Federal Aviation Administration, Federal Register*, Vol. 81, No. 1923, Washington, D.C., Jan. 2016.
- [13] Franssen, E., Van Wichen, C., Nagelkerke, N., and Lebre, E., "Aircraft Noise Around a Large International Airport and Its Impact on General Health and Medication Use," *Occupational and Environmental Medicine*, Vol. 61, No. 5, 2004, pp. 405–413.
- [14] Swift, H., "A Review of the Literature Related to Potential Health Effects of Aircraft Noise," Partnership for Air Transportation Noise and Emissions Reduction, Massachusetts Inst. of Technology PARTNERCOE-2010-003, Cambridge, MA, July 2010.
- [15] Ivan Djurek, Antonio Petosic, Sanja Grubesa and Mia Suhanek "Analysis of a Quadcopter's Acoustic Signature in Different Flight Regimes" *IEEE Access* Volume 8 2020, pp. 10662-10670
- [16] Magliozzi, B., Hanson, D. B., and Amiet, R. K., "Propeller and Propfan Noise," *Aeroacoustics of Flight Vehicles: Theory and Practice*, edited by H. H. Hubbard, Vol. 1, NASA Reference Publ. 1258, Hampton, VA, 1991, pp. 1–64.
- [17] Gutin, L., "On the Sound Field of a Rotating Propeller," *NACA TM-1195*, Oct. 1948.
- [18] Deming, A. F., "Noise from Propellers with Symmetrical Sections at Zero Blade Angle II," *NACA TN-679*, Dec. 1938.

- [19] Hanson, D. B., "Helicoidal Surface Theory for Harmonic Noise of Propellers in the Far Field," *AIAA Journal*, Vol. 18, No. 10, 1980, pp. 1213–1220. doi:10.2514/3.50873
- [20] Hanson, D. B., "Sound from a Propeller at Angle of Attack: A New Theoretical Viewpoint," *Proceedings: Mathematical and Physical Sciences*, Vol. 449, No. 1936, 1995, pp. 315–328.
- [21] Morfey, C. L., "Rotating Blades and Aerodynamic Sound," *Journal of Sound and Vibration*, Vol. 28, No. 3, 1973, pp. 587–617. doi:10.1016/S0022-460X(73)80041-0
- [22] Magliozzi, B., Metzger, F. B., Baush, W., and King, R. J., "A Comprehensive Review of Helicopter Noise Literature," *Federal Aviation Administration Rept. FAA-RD-75-79*, June 1975.
- [23] Farassat, F., and Succi, G. P., "A Review of Propeller Discrete Frequency Noise Prediction Technology with Emphasis on Two Current Methods for Time Domain Calculations," *Journal of Sound and Vibration*, Vol. 71, No. 3, 1980, pp. 399–419. doi:10.1016/0022-460X(80)90422-8
- [24] A. Guédel *Acoustique des ventilateurs*. CETIAT. PYC LIVRES, 1999
- [25] D. Croba, J.L. Kueny. Unsteady flow computation in a centrifugal pump coupling of the impeller and the volute. Fan Noise. An International INCE Symposium. Senlis (France). Proceedings, 1992.
- [26] D. Croba, J.L. Kueny, F. Hureau, J. Kermarec. Numerical and experimental unsteady flow analysis in centrifugal pumps. Impeller and volute interaction. Pump noise and vibrations. 1st International Symposium, Clamart (France), 1993.
- [27] S. Chu, R. Dong, J. Katz. The effect of blade-tongue interactions on the flow structure, pressure fluctuations and noise within a centrifugal pump. Pump noise and vibrations. 1st International Symposium, Clamart (France), 1993.
- [28] M.C. Thompson, K. Hourigan, A.N. Stokes. Prediction of the noise generation in a centrifugal fan by solution of the acoustic wave equation. Fan Noise. An International INCE Symposium. Senlis (France). Proceedings, 1992.
- [29] Howe M. S. Contribution to the theory of aerodynamic sound, with application to excess jet noise and the theory of the flute // *J. Fluid Mech.*— 1975.— 71, № 4.— P. 625–673.
- [30] M.J. Lighthill 1952 *Proceedings of the Royal Society, London A* 211, 564-587. On sound generated aerodynamically. Part I. General Theory
- [31] N. Curle The influence of solid boundaries upon aerodynamic sound. *Proc. Royal Soc. A* 231, p.505-514, 1955
- [32] Fowcs Williams, J. E., and Hawkings, D. L., "Sound Generation by Turbulence and Surfaces in Arbitrary Motion," *Philosophical Transactions of the Royal Society of London, Series A: Mathematical and Physical Sciences*, Vol. 264, No. 1151, 1969, pp. 321–342. doi:10.1098/rsta.1969.0031
- [33] F. Farassat and M.K. Myers 1988 *Journal of Sound and Vibration* 123, 451-461. Extension of Kirchhoff's formula to radiation from moving surfaces.
- [34] W.-S. Choi et al. / *International Journal of Naval Architecture and Ocean Engineering* 8 (2016) 235-242.
- [35] W.R. Sears some aspects of non-stationary airfoil theory and its practical application. *Journal of the aeronautical sciences*, vol. 8 (3), 1941
- [36] H. Atassi, G. Hamad Sound generated in a cascade by three-dimensional disturbances convected in a subsonic flow. Report NASA AIAA-81-2046, 1981
- [37] J.M. Tyler, T.G. Sofrin Axial flow compressor noise studies. *SAE Trans.*, Vol.70, 1962, pp. 309-332
- [38] Goldstein M.E. *Aeroacoustics: Transl. from English*. M.: Mechanical Engineering, 1981, 295 p.
- [39] S. Caro, S. Moreau Comparaison d'une technique 2D de type Sears avec un calcul instationnaire direct pour le calcul du bruit de raies d'un ventilateur. Bruit des ventilateurs à basse vitesse. Actes du colloque tenu à l'Ecole Centrale de Lyon les 8 et 9 novembre 2001

- [40] S. Caro, R. Sandboge, J. Iyer, Y. Nishio Presentation of a CAA formulation based on Lighthill's analogy for fan noise. Proceedings of 3rd International symposium on Fan Noise 2007, , Lyon, France, 19-21 September, 2007
- [41] Robert Sandboge, Karl Washburn and Chris Peak Validation of a CAA Formulation Based on Lighthill's Analogy for a Cooling Fan and Mower Blade Noise. Proceedings of 3rd International symposium on Fan Noise 2007, Lyon, France, 19-21 September, 2007
- [42] Zhu Y.J., Ou Y.H., Tian J. Experimental and Numerical Investigation on Noise of Rotor Blade Passing Outlet Grille. NCEJ 2008
- [43] De Reboul Silouane, Zerbib Nicolas, Heather Andrew Use OpenFOAM coupled with Finite and Boundary Element Formulations for Computational Aero-Acoustics for Ducted Obstacles. Inter Noise 2019
- [44] Ribner, H.S., The Generation of Sound by Turbulent Jets, Advances in Applied Mechanics, 1964, Volume 8, pages 103-182.
- [45] Колмогоров А.Н. Уравнения турбулентного движения несжимаемой жидкости. Изв. АН СССР, сер. физ., 6, №1-2, 56-58, 192.
- [46] Crow S.C. Aerodynamic Sound Emission as a Singular Perturbation Problem.- Studies in Applied Mathematics, 1970, vol. XLIX, No.1
- [47] Artamonov K.I. Thermohydroacoustic Stability. M.: Mechanical Engineering, 1982, 261 p. [in Russian]
- [48] Doak P. E. Fluctuating total enthalpy as the basic generalized acoustic field // Theor. Comp. Fluid Dyn.— 10.— 1998.— P. 115–133.
- [49] "FlowVision. User's guide". Version 3.10.02.
- [50] L. A. Bazhenova and A. G. Semenov Nature of the Source of Vortex Sound Flowing Around a Cylindrical Profile Acoustical Physics, 2014, Vol. 60, No. 6, pp. 678–686. © Pleiades Publishing, Ltd., 2014. Original Russian Text © L.A. Bazhenova, A.G. Semenov, 2014, published in Akusticheskii Zhurnal, 2014, Vol. 60, No. 6, pp. 645–655.



QUIET DRONES
International e-Symposium
on
UAV/UAS Noise
Remote from Paris – 19th to 21st October 2020

Drone Noise, A New Public Health Challenge?

**Antonio J Torija Martinez: A.J.TorijaMartinez@salford.ac.uk
Acoustics Research Centre, University of Salford, Manchester, UK**

Summary

There is a rapidly growing interest in manned and unmanned aerial vehicles of different size from small multi-rotor drones to Urban Air Mobility (UAM) vehicles. With the projected expansion of the sector, for a variety of applications from parcel delivery to transportation of people, it is very likely that urban and rural soundscapes will be altered by drone noise. This can lead to a significant source of community noise annoyance. This is the reason why it is widely accepted that noise is one of the largest limiting factors for public acceptance and adoption of drone technology. Unquestionable, if not tackled appropriately, the noise generated by drone operations might lead to significant tension with exposed communities. This paper aims to introduce the important uncertainty as to how communities will react to a new source of noise. Compared to conventional aircraft, drones generate an unconventional noise signature to which people are completely unfamiliar. Although with important broadband contributions, drone noise is highly tonal and has irritating frequency and amplitude modulations due to varying rotors rotational speeds. They will also flight closer to people and in a bigger number. An important factor to consider is that new communities, not currently affected by aircraft noise, will most likely be affected. Moreover, an overview on challenges and research gaps on noise effects of drones is provided:

- (1) It is uncertain whether the current evidence of health effects of aircraft noise will be of application. If not, new evidence will need to be gathered as to health effects of drone noise.
- (2) There are neither metrics able to account for the particular characteristics of drone noise nor information about acceptable levels.
- (3) There is no understanding on how the deployment of drones will affect the perception of current urban and rural soundscapes.

(4) Community annoyance will be different depending on context, e.g. drone delivering medicines to remote areas vs. drone delivering parcels to your neighbours

(5) For planning purposes, exposure-response functions for drone noise will need to be derived. This introduces the challenge of how to predict long-term effects.

1. Drones: A New Source of Noise

Most drone designs are markedly different from conventional aircraft. The different types and strengths of noise sources in drones compared to fixed wing aircraft and helicopters lead to significantly different noise signatures. Further, the sound produced by drones does not resemble qualitatively the sound generated by contemporary aircraft (Christian and Cabell, 2017).

Cabell et al. (2016) provide a comprehensive description of the basic spectral characteristics of the sound pressure level of a series of small multi-copters. As described by these authors, the sound of small multi-copters is characterised by the presence of multiple complex tones at harmonics of the blade passage frequency (of each rotor). Also, in multi-copter spectra there are significant sound levels at higher harmonics of the blade passage frequency, which seems to be caused by interaction noise from disturbed inflow due to other rotor blades or the fuselage (Magliozzi et al., 1991).

Figure 1 shows typical frequency spectra of an aircraft and a small quadcopter flyover, and a car pass-by. As shown in Figure 1, a typical fixed wing aircraft have a prominent tone at the blade passing frequency (at about 1 kHz in the example shown), with some harmonics at higher frequencies, and a substantial decay in high frequency content due to atmospheric absorption. Compared to a conventional fixed wing aircraft, the frequency spectrum of a small quadcopter contains a significant content in complex tones in the mid-to-high frequency region (between 400 Hz and 1 kHz in the example shown), and high sound level in the high frequency region that might be due to the electric motors (Cabell et al., 2016). This is in agreement with Whelchel et al. (2020) stating that noise of drone propellers is dominated by tonal noise at lower frequencies and broadband noise at higher frequencies. Alexander and Whelchel (2019) also suggested that the important mid-frequency broadband noise might be due to trailing edge noise from outer portions of the rotor diameter.

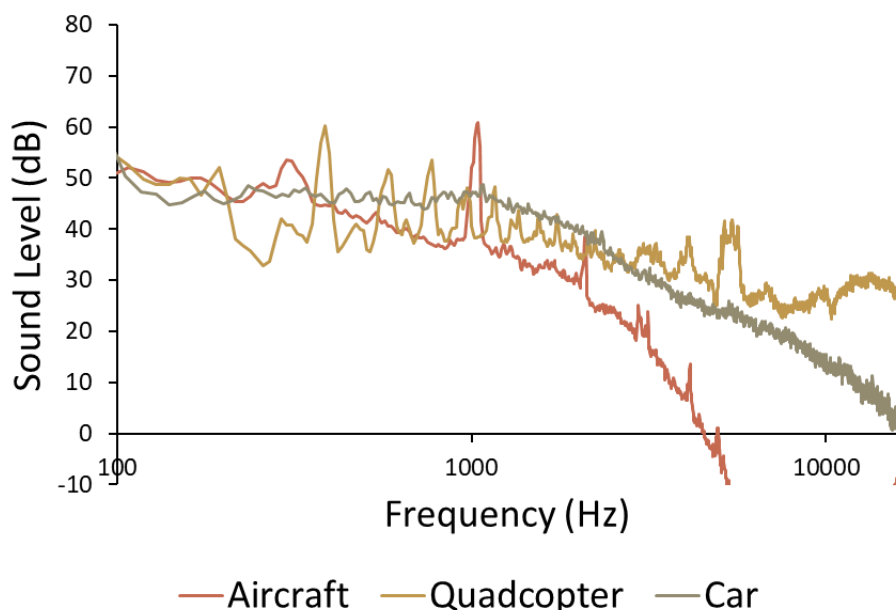


Figure 1. Typical frequency spectrum of an aircraft and a small quadcopter flyover, and a car pass-by, normalised to a L_{Aeq} of 65 dB(A)

Drones have specific noise features that lead to a significant uncertainty in the prediction of the resultant annoyance. For instance, the small tip-to-tip spacing between counter rotating propellers results in a significant source of noise due to blade interaction effects (Alexander et al., 2019; McKay et al., 2019; Torija et al., 2019). Moreover, ambient weather conditions have been found to have a significant impact on sound levels and character of drone noise (Alexander et al., 2019). As shown in Figure 2, tones below 1 kHz significantly differ between static hover and drone hovering outdoors due to varying rotor rotational speeds to maintain vehicle stability. Under typical outdoor conditions, rotors spin at different RPMs to compensate wind influence and ensure the stability of the vehicle. This leads to the maximum amplitudes of the tonal components to become weaker, but also to an increase in the number of tonal components (Alexander and Whelchel, 2019, Torija et al., 2019).

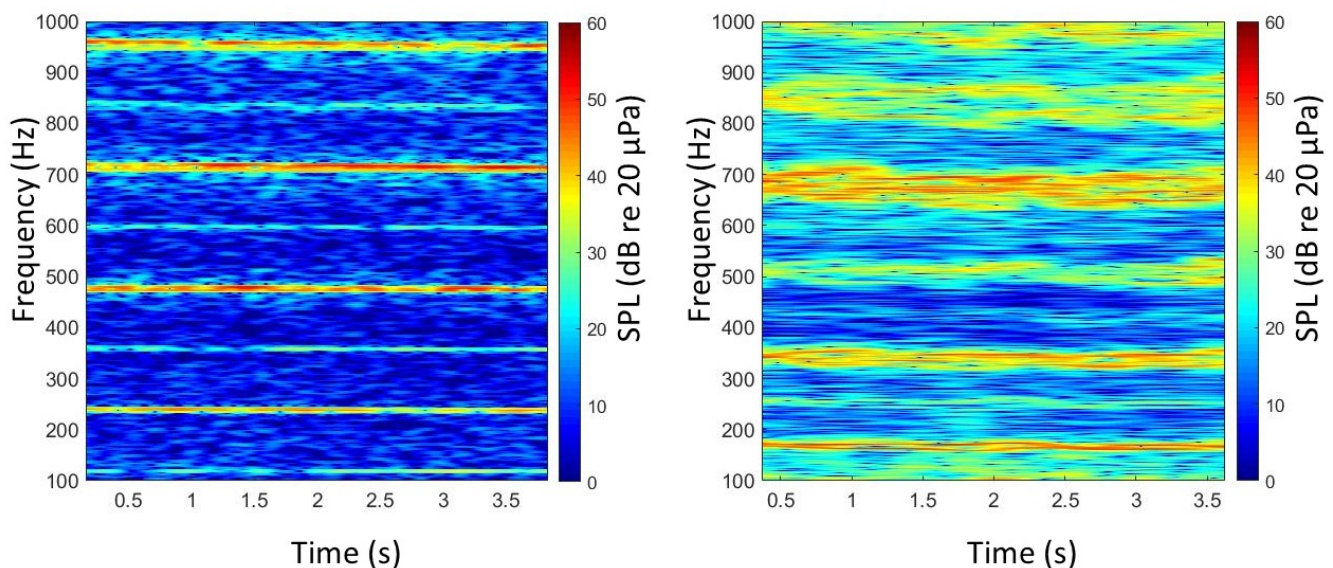


Figure 2. Spectrogram of a quadcopter hover measured in confined anechoic (left) and open environment (right) (Torija et al., 2019)

2. Is the Current Evidence of Health Effects of Aircraft Noise of Application to Drone Noise?

Aircraft noise is one of the most adverse environmental effects of aviation. There is substantial evidence of a strong relation between aircraft noise and annoyance (Basner et al., 2017). Based on current state of scientific knowledge, Basner et al. (2017) also found that there is sufficient evidence for marked negative effects of aircraft noise exposure in terms of cognitive impairment in children and sleep disturbance; and also that “*there is a good biological plausibility by which noise may affect health.*” In a recent paper, Clark et al. (2020) state that “*there is low quality evidence for a harmful effect of road traffic noise, aircraft noise, and railway noise on some cancer outcomes.*” The World Health Organization (WHO) suggest good evidence in the relation between aircraft noise and cardiovascular disease, sleep disturbance, annoyance and cognitive impairment. The WHO guidelines for protecting human health from exposure to aircraft noise:

- strongly recommends avoid exposure to more than 45 dB L_{den} , as “*this level is associated with adverse health effects,*” and

- Strongly recommends avoid night-time exposure to more than 40 dB L_{night} , as “*this level is associated with adverse effects on sleep*” (WHO, 2018).

Compared to conventional fixed wing aircraft and rotorcraft, small drones are expected to be quieter (Theodore, 2018). However, with the significant business opportunities, the expectation is that a substantial number of drones might inundate the skies of cities across the globe. Just in the UK, PWC¹ estimate that by 2030 there will be 76.233 drones flying in operation (Heathrow airport in London has 1,303 daily average flights). Further, drones will fly at relatively low altitudes over populated areas that have not normally been exposed to aircraft noise. With drones operating at low flight levels, and therefore a reduced atmospheric absorption, high frequency noise is likely to be an important factor for annoyance. Regarding UAM vehicles, increasing size will mean an increase in loudness. Notwithstanding the uncertainty about specific designs, it is expected that the sound generated by UAM vehicles, with dominance of complex tones, will be of similar character of drone sounds.

It is well known that non-acoustic factors such as fear, perceived control, trust in authorities and previous experience with or future expectations regarding noise have a strong contribution to individual annoyance reactions (Basner, et al., 2017; Sparrow et al., 2019). For the specific case of drones, a recent report² suggests safety, privacy and security, in addition to noise and visual pollution, as the main concerns with regards to the used of drones. Sparrow et al. (2019) conclude that “*There is preliminary evidence that the public may be concerned with these new noise sources intended for transportation and package delivery.*” For all the above, it seems unlikely that the current evidence of health effects of aircraft noise can be of application to drone noise. Further research is needed to understand the effects of this new source of noise on public health and wellbeing.

3. What are the Metrics and Acceptable Levels for Drone Noise?

Hitherto, there is no regulation establishing the necessary noise metrics for the certification and regulatory frameworks for the industry and governing bodies. A recent publication (Senzig and Marsan, 2018) suggests that current noise certification methods for fixed- and rotary-wing aircraft may not be suitable for certifying Unmanned Aerial Vehicles (UAVs). These authors also describe the main limitations of noise metrics to account for the specific characteristics of UAVs. For instance, current aircraft noise metrics assume a relatively constant noise source, and therefore might not be able to account for the perceptual effect of unstable noise (due to vehicle control system) during typical UAV manoeuvring operations. Torija et al. (2019a), found that the current metric for aircraft noise certification, i.e. Effective Perceived Noise Level (EPNL), is not able to account for the subjective response to aircraft noise with high number of tonal components evenly distributed along the frequency spectra.

Christian and Cabell (2017) investigated the performance of four noise metrics to account for the noise annoyance due to a series of UAVs and road vehicles: A-weighted Sound Exposure Level (SEL_A), C-weighted Sound Exposure Level (SEL_C), EPNL, and Loudness exceeded 5% of the time (L_5). They found that none of the four metrics tested was able to capture the subjective difference between the UAV and road vehicle sounds. This is in line with a research carried out by Torija et al. (2020) to investigate the noise perception of a hovering UAV in a series of urban scenarios. These authors found the participants’ responses on perceived annoyance highly influenced by acoustics factors particularly characteristic of small quadcopter noise or non-acoustic factors such as visual scene and expectation. Christian and Cabell (2017) suggest that a loitering correction (accounting for the time of exposure to UAV noise) and the addition of psychoacoustic measures as tonality can lead to a better performance in predicting noise annoyance of UAVs. However, qualitative characteristics of UAV sounds might also be relevant

¹ <https://www.pwc.co.uk/intelligent-digital/drones/Drones-impact-on-the-UK-economy-FINAL.pdf>

² <https://media.nesta.org.uk/documents/Flying-High-full-report-and-appendices.pdf>

for understanding the intrinsic annoyance of these vehicles, and also the perceptual differences with traditional transportation noise sources.

The European Commission has issued the Implementing Regulation (EU) 2019/945 “to provide citizens with high level of environmental protection, it is necessary to limit the noise emissions to the greatest possible extent.” The Annex Part 15 to this document states a maximum allowable sound power level of 85 dB for UAVs in the ‘open’ category. However, the sound power level is unable to account for all the typical acoustic features of UAVs (e.g. tonality, high frequency noise, etc) and the proposed maximum value does not seem related to public reaction. Therefore, more research is required to understand and predict the perception of UAV noise. Building upon this research, metrics optimised to UAV noise can be developed and acceptable levels can be proposed.

4. What will be the Influence of Drone Operations on Soundscape Perception?

Torija et al. (2020) investigated the effects of a hovering small quadcopter on the perception of a series of urban soundscapes. They found that in soundscapes with reduced road traffic noise, the participants taking part in their study reported a significantly higher perceived loudness and annoyance than in soundscapes highly impacted by road traffic noise, although the sound level of the quadcopter was held constant at 65 dBA across all scenarios. These results suggest that *“the concentration of drone operations along flight paths through busy roads might aid in the mitigation of the overall community noise impact caused by drones.”* However, these results also suggest that *as traffic varies over the day there will be times with low traffic volume when local residents experience the loudness and annoyance of drones much more”* (Eißfeldt, 2020). Torija et al. (2020) found that the reported annoyance with UAV noise is up to 6.4 times higher than without UAV noise, in locations with low road traffic volumes.

Therefore, public acceptance of drone operations will be primarily driven by the characteristics of the local soundscape, and the expectations of exposed communities. In other words, the noise impact generated by drones will be a function of the change in acoustic experience over the typical ambient sound at a particular time of day. Uber will consider background noise to plan routes and skyport locations, so Uber Air operations do not increase the ambient equivalent continuous sound level (L_{Aeq}) by more than 1.5 dBA³.

Further research is required to simulate different manoeuvring operations of drones in realistic audio-visual scenes (i.e. ecologically valid perceptual stimuli) to understand how the public will react to the introduction of these novel vehicles in their local soundscape. This research will aid regulators to define operating requirements for drones based on annoyance and acceptance.

5. How can Long-Term Effects of Drone Noise be Predicted?

The effects of transportation noise on individuals or a population is traditionally assessed using noise exposure-response relationships. These are empirically derived functions relating exposure metrics (e.g. Day-Night Level – DNL) and effects of noise exposure (e.g. percentage of highly annoyed persons). Well-established exposure-response relationships for transportation noise and annoyance (e.g. Miedema and Vos, 1998) have provided evidence for the development of noise regulation⁴ and definition of recommended noise exposure levels⁵. Exposure-response relationships have been derived for a series of auditory and non-auditory effects of noise on health (Basner et al., 2014).

³ <https://evtol.com/news/uber-elevate-community-engagement/>

⁴ <https://eur-lex.europa.eu/legal-content/EN/TXT/PDF/?uri=CELEX:32002L0049&from=EN>

⁵ https://www.euro.who.int/_data/assets/pdf_file/0008/383921/noise-guidelines-eng.pdf

As said above, it is highly unlikely that there will be enough evidence to derive exposure-response relationships for drone noise before wider communities are actually exposed to the noise of these vehicles. There have been some laboratory studies comparing noise perception of UAVs and other conventional transportation vehicles (Christian and Cabell, 2017; Torija et al., 2020). However, it is uncertain whether the findings of laboratory studies could be extrapolated to real scenarios. An alternative approach could be to apply ‘annoyance bonus’ or ‘annoyance penalties’, observed at laboratory when comparing drone noise with other sources of transportation noise, to standard transportation noise exposure relationships, in order to derive exposure-response functions for drones. However, still these derived drone noise exposure-response functions will need to be validated with field studies.

Therefore, innovative approaches are needed to derive exposure-response functions aiding regulators with the prediction of long-term exposure to drone noise.

6. Conclusions

This paper introduces and discusses the main challenges and research gaps on noise effects of drones. The paper outlines the main noise characteristics of drones, and states the need for further research to

- i. understand the effects of drone noise on public health and wellbeing,
- ii. develop metrics to assess community noise impact of drones,
- iii. define acceptable levels for drone noise,
- iv. inform best operational practices for drones with regard to noise profiles, and
- v. innovate in the approaches to predict long-term noise effects when drones operate at scale.

Bringing these research gaps is crucial to appropriately tackle noise issues associated with drones, and therefore protect quality of life and health of exposed communities.

References

- Alexander, W.N., and Whelchel, J., 2019, “Flyover Noise of Multi-Rotor sUAS.” In Proceedings of InterNoise 2019, Madrid, Spain.
- Alexander, W.N., Whelchel, J., Intaratep, N., and Trani, A. 2019. “Predicting community noise of sUAS.” In: Proceedings of 25th AIAA/CEAS Aeroacoustics Conference (AIAA 2019-2686). Delft, The Netherlands.
- Basner, M., Babisch, W., Davis, A., Brink, M., Clark, C., Janssen, S., Stansfeld, S. 2014. “Auditory and non-auditory effects of noise on health.” *Lancet*, 383(9925): 1325–1332.
- Basner, M., Clark, C., Hansell, A., Hileman, J.I., Janssen, S., Shepherd, K., Sparrow, V. 2017. “Aviation noise impacts: State of the science.” *Noise Health*, 19(87), 41-50.
- Cabell, R., Grosveld, F., and McSwain, R. 2016. “Measured noise from small unmanned aerial vehicles.” In: Proceedings of NOISE-CON 2016, Vol. 252, Institute of Noise Control Engineering, Providence, RI, USA.
- Christian, A. and Cabell, R. 2017. “Initial investigation into the psychoacoustic properties of small unmanned aerial system noise.” In: Proceedings of the 17th AIAA Aviation Technology, Integration, and Operations Conference (AVIATION 2017), Denver, CO, USA.
- Clark, C., Crumpler, C., Notley, H. 2020. “Evidence for environmental noise effects on health for the United Kingdom policy context: A systematic review of the effects of environmental noise on mental health, wellbeing, quality of life, cancer, dementia, birth, reproductive outcomes, and cognition.” *International Journal of Environmental Research and Public Health*, 17(2), 393.

- Eißfeldt, H. 2020. "Sustainable Urban Air Mobility supported with participatory noise sensing." *Sustainability*, 12(8), 3320.
- Magliozzi, B., Hanson, D.B., and Amiet, R.K. Propeller and propfan noise. In Harvey H. Hubbard, editor, *Aeroacoustics of Flight Vehicles: Theory and Practice: Volume 1: Noise Sources*, number NASA RP-1258, pages 1–64, 1991.
- McKay, R.S., Kingan, M.J., and Go, R. 2019. "Experimental investigation of contra-rotating multi-rotor UAV propeller noise." In: *Proceedings of Acoustics 2019*, Cape Schanck, Victoria, Australia.
- Miedema, H.M.E., and Vos, H. 1998. "Exposure-response relationships for transportation noise." *Journal of the Acoustical Society of America*, 104, 3432.
- Senzig, D.A., and Marsan M. 2018. "UAS Noise Certification," In *proceedings of Inter-Noise 2018*, paper in18_1855, Chicago, United States.
- Sparrow, V., Gjestland, T., Guski, R., Richard, I., Basner, M. et al. *Aviation Noise Impacts White Paper*. In: *ICAO 2019 Environment report Chapter 2 Aircraft noise 2019*.
- Theodore, C.R. 2018. "A summary of the NASA Design Environment for Novel Vertical Lift Vehicles (DELIVER) project." In: *Proceedings of the AHS International Technical Conference on Aeromechanics Design for Transformative Vertical Flight*, San Francisco, CA, USA.
- Torija, A.J., Roberts, S., Woodward, R., Flindell, I.H., McKenzie, A.R., and Self, R.H. 2019a. "On the assessment of subjective response to tonal content of contemporary aircraft noise." *Applied Acoustics*, 146, 190-203.
- Torija, A.J., Self, R.H., and Lawrence, J.L.T. 2019b. "Psychoacoustic characterisation of a small fixed-pitch quadcopter." In: *Proceedings of InterNoise 2019*, Madrid, Spain.
- Torija, A.J., Li, Zhengguang, Self, R.H. 2020. "Effects of a hovering unmanned aerial vehicle on urban soundscapes perception." *Transportation Research Part D: Transport and Environment*, 78, 102195.
- World Health Organization. *Environmental Noise Guidelines for the European Region*. WHO Regional office for Europe, Copenhagen. 2018
- Whelchel, J., Alexander, W.N., and Intaratep, N. 2020. "Propeller noise in confined anechoic and open environments." In: *Proceedings of AIAA Scitech 2020 Forum*, Orlando, FL, USA.



QUIET DRONES
International Symposium
on
UAV/UAS Noise
Remote from Paris – 19th to 21st October 2020

Achieving quiet flying passenger vehicles through numerical simulations, a LBM story

Dr. Wouter van der Velden, Gianluca Romani and Prof. Dr. Damiano Casalino
Dassault Systemes Deutschland GmbH, Meitnerstraße 8, 70563, Stuttgart, Germany
wouter.vandervelden@3ds.com

Summary

This paper describes multiple, fully automated, computational workflows for the evaluation of the acoustic environmental impact of vertical take-off and landing vehicles. Different scenarios are considered: (i) an isolated rotor for rotor performance studies, (ii) an isolated full vehicle undertaking quasi-static flow conditions, (iii) a vehicle hovering over an urban area, and (iv) an operational scenario of a vehicle undertaking an approach maneuver over a flat terrain. The aerodynamic performance and aeroacoustic sources are predicted by using the high-fidelity CFD solver SIMULIA PowerFLOW™ based on the Lattice-Boltzmann/Very-Large-Eddy-Simulation method. The acoustic propagation is computed using acoustic analogy formulations applied to the near-field flow field, with the exception of the urban scenario, for which the noise is extracted directly from the CFD simulation performed in a domain encompassing both the vehicle and the nearby urban city block. In this scenario, the effects of sound scattering due to the presence of several buildings is analyzed by comparing the noise levels on the surface of the buildings with those extracted on the same surface from another solution performed without buildings. Additionally, an integral approach based on the Ffowcs-Williams and Hawkings analogy is used to compute the noise on a hemisphere centered around the rotor and/or vehicle. This is used to compute the on-ground noise footprint for a prescribed, trimmed, flight trajectory path.

1. Introduction

As populations in megacities continue to grow, the existing traffic situation will become increasingly demanding. Millions of hours are wasted on the road worldwide, resulting in personal

and business related losses (Hoehner et al. 2012). The combined usage of Air Taxi Vehicle (ATV), Personal Air Vehicles (PAV) and delivery drones for small-size packages has the potential to radically improve commuters' mobility, with a positive impact on society, quality of life and environment. Therefore, the development of Urban Air Mobility (UAM) concepts, from vehicle design to traffic management, is attracting the interest of several stakeholders, like aircraft and car manufactures, regulators and agencies, research institutions and academia. The rapid growth of this topic in terms of industrial investments, research & development efforts and media coverage is usually referred to as the 3rd Aerospace Revolution. Many challenges need to be overcome in the following areas: (i) vehicle, e.g. battery endurance and propulsion efficiency, noise and safety, (ii) manufacturing, e.g. series production of composite structures with aerospace quality standards, (iii) operation, e.g. a specific Air Traffic Management (ATM) system able to manage both manned/unmanned and guided/autonomous vehicles, (iv) regulations, e.g. in connection with certification, operation and safety, (v) life-cycle management and maintenance and (vi) recycling.

From a vehicle design and prototyping point of view, many concepts have been already proposed by several companies and institutions, and they have the following common characteristics: (i) electrically propelled Vertical Take-Off and Landing (eVTOL) vehicles, (ii) with distributed propulsion consisting in lifting and thrusting rotors, (iii) with lifting surfaces to reduce the usage of batteries during cruise and (iv) cover a target distance of 60 miles. The two main engineering challenges can be easily defined, braking them down into (i) efficient usage of batteries for long flight range and (ii) low-noise operation in urban areas and ground proximity.

The design and optimization of eVTOL vehicles is strictly connected with the aero-mechanical behavior of the vehicle. More specifically, due to the strong connection between the maneuver and on-ground perceived noise, and between installed power and trajectories, the dynamic trim of the vehicle is a key element of any design and optimization process. The mission of Dassault Systemes (3DS) in the emerging UAM field is to develop virtual prototyping methods and software that allow to tackle all the engineering challenges in the 3DEXPERIENCE platform, including the dynamic trim of the vehicle. The present paper is specifically focused on the low-noise operation in urban areas and ground proximity challenge.

The optimization of take-off and landing procedures of an eVTOL vehicle is a difficult and interesting task due to the higher number of flight and operational control parameters compared to helicopters. A target mission profile under consideration by several institutions is a 60 miles' air-shuttle between an airport and the business city center. Analyses of the battery capacity reveal that lifting surfaces are required to limit the electric lift generation during take-off and landing and cover the target range. Therefore, the most viable eVTOL concepts are vehicles lifted by rotors that convert from a vertical to a horizontal axis. Some of these tilt-rotor concepts, like for instance one of the Common Reference Model (CRM) by Uber Elevate shown in, make use of additional lifting rotors during the conversion maneuver. Other concepts, like for instance the Vahana air taxi model developed by Airbus A³, make usage of tilting wings. The capability to tilt rotors and parts of the wing constitute an additional degree of freedom in the aero-mechanical and aeroacoustic optimization of a maneuver.

In multi-rotor configurations, Blade-Vortex Interaction (BVI) phenomena can take place at certain flight conditions when the tip vortices from one rotor are ingested by another rotor or by the rotor itself. For this kind of architectures, therefore, a low-noise procedure is one for which the occurrence of BVI conditions is minimized. Electrical motors enable the usage of variable speed rotors. This allows to adapt the rotational speed to different flight conditions to supply the required lift and thrust, while operating close to the optimal advance ratio. Compared to the control of the collective angle of a helicopter rotor blade, the rotational speed control can be used to better distribute the lift between the wings and the rotors during a conversion stage.

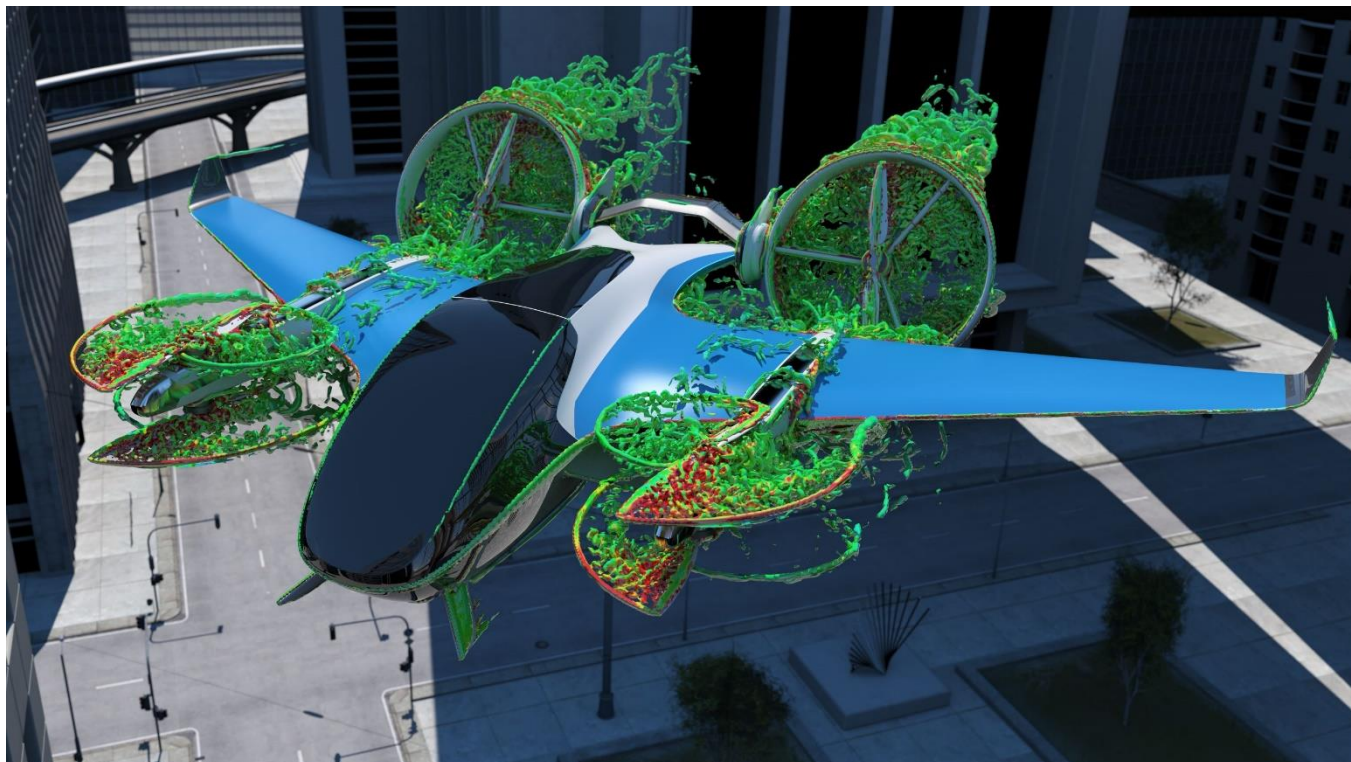


Figure 1: 3DS eVTOL demonstrated during transition maneuver

In the present study, a tilt-rotor concept developed by 3DS and illustrated in Fig. 1 is used; it comprises two front counter-rotating open rotors and two rear shrouded counter-rotating tilting rotors. This model is used as a test-bench for the development of multi-disciplinary workflows in the 3DEXPERIENCE platform involving different SIMULIA tools for structural, flight mission, aerodynamic and aeroacoustic analyses.

As already pointed out, the focus of the present paper is on the process of the aeroacoustic part of the workflow. Different scenarios are considered: (i) an isolated rotor for rotor performance studies, (ii) an isolated full vehicle undertaking quasi-static flow conditions, (iii) a vehicle hovering over a crowded urban area and (iv) an operational scenario of a vehicle undertaking an approach maneuver over a flat terrain. Each of these scenarios will be discussed and analyzed in the results sections. Prior to that, the underlying computational method is described, as well as details on the geometry and urban environment under consideration.

2. Methodology

All scenarios are prepared, simulated and post-processed by an automated workflow using SIMULIA PowerFLOW™, a high-fidelity CFD solver based on the Lattice-Boltzmann/Very-Large-Eddy-Simulation method (LB/VLES). The relaxation time and other parameters of the equilibrium distribution function are computed by considering scales related to the turbulent motion and to the strain rate and rotation of the resolved flow field. Such a procedure is based on the paradigm of a kinetic theory applied to a “gas of eddies”. As discussed by Chen et al. (2004), such an expanded analogy between the chaotic motion of particles and the chaotic motion of eddies leads to the fundamental observation that the Reynolds stresses, which are a consequence of the chaotic turbulent motion, have a non-linear structure and are better suited to represent turbulence in a state far from equilibrium, as in the presence of distortion, shear and rotation. In other words, although the relaxation time is computed using a two-equation transport model, the $k-\epsilon$ Re Normalization Group (RNG) model in PowerFLOW™ (Yakhot et al 1992, Teixeira 1998 and

Pervaiz and Teixeira 1999) is not used to compute an equivalent eddy viscosity, like in Reynolds-Averaged Navier Stokes (RANS) models, but it is used to recalibrate the Boltzmann model to the characteristic time scales of a turbulent flow motion.

SIMULIA PowerFLOW™ has been already used in the past for a variety of large aeroacoustic problems in a variety of ground-transportation and aerospace applications and a variety of Reynolds and Mach conditions and at various degree of complexity, from component level to full vehicle. Relevant to the present study are benchmark studies conducted for rotating devices (Perot et al 2012, Avallone et al 2018a, Casalino et al 2018, Gonzalez and Casalino 2018 and Casalino et al 2019a) and involving trailing-edge noise generation as a source of rotor/propeller broadband noise (Avallone et al 2018b). One of the crucial aspects of using this CFD solver for this application is the capability to manage complex geometries and multi-level rotations of parts, as a tilting counter-rotating rotor, in a simple and automated way from the user's point of view. This is primarily due to the capability of the software to generate automatically the surface and volume CFD mesh starting from faceted CAD geometries imported as separate entities in a specific reference system that can be both translated and rotated.

The aerodynamic noise generated by the rotation of the various propellers, as well as the interaction noise between the body and internal propellers is then predicted using an acoustic analogy based on the Ffowcs-Williams and Hawking's (FW-H) equation (Farassat and Succi 1983, Casalino 2003). Multiple averaged permeable surfaces around the aircraft geometry and wake are fitted to extract pressure, density and velocity as an input to the FW-H solver. The resulting predictions of far-field radiated noise are used to analyze the flow phenomena responsible for the noise generation and as input to the acoustic footprint calculator to predict full flight envelope noise information according to noise certification requirements (US Department of Transportation 1969+, Casalino et al 2012).

3. Workflow setup

Multicopter vehicles such as drones and VTOLs are highly complex and detailed vehicles, which could require up to a few weeks of engineering work to extract end to end (E2E) solutions for noise estimations. Therefore, automation of this full process is desired and required in order to meet customer targets. Within SIMULIA PowerFLOW™, process automation is feasible and can be easily implemented due to its nature to connect with any Python script before, throughout, and after a simulation.

A Multicopter Aero and Acoustic Simulation (MAAS) workflow process has been generated to automate all SIMULIA PowerFLOW™ features. The MAAS automated workflow is a multifunctional workflow for a large variation of different rotorcraft calculations, focusing on aerodynamic and/or aeroacoustic performance. The full process cycle is captured in the workflow, from pre-processing and simulation case generation, until post-processing and results comparison.

The following incomplete list provides examples of calculations the workflow can handle:

- isolated rotor, propeller, cooling fan or propulsive fan (e.g. axial and hover propellers);
- isolated rotor with collective and cyclic command angles (e.g. helicopter), including full automated trimming procedure;
- installed rotor with airframe components (e.g. a ducted fan shrouded rotor);
- N number of all above (e.g. interaction between installed front and rear rotors);
- full scale vehicle with all above under hover, conversion or cruise, e.g. Vertical Takeoff and Landing Vehicles (VTOL) or helicopters.

To showcase the process, 3DS eVTOL vehicle is used as depicted in Fig. 1. The electrical passenger VTOL vehicle designed by 3DS consists of eight, 1.2-meter radius propellers which contra-rotate to maintain balance and stability. The rear propellers are shrouded and tilted depending on the flight conditions. The total wing span is 15-meter-long, while the full fuselage is approximately 7-meter long. The full detailed and exact representation of the model is simulated using a total of 16 variable resolution layers (VRs). The VRs are placed onto regions of interest (e.g. propeller blades) according to the established best-practice PAV setup developed and distributed by 3DS.

4. Isolated rotor results

Prior to the full vehicle investigations, it is common to perform isolated rotor blade design studies. SIMULIA PowerFLOW™ is a suited tool to perform both quick and detailed aerodynamic and acoustic performance studies. The rotor of the 3DS eVTOL (Fig. 2) is investigated; a 1.2-meter radius, two bladed, fixed pitch rotor. Hover conditions at sea-level flow conditions with a RPM of 1,500 are simulated.



Figure 2: Geometry overview of the isolated rotor

The mean and unsteady surface data from the simulation is further analyzed by means of radial sections. Mean pressure distribution along multiple slices are reported in Fig. 3, while the integrated and sectional thrust and torque are plotted in Fig. 4.

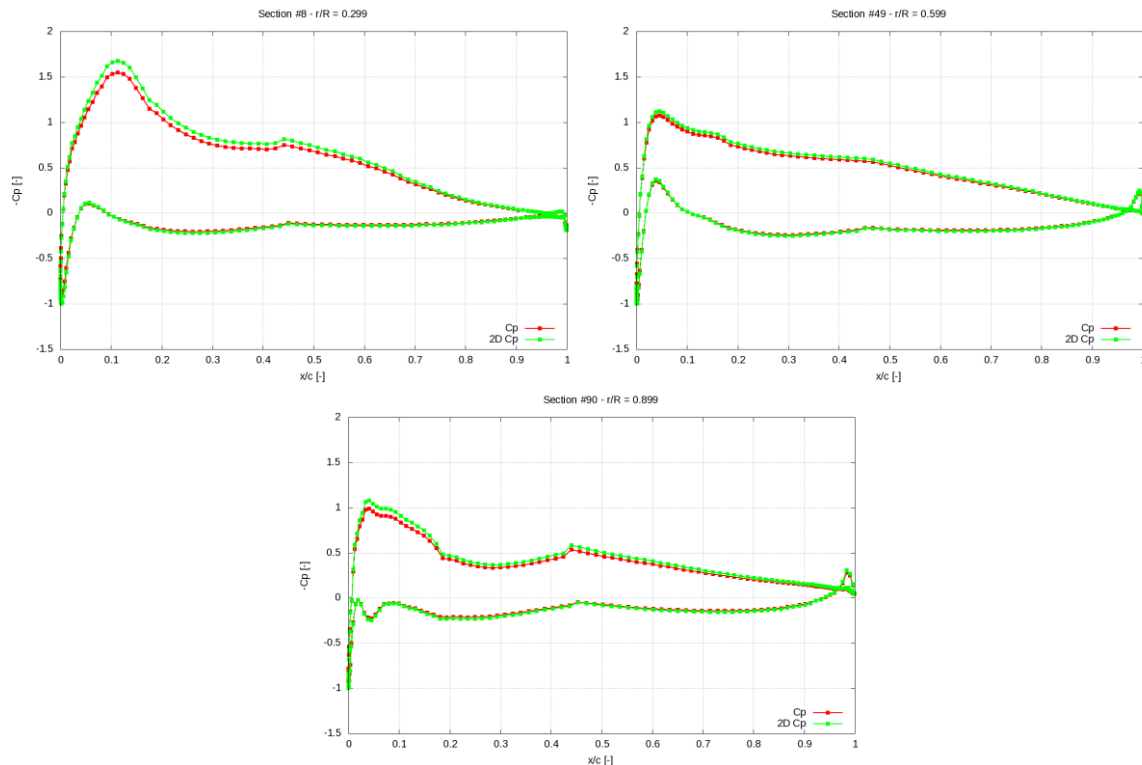


Figure 3: Mean pressure distribution along three spanwise cuts (top left) $r/R = 0.3$, (top right) $r/R = 0.6$ and (bottom) $r/R = 0.9$

The sectional thrust and torque increase with increasing radial section, as expected. The maximum sectional thrust and torque are already reached at 60% of the radius, with a drop seen at the tip due to local BVI. It is clear that this blade is not optimized for performance yet, and the change of the geometrical twist at the outer part of the blade would likely benefit the sectional thrust and torque conditions.

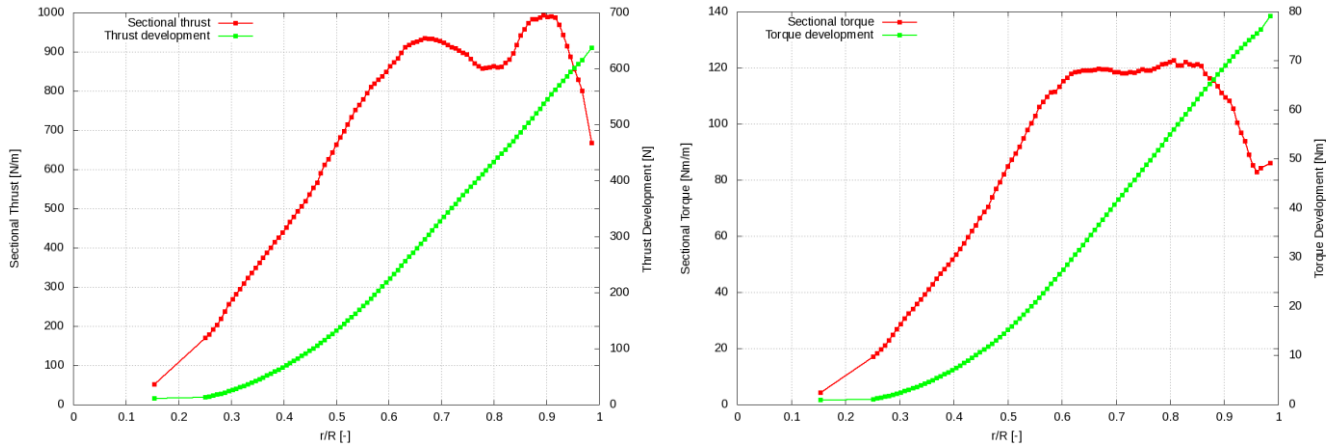


Figure 4: Radial force development; (left) thrust and (right) torque for the isolated rotor

A structured mesh, on which the results are projected after simulation, is used to identify the growth of Power Watt Level (PWL), an integrated quantity to highlight the overall tonal and broadband noise levels from the blade surface. Data from Fig. 5 is computed by means of sectional FW-H calculations on a full sphere of 225 microphones surround the isolated rotor.

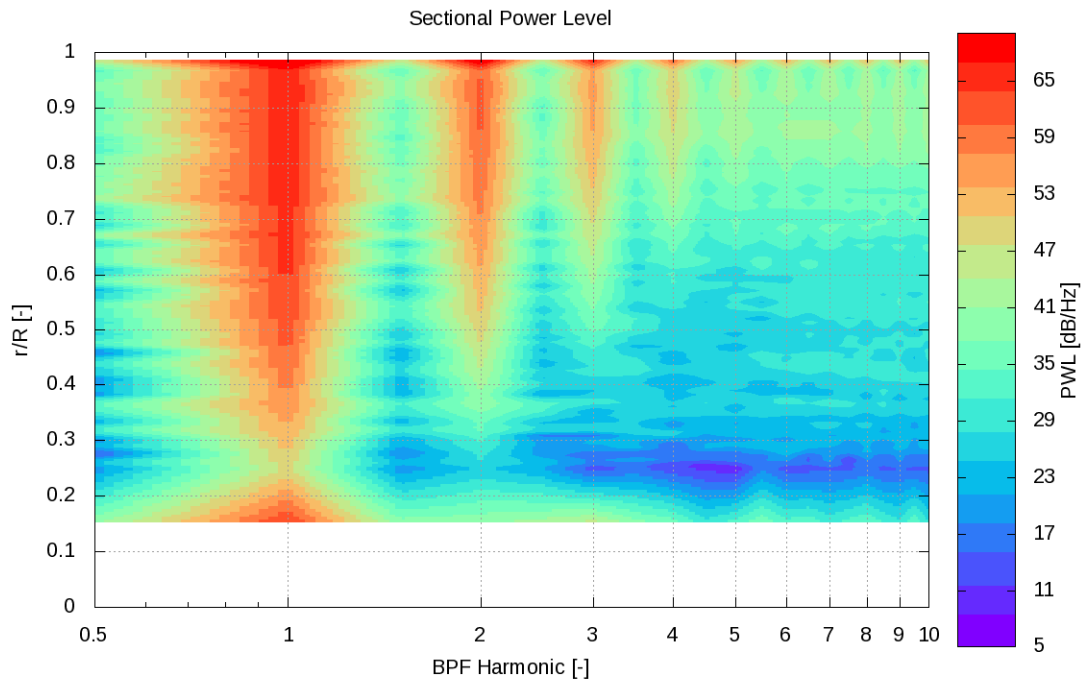


Figure 5: Sectional Power Watt Level map for the isolated rotor

The various harmonics are adequately captured up to the 5th BPF with the current mesh resolution (very coarse). The root part of the blade contributes only significantly to the first blade passing frequency, while closer to the tip, the contributions are the largest for all BPFs.

As BVI is expected based on the force development plots of Fig. 4, it would be good to investigate its impact on the sectional noise. For that, we qualitatively study the noise sources by means of computational beam-forming. In Fig. 6, both sky and ground view representations of the acoustic noise sources are plotted on top of the blade surface. The levels are relative to the maximum, i.e. only the largest sources are depicted.

The results indicated what was already expected; around 80% of the radius, the tip vortex of the previous blade hits the leading edge of the blade, causing a strong increase in BVI noise on both sides of the blade.

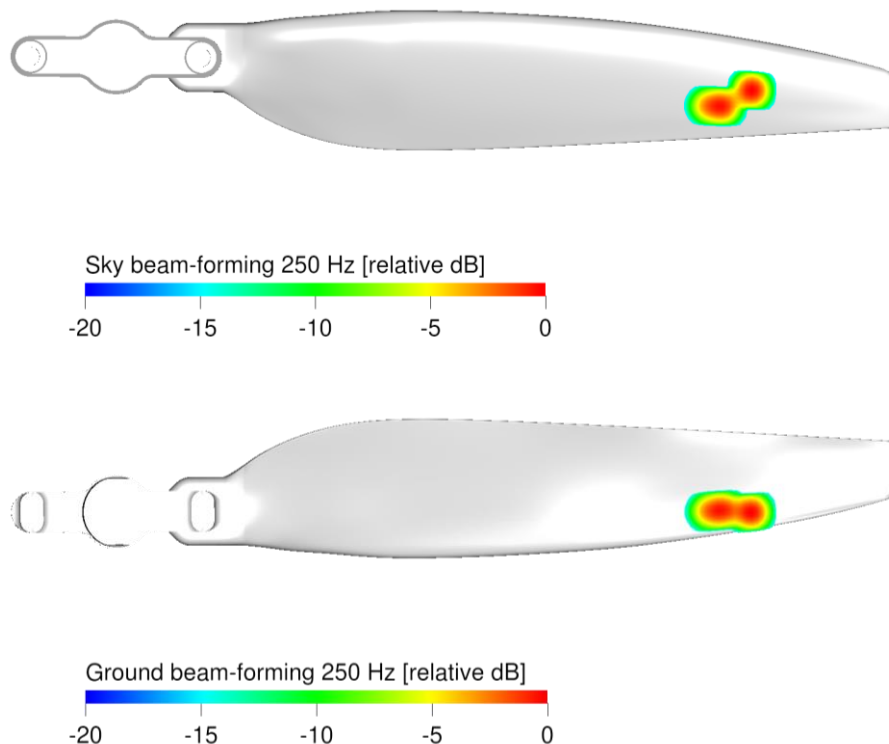


Figure 6: Computational beam-forming isolating the single blade; (top) sky oriented and (bottom) ground oriented

5. Installed configuration results

The sound generation of installed vehicles brings in complexity to the problem. The rotor wake may interact with the fuselage or another rotor and creating blade-vortex interaction (BVI), or rotor noise may be cancelled out by generating so-called anti-noise on port and starboard side respectively. In addition, noise emission can be limited, reduced or altered by using ducts or shrouds.

To give a good sense of the complexity of the flow solution, Fig. 7 highlights an instantaneous solution of iso-surfaces of λ_2 criterion, colored by the velocity magnitude, and time-derivative of the wall pressure field plotted in gray scale of the 3DS eVTOL under hover. The tip-vortex system is clearly highlighted by the coherent structure, which de-correlated further when down washed.

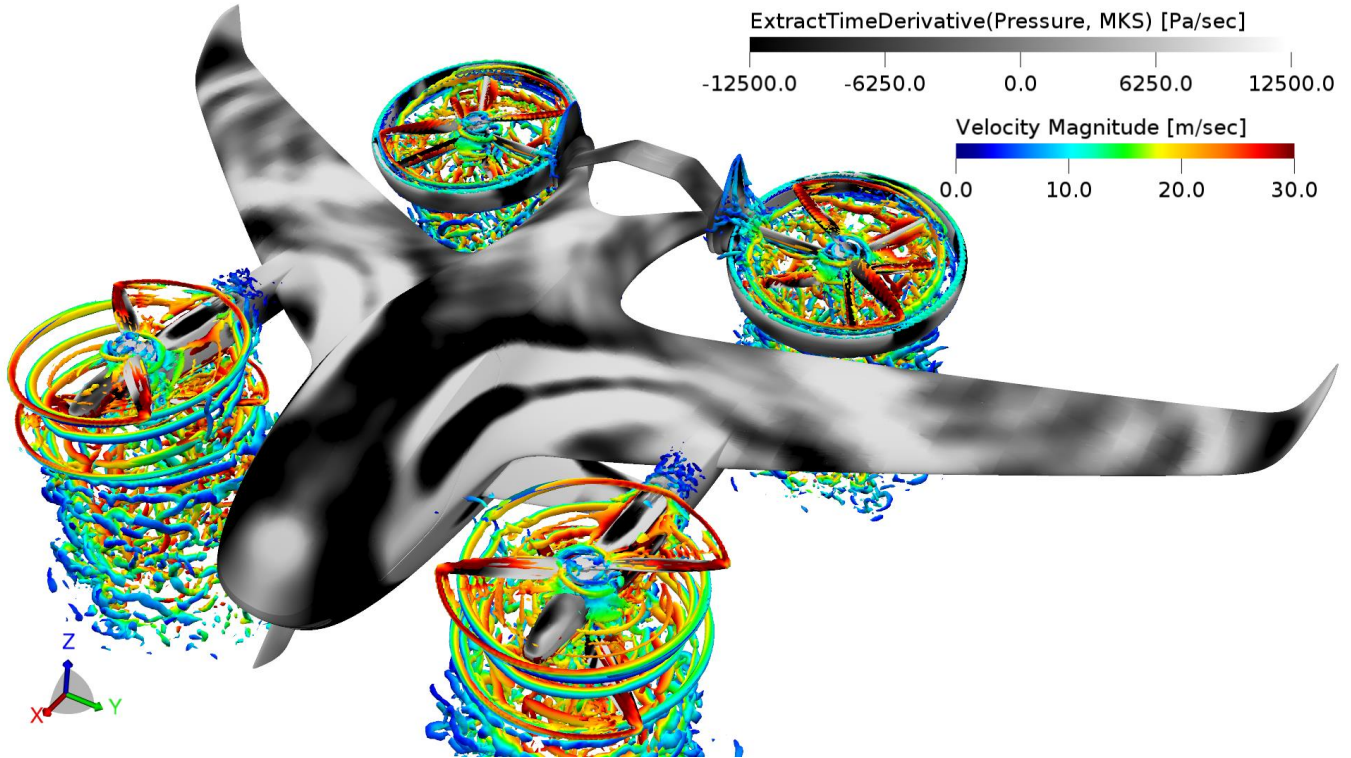


Figure 7: Instantaneous flow solution past the vehicle; λ_2 iso-surface superimposed to wall pressure time derivative

As hover does not create complex rotor-fuselage interaction condition for this configuration, forward flight cases are further qualitative studied. In detail, (i) the rotor speed and (ii) the rear rotor tilt angle are investigated.

Regarding the influence of the rotor speed, two horizontal flight cases with retracted front rotors, the same almost horizontal rear rotor axis and two different values of the rotor RPM are considered. The instantaneous acoustic fields are visualized as contour plots of the dilatation field in Fig. 8. As expected, the intensity of the acoustic waves is stronger for the higher RPM case.

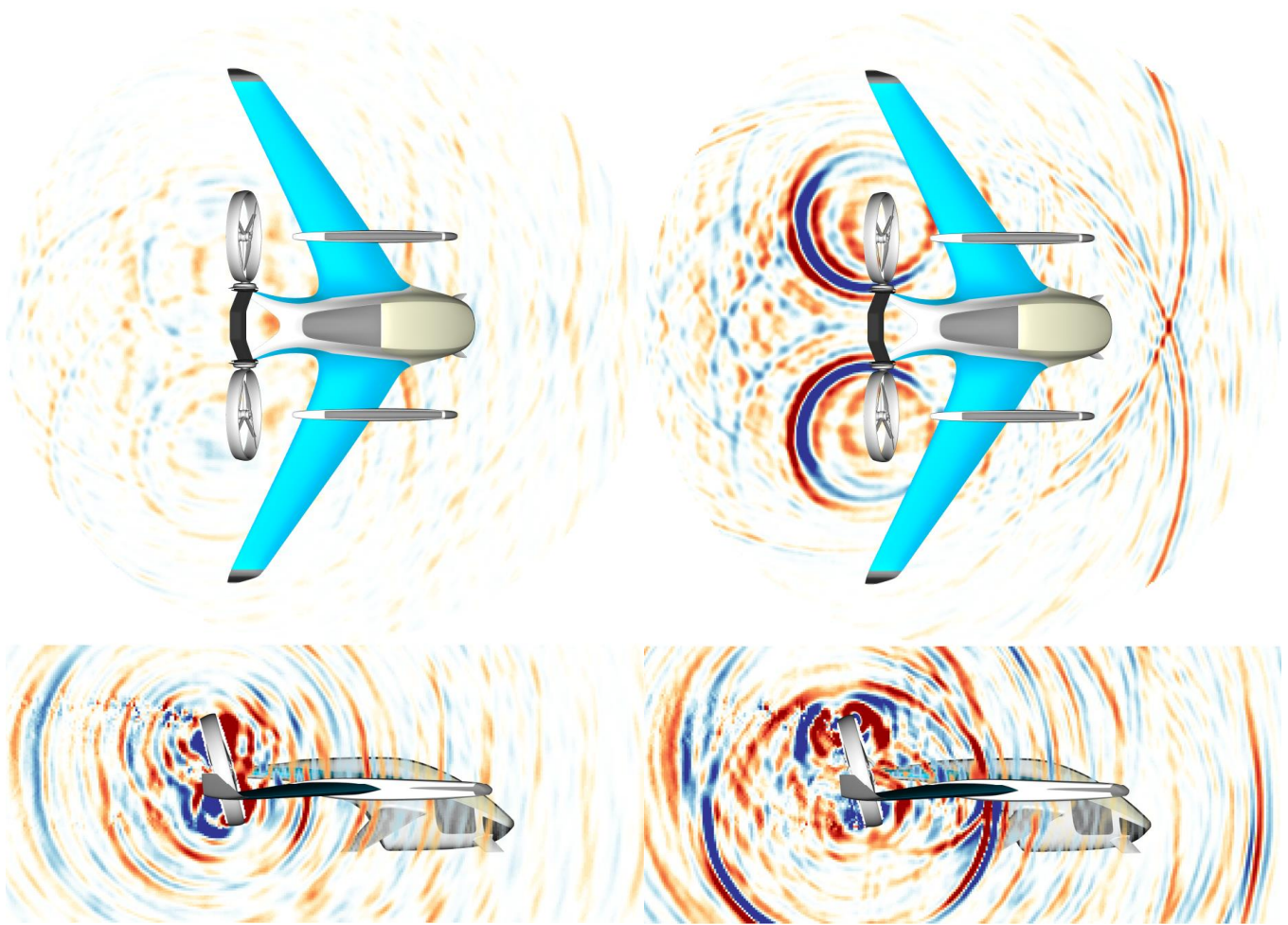


Figure 8: Instantaneous dilatation field for two different cases; (left) RPM = 1000, (right) RPM = 1500

Regarding the influence of the rear rotors tilt angle, two descending flight cases with the same flight speed, glide angle and rotor RPM and different values of the rear rotor tilt φ angle are considered. The instantaneous dilatation field is shown in Fig. 9. Although the intensity does not seem to vary significantly between the two cases, the directivity pattern reveals why higher tilt angles are associated with different on-ground noise levels. When the rotor axis is almost vertical, the noise exposure is limited to the time when the vehicle is close to the ground microphone. Whereas, when the rotor axis is almost horizontal, i.e. in cruise condition, the sound exposure is extended longer and more downstream.

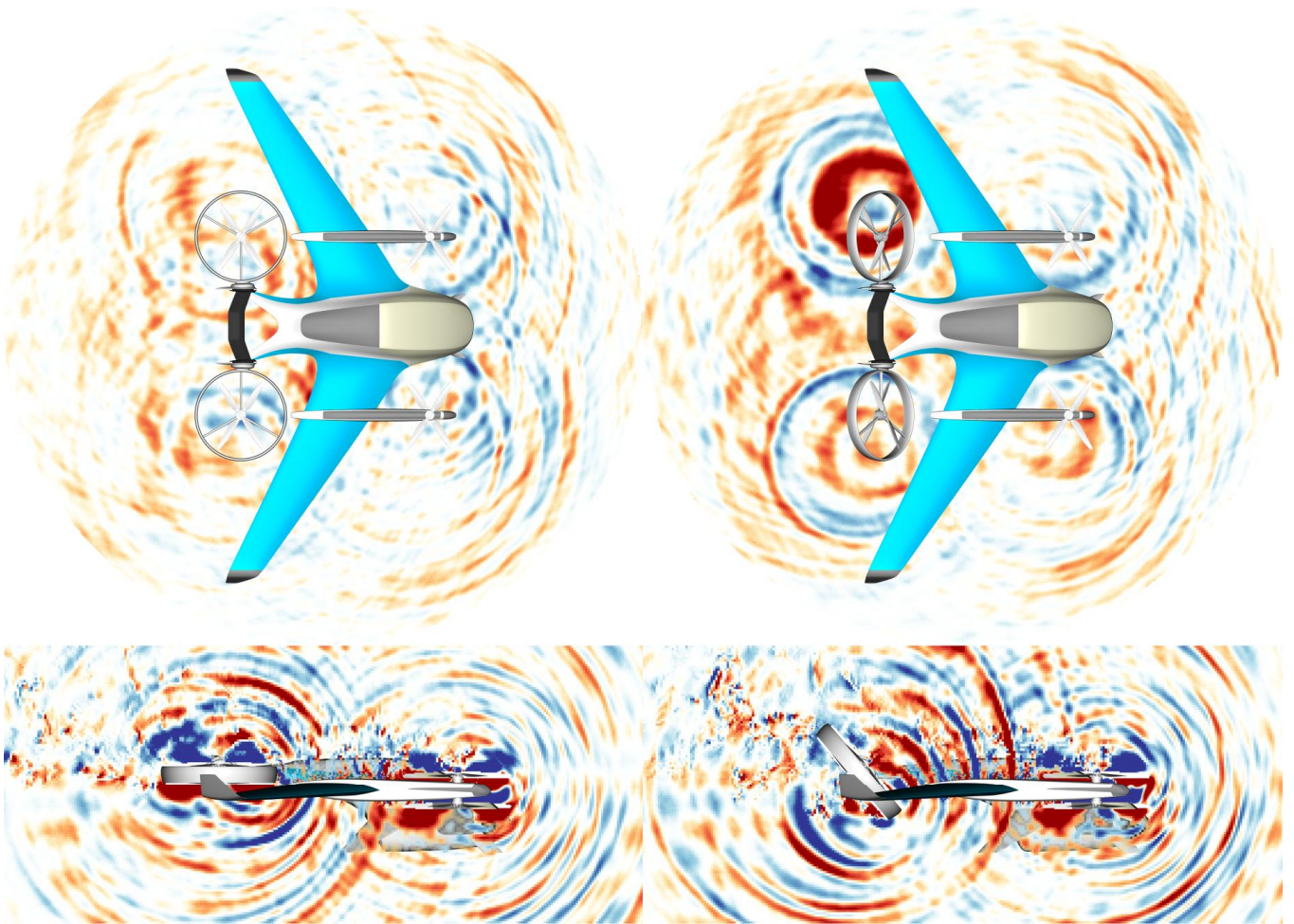


Figure 9: Instantaneous dilatation field for two different cases; (left) $\varphi = 0$ deg, (right) $\varphi = 50$ deg

Finally, it is interesting to compare two flight conditions at two different values of the angle of attack α . Multicopter systems can be affected by strong BVI effects for some specific values of the descending rate, if vortices shed from front rotors or parts of the fuselage are ingested by rear rotors. The present configuration can also incur in this situation. Fig. 10 shows iso-value surfaces of the λ_2 criterion for a level (top) and a descending flight (bottom) condition. The massive flow separation occurring in the second condition would necessarily result in BVI phenomena and thus additional noise generation.

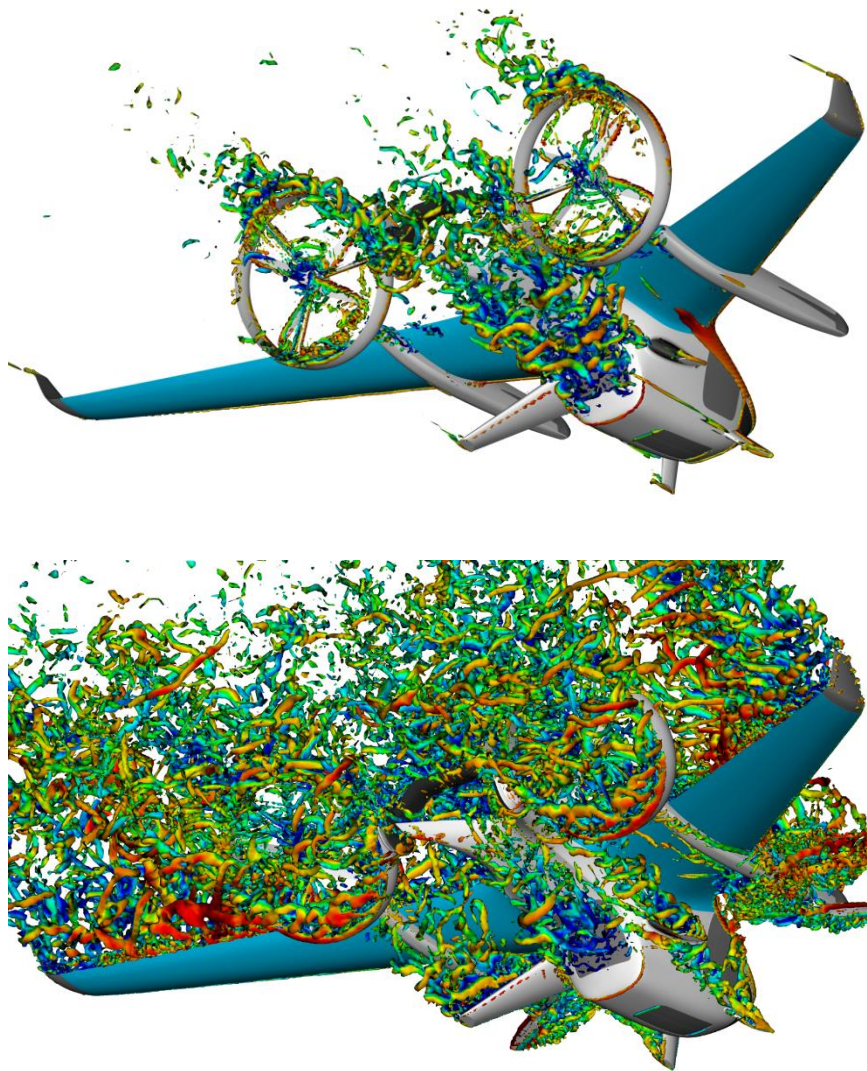


Figure 10: Instantaneous λ_2 iso-surfaces for two different cases; (top) $\alpha = 0$ deg, (bottom) $\alpha = 60$ deg

6. Urban environment results

In this section, the 3DS eVTOL vehicle in hover configuration is placed in proximity of a vertiport. The automatic mesh generation around the buildings is a key aspect, as well as the capability of the solver to propagate acoustic waves with low dissipation over long distances with a reduced number of grid points per acoustic wavelength.

The vertiport has been placed on the roof of one of the buildings of a fictitious but realistic urban city block. The block extends by 300 meters in both horizontal directions and by about 200 meters in altitude. The vehicle is located at about 160 meters from ground. An overview has been depicted in Fig. 11. The original aspect of this effort compared to previous analyses consists in extracting the acoustic field in a much large volume encompassing an urban setting directly from the transient CFD solution. No acoustic integral solution for the post-processing is therefore used.

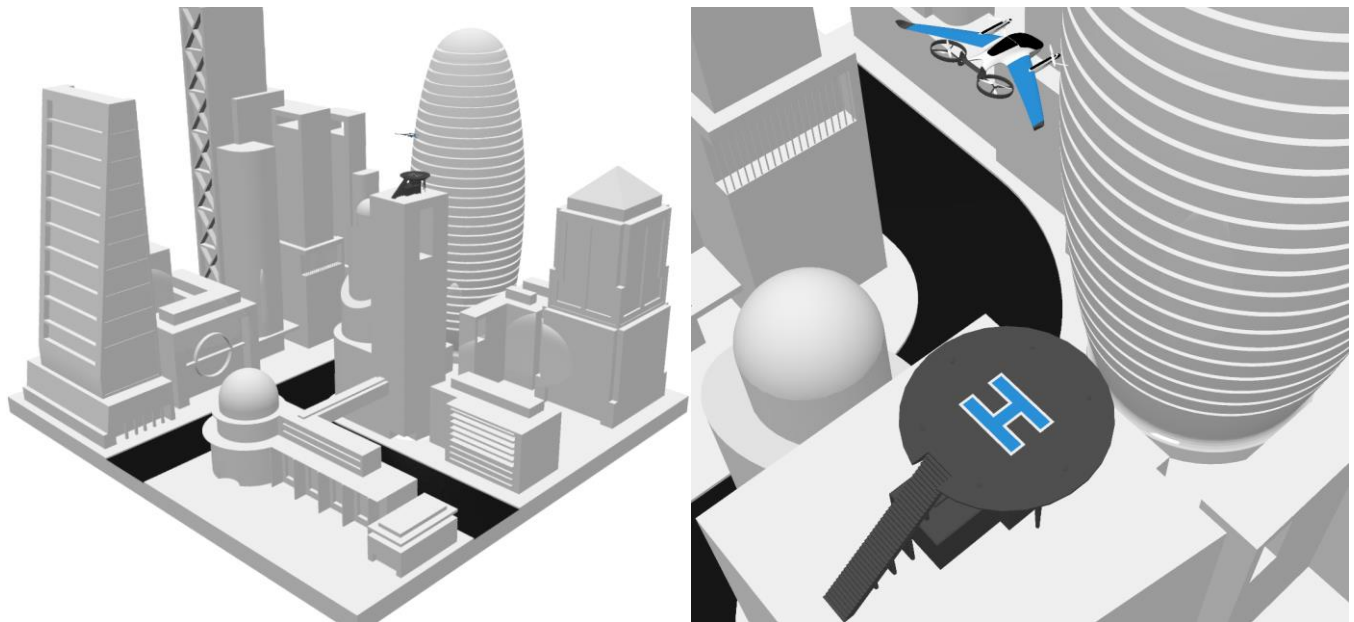


Figure 11: Illustration of the urban block, with a close-up view of the vertiport on the right

The complete urban block is embedded in a grid resolution region that corresponds to about 30 points per acoustic wavelength at the first Blade Passing Frequency BPF-1 (~ 40 Hz at 1,250 RPM). This resolution is sufficient to compute accurately the propagation of waves at BPF-2, which constitutes the dominant noise frequency of the employed counter-rotating rotors across the building block volume. Qualitative information can be derived from results at BPF-3.

The complete urban block is set on a flat solid ground. Two simulations are performed, both including the ground, and with and without the urban block. In the second simulation, the surface of the buildings is used as a fluid sampling surface upon which the static pressure is sampled and compared to the wall pressure of the first simulation. More details are found in the contribution by Casalino et al. (2019b).

The comparison between noise levels predicted with and without the buildings provides useful indications about the potential error made when the acoustic scattering effects of the buildings are neglected or not properly modelled. A qualitative illustration of the scattering effects due to the buildings is shown in Fig. 12 and Fig. 13, where an instantaneous field of the time-derivative of pressure on the surface of the buildings is shown for the two simulated case. As expected, the presence of shadow zones and strong wave interference patterns, also on parts directly exposed to the source, take place in the presence of the buildings.

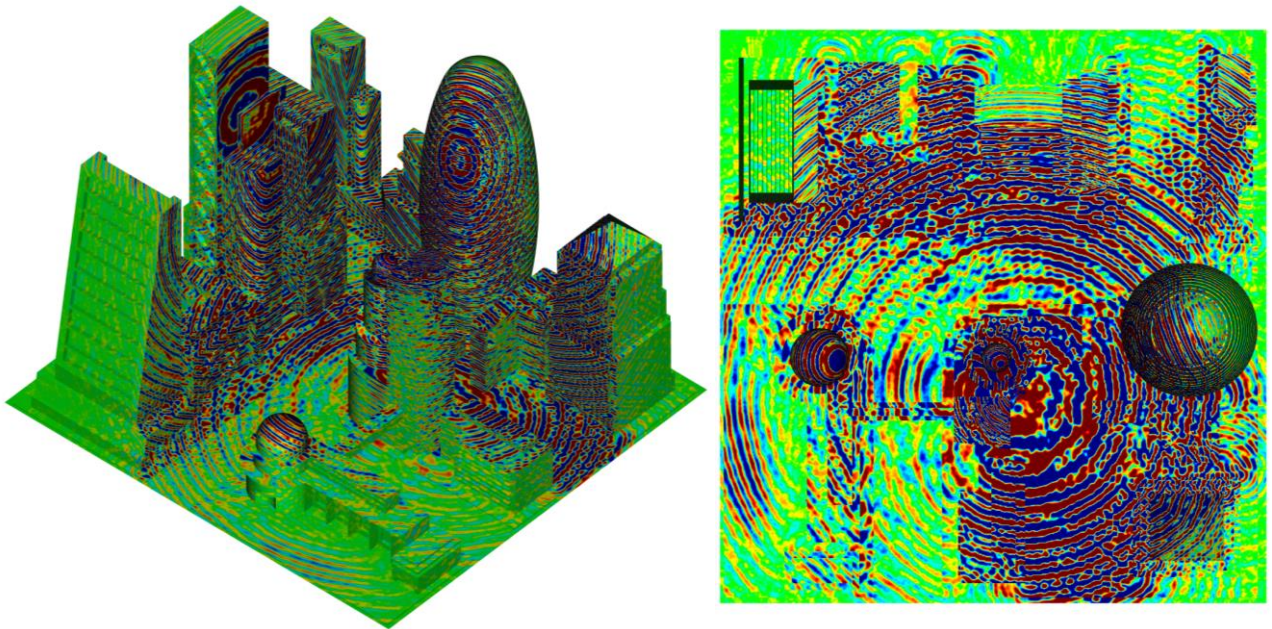


Figure 12: Pressure time derivative on the building surface, with building scattering

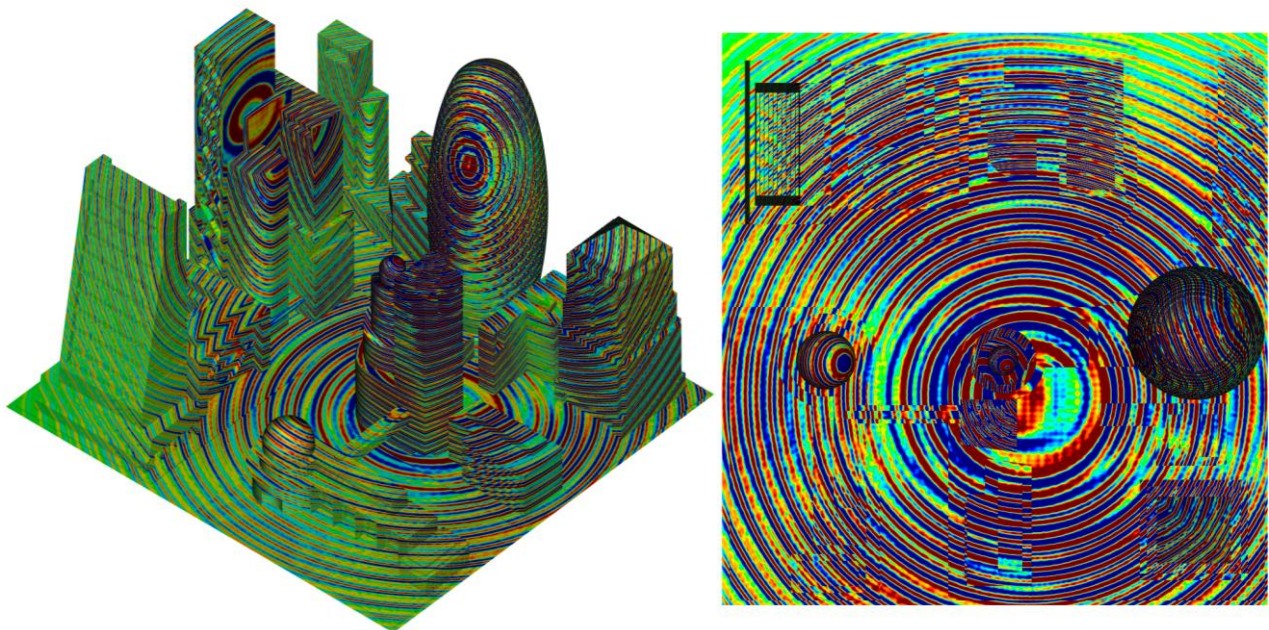


Figure 13: Pressure time derivative on the building surface, with building scattering

7. Flight envelope results

The trimming of the vehicle along the flight path is carried out by using a quasi-static approximation from a flow standpoint. The flight envelope is explored by performing 90 transient CFD simulations for different combinations of the flight Mach number, the angle of attack, the tilt angle of the rear rotors and the rotational speed of the four rotors, the two retracting counter-rotating lifting rotors in the front and the two tilting counter-rotating lifting/pushing rotors in the rear. This data was stored in a so-called Noise Hemisphere Database (NHD) from which, for each trajectory and waypoint, data was interpolated to extract the noise footprint. Details on the numerical description of the flight conditions, flight mechanics meta-model, trimming procedure, trajectory definition and NHD were already provided by Casalino et al. (2019c).

Three feasible flight trajectories were calculated with the meta-model, with their details highlighted in Fig. 14. For these trajectories, a point mass of 1500 kg was assumed for the vehicle, a horizontal distance of 300 meters was covered as well as a vertical distance of 425 meters. The full flight path was assumed to be taken place in a total duration of 60 seconds.

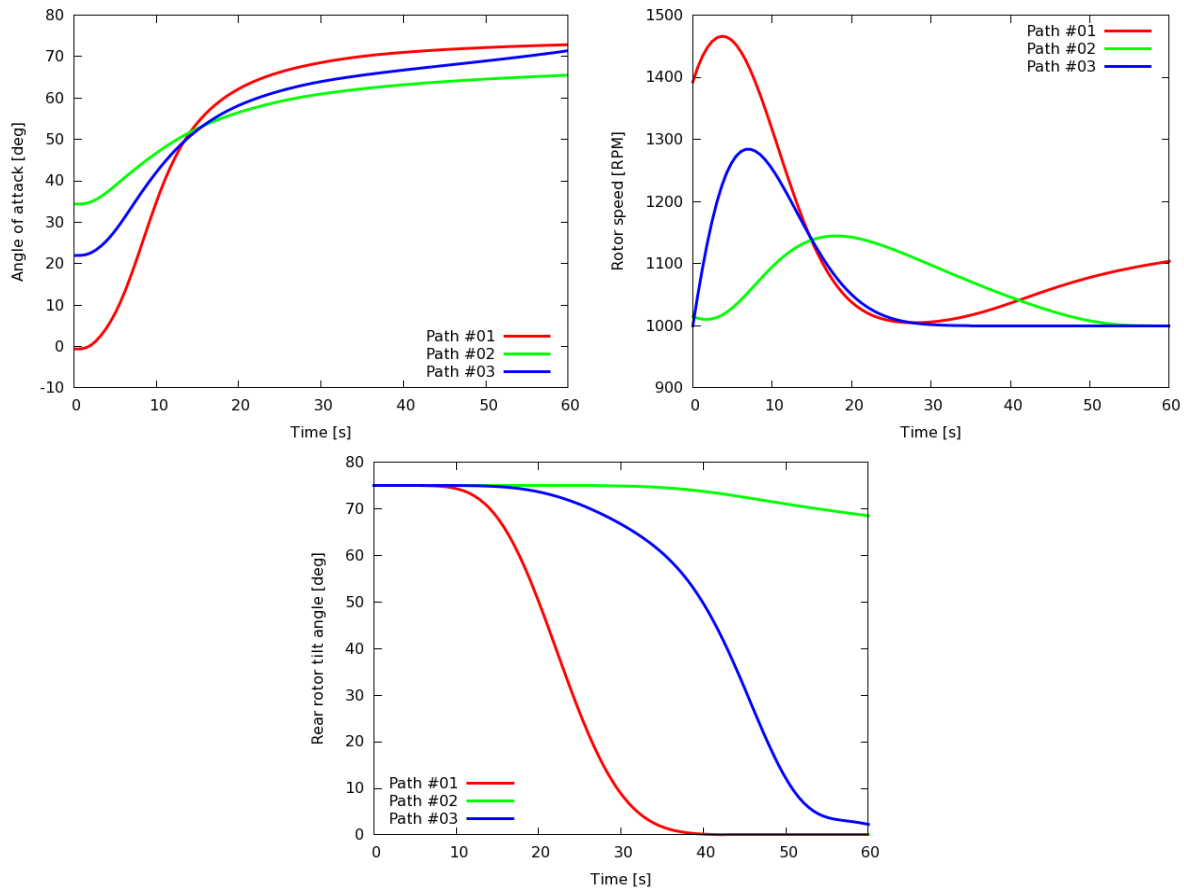


Figure 14: Trajectory definition by angle of attack (top left), rear rotor tilt angle (top right) and rotor speed (bottom)

The distribution of the lift between wing and rotor leads to significantly different evolutions of the rear rotor tilt angle and rotational speed. Interestingly, for path #2, the rear rotor axis reaches only an inclination of about 30 degrees with respect to the horizon at the end of the maneuver.

In order to investigate the fly-over noise at a carpet-centered position, the OASPL data over time as well as its SPL is plotted in Fig. 15. The three trajectory flight paths behave very differently in terms of OASPL. It is interesting to see that all paths obtain their highest levels after 18 seconds; this is the time when the vehicle is closest to the reference microphone. At this time instant, the amplitude varies with 6dB, with path #1 being the most silent and path #2 the noisiest trajectory. Quickly after fly-over, the OASPL drops rapidly for path #1. Path #3 behaves similarly, but the drop-off in noise is delayed until 40 seconds after the approach starts. For path #2, a less significant drop-off is visible and the vehicle keeps producing noise over 85 dB. Correlating this behavior back to the trajectory definition, there seems to be a strong influence on the directivity of the rear rotor tilt angle on the overall noise levels, in combination with the aircraft pitch angle.

Conversely, the influence of the rotor speed seems to be very weak: only a slight increase of the OASPL is observed for flight path #1 between 0 seconds and 10 seconds associated with the significantly higher value of the rotational speed. The SPL, on the right of Fig. 15 reveals what is expected: the trajectory with the highest OASPL emits the highest SPL noise levels. On average, there is a 20 dB overshoot of noise when path #2 is considered.

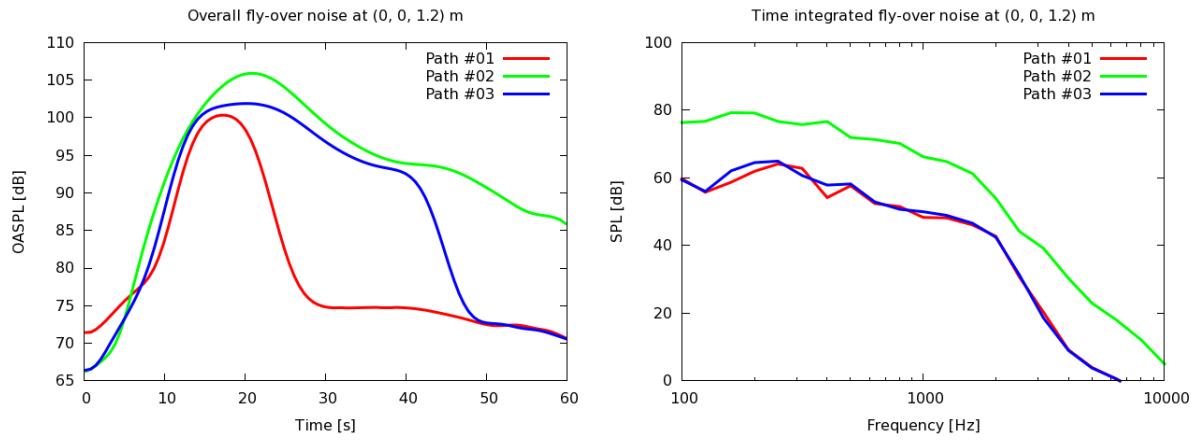


Figure 15: OASPL over time (left) and SPL integrated (right) at center ground location

As the noise levels change significantly along time, due to a combination of distance and aero-mechanical setting, it is expected that the impact on the ground is also different. The EPNL maps are plotted in Fig. 16 for the different flight trajectories. In the employed ground reference system, the vehicle is approaching the point on the map at $x = 150$ m from the negative values of the longitudinal coordinate ($x = -150$ m). As expected, #2 exhibits the highest noise footprint, with large areas exceeding the 110 EPNdB, while #1 shows the lowest noise contribution during the landing approach, overall lower than 100 EPNdB.

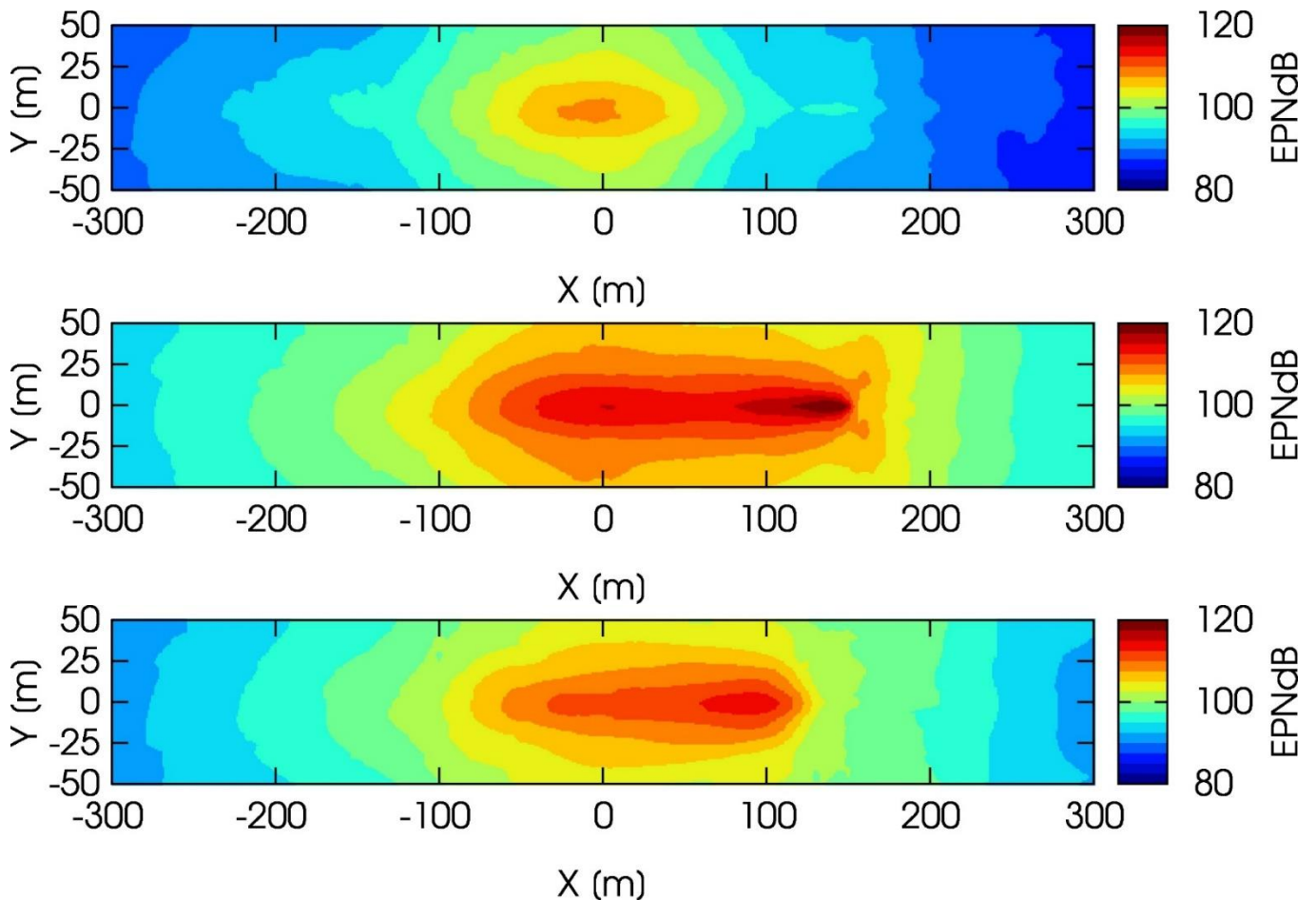


Figure 16: EPNL footprint map for #1 (top), #2 (middle) and #3 (bottom)

8. Conclusion

A fully automated, computational workflow for the evaluation of the acoustic environmental impact of vertical take-off and landing vehicles is presented. Different scenarios are considered: (i) an isolated rotor for rotor performance studies, (ii) an isolated full vehicle undertaking quasi static flow conditions, (iii) a vehicle hovering over a crowded urban area and (iv) an operational scenario of a vehicle undertaking an approach maneuver over a flat terrain.

The aerodynamic performance and aeroacoustic sources are predicted by using the high-fidelity CFD solver SIMULIA PowerFLOW™ based on the LB/VLES method. The acoustic propagation in quiescent air is extracted directly from the CFD simulation performed in a domain encompassing both the vehicle and the nearby urban city block. The effects of sound scattering due to the presence of several buildings is analyzed by comparing the noise levels on the surface of the buildings with levels extracted on the same surface from another solution performed without buildings. Additionally, an integral approach based on the Ffowcs-Williams and Hawkings analogy is used to compute the noise on a hemisphere centered around the rotor and/or vehicle. This is used to compute the on-ground noise footprint for a prescribed, trimmed, flight trajectory path.

References

- Avallone F, Casalino D and Ragni D (2018a) *Impingement of a Propeller Slipstream on a Leading Edge with a Flow-Permeable Insert: A Computational Aeroacoustic Study* International Journal of Aeroacoustics, Vol. 17, No. 6-8
- Avallone F, van der Velden W, Ragni D and Casalino D (2018b) *Noise reduction mechanisms of sawtooth and combed-sawtooth trailing-edge serrations* Journal of Fluid Mechanics, Vol. 848, 560-591
- Casalino D (2003) *An Advanced Time Approach for Acoustic Analogy Predictions* Journal of Sound and Vibration, Vol. 261, No. 4, 2003, 583-612
- Casalino D, Noelting S, Fares E, Van de Ven T, Perot F and Bres G A (2012) *Towards Numerical Aircraft Noise Certification: Analysis of a Full-Scale Landing Gear in Fly-Over Configuration* AIAA Paper 2012-2235
- Casalino D, Hazir A and Mann A (2018) *Turbofan Broadband Noise Prediction using the Lattice Boltzmann Method* AIAA Journal, Vol. 56, No. 2
- Casalino D, Avallone F, Gonzalez-Martino I and Ragni D (2019a) *Aeroacoustic Study of a Wavy Stator Leading Edge in a Realistic Fan/OGV Stage* Journal of Sound and Vibration, Vol. 442, 138-154
- Casalino D, van der Velden WCP, Romani G and Gonzalez-Martino I (2019b) *Aeroacoustic Analysis of Urban Air Operations using the LB/VLES Method*, AIAA Paper 2019-2662
- Casalino D, van der Velden WCP and Romani G (2019c) *Community Noise of Urban Air Transportation Vehicles*, AIAA Paper 2019-1834
- Chen H, Orszag S, Staroselsky I and Succi S (2004) *Expanded Analogy Between Boltzmann Kinetic Theory of Fluid and Turbulence* Journal of Fluid Mechanics, Vol. 519, 301-314
- Farassat F and Succi G P (1983) *The Prediction of Helicopter Discrete Frequency Noise* Vertica, Vol. 7, No. 4, 309-320
- Gonzalez-Martino I and Casalino D (2018) *Fan Tonal and Broadband Noise Simulations at Transonic Operating Conditions Using Lattice-Boltzmann Methods* AIAA Paper 2018-3919
- Hoehner C, Barlow C and Schootman, M (2012) *Commuting Distance, Cardiorespiratory Fitness, and Metabolic Risk* Am J Prev Med, Vol. 42, 571-578

Perot F, Kim M-S, Meskine M and Freed D (2012) *NREL wind turbine aerodynamic validation and noise predictions using LBM* AIAA Paper 2012-2287

Pervaiz M and Teixeira C M (1999) *Two Equation Turbulence Modeling with the Lattice-Boltzmann Method* ASME PVP Am Soc Mech Eng Press Vessels Pip Div, Vol. 397

Teixeira C M (1998) *Incorporating Turbulence Models into the Lattice-Boltzmann Method* International Journal of Modern Physics C, Vol. 9, 1159-1175

U.S. Department of Transportation (DOT) Federal Aviation Administration (FAA) (1969+) *Code of Federal Regulation (CFR) Title 14: Aeronautics and Space - Part 36. Noise Standards: Aircraft Type and Airworthiness Certification - Subpart B: Noise Levels for Transport Category and Jet Airplanes*

Yakhot V, Orszag S A, Thangam S, Gatski T B and Speziale C G (1992) *Development of Turbulence Models for Shear Flows by a Double Expansion Technique* Physics of Fluids A, Vol. 4, No. 7, 1510-1520



QUIET DRONES
International Symposium
on
UAV/UAS Noise
Remote from Paris – 19th to 21st October 2020

A study of the influence of support structure on drone noise

Simon Watkins, Nicola Kloet, Xu Wang
RMIT University, simon@rmit.edu.au

Summary

An overview of experimental work pertaining to the understanding and reduction of aerodynamically-generated noise from small multirotor unmanned aircraft system (UAS) of approximately 1-4 kg is given. The development of a quiet rig designed to drive a range of propellers with minimal interference noise from the motor and support systems is described. This permitted measurements on a range of isolated propellers where the effect of RPM and blade geometry on sound pressure level for a set thrust point. Noise levels (SPL and spectra up to 20,000 Hz) were measured in a semi-anechoic environment at a single point using a standard laboratory grade microphone system. Selected wake velocities were measured using a Cobra probe and mapped, which gave 3-D flow information. The flow measurements gave insights into the wake flows which impinge on typical drone support arms and generate an additional source of sound when compared to a propeller in isolation. The effects of a drone arm being introduced into the flow were evaluated for a range of shapes and sizes from the measurement data at upstream and downstream locations. While there is an increase in overall sound pressure level when a structure is introduced into propeller flow, the specifics of the geometry of the structure seem to have a relatively small effect when compared with other factors (such as RPM and distance between propeller and structure).

1. Introduction and Aims

Drones noise is predominantly aerodynamically generated, resulting from the interaction of the rotating propellers with the air. Whilst there is a large body of knowledge on propeller noise from larger manned aircraft, drone noise is generated at a much lower Reynolds number and a further noise source (not relevant to most manned aircraft) is the interaction of the wakes of the blades

impinging on the motor support structure or (depending upon motor support configuration) the wakes of the support structure impinging on the propeller blades.

The aim of this work is to measure the noise from a range of propellers typically used in multirotor drones of all-up weight of 1-4 kg and to investigate extra noise components arising from the interactions of the wakes of the propeller blades with the support structure (or the wakes of the support structures on the blades if the structures are upstream of the propellers).

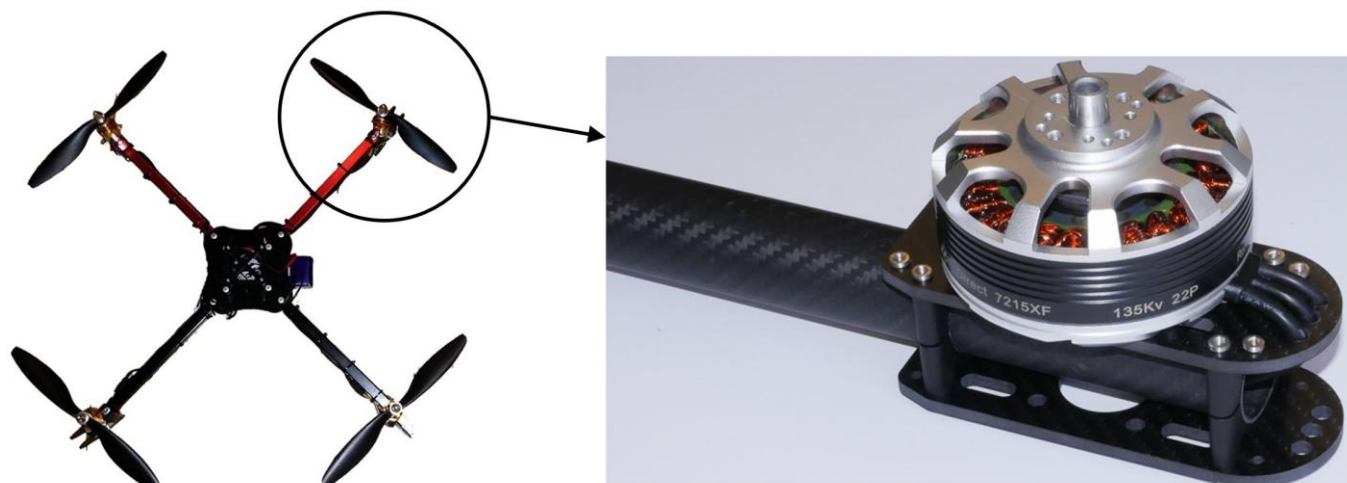
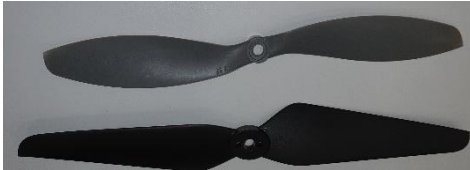


Figure 1 Typical drone (left) and close-up of motor and supporting structure (right).

2. Thrust RPM and Noise Measurement

Several propellers which would fit a typical multirotor UAS within the maximum take-off weight range of 1-4 kg were selected for this experiment. Two are presented here as case studies (shown in Table 1). These propellers are commercially available from reputable manufacturers.

Table 1 Propeller geometry and manufacturer specifications

Letter Designator	Diameter (inches)	Pitch (inches)	Manufacturer	Model	Propellers F (top) & J (bottom)
F	9	4.7	APC	Slow-fly	
J	9.5	4.5	T-Motor	AirGear	

An RC Benchmark 1580 Series thrust test stand dynamometer was used to performance benchmark as well as maintain thrust test points (and therefore constant RPM) during subsequent experiments. They were powered by a KDE 2315-980 kV motor and 55-amp ESC running on 16.4 volts DC power supply. While the RC Benchmark is a relatively open structure that should not cause a large amount of aerodynamic interference, it is known to generate noise under some conditions. For this reason, a customised low-noise drive system was developed.

2.1 Low Noise Drive System

This system separated the propeller from the rest of the drive system via a shaft extension of 10 propeller diameters and a sound insulating box. The shaft was supported by quiet bearing blocks and the box itself was made from layers of different sound absorbing materials: foam, particle board, and vinyl. The custom, low-noise system's acoustic output was compared to tests

completed on the RC Benchmark 1580 Series and has demonstrated a significant reduction at the required frequencies of interest.

2.2 Noise Measurement Technique and Equipment

Acoustic recordings were made with a B&K Sound Pressure Level (SPL) meter Type 2235 using a 1/2-inch microphone, Type 4176, mounted inside a custom microphone shield-box. The microphone was mounted 20 propeller radii, or 10 propeller diameters, away from the sound source according to the distance as shown in Figure 2. The propellers were mounted in a pusher configuration, with upstream air passing over the thrust test stand and exhaust air flowing away from the test stand. Prior testing confirmed that the acoustic directivity pattern was equal in all directions and measurements were taken in the far field.

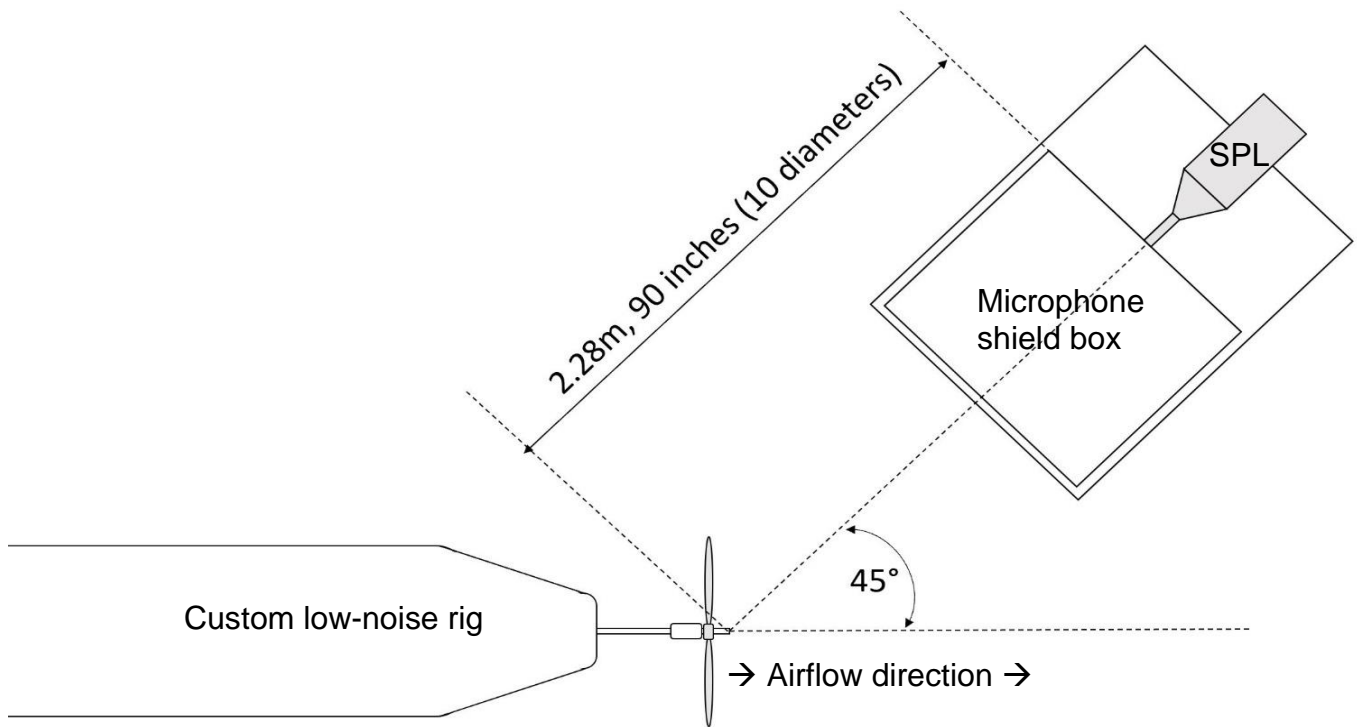


Figure 2 Experimental setup of acoustic recordings

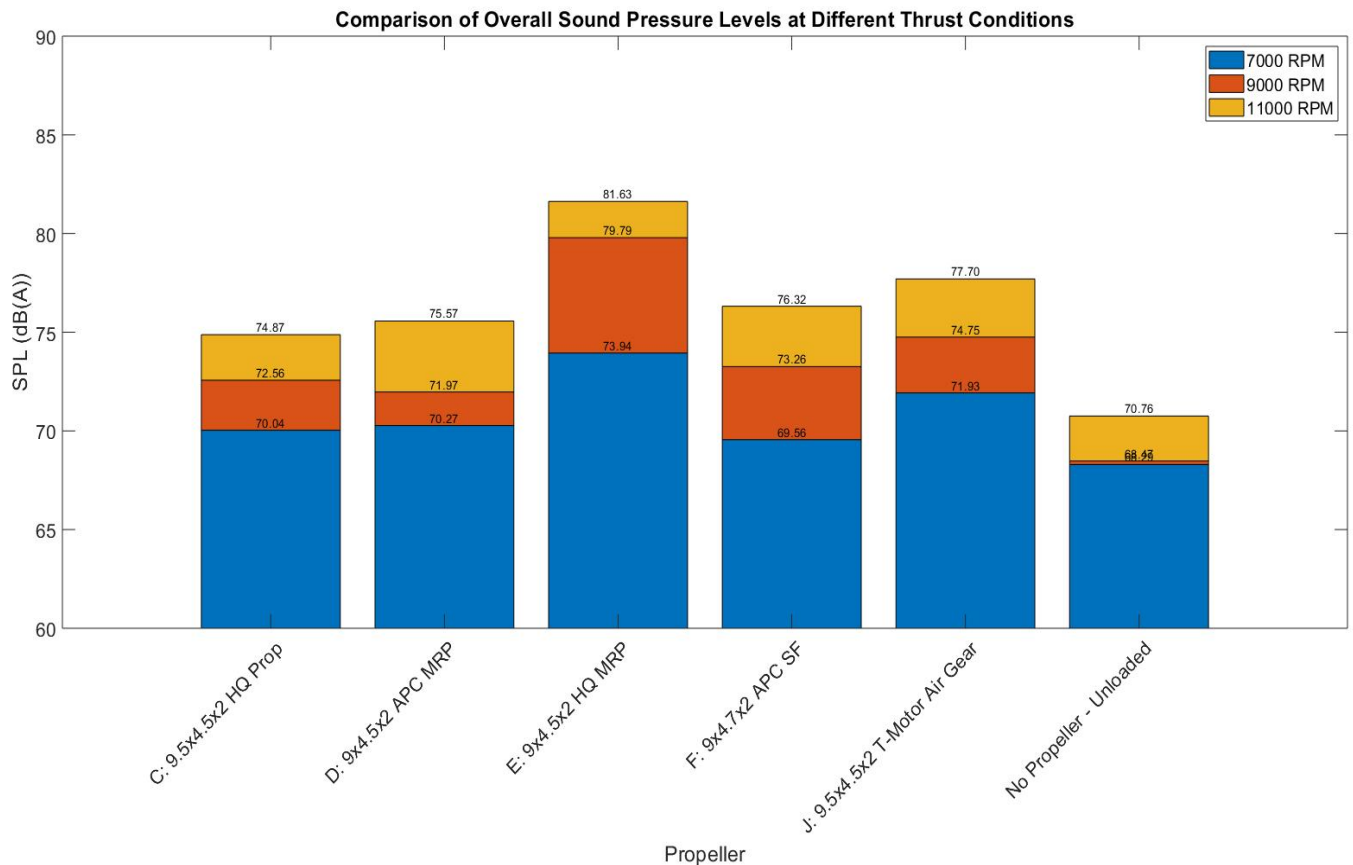


Figure 3 Overall sound pressure level measured for each propeller at given RPM condition

Figure 3 gives the overall sound pressure levels for five commercially available propellers running on the low-noise rig with no supporting structure present.

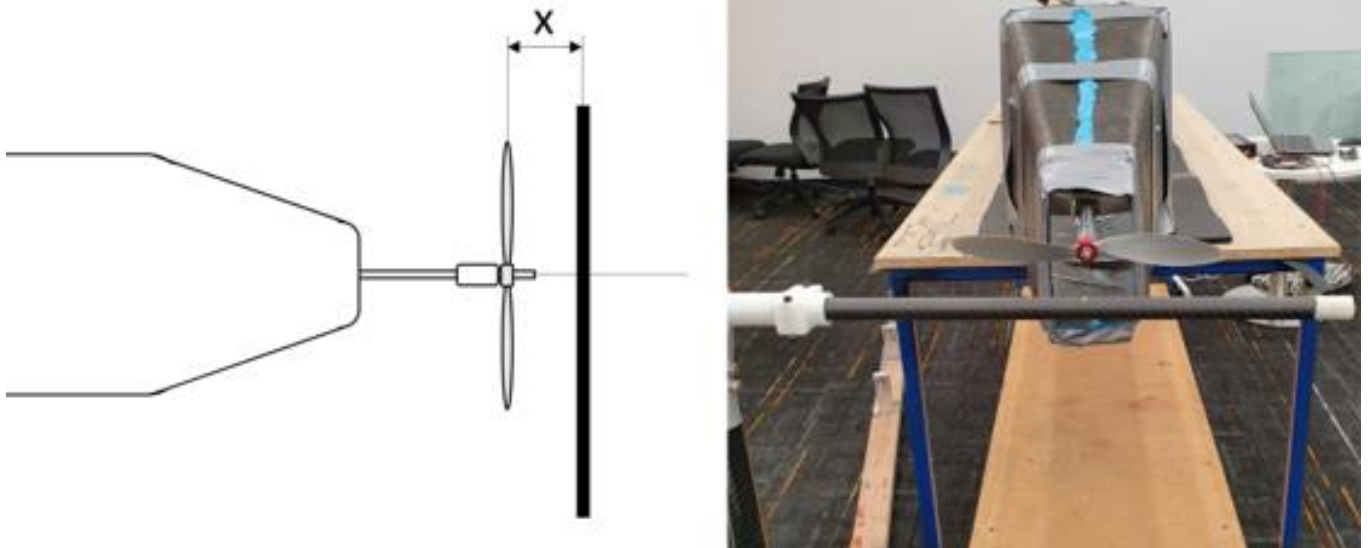


Figure 4 Diagram of x distance measured from propeller rotation plane (downstream is positive x) (LEFT) and image of 16mm diameter straight circular tube support structure in mounting location (RIGHT)

2.3 Support Structures and their Influences on Noise

Circular cross section structures were placed in the flow at varying distances from the propeller plane of rotation, see Figure 4. These supporting structures included straight circular tubes of 16mm OD, 30mm OD and a curved section 16mm OD (curve radius 114mm). These structures mimic a typical arm for a drone. Differing diameters and varying distances are compared in Figure 5 and Figure 6. It is seen from Figure 5 that for all the distances of the tube away from the

propeller, when the rotational speed of the propeller increases, the overall sound pressure level will increase. When the tube moves away from the propeller both down and up stream, the overall sound pressure level increases first and then decreases. The same trend of the overall sound pressure level over the distance can be observed Figure 6 where the upstream overall sound pressure levels show very little difference. In the downstream, the 16 mm outer diameter swept circular tube induces the lowest overall sound pressure level except that in the distance of 120 mm. The 30 mm outer diameter straight circular tube induces higher overall sound pressure level than the 16 mm outer diameter straight circular tube for all the distances except for the distance of 30 mm. The data points represented in these figures are the mean of three trials with a spread of +/- 1dB.

As the supporting structure is moved further from the propeller plane of rotation, the overall SPL decreases. By the time the structure is 120mm (approximately one propeller radius) downstream, it is equivalent to having no supporting structure present. Placing a supporting structure at an upstream location seems to have a slightly larger impact on the SPL than placing a supporting structure at a downstream location.

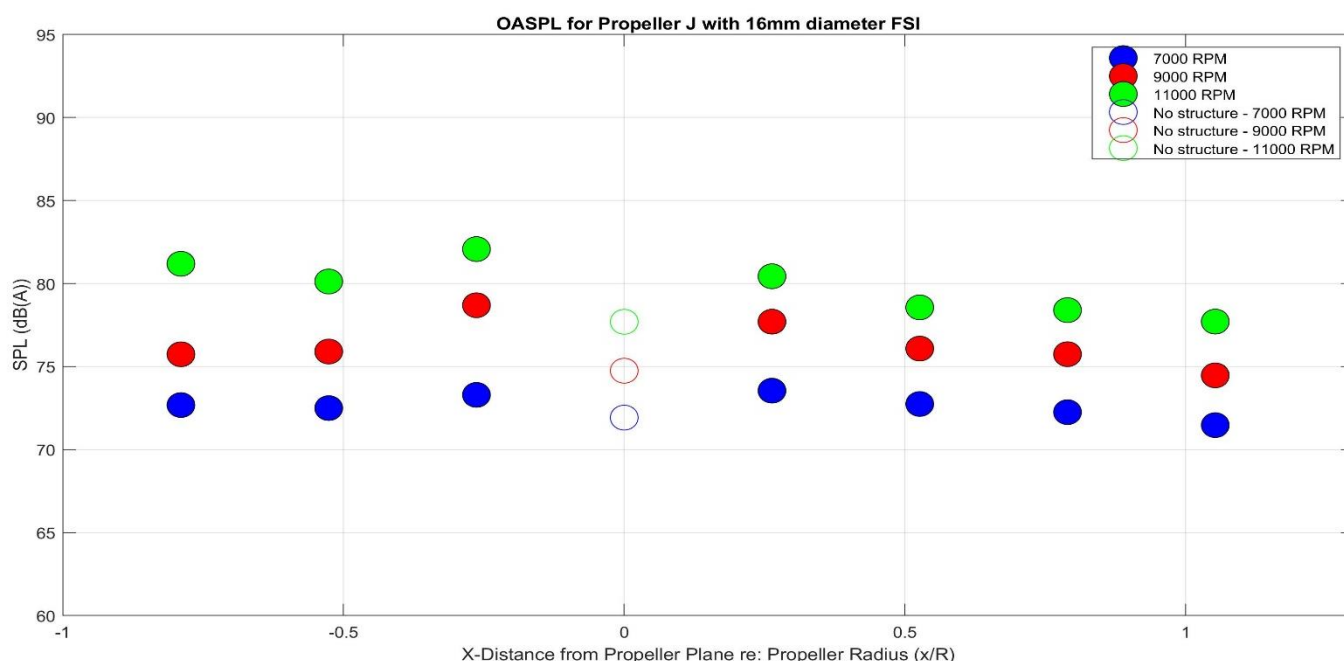


Figure 5 Overall Sound Pressure Level (OASPL) for propeller J at different RPM with a 16mm circular tube at different x distances from the propeller plane. (O-markers indicate sound with no supporting structure in the flow)

There is limited evidence to suggest that there is much to be gained from altering the type of supporting structure used. The overall SPL differs minimally between different supporting structures placed at the same location (as shown in Figure 6).

Comparing the spectral characteristics between the cases with and without support structures as shown in Figure 7, it is seen that there is an increase in the peak amplitude of the spectrum corresponding to the blade passing frequency at 300 Hz (this is discussed further in Section 2.5), and more generally a small increase across all peaks regardless of type of support structure.

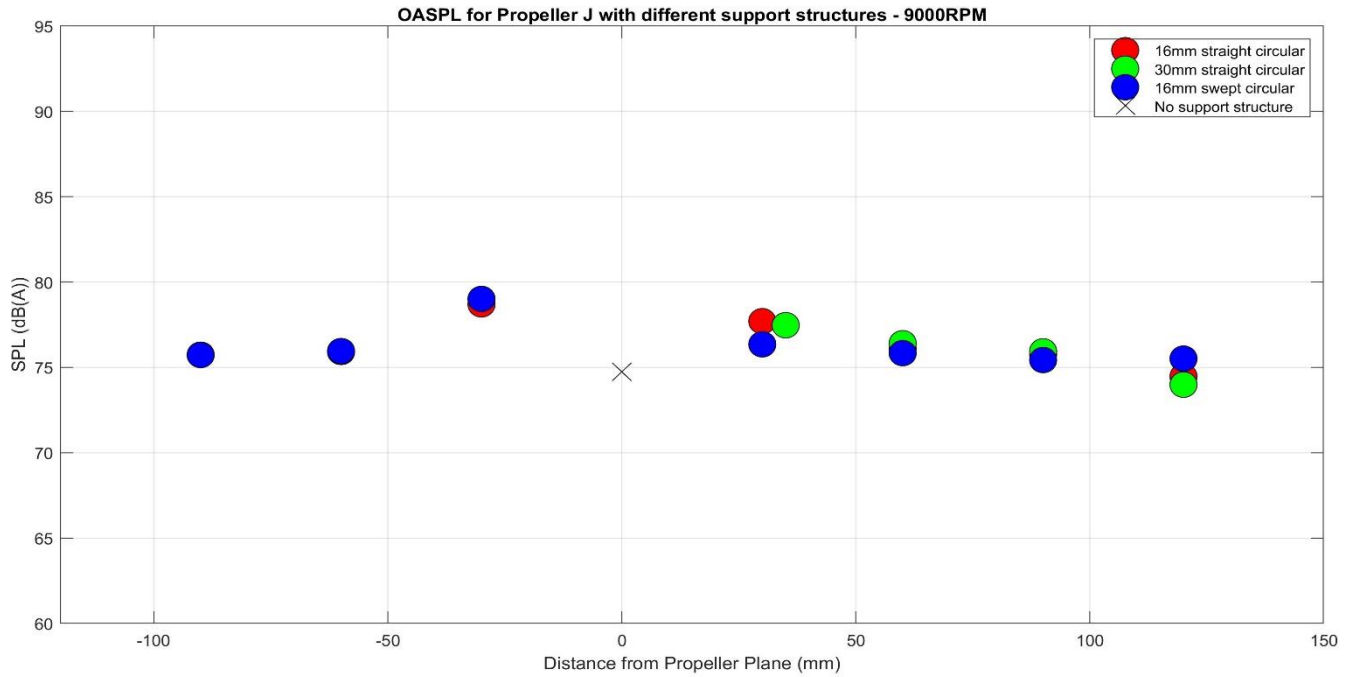


Figure 6 Comparison of overall sound pressure level for propeller J at 9000 RPM with different support structures at different spacing

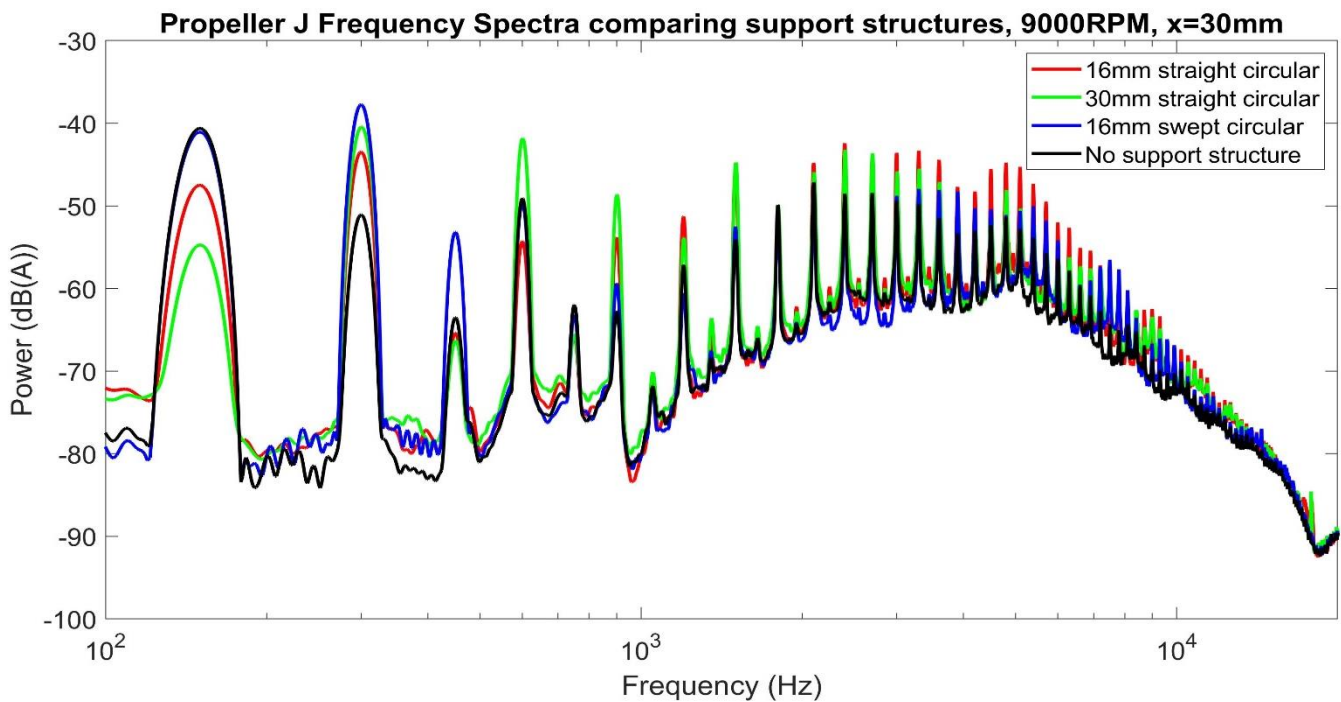


Figure 7 Spectra comparing different support structures at 30mm spacing for propeller J running at 9000 RPM

It is seen Figure 7 that at the blade passing frequency of 300 Hz, the peak SPL value of the spectrum for the case without the supporting structure is lowest. The peak SPL value of the spectrum for the case of the 30 mm outer diameter straight circular tube is larger than that for the case of the 16 mm outer diameter straight circular tube, the trend of which is consistent with that of the overall sound pressure level Figure 6. However, the 16 mm outer diameter swept circular tube induces the highest sound pressure peak value, which is different from the trend of the overall sound pressure levels from Figure 6. As the second order blade passing frequency of 300 Hz is our focused frequency. Therefore, it is believed that the 16 mm outer diameter swept circular tube induces the highest sound pressure peak value rather than the highest overall sound

pressure level. The sound pressure peak value at the second order blade passing frequency of 300 Hz is believed to be related to the blade aerodynamic noise component of the drone noise.

2.4 Flow Mapping

The velocity into, and out of, the propeller planes were mapped using a four-hole pressure probe known as a “Cobra” probe. The probe, a commercial product supplied by Turbulent Flow Instrumentation (TFI) (for overview see (Watkins, Mousely, & Hooper, 2002)), is capable of resolving the three orthogonal velocity components and local static pressure and is a robust and convenient alternative to hot-wire anemometry or PIV at the cost of a slight reduction in spatial and frequency resolution. The probe featured a 2.6mm head diameter with a pressure tap located on each of the surfaces of four faceted faces. The pressures from each tap are communicated to internal pressure transducers via 0.5mm ID tubing from which the velocities are calculated. This provides a robust system as the sensitive pressure transducers are removed from the pressure taps but introduces a distortion in frequency response and phase due to the tubing. This distortion is corrected in the TFI software using an inverse transfer function that is experimentally determined for each probe (for details see (Turbulent Flow Instrumentation Pty Ltd, 2018)). Each probe is factory calibrated with reliable performance for measuring velocity and flow angles up to 45° from the central axis yielding an effective cone of acceptance of $\pm 45^\circ$. In comparisons with hot-wire measurements, the TFI has a good verified dynamic response up to 1.5KHz (Mousley, Watkins, & Hooper, 1998).

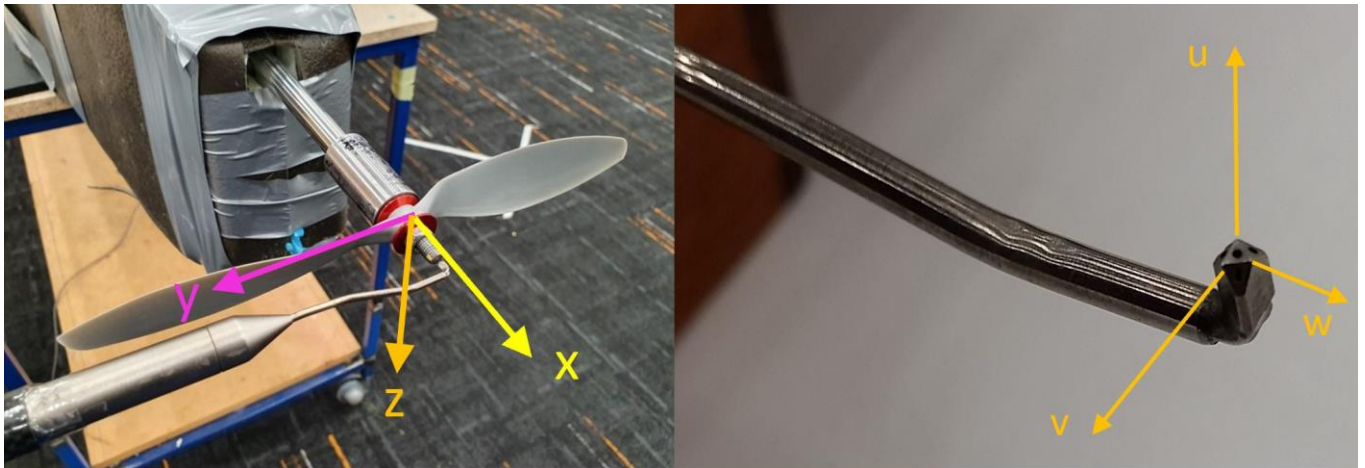


Figure 8 Left: axis direction for distance measurements. Cobra Probe traversed along y-axis (along propeller radius).
Right: Cobra Probe flow direction convention.

The probe was traversed from the propeller hub (centre) outwards in 10mm increments along the radius (y-direction), with the probe's u-axis aligned with the propeller x-axis. This measurement was taken at each position at a distance of 30mm downstream from the plane of rotation, similar to the method described in (Kloet, Watkins, & Wang, 2019).

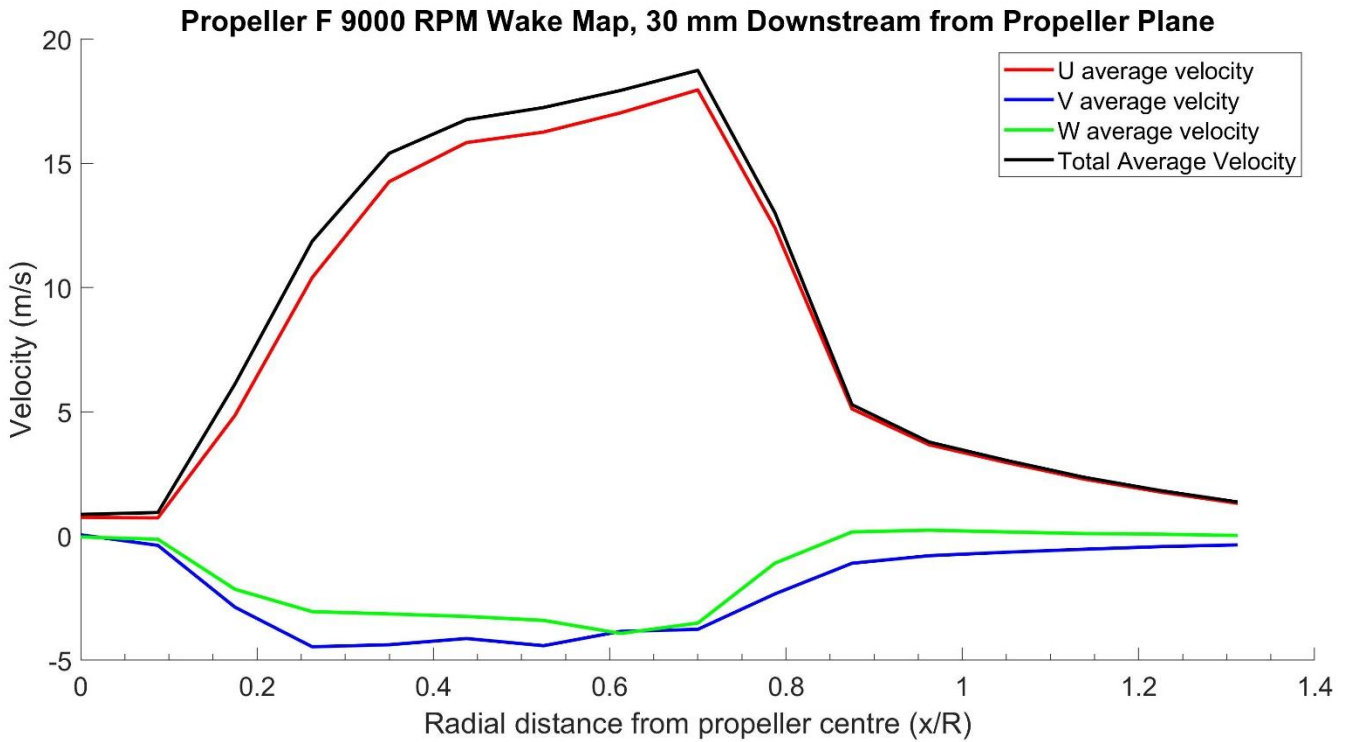


Figure 9 Time-averaged wake flow velocities for Propeller F at 9000 RPM, measured 30mm from propeller rotation plane, for different radial positions.

It is seen in Figure 8 that the U velocity component is dominant and is very close to the total velocity. The velocity component U and total velocity first increase with the radial distance from the propeller centre, reach the maximum values at a radial distance of $0.7R$ from the propeller centre, and then decrease with the distance. The V and W velocity components decrease with the radial distance from the propeller centre, reach their minimum values, then increase with the distance.

The flow information provided in Figure 10 and Figure 11 show that the flow is highly 3-dimensional in nature, with large amounts of swirl dependent on the direction of rotation of the propeller. It is seen Figure 11 that the time-averaged yaw and pitch wake flow angles first decrease with the radial distance from the propeller centre, reach minimum values at the radial distance of $0.18R$ from the propeller centre, then increase with the distance until reach the peaks at the distance of $0.45R$, then decrease with the distance until reach the other troughs, and then increase with the distance until reach the another peaks, finally decrease with the distance until reach the distance range limit of $1.3R$.

However examining the wake flows from Figure 9 to Figure 11 shows that the average flow velocity and direction varies considerably across the wake and is also turbulent. This investigation is ongoing as a part of a larger project.

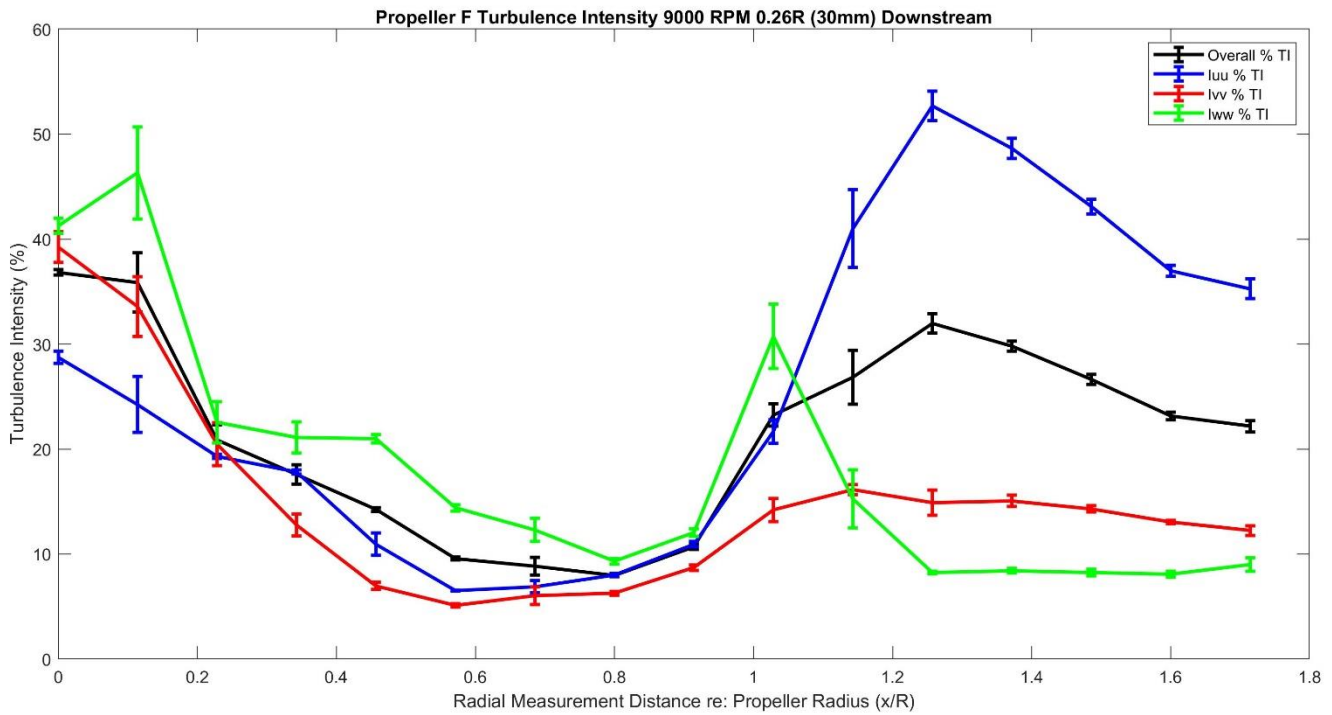
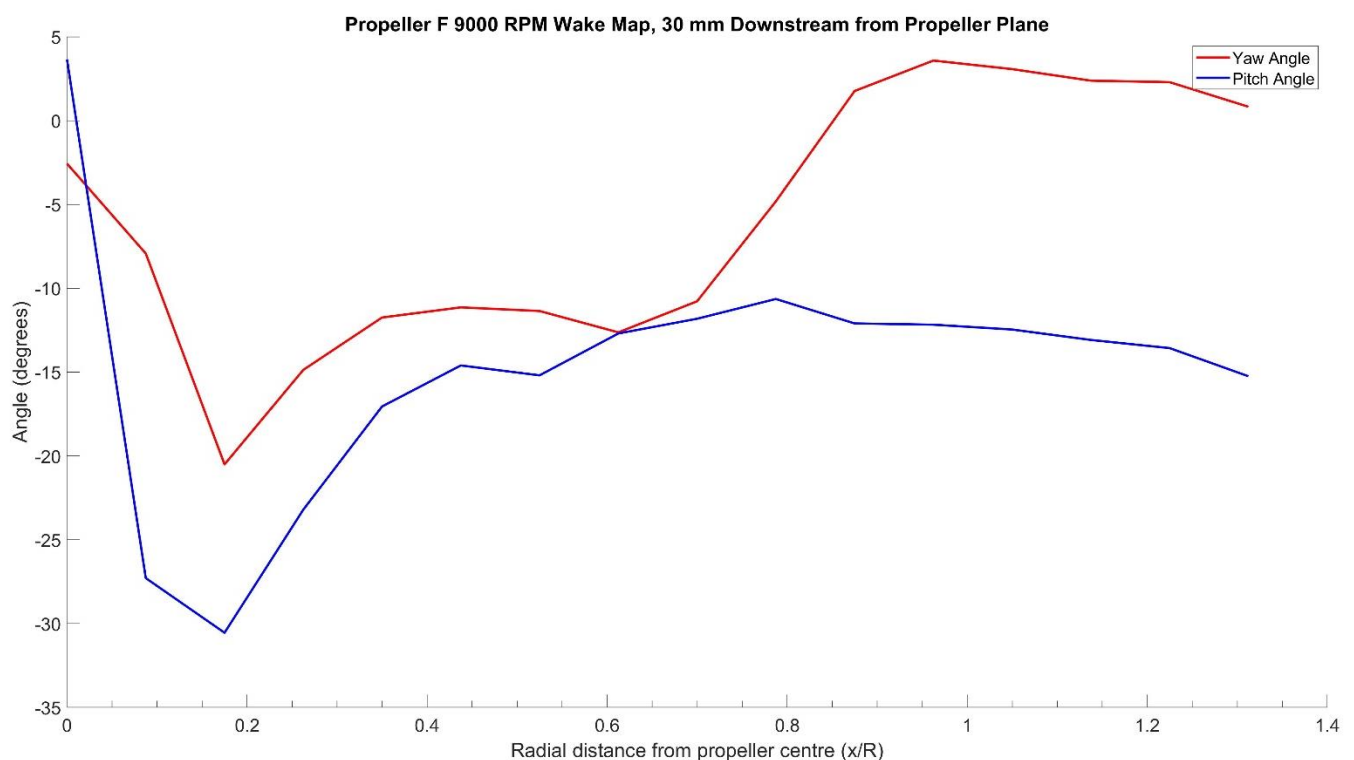


Figure 10 Percentage turbulence intensity for Propeller F at 9000 RPM as measured 30mm downstream from the propeller plane.

The turbulence intensity (indicating how unsteady the flow is) is lowest in the region where the overall flow velocity is highest. Moving in y-direction, you can see that the flow near the hub is, as expected, very low velocity and highly turbulent. As the main flow stream is traversed ($0.2 < x/R < 0.9$) the flow is of significantly higher velocity (Figure 9) and relatively smooth (shown by a low T.I. Percentage in Figure 10), and as the propeller tip is approached, the velocity drops significantly and the flow is relatively unsteady. Also note that the CP is a pressure-based velocity measuring instrument and so the accuracy for areas outside $0.2 < x/R < 0.9$ is reduced.



2.5 Methods to Minimise Noise from Support Structures

It is well known that bluff section cylinders (either square or circular such as drone support arms) shed vortices in smooth flow and that the resulting pressure fluctuations generate distinct tonal noise at frequencies that can be determined by the Strouhal Number.

$$St = \frac{N \cdot D}{U}$$

where N is the frequency of vortex shedding, D is the diameter, U is the mean flow velocity and St is the Strouhal Number. For circular cylinders the typical Reynolds numbers associated with these tests St is approximately constant at a value of 0.2, (Blevins, 1977). For square section cylinders the value varies between about 0.15 and 0.2 depending upon Reynolds number and orientation to the flow direction. Thus, the “extra” tonal noise sources can be predicted.

For the case of Propeller F, using an average wake flow velocity of 17.5 m/s and an approximate St value of 0.2, the predicted frequency is 219 Hz.

$$0.2 = \frac{N \cdot (0.016)}{17.5}$$

$$N = 219 \text{ Hz}$$

When comparing this to the blade passing frequency given by

$$BPF = \frac{n \cdot \omega}{60}$$

Where $n=2$ is the number of propeller blades and ω is the rotational speed (RPM). The predicted blade passing frequency for the same condition is 300Hz.

$$BPF = \frac{2 \cdot (9000)}{60}$$

$$BPF = 300 \text{ Hz}$$

This 300 Hz peak is visible in the spectral data for this condition for both the propellers (the case for Propeller F is shown in Figure 12), and an increase in the amplitude of this peak is clear when a supporting structure is introduced to the wake of the flow. The swept support structure demonstrates a larger peak than the straight structure at the blade passing frequency, however, the swept support structure induces a slightly lower sound pressure level than the straight support structure.

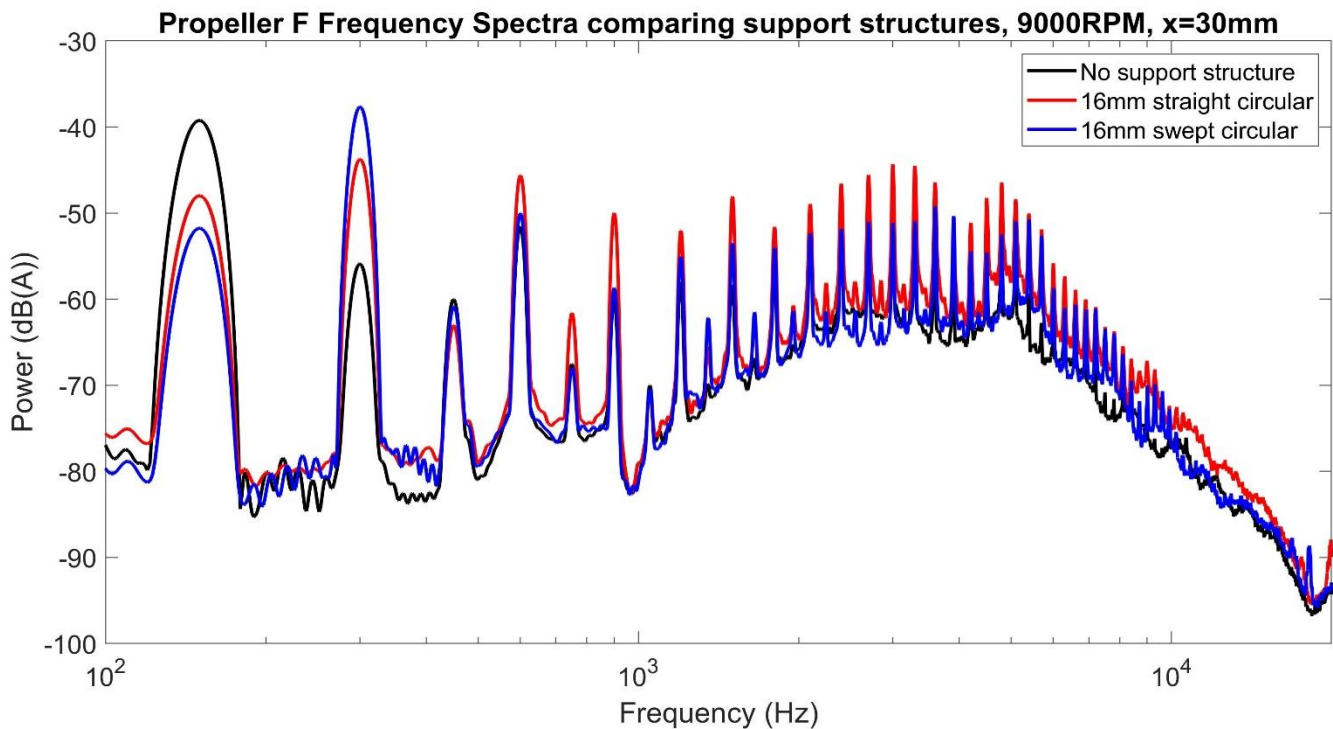


Figure 12 Frequency data for propeller F at 9000 RPM, comparing the acoustic spectra of a straight and swept supporting structure placed 30mm downstream.

There are similarities between drones and axial flow fans as both have support arms that bridge across the exhaust flow and support the motor. There is a large body of knowledge on how to make a low noise axial flow fan and some general rules from (Wallis, 2014). Very low noise fans are in mass production for a wide range of uses where low noise is highly desirable due to the proximity to humans (e.g. computer cooling and car radiator cooling fans etc). It is typical for such fans to not only have a different prime number of rotors and stators but also for the rotor, stator or both to be swept.

It is also relevant to note that a reduction of vortex shedding noise and vibration from bluff bodies can be achieved by reshaping the body to achieve streamlined flow and thus no periodic flow separation (e.g. by changing the shape to a aerofoil) or by reducing the 2-dimensional nature of the vortex shedding by putting strakes or spiral winds around a cylindrical structure (as evidence on stakes on circular chimney stacks and spiral winds around car radio antennae). Depending upon the level of tonal noise from flow interaction with the support structure these may be useful technique in the quest for even quieter drones.

3. Concluding Remarks

This study examined the acoustic effect of having a supporting structure in the wake of a multirotor propeller and investigated how the aerodynamics might affect these noise level outputs. Including a supporting structure of any sort slightly increases the overall sound pressure level, and the effect on sound generation can be altered by the distance the structure is placed away from the propeller rotation plane. There seems to be a limited effect on the sound due to the type of support structure used on the overall sound pressure level. Mapping of the propeller wakes indicated that the flows are highly 3D in nature, making it difficult to predict additional acoustic influences due to aerodynamic effects such as vortex shedding from the structure. This work is part of a larger project exploring a wider range of propellers and supporting structures. Additional flow mapping is also underway.

References

- Blevins, R. (1977). *Flow-induced Vibration*. New York: Van Nostrand Reinhold Co.
- Kloet, N., Watkins, S., & Wang, X. (2019). Aeroacoustic investigation of multirotor unmanned aircraft system (UAS) propellers and the effect of support structure. *InterNoise 2019* (pp. 3329-3340). Madrid, Spain: Institute of Noise Control Engineering.
- Mousley, P., Watkins, S., & Hooper, J. (1998). Use of a hot-wire anemometer to examine the pressure signal of a high-frequency pressure probe. *13th Australasian Fluid Mechanics Conference*, (pp. 395-399). Melbourne.
- Turbulent Flow Instrumentation Pty Ltd. (2018). *Cobra Probes*. Retrieved February 15, 2019, from <https://www.turbulentflow.com.au/Products/CobraProbe/CobraProbe.php>
- Wallis, R. (2014). *Axial Flow Fans: design and practice*. New York: Academic Press.
- Watkins, S., Mousely, P., & Hooper, J. (2002). Measurement of fluctuating flows using multi-hole probes. *Ninth International Congress on Sound and Vibration* (pp. 8-11). IIAV.



CidB

Centre d'information
sur le Bruit

QUIET DRONES
International e-Symposium
on
UAV/UAS Noise
Remote from Paris – 19th to 21st October 2020

Noise requirements of Unmanned Aircraft due to European Regulation 2019/945

Michael Wieland – michael.wieland@uavdach.org

Ronald Liebsch – ronald.liebsch@dji.com

Matthias Vyshnevskyy – matthias.vyshnevskyy@uavdach.org

1. Summary

The European Commission adopted the Regulation (EU) 2019/945¹ laying down the requirements for the design and manufacture of unmanned aircraft systems (UAS) intended to be operated under the rules and conditions defined in Implementing Regulation (EU) 2019/947². Before these UAS are made available on the EU market and put into service, they are required to pass CE certification. Sound power limits, the test code, and how the guaranteed sound power level is indicated for the consumer are included in the regulation (EU) 2019/945 and discussed in this report. Further, to specify design requirements and standard tests to comply with the regulation requirements, European Commission has requested CEN/CENELEC³ (delegated to ASD-STAN) to develop an EU harmonized Standard. The authors are members of the ASD-STAN D5 WG8 group Technical Report “TR Noise” and list findings to discuss the current regulation.

2. Background on EU Regulation 2019/945

Following the “basic regulation”⁴ (EU) 2018/1139, the delegated regulation (EU) 2019/945 and implementing regulation (EU) 2019/947 were adopted. These EU regulations adopted a risk-based approach for unmanned aircraft (UA) operations and as such do not distinguish between leisure or commercial activities. The regulations take into account the mass and specifications of the UAS and the operation the user intends to undertake. UAS whose operation under visual-line-of-sight (VLOS) conditions and below 25kg maximum take-off mass (MTOM) present the lowest risks belong to the ‘open’ category and may conduct operation without prior authorization by the competent authority⁵, and without submitting a declaration if operational and technical requirements are fulfilled.

UAS		Operation		Drone Operator/pilot		
Class	MTOM	Subcategory	Operational restrictions	Drone Operator registration	Remote pilot competence	Remote pilot minimum age
Privately built	< 250 g	A1 (can also fly in subcategory A3)	<ul style="list-style-type: none"> - may fly over uninvolved people (should be avoided when possible) - no fly over assemblies of people 	No, unless camera / sensor on board and a drone is not a toy	- no training needed	No minimum age
0					- read user's manual	16*, no minimum age if drone is a toy
Legacy drones (art. 20)						16*
1	< 900 g		<ul style="list-style-type: none"> - No expected fly over uninvolved people (if happens, should be reduced) - no fly over assemblies of people 	Yes	<ul style="list-style-type: none"> - read user's manual - complete online training - pass online theoretical exam 	16*
2	< 4 kg	A2 (can also fly in subcategory A3)	<ul style="list-style-type: none"> - no fly over uninvolved people - keep horizontal distance of 30 m from uninvolved people (it can be reduced to 5 m if low speed function is activated) 	Yes	<ul style="list-style-type: none"> - read user's manual - complete online training - pass online theoretical exam - conduct and declare a self-practical training - pass a written exam at the CAA (or at recognized entity) 	16*
3	< 25 kg	A3	<ul style="list-style-type: none"> - fly away from people - fly outside of urban area (150 m distance) 	Yes	<ul style="list-style-type: none"> - read user's manual - complete online training - pass online theoretical exam 	16*
4						
Privately built						
Legacy drones (art. 20)						

Figure 1 Drone requirements and limitations (source: EASA.europe.eu)

UAS design and operations should not be subject to 'traditional' aviation compliance procedures but must pass a certification process based on the CE principles defined in the EU Blue Guide⁶ for making products available on the EU market. The other two categories, 'specific' and 'certified' pose a higher risk and have therefore higher requirements. Technical requirements for UAS operated in the specific and certified category are still under development.

The 'open' category, also designated as category 'A', is further broken down into subcategories A1 to A3 of operations, where different kind of operational restrictions like "fly outside of urban areas" have been established. Within these subcategories, operational restrictions are linked to five different product classes C0 to C4 as shown in Figure 1. Whilst the subcategories mitigate the associated risk of operation by defining the required minimum distance to uninvolved persons and obligations with regards to the pilot (license, age, registration), the classes are basically related to the MTOM. For example, a UAS operated in subcategory A3 needs to stay 'far away' from people, and subsequently a C3 class UA does not need to be proven to be able to sustain flight loads and may literally fall apart at any time, because there will be no one around exposed to the hazard of being hit. Of course, such a UA is unlikely to become a commercial best-seller, but it is out of question that there is no over-regulation with regards to that.

Unfortunately, this is not the case with regards to noise as we will elaborate.

3. Technical Report Noise of ASD-STAN D5 WG8

For the 'open' category the rules for making UAS products available on the market shall be based on an assessment of the risk of operation and try to strike a balance between the obligations of UAS manufacturers and UAS operators in terms of safety, respect for privacy, the environment, protection against noise, and security⁷. Due to the demand to protect against noise, regulation (EU) 2019/945 includes requirements to measure the sound level of UA. For most UAS classes the regulation requires that the drone carries a label showing the guaranteed sound power level, and for some not to exceed certain sound levels.

Thereupon, the European Commission has requested a series of standards and technical reports⁸ on UAS classes to be used in the 'open' category in support of regulation (EU) 2019/945. These harmonized standards shall help to ensure a high level of safety in the operation of unmanned aircraft throughout the whole European Union. Given that such standards are, whenever possible, technology-agnostic and performance-based, they also promote equal conditions of competition among relevant economic operators dealing with UAS, in particular small and medium-sized enterprises. Indirectly, those standards also lead to lower production costs which benefits consumers in particular. It will give all Economic Operators (such as manufacturers, importers and distributors and their trade associations as well as bodies involved in the conformity assessment) a viable way to show compliance with the requirements as laid out in regulation (EU) 2019/945 and find commonality in compliance methods.

National UAS standardization bodies consolidate their opinions in ASD-STAN D5 WG8 to develop the requested harmonized set of standards and technical reports. It is planned to publish the first version of these standard as prEN 4709 series by mid 2021.

Noise minimization is an essential requirement mandated by Basic Regulation (EU) 2018/1139 for all kinds of aircraft, whether manned or unmanned. However, the noise test code, the noise limits and the definitions of the uncertainties used in regulation (EU) 2019/945 for the 'open' category have been inherited from the machinery directive 2000/14/EC⁹ and rely on internal production control using EN ISO 3744:2010¹⁰ to determine the noise emissions.

It shall be noted that directive 2000/14/EC itself is not listed amongst the applicable regulations dealing with unmanned aircraft – (EU) 2018/1139, 2019/947 and 2019/945 – and UAS in the 'open' category are thus neither implicitly nor explicitly considered as 'machines'. It shall be further noted that in accord with European Commission and EASA all safety of operation related aspects of UAS will be addressed either explicitly or by reference to IEC 62368-1¹¹ which is dealing with IT equipment rather than machinery.

ASD-STAN D5 WG8 is asked to deliver a Technical Report to the European Commission to discuss methods to improve the current requirements.

4. Noise test code of regulation (EU) 2019/945

Regulation (EU) 2019/945 lays down the requirements for the design and manufacture of unmanned aircraft systems intended to be operated in the open category. Part 13 describes the noise test code. For UA class C1, C2, C3 the manufacturer is required to determine the guaranteed A-weighted sound power level of the drone design.

To determine the A-weighted sound power level L_{WA} of a UA, the basic noise emission standard EN ISO 3744:2010 shall be used. The UA shall be hovering¹² 0.5m above a reflecting plane in the configuration as placed on the market. The UA shall be completely enclosed in a hemispherical measurement surface as par § 7.2.3 of EN ISO 3744:2010. Disregarding the shift of the noise source to 0.5m above ground, the measurement surface shall have its origin at the point O lying in the ground plane directly below the UA.

UA will be tested with and without accessories in all possible configurations.
 The European Commission defines sound power level L_{WA} as the A-weighted sound power in [dB] in relation to 1 pW as defined in EN ISO 3744:2010.

To determine the ‘measured sound power level’ the A-weighted surface time-averaged sound pressure level shall be determined at least three times for each UA configuration. If at least two of the determined values do not differ by more than 1 dB, further measurements will not be necessary. Otherwise, the measurements shall be continued until two values differing by no more than 1 dB are obtained. The surface time-averaged sound pressure level to be used for calculating the sound power level of a UA configuration is the arithmetic mean of the two highest values that do not differ by more than 1 dB.

The ‘guaranteed sound power level’ is determined in accordance with the requirements laid down in regulation (EU) 2019/945 Part 13 which includes the uncertainties due to production variation and measurement procedures. Within the CE conformity declaration, the manufacturer, or his authorized representative established in the community, confirms that according to the technical instruments applied and referred to in the technical documentation the guaranteed sound power level indicated is not exceeded.

The report shall contain the technical data necessary to identify the source under test as well as the noise test code and the acoustical data.
 The A-weighted sound power level value to be reported is the highest value of the different UA configurations tested rounded to the nearest whole number.

For multirotor UA of the open category, the European Commission defined the maximum sound power levels L_{WA} acceptable for UA of the class C1 and C2, while C3 have to indicate their sound power level only.

The maximum sound power levels will be reduced two years after entry into force, and again another two years later since the European Commission believes in technology development. Also, the Commission didn’t want to request the target value at once, to allow a fair and smooth transition phase for all UAS manufacturers.

Class C2 target will be limited to the target of C1, increased logarithmically to take the UA MTOM above 900gr into account (Figure 2).

PART 15

Maximum sound power level per class of UA (including transition periods)

UA class	MTOM m in gram	Maximum sound power level L_{WA} in dB		
		as from entry into force	as from 2 years after entry into force	as from 4 years after entry into force
C1 and C2	$m < 900$	85	83	81
C2	$900 \leq m < 4\,000$	$85 + 18,5 \lg \frac{m}{900}$	$83 + 18,5 \lg \frac{m}{900}$	$81 + 18,5 \lg \frac{m}{900}$

Where ‘lg’ is the base 10 logarithm.

Figure 2: Maximum sound power level for categories C1, C2 - (EU) 2019/945 amended by (EU) 2020/1058¹³

5. Findings and discussion about noise test code

UAS Industry involved in national standardization bodies discussed within ASD-STAN D5 WG8 working group the reliability and applicability of the sound power requirements. The critique focuses on the fact, that during normal operations with the UA maneuvering in all three dimensions, moving from one place to another, the noise emitted is not equal to the kind and level of noise the UA emits during hovering. Thus, the sound level reported does not reflect the performance of the UA during flight operations.

Further, it was noted that affected UA are typically operated 30-120m above persons (on the ground). Compared to lawnmowers, that operate within 2m to humans, the noise immersion for the operator and uninvolved people is much different, and in general much lower. Nevertheless, the noise limits for lawnmowers are much higher than those published for class C1 and C2 UA in (EU) 2019/945.

To reduce the noise of a UA, a manufacturer will need to change mass, material strength, size of propellers, rotation speed or velocity of the UA. In most cases, these changes reduce the safety buffers or discourage useful safety technology to be included in the UA.

Experts of the German Federal Ministry of Environment (UBA)¹⁴ have published a report in 2018, that complains about the decision to apply EN ISO 3744:2010 to measure the noise of UA. It states that UA have a wide range of different noise characteristics. The main noise components can be identified as the flow noise of the propeller blades. In addition to tonal components drone sounds can fluctuate in sound pressure level and be subjectively perceived as stutter, rattle, hum or hiss. Overall, the noise is strongly related to the flight mode of the drone. The performance during different power settings of the UA are not noticed by the current test code and lead to a misinformation of the consumer.

Hovering – ‘standing’ in the air - often has a completely different noise characteristic and composition than a fly-over or a turn. The noise ‘behavior’ changes significantly when a drone climbs, descends or changes direction of flight. The flight speed, the momentary wind force, the maneuvering load and acceleration also influence the noise ‘behavior’ of drones.

Tests show the various noise emission levels of UA available on the EU market (Figure 4).

Flight mode	No of tests	LAS MAX in db(A)	LWA in dB(A)	standard deviation
hovering 1.2m, microphone in 1.2m	9	57.8	83.3	0.9
hovering 8m, microphone in 5m	7	60.0	86.2	0.9
climbing from 1.2m to 8m, microphone in 3m	7	65.7	91.3	1.2
descending from 8m to 1.2m, microphone in 3m	10	66.0	91.5	0.8
passing in 5m, microphone in 1.2m	8	68.8	88.4	1.6
manoeuvring in 5m, microphone in 1.2m	7	73.8	93.4	1.3

Figure 3 Sound Power Levels of UA due to mode of operation (Source: UBA)

Julia Treichel and Steffen Körper of the UBA conclude that a suitable measuring method for determining a reproducible guaranteed sound power level within the framework of product approval is not yet available. The application of EN ISO 3744:2010, as requested by the EU Commission, only makes sense for hovering, i.e. the quietest operating condition. Besides, when measuring in enclosed spaces, many things such as the handling of the control unit, the dummy dimensions due to the directional characteristic or the size of the enveloping surface have not been conclusively clarified.

Further investigations are necessary to develop a uniform measurement procedure that also correctly represents the real emissions, whereby in particular measurements should be carried out in a reverberation chamber.

6. Findings of the Working Group TR Noise

While editing the technical report¹⁵ representatives of the UAS industry discussed findings beyond the test code. The EU commission excluded fixed wing UA from the sound level requirements which is against the fair EU market principle. Fixed wing and hybrid designs are arising, but an appropriate regulation is missing.

Also, the regulation does not define how to measure UA that are unable to hover. Many UA such as racing drones are unable to hover automatically. In addition, UA that rely on satellite navigation such as GPS cannot hover indoors, because closed rooms, reflection of buildings, and metal constructions obstruct satellite signals. Even the tripods of the microphone hemisphere could interfere with satellite signals and deny stable hovering of these UA.

In industrial areas outdoor testing of UA may be impacted by environmental noise. To determine the sound level EN ISO 3744:2010 requires a 10dB gap between expected noise level of the device test and the environmental noise. As seen in Figure 4 hovering is as quiet as $L_A=57,8 \text{ dB(A)}$. In an industrial area, UA manufacturer might not find an environment with $L_{A,env} \leq 47 \text{ dB(A)}$ for continuous control of their production.

Further, the working group for the technical report notes that there is no rationale for the noise limits imposed by regulation (EU) 2019/945. In particular, there are no studies on harmful effects of drone noise taking into account the different subjective perceptions of the 'behavior' of noise, not just on humans but also on wildlife.

Extra safety equipment adds weight to the UA. So, it is criticized that EU commission combined the noise limits with weight limits. Especially for class C1 where all UA between 250gr and 900gr are combined, this can lead to mismatches. A lighter UA without collision avoidance sensors will indicate lower noise emission values than a UA even of the same basic design with a lot of extra safety features that is heavier and thus louder.

Safety and privacy effects of noise have not been considered as well in the current regulation. Noise alerts humans and reduces accidents with UA or can avoid unaware recordings. Reducing the noise to a level, that is not louder than the environment might irritate humans as seen with electric cars. Low noise UA might be accused as spying tools. When very quiet UA appear near people who see but cannot hear the UA, it is expected that the reactions are rather negative.

Nevertheless, since 'open' category UA are limited to a maximum height above ground of 120m by law and forced to fly below this limit due to their application, noise level and the kind of sound emitted will influence acceptance and the operational approvals. In urban environments

and during the night, other limits are needed than industrial areas for safety inspection while the production machines are running next to it.

7. Conclusions

While it is undeniable that the test method required by regulation (EU) 2019/945 Part 13 can serve as to give an overall impression about the 'noisiness' of a product and allows to compare different products, it falls short of any assessment of operational noise levels.

Noise emissions and noise 'pollution' are relevant societal topics and the UA community should strive to find ways to define the right sound level for 'open' category operations and methods that allow fair and sustainable sound level measurements. The approach, to use a harmonized standard for open category UAS allows the manufacturer to produce cost-efficient UAS without assessing each device. Considering that regulation (EU) 2019/945 is adopted for the European mass market, for UAS which are used by consumers and professionals, the tool of a representative method to estimate the noise of a UA should not be changed.

Hovering condition to measure UA within a hemisphere as currently required by the regulation is one option. Working group TR Noise recommends evaluating indoor measurements using ISO 3745:2010. Also, ISO 3744:2010 Annex B should be considered as an applicable means to evaluate the sound power level in parallel to ISO 3744:2010 Annex F.

The working group recommends further research on noise level limits, the influence of UA noise on humans and wildlife, and noise 'pollution' of the environment when flying below 120m. The research should lead to an evaluation of current maximum sound levels. Also, the regulation should be extended and differentiate special operations. UA flown at night should meet different noise limits than UA used in industrial environments during working hours.

Finally, the Regulation (EU) 2019/945 applies for UAS of the 'open' category only. EC requested TR Noise group to provide proposals to improve the test code, and to adjust the noise limits. Experts are invited to consult working group to maximize the outcome of the TR Noise. For UAS of the specific and certified category TR Noise working group highly recommends defining new, more sophisticated test codes and noise limits, or to adjust existing codes for manned aircraft. The European Commission should prepare project funding for a set of research projects.

References

- ¹ COMMISSION DELEGATED REGULATION (EU) 2019/945 of 12 March 2019 on unmanned aircraft systems and on third-country operators of unmanned aircraft systems (OJ L 152, p.1); amended by COMMISSION DELEGATED REGULATION (EU) 2020/1058 of 27 April 2020
- ² COMMISSION IMPLEMENTING REGULATION (EU) 2019/947 of 24 May 2019 on the rules and procedures for the operation of unmanned aircraft (OJ L 152, p.45); amended by COMMISSION IMPLEMENTING REGULATION (EU) 2020/639 of 12 May 2020 and COMMISSION IMPLEMENTING REGULATION (EU) 2020/746 of 4 June 2020
- ³ CEN/CENELEC: European Committee for Standardization (CEN), the European Committee for Electrotechnical Standardization (CENELEC) <https://www.cencenelec.eu>
- ⁴ REGULATION (EU) 2018/1139 OF THE EUROPEAN PARLIAMENT AND OF THE COUNCIL of 4 July 2018 on common rules in the field of civil aviation and establishing a European Union Aviation Safety Agency, and amending Regulations (EC) No 2111/2005, (EC) No 1008/2008, (EU) No 996/2010, (EU) No 376/2014 and Directives 2014/30/EU and 2014/53/EU of the European Parliament and of the Council, and repealing Regulations (EC) No 552/2004 and (EC) No 216/2008 of the European Parliament and of the Council and Council Regulation (EEC) No 3922/91; SECTION VII „Unmanned aircraft“ and ANNEX IX „Essential requirements for unmanned aircraft“ (OJ L 212, 22.8.2020, p.1)
- ⁵ Source EASA: <https://www.easa.europa.eu/domains/civil-drones-rpas/drones-regulatory-framework-background> last check active 17.8.2020
- ⁶ EU Blue Guide: The ‘Blue Guide’ on the implementation of EU products rules 2016 (2016/C 272/01)
- ⁷ European Commission paves the way for safe, secure and green drone operations. 13.03.2020 https://ec.europa.eu/transport/modes/air/news/2019-03-12-drones_en last check active 17.08.2020
- ⁸ SHRAG: Draft standardisation request to the European Committee for standardisation as regards unmanned aircraft classes intended to be operated in the ‘open’ category of operations in support of Commission delegated Regulation (EU) 2019/945 of 12 March 2019 <https://ec.europa.eu/docsroom/documents/36363> last check active 17.08.2020
- ⁹ EU 2000/14/EC: Machinery directive of the European Parliament and of the Council of 8 May 2000 on the approximation of the laws of the Member States relating to the noise emission in the environment by equipment for use outdoors
- ¹⁰ EN ISO 3744:2010: Acoustics — Determination of sound power levels and sound energy levels of noise sources using sound pressure — Engineering methods for an essentially free field over a reflecting plane
- ¹¹ IEC 62368-1:2018 Audio/video, information and communication technology equipment - Part 1: Safety requirements
- ¹² ‘hovering’ means staying in the same geographical position in the air
- ¹³ COMMISSION DELEGATED REGULATION (EU) 2020/1058 of 27 April 2020 amending Delegated Regulation (EU) 2019/945 as regards the introduction of two new unmanned aircraft systems classes
- ¹⁴ Report about Investigation of noise of drones (german) <https://www.ingenieur.de/fachmedien/laermbekaempfung/laermschutz/untersuchung-der-geraeuschemission-von-drohnen/> last check active 17.8.2020



CidB

Centre d'information
sur le Bruit

QUIET DRONES
International e-Symposium
on
UAV/UAS Noise
Remote from Paris – 19th to 21st October 2020

3D Sound Source Tracking for Drones Using Direction Likelihood Integration

Taiki Yamada (Tokyo Institute of Technology): yamada@ra.sc.e.titech.ac.jp
Katsutoshi Itoyama (Tokyo Institute of Technology): itoiyama@ra.sc.e.titech.ac.jp
Kenji Nishida (Tokyo Institute of Technology): nishida@ra.sc.e.titech.ac.jp
Kazuhiro Nakadai (Tokyo Institute of Technology / Honda Research Institute Japan Co., Ltd.): nakadai@ra.sc.e.titech.ac.jp

Summary

In this paper, we present a 3D sound source tracking method by using multiple microphone arrays mounted to drones. Generally, microphone arrays have been utilized as a tool in signal processing for estimating a sound source direction. By mounting microphone arrays, drones will be able to search people calling for help in hazardous areas. However, the information of the sound source direction is insufficient to specify the sound source, which leads to the necessity to obtain the sound source location instead. Since it is difficult to obtain the 3D location using a single microphone array, recent studies show 3D sound source tracking based on triangulation techniques. In practice, due to large noise from a drone itself and unknown external noise, the direction estimation deteriorates. In addition, triangulation methods used in sound source location estimation is aggravated due to its discreteness. In this study, instead of triangulation, we propose to track the sound source location by estimating the likelihood distribution of the sound source location. Conventionally, when each microphone array localizes the sound source direction, it generally calculates the likelihood distribution of the sound source direction and takes the direction which has the highest likelihood. In our work, we propose to integrate the direction likelihoods of all microphone arrays and estimate the distribution of the location likelihood, rather than focusing only on the maximum likelihood. In this way, the sound source location distribution is represented in a non-Gaussian form, which is difficult via triangulation. The proposed method is evaluated through numerical estimation using real drone noise, comparing with other tracking methods based on triangulation. Simulation results demonstrates the effectiveness of the proposed method, which could track a 40 m far sound source with RMSE less than 4 m.

1. Introduction

In the field of acoustic scene analysis, localization of sound sources using microphone arrays has been actively studied, and it is expected to be a useful technique. For example, by combining with drones, drones can search for people buried under the rubble at the disaster site [1,2]. In general, a single microphone array is used to estimate the direction of the sound source, but instead of using a single microphone array, multiple microphone arrays allow us to estimate the sound source location by integrating estimated directions. One method for estimating sound source locations with multiple microphone arrays is shown by triangulation based on the sound source direction [3-5].

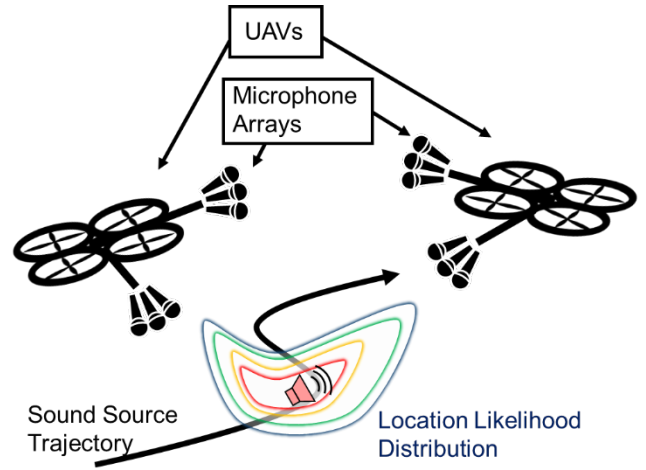


Figure 1 Overview of sound source tracking by microphone array mounted drones

However, when it comes to drone audition, sound sources to localize are far from drones in most cases, and drone noise may deteriorate direction estimation which worsens triangulations. Therefore, in this paper, we propose a sound source tracking method which localizes a sound source by estimating the distribution of location likelihood rather than estimating directions. In this way, the sound source location can be represented in a generic form and can be determined by information of all microphone arrays rather than pairs of microphone arrays. The rest of this paper is organized as follows. Section 2 explains the proposed method, and Section 3 evaluates the method through numerical simulations. The last section gives conclusions and future work.

2. Sound Source Tracking

This section proposes a sound source tracking method based on location likelihood estimation. The likelihood distribution of the location is obtained by integrating the likelihood distribution of sound source directions.

2.1 Settings

We consider tracking a sound source by multiple microphone arrays. We assume that N microphone arrays are mounted to drones which are numbered as follows.

$$MA_1, \dots, MA_N$$

The state of the n -th microphone array MA_n is described as below, and assumed as known.

$$\mathbf{m}_n(t) = [\mathbf{m}_{n,xyz}^T(t), \quad \mathbf{m}_{n,\phi\theta\psi}^T(t)]^T \quad (1)$$

$$\mathbf{m}_{n,xyz}^T(t) = [x_n(t), y_n(t), z_n(t)]^T \quad (2)$$

$$\mathbf{m}_{n,\phi\theta\psi}^T(t) = [\phi_n(t), \theta_n(t), \psi_n(t)]^T \quad (3)$$

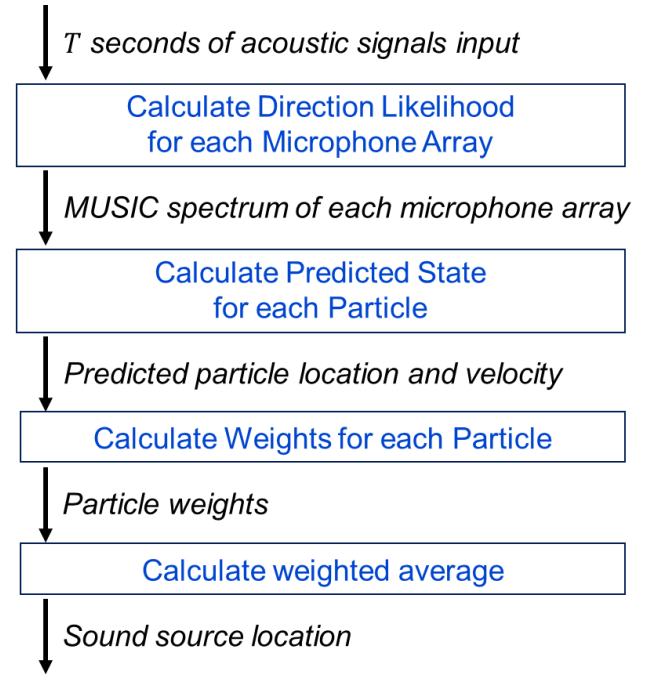
$x_n(t)$, $y_n(t)$, and $z_n(t)$ indicate the center of MA_n in the three dimensional coordinates and $\phi_n(t)$, $\theta_n(t)$, and $\psi_n(t)$ indicate the three dimensional rotational angles of MA_n . Each microphone array consists of M microphones. We assume the sound source to be a point source, and its location is described as below.

$$\mathbf{e}(t) = [x_e(t), y_e(t), z_e(t)]^T \quad (4)$$

The problem addressed in this paper is to estimate the sound source trajectory by estimating the sound source location $\mathbf{e}(t)$ from the n -th microphone array state $\mathbf{m}_n(t)$ and recorded sound signal at every T seconds.

2.2 Tracking method outline

This method is based on the integration of the direction likelihood distributions obtained by source direction estimation. In most cases, direction estimation methods calculates the likelihood $P(\phi, \theta)$ for each azimuth ϕ and elevation θ , and assume the direction with the largest $P(\phi, \theta)$ is the sound source direction. The approach of this method is to estimate the sound source location by converting the direction likelihood $P(\phi, \theta)$ of each microphone array into the likelihood of a three-dimensional location. Figure 2 illustrates a procedure of the proposed tracking method. This method estimates the sound source trajectory through particle filtering with each particle being given the location likelihood as its weight.



2.2.1 Estimation of direction likelihood distribution

There are indicators that can be regarded as likelihoods for sound source direction. The CSP (Cross-power Spectrum Phase) coefficients used in the CSP method [6], which is a method for estimating the Time Difference Of Arrival (TDOA) with two microphones, and the spatial spectrum obtained from the Delay-and-Sum beamformer includes scalar quantities whose parameters are the sound source direction, and they generally have a peak in the direction of the source [7]. In this paper, we use a MUSIC spectrum, which produces sharp peaks in the direction of the sound source, as the direction likelihood. The MUSIC method (MULTiple Signal Classification method) analyses the eigenspace of the spatial correlation matrix and estimates the source azimuth and elevation by using the orthogonality between the subspaces of the target sound source and the noise [10]. Let $\mathbf{a}(\omega, \phi, \theta) \in \mathbb{C}^M$ be the transfer function of a sound signal of a frequency component ω from a direction (ϕ, θ) , then the spatial spectrum which is known as MUSIC spectrum can be expressed as,

$$P(\phi, \theta) = \frac{1}{\omega_H - \omega_L + 1} \sum_{\omega=\omega_L}^{\omega_H} \frac{\mathbf{a}(\omega, \phi, \theta)^H \mathbf{a}(\omega, \phi, \theta)}{\mathbf{a}(\omega, \phi, \theta)^H \mathbf{E}_N(\omega) \mathbf{E}_N(\omega)^H \mathbf{a}(\omega, \phi, \theta)}, \quad (5)$$

where \mathbf{E}_N is the matrix consists of eigenvectors of the noise subspace of spatial correlation matrix. In general, the sound source direction is considered to be the direction where the MUSIC spectrum has peaks when estimating the direction. In this paper we regard the MUSIC spectrum as a direction likelihood of the sound source and we integrate the MUSIC spectrum obtained from each microphone array and convert them into a location likelihood of the sound source.

2.2.2 Converting to location likelihood distribution

Let $P_n(\phi, \theta)$ be the MUSIC spectrum calculated from MA_n . We express the likelihood distribution of the sound location by simply summing $P_n(\phi, \theta)$. Let an arbitrary three dimensional location be \mathbf{x} , and direction from \mathbf{x} to \mathbf{m}_n be (ϕ_n, θ_n) . Then, the location likelihood L at a location \mathbf{x} is described as following.

$$L(\mathbf{x}) = \sum_n P_n(\tilde{\phi}_n^{\text{round}}, \tilde{\theta}_n^{\text{round}}), \quad (6)$$

$$\tilde{\phi}_n^{\text{round}} = \text{round}(\tilde{\phi}_n), \quad \tilde{\theta}_n^{\text{round}} = \text{round}(\tilde{\theta}_n), \quad (7)$$

$$\begin{bmatrix} \cos \tilde{\phi}_n \cos \tilde{\theta}_n \\ \sin \tilde{\phi}_n \cos \tilde{\theta}_n \\ \sin \tilde{\theta}_n \end{bmatrix} = \mathbf{R}_n^{-1} \begin{bmatrix} \cos \phi_n \cos \theta_n \\ \sin \phi_n \cos \theta_n \\ \sin \theta_n \end{bmatrix}, \quad (8)$$

where $\text{round}(\cdot)$ is a function that rounds the direction according to the resolution of transfer function $\mathbf{a}(\omega, \phi, \theta)$ and \mathbf{R}_n is the rotation matrix representing the posture of MA_n . In other words, location likelihood $L(\mathbf{x})$ is the summation of direction likelihoods corresponding to directions towards \mathbf{x} seen from each microphone array.

2.2.3 Tracking based on location likelihood distribution

Finally, this method tracks the sound source location by particle filtering using $L(\mathbf{x})$. Let I be the number of particles, and \mathbf{x}_k^i, w_k^i be respectively the state and weight of the i -th particle. The state \mathbf{x}_k^i includes the location and the velocity of particle i .

$$\mathbf{x}_k^i = [x_k^i, y_k^i, z_k^i, \dot{x}_k^i, \dot{y}_k^i, \dot{z}_k^i]^T. \quad (9)$$

We use an excitation-damping model for prediction model [9].

$$\mathbf{x}_k^i = F \mathbf{x}_{k-1}^i + H \mathbf{v} \quad (10)$$

$$F = \begin{bmatrix} \mathbf{I} & T\mathbf{I} \\ \mathbf{0} & a\mathbf{I} \end{bmatrix}, \quad H = \begin{bmatrix} \mathbf{0} \\ b\mathbf{I} \end{bmatrix}, \quad (11)$$

$$\mathbf{v} \sim \mathcal{N}(\mathbf{0}, \mathbf{I}), \quad (12)$$

where $\mathbf{I} \in \mathbb{R}^3$ is an identity matrix and $\mathbf{0}$ is a zero matrix. Each particle gains weight proportional to $L(\mathbf{x}_{k,pos}^i)$, hence

$$w_k^i = w_{k-1}^i \frac{L(\mathbf{x}_{k,pos}^i)}{\sum_i L(\mathbf{x}_{k,pos}^i)}, \quad (13)$$

where $\mathbf{x}_{k,pos}^i = [x_k^i, y_k^i, z_k^i]^T$.

Resampling is necessary if effective particles are lesser than threshold N_{thr} . Hence, when

$$\frac{1}{\sum_i (w_k^i)^2} \leq N_{thr} \quad (14)$$

satisfies, weights of all particles will be reset to $1/I$.

Initialization of the particles is done by sampling from the distribution below.

$$\mathbf{x}_0^i \sim \mathcal{N}(\boldsymbol{\mu}_0, \boldsymbol{\Sigma}_0), \quad (15)$$

$$\boldsymbol{\mu}_0 = [\boldsymbol{\mu}_{0,pos}, 0, 0, 0]^T, \quad (16)$$

$$\boldsymbol{\Sigma}_0 = \begin{bmatrix} \sigma_{pos}^2 \mathbf{I} & \mathbf{0} \\ \mathbf{0} & \sigma_{vel}^2 \mathbf{I} \end{bmatrix}, \quad (17)$$

where $\boldsymbol{\mu}_{0,pos}$ is derived by performing triangulation based on direction estimation [4, 5]. After calculating the triangulation points, we can make the average point of them into $\boldsymbol{\mu}_{0,pos}$.

3. Evaluation

To evaluate the effectiveness and the performance of the proposed method, numerical simulation was performed by MATLAB.

3.1 Setup

We consider a scenario shown in Figure 3. There are two drones (black dots) with two microphone arrays (black circles) mounted on them, and both drones are hovering still at a height of 30 m. The target sound source to track is moving on a circle with a radius of 5 meters at a height of 1 meter. The velocity of the sound source is constantly π m/s. The horizontal distance between drones and the origin of coordinates are $l = 10, 20, 30, 40, 50$ m. Each microphone array is a sphere-shaped microphone array consisting of $M = 16$ microphones (Figure 4), and they record sound signals at 16 kHz, 24 bits. We estimate the sound source location every $T = 0.2$ seconds and track the sound source for 10 seconds. The MUSIC spectrum is calculated in 5-degree increments for both azimuth and elevation angles. Other parameters for the proposed method are listed in Table 1. We simulated 10 male voices, 10 female voices, and 10 white noise each, for a total of 30 different sounds. We also compare the tracking performance to two other methods. One is applying Kalman filtering to the average point of triangulation points [8], and another is performing particle filtering based on estimated directions [9].

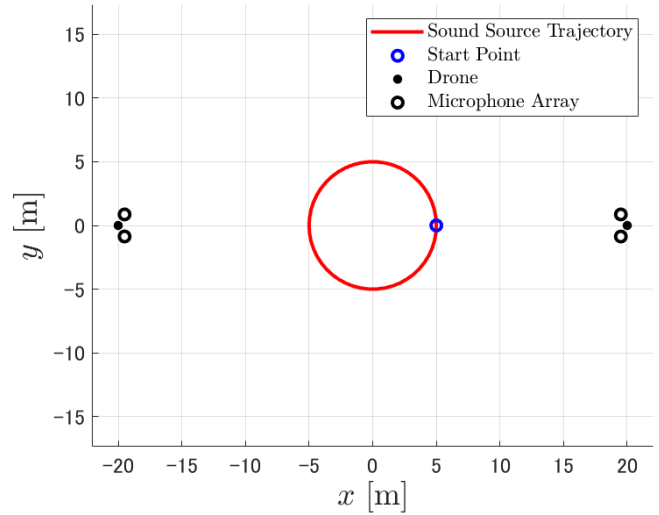


Figure 3 Top view of simulation scenario ($l = 20$ m)

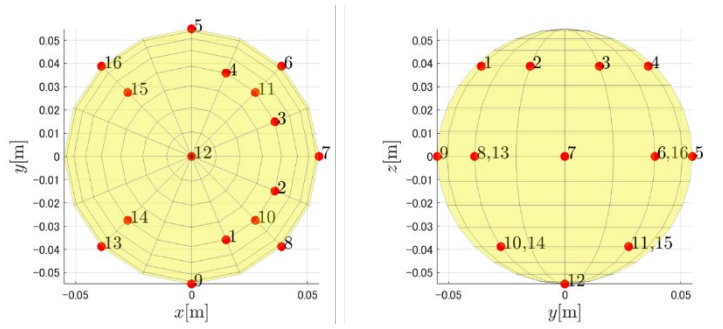


Figure 4 Location of the microphones in a microphone array

Table 1 List of variables used for sound source tracking

Variables	Value
a	0.5
b	3
I	500
N_{thr}	350
σ_{pos}^2	25
σ_{vel}^2	25

3.2 Results

Simulation results are shown in Figures 5 and 6. We can see from both figures that the proposed method is able to track a sound source. The first estimation is large especially in z direction. This is because the triangulation for initialization is unstable due to drone noise and the initial location is not near to the sound source. However, the proposed method seems to converges to the

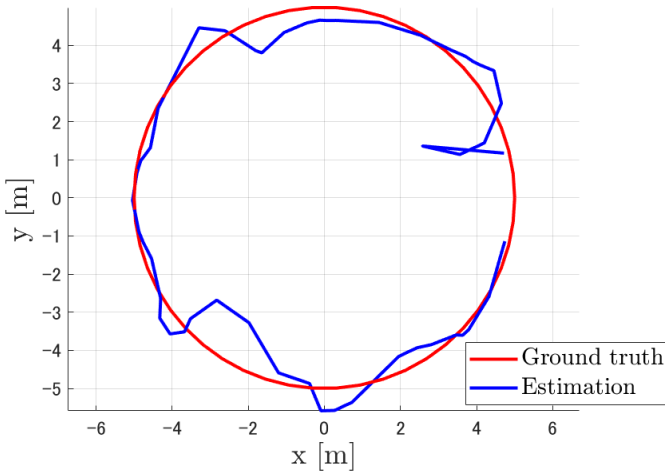


Figure 5 Top view of estimated trajectory

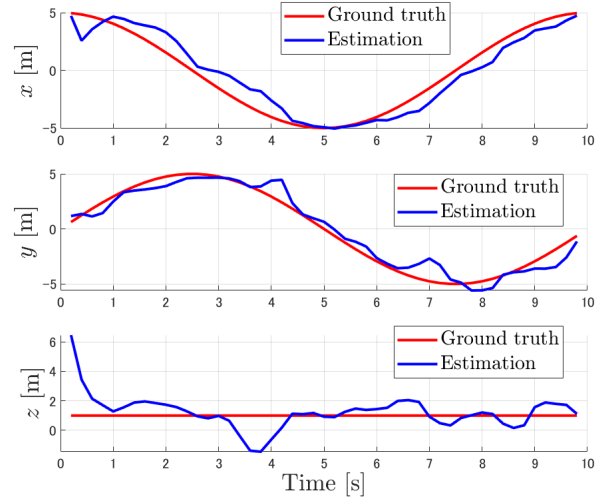


Figure 6 Location of estimated trajectory

ground truth despite the initial state. The tracking error is shown in Tables 2-4. Tables compare Root Mean Squared Error (RMSE), which is defined as below,

$$\text{RMSE} = \sqrt{\frac{1}{K} \sum \text{error}^2}, \quad (18)$$

where the error is the Euclidean distance between the estimated location and the ground truth and $\sum \text{error}^2$ is the sum of squares of all errors through 10-second simulation. K is the number of time steps through one simulation. We can see from Tables 2-4 that the proposed method tracked the sound source with least error in most cases compare to other methods. Since the proposed method tries to estimate the location likelihood instead of computing triangulation points, it is less affected by outliers of triangulation points, which could be seen from the results. We can also see that the RMSE increases as the horizontal distance becomes long, this is because the direction likelihood has a resolution, which also makes the location likelihood discrete. This discreteness will be noticeable as the sound source distance increases and worsens the location likelihood accuracy, which leads to high tracking error.

Table 2 Tracking RMSE in meters for each distance (Female voice)

	10 m	20 m	30 m	40 m	50 m
Proposed method	1.66	2.43	1.75	2.89	5.61
Method [8]	12.47	13.76	14.15	14.68	16.43
Method [9]	4.97	4.01	3.85	4.30	5.69

Table 3 Tracking RMSE in meters for each distance (Male voice)

	10 m	20 m	30 m	40 m	50 m
Proposed method	4.80	4.10	4.18	3.92	4.32
Method [8]	12.47	13.76	14.34	15.17	16.27
Method [9]	4.77	4.20	3.98	4.26	5.32

Least RMSE is written in red

Table 4 Tracking RMSE in meters for each distance (White noise)

	10 m	20 m	30 m	40 m	50 m
Proposed method	1.81	2.39	1.93	2.26	2.95
Method [8]	8.73	10.57	10.87	11.16	11.32
Method [9]	2.14	1.81	2.14	2.55	3.66

Least RMSE is written in red

4. Conclusions

In this paper, a sound source tracking method is proposed by integrating the direction likelihoods of the sound source into a location likelihood. The location likelihood is obtained by summing the direction likelihoods of microphone arrays. The proposed method is evaluated by numerical simulation, and it was found that the proposed method can track a moving sound source with error less than 4 m of RMSE for sound sources 40 m away. Evaluation in real-world environments is an issue for the future.

Reference

- [1] Nakadai, K. *et al.* (2017) *Development of microphone-array-embedded UAV for search and rescue task* 2017 IEEE International Conference on Intelligent Robots and Systems (IROS), pp. 5985–5990
- [2] Washizaki, K., Wakabayashi, M., and Kumon, M. (2016) *Position estimation of sound source on ground by multirotor helicopter with microphone array* 2016 IEEE/RSJ International Conference on Intelligent Robots and Systems (IROS), pp. 1980-1985
- [3] Brandstein, M. S., and Silverman, H. F. (1997). *A practical methodology for speech source localization with microphone arrays* Computer speech & language, 11(2), 91-126.
- [4] Gabriel, D., Kojima, R., Hoshiba, K., Itoyama, K., Nishida, K., and Nakadai, K. (2019). *2D sound source position estimation using microphone arrays and its application to a VR-based bird song analysis system* Advanced Robotics, 33(7-8), pp. 403-414.
- [5] Yamada, T., Itoyama, K., Nishida, K., and Nakadai, K. (2020). *Sound Source Tracking by Drones with Microphone Arrays* IEEE/SICE International Symposium on System Integration (SII), pp. 796-801
- [6] Knapp, C., and Carter, G. (1976). *The generalized correlation method for estimation of time delay* IEEE transactions on acoustics, speech, and signal processing, 24(4), pp. 320-327.
- [7] Valin, J. M., Michaud, F., and Rouat, J. (2006). *Robust 3D localization and tracking of sound sources using beamforming and particle filtering* 2006 IEEE International Conference on Acoustics Speech and Signal Processing Proceedings (Vol. 4, pp. IV-IV).
- [8] Potamitis, I., Chen, H., and Tremoulis, G. (2004). *Tracking of multiple moving speakers with multiple microphone arrays* IEEE Transactions on Speech and Audio Processing, 12(5), pp. 520-529.
- [9] Lauzon, J. S., Grondin, F., Létourneau, D., Desbiens, A. L., and Michaud, F. (2017). *Localization of RW-UAVs using particle filtering over distributed microphone arrays* 2017 IEEE/RSJ International Conference on Intelligent Robots and Systems (IROS) (pp. 2479-2484)
- [10] Schmidt, R. (1986). *Multiple emitter location and signal parameter estimation*. IEEE transactions on antennas and propagation, 34(3), pp. 276-280.



CidB

Centre d'information
sur le **Bruit**

**QUIET DRONES
International e-Symposium
on
UAV/UAS Noise
Remote from Paris – 19th to 21st October 2020**

Experimental Investigation of Noise Characteristics of Rotors

**Koichi Yonezawa, Central Research Institute of Electric Power Industry,
Center of Aerial Intelligent Vehicle, Chiba University, Japan:
koichi-y@criepi.denken.or.jp**

**Eiji Shima, Japan Aerospace Exploration Agency, Japan
Toshiyuki Nakata, Faculty of Engineering, Chiba University, Japan
Hao Liu, Faculty of Engineering, Chiba University, Japan
Yasutada Tanabe, Japan Aerospace Exploration Agency, Japan
Shigeru Sunada, Nagoya University, Japan
Hiroshi Tokutake, Kanazawa University, Japan**

Summary

Rotors for multi-rotor-type UAVs are required to be silent as well as highly efficient. Safety is also important. In the present study, ducted rotors were examined experimentally. In experiments, rotor thrust, aerodynamic torque and noise were measured. The following blade designs were examined in experiment: two kinds of two-bladed rotors with untwisted and twisted blades with a variable corrective pitch mechanism. One kind of the rotor duct geometry was examined. Although the duct increased the figure of merit of the rotor during hovering, the noise was also increased. Then the Helmholtz resonators were equipped on the duct wall and tested. The results showed that the noise increased as the rotational frequency increased, or the rotor duct was used. The Helmholtz resonator was not effective to suppress the noise. The influences of the blade twist, difference in the airfoil were also less than that of the rotational frequency.

1. Introduction

Multi-rotor-drones have been used in various field such as aerial photography, measurement, transportation, and disaster recovery. The drones are required to be highly efficient, safe, and silent. In order to improve the aerodynamic efficiency of the rotor, the ducted rotors were examined as well as the blade design (Avanzini et al. (2003), Ohanian III et al. (2011), Pflimlin

(2009), Penkov (2017), Tanabe et al (2019), Yonezawa et al. (2016,2017,2019)). The safety of the drone flight can be enhanced by improving flight control and navigation systems. In addition, high maneuverability of the aircraft should be important. In a series of our research and development, a quad-rotor-drone was developed. The rotor had a variable corrective pitch mechanism to improve the maneuverability. The rotor duct can be added as shown in Figure 1. It was confirmed that the aerodynamic efficiency of the rotor, the figure of merit was improved using the rotor duct as previously reported by several researchers. However, the noise level was also increased using the rotor duct. Loud noises of the rotor can disturb surrounding environment and can prevent missions of the drone itself. Therefore, it is quite important to reduce the noise. It is also important to understand the noise characteristics and mechanisms in order to realize the noise reduction (Tinney and Sirohi (2018)). In the present study, the noise characteristics of the ducted rotor were examined. Two kinds of blade design and a rotor duct were tested.

2. Experimental Method

2.1 Design of Blades and Duct

Two kinds of the rotor blades were tested: one was untwisted blade and the other was twisted blade. Geometries and design parameters were presented in Figure 2 and Table 1. Using the variable corrective pitch mechanism, the blade pitch angle could be changed between -20° and 20° . The rotational frequency of the rotor was fixed at 90 Hz during the flight and the thrust was adjusted by changing the blade pitch angle. The blades were made of carbon carbon fibre reinforced plastic (CFRP).



Figure 1 Quad rotor with ducted rotor (left) and variable corrective pitch mechanism



Figure 2 Blade geometries. untwisted blade (left) and twisted blade (right)

Table 1 Design parameters of rotor blades

	Untwisted blade	Twisted blade
Radius, R (m)		0.1905
Blade root chord length (m)		0.0665
Blade tip chord length (m)		0.0402
Rotational frequency, N (Hz)		90
Number of blades		2
Airfoil	NACA0009	OAF117
Twist angle (degree)	0	-21 (linear)
Tip clearance (m)		0.001 (0.0052 R)

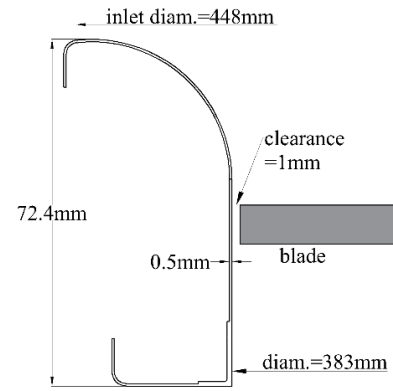
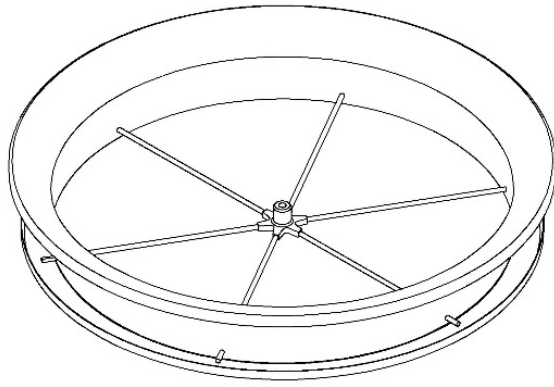


Figure 3 Geometry of the rotor duct

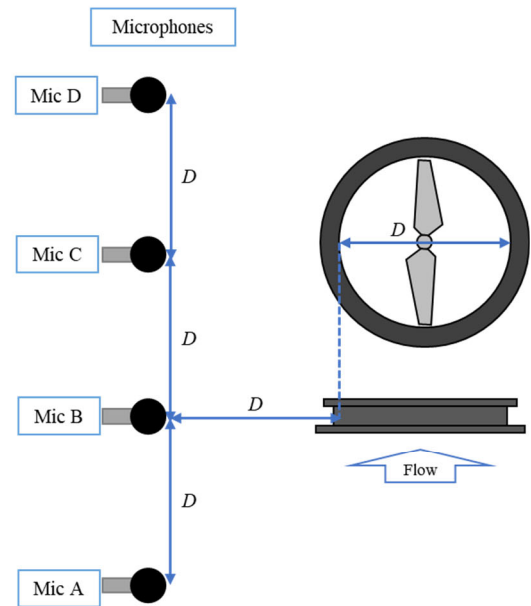
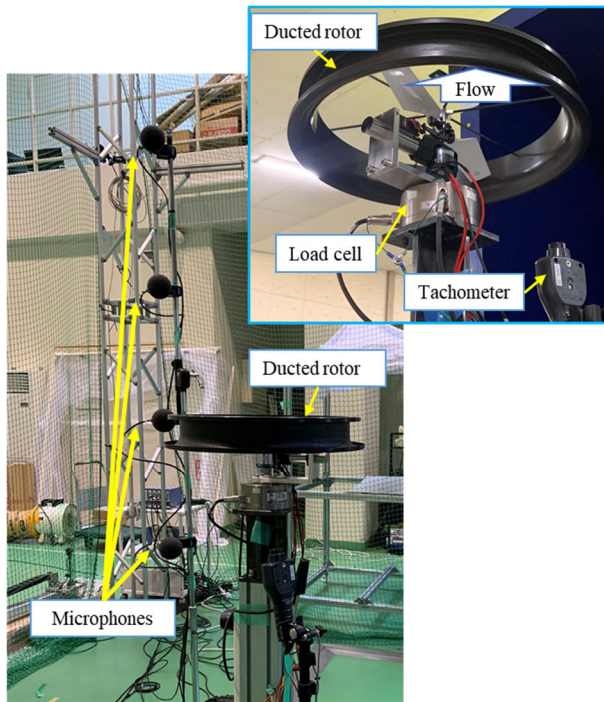


Figure 4 Experimental apparatus using variable pitch rotor unit

Figure 3 shows the geometry and main dimensions of the rotor duct. The duct was made of thin CFRP to reduce the mass. The total mass of the drone was 7.9 kg, which included the airframe, a Li-Po battery (6 cells, 10000mAh), and four ducts, and the mass of one duct was 0.165 kg. The duct was attached on the motor axis using a ball bearing. The duct can rotate with the rotor blades, but the rotational speed of the duct was much smaller than the blade rotation speed.

2.2 Measurement of Aerodynamic Forces and Noises Using Variable Pitch Rotor

Experiments were carried out using a single rotor, which was the same with that mounted on the quad-rotor-drone. The experimental apparatus is shown in Figure 4. The aerodynamic forces, thrust and axial torque were measured using a 6-component load cell. The rotor corrective pitch and the rotational speed were variable. Aerodynamic noise was measured using 4 microphones. The location of each microphone was shown in Figure 4. Mic A and B was located at upstream and the side of the rotor, respectively. Mics C and D were at downstream side. The experimental apparatus was put in a room and the noise could reflect on the room walls. The aerodynamic forces and noises were measured using a data recorder (Kyowa Electric Instruments, EDX-100A) with 20 kHz of sampling rate. Duration of each measurement was 10 s. The time-mean aerodynamics forces and allpass A-weighted sound pressure levels, L_{As} were estimated.

Table 2 Test conditions

Rotor configuration	Untwisted blade (UT)	without duct (open)
	Untwisted blade (UT)	ducted
	Twisted blade (T)	without duct (open)
	Twisted blade (T)	ducted
Fixed rotational freq., N	98 Hz	Thrust = 1.5, 1.75, 2, 2.25, 2.5 (kgf) =15,17, 20, 22, 25 (N)
	80 Hz	
Fixed corrective pitch	13.2 degree (UT-Open)	N = 50, 60, 70, 75, 80, 90 Hz
	12.8 degrees (UT-Ducted)	
	7.3 degree (T-Open)	
	8.6 degrees (UT-Ducted)	

Spectral analyses of the A-weighted sound waves were also carried out. Experiments were carried out at various conditions shown in Table 2.

2.3 Measurement of Aerodynamic Forces and Noises Using Small-Scale Rotor

The small-scale models were used to examine the method to noise reduction. The rotor blades and the duct were made using 3-D printers. The rotor radius was 0.1 m, which was 1/2 of the original rotor. The duct geometry was thick enough to consider to be rigid and the contour of the inner wall contour was similar to the original one. The experiments using the small-scale models were carried out in a soundproof room. The locations of the microphone were determined by the same manner with that in Figure 4.

As a noise reduction device, Helmholtz resonators were put on the duct wall as shown in Figure 6. The number of resonators was 300 and the resonance frequency was 1300 Hz.

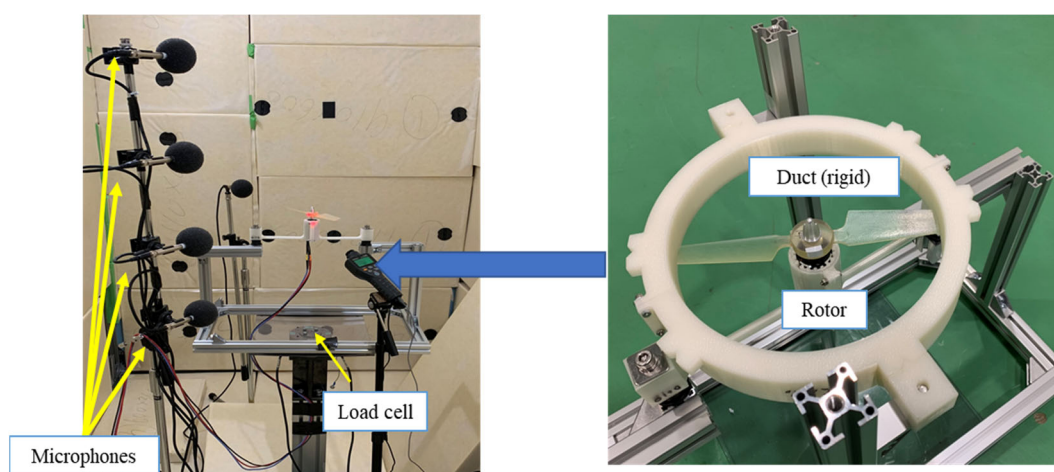


Figure 5 Small-scale test model

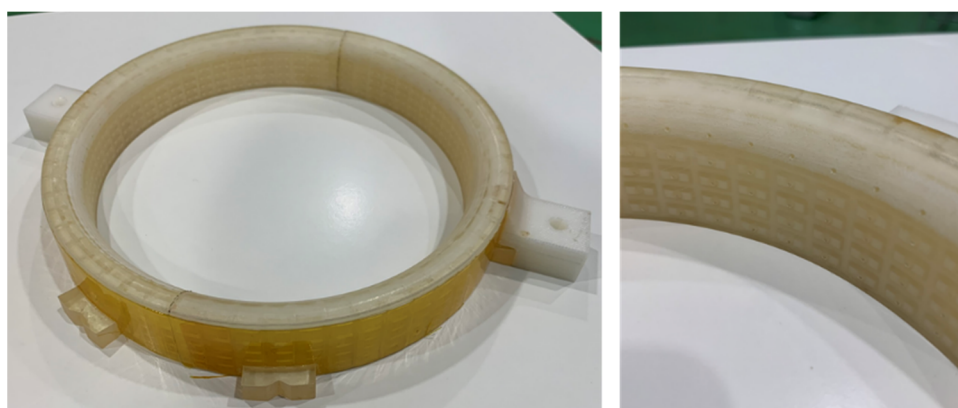


Figure 6 Duct with Helmholtz resonators

3. Result and Discussions

3.1 Experimental Results Using Variable Pitch Rotor

Aerodynamic characteristics of each rotor configuration were compared. The thrust and axial torque were normalized as follows:

$$\text{Thrust coefficient: } C_T = \frac{\text{Thrust}}{\rho (R\Omega)^2 \pi R^2} \quad (1),$$

$$\text{Torque coefficient: } C_Q = \frac{\text{Toque}}{\rho (R\Omega)^2 \pi R^3} \quad (2),$$

where, ρ , R , Ω are air density, radius of the rotor, and angular velocity of the rotor, respectively. Figure of merit, which is aerodynamic efficiency during hovering, was also obtained as follows:

$$\text{Figure of merit: } FoM = \frac{C_T^{3/2}}{\sqrt{2}C_Q} \quad (3).$$

Figure 7 shows relationships between the corrective pitch angle, θ of the rotor and the thrust coefficient, C_T for four kinds of rotor configurations. The values of θ using the untwisted blades were larger than those using the twisted blades comparing at identical C_T s. This is due to the difference in the adopted airfoils, NACA0009 and OAF117, as well as the twist of the blade. Relationships between FoM and C_T are shown in Figure 8. The measurements were carried out between θ of 0° and 18° . Comparing the untwisted and twisted blades for the open rotor cases, both the maximum FoM and C_T values of the twisted blades were larger than those of the untwisted blades. These differences became smaller for the cases of the ducted rotor. Both the

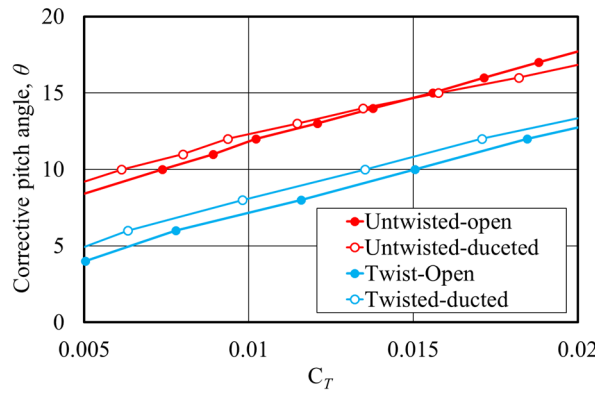


Figure 7 Corrective pitch angle vs. thrust coefficient

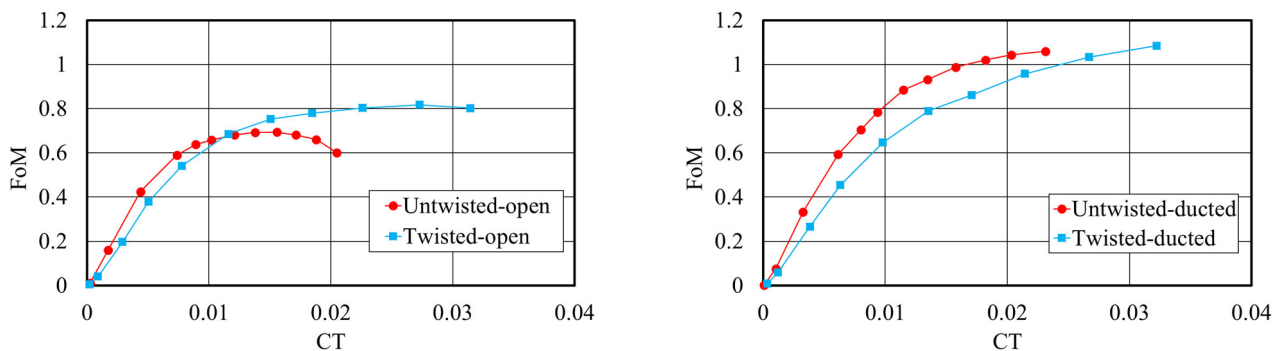


Figure 8 Aerodynamic characteristics of rotor. Open rotor (left) and ducted rotor (right) with untwisted and twisted blades are shown.

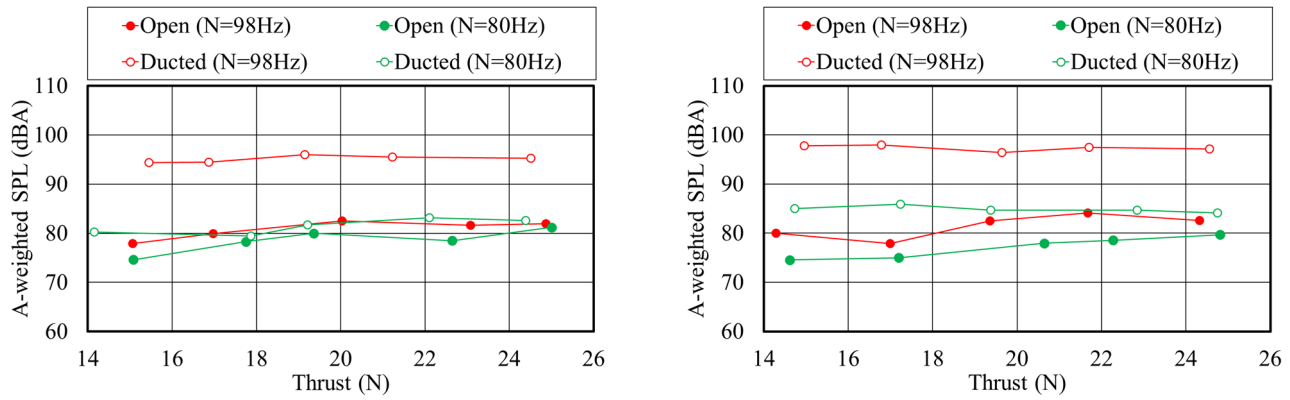


Figure 9 Allpass sound pressure level at “Mic C” for untwisted blade(left) and twisted blade(right). Rotor corrective pitch is varied, and revolution frequencies are fixed at 98 Hz and 80 Hz.

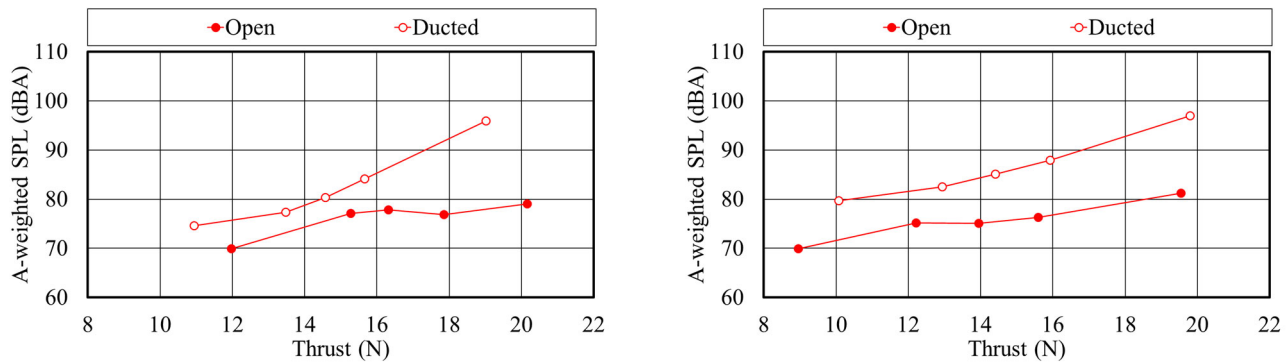


Figure 10 Allpass sound pressure level at “Mic C” for untwisted blade(left) and twisted blade(right). Rotor corrective pitch is fixed, and revolution frequency are varied.

maximum FoM and C_T values of the ducted rotor were larger than those of the open rotor with both untwisted and twisted blades.

Allpass sound pressure levels, SPLs were compared at the fixed rotational frequencies of the rotor, N s of 98 Hz and 80 Hz. The thrust values were varied by changing θ . Results were plotted as functions of the thrust values as can be seen in Figure 9. The range of the thrust, $Thrust = 15 - 25$ N, in Figure 9 corresponded to $C_T = 0.008 - 0.013$ for $N = 98$ and $C_T = 0.012 - 0.020$ for $N = 80$ Hz, respectively. The curves in these plots are almost flat, which means that the influence of the thrust and θ values on the allpass SPL were not significant. The allpass SPL values were affected by the value of N and the duct. As N increased, or using the rotor duct, the allpass SPL increased. Relationships between the allpass SPL and N are shown in Figure 10. The increasing rate of the allpass SPL increased as N increased as can be seen in Figure 10. Comparing the left and right figures in Figures 9 and 10, influences of the blade twist and airfoil were less significant than those of N and the duct.

Here, characteristics of sound directivity could not be examined well because of reverberant. This will be discussed in the next section using the small-scale model experiment in the soundproof room.

In order to understand the reason why the noise increased using the rotor duct, detailed analyses of the noises were carried out. The waveform of the sound pressure and its FFT result for the open rotor with twisted blade are shown in Figure 11. In the left figure, the waveform shows a periodic pattern with an approximate period of 0.005 s, which correspond to a period of the blade passing, $1/(2N)$. In the right figure, many spectral peaks can be seen at the frequencies of the blade passing and its harmonics. Powers broadband noise seems to be small around 40dBA.

The waveform of the sound pressure and its FFT result for the ducted rotor with twisted blade Figure 12. The operating condition, N and thrust value were identical to abovementioned the open rotor case. In the left figure, the periodicity of the waveform is not clear and waves with short period noticeable. In the right figure, many spectral peaks can be seen at the frequencies

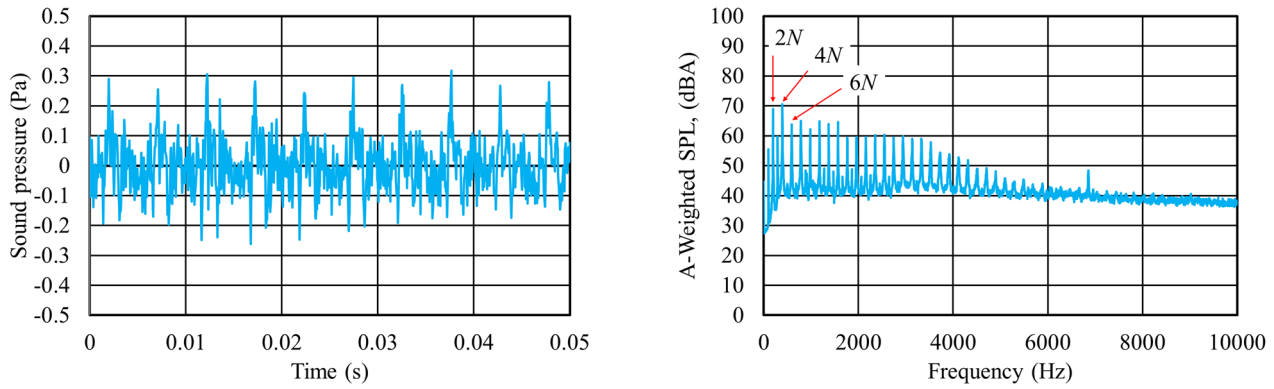


Figure 11 Temporal waveform (left) and FFT result (right) at “Mic C” for open rotor with twisted blade, N=5600, Thrust =17 N.

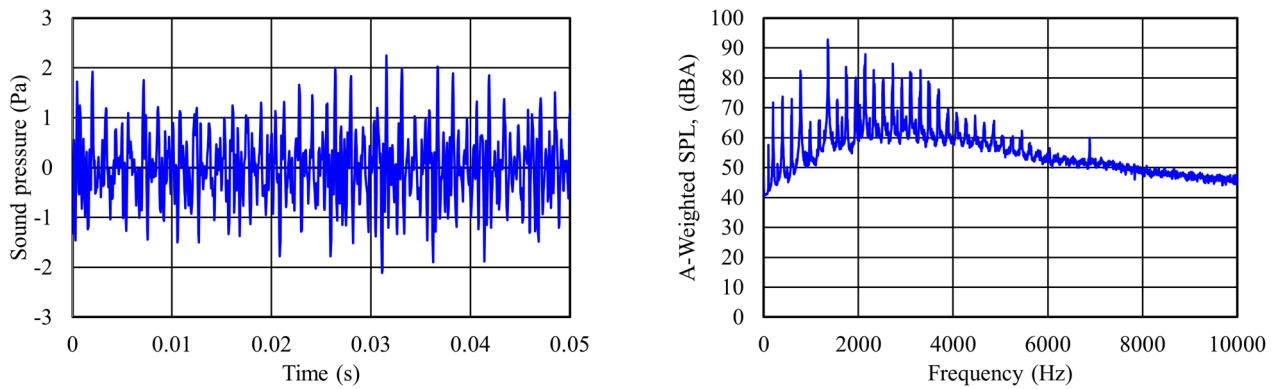


Figure 12 Temporal waveform (left) and FFT result (right) at “Mic C” for ducted rotor with twisted blade, N=5600, Thrust =17 N.

of the blade passing and its harmonics, which can be observed in the result of the open rotor. However, an appreciable difference can be seen in the power of the broadband noise. The larger peak of the broadband noise appears around 3000 Hz, and its range extends to 0-6000 Hz. According to these results, the noise level is affected by the rotational frequency and the duct. Since the influence of the rotational frequency is the most significant, the noise level of the ducted rotor can be reduced until similar level to the open rotor, by reducing the rotational frequency. By using the duct, the broadband noise increases as well as the blade passing components. Although the mechanisms have not been clarified, characteristics of turbulence and tip leakage vortices may cause the broadband noise. Further investigation is a future work.

3.2 Experimental Results Using Small Scale Model

Using the small-scale model, the directivity of noise was examined, and results can be seen in Figure 13. The allpass SPLs of the ducted rotor were totally larger than the open rotor as observed in the experiment using the actual drone rotor. For both cases of the open and ducted rotors, there are difference in the SPLs depending on the measuring locations. The SPL at Mic A, which was at the upstream side of the rotor, was the largest. On the other hand, the SPL at Mic B, which was at the side of the rotor was the smallest. According to these results, the duct did not function as a sound barrier.

As discussed in the previous section, one of the largest sources of the noise are the blade passing component and its harmonics. It is well known that Helmholtz resonator is effective to absorb tone noises. Then, the duct with Helmholtz resonators, with the resonance frequency of 1300 Hz, were examined. Allpass sound pressure levels are shown in Figure 14. The SPLs were totally increased using the Helmholtz resonators. Figure 15 shows FFT results of the noise at Mic C for the open rotor, the ducted rotor without resonators, and the ducted rotor with resonators. Comparing the results between the open rotor and the ducted rotor without resonators, the

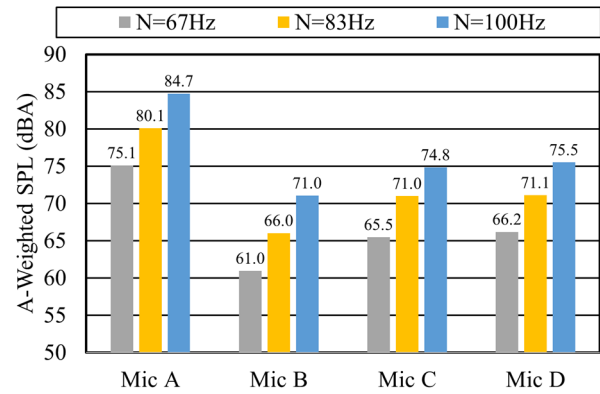
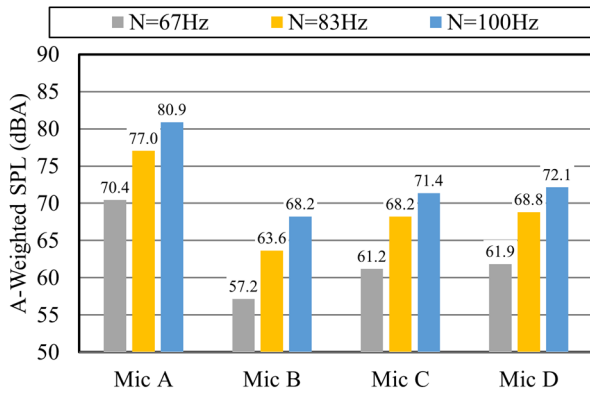


Figure 13 Allpass sound pressure levels at four points for open rotor (left) and ducted rotor (right) with twisted blades (Small-scale model, $\theta = 12^\circ$).

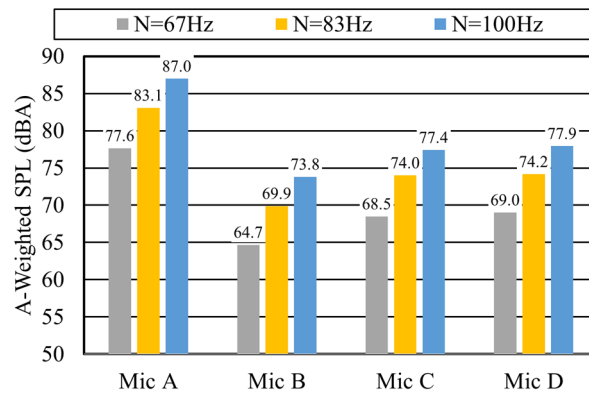
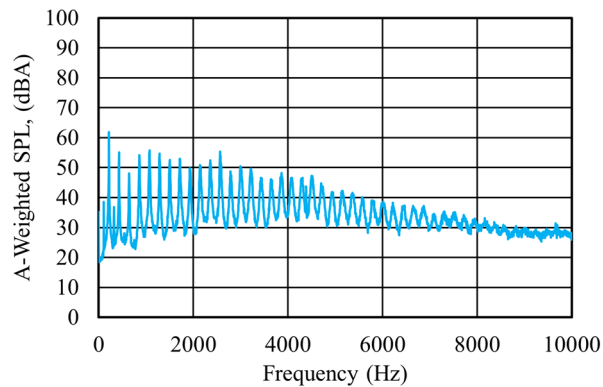
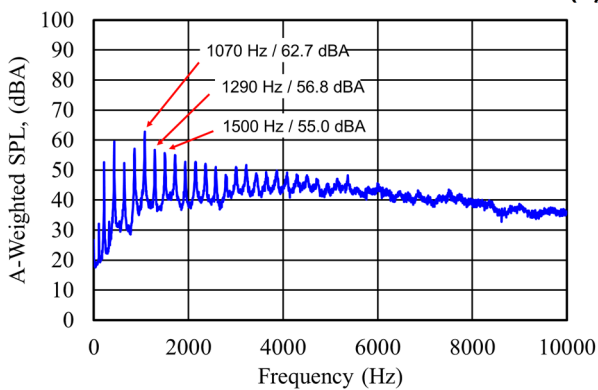


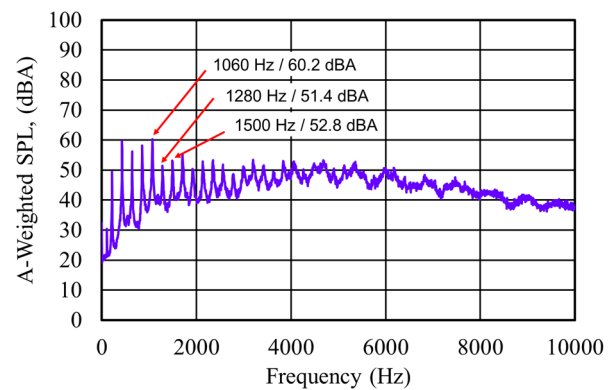
Figure 14 Allpass sound pressure levels at four points for ducted rotor with twisted blades and Helmholtz resonators (Small-scale model, $\theta = 12^\circ$).



(a) Open rotor



(b) Ducted rotor without resonator



(c) Ducted rotor with Helmholtz resonator

Figure 15 FFT results at “Mic C” (Small-scale model, $N = 100\text{Hz}$, $\theta = 12^\circ$).

broadband noise became larger by using the duct, which was identical to the results discussed in the previous section. For the ducted rotor with the resonators, the power spectra around 1300 Hz were smaller than those with the ducted rotor without resonators. However, the broadband noises more than 3000 Hz became larger by using the duct with resonators. This may be due to the increase of the surface roughness of the duct wall. Although the function of the Helmholtz resonator was observed as reduction of the tone noise level around 1300 Hz, it was concluded that the Helmholtz resonator was not effective to reduce the noises from the drone rotor.

4. Conclusions

Aerodynamic noise characteristics of the drone rotor was examined experimentally. The rotor with the variable corrective pitch mechanism was tested using two kinds of blades, which were the untwisted and twisted blades, and the rotor duct. By using the ducted rotor configuration, the figure of merit of the rotor becomes larger. However, the noise also became large using the ducted rotor in exchange for the advantage of the efficiency. The SPL was significantly affected by the rotational frequency of the rotor, and the influences of the blade twist, the airfoil adopted for the blade design and the corrective pitch angle were smaller. It was also confirmed that the increase in the SPL due to the duct could be cancelled without reducing the thrust, by reducing the rotational frequency and increasing the corrective pitch angle. Helmholtz resonators were mounted on the duct and examined. Although the function of the Helmholtz resonator was observed as reduction of the tone noise level around the resonance frequency, the Helmholtz resonators were not effective to reduce the noises.

References

- Avanzini, G, D'Angelo, S, (2003) Performance and Stability of Ducted-Fan Uninhabited Aerial Vehicle Model, *Journal of Aircraft*, 40(1), 86-93
- Ohanian, O S, Karni, E D, Londenbergl, W K, Gelhausenm P A, (2011) Ducted Fan Force and Moment Control via Steady and Synthetic Jets, *Journal of Aircraft*, 48(2) , 514-526
- Pflimlin, J-M, Binetti, P, Souères, P, Hamel, T, Trouchet, D. (2009) Modeling and attitude control analysis of a ducted-fan micro aerial vehicle, *Control Engineering Practice* 18(3), 209-218.
- Penkov, I and Aleksandrov, D (2017) Propeller shrouding influence on lift force of mini unmanned quadcopter, *International Journal of Automotive and Mechanical Engineering* 14(3), 4486-4495
- Tinney, C E, Sirohi, J, (2018) Multirotor Drone Noise at Static Thrust, *AIAA Journal* 56(7) 2816-2826.
- Tanabe, Y, Sugawara, H, Yonezawa, K, Sunada, S, Tokutake, H, (2019) Influence of Rotor Blade Twist on the Ducted Rotor Performance, 6th Asian Australian Rotorcraft Forum.
- Yonezawa, K, Yoshida, N, Sugiyama, K, Tokutake, H, Tanabe, Y, Sunada, S, (2016) Development of a Multicopter with Ducted and Variable Pitch Rotors, 5th Asian Australian Rotorcraft Forum.
- Yonezawa, K, Matsumoto, H, Sugiyama, K, Tokutake, H, Tanabe, Y, Sunada, S, (2017) Development of a Ducted Rotor for Multicopters, 6th Asian Australian Rotorcraft Forum.

Yonezawa, K, Matsumoto, H, Sugiyama, K, Tokutake, H, Tanabe, Y, Sunada, S, (2019) Aerodynamic Characteristics of a Quad-Rotor-Drone with Ducted Rotors, 6th Asian Australian Rotorcraft Forum.



QUIET DRONES
International e-Symposium
on
UAV/UAS Noise
Remote from Paris – 19th to 21st October 2020

Multi-rotor powered drone noise assessment

Xin Zhang

Department of Mechanical and Aerospace Engineering, The Hong Kong University of Science and Technology, Hong Kong, China, aexzhang@ust.hk

Siyang Zhong

Department of Mechanical and Aerospace Engineering, The Hong Kong University of Science and Technology, Hong Kong, China, zhongsy@ust.hk

Summary

This paper addresses noise and certification requirements of multi-rotor powered flying vehicles such as drones or unmanned vehicles that are now increasingly ubiquitous. As the vehicles' roles extend beyond leisure to commercial and industrial applications, their size and weight increase, and they operate increasingly close to urban areas, causing noise pollution and health damage. The noise problem was often neglected thus far in the headlong dash to growth by the industry. There are significant gaps in our understanding of the mechanisms of sound generation and shortfalls in our capability to evaluate the noise impact of multi-rotor powered unmanned vehicles. Noise impact assessment relies on accurate measurements and reliable noise models. Developments of measurement techniques and noise prediction methods are therefore timely and necessary. Some new features of the drone noise have been identified in recent fly and laboratory tests in the Advanced Aircraft Noise Technology Centre (AANTC) at HKUST. In this paper, we will discuss on the drone noise mechanisms and characteristics, offer views on noise certification and assessment conditions, and makes suggestions on assessment facilities and measurements requirements.

1. Introduction

The small unmanned aerial vehicles (UAV) or drones powered by multiple rotors are now increasingly ubiquitous [1] [2]. The roles of the vehicles are extending from recreational to commercial, scientific, agricultural, and other applications, including aerial photography, policing, survey, goods deliveries, construction monitoring, good deliveries, etc. The sizes and weight (due

to the lift requirement) of the drones are increased, causing serve noise pollution problem as the drones are often operated in populated urban regions. The drone noise could damage human health, disturb communication [3] and influence the wildlife [4]. Two significant sources of the drone noise are the motor noise and rotor noise [5]. The use of high-quality motors could reduce the motor noise, and, more importantly, may provide better aerodynamic performance to benefit the rotor noise reduction. The tonal noise of the rotor noise is due to the periodic motion of the blades, while the broadband noise is caused by complex turbulent flows. Both tonal and broadband contents have significant impacts on human. For example, the tonal noise, which is often in the low-frequency range, can cause annoy because human is sensitive to the pitch characteristics [6], and the broadband noise can affect the human brainstem auditory evoked response [7].

To reduce the environmental impact, noise regulations on drones to be delivered to the market are expected. Existing noise test codes such as the ICAO Annex 16-Volume 1 [8], contains Chapters on helicopters with a maximum take-off mass (MTOM) below 3,175kg and tilt-rotor vehicles that are often operated far above the urban region. They are remotely related to the drones that are usually of several to several tens of kilogram. The drones powered by multiple rotors are often operating at several meters about the ground. Also, the working environment of the drones may contain large acoustically reflecting structures such as buildings, making the ICAO test codes for heavier aircraft only based on ground measurement points unsuitable. For drones, the European Commission published a noise test code following the EN ISO 3744:2010 standards [9]. The test code measured the indoor and outdoor sound power level of the multi-rotor powered UAV in hovering. However, for the in-door tests, the tests do not contain guidelines in considering the flow recirculation in anechoic chamber tests [10]. The directivity characteristic should also be considered as people in the urban region may perceive drone noise from different directions to assess the environmental impact of drone noise. Also, the spectrum, directivity and strength of the drone noise can differ in different flight-phases of take-off, hovering, yawing, inflight and landing. Therefore, the assessment of the drone noise should be based on the enhanced understanding of noise mechanisms and characteristics.

Recently, a number of experiments have been conducted to investigate the rotor noise [11] [12] [13] [14] [15]. Some new features are identified, such as the importance of the flow recirculation effect in the anechoic chamber tests and the rotor unsteadiness on the noise generation. Considering that in practical applications, the imperfection of the motors and the blades made of injection moulding might experience oscillation, influencing the local flow and then alternating the noise generation. Therefore, there is a timely requirement to develop efficient noise prediction models with these effects considered to guide the quiet drone designs and to develop the noise regulations.

The remaining part of the paper will be organized as follow. Section 2 introduces some advances in the understanding of the drone noise. Section 3 offers some views on the noise certification and assessment conditions, and Section 4 is the conclusion.

2. Understanding the drone noise

Like other aeroacoustic problems, the drone noise source can be modelled/computed based on the acoustic analogy theories [16]. With the increasing power of the computers, it is now a popular approach to conducted high-fidelity numerical simulations to solve the flow governing equations. The mechanisms for the noise generation can be analysed using the comprehensive flow data obtained numerically. Figure 1 shows an example of simulating the aerodynamic flow and noise radiation from a drone powered by four rotors. The acoustic far-field properties, which is essential to assess the environmental impact, can be computed using the sound extrapolation methods such as the integral solution of the Ffowcs-Williams and Hawkings equations [16] or the indirect acoustic variable method to filter out the turbulent fluctuations [17]. However, the large-scale numerical simulations are still time-consuming, and the efficient post-processing of the large data

is also a practical issue. Therefore, simplified modelling and prediction methods, as well as the experiments, are still unreplaceable for the drone noise investigation.

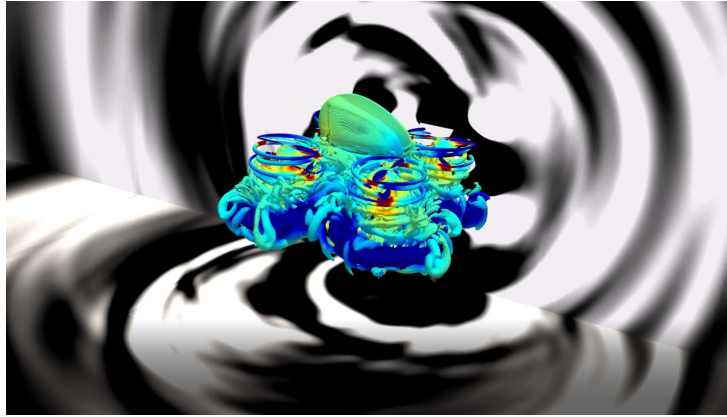


Figure 1: An example of investigating the near-field turbulent flow and sound radiation based on high fidelity numerical simulations.

For the tonal noise component, which is mainly caused by the rotatory motion of the rotors, high peaks are presented at the harmonics of the blade passing frequencies (BPF) in the noise spectra. Two common approaches to compute the rotor tonal noise are the time-domain approach based on Farassat Formulation 1A [18] and the frequency-domain method based on Hanson's model [19]. In the time-domain formulation, the modelled sources are experiencing rotational motion such that the temporal variation of the retarded time can modulate the noise radiation. By contrast, in the frequency-domain approach, equivalent distributed sources with varying phases in the area the rotor blades swept are assumed. Either way, a key step in predicting the tonal noise is to model the local velocity and aerodynamic loading efficiently and accurately, e.g. by high-fidelity numerical simulations or to use simplified approaches such as blade element and moment theory (BEMT). Figure 2 shows the comparison of the predictions of the first BPF noise of two different isolated rotors with experiments at various rounds per second (RPS). The experiments are conducted in the anechoic chamber at HKUST using an established rotor noise test rig. In the prediction based on the frequency-domain formulation [19], the steady flow variables (in the rotor-fixed coordinate) can be obtained by the BEMT method, as shown in Fig. 2 (Left), and the computation time is often less than one minute. The flow can also be computed using computational fluid dynamics (CFD), and close results with the experiments are also obtained, as shown in Fig. 2 (Right).

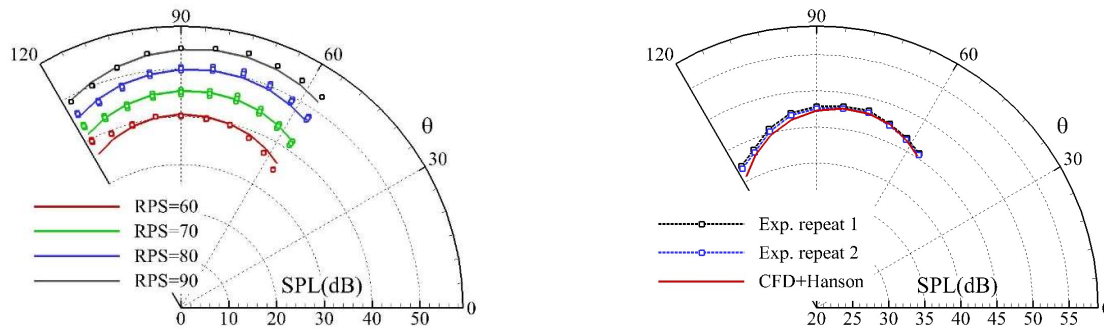


Figure 2: Comparison of the sound pressure level (SPL) at the first BPF of two different rotors at various rotation speeds predicted by the frequency-domain formulation and experiments. Left: APC 11x5 rotor using BEMT; Right: APC 9x5 rotor using CFD at 90RPS.

The computation for steady flows can be efficient. However, the rotor noise is sensitive to the realistic unsteady motions such that the noise at high-order BPF can be significantly influenced. The sources of the unsteady motion can be the imperfect performance of the motors, as also studied by McKay and Kingan [20], and due to the unsteady nature of the problem under realistic

flight conditions such as the time-varying superposed flows. As shown in Fig. 3 (Left), the practical rotors could experience fluctuated thrust and other aerodynamic forces. As a result, the tonal noise prediction can underestimate the noise at high-order BPF if only the mean steady flow is considered, as indicated by the green arrows in Fig. 3 (Right). By contrast, the prediction accuracy is improved if the unsteady motion is considered, as indicated by the blue arrows in the right figure of Fig. 3. The results highlight the necessity to consider the unsteady motion of real rotors when computing the sound. This fact also leads to a need to incorporate efficiently and accurately the unsteadies, which are often of small amplitudes, to the numerical simulations to capture the real acoustic processes.

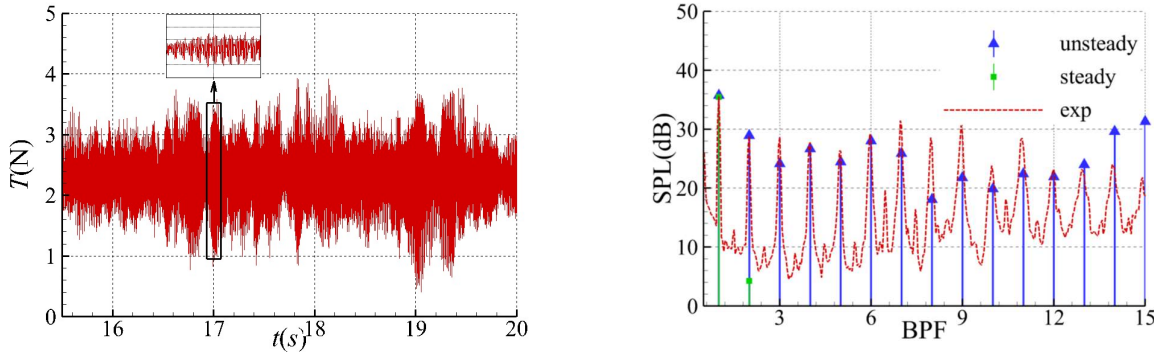


Figure 3: (Left) time signal of the measured thrust of a rotor in practice; (Right) a comparison of the predicted noise spectra with and without unsteady motion with the experiments.

Another cause of the unsteadiness can be the vibration of practical rotor blades under unsteady loads. For the commercial drones, the blades are often made of light materials such as elastic and carbon composite materials. At high speed, the more severe aerodynamic loading acting on the blade surface may lead to vibration or oscillation since the stiffness is relatively low. In this case, the noise generation can be significantly impacted since the local flows are disturbed. Figure 4 shows the comparison of the measured noise spectra of two geometrically identical rotors, one of which is of the high-stiffness metal (aluminium) and the other one is plastic. At the rotation speed of 60RPS, the measured noise spectra are close due to the identical geometry. By contrast, at 120RPS, the high BPF noise generated by the plastic can be 15dB higher than the metal blade, which is likely caused by the occurrence of the blade oscillations. At this speed, the characteristics of the broadband noise are also different. The impact of the blade oscillation on both aerodynamics and aeroacoustics is of the industrial concern, considering that the practical rotors are often operated above 100RPS. This effect should also be considered to predict and reduce the noise of real rotors.

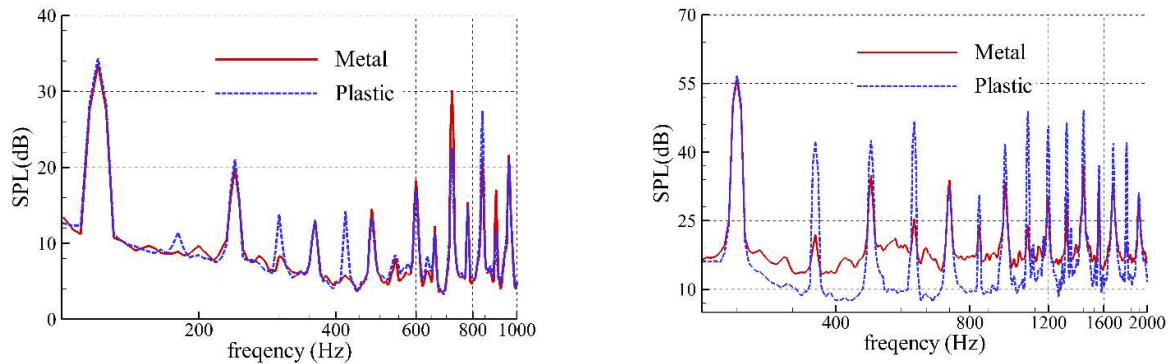


Figure 4: Comparison of the measured noise spectra of two rotors made of different materials at different rotation speeds. (Left): 60 RPS and (Right) 120 RPS.

The possible rotor broadband noise sources can be the turbulence (in boundary layer) scattering at the blade trailing edge, the blade-wake interaction and the blade-tip vortex interaction [21].

Accurate and efficient predictions of noise produced by different mechanisms are still challenging. For example, for the boundary layer scattering at the trailing edge, there are several methods to compute the sound. However, some of the methods require the local flow information such as the wall pressure spectra [22] and the mean flow gradients [23], which are often difficult to be accurately obtained in practical rotor applications. Another approach is based on a semi-empirical model of the airfoil self-noise [21]. For the small rotors, the Reynolds number is in the low-to-moderate range ($\sim 10^5$), and the flow condition is complex due to the separation and the rotatory motion. Figure 5 shows a comparison of the rotor trailing edge noise prediction with experiments. The predictions can capture the trend of the broadband noise spectra in the 1/3 octave. Also, the difference between the predicted and measured results in the directivity is smaller than 3dB at most observer angles. However, the prediction accuracy could also be impacted by the realistic factors. For example, if the blade-wake interaction or the blade-tip vortex interaction becomes more profound, their contribution should be considered for better prediction.

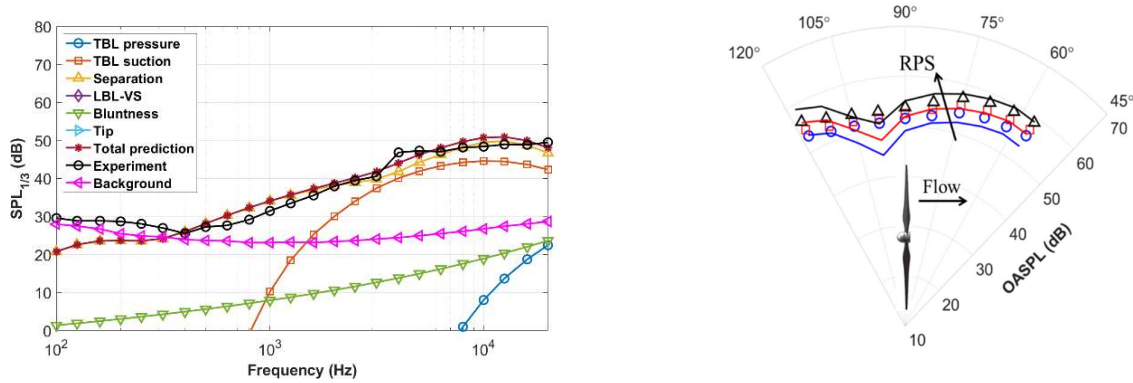


Figure 5: Comparison of the predicted rotor broadband noise with experiments. (Left) 1/3 octave spectra; (Right) directivity patterns at different RPS.

The complicated aeroacoustic mechanisms for both the tonal and broadband contents and the sensitive dependence with the realistic flow conditions can lead to complex drone noise characteristics in practice. Noise tests for different weight quadrotors have been conducted at AANTC in a large anechoic chamber facility under various flight conditions including hovering, yawing, inflight, climbing and descend to cover the complete flight mission [24]. Figure 6 (Top Left) shows a photograph of the experiment. Eighty 1/2-inch GRAS type-46AE free-field microphones were used, seventy-two of which were placed on the ground and eight were placed in the vertical direction to measure the acoustic signals at different observers. The distance of the microphones is larger than ten times of the drone diameter to ensure the far-field condition. Figure 6 (Top Right) clearly shows the significant difference of measured acoustic signals at different locations, i.e. vertical below, diagonally below and on the rotor plane. The difference in the amplitudes and the wave patterns confirms that observer locations should be considered when evaluating the environmental impact of drone noise. Also, the noise features are sensitive to the drone work condition. For example, Fig. 6 (Bottom Left) shows the acoustic spectrum at the observer on the rotor plane in hovering state. In the low-frequency range, clear tones at the harmonics of the BPF are found in the noise spectrum, while broadband noise is the major content at high frequency, i.e. higher than 2500Hz. However, when the drone is operated in the yawing condition, i.e. drone itself is rotating with respect to its center axis, dual peaks around the BPF harmonics in the spectra are measured at the same location, suggesting that the tonal noise characteristics are changed. The broadband content is also changed, and the impact on human health and annoyance can be different. For other flight conditions, besides the differences due to observer locations, the acoustic signals also preserve transient properties due to the drone motion, e.g. there are sudden changes in the spectrograms and pressure signals when the flight direction is reversed [24]. The results suggest that there is a need to consider the transient properties when characterizing the drone noise in practical applications since the drone flight states are often flexibly changed.

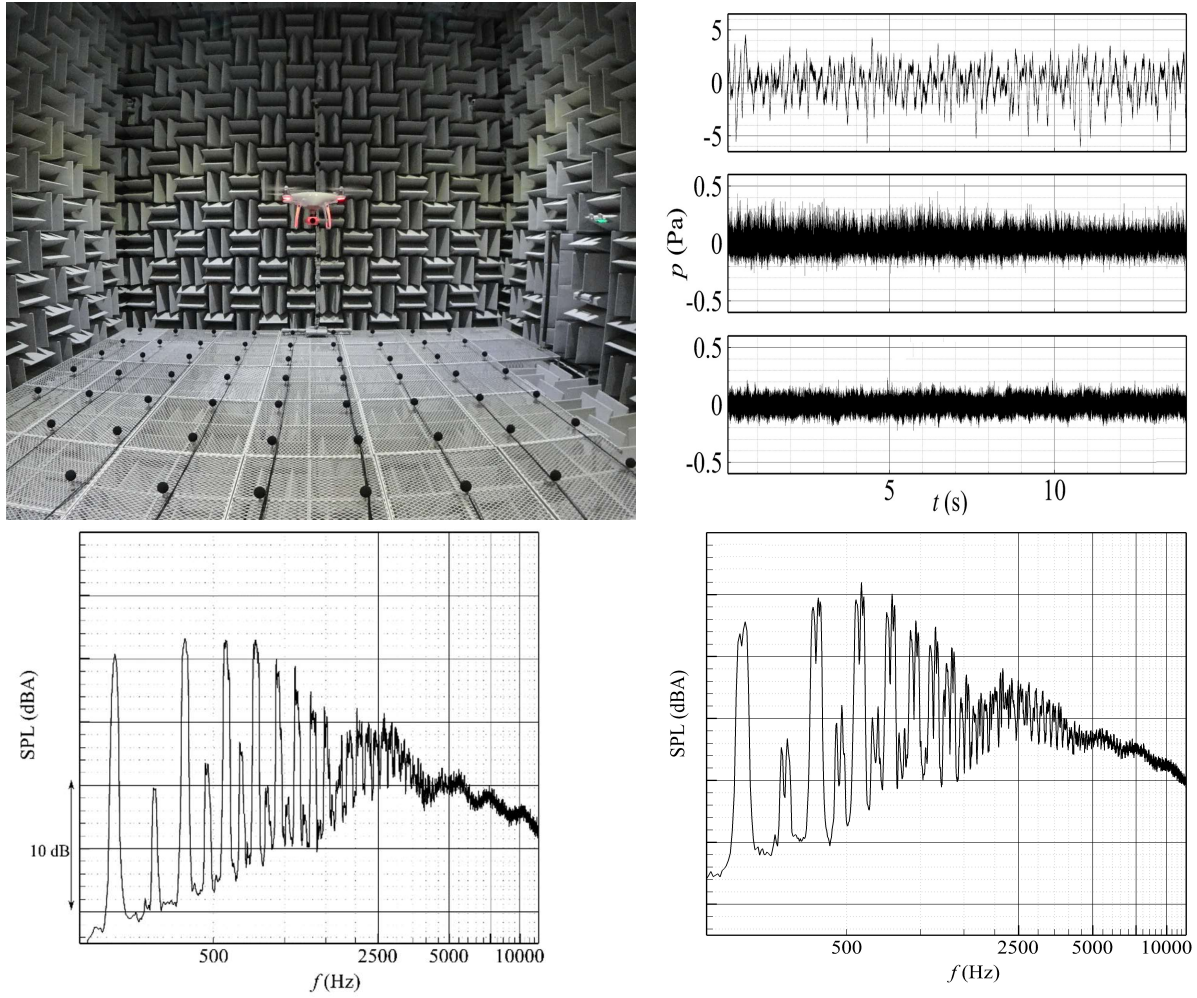


Figure 6: Acoustic characteristics of a quad-rotor in realistic flights. (Top left) Photograph of the experiment; (Top Right) the measured signals at different locations; (Bottom left) acoustic spectrum in hovering, and (Bottom right) the acoustic spectrum in yawing [24].

3. Drone noise assessment

It has been known that the drone noise is sensitive to the flow and flight conditions, and the impact on different observer location is quite different. To accurately assess the drone noise pattern, it is therefore needed to ensure that the acoustic test environment is controllable and sufficient number of measurements are made to capture the directivity properties. Additionally, the metric to characterize the drone noise impact should consider the tonal and broadband contents as they influence people's annoyance and health in different ways.

The measurements should be conducted at various observer points to capture the directional noise impacts, suggesting that the requirement and procedures for drone noise assessment will be different from helicopters based on only the group measurements. Figure 7 shows a schematic of the measurement points at various locations. Microphones should be placed on both the ground and in the vertical direction to capture the drone noise impacts at different locations. For the tests in flight conditions, additional microphones are needed in the flight directions as the relative distance and motion between the drone and the observers can also influence the property of the measured noise. High-precision equipment used for position tracking is required to provide the flight data. Synchronized measurements for acoustic, drone (including rotor) motion and drone location are needed. For the possible outdoor experiments, corrections are needed to account for the atmospheric factors, air temperature, wind correction and background noise.

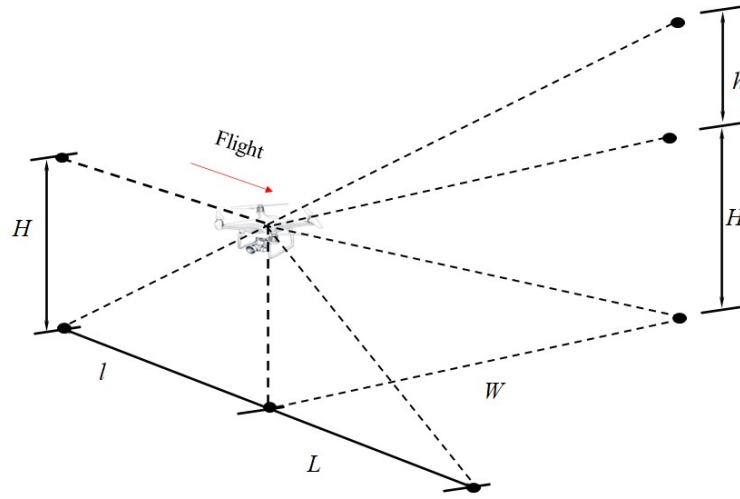


Figure 7: A schematic to show the requirement in drone noise assessment.

For the small drones (usually less than 5kg), the certified large anechoic chamber is preferred for the acoustic measurements due to the controlled condition and the low background noise. In this case, however, the recirculation effect [10] should be considered and removed for the rotor noise tests. The rotor operation will generate significant downwash velocity at the rotor plane to the wake region. The unsteady flow might be re-ingested by the rotor because of the finite size of the anechoic chamber. Despite the low amplitude, the unsteady motion can significantly impact the noise generation [25]. As a result, the tonal noise at higher BPF and the broadband noise can be clearly increased at a certain time from the experiment when the recirculation happens. As shown in Fig. 8, in the spectrogram of the rotor noise obtained by the short-time Fourier transform (STFT), the tonal noise only presents at the first BPF before $t = 4$ s. In contrast, high values at the higher BPF are observed after that. Similar results are found in the noise spectra computed using the measured data before and after the recirculation happens. The value at the first BPF is little impacted, while the higher BPF tones and broadband noise significantly differ. Considering that the recirculation does not happen in the outdoor flights the drones, the measured data before the recirculation are there recommended to assess the drone noise.

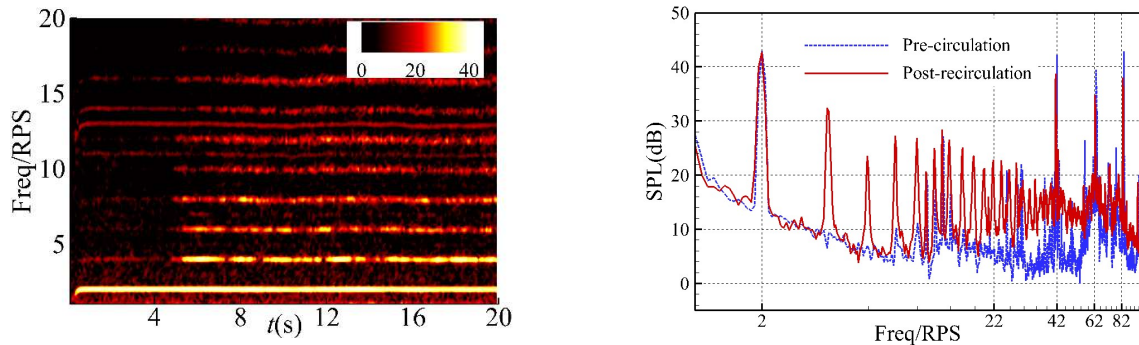


Figure 8: A demonstration of the recirculation effect on rotor noise measurement in anechoic chamber. (Left) The spectrogram obtained by STFT; (Right) a comparison of the noise spectra.

The understanding of drone noise characteristics based on the combined theoretical, numerical, and experimental research approaches can benefit the drone noise assessment. For example, based on the frequency domain formulation [19], the tonal noise at the first BPF by a rotor at different rotation speed can be computed. The computed sound levels can be well collapsed when they are scaled by Ω^{B+2} , where $\Omega = 2\pi \times \text{RPS}$ is the angular velocity and the B is the blade number, as shown in Fig. 9. The better understanding of the rotor noise based on the proposed scaling laws can verify the experimental tests and simplify the experiments. For example, if the directivity pattern is known in prior, the number of observer points can be greatly reduced. The

scaling laws can also be represented with respect to the thrust since $T \propto \Omega^2 D^4$, which may be more useful for practical applications since the dependence of designed payload and noise emission can be estimated. Similar scaling law studies can also be conducted for broadband noise. Our previous measurement in the large anechoic chamber also showed that for quad-rotor drones, the increase of the MTOM by 1kg could lead to noise increment approximately by 8dB, as shown in Fig. 10. The microphones were placed below (mics 1 and 2), on (mic 3) and above (mic 4) the rotor plane. The results highlight the need and provide guidance to certificate the noise radiation from drones with different MTOM.

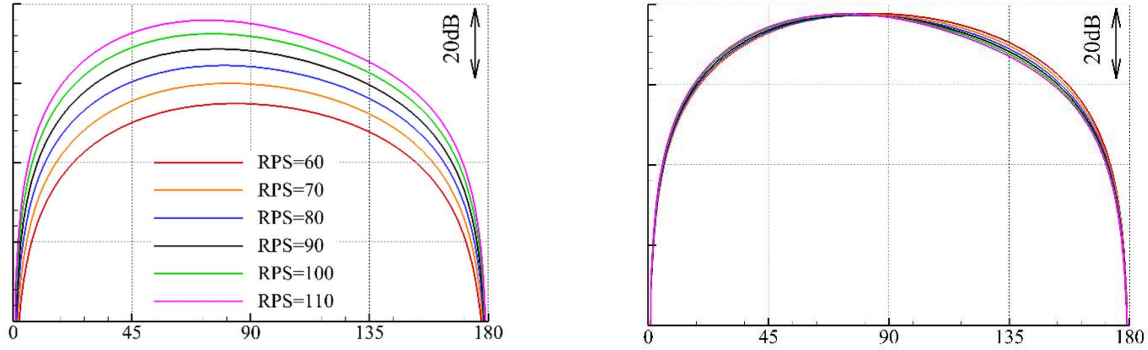


Figure 9: The tonal noise directivities of a rotor computed using the frequency domain formulation at different RPS. (Left) The original computed results; (Right) the results the sound pressure scaled by the rotation speed by Ω^{B+2} .

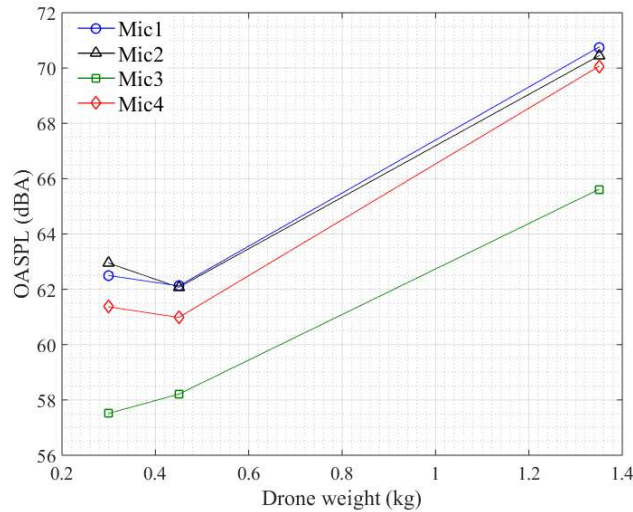


Figure 10: The dependence of the overall sound pressure level (OASPL) with the drone weight measured at different locations in a large anechoic chamber experiment.

In laboratory investigations of the drone/rotor noise, the acoustic analyses are often based on the SPL spectra. In practical applications to certify the drone noise, further data processing and additional noise metric might be needed. For example, a metric may need to account for the time-varying property due to the flight motion of the drones. In this case, the sound exposure level (SEL) that integrates the temporal A-weighted sound level over a period [26] can be used. This is suitable in the applications such as take-off, inflight and descent, and it considers the relative loudness perceived by the human ear. Also, the drone noise contains both tonal and broadband noise, and the “annoying” characteristic perceived by the observers could be different. A possible metric is based on the effective perceived noise level (EPNL) that has been employed for setting international noise standards for large aircraft [8]. The measurement is based the 1/3 octave bands, and an individual spectrum is investigated with tone-corrections.

4. Conclusions

The widening application of the multi-rotor powered drones will cause noise issue. Regulations on the drone noise are expected to reduce the environmental impact and to promote the development in the low-noise drone designs. The working environment and noise characteristics are quite different from other types of aircraft, making the existing noise certifications such as the ICAO Annex 16 for helicopters are unsuitable to certificate the drone noise. Some existing drone noise standard only examined the sound level of a hovering drone at a specified point. To this end, improved drone noise assessment should be based on the advances in understanding the noise mechanisms and characteristics.

With the increasing power of the computers, to conducting high-fidelity numerical simulation is becoming a popular approach to study the noise generation mechanisms. However, it should be combined with the analytical and experimental methods to capture acoustic physics in real applications efficiently. Predictions of both the tonal and broadband noise for rotors can be conducted, and the accuracy can be examined by comparing with experiments. The previous research also identified that the unsteady motions due to the motor performance and the likely blade oscillations could significantly alter the sound generation, requiring the development of efficient prediction models for practical drone noise assessment. The realistic flight tests of quadrotor drone in a large anechoic chamber facility showed that the noise feature could be significantly impacted by the location of the observer and the flight condition.

The improved understandings of the drone noise, for example, the development of scaling laws for the dependence of noise on the rotor speed and thrust, might be beneficial for designing the low-noise drones, simplifying the experimental measurements and certifying the drone noise. Some views on the drone noise assessment are given. The measurements are suggested to conduct at different observer points, rather than at a single point, to characterize the drone noise better. Also, for the rotor noise tests in anechoic chambers that can provide controlled flight condition and good acoustic environment, the effect of flow recirculation should be considered and removed. Also, the SEL and EPNL are probably the suitable noise metric to capture the transient property of the drone noise and the influence the tonal noise on human annoyance.

Acknowledgment

The authors wish to thank Mr. Hanbo Jiang, Dr. Ryu Fattah, Dr. Weijie Chen and Mr. Han Wu for the drone noise experiments. The work is supported by the Hong Kong Innovate Commission (ITS/387/17FP) and the Hong Kong Research Grant Council (RGC 16202520).

References

- [1] A. Luiceer, D. Tuner, D. H. King and S. A. Robinson, "Using an unmanned aerial vehicle (UAV) to capture microtopography of Antarctic moss beds," *Int. J. App. Earth Observation Geoinformation*, vol. 27, pp. 53-62, 2014.
- [2] D. Floreano and R. J. Wood, "Science, technology and the future of small autonomous drones," *Nature*, vol. 521, pp. 460-466, 2015.
- [3] A. W. Christian and R. Cabell, "Initial investigation into the psychoacoustic properties of small unmanned aerial system noise," *AIAA Paper 2017-4051*, 2017.
- [4] M. Mulero-Pázmány, S. Jenni-Eiermann, N. Strebel, T. Sattler, J. J. Negro and Z. Tablado, "Unmanned aircraft systems as a new source of disturbance for wildlife: A systematic review," *PloS one*, vol. 12, no. 6, p. e0178448, 2017.
- [5] D. L. Huff and B. S. Henderson, "Electric motor noise from small quadcopters: Part I- acoustic measurements," *AIAA Paper 2018-2952*, 2018.
- [6] U. Landstrom, E. Akerlund, A. Kjellberg and M. Tesarz, "Exposure levels, tonal components, and noise annoyance in working environments," *Environmental International*, vol. 21, pp. 265-275, 1995.

- [7] R. Burkard and K. Hecox, "The effect of broadband noise on the human brainstem auditory evoked response. I. Rate and intensity effects," *J. Acoust. Soc. Am.*, vol. 74, no. 4, pp. 1204-1213, 1983.
- [8] ICAO, "ICAO Annex 16: Environmental Protection," 2008.
- [9] U. E. I. 3744:2010, "Acoustics. Determination of sound power levels of noise sources using sound pressure. Engineering method in an essentially free field over a reflecting plane," 2010.
- [10] J. H. Stephenson, D. Weitsman and N. S. Zawdonay, "Effects of flow recirculation on unmanned aircraft system (UAS) acoustic measurements in closed anechoic chambers," *J. Acoust. Soc. Am.*, vol. 145, pp. 1153-1155, 2019.
- [11] N. S. Zwodny, D. D. Boyd and C. L. Burley, "Acoustic characterization and prediction of representative, small-scale rotary-wing unmanned aircraft system components," *AHS 72nd Annual Form*, 2016.
- [12] G. Sinibaldi and L. Marino, "Experimental analysis on the noise of propellers for small UAV," *Applied Acoustics*, vol. 74, p. 79-88, 2013.
- [13] Z. Ning, R. Wlezien and H. Hu, "An experimental study on small UAV propellers with serrated trailing edges," *AIAA Paper 2017-3813*, 2017.
- [14] J. Whelchel, W. N. Alexander and N. Intaratap, "Propeller noise in confined anechoic and open environments," *AIAA Paper 2020-1252*, 2020.
- [15] R. Fattah, W. J. Chen, H. Wu, Y. Wu and X. Zhang, "Noise measurements of generic small-scale propellers," *AIAA Paper 2019-2498*, 2019.
- [16] J. E. Ffowcs-Williams and D. L. Hawkings, "Sound generation by turbulence and surfaces in arbitrary motion," *Proc. R. Soc. A.*, vol. 264, pp. 321-342, 1969.
- [17] S. Y. Zhong and X. Zhang, "A generalized sound extrapolation method for turbulent flows," *Proc. R. Soc. A.*, vol. 474, p. 20170614, 2018.
- [18] F. Farassat and G. P. Succi, "A review of propeller discrete frequency noise prediction technology with emphasis on two current methods for time domain calculations," *J. Sound Vib.*, vol. 71, pp. 399-419, 1980.
- [19] D. B. Hanson and D. J. Parzych, "Theory for noise of propellers in angular inflow with parametric studies and experimental verification," *NACA CR No. 4499*, 1993.
- [20] R. McKay and M. J. Kingan, "Multirotor unmanned aerial system propeller noise caused by unsteady blade motion," *AIAA Paper 2019-2499*, 2019.
- [21] T. F. Brooks, D. S. Pope and M. A. Marcolini, "Airfoil self-noise and predictions," *NASA RP 1989-1218*, 1989.
- [22] R. K. Amiet, "Noise due to turbulent flow past a trailing edge," *J. Sound Vib.*, vol. 47, no. 3, pp. 387-393, 1976.
- [23] R. Parchen, "Progress report DRWA: a prediction scheme for trailing-edge noise based on detailed boundary layer characteristics," *TNO Rep. HAG-RPT-980023, TNO Institute of Applied Physics*, 1998.
- [24] T. Zhou, H. B. Jiang, Y. H. Sun, R. Fattah, X. Zhang, B. Huang and L. Cheng, "Acoustic characteristics of a quad-copter under realistic flight conditions," *AIAA Paper 2019-2587*, 2019.
- [25] S. E. Wright, "Discrete radiation from rotating periodic sources," *J. Sound Vib.*, vol. 17, no. 4, pp. 437-489, 1971.
- [26] IEC 60027-3:2002, "Letter symbols to be used in electrical technology - Part 3: Logarithmic and related quantities, and their units," 2002.



QUIET DRONES
International e-Symposium
on
UAV/UAS Noise
Remote from Paris – 19th to 21st October 2020

Assessment of the environmental impact of drone noise in virtual flights

Haoyu Bian¹, Ryu Fattah², Siyang Zhong¹, Xin Zhang^{*1,3}

1. Department of Mechanical and Aerospace Engineering, The Hong Kong University of Science and Technology, Clear Water Bay, Kowloon, Hong Kong SAR, China
2. Aerodynamics and Acoustics Facility, The Hong Kong University of Science and Technology, Clear Water Bay Road, Hong Kong SAR, China
3. HKUST-Shenzhen Research Institute, No.9 Yuexing First Road, South Area, Nanshan, Shenzhen, 518057, China

Summary

Drones are now ubiquitous in various civilian and industrial applications such as photography, logistics and agriculture for its low cost and high flexibility. The resultant noise issue is becoming more significant as the number and size of the drones are increasing. The environmental impact gets more attention from policymakers, urban planners and residents. To quantify the noise level, anechoic chambers and outdoor measurements are essential approaches, but they have limitations in efficiently and economically accounting for the impact of practical environments. While the numerical solutions of the fluid or wave governing equations can be computationally intensive for large and complex regions of interest. To this end, we developed an efficient noise computation platform Environmental Acoustic Ray Tracing Code (EnvARC) to assess the environmental impact of flying drones in realistic scenarios. It is based on the ray tracing method to capture the major acoustic physics, including the reflection of complex boundaries with different impedance, refraction of the non-uniform medium and atmospheric attenuation. A paraxial Gaussian beam method was implemented to fix the issues such as caustics and extreme shadow regions in the conventional ray tracing method. In this paper, this platform is verified by canonical outdoor propagation problems. A noise source model of a realistic quadcopter is

* Email: aexzhang@ust.hk

lumped to the platform to evaluate the environmental impact. Finally, virtual flights in realistic urban environments are conducted and the results are discussed.

1. Introduction

Drones have been significantly developed with a broad range of applications in the civilian sector, such as logistics, photography, engineering and environmental monitoring and preservation [1, 2]. The noise problem brought by the growing number and application of drones has arisen the concern of legislators on the proper regulation of drone flying. Since drones may fly in the proximity of buildings especially in missions of delivery and structure inspection, community residents also care about the noise level on the building facade. In this case, the full three-dimensional (3D) urban environment should be considered in the noise assessment. Therefore, an effective and efficient tool to evaluate the noise level of drones in the realistic complex urban environment is desired.

Field testing can give direct measurements while it may be inconvenient and inefficient, and the requirements for high-quality acoustic measurements can hardly be ensured. The numerical simulations to directly solve the sound propagation equations [3, 4] are still computationally expensive for the realistic problem with large propagation distances, especially at high frequencies. Additionally, Helmholtz equation solvers based on the boundary element method (BEM) should be coupled with specialized Green function for refractive media [5]. Other wave-based methods can suffer from difficulties when considering complex boundaries with varying impedance values or applied beyond the critical elevation angles, such as the fast field program (FFP) [6, 7] and parabolic equation (PE) [3, 8] solvers.

Geometric acoustic (GA) methods are known for their high efficiency in handling problems with boundary surfaces. However, the image source method [9] could be computationally inefficient when the boundary geometry is complex. Also, it is limited to the problems with a homogeneous medium. By contrast, the ray tracing method can incorporate the obstacle geometry, obstacle material property and the medium characteristic well, and it has been applied in both indoor and outdoor noise prediction [10, 11]. However, the method may suffer from unrealistic caustics and shadow regions [12]. Also, the determination of eigen rays in the 3D applications can lead to large computation time. Therefore, the Gaussian beam method that is based on the high-frequency asymptotic approximation of the wave equation [13] is often employed in combination with the ray tracing method. It can improve the accuracy due to the smoothing effect of the beams on the singularities of the ray-theoretic field. Also, the computation can be efficient since there is no need to search for the eigen rays [14].

This paper introduces an in-house code with an efficient implementation of the Gaussian beam method to efficiently investigate the drone noise impact on the environment. In Section 2, the numerical methods are outlined. In Section 3, the code is verified through the long-range outdoor propagation with a building model. In Section 4, the effects of the flying path and environmental characteristics on noise exposure in virtual flights are investigated. Finally, the acoustic mapping of drone noise in the realistic urban environment is demonstrated.

2. Numerical methods

The ENVIRONMENTAL Acoustic Ray Tracing Code (EnvARC) can assess the noise of drones in an arbitrary environment. The code allows the user-defined source models such that the drone noise model can be incorporated, and the acoustic properties of the boundaries such that the impedance of the terrain and buildings can be specified. The acoustic radiation of a source is modeled by the expansion of multiple Gaussian beams. The trajectory of each beam is governed by the ray tracing module. Through the dynamic ray tracing module, the Gaussian beam is

constructed with its transverse amplitude profile determined. Finally, at each observer point, the noise contribution by all nearby beams is integrated to obtain the acoustic field.

In the ray tracing part, piecewise rays are obtained from the Snell's law, which determines the ray direction change at the interface of two adjacent atmospheric layers. Within each layer, the sound speed is assumed to be constant. The change in the ray vector at the boundary of each segment is governed by:

$$\vec{t}_2 = V_2/V_1 [\vec{N} \times (-\vec{N} \times \vec{t}_1)] - \vec{N} \sqrt{1 - (V_2/V_1)^2 (\vec{N} \times \vec{t}_1) \cdot (\vec{N} \times \vec{t}_1)},$$

where the \vec{t} is the ray unit vector, V is the speed of sound, \vec{N} is the interface surface normal pointed towards the incident field, and the subscripts $(\cdot)_1$ and $(\cdot)_2$ respectively indicate the variables along the incident and refracted regions.

The dynamic ray tracing module is used to solve the following equations to obtain the 2×2 matrix \mathbf{P} and \mathbf{Q} [15]:

$$d\mathbf{Q}/ds = \mathbf{V}\mathbf{P}, \quad \frac{d\mathbf{P}}{ds} = -\mathbf{V}^{-2}\mathbf{V}\mathbf{Q},$$

where s is the arc length along the central ray and \mathbf{V} is the 2×2 matrix of the secondary derivatives of velocity V with respect to the ray-centered coordinate component q_I , whose elements are

$$V_{IJ} = (\partial^2 V(q_1, q_2, s) / \partial q_I \partial q_J)_{q_1=q_2=0}.$$

The acoustic pressure contribution of a single beam onto a specific observer can be calculated using [5]

$$p_{beam}(R') = p_{ray}(R) \exp \left[-i\omega \left(-T(R) - 1/2 \mathbf{q}^T(R') \text{Re}(\mathbf{M}(R)) \mathbf{q}(R') \right) \right] \\ \times \exp \left[-1/2 \omega \mathbf{q}^T(R') \text{Im}(\mathbf{M}(R)) \mathbf{q}(R') \right],$$

where R' is the observer point, R is the nearest point on the ray to R' , and T is the propagation time from ray origin to the point R . Complex matrix $\mathbf{M} = \mathbf{P}\mathbf{Q}^{-1}$ and \mathbf{q} is the ray-centered coordinate vector. The amplitude term p_{ray} is calculated using

$$p_{ray}(s) = \left[\frac{\rho(s)V(s)J(s_0)}{\rho(s_0)V(s_0)J(s)} \right]^{1/2} p(s_0).$$

The ray Jacobian term $J = \det(\mathbf{Q})$ can be determined in the dynamic ray tracing. p_0 is the initial value. The contributions by multiple Gaussian beams can be integrated as

$$p(R', \omega) = \iint \Phi(\gamma_1, \gamma_2) p_{beam}(R(\gamma_1, \gamma_2)) d\gamma_1 d\gamma_2.$$

Here, γ_1 and γ_2 are the ray coordinate components and $\Phi(\gamma_1, \gamma_2)$ is the weighting function [15].

3. Verifications

To verify the accuracy of the EnvARC code, we conducted the computation for a benchmark problem with time-harmonic monopole sources located at 15m above a flat ground, which is assumed to be an acoustically hard wall. The sound pressure level (SPL) distribution is plotted at the height of 10m with the horizontal distance from 0 to 1000m. The medium is assumed to be homogenous. Four frequencies of 100 Hz, 500 Hz, 1000Hz and 2000Hz are studied. In this case, the sound field can be analytically computed, and used to examine the accuracy of the EnvARC results. The predicted results are shown in Figure 1. For the result at low frequency, i.e. 100Hz, there is a slight difference at the large distance, which is probably due to that the ray-tracing method is originally proposed under the high-frequency assumption. Nevertheless, good agreements are obtained by both approaches and the EnvARC captures the interference patterns in the SPL profile fairly well.

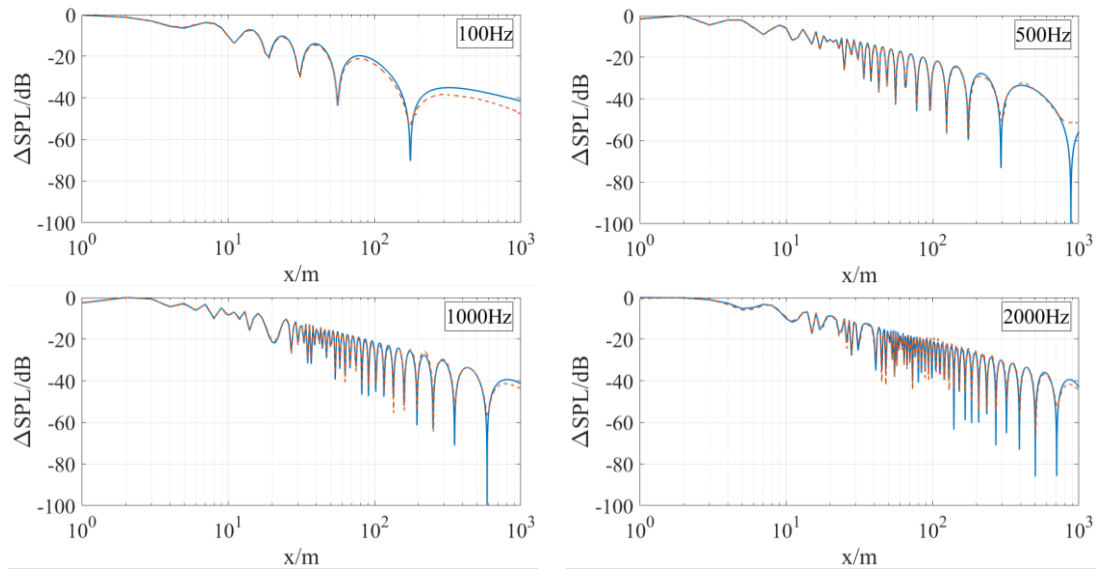


Figure.1 Predicted (---) and analytical (—) SPL profiles at the height of 10m with the monopole source located 15m above a planar ground surface at 100Hz, 500Hz, 1000Hz and 2000Hz.

Considering that the sound propagation at a large distance might be attenuated by the atmospheric absorption, especially at high frequency [16], the drone noise impact on the urban environment may be severer in the proximity of buildings near the source. Therefore, we study a simplified problem with a sound source near an obstacle with a dimension of $5\text{m} \times 5\text{m} \times 10\text{m}$ to mimic a building. The coordinate of the bottom surface center is $(17.5\text{m}, 17.5\text{m}, 0\text{m})$. The sound distributions at the frequencies of 50Hz and 100Hz are computed and compared with the results obtained by the finite element method (FEM), which is capable for the relatively low frequencies we are studying. The results at two planes with different orientations but crossing the source points are investigated. Figure 2 shows the results for the plane with the normal vector $(0,1,0)$, while Figure 3 shows the results on the plane with the normal vector $(1,1,0)$.

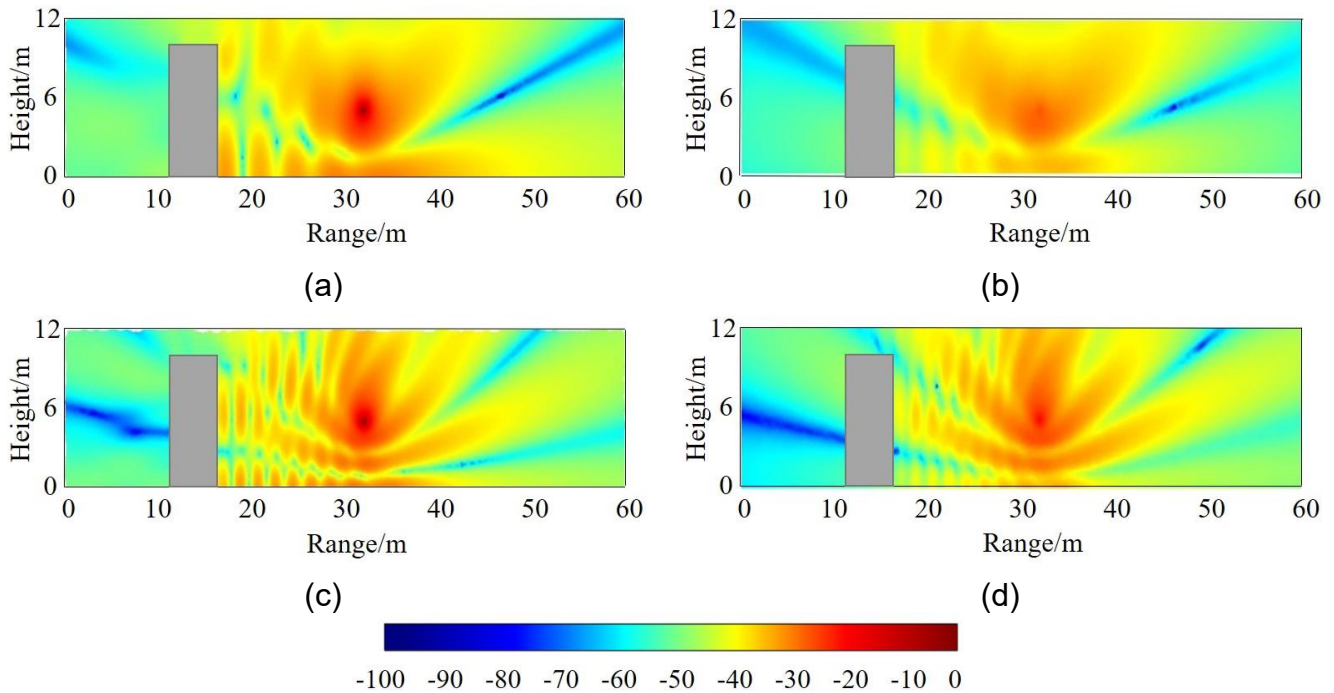


Figure.2 SPL map obtained from FEM and EnvARC over a vertical observation plane across the building center with the normal vector $(0,1,0)$. (a) FEM (50Hz) (b) EnvARC (50Hz) (c) FEM (100Hz) (d) EnvARC (100Hz).

Figure. 2 and 3 shows that similar acoustic interference patterns can be obtained using EnvARC compared with the FEM results for all case setups. When one of the building façades is directly facing the noise source, some rays are reflected in the same vertical plane and cause more regions encountering the constructive and destructive interference in Figure. 2. The edge of the building will reflect the rays to different azimuth angles, which makes the effect of the 3D environment more prominent in Figure. 3. It can be observed that EnvARC underestimates the noise level near the source, which may be caused by the singularity of the ray amplitude at the source point. Due to the summation procedure, the SPL map of EnvARC is smoother, especially for the lower frequency.

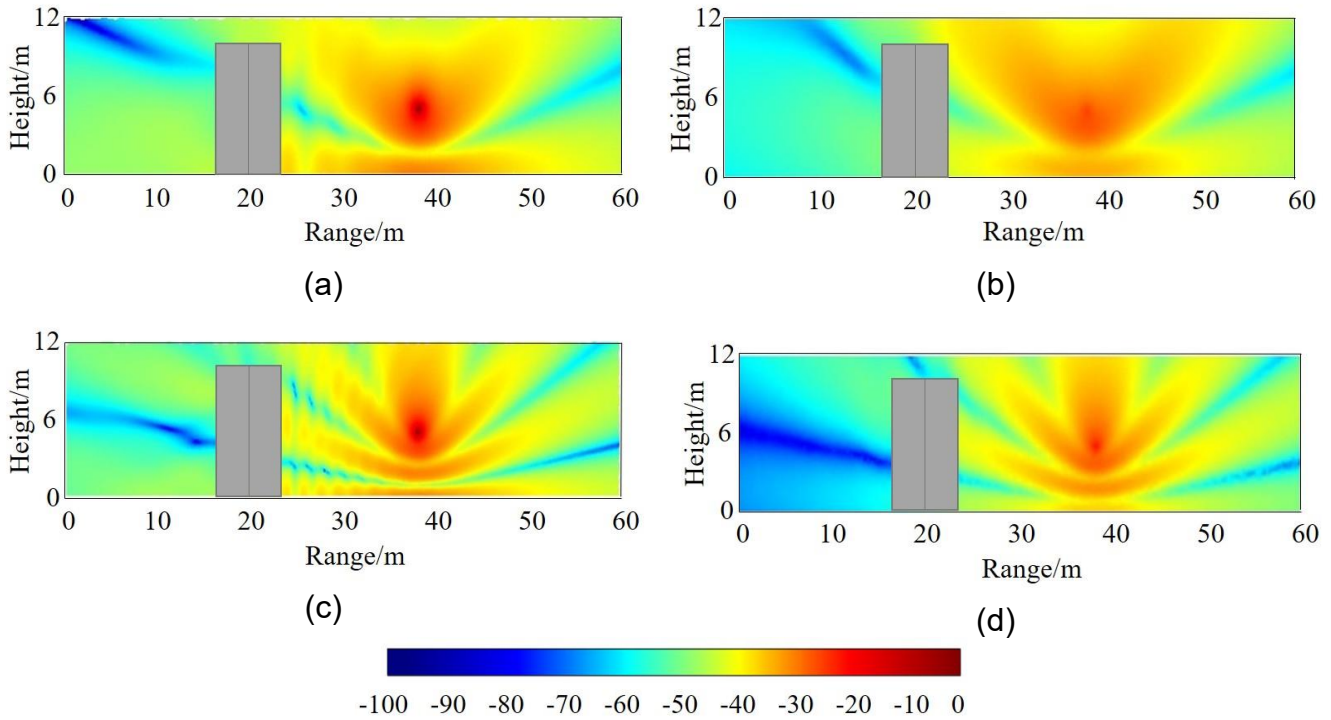


Figure.3 SPL map obtained from FEM and EnvARC over a vertical observation plane across the building center with the normal vector (1,1,0). (a) FEM (50Hz) (b) EnvARC (50Hz) (c) FEM (100Hz) (d) EnvARC (100Hz).

4. Applications in virtual flights

In this section, the EnvARC is used to investigate the effect of the flight path and boundary impedance for the noise radiation of a quadcopter. The source directivity is obtained from the Hanson's model for four propellers after summarizing the first four BPFs (200Hz, 400Hz, 400Hz and 800Hz) as shown in Figure. 4 (a). A simplified building with the dimension of 20m×30m×40m is located on an infinite planar ground. Three different paths between point A (50m, 0m, 1m) and point B (10m, 0m, 50m) are designed for a quadrotor (see Figure.4(b)), whose flight speed is assumed to be infinitely tending to zero. Only static simulation is run at different locations along these paths without considering the dynamic effect in the real flight.

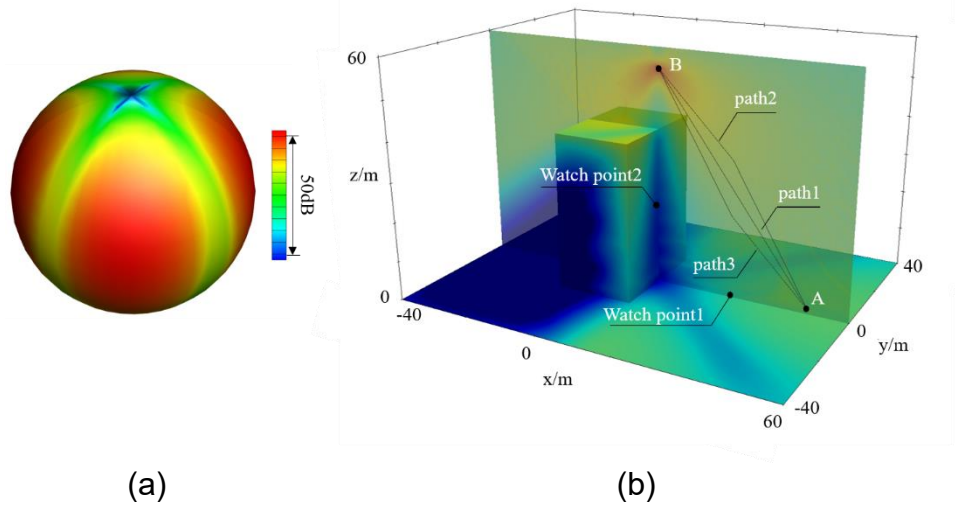


Figure.4 source model and case setup in virtual flights.

Two watchpoints are chosen on the ground of (30m, 0m, 0m) and the building surface (10m, 0m, 20m) to assess the noise impact of different drone flying paths. The SPL history at both watchpoints are plotted at the solid wall and impedance wall boundary condition for comparison in Figures 5 and 6. The flow resistivity used for the building is set as 4000 rays, while the ground is 200 rays to representing a grassland [17]. Both figures show that a finite impedance value can decrease the noise level received at the observers. Since the grassland is more absorptive than the building surface, the reflected rays by the ground can only affect observer 2 at the initial locations, causing the SPL for impedance wall dropping a little at first but almost recovering to the solid wall level afterwards. At observer 1, the change from flight path 1 to path 2 leads to an overall decrease in the SPL, and path 3 will increase the perceived noise at most of the source locations. This effect is not so obvious for observer 2, and different paths affect the noise peak location more than the overall noise level.

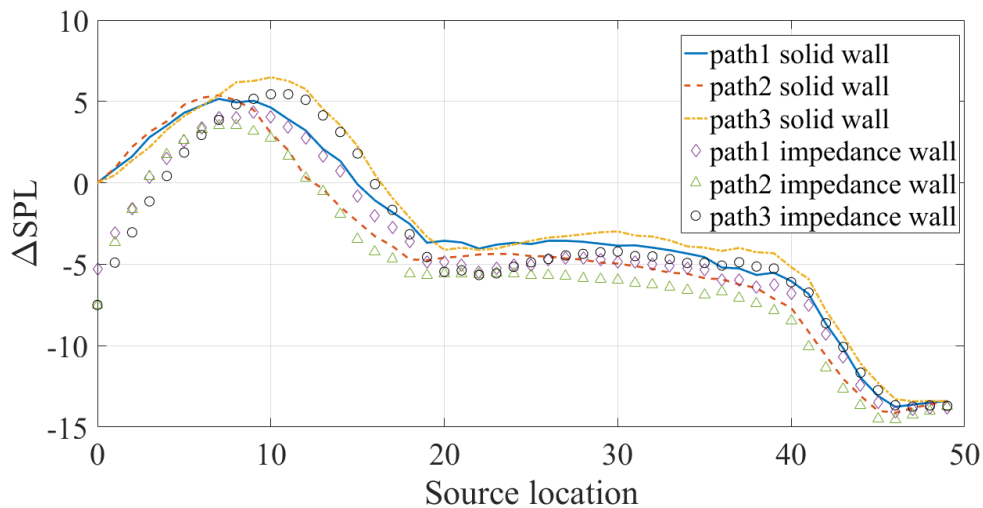


Figure.5 SPL history at watch point 1 in virtual flights of drones along three different paths for solid and impedance boundary.

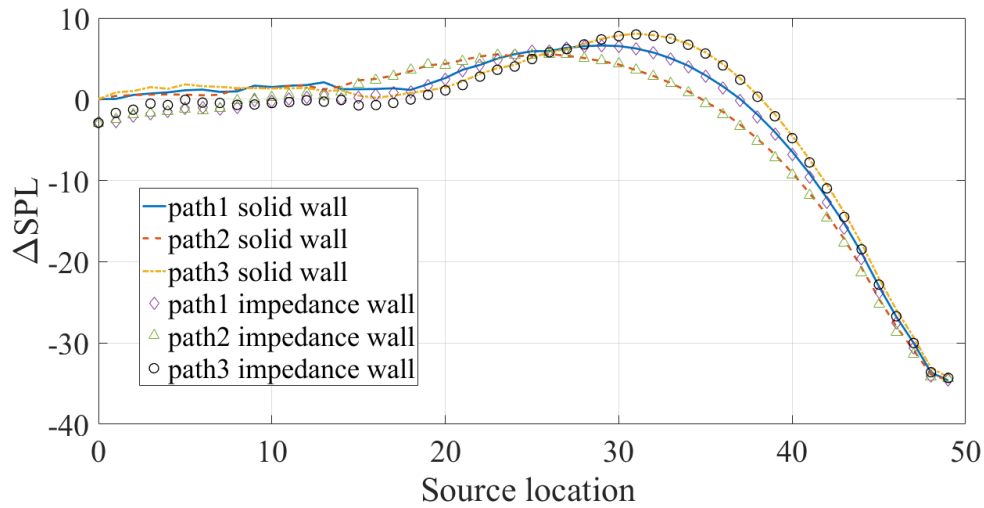


Figure.6 SPL history at watch point 2 in virtual flights of drones along three different paths for solid and impedance boundary.

5. Hovering drone in an urban environment

The capability of the EnvARC to assess the acoustic impact by a quad-rotor vehicle operating in a densely populated urban environment with complex geometry is demonstrated. The flight region has a size of 900mx930m. The tonal noise, which is the dominant source of drone noise at low frequency is computed by Hanson's model [18], which is also employed in the previous case shown in Figure 4 (a). A logarithmic sound speed profile is employed for the real atmospheric condition [19]. The atmosphere absorption is calculated according to the ISO standard [16] at the condition of 20°C, 70% humidity and 1 atm. The noise map for a drone hovering at the location (245, 661, 62) m is shown in Figure 7. The computation contains 2500 rays, and it costs 0.748 CPU hours. In another word, the computation can be finished within 1.87 minutes using 24 CPUs on a representative high-performance computer, suggesting that rapid and efficient virtual flights can be conducted to assess the drone noise impact on the environment with complex geometries.

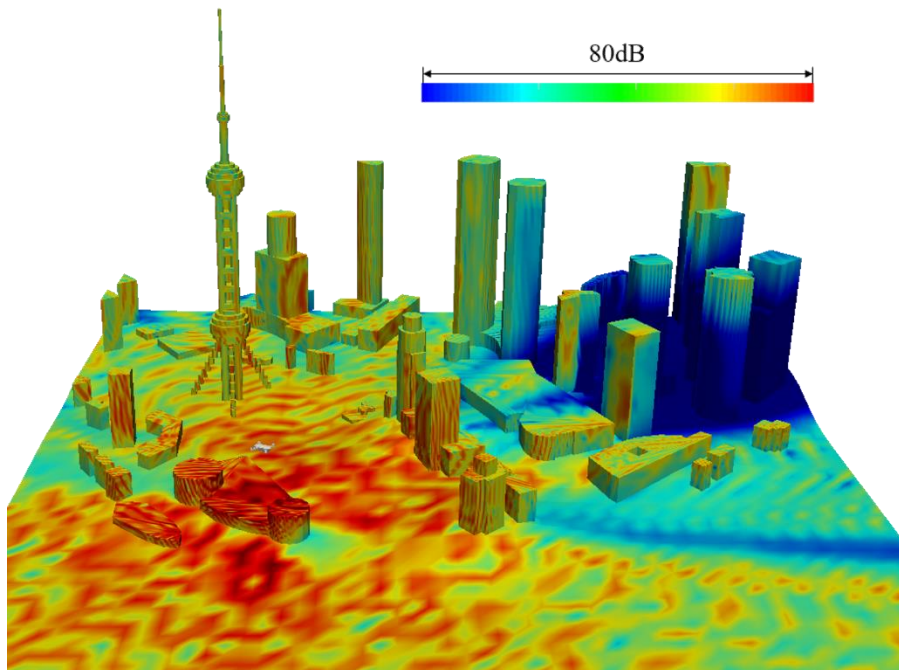


Figure.7 Noise exposure map of a hovering drone in an urban area.

6. Summary

In this work, a computationally efficient and robust simulation tool EnvARC was developed to provide quick and robust assessments of the noise effect of flying drones in complex environments with no need of practical outdoor measurements. The numerical method is based on acoustic ray tracing coupled with Gaussian beam method. The accuracy was demonstrated in the reflection test case. The developed code was applied to investigate the effect of the flying path and impedance wall on the noise exposure in virtual flights. It also gave a noise exposure map of a hovering drone in a realistic urban environment.

Acknowledgements

Bian Haoyu wishes to thank the Hong Kong University of Science and Technology (HKUST) for supporting part of his Ph.D thesis research. This work is supported by the Hong Kong Innovation and Technology Commission (ref. ITC/387/17FP), the National Natural Science Foundation of China (NSFC 11972029) and the Ministry of Science and Technology of China (SQ2018YFE010213). This work was performed at the Aerodynamics, Acoustics & Noise Control Technology Centre at HKUST.

References

1. Floreano, D. and Wood, R. J. Science, technology and the future of small autonomous drones, *Nature*, 521 (7553), 460–466, (2015).
2. Custers, B., *Future of drone use: opportunities and threats from ethical and legal perspectives*, Springer (2016).
3. Defrance, J., et al. Outdoor sound propagation reference model developed in the european harmonoise project, *Acta Acustica united with Acustica*, 93 (2), 213–227, (2007).
4. Ciskowski, R. D. and Brebbia, C. A., *Boundary element methods in acoustics*, Springer (1991).
5. Mo, Q., Yeh, H., Lin, M. and Manocha, D. Outdoor sound propagation with analytic ray curve tracer and Gaussian beam, *The Journal of the Acoustical Society of America*, 141 (3), 2289–2299, (2017).
6. Li, Y., Franke, S. and Liu, C. Numerical implementation of an adaptive fast-field program for sound propagation in layered media using the chirp z transform, *The Journal of the Acoustical Society of America*, 89 (5), 2068–2075, (1991).
7. Gdesen, A. Application of the safari model to sound propagation in the atmosphere, *The Journal of the Acoustical Society of America*, 87 (5), 1968–1974, (1990).
8. Gilbert, K. E. and White, M. J. Application of the parabolic equation to sound propagation in a refracting atmosphere, *The Journal of the Acoustical Society of America*, 85 (2), 630–637, (1989).
9. Allen, J. B. and Berkley, D. A. Image method for efficiently simulating small-room acoustics, *The Journal of the Acoustical Society of America*, 65 (4), 943–950, (1979).
10. Yang, L. and Shield, B. Development of a ray tracing computer model for the prediction of the sound field in long enclosures, *Journal of Sound and Vibration*, 229 (1), 133–146, (2000).
11. Alpkocak, A. and Sis, M. Computing impulse response of room acoustics using the ray-tracing method in time domain, *Archives of Acoustics*, 35 (4), 505–519, (2010).
12. Salomons, E. M., *Computational Atmospheric Acoustics*, Springer-Science & Business Media, B.V. (2001).
13. Cerveny, V. Expansion of a plane wave into gaussian beams, *Studia Geophysica et Geodaetica*, 26, 120–131, (1982).
14. Michael B. Porter. Beam tracing for two- and three-dimensional problems in ocean acoustics, *The Journal of the Acoustical Society of America*, 146 (3), (2019).
15. Cerveny, V., *Seismic ray theory*, Cambridge University Press (2005).
16. Standard, ISO 9613-1: Acoustics–Attenuation of sound during propagation outdoors–Part1: Calculation of the absorption of sound by the atmosphere, International Organization for

Standardization, 1993.

17. Embleton, T. F., Piercy, J. E., and Daigle, G. A., "Effective flow resistivity of ground surfaces determined by acoustical measurements," *The Journal of the Acoustical Society of America*, Vol. 74, No. 4, 1983, pp. 1239–1244.
18. Hanson, D. B., and Parzych, D. J., "Theory for noise of propellers in angular inflow with parametric studies and experimental verification," Technical Report CR 4499, NASA, 1993.
19. Salomons, E. M., Computational Atmospheric Acoustics, Springer-Science & Business Media, B.V. (2001).